Handbook of Fibrous Materials

Handbook of Fibrous Materials

Edited by
Jinlian Hu
Bipin Kumar
Jing Lu

Volume 1

WILEY-VCH

Handbook of Fibrous Materials

Edited by
Jinlian Hu
Bipin Kumar
Jing Lu

Volume 2

WILEY-VCH

Editors
Jinlian Hu
The Hong Kong Polytechnic University
Institute of Textiles and Clothing
Room QT715, Q Core, 7/F
Hung Hom
Kowloon 999077
Hong Kong S.A.R.
P.R. China

Bipin Kumar
Indian Institute of Technology Delhi
Department of Textile and Fibre Engineering
TX135, Hauz Khas
New Delhi 110016
India

Jing Lu
The Hong Kong Polytechnic University
Institute of Textiles and Clothing
Room QT807
Hung Hom
Kowloon 999077
Hong Kong S.A.R.
P.R. China

All books published by **Wiley-VCH** are carefully produced. Nevertheless, authors, editors, and publisher do not warrant the information contained in these books, including this book, to be free of errors. Readers are advised to keep in mind that statements, data, illustrations, procedural details or other items may inadvertently be inaccurate.

Library of Congress Card No.:
applied for

British Library Cataloguing-in-Publication Data
A catalogue record for this book is available from the British Library.

Bibliographic information published by the Deutsche Nationalbibliothek
The Deutsche Nationalbibliothek lists this publication in the Deutsche Nationalbibliografie; detailed bibliographic data are available on the Internet at <http://dnb.d-nb.de>.

© 2020 Wiley-VCH Verlag GmbH & Co. KGaA, Boschstr. 12, 69469 Weinheim, Germany

All rights reserved (including those of translation into other languages). No part of this book may be reproduced in any form – by photoprinting, microfilm, or any other means – nor transmitted or translated into a machine language without written permission from the publishers. Registered names, trademarks, etc. used in this book, even when not specifically marked as such, are not to be considered unprotected by law.

Print ISBN: 978-3-527-34220-4
ePDF ISBN: 978-3-527-34256-3
ePub ISBN: 978-3-527-34259-4
oBook ISBN: 978-3-527-34258-7

Cover Design Adam-Design, Weinheim, Germany
Typesetting SPi Global, Chennai, India
Printing and Binding Markono

Printed on acid-free paper

10 9 8 7 6 5 4 3 2 1

Contents

Volume 1

Preface *xix*

1 Fundamentals of the Fibrous Materials *1*
Jinlian Hu, Md A. Jahid, Narayana Harish Kumar, and Venkatesan Harun
1.1 Introduction *1*
1.1.1 What Are Fibrous Materials? *1*
1.2 Historical Evolution of Fibers *2*
1.3 Classification of Fibrous Materials *2*
1.4 Fundamental Characteristics of Fibrous Materials *6*
1.5 Morphological and Structural Properties of Fibrous Materials *7*
1.5.1 Plant or Natural Cellulosic Fibers *7*
1.5.2 Animal or Protein Fibers *7*
1.5.3 Regenerated Cellulosic Fibers *10*
1.5.4 Synthetic or Manufactured (Textile and Non-textile) Fibers *10*
1.6 Essential or Fundamental Properties of Fibrous Materials *10*
1.6.1 Physical Properties *10*
1.6.1.1 Mechanical Behavior of Fibrous Assemblies *11*
1.6.2 Chemical Properties *14*
1.6.3 Biological Properties *14*
1.6.4 Thermal Properties *14*
1.6.5 Other Desirable Properties *15*
1.7 Textile Processing *15*
1.7.1 Spinning *15*
1.7.1.1 Ring Spinning *16*
1.7.1.2 Rotor Spinning *17*
1.7.1.3 Friction Spinning *17*
1.7.1.4 Yarn Numbering System (Count) *17*
1.7.2 Fabric Manufacturing *18*
1.7.2.1 Weaving Process *18*
1.7.2.2 Knitting *19*
1.7.2.3 Nonwoven *19*
1.7.3 Wet Processing Technology *20*
1.7.3.1 Pretreatment Process *20*

1.7.3.2 Dyeing *20*
1.7.3.3 Dyeing Methods *20*
1.7.3.4 Dyes *20*
1.7.3.5 Finishing *21*
1.7.3.6 Printing *21*
1.8 Textile Applications *21*
1.8.1 Advanced Applications of Textile Material *21*
1.8.2 Functional Textile *22*
1.8.2.1 Water Repellent *22*
1.8.2.2 Water Vapor Permeability *23*
1.8.3 Applications of High-Performance Fibrous Materials *24*
1.8.3.1 Fibers for Automobile Composite *24*
1.8.3.2 Fibers as Building Materials *25*
1.8.3.3 Fibers for Auxetic Applications *25*
1.8.3.4 Fibers for Environmental Protection: Water Purification/Filtration *25*
1.8.3.5 Fibers for Optical Applications *26*
1.8.4 Application of Sensors/Actuators *26*
1.8.4.1 Fibers as Electronic Devices/Wearable Electronics/Energy Materials/Sensors and Actuators *26*
1.8.4.2 Fibers for Medical Compression *27*
1.8.4.3 Fibers for Health/Stress/Comfort Management *27*
1.8.4.4 Fibers for Thermal Protection *28*
1.8.4.5 Fibers for Radiation Protection *28*
1.8.5 Applications of Integrated Products *29*
1.8.5.1 Fibers for Tissue Engineering *29*
1.8.6 Sensitive and Smart Materials *30*
1.8.6.1 Fibers with Conductive Properties as Industrial Materials *30*
1.8.6.2 Memory Fibrous Materials *30*
1.8.7 Advantages of Fibrous Materials *30*
References *31*

2 Animal Fibers: Wool *37*
Xiao Xueliang
2.1 Introduction *37*
2.2 Classification of Wools *41*
2.2.1 Classification of Wool in Fineness *41*
2.2.2 Classification of Wool in Terms of Fiber Structure *41*
2.2.3 Classification of Wool in Terms of Fiber Type on Sheep Hair Layer *44*
2.2.4 Classification of Wool in Terms of Hair Picking Method and Original Hair Shape *44*
2.2.5 Classification of Wool in Terms of Wool Cut Season *45*
2.3 Processing of Wool Fibers and Yarns *45*
2.3.1 Primary Processing of Wool *45*
2.3.2 Yarn Spinning Process of Wool *46*
2.4 Chemical Compositions and Structural Characteristics of Wool *48*
2.4.1 Compositions of Wool *48*
2.4.2 Macromolecular Structure of Wool *49*

2.4.3 Morphology and Hierarchical Structure of Wool Fiber *50*
2.5 Properties of Wool *52*
2.5.1 Fineness of Wool *52*
2.5.2 Length of Wool Fiber *53*
2.5.3 Crimpness of Wool *55*
2.5.4 Friction and Felting Properties of Wool *56*
2.5.5 Wool Grease and Impurities *57*
2.5.6 Other Properties of Wool Fibers *59*
2.6 Quality Inspection and Evaluation of Wools *60*
2.6.1 Raw Wools from Sheep *60*
2.6.2 Fine Wool from China's Raw and Improved Sheep Breed *60*
2.6.3 Tops of Domestic Fine Wool and Its Improved Wool *60*
2.6.4 Inspection and Evaluation of Australia Wool *61*
2.6.5 Inspection and Evaluation of Wool Fabric *61*
2.7 Shape Memory Properties of Wool *63*
2.8 Future Trends of Application of Wool Keratin *70*
2.8.1 Extraction of Keratin from Wool for New Product Development *70*
2.8.2 Industrial Trends Relating to Sustainable Polymers *71*
2.8.3 Future Trends *71*
2.8.4 Sources of Further Information and Advice *72*
References *72*

3 Animal Fibers: Silk *75*
K. Murugesh Babu
3.1 Introduction to Silk and Silk Industry *75*
3.2 Types of Silk and Their Importance *78*
3.2.1 Mulberry *78*
3.2.1.1 Types of Mulberry Silk *79*
3.2.2 Non-mulberry *80*
3.2.2.1 Tasar *80*
3.2.2.2 Oak Tasar *81*
3.2.2.3 Eri *81*
3.2.2.4 Muga *82*
3.2.2.5 Anaphe Silk *82*
3.2.2.6 Fagara Silk *83*
3.2.2.7 Coan Silk *83*
3.2.2.8 Mussel Silk *83*
3.2.2.9 Spider Silk *83*
3.2.3 Fine Structure of Silk *83*
3.2.3.1 Longitudinal View *84*
3.2.3.2 Cross-Sectional View *84*
3.2.4 Amino Acid Composition *85*
3.2.5 Properties of Silk Fibers *86*
3.2.5.1 Tensile Properties *86*
3.2.5.2 Optical Properties *87*
3.2.5.3 Viscoelastic Behavior *88*
3.2.6 Applications *88*

3.2.6.1 Textile and Apparels *89*
3.2.6.2 Biomedical Field *90*
3.2.6.3 Fiber-Reinforced Composites *90*
3.3 Future Trends *91*
3.4 Summary *92*
References *92*

4 Cellulose Fibers *95*
Feng Jiang
4.1 Introduction *95*
4.2 Structure and Biosynthesis of Cellulose *95*
4.3 Nanoscaled Cellulose Fibers *100*
4.4 Submicron-Scaled Cellulose Fibers *107*
4.5 Macroscaled Cellulose Fibers *114*
4.6 Applications of Cellulose Fibers *118*
4.7 Conclusion and Perspectives *119*
References *119*

5 Chitosan Fibers *125*
Seema Sakkara, Mysore Sridhar Santosh, and Narendra Reddy
5.1 Introduction *125*
5.2 Extraction/Modification of Chitosan *127*
5.3 Fibers from Chitosan *131*
5.3.1 Production of Pure Chitosan Fibers *131*
5.3.2 Chitosan Blend Fibers *135*
5.3.3 Generating Hollow Chitosan Fibers *139*
5.3.4 Microfluidic Method of Producing Chitosan Fibers *140*
5.3.5 Application of Chitosan Fibers *140*
5.4 Electrospun Chitosan Fibers *145*
5.5 Regenerated Chitosan Fibers *151*
5.6 Conclusions *151*
Acknowledgments *152*
References *152*

6 Collagen Fibers *157*
Jinlian Hu and Yanting Han
6.1 Introduction *157*
6.2 Source and Structure of CF *157*
6.3 Isolation of Natural CF *160*
6.4 Spinning of CF *160*
6.4.1 Extraction of Collagen *160*
6.4.2 Electrospinning of CF *162*
6.4.3 Wet Spinning of CF *162*
6.4.4 Microfluidic Spinning of CF *164*
6.4.5 Collagen Composite Fiber *165*
6.5 Application of CF *165*
6.6 Perspectives *171*

References *171*

7 Electrospun Fibers for Filtration *175*
Xia Yin, Jianyong Yu, and Bin Ding
7.1 Introduction *175*
7.2 Fabrication Technologies *176*
7.2.1 Electrospinning *176*
7.2.2 Electro-netting *177*
7.3 Principles and Theories *178*
7.3.1 Fundamental Theory of Electrospinning *178*
7.3.2 Formation Mechanism of the Nanofiber/Net (NF/N) Membranes *180*
7.4 Structure and Properties *181*
7.4.1 Types and Structures of the Nanofiber Membranes *181*
7.4.2 Structures and Species of the Nanofiber/Net (NF/N) Membranes *183*
7.5 Application of Nanofibrous Membranes in Air Filtration *185*
7.5.1 Normal Temperature Filter *185*
7.5.1.1 Electrospun Nanofiber Membranes *185*
7.5.1.2 Electrospun Nanofiber/Net (NF/N) Membranes *191*
7.5.2 Medium-High Temperature Filter *196*
7.6 Future Trends *199*
References *199*

8 Aramid Fibers *207*
Manjeet Jassal, Ashwini K. Agrawal, Deepika Gupta, and Kamlesh Panwar
8.1 Introduction *207*
8.2 Preparation of Aromatic Polyamides *207*
8.2.1 Low Temperature Polycondensation *208*
8.2.2 Direct Polymerization in Solution Using Phosphites *210*
8.2.3 Copolyaramids *210*
8.3 Aramid Solutions *211*
8.4 Spinning of Aramid Fibers *214*
8.4.1 Dry Spinning *214*
8.4.2 Wet Spinning *214*
8.4.3 Dry-Jet-Wet Spinning *215*
8.4.4 Aramid Nanofibers *216*
8.4.5 Fiber Heat Treatment *216*
8.5 Influence of Structure on Properties *217*
8.5.1 Fiber Structure *217*
8.5.2 Fiber Properties *219*
8.5.2.1 Chemical Properties *219*
8.5.2.2 Mechanical Properties *220*
8.5.2.3 Thermal Properties *221*
8.6 Applications *222*
8.6.1 Composites with Soft Materials *222*
8.6.2 Advanced Composites *224*
8.6.3 Ultrafiltration and Hemodialysis *224*
8.6.4 Ropes and Cables *224*

8.6.5 Industrial Protective Apparel *225*
8.6.6 Ballistics *225*
8.6.7 Permselective Use *225*
8.6.8 Electrical Application *226*
8.6.9 Communication *226*
8.7 Future Trends *227*
References *227*

9 Conductive Fibers *233*
Tung Pham and Thomas Bechtold
9.1 Introduction *233*
9.2 Production of Conductive Fibers: Principles and Technologies *233*
9.2.1 Conductivity *233*
9.2.2 Metal Fibers: Coating and Deposition *234*
9.2.3 Intrinsically Conductive Polymers and Coating *239*
9.2.4 Carbon-Based Fibers (Carbon Black, Carbon Nanotubes, Graphene) *242*
9.2.5 Combination of Different Techniques *243*
9.3 Integration of Conductivity into Textile Structures *244*
9.3.1 Fiber Material Selection/Yarn Production *245*
9.3.2 Fabric Production *248*
9.3.3 Embroidery/Sewing *248*
9.3.4 Printing *249*
9.4 Applications/Examples *250*
9.4.1 Material Selection *250*
9.4.2 Washable Sensors (Example: Moisture Bed Sensor) *251*
9.4.3 Textile Electrodes *252*
9.4.4 Flexible Devices *253*
9.4.5 Wearable Electronics *253*
9.4.6 Summary and Future Trends *253*
References *254*

10 Phase Change Fibers *263*
Subrata Mondal
10.1 Introduction *263*
10.2 Phase Change Materials (PCMs) *264*
10.2.1 Principle of Phase Change Materials *264*
10.2.2 Various Types of Phase Change Materials *265*
10.2.2.1 Organic PCMs *266*
10.2.2.2 Inorganic PCMs *266*
10.2.2.3 Eutectic PCMs *267*
10.3 Phase Change Fibers *267*
10.3.1 How PCM Works with Fibrous Structures *267*
10.3.2 Microencapsulation of PCMs *268*
10.3.3 Techniques to Prepare Phase Change Fibrous Structures *270*
10.3.3.1 Coating of Encapsulated PCM on Fibrous Structure *270*

10.3.3.2 PCM Incorporated Fibrous Structure by Conventional Spinning *271*
10.3.3.3 Phase Change Fibers by Electrospinning *272*
10.4 Phase Change Fibers for Advanced Material Applications *274*
10.4.1 Phase Change Fibers for Advanced Textile Applications *274*
10.4.1.1 Sportswear *274*
10.4.1.2 Hospital Applications *274*
10.4.1.3 Beddings and Accessories *275*
10.4.1.4 Other Applications in Advanced Textiles *275*
10.4.2 Automotive Industries *275*
10.4.3 Electrical Applications *275*
10.4.4 Other Applications *276*
10.5 Summary *276*
References *276*

11 Bicomponent Fibers *281*
Rudolf Hufenus, Yurong Yan, Martin Dauner, Donggang Yao, and Takeshi Kikutani
11.1 Introduction *281*
11.2 Bicomponent Fiber Spinning Technologies *282*
11.2.1 Spin Pack Design *282*
11.2.2 Cross-Sectional Geometries *284*
11.2.3 Melt Spinning Equipment *285*
11.2.4 Special Spin Pack Designs *286*
11.3 Principles and Theories of Bicomponent Spinning *288*
11.3.1 Structure Formation During Spinning and Drawing *288*
11.3.2 Mutual Influence of Components on Orientation and Crystallinity *288*
11.3.3 Interfacial Adhesion *290*
11.3.4 Coextrusion Instabilities *291*
11.3.5 Encapsulation *292*
11.3.6 Volatiles *293*
11.3.7 Simulation and Modeling *293*
11.4 Post-treatment of Bicomponent Fibers *295*
11.5 Applications of Bicomponent Fibers *296*
11.5.1 Fibers as Bonding Elements in Nonwovens *296*
11.5.2 Microfibers *297*
11.5.3 Fibers with Special Cross Sections *297*
11.5.4 Fibers with High-Performance Core *298*
11.5.5 Fibers with Functional Surface *299*
11.5.6 Biodegradable Fibers *300*
11.5.7 Polymer Optical Fibers *301*
11.5.8 Electrically Conductive Fibers *301*
11.5.9 Liquid-Core Fibers *302*
11.5.10 Fibers for Fully Thermoplastic Fiber-Reinforced Composites *303*
11.5.11 Shape Memory Fibers *304*
References *304*

12 Superabsorbent Fibers *315*
Nuray Ucar and Burçak K. Kayaoğlu
12.1 Introduction *315*
12.2 Overview of Superabsorbent Fibers *316*
12.2.1 History of Superabsorbent Fibers *316*
12.2.2 Main Principle of Superabsorbency *316*
12.2.3 Polymer Materials *319*
12.2.4 Production Methods *319*
12.2.4.1 Mixing the Superabsorbent Material with Hydrophobic/Hydrophilic Material *320*
12.2.4.2 Directly Using a Superabsorbent Polymer for Superabsorbent Fiber Production *322*
12.2.5 Test Methods *325*
12.3 Application *327*
12.4 Future Scope and Challenges Ahead *329*
12.5 Summary *330*
References *331*

13 Elastic Fibers *335*
Lu Jing
13.1 Introduction *335*
13.1.1 Definition *335*
13.1.2 Classification *335*
13.2 Structure, Principles, and Characteristics *338*
13.2.1 Structure and Principle in Elasticity *338*
13.2.2 Structure and Principle in Other Performances *343*
13.3 New Development of Elastic Fibers *344*
13.3.1 Polyurethane Elastic Fiber *344*
13.3.2 Bicomponent Elastic Fiber *350*
13.3.3 Polyolefin Elastic Fiber *351*
13.3.4 Polyether-Ester Elastic Fiber *352*
13.3.5 Polyester Elastic Fiber *353*
13.4 Evaluation and Application *353*
13.5 Future Trends *356*
References *357*

14 Smart Fibers *361*
Dong Wang, Weibing Zhong, Wen Wang, Qing Zhu, and Mu Fang Li
14.1 Introduction *361*
14.1.1 Definition *361*
14.1.2 Research Status *361*
14.1.3 Classification *362*
14.2 Raw Materials and Preparation *362*
14.2.1 Raw Materials *362*
14.2.1.1 Metal Related *363*
14.2.1.2 Inorganic Nonmetallic and Polymer Related *364*

14.2.2 Preparations *365*
14.2.2.1 Spinning Methods *365*
14.2.2.2 Intelligentization Method *366*
14.3 Structure and Properties *367*
14.3.1 Primary Fiber Structure *368*
14.3.1.1 Conventional Fiber Structure *368*
14.3.1.2 Skin-Core Structure *369*
14.3.2 Multilayered Structure *369*
14.3.2.1 Coating with Single Layer *370*
14.3.2.2 Coating with No Less Than Double Layers *370*
14.3.3 Three-Dimensional Fiber-Based Structures *372*
14.3.3.1 Fabrics and Fiber-Based Membrane *372*
14.3.3.2 Aerogel *373*
14.4 Principles and Theories *373*
14.4.1 Shape Memory Fiber *373*
14.4.2 Fiber-Based Actuator *374*
14.4.3 Luminescence Fiber *375*
14.4.4 Color-Changed Fiber *376*
14.4.5 Thermoregulated Fiber *377*
14.5 Applications *377*
14.5.1 Smart Fibers Used in Textiles *377*
14.5.1.1 Smart Clothing *377*
14.5.1.2 Wearable Electronics *378*
14.5.2 Smart Fibers Used in Industrial *378*
14.5.2.1 Medical Supplies *378*
14.5.2.2 Sensors *380*
14.5.2.3 Energy Conversion *381*
14.5.3 Other Uses *381*
14.6 Future Trends *381*
References *383*

15 Optical Fibers *391*
Hiroaki Ishizawa
15.1 Introduction *391*
15.2 Fundamentals of Fiber Optics *392*
15.2.1 Fiber Optics Classification *392*
15.2.2 Manufacturing Process *392*
15.2.3 General Characteristics of Fiber Optics *394*
15.3 Optical Fiber Sensor *394*
15.3.1 Advantages of Optical Fiber Sensors *394*
15.3.2 Principles and Applications of Optical Fiber Sensors *395*
15.3.2.1 Temperature Measurement *395*
15.3.2.2 Oxygen Concentration Measurement *395*
15.3.2.3 Strain Measurement by Brillouin Optical Time Domain Reflectometry (B-OTDR) and Fiber Bragg Grating Sensors (FBG) *395*
15.3.2.4 Biomedical Measurement *397*

15.3.3 Principles and Application of the Vital Sign Measurement by FBG Sensor *398*
15.3.3.1 FBG Sensor Interrogator to Measure Human Vital Signs *398*
15.3.3.2 Pulse Wave Measurement *399*
15.3.3.3 Pulse Rate Measurement *400*
15.3.3.4 Respiratory Rate Measurement *400*
15.3.3.5 Blood Pressure Measurement by Pulse Transit Time Detection *401*
15.3.3.6 Partial Least Squares Regression Calibration for Blood Pressure Measurement *402*
15.4 Healthcare Monitoring by Using FBG Sensor *404*
15.4.1 FBG Sensor Application to Multi-vital Sign Measurement *404*
15.4.2 Fabrication of Smart Textiles *405*
15.5 Future Trends: As the Summary *406*
References *407*

16 Memory Fibers *411*
Harishkumar Narayana, Jinlian Hu, and Bipin Kumar
16.1 Introduction *411*
16.2 Morphology and Molecular Mechanism of Memory Polymers *412*
16.2.1 Nature of Transitions in MPs *413*
16.3 Evaluation of Shape Memory Properties *413*
16.4 Memory Polymers As Fibers (MPFs) *414*
16.4.1 Which Fibers Do Have Better Performance, Wet or Melt Spun? *415*
16.4.2 Effect of Post-spinning Operations on MP Fiber Properties *417*
16.4.2.1 Effect of Thermal Setting or Heat Treatment *417*
16.4.2.2 Influence of Drawing Process *420*
16.4.3 Other Type of MPU Fibers *421*
16.4.3.1 Smart Hollow Fibers *421*
16.4.3.2 Electro-responsive Fibers *421*
16.4.3.3 Electrospun Fibers *422*
16.5 Novel Stress Memory Behavior in MPs *422*
16.5.1 What Is Stress Memory? *422*
16.5.2 Mechanism of Stress Memory *423*
16.5.3 Components of Stress Memory *424*
16.6 Stress Memory Behavior in Memory Fibers *425*
16.7 Techniques of Characterization for Memory Fibers *428*
16.8 Potential Application of Stress Memory Fiber/Filaments *428*
16.9 Recent Advances in MP Fibers *430*
16.10 Future Trends *430*
References *430*

17 Textile Mechanics: Fibers and Yarns *435*
Zubair Khaliq and Adeel Zulifqar
17.1 Introduction *435*
17.2 Fiber *436*
17.2.1 Fiber Consumption *436*
17.3 Strength Contributing Fiber Parameters *438*

17.4 Mechanical Properties of Fiber *438*
17.4.1 Stress–Strain Curve *438*
17.4.2 Elastic Recovery, Work of Rupture, and Resilience *440*
17.4.3 Effects of Time, Temperature, and Moisture *440*
17.5 Yarn Classification *440*
17.6 Yarn Construction *441*
17.6.1 Ring-Spun Yarn *442*
17.6.2 Yarn Structure *443*
17.6.2.1 Carded and Combed Yarns *443*
17.6.2.2 Compact Yarn *444*
17.6.3 Rotor-Spun Yarn *445*
17.6.3.1 Yarn Structure *446*
17.6.4 Air Vortex Spun Yarn *446*
17.6.4.1 Yarn Structure *446*
17.6.5 Frictional Spun Yarn *448*
17.6.6 Mechanical Properties of the Yarn *448*
17.6.7 Important Parameters of Yarn Tensile Strength *448*
17.6.8 Strength–Comfort–Twist Relationship *451*
References *454*

18 Textile Mechanics: Woven Fabrics *455*
Adeel Zulifqar, Zubair Khaliq, and Hong Hu
18.1 Introduction *455*
18.1.1 Woven Fabric Structures *456*
18.1.1.1 Regular Woven Structures (Basic Weaves) *456*
18.1.1.2 Irregular Woven Structures *457*
18.1.2 Weave Factor *457*
18.1.3 The Myth of Crimp *458*
18.2 Woven Fabrics Geometrical Models *458*
18.3 Woven Fabric Mechanics, Theories, and Methodologies *460*
18.3.1 Tensile Deformation of Woven Fabrics *461*
18.3.1.1 Woven Fabric Behavior When Extended in Principal Directions *462*
18.3.1.2 Woven Fabric Behavior When Extended in Bias Direction *463*
18.3.1.3 Effect of Yarn Crimp and Yarn Friction Coefficient on Fabric Mechanical Properties *463*
18.3.1.4 Anisotropy of Woven Fabric Tensile Properties *464*
18.3.2 Compression Deformation of Woven Fabrics *465*
18.3.3 Shearing Deformation of Woven Fabrics *468*
18.4 Mathematical Modeling of Woven Fabric Constitutive Laws *469*
18.4.1 Constitutive Laws of Woven Fabric *470*
18.4.2 Computational Woven Fabric Mechanics *471*
18.4.2.1 Continuum Models *471*
18.4.2.2 Discontinuum Models *471*
18.4.3 Energy Methods for Woven Fabric Mechanics *472*
18.5 Conclusion *473*
References *474*

19 Fabric Making Technologies *477*
Tao Hua
19.1 Introduction *477*
19.2 Weaving *479*
19.2.1 Weaving Machines *479*
19.2.2 Woven Structures *481*
19.2.3 Properties *484*
19.2.4 Applications *484*
19.3 Knitting *485*
19.3.1 Knitting Machines *485*
19.3.2 Knitted Fabric Structures *486*
19.3.3 Properties *488*
19.3.4 Applications *489*
19.4 Nonwovens *490*
19.4.1 Manufacture of Nonwovens *490*
19.4.2 Properties *492*
19.4.3 Applications *493*
19.5 Braiding *493*
19.5.1 Braiding Processes and Machines *493*
19.5.2 Braided Structures and Properties *494*
19.5.3 Applications *495*
19.6 Future Trends *496*
References *496*

Volume 2

Preface *xv*

20 Chemical Characterization of Fibrous Materials *499*
Chi-wai Kan and Ka-po Maggie Tang

21 Soft Computing in Fibrous Materials *529*
Abhijit Majumdar, Piyali Hatua, and Mirela Blaga

22 Fiber-Shaped Electronic Devices *557*
Yang Zhou, Jian Fang, Yan Zhao, and Tong Lin

23 Fibers for Optical Textiles *593*
Dana Křemenáková, Jiri Militky, and Rajesh Mishra

24 Fibers as Energy Materials *649*
Jiadeng Zhu, Esra Serife Pampal, Yeqian Ge, Jennifer D. Leary, and Xiangwu Zhang

25 Fiber-Based Sensors and Actuators *681*
Xiaomeng Fang, Kony Chatterjee, Ashish Kapoor, and Tushar Ghosh

26 **Textile-Based Electronics: Polymer-Assisted Metal Deposition (PAMD)** *721*
Casey Yan and Zijian Zheng

27 **Fibers for Medical Compression** *749*
Bipin Kumar, Harishkumar Narayana, and Jinlian Hu

28 **Electrospun Nanofibers for Environmental Protection: Water Purification** *773*
Hongyang Ma, Christian Burger, Benjamin Chu, and Benjamin S. Hsiao

29 **Fibers for Filtration** *807*
Govindharajan Thilagavathi and Siddhan Periyasamy

30 **Fibrous Materials for Thermal Protection** *831*
Gouwen Song and Yun Su

31 **Comfort Management of Fibrous Materials** *857*
Chengjiao Zhang and Faming Wang

32 **Fibers for Radiation Protection** *889*
Boris Mahltig

33 **Fibrous Materials for Antimicrobial Applications** *927*
Yue Deng, Yang Si, and Gang Sun

34 **Fibers for Auxetic Applications** *953*
Hong Hu and Adeel Zulifqar

Index *973*

Contents

Volume 1

Preface *xix*

1 **Fundamentals of the Fibrous Materials** *1*
Jinlian Hu, Md A. Jahid, Narayana Harish Kumar, and Venkatesan Harun

2 **Animal Fibers: Wool** *37*
Xiao Xueliang

3 **Animal Fibers: Silk** *75*
K. Murugesh Babu

4 **Cellulose Fibers** *95*
Feng Jiang

5 **Chitosan Fibers** *125*
Seema Sakkara, Mysore Sridhar Santosh, and Narendra Reddy

6 **Collagen Fibers** *157*
Jinlian Hu and Yanting Han

7 **Electrospun Fibers for Filtration** *175*
Xia Yin, Jianyong Yu, and Bin Ding

8 **Aramid Fibers** *207*
Manjeet Jassal, Ashwini K. Agrawal, Deepika Gupta, and Kamlesh Panwar

9 **Conductive Fibers** *233*
Tung Pham and Thomas Bechtold

10 **Phase Change Fibers** *263*
Subrata Mondal

11 Bicomponent Fibers *281*
Rudolf Hufenus, Yurong Yan, Martin Dauner, Donggang Yao, and Takeshi Kikutani

12 Superabsorbent Fibers *315*
Nuray Ucar and Burçak K. Kayaoğlu

13 Elastic Fibers *335*
Lu Jing

14 Smart Fibers *361*
Dong Wang, Weibing Zhong, Wen Wang, Qing Zhu, and Mu Fang Li

15 Optical Fibers *391*
Hiroaki Ishizawa

16 Memory Fibers *411*
Harishkumar Narayana, Jinlian Hu, and Bipin Kumar

17 Textile Mechanics: Fibers and Yarns *435*
Zubair Khaliq and Adeel Zulifqar

18 Textile Mechanics: Woven Fabrics *455*
Adeel Zulifqar, Zubair Khaliq, and Hong Hu

19 Fabric Making Technologies *477*
Tao Hua

Volume 2

Preface *xv*

20 Chemical Characterization of Fibrous Materials *499*
Chi-wai Kan and Ka-po Maggie Tang
20.1 Introduction *499*
20.2 Chemical Finishing of Fibrous Materials for Advanced Applications *500*
20.2.1 Electronic Textiles *500*
20.2.1.1 Conductive Fibers *500*
20.2.1.2 Conductive Fabrics *500*
20.2.1.3 Conductive Inks *500*
20.2.2 Medical Textiles *501*
20.2.2.1 Add into the Initial Polymer Solution or Chemical Chain Prior to Fiber Extrusion *503*
20.2.2.2 During Textile Finishing *504*

20.2.3 Self-Cleaning Textiles *506*
20.3 Principles and Methods in Chemical Characterization of Fibrous Materials *507*
20.3.1 Fourier Transform Infrared (FTIR) Spectroscopy *507*
20.3.2 X-Ray Diffraction (XRD) *509*
20.3.3 X-Ray Photoelectron Spectroscopy (XPS) *511*
20.3.4 X-Ray Fluorescence *512*
20.3.5 Chromatographic Methods *512*
20.3.6 Energy-Dispersive X-Ray Analysis (EDX) *513*
20.3.7 Scanning Electron Microscope (SEM) *515*
20.3.8 Atomic Force Microscopy (AFM) *515*
20.4 Performance, Evaluations, and Applications of Chemical Treatment on Fibrous Materials *515*
20.4.1 Electronic Textiles *515*
20.4.1.1 Fashion Statements *515*
20.4.1.2 Utility Functions *515*
20.4.2 Medical Textiles *518*
20.4.3 Self-Cleaning Textiles *519*
20.5 Performance Tests *521*
20.6 Conclusion *522*
Acknowledgment *522*
References *522*

21 Soft Computing in Fibrous Materials *529*
Abhijit Majumdar, Piyali Hatua, and Mirela Blaga
21.1 Introduction *529*
21.2 Soft Computing Techniques *530*
21.2.1 Artificial Neural Network (ANN) *530*
21.2.1.1 Back-Propagation Algorithm *532*
21.2.1.2 Levenberg–Marquardt Algorithm *533*
21.2.1.3 Important Parameters of Artificial Neural Network *534*
21.2.2 Fuzzy Logic *535*
21.2.2.1 Types of Fuzzy Inference System *538*
21.2.3 Genetic Algorithm *539*
21.2.4 Hybrid Systems *541*
21.2.4.1 Adaptive Network-Based Fuzzy Inference System (ANFIS) *541*
21.3 Applications of Soft Computing in Fibrous Materials *544*
21.3.1 Applications in Yarn Manufacturing *544*
21.3.1.1 Yarn Engineering and Process Optimization *544*
21.3.2 Applications in Fabric Property Prediction *545*
21.3.2.1 Prediction of Mechanical Properties of Fabrics *546*
21.3.2.2 Prediction of Transmission Properties of Fabrics *546*
21.3.2.3 Modeling of Fabric UV Protection *547*
21.3.2.4 Applications in Nonwoven Fabrics *551*
21.4 Conclusions *551*
References *552*

22 Fiber-Shaped Electronic Devices *557*
Yang Zhou, Jian Fang, Yan Zhao, and Tong Lin
22.1 Introduction *557*
22.2 Fiber-Shaped Electronic Devices *558*
22.2.1 Twisted Fiber Devices (TFDs) *559*
22.2.2 Fiber Electrode Wrapped Fiber Devices (FEWFDs) *560*
22.2.3 Sheath–Core Single Fiber Devices (SCSFDs) *561*
22.2.4 Parallel Coil Fiber Devices (PCFDs) *561*
22.3 Electrode Materials *562*
22.3.1 Metals and Metal Oxides *562*
22.3.2 Carbon-Based Materials *564*
22.3.3 Conducting Polymers *565*
22.4 Applications *566*
22.4.1 Energy Harvesters *566*
22.4.1.1 Thermal Energy Harvesters *566*
22.4.1.2 Solar Cells *568*
22.4.1.3 Mechanical Energy Harvesters *570*
22.4.2 Energy Storage *572*
22.4.2.1 Supercapacitors *572*
22.4.2.2 Fiber-Shaped Li-Ion Battery *575*
22.4.3 Electrochromic Fibers *577*
22.4.4 Transistors *580*
22.4.5 Fiber-Shaped Electroluminescent Device *581*
22.4.6 Fiber-Shaped Sensors *582*
22.4.7 Characterization Techniques and Key Parameter *583*
22.5 Conclusions *584*
References *584*

23 Fibers for Optical Textiles *593*
Dana Křemenáková, Jiri Militky, and Rajesh Mishra
23.1 Introduction *593*
23.2 Principles of Fibers Optics *595*
23.3 Materials of POF *604*
23.3.1 Core *604*
23.3.2 Cladding *608*
23.3.3 Jacket *608*
23.4 Side-Emitting POF *609*
23.4.1 SEPOF Based on Difference Between Refractive Indexes *610*
23.4.2 SEPOF Based on Multiple Micro-bending *612*
23.4.3 Modifications of POF Structure *616*
23.4.4 Local Side Emission *620*
23.5 Properties of POF *622*
23.5.1 Optical Attenuation *623*
23.5.2 Mechanical Properties *627*
23.5.3 Thermal Properties *635*
23.6 Illumination Systems Using POF *636*
23.7 LIHS Applications *642*

23.8 Conclusion *643*
References *644*

24 Fibers as Energy Materials *649*
Jiadeng Zhu, Esra Serife Pampal, Yeqian Ge, Jennifer D. Leary, and Xiangwu Zhang
24.1 Introduction to Fibers as Energy Materials *649*
24.2 Fundamental Principles *649*
24.2.1 Basic Terms Related to Energy *650*
24.2.2 Principles of Lithium-Ion Batteries *650*
24.2.3 Principles of Supercapacitors *651*
24.3 Characterization, Structure, and Fabrication of Fibrous Energy Materials *652*
24.3.1 Commonly Used Characterization Techniques for Fibrous Energy Materials *653*
24.3.2 Fibrous Structures of Electrodes *653*
24.3.2.1 Continuous Fibers *653*
24.3.2.2 Carbon Fibers Containing Nanoparticles *653*
24.3.2.3 Porous and Tubular Fibers *654*
24.3.3 Fibrous Structures of Separators *656*
24.3.4 Fabrication Approaches *657*
24.4 Applications to Batteries, Supercapacitors, and Energy Harvesting *659*
24.4.1 Batteries *659*
24.4.2 Supercapacitors *665*
24.4.3 Energy Harvesting Devices *667*
24.5 Future Trends *672*
References *672*

25 Fiber-Based Sensors and Actuators *681*
Xiaomeng Fang, Kony Chatterjee, Ashish Kapoor, and Tushar Ghosh
25.1 Introduction *681*
25.2 Fibers as Actuators and Sensors *682*
25.3 Fundamental Principle and Types of Fiber Actuators *683*
25.3.1 Shape Memory Materials *683*
25.3.2 Piezoelectric Materials *684*
25.3.3 Electrically Conducting Polymers *686*
25.3.4 Dielectric Electroactive Polymers *688*
25.3.5 Carbon Nanotubes *689*
25.3.6 Twisted/Coiled Fibers *694*
25.3.7 Other Types *694*
25.4 Fundamental Principle and Types of Fiber Sensors *694*
25.4.1 Strain and Pressure Sensors *696*
25.4.1.1 Piezoresistive Type *696*
25.4.1.2 Capacitive Type *699*
25.4.1.3 Piezoelectric Type *700*
25.4.1.4 Optical Type *704*

25.4.2 Humidity and Temperature Sensors *705*
25.4.3 Chemical Sensors *705*
25.5 Conclusions and Outlook *709*
References *710*

26 Textile-Based Electronics: Polymer-Assisted Metal Deposition (PAMD) *721*
Casey Yan and Zijian Zheng
26.1 Introduction *721*
26.1.1 The Rise of Textile-Based Electronics *721*
26.1.2 The Essential: High-Performance Conductive Textiles *722*
26.1.3 Fabrication of Metallic Textiles and the Challenges *723*
26.1.4 Polymer Brushes Tackle Metal/Textile Interfacial Challenge *724*
26.2 Polymer-Assisted Metal Deposition (PAMD) *726*
26.2.1 What Are Polymer Brushes? *726*
26.2.2 Mechanism of PAMD *728*
26.2.3 Brush Selection for ELD *731*
26.2.3.1 Cationic Polymer Brushes *731*
26.2.3.2 Anionic Polymer Brushes *732*
26.2.3.3 Nonionic Polymer Brushes *733*
26.2.3.4 Advantages of Using Polymer Brushes as ELD Platform *733*
26.2.3.5 Fabrication of Metallic Textiles via PAMD *734*
26.3 Strategy to Fabricate Patterned Metallic Traces in PAMD *736*
26.3.1 Why Patterning Is Required? *736*
26.3.2 Catalytic Moiety Ink Patterning *736*
26.3.3 Copolymer Ink Patterning *738*
26.4 Applications in Textile-Based Electronics *739*
26.4.1 Supercapacitor *739*
26.4.2 Triboelectric Nanogenerator *742*
26.4.3 Solar Cell *742*
26.5 Conclusion, Future Outlook, and Challenges *745*
References *746*

27 Fibers for Medical Compression *749*
Bipin Kumar, Harishkumar Narayana, and Jinlian Hu
27.1 Introduction *749*
27.2 Compression Therapy *750*
27.2.1 Pathophysiology and Implications of Chronic Venous Disorders *750*
27.2.2 Need for External Pressure and Its Physiopathology *752*
27.3 Role of Fibers in Compression Therapy *753*
27.3.1 Fiber-Based Compression Modalities *753*
27.3.2 Compression Requirements *754*
27.3.3 Practical Challenges *755*
27.4 Theoretical Insights into Pressure Prediction *756*
27.5 Fibrous Material and Construction Used in Compression and Their Performance *758*
27.6 Innovation in Compression Products *762*

27.7 Shape Memory Fibers for Compression *765*
27.8 Conclusions *768*
References *768*

28 Electrospun Nanofibers for Environmental Protection: Water Purification *773*
Hongyang Ma, Christian Burger, Benjamin Chu, and Benjamin S. Hsiao
28.1 Introduction *773*
28.2 Characters of Electrospun Nanofiber Scaffold *775*
28.2.1 Porosity *775*
28.2.2 Pore Size *777*
28.2.3 Surface Area *778*
28.2.4 Pore Geometry *779*
28.2.5 Mechanical Properties *781*
28.2.6 Materials *782*
28.3 Applications of Electrospun Nanofibrous Composite Membranes *783*
28.3.1 As a Barrier Layer *783*
28.3.1.1 Size Exclusion *783*
28.3.1.2 Adsorption *785*
28.3.2 As a Support Layer *788*
28.3.2.1 Ultrafiltration *789*
28.3.2.2 Nanofiltration and Reverse Osmosis *795*
28.3.2.3 Other Applications *797*
28.4 Conclusions *799*
28.5 Future Prospects *799*
Acknowledgments *799*
References *800*

29 Fibers for Filtration *807*
Govindharajan Thilagavathi and Siddhan Periyasamy
29.1 Introduction *807*
29.2 Filtration and Filter Media *808*
29.2.1 Types of Filtration *809*
29.2.2 Filtration Theories *809*
29.2.3 Requirements of Filter Media *810*
29.3 Fibrous Materials as Filter Media *811*
29.3.1 Classification of Fibers *811*
29.3.2 Fine and Morphological Structures of Fibers *811*
29.4 Forms of Fibrous Substrates for Filtration *814*
29.4.1 Roving and Yarns *814*
29.4.2 Interlaced Fabrics *815*
29.4.3 Nonwovens *816*
29.4.4 Interloped Fabrics *816*
29.4.5 Fibrous Membranes *817*
29.5 Fibers in Filtration Applications *817*
29.6 Factors Governing the Performance of Fibrous Filter Media *823*
29.6.1 Role of Cross Section of the Fiber *823*

29.6.2 Role of Pore Size *825*
29.7 Characterization of Filter Media *826*
29.8 Future Prospects *827*
References *828*

30 Fibrous Materials for Thermal Protection *831*
Gouwen Song and Yun Su
30.1 Introduction *831*
30.2 Performance Requirements of Thermal Protective Clothing *832*
30.3 Fibrous Materials Suitable for Thermal Protection *833*
30.3.1 Chemically Modified Flame Retardant Fibers *835*
30.3.2 Inherently Flame Retardant Fibers *836*
30.4 Performance Standards and Evaluation Method Development *839*
30.4.1 Flammability Test *839*
30.4.2 Thermal Protective Performance Evaluation *841*
30.4.2.1 Benchtop Testing *842*
30.4.2.2 Full-Scaled Manikin Testing *845*
30.5 Influencing Factors of Thermal Protective Performance *847*
30.5.1 Effect of Fabric Basic Properties *847*
30.5.2 Effect of Air Gap Size *848*
30.5.3 Effect of Moisture Content *849*
30.6 Future Trends *849*
References *850*

31 Comfort Management of Fibrous Materials *857*
Chengjiao Zhang and Faming Wang
31.1 Introduction *857*
31.2 Human Thermal Regulation and Heat Transfer Mechanisms *857*
31.3 Clothing Comfort *860*
31.4 Heat and Moisture Transfer Through Textiles *861*
31.4.1 Heat Transfer Through Textiles *861*
31.4.2 Moisture Transfer Through Textiles *862*
31.5 Assessment of Materials and Clothing *863*
31.5.1 Material and Fabric Testing *864*
31.5.2 Full-Scale Clothing Testing *866*
31.5.3 Clothing Thermal Insulation *866*
31.5.4 Clothing Vapor Resistance *868*
31.5.5 Human Trials *870*
31.5.6 Fiber and Thermal Comfort *871*
31.6 Fabric and Thermal Comfort *872*
31.7 Personal Conditioning Clothing for Improving Wear Comfort *874*
31.7.1 Personal Cooling Clothing System *874*
31.7.2 Personal Heating Clothing System *876*
31.7.3 Smart Heating Sleeping Bag *877*
31.8 Conclusions *879*
References *879*

32 Fibers for Radiation Protection *889*
Boris Mahltig
32.1 Introduction *889*
32.2 Structures and Properties of Fibers for Radiation Protection *892*
32.3 Functions, Performance, Evaluations, and Applications *906*
32.3.1 Radiowave/Microwave Shielding *906*
32.3.2 IR Shielding/Heat Management *910*
32.3.3 UV and IR Protection *912*
32.3.4 X-Ray Shielding *914*
32.4 Future Trends *918*
Acknowledgments *918*
References *919*

33 Fibrous Materials for Antimicrobial Applications *927*
Yue Deng, Yang Si, and Gang Sun
33.1 Introduction *927*
33.1.1 Basic Principles *927*
33.1.2 Brief History *927*
33.2 Quaternary Ammonium Compound Modified Fabrics *928*
33.2.1 Antimicrobial Mechanism of QACs *929*
33.2.2 Environmental Impact *929*
33.2.3 Conclusions *930*
33.3 *N*-Halamine Modified Fabrics *930*
33.3.1 Basic Principles *931*
33.3.2 Modification Method *931*
33.3.2.1 Cross-linking *931*
33.3.2.2 Grafting *932*
33.3.2.3 Coating *932*
33.3.2.4 Reactive Reagent Treating *932*
33.3.2.5 Electrospinning *933*
33.3.3 Conclusions and Future Trend *933*
33.4 Metals and Metal Oxide Modified Fabrics *933*
33.4.1 Silver *934*
33.4.2 Oligodynamic Effects of Metals *934*
33.4.3 Titanium Dioxide *934*
33.4.4 Conclusions and Future Trend *935*
33.5 Photoactive Chemical Modified Fabrics *935*
33.5.1 LAAAs and Photoinduced Biocidal Effect *935*
33.5.2 Textile Modification with TiO_2 *936*
33.5.3 Organic Photoactive Reagents *936*
33.5.4 Conclusions and Future Trend *937*
33.6 Natural Antimicrobial Polymers *938*
33.6.1 Hyaluronic Acid *938*
33.6.2 Gelatin *939*
33.6.3 Alginate *939*
33.6.4 Chitosan *940*
33.6.5 Conclusions and Future Trend *941*

33.7 Conclusions *941*
References *942*

34 Fibers for Auxetic Applications *953*
Hong Hu and Adeel Zulifqar
34.1 Introduction *953*
34.2 Auxetic Structures and Geometries *954*
34.2.1 Auxetic Geometries *955*
34.2.1.1 Re-entrant Geometries *955*
34.2.1.2 Rotating Rigid Geometry *955*
34.2.1.3 Nodule and Fibril-Based Structure *956*
34.2.1.4 Chiral-Based Auxetic Geometries *956*
34.2.1.5 Foldable Geometries *957*
34.3 Auxetic Polymeric Fibers and Materials *958*
34.3.1 Liquid Crystalline Polymers and Auxetic Monofilaments *958*
34.3.2 Auxetic Polymeric Fibers *960*
34.3.3 Auxetic Polypropylene Fibers *960*
34.3.3.1 Large-Scale Production of Auxetic PP Fibers *960*
34.3.3.2 Testing of Auxetic Behavior of PP Fibers *962*
34.3.4 Auxetic Polyethylene *963*
34.3.5 Auxetic Polyester Fibers *964*
34.3.6 Auxetic Polyamide Fibers *965*
34.3.7 Moisture-Sensitive Auxetic Fibers *966*
34.4 Properties and Applications of Auxetic Fibers *967*
34.5 Conclusions *968*
References *969*

Index *973*

Preface

The art of using a fiber material is as old as human civilization. Initially, they were primarily used to make textiles such as yarn or fabric, serving the basic requirement of garment, storage, protection, building, ropes, fishing nets, etc. In textile industry, fibers are characterized by having a length at least 100 times its diameter (ASTM D123-15) and offer several unique features due to its unique configuration – high flexibility, high specific surface area, easy transformability into textile structures, and high load-bearing ability along axial direction – which makes them perfect material for apparel use. Further with the development of advanced materials and their technologies, it is now possible to generate novel fibers, which may not possess the same properties like textile fibers (cotton, PET, Nylon, wool) but have unique functions such as shape memory, superhydrophobicity, phase change, optics, and conductivity that could solve new scientific and technological challenges of different advanced fields. This book focuses on the research and development in fibrous materials and innovative application potentials. Each of the chapters is exclusive and selectively chosen, edited by the internationally recognized experts in the field to cover latest developments and future trends in their fields.

Chapter 1 introduces the different types of fibrous materials including natural and synthetic fibers and their fundamental characteristics. Chapters 2–6 include topics from animal fibers (wool, silk, collagen, chitosan) and plant fibers (cellulose). Chapters 7–16 focus on research and application of different synthetic fibers including electrospun fibers, aramid fibers, conductive fibers, phase change fibers, bicomponent fibers, superabsorbent fibers, elastic fibers, smart fibers, optical fibers, and memory fibers. Chapters 17–19 describes the scientific principles and technologies for converting fibrous materials into textile yarns and fabrics. Chapters 20 and 21 list some characterization methods for analyzing fibrous materials and their structures. More emphasis is given on the wide application potential and scope of advanced fibrous materials in electronics (Chapter 22), optics (Chapter 23), energy (Chapter 24), sensors and actuators (Chapter 25), wearable (Chapter 26), medical (Chapter 27), environmental protection (Chapter 28), filtration (Chapter 29), protection (Chapters 30 and 32), health (Chapter 33), and auxetic (Chapter 34).

The content has been designed to cover different types of advanced fibers, their materials, and devices as well as different properties, diversified functions, and applications.

Finally, we would like to acknowledge the time and efforts of our contributors, who are experts in the respective areas described in this book.

Jinlian Hu
The Hong Kong Polytechnic University

1

Fundamentals of the Fibrous Materials

Jinlian Hu, Md A. Jahid, Narayana Harish Kumar, and Venkatesan Harun

The Hong Kong Polytechnic University, Institute of Textiles and Clothing, Room TQ715, Q Core 7/F, Hung Hom, Kowloon 999077, Hong Kong S.A.R., P.R. China

1.1 Introduction

1.1.1 What Are Fibrous Materials?

A fiber is a material that is defined by Textile Institute [1] as units of matter characterized by flexibility and fineness and a high ratio of length to thickness. In different fields, fibers have very broad meaning such as those for food supplements and fibers in plants or in human body. A fiber is more often referred to the basic unit of making textile yarns and fabrics. Textile fibers should have some specific properties though. For example, cotton plant contains fibers that are strong and soft enough to be spun into yarns that can be woven or knitted into a fabric by textile processing, but human hair is not a textile fiber because it cannot fill up the above properties. So, we can say all textiles are made of fibers, but not all fibers can be used to make textiles. The important requirements for fibers to be twisted into a yarn include a length of at least 5 mm, cohesiveness, flexibility, and sufficient strength, and other important properties include elasticity, fineness, uniformity, luster, and durability. It is also important to remember that all textile fibers are not created equally [2]. Each fiber contains different qualities and will result in a different textile. Some retain heat better than others; some hold dye very well; some are more durable, while some are more comfortable [3].

The origin of fibrous materials may be of organic, inorganic, or metal. They are fine structures that are formed by joining component atoms into molecules. Fibrous materials can be grouped into two major categories: natural and chemical or man-made fibers. The growth of natural fibers is slow and controlled under genetics from fast production of manufactured fibers in terms of structures. Natural fibers include plant or vegetable fibers (such as cotton, flax, ramie, jute, and hemp), animal fibers (such as silk, wool, and hair fibers), and mineral fibers (such as asbestos). Synthetic fibers include regenerated fibers (such as viscose and acetate), synthetics (such as polyester, polyamides, polyolefins), and inorganic fibers such as glass and carbon fibers with completely amorphous or microcrystalline structures [4]. Another class is high-performance fibers that are manufactured ones with improved tensile and other mechanical properties.

Handbook of Fibrous Materials, First Edition. Edited by Jinlian Hu, Bipin Kumar, and Jing Lu.
© 2020 Wiley-VCH Verlag GmbH & Co. KGaA. Published 2020 by Wiley-VCH Verlag GmbH & Co. KGaA.

Finally, smart fibers are an emerging class of fibrous structures that are responsive to stimulus or an environment, tailored with advanced functionalities for many applications.

1.2 Historical Evolution of Fibers

Natural fibers are abundantly available in nature that are biodegradable and sustainable and have played a key role in the human race since nearly 7000 BC [5]. Human beings have been using the fibers from many ages for which there are no records, which itself is a distinct proof that fiber is present from several hundreds of years. The first choice for the human beings to use is natural fibers. Production of synthetic fibers was beginning only in 1910 by commercially producing the rayon fiber, and this was the result of technological development that has not stopped yet on the present era. Natural fibers have been used in many cultures traditionally across the globe in making utilitarian products. Fibrous materials can be obtained naturally from many resources such as plants, leaf, seeds, bark, stem, and grass. Flax is believed to be the oldest fiber and it was obtained in dates back to 6000 BC. Egyptians started to wear the cotton since 4000 BC, and later revolutionary changes occurred to discover ginning and production of different variety of cotton products. Wool fiber was also discovered around 3000 BC, and then around 40 breeds were explored to produce wide range of wool fibers. Dates back to 2500 BC, silk fiber is believed that it was first discovered by a Chinese princess that was obtained from the cocoons of silk worms. The silk processing was found to be kept secret for almost 3000 years and then started to spread all over the world in the later stage.

Even though natural fibers were comfortable and biodegradable, they had some drawbacks such as wrinkling of cotton and flax and delicate handling of silk and wool fibers receptive to shrinkage and moth attack. Growing needs of human race and these disadvantages of fibers paved the way to produce the first man-made fiber with revolutionary technological efforts into rayon, which is known as artificial silk to the present era. In the later stages, other man-made fibers such as acetate, nylon, acrylic, polyester, spandex, polypropylene, lyocell, and microfibers were produced with rapid transformation from science to market and end users around the world. The complete developments in the evolution of human civilization (Figure 1.1) and textile fiber (Figure 1.2) are presented below [6].

1.3 Classification of Fibrous Materials

A comprehensive classification of fibrous materials is depicted in Figure 1.3. Nature offers us abundant resources for getting fibrous materials that grow in various geographical locations and altitudes. Fibrous materials can be further classified into textile and non-textile fibers. The internal characteristics that are suitable for processing from fibers [7] to yarn, fabric, and other utilitarian products can be termed as textile fibers [8, 9]. However, the properties of fibers

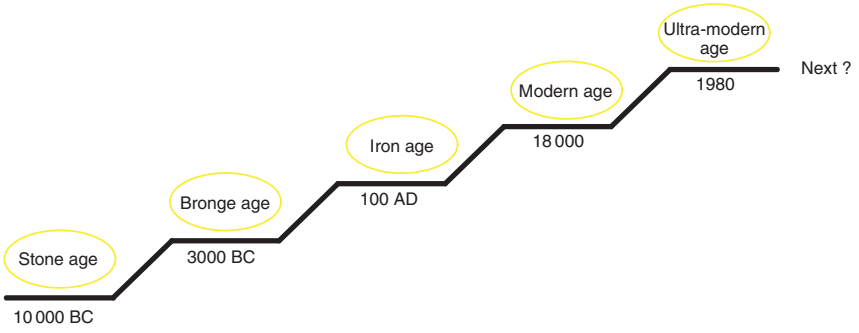


Figure 1.1 Evolution of human civilization.

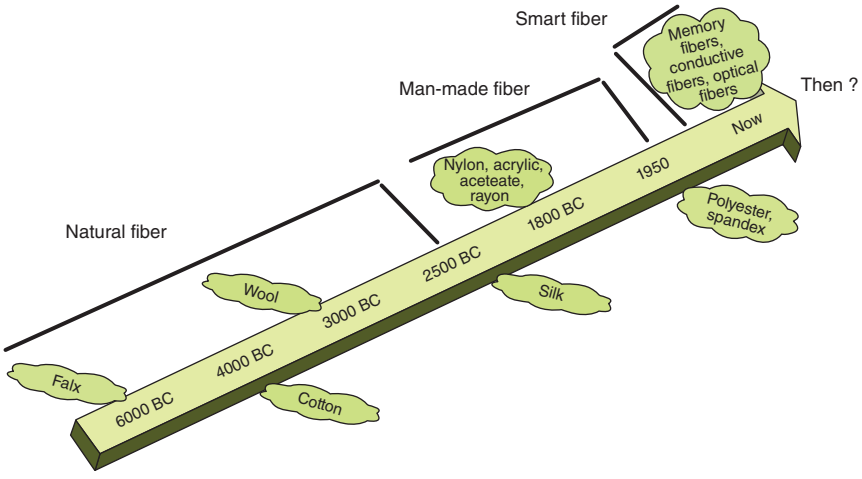


Figure 1.2 Evolution of textile fibers.

that are not suitable for clothing could be considered as non-textile fibers and have been found broad horizon of arenas to fulfill the human desired needs in many ways. Non-textile natural fibers are also used in building materials, animal and human food, ecofriendly cosmetics, agro-fine chemicals, and sources of energy.

Fibers can be classified into two major groups as natural and man-made or manufactured ones. Natural fibrous materials are basically from three origins; they are cellulosic/lignocellulosic (from plants), protein, and mineral, which is decided by the chemical composition and fiber morphology. Cellulosic fibers constitute long-chain molecule joined together with glucose rings by valence bonds and hydroxyl groups linked by hydrogen bonds in its chemical structure. Other cellulosic fibers such as flax, jute, hemp, ramie and sisal differ from cotton in various ways. Normally larger proportion of impurities contains in their structure. They are multicellular fibers composed of microscopic individual cells bonded together and running along the strands in the plant or leaf. Hair fibers are also termed as protein fibers that are morphologically formed by

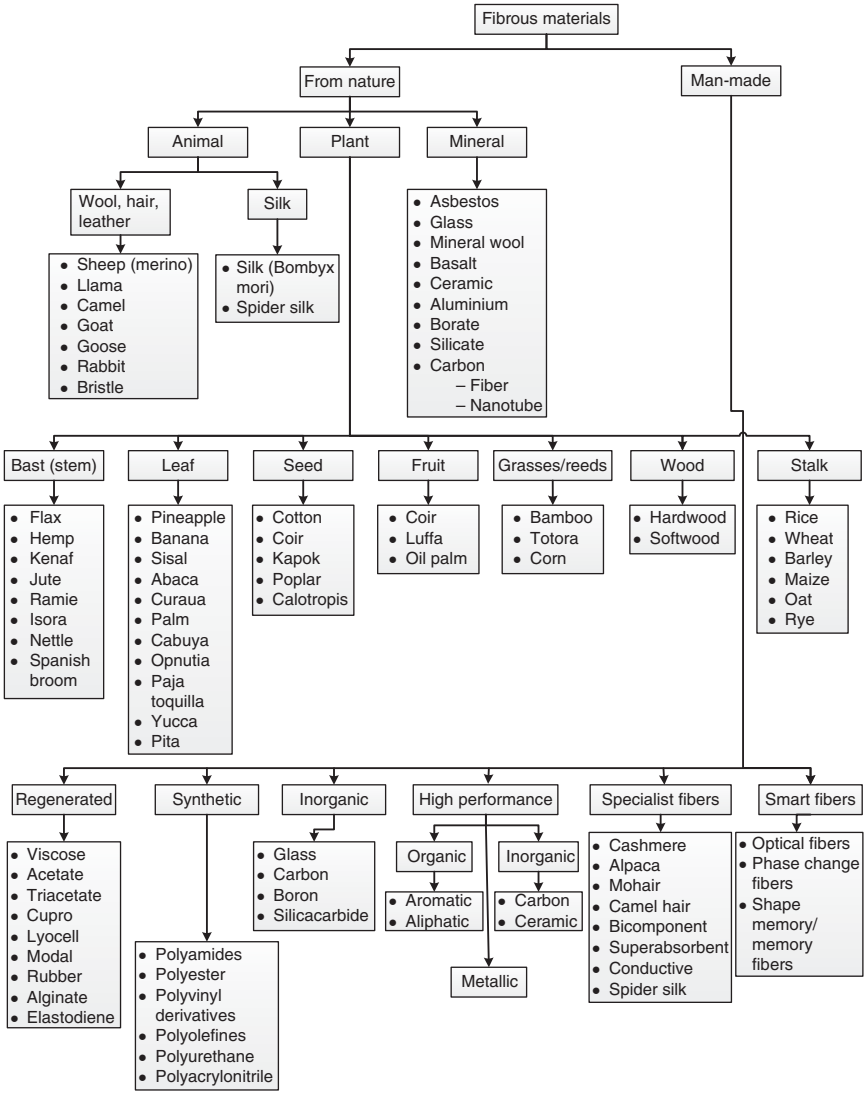


Figure 1.3 Classification of fibrous materials.

the polymerization of amino acids (NH_2–CHR–COOH) by peptide linkage (–CO–NH–) into long-chain molecules such as silk and wool. Mineral fibers are obtained from the naturally available inorganic substances such as rock, clay, and slag. Another group of fibers that have changed the world with revolutionary scientific discovery of mankind is man-made or manufactured fibers. Different classes of manufactured fibers are grouped in Figure 1.4, which includes fibers from natural polymers (regenerated or artificial or modified celluloses), synthetic polymers, and organic and inorganic substances. Regenerated fibers such as viscose rayon, acetate, and triacetate are produced from the celluloses that are

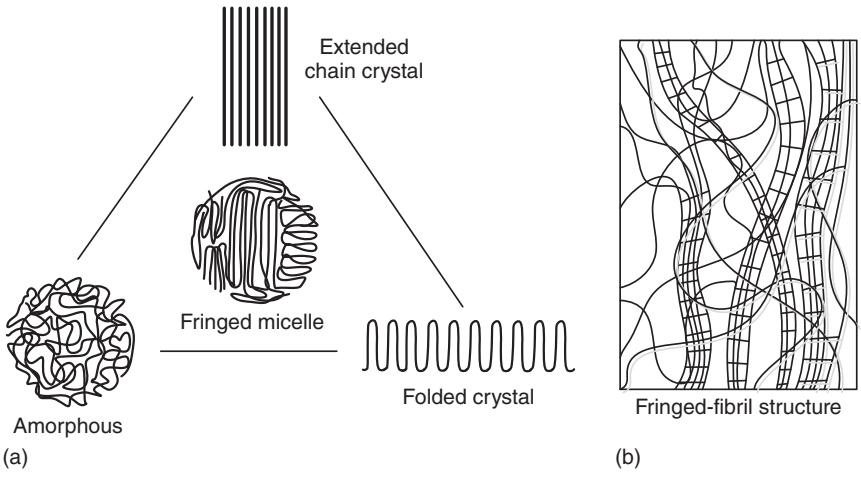


Figure 1.4 Phases of polymeric chains in fibrous materials. Source: Adapted from Morton and Hearle 2008 [2] and Kajiwara 2009 [26].

chemically regenerated from the natural resources such as wood pulp. The major difference in this class of fibers is thinning down or reducing the degree of polymerization by chemical modification of native cellulose. However, alginate fibers are produced from the alginic acid that can be obtained from seaweed. The acid is subjected to degradation and neutralization process to form the metallic salts that form the highly oriented and highly crystalline alginic acid fibers [3]. Synthetic fibers are spun from the polymers that are synthesized using monomers joined together by covalent bonds via process called polymerization. Polymerization could proceed with several variations, and thus they can be classified in various ways as listed in Figure 1.4 under synthetic group. High-performance fibers are of two types, namely, organic and inorganic. Glass is an inorganic with unoriented and amorphous network based fiber, which has a long history as decorative product. Carbon fibers are basis for making composites that are made of acrylic or cellulose precursors via carbonization. The high temperature ceramic fibers are produced by using organosilicon polymers or viscous liquid with aluminum salts. Discovery of liquid crystals led the way to produce fibers with almost perfect crystallinity, almost perfect orientation, and fully extended molecular chains. Aromatic and aliphatic polymers used to produce Kevlar and Nomex that are also called as aramid fibers. Liquid crystals can also be formed from polyethylene to produce ultrahigh molecular weight polyethylene to get highest strength. Specialty fibers are of normally hair fibers such as cashmere, camel hair, alpaca, and mohair. These fibers are generally straighter and smoother than wool [10–12]. Other specialist fibers that are produced by advanced and distinguished technology such as hollow fibers, bicomponent fibers [13, 14], superabsorbent fibers [15, 16], and conductive fibers [17]. Hollow and bicomponent fibers are generally spun using different types of spinnerets. Superabsorbent fibers are produced using acrylic-based products and characterized by improved liquid or fluid transportation that are

used in medical, textiles, food packaging, and technical textiles. Other advanced fibers can also be considered as specialist fibers, but they are listed under smart fibers that are stimulus responsive such as optical fibers, phase change fibers, and shape memory fibers. Optical fibers are made of polymer or glass core materials with hollow core along the length for applications such as photonics and sensors, and they are called as bandgap fibers [18]. Phase change fibers are generally composed of thermoplastic polymer and luminescent materials as a composite structure [19]. Another smart fiber is considered as one of the most important class of stimuli responsive materials, i.e. shape memory polymeric (SMP) fibers. SMPs are made of segmented polyurethanes with custom tailorable switching or transition temperatures that can be spun via different spinning methods such as melt spinning, dry spinning, wet spinning, reaction spinning, and electrospinning process [20–23].

Increased demand and population explosion is alarming the world to look up for an alternative material that is sustainable and biodegradable. Researchers and industrial inventors may invent futuristic advanced material-based fibers for upcoming days. This is unstoppable and essential for groundbreaking revolutionary technological advancements for this present competent world to prepare for better future.

1.4 Fundamental Characteristics of Fibrous Materials

The era of synthetic fibers was beginning around ten decades ago, and until that time the usage of natural fibers was most popular owing to their natural properties useful for mankind. These natural properties were being considered as benchmark to consider a fiber to be useful in the production of textile materials [24]. These properties are imperative for textile processing and they can be divided as follows [6]. They are primary properties (such as staple, strength, elasticity, fineness, uniformity, and spinning quality) and secondary properties that are desirable. Fibers that are useful in textile processing should be elastic between 5% and 50% breaking elongation. Other non-textile materials like inorganic fibers such as glass, ceramic, and fully crystalline objects are neither flexible nor extensible. The materials that meet this requirement would be almost partially oriented, partially crystalline, and linear molecular arrangements. Functional applications need high-performance fibers that differ from textile fibers with high strength and low extension. Almost they are linear polymers and added with inorganic networks to integrate the flexibility. Elastomeric fibers are used for high stretch applications. There is also other sort of fibers that are interesting such as those in living organisms, wood fibers used for papers, and various tissues. In addition to general characteristics, there are other important features that characterize the fibers, and they are degree of order, degree of localization of order, length/width ratio of localized units, degree of orientation, size of localized units, and molecular extent in a fiber assembly [3]. Fibrous strand is composed of fibrils that are an assembly of polymer molecules and a primary unit called microfibril that is almost identical in all natural fibers. Man-made fibers also show a similar element

in the structure [25]. Hess and Kiessing [27] suggested a schematic fringed micelle model to elucidate the structure of microfibrils of synthetic fibers as shown in Figure 1.4. The microfibril basically constitutes crystalline region (ordered polymer chains along the axis) and amorphous region (randomly oriented or less ordered), and an individual polymeric chain interconnects the two regions (Figure 1.4a). Hearle [27–29] proposed a fringed fibril structure (Figure 1.4b) for low crystalline fibers, which can be seen in stiffer molecular chains such as cellulose. This model combines fibrillar form and the concept in fringed micelle structure having distinct crystalline and non-crystalline portions with molecular chains running through each region continuously. High-performance fibers with highly crystallinity have more closely packed fibrillar structure. Natural fibers have specific fibrillar forms and wool with fibrils separated by various matrices.

1.5 Morphological and Structural Properties of Fibrous Materials

The structure of fibrous materials varies in several ways and depends on how actually they are formed whether naturally or artificially. Natural fibers grow slowly and are controlled under genetics to yield different structures, which vary from fastest passage of synthetic fiber production.

1.5.1 Plant or Natural Cellulosic Fibers

An essential feature of natural fibers is that they are aggregated into finer microfibrillar structures (Figure 1.5a,b). According to biological validation, during the growth glucose rings are joined together to form long-chain molecules of cellulose. The thickness of these natural microfibrils is about 4 nm. The molecular alignment takes place in parallel direction of crystal lattice with no chain folding. The crystallization occurs due to minimization of free energy, and forceful attractions are at the edge of molecules likely to form a ribbonlike structure (Figure 1.5a). Microfibrils are almost flexible and attract each other with strong hydrogen bonding at molecular edges or between the faces by weak van der Waals force. Cotton fibers show irregular, convoluted long ribbonlike structure, covered with cuticle, primary wall, and lumen at the center in a cross-sectional view (bean shape) (Figures 1.5a and 1.6a). Apart from cotton, other cellulosic fibers including jute, ramie, hemp, and flax are also multicellular fibrous structures. Smaller fibrillar cells run along the length from the stem or leaf as shown in Figure 1.5. The fibrils spiral around the fibers and are parallel to axis in all natural cellulosic fibers. However, in bast fibers, the spiral angle is reduced, and structures are highly oriented to fetch high strength with less extensibility.

1.5.2 Animal or Protein Fibers

Silk, wool, or hair fibers are considered as protein fibers originated from the living animals. Groups of amino acids combine into long-chain molecules

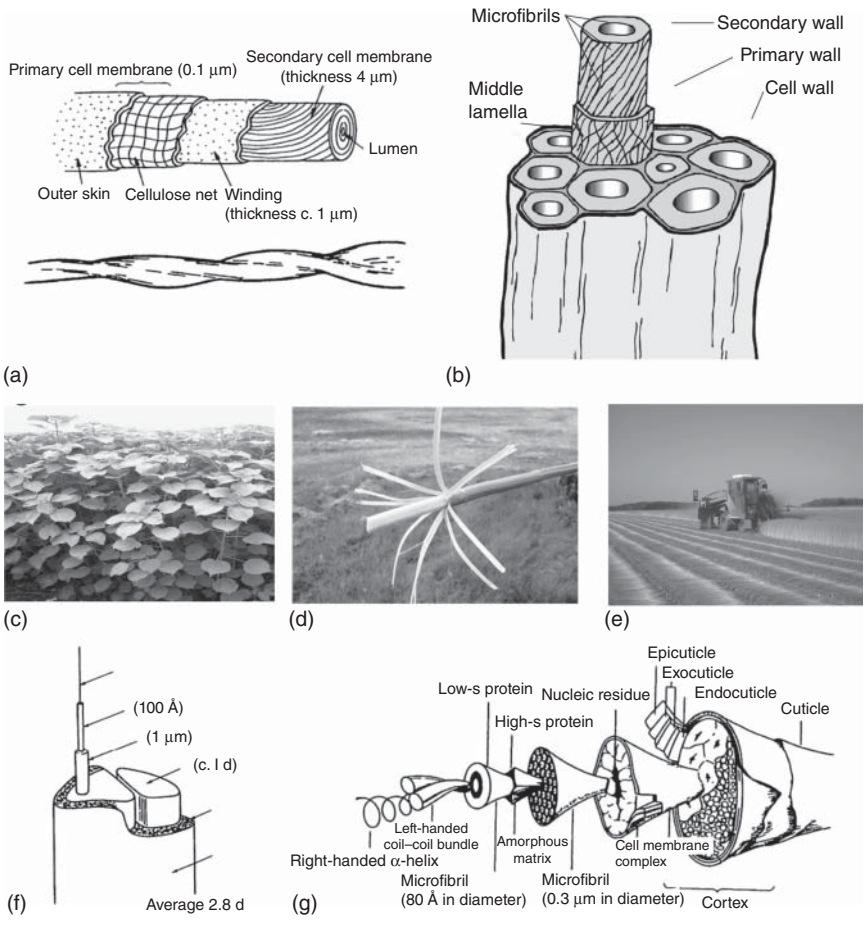


Figure 1.5 Structural and photographical images of natural and animal fibers. (a) Cotton. (b) Jute. (c) Ramie. (d) Hemp. (e) Flax. (f) Silk. (g) Wool. Source: Adapted from Kajiwara 2009 [26], Kozasowski et al. 2012 [30], and Roy and Lutfar 2012 [31, 32].

with polypeptide linkages to form protein fibers. The major protein of silk fiber is fibroin molecule that is 140 nm long with other 17 nm long segments composed of tyrosine and other concentrated side groups, with rest being fully glycine, alanine, and serine acids. Silk is spun by silkworm and constitutes two triangular fibroins covered with a sericin gum (Figures 1.5f and 1.6a). Hair or wool fibers show the most complex structures among any other fibrous materials (Figure 1.5g). The major protein in hair fibers is keratin that consists of several proteins. Wool fibers with α-keratin protein tend to reverse transformation when stretched to form β-keratin. α-Helix consists multiple twisted molecules, two chains makes a dimer, two dimers into a protofilament, two protofilaments a protofibrils, two protofibrils a half filament, and two half filaments gives an intermediate filament having 32 molecules in cross section [3].

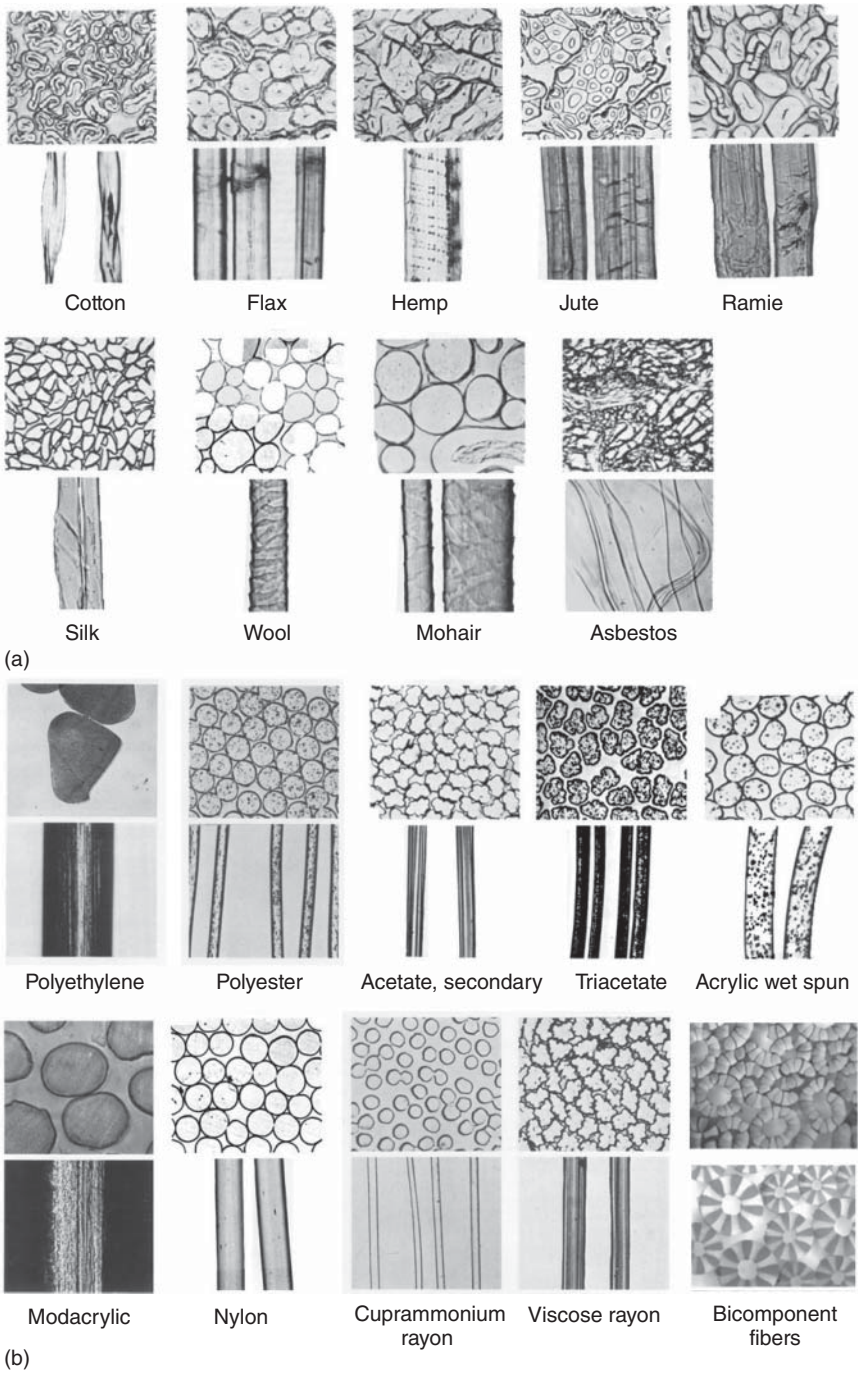


Figure 1.6 Microscopic structural images of fibrous materials. (a) Longitudinal and cross-sectional view of natural fiber. (b) Longitudinal and cross-sectional view of man-made fiber. Source: Adapted from Prahsarn et al. 2016 [14] and AATCC 2013 [34].

1.5.3 Regenerated Cellulosic Fibers

The degree of polymerization is reduced and of the order of 500 compared to native cellulose. The crystalline region is less and of about one third of the total. However, the degree of orientation totally depends on the drawing during spinning. There are diverse forms of rayon with irregular shapes in the cross section (Figure 1.6b). Viscose rayon is formed by intermediate cellulosic xanthate, whereas acetate fibers are treated to replace the hydroxyl groups with acetyl groups. They have good dimensional stability and high softening point and are crease resistant with heat-set ability [3].

1.5.4 Synthetic or Manufactured (Textile and Non-textile) Fibers

Synthetic fibers lack in terms of their structural features. Spinning conditions and the spinneret being used decides the fiber cross section. Melt-spun fibers using circular spinneret shows circular shape and other shapes from shaped spinneret. However, fibers from solution spinning have different shapes such as acrylic fibers (dumbbell shape) due to mass transfer or loss of solvent (Figure 1.6). The longitudinal and cross-sectional views of other synthetic fibers are shown in Figure 1.6b [13].

Other additives such as pigments, delustrants, and antistatic agents can also be included to achieve desired properties. Most of the non-textile fibers that are required for engineering uses need high stiffness and strength and high-performance (high-modulus, high-tenacity [HM-HT]) fibers are the best choice for this. The presence of covalent strong chemical bonding gives high mechanical and chemical resistance to ceramic fibers. Ceramic fibers contain mixture of components such as silica, SiO_2, carbon, Al_2O_3, and B_2O_3. Carbon fibers are composed of graphite crystal lattice, and the carbon atoms are held together by covalent bonds. Aramid (para) fibers such as Kevlar and Twaron are composed of aromatic polyamide, poly(*p*-phenylene terapthalamide) (PPTA). These fibers are highly oriented with fully extended chains and high crystallinity [3].

1.6 Essential or Fundamental Properties of Fibrous Materials

The fundamental composition and morphological structure vary from fiber to fiber, and there are some important properties to be considered to intelligently utilize them into different applications for human needs. Fundamental properties of fibrous materials are most necessary to distinguish them from each other and find out other desirable properties via standard testing conditions.

1.6.1 Physical Properties

Primary processing of any fibrous material is to be decided by their physical properties such as fiber length, elongation, tenacity, moisture sorption and swelling

behavior, color, luster, electrical behavior, specific gravity or density, and solubility. Fiber length of natural fibers varies, and they differ in their staple length except continuous filament such as silk. Physical properties of synthetic fibers can be tailor-made according to end user requirements. Physical properties of fibers materials are shown in Table 1.1.

1.6.1.1 Mechanical Behavior of Fibrous Assemblies

Textile fibrous materials differ from conventional engineering materials in different ways owing to their unique mechanical behaviors. Based on such behaviors, it is possible to predict general fashion and expected behavior to obtain the necessary characteristics. Fibrous materials are highly anisotropic, easy to deform, and inhomogeneous and have larger strains and displacement at lower stress and nonlinear and plastic nature at low stress and in room temperature. Hence they do provide essential characteristics suitable for the movement of human body, perception satisfaction, and other psychological and physiological requirements [1].

It is imperative to comprehend the behavior of fibers in a unit of assembly employed for multidirectional deformations. Figure 1.7 shows the complicated geometrical structure of a fibrous assembly, textile woven fabrics, which is an integration of warp and weft yarns through intersection points. The passage of fibrous strand in the cross-sectional shape is crimped and irregular with protruding the fibers from the strand surfaces. Porus structure of woven fabric is decided by the distance between two adjacent yarns differentiates from the continuum engineering material such as metallic sheets. Pierce has simplified and idealized the cross-sectional shape and physical properties of yarn assemblies through theoretical modeling approach [1].

Nonlinear Stress–Strain Behavior of Textile Fibrous Assembly The mechanical behavior of woven fabric structures is complicated upon deformation, and their typical stress–strain curves are depicted in the Figure 1.8, which shows tensile, bending, and shear deformations. The tensile stretching (Figure 1.8a) shows larger strain even at small force, and this is ascribed to straightening of crimped length of yarns in the woven structure. A typical fabric has a tensile modulus in the order of 10 MPa as compared to steel that is around 2×10^5 MPa. The woven fibrous assemblies are more prone to bending deformations under the transverse loading (Figure 1.8b). The bending stiffness of the fibrous strand to that of a solid rod of the same cross section can be easily determined assuming the slippage between the fibers is unconstrained. That is, $\alpha(\gamma/R)^2$, where α is denoted as porosity ratio and R and γ are the radii of the yarn and its constituent fibers, respectively. For a typical yarn that contains 100 fibers, this ratio is $\sim 1 : 10\,000$. Thus, it is possible to develop a thick yarn with more flexibility and is advantageous to have less bending stiffness in the woven fibrous structure. As mentioned earlier, the geometry of the woven fabrics is complicated, and when these materials are subjected into deformation, interesting phenomena could be seen, which is distinguished from conventional engineering materials. They are as follows:

(1) *Nonlinear stress–strain trend*: When the woven fibrous material is subjected to small strains, the corresponding stress will be nonlinear, which contrasts

Table 1.1 Properties of different types of textile fiber [6, 26, 30, 31].

Family/ group	Fibers	Tensile strength (cN/dtex)		Elongation (%)	Specific gravity (g/cm^3)	Young's modulus (cN/dtex)	Moisture regain (%)
		Dry	Wet	Dry			
Natural fibers	Cotton	2.3–4.3	2.9–5.6	3–7	1.54	60–82	8.5
	Jute	5.4–8.71	—	1–1.8	1.48	—	13.8
	Silk	2.6–3.5	1.9–2.5	15–25	1.33	44–88	11
	Wool	0.9–1.5	0.7–1.4	25–35	1.32	10–22	15
Regenerated fibers	Viscose rayon	1.5–2.0	0.7–1.1	18–24	1.50–1.52	57–75	11
	Triacetate	1.1–1.2	0.6–0.8	25–35	1.30	26–40	3.5
Synthetic fibers	PET	3.8–5.3	3.8–5.3	20–32	1.38	79–141	0.4
	Polyacrylonitrile	2.2–4.4	1.8–4.0	25–50	1.14–1.17	34–75	2
	Polyvinyl chloride	1.11–3.33	1.11–3.33	10–125	1.33–1.40		
	PTFE	1.11–2.22		10–30	2.1–2.3		0
	Nylon 6	4.2–5.7	3.7–5.2	28–45	1.14	18–40	4.5
	Nylon 6,6	4.4–5.7	4.0–5.3	25–38	1.14	26–46	4.5
	Vinylon (PVA)	3.5–5.7	2.8–4.6	12–26	1.26–1.30	53–79	5
	Polypropylene	4.0–6.6	4.0–6.6	30–60	0.91	35–106	0
	Polyethylene	4.4–7.9	4.4–7.9	8–35	0.94–0.96	—	0
	Polyurethane	0.5–1.1	0.5–1.1	450–800	1.0–1.3	—	1
Aramid fibers	Kevlar	8.8–24.44	7.7–23.33	3–20	1.45	133.3–144.4	3
	Nomex	6.66–13.33	5.55–12.22	20–30	1.38	125.5–133.3	3.5
High-performance fibers	Polycarbonate	4.44–5.55	—	20–45	1.23	—	0.4
	PBI	2.88–3.33	2.33–2.77	25–30	1.43	50–66	15
	Sulfur	3.33–3.88	—	25–35	1.37	33–44	0.6
Inorganic	Carbon	22.2–27.7	—	1–2	1.7–1.8	—	—
	Glass	6.6–11.1	5.5–8.8	—	2.5–2.6	—	0.5

PET, polyester; PTFE, poly(tetrafluoroethylene); PBI, polybenzimidazole.

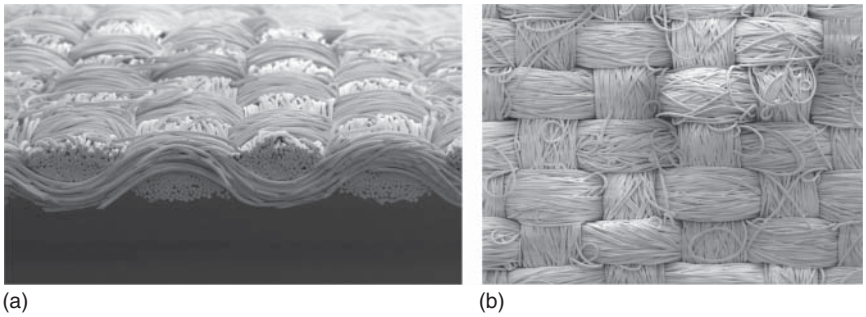


Figure 1.7 Structural photographic images of plain woven fibrous assembly. (a) Cross-sectional image. (b) Surface image. Source: Adapted from Denton and Daniels 2002 [1].

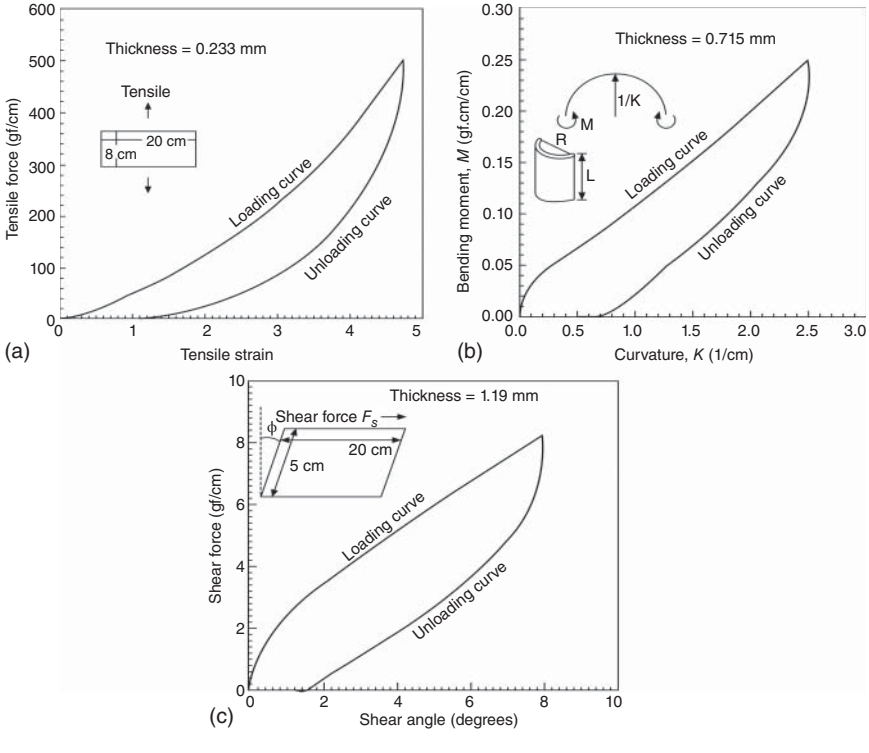


Figure 1.8 Typical stress–strain plots for woven fabrics. (a) Plot of stress vs. strain. (b) Plot of moment vs. curvature. (c) Plot of shear force vs shear angle. Source: Adapted from Hu 2004 [9].

with that of conventional engineering material with linear trend. The stress–strain curve in fabrics is nonlinear up to small strains, and it becomes linear beyond the critical stress region. This critical region is higher for tensile deformation and very low or nearly zero for bending and shear deformations. Due to porous and crimped nature of fibrous assembly in the woven fabrics, they tend to become straightened upon deformations, thus showing nonlinear trend during the consolidation process. Once the consolidation and reorientation is done, the stress–strain trend shows the linear that is like a solid conventional engineering material.

(2) *Irrecoverable deformation*: Woven textile fibrous assembly shows loops between the loading and unloading curves as shown in the Figure 1.8. It can be seen that, in three of the cases such as tensile, bending, and shear, the deformed length is not able to recover back to their original state. This is denoted as irreversible or irrecoverable deformation occurs at small stresses. This phenomenon differs from the conventional engineering material where the inelastic deformation occurs at high stress level where the failure may happen.

Textile fibrous assemblies do obviously differ from those conventional engineering materials in many ways such as inhomogeneous, anisotropic, and nonlinear behaviors. Complicated mechanical response occurs at low stress and room temperature for fabrics, whereas this happens at high temperature and high stress for engineering materials.

1.6.2 Chemical Properties

Natural and synthetic fibers have different chemical properties such as affinity and inertness to various chemicals. In general, most of the cellulosic fibers are resistant to alkalis and protein fibers to acids. There are some important chemical properties to be considered such as effect of acids, effect of alkalis, effect of oxidizing agents, effect of light or sunlight, and effect of insects.

1.6.3 Biological Properties

Biological properties of fibrous materials play an important role in some very specific applications. These properties include resistance to moths, mildews, and microorganisms, biodegradability, and biocompatibility of fibrous structures. Biodegradable natural or synthetic polymeric fibers such as silk, collagen fibers, and polyurethanes are used for implants and tissue engineering.

1.6.4 Thermal Properties

Fibrous materials are thermoset (natural fibers) or thermoplastic (manufactured) in nature. Thermal properties such as softening point, glass transition temperature, melting temperature, and degradation point or decomposition temperature range are important to be considered for processing or applications.

1.6.5 Other Desirable Properties

Manufactured fibers are modified into broad horizon of materials suitable for vivid smart applications needing desirable properties such as optical performance (photonics), electrical properties (energy storage), phase change behavior, and shape memory properties (memory behavior).

1.7 Textile Processing

Textile manufacturing or processing is a very complex process. The area of textile manufacturing process is too long (Figure 1.9). It starts from fiber to finished products. Fiber is the main material for textile product; properties of textile products mainly depend on fiber type. Textile fiber has few special features that vary between fibers and textile fiber. Textile fiber can be twisted into a yarn or made into a fabric by various methods like weaving, knitting, nonwoven, and braiding. Textile fiber needs to be stronger enough to hold their shape, flexible enough to be shaped into a yarn or fabric, elastic to stretch enough, and durable enough to last [33, 34].

1.7.1 Spinning

Spinning is the first step of textile product processing. The process of making yarns from the textile fiber is called spinning. Spinning is the twisting together of fibers to form yarn. There are different types of spinning process: ring spinning, rotor spinning, friction spinning, etc. Ring spinning is the most commonly and widely used spinning process.

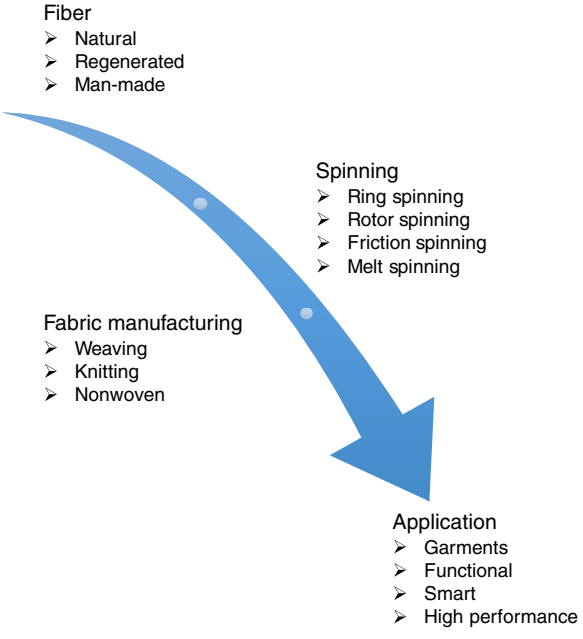


Figure 1.9 Flow process chart of textile manufacturing.

1.7.1.1 Ring Spinning

Ring spinning is a continuous system of spinning in which twist is inserted into a yarn by using a circulating traveler in ring spinning; the roving is first attenuated by using drawing rollers and then spun and wound around a rotating spindle, which in its turn is contained within an independently rotating ring flyer. Ring spinning is the mostly used spinning process. Ring spinning processes are as follows:

Blow room: The section where the supplied compressed bale is turn into a uniform lap of particular length by opening, cleaning, blending, or mixing is called blow room section. It is the first step of spinning process. It is even feed of material to the card.

Carding: It is the heart of spinning process. This is where the flock from bales will be open into individual fiber. Thus, it will ease to remove the excess impurities on the fiber surface. At this point, short fiber that is not suitable for production in terms of length requirements will be removed. Carding is one of the most important operations in the yarn processing as it directly determines the final features of the yarn. The main objectives of the carding can be summarized as opening the tufts into individual fibers, eliminating all the impurities contained in the fiber that were not removed in the previous cleaning operations, selecting the fibers based on length and eliminating the shortest ones, removing the neps, and parallelizing and stretching the fiber.

Drawing: At this stage, the sliver will be pulled in lengthwise direction over each other. Thus, it will cause it to be stronger and thinner in production, which is very important in evenness of the yarn. Card slivers fed to the drawing machine have some degree of unevenness. The drawing machines are very much important in the yarn manufacturing process. One of the main and most important tasks of the draw frame is improving evenness.

Combing: The cotton sliver produced by the card contains several contaminants that obstruct with the spinning of fine high and good quality yarns. This is a process where the yarn will be straightened again so that they are arranged in parallel manner. While at the same time, the remaining of short fiber will be removed completely from the fiber. The main functions of the comber are to remove a substantial amount of the short fiber as "noil" and eliminate the smallest trash particles and neps.

Roving manufacturing: In this stage, sliver will be further drafted and twist will be inserted to produce roving sliver. Enough twist is given to keep the fibers together but still has no tensile strength. The roving in bobbins is placed in spinning frame where it passes several sets of roller that run at high speed to convert into yarn forms.

Ring spinning: The ring spinning is the most broadly used form of spinning machine due to significant advantages in comparison with the new spinning processes. The ring spinning machine is used in the textile industry to continuously twist staple fibers into yarn and then wind it onto bobbins. The following are the core objectives of ring spinning:

- To draft the roving fed to the ring spinning frame, i.e. to convert roving into very fine strand called yarn.

- To improve strength to the yarn by inserting the necessary amount of twist.
- To collect twisted strand called yarn onto handy and transportable package by winding the twisted thread on a cylindrical bobbin or tube.

Cone winding: In the spinning process, winding is the last step. After winding yarn packages are used for making woven or knitted fabric. Winding process can be defined as the transfer of spinning yarn from one package to another large package (cone). A process of assemble yarn on a package to facilitate the next process is called as winding.

1.7.1.2 Rotor Spinning

In rotor spinning, sliver is fed into the opening end of rotor; then fed sliver is opened into single fibers, and then the singled fibers are reassembled, twisted, and wound on a package. Moreover, sliver from the carding machine goes into the rotor, is twisted into yarn and comes out, wrapped up on a cone shaped bobbin; so there is no roving stage in rotor machine and no need to use the auto-coner to winding the yarn in a cone because output of rotor machine is sliver to yarn into a cone shaped package. Advantages of rotor machine are less labor, less time, and high productivity compared with ring spinning. But the disadvantages are low strength, difficult to produce fine yarn, and difficult to keep spinning condition constant.

1.7.1.3 Friction Spinning

Friction spinning system is an open-end system or a "core-type" spinning system, where the yarn formation takes place by the frictional forces. In friction spinning, fibers are supplied onto the drum surface, which transport it and stack fiber to the fiber bundle circulating between two surfaces passing in opposite directions; then opening or individualization of fibers will happen, followed by reassembling of single fiber and then twisting of assembled fiber by frictional force, winding the final yarn. Advantages of friction spinning are excellent yarn regularity, lower preparation and spinning cost, and very high twist insertion rate, and few disadvantages are low yarn strength, high air consumption leading to high power consumption, and friction spun yarns having higher snarling tendency.

1.7.1.4 Yarn Numbering System (Count)

Count is a numerical value, which expresses the coarseness or fineness (diameter) of the yarn and indicates the relationship between length and weight (the mass per unit length or the length per unit mass) of that yarn. The fineness of the yarn is usually expressed in terms of its linear density or count.

According to Textile Institute, "Count is a number indicating the mass per unit length or the length per unit mass of yarn."

There are a number of systems and units for expressing yarn fineness. But they are classified as follows:

Direct count system: The weight of a fixed length of yarn is determined. The common features of all direct count systems are that the length of yarn is fixed and the weight of yarn varies according to its fineness. In the direct system, the higher the yarn count number, the heavier or thicker the yarn. It is based on the fixed length system. This system is generally used for jute or silk yarn.

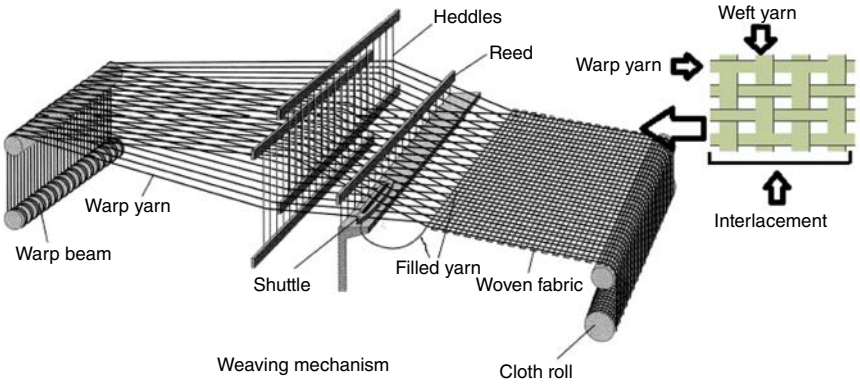


Figure 1.10 Weaving mechanism. Source: Reproduced with permission from https://textilechapter.blogspot.com/2017/03/weaving-loom-principle-mechanism.html.

Indirect count system: In an indirect yarn counting system, the yarn number or count is the number of "units of length" per "unit of weight" of yarn. This means the higher the yarn count number, the finer or thinner the yarn. It is based on the fixed weight system. This system is generally used for cotton, woolen, worsted, and linen yarn [35–37].

1.7.2 Fabric Manufacturing

1.7.2.1 Weaving Process

Weaving is one of the major processes of making fabric. In it, two individual sets of yarns called the warp and weft are interlaced with each other to form a fabric (Figure 1.10). Yarn is a long continuous length of interlocked fibers. The lengthwise yarns that run from the back to the front of the loom are called the warp. The crosswise yarns are the filling or weft. A loom is a device for holding the warp threads in place while the filling threads are woven through them. Yarns made from natural fibers like cotton, silk, and wool and synthetic fibers such as nylon and Orlon are commonly used for weaving textile. Before start weaving we have some work like weaving preparation. In weaving preparation work, we must do the following:

- *Warping*: A process of transferring the warp yarn from the single yarn packages to an even sheet of yarn representing hundreds of ends and then winding onto a warp beam.
- *Sizing/slashing*: Sizing of yarn is carried to improve its strength and produce a smooth surface.

To interlace the warp and weft yarn, there are three operations often called primary motions that are necessary:

Shedding: The process of separating the warp yarn into two layers by raising the harness to form an open area between two sets of warps.

Picking: The process of inserting the filling yarn through the shed by means of the shuttle less while the shed is opening.

Beating: The process of pushing the filling yarn into the already woven fabric at a point known as the fell and done by the reed.

Taking up and letting off: With each shedding, picking, and beating operation, the new fabric must be rolled on the cloth beam that is called "taking up." At the same time, the warp yarns must be open from the warp beam that is called "letting off" [38–40].

1.7.2.2 Knitting

Knitting is a method by which yarn is turned to create a textile or fabric. Knitting is the process through which the yarn is turned into knitted fabric by joining consecutive row of loops (course and wales) using different types of knitting machines. In knitted loop terminology, a course of knit is a mainly horizontal row of needle loops produced by adjacent needles during the same knitting cycle. Wales of knit are a mainly vertical column of interlaced needle loops generally produced by the same needle at successive knitting cycles.

Mainly two different types of knitted fabric are produced. They are as follows.

Warp Knitting The general direction of path of yarn is along the length of the fabric. Warp knit fabrics are constructed with yarn loops formed in a vertical or warp direction. Warp knitting are four types. They are tricot knit, Raschel knit, crochet knit, and milanese knit. Warp knitted fabrics are normally using inner wears (brassieres, panties, sleepwear), sportswear lining, and household (mattress, mosquito nets).

Weft Knitting The general direction of path of yarn is across the length of fabric. Weft knitted fabrics is categorized by a series of horizontal loops formed by horizontally running threads and binds with previously formed series of loops of the same thread. End uses of weft knitting are underwear, T-shirts, sportswear, baby clothes, jumpers, scarves, hats, gloves, etc. https://textilechapter.blogspot.com/2017/03/weaving-loom-principle-mechanism.html [41].

1.7.2.3 Nonwoven

Nonwoven fabric is a fabric-like material made from long fibers, bonded together by chemical, mechanical, heat, or solvent treatment or using proper moisture or heat rather than by spinning, weaving, and braiding. Nonwoven fabric is a molded product with planar structure made by interweaving natural, chemical, and metal fibers according to their mutual characteristics to form a web in the shape of a sheet and bonding them together by mechanical or physical means. Nonwovens may be a limited life, single-use fabric or a very durable fabric. Nonwoven fabrics provide specific functions such as absorbency, liquid repellency, resilience, stretch, softness, strength, flame retardancy, wash ability, cushioning, filtering, bacterial barriers, and sterility [42].

1.7.3 Wet Processing Technology

1.7.3.1 Pretreatment Process

Natural fibers and synthetic fibers both contain primary impurities that are contained naturally and secondary impurities that are added during different process like spinning, knitting, and weaving processes. Textile pretreatment is the series of cleaning operations. All impurities that cause unfavorable effect during dyeing and printing are removed in pretreatment process. Pretreatment processes include desizing, scouring, and bleaching that make dyeing processes easy. Desizing is for the removal of the size coating after weaving. Desizing with enzymes ensures complete removal of starch-based sizes, which means excellent batch-to-batch dyeing reproducibility and evenness. Scouring is a cleaning process used to remove impurities (wax, oil) on fibers, yarns, or cloth. Bleaching is decolorizing the impurities that mask the natural whiteness of fibers to obtain white cloth and increase the ability of the fabric to absorb dyestuffs uniformly.

1.7.3.2 Dyeing

The process of applying color to fiber, yarn, or fabric is called dyeing. Dyeing is the process of giving colors to a textile material through a dye (color). Dyeing can be done at any stage of the manufacturing of textile: fiber, yarn, fabric, or a finished textile product including garments and apparels. The property of color fastness depends upon two factors: selection of proper dye according to the textile material to be dyed and selection of the method for dyeing the fiber, yarn, or fabric.

1.7.3.3 Dyeing Methods

Color is applied to fabric by different methods of dyeing for different types of fiber and at different stages of the textile production process. Mostly used methods are fabric dyeing and yarn dyeing. When a dye is applied directly to the fabric without the aid of an affixing agent, it is called direct dyeing. When dyeing is done after the fiber has been spun into yarn, it is called yarn dyeing. Yarn dyeing is slightly different from woven or knit dyeing. Yarns are dyed in package form by yarn dyeing process.

1.7.3.4 Dyes

Dyes are used for coloring the fabrics. Dyes are molecules that absorb and reflect light at specific wavelengths to give human eyes the sense of color. There are two major types of dyes: natural and synthetic dyes. The natural dyes are extracted from natural substances. Synthetic dyes are made in a laboratory. Chemicals are synthesized for making synthetic dyes. Mostly used dyes are reactive dyes (used for dyeing cellulose fibers and protein fiber), direct dyes (used for dyeing wool, silk, nylon, cotton, rayon, etc.), vat dyes (used for dyeing wool, nylon, polyesters, acrylics, and modacrylics), disperse dyes (used to dyeing nylon, cellulose triacetate, and acrylic fibers), sulfur dyes (used for dyeing cotton and linen, viscose, and jute), basic dyes (used for dyeing cotton, linen, acetate, nylon, polyesters, acrylics, and modacrylics) [43–46].

1.7.3.5 Finishing

In textile manufacturing, finishing refers to the processes that convert the woven or knitted cloth into a usable material and more specifically to any process performed after dyeing the yarn or fabric to improve the look, performance, or hand feel of the finish textile. To impart the required functional properties to the fiber or fabric, it is customary to subject the material to different type of physical and chemical treatments. For example, wash and wear finish for a cotton fabric is necessary to make it crease-free or wrinkle-free. In a similar way, mercerizing, singing, flame retardant, water repellent, waterproof, antistatic finish, peach finish, etc. are some of the important finishes applied to textile fabric [47].

1.7.3.6 Printing

Textile printing is the process of applying color to fabric in definite patterns or designs. In a proper printed fabric, the color is affixed to the fiber, so that it may not be affected by washing and friction. The dyes used for printing mostly include vat, reactive, naphthol, and disperse colors, which have good fastness properties. The pigments, which are not truly dyes, are also used extensively for printing. These colors are fixed to the fiber through resins that are very resistant to laundering or dry-cleaning. Mostly used printing methods are direct printing, discharge printing, resist printing, roller printing, block printing, screen printing, transfer printing, and electrostatic printing [48, 49].

1.8 Textile Applications

Textile structures are now being used for various applications due to their unique advantages. In fact, we can divide their applications into apparel, technical textile, and functional and smart textiles. Apparel manufacturing industries include establishment that process fiber into fabric and fabric into clothing, and other textile products includes shirt, pant, socks, shoes, bra, etc. Technical textiles are indicated to be the quickest improving sector of the textile industry. Functional or technical textiles are the textiles that have been developed to fulfill the high-performance requirement in industries other than conventional clothing [50, 51]. Applications of advanced textiles will be discussed below. The applications of textile materials are presented in Figure 1.11.

1.8.1 Advanced Applications of Textile Material

In this exiting era of advanced materials, we are seeing their widespread contribution in diversified areas, starting from clothing sector to biomedical field, civil engineering, filtration, fiber optics, aerospace, automobile industries, and energy storage and harvesting applications. The convergence of different science and engineering fields is a reason for these astonishing results. Advanced materials are driven by special technical functions that require specific performance properties unique to these materials. Based on their functionality they can be classified into materials for functional, high performance, sensors/actuators,

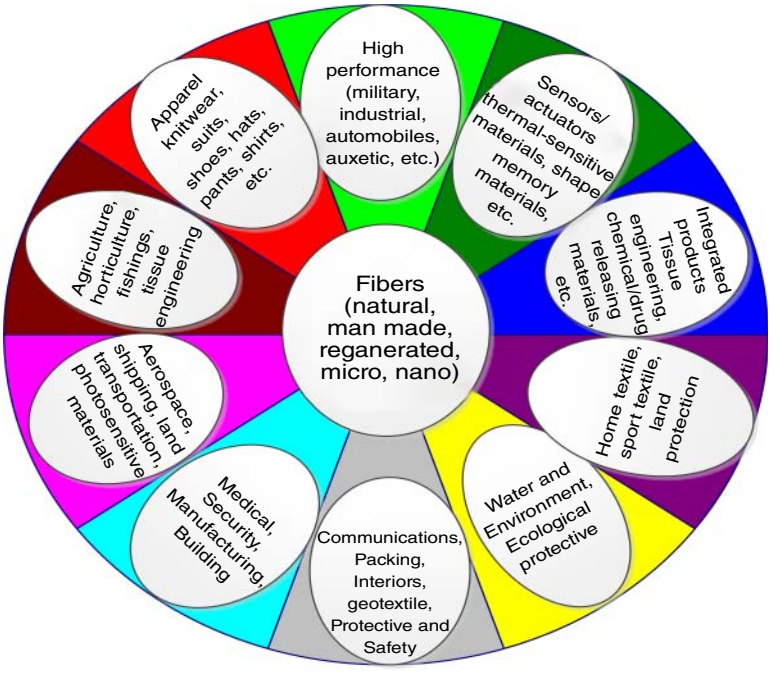


Figure 1.11 Applications of textile materials.

integrated assemblies, and sensitive/smart. Functional materials include water repellent/waterproof, crease resistance, flame retardant, water vapor permeability, etc. High-performance materials usually exhibit high modulus and strength and are used in areas like military, industrial, automobiles, building, auxetics, and land protection applications. The sensors and actuators include fiber optics, nanomaterials, microcapsules, and intelligent membranes/coatings. For integrated products, photonics, tissue engineering, chemical/drug releasing materials are used. Sensitive and smart materials include conductive materials, memory materials, photonic materials, etc. The advanced application of textile materials is shown in Figure 1.12.

1.8.2 Functional Textile

Functional textiles are a class of textiles with integrated property of adjusting textiles according to requirements and functions such as temperature and humidity responsive, water repellent, water vapor permeable, flame retardant, etc. The widely used fibers for functional textiles are viscose, polyester, and polyurethane fibers. The properties of functional textiles are shown in Figure 1.13.

1.8.2.1 Water Repellent

Water repellent is the special type of finishes that repel water, oil, and dry dirt. Water repellent properties are very important for garments, home, and technical textiles. The aim of water-repellent finishes is that the drop of water on the fabric

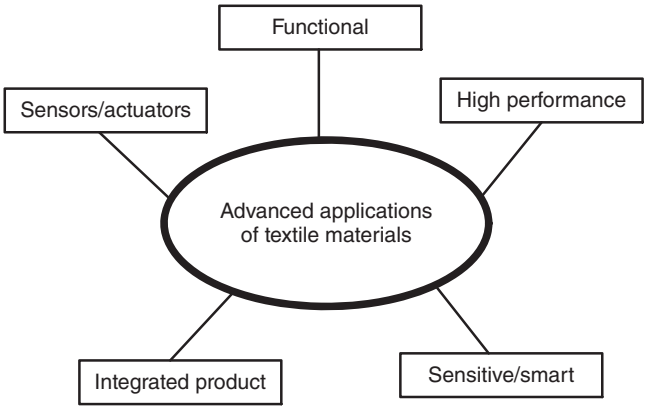


Figure 1.12 Advanced applications of textile materials.

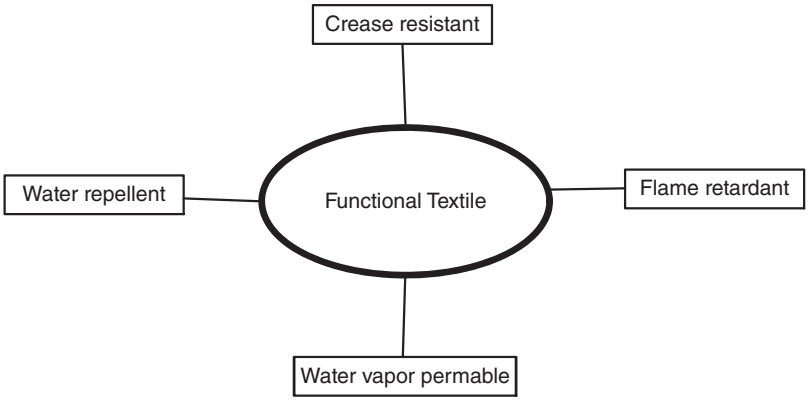


Figure 1.13 Properties of functional textile.

surface should not spread and should not wet the textile; wetting will happen only when the droplet is absorbed by textile. Water repellency is attained by using different products, but oil repellency is achieved only by using fluorocarbon polymers. In water-repellent fabric it is expected that the drop of water will stay on the surface and easily can drips off or it can be brushed off. The air permeability of the finished fabric should not be significantly affected because of water repellency, so water-repellent fabric maintains air permeability. In waterproof breathable fabric, droplet of water should not penetrate into textile, but perspiration should penetrate into textile. In the waterproof breathable fabric coating with micropores, size is small for water droplets to penetrate, and at the same time pores are big enough for perspiration vapor.

1.8.2.2 Water Vapor Permeability

Water vapor permeability is the property of a textile material that allows the passage of water vapor through fabric. It is very important for the textiles used for garment applications to transport the vapour especially when the temperature

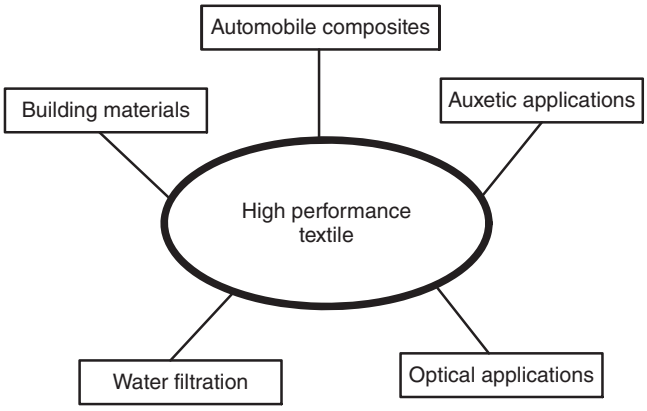


Figure 1.14 Application of high-performance textile.

is high. For getting water vapor (perspiration) permeability properties, we need to coat the fabric by special type of polymer. Water vapor permeability property will help us to avoid physiological problems. Nowadays there are a wide range of woven, laminated, or coated fabrics which are water vapor permeable and waterproof [52–54].

1.8.3 Applications of High-Performance Fibrous Materials

Fiber-reinforced composite materials have been playing an important role for many decades. There are many potential applications of high-performance fibrous materials such as automobile industry, building materials, auxetic application, water filtration, and optical applications. The different applications of high-performance fibrous materials are shown in Figure 1.14.

1.8.3.1 Fibers for Automobile Composite

The polymeric composite materials are widely being used in automotive industry. Fiber mat thermoplastics and compression-molded thermoset polymers are used to manufacture large parts of automotive industries. Composites used for nonstructural functional components are composed of glass fiber-reinforced plastics in the range of 10–50% reinforcement. Such nonstructural composites are used in pedal systems, mirror housing, and so on. To improve the fuel efficiency, hybrid valve lifter used in automotive internal combustion engine was made from carbon fiber/phenolic composite and steel. Semi-structural composites like sheet-molded compounds (SMC) are increasingly used in automotive industry for manufacturing low mass body panels with high strength to weight ratio. The materials that replaced steel with high strength to mass ratio are aluminum, glass SMC, and carbon SMC. Structural polymer composites that are studied have been gradually replacing metal components due to their reduced weight and durability and their resistance to crash. Carbon, glass, aramid, and graphite fiber-reinforced polymers and nanocomposites were studied for impact energy absorption, durability, and crushing behavior.

1.8.3.2 Fibers as Building Materials

Natural and synthetic fibers are used as building materials. They are used in constructing bridges, roads, nonstructural gratings and claddings, structural systems for industrial buildings, roof structures, tanks and thermal insulators, etc. High-performance synthetic fibers are more suitable fibers for building materials. Fibers like nylon, polyester, polypropylene, and aramid fibers are widely used as reinforcements for building materials. Natural fibers like jute, hemp, ramie, and flax are used as reinforcement in building materials. Lower cost of textiles and less energy required to make them most suitable for building materials. Among other natural fibers, jute is widely used as reinforcing fiber in composites for civil engineering applications due to its low specific gravity and high specific modulus when compared with glass.

1.8.3.3 Fibers for Auxetic Applications

The auxetic effect improves the material's mechanical properties, such as enhancement in fracture toughness, shear moduli, and indentation resistance, and allows porosity and permeability variation (under pressure) and dome shape. Due to this wide range of characteristics, auxetic materials can be used in various areas, including medicine, architecture, civil engineering, sport clothing, high-performance equipment, protection against explosives, insulation, and filters. Therefore, the use of high-performance fibers in advanced fibrous architectures like auxetic structures may offer lightweight, excellent mechanical performance and several interesting characteristics that can fulfill the explicit demands imposed by several advanced technical sectors. Auxetic structures for high-performance applications are currently studied using polyester, aramid, carbon, nylon fibers, and shape memory materials [55, 56].

1.8.3.4 Fibers for Environmental Protection: Water Purification/Filtration

There are many examples of using fibers in water treatment process. The advanced fiber technologies led separation membranes made of ultrafine fibers, ion exchange fibers, hollow fiber membranes, and aromatic polyamides in reverse osmosis membrane materials. These membrane technologies are used in many application fields from small-scale home water purification to large-scale filtration of fresh water from seawater sources. Microfine filtration membranes, ultrafine membranes, and reverse osmosis membranes made using the fiber technologies are used to remove small impurities like red rust, bacteria, particles, chemical products and salts from water. Many kinds of natural, inorganic, metallic, and synthetic fibers have been used in filtration. Synthetic fibers have played a significant role in the growth of several segments in the filtration industry. Nonwoven fabrics have been successfully used in the industry as membrane support for microfine, ultrafine, and reverse osmosis filtration. Filters with large surface area and many fine pores are required to filter fine particles. Large surface area can be achieved by using micro- and nanofibers. Hydrophilic or hygroscopic fibers are used to improve or reduce the particle adhesion to the filters. To prevent generation of static charge in filters, conductive fibers like carbon and metallic fibers are used. In hot gas filtration

and high temperature filtration and other processes mineral, ceramic or metal fibers are used as filter materials.

1.8.3.5 Fibers for Optical Applications

Optical fibers are those very fine long glass fibers that allow light signals to travel through. The demand for fiber optics has grown enormously. They are used as network carriers; in data transmission, transmitting broadband signals, intelligent transportation systems, and biomedical industry as telemedicine devices for transmitting digital diagnostic images; and in detecting target biomolecules like enzymes, antibodies, and oligonucleotides. It is also used in military and space and automotive sectors. Optical fibers are usually made up of molten solution of silica or silicon dioxide with other materials such as arsenic, quartz, etc. Polymeric optical fibers can be doped with photosensitive material to change the refractive index when exposed to bright light usually in UV range of spectrum. A structured fiber with combination of cores, holes, and electrodes is used for variety of specialty applications. Optical fiber for imaging is made of multiple noninteracting cores, which is used in endoscopes to directly image internal organs. The use of capillary tube-based optical fibers is used for proteomic and genomic studies. Photonic crystal-based fiber optics is used to study light interactions. Fiber-optic biosensors (FOBS) work as a transduction element and depend on optical transduction mechanisms for detecting biomolecules. They are used for applications such as detection of pathogens, medical diagnosis based on protein or cell concentration, and real-time detection of DNA hybridization. Fiber-optic chemical sensors (FOCS) are used in sensing gases and vapors, medical and chemical analysis, marine and environmental analysis, molecular biotechnology, industrial production monitoring and bioprocess control, and automotive industry.

1.8.4 Application of Sensors/Actuators

1.8.4.1 Fibers as Electronic Devices/Wearable Electronics/Energy Materials/Sensors and Actuators

Wearable electronics is one of the widely spoken technologies in smart textile arena. The functionality of the fabric is due to the electronics and interconnections woven between them. Future generation of wearable electronics focuses on the systems to be worn directly on human body. Wearable electronic systems developed using conductive fibers have shown promising results. The technical possibility for building the electronic functions as integral part or on the surface of the fiber is scientifically proven. The development of soft and flexible fiber-based conductive and semiconductive materials is essential. Conductive polymeric fibers are one of the promising materials due to their extremely flexible nature. It also can be blended with variety of composite materials to achieve unique electronic, optical, electrical, and magnetic properties. Π-Conjugated nanoscaled organic molecules was investigated for sensors, transistors, flexible electronic devices, and field emission display in textiles [57]. Polyaniline and polypyrrole-based nanofibers show high conductivity properties at room temperature [58–60]. Poly-(3,4-ethylenedioxythiophene) (PEDOT) is

one of the conductive polymers with high conductivity and solution process ability. The application of this polymer as electrodes for wearable capacitors or photodiodes is currently being explored. Carbon-based nanomaterials due to their intrinsic carrier mobility are used as channel materials in transparent electrode and field-effect transistors. Porous carbon materials like graphene, carbon nanotubes (CNTs), carbon fibers, and carbon aerogels are frequently used in wearable electronics due to their large specific surface area and better mechanical properties. Metallic nanoparticles or nanowires possess high conductivity and are very much suitable for wearable electronics. Metallic nanowires are used to develop fiber-based piezoelectric nanogenerator by coating silver on highly stretchable polyamide fabric [57]. Fiber-based electrodes made of CNTs, metals, or alloys like copper and stainless steel are light, foldable, durable, and flexible, thus more suitable for wearable electronics. Integrating sensors with conductive fibers in the fabrics can be used to monitor electrocardiogram (ECG), electromyography (EMG), and electroencephalography (EEG) [61, 62]. Fabric integrated with luminescent elements could be used for biophotonic sensing; shape-sensitive fabrics is used to sense the movement and used with EMG to obtain muscle fitness data. Integrated carbon electrodes in fabrics help to detect environmental features such as oxygen, salinity, moisture, and contaminants. Strain fabric sensing technology uses conductive yarns to record motion or flexing, pressure, and stretching or compression [63]. Merely conductive yarns of specific length are also used to make fabric antennas by stitching them together with nonconductive fabrics [64].

1.8.4.2 Fibers for Medical Compression

Compression garments are used to apply certain pressure on different parts of body. They are specially used for medical treatments, sports, and body shaping purposes. Medical compression garments are used to treat scars, muscular sprains, and low blood pressure and to quicken healing process for deep vein thrombosis patients [65]. Medical compression systems are usually made using fibers like polyester, polyamide elastane. Recent studies about application of shape memory fibers and alloys in the medical compression have gained attention [55, 66–69]. Shape memory materials are actuated using electrical current and body heat to provide compression effect. Segmented polyurethane-based shape memory fibers have shown promising results, and they have gained advantage over shape memory alloys due to their lightweight, flexibility, comfort, and easy actuation without any additional devices [70].

1.8.4.3 Fibers for Health/Stress/Comfort Management

Fibers within the human body serve as an inspiration for development of different kind of advanced materials. Hollow fibers are used in artificial lung and blood vessels. There are several studies which focus on the production of artificial liver, pancreas, skin, muscle, and nervous systems. Lightweight, sweat-absorbent, and easy dry fibers are developed for sportswear application to keep the wearer feel comfortable during workout. Fibers that can retain heat allow the water vapor from the body to pass through and repel water and are developed to protect people from extreme cold weather conditions. Breathable

shape memory polyurethanes fibers and films that can respond according to the microclimatic condition between the clothing and body of the wearer are used. Antibacterial fibers are used in clothing, hospital wear, and wound care bandages to prevent contamination and bad odors caused due to bacteria. Fibers used in comfort applications must have the following properties: absorption of sweat, high water absorbency/quick dry bacteria-free/moss-free, microbe controlling, insect/tick repellent, heat retention/storage, moisture retention, moisture absorption, coolness, tranquilizer moisture permeable/water repellent, deodorant, antibacterial, electric control, UV shielding, electromagnetic wave shielding, insulation, lightweight, fitness to skin, high touch, stretch, soil-free/soil release, and shape stability.

1.8.4.4 Fibers for Thermal Protection

Fibers used for flame and thermal protection play a vital role in providing protection to workers engaging in high temperature environments, military clothing, home furnishing materials, and building materials and for firefighters. The protective clothing made using these fibers must have insulation properties and dimensional stability. Flame-resistant viscose fibers are produced by doping the spinning solution before extrusion using phosphorus-based additives (Lenzing FR®), polysilicic acid, and clay nanocomposites (TENCEL®). Flame-retardant polyester and acrylics are produced using FR comonomers during copolymerization, introducing flame-retardant additives during extrusion and flame-retardant finishes. Aromatic polyamides and meta-aramid fibers are used for protective clothing for astronauts, tank crews, and fighter pilots. Nonwoven meta-aramids are used in thermal insulation and hot gas filtration purposes. Para-aramids are specifically used for ballistic and flame protection applications. Polyimide fiber is an aromatic copolyamide sold in the brand name P84®. It has Limiting Oxygen Index (LOI) of 36–38% and is used in the production of protective clothing, hot gas filtration, sealing materials, and aviation materials.

1.8.4.5 Fibers for Radiation Protection

The need for special protective clothing is inevitable to protect people exposed to radioactive rays, UV radiation, and electromagnetic radiations. Woven cotton, polyester/cotton, and polyester/nylon fabrics with twill and sateen weave and nonwoven fabrics are used to protect people from α, β, and γ radiation environments. The fabric acts as a barrier between human skin and nuclear radiation emitted from radioactive source. Closely woven fabrics made up of wool and polyester have high UV absorption and protect skin from UV-A and UV-B radiations. Humans are exposed to different kinds of electromagnetic radiation extending from 1 to 10 000 mHz emitted by various sources, for example, cell phones, microwave ovens, and radar signal communication systems. When exposed at higher levels, these waves will cause abnormal chemical activities in body that produces cancer cells. It also obstructs the capability of cells for regeneration of DNA and RNA. To tackle this problem conductive materials are used to shield electromagnetic and static charges. General textile fibers have sufficient resistivity to shield electromagnetic radiation. The resistivity required for dissipating and shielding electrostatic charges is achieved through

conductive coatings on fabric, fibers doped with carbon black, carbon fibers, and metal fibers. The conductive fibers or yarns are incorporated in fabrics to produce conductive garments to resist static charges.

1.8.5 Applications of Integrated Products

1.8.5.1 Fibers for Tissue Engineering

Tissue engineering concept was born when several investigators realized that when cell are placed close enough to each other, they form structures identical with those formed by such cells in a living body. This, apparently, may be achieved thanks to signals that living cells can exchange with the neighboring ones. Various disciplines, such as materials science, cell biology, reactor engineering, and clinical research, are contributors of tissue engineering. Advanced tissue engineering involves the use of polymeric materials implanted at the defective site. The defective sites are usually supported by scaffolds. They provide the framework for the cells to attach, proliferate, and form results in the formation of extracellular matrix. Biodegradable natural and synthetic fibers as well as some nonbiodegradable polymeric fibers are currently used for tissue engineering. Polylactides, polyglycolides, polycaprolactone (PCL), and their copolymers have been often used for the preparation of scaffolds for cartilage tissue engineering. However, their hydrophobicity, the acidity of their decomposition products, and the self-acceleration of their degradation have constituted serious drawbacks. Chitosan and alginate are nontoxic, biodegradable, biocompatible polymer and does not have these disadvantages. The use of natural polysaccharide like alginates that are extracted from algae has shown promising growth in tissue engineering and wound dressing applications. Alginate fibers and dressings as wound care products are resistant to bacterial attack, antiviral, antifungal, nontoxic, high absorbent, hemostatic, non-allergic, breathable, biocompatible and can blended with medicines. Alginate nanofibers were produced by electrospinning technique in the presence of various synthetic polymers and/or surfactants and sometimes in combination with chitosan offer better cell adhesion properties [71, 72]. Bio-artificial scaffolds made of *Chlamydomonas reinhardtii* single-cell green alga mixed with fibrinogen have shown excellent in vitro biocompatibility and photosynthetic activity, and the algae survived for five days in vivo. These kinds of photosynthetic scaffolds can be implanted in full skin defects and can be used in the generation of chimeric tissue composed of mammalian and photosynthetic cells in vivo [73]. Chitosan, a unique biopolymer derived from chitin, exhibits outstanding properties along with excellent biocompatibility and biodegradability. Chitosan and its blends with sodium alginate, tropocollagen, cellulose, sodium hyaluronate, sodium chondroitin sulfate, poly(acrylic acid), and synthetic polymers like PEO,UMHMWPEO, PVA, PLA, and PVP are used to produce nanofiber mats for tissue engineering and wound healing applications [74]. Collagen fibrils and their networks form a highly organized 3D scaffold to surround the cells. It ensures structural and biological integrity of ECM. Collagen can form fibers with high tensile strength and stability. The hollow fiber made using collagen tubing is used for cell culture nerve regeneration [75]. The unique structure of silk,

versatility in processing, biocompatibility, availability of different biomaterial morphologies, options for genetic engineering of variations of silks, the ease of sterilization, thermal stability, surface chemistry for facile chemical modifications, and controllable degradation features make silks promising biomaterials for many clinical functions. Silk fibrous materials are used as scaffolds for tissue engineering and sutures.

1.8.6 Sensitive and Smart Materials

1.8.6.1 Fibers with Conductive Properties as Industrial Materials

Conductive fibers are lightweight alternatives to heavy copper wiring in variety of areas where weight is a concern especially in aerospace technologies. Inherently conductive fibers include metallic fibers, carbon fibers, and conjugated polymeric fibers. Treated conductive fibers are conductive-filled fibers and conductive-coated fibers. Metallic fibers are developed from metals or metal alloys. These fibers have very high conductivity, but they possess low flexibility, stiffness, and high weight. Carbon fiber and its composites possess conductivity like that of metals with high strength, stiffness, and lower weight. Conjugated polymers like PEDOT fibers have high conductivity values from 150 to 250 s/cm. Polymeric fibers filled with conductive fillers like metallic powder, carbon black, CNT, graphene, or conjugated polymer powder are used as conductive fibers. The conductive fibers that can be produced by coating insulating materials with highly conductive materials, such as metals, metal alloys, carbon black, carbon nanotubes, and ICPs, are known as conductive-coated fibers. To apply metallic coatings, sputtering, vacuum deposition, electroless plating, carbonizing, and filling or loading fibers are the most extensively used methods. Potential applications of conductive fibers include power lines; aircraft and aerospace wiring systems; harnesses for automotive wiring; wires for missile guidance; electrotextiles for medical, military, and consumer applications; lightweight deployable antennas; thermal blankets and clothing; flexible keyboards; giant-area flexible circuits for energy harvesting; electrostatic charge dissipation; and battlefield monitoring and reporting of vital signs and wound locations on soldiers.

1.8.6.2 Memory Fibrous Materials

Smart textile is the development of textile having sensing, reacting, and adapting capabilities. Materials or structure that sense react to external stimuli or condition such as thermal, chemical, mechanical, or other sources. Shape memory material can move to temporary shape by external stimulus, and it can come back to its original shape with right stimulus. Memory materials include water vapor permeability textile, ventilation textile, medical textile, thermal protective textile, etc.

1.8.7 Advantages of Fibrous Materials

Fibrous materials have been used from many centuries in the application of clothing and other utilitarian products. Natural fibers are abundantly available in different geological locations with various altitudes in the world, and they are easily processable. Synthetic fibers can be produced with customized

parameters according to specific end use without much trouble. The revolutionary breakthrough of research in science and technology in the twenty-first century leads to the use of both natural and synthetic fibrous materials in vivid multidisciplinary applications, owing to their several advantages. This is the era of synthetic fibers now, and it offers platform to tailor their properties suitable to put them into proper end use. Synthetic fibers can be produced into micro-, macro-, and nano-sizes with novel functionalities, which is reliable to produce in mass with low material cost. Fibers do offer several advantages over other materials such as lightweight (less density), superior stretch ability, toughness (e.g. regenerated spider silk), high tensile strength (e.g. silk), high specific surface area, vibration damping capability [77], energy storage ability [78], super absorbency [16] and memory behavior (e.g. shape or stress memory) [79, 80], self-healing [81], biodegradability [82], biocompatibility (e.g. tissue engineering and implants) [83, 84], insulation capability [33], chemical inertness, antimicrobial [85], flame retardancy [86], biomimicking [87], etc. These several advantages of fibrous materials enable one to make them into substrates by traditional textile processing technologies such as weaving, knitting, nonwoven webs, and braiding due to their excellent flexibility and strength. These substrates made from fibers have been employed into various multidisciplinary areas including electronics, construction, power harvesting, aerospace, medical, transportation, and industrial high-performance materials. Both natural and synthetic fibers are needed in daily life to the human being, and smart fibers are considered as futuristic material to prepare well for needs of tomorrow's challenging and sustainable days. Hence fibers play a very vital role in fulfilling our requirements on this planet.

References

1 Denton, M.J. and Daniels, P.N. (2002). *Textile Terms and Definitions*, 11e. Manchester: The Textile in Institute.
2 Morton, W.E. and Hearle, J.W.S. (2008). *Physical Properties of Textile Fibers*, Woodhead Publishing in Textiles. England: Woodhead Publishing Limited.
3 Collier, B.J., Bide, M.J., and Tortora, P.G. (2009). *Understanding Textiles*, 7e. Pearson/Prentice Hall.
4 Houck, M.M. (2009). *Identification of Textile Fibers*, Woodhead Publishing in Textiles. Cambridge: Woodhead Publishing Limited.
5 Blackburn, R. (2005). *Biodegradable and Sustainable Fibers*, Woodhead Publishing Series in Textiles. Woodhead Publishing.
6 Mishra, S.P. (2000). *Fiber Science and Technology*. New Delhi: New Age International (P) Limited.
7 Saville, B.P. (1999). 3 - Fiber dimensions. In: *Physical Testing of Textiles*, 44–76. Woodhead Publishing.
8 Hearle, J.W.S. and Backer, P.G.S. (1969). *Structural Mechanics of Fibers, Yarns, and Fabrics*. Wiley-Interscience.
9 Hu, J.L. (2004). *Structure and Mechanics of Woven Fabrics*, Woodhead Publishing in Textiles. CRC Press; Woodhead Publishing.

10 Yang, Q.X. and Li, G.Q. (2014). Spider-silk-like shape memory polymer fiber for vibration damping. *Smart Materials and Structures* 23 (10).
11 Haigh, H.S. (2009). Speciality fibers. *Journal of the Textile Institute Proceedings* 40 (8): 794–813.
12 Das, T. and Ramaswamy, G.N. (2006). Enzyme treatment of wool and specialty hair fibers. *Textile Research Journal* 76 (2): 126–133.
13 Vineis, C., Aluigi, A., and Tonin, C. (2011). Outstanding traits and thermal behaviour for the identification of speciality animal fibers. *Textile Research Journal* 81 (3): 264–272.
14 Prahsarn, C., Klinsukhon, W., Padee, S. et al. (2016). Hollow segmented-pie PLA/PBS and PLA/PP bicomponent fibers: an investigation on fiber properties and splittability. *Journal of Materials Science* 51 (24): 10910–10916.
15 Tallury, S.S., Behnam, P., Melissa, A.P., and Richard, J.S. (2016). Physical microfabrication of shape-memory polymer systems via bicomponent fiber spinning. *Macromolecular Rapid Communications* 37 (22): 1837–1843.
16 Kim, G.H., Youk, J.H., Kim, Y.J., and Im, J.N. (2016). Liquid handling properties of hollow viscose rayon/super absorbent fibers nonwovens for reusable incontinence products. *Fibers and Polymers* 17 (7): 1104–1110.
17 Beskisiz, E., Ucar, N., and Demir, A. (2009). The effects of super absorbent fibers on the washing, dry cleaning and drying behavior of knitted fabrics. *Textile Research Journal* 79 (16): 1459–1466.
18 Lee, T.W., Han, M., Lee, S.E., and Jeong, Y.G. (2016). Electrically conductive and strong cellulose-based composite fibers reinforced with multiwalled carbon nanotube containing multiple hydrogen bonding moiety. *Composites Science and Technology* 123: 57–64.
19 Schmidt, M.A., Argyros, A., and Sorin, F. (2016). Hybrid optical fibers - an innovative platform for in-fiber photonic devices. *Advanced Optical Materials* 4 (1): 13–36.
20 Xi, P., Tianxiang, Z., Lei, X. et al. (2017). Fabrication and characterization of dual-functional ultrafine composite fibers with phase-change energy storage and luminescence properties. *Scientific Reports* 7 (1): 1–9.
21 Meng, Q.H., Hu, J.L., and Yeung, L. (2007). An electro-active shape memory fiber by incorporating multi-walled carbon nanotubes. *Smart Materials and Structures* 16 (3): 830–836.
22 Meng, Q.H. (2009). The influence of heat treatment on the properties of shape memory fibers. II. Tensile properties, dimensional stability, recovery force relaxation, and thermo mechanical cyclic properties. *Journal of Applied Polymer Science* 111 (3): 1156–1164.
23 Meng, Q.H. (2007). Morphology, phase separation, thermal and mechanical property differences of shape memory fibers prepared by different spinning methods. *Smart Materials and Structures* 16 (4): 1192–1197.
24 Meng, Q.H., Hu, J.L., Zhu, Y. et al. (2007). Polycaprolactone-based shape memory segmented polyurethane fiber. *Journal of Applied Polymer Science* 106 (4): 2515–2523.
25 Pan, N. and Gibson, P. (2006). *Thermal and Moisture Transport in Fibrous Materials*. Cambridge: Woodhead Publishing Limited.

26 Kajiwara, K. (2009). Synthetic textile fibers: structure, characteristics and identify cation. In: *Identification of Textile Fibers* (ed. M.M. Houck), 68–87. Cambridge: Woodhead Publishing Limited.

27 Hess, K. and Naturwissenschaft, H.K. (1944). Over-long-term interferences and micellar fiber refinement in fully synthetic fibers (polyamides and polyesters). *Journal of Physical Chemistry* A193 (171): 196.

28 Hearle, J.W.S. (1958). You have full text access to this content fringed fibril theory of structure in crystalline polymers. *Journal of Polymer Science* 28 (117): 432–435.

29 Hearle, J.W.S. (1963). The fine structure of fibers and crystalline polymers. I. Fringed fibril structure. *Journal of Polymer Science* 7 (4): 1175–1192.

30 Kozasowski, R.M., Mackiewicz-Talarczyk, M., and Allam, A.M. (2012). 5 - Bast fibers: flax A2 - Kozłowski, Ryszard M. In: *Handbook of Natural Fibers*, 56–113. Woodhead Publishing.

31 Roy, S. and Lutfar, L.B. (2012). 3 - Bast fibers: jute A2 - Kozłowski, Ryszard M. In: *Handbook of Natural Fibers*, 24–46. Woodhead Publishing.

32 Roy, S. and Lutfar, L.B. (2012). 4 - Bast fibers: ramie A2 - Kozłowski, Ryszard M. In: *Handbook of Natural Fibers*, 47–55. Woodhead Publishing.

33 Koh, E. and Lee, Y.T. (2017). Antimicrobial activity and fouling resistance of a polyvinylidene fluoride (PVDF) hollow-fiber membrane. *Journal of Industrial and Engineering Chemistry* 47: 260–271.

34 AATCC (2013). *Fiber analysis: qualitative*.

35 Edward, L.G. (1966). *Natural and Manmade Textile Fibers: Raw Material to Finished Fabric*, 1e. New York: Duell, Sloan and Pearce.

36 Lawrence, C.A. (2010). *Advances in Yarn Spinning Technology*. Cambridge: Woodhead Publishing Ltd.

37 Mahadevan, M.G. (2009). Textile spinning, weaving and designing. In: *Chandigarh*, 1e. Abhishek Publications.

38 Vasudeo, K.M. (2013). *Fundamentals of Yarn Winding*. New Delhi: Woodhead Publishing.

39 Ormerod, A. and Sondhelm, W.S. (1995). *Weaving: Technology and Operations*. Manchester: The Textile Institute.

40 Abhijit, M. (2017). *Principles of Woven Fabric Manufacturing*. Boca Raton, FL: CRC Press.

41 Belal, S.A. (2009). *Understanding Textiles for a Merchandiser*, 1e. Dhaka: BMN3 Foundation.

42 Chandra, R.S. (2012). *Fundamentals and Advances in Knitting Technology*. New Delhi: Woodhead Publishing India Pvt.

43 Spencer, D.J. (2001). *Knitting Technology*, 3e. Cambridge: Woodhead Publishing.

44 Albrecht, W. and Fuchs, H.W. (2003). *Nonwoven Fabrics*. Weinheim: Wiley-VCH.

45 Gürses, A., Açıkyıldız, M., Güneş, K., and Gürses, M.S. (2016). *Dyes and Pigments*. Switzerland: Springer.

46 Fu, J. (2013). *Dyeing: Processes, Techniques, and Applications*. Hauppauge, NY: Nova Science Publishers, Inc.

47 Clark, M. (2011). *Handbook of Textile and Industrial Dyeing*. Cambridge: Woodhead Publishing.

48 Arthur, B.D. (2001). *Basic Principles of Textile Coloration*. Bradford: Society of Dyers and Colorists.

49 Trotman, E.R. (1975). *Dyeing and Chemical Technology of Textile Fibers*, 5e. London: Griffin.

50 Kate, W. (1997). *Fabric Dyeing & Printing*. Loveland, CO: Interweave Press.

51 Yohanan, P. (1990). *Dyeing and Printing: A Handbook*. London: Intermediate Technology.

52 Thakur, S., Jahid, M.A., and Hu, J.L. (2018). Mechanically strong shape memory polyurethane for water vapour permeable membranes. *Polymer International* 67: 1386–1392.

53 Jahid, M.A., Hu, H.L., and Zhou, H. (2018). *Smart Textile Coatings and Laminates*, Chapter 6, 155–173.

54 Jahid, M.A., Hu, J.L., Wong, K.H. et al. (2018). Fabric coated with shape memory polyurethane and its properties. *Polymers* 10: 681.

55 Nayak, R. and Padhye, R. (2015). *Garment Manufacturing Technology*. Sawston, Cambridge: Woodhead Publishing, an imprint of Elsevier.

56 Koncar, V. (2016). *Smart Textiles and Their Applications*. Duxford: Woodhead Publishing.

57 Horrocks, A.R. and Anand, S.C. (2016). *Handbook of Technical Textiles*, 2e. Cambridge: Woodhead Publishing in association with the Textile Institute, Woodhead Publishing is an imprint of Elsevier.

58 Meng, Q. and Hu, J.L. (2008). A temperature-regulating fiber made of PEG-based smart copolymer. *Solar Energy Materials and Solar Cells* 92 (10): 1245–1252.

59 Zhu, Y., Hu, J.L., and Yeung, K.W. (2009). Effect of soft segment crystallization and hard segment physical crosslink on shape memory function in antibacterial segmented polyurethane ionomers. *Acta Biomaterialia* 5 (9): 3346–3357.

60 Jang, S.Y., Seshadri, V., Khil, M.S. et al. (2005). Welded electrochromic conductive polymer nanofibers by electrostatic spinning. *Advanced Materials* 17 (18): 2177–2180.

61 Huang, K., Wan, M., Long, Y. et al. (2005). Multi-functional polypyrrole nanofibers via a functional dopant-introduced Process. *Synthetic Metals* 155 (3): 495–500.

62 Huang, J. and And Kaner, R.B. (2004). Nanofiber formation in the chemical polymerization of aniline: a mechanistic study. *Angewandte Chemie International Edition* 43 (43): 5817–5821.

63 Zeng, W., Tao, X.M., Chen, S. et al. (2013). Highly durable all-fiber nanogenerator for mechanical energy harvesting. *Energy & Environmental Science* 6 (9): 2631–2638.

64 Coosemans, J., Hermans, B., and Puers, R. (2006). Integrating wireless ECG monitoring in textiles. *Sensors and Actuators A: Physical* 130: 48–53.

65 Custodio, V., Herrera, F.J., Lopez, G., and Moreno, J.I. (2012). A review on architectures and communications technologies for wearable health-monitoring systems. *Sensors* 12 (10): 13907–13946.

66 Pacelli, M., Taccini, N., and Paradiso, R. (2006). Sensing fabrics for monitoring physiological and biomechanical variables: E-textile solutions. *2006 3rd IEEE/EMBS International Summer School on Medical Devices and Biosensors.*

67 Salonen, P. and Hurme, L. (2003). A novel fabric WLAN antenna for wearable applications. *IEEE Antennas and Propagation Society International Symposium. Digest. Held in conjunction with: USNC/CNC/URSI North American Radio Sci. Meeting (Cat. No.03CH37450).*

68 Wang, L., Felder, M., and Cai, J. (2011). Study of properties of medical compression fabrics. *Journal of Fiber Bioengineering & Informatics* 4 (1): 15–22.

69 Kumar, B., Hu, J.L., and Pan, N. (2016). Smart medical stocking using memory polymer for chronic venous disorders. *Biomaterials* 75: 174–181.

70 Kumar, B., Hu, J.L., and Pan, N. (2016). Memory bandage for functional compression management for venous ulcers. *Fibers* 4 (1): 10.

71 Moein, H. and Menon, C. (2014). An active compression bandage based on shape memory alloys: a preliminary investigation. *Biomedical Engineering Online* 13: 135.

72 Zhu, Y., Hu, J.L., Yeung, K.W. et al. (2007). Effect of cationic group content on shape memory effect in segmented polyurethane cationomer. *Journal of Applied Polymer Science* 103 (1): 545–556.

73 Rinaudo, M. (2014). Biomaterials based on a natural polysaccharide: alginate. *TIP* 17 (1): 92–96.

74 Jeong, S.I., Krebs, M.D., Bonino, C.A. et al. (2010). Electrospun alginate nanofibers with controlled cell adhesion for tissue engineering. *Macromolecular Bioscience* 10 (8): 934–943.

75 Schenck, T.L., Hopfner, U., Chavez, M.N. et al. (2015). Photosynthetic biomaterials: a pathway towards autotrophic tissue engineering. *Acta Biomaterialia* 15: 39–47.

76 Croisier, F. and Jérôme, C. (2013). Chitosan-based biomaterials for tissue engineering. *European Polymer Journal* 49 (4): 780–792.

77 Chattopadhyay, S. and Raines, R.T. (2014). Review collagen-based biomaterials for wound healing. *Biopolymers* 101 (8): 821–833.

78 Deng, J., Ye, Z., Yang, Z. et al. (2015). A shape-memory supercapacitor fiber. *Angewandte Chemie International Edition* 54 (51): 15419–15423.

79 Narayana, H., Hu, J.L., Kumar, B. et al. (2017). Stress-memory polymeric filaments for advanced compression therapy. *Journal of Materials Chemistry B* 5 (10): 1905–1916.

80 Tonazzini, A., Stefano, M., Bryan, S. et al. (2016). Variable stiffness fiber with self-healing capability. *Advanced Materials* 28 (46): 10142–10148.

81 Emmert, M., Patrick, W., Miranda, R.G., and Doris, H. (2017). Nanostructured surfaces of biodegradable silica fibers enhance directed amoeboid cell migration in a microtubule-dependent process. *RSC Advances* 7 (10): 5708–5714.

82 Akbari, M., Tamayol, A., Bagherifard, S. et al. (2016). Textile technologies and tissue engineering: a path toward organ weaving. *Advanced Healthcare Materials* 5 (7): 751–766.

83 O'Connor, R.A. and McGuinness, G.B. (2016). Electro spun nanofibre bundles and yarns for tissue engineering applications: a review. *Proceedings of*

the Institution of Mechanical Engineers, Part H: Journal of Engineering in Medicine 230 (11): 987–998.

84 Korjenic, A., Zach, J., and Hroudova, J. (2016). The use of insulating materials based on natural fibers in combination with plant facades in building constructions. *Energy and Buildings* 116: 45–58.

85 Shukla, A., Basak, S., Ali, S.W., and Chattopadhyay, R. (2017). Development of fire retardant sisal yarn. *Cellulose* 24 (1): 423–434.

86 Zhang, K., Fan, L., Yan, Z. et al. (2012). Electrospun biomimic nanofibrous scaffolds of silk fibroin/hyaluronic acid for tissue engineering. *Journal of Biomaterials Science Polymer Edition* 23 (9): 1185–1198.

87 Weng, W., Chen, P., He, S. et al. (2016). Smart electronic textiles. *Angewandte Chemie International Edition* 55 (21): 6140–6169.

2

Animal Fibers: Wool

Xiao Xueliang

School of Textiles and Clothing, Jiangnan University, Lihu Road 1800, Binhu, Wuxi 214122, Jiangsu, P.R. China

2.1 Introduction

In animal fibers, natural hairs have a huge number of family members. In terms of sources, there are sheep hair (wool), goat hair (guard hair and cashmere), camel hair (camel guard hair and camel cashmere), alpaca hair (vicuna hair and Peru wool), rabbit hair (e.g. Angora rabbit hair), and other animal hairs (e.g. ox hair, horse hair, yak hair, and deer velvet) rarely mentioned. Among these hairs, sheep hair fiber, namely, "wool," as shown in Figure 2.1, is a kind of the most important natural protein fiber and is also an important textile material that has a number of excellent properties, such as good elasticity, high water absorption, natural wavy crimpness, good warmth retention, difficult stained, gentle luster, etc. These properties endow wools with different unique styles. The high-grade clothing made of wools, like cassimere and medium tweed, can be spring and autumn fabrics with hand feel of slippery waxy, rich bone, good elasticity, surface clean, and natural shine, while all kinds of thick wool coats have a feel of rich texture, plumply, strong warmth retention, etc.

Wool fibers can be used for technical products, such as woolen cloth, felt, blanket, cushion material, etc. Furthermore, many decorative textiles made of wool, such as tapestry and wool carpet, give people a precious gorgeous feel [1]. Wool has unique physical and chemical properties that perform extremely versatile due to the special wool compositions and macromolecule spatial structure especially the molecular conformation. For example, the high temperature of heat setting (>100 °C) on wool products can permanently set the wool shape for the change of molecular conformation that cannot backward the wool original shape ever. Moreover, because of high moisture absorbing properties for the large amount of hydroxyl groups on the hair macromolecular chains, wool can be warm or cool in terms of casual or formal format that makes people feel comfortable to wear actively and passively. Moreover, because wool is a natural protein fiber, the use of such fiber in textile can be considered by consumers to be sustainable, renewable, and environmental friendly. Therefore, like cotton, wool is also one of the most popular natural and

Handbook of Fibrous Materials, First Edition. Edited by Jinlian Hu, Bipin Kumar, and Jing Lu.
© 2020 Wiley-VCH Verlag GmbH & Co. KGaA. Published 2020 by Wiley-VCH Verlag GmbH & Co. KGaA.

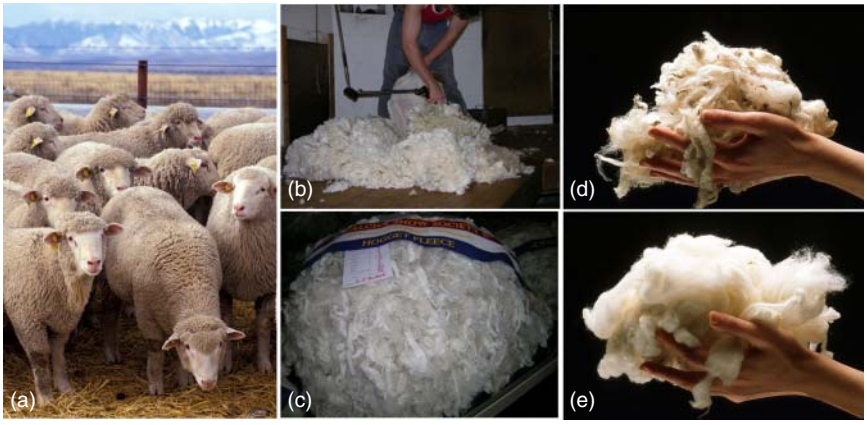


Figure 2.1 Wool fibers from sheep, (a) sheep before shearing, (b) fine Merino shearing, (c) champion hogget fleece (Walcha Show), (d) raw wools before processing, and (e) processed wools. Source: From https://ipfs.io/ipfs/QmXoypizjW3WknFiJnKLwHCnL72vedxjQkDDP1mXWo6uco/wiki/Wool.html.

sustainable fibers by present consumer and retail who demand for all kinds of clothing.

However, due to the decreased number of total sheep around the world, wool's productivity over all the global market share has declined a little during the last 10 years, as shown in the tendency in Figure 2.2.The percentage of wool (now a minority fiber) that takes around only 1.9% of world fiber production [2] decreases slightly in the very large textile fiber market. However, wool is still the number one of protein fibers in weight measure that is used in textile industry. Wool does, however, play a significant role in the market of men's suiting, knitwear, and carpets, as well as the area of unique properties that wool can supply with the excellent appearance, comfort, and durability that cannot be satisfied by other natural and chemical fibers.

Australia produces the highest amount of wool (around 1/3 of world total output) and is also the number one of countries that exports wool to other countries. The second highest production of wool per year in the world is New Zealand, followed by Argentina, Uruguay, South Africa, Russia, and United Kingdom. China's wool production is also the highest one in the world; however, China is also a big consumer country of wool. Every year, China has to import a large amount of wool from Australia [1].

Here, take China's wool as an example to demonstrate wool's category, distribution, and quality because China is a typical country that is so vast to span the climate regions of frigid, temperate, subtropical, and tropical. Wool's type and quality are versatile in comparison with relatively pure types of other countries' wool. It was reported that, since the 1970s, China's number of sheep has been increased to four times higher, indicating that the amount of produced wool has a great development. However, 20% of fine wools (high quality of wool) are still

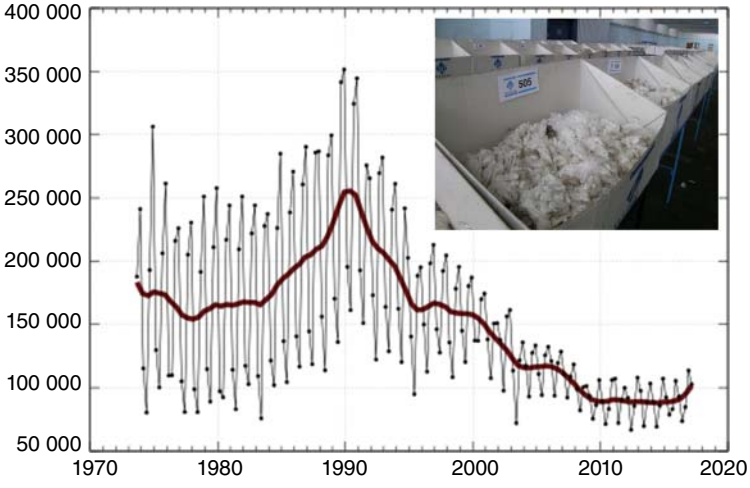


Figure 2.2 Wool received by Australian brokers and dealers (tons/quarter) since 1973 (Toby Hudson, Own work; this image is based on Australia Bureau of Statistics data) and the inset image showing Merino wool samples for sale by auction (Newcastle, New South Wales). Source: From https://ipfs.io/ipfs/QmXoypizjW3WknFiJnKLwHCnL72vedxjQkDDP1mXWo6uco/wiki/Wool.html.

required importation. For domestic wool, most of China's wools are supplied from husbandry areas of Xinjiang, Inner Mongolia zone, and Gansu province. In this case, China's wool has many types according to the wool's fineness (in diameter measure), for example, superfine, semi-fine, and coarse wool. The domestic wool also has home wool and improved wool according to the wool quality, where the latter has improved fine wool and semi-fine wool from hybrid breed of sheep while the former is only from Mongolia, Tibet, and Hakelong types. Table 2.1 compares the quality of China's wool according to the types and wool mechanical properties.

Beyond semi-fine wool, when wool's diameter is larger than 40 μm; this hair is called guard hair. The wools from Inner Mongolia, Tibet, Hazake sheep, etc. have a proportion of guard hairs that have a function of protection of superfine hairs for warmth retention. When producing guard hairs, it is inevitable to include some fine and superfine hairs and even dead wool inside; thus the quality and property of guard hair products are variable. Thus, these hairs are commonly used for wool blanket, carpet, tapestry, etc. In Table 2.1, most fine wools are from improved sheep after several generations of cross breeding. For example, Xinjiang fine wool is the first improved wool from the sheep after hybridization of China's Hazake female sheep and Russian Lanbuliye and Caucasian male sheep. The Xinjiang wool has fineness of below 0.6 tex and length of 6–7 cm and oil/grease content of 7–10%. China's northeast fine wool is from the sheep after

Table 2.1 Quality of main China's wools.

Wool types (production area)		Productivity per year (kg/sheep)		Wool count	Wool fiber length (cm)	Tenacity		Net wool rate (%)
		Male sheep	Female sheep			Strength (cN)	Elongation at break (%)	
Fine wool (fiber diameter <25 μm)	Xinjiang	10.1–11.5	3–4	60–66	6–7	3.9–4.9	30–38	44
	Northeast	13–14	5–6	60	7–8	5.9–9.8	40–47	35
	Inner Mongolia	12	5.5	60–64	6–7	7.8–11.8	25–30	47
	Gansu	9–10	4–4.7	60–64	7–8	5.9	40–45	35
	Merino	14–15	5–6	60–64	7–8	5.9–10.8	45	48
	Qinghai	8–8.5	3–4	60–64	7–8	4.9–7.9	30–35	45
Semi-fine wool (diameter 25–40 μm)	Qinghai	5	3.2	46–58	8–10	9.8–17.6	34–40	55
	Northeast	4.6	3.7	56–58	8–9.5	9.8–11.8	35	53
	Inner Mongolia	—	—	48–60	6–9	9.8–15.7	38	50
	Anhui	7–12	5–6	56–58	9–15	9.8	42	45

several hybridization generations of American Lanbuliye sheep and Inner Mongolia sheep and Lanbuliye and Caucasian male sheep. The related wool has fineness of below 0.55 tex (wool count of 60–64) and length of 7–8 cm, and such wool shows high tenacity and good luster. China's wool from Inner Mongolia is cut from the sheep after several hybridization generations of Xinjiang female sheep, Corriedale male sheep, and Caucasian male merino. The wool has fineness of below 0.55 tex (wool count of 60–64) and length of 6–7 cm. While China's merino seems have better quality with fineness of below 0.6 tex and length of beyond 8 cm, and such wool shows strong tenacity, good luster, crimpness, and appropriate oil content.

In comparison with China's wool in Table 2.1, Table 2.2 lists the wool's type and properties, such as productivity, wool count, wool length, sheep body weight, and fertility, from other countries and regions that produce the most amount of wool in the world. The wool has been classified as fine wool (fiber diameter < 25 μm) and semi-fine wool (fiber diameter is in the range of 25–40 μm) and long wool, which means the fiber length is larger than 10 cm. After comparison, it is found that Australia Merino wool (strong type) shows highest productivity per year, higher wool count, and long wool fiber, indicating the Australia Merino wool is of high importance in wool market.

2.2 Classification of Wools

There are many classification methods of wool in terms of wool fineness, fiber structure, fiber type on hair coat, wool picking and original wool shape, and the wool cut seasons, as shown in the classification branches in Figure 2.3. According to Figure 2.3, the detailed description of the classification has been divided into five sections.

2.2.1 Classification of Wool in Fineness

(1) *Botany wool*: The diameter of botany wool is in the range of 10–25 μm.
(2) *Medium wool*: The diameter of medium wool is in the range of 25–40 μm; the length of such wool has a range below the value of 15 cm.
(3) *Coarse wool*: The diameter of coarse wool is in the range of 40–70 μm; the length of such wool is also less than 15 cm.
(4) *Long wool*: The length of such wool is in the range of 15–30 cm, and the diameter of most of such wool is more than 37 μm.

2.2.2 Classification of Wool in Terms of Fiber Structure

(1) *Down wool hair*: Such wool has layers of only epidermis and cortical without medullary substance, as shown in the cross section of a down wool hair in Figure 2.4a. Because there is no medulla layer, the quality and spinning performance of such wool is excellent due to better elasticity and fineness for high combining force with each other.

Table 2.2 Type and property of wools from the main production country.

Wool types			Productivity per year (kg/sheep)		Wool count	Wool length (cm)	Body weight (kg)		Fertility rate (%)
			Male sheep	Female sheep			Male sheep	Female sheep	
Fine wool (<25 μm)	Australia merino	Fine hair	6.3–9	2.7–4.5	64–90	5.8–10	59–76	36–63	105–135
		Intermediate	8–12	3.6–9	60–75	7.5–11	68–90	45–63	105–135
		Strong type	10–15	4–8	56–70	7.5–13	79–114	54–72	105–135
	Russia merino		10–12	5–7	64–70	7.5–10	90–100	50	135
	Germany merino		7–8	5	60–64	7–10	125–150	100–130	120
	Askanya sheep		10–14	5.5–6	64–70	7.8–8	100–120	60–65	145–160
	South Africa merino		5.6–9.6	4.5–8.2	64–70	7.5–10	70–90	36–55	105–130
	Caucasian merino		10–11	5.8–6.5	64–70	7–8	90–100	55–60	105–110
	Lanbuliye sheep		7–10	4–5	64–80	6–8	70	50–60	130–140
	Tebuli sheep		5.5–11	3.6–7.2	60–70	6.4–9	68–120	57–73	120
Semi-fine wool (25–40 μm)	Corriedale sheep		7.5	4.5	50–70	7.5–10	60–100	30–65	125–140
	Pohl Wass sheep		7.5	4	58–60	10–12	75	55	110–130
	Tsigai sheep		5.5–6	4.3–4.5	46–56	8–9	70–78	52–55	105–120
Long hair wool (length > 10 cm)	Romney Marsh sheep		12–14	6–9	40–46	15–20	130–140	110–120	105–145
	Leicester sheep		4.5		46–56	14–20	100–150	80–90	120–165
	Border area of Leicester sheep		3.5–4.5		44–48	18–23	90–100	60–80	150–200
	Lincoln sheep		5.5		36–44	30	138	110	125–160

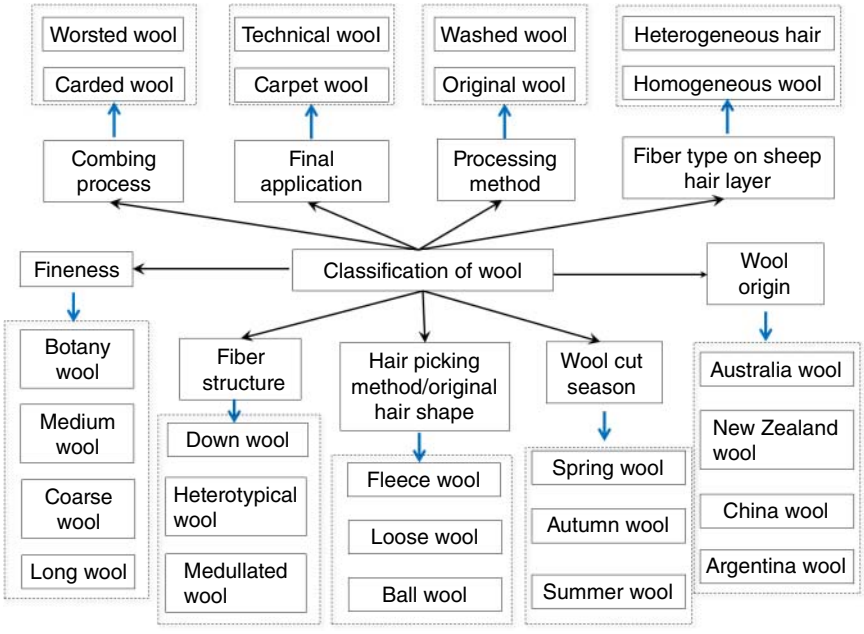
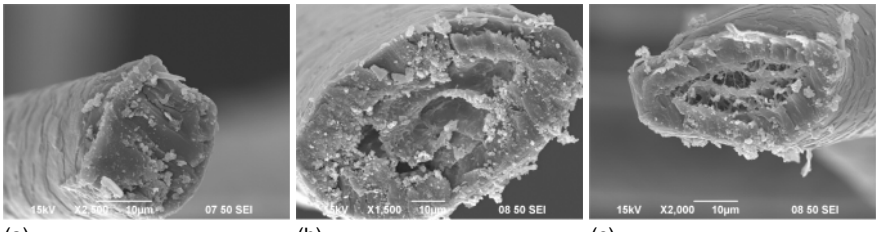


Figure 2.3 Classification of wool in terms of different parameters.



(a) (b) (c)

Figure 2.4 SEM images of cross sections of (a) down wool, (b) heterotypical wool, and (c) medullated wool.

(2) *Heterotypical wool fiber*: Such wool fiber has discontinuous medulla, as shown in Figure 2.4b. Meantime, the wool has both the characteristics of down wool hair and coarse wool. In a bundle of such wool fibers, the difference of fiber thickness is large, and the performance of the yarn using heterotypical fiber is worse than the yarn made of down hair because of large deviation of fiber performance.
(3) *Medullated wool*: Such wool fiber has a continuous medulla layer, as shown in Figure 2.4c. With the different content of medullary substance, such wool has many types of performance fibers, such as bristles, wool, hair, dry wool cavity, and dead wool, in which the dry and dead wool have relatively low spinning value for their poor mechanical properties.

2.2.3 Classification of Wool in Terms of Fiber Type on Sheep Hair Layer

(1) *Homogeneous wool*: Such wools from a sheep body are made of the same wool fiber. Thus, the fineness and length of wools are basically the same values. In terms of fineness, homogeneous wool belongs to high-count wool. Generally speaking, the quality of homogeneous wool is rather good compared with other types of wool.
(2) *Heterogeneous hair*: Such wools on a sheep body are made of two or more types of hair fibers with different wool length and fineness. Heterogeneous hair normally has different grades of hairs according to the gross content of coarse cavity. The yarn spinning using such wools requires more factors that should be considered, such as yarn strength, evenness, and hairiness.

2.2.4 Classification of Wool in Terms of Hair Picking Method and Original Hair Shape

(1) *Fleece wool*: Such wool fibers that cut from sheep body connect each other and can form a sheet of hair coat, called "fleece hair," as shown in Figure 2.5. The fleece hair is classified as closed hair and open hair. From outside appearance, the closed fleece hair looks like a complete assembly of wool fibers, while the open fleece hair looks like a bulgy wool braid from the appearance, and the hair bottom connects each other, and the hair top does not link each other within open appearance.
(2) *Loose wool*: The loose wool means that the wool fibers just cut from a sheep body and do not link each other, which does not form a hair sheet.
(3) *Ball wool*: When sheep is in an unhairing season, people would like to comb wool fibers from sheep body by means of comb-like tools. These wool fibers are called "ball wool." Usually, cashmere is a kind of ball wool. Thus, "ball wool" can be used for high-level wool products.



Figure 2.5 Fleece of fine New Zealand Merino wool and combed wool top on a wool table. Source: From https://ipfs.io/ipfs/QmXoypizjW3WknFiJnKLwHCnL72vedxjQkDDP1mXWo6uco/wiki/Wool.html.

2.2.5 Classification of Wool in Terms of Wool Cut Season

(1) *Spring wool*: The wool obtained from sheep in spring season usually is fine and long, the content of fine fluff is high, and the content of fatty oil on fiber surface is also high. The performance of such wool is outstanding for making end-use textiles.
(2) *Autumn wool*: The wool obtained from sheep in autumn season usually is coarse and short, but the luster is good and color is white. The wool quality is followed by spring wool.
(3) *Summer wool*: The wool obtained from sheep in summer season is like autumn wool, fibers are short and coarse, and the content of dead wool is high, and the quality of wool is relatively poor.

In addition, there are many kinds of wool classification methods, for example, wool can be classified as worst wool and carded wool in terms of combing process in yarn spinning. Wool can be classified as carpet wool and technical wool in terms of final application. Wool can be classified as original wool and washed wool in terms of processing method. Wool can be classified as fine wool, semi-fine wool, coarse wool, and long fiber wool in terms of pastoral sheep breed. Wool can be classified as Australia wool, New Zealand wool, China wool, etc. in terms of country of origin.

2.3 Processing of Wool Fibers and Yarns

2.3.1 Primary Processing of Wool

Primary processing of wool fibers include two main steps, namely, the cleaning process and conditioning process, for the post-manufacturing processes along the whole textile engineering, because there are many impurities in hair fibers that just combed from sheep. The primary processing method comprises the following steps: *shearing → sorting and classification → grading and package → wool washing → carbonization (wash hair) → final pack*.

(1) *Wool shearing and wool sorting processes*: The shearing process of sheep is usually carried out in spring. Fine wool and semi-fine wool are usually obtained once a year, while coarse wool can be obtained from sheep twice a year. Normally the shearing process takes place in spring and autumn. The just sheared hairs are connected together to become a whole set of wools. This connection is easily sorted out for post-treatment. The sorting process is for better rationally use of raw materials. In order to use the good selected wool for good end use, the sheared hairs are sorted according to the wool quality, including the division of different grades of wool into different qualities of piled hair separately. In the sorting process of defective wool, two kinds of miscellaneous grass shearing are separated; these works are usually completed manually.

(2) *Washing and weeding of wool*: The purpose of washing wool fibers is to wash the wool fatty film from the wool fiber surface, sheep deposited sweaty spots and sand, and other dirt stuff in wools. The key of washing wools is to remove the fatty materials on fibers (lanolin). The main method of washing process to raw wools is to employ detergent that contains surface active agent. The commonly used detergent is mainly soap alkali and synthetic detergent solutions. After washing process of wool, the cleaned wool although has pressured for removing water, the wools generally still contains about 40% weight of water, therefore, after washing process of wool, the wet cleaned wools must have a drying process for later storage and transportation. At the present, the factory of preliminary wool treatment usually employs the combination of opening and washing processes together for opening wool package, washing fatty films, drying wet washed wools, and then finally obtaining the dry cleaned wools for the post wool manufacturing.
Some tips should be noted in washing process, because some impurities from plants are in raw wools, such as leaves, seeds, and burr, which are referred to as the grass complex, and usually these impurities are entangled with wool fibers. In practice, it is not easy to remove them in opening wool package and washing wool processes. The method of removing plant impurities is usually performed by chemical method that is called "carbonization." The principle of this chemical method is due to the different acid resistance in which wool is a good acid-resistant material, while plant impurities are not such materials. Using this method, raw wool fibers containing grass impurities are soaked into sulfuric acid solution; thus, the impurities are carbonized into inorganic carbons. Then the wool fibers are dried and compressed that the carbonized impurities are fragile to be collapsed and separated from the processed wools. This chemical processing can reduce the impurity content of grass from raw wool significantly. For China's wool, before carbonization, the wool miscellaneous grass carbonization rate is in 1–2% (China short hair 2–4%). For Australasian wool, the value is around 1%; after carbonization, the wool containing grass mixed rate decreased to 0.1% (China short hair below 0.2%).

2.3.2 Yarn Spinning Process of Wool

In woolen spinning, slubbings, which are lightweight continuous strands of staple fibers, instead of slivers are produced directly from carding. These are spun directly into yarns typically using ring or mule spinning systems. The spinning process of wool is relatively complicated compared with cotton spinning, for example, there are more combing steps in wool spinning for high grade of wool products. However, their processing principles are similar, i.e. combing for orientation of fibers along the sliver axis and twisting for improvement of yarn strength. Herein, the worsted spinning process is similar to the combed cotton spinning process in that the yarns are carded, gilled (a process similar to drafting



Figure 2.6 Wool fibers in format of slivers, single yarn, or plied structural yarns. Source: From https://ipfs.io/ipfs/QmXoypizjW3WknFiJnKLwHCnL72vedxjQkDDP1mXWo6uco/wiki/Wool.html.

but using pins to support and comb the fibers as they are drawn), combed, gilled again, formed into a roving, and then spun. Woolen and worsted spinning processes are not constrained to wool fibers but can be used for synthetic fibers of similar length and fineness to wool fibers that would normally be spun using them. Normally, long staple yarns combed and produced using the worsted spinning process are called worsted yarns, and long staple produced on the woolen system without combing are called woolen yarns, as shown in some different wool yarn forms in Figure 2.6.

For example, a worsted spinning process for sliver dyeing product is described as follows (Example (1)). It can be seen that a very complicated process has been shown from wool raw material to final wool yarns (dyed) for weaving or knitting and many gilling and combing processes are arranged during the yarn spinning because of the removal of impurities and short fibers and improvement of orientation of wool fibers for better yarn quality:

(1) Wool selection → opening packing → washing → drying → mixing wools → oiling → carding → first gilling for wool sliver → second gilling of wool tops → third gilling of wool tops → combing → fourth gilling of wool tops → last gilling of wool tops → (wool tops completed) → balling → coiling in cans → dyeing for tops → dehydration → rewashing → combing of mixed tops → first gilling of pre-spinning → third gilling of wool tops → recombing → fourth gilling → mixing tops → last gilling of wool tops (re-combing of wool tops) → first combing of pre-spinning → second → … → fourth combing of pre-spinning → roving → spinning → plying → twisting → streaming → winding (post-spinning) → (automatic spinning → electronic plying → doubling twisting).
(2) Pre-treatment → first carding → first gilling → second combing → second gilling → … → spinning → post-treatment (waxing, bleaching, washing, or coloring).

Example (2) is a simplified process for wool spinning without dyeing before spinning; this is a normal case for most wool mills because of relatively shorter

processes. Thus, the wool yarn quality is varied, depending on the number of gilling or effective combing processes.

2.4 Chemical Compositions and Structural Characteristics of Wool

2.4.1 Compositions of Wool

The main composition of wool fiber is a kind of insoluble protein, known as α-keratin. The fundamental chemical composition of α-keratin is elements of carbon (49–52% in weight), oxygen (17.8–23.7%), nitrogen (14.4–21.3%), hydrogen (6.0–8.8%), sulfur (2.2–5.4%), and ash (metal oxide 0.16–1.01%). The α-keratin of wool fiber is made up of many kinds of α-amino acids, and the contents of various α-amino acids are shown in Table 2.3.

Table 2.3 Content (%) of α-amino acids in natural proteins.

Amino acid	Wool fiber	Silk fibroin	Mulberry silk gum	Tussah fibroin	Casein	Soybean protein
Glycine	3.10–6.50	37.5–48.3	1.1–8.8	20.3–24.0	0.5	4.00–7.77
Alanine	3.29–5.70	26.4–35.7	3.5–11.9	34.7–39.4	1.9	4.31–4.85
Leucine	7.43–9.75	0.4–0.8	0.9–1.7	0.4	9.7	7.71–9.60
Isoleucine	3.35–3.75	0.5–0.9	0.6–0.8	0.4	9.7	4.40–5.27
Phenylalanine	3.26–5.86	0.5–3.4	0.3–2.7	0.5	3.9	5.70–6.12
Valine	2.80–6.80	2.1–3.5	1.2–3.1	0.6	8.0	3.93–5.72
Proline	3.40–7.20	0.4–2.5	0.3–3.0	0.3	8.7	5.32–6.78
Lysine	2.80–5.70	0.2–0.9	5.8–9.9	0.2	6.2	4.67–5.56
Histidine	0.62–2.06	0.14–0.98	1.0–2.8	2.2	2.5	1.30–1.63
Arginine	7.90–12.10	0.4–1.9	3.7–6.1	9.2–13.3	3.7	7.46–9.15
Tryptophan	0.64–1.80	0.1–0.8	0.5–1.0	1.8–2.1	0.5	0.12–0.47
Serine	2.90–9.60	9.0–16.2	13.5–33.9	9.8–12.2	5.0	4.32–4.83
Threonine	5.00–7.02	0.6–1.6	7.5–8.9	0.1–1.1	3.5	3.21–4.12
Tyrosine	2.24–6.76	4.3–6.7	3.5–5.5	3.6–4.4	5.4	0.11–0.24
Hydroxyproline	—	1.5	—	—	0.2	0.11–0.24
Aspartic acid	2.12–3.29	0.7–2.9	10.4–17.0	4.2	6.0	10.89–13.87
Asparagine	3.82–5.91	0.7–2.9	10.4–17.0	4.2	6.0	10.89–13.87
Glutamate	7.03–9.14	0.2–3.0	1.0–10.1	0.7	21.6	20.96–24.71
Glutamine	5.72–6.86	0.2–3.0	1.0–10.1	0.7	21.6	20.96–24.71
Cystine	10.84–12.18	0.03–0.9	0.1–1.0	—	0.4	0.00
Cysteine	1.44–1.77	—	—	—	—	0.00
Methionine	0.49–0.71	0.03–0.2	0.1	—	3.3	0.91–1.76

2.4.2 Macromolecular Structure of Wool

Wool is composed of α-keratin proteins. It is found from experimental [1] that wool can be dissolved easily by acid (H^+) or caustic soda (OH^{1-}) solutions, and the final unit after hydrolysis of wool is α-amino acid. It is well known that the molecular formula of α-amino acids is –COOH–CHR–NH–, in which R represents a variety of substituents (pendant group). The groups of hydroxyl (–OH), amino (–NH), carboxyl (–COOH), and disulfide bonds (DBs) (–S–S–) on the backbone of peptide (–CO–NH–) macromolecule chains are the functional element groups in the protein fibrils, which determine the properties of wool fiber, such as resistance of acid and alkali, moisture absorption, and many other physical properties like mechanical properties.

The proportion of α-amino acids in protein fibrils was significantly different in terms of the species of protein type, sheep growth conditions, growth sites, and harvest seasons. In 20 kinds of α-amino acid (main compositions) of wool fibers as listed in Table 2.3, arginine (two amino acids), aspartic acid, proline (two amino acid), glutamic acid, aspartic acid (hydroxy acid), and cystine (sulfur-containing amino acids) are the highest content (>30%) of amino acids in wool. Furthermore, as to the wool keratin backbone, some branches of backbone connect each other with horizontal linkage bonds such as salt bonds, DBs, hydrogen bond, and space. These bonds can enhance the strength of wool fibrils significantly.

The macromolecular compositions and structure of α-keratin proteins in wool fiber are shown in Figure 2.7, where the macromolecule chains may pass across the amorphous area and crystalline area alternatively, in which the crystalline

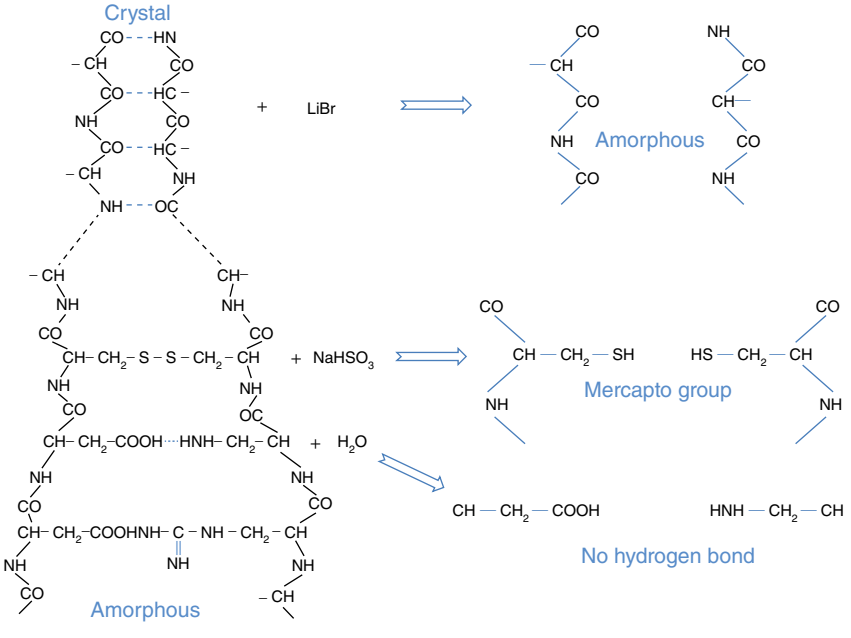


Figure 2.7 Two-dimensional macromolecular structure of wool fiber and interaction with a few chemical solutions.

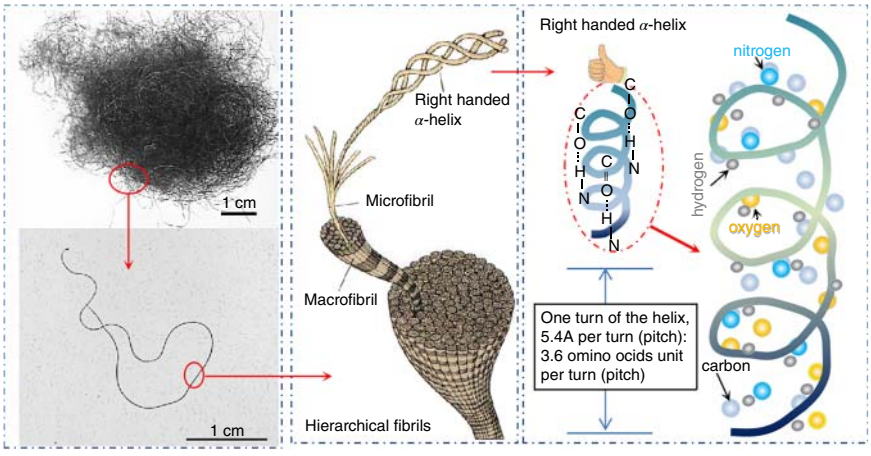


Figure 2.8 The right-hand spatial structure of α-keratin macromolecular chain and chemical compositions along a molecule chain. Source: Adapted from http://www.fzfzjx.com/tech_news/detail-4048.html[4].

phase is made of regular structural molecules and the amorphous phase is made of macromolecule chains and other matrix materials. For the two phases, experimental data [30] showed that LiBr solution can dissolve the wool crystalline phase into amorphous molecule chains and $NaHSO_3$ dilute solution (a reductant) can break down the DBs of two branches and aqueous molecules can break down the hydrogen bonds at intra- and inter-keratin macromolecules, respectively.

The natural protein fiber has two kinds of spatial structure, i.e. α-helical structure and β-sheeted structure. The silk fiber mainly contains β-sheeted structural proteins, which is in linear zigzag shape that has repeatable unit of angles and amino acid unit. While the α-keratin shows the helical conformation, which is one of the most common protein structures that encountered in nature, namely, α-spiral keratin protein as shown in a schematic illustration in Figure 2.8. The helical spatial structure obeys right-hand rule in spatial sequence. In the helical spatial structure, the molecular backbone, salt bond, DB, and hydrogen bond are linked to form a stable spiral structure, in which hydrogen bonds are existed at intra- and intermolecular chains, while DBs only existed between intermolecular chains.

2.4.3 Morphology and Hierarchical Structure of Wool Fiber

The external shape of a wool fiber is like a python that the main part is a long cylinder with scaly surface. The wool root is slightly coarser than the wool head. From any cross section of wool in the middle of hair fiber, the wool has clearly three components that are epidermis (scales), cortex, and medulla layers, where the scaly surface is a very thin layer of tile overlapping structure, as shown in the scale cortex (four layers of cuticles) in Figure 2.9.

Under the scaly surface, the cortex layer takes the main component of wool (95% in weight) that is usually composed of positive cortex and inner

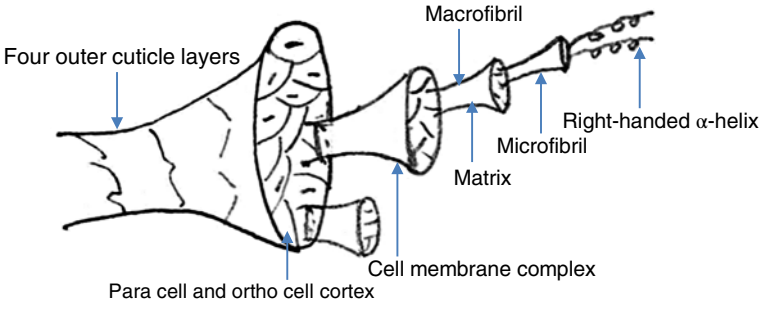


Figure 2.9 A typical hierarchical structure of wool fiber.

cortex. From the view of hierarchical structure, the cortex is in the scale of top macroscale structure that is made of macrofibrils and substance that is in the space between macrofibrils. The macrofibrils are made of fibrils and microfibrils, while the latter are made of photofibrils and, at the final microscale, are coils of macromolecule chains (in helical conformation), as shown in a typical hierarchical structure in Figure 2.9. In the center of each wool fiber, there is usually a center porous medulla. Medulla is a kind of biodegradable cellular materials in the form of porous medium and continuous or discontinuous cavities that benefit the hair warmth retention. The difference of scaly surface, cortex, and medulla displays at the configuration that is resulted from the volume ratio and texture of cortex and medulla. The detailed descriptions of the three components are as follows:

(1) *Cuticle layer*: The cuticle layer, also known as the scaly layer, consists of a piece of keratin cells, coated on the surface of wool fiber. The average thickness of wool cuticle layer is in the range of 0.2–2 μm, width is in the range of 25–30 μm, and height is in the range of 35.5–37.5 μm. The root of cuticle layer is attached to the hair trunk, and the tip extends out of the surface and points to the mouth of the hair when the hair is dry. The main function of the scale layer is to protect the wool from the external environmental conditions. The density and degree of scale attachment have great influence on the gloss and surface properties of wool. The scales of a fine wool are usually arranged closely and covered by a ring, and the protruding end is prominent. The scales of a coarse wool is arranged in a thin and cracked cover layer. In addition, due to the existence of the scale layer, the wool has an evident feature of felting that related wool products are narrowed down easily in size after washing.

(2) *Cortex layer*: The cortical layer is the main component of wool fiber, which determines the physical and chemical properties of wool. The cortical layer is composed of two kinds of different cortical cells, namely, the bilateral structure of orthocortex and partial cortex, and the two cortical cells have conversion position along the fiber axis so that the natural wool fiber crimpness is formed. If there is a large difference in the proportion of the orthocortex and partial cortex, the wool's crimpness is not obvious. The orthocortex (soft

cortex) structure is loose, it is in the outer side of wool coiling arc, and its sulfur content is less. The orthocortex is inactive with reaction of enzyme and chemical reagent, causing wool with good moisture absorption and dyeing ability. However, the partial cortex (cortex) is in a more compact state, which is in the inner side of the crimpness arc, and the sulfur content in partial cortex is high that gives wool an easy affinity of acid dyes and poor response to chemical reagents. The experience tells us [5] that the good grown wool hair would have higher content of cortical layer, leading to the better quality of wool fiber. As a consequence, the strength of crimpness and elasticity of wool are all better than the wool from poorer growth environment. Some wool fibers also have natural pigments in their cortex layer, causing that these wools are difficult to remove the inherent colors before dyeing.

(3) *Medulla layer*: Usually, there is a continuous cavity in wool center that is composed of loosely structured and air-filled keratinocytes. The cells in this layer are poorly linked and dark black. The medulla layer influences the strength, crimpness, and elasticity of wool fiber and affects the consequential spinning process. Generally, the wool fibers in high quality have no medullary layer or only intermittent medullary layer. The coarser the wool fiber, the larger proportion of medulla layer will be. Experience tells us [6, 7] that the more medulla layer of wool is more brittle and easier to break under stretching.

2.5 Properties of Wool

In this section, a few physical properties are discussed in detail to interpret the wool performance in end use of clothing and decorative and technical textiles, including wool's fineness, length, crimpness, friction and felting properties, content of grease and impurities, and other physical properties.

2.5.1 Fineness of Wool

The fineness of wool mainly depends on the factors of variety, age, gender, growth position, and feeding conditions of sheep. The cross section of wool fiber is approximately circular, and the fineness of wool fiber is usually expressed in diameter; the unit is micron (μm), as shown in a well-known diameter range for defining the wool fineness in Figure 2.10b, where the superfine wool is defined of diameter below 20 μm. Most wools have the diameter in the range of 20–50 μm, called fine wool, and fine wool accounts for the most productivity as shown in Figure 2.10a. Wool fineness varies greatly, the minimum diameter of villus is 7 μm, and the maximum diameter can be up to 240 μm. One wool has its diameter great variation usually that can reach up to 5–6 μm; the coarser wool would have more uneven fineness. The normal cross section of fine wool is approximately circular, the aspect ratio of the section is "1 : 1.2" without medullary layer. The cross section of the setae is oval, containing medulla layer, and the aspect ratio is "1.1 : 2.5." The cross section of dead wool is usually flat, and the ratio of the length and width for such section is more than 3.

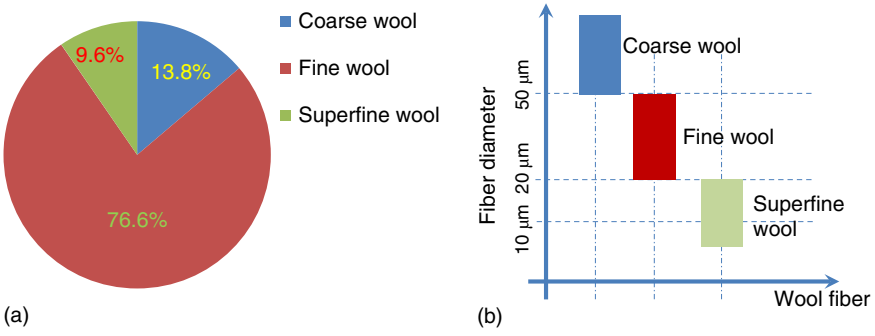


Figure 2.10 Wool productivity and wool fineness distribution. (a) China wool production in 2014. Source: Data from http://big5.qianzhan.com. (b) Diameter range for defining wool's fineness.

Fineness is an important index to determine the quality and application value of wool. Generally, the finer of wool would have smaller dispersion of wool bundles, the higher of relative strength of wool would have greater degree of curvature, the larger of scale density of wool would have the higher lipid and lanoline content, but the length is relatively short. The fineness of wool fiber has a great influence on the quality and style of final wool products. Worsted wool products are usually produced using homogeneous fine wool fibers, while woolen products are normally produced using semi-fine or modified wool fibers. Some wool cords are normally using semi-fine wools in the count range of 46–58, and underwear fabrics are using superfine wools. Experience tells us [5, 8] that the finer wool fibers would lead to more knots in the process of spinning and easier surface pilling on fabric.

Apart from the diameter as an index to measure the fineness of wool, there are still other factors such as linear density, metric count, and quality count to measure the wool fineness. For example, for the wools with the average diameter of 11–70 μm and the coefficient of variation of diameter of 20–30%, the corresponding linear density is in the range of 1.25–42 μm.

The quality count of wool simplified was called "count," which is an important measure index in wool long-term production. At present, the classification of wool in textile industry and international trade and the establishment of the strip processing technology are all based on the wool's count. In the early stage, the quality of wool is mainly assessed by subjective method. According to the situation of that time, fineness of the actual count number of wool spinning was called the quality count, in order to express the real apparent quality of wool. Now the quality count of wool only means the fineness of wool. Different countries have different definitions of quality counts for different wool fibers. In China, the wool count quality and the corresponding average diameter are shown in Table 2.4.

2.5.2 Length of Wool Fiber

Due to the existence of natural crimp, the length of wool fiber is divided into natural length and stretched length. Generally, the length of wool bundle is used to

Table 2.4 Relationship of wool quality count and average diameter of China's wool.

Quality count number	Average diameter (μm)	Yarn count that can be spun
70	18.1–20.0	More than 64
66	20.1–21.5	52–60
64	21.6–23.0	45–52
60	23.1–25.0	45–52
58	25.1–27.0	36–45
56	27.1–29.0	32–34
50	29.1–31.0	28–32
48	31.1–34.0	
46	34.1–37.0	
44	37.1–40.0	
40	40.1–43.0	
36	43.1–55.0	
32	55.1–67.0	

describe the natural length of wool bundle, while the stretched length is employed to evaluate the wool quality. Natural length refers to the straight distance between the two ends of wool under natural crimp. Stretched length refers to the length of wool fiber after the removal of the crimp. Wool fiber length depends on the factors such as sheep breed, age and gender, feeding conditions, shearing numbers, and seasons. The length of fine wool is generally in the range of 6–12 cm, and the length of semi-fine wool is 7–18 cm, and the length of long wool (fleece) is in the range of 15–30 cm. Moreover, from the same sheep, it is found that the wool fiber would be long when it is from the sheep's shoulder, neck, and back, while the hair is short when it is from sheep's head, legs, and abdomen.

The effect of wool length on its yarn quality is not as important as wool fineness. However, when wool fineness is the same value, it is found that the longer the wool would give higher count of spun yarns. Meanwhile, when wool count is constant, the woolen yarn strength is stronger, and yarn is more even with the increase of wool length. In the spinning process, the stretched wool below the length of 3 cm, e.g. short wool, should be controlled strictly; otherwise, the involvement of such short wools in spinning would lead to poor quality of woolen yarns, for example, such wools involvement easily forms yarn slub, thick and thin section, big belly yarn, etc. For the measurement of raw wool fibers, it is normally to take a simple method from the bundle length, for example, to measure the length of 30 wool bundles to calculate the average length, variance, and coefficient of variation of wools, as shown in a typical tool for measuring wool length in Figure 2.11.

On the other hand, for the wool sliver or washed wool hairs after combing process, it is usually to employ a length analyzer to measure the length of wool fibers.

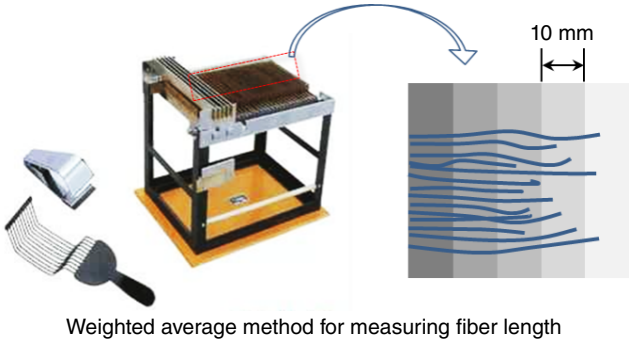


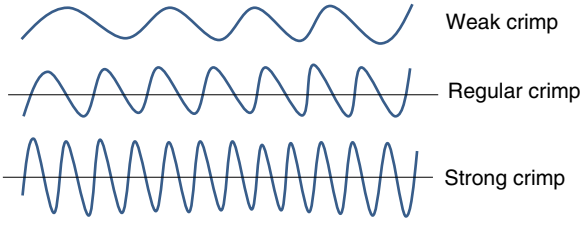
Figure 2.11 A set of typical measure tool for wool length.

For example, for a wool bundle sample of 2 g, from long to short wool bundle in the group of 10 mm, each group of wools is weighed; thus, the values of weighted average length, variance, or coefficient of variation of main hair length and content rate of short hair can be obtained based on such method.

2.5.3 Crimpness of Wool

Wool fiber has natural periodic curly crimpness along the direction of fiber axis. The degree of wool crimpness is related to the factors such as the sheep breeds, wool fineness, and wool fleece location. Thus, the wool crimpness has a great reference to judge the fineness, homogeneity, and uniformity of wool. According to the definition of crimpness, the shape of wool's crimpness is divided into three types: weak crimp, regular crimp, and strong crimp; this can be shown in Figure 2.12. Usually, weak crimpness refers to a crimp less than half a circle, and most part of such wool is in straight state along the fiber length direction; the number of wool coiling is small. The majority of the semi-fine wool fibers belongs to this type of weak crimpness; the ratio of wave width to wave height is usually in the range of "4–5." The regular crimp refers to the curly shape of semicircle. The majority of fine wool belongs to this type of crimpness, which is mostly used in worsted spinning. The ratio of wave width to wave height is in the range of "3–4." Strong crimp of wool has higher amplitude of coils, and the coiling number of wool is high; some abdominal wool hair belongs to this type of crimpness. This kind of wool is usually used for woolen spinning; the ratio of wave width to wave height is less than 3.

Figure 2.12 Illustration of crimped shape of wool fiber along fiber axis.



The shape of wool's crimpness refers to wool's distribution of orthocortex and partial cortex. The cortical layer of fine wool is composed of two kinds of cortical cells, which is in bilateral structure and present conversion position along the fiber axis. Thus, this conversion of two cortex cells leads to the crimpness. Scientifically, the number of wool fiber crimps is a measure for the crimpness with unit of number per centimeter; the fine wool usually has such parameter in the range of 6–9 cm^{-1}. There are also other indexes of wool fiber for crimped rate, such as the index of elasticity of wool fiber, the recovery rate, and the elastic recovery rate.

2.5.4 Friction and Felting Properties of Wool

In the normal conditions, the surface of wool covers scales, the root of which attaches to the wool stem. The tip of wool scale is out of the stem and points to the wool fiber head. Due to the characteristic feature of scale, the friction factor is different when sliding takes place in different directions. Common sense tells us that the frictional coefficient is much larger for friction happens reversed to the scale grown direction than the direction takes place along the grown direction of scale. This characteristic is called directional frictional effect and can be denoted by terms of frictional effect and scaly degree.

The frictional property of wool fiber is the basis of wool product felting. Under the conditions of high temperature and moisture or some chemical reagents, the wool products (wool yarns or fabrics) are usually pressed and rubbed repeatedly or periodically by external mechanical forces, for example, wool fabric usually appears frictional behavior after washing process. This is performed of wool products within gradual contraction in size. Some wool fibers are entangled with each other. This property is known as wool "felting." The main reason is, first, directional friction effect of wool fiber. This effect means the aggregation of fibers when subjected to the repeated external forces that the frictional force is much greater when inter-fibers motion is against scale direction than along the scale direction. This inter-fibers motion would always keep a direction to the wool fiber root. Second, the existence of natural crimpness would lead to the mutual movement of wool fibers irregular, and such natural crimpness of wool would cause inter-fibers easily to be entangled. Finally, the wool fiber itself has a good elasticity, which means when an external force is exerted to the wool fiber, the fiber is stretched by force and is contracted when the force is removed. The repeated creep of stretching and contraction of wool fiber results in the fiber curling and winding. Thus, it can be seen that the directional friction effect, coiling, and elasticity are the intrinsic causes of wool fulling. The effects of heat and humidity, chemical reagent, and external force are the main external factors on wool fulling.

After a fulling finishing process of wool fabric, the length of fabric is shrunk; the thickness and the tightness are thereafter increased. The fabric surface is then exposed with a layer of fluff, which causes the fabric with advantages of beautiful appearance, rich and soft hand feeling, and improved thermal insulation performance. To use such wool fulling, we can also put some loose short wool fibers together under certain mechanical forces to make certain shape and density wool felts; this method is called "felting." Some wool products, such as boots,



Figure 2.13 Wool blanket, belt, and fabrics manufactured using wool friction and felting properties.

hat, blankets, and other end-use wool products, are mainly made by using the felting process.

The fulling property leads to wool products with a unique style; on the other hand, fulling is also the main reason of wool fabric in size contraction and deformation after longtime wearing or washing. Here, in washing process, the factors of machine rubbing, warm water, and detergent usually promote the shrinkage of wool fiber and products. Wool knitted fabric in the wearing process is easily produced of felting, fuzzing, and pilling phenomenon at the fabric positions encountering with human sweat and friction easily. Most worsted wool fabrics and knitted fabrics require clear lines and stable shape, which are required to reduce or eliminate the wool fulling property. Therefore, some high-grade wool products require wool shrink-proof processing before they get into market, as shown in some wool products in Figure 2.13.

There are two kinds of methods for wool shrink-proof treatment: "oxidation" and "resin." Oxidation method, also known as the degradation method, is to eliminate the wool surface scales. The corrosion of scale agents usually has oxidants, such as sodium hypochlorite, chlorine, chloramine, potassium hydroxide, potassium permanganate, and other chemical reagents. Among these agents, the most commonly used oxidant is the chlorine oxidation agent, also known as chlorination. Resin method is to coat the wool fiber with a resin thin film that can reduce or eliminate the friction effect between the wool fibers or to make the fibers bonding each other at the crosshead position. This can restrict the mutual movement of wool fibers significantly, making the coated wool fibers loss of fulling. Here, the normally used resins include urea formaldehyde, melamine formaldehyde, silicone, polyacrylic resin, etc. Sometimes, the two mentioned methods are combined to use to enhance the anti-felting effect of treatment.

2.5.5 Wool Grease and Impurities

(1) *Wool grease*: The grease of wool is composed of two parts, namely, lanolin and perspiration, which are secreted by the sebaceous glands and sweat glands in the surface skin of sheep. Grease is a grease coating of wool fiber, which can protect wool from heavy sunshine and rain. Sweat can, to some extent,

Table 2.5 Lipid content (%) of wool fiber.

Wool type	Content of wool grease (%)	Content of wool sweat (%)
China's fine wool	10–20	7–10
China's domestic wool	3–7	8–11
Australian Merino wool	14–25	4–8

prevent wool felting but usually makes wool fibers adhesive to each other, so that prevents the external material into the fleece wool, only left a limited depth of black pollution layer at the tip of wool hair. Lack of wool grease, the wool's hand feel is stiff and rough without normal luster of wool fibers; meanwhile, the wool has poor resistance to wind erosion and is easy to be dyed unevenly. Lanolin is composed of high-level fatty acids and high-level alcohols. The physical and mechanical properties, chemical properties, and amino acid content of wool fibers are related to the content of grease and the color of lanolin. On the other hand, there is a great difference of wool's grease content depending on the variety, age, and growth environment of sheep. And different fineness of wool also has different contents of grease. For example, fine wool with content of fatty grease is more than 20%, while the coarse wool has such content below 10%; moreover, wool from sheep body side has higher content of fatty grease. Table 2.5 shows the contents of grease and sweat of wool fibers from China and Australia.

Furthermore, the color of wool lanolin is different depending on the sheep breeds and contents of grease and sweaty materials. Usually, the best quality of wool grease manifests white and light yellow colors; other colors such as yellow, orange, deep brown, and tea brown show poorer quality. The influence of different grease colors on wool quality is different. According to the color of wool, grease can identify the quality of wool, for example, wool quality with white or light milk color of grease is better than the color of yellow or darker yellow of grease and fatty materials.

The wool grease has strong anti-chemical and antimicrobial performances, which cannot be corrupted, and wool grease can infiltrate into human skin; thus, it is usually used for the matrix of some cosmetics and skin care products. This material can also be used for treatment of human burn injury or be used as anti-rust agent in industry. The wool grease (or lanolin) is a by-product of wool scouring process; it has very high value in potential applications. This valued material is usually recycled from the washed wool detergent. The main components of wool grease and sweat are inorganic salts, for example, potassium carbonate accounts for 78.5–86%, potassium sulfate accounts for 3–5%, potassium chloride accounts for 3–5%, a part of insoluble substances accounts for 3–5%, and other organic matter was 3–5%. The content of wool sweat is generally 4–20%, and its aqueous solution is alkaline.



Figure 2.14 Impurities of raw wool.

(2) *Impurities of wool*: As shown in Figure 2.14, the impurities of wool are those that are attached to the wool, such as muddy sand, dust, manure, and some plant impurities (which is the most harmful to wool, such as alfalfa seeds). The raw wools are the hairs directly cut from sheep body. With impurities in raw wool, the quantity and type of impurities have great differences because of various sheep breeds, rearing conditions, and the local climates.
"Net raw wool rate" refers to the raw wool after processes of cleaning and removal of grease and sweat, vegetable matter, sand, and ash, and the pure wool weight is transferred to certain moisture regain (%), certain concentrate of fatty material and ash, and then the weight percentage of such pure wool to the weight of raw wool. The net raw wool rate is an important index to evaluate the economic value of wool, which is closely related to the cost of wool manufacture factory and the amount of wool used in textile industry. In our country, the raw wool has a high content level of impurity and a low level of net raw wool rate.

2.5.6 Other Properties of Wool Fibers

α-Keratin protein is the main composition of wool fiber; therefore, wool fiber is more acid resistance other than alkali resistant. Experimental data [9] showed that wool in dilute sulfuric acid boiling environment for a few hours has no damage. Under room temperature, the strength of wool is almost not affected in 80 wt% sulfuric acid solution for a short time, and other weak acids such as acetic acid, formic acid, and organic acid are the dyeing accelerant in the dyeing process of wool. The effect of alkali on wool's property is more severe than that of acid. With the increase of alkali concentration, temperature, and prolonging of treatment time, the damage of wool is getting more serious. The alkali normally turns the wool to be yellow, decreased sulfur content, and is partially dissolved. Compared with other natural fibers, the tensile strength of wool fiber is the smallest, and the elongation rate is the largest, indicating that the elastic recovery of wool is the best. Moreover, the hygroscopicity of wool is the highest in natural fibers; its moisture regain reaches up to 15–17% under the general atmospheric conditions. The main reason is a large amount of hydrophilic groups existed in wool macromolecules.

Wool fiber has a relative lower value of thermal conductivity, and natural crimpness of wool increases the storage of still air among wool products. Therefore, the warmth retention of wool textiles is excellent. Wool performs worse than other general fibers in heat resistance, for example, woof would become yellow and stiff under 100–105 °C of dry heat conditions that leads to complete removal of water from hair fiber after drying. When the heating temperature rises to 120–130 °C, the wool fibers begin to collapse. The practice experience [10] shows that the effect of wool fiber can be shape set permanently under certain heat and moisture conditions. In addition, worms like wool fibers and the end-use products very much and damage them after a while of storage, because the wool protein molecules are good food of worms.

2.6 Quality Inspection and Evaluation of Wools

2.6.1 Raw Wools from Sheep

According to national standard (China) "GB1523-93," raw wool cut from sheep should be grading and counting. There are four assessment index to grade the fine raw wools, that is, fineness, length, height of the hair bundle, and content of coarse/dead hair, in which the lowest value of evaluated index is to determine the count of wool. Here, the wool fineness is the main assessment index. The wool from improved sheep breed is usually graded through wool length, coarse cavity hair, and dry-dead hair to be the evaluation criteria, in which the lowest one is defined as the wool grade. The appearance of raw wool is a reference index, which is the hair assessment for middle level of wools.

2.6.2 Fine Wool from China's Raw and Improved Sheep Breed

The fine wool from domestic and modified sheep breeds has grading types, called "count wool." For homogeneous wool, wool is graded by fineness like in 70s, 66s, 64s, and 60s. Another one is called "grade wool," which is based on homogeneous and heterogeneous media, according to the content of coarse medullated hair. The raw wool is divided into grade one, two, three, four A, four B, and five. For washed wools, they are divided into first class and second class. Herein, there are two conditions for the determination of wool class, that is, the content of soil in wool such as the rate of soil contamination and the rate of felting. The lowest value is the grading class for the wool products. There are three items for wool production factory to ensure the grading class, that is, the oil content, moisture regain, and rate of residual alkali.

2.6.3 Tops of Domestic Fine Wool and Its Improved Wool

The tops of China's wool and its improved wool are divided into count wool tops and improved graded wool tops. The count of wool tops is graded according to the wool's fineness; there are 70s (18.1–20.0 μm), 66s (20.1–21.5 μm), 64s (21.6–23.0 μm), and 60s (23.1–25.0 μm). The grade of wool tops is determined

according to the content of coarse cavity wool; there are grade one, two, three, four A, four B, and five.

The technical indexes of wool count tops and improved wool tops have physical indexes and appearance defections. The physical indicators include discretion of fineness, content of coarse cavity wool, weighted average length, variation of coefficient of wool length, content of short wool below 30 mm, weight tolerance, and weight unevenness. The appearance defection indexes include wool grain, wool piece, flax, and other grass fiber. According to the test results, the wool tops are divided into grade one, two, and so on.

2.6.4 Inspection and Evaluation of Australia Wool

Australia is the world's largest producer of fine wool. Australia has mature objective inspection and evaluation system, including the feel visual subjective evaluation system before wool packing process and objective evaluation system for wool quality after wool package into commercial circulation (auction). At the present, the subjective evaluation system is being objective gradually, for example, the original subjective measurement of raw wool fiber length and fineness uniformity using DFDA200 method. The objective evaluation system is mainly aimed at wool fineness and cleaning rate (for the first inspection certificate), taking into account the strength of wool, length, and weak section inspection (for the second inspection certificate). Here, the first inspection certificate includes parameters like average fiber diameter, diameter variation coefficient, and the content of crude fiber, as well as wool wash rate (wool matrix), total impurity content, and impurity content of three parties. Currently, the first inspection of certificate has reached a rate of more than 99%. The second inspection certificate includes the index of strength and length of hair bundle, weight of the break point, etc. Currently, the second certificate inspection has reached a test rate of more than 60%.

The abovementioned inspections on Australia wool's quality are carried out in Australian Wool Testing authority (AWTA). All related tests are performed under objective measurements. The test results are given to wool auction center in the format of data table, and a variety of software for data analysis can be used for forecast, including the wool market price and analysis of processing performance.

2.6.5 Inspection and Evaluation of Wool Fabric

Similarly with quality inspection of wool fiber and top, the inspection and evaluation of wool fabric is also based on the wool product test standard or agreement with customer to do the grading evaluation. The grading evaluation of fabric usually has two aspects of evaluations that are apparent faults and inherent quality. The fabric apparent faults are performed under subjective sensory detection method, i.e. a comparison between the fabric sample and standard sample that based on the quality grading standard for marking the fabric faults. The inherent quality of wool fabric has many objective parameters, for example, breaking strength and breaking elongation, warp and weft density, and gram weight per

square meter, and these inherent parameters can be measured by specific test device for grading evaluation based on particular quality evaluation standard. For some special performance, functions, and requirements of wool textiles, the evaluation system should be established according to the lowest value during different aspects of inspection and evaluation. Here, take worsted wool fabric as an example to demonstrate the grading system for wool fabrics. Technical requirements for worsted fabrics include safety requirements, product quality, inherent quality, and appearance quality. The safety requirements of worsted fabrics should meet the regulations of GB 18401 of "National Fundamental Safety Technical Standard for Textiles." The product quality of wool worsted fabric includes the fabric surface, hand feel, and luster. The fabric internal quality involves physical indicators and color fastness. The fabric appearance quality includes localized defect and scattered defects.

The quality grading of worsted fabric is divided into high-class product, grade A, grade B, and others below grade B that are classified into offgrades. Fabrics made of combed wool yarns are metering based on the unit of fabric piece. Thus, the fabric quality is assessed and evaluated by three combining factors of fabric weight, inherent quality, and appearance quality and graded finally according to the lowest marking value of them. Here, if two or two more indexes of the three evaluation items are grade B at the same time, the product will be reduced to offgrades.

The length of wool worsted fabric should be longer than 12 m. While the net length of wool worsted fabric beyond 17 m can be composed of two sections, but the shortest part is not less than 6 m. When matching two pieces of fabric, they should be the same grade and the same color and luster.

For sample processing by buyer, the producers should establish seal sample according to the buyer's requirements and confirm the seal by both parties. In inspection, it should be graded carefully by comparing every piece of sealed sample. The samples that apparently worse than grade A should be classified as grade B, and those significantly worse than grade A are classified as grade C. The inherent grades of worsted fabric are assessed comprehensively using physical indicators and dyeing fastness. The lowest value of the two indicators determines the final fabric grade. Physical indicators of worsted fabric are graded in accordance with Table 2.6, and dyeing fastness is in accordance with Table 2.7. The change rate in size of "machine washable" products can be referred to Table 2.8. The appearance of defects, evaluation, and grading of wool worsted products are detailed listed and compared in Table 2.9, where the comparison was performed along warp and weft directions and degree of faults on fabric surface was also classified as four levels, including appearance faults and scatter faults.

In terms of influence on the end use and the appearance of different problems, the appearance defects of wool worsted fabric can be divided into two types of quality issues: local appearance defects and distributed appearance defects. Here, we would not discuss the defects in detail because of its strong professional description. The appearance of defects, evaluation, and grading are listed in Table 2.9.

Table 2.6 Physical requirements of wool worsted fabric.

Item		High-level class	Grade one	Grade two
Deviation of fabric width (cm) ≤		2	2	5
Tolerance of fabric weight per square meter (%)		−4 to +7	−5 to +7	−14 to +10
Static dimension variation rate (%)≥		−2.5	−3.0	−4.0
Fiber content (%)	Content allowance of wool fiber in wool blended products	−3 to +3	−3 to +3	−3 to +3
Pilling (level) ≥	Suede face	3–4	3	3
	Smooth face	4	3–4	3
Breaking strength (N)≥	(7.3tex*2)*(7tex*2) (80S/2*80S/2) and single weft no less than 14.5tex (40S)	147	147	147
	Other	196	196	196
	Normal worsted wool products	15	10	10
	(8.3tex*2)*(8.3tex*2) (70S/2*70S/2) and single weft no less than 16.7tex (35S)	12	10	10
Dimension change rate of fabric under steam (%)		−1 to +0.5	−1 to +0.5	—
Deformation of fabric in water (level)≥		4	3	3
Degree of fabric fracture (mm) ≥		6	6	8

(1) In order to improve the spinning performance and durability of wool products, the "pure" wool products are allowed to blend with 5% of synthetic fiber. For wool products with decorative fiber products (decorative fiber must be visible with adornment effect), the non-wool fiber content should be less than 7%. But the sum content of both high-performance and decorative fibers should not exceed 7%.
(2) Functional fiber and cashmere in the final wool products show the content less than 10%; the decrease of the content should not be higher than that of tagging content of 30%.
(3) The fiber in the linkage of two-layer fabric is not considered in the examination.
(4) Content of embedded threads lower than 5% is not considered in the examination.
(5) The degree of fabric fracture in the leisure clothes is 10 mm.

2.7 Shape Memory Properties of Wool

For thousands of years, wool has been merely considered as a textile fiber with outstanding performances for its excellent elasticity and thermal insulation. These properties are ascribed to the wool hierarchical structure with macro- and microfibrils and helical coils, which are wrapped by cortex and cuticles outside as shown in Figure 2.9. In addition, as shown schematically in Figure 2.7, the structural components of hydrogen and DBs in crystals and amorphous regions play key roles for the advanced properties. A hydrogen bond is an electrostatic attraction between polar molecules. It is not actually a true bond but a particularly strong dipole–dipole attraction. However, DB is a strong covalent cross-linker between hair molecules (can be characterized by Raman

Table 2.7 Color fastness requirements of wool worsted fabric.

Item		High-level class	Grade one	Grade two
Color fastness to light ≥	≤1/12 standard depth of color (light)	4	3	3
	≥1/12 standard depth of color (dark)	4	4	3
Color fastness to water ≥	Color change	4	3–4	3
	Staining felt	3–4	3	3
	Other adjacent fabric staining	3–4	3	3
Color fastness to perspiration ≥	Color change (acidic)	4	3–4	3
	Staining felt (acidic)	4	4	3
	Other adjacent fabric staining (acidic)	4	3–4	3
	Color change (alkalinity)	4	3–4	3
	Staining felt (alkalinity)	4	4	3
	Other adjacent fabric staining (alkalinity)	4	3–4	3
Color fastness to ironing ≥	Color change	4	4	3–4
	Staining felt	4	3–4	3
Color fastness to rubbing ≥	Dry friction	4	3–4	3
	Wet friction	3–4	3	2–4
Color fastness to washing ≥	Color change	4	3–4	3–4
	Staining felt	4	4	3
	Other adjacent fabric staining	4	3–4	3
Color fastness to dry washing ≥	Color change	4	4	3–4
	Solvent change	4	4	3–4

(1) Color fastness to washing and color fastness to rubbing are not considered in "dry washing only."
(2) Color fastness to dry washing is not considered for "careful hand washing" and "machine washable."

Table 2.8 Dimensional stability to washing requirements of worsted wool fabric in "machine washable."

Item		High-level class, grade one, grade two	
		Suit, pants, coat, overcoat, one-piece dress, jacket, skirt	Shirt, evening dress
Dimensional change rate to relaxation (%)	Width	−3	−3
	Length	−3	−3
	Washing procedure	1*7A	1*7A
General dimensional change rate (%)	Width	−3	−3
	Length	−3	−3
	Edge	−1	−1
	Washing procedure	3*5A	3*5A

Table 2.9 Appearance of defects, evaluation, and grading of wool worsted products.

Fabric faults		Degree of faults appearing on fabric	Local braiding	Scatter degradation	Remarks
Warp direction	(1) Coarse yarn, fine yarn, doubling yarn, loose yarn, tight yarn, wax yarn, local narrowed area of fabric surface	Obvious 10–100 cm; >100 cm; spread all over per 100 cm; scatter all the pieces	1 1	Grade two Shuffs	
	(2) Oil yarn, dirty yarn, jute, yarn exchange between face and back, selvage press mark, cut mark	Obvious 5–50 cm; >50 cm, per 50 cm; scatter all; spread all over	1 1	Grade two Shuffs	
	(3) No warping yarns, dead crease	Obvious 5–20 cm warp; >20 cm, per 20 cm; scatter all	1 1	Shuffs	
	(4) Barre, crease, barring, print of warping exchange, selvage depth, depth of fabric ends	Obvious 40–100 cm; >100 cm, per 100 cm; spread all over; scatter all the pieces	1 1	Grade two Shuffs	Grade two for (selvage depth 4)
	(5) Streakiness, color tone	Obvious 20–100 cm; >100 cm, per 100 cm; spread all over; scatter all the pieces	1 1	Grade two Shuffs	
Warp direction	(6) Bristle mark	Obviously 20 cm or less; >20 cm per 20 cm; spread all over	1 1	Shuffs	
	(7) Clip mark, broken selvage	Obvious 2–10 cm; >100 cm per 100 cm; spread all over; scatter all the pieces	1 1	Grade two Shuffs	
	(8) Thorn flash, edge friction, hairy edge character incomplete, edge character seriously stained, bleached fabric edge stitch, white edge depth more than 1.5 cm needle, needle embroidery, flounces, dense edge	Obvious 0–100 cm; >100 cm per 100 cm; scatter all	1 1	Grade two	
Weft direction	(9) Coarse yarn, fine yarn, doubling yarn, loose yarn, tight yarn, exchange mark of yarn	Obvious 10 cm to all; spread all over; scatter all the pieces	1	Grade two Shuffs	

Table 2.9 (Continued)

Fabric faults		Degree of faults appearing on fabric	Local braiding	Scatter degradation	Remarks
	(10) Mispick, oil yarn, dirty yarn, jute, small braid yarn	Obvious 5 cm to all; spread all over; scatter all the pieces	1	Grade two Shuffs	
Weft direction	(11) Thick places, weft shallow, hard joining stencil mark, severe press mark, yarn uniformization	Obviously 20 cm and less warp >20 cm; spread all over; scatter all the pieces	1 1	Grade two Shuffs	
	(12) Thin places of fabric, loom bar, wrong construction, mat-up, loose weave, mottled, hole repair mark, hole correction mark, big belly yarn, warp bar	Obviously 10 cm or less warp; >10 cm per 10 cm; spread all over	1 1	Shuffs	Big belly yarn 1 cm for start point 0.5 cm mottled for note 2
	(13) Bore chafed yarn	2 cm (including 2 cm); spread all over	1	Shuffs	
	(14) Combed hair, knot, grass, dead hair, overshot, loose pattern	Spread all over; scatter all the pieces		Grade two Shuffs	
	(15) Bias of fabric face	Plain fabric: 4 cm Plaid fabric: 3 cm, 40–100 cm, >100 cm per 100 cm. Plain fabric: 4–6 cm scatter all; spread over 6 cm. Plaid fabric: 3–5 cm scatter all; spread over 5 cm	1 1	Grade two Shuffs Grade two Shuffs	High-level fabric product plaid fabric from 2 cm; plain fabric from 3 cm

(1) Fabric faults in the area from edge to less than 1.5 cm of fabric (a line refers to the inner cloth within 0.5 cm depth edge of defects) in the identification of fabric goods are not considered as fabric faults; however, the hole, broken edge, edge burr, edge wear, bleaching, and stitch defect edge character on the edge of fabric should be checked; if the defect length extends to the inner part of fabric, this should be considered to inspect together.

(2) For the appearance faults of wool fabric, in the case of exceeding the above provisions of special circumstances, it can be sorted out according to the extent of their impact on the use of similar defects in the evaluation of the relevant provisions of the discretion.

(3) For the scatter appearance faults, especially the serious impact on fabric wearability, it should be set price according to quality.

(4) The top grade of wool products should not have more than 1 cm of broken hole, spider web, rolling shuttle, and serious weft bar.

spectroscopy) [11] that can control the hair elasticity [5, 8]. Keten et al. reported that both hydrogen bonds and DBs in the amorphous regions of animal hair can be reversible under certain environmental conditions such as redox agents, water, and heat [12, 13], which lead to the conversion of temporary and permanent shrinkage macroscopically [14]. In addition, ~40% of the crystallinity in wool is proven to be too hard to cleave and has been studied by textile researchers using X-ray diffraction (XRD) that the crystalline phase of wool is made of very dense hydrogen bonds [7, 15, 16].

Shape memory polymers (SMPs) are a kind of smart polymers characterized by their stimuli-responsive behavior adapting to our human demands. SMPs can be described in terms of netpoint-switch structure as refer to the work [17] where their permanent shape is determined by netpoints and reversible bonds in the amorphous region acting as a switch unit that leads to temporary shape. Even though there are a few latest reports of triple stimuli-responsive SMPs [18–21], SMPs have one stimulus in most existing cases. However, Schattling et al. [22] stressed the rising importance of developing multi-stimuli-responsive polymers that are called "all-in-one talents" in many industries, such as life sciences for comparable natural adaptability and information technology for the parallel writing of information to give a dramatic increase of memory density. They believed that the addition of one more stimulus in a polymer can improve the degree of control, provide more free choice, and increase the level of intricacy, which in turn enhances the adaptability of a material to different environments by more intelligent functions. However, developing such multi-responsive talented polymers requires new technologies that may be beyond our normal imagination. On the other hand, nature is full of wisdom, and we may learn tricks even from a very common subject such as animal hair fiber [3]. For example, an interesting shape memory (SM) phenomenon of a dry wool yarn is usually encountered in textile industry, where the yarn contracts by 20% in water after being pretreated using reducing agent ($NaHSO_3$) and pre-stretched to 30% strain [23]. It is believed that this is the SM of wool responsive to redox and water.

For hydrogen bonds in polymers, they can be very strong acting as dense physical cross-linking, which are difficult to cleave such as in a hard polymer crystal phase. This is well known, and they are widely used as netpoints in many SMPs where hydrogen bonding-based crystal acts as netpoint for the purpose of shape recovery [24, 25]. When they are not that strong, they may be reversibly dissociated and re-formed under conditions such as heat and water [26–28], which can be used as switch in SMPs. For example, it is found that the glass transition temperature (T_g) of wool is decreased with the increase of water content (Figure 2.15a) [6], due to the collapse of a large amount of HBs in the amorphous region for the cause of aqueous molecules. It is also observed that the collapsed HBs in the amorphous region can be re-formed when the wet wool is dried. This indicates the HBs are reversible, with and without water alternatively [29]. Thus, HB is the key behind water-responsive SM and plays a main role in the water-driven shape recovery process [27, 30, 31]. Furthermore, Jung and So observed a water-responsive SM in a poly(ethylene glycol) (PEG)-based polyurethane where the crystalline segment was dissolved by water due to the disappearance of HBs [32]. Using high molecular weight of

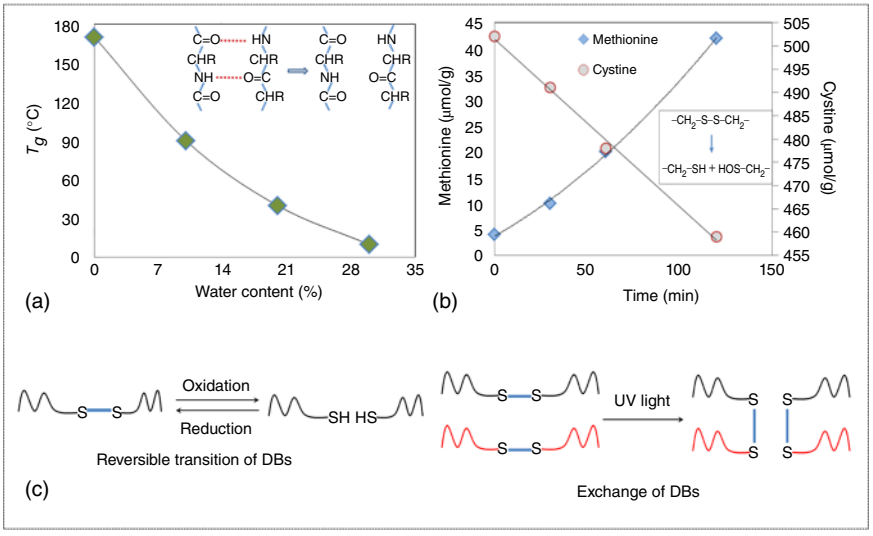


Figure 2.15 Physical properties of wool. (a) Effect of water content on wool glass transition temperature. (b) Effect of reducing reaction on amount of disulfide bonds (DBs). (c) Reversible transition of DBs in redox reaction and exchange of DBs among macromolecules under UV light.

PEG, another shape recovery of 99% copolymer was synthesized through HB switches [33]. A simple and controllable triple-SM supramolecular composite was also developed successfully through HB switches between a polymer and mesogenic units [34] where the HBs enable broad and independent control of both T_g and cross-link density [35].

For DBs, it is found that it can be broken when reducing agent is applied because a decreased amount of cysteine and increased methionine were observed throughout the reducing reaction as shown in Figure 2.15b [1]. This is because DBs can be cleaved to form two thiol groups in reducing solution. In turn, the broken DBs can be reversed by an oxidation reaction [36]. DBs are a type of dynamic covalent bonds responsive to redox and different light triggers, which form the basis as switch in SMPs. As shown in Figure 2.15c, reversible change happens between DBs and thiols where DBs are cleaved to thiol groups by a reduction reaction and re-formed by an oxidation reaction [37]. This reversible change can be found in responsive polymer capsules and micelles and gels for applications such as drug delivery [38–40]. DBs have another type of reversibility: exchange reaction that can lead to the healing ability of a polymer driven by UV and visible light as shown in Figure 2.15c [41–44]. As far as SMPs are concerned, there are only two reports in literature: a thermally responsive SMP was reported with semicrystalline and covalently cross-linked network where DBs were used for self-healing function only under UV light [45]. Thus, only one SMP reported in the literature has utilized DBs as a switch responsive to redox treatment where cellulose derivatives with cross-linkable mercapto groups were used [46]. Strictly speaking, the use of DBs in SMPs as netpoints has not been reported yet, but they are strong chemical bonds that are stable under some

conditions and can be used as netpoints in SMPs as evidenced in wool, where they control its elasticity under normal environmental conditions [5]. Moreover, it is also clear that DBs could act as reversible switches, having self-healing capability [47] when exchange reactions take place among macromolecules under light, particularly in UV light conditions.

In a report, wool was investigated on its multi-stimuli-responsive SM behaviors and for corresponding mechanisms in molecular and structural networks. The innate shape of a wool hair can be recovered in varying degrees through different stimuli effect on the fixed deformation, which is a typical multi-stimuli SM material. High temporary shape fixation (>0.8) and shape recovery (>0.5) of wool exposure on water and redox agent demonstrated that wools are smart α-keratin fibers stimulated by water and redox. However, low temporary shape fixation under heat (0.55) and low shape recovery (0.23) under UV illuminating indicates that wools have less SM abilities under stimuli of heat and UV light. The single tensile of wool interpreted well for the effect of each stimulus on the switch (assuming netpoint intact after stimuli) open and close. XRD and DSC characterizations of wool under four stimuli showed that the crystalline phase can be viewed as an invariable component during SM program. However, Raman spectra showed the DBs in breakage when wool faces UV light and reductant ions and in variation under the stimuli of water and heat, indicating these bonds act as switch unit for stimuli of UV light and redox agent and as netpoint for water and heat. FTIR characterization for HBs of wool through the variations of characteristic peaks in wavenumber shifting and intensity ratio showed that these bonds could act as switch for the stimuli of heat, water, and redox agent in each SM behavior. Based on this, a twin-netpoint-switch structure model for wool was proposed, as shown in Figure 2.16, for interpreting the different SM abilities of the hair when exposed to different external stimuli, where a twin-netpoint/single-switch structure is for the stimulus of water, heat,

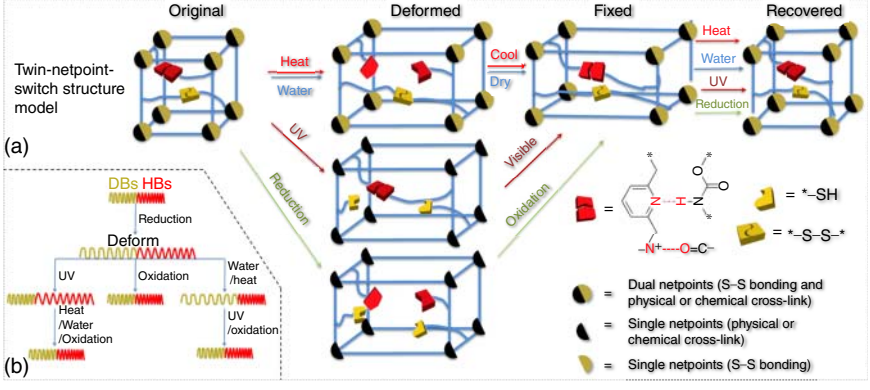


Figure 2.16 (a) Twin-net-switch structural model of wool for SM abilities. (b) Variation of three key components under four types of stimuli where reductant can open both switches (DBs and HBs), HBs can be closed using oxidant, water, and heat, and DBs can be re-formed using UV and oxidant.

and UV light and a single-netpoint/twin-switch structure is for the stimulus of redox agent.

2.8 Future Trends of Application of Wool Keratin

When considering the application of wool beyond textiles, it is of importance to first consider the materials from which wool is made up, such as the inner components for SM applications. Once the macroscopic wool as a fiber is not fundamental in defining the application, then it comes down to the base materials from which the fiber is formed to define the relevant applications.

From the view of macroscopic and microscopic scales, both characteristics of wool have been extensively reviewed [48, 49]. By far the most important material in this consideration is keratin protein, defined by the US National Library of Medicine as "A class of fibrous or sclera proteins important both as structural proteins and as keys to the study of protein conformation." The family represents the principal constituent of epidermis, hair, nails, horny tissues, and the organic matrix of tooth enamel. It is clear from the definition that keratin proteins, in many forms, are widely present in biological systems, in the hair, skin, nails, and other tissues.

This widespread occurrence in nature, as a tough, physical material from which to build structures, is of significance when considering the advanced applications of wool. The tenacity of wool, the resilience of our nails, and the barrier characteristics of our skin tell us much about the features that we can look for in advanced applications of wool-derived keratins. While keratin may account for up to 95% of the dry matter of a wool, the other components are also of note for their interesting characteristics. Considered as an ordered collection of elongated cells, rich in multiple types of keratin proteins, the wool structure is brought together by the cell membrane complex, the material that defines the cell boundaries and a key element in keeping the cells together in a strong and ordered fibrous alignment.

2.8.1 Extraction of Keratin from Wool for New Product Development

Beyond the fiber, advanced applications of wool utilize the keratin protein from which the fiber is constructed. The first step, then, in development of these materials is isolation of that protein in a versatile form that can be further manipulated into the desired applications. Wool, by its nature, is a tough insoluble material evolved by nature to be robust and resistant to degradation. Its conversion to a state where it can be widely manipulated is not straightforward, and this has been a key reason that keratin protein has not been exploited commercially as a material in the way that other biopolymers have been, such as collagens, alginates, celluloses, and starches. The simplest way to isolate a soluble from of keratin from the source fiber is to apply conventional methods of hydrolysis, using acid, alkali, or enzymatic digestion of the peptide bonds to create a mixture of peptides and amino acids that have retained none of the secondary or tertiary structure of the core protein.

In most cases, these processes also destroy many of the core amino acids. Although this harsh processing destroys many of the unique characteristics of protein, it has provided a route for several developments, such as the historic industrial uses explored below. In order to progress beyond these limited applications of keratin-derived peptides, hydrolysates, and amino acids, a series of processes for the isolation of keratin proteins from wool that maintain core features of the protein and its structure have been developed [50, 51]. Most of the processes do not hydrolyze the peptide linkages, and this allows the keratin proteins that are produced to retain a form and function similar to the native keratins. By maintaining the structural and chemical complexity of the native proteins, by having substantial fibrous proteins that naturally form robust and ordered materials, and with chemically active amino acid components such as cystine present in abundance, then advanced applications in a range of areas may be developed. The development of technology to achieve these forms of keratin is a key to the creation of advanced applications of wool.

2.8.2 Industrial Trends Relating to Sustainable Polymers

Advanced applications of wool keratins can be considered in a similar manner to developments undertaken elsewhere into biopolymer- or biologic-derived materials. The factors influencing the developments come primarily from the commercial arena, which is in turn driven by opportunities created by innovation and importantly environmental and legislative factors. Global interest in sustainably produced materials and full life cycle analysis of products has driven interest and investment in biological materials. Biopolymers, as alternatives to synthetic plastics, have been the promise of white biotechnology for several decades, with Biopol™ from Monsanto as an early example of a promising technology that has not yet had the appropriate alignment of technological, environmental, and legislative factors to drive enough commercial interest to lead to success. NatureWorks™ from Cargill Dow, used from packaging to fiber applications, is an example of a biopolymer material for which there is rapidly increasing consumer interest. The development was made possible by advanced biotechnology, but its continued development is driven by a commercial need to find biological alternatives to oil-derived synthetic polymers because of legislative and economic pressure on oil. While price signals are important, there is increasing pressure on landfill that is being progressively occupied by synthetics derived from oil. These same drivers create strong opportunities for other natural biopolymers with an established biological function as a material. Advanced applications from wool keratin are emerging to capture this opportunity.

2.8.3 Future Trends

The future advanced uses of wool keratins may be in two distinct areas. The first is medical technology. Developments will be driven by science and improved healing outcomes. Recent academic research into the previously unknown biological role of keratins in body was identified through the work of Coulombe, Omary,

and others [52, 53]. This has determined that keratin in body plays more than a physical role but is essential in the transportation of signaling peptides crucial for the growth and differentiation of cells. Coupled with the developing technology for the creation of medical devices from keratin, substantial advanced uses of wool will develop in the medical area. This is already commencing in the areas of wound care and orthopedics, and the natural evolution into other areas of medical care will follow.

The second area of advanced use is in industrial technology and will be driven by legislation and commercial necessity. With the price of oil on a sustained sharp increase over recent years, and a flow-on effect to all oil-derived materials, coupled with harsher environmental legislation being established globally relating to both carbon neutrality and source and waste management, the focus on biopolymers will naturally increase sharply. Keratin is one of nature's most successful materials; it was evolved to be versatile, tough, and protective, and as a natural protein, there are wide opportunities in a range of industrial areas. Robust materials, such as plastics, to the less obvious industrial speciality chemicals that are also derived from a synthetic backbone are all a likely development for advanced uses of wool. None of these future applications requires the fiber to maintain its fibrous form, but all utilize the complex fundamental structure that the wool fiber is based on.

2.8.4 Sources of Further Information and Advice

Further information on the structural components of wool can be gained from Marshall et al. [49] and Gillespie [48]. The biological role of keratin in the skin and other tissues is the subject a variety of publications including Kim et al. [53] and Omary and Ku [52]. The use of keratin in applications beyond the conventional fiber is the subject of numerous patent applications (see, for example, [51], and [50]). Biopolymer trends and the importance of both technology and legislation is well documented by the Greentech organization (www.greentech.org).

References

1 Yao, M. (2009). *Textile Materials*. Beijing: China Textile Press.
2 IWTO (2016). World's fibers production and distribution, Forward – The Economist, 2018. https://www.qianzhan.com/analyst/detail/220/180704-ede538d7.html.
3 Xiao, X. and Hu, J. (2016). *Scientific Reports* 6: 26393.
4 *The Macromolecular Structure of Wool Fiber*. http://www.fzfzjx.com/tech_news/detail-4048.html (accessed 22 June 2010).
5 Harris, M., Mizell, L.R., and Fourt, L. (1942). *Industrial and Engineering Chemistry* 34 (7): 833–838.
6 Wortmann, F.J., Rigby, B.J., and Phillips, D.G. (1984). *Textile Research Journal* 54: 6–8.
7 Lotay, S.S. and Speakman, P.T. (1977). *Nature* 265: 274–276.
8 Lindley, H. (1957). *Textile Research Journal* 27: 690–695.

9 Hearle, J.W. (2000). *International Journal of Biological Macromolecules* 27 (2): 123–138.
10 Okajima, S. and Kikuchi, K. (1956). *Fiber* 12 (12): 899–902.
11 Akhtar, W. and Edwards, H.G.M. (1997). *Spectrochimica Acta Part A: Molecular and Biomolecular Spectroscopy* 53 (7): 1021–1031.
12 Chapman, B.M. (1970). *Journal of the Textile Institute* 61 (9): 448–457.
13 Keten, S., Chou, C.C., Van Duin, A.C.T., and Buehler, M.J. (2012). *Journal of the Mechanical Behavior of Biomedical Materials* 5: 32–40.
14 Astbury, W.T. and Woods, H.J. (1934). *Philosophical Transactions of the Royal Society of London, Series A: Mathematical, Physical and Engineering Sciences* 232: 333–394.
15 Wu, B., Yi, Y., Xu, T., and Lei, H. (2012). *2nd International Conference on Electronic & Mechanical Engineering and Information Technology (EMEIT-2012)*, 1405–1408. Paris, France: Altantis Press.
16 Samways, C. and Hastings, G.W. (1970). *Nature* 225: 634–635.
17 Hu, J.L. and Chen, S.J. (2010). *Journal of Materials Chemistry* 20 (17): 3346–3355.
18 Chen, J., Zhang, S., Sun, F. et al. (2016). *Polymer Chemistry* 7: 2947–2954.
19 Kumpfer, J.R. and Rowan, S.J. (2011). *Journal of the American Chemical Society* 133: 12866–12874.
20 Wang, L., Yang, X., Chen, H. et al. (2013). *Polymer Chemistry* 4: 4461–4468.
21 Tao, Z., Peng, K., Fan, Y. et al. (2016). *Polymer Chemistry* 7: 1405–1412.
22 Schattling, P., Jochum, F.D., and Theato, P. (2014). *Polymer Chemistry* 5: 25–36.
23 Hu, J.L., Zhu, Y., Huang, H.H., and Lu, J. (2012). *Progress in Polymer Science* 37 (12): 1720–1763.
24 D'hollander, S., Van Assche, G., Van Mele, B., and Du Prez, F. (2009). *Polymer* 50: 4447–4454.
25 Zhang, T., Wen, Z., Hui, Y. et al. (2015). *Polymer Chemistry* 6: 4177–4184.
26 Ratna, D. and Karger-Kocsis, J. (2008). *Journal of Materials Science* 43: 254–269.
27 Zhang, S., Yu, Z.J., Govender, T. et al. (2008). *Polymer* 49 (15): 3205–3210.
28 Huang, W.M., Yang, B., An, L. et al. (2005). *Applied Physics Letters* 86: 114101–114103.
29 Eaves, J.D., Loparo, J.J., Fecko, C.J. et al. (2005). *Proceedings of the National Academy of Sciences of the United States of America* 102 (37): 13019–13022.
30 Fan, K., Huang, W.M., Wang, C.C. et al. (2011). *Express Polymer Letters* 5 (5): 409–416.
31 Xiao, X. and Hu, J. (2016). *International Journal of Chemical Engineering* 1 (12): UNSP 4803254
32 Jung, Y.C. and So, H.H. (2006). *Journal of Macromolecular Science, Part B: Physics* 45 (6): 1189–1190.
33 Liu, G., Guan, C., Xia, H. et al. (2006). *Macromolecular Rapid Communications* 27: 1100–1104.
34 Chen, H., Liu, Y., Gong, T. et al. (2013). *RSC Advances* 3: 7048–7056.
35 Ware, T., Hearon, K., Lonnecker, A. et al. (2012). *Macromolecules* 45: 1062–1069.

36 Wedemeyer, W.J., Welker, E., Narayan, M., and Scheraga, H.A. (2000). *Biochemistry* 39 (15): 4208–4216.

37 Zheng, M., Aslund, F., and Storz, G. (1998). *Science* 279: 1718–1721.

38 Dailing, E.A., Nair, D.P., Setterberg, W.K. et al. (2016). *Polymer Chemistry* 7: 816–825.

39 Kakizawa, Y., Harada, A., and Kataoka, K. (1999). *Journal of the American Chemical Society* 121: 11247–11248.

40 Yan, Y., Wang, Y., Heath, J.K. et al. (2011). *Advanced Materials* 23: 3916–3921.

41 Fairbanks, B.D., Singh, S.P., Bowman, C.N., and Anseth, K.S. (2011). *Macromolecules* 44 (8): 2444–2450.

42 Otsuka, H., Nagano, S., Kobashi, Y. et al. (2010). *Chemical Communications* 46: 1150–1152.

43 Canadell, J., Goossens, H., and Klumperman, B. (2011). *Macromolecules* 44 (8): 2536–2541.

44 Amamoto, Y., Otsuka, H., Takahara, A., and Matyjaszewski, K. (2012). *Advanced Materials* 24: 3975–3980.

45 Michael, B.T., Jaye, C.A., Spencer, E.J., and Rowan, S.J. (2013). *ACS Macro Letters* 2: 694–699.

46 Aoki, D., Teramoto, Y., and Nishio, Y. (2007). *Biomacromolecules* 8: 3749–3757.

47 Chang, R., Huang, Y., Shan, G. et al. (2015). *Polymer Chemistry* 6: 5899–5910.

48 Gillespie, J.M. (1983). *Biochemistry and Physiology of the Skin*, 1e (ed. L.A. Goldsmith), 475. Oxford University Press.

49 Marshall, R.C., Orwin, D.F.G., and Gillespie, J.M. (1991). *Electron Microscopy Reviews* 4: 47–49.

50 Smith, R.A., Blanchard, C.R., and Timmons, S.F. (1997). US Patent 5, 932, 552

51 Kelly, R.J., Worth, G.H., Roddick-Lanzilotta, A.D. et al. (2002). US Patent 7, 148, 327.

52 Omary, M.B. and Ku, N.O. (2006). *Nature* 441 (7091): 296–298.

53 Kim, S., Wong, P., and Coulombe, P.A. (2006). *Nature* 441 (7091): 362–365.

3

Animal Fibers: Silk

K. Murugesh Babu

Bapuji Institute of Engineering and Technology (Affiliated to Visvesvaraya Technological University, Belgaum), Department of Textile Technology and Research Centre, Davangere, 577004, Karnataka, India

3.1 Introduction to Silk and Silk Industry

Silk is one of the oldest fibers known to man. Silk is an animal fiber produced by certain insects to build their cocoons and webs. Although many insects produce silk, only the filament produced by the mulberry silk moth *Bombyx mori* and a few others in the same genus is used by the commercial silk industry [1]. The silk produced by other insects, mainly spiders, is used in a small number of other commercial capacities, for example, weapon and telescope cross hairs and other optical instruments [2].

Silks belong to a group of high molecular weight organic polymers characterized by repetitive hydrophobic and hydrophilic peptide sequences [3]. Silks are fibrous protein polymers that are spun into fibers by some arthropods such as silkworms, spiders, scorpions, mites, and fleas [3, 4]. There are thousands of silk-spinning insects and spiders, yet only a few have been investigated in detail. Silks differ in composition, structure, and properties depending on their specific source and function [3, 5, 6]. They are naturally produced by spiders or insects, such as *Nephila clavipes* and *B. mori*, respectively [7, 8]. Silkworm fibers are classified as domestic and wild silk. Wild silks are produced by caterpillars other than the mulberry silkworm, and they differ from the domesticated varieties in color, size, and texture. The cocoons gathered in the wild usually have been damaged by the emerging moth before the cocoons are gathered, so the silk thread that makes up the cocoon has been torn into shorter lengths. Domestic silkworms like *B. mori* are commercially reared, and the pupae are killed by dipping them in boiling water before the adult moths emerge, allowing the whole cocoon to be unraveled as one continuous thread. There are other commercially exploited silkworms other than *B. mori* that can be used to rear the silk known as non-mulberry silkworms like *Antheraea mylitta* (tasar),

Handbook of Fibrous Materials, First Edition. Edited by Jinlian Hu, Bipin Kumar, and Jing Lu.
© 2020 Wiley-VCH Verlag GmbH & Co. KGaA. Published 2020 by Wiley-VCH Verlag GmbH & Co. KGaA.

Philosamia ricini (eri), and *Antheraea assama* (muga). Silks are also produced by spiders and insects that secret glycine-rich silks characterized by their unique synthesis and processing features, as well as strength and extensibility.

The silk filament contains 72–81% fibroin, 19–28% sericin, 0.8–1.0% fat and wax, and 1.0–1.4% coloring matter and ash of the total weight. The silkworm extrudes the liquid fiber from the two excretory canals of sericteries that unite in the spinneret in its head, each of them termed as brin. The two brins cemented together in the spinneret by sericin become a single continuous fiber called the bave or filament. The seric bave is thus made by the union of two brins held together by sericin [9]. Fibroin is a valuable protein along with sericin, which acts as a glue to fix fibroin fiber together in a cocoon. Sericin and fibroin protein is useful because of its properties and has been found to possess various biological functions.

The molecular weight of sericin ranges from 10 to 310 kDa, and that of fibroin ranges from 300 to 450 kDa [10, 11], but silk produced by spiders is mechanically superior to any insect silk. However, spider silk differs in many aspects from those produced by mulberry silkworms. The fibroin is a protein dominated in composition by the amino acids glycine, alanine, and serine, which form antiparallel β sheets in the spun fibers [12–14]. But only the silk of moth caterpillars has been used widely for textile manufacture and other applications. The main difference between spider and mulberry silkworm silks is that dragline spider silks are mechanically superior, but better water resistance and availability make silkworm silks more prominent. The choice of silk for a particular application must therefore include careful consideration of the desired properties.

Genetically, silks are characterized by a combination of highly repetitive primary sequences that lead to significance in secondary structure, which provides unique mechanical properties. Because of these impressive properties, combined with their biocompatibility and relative environmental stability, silks have been used as an important set of material options in the fields of controlled release and for biomaterials, in addition to their uses as textile materials [15].

The structure of silk is shown in Figure 3.1. Silk of *B. mori* is composed of the proteins fibroin and sericin and matters such as fats, wax, sand pigments, and minerals. Fibroin in the *B. mori* comprises a high content of the amino acids glycine and alanine, 42.8 and 32.4 g, respectively, as shown in Table 3.1. The key amino acids in sericin are serine (30.1 g), threonine (8.5 g), aspartic acid (16.8 g), and glutamic acid (10.1 g).

Table 3.1 shows that there are different proportions of amino acid residues in fibroin. Fibroin has high proportion of alanine, glycine, and serine. A small amount of cystine residues give a very small amount of sulfur in the fiber. Fibroin contains only a small amount of amino acid side chains. The amounts of acid and alkali that can be absorbed by silk are relatively lower than those absorbed by wool (c. 0.2 equiv/kg of silk). The isoelectric point of silk fiber is around pH 5. There is a low proportion of amino acid residue with large side chain. In silk hydrogen bonding is important in fibroin. An X-ray structure analysis of the crystalline domain of fibroin shows that the peptide chains pack in fully extended forms [16] (Figure 3.2).

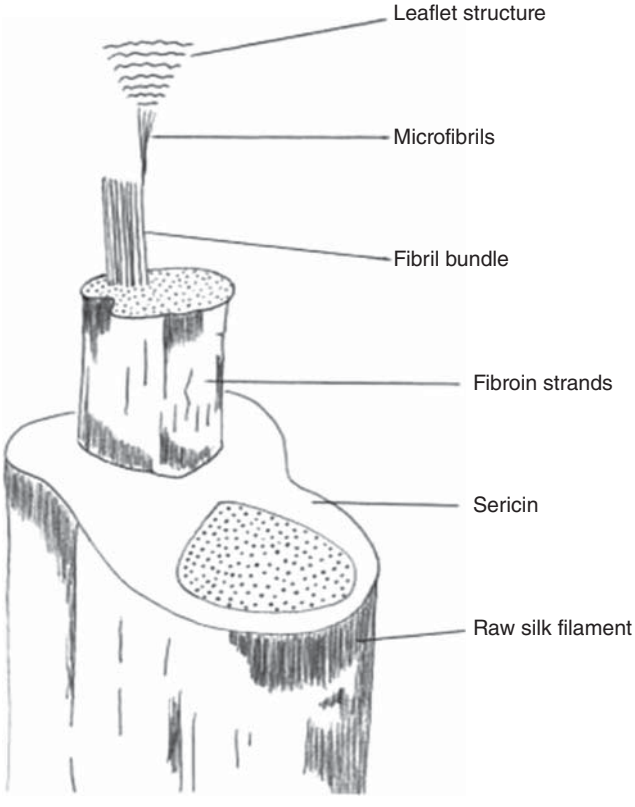


Figure 3.1 Structure of silk.

Table 3.1 Amino acid composition of fibroin and sericin.

Amino acids	Fibroin	Sericin	Amino acids	Fibroin	Sericin
Glycine	42.8	8.8	Glutamic acid	1.7	10.1
Alanine	32.4	4.0	Serine	14.7	30.1
Leucine	0.7	0.9	Threonine	1.2	8.5
Isoleucine	0.9	0.6	Phenylalanine	1.2	0.6
Valine	3.0	3.1	Tyrosine	11.8	4.9
Arginine	0.9	4.2	Proline	0.6	0.5
Histidine	0.3	1.4	Methionine	0.2	0.1
Lysine	0.5	5.5	Tryptophan	0.5	0.5
Aspartic acid	1.9	16.8	Cystine	0.1	0.3

Values are given as gram of amino acid per 100 g of protein.
Source: Tanaka et al. 1999 [10].

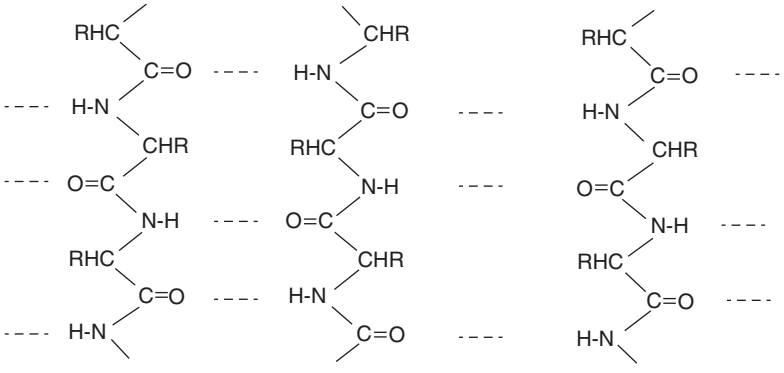


Figure 3.2 Crystal structure of the polypeptide bond in the silk fibroin. Source: Guljarni 1992 [31]. Reproduced with permission of John Wiley & Sons.

3.2 Types of Silk and Their Importance

Silk is mainly divided into two types:

- Mulberry silk (*B. mori*), also called cultivated silk.
- Non-mulberry silk.

3.2.1 Mulberry

Mulberry silk is also known as cultivated silk and bombyx silk, but mulberry silk is the most commonly used term. It is also sometimes referred to it by its type, which is thrown or reeled silk [17]. Figure 3.3 shows the mulberry worm and the cocoons.

The bulk of the commercial silk produced in the world comes from mulberry silk. Mulberry silk comes from the silkworm *B. mori*, which solely feeds on the leaves of mulberry plant. These silkworms are completely domesticated and reared indoors. In India, the major mulberry silk producing states are Karnataka, Andhra Pradesh, West Bengal, Tamil Nadu, and Jammu Kashmir, which together



Figure 3.3 Mulberry silkworms and cocoons.

Table 3.2 World raw silk production (tonnes).

Country	2002	2003	2004	2005	2006	2007	2008	% Share
China	68 600	94 600	102 560	105 360	130 000	108 420	98 620	81.24
India	16 319	15 742	16 500	17 305	18 475	18 320	18 370	15.13
Japan	394	287	263	150	150	105	95	0.08
Brazil	1607	1563	1512	1285	1387	1220	1177	0.97
Korea Republic	154	150	150	150	150	150	135	0.11
Uzbekistan	1260	950	950	950	950	950	865	0.71
Thailand	1510	1500	1420	1420	1080	760	1100	0.91
Vietnam	2200	750	750	750	750	750	680	0.56
Others	3814	1500	1500	1500	1000	500	350	0.29
Total	95 858	117 042	125 605	128 870	153 942	131 175	121 392	100.00

Figures of India is for financial year April to March.
Source: ISC website www.inserco.org SS:08-09-2009.

accounts for 92% of country's total mulberry raw silk production [17]. World raw silk production is shown in Table 3.2.

3.2.1.1 Types of Mulberry Silk

B. mori, the domesticated silkworm, has been reared for over 2000 years. During this long history, many mutations have occurred. The mutants have been further classified with each other resulting in a combination of various genes producing a large number of silkworm races. The silkworm races are classified on the basis of:

(1) Place of origin
(2) Voltinism
(3) Molting

Place of Origin

Indian Races These races are aboriginal in India and Southeast Asia. The larval stage is longer and they are robust against high temperature and humidity. The size of the cocoon and larvae is small. In many cases, the cocoon is spindle shaped, and the cocoon color is green, yellow, or white. The cocoon shell is thin with less shell percentage. They are mainly multivoltines.

Japanese Races These races are aboriginal in Japan. The larvae are robust. The cocoon is in peanut shape. The sizes of the larvae do not correspond with the long larval duration. The cocoon color is usually white, but few are also green or yellow in color. The ratio of double cocoons is more. The quality of the silk filament is inferior and it is thick and short. They are univoltine or bivoltine.

Chinese Races These races are aboriginal in China. The larvae are robust against high temperature but weak against high humidity. The larvae are plain and active. They voraciously eat mulberry leaves and grow quickly. The cocoon shape is, in

many cases, elliptical spherical and spindle shaped in few cases. The cocoon color is white, golden yellow, green, red, or beige. The cocoon filament is fine and reelability is good. They are univoltine, bivoltine, and multivoltine.

European Races These races are aboriginal in Europe and Central Asia. Larval duration is long and they actively eat mulberry leaves. Larvae are weak against high temperature and high humidity. The cocoon size is big with a little constriction. The cocoon reelability is good.

Voltinism According to voltinism, silkworms are classified into (a) univoltines, (b) bivoltines, and (c) multi- or polyvoltines.

Univoltines These races have only one generation in a year. The body size of larvae is large. The cocoon weight, shell weight, shell ratio, and cocoon filament weight are high. The cocoon filament quality is good.

Bivoltines These races have two generations in a year; the silkworms are more uniform and strong. The cocoon weight, cocoon shell weight, shell ratio, and cocoon filament weight are less compared with univoltines. Larvae are robust compared with univoltines.

Multivoltines The life cycle is short. They have many generations in a year. Larvae are robust and can withstand high temperature. The size of cocoons is small. The cocoon weight, shell ratio, and cocoon filament weight are less than bivoltines. Cocoon filament is fine.

Molting Based on molting, silkworms are classified into (a) trimolters, (b) tetramolters, (c) pentamolters, rarely bimolters, and hexamolters. Tetramolters are mainly reared for commercial purposes.

Thai silk is only one of the mulberry silkworm (*B. mori*) silks, but it differs somewhat in appearance and is yellower in color. The filament is coarser and has more silk gum (e.g. up to 37%) than normal mulberry silk (e.g. 20–25%) [11, 18]. These characteristics cause Thai silk to have its own style after weaving. Thai silk products are mainly produced by domestic industries in the northern and north east part of Thailand.

3.2.2 Non-mulberry

A large number of species (400–500) are used in the production of non-mulberry silks, but only about eighty have been commercially exploited in Asia and Africa, chiefly in tribal communities. The major varieties of non-mulberry silk are described below [1].

3.2.2.1 Tasar

Tasar silk, popularly known as "Dasali Pattu," is a wild silk reeled from tasar cocoons. Tasar (tussah) is a copperish, coarse silk mainly used for furnishings and interiors. It is less lustrous than mulberry silk, but has its own feel and appeal.



Figure 3.4 Tasar silkworm and cocoon.

Tasar silk is generated by the silkworm *A. mylitta*, which mainly thrive on food plants Asan (*Terminalia tomentosa*) and Arjun (*Terminalia arjuna*). The rearing is conducted in nature on the trees in the open areas. In India, tasar silk is mainly produced in the states of Bihar, Jharkhand, Chhattisgarh, and Orissa, besides Maharashtra, West Bengal, and Andhra Pradesh. Tasar culture is the mainstay for many a tribal community in India [1]. Figure 3.4 shows the tasar worm and the cocoons.

3.2.2.2 Oak Tasar

Oak tasar is a finer variety of tasar generated by the silkworm *Antheraea proylei* J in India, which feeds on natural food plants of oak, found in abundance in the sub-Himalayan belt of India, covering the states of Manipur, Himachal Pradesh, Uttar Pradesh, Assam, Meghalaya, and Jammu and Kashmir. China is the major producer of oak tasar in the world, and this comes from another silkworm known as *Antheraea pernyi*.

3.2.2.3 Eri

Eri silk is known as "Ahimsa silk." Also known as endi or errandi, eri is a multivoltine silk spun from open-ended cocoons, unlike other varieties of silk. Eri silk is the product of the domesticated silkworm *P. ricini*, which mainly thrive on food plants castor and tapioca, kessera, papaya, etc. Eri cocoon is open mouthed; the filament is discontinuous and thus can be used only for spinning. Like tasar, the cocoon varies in color, size, and softness. The soft cocoons are better for mechanical spinning and slightly hard and bigger cocoons for hand spinning [19]. A picture of the worm and the cocoons is presented in Figure 3.5.

Eri silk has the unique dual characteristics of the softness of silk and the warmth of the wool and holds a lot of promise as a commercial venture. Ericulture is a household activity practiced mainly for protein-rich pupae, a delicacy for the tribal. Resultantly, the eri cocoons are open mouthed and are spun. The silk is used indigenously for preparation of chaddars (wraps) for own use by these tribals. In India, this culture is practiced mainly in the northeastern states and Assam. It is also found in Bihar, West Bengal, and Orissa [18].

The eri silk production in India is 1483 Metric Tonnes per annum mainly with 90% from northeast states. It provides gainful employment to the people with



Figure 3.5 Eri silkworm and cocoons.



Figure 3.6 Muga silkworm and cocoons.

emphasis on women folk in rural areas where poverty and unemployment are concentrated.

3.2.2.4 Muga

This golden yellow-colored silk is prerogative of India and the pride of Assam state. It is obtained from semidomesticated multivoltine silkworm *Antheraea assamensis*. These silkworms feed on the aromatic leaves of Som and Soalu plants and are reared on trees similar to that of tasar. Muga culture is specific to the state of Assam and an integral tradition and culture of that state. The muga silk and high value product is used in products like sarees, mekhalas, chaddars, etc. Figure 3.6 shows the muga silkworm and the cocoons.

3.2.2.5 Anaphe Silk

This silk of southern and central Africa is produced by silkworms of the genus *Anaphe*: *A. moloneyi* Druce, *A. panda* Boisduval, *A. reticulata* Walker, *A. carteri* Walsingham, *A. venata* Butler, and *A. infracta* Walsingham. They spin cocoons in communes, all enclosed by a thin layer of silk. The tribal people collect them from the forest and spin the fluff into a raw silk that is soft and fairly lustrous. The silk obtained from *A. infracta* is known locally as "book," and that from *A. moloneyi* as "tissnian-tsamia" and "koko." The fabric is elastic and stronger than that of mulberry silk. Anaphe silk is used in velvet and plush.

3.2.2.6 Fagara Silk

Fagara is obtained from the giant silk moth *Attacus atlas* L. and a few other related species or races inhabiting the Indo-Australian biogeographic region, China, and the Sudan. They spin light-brown cocoons nearly 6 cm long with peduncles of varying lengths (2–10 cm).

3.2.2.7 Coan Silk

The larvae of *Pachypasa otus* D., from the Mediterranean biogeographic region (southern Italy, Greece, Romania, Turkey, etc.), feed primarily on trees such as pine, ash, cypress, juniper, and oak. They spin white cocoons measuring about 8.9×7.6 cm. In ancient times this silk was used to make the crimson-dyed apparel worn by the dignitaries of Rome; however, commercial production came to an end long ago because of the limited output and the emergence of superior varieties of silk.

3.2.2.8 Mussel Silk

Where the non-mulberry silks previously described are of insect origin, mussel silk is obtained from a bivalve, *Pinna squamosa*, found in the shallow waters along the Italian and Dalmatian shores of the Adriatic. The strong brown filament or byssus is combed and then spun into a silk popularly known as "fish wool." Its production is largely confined to Taranto, Italy.

3.2.2.9 Spider Silk

Spider silk is another non-insect variety. It is not only soft and fine but also strong and elastic. The commercial production of this silk comes from certain Madagascan species, including *Nephila madagascariensis*, *Miranda aurantia*, and *Eperia*. The spinning tubes (spinerules) are in the fourth and fifth abdominal part to a frame, from which the accumulated fiber is reeled out four or five times a month.

Because of the high cost of production, spider silk is not used in the textile industry; however, durability, resistance to extremes of temperature, and humidity make it indispensable for cross hairs in optical instruments [1].

3.2.3 Fine Structure of Silk

Silk fibers (*B. mori*) spun out from silkworm cocoons consist of fibroin in the inner layer and sericin in the outer layer. Each raw silk thread has a lengthwise striation, consisting of two fibroin filaments of 10–14 m each embedded in sericin. The chemical compositions are, in general, silk fibroin of 75–83%, sericin of 17–25%, waxes of about 1.5%, and others of about 1.0% by weight. Silk fibers are biodegradable and highly crystalline with well-aligned structure. It has been known that they also have higher tensile strength than glass fiber or synthetic organic fibers, good elasticity, and excellent resilience. Silk fiber is normally stable up to 140 °C, and the thermal decomposition temperature is greater than 1500 °C. The densities of silk fibers are in the range of 1320–1400 kg/m^3 with sericin and 1300–1380 kg/m^3 without sericin. Silk fibers are also commercially available in a continuous fiber type.

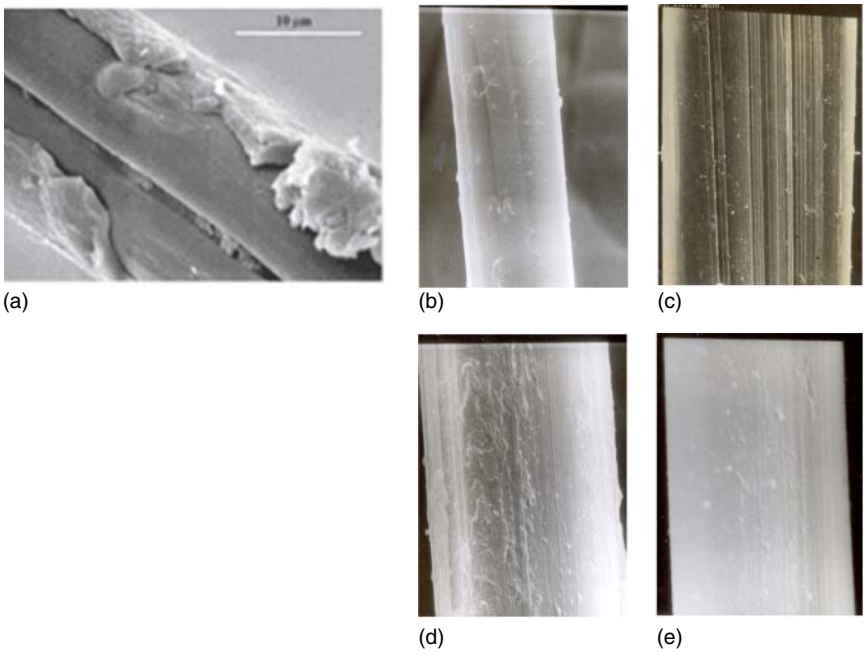


Figure 3.7 (a) Longitudinal view of silk fibers (undegummed). Longitudinal view of silk fibers (degummed). (b) Mulberry. (c) Tasar. (d) Muga. (e) Eri.

3.2.3.1 Longitudinal View

Scanning electron micrographs of longitudinal views of undegummed and degummed silk fibers are presented in Figure 3.7a,b, respectively.

It may be observed that mulberry silk shows a more or less smooth surface (Figure 3.7b), whereas non-mulberry silks such as tasar, muga, and eri (Figure 3.7c–e) all have striations on their surface compared with mulberry.

3.2.3.2 Cross-Sectional View

Scanning electron micrographs of cross section of silk fibers are presented in Figure 3.8. The cross section of silk fiber, which is made up of two types of protein, namely, sericin and fibroin, is shown in figure. It is found that two strands of fibroin filaments are enveloped by nonfibrous sericin. When a strand of fibroin filament is enlarged for its inner structure, it appears like a bundle of fibrils in which a large number of fibrils are accumulated [20].

There are variations depending upon the variety of silkworms and also among the individual cocoons. It may be observed that, in this respect, the mulberry and non-mulberry silks exhibit an altogether different cross-sectional morphology. The mulberry silks show a more or less triangular cross section and a smooth surface (Figure 3.8a). Among the non-mulberry varieties, tasar and muga exhibit an elongated rectangular- or a wedge-shaped cross section and a large cross-sectional area (Figure 3.8b,c). The eri silk has a more or less triangular shape (Figure 3.8d).

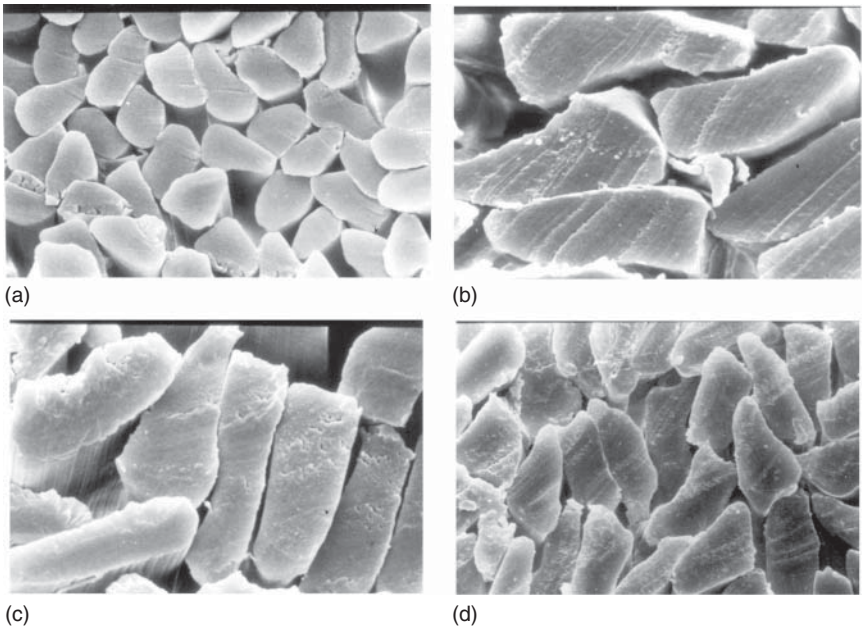


Figure 3.8 Cross-sectional view of silk fibers (degummed). (a) Mulberry. (b) Tasar. (c) Muga. (d) Eri.

Usually in the case of the cocoon fibers of domestic silkworms like mulberry and eri, the cross section is irregular ranging from triangular shape to circular shape. Moreover, even in the same fibroin filament, there are variations in the cross-sectional area depending upon the level of the cocoon layer.

3.2.4 Amino Acid Composition

The amino acid composition varies in different varieties of silk. Three major amino acids such as serine, glycine, and alanine may be found in mulberry and non-mulberry varieties. Among the other major amino acids present are tyrosine and valine. In general, in mulberry silks, glycine, alanine, and serine together constitute about 82%, of which about 10% is serine. Tyrosine and valine may be considered next to these at about 5.5% and 2.5%, respectively. The overall composition of acidic amino groups (i.e. aspartic and glutamic acids) in the mulberry variety is greater than that of the basic amino acids. The other important aspect is the composition of amino acids with bulkier side groups. The presence of bulky side groups can hamper close packing of molecules and hinder crystallization process. In general, a large portion of the mulberry fibroin is made up of simple amino acids such as glycine and alanine, suggesting a favorable condition for crystallization [21].

Compared with the mulberry silks, the total amount of glycine, alanine, and serine constitute about 73% in the non-mulberry variety, less by about 10%. All the non-mulberry silks exhibit a high proportion of alanine compared with that in the mulberry variety. The proportion of alanine is about 34% in tasar, 36% in eri,

Table 3.3 Amino acid composition of silk fibers.

Amino acid composition (mol%)				
Amino acid	***Bombyx mori* (mulberry)**	***Antheraea mylitta* (tasar)**	***Antheraea assama* (muga)**	***Philosamia ricini* (eri)**
Aspartic acid	1.64	6.12	4.97	3.89
Glutamic acid	1.77	1.27	1.36	1.31
Serine	10.38	9.87	6.11	8.89
Glycine	43.45	27.65	28.41	29.35
Histidine	0.13	0.78	0.72	0.75
Arginine	1.13	4.99	4.72	4.12
Threonine	0.92	0.26	0.21	0.18
Alanine	27.56	34.12	34.72	36.33
Proline	0.79	2.21	2.18	2.07
Tyrosine	5.58	6.82	5.12	5.84
Valine	2.37	1.72	1.5	1.32
Methionine	0.19	0.28	0.32	0.34
Cystine	0.13	0.15	0.12	0.11
Isoleucine	0.75	0.61	0.51	0.45
Leucine	0.73	0.78	0.71	0.69
Phenylalanine	0.14	0.34	0.28	0.23
Tryptophan	0.73	1.26	2.18	1.68
Lysine	0.23	0.17	0.24	0.23

and 35% in muga. This value is consistent but is lower than that particularly for muga (~44%). On the other hand, the glycine content in these varieties is about 27–29%, which is lower than that found in the mulberry varieties (~43%).

In addition, the non-mulberry varieties have a substantial proportion of amino acids with bulky side groups, especially aspartic acid (4–6%) and arginine (4–5%), which means that not only the acidic but also basic amino acid levels are greater. It is interesting to note the presence of sulfur-containing amino acids (i.e. cystine and methionine) in all the varieties of silk. Methionine content in non-mulberry silks is slightly higher (0.28–0.34%) compared with that found in mulberry varieties (0.11–0.19%), whereas the cystine content is comparable [21]. Amino acid composition of different varieties of silk is presented in Table 3.3.

3.2.5 Properties of Silk Fibers

3.2.5.1 Tensile Properties

The tensile properties of different varieties of silks in terms of tenacity, elongation at break, and initial modulus have been determined by a number of workers [22–26].

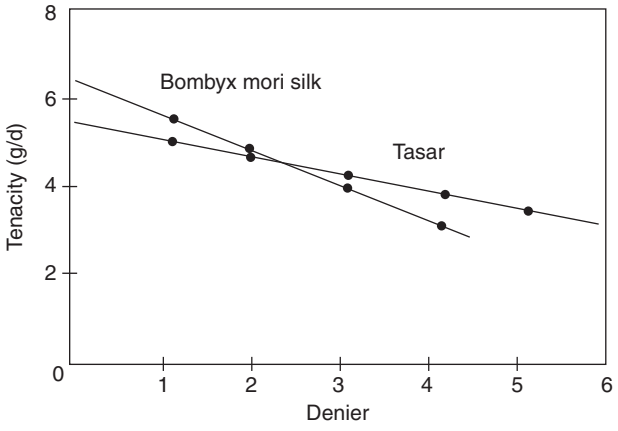


Figure 3.9 Tenacity vs. denier thread relationship.

Studies conducted on some mulberry and non-mulberry varieties by E. Iizuka et al. reveal that the tenacity, elongation at break, and modulus are all dependent on the linear density of the filament and the linear density or the mean size in turn depends on the silkworm race. The tenacity is found to be linearly related to the linear density of the filament (Figure 3.9). The correlation is negative, i.e. as the linear density increases, tenacity decreases. Similar trend has been observed for modulus too. Elongation on the other hand increases with an increase in linear density.

The tenacity ranges from 2.5 to 4.82 g/d for Japanese and Chinese mulberry varieties, 2.4–4.32 g/d for Indian mulberry varieties, and 3.74–4.6 g/d for Indian tasar varieties [25]. In a study on chemical structure and physical properties of *A. assama* (muga) silk, it has been reported that the tenacity of muga varies from 3.2 to 4.95 g/d [22, 24]. Another important non-mulberry variety, eri, showed lowest tenacity value, ranging from 2.3 to 4.0 g/d [26].

Elongation at break, on the other hand, showed a higher value for all the non-mulberry silks compared with mulberry varieties. The values range from 31% to 35% for tasar, 34% to 35% for muga, and 29% to 34% for eri silks, respectively. The elongation values for mulberry varieties ranged from 19% to 24%. Some of the mechanical properties of different varieties of silk are summarized in Table 3.4.

3.2.5.2 Optical Properties

Silk fibroin extracted from silkworm cocoons is a unique biopolymer that combines biocompatibility and implantability, along with excellent optical properties. Silk may be used as an optical material for applications in biomedical engineering, photonics, and nanophotonics. Silk can be nanopatterned with features smaller than 20 nm. This allows manufacturing of structures such as (among others) holographic gratings, phase masks, beam diffusers, and photonic crystals out of a pure protein film. The properties of silk allow these devices to be "biologically activated" offering new opportunities for sensing and biophotonic components.

Table 3.4 Mechanical properties of different varieties of silk.

Variety	Sex	Dynamic modulus (10^{10} dyn/cm^2)	tan δ	Tenacity (g/d)	Elongation (%)
Shunreix shougetsu (mulberry)	M	1.847	—	5.265	20.36
	F	1.808	—	5.207	21.48
A. mylitta (tropical tasar)	M	1.132	0.030	3.412	31.36
	F	1.087	0.035	3.256	31.12
A. proylei (temp. tasar)	M	1.305	0.023	4.123	31.45
	F	1.087	0.025	4.128	31.48
A. assama (muga)	M	1.205	0.020	3.170	34.83
	F	1.230	0.023	3.823	34.10

Many interesting bio-optical devices can be fabricated by doping silk films with fluorescent materials (such as quantum dots shown above). Ways can be explored to enhance the light emission by patterning the silk film surfaces, as well as making tunable wavelength devices and printing specific patterns on silk film surfaces.

Luster associated with silk is due partly to the influence on the pattern of light – reflection of its triangular shape. In an attempt to understand the optical properties of silk, many researchers have determined the refractive index and birefringence of fibers. The refractive index of silk generally varies through its cross section. The birefringence (n) value varies from 0.051 to 0.0539, mulberry silk and 0.030 to 0.034 for non-mulberry silks [27].

3.2.5.3 Viscoelastic Behavior

Silk fiber exhibits viscoelastic behavior. Time-dependent mechanical properties of silk fibers such as stress relaxation, creep, creep recovery, etc. have also been the subject of interest. Creep is a phenomenon associated with time-dependent extension under an applied load. The complementary effect is stress relaxation under a constant extension.

Creep and stress relaxation behavior of silk has been reported [28]. The instantaneous extension and secondary creep are both higher for tasar silk compared with those for mulberry silk. The stress relaxation was also found to be more in non-mulberry silks than in mulberry silk.

Silk has also been shown to exhibit inverse stress relaxation phenomenon [28]. The inverse relaxation could be observed for both mulberry and tasar silks when the level of strain was maintained below a certain value. Inverse relaxation becomes higher with the increase in peak tension. Cyclic loading has been found to reduce the extent of inverse relaxation.

3.2.6 Applications

Silk is one of the most beautiful fabrics available, with a long and colorful history and changing applications in the world today. Be it for gowns, medical use, home decor, and more, the use of silk is a wide and varied topic.

3.2.6.1 Textile and Apparels

Silk's good absorbency makes it comfortable to wear in warm weather and while active. Its low conductivity keeps warm air close to the skin during cold weather. It is often used for clothing such as shirts, blouses, formal dresses, high fashion clothes, negligees, pajamas, robes, skirt suits, sundresses, and kimonos. Silk's elegant, soft luster and beautiful drape makes it perfect for many furnishing applications. It is used for upholstery, wall coverings, window treatments (if blended with another fiber), rugs, bedding, and wall hangings.

Silk has several uses in daily life. It is a common cloth used for high-end garments, including wedding gowns and blouses. It appears frequently in accessories like handbags and headbands and scarves. Because of its luster and texture, it also is commonly used for home decoration, especially as sheets, bedding, curtains, and cushions. It is also used for warmth and skiing garments because of its remarkable ability to retain heat; paradoxically, it also is a popular summer cloth because it keeps the wearer cool in warmer weather.

Silk continues to be used as a material to produce fine dresses. Chinese women continue to have their wedding cheongsam dresses made out of silk. They choose this material because it is one of the finest materials known in ancient Chinese culture. Delicately woven dragons, flowers, and butterflies are sewn into the silk dresses. The material is thick so it allows a woman to look leaner and have cleaner lines. Additionally, the shininess of the material is very flattering and alluring. Women's evening gowns are also made of silk. It also falls well and is a material that is slightly warmer allowing the women's body to feel a bit of warmth, even as she wears a sleeveless gown in the winter.

Silk shirts remain popular among women. Especially for women's blouses, silk is a great material. It is seen as more classic and flattering since it drapes a woman's body. Additionally, the thinness of the material allows women to easily tuck the shirt into their skirts or wear a jacket on top without having the jacket look bulky. For men, silk shirts are becoming more and more popular. Men have started wearing silk short sleeve shirts as well as long sleeve shirts. Men used to only wear silk shirts for the evening, but the lightness of the material has made it a popular alternative to cotton.

Silk is also used very frequently for pajamas. Silk pajamas feel soft and smooth and very comfortable while sleeping. Both men's and women's pajamas are now made of this fine thread. For women, silk is often used to make lingerie as well. Using this fine thread has become a great option since it is smooth, tends not to catch on your hair, and is very breathable for the body.

Silk scarves have also been around for a long time. The number of gorgeous patterns and designs on the scarves has made these items very expensive. Women tend to tie the scarf around their necks for warmth and for style. Men tend to carry one in their pocket as an alternative to the cotton handkerchief. Be prepared to pay more for a silk scarf with a fancy design.

More and more, manufacturers of bedding have started to make silk sheets and silk pillowcases. The health benefits of silk are starting to be more widely known. Sleeping on them helps prevent coughing and sneezing, especially for those allergic to dust mites who do not like silk. Additionally, sleeping on silk sheets is sometimes beneficial to women's hair, helping it to have less tangles and

less split ends. Beyond the solid color sheets, many makers of luxurious bedding are now offering their own version of sheets with lots of different patterns and designs in stores.

Silk has come a long way since the Silk Road. It is still a highly sought-after material. Having pieces of fine clothing or a scarf or even a silk sheet is often seen as the ultimate extravagance.

3.2.6.2 Biomedical Field

Silk, and especially *B. mori* silk, has a very long history in biomedical applications. In recent years, the reported exceptional nature of silk leads to increased interest in silk for biomedical applications [29]. Silk fibroin has been increasingly studied for new biomedical applications due to the biocompatibility, slow degradability, and remarkable mechanical properties of the material. In addition, the ability to now control molecular structure and morphology through versatile processability and surface modification options has expanded the utility for this protein in a range of biomaterial and tissue engineering applications. Silk fibroin in various formats (films, fibers, nets, meshes, membranes, yarns, and sponges) has been shown to support stem cell adhesion, proliferation, and differentiation in vitro and promote tissue repair in vivo. In particular, stem cell-based tissue engineering using 3D silk fibroin scaffolds has expanded the use of silk-based biomaterials as promising scaffolds for engineering a range of skeletal tissues like bone, ligament, and cartilage, as well as connective tissues like skin [30]. More recent studies with well-defined silkworm silk fibers and films suggest that the core silk fibroin fibers exhibit comparable biocompatibility in vitro and in vivo with other commonly used biomaterials such as polylactic acid and collagen [3].

Silk from the silkworm *B. mori* has been used as biomedical suture material for centuries. The unique mechanical properties of these fibers provide important clinical repair options. Silk has been used in native fiber form as sutures for wound ligation and became the most common natural suture, surpassing collagen over the past 100 years [3]. Silk sutures are used in ocular, neural, and cardiovascular surgeries, as well as a variety of other tissues in the body. Silk's knot strength, handling characteristics, and the ability to lie low to the tissue surface make it a popular suture in cardiovascular applications. The above features of silk fibroin have led to the recent emergence of silk-based biomaterials for a wide range of cell and tissue studies such as scaffolds, films, sponges, hydrogels, bone materials, cardio vascular devices, etc.

3.2.6.3 Fiber-Reinforced Composites

Silk is a fiber with remarkable mechanical properties. This unique characteristic of silk has led its use in fiber-reinforced composites for various applications. Silk yarn is easily available as the waste product of textile industry, so the composite is cost effective and perfect utilization of waste product. Though the silk is extensively used as a valuable material for textile purposes, in recent years it is being widely considered as a reinforcing material for composites made from epoxy and other biodegradable biopolymeric resins. The organization of silk fibers can contribute significantly to the impact resistance by ensuring either or both a sufficient strength of the composite and a good deformability of the composite.

3.3 Future Trends

With improved analytical techniques, together with the tools of biotechnology, a new generation of silk-related materials is envisioned that depart from traditional textiles and medical sutures, which are currently the focus for these materials. These proteins are already finding broadened applications in medical fields as biomaterials. The unique and remarkable mechanical properties of silks have already prompted studies for their application in high-performance materials, as well as modes to mimic these features through more traditional synthetic organic polymer chemistry routes. Since the specifics of the silks can be modulated through genetic manipulation, through processing and through choice of starting protein, a great deal of control of structure, morphology, and functional attributes in materials derived from these proteins can be obtained. This control is already exploited in the biomaterials arena and suggests that this family of novel proteins can serve as an important blueprint for understanding structure–function relationships as well as for new and novel materials. A number of consumer products are already promulgated based on silks, including cosmetics, hair replacements, and shampoos, among others. Sutures, biomaterials for tissue repairs, wound coatings, artificial tendons, bone repair, and related needs may be possible applications since silks are biocompatible and slowly degrade in the human body. Genetically engineered silks have also been commercialized as cell culture plate coatings to improve cell adhesion. Genetic variants of silks are also actively pursued as controlled-release systems to deliver pharmaceuticals in a variety of systems.

New trends in production and applications of silk have to be deployed for maintaining a sustainable market for silk. As a result researchers in Japan have developed fluorescent silks. The world's first silks exhibiting fluorescence and other pioneering properties have been successfully developed as a result of transgenic silkworm research conducted by Japanese researchers. Fluorescent silk thread is made by pulling threads from cocoons made by silkmoth larvae (silkworms). Researchers have now developed three lines of transgenic silkworms. The first line produces silk threads that emit green, red, or orange fluorescent light. These threads were created by introducing into silkworm egg genes that promote the generation of fluorescent proteins. It has been possible to achieve green fluorescence using genes extracted from jellyfish, a technique developed by Nobel Prize-winning chemist Osamu Shimomura, and red and orange fluorescence with genes extracted from coral, a technique that has already been used in commercial applications. The fluorescent silk threads have great potential for use in the fashion industry, and there is expected to be considerable demand for them from producers of high-end apparel.

Though the traditional practices make silk to construct only textiles, the new approach extends its application toward nutritional, cosmetic, pharmaceutical, biomaterial, biomedical and bioengineering, automobile, house building, and art craft applications. The inclination rightly suits to silk due to faster production rate and increasing global demand for its variable eco-friendly composites and viable contributing impact on value, employment, and environmental safety. This move, however, requires more of awareness among stakeholders, trainings, and

idea exchange between entrepreneurs, besides service accessibility to consumers. The celebration of International Year of Natural Fibres 2009 will create awareness on insect-based natural fiber, silk for its continued use, and innovative research during the year and beyond.

3.4 Summary

Although substitution of natural materials has been underway for several decades, natural silks remain commercially important because of their unique properties, as well as their relative environmental stability and biocompatibility and consumer preferences. The industries should look at the utilization of silk fiber in total for innovative marketable products of modern society's application and appreciation, which facilitate its all-round development. Though, traditionally, silk is used for making textiles, the new approaches must be attempted to extend the application of silk in nutritional, cosmetic, pharmaceutical, biomedical and bioengineering, automobile, house building, and art craft products. During the past decade a great deal of progress has been made in understanding silk genetic and protein structures. On the other hand, materials scientists have long been fascinated by structure–function relationships in silk proteins. Since the exploration of biomaterial applications for silks, aside from sutures, is only a relatively recent advance, the future for this family of structural proteins to impact clinical needs appears promising.

References

1 Jolly, M.S., Sen, S.K., Sonwalker, T.N., and Prasad, G.K. (1979). Non-mulberry silks. In: *Manual on Sericulture* (eds. G. Rangaswami, M.N. Narasimhanna, K. Kashivishwanathan, et al.), 1–178. Rome: Food and Agriculture Organization of the United Nations.
2 Spring, C. and Hudson, J. (2002). *Silk in Africa*. Seattle, WA: University of Washington Press.
3 Altman, G.H., Diaz, F., Jakuba, C. et al. (2003). Silk-based biomaterials. *Biomaterials* 24: 401–416.
4 Craig, C.L. (1997). Evolution of arthropod silks. *Annual Review of Entomology* 42: 231–267.
5 Craig, C.L., Hsu, M., Kaplan, D., and Pierce, N.E. (1999). A comparison of the composition of silk proteins produced by spiders and insects. *International Journal of Biological Macromolecules* 24: 109–181.
6 Sheu, H.S., Phyu, K.W., Jean, Y.C. et al. (2004). Lattice deformation and thermal stability of crystals in spider silk. *International Journal of Biological Macromolecules* 34: 325–331.
7 Becker, N., Oroudjev, E., Mutz, S. et al. (2003). Molecular nanosprings in spider capture-silk threads. *Natural Materials* 2: 278–283.
8 Bell, F.I., McEwen, I.J., and Viney, C. (2002). Fibre science: supercontraction stress in wet spider dragline. *Nature* 416: 37.

9 Carboni, P. (1952). *Silk, Biology, Chemistry and Technology*. London: Chapman & Hall Ltd.

10 Tanaka, K., Kajiyama, N., Ishikura, K. et al. (1999). Determination of the site of disulfide linkage between heavy and light chains of silk fibroin produced by *Bombyx mori*. *Biochimica et Biophysica Acta (BBA) - Protein Structure and Molecular Enzymology* 1432: 92–103.

11 Zhou, C.Z., Confalonieri, F., Medina, N. et al. (2000). Fine organization of Bombyx mori fibroin heavy chain gene. *Nucleic Acids Research* 28: 2413–2419.

12 Asakura, T. and Kaplan, D.L. (1994). Silk production and processing. In: *Encyclopedia of Agricultural Science*, vol. 4 (eds. C.J. Arntzen and E.M. Ritter), 1–11. New York: Academic Press.

13 Asakura, T., Yao, J., Yamane, T. et al. (2002). Heterogeneous structure of silk fibers from *Bombyx mori* resolved by ^{13}C solid-state NMR spectroscopy. *Journal of the American Chemical Society* 124: 8794–8795.

14 He, S.J., Valluzzi, R., and Gido, S.P. (1999). Silk I structure in *Bombyx mori* silk foams. *International Journal of Biological Macromolecules* 24: 187–195.

15 Yao, J. and Asakura, T. (2004). Silks. In: *Encyclopedia of Biomaterials and Biomedical Engineering*, 1363–1370. Marcel Dekker Inc.

16 Sonthisombat, A. and Speakman, P.T. (2004). *Silk: Queen of Fibres - The Concise Story by Speakman*. Department of Textile Engineering, Faculty of Engineering, Rajamangala University of Technology Thanyaburi (RMUTT).

17 Mahadevappa, D., Halliyal, V.G., Shankar, D.G., and Bhandiwad, R. (2001). *Mulberry Silk Reeling Technology*. India: Oxford and IBH Publication Co.

18 Dhavalikar, R.S. (1962). Amino acid composition of Indian silk fibroins and sericins. *Journal of Science and Industrial Research* 21(C): 261–263.

19 Sonwalker, T.N. (1969). Investigations on degumming loss and spinning performance of pierced and cut cocoons in silk worm, *Bombyx Mori*-L. *Indian Journal of Sericulture* 7 (1): 61.

20 Minagawa, M. (2000). *Structure of Silk Yarn*, vol. I (ed. N. Hojo), 185–208. New Delhi: Oxford & IBH Publishing Co. Pvt. Ltd.

21 Sen, K. and Murugesh Babu, K. (2004). Studies on Indian silk. I. Macrocharacterization and analysis of amino acid composition. *Journal of Applied Polymer Science* 92: 1080–1097.

22 Freddi, G., Gotoh, Y., Mori, T. et al. (1994). Chemical structure and physical properties of *antheraea assama* silk. *Journal of Applied Polymer Science* 52: 775–781.

23 Iizuka, E. (1994). Physical properties of antheraea silks. *International Journal of Wild Silkmoth and Silk* 1 (2): 143–146.

24 Iizuka, E., Okachi, Y., Shimizu, M. et al. (1993). Chemo and bioassay of high yielding triploids and diploids of mulberry (*Morus* Spp.). *Indian Journal of Sericulture* 32 (2): 175–183.

25 Iizuka, E. (1995). Size dependency of the physical properties of *Bombyx* silk. *Journal of Sericultural Science of Japan* 65 (2): 102–108.

26 Iizuka, E. and Itoh, H. (1997). Physical properties of eri **silk**. *International Journal of Wild Silkmoth and Silk* 3: 37–42.

27 Tsukada, M., Freddi, G., Minoura, N., and Allara, G. (1994). Preparation and application of porous silk fibroin materials. *Journal of Applied Polymer Science* 54: 507–514.
28 Das, S. (1996). Studies on tasar silk. PhD thesis. IIT, Delhi.
29 Hakimi, O., Knight, D.P., Vollrath, F., and Vadgama, P. (2007). Spider and mulberry silkworm silks as compatible biomaterials. *Composites Part B: Engineering* 38: 324–337.
30 Wang, Y., Kim, H.-J., Vunjak-Novakovic, G., and Kaplan, D.L. (2006). Stem cell based tissue engineering with silk biomaterials. *Biomaterials* 27: 6064–6082.
31 Guljarni, M.L. (1992). Degumming of Silk. *Review of Progress in Colouration.* 22: 79–89.

4

Cellulose Fibers

Feng Jiang

University of British Columbia, Department of Wood Science, Sustainable Functional Biomaterials Lab, 2424 Main Mall, Vancouver, BC, Canada

4.1 Introduction

Cellulose, as the most abundant polymeric material on Earth with approximately 75 billion tons annual production, originates from varied sources including plants, marine animals (tunicates), bacteria, fungi, algae (*Cladophora* green algae), and protozoans, with plants being the dominant source [1, 2]. The term "cellulose" was first introduced in 1839 by scientists in French Academy of Sciences to describe the solid fibrous substance in plant tissues that is insoluble in acids, ammonia, alcohol, and ether, which was first discovered by the French chemist Anselme Payen in the prior year [3]. Among all fibrous substance, cellulose fiber is one of the earliest materials being utilized in daily life, either as building and clothing materials thousands of year ago or as chemical raw materials for the past 150 years. In fact, cellulose nitrate through esterification reaction with nitric acid has been widely recognized as the first thermoplastic polymer that, when plasticized by camphor, was marketed by Hyatt Manufacturing Company as "celluloid" in 1870 [3, 4].

4.2 Structure and Biosynthesis of Cellulose

Although cellulose has been discovered and utilized as chemical raw material in the nineteenth century, its structure was not completely revealed until 1920s when Hermann Staudinger discovered that small molecules could link with each other via primary valence bonds to form macromolecules [5, 6]. Cellulose, with the molecular formula of $C_6H_{10}O_5$, has been well accepted as a type of linear homopolymer consisting of β-D-glucopyranose repetitively linked together through C4 and anomeric C1 hydroxyl groups via β-1-4 glycosidic linkage, irrespective of its origins [3, 7–9]. In cellulose chain, the glucopyranose unit adopts a $^4C_1$ chair conformation with adjacent unit rotating 180° with each other, forming a cellobiose repeating unit with 10.3 Å distance (Figure 4.1). The linear chain structure is stabilized by two types of intramolecular hydrogen

Handbook of Fibrous Materials, First Edition. Edited by Jinlian Hu, Bipin Kumar, and Jing Lu.
© 2020 Wiley-VCH Verlag GmbH & Co. KGaA. Published 2020 by Wiley-VCH Verlag GmbH & Co. KGaA.

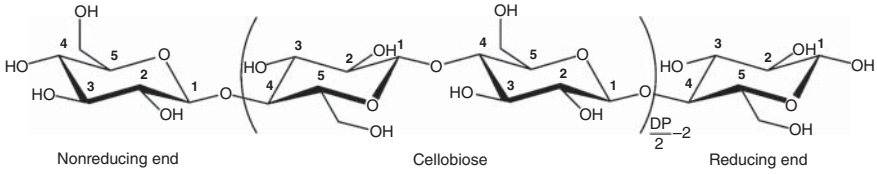


Figure 4.1 Molecular structure of cellulose showing repeating cellobiose unit, reducing and nonreducing ends. Source: Habibi et al. 2010 [2]. Reprinted with permission of American Chemical Society.

bonds, originating from O(3′)-H hydroxyl to O(5) ring oxygen and O(2)-H hydroxyl to O(6′) hydroxyl. The degree of polymerization (DP) of cellulose is highly dependent on the source, varying from 500 to 2000 for wood pulp, 10 000–15 000 for cotton, and as high as 44 000 for *Valonia* [5, 10]. Besides, the DP is also subject to change from chemical treatment, rendering lowered value of 250–500 for regenerated cellulose and 150–300 for acid-hydrolyzed microcrystalline cellulose [3, 11]. Condensation polymerization between C_4 and anomeric C_1 hydroxyls linked glucose unit in a unidirectional fashion that the cellulose chain is chemically asymmetric with one end adopting a reducing hemiacetal group (C_1) and another bearing a nonreducing hydroxyl group (C_4), regardless of the chain length.

Cellulose biosynthesis has been proposed to through multiple subunits cellulose synthases according to Preston's "ordered granule hypothesis" in 1964 [12], which was not confirmed until Brown and Montezinos observed linearly organized terminal complexes (TCs) at the end of cellulose microfibrils in the freeze fracture of plasma membrane from green algae *Oocystis apiculata* in 1976 [13]. These linear TCs are mostly found in varied algae species, such as *Valonia*, *Boergesenia*, *Glaucocystis*, *Erythrocladia*, and *Vaucheria* [14]. From the electron microscopy images of freeze-fracture surface of *Zea mays* plasma membrane, Mueller et al. successfully observed globular TCs composed of subunits associated at the end of cellulose microfibrils [15]. Rosette-shaped TCs were further confirmed, presenting as sixfold symmetrical subunits aggregates in the corn mesocotyl plasma membrane [16]. The rosette TC is predominantly present in all land plants including mosses, ferns, higher plants, and advanced algae [14]. Each rosette TC is composed of six subunits, arranged in hexagonal shape with average diameter of 25–30 nm in the plasma membrane, with each subunit having a diameter of approximately 8 nm (Figure 4.2a) [17, 19, 20]. Cellulose biosynthesis in rosette TC is through cellulose synthase enzyme (CeSA), which polymerizes glucan chains at the nonreducing end (Figure 4.2b). A hexamer of CeSAs is present within one rosette subunit, and with a sixfold subunit rosette, 36 glucan chains could be extruded and bound with each other to form cellulose microfibrils [18, 20]. The width of the microfibrils with 36 glucan chains is around 3.5 nm for higher plant [20], whereas 1200–1400 perfectly packed glucan chains assembled into 28 nm wide single crystal has also been reported in *Valonia macrophysa* [21].

Glucan chains, once being extruded from CeSA via polymerization of UDP-α-glucose, do not present as individual molecules or fold into more thermodynamically stable cellulose II crystalline structure. Instead, the glucan

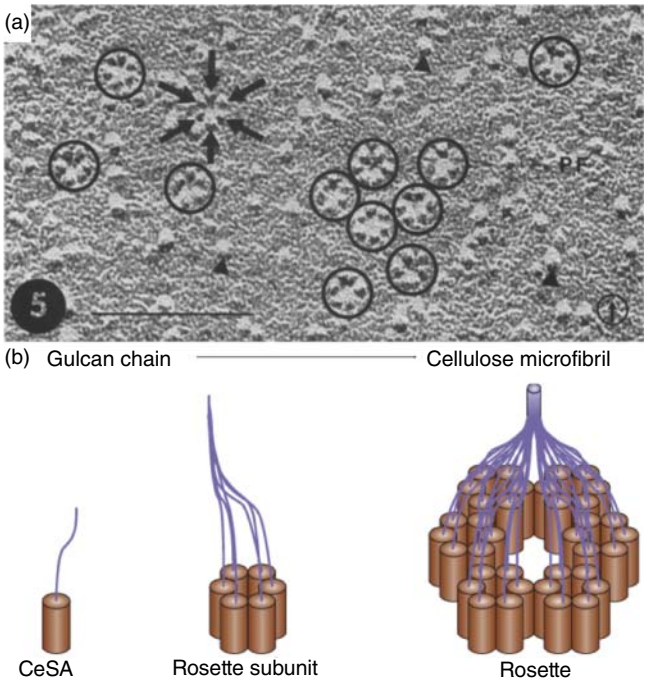


Figure 4.2 (a) Plasmatic fracture face of plasma membrane of a developing xylem vessel elements in root of cress, *Lepidium sativum* L., showing rosette TCs with six subunit (arrows) and irregular clustering (encircled rosettes) (magnification: 430 000×). Source: Herth 1985 [17]. Reprinted with permission of Springer-Verlag. (b) Schematic of cellulose synthesis from rosette TCs. Each rosette TC is comprised of six subunits, each of which contains hexamer of CeSA. A single β-(1,4)-glucan chain is synthesized from each CeSA, which is bound into six-chain fibrils. Within the rosette TC, 36 glucan chains could assemble into cellulose microfibrils. Source: Cosgrove 2005 [18]. Reprinted with permission of JSPP.

chains synthesized within the same TCs tend to crystallize with each other to form cellulose I crystalline structure. The preferential adoption of less stable cellulose I structure over the thermodynamically more stable cellulose II in native cellulose suggests that the crystalline structure could be confined by the synthetic TCs, limiting chain mobility by immediate crystallization following chain polymerization [7]. Depending on the source of cellulose, the native cellulose I crystalline structure includes two types of polymorphs of Iα and Iβ [22, 23]. In general, Iα-rich structure could be found in cellulose secreted by algae [23, 24] and bacteria [23, 25], accounting for as high as 64% of the crystalline polymorphs [25, 26]. However Iβ is predominantly present in higher plant [27] or the exclusive polymorph in tunicate [28]. Cellulose Iα is less thermodynamically stable than cellulose Iβ and could be transformed to Iβ by annealing at high temperature (260 °C) steam [29], NaOH solution [24], or varied organic solvents [30].

Both cellulose Iα and Iβ coexist in most of native cellulose, except in tunicate [31] or hydrothermally annealed *Valonia* cellulose [32] where pure Iβ crystal

structure could be observed. Electron diffraction of tunicate or annealed *Valonia* cellulose showed symmetric diffraction spots patterns in the four quadrants, corresponding to a two-chain $P2_1$ monoclinic unit cell for cellulose Iβ [31]. The unit cell of Iβ has dimensions of $a = 0.801$ nm, $b = 0.817$ nm, c (chain axis) $= 1.036$ nm, $\alpha = \beta = 90°$, $\gamma = 97.3°$, cell volume $= 0.6725\,\text{nm}^3$, and density of $1.599\,\text{g/cm}^3$ (Figure 4.3a,b) [34]. However, electron diffraction of *Valonia* and *Microdictyon tenuous* cellulose showed extra diffraction spots other than the monoclinic unit cells observed in tunicate, asymmetrically distributed in the four quadrants in every layers except for the equator [31].

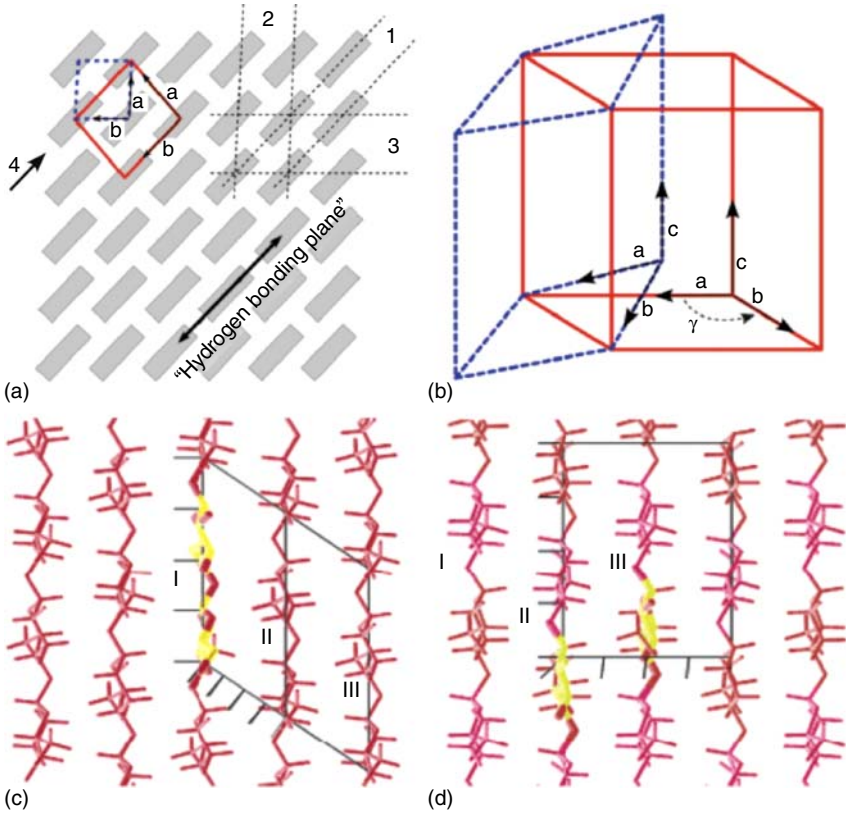


Figure 4.3 Schematic of unit cells for cellulose Iα (triclinic, dashed line) and Iβ (monoclinic, solid line). (a) Cross-sectional projection along the *c*-axis of a 36-chain cellulose I crystals showing parallelogram shape of both unit cells. The glucan chains in cellulose I crystals are arranged in the same manner when looking down the *c*-axis, sharing the same lattice planes of 1, 2, and 3 with corresponding *d*-spacings of 0.39, 0.53, and 0.61. The lattice planes for 1, 2, and 3 are designated as $(110)_t$, $(010)_t$, and $(100)_t$ for Iα and $(200)_m$, $(110)_m$, and $(1\bar{1}0)_m$ for Iβ. (b) Relative configuration of one-chain triclinic unit cell (Iα, blue dashed line) and two-chain monoclinic unit cell (Iβ, red solid line). Source: Moon et al. 2011 [1]. Reprinted with permission of Royal Society of Chemistry. (c) Crystal structure of cellulose Iα. (d) Iβ perpendicular to the chain axis and in the plane of hydrogen-bonded sheet (110 for Iα and 200 for Iβ). The cellulose chains are represented by red skeletal models. Source: Nishiyama et al. 2003 [33]. Reprinted with permission of American Chemical Society.

These asymmetrical diffraction spots is from a one-chain P1 triclinic unit cell for cellulose Iα, with corresponding dimensions of $a = 0.674$ nm, $b = 0.593$ nm, c (chain axis) = 1.036 nm, $\alpha = 117°$, $\beta = 113°$, $\gamma = 81°$, cell volume = 0.3395 nm^3, and density of 1.582 g/cm^3 (Figure 4.3a,b) [34]. All glucan chains within cellulose I crystals are assembled in the so-called "parallel-up" fashion, indicating that the chains are oriented with the $1 \rightarrow 4$ glycosidic linkage pointing to the same positive c-axis direction of the unit cell. Although glucan chains packing within cellulose Iα and Iβ are nearly identical when looking down the c-axis, they have different displacement along the c-axis that helps to differentiate their structures, which could be visualized by looking perpendicular to the c-axis and along the hydrogen-bonded planes (Figure 4.3c,d). The second hydrogen-bonded sheet (II) in both cellulose Iα and Iβ shifted one quarter of c-axis "up" relative to the first sheet (I), whereas the third sheet (III) continuously shifted "up" and "down" relative to sheet II in cellulose Iα and Iβ, respectively [33]. Therefore, the cellobiose repeat units demonstrated a diagonally shifted arrangement in Iα and staggered arrangement in Iβ.

Besides the native cellulose I structure, there also exist another five different polymorphs (II, III_I, III_{II}, IV_I, and IV_{II}) that could be interconverted [7]. As mentioned in Section 4.2 on cellulose biosynthesis, cellulose I is not a thermodynamically stable state that the glucan chains prefer to form if not being regulated by the synthetic TCs. Instead, cellulose II is the most stable polymorph that could be irreversibly converted from cellulose I by either dissolution and regeneration or mercerization by sodium hydroxide solution [2, 3]. Cellulose II adopts a two-chain $P2_1$ monoclinic unit cell structure with dimensions of $a = 0.810$ nm, $b = 0.903$ nm, c (chain axis) = 1.031 nm, $\alpha = \beta = 90°$, and $\gamma = 117.10°$ [35]. In contrast to the parallel-up chain arrangement, cellulose II adopts antiparallel chain arrangement that could favor more stronger hydrogen-bonding patterns, leading to stable structure [7, 36]. Cellulose III_I and III_{II} could be obtained by treating the respective cellulose I and II with ammonia or amines, which could be further converted to cellulose IV_I and IV_{II} by heating up to 260 °C in glycerol [2].

The crystalline structure of native cellulose I is held together by both intra- and interchain hydrogen bonding. The intrachain O3–H···O5 hydrogen bonds are prevalent in both cellulose Iα and Iβ structure, but with different types of alteration in H···O bond distance and O–H···O bond angles (Figure 4.4) [33]. Within the two-chain monoclinic unit cell in cellulose Iβ, the alteration could be observed between origin and center chains, with respective bond distances of 1.966 and 1.752 Å and bond angles of 137.08° and 162.23°. However, in the one-chain triclinic unit cell structure of cellulose Iα, the alteration is down the same chains with the values of 2.072 and 1.954 Å for bond distances, as well as 137.59° and 163.94° for bond angles. Intrachain O2–H···O6 hydrogen bonds are also present in both cellulose Iα and Iβ, but with a shorter bond distance in the former case. These intrachain hydrogen bonds help to lock the glucosyl units in the opposite position to form a flat-ribbon chain configuration [37]. Interchain hydrogen bonds involving O6–H···O3 and O2–H···O6 could help to link the glucan chains edge to edge to form a flat sheet. However, the occurrence of these interchains hydrogen bonds is found to be at different chain position in cellulose Iβ (i.e. both are present in the center chains, whereas only O6–H···O3 is present

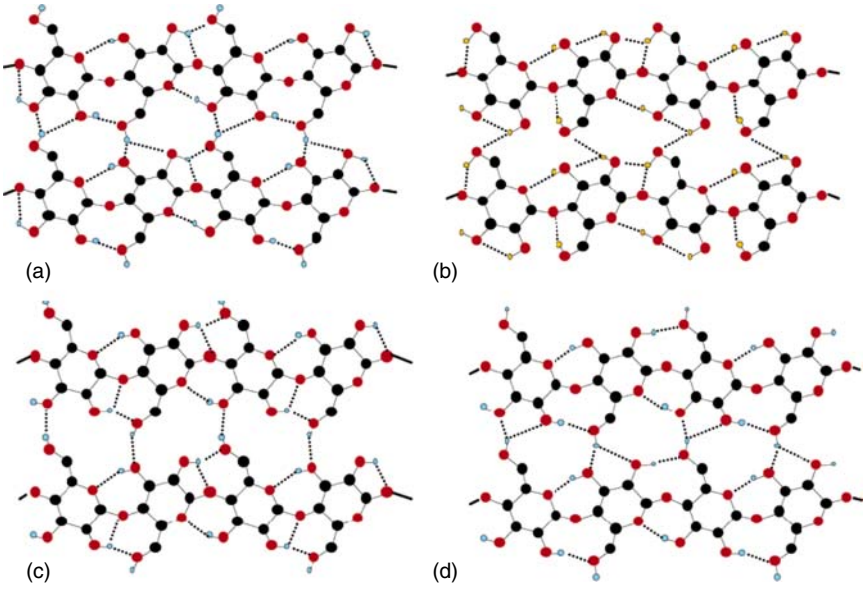


Figure 4.4 (a, b) The two alternative hydrogen-bond networks in cellulose Iα [33]. (c, d) The dominant hydrogen-bond network in cellulose Iβ: (c) chains at the origin of the unit cell; (d) chains at the center of the unit cell. Source: Sturcova et al. 2004 [37]. Reprinted with permission of American Chemical Society.

in the origin chains) or at dynamical balance in the same chains in cellulose Iα [38]. As all hydroxyls are located in the equatorial position of the glucopyranose rings, only intrachain and intrasheet hydrogen bonding could be formed in cellulose I, without signs of intersheet O–H· · ·O hydrogen bonding [39]. Therefore, the hydrogen-bonded sheets are assembled together by hydrophobic interactions and weak C–H· · ·O bonds [38, 40].

4.3 Nanoscaled Cellulose Fibers

Cellulose fiber represents a hierarchical structure consisting of fibers with progressively increased diameters, including the finest elementary fibrils of 1.5–3.5 nm wide, microfibrils of 10–30 nm wide, microfibrils bundles of 100 nm, and the macroscopic cellulose fibers on the order of microns (Figure 4.5) [3, 8]. With the aid of negative contrast electron microscopic technique, Muhlethaler has successfully observed finest fibrils with averaged 3.5 nm width along the axis [44], which was regarded as elementary fibrils following Frey-Wyssling's terminology [45]. Elementary fibrils have been considered as a universal structural unit in native cellulose that has been observed in varied sources including cotton, ramie, jute, and wood [43]. Microfibrils are assembled from the coalescence of these elementary fibrils to reduce the surface free energy, with general diameter of less than 35 nm [46]. The cellulose microfibrils are characterized as paracrystalline structures consisting of numerous cellulose I

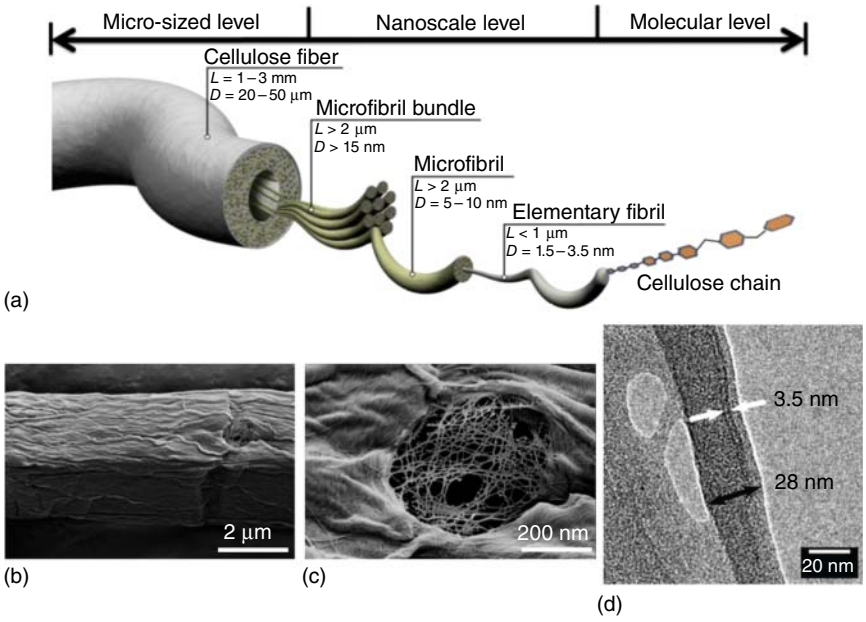


Figure 4.5 (a) Schematics of hierarchical structure of wood cellulose fibers. Source: Zhu et al. 2014 [41]. Reprinted with permission of Royal Society of Chemistry. SEM images of *Eucalyptus* fibers showing the (b) gross fiber surface and (c) microfibrils on the surface. Source: Chinga-Carrasco et al. 2011 [42]. Reprinted with permission of Microscopy Society of America. (d) TEM image of an individual microfibril of *Pinus radiata*. The black arrow indicates the boundaries of a microfibrils of 28 nm wide, and the white arrows indicate a single elementary fibrils of 3.5 nm wide. Source: Chinga-Carrasco 2011 [43]. Reprinted with permission of Springer.

crystallites stringed together by the amorphous cellulose chains. Both the degree of crystallinity and crystallite dimensions vary from different cellulose sources, with the algae cellulose generally having higher crystallinity and larger crystallite dimensions (Table 4.1).

Owing to the intermittent crystalline and amorphous regions, the cellulose microfibrils demonstrated superb flexibility owing to the amorphous chains, as well as high stiffness due to the highly crystalline crystallites. Young's modulus of crystalline cellulose Iβ has been reported in the range of 120–220 GPa, depending not only on the sources of origin but also the characterization techniques [1, 47, 48]. Young's modulus of long cellulose microfibrils or elementary fibril are also source and measurement technique dependent, with reported value of ~150 GPa for the tunicate microfibrils (8 nm thick and 20 nm wide) from three-point bending measurement by atomic force microscopy (AFM) [49] and 78 and 114 GPa for bacterial cellulose (BC) (30–90 nm wide) using the same AFM bending techniques [50] and Raman spectroscopic techniques [51], respectively. Although elastic modulus has been well characterized by either theoretical or experimental methods since the 1930s [52], mechanical strength of the cellulose microfibrils has been scarcely reported. The strength of cellulose microfibrils has only been recently estimated based on the model

Table 4.1 Degrees of crystallinity (x_c), crystallite sizes ($D_{(hkl)}$), and lateral dimensions (d) of microfibrils of native cellulose.

Cellulose source	x_c (%)	Crystallite sizes (nm)			d (nm)
		$D_{(110)}$	$D_{(110)}$	$D_{(020)}$	
Algal cellulose	>80%	10.1	9.7	8.9	10–35
Bacterial cellulose	65–79	5.3	6.5	5.7	4–7
Cotton linters	56–65	4.7	5.4	6.0	7–19
Ramie	44–47	4.6		5.0	3–12
Flax	44 (56)[a)]	4–5	4–5	4–5	3–18
Hemp	44 (59)[a)]	3–5	3–5	3–5	3–18
Dissolving pulp	43–56			4.1–4.7	10–30

a) Degree of crystallinity relative to cellulose.
Source: Klemm et al. 2005 [3]. Reproduced with permission from John Wiley & Sons.

for sonication-induced fragmentation method as 1.6–3 GPa for wood cellulose and 3–6 GPa for tunicate cellulose [53]. The mechanical properties of cellulose microfibrils are comparable to those of multiwalled carbon nanotube and synthetic Kevlar fibers [1, 53]. However, the biological origin of these sustainable nanomaterials has driven researchers to explore varied techniques to obtain these nanoscaled cellulose fibers.

As cellulose microfibrils are intimately imbedded in lignocellulosic matrix with tight association with each other as well as the lignocellulosic matrices, isolation of individual cellulose microfibrils needs to be assisted with various means to disrupt these interfibrils association, i.e. via a "top-down" route to individualize the microfibrils from the large cellulose fibers. Currently, several techniques have been proven effective in isolating these cellulose microfibrils, including (I) mechanical shearing to physically disrupt the interfibril bondings (microfluidization, homogenization, ultrasonication, high-speed blending, aqueous counter collisions [ACC], twin-screw extruding, and grinding), (II) chemical treatments to reduce the hydrogen bonding capacities between the microfibrils (oxidation, quaternization, acid hydrolysis), (III) biological treatment to breakdown cellulose chains (enzymatic hydrolysis by cellulase), and (IV) a combination of these techniques for more efficient and synergistic results [54].

Although the terminology of cellulose microfibrils is most commonly used in describing the bundled elementary fibrils of 3–10 nm wide formed during biosynthesis in cell wall, "microfibrillated cellulose (MFC)" was firstly used to describe the cellulose fibrils disintegrated from plant cell walls by homogenization treatment, which demonstrated gel-like characteristics in water with pseudoplastic and thixotropic properties [55, 56]. Therefore, "microfibrillated cellulose" should not be confused with the "cellulose microfibrils," as the former usually has diameters of around 20–40 nm or even greater, consisting of multiple "microfibrils" packed together [57]. MFCs are generally defibrillated from cellulose fibers by the high shearing force created by repetitive mechanical treatment to break the hydrogen bonds and disintegrate into microfibril bundles.

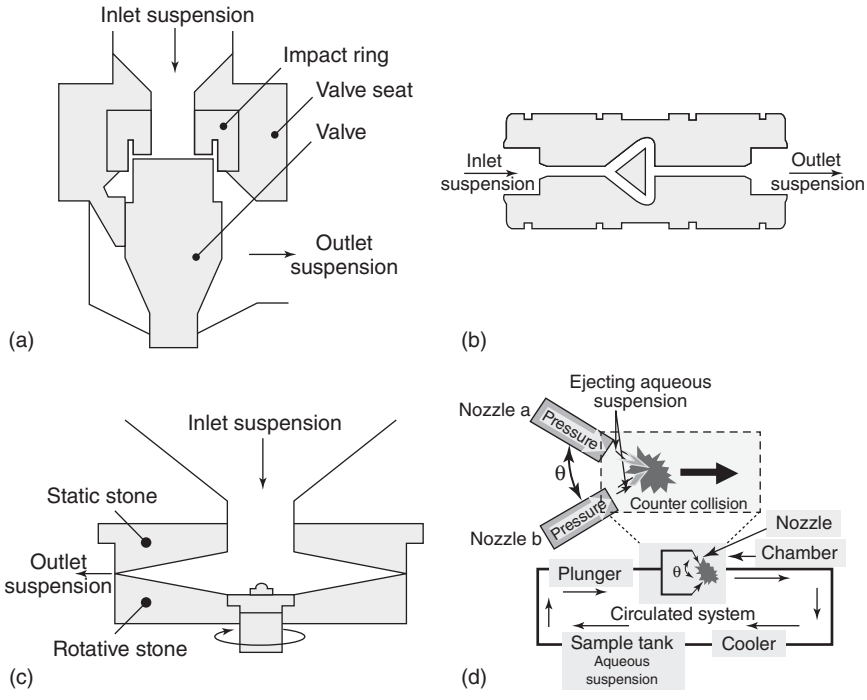


Figure 4.6 Schematics of the working principle of (a) homogenizer, (b) microfluidizer, (c) grinder; Source: Nechyporchuk et al. 2016 [59]. Reprinted with permission of Elsevier, and (d) aqueous counter collisions. Source: Kondo et al. 2014 [60]. Reprinted with permission of Elsevier.

High-pressure homogenization is firstly used to produce MFC back in the 1980s and remains being actively used nowadays [55, 58]. During homogenization, high shear and impact forces are exerted on cellulose fiber slurries when passing through the small gaps between the impact ring and spring-loaded valve (Figure 4.6a), achieving microfibril defibrillation [59]. Microfluidizer represents another technique for processing MFC by passing the cellulose suspension through a Z- or Y-shaped chamber under high pressure (150–210 MPa), exerting strong shear and impact forces against the channel walls (Figure 4.6b) [59, 61, 62]. As another commonly used technique, grinding processes MFC by passing the cellulose slurry through the static and rotative stones with adjustable inter-disk spacing, which generates shearing forces to disintegrate the microfibrils (Figure 4.6c) [59, 63, 64]. Recently, Kondo and coworkers developed another setup called "aqueous counter collision" to produce MFC, which creates high-speed head-on collision of two jets of aqueous cellulose suspension to pulverize the large cellulose fibers into smaller MFCs (Figure 4.6d) [60, 65, 66]. The high energy consumption on the order of 100 kWh/kg has been considered as the major barrier for mass production of MFC, especially with the high-pressure homogenization process [67]. However, it is found that microfluidization, ACC, and micro-grinding processes are more energy efficient, consuming significantly less energy than homogenization [60, 64, 66, 68]. Besides those most widely used

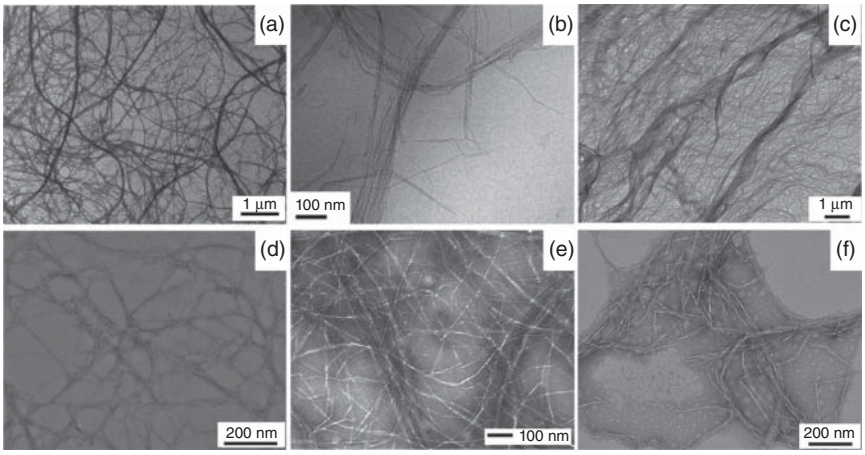


Figure 4.7 TEM images of mechanically derived microfibrillated cellulose: (a) high-speed homogenizer; Source: Dufresne et al. 1997 [73]. Reprinted with permission of John Wiley & Sons, Inc., (b) microfluidizer; Source: Taipale et al. 2010 [62]. Reprinted with permission of Springer, (c) grinding; Source: Jonoobi et al. 2012 [64]. Reprinted with permission of Elsevier, (d) ACC; Source: Jiang et al. 2016 [66]. Reprinted with permission of American Chemical Society, (e) ultrasonication; Source: Chen et al. 2014 [74]. Reprinted with permission of John Wiley & Sons, Inc., and (f) high-speed blending. Source: Jiang and Hsieh 2013 [71]. Reprinted with permission of Elsevier.

techniques, MFC production has also been reported using other technique such as ultrasonication [69, 70] and high-speed blending [71, 72].

The morphologies of MFC defibrillated using the common mechanical means are present in Figure 4.7, showing ultralong cellulose fibrils with heterogeneous diameter distribution ranging from 10 to 50 nm. The exact fibril diameters depend on the source of cellulose, treatment parameters such as pressure and treatment cycles/times, and separation procedures (centrifugation and filtration). Nevertheless, MFCs are considered as cellulose microfibril bundles containing multiple elementary fibrils bonded together via interfibril hydrogen bonding. As no chemical is used during mechanical defibrillation, MFCs show several advantages such as no surface modification, high aspect ratios, and exceptional thermal stability comparable to the original cellulose fibers [66, 71]. For more complete review on the preparation and properties of MFC, the readers could refer to recent reviews by Lavoine et al. [75] and Nechyporchuk et al. [59].

Although microfibril bundles of several tens of nanometers have been successfully isolated with the aid of mechanical means in the 1980s, due to the presence of numerous strong interfibril hydrogen bonds, isolation of elementary fibrils has remained a grand challenge until the beginning of this century. The prerequisite for isolating the finest elementary fibrils is to break the interfibril hydrogen bonds by varied chemical treatments, among which selective surface oxidation by 2,2,6,6-tetramethyl-1-piperidinyloxy (TEMPO) treatment represents the most effective one [67, 76]. TEMPO-mediated oxidation of native cellulose is commonly carried out at elevated pH of 10–11 using NaClO as the primary oxidant and TEMPO/NaBr as catalyst. This reaction has been proven to be highly

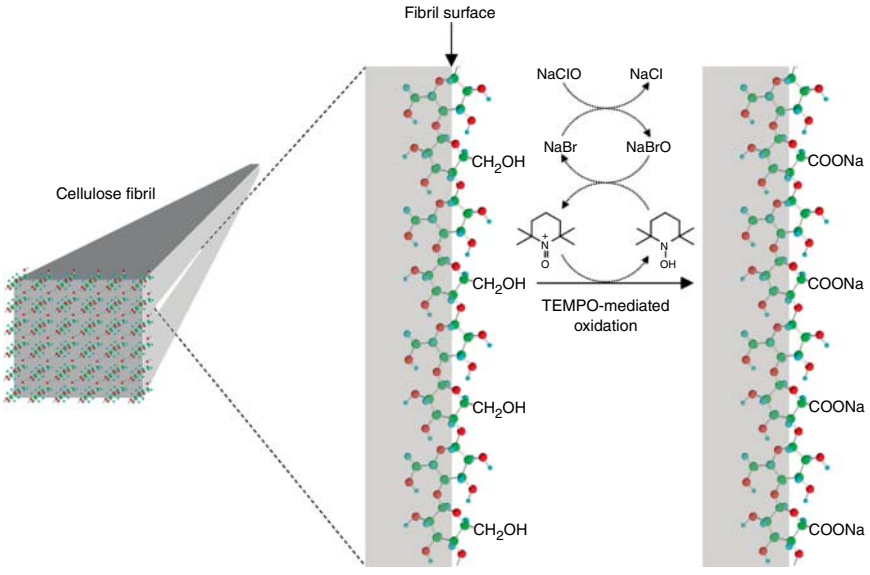


Figure 4.8 Schematic model of oxidation of C6 primary hydroxyl on cellulose microfibril surfaces by TEMPO oxidation. Source: Okita et al. 2010 [77]. Reprinted with permission of American Chemical Society.

regioselective that could only oxidize the C6 hydroxymethyl groups of cellulose (Figure 4.8) [9]. However, unlike regenerated cellulose where clear solution of cellouronic acids is obtained after oxidation [78], TEMPO oxidation could hardly convert the native cellulose I into soluble products [71, 79]. Therefore, further mechanical treatment is necessary to obtain individualized cellulose nanofibrils (CNFs), including magnetic stirring [80], high-speed blending [79, 81], and ultrasonication [82], but at significantly reduced energy consumption as compared with mechanical defibrillation alone [67].

The CNFs obtained from TEMPO oxidation appear as homogeneous long fibrils with lateral dimensions depending on the cellulose sources and extent of oxidation (Figure 4.9a–c). CNFs from wood showed uniform width of a few nanometers, whereas tunicin and BC demonstrated significantly wider fibril dimensions. Nevertheless, the lateral dimension of the CNFs derived from TEMPO oxidation is almost similar to the lateral crystallite dimension as determined from the wide- and small-angle X-ray diffraction measurements [79, 81]. Successful isolation of the elementary fibrils requires breaking the interfibril hydrogen bonds, which could also be achieved by other chemical or biological treatments, other than the mostly investigated TEMPO oxidation. Carboxymethylation of softwood dissolving pulp using monochloroacetic acid could liberate CNFs of 5–15 nm wide and over 1 μm long (Figure 4.9d), due to the electrostatic repulsion caused by the negatively charged surface carboxymethyl groups [83]. Besides these anionization reactions, cationization reaction can introduce positive charges on the surface of elementary fibrils, breaking the hydrogen bonds and facilitating its

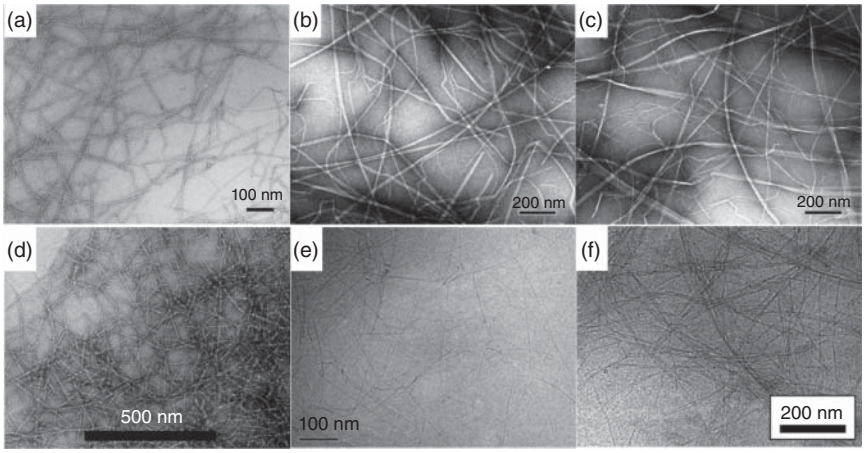


Figure 4.9 Transmission electron microscopy images of cellulose nanofibrils defibrillated via combined chemical–mechanical treatment. TEMPO oxidation of (a) wood, (b) tunicin, and (c) bacterial cellulose; Source: Saito et al. 2006 [81]. Reprinted with permission of American Chemical Society, (d) carboxymethylation; Source: Wagberg et al. 2008 [83]. Reprinted with permission of American Chemical Society, (e) quaternization; Source: Olszewska et al. 2011 [84]. Reprinted with permission of Springer, and (f) enzymatic hydrolysis. Source: Paakko et al. 2007 [85]. Reprinted with permission of American Chemical Society.

liberation by mechanical treatment. Quaternization of dissolving pulp with *N*-(2-3-epoxypropyl)trimethylammonium chloride has shown to introduce 354 μEq/g of positively charged quaternary amine to the elementary fibrils, which have been liberated as individual fibrils of 2.5–3 nm, close to the elementary fibrils from Norway spruce 2.5 ± 0.2 nm obtained from TEM and small- and wide-angle X-ray scattering [84, 86]. Besides introducing charged species on the microfibril surface, enzymatic hydrolysis by endoglucanase has also found to be able to introduce interfibril defects that could facilitate mechanical defibrillation, yielding individual nanofibrils of c. 5 nm and thicker bundles of 10–20 nm wide [85].

All of these aforementioned defibrillation methods include a top-down process that involves liberating the preassembled plant cellulose fibers into the individual elementary fibrils. Due to the strong interfibrils and interspecies association, chemical and energy-intensive mechanical treatments are required to remove the lignin/hemicellulose as well as to individualize the cellulose microfibrils. On the other hand, chemically pure cellulose free of lignin, pectin, and hemicellulose could be obtained by biosynthesis from the gram-negative, aerobic microorganism (*A. xylinum*) using D-glucose as the carbon sources or a "bottom-up" process (Figure 4.10) [3, 87]. The first discovery of BC synthesized by *A. xylinum* was made in 1886 by Brown, who found a gelatinous translucent membrane formed during vinegar fermentation on the surface of medium broth, which has been identified with the same chemical structure of plant cellulose [88]. The synthesis of BC starts with glucose, which could be transformed into UDP (guanosine triphosphate)-glucose via glucose-6-phosphate and glucose-1-phosphate, followed by polymerization reaction mediated by cellulose synthase to add the

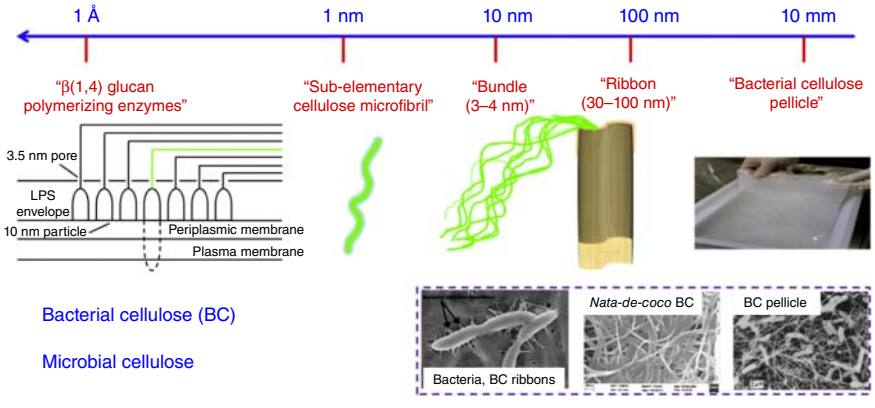


Figure 4.10 Hierarchical structure of bacterial cellulose. Source: Lin and Dufresne 2014 [52]. Reprinted with permission of Elsevier.

UDP-glucose to the end of glucan chains by cellulose synthase (TCs) [87]. Similar to plant cellulose, BC is also synthesized through TCs. However, in contrast to the rosette-shaped TCs found in the plasma membrane of higher plant, the BC TCs are linearly arranged on the cell surface of bacteria, with a basket-shaped structure. Each basket-shaped structure could synthesize 16 glucan chains through the catalytic sites, assembling into sub-elementary fibrils containing four mini-sheets, approximately 1.5 nm wide. One linear TC contains three basket-shaped subunits, linearly positioned parallel to the longitudinal axis of the bacteria. Therefore, the secreted sub-elementary fibrils could assemble with each other to form a ribbon like elementary microfibrils, which further assemble into larger ribbon-like fibers of approximately 40–50 nm wide [87, 89]. The flat-ribbon-like BC nanofibers intertwine with each other to form BC pellicles to float on the oxygen-rich surface of the media, with the pellicle protecting the cells from lethal effects of ultraviolet radiation and other harsh environments [87, 90]. BC contains both Iα and Iβ, with over 80% being dominant by cellulose Iα and crystallinity as high as 84–89% [91]. BC has extremely long fibers of approximately 1–9 μm, with DP as high as 14 000–16 000 [92], depending on the cultivation conditions and bacterial strains. Due to its high crystallinity and extraordinary hydrogen bonding systems, BC is extremely strong with Young's modulus of 78 GPa measured on a single BC fiber using three-point bending AFM technique [50]. BC nanofibers could also be further broken down into smaller nanofibrils by ACC [65] or TEMPO oxidation treatments [93], showing reduced diameters to 30 and 15–40 nm, respectively. Further reduction in the diameters of bacterial CNFs into elementary fibrils has not been reported, possibly due to the strong interfibril hydrogen bonding.

4.4 Submicron-Scaled Cellulose Fibers

Precise dimensional control of the linear cellulose fibers is intriguing considering that numerous properties of cellulose fibers are dependent on the

fiber dimensions, such as specific surface area, surface functionality, porosity, permeability, and mechanical properties. However, in nature, except for BC where the strands of cellulose nanofilaments secreted by different bacteria are well separated with each other within the pellicles, all plant cellulose fibers lose such delicacy of well-separated nanocellulose. Instead, due to the high specific surface areas of cellulose elementary microfibrils and the large availability of surface polar hydroxyl groups, they readily assemble with each other to form large macroscopic fibers of hundreds of microns wide. Therefore, it has drawn great attention in designing macroscopic cellulosic fibrous materials with imbedded submicron or even nanoscaled cellulose fibers to harness both the intrinsic nanoscale properties and the easy-to-handle macroscopic properties. Several approaches have been developed to design this type of materials, mainly involving controlled assembly of the cellulose chains into continuous fibrous structure. In this section, two of the most adopted approaches will be reviewed, including electrospinning and self-assembly.

Since its invention, electrospinning has evolved as an efficient technique in fabricating continuous polymeric micro/nanofibers, with the fiber diameters ranging from less than 100 nm to up to a few microns [94]. During electrospinning, the polymer solution was subject to electric filed, which charges the solution to induce charge repulsion. This charge repulsion, together with the contraction of the surface charges to the counter electrode, exerts a force on the surface of polymer solutions to overcome the surface tension. At sufficient large electric field, the jet of polymer solution could be ejected and fly toward the metal collector, forming polymer nanofiber membranes once the solvent evaporates [95]. The prerequisite of electrospinning polymeric nanofibers is to form a homogeneous solution, which represents the greatest challenge for cellulose, considering the strong intramolecular and intermolecular hydrogen bonding that prevent it dissolving into common solvents or melting. Several solvent systems, which have been successfully used in cellulose fiber spinning, were found to be suitable for electrospinning of native cellulose, including *N*-methylmorpholine-*N*-oxide/water (NMMO/H_2O) [96, 97], lithium chloride/dimethylacetamide (LiCl/DMAc) [96, 98], ionic liquid [99–101], and ionic liquid cosolvent system [100, 102, 103]. The common problem with these solvent systems is their low volatility that cannot evaporate completely when traveling from the spinneret to the collector [104]. Besides, some solvent systems also contain nonvolatile salts such as LiCl and ionic liquids that could not be evaporated from the electrospun fibers. Therefore, specific collector design is required to effectively remove the solvents, including using a heated collector (~100 °C) for LiCl/DMAc to enhance evaporation of DMAc, followed by coagulation with water to remove the LiCl salt, resulting a dry and stable mat of cellulose fibers with diameters as small as 150 nm (Figure 4.11a) [96, 98]. As a contrast, electrospinning of cellulose nanofibers from NMMO/H_2O system requires a lower temperature collector (9–10 °C) to promote fast solidification of fibers, followed by the same coagulation with water bath to remove the solvent, obtaining uniform cellulose fibers of less than 1 μm wide (Figure 4.11b) [96]. Nontoxic room temperature ionic liquid 1-ethyl-3-methylimidazolium acetate ([C_2min][CH_3CO_2]) was also used to dissolve cellulose to electrospun

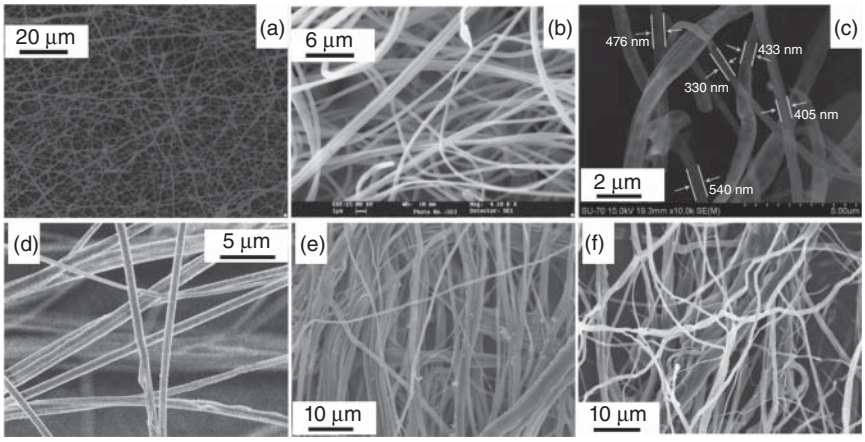


Figure 4.11 Electrospun pure cellulose nanofibers from different solvent systems: (a) 3% (w/w) cellulose/8% LiCl/DMAc; Source: Kim et al. 2005 [98]. Reprinted with permission of John Wiley & Sons, Inc., (b) 9 wt% cellulose/NMMO/H_2O, $T_{nozzle} = 50\,°C$; Source: Kim et al. 2006 [96]. Reprinted with permission of Elsevier, (c) 8 wt% cellulose in [C_2min][CH_3CO_2] ionic liquid; Source: Freire et al. 2011 [99]. Reprinted with permission of Royal Society of Chemistry, (d) 5 wt% cellulose in AMMIMCl/DMSO (1 : 2 ratio); Source: Xu et al. 2008 [103]. Reprinted with permission of Elsevier, (e) 6.3 wt% cellulose in [C_2min][OAC]/DMF (1 : 1 ratio); Source: Ahn et al. 2012 [102]. Reprinted with permission of Elsevier, and (f) 6.3 wt% cellulose in [C_2min][OAC]/DMAc (1 : 1 ratio). Source: Ahn et al. 2012 [102]. Reprinted with permission of Elsevier.

fibers using grounded water bath as collector to remove ionic liquid in order to prevent fiber fusion (Figure 4.11c) [99]. The average diameter of as-spun cellulose nanofibers was 470 nm, which could be further reduced to 120 nm with addition of a surface active ionic liquid 1-decyl-3-methylimidazolium chloride as cosolvent. Due to its high viscosity and nonvolatility, electrospinning cellulose in pure ionic liquid is a great challenge. Therefore, the common practice is to add a volatile cosolvent to lower the surface tension and viscosity of ionic liquid. Adding DMSO as a cosolvent to 1-allyl-3-methylimidazolium chloride (AMIMCl) has found to increase the conductivity and decrease the surface tension and viscosity, which therefore could produce stable fibers of 500–800 nm (Figure 4.11d) [103]. Besides DMSO, DMF and DMAc were also mixed with ionic liquid (1-ethyl-3-methylimidazolium acetate) to assist cellulose electrospinning [102]. It was found that cellulose dissolved in pure ionic liquid could not form a stable Taylor cone, a prerequisite in obtaining nanofibers. Adding either DMF or DMAc could significantly improve the spinnability, showing uniform cellulose nanofibers with average diameters less than 600 nm at 1 : 1 solvent ratio (Figure 4.11e,f). Recently, a new solvent system NaOH/urea was developed to dissolve cellulose and explored on the suitability in electrospinning thereafter. However, it was found that electrospinning cellulose dissolved in NaOH/urea could not produce fibers, and nanofibers could only be formed when other fiber-forming facilitating polyol binders such as polyethylene glycol (PEG) and polyvinyl alcohol (PVA) [105]. As direct electrospinning cellulose nanofibers from dissolved cellulose solution remains a challenge due to the

limited solvent system and their low volatility or nonvolatility, it is much easier to obtain regenerated cellulose nanofibers by post-hydrolysis of cellulose acetate nanofibers. Cellulose acetate nanofibers has been successfully electrospun from mixed acetone/DMAc or acetic acid/DMAc solvent, which could be further converted to regenerated cellulose by deacetylation to remove the acetyl groups [106].

These submicron-wide fibers derived from electrospinning requires complicated processes including dissolution, electrospinning, and post-coagulation, requiring tremendous amount of solvents and energy. Besides, these dissolution and regeneration treatment of cellulose disrupt the native hydrogen bonding between cellulose chains, rendering change of crystal structure from native cellulose I to regenerated cellulose or cellulose II. Therefore, it has drawn a great interest in searching for a more facile and greener method in deriving continuous submicron cellulose fibers with well-preserved cellulose I crystal structures. This search has been fruitful during the past decade, with the booming of researches in nanocellulose. Essentially, the native cellulose I nanocellulose (including CNFs and cellulose nanocrystals [CNCs]) has found to be able to assemble with each other during freezing and freeze-drying, forming assembled submicron-wide fibers or nanofibers. The pioneering work on nanocellulose assembly was reported by Paakko et al. in 2008, showing that the enzymatic hydrolyzed cellulose I nanofibers (5–10 nm wide) could aggregate into hierarchical structures containing interconnected fibrillar networks of approximately 30 nm wide (Figure 4.12) [107].

The intriguing phenomenon of nanocellulose assembly has been extensively investigated, and the formation of ice crystals during freezing and its subsequent sublimation has been identified as the driving force for the assembly. Starting from homogeneously dispersed aqueous nanocellulose suspension, the assembly of nanocellulose takes advantages of ice nucleation and crystal growth, which could segregate the nanocellulose into isolated regions. The locally concentrated high specific surface nanocellulose could thereafter assemble with each other via hydrogen bonding and van der Waals force into fibrous or

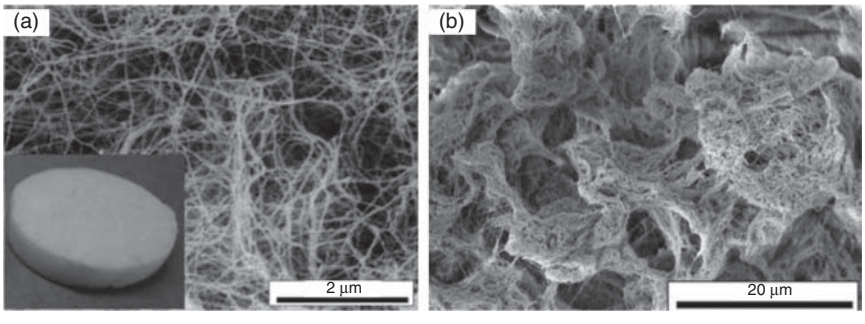


Figure 4.12 SEM micrographs of the aerogels as prepared by quickly freezing the aqueous nanofibrillar gel in liquid propane and extracting the water from the frozen state. (a) Higher magnification showing the fibrillar aerogel skeleton. Inset: 3 mm thick aerogel specimen. (b) Lower magnification showing the hierarchical porosity. Source: Paakko et al. 2008 [107]. Reprinted with permission of Royal Society of Chemistry.

dense film-like structures, depending on a series of factors, such as freezing temperature, nanocellulose concentration, aspect ratio, surface chemistry, crystal structure, and dispersing medium [108–111]. Among them, assembled fibrous forms are commonly obtained by extremely low freezing temperature such as liquid nitrogen (−196 °C) or liquid propane (−180 °C), where smaller ice crystals could be formed to segregate nanocellulose into thinner bundles between ice crystals to form submicron fibers. In contrast, relative higher freezing temperature such as the freezing in the freeze-dryer cooling chamber (−50 °C) or freezer (−20 °C) could lead to nanocellulose assembly into larger two dimensional sheets, due to the growth of large ice crystals at higher freezing temperature [107, 111, 112]. The formation of submicron fibers is also highly dependent on the starting concentration of nanocellulose suspensions, which shows that submicron fibers could only be obtained when the nanocellulose concentration is lower than certain critical concentrations [113]. Essentially, at lower concentration, the nanocellulose has lower local concentration and is well separated by the ice crystals, confining the lateral assembly of nanocellulose into submicron fibers. When the concentration is high, higher local concentration between ice crystals is also expected, which could reduce the nanocellulose spacing and promote more lateral association between nanocellulose to form 2D sheetlike structures (Figure 4.13). The critical concentration in forming submicron fibers shows significant variation for different types of nanocellulose, primarily due to the surface chemistry of the nanocellulose. It was found that CNCs tend to form submicron fibers at concentrations below 0.5 wt%, whereas the TEMPO-oxidized CNFs could only form submicron fibers at concentrations below 0.05 wt%, at least 1 magnitude lower than that for CNCs [111]. The reason that CNFs tend to assemble into film-like structures at much lower concentration is due to the stronger hydrogen bonding capacity of the surface carboxylate groups as compared with the hydroxyl groups for pure cellulose. The same concentration-dependent assembling properties were also observed

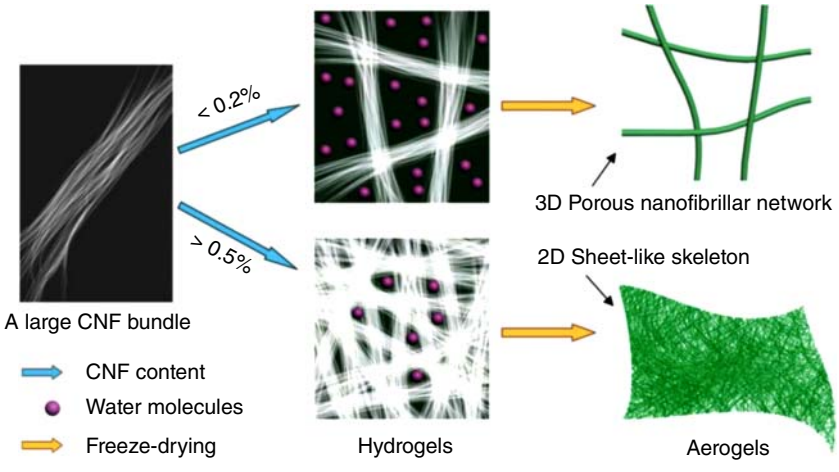


Figure 4.13 Schematics of the effect of CNF content on the assembled morphologies. Source: Chen et al. 2011 [108]. Reprinted with permission of Royal Society of Chemistry.

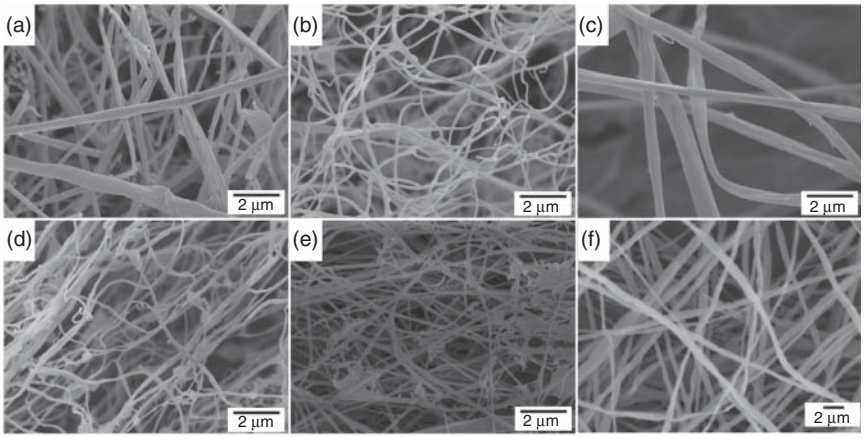


Figure 4.14 SEM image of self-assembled submicron fibers from varied nanocellulose. (a) CNCs at 0.1 wt%; Source: Jiang and Hsieh 2013 [71]. Reprinted with permission of Elsevier, CNFs at 0.1 wt% with (b) 0.59 and (c) 1.29 mol/g surface carboxyl groups. Source: Jiang et al. 2013 [79]. Reprinted with permission of Royal Society of Chemistry. (d) CNFs from high-speed blending at 0.05 wt%. Source: Jiang and Hsieh 2013 [71]. Reprinted with permission of Elsevier. (e) CNFs from aqueous counter collision treatment at 0.1 wt%. Source: Jiang et al. 2016 [66]. Reprinted with permission of American Chemical Society. (f) CNFs from ultrasonication. Source: Chen et al. 2014 [74]. Reprinted with permission of John Wiley & Sons, Inc.

for ultrasonication-treated CNFs that resemble to pure cellulose without surface chemistry modification, showing that submicron fibers could be obtained at concentration below 0.2 wt% [108].

Regardless of the type of nanocellulose and their respective surface chemistries, submicron fibers could be exclusively obtained when freezing at extremely low temperature (−196 °C using liquid nitrogen) and nanocellulose concentration (preferably <0.1%). Freeze-drying of various nanocelluloses leads to similar white and fluffy fibrous mass, which differ in microscopic morphologies with regard to the nanocellulose characteristics. Due to the higher crystalline and rigid rodlike structure, CNCs usually assemble into straight fibers of 300–400 nm wide (Figure 4.14a) [71]. The surface of the assembled CNC fibers appeared to be undulated with aligned CNC bundles and showed exceptional stability in water by handshaking or gentle mechanical stirring, which could be ascribed to the tight association of the CNCs through abundant inter-crystal hydrogen bonds [114]. Unlike highly crystalline rigid rodlike CNCs, the CNFs isolated either from TEMPO oxidation or mechanical shearing contain both crystalline and amorphous regions, showing significantly enhanced flexibility with higher aspect ratios. Therefore, curved and flexible submicron fibers could be obtained by assembling these longer CNFs (Figure 4.14b–f). The self-assembled morphologies of TEMPO-oxidized CNFs depend highly on the amount of surface charges as well as the degree of surface carboxyl protonation, i.e. the ratios of carboxylate to carboxylic acid [79, 115]. With increased amounts of surface carboxylate groups or degree of protonation at fixed surface carboxylate groups, the diameters of the assembled submicron fibers tend to increase or even evolve into film-like structure, due to the stronger hydrogen bonding

capacity of the protonated carboxylic acid groups. Ultrafine submicron fibers with average diameters of 120–140 nm have been successfully assembled from TEMPO-oxidized CNFs with low surface charge density of 0.59 mmol/g [79] or with less than 10% of protonated carboxylic groups at high surface charge density of 1.29 mmol/g [115]. Mechanically defibrillated CNFs preserve the surface hydroxyls without any chemical alteration, therefore most resembling the elementary cellulose microfibrils in plants. These uncharged CNFs were found to be able to assemble into most uniform submicron fibers, with lateral dimensions ranging from 120 to 150 nm (Figure 4.14d–f) [66, 69, 74].

Due to the prevalent surface polar groups on the nanocellulose, such as hydroxyls and carboxyls, nanocelluloses extensively assemble with each other into continuous submicron fibers with diameters ranging from 100 to 500 nm, signifying a facile process in obtaining fibrous materials. However, the extensive assembly inevitably reduces the specific surface area of these nanomaterials, which is considered the most interesting properties of the nanocellulose. In order to preserve these nanoscale dimensions, *tert*-butanol is commonly used as a cosolvent to inhibit the interfibril hydrogen bonding, therefore leading to much finer assembled nanofibers [111, 116]. With addition of respective 93 and 50 vol% *tert*-butanol, both CNCs and CNFs could assemble into relatively homogeneous nanofibers of approximately 40 nm wide (Figure 4.15) [111]. Due to the less interfibril association, these assembled nanofibers are found to be much more

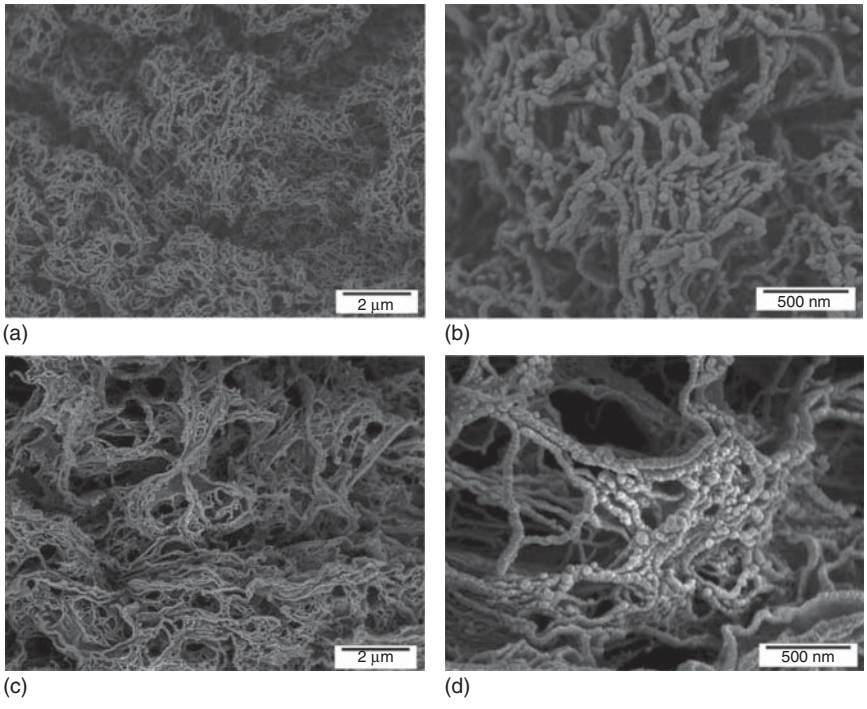


Figure 4.15 Nanofibers assembled from freezing (−196 °C) and freeze-drying of (a, b) 0.1% CNC in 93/7 *tert*-butanol/water and (c, d) 0.1% CNF in 50/50 *tert*-butanol/water. Source: Jiang and Hsieh 2014 [111]. Reprinted with permission of American Chemical Society.

easily redispersed into various solvent systems. The clearly reduced assembled fiber diameters could be ascribed to the different hydrogen bonding capacity between *tert*-butanol and water with nanocellulose and the steric hindrance of *tert*-butanol-bound nanocellulose surfaces. Each *tert*-butanol molecule could hydrogen bond to only one nanocellulose surface hydroxyl or carboxyl, preventing it from further hydrogen bonding or polar interaction, while the three bulky methyl groups add steric hindrance to limit inter-nanocellulose association. As a result of this inhibition on the self-assembly, the specific surface area of the fibrous mass could be significantly improved, showing as high as 350 m^2/g [110, 117].

In essence, submicron-wide cellulose fibers could be facilely obtained through either electrospinning of dissolved cellulose in carefully selected solvent systems or by direct self-assembly of aqueous dispersion of nanocellulose suspension. Compared with the electrospinning process, freeze-drying-assisted self-assembly demonstrates several advantages including less solvent consumption, easier procession, nontoxic solvent system, better control on the fibers' morphologies (ranging from several tens of nanometers to a few hundred nanometers), and preservation of the native cellulose I crystalline structure.

4.5 Macroscaled Cellulose Fibers

Macroscaled continuous cellulose fibers play a critical role in modern society, finding practical applications in textile, membrane, filtration, and reinforced composites. As a naturally abundant biopolymer, cellulose fibers have been used in clothing, construction, papermaking, and fishing for thousands of years. Until nowadays, cotton, a type of highly crystalline plant cellulose fibers, is still one of the major raw materials for textile industry. As the majority of cellulose on Earth is short fibers from trees, it is necessary to further process these short fibers into continuous filaments for more practical applications. Traditional cellulosic fiber process produces regenerated cellulose relying on viscose and cuprammonium rayon and Lyocell processes, all requiring heavy hazardous chemical dosage to derivatize or dissolve cellulose (xanthogenation for viscose, dissolution in cuprammonium and *N*-methylmorpholine-*N*-oxide for rayon and Lyocell, respectively), as well as regenerate into cellulose fibers [118, 119]. Therefore, these processes pose great environmental effects, and much greener and more environmental benign processes are being sought to process macroscaled cellulose fibers. Recently, a novel NaOH/urea aqueous solvent systems was developed to successfully dissolve cellulose, which is much greener compared with the previous organic solvent system [118, 120]. Wet spinning of cellulose dissolved in NaOH/urea generated continuous cellulose fibers with circular cross section and smooth surface, significantly different from the lobulated shape of the viscose rayon, but similar to cuprammonium rayon and Lycocell fibers [118]. Besides, the cellulose fibers spun from NaOH/urea solution showed homogeneous smooth surface without signs of fibrillation, a common problem for Lyocell fibers. Drawing has shown to improve the cellulose

molecular orientation and tensile strength, with the mechanical properties being approximate to the viscose rayon. However, this dissolution–regeneration process inevitably converted the native cellulose I to cellulose II structure, which could lead to deteriorated mechanical properties. Besides, stringent processing conditions are generally required for this process due to the narrower temperature window for dissolution, making scaling up a great challenge.

In contrast to dissolved cellulose where the crystalline structures are destroyed through interactions with solvent molecules, both CNCs and CNFs well preserve the native cellulose I crystalline structure, which lead to extraordinary mechanical properties including high modulus of 120–220 GPa [47–49] and strength of 3–6 GPa [53]. Therefore, great efforts have been devoted in fabricating macroscaled fibers out of these mechanically strong nanocellulose, aiming at transferring the exceptional mechanical properties of cellulose I nanocellulose to their assembled macrofibers. Wet extrusion of CNF aqueous suspensions into coagulation bath containing water miscible organic solvent (such as acetone, ethanol, tetrahydrofuran [THF], and dioxane) has been applied to fabricate macrofibers (Figure 4.16a,b). During this process, the aqueous CNF suspensions solidify when contacting the non-dispersing exchange solvent, forming a skin at the surface of the extruded fibers. Shearing force induced by extrusion could lead to preferential orientation of CNFs along the macrofibers, showing modest birefringence when being observed under crossed polarizers (Figure 4.16c). However, pure shearing force induced by extrusion is insufficient for complete nanofibril alignment, therefore resulting in moderate mechanical properties

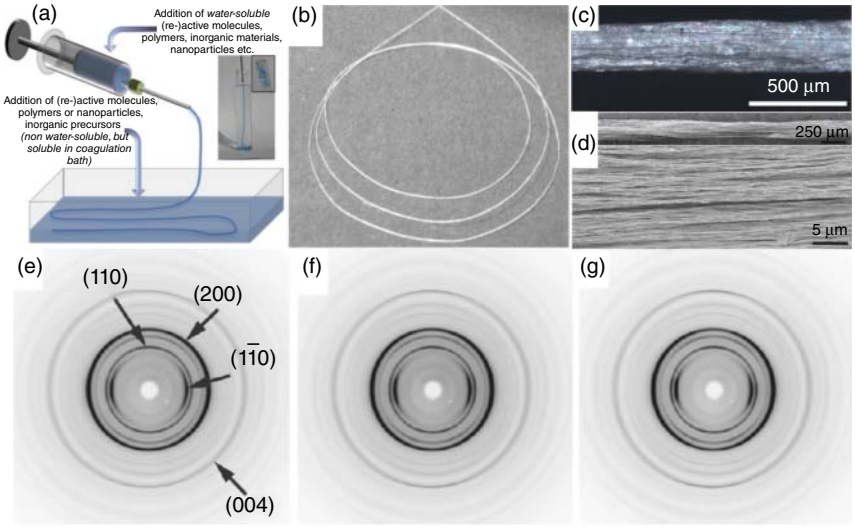


Figure 4.16 (a) Preparation of NFC macrofibers based on extrusion of NFC hydrogels into a coagulation bath and drying. (b) Photograph of a 1 mm long macrofiber of c. 0.2 mm diameter. (c) Optical microscopy image of the macrofibers with cross polarizers. (d) SEM images of macrofibers. Source: Walther et al. 2011 [121]. Reprinted with permission of John Wiley & Sons, Inc. X-ray fiber diagrams of the tunicate fibers spun at rates of (e) 0.1, (f) 1, and (g) 10 m/min. Source: Iwamoto et al. 2011 [122]. Reprinted with permission of American Chemical Society.

of 22.5 GPa for Young's modulus and 275 MPa for tensile strength, yet still 1 order of magnitude higher than typical rayon fibers. Although post-drawing was proposed in this study to improve the alignment of nanofibrils, it was not experimentally carried out to examine this hypothesis. Besides the less preferential alignment along the fiber axis, the macrofibers showed estimated porosity of 10%, with numerous nanopores in the size up to 25 nm being observed on the surface of SEM imaging (Figure 4.16d), which could also lead to the inferior mechanical properties. In another contemporary work, similar wet-spinning strategy was used to spin macrofibers out of TEMPO-oxidized CNFs in an acetone coagulation bath, focusing more on the shear force-induced alignment by varying the spinning speed from 0.1 to 100 m/min [122]. The X-ray diffractograms of the spun fibers showed equatorial arcs corresponding to (110), $(1\bar{1}0)$, and (200) diffractions and a meridian arc corresponding to (004) (Figure 4.16e–g). The orientation index of the wood fibers increased with increasing spinning speed, indicating better alignment of the nanofibers along the fiber axis. Correspondingly, the tensile strength and Young's modulus also increased with increasing orientation index, reaching 321 MPa and 23.6 GPa, respectively. This positive correlation between orientation index and mechanical properties is due to the anisotropy in mechanical properties for cellulose nanofibers, with estimated 150 GPa [49] and 18–50 GPa [48] Young's modulus at the respective longitudinal and transverse directions.

Wet-stretching-induced CNF orientation was investigated on wet-spun TEMPO-oxidized cellulose macrofibers coagulated in THF [123]. The wet stretching was conducted using a home-built computer-controlled device (Figure 4.17a), leading to a stretch ratio up to 0.3. Better CNF alignment could be clearly confirmed from the SEM image of the cross sections (Figure 4.17b), as well as increased orientation index from the 2D wide-angle X-ray diffraction. Quadruple increment in Young's modulus from 8.2 to 33.7 GPa and more than doubled increase of tensile strength from 118 to 289 MPa could be obtained by wet stretching, indicating simultaneous stiffening and strengthening with increasing stretching ratio (Figure 4.17c). Although wet stretching could lead to significant increase in mechanical properties owing to improved fibril alignment, the 289 MPa tensile strength is only moderately higher than the previously reported 275 MPa [121], possibly due to the variation of the starting materials. However, wet stretching indeed enhances the stiffness of the macrofibers as evidenced from the over 10 GPa Young's modulus increase. Hydrodynamic alignment was applied to force the CNF aligned in the flow direction, which was immediately fixed by electrolyte diffusion to aligned structure, as shown in the schematic in Figure 4.17d [124]. To obtain homogeneous and smooth gel fibers, the timing for ion diffusion-induced gel fixation has to be fit between the hydrodynamic alignment and the relaxation caused by Brownian diffusion. Compared to the previously reported porous fiber structures, this hydrodynamically aligned and fixed fibers showed void-free cross sections, and individual nanofibers could not be observed, suggesting a much denser and compact structure (Figure 4.17e,f). Due to the dual effects of alignment and fixation, the fibers are mechanically strong and stiff with tensile strength as high as 490 MPa and Young's modulus of 18 GPa (Figure 4.17g), with tensile strength surpassing

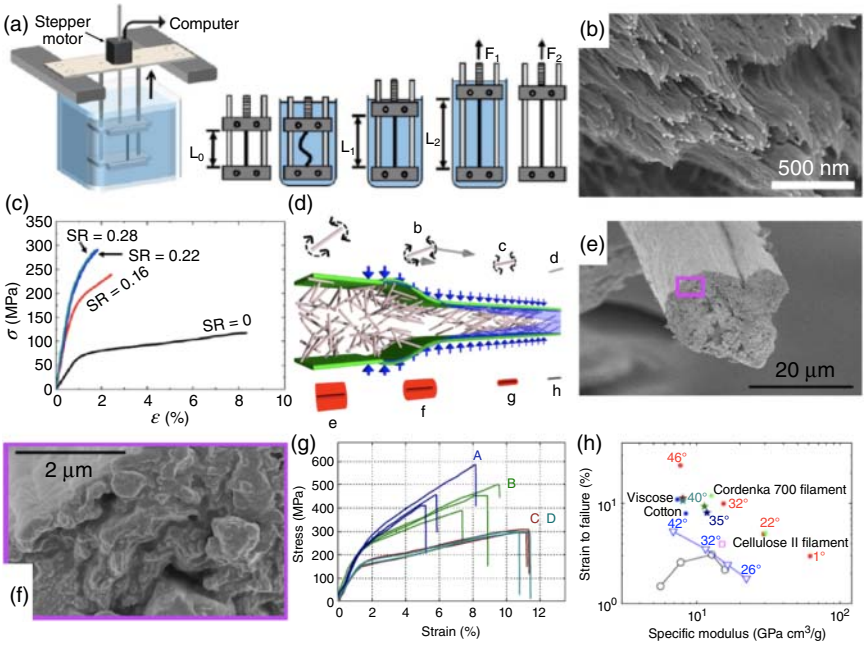


Figure 4.17 (a) Schematic drawing for the computer-controlled wet-stretching device into which a fiber can be clamped and immersed into a liquid and stretched using controlled strain rates; the right-hand side shows the various states during wet stretching. (b) SEM image of cross sections of stretched (SR = 0.28) NFC macrofibers. (c) Stress–strain curves of NFC macrofibers at different SR. Source: Torres-Rendon et al. [123]. Reprinted with permission of American Chemical Society. (d) Illustration of the hydrodynamic assembly process. Source: Hakansson et al. 2014 [124]. Reprinted with permission of Macmillan Publishers Limited. (e, f) SEM images of the filament. (g) Stress–strain plot of filaments. (h) Strain-to-failure versus specific Young's modulus for cellulose pulp fibers, filaments, and films made from CNF and the hydrodynamically assembled filaments of this study. The angle represents the angle of the CNF toward the filament or fiber axis in the case of filaments and toward the tensile testing axis in the case of films. Source: Reprinted with permission of Hakansson et al. 2014 [124]. https://www.nature.com/articles/ncomms5018. https://creativecommons.org/licenses/by/3.0/. Licensed under CCBY 3.0.

all the previously assembled cellulose nanofibers. The cellulose fiber is stronger than the strongest commercially available cellulose filament, owing to the much stiffer cellulose I structure as compared with the cellulose II structure in the regenerated cellulose filaments (Figure 4.17h).

Although wet-spinning CNF is much greener than the predominant spinning regenerated cellulose, it generally involves solvent in the coagulation step. In recent years, dry spinning has been reported to directly spin concentrated CNF aqueous suspension followed by drying in air [125]. The mechanical properties of these dry-spun CNF filaments are determined to be around 222 MPa for tensile strength and 12.6 GPa for Young's modulus, comparably lower than the wet-spun cellulose filaments. However, these dry-spun fibers are more uniform and clearly advantageous considering no chemical coagulation is needed.

4.6 Applications of Cellulose Fibers

With the booming of nanocellulose isolation and advanced characterization techniques, exploring and expanding the applications of these nanoscaled cellulose fibers have been exponentially grown during the past decade, which has expanded essentially in every aspects of human life, including energy, electronics, environmental remediation, and biomedical applications. In this section, these emerging applications for cellulose fibers will be summarized, and due to the limited pages of this chapter, the readers will be directed to respective review papers for more comprehensive analytical summaries on these aspects.

With the rapid development of portable and wearable electronics, energy storage devices have become an essential part of human life. The application of cellulose fibers in energy storage devices has offered several advantages that include biodegradability, flexibility, and lightweight. Therefore, this has sparked tremendous research interests by using cellulose fibers in varied energy storage devices such as lithium ion battery [126] and supercapacitors [127]. The applications of cellulose fibers in supercapacitors has recently been reviewed by Aleman and coworkers [128], showing the promising performance of cellulose fibers as supporting materials, template, separator, and electrolytes.

With increasing environmental deterioration due to the anthropogenic activities, it is of critical importance to remediate the deteriorated natural resources, such as water, air, and soil, by using naturally occurred cellulosic materials. Due to the large surface area and abundantly available surface functional groups, nanocellulose fibers have been widely used in water contaminant removal for water regeneration, including oil contaminant [113, 129], heavy metals [130], and dyes [74, 131], as well as antibacterials [132]. Beyond water treatment, air pollution has also been remediated by nanocellulose-based fibrous materials, such as for use in CO_2 absorption in response to global warming issues [133], and air filter for particle removal [134]. For more comprehensive review on using cellulose nanomaterials on water treatment, the readers could refer to the recent reviews by Wiesner and coworkers [135] and Liu et al. [136].

Due to the excellent biocompatibility, hemocompatibility, biodegradability, and low toxicity, nanocellulose fibers have generally been considered as a safe nanomaterial to be applied in biomedical applications. The applications of nanocellulose fibers in biomedical areas have spanned from the molecular level to macroscopic level, with most works having been extensively reviewed by Lin and Dufresne [52]. From the molecular or nanoscale level, the nanocellulose has been used for fluorescent labeling, cellular culture, drug delivery, enzyme/protein immobilization, and DNA carrier by utilizing the readily available surface functional groups. Besides, the nanocellulose has also been used as tissue bioscaffolds, tissue substitutes, tissue repair materials, and antibacterial wound dressing. The application of macroscaled nanofibrillated cellulose threads decorated with human stem cell has been demonstrated as a suitable surgical bionanomaterials for treating postoperative inflammation and chronic wound healing issues [137].

4.7 Conclusion and Perspectives

Cellulose fibers are the oldest fibrous materials being used by human beings and have been the subject of technical revolution throughout the human history. Currently, cellulose fibers are still widely used in various areas including textile, paper, printed electronics, constructions, and fiber-reinforced composite. Traditionally, continuous cellulosic fibrous materials are predominantly fabricated out of regenerated cellulose or cellulose derivatives, which requires copious amount of solvents to dissolve or derivatize cellulose, creating serious environmental side effects. Besides, the strong and stiff native cellulose I crystalline structures were destroyed during these solvent processing, thus limiting the mechanical properties of the final materials. With the continuous advancement of nanotechnologies in bio-based materials, nanocellulose with well-preserved native cellulose I crystalline structures has drawn great attentions in fabricating fibrous mass. The nanocelluloses are generally a few nanometers wide, approaching the size of single elementary fibrils, and up to micrometers long. The mechanical properties of these nanocelluloses are exceptionally high, with respective Young's modulus of 150 GPa and strength of 3–6 GPa, approaching to or even higher than carbon nanotube or Kevlar fibers. Therefore, it draws great interests in transforming these nanoscale building blocks to the macroscopic fibrous materials, including 2D macrofibers and 3D fibrous mass or aerogels. Although success has been well documented in fabrication of macroscopic fibrous materials from nanocellulose, numerous favorable traits of the nanocellulose have been lost during the transformation, such as the high specific surface area and excellent mechanical properties, just to name a few. The best reported tensile strength of the cellulose filaments is less than 500 MPa, much lower than the 3–6 GPa of the nanocellulose building block. Therefore, in the perspective of fabricating advanced fibrous materials from nanocellulose, several approaches warrant further investigations, including isolating nanocellulose with high mechanical properties and fewer defects, modulating the nanocellulose assembly to transfer the nanoscale characteristics to the macroscopic counterparts and to develop hybrid materials out of nanocellulose and other functional materials. Besides, further expanding the potential applications of the cellulose fibers at different scales is needed to justify the designing of these naturally occurred cellulosic fibrous materials for more functionalities.

References

1 Moon, R.J., Martini, A., Nairn, J. et al. (2011). *Chemical Society Reviews* 40: 3941.
2 Habibi, Y., Lucia, L.A., and Rojas, O.J. (2010). *Chemical Reviews* 110: 3479.
3 Klemm, D., Heublein, B., Fink, H.P., and Bohn, A. (2005). *Angewandte Chemie International Edition* 44: 3358.
4 Roy, D., Semsarilar, M., Guthrie, J.T., and Perrier, S. (2009). *Chemical Society Reviews* 38: 2046.

5 Zugenmaier, P. (2008). *Crystalline Cellulose and Cellulose Derivatives: Characterization and Structures*, 7. Berlin Heidelberg: Springer-Verlag.
6 Staudinger, H. (1920). *Berichte der Deutschen Chemischen Gesellschaft* 53: 1073.
7 Osullivan, A.C. (1997). *Cellulose* 4: 173.
8 Zhu, H.L., Luo, W., Ciesielski, P.N. et al. (2016). *Chemical Reviews* 116: 9305.
9 Habibi, Y. (2014). *Chemical Society Reviews* 43: 1519.
10 Wertz, J.-L., Bedue, O., and Mercier, J.P. (2010). *Cellulose Science and Technology*, 21. Lausanne, Switzerland: EPFL Press.
11 Battista, O.A., Coppick, S., Howsmon, J.A. et al. (1956). *Industrial and Engineering Chemistry* 48: 333.
12 Preston, R.D. (1964). *Formation of Wood in Forest Trees* (ed. M.H. Zimmerman), 169. Academic Press.
13 Brown, R.M. Jr., and Montezinos, D. (1976). *Proceedings of the National Academy of Sciences of the United States of America* 73: 143.
14 Brown, R.M. Jr., (1996). *Journal of Macromolecular Science, Part A Pure and Applied Chemistry* 33: 1345.
15 Mueller, S.C., Brown, R.M., and Scott, T.K. (1976). *Science* 194: 949.
16 Mueller, S.C. and Brown, R.M. (1980). *Journal of Cell Biology* 84: 315.
17 Herth, W. (1985). *Planta* 164: 12.
18 Cosgrove, D.J. (2005). *Nature Reviews Molecular Cell Biology* 6: 850.
19 Saxena, I.M. and Brown, R.M. (2005). *Annals of Botany* 96: 9.
20 Herth, W. (1983). *Planta* 159: 347.
21 Sugiyama, J., Harada, H., Fujiyoshi, Y., and Uyeda, N. (1985). *Planta* 166: 161.
22 Atalla, R.H. and VanderHart, D.L. (1999). *Solid State Nuclear Magnetic Resonance* 15: 1.
23 Atalla, R.H. and Vanderhart, D.L. (1984). *Science* 223: 283.
24 Yamamoto, H. and Horii, F. (1993). *Macromolecules* 26: 1313.
25 Yamamoto, H. and Horii, F. (1994). *Cellulose* 1: 57.
26 Vanderhart, D.L. and Atalla, R.H. (1984). *Macromolecules* 17: 1465.
27 Kataoka, Y. and Kondo, T. (1999). *International Journal of Biological Macromolecules* 24: 37.
28 Helbert, W., Nishiyama, Y., Okano, T., and Sugiyama, J. (1998). *Journal of Structural Biology* 124: 42.
29 Horii, F., Yamamoto, H., Kitamaru, R. et al. (1987). *Macromolecules* 20: 2946.
30 Debzi, E.M., Chanzy, H., Sugiyama, J. et al. (1991). *Macromolecules* 24: 6816.
31 Sugiyama, J., Persson, J., and Chanzy, H. (1991). *Macromolecules* 24: 2461.
32 Sugiyama, J., Okano, T., Yamamoto, H., and Horii, F. (1990). *Macromolecules* 23: 3196.
33 Nishiyama, Y., Sugiyama, J., Chanzy, H., and Langan, P. (2003). *Journal of the American Chemical Society* 125: 14300.
34 Sugiyama, J., Vuong, R., and Chanzy, H. (1991). *Macromolecules* 24: 4168.
35 Langan, P., Nishiyama, Y., and Chanzy, H. (2001). *Biomacromolecules* 2: 410.
36 Sarko, A. and Muggli, R. (1974). *Macromolecules* 7: 486.
37 Sturcova, A., His, I., Apperley, D.C. et al. (2004). *Biomacromolecules* 5: 1333.

38 Nishiyama, Y., Langan, P., and Chanzy, H. (2002). *Journal of the American Chemical Society* 124: 9074.
39 Qian, X.H., Ding, S.Y., Nimlos, M.R. et al. (2005). *Macromolecules* 38: 10580.
40 Jarvis, M. (2003). *Nature* 426: 611.
41 Zhu, H.L., Fang, Z.Q., Preston, C. et al. (2014). *Energy & Environmental Science* 7: 269.
42 Chinga-Carrasco, G., Yu, Y.D., and Diserud, O. (2011). *Microscopy and Microanalysis* 17: 563.
43 Chinga-Carrasco, G. (2011). *Nanoscale Research Letters* 6: 417.
44 Muhlethaler, K. (1967). *Annual Review of Plant Physiology* 18: 1.
45 Frey-Wyssling, A. (1954). *Science* 119: 80.
46 Peterlin, A. and Ingram, P. (1970). *Textile Research Journal* 40: 345.
47 (a) Diddens, I., Murphy, B., Krisch, M., and Muller, M. (2008). *Macromolecules* 41: 9755. (b) Sturcova, A., Davies, G.R., and Eichhorn, S.J. (2005). *Biomacromolecules* 6: 1055.
48 Lahiji, R.R., Xu, X., Reifenberger, R. et al. (2010). *Langmuir* 26: 4480.
49 Iwamoto, S., Kai, W.H., Isogai, A., and Iwata, T. (2009). *Biomacromolecules* 10: 2571.
50 Guhados, G., Wan, W.K., and Hutter, J.L. (2005). *Langmuir* 21: 6642.
51 Hsieh, Y.C., Yano, H., Nogi, M., and Eichhorn, S.J. (2008). *Cellulose* 15: 507.
52 Lin, N. and Dufresne, A. (2014). *European Polymer Journal* 59: 302.
53 Saito, T., Kuramae, R., Wohlert, J. et al. (2013). *Biomacromolecules* 14: 248.
54 Abitbol, T., Rivkin, A., Cao, Y.F. et al. (2016). *Current Opinion in Biotechnology* 39: 76.
55 (a) Turbak, A.F., Snyder, F.W., and Sandberg, K.R. (1983). *Journal of Applied Polymer Science, Applied Polymer Symposium* 37: 815. (b) Herrick, F.W., Casebier, R.L., Hamilton, J.K., and Sandberg, K.R. (1983). *Journal of Applied Polymer Science, Applied Polymer Symposium* 37: 797.
56 Klemm, D., Kramer, F., Moritz, S. et al. (2011). *Angewandte Chemie International Edition* 50: 5438.
57 Svagan, A.J., Samir, M., and Berglund, L.A. (2008). *Advanced Materials* 20: 1263.
58 (a) Nakagaito, A.N. and Yano, H. (2004). *Applied Physics A: Materials Science & Processing* 78: 547. (b) Nakagaito, A.N. and Yano, H. (2005). *Applied Physics A: Materials Science & Processing* 80: 155. (c) Iwamoto, S., Abe, K., and Yano, H. (2008). *Biomacromolecules* 9: 1022.
59 Nechyporchuk, O., Belgacem, M.N., and Bras, J. (2016). *Industrial Crops and Products* 93: 2.
60 Kondo, T., Kose, R., Naito, H., and Kasai, W. (2014). *Carbohydrate Polymers* 112: 284.
61 (a) Zimmermann, T., Pohler, E., and Geiger, T. (2004). *Advanced Engineering Materials* 6: 754. (b) Zimmermann, T., Bordeanu, N., and Strub, E. (2010). *Carbohydrate Polymers* 79: 1086.
62 Taipale, T., Osterberg, M., Nykanen, A. et al. (2010). *Cellulose* 17: 1005.
63 (a) Iwamoto, S., Nakagaito, A.N., and Yano, H. (2007). *Applied Physics A: Materials Science & Processing* 89: 461. (b) Abe, K. and Yano, H. (2009).

Cellulose 16: 1017. (c) Abe, K., Iwamoto, S., and Yano, H. (2007). *Biomacromolecules* 8: 3276. (d) Wang, Q.Q., Zhu, J.Y., Gleisner, R. et al. (2012). *Cellulose* 19: 1631.

64 Jonoobi, M., Mathew, A.P., and Oksman, K. (2012). *Industrial Crops and Products* 40: 232.

65 Kose, R., Mitani, I., Kasai, W., and Kondo, T. (2011). *Biomacromolecules* 12: 716.

66 Jiang, F., Kondo, T., and Hsieh, Y.L. (2016). *ACS Sustainable Chemistry & Engineering* 4: 1697.

67 Isogai, A., Saito, T., and Fukuzumi, H. (2011). *Nanoscale* 3: 71.

68 Spence, K.L., Venditti, R.A., Rojas, O.J. et al. (2011). *Cellulose* 18: 1097.

69 Chen, W.S., Yu, H.P., and Liu, Y.X. (2011). *Carbohydrate Polymers* 86: 453.

70 Chen, W.S., Yu, H.P., Liu, Y.X. et al. (2011). *Cellulose* 18: 433.

71 Jiang, F. and Hsieh, Y.-L. (2013). *Carbohydrate Polymers* 95: 32.

72 Uetani, K. and Yano, H. (2011). *Biomacromolecules* 12: 348.

73 Dufresne, A., Cavaille, J.Y., and Vignon, M.R. (1997). *Journal of Applied Polymer Science* 64: 1185.

74 Chen, W., Li, Q., Wang, Y. et al. (2014). *ChemSusChem* 7: 154.

75 Lavoine, N., Desloges, I., Dufresne, A., and Bras, J. (2012). *Carbohydrate Polymers* 90: 735.

76 Isogai, A. (2013). *Journal of Wood Science* 59: 449.

77 Okita, Y., Saito, T., and Isogai, A. (2010). *Biomacromolecules* 11: 1696.

78 Isogai, T., Yanagisawa, M., and Isogai, A. (2009). *Cellulose* 16: 117.

79 Jiang, F., Han, S., and Hsieh, Y.-L. (2013). *RSC Advances* 3: 12366.

80 Saito, T., Kimura, S., Nishiyama, Y., and Isogai, A. (2007). *Biomacromolecules* 8: 2485.

81 Saito, T., Nishiyama, Y., Putaux, J.L. et al. (2006). *Biomacromolecules* 7: 1687.

82 (a) Li, Q. and Renneckar, S. (2009). *Cellulose* 16: 1025. (b) Li, Q.Q. and Renneckar, S. (2011). *Biomacromolecules* 12: 650.

83 Wagberg, L., Decher, G., Norgren, M. et al. (2008). *Langmuir* 24: 784.

84 Olszewska, A., Eronen, P., Johansson, L.S. et al. (2011). *Cellulose* 18: 1213.

85 Paakko, M., Ankerfors, M., Kosonen, H. et al. (2007). *Biomacromolecules* 8: 1934.

86 Jakob, H.F., Fengel, D., Tschegg, S.E., and Fratzl, P. (1995). *Macromolecules* 28: 8782.

87 Klemm, D., Schumann, D., Udhardt, U., and Marsch, S. (2001). *Progress in Polymer Science* 26: 1561.

88 (a) Brown, A. (1886). *Journal of the Chemical Society* 49: 172. (b) Brown, A. (1886). *Journal of the Chemical Society* 49: 432.

89 Brown, R.M. (1996). *Journal of Macromolecular Science Pure and Applied Chemistry* A33: 1345.

90 Huang, Y., Zhu, C.L., Yang, J.Z. et al. (2014). *Cellulose* 21: 1.

91 Czaja, W., Krystynowicz, A., Bielecki, S., and Brown, R.M. (2006). *Biomaterials* 27: 145.

92 (a) Wu, Z.Y., Liang, H.W., Chen, L.F. et al. (2016). *Accounts of Chemical Research* 49: 96. (b) Tahara, N., Tabuchi, M., Watanabe, K. et al. (1997). *Bioscience Biotechnology and Biochemistry* 61: 1862.

93 Yao, J., Chen, S., Chen, Y. et al. (2017). *ACS Applied Materials & Interfaces* 9: 20330.
94 Doshi, J. and Reneker, D.H. (1995). *Journal of Electrostatics* 35: 151.
95 Huang, Z.M., Zhang, Y.Z., Kotaki, M., and Ramakrishna, S. (2003). *Composites Science and Technology* 63: 2223.
96 Kim, C.W., Kim, D.S., Kang, S.Y. et al. (2006). *Polymer* 47: 5097.
97 Kulpinski, P. (2005). *Journal of Applied Polymer Science* 98: 1855.
98 Kim, C.W., Frey, M.W., Marquez, M., and Joo, Y.L. (2005). *Journal of Polymer Science Part B: Polymer Physics* 43: 1673.
99 Freire, M.G., Teles, A.R.R., Ferreira, R.A.S. et al. (2011). *Green Chemistry* 13: 3173.
100 Quan, S.L., Kang, S.G., and Chin, I.J. (2010). *Cellulose* 17: 223.
101 Viswanathan, G., Murugesan, S., Pushparaj, V. et al. (2006). *Biomacromolecules* 7: 415.
102 Ahn, Y., Hu, D.H., Hong, J.H. et al. (2012). *Carbohydrate Polymers* 89: 340.
103 Xu, S.S., Zhang, J., He, A.H. et al. (2008). *Polymer* 49: 2911.
104 Frey, M.W. (2008). *Polymer Reviews* 48: 378.
105 Qi, H.S., Sui, X.F., Yuan, J.Y. et al. (2010). *Macromolecular Materials and Engineering* 295: 695.
106 Liu, H.Q. and Hsieh, Y.L. (2002). *Journal of Polymer Science Part B: Polymer Physics* 40: 2119.
107 Paakko, M., Vapaavuori, J., Silvennoinen, R. et al. (2008). *Soft Matter* 4: 2492.
108 Chen, W.S., Yu, H.P., Li, Q. et al. (2011). *Soft Matter* 7: 10360.
109 Han, J.Q., Zhou, C.J., Wu, Y.Q. et al. (2013). *Biomacromolecules* 14: 1529.
110 Sehaqui, H., Zhou, Q., and Berglund, L.A. (2011). *Composites Science and Technology* 71: 1593.
111 Jiang, F. and Hsieh, Y.-L. (2014). *ACS Applied Materials & Interfaces* 6: 20075.
112 Jiang, F. and Hsieh, Y.-L. (2014). *Journal of Materials Chemistry A* 2: 350.
113 Jiang, F. and Hsieh, Y.-L. (2014). *Journal of Materials Chemistry A* 2: 6337.
114 Lu, P. and Hsieh, Y.L. (2012). *Carbohydrate Polymers* 87: 564.
115 Jiang, F. and Hsieh, Y.L. (2016). *ACS Sustainable Chemistry & Engineering* 4: 1041.
116 Jiang, F. and Hsieh, Y.-L. (2015). *Carbohydrate Polymers* 122: 60.
117 Saito, T., Uematsu, T., Kimura, S. et al. (2011). *Soft Matter* 7: 8804.
118 Cai, J., Zhang, L.N., Zhou, J.P. et al. (2004). *Macromolecular Rapid Communications* 25: 1558.
119 Lundahl, M.J., Klar, V., Wang, L. et al. (2017). *Industrial and Engineering Chemistry Research* 56: 8.
120 Cai, J., Zhang, L.N., Zhou, J.P. et al. (2007). *Advanced Materials* 19: 821.
121 Walther, A., Timonen, J.V.I., Diez, I. et al. (2011). *Advanced Materials* 23: 2924.
122 Iwamoto, S., Isogai, A., and Iwata, T. (2011). *Biomacromolecules* 12: 831.
123 Torres-Rendon, J.G., Schacher, F.H., Ifuku, S., and Walther, A. (2014). *Biomacromolecules* 15: 2709.
124 Hakansson, K.M.O., Fall, A.B., Lundell, F. et al. (2014). *Nature Communications* 5: 4108.

125 (a) Hooshmand, S., Aitomaki, Y., Norberg, N. et al. (2015). *Acs Applied Materials & Interfaces* 7: 13022. (b) Shen, Y.F., Orelma, H., Sneck, A. et al. (2016). *Cellulose* 23: 3393.
126 (a) Huang, F.L., Xu, Y.F., Peng, B. et al. (2015). *ACS Sustainable Chemistry & Engineering* 3: 932. (b) Chiappone, A., Nair, J.R., Gerbaldi, C. et al. (2011). *Journal of Power Sources* 196: 10280.
127 (a) Yang, X., Shi, K.Y., Zhitomirsky, I., and Cranston, E.D. (2015). *Advanced Materials* 27: 6104. (b) Shi, K.Y., Yang, X., Cranston, E.D., and Zhitomirsky, I. (2016). *Advanced Functional Materials* 26: 6437. (c) Nystrom, G., Marais, A., Karabulut, E. et al. (2015). *Nature Communications* 6.
128 Perez-Madrigal, M.M., Edo, M.G., and Aleman, C. (2016). *Green Chemistry* 18: 5930.
129 Jiang, F. and Hsieh, Y.-L. (2017). *ACS Applied Materials & Interfaces* 9: 2825.
130 (a) Zhu, H., Yang, X., Cranston, E.D., and Zhu, S.P. (2016). *Advanced Materials* 28: 7652. (b) Ma, H.Y., Hsiao, B.S., and Chu, B. (2012). *ACS Macro Letters* 1: 213.
131 Pei, A., Butchosa, N., Berglund, L.A., and Zhou, Q. (2013). *Soft Matter* 9: 2047.
132 Wang, M.S., Jiang, F., Hsieh, Y.-L., and Nitin, N. (2014). *Journal of Materials Chemistry B* 2: 6226.
133 (a) Gebald, C., Wurzbacher, J.A., Tingaut, P. et al. (2011). *Environmental Science and Technology* 45: 9101. (b) Sehaqui, H., Galvez, M.E., Becatinni, V. et al. (2015). *Environmental Science and Technology* 49: 3167.
134 Nemoto, J., Saito, T., and Isogai, A. (2015). *ACS Applied Materials & Interfaces* 7: 19809.
135 Carpenter, A.W., de Lannoy, C.F., and Wiesner, M.R. (2015). *Environmental Science and Technology* 49: 5277.
136 Liu, H.Z., Geng, B.Y., Chen, Y.F., and Wang, H.Y. (2017). *ACS Sustainable Chemistry & Engineering* 5: 49.
137 Mertaniemi, H., Escobedo-Lucea, C., Sanz-Garcia, A. et al. (2016). *Biomaterials* 82: 208.

5

Chitosan Fibers

Seema Sakkara, Mysore Sridhar Santosh, and Narendra Reddy

Centre for Incubation, Innovation, Research and Consultancy, Jyothy Institute of Technology, Thathaguni Post, Bengaluru 560082, India

5.1 Introduction

Chitosan (derived from the raw material chitin) is one of the most abundantly available biopolymers, next only to cellulose. Worldwide, about 22 000 tons of chitosan are produced and the quantity is increasing each year. The market value of chitosan is expected to reach US$4.4 billion by 2020. Typically, industrial grade chitosan having acetylation degrees ranging from 75% to 85% sells at a price of about US$3.50–4.00 kg^{-1}. However, high purity medical grade chitosan is reported to sell at prices up to US$25,000 kg^{-1}. Although most chitosan is derived from chitin found in shrimp, crab, and shells of other marine animals, some fungi such as *Aspergillus niger*, *Mucor rouxii*, and *Penicillium notatum*; microorganisms such as algae, yeast, and others; and insects such as scorpions and spiders (Table 5.1) [1] have also been used to produce chitosan. In terms of structure (Figure 5.1), chitosan has typical features of polysaccharides [2]. The basic unit in chitosan consists of a β-(1-4)-linked D-glucose units. However, unlike cellulose, the hydroxyl at position C-2 of cellulose is replaced by acetamide group, and chitosan contains about 5–8% of nitrogen due to the acetamide group [3]. An FTIR spectrum of chitosan is given in Figure 5.2. An absorption band at 3439 cm^{-1} is seen due to the stretching vibration of the –OH and $–NH_2$ bonds, and the peaks at 1659, 1379, and 1321 cm^{-1} are due to the presence of tertiary amine. The bands in the region of 1460–1200 cm^{-1} and 1160–1000 cm^{-1} are from the COH and COC groups, respectively [4]. Stretching vibrations of amide I and II and bending vibrations from amide III bonds are responsible for the bands at 1659, 1599, and 1321 cm^{-1}.

One of the most notable characteristics of chitosan is its solubility in acidic solutions [1]. Some of the common solvents used to dissolve chitosan are listed in Table 5.2. Recently, water-soluble chitosan has also been developed. Primary applications of chitosan are in agrochemicals, water treatment, medicine,

Handbook of Fibrous Materials, First Edition. Edited by Jinlian Hu, Bipin Kumar, and Jing Lu.
© 2020 Wiley-VCH Verlag GmbH & Co. KGaA. Published 2020 by Wiley-VCH Verlag GmbH & Co. KGaA.

Table 5.1 Sources used for production of chitosan.

Sea animals	Insects	Microorganisms
Annelida	Scorpions	Green algae
Mollusca	Spiders	Yeast
Coelenterata	Brachiopods	Fungi
Crustaceans	Ants	Mycelia penicillium
• Lobster	Cockroaches	Brown algae
• Crab	Beetles	Spores
• Shrimp		*Chytridiaceae*
• Prawn		Ascomydes
• Krill		*Blastocladiaceae*

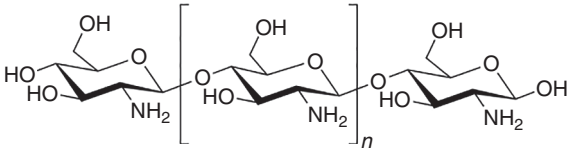


Figure 5.1 Structure of chitosan.

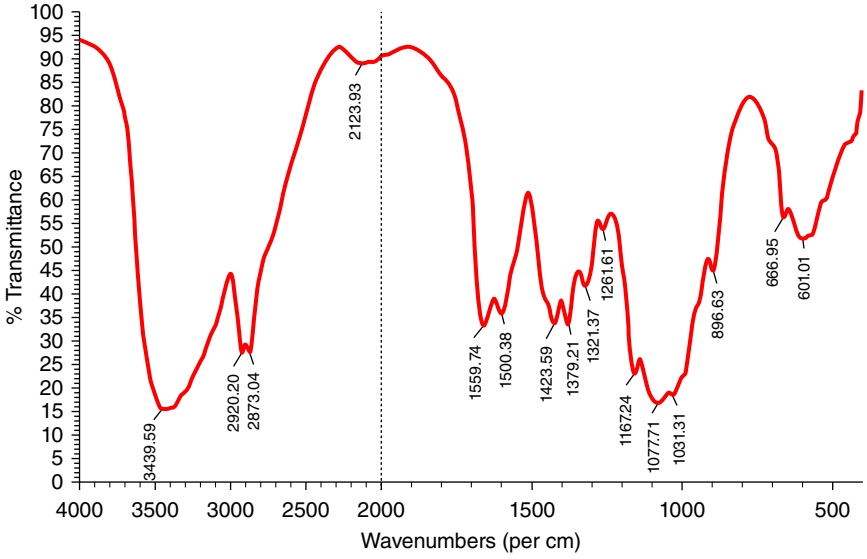


Figure 5.2 FTIR spectrum of chitosan shows the distinct peaks. Source: Chen et al. 2011 [4]. Reproduced with permission from Elsevier.

cosmetics, and others (Table 5.3) [5]. Since chitosan is widely available, is easily soluble, and has unique properties, it has been made into various products and considered for several applications. In addition to films, hydrogels, sponges, etc., considerable efforts have also been made to produce solution spun, electrospun, and regenerated chitosan fibers. Since fibrous materials are preferred for medical applications and chitosan has inherent antibacterial properties, most

Table 5.2 Common solvent/solvent mixtures used to dissolve chitosan.

Solvents
Aqueous acetic acid
Trifluoroacetic acid
Aqueous acetic acid/dimethylformamide
Aqueous acetic acid/dimethyl sulfoxide
1,1,1,3,3,3,-Hexafluoroisopropanol (HFIP)
HFIP/formic acid
Tetrahydrofuran/dimethylformamide
$CHCl_3$
Lithium hydroxide (LiOH)
Glycine chloride

Table 5.3 Various forms and applications of chitosan.

Form of chitosan	Application
Beads, microspheres, nanoparticles	Drug delivery, enzyme immobilization, gene delivery
Coatings	Surface modifications, textile finishes
Fibers, nanofibers, nonwovens	Medical textiles, suture, bone regeneration, nerve tissue engineering, wound healing
Films	Wound care, dialysis membrane, wound dressing and antimicrobial membranes
Powder	Absorbent for pharmaceutical and medical, surgical glove powder, enzyme immobilization
Sponge	Mucosomal hemostatic dressing, drug delivery, enzyme entrapment and artificial skin
Solution	Cosmetics, bacteriostatic, hemostatic agents, anticoagulants and antitumor agents
Gels	Implants, coating, tissue engineering
Tablets and capsules	Disintegrating agent, delivery vehicles

of the studies on chitosan fibers have been intended for medical applications. Also, in chitosan, there are one primary amino and two free hydroxyl groups for each building (C6) unit, making chitosan positively charged. Hence, negative charge-carrying metal ions such as cobalt are easily attracted and make chitosan an ideal material for separation of metals from wastewater [4].

5.2 Extraction/Modification of Chitosan

Chitosan is extracted from chitin using various physical, chemical, and other approaches. Typically, chitin is deacetylated to various degrees using alkaline conditions. In the conventional approach, chitin is treated with 3 M hydrochloric

Table 5.4 Comparison of the apparent viscosities (cP) of extracted and commercial chitosan at different temperatures.

Temperature (°C)	Extracted chitosan	Commercial chitosan
20	56.5 ± 0.14	38.2 ± 0.03
25	46.1 ± 0.07	31.9 ± 0.00
30	38.2 ± 0.02	27.1 ± 0.01
35	31.7 ± 0.06	23.3 ± 0.0
40	26.7 ± 0.01	20.4 ± 0.0

Source: Kucukgulmez et al. 2011 [8]. Reproduced with permission from Elsevier.

acid to remove calcium carbonate. Later, the materials are treated with 10% sodium hydroxide at 80 °C for two hours to remove proteins. Deacetylation of the chitosan is achieved by treating with 50% sodium hydroxide at 100 °C for 2.5 hours. Under similar conditions, chitosan with antibacterial and antifungal properties was extracted from two Tunisian crustacean species [6]. Shrimp shells were used as a source of chitosan and treated with 1 M NaOH for 24 hours and later demineralized using 1 M HCl and deprotonized using 1 M NaOH for 24 hours. Later, chitosan was discolored using $KMnO_4$ and oxalic acid to get the chitin powder [7]. Up to 89% deacetylation could be achieved. The extracted chitosan was grafted onto rayon to improve the antibacterial and antimicrobial properties [6]. Using a similar approach, chitosan was extracted from *Metapenaeus stebbingi* shells. About 17.5% of the weight of the shells could be obtained as chitosan with properties shown in Tables 5.4 and 5.5. It was suggested that the shells could be an inexpensive source to produce chitosan at high efficiency [8]. Although alkalis and acids have been extensively used to extract keratin, the type of acid and extraction conditions determine the properties of the chitosan obtained [9]. This was substantiated when chitosan was extracted from 15-day biomass of *Agaricus* sp., *Pleurotus* sp., and *Ganoderma* sp. [9]. Similarly, fungal-based chitosan was extracted, purified, and characterized from *Aspergillus brasiliensis*. A degree of deacetylation of 81.3%, molecular weight of 310 000 Da, and 96% solubility in 1% acetic acid was obtained for the chitosan [10].

Table 5.5 Characteristics of the chitosan extracted from *Metapenaeus stebbingi* shells compared with commercial chitosan.

	Extracted chitosan	Commercial chitosan
Yield (%)	17.5 ± 0.6	—
Moisture (%)	1.3 ± 0.08	1.07 ± 0.09
Ash (%)	0.6 ± 0.03	0.59 ± 0.07
Deacetylation degree (%)	92.2 ± 2.7	86.92 ± 1.62
Molecular weight (kDa)	2.2 ± 0.03	3.52 ± 0.02
Water binding capacity (%)	713 ± 12.0	493 ± 10.10
Fat binding capacity (%)	531 ± 12.3	383 ± 10.02

Source: Kucukgulmez et al. 2011 [8]. Reproduced with permission from Elsevier.

Many attempts have been made to develop alternative technologies for extraction of chitosan since the conventional process of extracting chitosan consumes considerable time and energy. Microwave irradiation was considered as a solution to extract chitosan rapidly at low cost. Using similar chemicals, chitin was heated for eight minutes in a microwave to demineralize, deprotenize, and deacetylate the chitin. Compared with the conventional approach that takes six hours and 30 minutes, the entire conversion from chitin to chitosan with same level of deacetylation took only 24 minutes [11]. A degree of deacetylation of 82.7% was achieved similar to that of conventional heating. However, chitosan obtained using microwave heating had higher molecular weight but similar crystallinity. It was suggested that microwave heating was an environmentally friendly and inexpensive approach to extract chitosan from shrimp shells (Tayel et al. 2016). Microwave extraction was also used to obtain chitosan from marine sources in the Arabian Gulf [12]. Figure 5.3 shows the schematic of the process used for the microwave extraction. Similar to previous studies on using microwave extraction, the chitosan obtained from the microwave method had higher molecular weight and crystallinity.

Micelia waste from *A. niger* was used as a source of chitosan and extracted using enzymes. Instead of using acid or alkali, lysozymes, snailase, neutral protease, and chitin deacetylase were used for the extraction. Enzymatic method produced chitosan with considerably higher molecular weight but similar level of deacetylation (Table 5.6), leading to an environmentally friendly approach [13].

Chitosan has been extensively modified to make it soluble in water and other common solvents, improve properties, and make it suitable for various medical applications [14]. Carboxymethylation is one of the most common approaches of modifying chitosan. Some of the chitosan derivatives and brief method to obtain carboxymethylated chitosans are shown in Figure 5.4, and the properties of the modified chitosans are in Table 5.7. In addition to carboxymethylation, chitosan has been acylated, alkylated, and grafted with various chemicals and

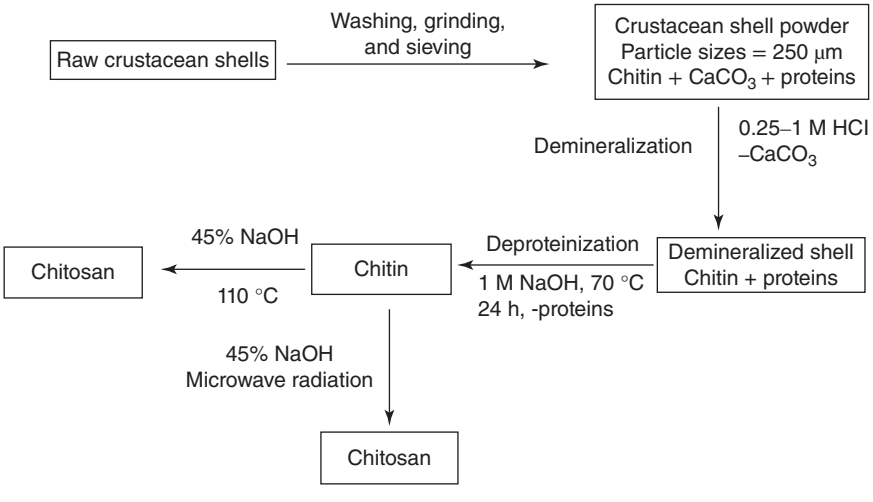


Figure 5.3 Schematic of the process of extraction of chitosan from chitin using microwave heating. Source: Sagheer et al. 2009 [12]. Reproduced with permission from Elsevier.

Table 5.6 Comparison of the properties of chitosan obtained using the conventional chemical approach and the enzymatic method.

Parameter	Chemical method	Enzymatic method
Degree of deacetylation (%)	76.8	73.6
Molecular weight (kDa)	84.04	268
Content of glucosamine (%)	82.7	94.4
Ash (%)	0.370	0.283

Source: Cai et al. 2006 [13]. Reproduced with permission from Elsevier.

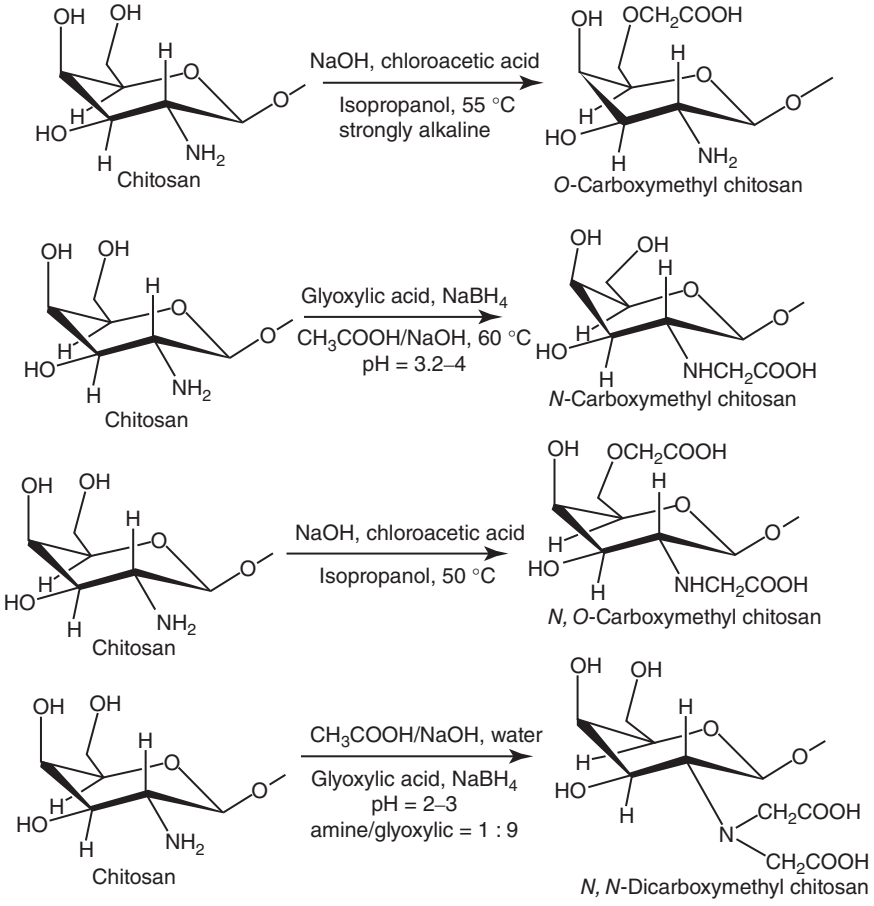


Figure 5.4 Structure of chitosan after various carboxymethylations. Source: Upadhyaya et al. 2013 [14]. Reproduced with permission from Springer Nature.

Table 5.7 Properties of various forms of chemically modified chitosans.

Derivatives	Subtypes	Important properties
Quaternized chitosan	*N,N,N*-Trimethyl chitosan (TMC)	Good absorption efficiency, mucoadhesion
Carboxyalkyl chitosan	*N,O*-Carboxymethyl chitosan (*N,O*-CMC)	Better gelling property, with high water retentivity and less immunogenicity
Hydroxyalkyl chitosan	Hydroxyethyl chitosan	Hydrophilic nature, increase in moisture absorption rate
	Hydroxypropyl chitosan	High inhibition rate of bacteria
Thiolated chitosan	Chitosan-4-thio-butylamidine	Increase in porous structure and solubility
	Chitosan-thioglycolic acid	Excellent gelling property
Sulfated chitosan	2-*N*, 6-*O*-sulfated chitosan (26SCS)	Inhibits blood coagulation
Semisynthetic resins of chitosan	Copolymer of chitosan with methyl methacrylate	Good mechanical and nanoporous structure used in drug delivery
Sugar derivatives of chitosan	Glucosamine chitosan	Increase in water solubility and antimicrobial property
Glutaraldehyde chitosan		Form a biocompactible and biostable complex
Chitosan-ascorbate conjugate		Good antioxidant property with scavenging and chelating capacity

Source: Upadhyaya et al. 2013 [14]. Reproduced with permission from Elsevier.

polymers [14]. Other than these conventional approaches, low temperature plasma and electron beam including γ-irradiation have been done to modify the properties of chitosan. Treating with plasma enhanced the medical applications of chitosan, whereas γ-irradiation reduced the molecular weight and also affected the ability to promote cell attachment and growth [15].

5.3 Fibers from Chitosan

5.3.1 Production of Pure Chitosan Fibers

Chitosan has been made into fibers using various techniques. In one of the earliest studies on producing fibers from chitosan, about 5% chitosan was dissolved in 2% acetic acid solution and extruded into a coagulation bath consisting of NaOH. Coagulated fibers were drawn to various ratios to improve their mechanical properties. Mechanical properties and fineness of the fibers was dependent on the draw ratio. Fineness decreased from 14.7 to 6.4 tex, and tenacity varied between 0.17 and 0.19 N/tex, and elongation increased substantially from 4.9% to 8.7%. Chitosan fibers were reconverted into chitin fibers by treating with acetic anhydride [16]. To further improve the antimicrobial properties of chitosan,

silver-containing compound was mixed and extruded with the fibers. The silver particles were found to be uniformly distributed along the fiber and increased the antimicrobial activity substantially.

Common approach of developing chitosan fibers is to dissolve the polymer in acetic acid and extrude into NaOH coagulation to form the fibers. In an alternative technique, chitosan having a viscosity average molecular weight of 3.0×10^6 Da and 65% of deacetylation was dissolved using ionic liquids (7.2% LiOH) and 6.0 wt% urea. Dissolved solution was extruded into a coagulation bath consisting of 6–8% sulfuric acid/aqueous ethanol at 40–50 °C and later into a bath containing water. Fibers obtained using the ionic dissolution method had higher thermal stability with a decomposition temperature of 304 °C compared with 295 °C for the normal fibers. Morphologically, the fibers had a rough surface and dense structure. Tensile strength of the fibers was 134 MPa, and elongation was 11.8%, about 20% higher strength compared with the fibers developed using the conventional approach [17]. In another study, glycine chloride was used as an ionic liquid to dissolve chitosan and produce fibers with improved properties [17]. Fibers were extruded into a sodium sulfate/ethanol bath and freeze-dried immediately. Chitosan I crystal form was retained, and fibers produced had tenacity of 3.8 cN/dtex compared with 0.9 cN/dtex obtained for chitosan fibers dissolved using acetic acid. Considerable variations were observed in the tensile properties depending on the conditions used to produce the fibers (Table 5.8). In addition, the ionic liquid could be recovered completely, leading to a green process of producing chitosan fibers.

Chitosan fibers were produced by dissolving in acetic acid–methanol mixture and extruding into various coagulations baths. The chitosan was also modified using vanillin and other aldehydes. Some of the properties of the unmodified and modified chitosan fibers are listed in Table 5.8. Tensile strength and elongation varied considerably when the molecular weight or the coagulation conditions or

Table 5.8 Variations in the properties of chitosan filaments with change in spinning conditions and extent of stretching.

Solvent	Coagulation bath	Stretching	Filament fineness (dtex)	Tenacity (g/tex)	Elongation (%)
2% AcOH + MeOH	10% NaOH + 30% AcONa	No	10.0	1.27	13.0
2% AcOH	10% NaOH + 30% AcONa	No	14.9	0.68	12.6
2% AcOH + MeOH	10% NaOH + 30% AcONa	Yes	4.2	1.43	17.3
2% AcOH	10% NaOH + 30% AcONa	Yes	8.4	0.87	23.0
2% AcOH + MeOH	10% NaOH + 30% Na_2SO_4	No	9.0	0.73	13.6
2% AcOH	10% NaOH + 30% Na_2SO_4	No	8.8	0.98	21.4
2% AcOH + MeOH	10% NaOH + 30% Na_2SO_4	Yes	7.1	1.38	16.5
2% AcOH	10% NaOH + 30% Na_2SO_4	Yes	10.0	1.17	28.1
2% Oxalic acid	10% NaOH + 30% AcONa	No	6.2	0.85	15.1

Source: Hirano et al. 1999 [18]. Reproduced with permission from Elsevier.

Table 5.9 Tensile properties of chitosan films in the dry and wet condition.

Concentration of sodium acetate (%)	Condition of measurement	Tenacity		Elongation		Initial modulus at 2% extension	
		Mean (g/d)	CV (%)	Mean (%)	CV (%)	Mean (g/d)	CV (%)
0	Dry Wet	1.30 1.21	9.3 5.6	15.4 14.6	10.6 9.9	31.9 23.9	9.7 4.3
5	Dry Wet	1.35 1.25	8.9 9.5	15.4 14.3	13.2 12.8	32.5 24.2	4.3 9.5
10	Dry Wet	1.43 1.33	6.7 5.6	13.2 14.6	10.9 12.8	35.8 24	5.4 7.0
15	Dry Wet	1.42 1.31	7.9 4.2	13.2 14.2	11.2 11.8	36.1 25.4	8.5 9.9
20	Dry Wet	1.44 1.35	6.6 10.3	13.6 14.7	10.7 14.4	36.3 28.6	7.8 9.4

Source: Lee et al. 2007 [19]. Reproduced with permission from Elsevier.

the type of aldehyde modifications were changed [18]. Also, stretching caused large variations in the fiber diameters. For instance, increasing molecular weight of chitosan from 14 to 24×10^4 kDa increased tenacity from 0.8 to 1.1 g/dtex, but the elongation did not show any consistent trend. Post-treatment of chitosan with aldehydes was suggested to be a better approach for producing chitosan fibers with improved properties [18]. Chitosan dissolved in acetic acid and having a viscosity of 52 700 cP at 25 °C was extruded into a coagulation bath of 1 M KOH and later into methanol. Dried fibers were immersed into cross-linking solutions (glyoxal or glutaraldehyde) of various concentrations. Considerable changes in the mechanical properties and decrease in swelling were observed after cross-linking (Table 5.9). It was suggested that a Schiff's base reaction occurred between chitosan and the aldehydes and specifically between the chitosan free amine and a hemiacetal [20].

In another study, glyoxal was used as a cross-linking agent for chitosan fibers obtained using 3.5% chitosan solution to improve properties of the fiber [21]. Considerable increase in tensile properties was observed depending on the processing conditions used. A tenacity of about 2.1 cN/dtex (1.0 cN/dtex before cross-linking) was obtained using a glyoxal concentration of 4%. Acetalization and Schiff base reaction were considered to be the reasons for the improved mechanical properties. A one-step fiber production and cross-linking was achieved by extruding chitosan solution into sodium acetate solution containing epichlorohydrin as the cross-linking agent [19]. Increasing the concentration of sodium acetate continually increased the dry and wet strength of the chitosan fibers (Table 5.10). Heat of decomposition also showed substantial increase, and fibers had a smooth cross section after cross-linking. In an earlier study on using epichlorohydrin to cross-link chitosan, strength of the fibers increased from 1.3 to 1.5 g/den with substantial decrease in elongation from 10.4% to 8.7%. However, there was considerable increase in wet strength of the fibers from 0.7 g/den before cross-linking to as much as 1.2 g/den after cross-linking. In another study, chitosan with deacetylation of 95% was made into fibers using acetic acid as the solvent. Fibers obtained were modified by treating with solutions containing phthalate and phosphate ions. Properties of the fibers were

Table 5.10 The variation of dry fiber mechanical properties with concentration of dialdehyde (1 hour, 25.8 °C).

Concentration of dialdehyde[a] (mol/dl), pH	Modulus (g/den)[b),c)]	Tenacity (g/den)[d)]	Elongation at break (%)
Glutaraldehyde control (water)	45.19 ± 0.77	1.44 ± 0.02	27.61 ± 2.53
7.64 E-5, 5.5	49.94 ± 1.94	1.71 ± 0.02	11.94 ± 1.05
1.46 E-4, 5.0	51.73 ± 0.68	1.94 ± 0.03	10.67 ± 0.77
6.40 E-4, 4.5	59.78 ± 1.38	2.09 ± 0.06	6.75 ± 0.76
1.27 E-2, 4.0	77.99 ± 1.35	2.19 ± 0.06	5.94 ± 0.28
2.44 E-2, 3.9	78.58 ± 4.46	2.23 ± 0.02	3.71 ± 0.25
5.22 E-2, 3.6	78.27 ± 4.37	2.21 ± 0.00	3.32 ± 0.13
9.88 E-2, 3.3	75.18 ± 0.23	1.64 ± 0.04	2.40 ± 0.09
2.20 E-1, 3.3	64.62 ± 2.70	1.22 ± 0.02	2.32 ± 0.13
Glyoxal control (water)	49.22 ± 0.77	1.44 ± 0.01	28.69 ± 2.25
1.71 E-4, 5.5	48.78 ± 2.05	1.68 ± 0.03	11.40 ± 0.30
3.32 E-4, 5.1	52.01 ± 2.19	1.93 ± 0.04	9.00 ± 1.47
6.29 E-4, 4.7	56.56 ± 4.38	1.96 ± 0.14	7.33 ± 1.30
1.38 E-3, 4.4	71.42 ± 2.73	2.20 ± 0.04	5.88 ± 0.30
2.10 E-3, 4.1	72.76 ± 0.38	2.20 ± 0.21	5.02 ± 1.46
2.75 E-3, 3.9	71.93 ± 5.16	2.35 ± 0.14	5.45 ± 0.87
5.25 E-3, 3.8	79.03 ± 6.22	2.42 ± 0.09	4.92 ± 1.05
2.58 E-2, 3.4	86.66 ± 5.14	2.46 ± 0.01	4.81 ± 0.09
5.08 E-2, 3.1	90.18 ± 5.86	2.53 ± 0.1	4.35 ± 0.32
1.00 E-1, 2.8	92.18 ± 1.16	2.46 ± 0.02	4.28 ± 0.99
2.17 E-1, 2.6	89.13 ± 1.90	2.35 ± 0.00	3.21 ± 0.00

a) Testing conditions were at 65% RH and 20 °C.
b) Fiber denier 5 20.7 dtex or 18.6 denier.
c) Gauge length was set at 2.3 cm.
d) Breaking strength, in grams force, is calculated by multiplying the tenacity by the denier.
Source: Knaul et al. 1999 [20]. Reproduced with permission from John Wiley & Sons.

highly dependent on the pH, immersion time and temperature [22]. Further, drawing of the fibers decreased the denier and elongation but considerably increased the strength due to the better alignment/orientation of the crystals in chitosan.

Common methods of wet spinning produce chitosan fibers that are several magnitudes higher than 10 µm in diameter. To produce fibers of less than 10 µm, a novel method of extruding chitosan solution into a bath consisting of sodium chitosan and STPP leading to formation of stable fibers that had compressive strength of 2400 kPa in dry and 280 kPa in the wet condition considered to be suitable for medical applications was developed [23]. In a similar approach called electro-wet spinning, submicron fibers were produced by dissolving 2% chitosan

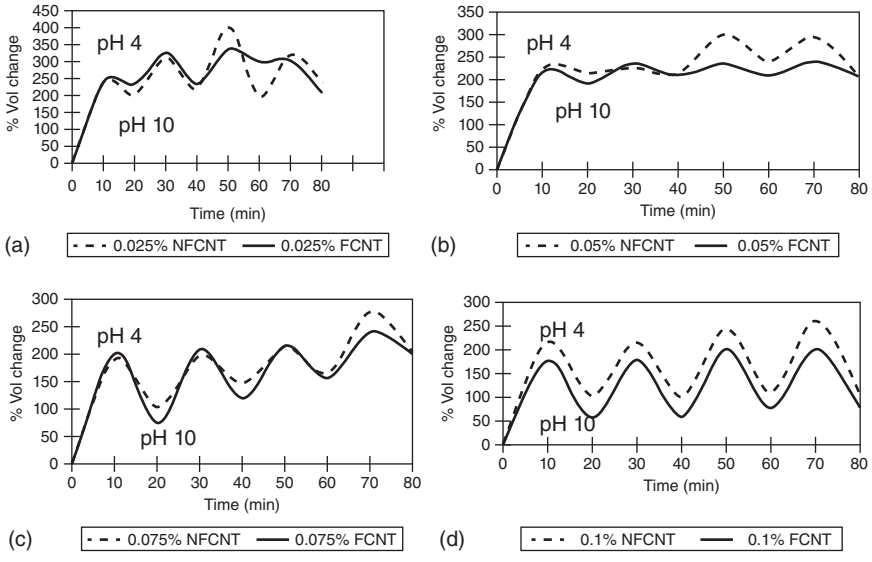


Figure 5.5 Changes in the pH response of chitosan fibers with different levels of single-walled carbon nanotubes. Source: Ozarkar et al. 2008 [25]. Reproduced with permission from Institute of Physics. (a) 0.025% NFCNT and 0.025%FCNT, (b) 0.05% NFCNT and 0.05% FCNT, (c) 0.075% NFCNT and 0.075% FCNT, and (d) 0.1% NFCNT and 0.1% FCNT.

in 2% acetic acid and extruding the solution into a coagulation bath consisting of ethyl alcohol and sodium hydroxide under an applied electric field [24]. Chitosan fibers developed were electroactive and had response time of less than 10 seconds and also showed reversible electroactuated contraction at low voltages (1.5 V) [24]. Better biocompatibility and stimuli-responsive properties of these materials were considered to be suitable for use as artificial muscles, biosensors, or artificial organs. Chitosan fibers reinforced with single-walled carbon nanotubes were also found to have electroresponsive properties. Reinforcing chitosan fibers with the carbon nanotubes increased the strength of the fibers from 96 to 226 MPa even at a nanotube concentration of 0.2 wt% [25]. Electric response and swelling of the fibers was dependent on the pH and other parameters (Figure 5.5).

5.3.2 Chitosan Blend Fibers

Since pure chitosan has limited applications and properties mainly due to its inferior mechanical properties, several researchers have attempted to produce blends of chitosan with various polymers. Many methods such as cross-linking and addition of inorganic or organic fillers have also been used to increase the mechanical properties of chitosan fibers. In a different approach, chitin nanocrystals made through acid treatment of chitin and having high surface area and modulus and biocompatibility were incorporated into chitosan solution and wet-spun into fibers. Nanocrystals were found to be uniformly distributed in the fibers and substantially increased the strength and modulus but decreased the elongation

up to 5 wt% in the fibers [26]. Highest strength of 2.2 cN/dtex and modulus of 146 cN/dtex was reported.

Bicomponent electrospun fibers were developed using a combination of chitosan (82.5% deacetylated) and PVA. Chitosan dissolved in acetic acid was mixed with PVA solution in various ratios and electrospun into fibers. However, the presence of chitosan hindered fiber formation, and it was not possible to obtain uniform fibers above a chitosan content of 25%. To overcome this limitation, chitosan was hydrolyzed using sodium hydroxide to substantially decrease the molecular weight and increase the chitosan content in the fibers. By decreasing the molecular weight of chitosan from 1500 dkDa to 800 kDa through alkaline hydrolysis, it was possible to obtain uniform bicomponent fibers (20 nm in diameter), having chitosan content up to 50%. Further, the PVA component in the fibers was removed by treating with NaOH, resulting in porous fibers.

A composite fibrous scaffold suitable for bone tissue engineering was fabricated by combing chitosan, polylactic acid, and hydroxyapatite. Both chitosan and HA were uniformly distributed in the PLA matrix, leading to improved the degradation of PLA. Bone mesenchymal stem cells had good affinity and grew along the direction of the chitosan fibers suggesting their suitability for bone tissue engineering [27]. Chitosan fibers blended with hyaluronan were produced using wet spinning method for potential use as scaffolds for ligament tissue engineering [28]. Chitosan used for fiber production had a molecular weight of 600 000 and deacetylation degree of 81%. Solution was extruded into methanol to form the fibers. Inclusion of HA in chitosan increased mechanical properties and also biological activity, making the fibers suitable for ligament tissue engineering.

Composite fibers composed of chitosan and *O*-hydroxyethyl chitosan fibers were prepared by blending *O*-hydroxyethyl chitosan xanthate and cellulose xanthate using the viscose production process [29]. The chitosan ester was prepared using sodium hydroxide and carbon disulfide. Chitosan ester prepared was blended with various ratios of cellulose xanthate and wet-spun into fibers. Properties of the fibers and their activity against *Escherichia coli* were measured. Properties of the blend fibers (Table 5.11) were similar to that of viscose rayon except wet elongation, which increased significantly as the chitosan ratio was increased. The presence of chitosan imparted excellent antibacterial activity against *E. coli* and also increased the antistatic properties [29].

Table 5.11 Comparison of the properties of cellulose/*O*-hydroxyethyl chitosan fibers with viscose rayon [29].

Fiber	Tensile strength (cN/dtex)		Elongation at break (%)		Moisture absorption (%)	Mass specific resistance (Ωg/cm, × 10^8)
	Dry	Wet	Dry	Wet		
Viscose rayon	3.06	2.70	19.0	17.9	13.01	4.7
CHCFs-3	3.04	2.66	21.2	19.4	13.23	4.3
CHCFs-4	3.01	2.61	22.5	21.2	13.40	4.2
CHCFs-6	2.97	2.55	22.9	24.5	13.55	4.0

Source: Xu et al. 2010 [29]. Reproduced with permission from Elsevier.

Table 5.12 Properties of papain purified using the chitosan/nylon hybrid fibers.

Protein content (mg)	Specific activity (U/mg)	Purification (fold)
15.1	6.67	—
1.3	6.17	0.93
1.1	7.08	1.06
0.7	9.76	2.46
0.4	16.41	4.79
0.3	31.95	2.87
0.2	13.27	1.99

Source: Zhang et al. 2010 [30]. Reproduced with permission from Springer Nature.

Chitosan/nylon 6 hybrid fibers with diameters in the range of 80–310 nm were developed through electrospinning by dissolving the polymers using a 90/10 (v/v) mixture of HFIP/formic acid. Membranes obtained were immobilized with cibacron Blue F3G through nucleophilic reaction. Ability of the immobilized membranes to purify papain was investigated [30]. An equilibrium adsorption capacity of 93.5 mg/g of papain was obtained, and most of the adsorbed papain could be eluted depending on the pH and other conditions (Table 5.12). It was suggested that the membranes could be used for industrial purification of papain due to their high affinity and regeneration potential.

To exploit the advantages of natural and synthetic polymers for medical applications, chitosan was blended with poly(caprolactone) and made into nanofibers. The two polymers were blended by dissolving in mixture of 3/7 acetic acid/formic acid. It was observed that addition of PCL substantially increased the electrospinnability of chitosan [31] due to favorable change in viscosity. Blend fibers had diameters of about 154 nm and an ultrafine nanofiber web could be obtained. In a similar approach, chitosan was blended with poly(lactic acid) in a core–shell form using coaxial electrospinning [32]. Nonwoven fibrous mats were obtained with PLA as the core and chitosan as the sheet. Blend fibers had an average diameter of 236 nm and exhibited excellent antibacterial activity up to 100% against *E. coli*.

To improve the mechanical properties and applicability of chitosan, chitosan fibers modified with hydroxyapatite were combined with nanoparticles of hydroxyapatite (HAp) and tricalcium phosphate (β-TCP). Fibers were produced by extruding the mixture into aqueous NaOH solution and later washed using ethanol–water solution [33]. Some of the properties of the chitosan fibers containing various levels of the nanoparticles are listed in Tables 5.13 and 5.14. Inclusion of the individual nanoparticles increased the linear density and decreased the tenacity of the fibers, whereas the nanoparticle complex did not decrease the tenacity. However, it was reported that the presence of the nanoparticles facilitated smoother production of the fibers during extrusion [33]. In a similar approach, various (2, 4, or 6%) graphene oxides were added into 10% chitosan dissolved in acetic acid and made into fibers using the wet spinning

Table 5.13 Some properties of chitosan solutions containing hydroxyapatite (HAp) and tricalcium phosphate (ß-TCP) particles.

	Percentage of solution used (%)			Concentration of				
Solution code	A	B	C	ß-TCP (wt%)	HAp (wt%)	Acetic acid (wt%)	Chitosan (wt%)	Dynamic viscosity/ temperature (Pa/°C)
Chit 58	100	—	—	—	—	3.00	5.16	19 000/52
MCT 6	83.3	16.7	—	0.333	—	2.75	4.50	7500/49
MCT 7	83.3	—	16.7	—	0.330	2.75	4.63	9250/49
MCT 8	71.4	14.3	14.3	0.286	0.283	2.36	4.46	4500/52
MCT 11	62.5	25.0	12.5	0.707	0.252	2.10	4.01	1750/51

Source: Wawro et al. 2011 [33]. https://www.mdpi.com/1422-0067/12/11/7286 and http://creativecommons.org/licenses/by/3.0/. Licensed under CCBY 3.0.

Table 5.14 Influence of HAp, β-TCP, and HAp/ β-TCP on the mechanical properties of chitosan fibers.

Parameter	Chitosan	MCT6	MCT7	MCT8	MCT11
Linear density (dtex)	4.39	4.48	5.14	5.41	4.16
Breaking force (cN)	3.61	3.51	2.46	2.91	3.35
Tenacity (cN/tex)	8.22	7.83	4.79	5.38	8.05
Elongation at break (%)	17.0	22.0	9.9	11.0	12.0
Tenacity, wet (cN/tex)	6.38	4.93	3.46	4.58	6.86
Elongation, wet (%)	7.8	7.3	7.8	6.1	8.0

Source: Wawro et al. 2011 [33]. https://www.mdpi.com/1422-0067/12/11/7286 and http://creativecommons.org/licenses/by/3.0/. Licensed under CCBY 3.0.

approach [34]. Considerable changes in the morphology and tensile properties were observed due to the presence of graphene oxide. Tensile strength increased from 96 to 168 MPa when the graphene oxide content was increased from 0% to 6%. However, elongation of the fibers decreased with increasing graphene. The blend fibers spontaneously absorbed fuchsin acid dye through an exothermic process. It was suggested that the graphene oxide-containing chitosan fibers would be suitable for removal of dyes from aqueous solutions [34].

Composite chitosan-poly(lactide-co-glycolide) (PLGA) fibers were developed by dissolving the two polymers in a blend of methylene chloride and HFIP. Dissolved polymers were extruded into a methanol bath. Similar approach was also used to produce PLGA-dispersed chitosan blend fibers that were formed into a mat. The fibers obtained had diameters of 30 µm, and the micropores formed in the fibers had diameters in the range of 150–200 µm [35]. Addition of methylene chloride was necessary to completely dissolve chitosan in HFIP. Combing PLGA and chitosan resulted in desired degradability and mechanical properties. Chondrocytes loaded on the blend scaffolds showed active growth and potential for tissue engineering applications [35].

In another study, chitosan and poly(vinyl alcohol) blend fibers were prepared by dissolving chitosan in acetic acid and PVA in water. The two polymers were combined in various ratios and then extruded into a coagulation bath consisting of 6% sodium hydroxide [36]. Blends containing 60% chitosan had highest strength, moisture absorption, and antibacterial properties against *E. coli* and *Staphylococcus aureus*. Instead of a binary blend, a tertiary blend of chitosan/PLA and collagen was prepared for potential use for cartilage tissue engineering. A highly porous scaffold was obtained with good potential for cell attachment and viability [37].

5.3.3 Generating Hollow Chitosan Fibers

Hollow chitosan fibers were prepared as potential carriers for various biomolecules [38]. To obtain the hollow structure, outside layer of the fibers was coagulated first, and later, the core of the fiber was removed by passing air and then treating with 1 M NaOH solution. Internal diameter of the hollow fibers was $400 \pm 20\,\mu m$ (Figure 5.6) with a wall thickness of about $60 \pm 5\,\mu m$, and standard length was 0.5 m. Fibers were immersed in a solution containing various biomolecules, and the diffusion properties were studied. pH was found to have major effect on the diffusion compared with permeate concentration or flow rate. Diffusion of biomolecules such as tryptophan, vitamin B12, and chloramphenicol was dependent on the molecular weight. Since the fiber was hollow, the structure collapsed upon immersion in the media and had limited permeability. The hollow fibers were considered to be suitable for delivery of enzymes, catalysis, and nerve regeneration [38]. A dry–wet spinning approach was used to prepare hollow chitosan fibers, and the fibers obtained were cross-linked using glutaraldehyde [39]. In this method, a 5.5% chitosan solution was extruded through a spinneret having an outer and inner diameter of 2 and 1 mm, respectively, and passed into a coagulation bath containing 10% NaOH. Two different flow rates of bore fluid were used to create the hollow structure. Fibers obtained were cross-linked with glutaraldehyde, which helped to improve the tensile properties (strength up to 50 MPa) up to a glutaraldehyde

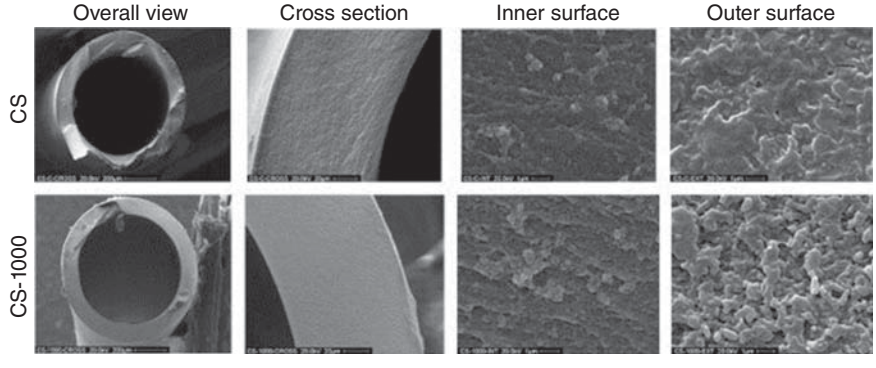


Figure 5.6 Scanning electron images of the morphology of pure and cross-linked chitosan fibers. Source: Tasselli et al. 2013 [39]. Reproduced with permission from Elsevier.

concentration of 200 g/l. Figure 5.11 shows the morphology of the chitosan fibers before and after cross-linking [39]. Cross-linking made the fibers rougher but increased the resistance to swelling. Sorption capacity of the fibers for dyes decreased with increasing level of cross-linking since the available sites would be consumed for cross-linking. However, the fibers could be regenerated using NaOH and reused for dye sorption [39].

5.3.4 Microfluidic Method of Producing Chitosan Fibers

Conventional approach of producing chitosan fibers used harsh chemicals that will kill cells. To incorporate cells into fibers, a microfluidic approach was used, and chitosan–alginate fibers intended for tissue engineering applications were developed [40]. Figure 5.7 shows a schematic process of producing chitosan–alginate fibers loaded with HepG2 cells. Diameter of the fibers could be controlled within 100 μm. Cells could be easily encapsulated within the fibers, and the presence of alginate promoted the attachment, growth, and proliferation of cells. Microfluidic approach of producing chitosan fibers also allowed spatial control of the spreading of the cells that would be beneficial for tissue engineering [40].

5.3.5 Application of Chitosan Fibers

Chitosan fibers have been extensively used for medical, textile, environmental, and cosmetic applications mainly due to their antimicrobial property. Novel

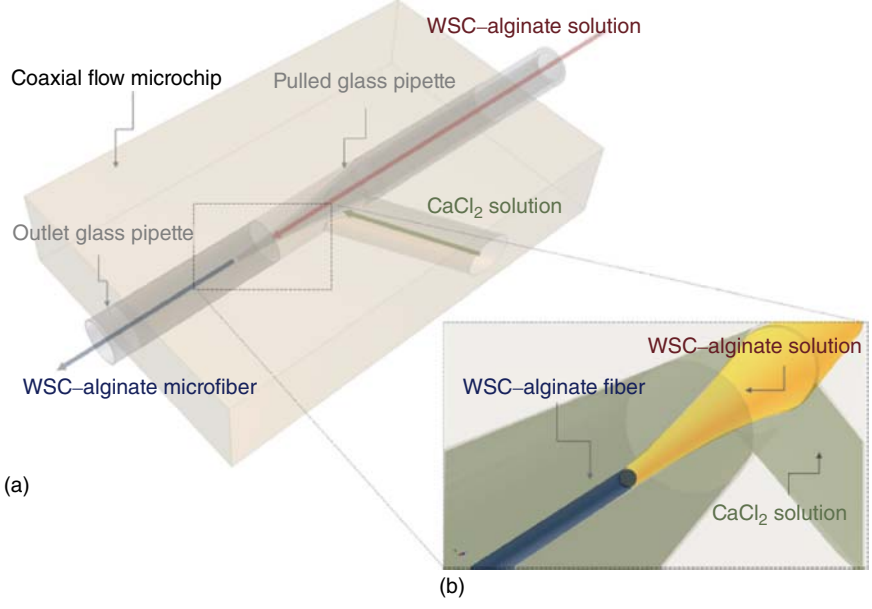


Figure 5.7 Schematic representation of the microfluidic approach of producing chitosan fibers. (a) Schematic for the microfluidic device and (b) detailed view of fiber forming section. Source: Lee et al. 2011 [40]. Reproduced with permission from American Institute of Physics.

chitosan fibers with ability to release various fragrances were prepared by treating with various aldehydes [41]. Strength and elongation of the fibers decreased due to the treatment with aldehydes, but controlled release of the fragrance could be felt in the atmosphere [41]. These fibers were suggested to be suitable for cosmetics, air filters, and textiles. To improve the antimicrobial properties, chitosan fibers were treated with zinc and silver, and the activity against *E. coli*, *S. aureus*, and *Bacillus subtilis* were tested. Up to 100% reduction in bacterial activity was achieved with silver-containing fibers providing the highest resistance [42]. Silver and zinc ions in the fibers could be released into solution, and the extent of release could be controlled depending on the loading and unloading conditions.

An attempt was made to produce chitosan fibers suitable for medical applications without the use of cytotoxic cross-linking agents. Production parameters of chitosan fibers were varied to obtain optimum conditions and desired mechanical properties. Instead of the conventional approach, fibers were immersed in 10% or 25% ammonia solution [43]. Further, fibers were cross-linked using heparin and annealed to improve mechanical properties and stability. Extrusion into ammonia solution increased the crystallinity and hence tensile strength by more than 200%. Changes in the tensile properties of the fibers at various conditions are shown in Figure 5.6. In addition to providing desired mechanical properties, the fibers were also found to support the attachment and growth of valvular interstitial cells (VIC) after 10 days of culture [43]. It was suggested that fibrous chitosan scaffolds with tunable mechanical properties could be produced using this approach [43].

Chitosan fibers were carboxymethylated by treating with chloroacetic acid to impart chelating properties and improve sorption of Cu (II) ions [44]. Degree of carboxymethylation varied from 12% to 40% depending on the conditions used during modification. Sorption capacity of Cu(II) ions was also dependent on the time, pH, temperature, amount of sorbent, etc. (Table 5.15) [44]. Up to 148 mg of Cu(II) was sorbed per mg of fiber when the carboxymethylation was 40%. To improve moisture absorption and retentivity, *N*-acyl chitosans were prepared using *N*-acetylated, *N*-maleyl, and *N*-succinyl chitosan in glycine chloride [34]. Changes in the moisture sorption of chitosan after different chemical modifications are depicted in Figure 5.8. Moisture sorption capacity of the fibers was dependent on the degree of substitution with high DS providing better sorption. Ability to control the mechanical properties and moisture sorption was suggested to be suitable for use in hernioplasty, saturation. or wrinkle filling [34].

Chitosan fibers having a linear density of 1.23 mg/cm, strength of 1.46 g/d, and extensibility of 12.1% were made into a scaffold (Figure 5.9) for attachment, spreading, and differentiation of osteoblasts [45]. Fibers in the scaffold had average diameter of 20 μm with a flaky surface. The scaffolds were coated with collagen to improve cell attachment and growth. Excellent attachment and proliferation of murine osteoblasts was observed, and it was suggested that the scaffolds were suitable for culture of human normal and stem cells [45].

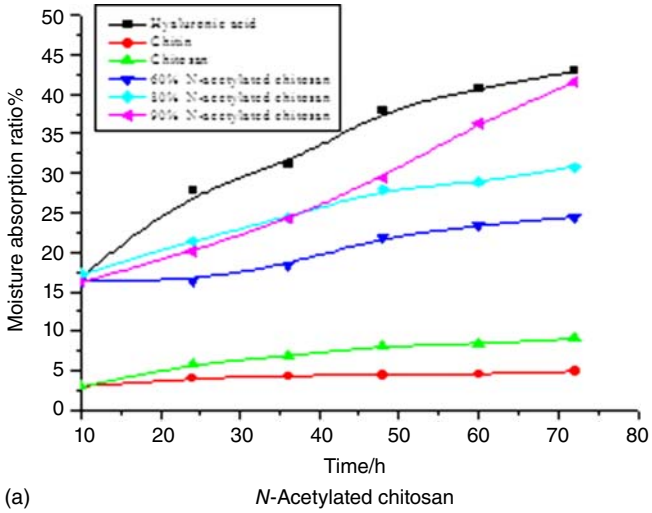
Wound dressings are one of the most common applications of chitosan fibers and fabrics due to the inherent antibacterial, biocompatible, and excellent

Table 5.15 Effect of various conditions on the removal efficiency of Cu(II) by the chitosan fibers.

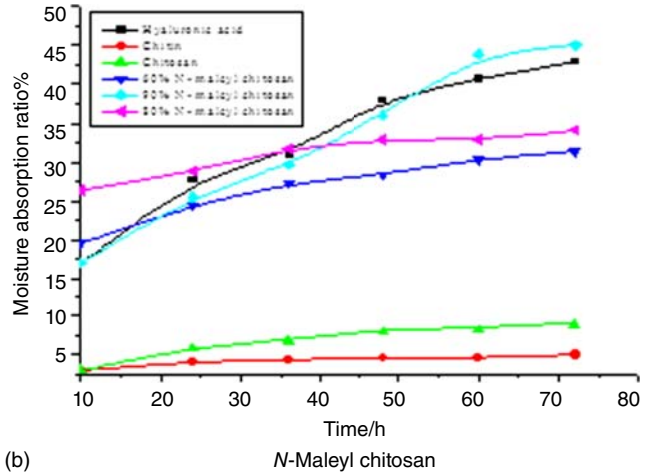
	Cu(II) concentration after treatment (mg/l)	Cu (II) removal (%)	Absorption capacity (mg Cu(II)/g fiber)
Temperature (°C)			
25	7.7	95.2	76.1
37	64.2	59.9	47.9
55	127.6	20.2	16.2
70	83.2	48.0	38.4
95	21.2	86.8	69.4
Amount of fiber (g)			
0.050	85.9	46.3	148.1
0.100	34.2	78.6	125.7
0.150	8.7	94.5	100.8
0.200	14.3	91.1	72.9
0.250	8.1	95.0	60.8
pH			
2	49.4	69.1	55.3
4	22.2	86.1	68.9
7	22.2	86.1	68.9
9	33.6	79.0	63.2
11	24.9	84.4	67.5
Time (h)			
0.25	62.2	61.1	48.9
0.5	75.3	53.0	42.4
1	50.4	68.5	54.8
2	44.2	72.3	57.9
5	7.7	95.2	76.1
8	9.8	93.9	75.1
15	17.0	89.4	71.5
24	14.2	91.1	72.9

Source: Qin et al. 2006 [44]. Reproduced with permission from John Wiley & Sons.

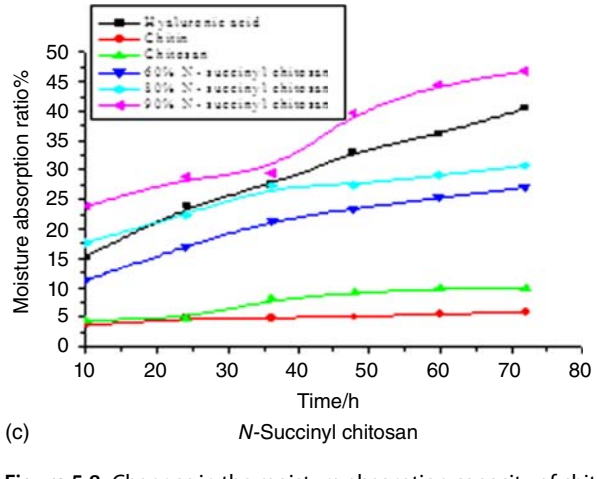
biosorption properties. To further improve the antibacterial properties of chitosan, colloidal silver nanoparticles were incorporated into fibers [46]. Amount of silver in the fibers was controlled at 130 and 167 mg/kg. Properties of the fibers including tensile strength and elongation were affected due to the inclusion of silver. Increasing amount of silver in the fibers increased the bactericidal activity against *S. aureus* and *E. coli*. The fibers were also considered as nonconductive and suitable for preparation of bandage and other medical materials [46]. Chitosan-based heart valve scaffolds were developed using chitosan fibers



(a) *N*-Acetylated chitosan

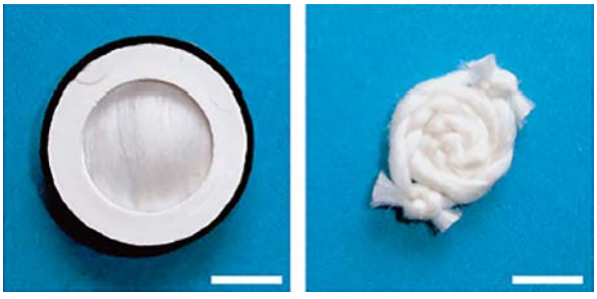


(b) *N*-Maleyl chitosan



(c) *N*-Succinyl chitosan

Figure 5.8 Changes in the moisture absorption capacity of chitosan fibers modified using various approaches. (a) N-acetylated chitosan, (b) Nmaleyl chitosan, and (c) N-succinyl chitosan. Source: Li et al. 2013 [34]. Reproduced with permission from John Wiley & Sons, Inc.



(a) (b)

Figure 5.9 Digital image of a scaffold made using chitosan fibers and suitable for tissue engineering. Left image shows chitosan fibers fixed inside a holder and right image is stand-alone chitosan fibers. (a) Chitosan fibers fixed inside a holder and (b) stand-alone chitosan fibers. Source: Heinemann et al. 2008 [45]. Reproduced with permission from American Chemical Society.

cross-linked with heparin [43]. Addition of fibers into the scaffold increased the strength (220 kPa) and stiffness equivalent to radial values of human pulmonary valve leaflets. Unreinforced scaffolds had strength of 58 kPa compared with 750 kPa for the reinforced scaffolds. Similarly, the strain of the fibers was 20% compared with 90% for the scaffold. It was suggested that the mechanical properties of the scaffold could be controlled as per requirement. Chitosan-based composite nanofibrous membranes were prepared by blending chitosan, PLA, and silk nanoparticles and electrospinning. *N*-carboxymethylation of chitosan was done to make chitosan soluble in water and compatible with PVA. Strong interactions were observed between the components in the fibers, and inclusion of silk nanoparticles promoted attachment and growth of mouse fibroblasts. Hence, the scaffolds were considered suitable as wound dressings [47].

Fiber meshes intended for tissue engineering were prepared from 85% deacetylated chitosan. Dissolved chitosan was extruded into a coagulation bath containing sodium sulfate and sodium hydroxide and later drawn to increase the orientation. The fibers were subject to bioactivity, biocompatibility, and cytotoxicity tests [48]. Morphological analysis showed that the fibers were oriented in one direction and had smooth but striated surface. Fibers had a tensile strength of 205 MPa and elongation of 8.5%. When immersed into body fluids, the fibers were able to initiate the formation of calcium phosphate suggesting bioactivity. Osteoblasts seeded on the fiber meshes had excellent attachment, growth, and proliferation (Figure 5.10).

Various flavonoids were grafted onto chitosan fibers using tyrosinase as the cross-linking agent and studied for their potential to improve antimicrobial and antioxidant properties [49]. Compared to ungrafted chitosan, higher antioxidant activity ranging from 0.5% to 88% was determined depending on the type of flavonoid and assay method used [49] (Table 5.16). The use of an enzyme and natural antioxidant to impart antibacterial and antioxidant properties was considered highly suitable for medical applications.

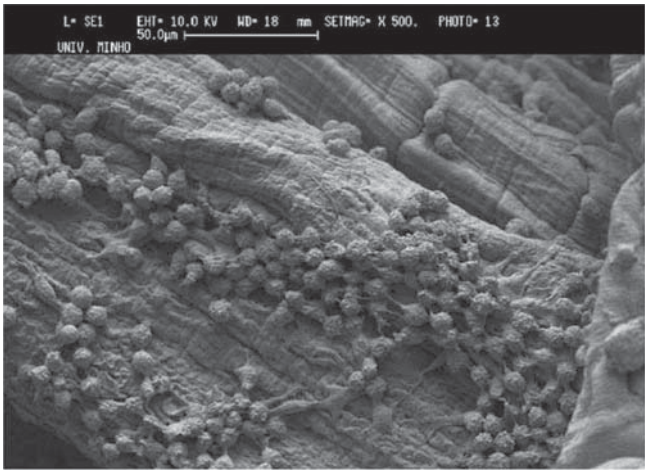


Figure 5.10 SEM images shows substantial proliferation of osteoblast cells on the surface of the chitosan fiber meshes after seven days of culture. Source: Tuzlakoglu et al. 2004 [48]. Reproduced with permission from John Wiley & Sons.

5.4 Electrospun Chitosan Fibers

Nanofibers have high surface area and can hence sorb higher levels of chemicals and pollutants. Also, nanofibers mimic the nature of the extracellular matrix in the human body and hence are preferred for medical applications. Chitosan has been widely studied for developing nanofibers for various applications (Table 5.17). Nanofibers with average diameter as low as 66 nm were developed by dissolving 75% deacetylated chitosan in a mixture of trifluoroacetic acid and dichloromethane [51]. Electrospinning conditions and the ratio of the two solvents significantly affected the properties of the electrospun fibers. A chitosan concentration of 8% and acetic acid to dichloromethane ratio of 80 : 20 produced fiber mats with the lowest thickness when a voltage of 30 kV and needle diameter of 0.5 µm was used [51]. In a process termed "electrohydrodynamic processing," chitosan grafted with L-lactide was made into fibrous substrates for potential use as tissue engineering scaffolds [52]. Grafted chitosan was dissolved using ethyl acetate and 2-butanone and electrospun into fibers. Hydrophilicity and rate of biodegradation of the scaffolds could be controlled by varying the L-lactide to chitosan ratio. Viability and proliferation of cells was higher on the grafted scaffolds. However, higher levels of lactic acid reduced the pH of the media, resulting in cytotoxicity [52]. Chitosan nanofibers have also been used as sorbent for various metals. To produce the fibers, chitosan was dissolved in HFIP and extruded using a voltage of 8 kV and tip to collector distance of 7 cm. Fiber mats were immersed in metal solutions, and various sorption conditions were studied [53]. Sorption of metal ions by the chitosan fibers was dependent on the sorption conditions, and up to 100% sorption could be achieved. The fibers also showed selectivity toward various metal ions with the following order Cu > Fe > Ag > Cd and were found to be suitable for use in solid-phase extraction cartridges [53].

Table 5.16 Antioxidant activity of chitosan fibers grafted with various flavonoids.

Antioxidant activity	Catechin	Epicatechin	Epigallocatechin	Epigallocatechin gallate	Fisetin	Quercetin	Rutin	Hesperidin	Daidrein
Total antioxidant activity	13.9 ± 0.02	10.6 ± 0.03	69.9 ± 0.5	15.1 ± 0.05	—	—	3.1 ± 0.05	4.2 ± 0.05	20.7 ± 0.03
DPPH/free radical scavenging	87.4 ± 0.03	88.5 ± 0.04	—	53.9 ± 0.03	41.1 ± 0.1	24.2 ± 0.08	6.6 ± 0.1	7.9 ± 0.02	2.5 ± 0.01
ABTS radical cation assay	8.5 ± 0.04	21.0 ± 0.03	20.0 ± 0.05	26.8 ± 0.02	3.4 ± 0.0	25.5 ± 0.03	17.9 ± 0.01	21.3 ± 0.05	26.9 ± 0.03
Superoxide anion scavenging activity	36.9 ± 0.05	1.1 ± 0.05	73.9 ± 0.08	35.1 ± 0.03	32.9 ± 0.3	38.9 ± 0.07	—	48.9 ± 0.02	19.7 ± 0.04
Ferrous metal ion chelating activity	0.46 ± 0.03	4.18 ± 0.04	10.9 ± 0.05	—	—	8.8 ± 0.04	3.6 ± 0.04	12.2 ± 0.05	—

Source: Sousa et al. 2009 [49]. Reproduced with permission from Elsevier.

Table 5.17 Examples of methods used to process chitosan into nanofibers and their potential applications [50].

Polymer	Solvents	Average fiber diameter (nm)	Application
Chitosan	aq AA	130	—
Chitosan	TFA/DCM	130 ± 10	—
Chitosan	TFA/DCM	126 ± 20	Tissue engineering
Chitosan (neutralized with K_2CO_3 solution)	TFA	235	Filtration
Chitosan/PVA (removing PVA with 0.5 M NaOH)	aq AA	80–150	Enzyme immobilization
Chitosan/PVA	aq AA	99 ± 21	Wound dressings
Chitosan/PEO	aq AA	80 ± 35	Filtration
Chitosan/UHMWPEO (10%)	aq AA/DMSO	138 ± 15	—
Chitosan/UHMWPEO (20%)	aq AA/DMSO	102 ± 14	—
Chitosan/PET	TFA	500–800	Wound dressings
Chitosan/PCL	HFIP	450 ± 110	Bone tissue engineering
Chitosan/nylon-6	HFIP/FA	80–310	Filtration
Chitosan/PVA-PLGA (by multi-jet electrospinning method)	aq AA THF/DMF	275 ± 175	Tissue engineering
Chitosan/collagen/PEO (cross-linked by GA vapor)	aq AA	398 ± 76	Wound dressings
H-CS	$CHCl_3$	640–3930	Skin tissue engineering
Q-CS/PVP (cross-linked by UV irradiation)	Water	2400 ± 640	Wound dressings
CS-HOBt/PVA	Water	190–282	Drug delivery
Chitosan/HAp/PVA	aq AA/DMSO	100–700	Bone tissue engineering
Chitosan/gelatin/AgNPs	aq AA	220–400	Wound dressings
CS-g-AA/PaNPs	aq AA	70–200	Catalyst

THF, tetrahydrofuran; aq AA, aqueous acetic acid solution; DMSO, dimethyl sulfoxide; DMF, dimethylformamide; HFIP, 1,1,1,3,3,3-hexafluoro-2-propanol.

Low (70 000 Da), medium (190 000–310 000 Da), and high molecular weight (500 000–700 000 Da) chitosan was dissolved in trifluoroacetic acid and electrospun into fibers. High molecular weight chitosan produced fibers with diameter of 108 nm compared with about 77 nm for the other two molecular weight range. Although the fibers had acceptable mechanical properties, they instantly dissolved in water or acetic acid. To improve the stability, the fibers were cross-linked using glutaraldehyde vapors [54]. Cross-linking resulted in substantial decrease in strength (from 4 to 1.2 MPa) and elongation of the fibers.

However, the cross-linked fibers were found to be stable in water, acetic acid, and NaOH solutions [54]. Glutaraldehyde vapors were considered suitable for cross-linking chitosan nanofibers, but the effect of cross-linking on cells and hence biocompatibility was not assessed. Schiffman et al. also demonstrated that a one-step cross-linking and electrospinning of chitosan could be done that was 25% faster and also produced finer fibers. Glutaraldehyde solution was combined with the chitosan solution and electrospun. Cross-linking occurred during electrospinning, thereby avoiding the need for an additional cross-linking step [55]. Cross-linked fibers were stable to acetic acid, water, and NaOH for up to 72 hours. However the biocompatibility/cytotoxicity of these fibers was not evaluated.

Highly aligned nanofibers desirable for use in textile, energy, environment, and bioengineering were developed from chitosan using a novel centrifugal electrospinning system (Figure 5.11) [56]. Increasing speed produced fibers with better alignment that were also shown to have better piezoelectric properties for PVDF fibers. No results were presented for chitosan fibers.

To prepare chemically stable chitosan membranes, carbon black having an average size of 67 nm was mixed with chitosan (190–310 kDa) dissolved using trifluoroacetic acid. Solutions containing up to 62% carbon black were electrospun to form membranes, which were cross-linked using glutaraldehyde. Inclusion of the carbon black changed the color of the membranes (Figure 5.12) but did not change the morphology of the fibers [57]. Although uncross-linked membranes dissolved immediately, the cross-linked membranes had excellent stability in acidic, basic, or aqueous solutions for up to 20 days. Conductivity of

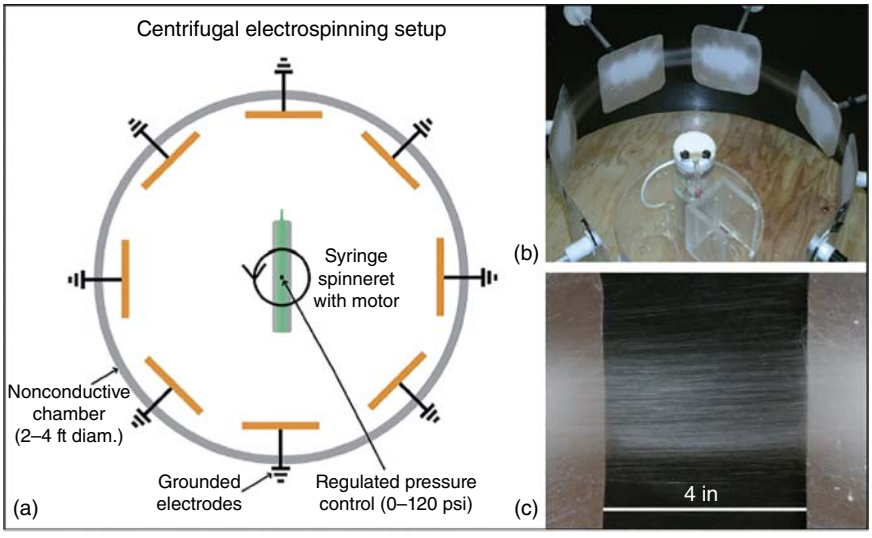


Figure 5.11 New method of centrifugal electrospinning using different collectors and rotating needle. (a) Schematic representation of the system configuration, (b) photograph of the CE system with deposited PVDF nanofibers, and (c) electrospun PVDF fibers deposited across a four-inch gap between two grounded electrodes. Source: Edmondson et al. 2012 [56]. Reproduced with permission from Royal Society of Chemistry.

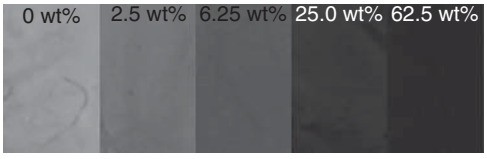


Figure 5.12 Images of chitosan membranes containing various levels of carbon black shows considerable change in color due to the addition of the carbon black. Source: Schiffman et al. 2011 [57]. Reproduced with permission from Elsevier.

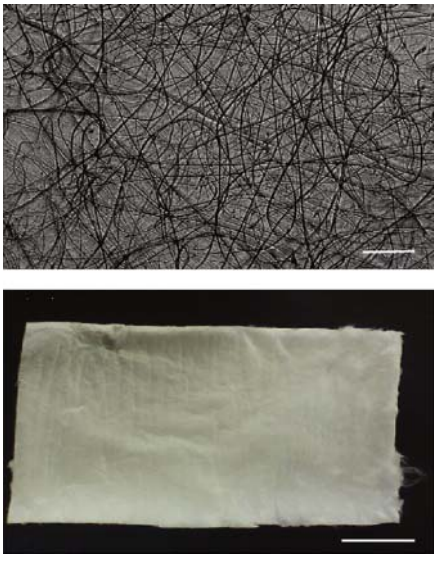


Figure 5.13 Digital image of the morphology of the fibers and picture of the fibrous chitosan mat produced by electrospinning. Source: Frohbergh et al. 2012 [58]. (a) Electrospun chitosan microfibers and (b) fibrous mat from the chitosan fibers. Reproduced with permission from Elsevier.

the membranes increased nearly three times when 2.5% or 6.25% carbon black was present, but the tensile strength and elongation decreased substantially. Good chemical stability and ability to control the conductivity were considered to be desirable for electrochemical applications [57].

Composite electrospun fibers intended for bone tissue engineering were made by adding hydroxyapatite nanocrystals into chitosan solution [58]. Electrospun mats obtained (Figure 5.13) were cross-linked with genipin to increase water stability. The scaffolds were soaked in the genipin solution in PBS for 24 hours for the cross-linking to occur. The presence of hydroxyapatite significantly promoted the formation of bone tissue, and cross-linking increased the modulus up to fourfolds (142 ± 13 MPa). Modulus of the fibrous scaffold was considered to be similar to that of natural periosteum. Attachment, growth, proliferation, and mRNA expression of osteoblast cells suggested that the scaffolds could be useful for repair and regeneration of maxillofacial defects and injuries [58]. Since electrospun fibers are more susceptible to moisture and disintegrate in aqueous systems, it is necessary to cross-link or modify them with chemical and physical approaches as discussed earlier. Instead of the conventional covalent

cross-linkers, Kiechel et al. used glycerol phosphate (GP), tripolyphosphate (TPP), and tannic acid (TA) as new set of noncovalent cross-linkers [59]. Type of cross-linker used influenced the stability, fiber diameters, and hence application. Cross-linking could be done in a one- or two-step process depending on the cross-linker. The cross-linked nanofiber membranes were suggested to be suitable for tissue engineering and drug delivery applications [59].

Three-dimensional electrospun chitosan mats were prepared using trifluoroacetic acid as the solvent. The fiber mats obtained were treated with fibronectin to promote the attachment and growth of primary ventricular cardiomyocytes and also co-cultured with microvascular endothelial cells or fibroblasts [60]. It was found that the 3D chitosan scaffolds supported the attachment and growth of cells and could form cardiac tissue constructs similar to native heart tissue. It was suggested that co-culture of cells could maintain the properties of the individual cells in long-term use [60].

Core–shell polylactic acid/chitosan fibers were produced by electrospinning using sodium dodecyl sulfate [17]. Chitosan was modified using SDS and later dissolved along with PLA using dichloromethane and dimethyl sulfoxide, and the solution was electrospun into fibers. Cross-linking of the fibers was done using glutaraldehyde vapors, and the scaffolds obtained were used as substrates for mouse fibroblast cells (L929). SDS on the fibers was removed to create porous substrates that promoted the attachment, growth, and proliferation of the cells. Shape and proliferation of the cells suggested that the fibers would be suitable for tissue engineering and wound healing [17]. Instead of using cross-linking agents, Pangon et al. demonstrated that addition of chitin whiskers into chitosan/PVA blends substantially improved the mechanical properties. In addition, biomineralization with hydroxyapatite leads to the promotion of the attachment and growth of osteoblast cells. It was suggested that the chitosan/chitin/PVA hydroxyapatite blends would be ideal for bone tissue engineering [61]. In a similar approach, biomimetic scaffolds mimicking the structure of the extracellular matrix were prepared by combining chitosan with collagen. Various ratios of collagen and chitosan were dissolved in a 90/10 mixture of 1,1,1,3,3,3-hexafluoroisopropanol/trifluoroacetic acid and electrospun into fibers and later cross-linked with glutaraldehyde (Chen et al. 2010). Fibers in the blend had average diameter of 434–691 nm, and cross-linking stabilized the morphology of the scaffolds. Both endothelial and smooth muscle cells had excellent proliferation on the nanofibers suggesting their suitability for tissue engineering and regeneration of blood vessel and nerve tissues (Chen et al. 2010).

Conducting nanofibers were obtained by blending plasma-modified chitosan with poly(3,4-ethylenedioxythiophene) using PVA as a supporting polymer. Plasma-modified chitosan and PEDOT were dissolved using 0.5 M acetic acid and later combined with PVA dissolved in water to form the blend solution for electrospinning [62]. Plasma modification provided better antibacterial activity and formation of finer fibers. Electrochemical studies showed that the blend fibers had electroactive properties and could be useful for biomedical applications [62] (Figure 5.14).

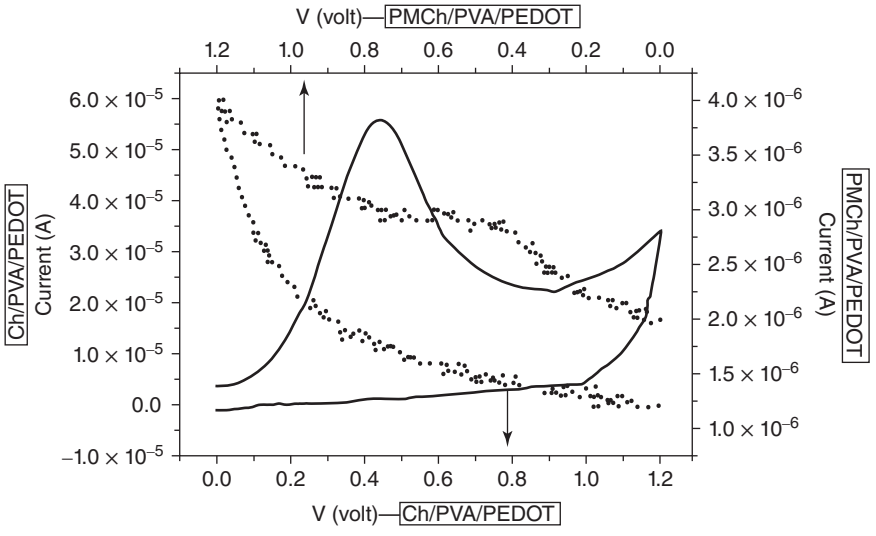


Figure 5.14 Properties of the chitosan/PVA/PEDOT blend fibers. Source: Kiristi et al. 2013 [62]. Reproduced with permission from Elsevier.

5.5 Regenerated Chitosan Fibers

In addition to the natural micro- and electrospun fibers, researchers have also produced regenerated chitosan fibers. For this, chitosan was dissolved in a binary ionic liquid and regenerated using a wet and dry spinning technique [63]. Chitosan (5%) was dissolved and heated at 80 °C to have a viscosity of 5 Pa. Solution was extruded through a 60 μm diameter spinneret at a pressure of 0.4 MPa and coagulated first using ethanol and later using 5% sodium hydroxide solution. The fibers obtained had a strength of 2.1 cN/dtex and modulus of 83.5 cN/dtex, much stronger than the common chitosan fibers [63].

5.6 Conclusions

Chitosan is one of the few biopolymers that has been extensively studied and used for medical, environmental, energy, textile, and other applications. Inherent antimicrobial activity, easy solubility, and ability to be made into various forms are some of the advantages of chitosan. However, stability in aqueous environments and mechanical properties of chitosan-based products are concerns for many applications. Despite considerable efforts on chemical and physical modifications including cross-linking, achieving the desired level of properties in chitosan-based products is a challenge. In addition to conventional solution spinning, chitosan has been made into electrospun fibers with properties suitable for skin and bone tissue engineering. Several studies have demonstrated that chitosan fibers can be used for controlled release of drugs and sorption of pollutants from wastewater. Chitosan has also been blended with various

biopolymer and synthetic polymers to develop fibers for specific applications. Similarly, a few studies have been done on developing regenerated chitosan fibers. Recent studies have focused on using additives such as graphene oxide, carbon nanotubes, and carbon black to improve the applicability of chitosan. New technologies such as microwave heating that substantially reduces the extraction time and hence cost and use of unconventional sources of chitin such as plants and fungi provide an opportunity to explore new applications for chitosan fibers.

Acknowledgments

Authors thank the Centre for Incubation, Innovation, Research and Consultancy and Jyothy Institute of Technology for their support to complete this work. Narendra Reddy thanks the Department of Biotechnology, Ministry of Science and Technology, Government of India for support through the Ramalingaswami Reentry Fellowship. M. S. Santosh thanks Karnataka Council for Technological Upgradation for funding part of this work.

References

1 Rinaudo, M. (2006). Chitin and chitosan: properties and applications. *Progress in Polymer Science* 31: 603–632.
2 Boamah, P.O., Huang, Y., Hua, M. et al. (2015). Sorption of heavy metal ions onto carboxylate chitosan derivatives – a mini-review. *Ecotoxicology and Environment Safety* 116: 113–120.
3 Islam, S., Bhuiyan, M.A.R., and Islam, M.N. (2016). Chitin and chitosan: structure, properties and applications in biomedical engineering. *Journal of Polymers and the Environment* 25: 854–866.
4 Chen, G., Mi, J., Wu, X. et al. (2011). Structural features and bioactivities of the chitosan. *Journal of Biological Macromolecules* 49: 543–547.
5 Younes, I. and Rinaudo, M. (2015). Chitin and chitosan preparation from marine sources. Structure properties and applications. *Marine Drugs* 13: 1133–1174.
6 Liman, Z., Selmi, S., Sadok, S., and Abed, A.E. (2011). Extraction and characterization of chitin and chitosan from crustacean byproducts: biological and physiochemical properties. *African Journal of Biotechnology* 40 (4): 640–647.
7 Teli, M.D. and Sheikh, J. (2012). Extraction of chitosan from shrimp shells waste and application in antibacterial finishing of bamboo rayon. *International Journal of Biological Macromolecules* 50: 1195–1200.
8 Kucukgulmez, A., Celik, M., Yanar, Y. et al. (2011). Physiochemical characterization of chitosan extracted from *Metapenaeus stebbingi* shells. *Food Chemistry* 126: 1144–1148.
9 Kannan, M., Nesakumari, M., Rajarathnam, K., and Singh, R.A.J.A. (2010). Production and characterization of mushroom chitosan under solid-state fermentation conditions. *Advance Biological Research* 4 (1): 10–13.

10 Tayel, A.A., Ibrahim, L.A.S., Al-Saman, M.A., and Moussa, S.H. (2014). Production of fungal chitosan from date wastes and its application as a biopreservative for minced meat. *International Journal of Biological Macromolecules* 69: 471–475.

11 Knidri, H.E., Khalfaouy, R.E., Laajeb, A. et al. (2016). Eco-friendly extraction and characterization of chitin and chitosan from the shrimp shell waste via microwave irradiation. *Process Safety and Environmental Protection* 104: 395–435.

12 Sagheer, F.A.A., Al-Sughayer, M.A., Muslim, S., and Elsabee, M.Z. (2009). Extraction and characterization of chitin and chitosan from marine sources in Arabian Gulf. *Carbohydrate Polymers* 77: 410–419.

13 Cai, J., Yang, J., Du, Y. et al. (2006). Enzymatic preparation of chitosan from the waste *Aspergillus niger* mycelium of citric acid production plant. *Carbohydrate Polymers* 64: 151–157.

14 Upadhyaya, L., Singh, J., Agarwal, V., and Tewari, R.P. (2013). Biomedical applications of carboxymethyl chitosans. *Carbohydrate Polymers* 91: 452–466.

15 Demina, T.S., Gilman, A.B., Akopova, T.A., and Zelenetskii, A.N. (2014). Modification of the chitosan structure and properties using high energy chemistry methods. *High Energy Chemistry* 48 (5): 293–302.

16 East, G.C. and Qin, Y. (1993). Wet spinning of chitosan and the acetylation of chitosan fibers. *Journal of Applied Polymer Science* 50: 1773–1779.

17 Li, L., Yuan, B., Liu, S. et al. (2012). Preparation of high strength chitosan fibers by using ionic liquid as spinning solution. *Journal of Materials Chemistry* 22: 8585–8594.

18 Hirano, S., Nagamura, K., Zhang, M. et al. (1999). Chitosan staple fibers and their chemical modification with some aldehydes. *Carbohydrate Polymers* 38: 293–298.

19 Lee, S., Park, S., and Kim, Y. (2007). Effect of the concentration of sodium acetate (SA) on crosslinking of chitosan fiber by epichlorohydrin (ECH) in a wet spinning system. *Carbohydrate Polymers* 70: 53–60.

20 Knaul, J.Z., Hudson, S.M., and Creber, K.A.M. (1999). Crosslinking of chitosan fibers with dialdehydes: proposal of a new reaction mechanism. *Journal of Polymer Science Part B: Polymer Physics* 37: 1079–1094.

21 Yang, Q., Dou, F., Liang, B., and Shen, Q. (2005). Studies of crosslinking reaction on chitosan fiber with glycerol. *Carbohydrate Polymers* 59: 205–210.

22 Knaul, J.Z., Hudson, S.M., and Creber, K.A.M. (1999). Improved mechanical properties of chitosan fibers. *Journal of Applied Polymer Science* 72: 1721–1732.

23 Pati, F., Adhikari, B., and Dhara, S. (2011). Development of ultrafine chitosan fibers through modified wet spinning technique. *Journal of Applied Polymer Science* 121: 1550–1557.

24 Lee, C.K., Kim, S.J., Kim, S.I. et al. (2006). Preparation of chitosan microfibers using electro-wet-spinning and their electroactuation properties. *Smart Materials and Structures* 15: 607–611.

25 Ozarkar, S., Jassal, M., and Agrawal, A.K. (2008). pH and electrical actuation of single walled carbon nanotube/chitosan composite fibers. *Smart Materials and Structures* 17: 055016–055025.

26 Yan, W., Shen, L., Ji, Y. et al. (2014). Chitin nanocrystal reinforced wet-spun chitosan fibers. *Journal of Applied Polymer Science* 131: 40852–40858.

27 Zhao, J., Luo, C., Han, W. et al. (2012). Fabrication and properties of poly(L-lactide)/hydroxyapatite/chitosan fiber ternary composite scaffolds for bone tissue engineering. *Journal of Polymer Engineering* 32: 283–289.

28 Funakoshi, T., Majima, T., Iwasaki, N. et al. (2005). Novel chitosan based hyaluronan hybrid polymer fibers as a scaffold in ligament tissue engineering. *Journal of Biomedical Materials Research* 74A: 338–346.

29 Xu, X., Zhuang, X., Cheng, B. et al. (2010). Manufacture and properties of cellulose/O-hydroxyethyl chitosan blend fibers. *Carbohydrate Polymers* 81: 541–544.

30 Zhang, H., Wu, C., Zhang, Y. et al. (2010). Elaboration, characterization and study of a novel affinity membrane made from electrospun hybrid chitosan/nylon-6 nanofibers for papain purification. *Journal of Materials Science* 45: 2296–2304.

31 Schueren, L.V., Steyaert, I., Schoenmaker, B.D., and Clerck, K.D. (2012). Polycaprolactone/chitosan blend nanofibers electrospun from an acetic acid/formic acid solvent system. *Carbohydrate Polymers* 88: 1221–1226.

32 Nguyen, T.T.T., Chung, O.H., and Park, J.S. (2011). Coaxial electrospun poly(lactic acid)/chitosan (core/shell) composite nanofibers and their antibacterial activity. *Carbohydrate Polymers* 86: 1799–1806.

33 Wawro, D. and Pighinelli, L. (2011). Chitosan fibers modified with Hap/β-TCP nanoparticles. *International Journal of Molecular Sciences* 12: 7286–7300.

34 Li, L., Yuan, B., Liu, S. et al. (2013). N-Acyl chitosan and its fiber with excellent moisture absorbability and retentivity: preparation in a novel [Gly]Cl/water homogenous system. *Journal of Applied Polymer Science* 129: 3282–3289.

35 Shim, I.K., Lee, S.Y., ParK, Y.J. et al. (2008). Homogenous chitosan-PLGA composite fibrous scaffolds for tissue engineering. *Journal of Biomedial Materials Research* 247: 247–255.

36 Qu, L.J., Guo, X.Q., Tian, M.W., and Lu, A. (2014). Antimicrobial fibers based on chitosan and polyvinyl-alcohol. *Fibers and Polymers* 15 (7): 1357–1363.

37 Haaparanta, A.M., Järvinen, E., Cengiz, I.F. et al. (2014). Preparation and characterization of collagen/PLA, chitosan/PLA, and collagen/chitosan/PLA hybrid scaffolds for cartilage tissue engineering. *Journal of Materials Science: Materials in Medicine* 25 (4): 1129–1136.

38 Peirano, F., Vincent, T., and Guibal, V. (2008). Diffusion of biological molecules through hollow chitosan fibers. *Journal of Applied Polymer Science* 107: 3568–3578.

39 Tasselli, F., Mirmohseni, A., Dorraji, M.S.S., and Figoli, A. (2013). Mechanical, swelling and adsorptive properties of dry-wet spun chitosan hollow fibers crosslinked with glutaraldehyde. *Reactive and Functional Polymers* 73: 218–223.

40 Lee, R., Lee, K.H., Kang, E. et al. Microfluidic wet spinning of chitosan-alginate microfibers and encapsulation of HepG2 cells in fibers. *Biomicrofluidics* 5: 0222208.

41 Hirano, S. and Hayashi, H. (2003). Some fragrant fibres and yarns based on chitosan. *Carbohydrate Polymers* 54: 131–136.

42 Qin, Y., Zhu, C., Chen, J. et al. (2006). The absorption and release of silver and zinc ions by chitosan fibers. *Journal of Applied Polymer Science* 101: 776–771.

43 Albanna, M.Z., Bou-Akl, T.H., Walters, H.L., and Matthew, H.W.T. (2012). Improving the mechanical properties of chitosan-based heart value scaffolds using chitosan fibers. *Journal of the Mechanical Behavior of Biomedical Materials* 5: 171–180.

44 Qin, Y., Hu, H., Luo, A. et al. (2006). Effect of carboxymethylation on the absorption and chelating properties of chitosan fibers. *Journal of Applied Polymer Science* 99: 3110–3115.

45 Heinemann, C., Heinemann, S., Bernhardt, A. et al. (2008). Novel textile chitosan scaffolds promote spreading, proliferation and differentiation of osetoblasts. *Biomacromolecules* 9: 2913–2920.

46 Wawro, D., Stepleweski, W., Sobczak, E. et al. (2012). Antibacterial chitosan fibers containing silver nanoparticles. *Fibers and Textiles in Eastern Europe* 68 (96): 24–31.

47 Zhou, Y., Yang, H., Liu, X. et al. (2013). Electrospinning of carboxyethyl chitosan/poly (vinyl alcohol)/silk fibroin nanoparticles for wound dressings. *International Journal of Biological Macromolecules* 53: 88–92.

48 Tuzlakoglu, K., Alves, C.M., Mano, J.F., and Reis, R.L. (2004). Production and characterization of chitosan fibers and 3-D fiber mesh scaffolds for tissue engineering applications. *Macromolecular Bioscience* 4: 811–819.

49 Sousa, F., Guebitz, G.M., and Kokol, V. (2009). Antimicrobial and antioxidant properties of chitosan enzymatically functionalized with flavonoids. *Process Biochemistry* 44: 749–756.

50 Sun, K. and Li, Z.H. (2011). Preparations, properties and applications of chitosan-based nanofibers fabricated by electrospinning. *Express Polymer Letters* 5 (4): 342–361.

51 Areias, A.C., Gomez-Tejedor, J.A., Sencadas, V. et al. (2012). Assessment of parameters influencing fiber characteristics of chitosan nanofiber membrane to optimize fiber mat production. *Polymer Engineering and Science* 52 (6): 1293–1300.

52 Skotak, M., Leonov, A.P., Larsen, G. et al. (2008). Biocompatible and biodegradable ultrafine fibrillary scaffold materials for tissue engineering by facile grafting of L-Lactide onto chitosan. *Biomacromolecules* 9: 1902–1908.

53 Horzum, N., Boyaci, E., Eroglu, A.E. et al. (2010). Sorption efficiency of chitosan nanofibers toward metal ions at low concentrations. *Biomacromolecules* 11: 3301–3308.

54 Schiffman, J.D. and Schauer, C.L. (2007). Crosslinking chitosan nanofibers. *Biomacromolecules (a)* 8: 594–600.

55 Schiffman, J.D. and Schauer, C.L. (2007). One-step crosslinking of crosslinked chitosan fibers. *Biomacromolecules (b)* 8: 2665–2667.

56 Edmondson, D., Cooper, A., Jana, S. et al. (2012). Centrifugal electrospinning of highly aligned polymer nanofibers over a large area. *Journal of Materials Chemistry* 22: 18646–18652.

57 Schiffman, J.D., Blackford, A.C., Wegst, U.G.K., and Schauer, C.L. (2011). Carbon black immobilized in electrospun chitosan membranes. *Carbohydrate Polymers* 84: 1252–1257.

58 Frohbergh, M.E., Katsman, A., Botta, G.P. et al. (2012). Electro spun hydroxyapatite-containing chitosan nanofibers crosslinked with genipin for bone tissue engineering. *Biomaterials* 33: 9167–9178.

59 Kiechel, M.A. and Schauer, C.L. (2013). Non-covalent crosslinkers for electro spun chitosan fibers. *Carbohydrate Polymers* 95 (1): 123–133.

60 Hussain, A., Collins, G., Yip, D., and Cho, C.H. (2013). Functional 3-D cardiac co-culture model using bioactive chitosan nanofiber scaffolds. *Biotechnology and Bioengineering* 110: 637–647.

61 Pangon, A., Saesoo, S., Saengkrit, N. et al. (2016). Hydroxyapatite-hybridized chitosan/chitin whisker bionanocomposite fibers for bone tissue engineering applications. *Carbohydrate Polymers* 144: 419–427.

62 Kristi, M., Oksuz, A.U., Oksuz, L., and Ulusoy, S. (2013). Electrospun chitosan/PEDOT nanofibers. *Materials Science and Engineering C* 33: 3845–3850.

63 Ma, B., Qin, A., Li, X., and He, C. (2013). High tenacity regenerated chitosan fibers prepared by using the binary ionic liquid solvent (Gly-HCl)-[Bmim]Cl. *Carbohydrate Polymers* 97: 300–305.

6

Collagen Fibers

Jinlian Hu and Yanting Han

Institute of Textiles and Clothing, The Hong Kong Polytechnic University, Hung Hom, Kowloon, Hong Kong, China

6.1 Introduction

Type I collagen fiber (CF) is one of the most abundant structural proteins in vertebrates. It exists in animal bones, tendons, cartilage, interosseous membrane, skin, ligaments, and other connective tissue, accounting for 25% or more (up to 35%) of total protein [1]. As the basic unit of CFs, individual collagen triple helices further assemble in a complex and hierarchical manner, which results in the macroscopic fibers and networks. Collagen fibril normally has a diameter of 10–500 nm. It is further gathered into small fibril bundle with a diameter of 1–2 μm by glycoproteins and proteoglycans [2]. Through covalent cross-linking, collagen fibrils can be formed into CFs [3]. Due to its short length, natural CF is different from the conventional fibers, which can be easily applied in textile fields. Thus, to adapt to human demands, regenerated CFs with specific properties are obtained by spinning methods with collagen protein extracted from substrates. Because of its excellent biocompatibility and biodegradability, and weak antigenicity, collage is regarded as suitable material for bio-applications. Besides, CFs possess affinity to chemicals and mental ions, which expand its application to various fields.

6.2 Source and Structure of CF

CF comes from most tissues of animal in different arrangements to play different functions (Figure 6.1). These tissues included tendons and ligaments. Tendons consist of bundles of collagenous fiber arranged in parallel, forming cords that have great tensile strength, thus to anchor or bind muscles to bones. The distinctive structural feature of fibrillar collagens is 300 nm uninterrupted triple helical structure, aggregating themselves into highly ordered fibrils with a typical quarter-staggered fibril array. In tissue, CF influences the mechanical properties based on fibril arrangement.

Handbook of Fibrous Materials, First Edition. Edited by Jinlian Hu, Bipin Kumar, and Jing Lu.
© 2020 Wiley-VCH Verlag GmbH & Co. KGaA. Published 2020 by Wiley-VCH Verlag GmbH & Co. KGaA.

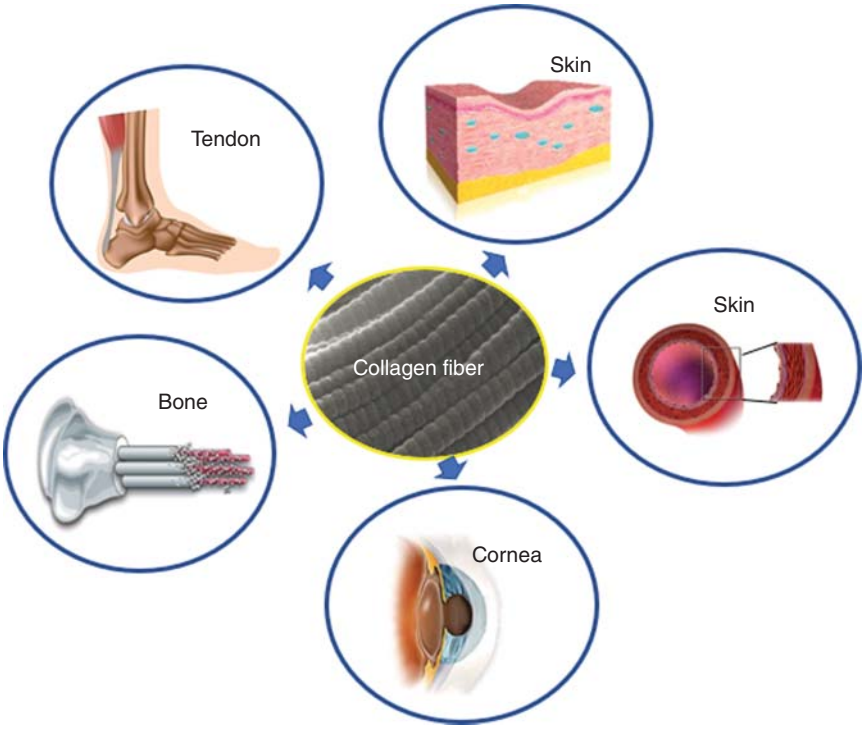


Figure 6.1 CF in different tissues.

The defining feature of collagen is a right-handed triple helix in which three parallel peptides in a left-handed triple helix are held together in a helical conformation by hydrogen bonds. At present, nineteen types of collagen have been identified, among which seven types of collagen have fibrous structure. The collagen used nowadays is mainly derived from the skin of vertebrates, which contains mainly type I collagen. In this chapter, we only focus on fibrils and fibers composed of type I collagen.

As shown in Figure 6.2, CFs have the hierarchical structure. In fibrillar collagen, collagen triple helix, known as tropocollagen (TC), assemble into fibrils, which agglomerate to form fibers. These fibril-forming collagens have large sections of homologous sequences. Individual TC monomers are arranged into microfibril, and individual microfibrils are packaged into collagen fibril, namely, the fibrillogenesis of collagen. Due to the enhanced effect of fibrillogenesis, collagen fibrils show good thermal stably. The strong macromolecular structure assembled in a complex, hierarchical manner provides CF and its network the ability to support stress multidimensionally.

The primary structure of collagen is the sequence structure of peptide chain. Collagen has a most unusual repetitious tripeptide sequence of Gly-X-Y, in which X can be any amino acid but is frequently a proline while Y is frequently a hydroxyproline or hydroxylysine. Collagen also contains some alanine, serine, arginine, and a small amount of methionine. Glycine is located inside the triple

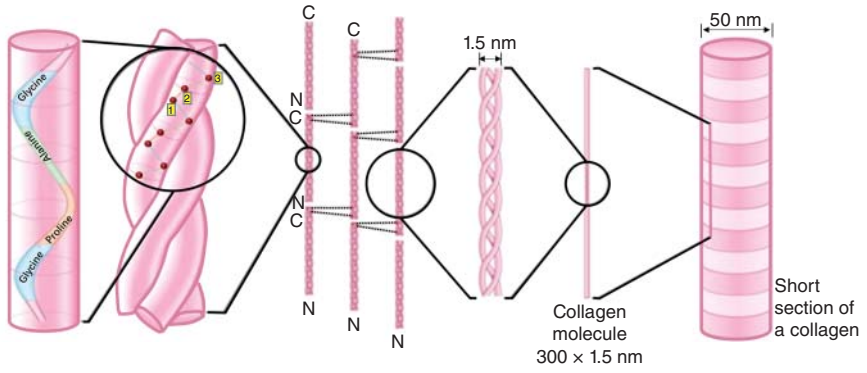


Figure 6.2 Hierarchical structure of CF.

helix bundle, providing a rotatable flexibility for the molecular chain, while proline increases the rigidity of the polypeptide chain, which results in the formation of a nonspherical conformation. Hydroxyproline is present in the triple helix bundle domain of collagen proteins. It provides additional hydrogen bonding capability that stabilizes the mature protein. Within the triple helix domains of nonfibrillar collagens, the repeated sequence is disrupted at certain location.

The secondary structure of the protein involves the folding ways of the polypeptide chain. Three left-handed helical (non-α spiral) polypeptide chains are intertwined to form a tropocollagen with a right-handed triple helix structure. Each peptide chain has about 1000 amino acid residues with a relative molecular mass between 92 000 and 100 000, so the relative molecular mass of the entire collagen molecule is about 300 000. In the formation of single-stranded spiral, hydrogen bonds cannot be generated within each peptide chain residues. However, when the peptides are stranded into three strands of helical chain, hydrogen bonds are formed between each peptide chain, resulting in a stable triple helix structure.

The tertiary structure of collagen refers to the three-dimensional (3D) position of the tropocollagen when forming the collagen microfibrils. Based on the secondary structure, the tropocollagen is further curly folded by the secondary bond to form a specific conformation. The tertiary structure of collagen reveals the role of secondary bonds between peptide chains in protein molecules, such as hydrogen bonds, ionic bonds, van der Waals forces, and hydrophobic bonds generated by nonpolar and polar groups on the side chain of amino acid residues. In addition to the secondary bonds, there are aldehydes condensation, aldol condensation, and aldol-histidine cross-linking between collagen molecules, which allows the individual polypeptides to be firmly connected, thus to imbue the fiber with exceptional strength and rigidity [4, 5].

The quaternary structure of collagen refers to that collagen microfibrils, which are arranged in parallel into a bundle through the covalent cross-linking to form the collagen fibrils with good stability, flexibility, and toughness [1]. By end-to-end aggregation, collagen fibrils will further gather into a bundle of CF [6]. It is observed that dark and white stripes are distributed in the entire CF.

The intermolecular distance was 67 nm, and the longitudinal distance between adjacent molecules was 40 nm. CFs generally covalently cross-linked by histidine and lysine between the C-terminus and the N-terminus. Due to the isolable and insolubility of individual natural microfibrils and fibrils, it is difficult to use most standard structure-determination techniques to identify the accurate features of collagen structure.

6.3 Isolation of Natural CF

Different from the cocoon silk that is continuous long independent fiber that can be reel off after degumming and collected by roller, CF in tissue is either discontinuous or usually intertwined with each other, leading to the difficulty to collect the CF using traditional method in textile fields. Research work has been carried out in development of newer methods to obtain CF from animal skin. However, as the protein, CF goes through denaturation and hydrolysis into gelatin under harsh conditions such as high temperature and strong acid and enzyme. Thus, physical treatment under moderate condition is preferred to obtain CF. Liao et al. [7] prepared the CF from animal skin through a series of procedures of leather processing including liming, splitting, deliming, bating, and pickling and then the grinding and sieving processes. Obtained CF has a size with 1–4 μm in diameter and 0.5–1 mm in length, which was used for metal ion absorption. J.D. Ambrósio et al. [8] prepared short leather fiber with size between 0.25 and 1.68 mm by smash and sieves as filler as enhancer. Joseph et al. [9] reported that leather fiber with average diameter of 4.5 μm and length of 258.5 μm is available from tanneries. However, strictly speaking, leather fiber is the chemically modified CF because tanning agents are reacted with collagen for stability. To prepare the pure long CF, spinning methods are adopted.

6.4 Spinning of CF

6.4.1 Extraction of Collagen

Natural collagen is usually extracted from tissues such as skin, tendons, and bones. The dissolution of collagen is, however, impeded by the low solubility of natural collagen due to its covalent cross-links including Schiff base [10], which formed a stably fiber network. Therefore, chemical/biological agents are used to cleave the covalent bonds and get the CF dissolved. To date, the noncovalent-bonded collagen can be obtained by mainly three widely used methods: acid extraction, alkali extraction, and enzyme extraction. The most common solvent systems include a neutral salt solution (0.15–0.20 M NaCl) and dilute acid solution (0.5 M acetic acid):

(1) *Enzyme*: For insoluble collagen, pepsin is able to cleave the cross-linked regions at the telopeptide without damaging the integrity of the triple helix, and then the collagen can be extracted by further treatment. Briefly, raw

materials are suspended in 0.5 mol/l acetic acid in the presence of pepsin. The extraction of collagen with limited pepsin digestion contributes to a higher yield. Due to the high activity of enzyme, enzyme extraction is highly efficient and nonpolluting. As enzyme is sensitive to temperature and pH, the control of the reaction process is essential.

(2) *Acid extraction*: Acid acetic acid, sulfuric acid, citric acid, and hydrochloric acid are commonly used for acid extraction. Acid will make partial hydrolysis of collagen to get small molecules of collagen [11]. Generally, collagen is extracted using 0.5 M acetic acid solution, which proved to be effective without too much damage to triple helix structure of collagen. The extraction normally is conducted for 16 hours with intermittent stirring. The collagen solution after centrifugation is salt out by solution of NaCl. To further purify the collagen, it can be redissolved in acetic acid and reprecipitated as described above. To avoid the degradation of collagen, temperature should be as lower as possible [12], for example, 15 °C.

(3) *Alkali extraction*: Alkali sodium hydroxide, calcium hydroxide, sodium carbonate, and lime are commonly used. The steps for alkali extraction of CFs are similar to acid extraction, but large amount of alkali consumption will result in environment pollution. There is a standard method for alkali extraction of collagen. Briefly, raw materials are shaken in 0.5 M NaOH containing 10% NaCl at 4 °C [13]. After the CF is dissolved, the collagen is recovered by salting out, purified by redissolving in acid, dialyzed against 0.01 M acetic acid, and lyophilized. Practically, in the process of preparing the collagen, a variety of ways are combined and used to achieve the best effect. For example, acid extraction and alkali extraction can be combined together to improve the extraction efficient process.

Owing to the excellent biological features and physiochemical properties of collagen, it has been among the most widely used biomaterials for biomedical applications particularly when delivered in the form of gels, films, injectables, and coatings. To further extend the utility of collagen for use in medical devices and to address issues such as fixation in defect sites and stability for tissue engineering (TE) and guided bone regeneration (GBR), the ability to manufacture mechanically robust fibers and fabrics is important. To date, mainly three spinning methods including wet spinning, electrospinning, and microfluidic spinning (Figure 6.3) have been reported to prepare CFs.

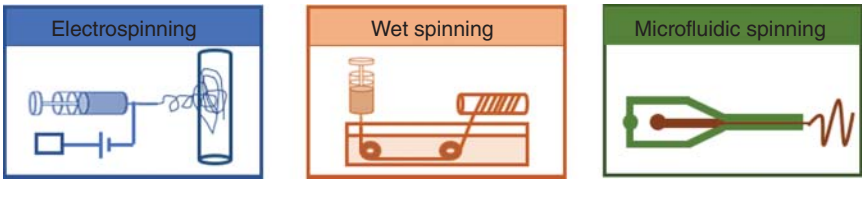


Figure 6.3 Spinning methods used to prepare CF.

6.4.2 Electrospinning of CF

Electrospinning is a process that uses an electric field to control the formation and deposition of polymers. This process is remarkably efficient, rapid, and inexpensive [14]. Generally, in electrospinning, the collagen solution is fed through a thin needle opposite to a collecting plate or target. When a high voltage is applied to the solution, a jet is formed as soon as the applied electric field strength overcomes the surface tension of the solution. When traveling toward the grounded collecting plate, the jet becomes thinner as a consequence of solvent evaporation, and fibers are formed. Splaying of the fibers because of splitting of the jet can occur as well. The fibers are deposited on the grounded target as a nonwoven highly porous mesh. Placing a rotating collector between the needle and the grounded plate allows deposition of the fibers on the collector with a certain degree of alignment. Mats with randomly oriented or aligned fibers can be formed by using a stationary or a rotating collector. Fibers with diameters in the range of 100 nm to few micrometers can be created depending on the polymer physical properties (e.g. viscosity, electrical conductivity, and surface tension), applied electric field, polymer flow rate, and the distance between the needle tip and the collector.

The possibility to produce meshes with a high surface area makes electrospinning an ideal solution for applications, which require seeding of cells, like vascular tissue engineering. Moreover, the architecture of the produced nonwoven meshes is similar to that found in most natural extracellular matrices, thus enhancing the applicability of these scaffolds [15]. Therefore, the electrospinning process has the potential to produce collagen fibrils that closely mimic, and at some points may even fully reproduce, the structural and biological properties of the natural polymer [16]. Matthews et al. [17] used hexafluoro-2-propanol (HFP) as solvent; the viscosity and conductivity of the solution, the spinning voltage, the flow rate, and the collecting distance were adjusted in preliminary experiments to optimize the electrospinning conditions. During electrospinning of an 8% w/v collagen solution in HFP, jet formation was first observed at 12 kV. Increasing the voltage to values between 19 and 21 kV offered stable operating conditions to electrospin continuously for more than three hours. Dry CFs could be collected at a distance of ~15 cm on a grounded plate with evaporation of HFP. It is noted that the CFs produced by this method using the mentioned parameters have similar dimensions as native collagen fibrils and range from 100 to 600 nm (Figure 6.4). Although strong organic solvent such as HFP may influence the structure of electrospinning of collagen, it is proved that only minor differences between structures of collagen electrospun from HFP and structures of collagen electrospun from phosphate buffered saline (PBS)-based solutions. The bending moduli of the electrospun fibers ranged from 1.3 to 7.8 GPa at ambient conditions and ranged from 0.07 to 0.26 MPa when immersed in PBS buffer.

6.4.3 Wet Spinning of CF

Among the various fiber manufacturing processes available, wet spinning has the potential to convert biomolecules into fibers without need for high voltage

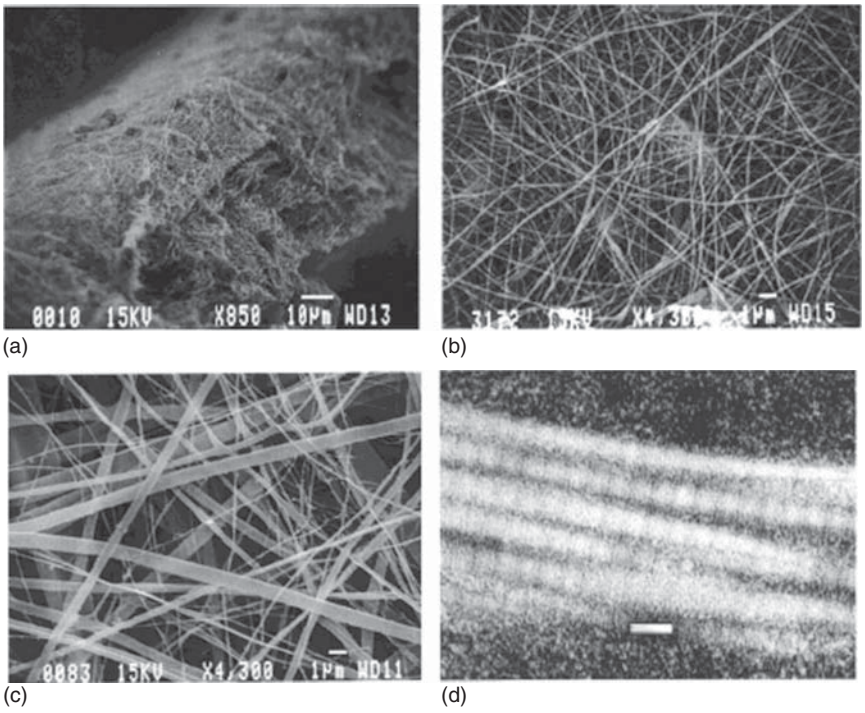


Figure 6.4 Calfskin type I collagen electrospun onto a static, cylindrical mandrel. Source: Matthews et al. 2002 [17]. Reproduced with permission from American Chemical Society.

during manufacture and is less likely to be associated with denaturation. Wet spinning is conventional methods to produce man-made fibers such as viscose rayon. This fiber spinning technology is based on nonsolvent-induced phase separation, whereby polymer dope solutions are extruded through a spinneret into a nonsolvent coagulation bath in which it continuously polymerizes so as to form a solid long fiber.

The coagulation bath must be either a poor solvent or a nonsolvent with respect to the polymer. The diameter of fibers can be tuned by changing the needle(s) diameter, the polymer composition, and its volumetric flow rate [18]. Traditional wet and dry spinning processes have been most commonly used to produce protein fibers including CF.

Hirano et al. [19] described the production of chitosan–CFs by wet spinning from an aqueous 2% acetic acid–methanol solution spun into an aqueous 5% ammonia solution containing 40–43% ammonium sulfate. Continuous fibers with an average diameter of 36 µm were produced. In a method reported by Fofonoff and Bell [20], CFs with diameter more than 100 µm were prepared by wet spinning from an aqueous 0.05% acetic acid (0.5 M) solution into a coagulating bath consisting of alkaline alginic acid/boric acid (pH 8–10) with heating at 35±2°C. CF can be formed by polymerization when the acid in the collagen is neutralized upon contact with the neutralizing solution [21]. The obtained fibers are subsequently dehydrated in acetone and ethanol baths. The morphology

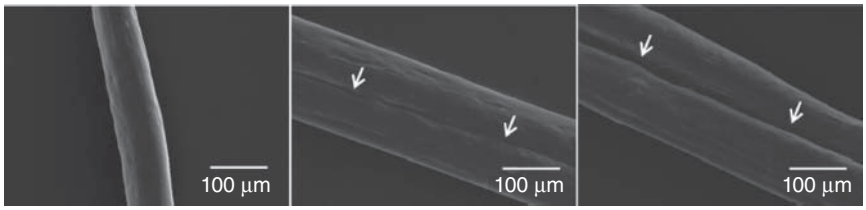


Figure 6.5 SEM images of fibers wet spun from suspensions with varied collagen concentration: (a) 1.2%, (b) 1.4%, and (c) 1.6% collagen (w/v) suspensions. Surface striations (marked with arrow) are observed in fibers derived from wet spinning suspensions with increased collagen concentrations. Source: Arafat et al. 2015 [21]. Reproduced with permission from Elsevier.

of thus obtained fibers depends on the collagen concentration (Figure 6.5). An additional example is provided by Furukawa et al. [22] in which solubilized collagen is spun through a spinneret into a coagulating bath comprising an aqueous solution of an inorganic salt, such as sodium sulfate, sodium chloride, ammonium sulfate, magnesium chloride, or aluminum sulfate. To enhance the CF properties, different strategies were successful as cross-linking and stretching of the filaments. By controlling the spinning conditions, different physical parameters can be achieved. Therefore, the quality of the fibers prepared from collagen dispersion is up to the composition and concentration of the coagulation bath and the spinneret design. In addition, post cross-linking treatment is proved to be effective method to improve the stability of CF against trypsin digestion. For example, using chemical agent such as glutaraldehyde, polyethylene glycol (PEG) in a solution for cross-linking acceptable low proliferation inhibition was observed interpreted as low cytotoxic effect [21, 23].

6.4.4 Microfluidic Spinning of CF

Microfluidic spinning is defined as the formation of fibers in a microchannel using a coaxial flow of a prepolymer and a cross-linking agent. In general, microfluidics deals with the processing of small amounts of fluids in channels with dimensions of tens to hundreds of micrometers, which are mostly embedded in small chips regularly consisting of polydimethylsiloxane (PDMS). This is similar to wet pinning, except that the cross-linking agent is supplied by the coaxial flow directly instead of the bath. To prevent polymerization inside of the system, the streams need to be coaxed close to the nozzle, which can be achieved by using microfluidic systems made by microfabrication techniques. The short distance of coaxial flow facilitates the formation of cell-laden fibers as the cells are only briefly exposed to a high shear stress [24]. Therefore, microfluidic spinning method is a promising platform for continuous fabrication of fibers with tunable morphological, structural, and chemical features. The diameters of the fabricated fibers can vary from ten to several hundreds of micrometers, depending on parameters such as flow rates of core and sheath solutions, channel dimensions, and solutions viscosities. The rotation speed of the collecting roller may also affect the fiber diameter as it imposes an external elongation stress on

the fiber. In general, the size of the fibers fabricated with microfluidic systems is smaller than wet spinning but larger than electrospun fibers.

Microfluidic fiber spinning methods have been used to incorporate CFs. In comparison with blended fibers, the endless, plain CFs would be highly desirable due to a better performance including an expected higher mechanical stability, better biocompatibility, and less complexity in processing. Enomoto et al. [25] prepared the CF with a diameter from 8 to 30 μm by microfluidic spinning system with phosphate buffer. The obtained CF showed good bioactivity. Haynl et al. [26] reported that microfibers produced by microfluidic methods exhibited tensile strength and Young's modulus exceeding that of fibers produced in classical wet spinning devices and even that of natural tendon, and they showed lower diameters (Figure 6.6). It can be assumed that the smaller diameters of our microfibers led to increased mechanical stability due to better longitudinal orientation of collagen fibrils and less defect structures like voids, entanglements, free chain ends, and foreign particles in contrast to the situation in bigger diameter fibers.

6.4.5 Collagen Composite Fiber

CF in an electrospun form usually lacks mechanical integrity upon hydration. Previously established methods of cross-linking with glutaraldehyde, successful in increasing the strength of the electrospun structures, also carry an enhanced risk of cytotoxicity and calcification when used in vivo under inadequate removing of unreacted glutaraldehyde molecules. Thus, in addition to avoid denaturation of the native triple helical structure and the instability of regenerated collagen materials in the hydrated state, polymer component with stability is complexed with collagen to generate enhanced composite fibers while maintaining a high level of bioactivity through the presence of collagen. On the other hand, blending of collagen with synthetic polymers can provide methods to tailor mechanical and bioactive properties of the spinning scaffolds. The commonly used polymers for preparing collagen composite fiber include poly(lactic acid) (PLA) [27], polyurethane (PU) [28], polycaprolactone (PCL) [29], polydioxanone (PDO) [30], hydroxyapatite (HAP) [31], chitosan [32], poly(*N*-isopropyl acrylamide) [33], etc.

6.5 Application of CF

In addition to its high affinity and biodegradable, CF shows outstanding strength and flexibility. At present, the application CF is divided into two categories: one is based on the biological properties of collagen including its good biocompatibility and low antigenicity and biodegradability, which is suitable for cosmetics, biomedical materials, tissue engineering materials, and drug release fields, and the other is based on the unique fiber performance, such as good mechanical properties and highly chemical reactivity, making the CF preferable material for paper, textile, adsorbing materials, etc.

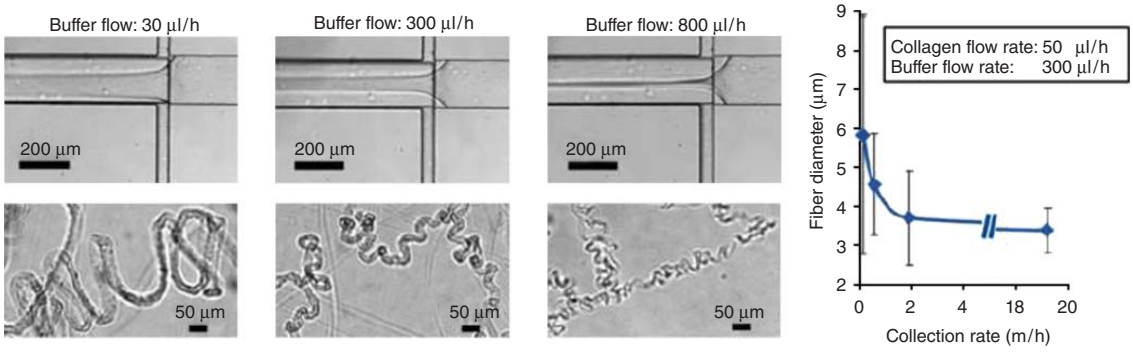


Figure 6.6 Using a constant collagen flow (here, 50 µl/h) and varying buffer flow rates enables the extrusion of microfibers into water with adjustable diameters. Source: Haynl et al. 2016 [26]. Reproduced with permission from American Chemical Society.

(1) *Bio-application*: Because of collagen's good mechanical stability, biocompatibility, biodegradability, low immunogenicity, and ability to promote cellular attachment and growth, collagenous materials, especially fibers, are used in medical and biomedical applications such as drug delivery [34], wound healing [35], and tissue engineering [36]. Rapid expansion of understanding of the excretal cellular matrix and progress toward the generation of synthetic matrix components suggests that synthetic CFs offer compelling advantages over traditional polymers for soft tissue repair and replacement. The CFs obtained by mechanical or chemical treatment still retain the structural characteristics and properties of natural CFs. CFs are regarded as a "green" fiber, which has been widely used in various fields. The CF extracted from the natural materials by acid, alkali, and enzymatic methods is a natural linear polymer whose amino acid composition is very close to that of the human tissues, so it can be applied on field of medical and healthcare such as burns and orthopedics, beauty, trauma treatment, tissue repair, and wound hemostasis.

(2) *Fiber as enhancer*: One alternative for natural CF, especially leather fiber, is to incorporate the fiber as filler in thermosetting and thermoplastic polymers. J.D. Ambrósio et al. [8] prepared the composites with recycled poly(vinyl butyral) (PVB) and wet blue leather fiber. PVB showed good interfacial adhesion with leather fibers. Increasing the leather fibers led to a significant increase in the tensile modulus while a reduction in the tensile strain in breaks. In the work of Joseph et al. [9], the waste leather fiber-filled polycaprolactone (PCL) composites were prepared by twin-screw extrusion. Addition of leather fibers resulted in improvement of tensile modulus of neat PCL and reduction in percentage crystallinity of PCL matrix. Leather fibers also increased the water uptake. They suggested that these biodegradable composites could be used to develop low-cost materials suitable for applications in wearing products and bags.

(3) *Metal adsorption application*: Calfskin that shows highly reactivity to tannins is utilized to prepare natural CF membrane for immobilization of tannins for adsorption metal ions in solution [37, 38] as shown in Figure 6.7. Vegetable tannins have multiple adjacent phenolic hydroxyls and exhibit specific affinity to metal ions. Thus, they promise to be a versatile agent for the treatment of metal ions containing wastewater. However, vegetable tannins are water-soluble compounds, which restrict their practical application. Due to the highly reactive activity to tannins, animal skin including calfskin is used to immobilize tannins. Attempts had been made to immobilize tannins onto various water-insoluble matrices.

Liao et al. [7] prepared a novel adsorption membrane by immobilizing condensed vegetable tannins onto CF membrane; these tannin-immobilized membranes possess proper physical properties and excellent adsorption and desorption characteristics for UO^{2+}. The effectiveness and practicability of tannin-immobilized membrane in the recovery of UO^{2+} from aqueous solution are obvious. Later, they found that tannin-immobilized CF matrixes are effective adsorbents in the recovery of Au(III) from aqueous solutions. Because the B ring of bayberry tannins is a pyrogallol structure, whereas the

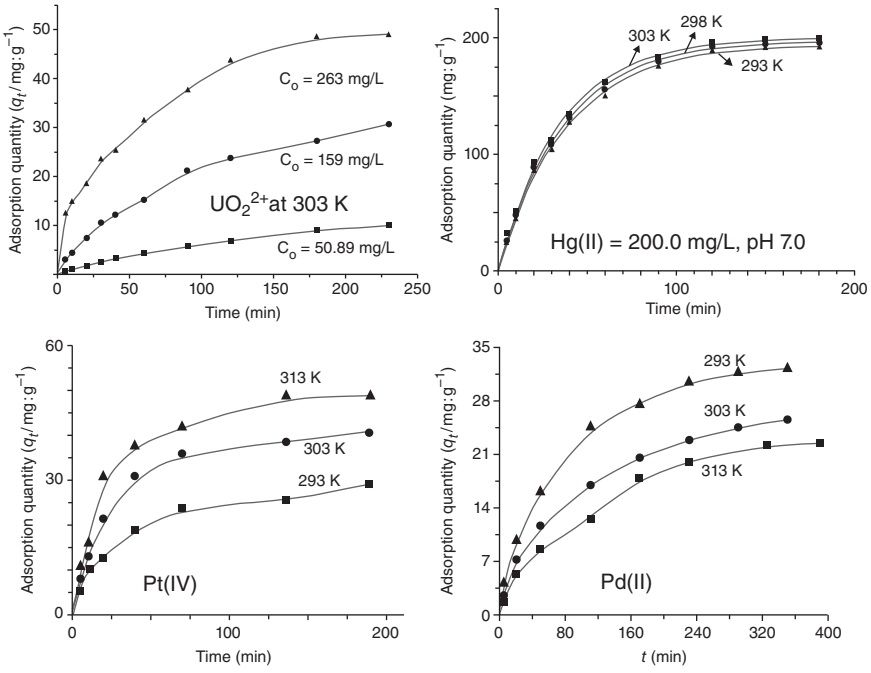


Figure 6.7 Absorption rate of modified skin CF to different metal ions ([7], [37], [38]).

B ring of larch tannins is a catechol structure, bayberry tannins have a higher reaction activity with Au(III). Therefore, immobilized bayberry tannins have a higher adsorption capacity for Au(III) than immobilized larch tannins [39]. Besides, the adsorption of other metal ions including platinum(IV) and palladium(II) on bayberry tannin-immobilized CF (BTICF) membrane was investigated [37]. Results showed that the membrane exhibits ability of selective adsorption to Pt(IV) and Pd(II) in the mixture solutions of metal ions.

(4) *Template for synthetic metal fiber*: According to the principles of leather processing, CF that contains abundant functional groups, like –OH, –COOH, and $–NH_2$, is ready to react with some metal ions, such as Cr(III), Al(III), Zr(IV), Ti(IV), and so forth. Hence, the metal fibers are supposed to generate via the reaction between metal ion and skin CF. On the basis of this idea, Deng et al. [40] synthesized the alumina fiber by reaction between Al(III) and CF from animal skin that was first stabilized by vegetable tannins to enhance its fixing capacity to Al(III). In their research, hierarchical alumina fiber (Figure 6.8) with ordered mesoporous distribution was successfully prepared. This metal fiber showed their improve abilities to be used as catalyst or catalyst support with high activity and selectivity owing to its high surface area and shape-selective properties [40, 41, 43]. Base on this method, hierarchical mesoporous ZrO_2 fiber and TiO_2 fiber were also successfully synthesized by using CF as template as shown in Figure 6.8 [41, 42]. Therefore, animal skin including calfskin can be used to prepare CF for general template to synthesize porous metal oxide fibers.

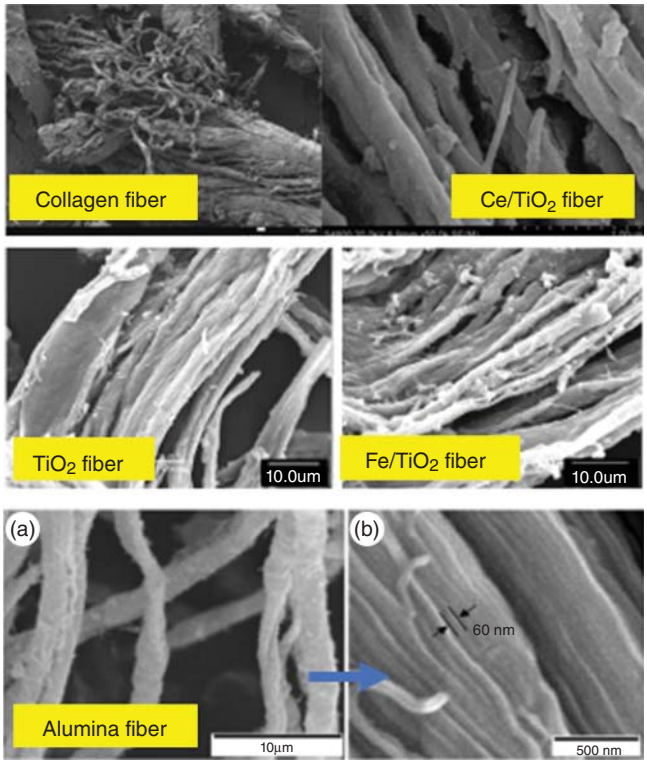


Figure 6.8 SEM of skin CF and metal fibers using CF as templates ([40–42]).

(5) *Metal nanoparticle supporter*: Due to the affinity to metal ions, water insolubility, hydrophilicity, flexibility, and softness, CF from animal skin is promising candidate of biopolymers for preparing supported metal nanoparticles. Wu et al. [44] use CF as a natural polymeric support to synthesize a novel palladium (Pd) nanoparticle catalyst. To achieve a stable immobilization of Pd on CF support, they used epigallocatechin-3-gallate (EGCG) to graft onto CF surface, acting both as dispersing and stabilizing agent for Pd nanoparticles. This EGCG-CF nanocatalyst presented high activity and selectivity for the liquid hydrogenation of allyl alcohol and retained the catalytic efficiency after recycling for five times. Later, Wu et al. [45] further used this method to prepare size-controlled gold nanoparticles (AuNPs) supported on CF, which was successfully applied as catalyst for 4-nitrophenol reduction. In addition to catalyst, metal nanoparticle-loaded skin CFs can also be used as high-performance microwave absorption. Guo et al. [46] designed and fabricated the controllable Ag@Ni core–shell NPs assembled in the hierarchical intertexture of skin CF stabled with bayberry tannin (SCF-BT) by a simple one-step route (Figure 6.9). This modified CF exhibited excellent microwave absorption performance in the whole X-band and C-band and some part of the S-band due to its multiple defective site polarization and interfacial polarization, as well as significant eddy current effect and anisotropic energy for the microwave energy dissipation.

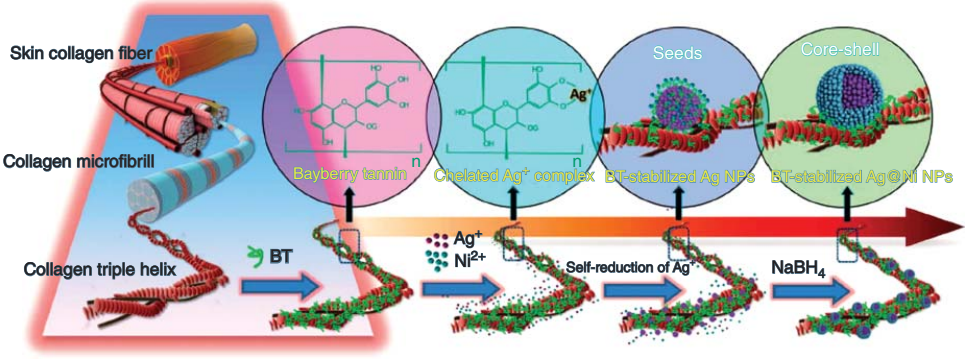


Figure 6.9 Schematic diagram showing the preparation mechanism of the one-step seeding growth of Ag@Ni core–shell NPs on skin CF. Source: Guo et al. 2012 [46]. Reproduced with permission from Royal Society of Chemistry.

6.6 Perspectives

Due to its unique structure, CF exhibits outstanding mechanical and biological properties, which has significantly benefited the development of functional materials, which is incomparable to synthetic polymers. According to the current development and based on our own understanding, perspectives are given for future development of CF:

(1) *Structure functions*: Although the molecule structure has been widely studied, the functions, especially its intrinsic smart behavior in materials' point of view, are rarely explored. Hence, more properties and smart function of CF regarding to its hierarchical structure from micro to macro can be investigated. For example, environmental (e.g. pH, thermo, magnetic, etc.) stimulus response of CF should be intensively studied for their potential application.
(2) *Preparation methods*: To date, CF with controllable length and diameter can be only achieved by spinning methods. Although the spinning method provides facile path to prepare CF, the regenerated structure of spun CF can be different from natural CF, which would weak its natural properties. Therefore, more efforts can be paid on how to obtain CF without breaking its natural structure and thus how to utilize the CF to prepare materials in various formats.
(3) *Multifunctions and high performance*: To meet the ever-increasing demand for novel materials, multifunctions and high performance should be realized on CF-based materials. For example, by chemical modification and/or compositing technology, the novel CF or its composites would exhibit enhanced property due to the synergistic effect resulting from natural CF and polymers.
(4) *Extended applications*: Generally, the application of CF, especially by spinning method, is focused on biological application such as wound dressing and scaffold. Some other potential application including metal and microwave absorption has been reported; however, the complex and high-cost preparation process limited its practical development. As major component of skin, CF should have advantages when applied in files such as artificial skin. Besides, the environmental stimuli-responsive behavior of CF may also contribute to its application as robotic sensors. On the other hand, back to its fiber form, 3D fibrous network can be achieved by CF, which could have broad range of application as covering materials to provide strength, flexibility, protectiveness, permeability, etc.

References

1 Buehler, M.J. (2006). Nature designs tough collagen: explaining the nanostructure of collagen fibrils. *Proceedings of the National Academy of Sciences of the United States of America* 103: 12285–12290.
2 Giudici, C., Viola, M., Tira, M.E. et al. (2003). Molecular stability of chemically modified collagen triple helices. *FEBS Letters* 547: 170–176.

3 Ushiki, T. (2002). Collagen fibers, reticular fibers and elastic fibers. A comprehensive understanding from a morphological viewpoint. *Archives of Histology and Cytology* 65: 109–126.

4 Drach, B., Kuksenko, D., and Sevostianov, I. (2016). Effect of a curved fiber on the overall material stiffness. *International Journal of Solids and Structures* 100–101: 211–222.

5 Eppell, S.J., Smith, B.N., Kahn, H., and Ballarini, R. (2006). Nano measurements with micro-devices: mechanical properties of hydrated collagen fibrils. *Journal of the Royal Society, Interface* 3: 117–121.

6 Raspanti, M., Viola, M., Sonaggere, M. et al. (2007). Collagen fibril structure is affected by collagen concentration and decorin. *Biomacromolecules* 8: 2087–2091.

7 Liao, X., Ma, H., Wang, R., and Shi, B. (2004). Adsorption of UO_2^{2+} on tannins immobilized collagen fiber membrane. *Journal of Membrane Science* 243: 235–241.

8 Ambrósio, J.D., Lucas, A.A., Otaguro, H., and Costa, L.C. (2011). Preparation and characterization of poly(vinyl butyral)-leather fiber composites. *Polymer Composites* 32: 776–785.

9 Joseph, S., Ambone, T.S., Salvekar, A.V. et al. (2015). Processing and characterization of waste leather based polycaprolactone biocomposites. *Polymer Composites* 38: 2889–2897.

10 Eyre, D.R., Paz, M.A., and Gallop, P.M. (1984). Cross-linking in collagen and elastin. *Annual Review of Biochemistry* 53: 717–748.

11 Kittiphattanabawon, P., Benjakul, S., Visessanguan, W. et al. (2005). Characterisation of acid-soluble collagen from skin and bone of bigeye snapper (*Priacanthus tayenus*). *Food Chemistry* 89: 363–372.

12 Nalinanon, S., Benjakul, S., and Kishimura, H. (2010). Collagens from the skin of arabesque greenling (*Pleurogrammus azonus*) solubilized with the aid of acetic acid and pepsin from albacore tuna (*Thunnus alalunga*) stomach. *Journal of the Science of Food and Agriculture* 90: 1492–1500.

13 Sadowska, M., Kołodziejska, I., and Niecikowska, C. (2003). Isolation of collagen from the skins of Baltic cod (*Gadus morhua*). *Food Chemistry* 81: 257–262.

14 Huang, Z.-M., Zhang, Y.-Z., Kotaki, M., and Ramakrishna, S. (2003). A review on polymer nanofibers by electrospinning and their applications in nanocomposites. *Composites Science and Technology* 63: 2223–2253.

15 Yang, L., Fitie, C.F., van der Werf, K.O. et al. (2008). Mechanical properties of single electrospun collagen type I fibers. *Biomaterials* 29: 955–962.

16 Sell, S.A., McClure, M.J., Garg, K. et al. (2009). Electrospinning of collagen/biopolymers for regenerative medicine and cardiovascular tissue engineering. *Advanced Drug Delivery Reviews* 61: 1007–1019.

17 Matthews, J.A., Wnek, G.E., Simpson, D.G., and Bowlin, G.L. (2002). Electrospinning of collagen nanofibers. *Biomacromolecules* 3: 232–238.

18 Yaari, A., Schilt, Y., Tamburu, C. et al. (2016). Wet spinning and drawing of human recombinant collagen. *ACS Biomaterials Science & Engineering* 2: 349–360.

19 Hirano, S., Zhang, M., Nakagawa, M., and Miyata, T. (2000). Wet spun chitosan–collagen fibers, their chemical *N*-modifications, and blood compatibility. *Biomaterials* 21: 997–1003.

20 Fofonoff, T.W. and Bell, E. (1999). Method for spinning and processing collagen fiber. Google Patents.

21 Arafat, M.T., Tronci, G., Yin, J. et al. (2015). Biomimetic wet-stable fibres via wet spinning and diacid-based crosslinking of collagen triple helices. *Polymer* 77: 102–112.

22 Furukawa, M., Takada, M., Murata, S., and Sasayama, A. (1994). Process for producing regenerated collagen fiber. Google Patents.

23 Tronci, G., Kanuparti, R.S., Arafat, M.T. et al. (2015). Wet-spinnability and crosslinked fibre properties of two collagen polypeptides with varied molecular weight. *International Journal of Biological Macromolecules* 81: 112–120.

24 Lee, P., Lin, R., Moon, J., and Lee, L.P. (2006). Microfluidic alignment of collagen fibers for in vitro cell culture. *Biomedical Microdevices* 8: 35–41.

25 Enomoto, S., Yajima, Y., Watabe, Y. et al. (2015). One-step microfluidic spinning of collagen microfibers and their application to cell cultivation. In: *2015 International Symposium on Micro-NanoMechatronics and Human Science (MHS)*, 1–4. IEEE.

26 Haynl, C., Hofmann, E., Pawar, K. et al. (2016). Microfluidics-produced collagen fibers show extraordinary mechanical properties. *Nano Letters* 16: 5917–5922.

27 Yang, F., Murugan, R., Wang, S., and Ramakrishna, S. (2005). Electrospinning of nano/micro scale poly(L-lactic acid) aligned fibers and their potential in neural tissue engineering. *Biomaterials* 26: 2603–2610.

28 Chen, R., Huang, C., Ke, Q. et al. (2010). Preparation and characterization of coaxial electrospun thermoplastic polyurethane/collagen compound nanofibers for tissue engineering applications. *Colloids and Surfaces B: Biointerfaces* 79: 315–325.

29 Phipps, M.C., Clem, W.C., Grunda, J.M. et al. (2012). Increasing the pore sizes of bone-mimetic electrospun scaffolds comprised of polycaprolactone, collagen I and hydroxyapatite to enhance cell infiltration. *Biomaterials* 33: 524–534.

30 McClure, M.J., Sell, S.A., Simpson, D.G., and Bowlin, G.L. (2009). Electrospun polydioxanone, elastin, and collagen vascular scaffolds: uniaxial cyclic distension. *Journal of Engineered Fibers and Fabrics* 4: 18–25.

31 Teng, S.-H., Lee, E.-J., Wang, P., and Kim, H.-E. (2008). Collagen/hydroxyapatite composite nanofibers by electrospinning. *Materials Letters* 62: 3055–3058.

32 Chen, Z., Wang, P., Wei, B. et al. (2010). Electrospun collagen–chitosan nanofiber: a biomimetic extracellular matrix for endothelial cell and smooth muscle cell. *Acta Biomaterialia* 6: 372–382.

33 Chen, M., Dong, M., Havelund, R. et al. (2010). Thermo-responsive core–sheath electrospun nanofibers from poly(*N*-isopropylacrylamide)/polycaprolactone blends. *Chemistry of Materials* 22: 4214–4221.

34 Zeng, J., Xu, X., Chen, X. et al. (2003). Biodegradable electrospun fibers for drug delivery. *Journal of Controlled Release* 92: 227–231.

35 Chen, J.-P., Chang, G.-Y., and Chen, J.-K. (2008). Electrospun collagen/chitosan nanofibrous membrane as wound dressing. *Colloids and Surfaces A: Physicochemical and Engineering Aspects* 313: 183–188.

36 Li, M., Mondrinos, M.J., Gandhi, M.R. et al. (2005). Electrospun protein fibers as matrices for tissue engineering. *Biomaterials* 26: 5999–6008.

37 Ma, H.-w., Liao, X.-P., Liu, X., and Shi, B. (2006). Recovery of platinum(IV) and palladium(II) by bayberry tannin immobilized collagen fiber membrane from water solution. *Journal of Membrane Science* 278: 373–380.

38 Huang, X., Liao, X., and Shi, B. (2009). Hg(II) removal from aqueous solution by bayberry tannin-immobilized collagen fiber. *Journal of Hazardous Materials* 170: 1141–1148.

39 Liao, X., Zhang, M., and Shi, B. (2004). Collagen-fiber-immobilized tannins and their adsorption of Au(III). *Industrial and Engineering Chemistry Research* 43: 2222–2227.

40 Deng, D., Tang, R., Liao, X., and Shi, B. (2008). Using collagen fiber as a template to synthesize hierarchical mesoporous alumina fiber. *Langmuir* 24: 368–370.

41 Xiao, G., Huang, X., Liao, X., and Shi, B. (2013). One-pot facile synthesis of cerium-doped TiO_2 mesoporous nanofibers using collagen fiber as the biotemplate and its application in visible light photocatalysis. *The Journal of Physical Chemistry C* 117: 9739–9746.

42 Cai, L., Liao, X., and Shi, B. (2010). Using collagen fiber as a template to synthesize TiO_2 and Fe_x/TiO_2 nanofibers and their catalytic behaviors on the visible light-assisted degradation of orange II. *Industrial and Engineering Chemistry Research* 49: 3194–3199.

43 Xiao, G., Zhou, J., Huang, X. et al. (2014). Facile synthesis of mesoporous sulfated Ce/TiO_2 nanofiber solid superacid with nanocrystalline frameworks by using collagen fibers as a biotemplate and its application in esterification. *RSC Advances* 4: 4010–4019.

44 Wu, H., Wu, C., He, Q. et al. (2010). Collagen fiber with surface-grafted polyphenol as a novel support for Pd(0) nanoparticles: synthesis, characterization and catalytic application. *Materials Science and Engineering C* 30: 770–776.

45 Wu, H., Huang, X., Gao, M. et al. (2011). Polyphenol-grafted collagen fiber as reductant and stabilizer for one-step synthesis of size-controlled gold nanoparticles and their catalytic application to 4-nitrophenol reduction. *Green Chemistry* 13: 651–658.

46 Guo, J., Wang, X., Miao, P. et al. (2012). One-step seeding growth of controllable Ag@Ni core–shell nanoparticles on skin collagen fiber with introduction of plant tannin and their application in high-performance microwave absorption. *Journal of Materials Chemistry* 22: 11933–11942.

7

Electrospun Fibers for Filtration

Xia Yin[1], *Jianyong Yu*[2], *and Bin Ding*[1,2]

[1] *Key Laboratory of Textile Science & Technology, Ministry of Education, College of Textiles, Donghua University, Shanghai 201620, China*
[2] *Innovation Center for Textile Science and Technology, Donghua University, Shanghai 200051, China*

7.1 Introduction

With the rapid growth of industrialization, urbanization, and modern agricultural development, environmental pollution is becoming more and more serious [1–3]. Among them, air pollution is a major health hazard that is responsible for respiratory diseases, tuberculosis, allergies, and asthma [4–6]. Besides the harmful gas, the suspended dusts are generally considered to contribute to air pollution, the size of which are 0.01–100 μm, and the smaller particle, the deeper it can enter into respiratory tract. In particular, the fine particles (PM with an aerodynamic diameter of 2.5 μm or less [PM2.5]) in the air are the most important air pollutants, having a negative impact on both industrial production and the health of human beings [7–10]. Therefore, finding effect way to achieve the protection and control of air pollution, especially the PM2.5 pollution, is an urgent issue to solve.

As for the sources of the fine particles, they are emitted mainly by anthropogenic activities, for example, vehicle exhaust, industrial production, biomass burning, secondary nitrate and secondary sulfates, etc., which can be grouped as normal and medium-high temperature particles according to the conditions that the particles are produced [11]. Due to the recognized threats of fine particles to the production facilities and human bodies, many prevention measures are taken to solve this problem: source control, usage of clean energy, air filtration technologies, and so on [12]. Among them, air filtration technology is the most widely used method for its high performance, low energy consumption, wide application range, and low cost. Traditional air filtration materials made of gauze can trap particles with bigger size and have very good air permeability, but they have almost no effect for particles with less than the order of magnitude of submicron [13]; nonwoven fibrous membranes (based on different fibers like glass, polypropylene [PP], polyester, and polyethylene [PE], etc.), which bear disordered arrangement of fibers, have relatively higher filtration efficiency [14], but their structure characteristics of still thicker fiber and larger pore size lead to

Handbook of Fibrous Materials, First Edition. Edited by Jinlian Hu, Bipin Kumar, and Jing Lu.
© 2020 Wiley-VCH Verlag GmbH & Co. KGaA. Published 2020 by Wiley-VCH Verlag GmbH & Co. KGaA.

limited filtration performance for ultrafine particles [15]. We can enhance the filtration efficiency of nonwoven fibrous membranes by increasing the fiber density of the membranes, but this way, the air permeability would be sacrificed [16, 17]. Therefore, achieving air filtration materials with higher filtration efficiency and at the same time with the lower pressure drop is always a difficult problem faced.

For fibrous filter media, it is easy to understand that the smaller the fiber diameter, the better filtration efficiency it will achieve. Meanwhile, the theory called "slip effect" tells us that when the diameter of fiber is small, the airflow would bypass the fiber so that cause less resistance against airflow, consequently leading to a smaller pressure drop across the fibrous media [18–20]. Thus, nanofibers become very promising to form filter media with high filtration performance for ultrafine particles. So far, a variety of techniques such as drawing, template synthesis, phase separation, islands in a sea, self-assembly, electrospinning, and solvothermal synthesis have been developed to fabricate nanofibers [21–26]. Comprehensively considering the complexity of the equipment, processing controllability, spinnable fiber range, structural controllability, productivity, and cost, electrospinning is often regarded as the preferred method to prepare uniform nanofibers in a continuous process and at a long length scales [27–29]. Electrospun nanofibrous membranes possess several intriguing features such as smaller pore size, higher porosity, remarkable specific surface area (SSA), and interconnected porous structure that make them very attractive in air filtration area including disposable respirators, automotive cabin air filters, industrial filter paper, cleanroom air purification systems, indoor air purifiers, and so on [14, 30–32].

Taking advantage of abovementioned fascinating features of electrospun nanofibrous membranes, the electrospinning technique is of huge interest for use in air filtration fields. Actually, there is another technique so-called electro-netting; strictly speaking, it can be regarded as the derived nanofabrication method from the technology of electrospinning. The diameter of nanofibers made by electro-netting can fall below 50 nm, further reduced than electrospun fibers (average diameter 100–500 nm) [33]. Thus, this technique of electro-netting attracted more attentions of researchers in recent years for their application in filtration area. In this chapter, two nanofabrication technologies, electrospinning and electro-netting, will be introduced, including the structures and properties of nanofibrous membranes that they can fabricate, the principle and formation mechanisms of each method, and their application in air filtration area for trapping both normal temperature and medium-high temperature ultrafine particles.

7.2 Fabrication Technologies

7.2.1 Electrospinning

Electrospinning, also named as electrostatic spinning, is a simple but effective and highly versatile technique that has been widely used to fabricate micro- and nanoscale fibers. This is a kind of technology that micro/nanofibers are formed

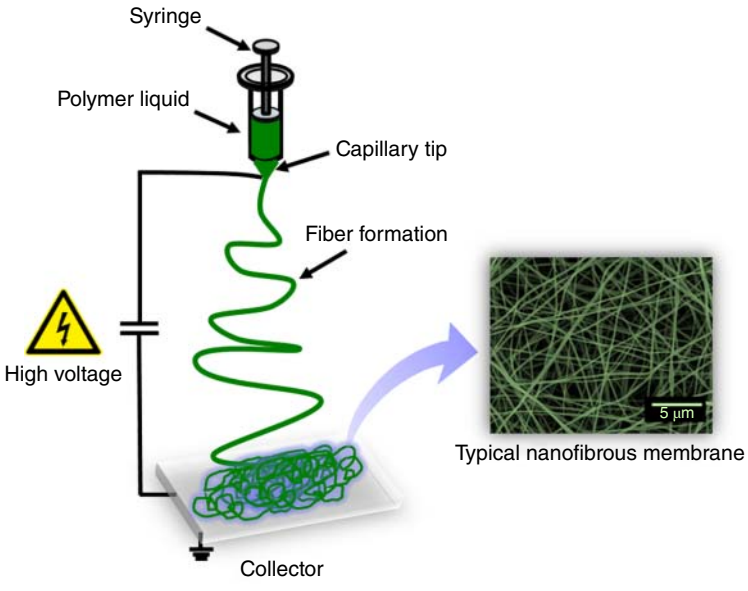


Figure 7.1 Schematic diagram of the basic setup for electrospinning.

from polymeric solutions or melts under the application of an electric field [34]. The schematic diagram to demonstrate the process of electrospinning is shown in Figure 7.1. During the electrospinning, the polymer liquid (a solution or melt) is put in the syringe that will push the liquid out from the tip with a certain speed, and a high voltage electric field (typically 10–50 kV) is applied to the polymer liquid. Gradually increasing the intensity of the electric field, a jet is drawn from the spinneret under a constant flow rate flying toward the collector; between the syringe tip and the collector, the solvent gradually evaporates and the polymer solidifies, and finally the solid micro/nanofiber is collected as an interconnected mats (as shown in Figure 7.1) on the oppositely charged grounded collector [35]. The diameters of the formed polymer fibers are from micrometers to few tens nanometers depending on different polymer type and technological conditions.

The process parameters that would influence the electrospinning include polymer solution properties (polymer type, solution concentration, solution viscosity, solution conductivity, etc.), spinning parameters (electric voltage, injection speed, collecting distance, etc.), and environmental parameters (mainly ambient temperature and ambient humidity).

7.2.2 Electro-netting

Since always accompanied with electrospinning, electro-netting is also called electrospinning/netting (ESN) process. As a variant of electrospinning process, this technique involves more higher voltage to induce the formation of not only a liquid jet but also the phase separation-induced splitting of small charged droplets between the syringe tip and the grounded collector, as shown in Figure 7.2a. Through this technique of electro-netting, a two-dimensional (2D)

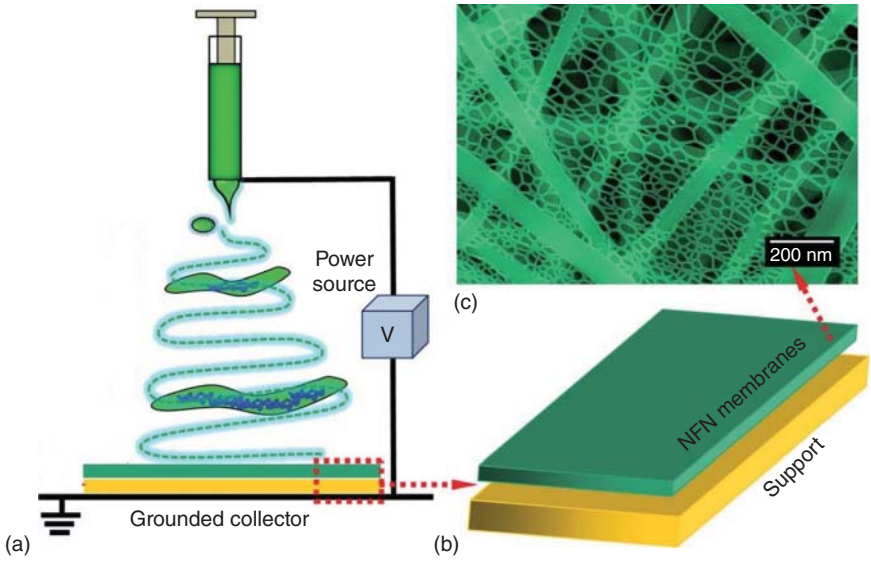


Figure 7.2 Setup for electro-netting and its formed NF/N membrane. (a) Setup for electro-netting. (b) NF/N membranes on support material. (c) Typical Field Emission Scanning Electron Microscope (FE-SEM) image of NF/N membranes. Source: Wang et al. 2012 [94]. Reproduced with permission of Royal Society of Chemistry.

spider-web-like-structured nanonets are fabricated between the primary electrospun fibers to construct a kind of aggregate structure termed as "electrospun nanofiber/net (NF/N) membranes" [33, 94] (shown in Figure 7.2c). This membrane possesses the unique "nanonet" structure comprising interlinked ultrathin nanowires with diameter of only 5–40 nm, which break the limitation of common electrospun fibers usually with large average diameter (100–500 nm) [36].

The origins of this novel one-step ESN process can be traced to the year of 2006 through a research article published in the journal of "Nanotechnology" by Ding et al. [37]. Compared with electrospinning, electro-netting needs more rigorous technological requirements, thus leading to the controllable preparation even harder. The formed inimitable NF/N structure exhibits many fascinating characteristics, such as extremely small diameter, super large SSA, and high porosity, which make it an attractive candidate in filtration, sensing, body protection, and many other environment, energy, and healthcare fields.

7.3 Principles and Theories

7.3.1 Fundamental Theory of Electrospinning

Although the setup for electrospinning is quite simple, the fundamental theory behind is very complex involving electric field, fluid rheology, polymer physics and chemistry, electrostatics, etc. [38, 39]. At first, the formation of micro/nanofibers by electrospinning was often thought to be caused by splitting

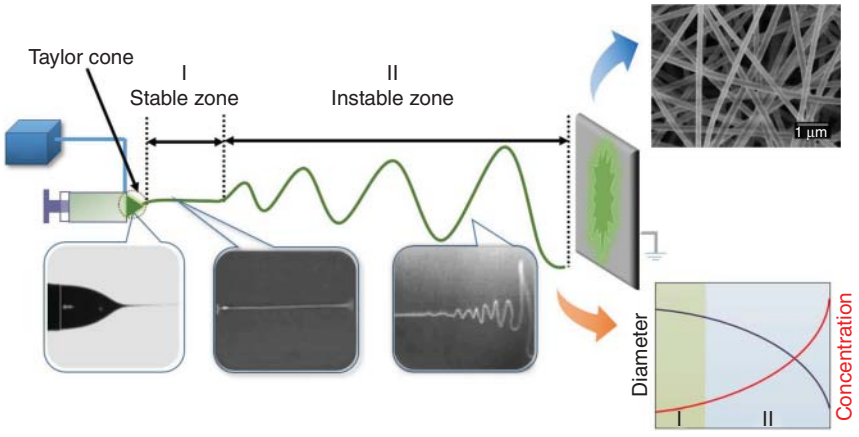


Figure 7.3 Fundamental theory and dynamic evolving process of electrospinning. Source: Wang et al. 2006 [46]. Reproduced with permission of American Chemical Society.

or splaying of the electrified jet as a result of repulsion between surface charges. With further research, it is indicated that the formation process actually is a dynamic evolving process, mainly controlled by the interaction of several physically unstable processes in electric field [40, 41]. The fundamental theories on electrospinning mainly can be described by three zones: (i) Taylor cone zone, (ii) jet stable zone, and (iii) jet in flight-instability zone, as shown in Figure 7.3.

During the electrospinning, the syringe is filled with a melt or blend polymer solution. When high voltage is applied, the solution becomes highly charged; the solution droplet at the syringe tip then will suffer two major types of forces: the surface tension and electrostatic repulsion force. When the voltage is increased to the critical value and any further increase will destroy the equilibrium, the hemispherical surface of the liquid at the tip elongates to form a conical shape, usually with a half angle of 49.3°, referred to as the Taylor cone [42, 43] (see insert in Figure 7.3). Just after this moment, the repulsive force of the charged polymer overcomes the surface tension of the solution, and as a result, a charged jet erupts from the tip of the Taylor cone and moves toward the collector.

After the charged jet ejecting from the Taylor cone, the jet first follows a straight path in the direction of the counter electrode. In this stable zone, the jet diameter decreases typically due to evaporation of the solvents and longitudinal deformations induced by electric forces [44, 45]. Following, the jet will bend and turn sideways and begin to perform spiraling (see insert in Figure 7.3); the electric forces continue to stretch and thin the jet by large ratios. It is revealed by researchers that as the diameter of the jet decreases, the path of the jet again becomes unstable and a new, smaller diameter electrical bending instability occurred [40, 46]. A succession of three or more smaller diameter bending instabilities is often observed before the jet solidified. Thanks to these instabilities, finally the length of the fiber increases enormously, and their cross-sectional diameter decreases to a fraction of a micron. Thus, during the whole process of fabrication, from the syringe tip to the collector, the solvent gradually evaporates so that the polymer

concentration increases, and the fiber diameter decreases to the final microscale or even nanoscale (the corresponding change curve is shown in Figure 7.3.).

7.3.2 Formation Mechanism of the Nanofiber/Net (NF/N) Membranes

When the fantastic NF/N membrane with special spider-web-like structure was first demonstrated by Ding et al., its potential application value trigged enormous researchers to explore the spinnable polymers, influencing parameters, morphology, and so on; they also wanted to reveal what happened to the charged polymer jets and droplets during such small distance between the syringe tip and grounded collector and how to control the final collected structure [47]. However, the formation mechanism of NF/N structures is complex, and the consensus on it has not been reached yet.

In order to enrich the polymer species, develop more functional features, and broaden the applied fields for the polymeric nanonets, the systematic formation mechanism of the NF/N structure is eager to be created to achieve the controllable fabrication. Up to now, there are mainly four possible mechanisms proposed to explain the formation of the nanonet structure: (i) ions initiated splitting up of the electrospun fibers, (ii) intermolecular hydrogen bonding, (iii) intertwining among branching jets, and (iv) phase separation of charged droplets. The first one was proposed by Kim et al. [48], believing that nanonets are formed by the joints between many fibers and the possible joints occur at the apex of Taylor cone; the second one focuses on the hydrogen bonding, which possibly offers the link force for the interconnected fibers [49]. These two mechanisms do provide some qualitative and possible explanation for the nanonet formation, but the first one is just suitable for salt addition system, while the second one is only for PA-6/oligomer system [33]. The third plausible mechanism of nanonets is "intertwining among branching jets," pointed out by Tsou et al., who attributed the nanonet formation to the enormous tiny subsidiary jets [50], but it ignores that the tiny jets may not be strong enough to withstand the huge electric traction force during flying process. The last mechanism based on phase separation of charged droplets is regarded as the most comprehensive one so far, which systematically analyzes the forces exerted on the charged liquid and droplets to reveal the complex formation process for the nanonets [37, 51], and thus will be described next.

The mechanism of "phase separation of charged droplets" was first proposed by Ding et al. in 2006 after the observation of the defect poly(acrylic acid) (PAA) films and partly split PAA nanonets [37]. In a simple word, this mechanism states that the formation of nanonets is due to the phase separation of charged droplets generated between the syringe tip and grounded collector. They suggested that during the electro-netting process, besides the formation of polymer solution jet, it also sprayed some small charged droplets under a higher electric field [52] (see the schematic diagram illustrating the possible formation procedure of nanonets shown in Figure 7.4): having experienced instability and elongation process, the polymer solution jets become very long and thin and eventually form the polymer nanofibers; while, for small charged droplet, it deforms significantly to a thin liquid film, then the rapid phase separation leads the solvent part into pores, and the spider-web-like nanonet structure is gradually formed and collected.

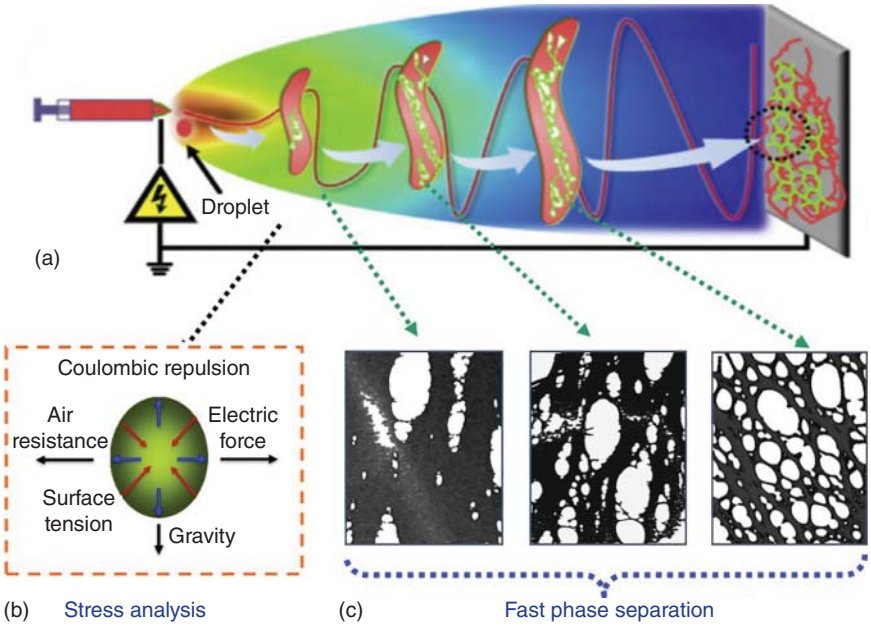


Figure 7.4 (a) Schematic diagram of electro-netting process. (b,c) The forces acting on the charged droplet and the possible process of nanonet formation during ESN process. Source: Wang et al. 2011 [54]. Reproduced with permission of The Royal Society of Chemistry.

After the charged droplets with microscale generated accompanying with the polymer solution jets, there are various forces exerted on the droplets under the electric field: electrostatic force, gravity, surface tension, drag force (air resistance), coulombic repulsion force, and viscoelastic force [53, 54], as shown in Figure 7.4b. The electrostatic force aims to carry the charged droplet from syringe tip to the grounded collector with a certain accelerated speed; the drag force between the surrounding air and the charged droplet would deform the droplets into films; the coulombic repulsion force acts an opposite function with surface tension and viscoelastic forces of the droplet. On the one hand, the coulombic repulsion force would like to expand the droplet; on the other hand, the droplet's surface tension and viscoelastic forces will contract it. During the electro-netting process, with the increasing moving speed of the charged droplet, the exerted drag force and the coulombic repulsion forces will be reinforced, so that leads to further expansion and distortion of the thin film. And at the same time, the fast phase separation causes the solvent part into pores (shown in Figure 7.4c); thus, the spider-web-like nanonet structure is finally constructed and collected.

7.4 Structure and Properties

7.4.1 Types and Structures of the Nanofiber Membranes

As a nanofabrication technique, electrospinning has been widely used due to not only simplest setup but also large number of spinnable material types

and versatile structures and properties of nanofiber membranes. A variety of materials such as polymers (natural polymers like silk, chitin, chitosan, etc. and synthetic polymers like nylon 6, polystyrene, polyurethane, etc.) [55–58], ceramics (e.g. TiO_2, SiO_2, ZnO, etc.) [59, 60], carbon (including PAN based, polybenzoxazine based, polybenzimidazole based, and so on) [61, 62], and even metals [63] have been electrospun into uniform fibers with well-controlled sizes, compositions, and morphologies. In most situations, electrospun nanofibers are usually smooth solid fibers, and they are collected as nonwoven membranes with randomly arranged structures (as shown in Figure 7.6a); this kind of membrane structure is superior for filtration application because of thin fiber diameter, smaller pore size, and higher porosity. In order to explore the application of electrospun nanofibers, more and more researchers tried to develop nanofibers with versatile structures and morphologies through controlling processing parameters. So far, many kinds of novel structures have been successfully fabricated, including single fiber structure and aggregate structure.

The single fiber structure is important because it will directly influence the structure and property of the aggregated nanofiber membranes. For example, the cross-sectional shape and size, the pore distribution, and the internal structure of the single fiber will determine the porosity, SSA, and even physical and chemical properties of nanofiber membranes. So far, by regulating processing parameters including (i) the solution properties such as solution concentration, viscosity, elasticity, conductivity, and surface tension; (ii) spinning parameters like electric voltage, injection speed, collecting distance between syringe tip and ground collector, etc.; and (iii) the ambient parameters such as ambient temperature, ambient humidity, and air velocity, researchers can obtain single nanofibers other than smooth solid structure, but with bead-on-string, ribbon-like [64], helical [65], porous [66], core–shell [67], multichannel tubular [68], tube-in-tube [69], necklace-like [70], rice-grain shape [71], multicore cable-like [72], nanowire-in-microtube [73], and hollow [74] structures, as shown in the Figure 7.5a–l. These different structures can be used in various application fields: for example, the porous structure is suitable in application of adsorption field due to its high SSA; the multichannel tubular and hollow structures, because of the inner still air, can be used for thermal productive garments.

In addition to rich structures of single fiber, different nanofiber assembly morphologies were also reported via control of the processing conditions or collecting methods to produce fibrous nonwovens with versatile structures besides random oriented structure; the main patterns of them are shown in Figure 7.6. For instance, by using the rotating roller with high speed as collector, nanofibers were strongly stretched by such high speed to be aligned among the rotating orientation. Thus the highly aligned nanofibers were successfully fabricated, as shown in the Figure 7.6b; the uniform mesh-like patterning nanofibers can be fabricated by using electroconductive collector with woven structure, which is displayed in Figure 7.6c [75], and the fantastic spider-web-like nanofiber/net (shown in Figure 7.6d) can be prepared by the process of electro-netting. Therefore, we can obtain nanofibrous membranes with rich polymer type, various single fiber structures, and assembly morphologies to be highly attractive to numerous applications including filters, textiles, composites, sensors, biotechnology, and so on.

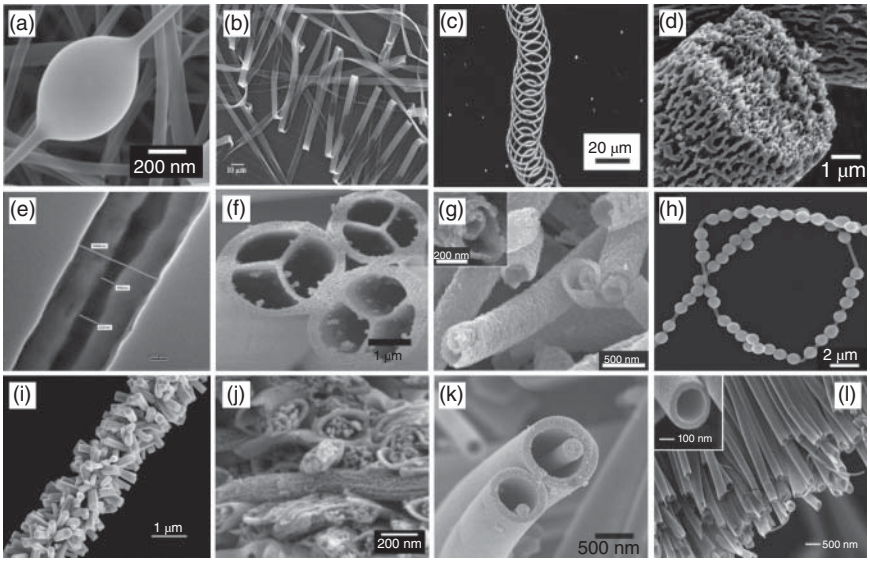


Figure 7.5 Various single fiber structures obtained by electrospinning. (a) Bead on string. (b) Ribbon-like. Source: Koombhongse et al. [64]. Reprinted with permission of John Wiley & Sons, Inc. (c) Helical. Source: Kessick and Tepper 2004 [65]. Reprinted with permission of American Institute of Physics. (d) Porous [67]. Source: Adapted from Ding et al. 2008 [66]. (e) Core-shell. Source: Sun et al. 2003 [67]. Reprinted with permission of John Wiley & Sons, Inc. (f) Multichannel tubular. Source: Zhao et al. 2007 [68]. Reprinted with permission of American Chemical Society. (g) Tube in tube. Source: Mou et al. 2010 [69]. Reprinted with permission of American Chemical Society. (h) Necklace-like. Source: Jin et al. 2009 [70]. Reprinted with permission of American Chemical Society. (i) Rice grain-shaped. Source: Shengyuan et al. 2011 [71]. Reprinted with permission of Royal Society of Chemistry. (j) Multicore cable-like. Source: Kokubo et al. 2007 [72]. Reprinted with permission of IOP Publishing Ltd. (k) Nanowire in microtube. Source: Chen et al. 2010 [73]. Reprinted with permission of American Chemical Society. (l) Hollow structures. Source: Li and Xia 2004 [74]. Reprinted with permission of American Chemical Society.

7.4.2 Structures and Species of the Nanofiber/Net (NF/N) Membranes

As mentioned previously, the technology of electro-netting needs higher requirements in processing control compared with electrospinning. Although a very broad range of polymers have been electrospun into micro- or nanofibers by electrospinning, it is founded that not all of those spinnable polymers can be fabricated into spider-web-like NF/N-structured membranes. However, with continuous efforts that have been applied to NF/N membranes, many kinds of polymer systems, such as polymers soluble and spinnable from water, biocompatible and biodegradable polymers, and polymer blends, can be successfully obtained with NF/N structure [33]. Some typical morphologies of NF/N membranes based on different polymer systems are shown in Figure 7.7.

Similar to the technology of electrospinning, many parameters including solution parameters, process parameters, and ambient parameters will influence the phase separation process during the electro-netting and the gained morphologies of NF/N membranes. Although a general knowledge of formation mechanism

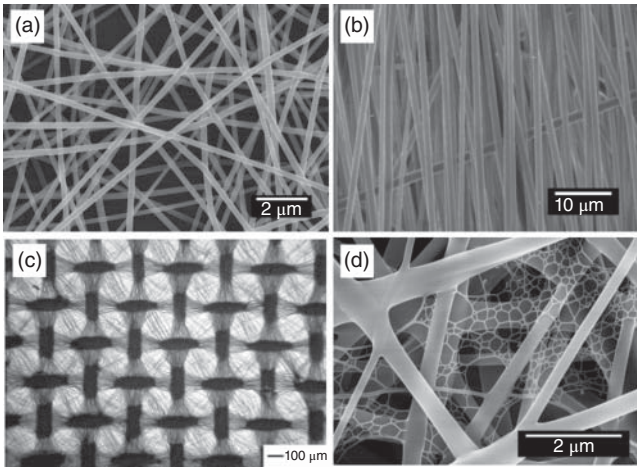


Figure 7.6 Different aggregate structure of electrospun nanofiber. (a) Random oriented. (b) Aligned. Source: Mathew et al. 2006 [116]. Reprinted with permission of John Wiley & Sons, Inc. (c) Patterned. Source: Reprinted with permission of Zhang and Chang 2007 [75]. Copyright 2007 Wiley-VCH Verlag GmbH & Co. (d) Spider-web-like nanofiber/net structures. Source: Reprinted with permission of Wang et al. 2009 [117]. Copyright 2010 IOP Publishing Ltd.

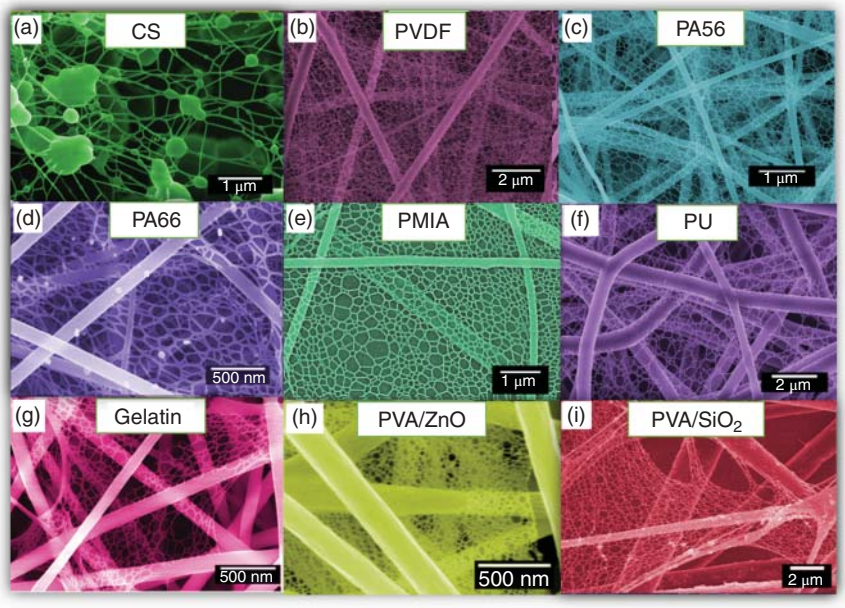


Figure 7.7 Several typical NF/N membranes based on different polymer systems. (a) CS. (b) PVDF. (c) PA-56. (d) PA-66. (e) PMIA. (f) polyurethane (PU). Source: Reprinted with permission of Hu et al. 2011 [54]. Copyright 2011 Wiley-VCH Verlag GmbH & Co. (g) Gelatin. Source: Reprinted with permission of Wang et al. 2011 [118]. Copyright 2011 Elsevier Ltd. (h) polyvinyl acetate (PVA)/ZnO. Source: Reprinted with permission of Ding et al. 2008 [119]. 2008 Elsevier B.V. (i) PVA/SiO_2. Source: Ding et al. 2010 [120]. Reproduced with permission of Elsevier.

and influencing factors of NF/N membranes has been known, the relationship between spinnable polymers and NF/N membranes is yet to be revealed. Recently, Ding's laboratory successfully fabricated the first pure-inorganic NF/N membranes (SiO_2, TiO_2, etc.) and even the first carbon NF/N membranes in the world, which will intensively broaden the application field of NF/N membranes. In addition to develop new types of NF/N membranes, researchers also engaged in controllable fabrication and structure optimization of the NF/N membranes, such as regulating the fiber and nanowire diameter, pore width, coverage rate of nanonets, and so on.

7.5 Application of Nanofibrous Membranes in Air Filtration

Due to many outstanding structural advantages of nanofibrous membranes, such as finer fiber diameter, smaller pore size, higher surface area to volume ratio, higher porosity, and vast possibilities for surface functionalization, nanofibrous membrane-based filter media (usually with random oriented nonwoven structure) are considered to be much promising in air filtration fields. According to the temperature of particle source, current electrospun nanofibrous filters can be divided into two groups: normal temperature filter and medium-high temperature filter.

7.5.1 Normal Temperature Filter

Normal temperature filtration media are those filters that can be conveniently used under 150 °C for a long time. They are usually the core filtration part of indoor air purifier, vehicle cabin filters, building filters, and personal respiratory protection products. The materials used for these filtration applications (no need to resist high temperature) can be natural polymers, synthetic polymers (mostly used like PA, PAN, PU, PVA, PEO, etc.) [76–80], polymer blends [81, 82], and polymer incorporated with functional materials [83, 84]. Among those normal temperature filters made by various polymer systems, if we classify them according to structure, there are mainly electrospun nanofiber membranes and electrospun NF/N membranes.

7.5.1.1 Electrospun Nanofiber Membranes

Nanofiber Filters with High Efficiency and Low Pressure Drop Compared with traditional filtration materials made of cotton cloth or gauze, nanofibrous membranes have more thinner fiber diameter and smaller pore size, so that they can trap even finer pollutant particles in the air. Gibson et al. [85] firstly fabricated PA-66 nanofibrous membranes for filtration use and revealed that they were extremely efficient at trapping airborne particles with diameter between 0.5 and 200 μm. Li et al. [86] prepared PA-6 electrospun nanofibers with diameter in the range of 120–700 nm; this fabricated nanofibrous membrane has filtration efficiency of above 80% for the airborne particles of 0.5 μm, which is much higher than that of

traditional filtration materials. By further adjusting processing parameters, Ahn et al. [87] obtained PA-6 thinner fiber (average diameter of 80 nm) membrane with improved filtration efficiency of 99.99%, but its air pressure drop was too high (larger than 500 Pa). It is found that raising filtration efficiency and reducing pressure drop are always a pair of contradictory body when trying to improve the performance of nanofibrous filtration membranes. Thus, the achievement of air filters with both high efficiency and low pressure drop is always a challenge that researchers face these years.

According to the "slip effect," it is known that the thinner the fiber, the higher filtration efficiency, and meanwhile, if the diameter of fiber decreases close to the mean free path of air molecules (65.3 nm), the air will stride over the fiber so that the air pressure drop of the filtration materials can be dramatically reduced [88]. However, if the fiber assembly pack is too dense, it will destroy this "slip effect." Therefore, a good balance should be made between the fiber structure and assembly structure. Through careful controlling over the diameters of electrospun polyacrylonitrile fibers and aperture size of fiber assembly, Zhao et al. [89] reported novel slip-effect functional nanofibrous membranes with decreased air resistance (reduction rate of 40%) due to the slip flow of air molecules and indicated the optimal fiber diameter and pore size that are validated both theoretically and experimentally. In order to obtain the fibers with diameter in the vicinity of mean free path of air molecules, authors in this chapter selected polyacrylonitrile (PAN) with low molecular weight as electrospun polymer and lithium chloride (LiCl) to enhance the solution conductivity to obtain the bead-free nanofibers. According to the drag theory, the relationship between pore structure and slip effect was intensively investigated (shown in Figure 7.8): with decreasing of fiber diameter, the average pore size of the membrane decreases, and the drag force reduces as well, but if the fiber diameter and pore size continuously go down (e.g. fiber diameter lower than 70 nm), the drag force will then increase. That means too close

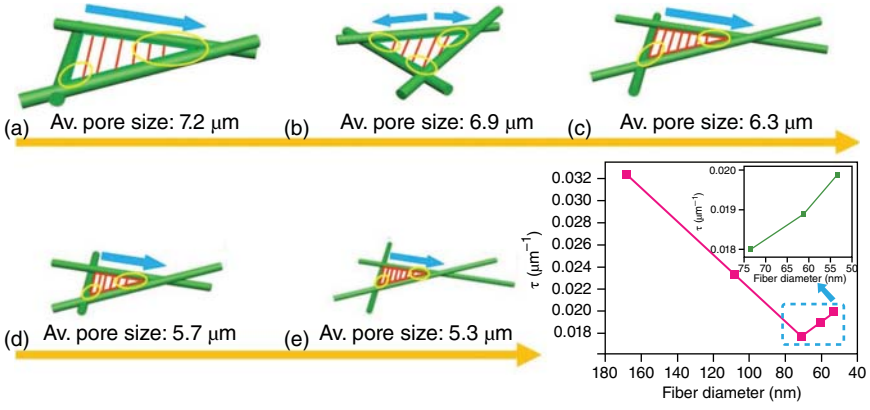


Figure 7.8 The relationship between pore structure and slip effect. The average pore size reduces with the decreasing of fiber diameter: (a) 168, (b) 108, (c) 71, (d) 60, and (e) 53 nm. (f) Equilibrium factor of PAN fibrous membranes with different fiber diameter. Source: Zhao et al. 2016 [89]. https://www.nature.com/articles/srep35472#rightslink; http://creativecommons.org/licenses/by/4.0/. Licensed under CCBY 3.0.

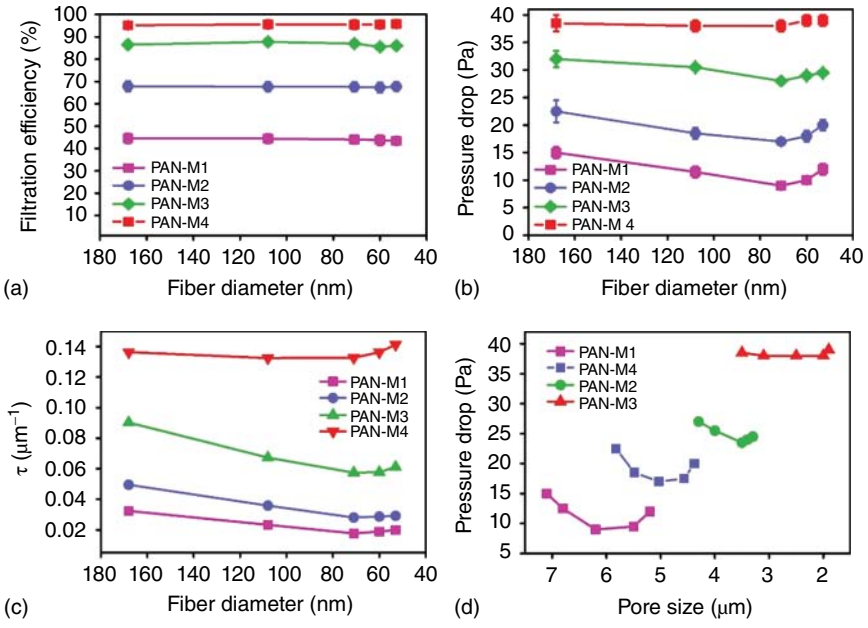


Figure 7.9 The influence of fiber diameter and pore size of the several PAN membranes on the filtration properties. (a) Filtration efficiency for several PAN membranes. (b) Pressure drop change with different fiber diameter. (c) Equilibrium factor change of PAN fibrous membranes with different fiber diameter. (d) Structure–function relationship between pressure drop and pore size. Source: Zhao et al. 2016 [89]. https://www.nature.com/articles/srep35472#rightslink; http://creativecommons.org/licenses/by/4.0/. Licensed under CCBY 3.0.

distance between two adjacent fibers will restrain the airflow and thus result in the increasing of the air pressure drop.

To further investigate the critical value of the fiber diameter and pore size of PAN nanofibrous membranes, Zhao et al. [89] then fabricated several PAN fibrous membranes with nearly identical filtration efficiencies by controlling the electrospinning time, as illustrated in Figure 7.9a (the points with the same color have nearly identical filtration efficiencies but with different fiber diameters). It is found that the fiber diameters between 60 and 100 nm are most effective for slip flow (achieving lowest pressure drop and drag force; see Figure 7.9b,c); if the pore size is too small (less than 3.5 μm), the air pressure drop of the nanofibrous membrane will be the same no matter how the fiber diameter changes (see Figure 7.9d). Thus the pore size should be larger than 3.5 μm for constructing slip-effect functional nanofibrous membranes. Ultimately, the fabricated PAN membranes displayed low air resistance of only 29.5 Pa, high purification efficiency of 99.09%, good transmittance of 77%, and long service life.

Instead of further reducing the fiber diameter and at the same time to keep higher porosity of the membrane to improve the filtration performance, some other researchers focused on fabricating electreted nanofibrous membranes to improve its filtration efficiency by electrostatic effect without deteriorating the pressure drop. Yeom et al. [84] prepared PA-6/boehmite nanofibrous

membranes; this membrane had better filtration efficiency than pure PA-6 membrane when both membranes had almost the same air pressure drop. Cho et al. [83] added TiO_2 electreted nanoparticles when electrospinning PAN nanofibrous membranes and successfully fabricated PAN/TiO_2 nanofibrous membrane with higher filtration efficiency and lower air pressure drop. Recently, Wang et al. [90] reported a novel electret nanofibrous membrane with rich charges and desirable charge stability by using polyvinylidene fluoride (PVDF) as the matrix polymer and polytetrafluoroethylene nanoparticles (PTFE NPs) as the charge enhancer through the in situ charging technology of electrospinning. By adjusting the concentration of PTFE NPs (22 wt% PVDF polymer solution containing 0, 0.01, 0.05, and 0.1 wt% of PTFE NPs was prepared) and the applied voltage (four injection energy level as 20, 30, 40, and 50 kV, respectively) during electrospinning, it was found that the optimal employment of PTFE NPs should be 0.05 wt% and 40 kV was the best applied voltage. The electreted PVDF/PTFE nanofibrous membranes they fabricated were endowed with elevated surface potentials from 0.42 to 3.63 kV and had better charge stability (reduced decrement of charges from 75.4% to 17.5%).

Meanwhile, they also proposed the electret mechanism of this PVDF/PTFE nanofibrous membrane [90]. They thought there were four kinds of charge format: volume charges, surface charges, polarized dipole, and interfacial polarization between PVDF nanofibers and PTFE nanoparticles, as shown in Figure 7.10a–d. The good electreted effect of PVDF/PTFE nanofibrous membranes was attributed to, on the one hand, the strong polarity of fluorine-containing polymer (polarized dipole produced is much stable than volume charge and surface charge) and, on the other hand, the extra interfacial polarization between PVDF nanofibers and PTFE nanoparticles. With the increase of the concentration of PTFE NPs and injection energy, the electreted effect of PVDF/PTFE nanofibrous membranes was significantly improved. Finally, the resultant PVDF/PTFE nanofibrous membrane reached a

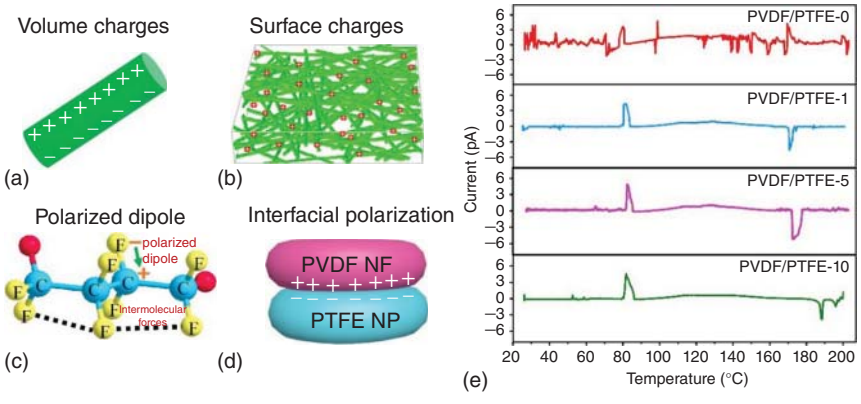


Figure 7.10 Schematic description of electric charge categories existing in PVDF nanofibrous membranes containing various PTFE NP concentrations. (a) Volume charges. (b) Surface charges. (c) Polarized dipole. (d) Interfacial polarization. (e) Thermally stimulated current spectra of PVDF fibrous membranes containing various PTFE NP concentrations. Source: Wang et al. 2016 [90]. Reprinted with permission of American Chemical Society.

high filtration efficiency of 99.972%, a low pressure drop of 57 Pa, and superior long-term service performance.

Nanofiber Filters with Functional Properties Besides the efforts made in the direction of achieving filtration materials with high efficiency and low pressure drop, researchers also did many work on developing air filters with functional properties.

One of the most important functions we concern about the filtration materials is mechanical property during the practical application; thus many mechanically enhanced nanofibrous membranes were continuously reported. Liu et al. [91] prepared polyacrylonitrile/poly(acrylic acid) (PAN/PAA) nanofibrous membranes as filter medium by electrospinning; the tensile strength of this blended nanofibrous mat improved as increasing PAA content, from 3.8 to 6.6 MPa, higher than pristine PAN. Wang et al. [82] fabricated tortuously structured polyvinyl chloride (PVC)/PU fibrous filtration medium with robust mechanical performances. They prepared blended solutions with different weight ratios of PVC/PU (10/0, 9/1, 8/2, and 7/3) and found that the increasing PU contents not only increased the average fiber diameter but also showed gradually increased adhesion among the adjacent fibers (as shown in Figure 7.11, indicated by dotted circle). When the weight ratio of PVC/PU was 8/2, the interfacial compatibility of PVC/PU reached to the optimum state, and the PVC/PU membranes showed the maximum tensile strength of 9.9 MPa. The as-prepared membranes showed filtration efficiency (99.5%) and pressure drop (144 Pa) performance for 300–500 nm sodium chloride aerosol particles.

In order to obtain mechanically enhanced air filters without sacrificing filtration performance, recently, Zhang et al. [92] combined multi-jet electrospinning and physical bonding process to create anti-deformed poly(ethylene oxide)@polyacrylonitrile/polysulfone (PEO@PAN/PSU) composite membranes with binary structures for effective air filtration. This membrane allows the ambiguous fiber framework including thin PAN nanofibers and fluffy PSU microfibers, and the mixed PEO component will be melted as bonding points between fibers after heat treatment (see the fabrication procedure in Figure 7.12). With increasing PEO concentration, the number of point-shaped bonding structures

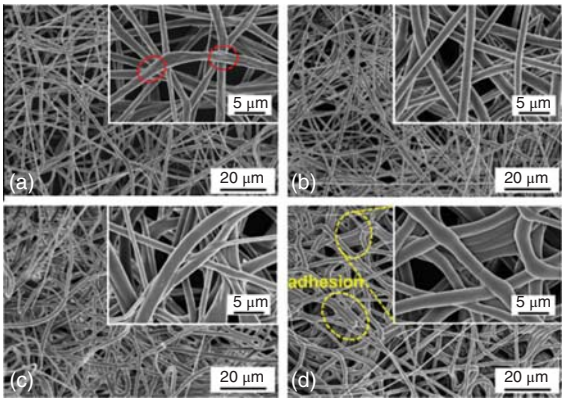


Figure 7.11 FE-SEM images of PVC/PU membranes fabricated with varied weight ratios of PVC/PU: (a) 10/0, (b) 9/1, (c) 8/2, and (d) 7/3. Source: Wang et al. 2013 [82]. Reprinted with permission of Elsevier.

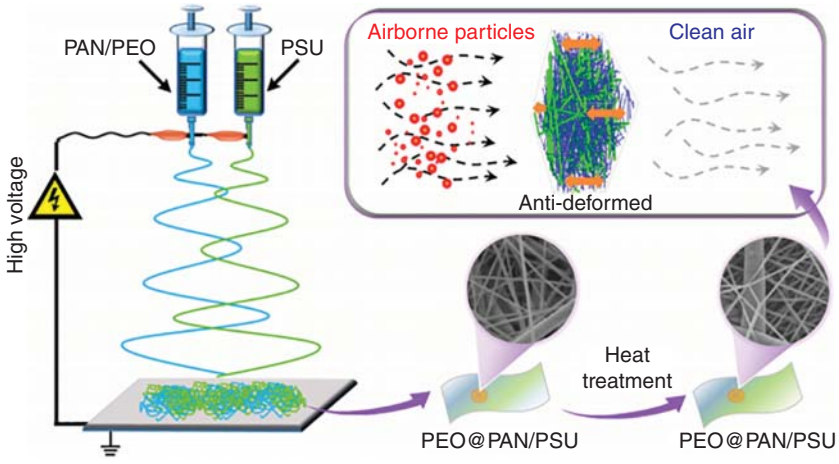


Figure 7.12 Schematic illustration of the fabrication procedure of the anti-deformed PEO@PAN/PSU composite membranes, including the multi-jet electrospinning device and physical bonding (heat treatment) process. Source: Zhang et al. [92]. Reprinted with permission of American Chemical Society.

increased dramatically; thus the mechanical properties of the membrane were strengthened. It was found that when the PEO concentration was of 1.5 wt%, the filtration efficiency of the PEO@PAN/PSU membrane would keep the same before and after the compacting treatment; in other words, the membrane's structural deformation can be neglected even under some external force. With the integrated features of small pore size, high porosity, and point-shaped bonding structure, the resultant composite membrane exhibited robust mechanical properties (8.2 MPa), high filtration efficiency of 99.992%, low pressure drop of 95 Pa, and desirable quality factor of 0.1 Pa^{-1}, and most importantly, it can avoid the potential safety hazards caused by unexpected structural collapsing under external forces during the practical application.

Besides the improvement of mechanical properties, air filtration materials can be endowed with other functions. For example, Wang et al. [93] report a novel superamphiphobic nanofibrous membrane by the combination of electrospun PAN/PU nanofibers and a new synthesized fluorinated polyurethane (FPU) containing terminal perfluoroalkane segment to achieve oil and non-oil aerosol particle filtration (see Figure 7.13). The introduction of low surface energy FPU enabled the PAN/PU composite membranes to have both superhydrophobicity and superoleophobicity. By tuning the solution composition, hierarchical structure, and the FPU content, the as-prepared membrane obtained excellent superamphiphobic properties of a water contact angle of 154° and an oil contact angle of 151°. Meanwhile, this kind of membrane can capture a range of different oil aerosol particles in a single-unit operation with filtration efficiency larger than 99.9%. Therefore, it is very promising in the filtration performance toward oil and non-oil aerosol particles and can be used in industry, respiratory protection equipment, and numerous air filtration fields.

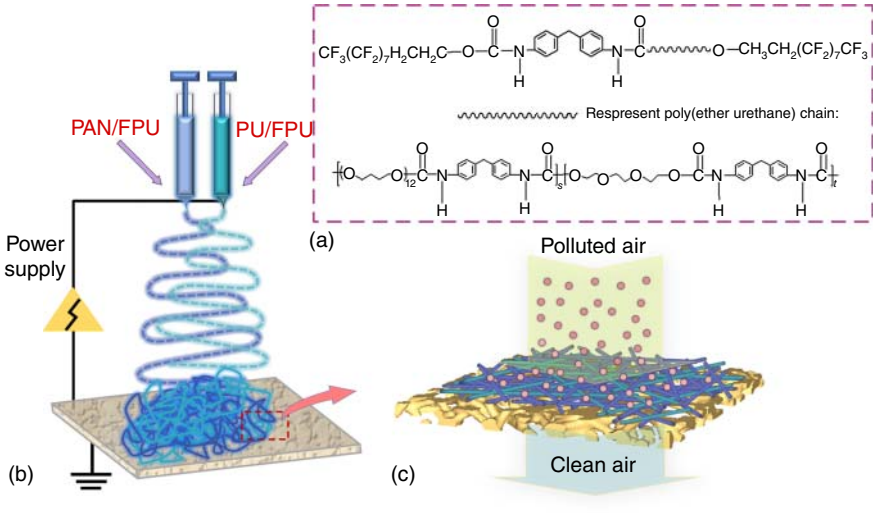


Figure 7.13 Schematic illustration of the fabrication procedure of the superamphiphobic nanofibrous membrane. (a) Illustration of the chemical structure of as-synthesized FPU. (b) Electrospinning device for the preparation of the filter membranes. (c) Filtration process of the superamphiphobic membranes for aerosol particles. Source: Wang et al. 2014 [93]. Reprinted with permission of Elsevier.

7.5.1.2 Electrospun Nanofiber/Net (NF/N) Membranes

In addition to the above electrospun nanofiber membranes fabricated by electrospinning, as mentioned previously, another promising technology of electro-netting is also widely used for air filter construction due to finer fiber diameter, smaller pore size, and higher porosity of the NF/N membranes.

For instance, Wang et al. [94] firstly created a two-tier composite structure as a novel airborne particulate filtration medium: the polyamide-66 (PA-66) NF/N membrane composed of traditional electrospun nanofibers and 2D spider-web-like nanonets as the top layer and the conventional nonwoven PP structure as the support (as shown in Figure 7.14). By regulating the solution properties (mainly the kinds of salt and salt concentration) and several electro-netting process parameters (such as applied voltage, ambient temperature, and humidity), the optimal nanonets with a high coverage rate (over 95%) and a layer-by-layer packing structure were finally achieved under a voltage of 30 kV, ambient temperature of 25 °C, and relative humidity (RH) of 25%. Owing to several fascinating features such as extremely small diameter, high porosity, and controllable coverage rate, the resultant two-tier composite filtration medium showed high filtration efficiency (up to 99.9%) toward NaCl aerosols, low pressure drop, facile filter cleaning, and more lightweight.

In order to further improve the filtration efficiency, Liu et al. [95] fabricated a bio-based polyamide-56 nanofiber/net (PA-56 NF/N) membrane with bimodal structures for effective air filtration via one-step ESN. This filtration medium contained completely covered 2D ultrathin (20 nm) nanonets and bonded scaffold fibers to improve the mechanical properties of the membrane.

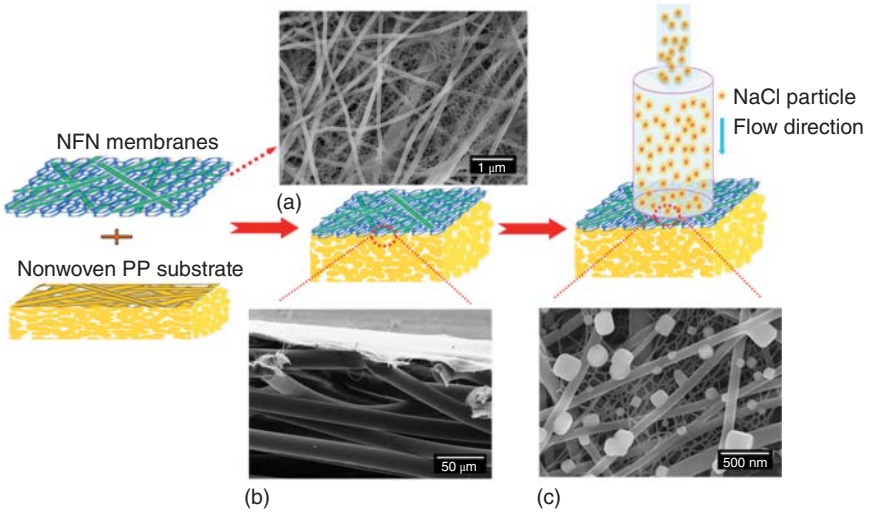


Figure 7.14 Schematic diagrams illustrating the fabrication of an NF/N layer deposited on the nonwoven PP substrate and the filtration process of the composite membrane. (a) FE-SEM image of PA-66 NF/N membranes deposited on the PP scaffold. FE-SEM images of the composite membrane. (b) Cross section before filtration. (c) Top view after filtration. Source: Wang et al. 2012 [94]. Reproduced with permission of Royal Society of Chemistry.

Through tuning the solution concentration and regulating the weight ratio of $HCOOH/CH_3COOH$, the optimal structure with high coverage of nanonets and stable bonded scaffold fibers was finally constructed. Taking advantages of extremely thin diameter, high porosity, and bonded scaffold, the resultant PA-56 NF/N membranes exhibit robust mechanical strength of 11.02 MPa, high filtration efficiency of 99.995%, pressure drop of 111 Pa, large dust holding capacity of 49 g/m^2, and long service life (dust-cleaning regeneration ability) for filtrating ultrafine airborne particles.

Although NF/N membranes with ultrathin fiber diameter can achieve higher filtration efficiency, the tiny pore size usually results in relatively high pressure drop. How to fabricate filter medium having higher filtration efficiency but at the same time with lower air pressure drop is always a challenging problem. Thus, many researchers tried ways to construct NF/N membrane that avoid dense packing structure to improve the filtration performance. For instance, Wang et al. [96] prepared an ultra-lightweight (2.94 gm^{-2}) nylon 6–polyacrylonitrile nanofiber/net binary (N6–PAN NNB)-structured membrane via multi-jet spinning (see Figure 7.15). The combination of high coverage N6 nanonets and low packing density of PAN nanofibers enabled the resultant NNB composite membrane to act as an efficient filtration medium. It is found that when the concentration of N6 solutions was 15 wt%, and the fiber spinning jet ratio of N6/PAN reached 2/2, the composite membrane exhibited high filtration efficiency (99.99%) and desirable quality factor (0.1163 Pa^{-1}) even under a high flow rate (90 l/min), better than the commercial glass fiber and melt-blown PP fiber-based media. Meanwhile, this as-prepared composite membrane showed

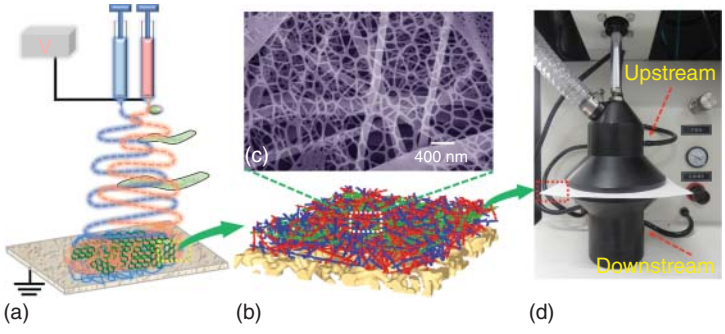


Figure 7.15 (a) The fabrication process of N6–PAN NNB composite membranes on a nonwoven substrate by multi-jet spinning. (b) Representation of the formed N6–PAN NNB composite membrane (N6 nanofibers are in red; N6 nanonets are in green; and PAN nanofibers are in blue) and nonwoven substrate (yellow part). (c) Typical FE-SEM image of the membrane. (d) Illustration of the filtration process of N6–PAN NNB composite filter medium. Source: Wang et al. [96]. Reprinted with permission of Royal Society of Chemistry.

a deep bed filtration pattern, rather than the surface filtration pattern of the N6 NF/N membrane, which was investigated by the way of three-dimensional computer simulation.

Different from incorporating low packing density of nanofibers into the NF/N membranes, Yang et al. [97] created a sandwich-structured polyamide-6/polyacrylonitrile/polyamide-6 (PA-6/PAN/PA-6) composite membrane for effective air filtration via sequential spinning. This composite membrane had three layers (see Figure 7.16): the upper and bottom PA-6 NF/N layers with ultrathin (~20 nm) nanonets and the middle PAN bead-on-string fiber layer as cavity structure. The existence of the middle PAN layer cannot only reduce the packing density of the whole composite membrane but also

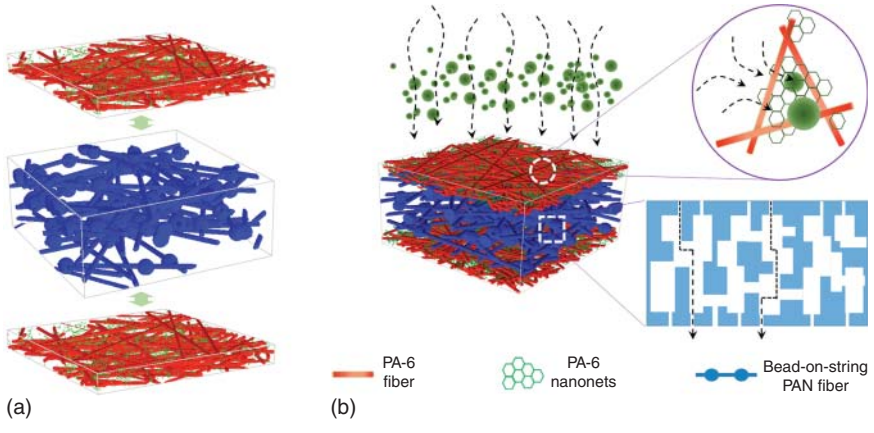


Figure 7.16 (a) Illustration of the sandwich-structured PA-6/PAN/PA-6 composite membrane. (b) Schematic diagram showing the filtration process of PA-6/PAN/PA-6 composite media for 300–500 nm NaCl airborne particles. Source: Yang et al. [97]. Reprinted with permission of Elsevier.

function as a support to strengthen the filter medium. By tuning the solution concentration and voltage applied, the number and size of the beads for the PAN layer were finely controlled, while by varying the weight ratio of PA-6 NF/N layers and PAN layer, the sandwich-structured composite filtration medium was finally optimized. Attributed to the integrated properties of ultrathin diameter offered by PA-6 NF/N layers, and stable cavity structure provided by PAN bead-on-string fiber layer, the resultant sandwich-structured PA-6/PAN/PA-6 composite membranes exhibit robust mechanical properties (tensile strength of 7.28 MPa, toughness of 1.77 MJ/m^3, and Young's modulus of 130.4 MPa) and much high filtration efficiency of 99.9998% with pressure drop of 117.5 Pa for 300–500 nm airborne particles. These novel composite membranes were regarded very promising in wide application fields of indoor air clean, engine intake, respirator, and heating, ventilation, and air conditioning, etc.

Zhang et al. [98] then tried a new strategy to create microwave-structured polyamide-6/poly(*m*-phenylene isophthalamide) nanofiber/net (PA-6/PMIA NF/N) membranes by combining the electro-netting and thicker staple fiber intercalating process. The embedded PMIA staple fibers, because of more thicker fiber diameter, constructed a cavity structure (microwave fluctuation and high-loft structures due to the supporting effect of the staple fibers) for the NF/N membranes so as to reduce the packing density. By optimizing the PA-6 concentrations and PMIA staple fiber arrangement, the resulting PA-6/PMIA NF/N filtration medium can efficiently filter ultrafine airborne particles with high filtration efficiency of 99.995%, low pressure drop of 101 Pa, and large dust-holding capacity of $>50\ g/m^2$. Thus, it is proved that the way of embedding thicker fiber into NF/N membranes to build cavity structure is creative and effective. However, the staple fibers are short and randomly distributed, which somewhat limit the controllable fabrication and stability of the membranes. In order to construct more stable cavity structure, recently, the authors introduced filament into the NF/N membranes [99]; they allowed polyethylene terephthalate (PET) filaments to orderly embed into 2D PA-6 nanonet layer (see Figure 7.17) to construct a ripple-like composite membrane for effective air filtration. The pleat span provided by single filament enlarged with the increasing of filament diameter (see Figure 7.17h). By adjusting the filament diameter and interval gap, the membrane structure for the optimized filtration performance was obtained. It was found that the as-prepared ripple-like PA-6 NF/N filtration medium can filter the ultrafine airborne particles (300–500 nm) with high efficiency of 99.996% and lower air pressure drop of only 95 Pa due to its extremely small pore size (≈0.35 μm) provided by PA nanonets and high porosity (92.5%) supplied by the built stable cavity structures.

In addition to construct stable cavity structure for NF/N filtration medium to achieve low air pressure drop, Zhang et al. [100] reported a highly integrated polysulfone/polyacrylonitrile/polyamide-6 (PSU/PAN/PA-6) filtration medium for multilevel physical sieving airborne particles via sequential spinning. This integrated air filter had three layers: the PSU microfiber (diameter of ~1 μm) layer, middle PAN nanofiber (diameter of ~200 nm) layer, and PA-6 nanonets

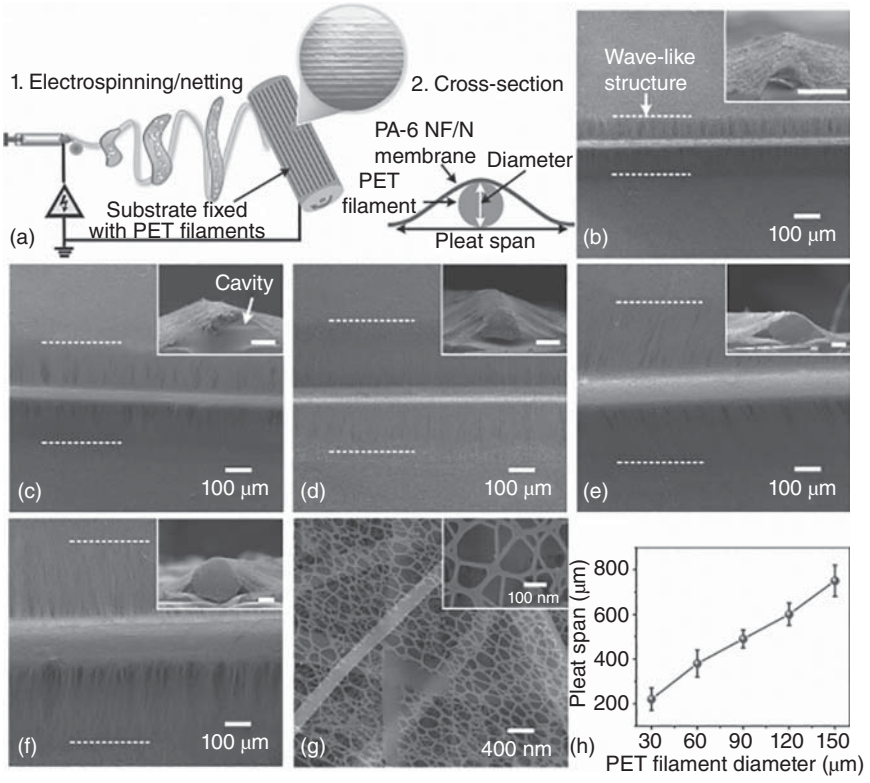


Figure 7.17 (a) Schematic showing (1) the fabrication process of the ripple-like PA-6 NF/N membrane and (2) the cross section of the PET embedded PA-6 NF/N filter. SEM images of PA-6 NF/N membranes embedded with PET filaments with various diameters of (b) 30, (c) 60, (d) 90, (e) 120, and (f) 150 μm and certain framework gap of 1 mm. Insets are the corresponding images of their cross-sectional views (the scale bar is 50 μm). (g) FE-SEM image of PA-6 nanonets. (h) The pleat span provided by single PET filament with various diameters. Source: Zhang et al. 2017 [99]. Reprinted with permission of John Wiley & Sons, Inc.

(diameter of ~20 nm) layer (see Figure 7.18). Different layers have varied pore structures and porosity so that the combined multilayer structure enables the filter to work efficiently to cut off penetration of particles with a relatively wide range without sacrificing the air pressure drop. Owing to the elaborate gradient structure and excellent hydrophobicity (Water contact angle of ~130°), such as-prepared highly integrated filter can have a high efficiency of 99.992%, a low pressure drop of 118 Pa, and a robust Quality factor value of 0.08 Pa^{-1} for filtrating the 300 nm NaCl particles. Moreover, it is worthy to mention that the filtration performance was exhibited after treatment of removing electric charges of the membrane. That means this integrated filtration medium traps airborne particles only in the way of physical sieving manner; it can avoid the potential safety hazards caused by unexpected electret failure. Thus, this kind of integrated air filters will be more stable and can be used even in the special filtration environment of high airflow speed and high humidity.

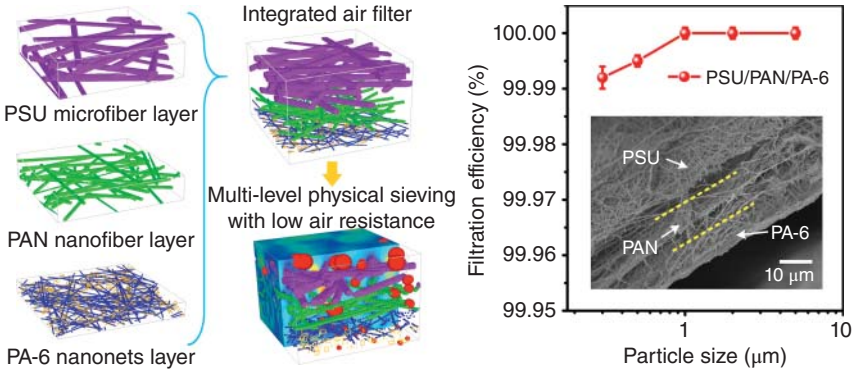


Figure 7.18 The left part: Illustration of the integrated air filter containing three layers (the upper PSU microfiber layer, middle PAN nanofiber layer, and the bottom PA-6 nanofiber/nets layer). The right part: The filtration efficiency of the integrated filter for trapping airborne particles with different size. Source: Zhang et al. 2016 [100]. Reprinted with permission of American Chemical Society.

7.5.2 Medium-High Temperature Filter

Besides dealing with airborne articles with normal temperature (usually for personal protecting area like indoor air cleaner, respirator, window gauze, etc.), filters used for the source control (e.g. automobile exhaust and most industrial dedusting processes such as coal fired boilers, municipal waste incinerators, etc.) are often required to operate within a range between 150 and 260 °C or even higher under some extreme environments. Polymers that are mentioned above for normal temperature filtration such as PA-6, PAN, and PU nanofibrous membranes cannot fulfill the requirements of medium-high temperature filtration. Only those polymers with excellent thermal stability (higher than 200 °C) such as polyethersulfone (PES) [101], polyetherimide [102], polyimide [103], and polymeta-phenylene isophthalamide [104] have feasibility to achieve medium-high temperature filtration.

Nakata et al. [101] prepared PES (glass transition temperature up to 220 °C) nanofibrous membranes as the high heat-resistant air filters. They found that the diameter profile of electrospun PES membrane was obviously affected by PES concentration, feeding rate, and needle-collector distance. After evaluating the filtration properties of PES nanofibrous membranes made by various electrospinning processes, it was found that both the filtration efficiency and pressure drop were significantly decreased over the pore size of 3.0 μm. When the average pore size was 3.2 μm, the PES membranes exhibited the best filtration performance with the high filtration efficiency (99.9998%) and low pressure drop (215 Pa) for removing 300 nm particles, which can meet the High efficiency particulate air Filter (HEPA) requirement. Li et al. [105] reported a novel hierarchical-structured polyetherimide–silica (PEI-SiO_2) nanofibrous membrane by a single-step strategy. The introduction of SiO_2 particles provided the membrane with not only electreted effects but also promising superhydrophobicity. Moreover, unlike other filtration media, such prepared

membrane can be treated at 200 °C for 30 minutes without sacrificing filtration efficiency and pressure drop, which thus expanded the scope of application in air filtration fields.

However, the thermal stability of polymers is still limited so that they cannot be directly used as filtration media working under high temperature over 1000 °C. Thus, in the field of high temperature filtration, more effective and stable heat-resistant materials are needed to deal with high temperature waste from process and power industries and other extreme environments. We all know that ceramic materials have excellent resistance against corrosion, chemical erosion, and heat treatment. Therefore, using electrospun ceramic nanofibrous membranes with extremely high thermal stability and nanoscale fiber as the high temperature filtration media attracted particular attentions these years. So far, many different kinds of ceramic nanofibers such as SiO_2, Al_2O_3, ZrO_2, etc. [106–108] had been fabricated, but the common problem they all faced is the brittleness of the ceramic nanofibers. Then, considerable efforts have been made to fabricate flexible ceramic nanofibers, and some good achievements have been obtained [109–113], which actually shed the light on their successful application for high temperature filtration.

For instance, Mao et al. [114] fabricated a novel silica nanofibrous (SNF) membranes with remarkable flexibility and thermal stability as high temperature filtration media by the combination of electrospinning and sol–gel methods (the schematic illustration of the fabrication process; see Figure 7.19). Through regulating the precursor fiber composition and calcination temperature, the optimal SNF membrane was obtained with good flexibility (0.0156 gf cm), relatively high tensile strength (5.5 MPa), and tensile modulus (114 MPa), which also showed excellent filtration performances toward 300–500 nm sodium chloride aerosols in terms of a high filtration efficiency (99.99%) and relatively low pressure drop (163 Pa). Most importantly, this kind of filtration medium

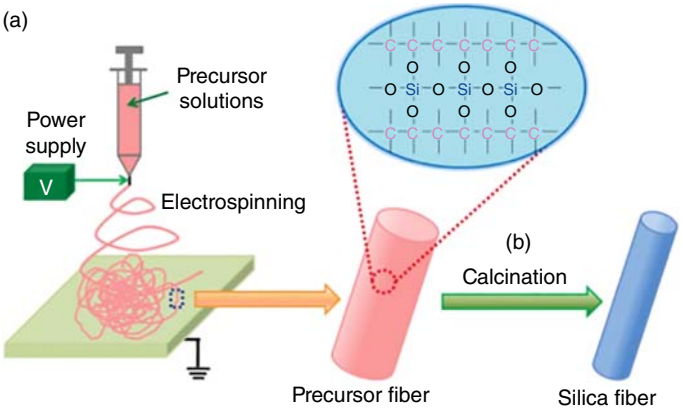


Figure 7.19 Schematic illustration of the fabrication process of silica nanofibrous membranes by the first step of (a) electrospinning and then (b) the calcination process. Source: Mao et al. 2012 [114]. Reproduced with permission of Royal Society of Chemistry.

exhibited excellent thermal stability up to 1000 °C; thus it has great potential for applications as high temperature filtration media to trap ultrafine particles. In order to further improve the application performance, recently, the authors successfully prepared flexible and highly temperature-resistant polynanocrystalline yttria-stabilized zirconia (YSZ) nanofibrous membranes by the combination of electrospinning and heat treatment process [115]. They used zirconium acetate (Zr: 15–16 wt%), yttrium nitrate hexahydrate, and poly(vinylpyrrolidone) (PVP) (molecular weight = 1 300 000) as a precursor solution. The mechanical properties of the YSZ membranes could be controlled by tuning the morphology and crystallite size of the fiber, from brittleness to flexibility. The filtration performances of the YSZ nanofibrous membranes with different fiber diameter were also carefully investigated (see Figure 7.20), and it was found that when the average fiber diameter of the YSZ membranes was 382 nm, the prepared membrane exhibited excellent performance: bending resistance of 400 times, heat resistance of 1473 K, and high filtration efficiency of 99.996% for 300–500 nm NaCl particles. Thus, this reported inorganic flexible nanofibrous membranes were regarded by authors as promising high temperature filtration membranes for a wide range of fields such as metallurgy, steel, electric power, and cement industries.

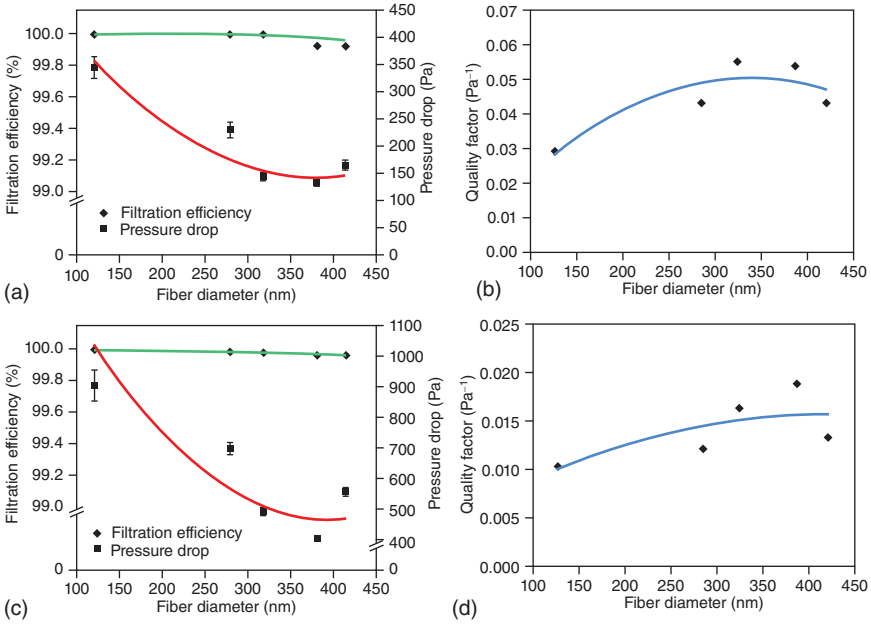


Figure 7.20 Filtration performance of the YSZ nanofibrous membranes with different fiber diameter. (a) Filtration efficiency and pressure drop. (b) Quality factor of the YSZ nanofibrous membranes with different fiber diameter under a face velocity of 32 l/min, respectively. (c) Filtration efficiency and pressure drop. (d) Quality factor of the relevant membranes with different fiber diameter under a face velocity of 85 l/min, respectively. Source: Mao et al. 2012 [115]. Reprinted with permission of American Ceramic Society.

7.6 Future Trends

Nanofibrous membranes fabricated by electrospinning and electro-netting, due to the integrated good properties of fine fiber diameter, tiny pore size, high porosity, and SSA, have been widely regarded as an attractive option for ultrafine particle filtration. In the past ten years, researchers made great efforts on structure design, controllable fabrication, and performance optimization of the nanofibrous filtration membranes and have already achieved many developments in fabricating membranes with both higher filtration efficiency and lower air pressure drop. However, further improving the filtration performance and realizing functionalization of the nanofibrous filters are still challenging, and many practical problems are waiting to be solved. For instance, the mechanical properties (tensile, compression, and abrasion properties) of nanofibrous membranes are relatively poor for the practical use; thus mechanical property enhanced nanofibrous membranes by creating special structure, or chemical modification must be a direction of development in the future. The processes of electrospinning and electro-netting actually can endow nanofibrous membranes with electret effects, and the resultant electrostatic effect will improve the filtration efficiency without sacrificing air pressure drop, so constructing stable and efficient electreted nanofibrous membranes will shred the light on the achievement of air filtration materials with further high performance. In addition, the functionalization of the air filters should be another direction of development, such as air filters with moisture resistant, harmful gas removing, superamphiphobic, and so on.

References

1 Macpherson, C.C. (2013). Climate change matters. *Journal of Medical Ethics* 40 (4): 288–290.
2 Holmes, C.D. (2014). Air pollution and forest water use. *Nature* 507 (7491): E1–E2.
3 Kjellstrom, T., Butler, A.J., Lucas, R.M. et al. (2010). Public health impact of global heating due to climate change: potential effects on chronic non-communicable diseases. *International Journal of Public Health* 55 (2): 97–103.
4 Fajersztajn, L., Veras, M., Barrozo, L.V. et al. (2013). Air pollution: a potentially modifiable risk factor for lung cancer. *Nature Reviews Cancer* 13 (9): 674–678.
5 World Health Organization. (2017). 7 million premature deaths annually linked to air pollution (March 25, 2014) https://www.who.int/mediacentre/news/releases/2014/air-pollution/en/
6 Lave, L.B. and Seskin, E.P. (2013). *Air Pollution and Human Health*. Taylor & Francis London, UK.
7 Querol, X., Alastuey, A., Rodriguez, S. et al. (2001). Monitoring of PM10 and PM2. 5 around primary particulate anthropogenic emission sources. *Atmospheric Environment* 35 (5): 845–858.

8 Rodrıguez, S., Querol, X., Alastuey, A. et al. (2004). Comparative PM10–PM2. 5 source contribution study at rural, urban and industrial sites during PM episodes in Eastern Spain. *Science of the Total Environment* 328 (1): 95–113.

9 Oberdörster, G., Ferin, J., Gelein, R. et al. (1992). Role of the alveolar macrophage in lung injury: studies with ultrafine particles. *Environmental Health Perspectives* 97: 193.

10 Yim, S.H. and Barrett, S.R. (2012). Public health impacts of combustion emissions in the United Kingdom. *Environmental Science & Technology* 46 (8): 4291–4296.

11 Peukert, W. (1998). High temperature filtration in the process industry. *Filtration & Separation* 35 (5): 461–464.

12 Song, Y., Zhang, Y., Xie, S. et al. (2006). Source apportionment of PM2. 5 in Beijing by positive matrix factorization. *Atmospheric Environment* 40 (8): 1526–1537.

13 Donovan, R.P. (1985). *Fabric Filtration for Combustion Sources*, 1e. New York and Basel: Marcel Dekker, Inc.

14 Wang, C.-S. and Otani, Y. (2012). Removal of nanoparticles from gas streams by fibrous filters: a review. *Industrial & Engineering Chemistry Research* 52 (1): 5–17.

15 Adiletta, J.G. (1999) Fibrous nonwoven web. US Patent 5,954,962.

16 Shim, W.S. and Lee, D.W. (2013). Quality variables of meltblown submicron filter materials. *Indian Journal of Fiber &Textile Research* 38: 132–137.

17 Liu, Y., Cheng, B., Wang, N. et al. (2012). Development and performance study of polypropylene/polyester bicomponent melt-blowns for filtration. *Journal of Applied Polymer Science* 124 (1): 296–301.

18 Hung, C.-H. and Leung, W.W.-F. (2011). Filtration of nano-aerosol using nanofiber filter under low Peclet number and transitional flow regime. *Separation and purification technology* 79 (1): 34–42.

19 Yoon, K., Hsiao, B.S., and Chu, B. (2008). Functional nanofibers for environmental applications. *Journal of Materials Chemistry* 18 (44): 5326–5334.

20 Ma, H., Hsiao, B.S., and Chu, B. (2011). Thin-film nanofibrous composite membranes containing cellulose or chitin barrier layers fabricated by ionic liquids. *Polymer* 52 (12): 2594–2599.

21 Liu, X. and Ma, P.X. (2009). Phase separation, pore structure, and properties of nanofibrous gelatin scaffolds. *Biomaterials* 30 (25): 4094–4103.

22 Suzuki, A. and Arino, K. (2012). Polypropylene nanofiber sheets prepared by CO_2 laser supersonic multi-drawing. *European Polymer Journal* 48 (7): 1169–1176.

23 Tanaka, S., Doi, A., Nakatani, N. et al. (2009). Synthesis of ordered mesoporous carbon films, powders, and fibers by direct triblock-copolymer-templating method using an ethanol/water system. *Carbon* 47 (11): 2688–2698.

24 Wang, D., Sun, G., and Chiou, B.S. (2007). A high-throughput, controllable, and environmentally benign fabrication process of thermoplastic nanofibers. *Macromolecular Materials and Engineering* 292 (4): 407–414.

25 Qiu, P. and Mao, C. (2010). Biomimetic branched hollow fibers templated by self-assembled fibrous polyvinylpyrrolidone structures in aqueous solution. *ACS Nano* 4 (3): 1573–1579.

26 Wang, X. and Li, Y. (2002). Selected-control hydrothermal synthesis of α-and β-MnO_2 single crystal nanowires. *Journal of the American Chemical Society* 124 (12): 2880–2881.

27 Fong, H., Chun, I., and Reneker, D. (1999). Beaded nanofibers formed during electrospinning. *Polymer* 40 (16): 4585–4592.

28 Ding, B., Kimura, E., Sato, T. et al. (2004). Fabrication of blend biodegradable nanofibrous nonwoven mats via multi-jet electrospinning. *Polymer* 45 (6): 1895–1902.

29 Wu, J., Wang, N., Zhao, Y. et al. (2013). Electrospinning of multilevel structured functional micro-/nanofibers and their applications. *Journal of Materials Chemistry A* 1 (25): 7290–7305.

30 Thavasi, V., Singh, G., and Ramakrishna, S. (2008). Electrospun nanofibers in energy and environmental applications. *Energy & Environmental Science* 1 (2): 205–221.

31 Sahay, R., Kumar, P.S., Sridhar, R. et al. (2012). Electrospun composite nanofibers and their multifaceted applications. *Journal of Materials Chemistry* 22 (26): 12953–12971.

32 Zhou, C., Chu, R., Wu, R. et al. (2011). Electrospun polyethylene oxide/cellulose nanocrystal composite nanofibrous mats with homogeneous and heterogeneous microstructures. *Biomacromolecules* 12 (7): 2617–2625.

33 Wang, X., Ding, B., Sun, G. et al. (2013). Electro-spinning/netting: a strategy for the fabrication of three-dimensional polymer nano-fiber/nets. *Progress in Materials Science* 58 (8): 1173–1243.

34 Reneker, D.H. and Chun, I. (1996). Nanometre diameter fibres of polymer, produced by electrospinning. *Nanotechnology* 7 (3): 216.

35 Bhardwaj, N. and Kundu, S.C. (2010). Electrospinning: a fascinating fiber fabrication technique. *Biotechnology advances* 28 (3): 325–347.

36 Lin, K., Chua, K.-N., Christopherson, G.T. et al. (2007). Reducing electrospun nanofiber diameter and variability using cationic amphiphiles. *Polymer* 48 (21): 6384–6394.

37 Ding, B., Li, C., Miyauchi, Y. et al. (2006). Formation of novel 2D polymer nanowebs via electrospinning. *Nanotechnology* 17 (15): 3685.

38 Greiner, A. and Wendorff, J.H. (2007). Electrospinning: a fascinating method for the preparation of ultrathin fibers. *Angewandte Chemie International Edition* 46 (30): 5670–5703.

39 Li, Z. and Wang, C. (2013). *Effects of Working Parameters on Electrospinning*. Heidelberg: Springer.

40 Wendorff, J.H., Agarwal, S., and Greiner, A. (2012). *Electrospinning: Materials, Processing, and Applications*. Chichester: Wiley.

41 Teo, W.E. and Ramakrishna, S. (2006). A review on electrospinning design and nanofibre assemblies. *Nanotechnology* 17 (14): R89–R106.

42 Higuera, F.J. (2003). Flow rate and electric current emitted by a Taylor cone. *Journal of Fluid Mechanics* 484 (484): 303–327.

43 Xie, J. and Wang, C.H. (2007). Encapsulation of proteins in biodegradable polymeric microparticles using electrospray in the Taylor cone-jet mode. *Biotechnology and Bioengineering* 97 (5): 1278–1290.

44 Han, T., Reneker, D.H., and Yarin, A.L. (2007). Buckling of jets in electrospinning. *Polymer* 48 (20): 6064–6076.

45 Reneker, D.H. and Yarin, A.L. (2008). Electrospinning jets and polymer nanofibers. *Polymer* 49 (10): 2387–2425.

46 Wang, C., Hsu, C., Lin, J. (2006). Scaling laws in electrospinning of polystyrene solutions. *Macromolecules* 39 (22): 7662–7672.

47 Ding, B., Wang, M., Wang, X. et al. (2010). Electrospun nanomaterials for ultrasensitive sensors. *Materials Today* 13 (11): 16–27.

48 Barakat, N.A.M., Kanjwal, M.A., Sheikh, F.A. et al. (2009). Spider-net within the N6, PVA and PU electrospun nanofiber mats using salt addition: novel strategy in the electrospinning process. *Polymer* 50 (18): 4389–4396.

49 Pant, H.R., Bajgai, M.P., Nam, K.T. et al. (2010). Formation of electrospun nylon-6/methoxy poly (ethylene glycol) oligomer spider-wave nanofibers. *Materials letters* 64 (19): 2087–2090.

50 Tsou, S.Y., Lin, H.S., and Wang, C. (2011). Studies on the electrospun Nylon 6 nanofibers from polyelectrolyte solutions: 1. Effects of solution concentration and temperature. *Polymer* 52 (14): 3127–3136.

51 Chun, J.Y., Hong, G.P., Surassmo, S. et al. (2014). Study of the phase separation behaviour of native or preheated WPI with polysaccharides. *Polymer* 55 (16): 4379–4384.

52 Mit-uppatham, C., Nithitanakul, M., and Supaphol, P. (2004). Ultrafine electrospun polyamide-6 fibers: effect of solution conditions on morphology and average fiber diameter. *Macromolecular Chemistry and Physics* 205 (17): 2327–2338.

53 Grimm, R.L. and Beauchamp, J. (2005). Dynamics of field-induced droplet ionization: time-resolved studies of distortion, jetting, and progeny formation from charged and neutral methanol droplets exposed to strong electric fields. *The Journal of Physical Chemistry B* 109 (16): 8244–8250.

54 Wang, X., Ding, B., Yu, J., et al. (2011). Electro-netting: fabrication of two-dimensional nano-nets for highly sensitive trimethylamine sensing. *Nanoscale* 3 (3): 911–915.

55 Ding, B., Kim, H.Y., Lee, S.C. et al. (2002). Preparation and characterization of nanoscaled poly (vinyl alcohol) fibers via electrospinning. *Fibers and Polymers* 3 (2): 73–79.

56 Kim, B., Park, H., Lee, S.-H. et al. (2005). Poly (acrylic acid) nanofibers by electrospinning. *Materials Letters* 59 (7): 829–832.

57 Li, X., Lin, L., Zhu, Y. et al. (2013). Preparation of ultrafine fast-dissolving cholecalciferol-loaded poly (vinyl pyrrolidone) fiber mats via electrospinning. *Polymer Composites* 34 (2): 282–287.

58 Chen, C., Wang, L., and Huang, Y. (2007). Electrospinning of thermo-regulating ultrafine fibers based on polyethylene glycol/cellulose acetate composite. *Polymer* 48 (18): 5202–5207.

59 Li, D. and Xia, Y. (2003). Fabrication of titania nanofibers by electrospinning. *Nano Letters* 3 (4): 555–560.

60 Fan, M., Hui, W., Li, Z. et al. (2012). Fabrication and piezoresponse of electrospun ultra-fine Pb ($Zr_{0.3}$, $Ti_{0.7}$) O_3 nanofibers. *Microelectronic Engineering* 98: 371–373.

61 Deng, L., Young, R.J., Kinloch, I.A. et al. (2013). Carbon nanofibres produced from electrospun cellulose nanofibres. *Carbon* 58: 66–75.

62 Yan, H., Mahanta, N.K., Wang, B. et al. (2014). Structural evolution in graphitization of nanofibers and mats from electrospun polyimide–mesophase pitch blends. *Carbon* 71: 303–318.

63 Khalil, A., Hashaikeh, R., and Jouiad, M. (2014). Synthesis and morphology analysis of electrospun copper nanowires. *Journal of Materials Science* 49 (8): 3052–3065.

64 Koombhongse, S., Liu, W., and Reneker, D.H. (2001). Flat polymer ribbons and other shapes by electrospinning. *Journal of Polymer Science Part B* 39 (21): 2598–2606.

65 Kessick, R. and Tepper, G. (2004). Microscale polymeric helical structures produced by electrospinning. *Applied Physics Letters* 84 (23): 4807–4809.

66 Ding, B., Li, C., Du, J., and Shiratori, S. (2008). *Nanotechnology Research: New Nanostructures, Nanotubes and Nanofibers* (ed. X. Huang). New York: Nova Science Publishers, Inc.

67 Sun, Z., Zussman, E., Yarin, A.L. et al. (2003). Compound core–shell polymer nanofibers by co-electrospinning. *Advanced Materials* 15 (22): 1929–1932.

68 Zhao, Y., Cao, X., and Jiang, L. (2007). Bio-mimic multichannel microtubes by a facile method. *Journal of the American Chemical Society* 129 (4): 764–765.

69 Mou, F., Guan, J.-G., Shi, W. et al. (2010). Oriented contraction: a facile nonequilibrium heat-treatment approach for fabrication of maghemite fiber-in-tube and tube-in-tube nanostructures. *Langmuir* 26 (19): 15580–15585.

70 Jin, Y., Yang, D., Kang, D. et al. (2009). Fabrication of necklace-like structures via electrospinning. *Langmuir* 26 (2): 1186–1190.

71 Shengyuan, Y., Peining, Z., Nair, A.S. et al. (2011). Rice grain-shaped TiO_2 mesostructures-synthesis, characterization and applications in dye-sensitized solar cells and photocatalysis. *Journal of Materials Chemistry* 21 (18): 6541–6548.

72 Kokubo, H., Ding, B., Naka, T. et al. (2007). Multi-core cable-like TiO_2 nanofibrous membranes for dye-sensitized solar cells. *Nanotechnology* 18 (16): 165604.

73 Chen, H., Wang, N., Di, J. et al. (2010). Nanowire-in-microtube structured core/shell fibers via multifluidic coaxial electrospinning. *Langmuir* 26 (13): 11291–11296.

74 Li, D. and Xia, Y. (2004). Direct fabrication of composite and ceramic hollow nanofibers by electrospinning. *Nano Letters* 4 (5): 933–938.

75 Zhang, D. and Chang, J. (2007). Patterning of electrospun fibers using electroconductive templates. *Advanced Materials* 19 (21): 3664–3667.

76 Kim, G.T., Ahn, Y.C., and Lee, J.K. (2008). Characteristics of Nylon 6 nanofilter for removing ultra fine particles. *Korean Journal of Chemical Engineering* 25 (2): 368–372.

77 Mei, Y., Wang, Z., and Li, X. (2013). Improving filtration performance of electrospun nanofiber mats by a bimodal method. *Journal of Applied Polymer Science* 128 (2): 1089–1094.

78 Sambaer, W., Zatloukal, M., and Kimmer, D. (2011). 3D modeling of filtration process via polyurethane nanofiber based nonwoven filters prepared by electrospinning process. *Chemical Engineering Science* 66 (4): 613–623.

79 Qin, X.H. and Wang, S.Y. (2008). Electrospun nanofibers from crosslinked poly (vinyl alcohol) and its filtration efficiency. *Journal of Applied Polymer Science* 109 (2): 951–956.

80 Patanaik, A., Jacobs, V., and Anandjiwala, R.D. (2010). Performance evaluation of electrospun nanofibrous membrane. *Journal of Membrane Science* 352 (1): 136–142.

81 Yun, K.M., Suryamas, A.B., Iskandar, F. et al. (2010). Morphology optimization of polymer nanofiber for applications in aerosol particle filtration. *Separation and Purification Technology* 75 (3): 340–345.

82 Wang, N., Raza, A., Si, Y. et al. (2013). Tortuously structured polyvinyl chloride/polyurethane fibrous membranes for high-efficiency fine particulate filtration. *Journal of Colloid and Interface Science* 398: 240–246.

83 Cho, D., Naydich, A., Frey, M.W. et al. (2013). Further improvement of air filtration efficiency of cellulose filters coated with nanofibers via inclusion of electrostatically active nanoparticles. *Polymer* 54 (9): 2364–2372.

84 Yeom, B.Y., Shim, E., and Pourdeyhimi, B. (2010). Boehmite nanoparticles incorporated electrospun nylon-6 nanofiber web for new electret filter media. *Macromolecular Research* 18 (9): 884–890.

85 Gibson, P., Schreuder-Gibson, H., and Rivin, D. (2001). Transport properties of porous membranes based on electrospun nanofibers. *Colloids and Surfaces A* (187): 469–481.

86 Li, L., Frey, M.W., and Green, T.B. (2006). Modification of air filter media with nylon-6 nanofibers. *Journal of Engineered Fibers and Fabrics.* 1: 1–22.

87 Ahn, Y., Park, S., Kim, G. et al. (2006). Development of high efficiency nanofilters made of nanofibers. *Current Applied Physics* 6 (6): 1030–1035.

88 Przekop, R. and Gradoń, L. (2008). Deposition and filtration of nanoparticles in the composites of nano-and microsized fibers. *Aerosol Science and Technology* 42 (6): 483–493.

89 Zhao, X., Wang, S., Yin, X. et al. (2016). Slip-Effect functional air filter for efficient purification of $PM_{2.5}$. *Scientific Reports* 6: 35472.

90 Wang, S., Zhao, X., Yin, X. et al. (2016). Electret polyvinylidene fluoride nanofibers hybridized by polytetrafluoroethylene nanoparticles for high-efficiency air filtration. *ACS Applied Materials & Interfaces* 8 (36): 23985–23994.

91 Liu, Y., Park, M., Ding, B. et al. (2015). Facile electrospun Polyacrylonitrile/poly (acrylic acid) nanofibrous membranes for high efficiency particulate air filtration. *Fibers and Polymers* 16 (3): 629–633.

92 Zhang, S., Liu, H., Yin, X. et al. (2016). Anti-deformed polyacrylonitrile/polysulfone composite membrane with binary structures for effective air filtration. *ACS Applied Materials & Interfaces* 8 (12): 8086–8095.

93 Wang, N., Zhu, Z., Sheng, J. et al. (2014). Superamphiphobic nanofibrous membranes for effective filtration of fine particles. *Journal of Colloid and Interface Science* 428: 41–48.

94 Wang, N., Wang, X., Ding, B. et al. (2012). Tunable fabrication of three-dimensional polyamide-66 nano-fiber/nets for high efficiency fine particulate filtration. *Journal of Materials Chemistry* 22 (4): 1445–1452.

95 Liu, B., Zhang, S., Wang, X. et al. (2015). Efficient and reusable polyamide-56 nanofiber/nets membrane with bimodal structures for air filtration. *Journal of Colloid and Interface Science* 457: 203–211.

96 Wang, N., Yang, Y., Al-Deyab, S.S. et al. (2015). Ultra-light 3D nanofibre-nets binary structured nylon 6–polyacrylonitrile membranes for efficient filtration of fine particulate matter. *Journal of Materials Chemistry A* 3 (47): 23946–23954.

97 Yang, Y., Zhang, S., Zhao, X. et al. (2015). Sandwich structured polyamide-6/polyacrylonitrile nanonets/bead-on-string composite membrane for effective air filtration. *Separation and Purification Technology* 152: 14–22.

98 Zhang, S., Liu, H., Yu, J. et al. (2016). Microwave structured polyamide-6 nanofiber/net membrane with embedded poly (m-phenylene isophthalamide) staple fibers for effective ultrafine particle filtration. *Journal of Materials Chemistry A* 4 (16): 6149–6157.

99 Zhang, S., Liu, H., Zuo, F. et al. (2017). A controlled design of ripple-like polyamide-6 nanofiber/nets membrane for high-efficiency air filter. *Small*: 1603151.

100 Zhang, S., Tang, N., Cao, L. et al. (2016). Highly integrated polysulfone/polyacrylonitrile/polyamide-6 air filter for multilevel physical sieving airborne particles. *ACS Applied Materials & Interfaces* 8 (42): 29062–29072.

101 Nakata, K., Kim, S.H., Ohkoshi, Y. et al. (2007). Electrospinning of poly (ether sulfone) and evaluation of the filtration efficiency. *Sen'i Gakkaishi* 63 (12): 307–312.

102 Moon, S., Choi, J., and Farris, R.J. (2008). Preparation of aligned polyetherimide fiber by electrospinning. *Journal of Applied Polymer Science* 109 (2): 691–694.

103 Fukushima, S., Karube, Y., and Kawakami, H. (2010). Preparation of ultrafine uniform electrospun polyimide nanofiber. *Polymer Journal* 42 (6): 514–518.

104 Huang, C., Chen, S., Reneker, D.H. et al. (2006). High-strength mats from electrospun poly (p-Phenylene Biphenyltetracarboximide) nanofibers. *Advanced Materials* 18 (5): 668–671.

105 Li, X., Wang, N., Fan, G. et al. (2015). Electreted polyetherimide–silica fibrous membranes for enhanced filtration of fine particles. *Journal of Colloid and Interface Science* 439: 12–20.

106 Shao, C., Kim, H., Gong, J. et al. (2002). A novel method for making silica nanofibres by using electrospun fibres of polyvinylalcohol/silica composite as precursor. *Nanotechnology* 13 (5): 635.

107 Yu, H., Guo, J., Zhu, S. et al. (2012). Preparation of continuous alumina nanofibers via electrospinning of PAN/DMF solution. *Materials Letters* 74: 247–249.

108 Zhao, Y., Tang, Y., Guo, Y. et al. (2010). Studies of electrospinning process of zirconia nanofibers. *Fibers and Polymers* 11 (8): 1119–1122.

109 Guo, M., Ding, B., Li, X. et al. (2009). Amphiphobic nanofibrous silica mats with flexible and high-heat-resistant properties. *The Journal of Physical Chemistry C* 114 (2): 916–921.

110 Zhao, F., Wang, X., Ding, B. et al. (2011). Nanoparticle decorated fibrous silica membranes exhibiting biomimetic superhydrophobicity and highly flexible properties. *RSC Advances* 1 (8): 1482–1488.

111 Wang, X., Cui, F., Lin, J. et al. (2012). Functionalized nanoporous TiO_2 fibers on quartz crystal microbalance platform for formaldehyde sensor. *Sensors and Actuators B* (171): 658–665.

112 Yang, L., Raza, A., Si, Y. et al. (2012). Synthesis of superhydrophobic silica nanofibrous membranes with robust thermal stability and flexibility via in situ polymerization. *Nanoscale* 4 (20): 6581–6587.

113 Han, W., Ding, B., Park, M. et al. (2015). Facile synthesis of luminescent and amorphous La_2O_3–ZrO_2: Eu^{3+} nanofibrous membranes with robust softness. *Nanoscale* 7 (34): 14248–14253.

114 Mao, X., Si, Y., Chen, Y. et al. (2012). Silica nanofibrous membranes with robust flexibility and thermal stability for high-efficiency fine particulate filtration. *RSC Advances* 2 (32): 12216–12223.

115 Mao, X., Bai, Y., Yu, J. et al. (2016). Flexible and highly temperature resistant polynanocrystalline zirconia nanofibrous membranes designed for air filtration. *Journal of the American Ceramic Society* 99 (8): 2760–2768.

116 Mathew, G., Hong, J., Rhee, J. et al. (2006). Preparation and anisotropic mechanical behavior of highly-oriented electrospun poly (butylene terephthalate) fibers. *Journal of Applied Polymer Science* 101 (3): 2017–2021.

117 Wang, X., Ding, B., Yu, J. et al. (2009). A highly sensitive humidity sensor based on a nanofibrous membrane coated quartz crystal microbalance. *Nanotechnology* 21 (5): 055502.

118 Wang, X., Ding, B., Yu, J. et al. (2011). Large-scale fabrication of two-dimensional spider-web-like gelatin nano-nets via electro-netting. *Colloids and Surfaces B* 86 (2): 345–352.

119 Ding, B., Ogawa, T., Kim, J. et al. (2008). Fabrication of a super-hydrophobic nanofibrous zinc oxide film surface by electrospinning. *Thin Solid Films* 516 (9): 2495–2501.

120 Ding, B., Li, C., Wang, D. et al. (2010). *Fabrication and Application of Novel Two-Dimensional Nanowebs via Electrospinning*, Nanotechnology: Nanofabrication, Patterning, and Self Assembly, 51–69. New York: Nova Science Publishers, Inc.

8

Aramid Fibers

Manjeet Jassal, Ashwini K. Agrawal, Deepika Gupta, and Kamlesh Panwar

Indian Institute of Technology, Department of Textile Technology, New Delhi, 110016 Delhi, India

8.1 Introduction

As per the US Federal Trade Commission, aramid fibers, or aromatic polyamides, are manufactured fibers that have at least 85% of the amide linkages attached directly to two aromatic rings. These were the first organic fibers to be used for reinforcement in advanced composites. Due to their outstanding thermal and mechanical properties, these fibers have been able to displace inorganic fibers and metal wires from the market of high-performance applications. These fibers have been used widely in areas such as protective clothing for hostile environment that are exposed to heat, chemicals, and radiations.

It was due to their inability to dissolve in a solvent and no melting point that the production of first aramid fiber took place long after the commercialization of nylon in 1938. DuPont launched the very first aramid fiber under the trade name Nomex® in 1960. It was the first *m*-aramid fiber with very high temperature resistance. In order to achieve further superior properties, the attention was drawn toward *p*-aramid fibers leading to the development of Kevlar® in 1971. A similar *p*-aramid, Twaron, was launched by Teijin toward the end of 1980s.

DuPont Co. (USA) is world's leading producer of *m*-aramid fibers (under the trade name Nomex). Teijin (Japan) is the only other producer of *m*-aramid fibers (under the trade name Teijinconex). DuPont Co. (USA) is world's leading producer of *p*-aramid fibers also, followed by Teijin (Japan), which is the second largest producer. Other major producers include Rhône-Poulenc (France), Toray Industries Inc. (Japan), Acordis, and Akzo Nobel (NV, Netherlands). The history of the development of the aramid fibers is summarized in Figure 8.1. Several reviews [1–10] are available on the synthesis, spinning, properties, and applications of aramid fibers.

8.2 Preparation of Aromatic Polyamides

Due to their characteristic features such as rigid structures, no melting point, and inability to dissolve in a solvent, aramids could not be prepared by melt spinning

Handbook of Fibrous Materials, First Edition. Edited by Jinlian Hu, Bipin Kumar, and Jing Lu.
© 2020 Wiley-VCH Verlag GmbH & Co. KGaA. Published 2020 by Wiley-VCH Verlag GmbH & Co. KGaA.

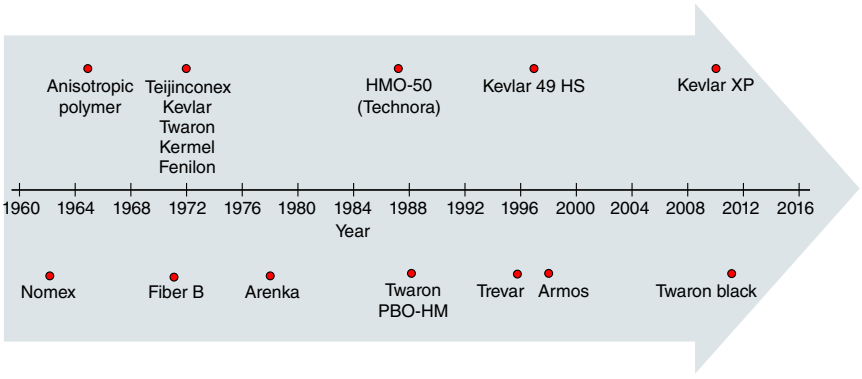


Figure 8.1 Timeline of important historical developments of aramid fibers.

and conventional bulk polymerization. Instead, the aromatic polyamides are mainly synthesized by low temperature polycondensation and direct polycondensation in solution using phosphites [11–13]. Aramids could be synthesized in the form of AB homopolymers with reaction between an amine group and a carboxylic acid halide group or AABB aramids by reaction between aromatic diamines and diacids or diacid chlorides.

8.2.1 Low Temperature Polycondensation

Due to low reactivity of aromatic diamines toward aromatic dicarboxylic acids, aromatic diacid chlorides are generally used for the synthesis of aramids. Low temperature polycondensation is carried out at temperatures below 50 °C to avoid degradation, side reaction, and cross-linking.

The basic reaction involved in the synthesis of aramids by low temperature polycondensation is shown in Figure 8.2.

Based on these reactions, the synthesis of Nomex (*m*-aramid) and Kevlar (*p*-aramid) [14] could be shown in Figures 8.3 and 8.4, respectively.

Generally, 5–20 wt% initial monomer concentration is used with equimolar ratios of diamines and diacid chloride. Solvent is selected either from

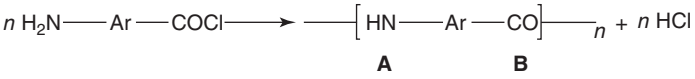


Figure 8.2 Reaction mechanism for the synthesis of aramids by low temperature polycondensation.

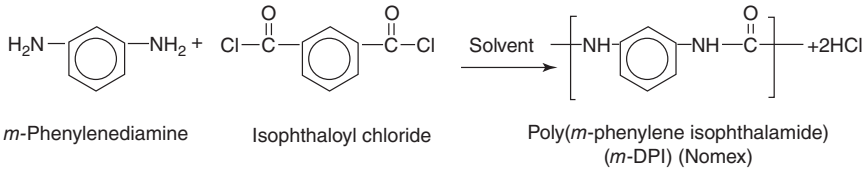


Figure 8.3 Reaction mechanism for the synthesis of Nomex (*m*-aramid).

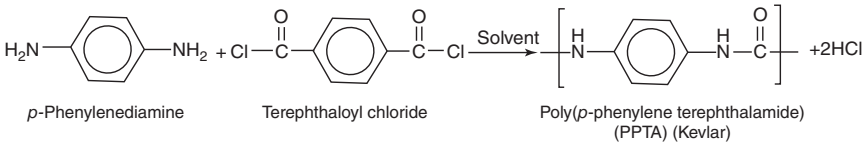


Figure 8.4 Reaction mechanism for the synthesis of Kevlar (*p*-aramid).

halogenated nonaromatic hydrocarbons (such as methyl ethyl ketone, chloroform, methylene chloride, dimethylcyanamide, and acetonitrile) or amide (such as *N*-methyl-2-pyrrolidone, dimethylacetamide, tetramethyl urea, and hexamethylphosphoramide). The incorporation of aryl-ether linkages in aramid structure has been reported [15–17] to increase its solubility and processability without significantly altering their thermal properties. Similarly, various other approaches such as incorporation of other flexible functionalities [18–20], *N*-alkylation of the backbone, and introduction of bulky pendant groups [21–23] have been explored for improving the solubility of the aramids.

Low temperature polycondensation could be carried out by two different methods: interfacial polycondensation and solution polycondensation. In the case of interfacial polycondensation, the monomers are dissolved in two different immiscible solvents, and the reaction is carried out at the interface. However, in solution polycondensation, reaction is carried out in an inert organic solvent. As the interfacial polycondensation is diffusion dependent, high molecular weight polymers with a broad molecular weight distribution are synthesized. Due to this reason, solution polycondensation is preferred to interfacial polycondensation.

The properties of the synthesized polymer depend upon various factors such as the solubility–concentration–temperature relationship and the salt concentration. The molecular weight of the final polymer is dependent upon the stoichiometry of the solvent and reactant mixture. The inherent viscosity is highest at an optimum reactant concentration, although it decreases on both decreasing and increasing concentration from the optimum value. The viscosity drop at low reactant concentration is due to the occurrence of side reactions. However, at high reactant concentration, the viscosity drop is due to reduced mobility of reactant as a result of gelation much before high inherent viscosity is achieved. A suitable solvent could be useful in delaying the gelation until high molecular weight is attained. Also, small amounts of various alkaline and alkali earth metal salts such as lithium hydroxide, lithium chloride, calcium hydroxide, and calcium chloride are used to increase the solvating power of organic solvents [23, 24]. As the polymerization reaction is an exothermic process, so at high reactant concentration, the large amount of heat released causes an increase in side reactions, thus reducing the inherent viscosity. So, the temperature of the reaction is generally kept very low (0 to −15 °C), thus reducing side reactions and increasing the inherent viscosity.

As a large amount of salt is generated during low temperature polycondensation reaction that further neutralizes HCl, the process requires expensive corrosion-resistant materials adding significantly to the cost of the process. The acid dichloride, being highly active, must be stored in refrigerator under dry conditions to avoid their hydrolysis.

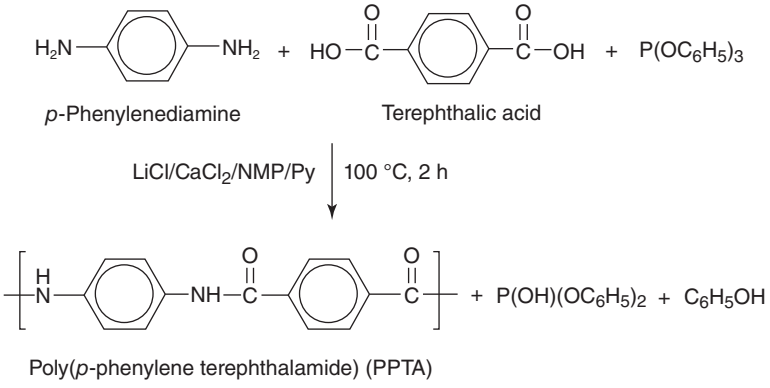


Figure 8.5 Reaction mechanism for the synthesis of poly(*p*-phenylene terephthalamide) (PPTA) through direct polycondensation.

8.2.2 Direct Polymerization in Solution Using Phosphites

Synthesis of aramids using aromatic diacids and aromatic diamines is a straightforward and direct synthesis method. Diacids are reasonably cheap materials but show lesser activity toward diamines. As a result, their reaction with diamines is carried out in the presence of certain catalysts (generally phosphorus- or sulfur-based compounds) [25–27]. These catalysts activate the diacids forming an N-P type intermediate and thus completing the polycondensation. The reaction mechanism for the synthesis of aramids by direct polycondensation is shown in Figure 8.5.

Shoji et al. [28] reported the synthesis of aramids using diacids and diamines with ether linkage. The presence of ether linkages led to an increase in the polymer mobility that, on the other hand, reduced the glass transition temperature as well as melting point of the synthesized aramid. Polycondensation of isophthalic acid with 3,4′-oxydianiline led to the formation of high molecular weight aramids. The group further synthesized high molecular weight aramid using aromatic diacid and 4,4′-oxydianiline by bulk polycondensation.

Besides polycondensation, aramids are also synthesized by low temperature hydrogen transfer reactions. This reaction occurs in between a diacid and diisocyanate forming an intermediate polymer, which on removal of carbon dioxide on subsequent heating leads to the formation of aromatic polyamide. The reaction mechanism for hydrogen transfer reaction is shown in Figure 8.6. However, this is not the commonly used reaction for the synthesis of aramids because of the higher cost of diisocyanates and the difficulty in eliminating all the carbon dioxide.

8.2.3 Copolyaramids

Aramids possess very high melting point and show inability to dissolve in a solvent, which make their processing very difficult. In order to improve their processability, copolymers of aramids are synthesized [29–31]. The incorporation of diamines with significantly distant amino groups leads to lowered spatial

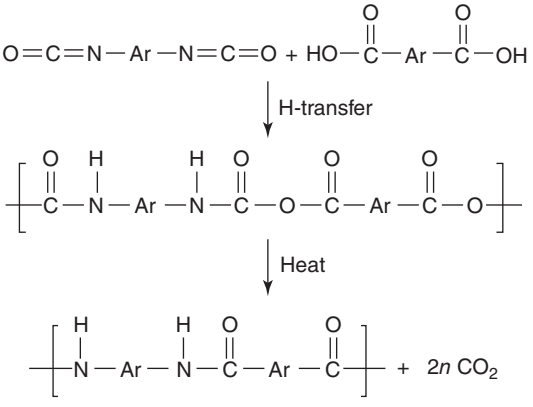


Figure 8.6 Reaction mechanism for the synthesis of aramids by hydrogen transfer reaction.

Table 8.1 Polymerization conditions for certain copolyaramids.

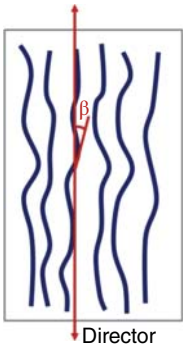
Monomers	Solvent	Polymer	η_{inh}
1. *p*-Phenylenediamine Terephthaloyl chloride Isophthaloyl chloride	HMPA/NMP	95/5 Copoly(*p*-phenylene terephthalamide/isophthalamide)	4.48, 3.9
2. *p*-Phenylenediamine *p*-Phenylene diisocyanate Terephthaloyl chloride	HMPA/NMPLiCl	90/10 Copoly(*p*-phenylene *p*-phenylene diisocyano terephthalamide)	1.83
	HMPA/NMPLiCl	95/5 Copolymer	2.87
	HMPA/NMPLiCl	80/20 Copolymer	2.82
3. *p*-Phenylenediamine 2,5-Bis(*p*-aminophenyl)-1,3,4-oxadiazole Terephthaloyl chloride	HMPA/NMPLiCl	Copoly(*p*-phenylene)/2,5-bis-(*p*-aminophenyl)-1,3,4-oxadiazo terephthalamide	4.48
4. *p*-Phenylenediamine 2-Chloro-*p*-phenylenediamine Terephthaloyl chloride	DMAC/Li_2CO_3	50/50 Copoly(*p*-phenylene/2-chloro-*p*-phenylene terephthalamide)	3.85

HMPA, hexamethyl phosphoric triamide; DMAC, dimethyl acetamide; NMP, *N*-methyl-2-pyrrolidone.
Source: With prior permission from Indian Journal of Fibre & Textile Research.

density of hydrogen bonding and rate of crystallization. On the other hand, the fiber drawability could be improved by using another comonomer with two phenylene groups connected with a single atom. The polymerization conditions for copolyaramids are summarized in Table 8.1.

8.3 Aramid Solutions

Aramid polymers exhibit high melting point, and often their decomposition temperature is higher than their melting temperature. This makes the fiber processing



β = 9–12°

High molecular orientation

Figure 8.7 Directional orientation of rodlike molecules of PPTA.

of aramids via melt spinning unfeasible. Therefore aramid fibers are made by solution spinning. However, dissolution of aramids is also challenging because of their rigid structure. It is generally achieved by the use of highly polar solvents without or with inorganic salts or strong acids. Isotropic solutions of aramids can be produced by dissolving homopolymers (e.g. poly(*m*-phenylene isophthalamide) (*m*-DPI)) in solvents such as *N*-methyl-2-pyrrolidone (NMP) and DMAc. In the case of *p*-aramids, solubility can be increased by copolymerization as explained previously. As mentioned earlier, *p*-aramids dissolve in highly polar solvents containing inorganic salts and strong acids. They form isotropic solutions only at low polymer concentrations. For example, poly(*p*-phenylene terephthalamide) (PPTA) forms isotropic solutions at concentrations lower than 10 wt% and ambient temperature.

One of the distinctive features of semirigid polymer is that they exhibit molecular orientation when subjected to external forces such as electrical, magnetic, shear, and elongational flow. The above characteristics are shown in lyotropic solutions such as poly(*p*-benzamide) and PPTA [32]. Figure 8.7 shows the molecular orientation of rodlike molecules of PPTA along the direction or axis of orientation, with degree of orientation described by β that ranges from 9° to 12°.

As mentioned earlier factors such as concentration of solution, solvent, molecular weight of polymer, and temperature affect the orientation and phase behavior in lyotropic nematic polymer solutions. Example of a lyotropic solution is that of PPTA in 100% sulfuric acid where the viscosity and molecular arrangement are the function of concentration as shown in Figure 8.8. With increasing concentration the molecular orientation increases, leading to the formation of smectic and nematic phases in liquid crystals (Figure 8.8a). From Figure 8.8b it can be seen that initially the viscosity increases with increase in the concentration and solution shows little or no orientation of crystal domains. On further increasing the concentration (18–23% PPTA), the viscosity decreases, since in this region the crystal domains perfectly orient showing anisotropic behavior. This particular concentration region where the viscosity is lowest (i.e. formation of nematic liquid crystal) and the polymer is highly oriented is of interest for spinning. Unlike the case of isotropic polymers where an increase in the viscosity is expected with concentration, lyotropic solutions show decrease in the viscosity as a result of formation of nematic liquid crystal phase.

For solution spinning, low viscosity at high polymer concentration is required. Figure 8.9 shows a phase diagram for PPTA in 100% sulfuric acid. As mentioned

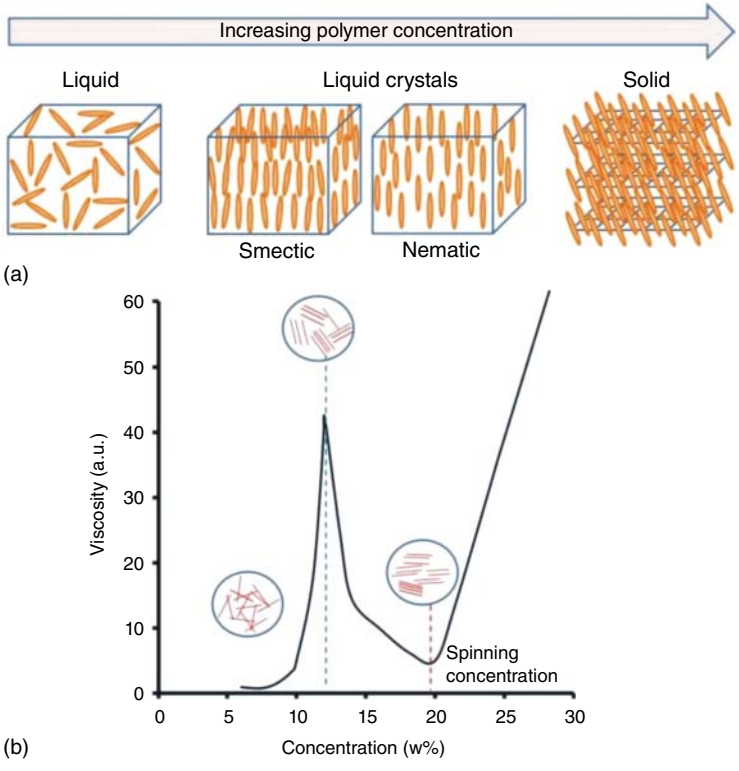


Figure 8.8 (a) Structure of lyotropic nematic phase with respect to concentration. (b) A typical viscosity vs. concentration curve for lyotropic solutions.

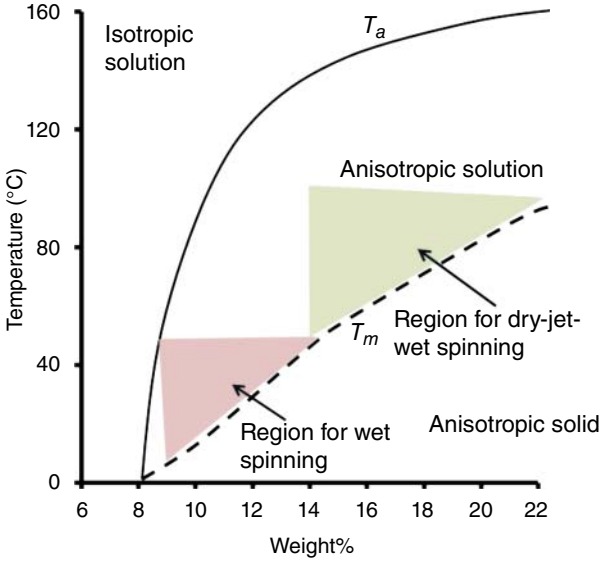


Figure 8.9 Phase diagram of anisotropic solution of PPTA in 100% H_2SO_4.

earlier, critical concentration is dependent on the molecular weight and temperature. These dopes at high concentration of 18–23% are solid up to about 80 °C. Therefore, they are required to be melted prior to spinning. On the other hand, for coagulation at low temperatures, dry-jet-wet spinning is done. In this process of spinning of PPTA in nematic phase, fiber precipitation occurs in the air gap, and the acid is removed in the coagulation bath. It is also evident from the phase diagram (Figure 8.9) that up to concentrations of 10%, dope viscosity remains low and such dopes can be wet-spun.

8.4 Spinning of Aramid Fibers

The spinning of aramid fibers can be done using dry spinning, wet spinning, or dry-jet-wet spinning process.

8.4.1 Dry Spinning

The dry spinning of aramid fibers is done by extruding the polymer solution through a spinneret mounted above a heated column. The polymer solution is extruded in the presence of hot inert gas (or air), and solvent gets evaporated from the emergent fiber. The solidified fiber is collected at the bottom of the column.

The process for dry spinning of Nomex fibers from dimethylformamide (DMF), and DMAc solutions was developed by DuPont. Nomex, derived from the *m*-aramid polymer solution, is disoriented when in solution, unlike *p*-aramid (e.g. Kevlar). The fibers get roughly orientated during the extrusion of the solution; however it exhibits poorer strength as compared with its *p*-aramid counterpart. The extent of fiber orientation can be increased by increasing the shear rate through the spinneret capillary. However, inhomogeneity is developed due to solvent diffusion and formation of skin due to fast solvent evaporation from surface than from bulk. The as-spun fibers are drawn to enhance their physical properties. Typical mechanical properties of fibers are on the order of 0.6 GPa with a 30% elongation at break.

8.4.2 Wet Spinning

In the wet spinning process, spinneret is submerged in the coagulation bath containing solvent and non-solvent. Polymer–solvent and non-solvent interaction affects the structure and leads to the ultimate properties. Important variables that control this process are polymer concentration, solution composition and its temperature, composition and temperature of coagulating solution, the rate of extrusion, and the residence time in the coagulating bath. The isotropic solution, spun by wet spinning, is exposed to the coagulant as soon as it exits the spinneret nozzle, preventing the solution from complete attenuation and hence resulting in low tenacity, intermediate modulus, and high elongation. Aramids such as Kevlar and Teijinconex have been spun using wet spinning process.

8.4.3 Dry-Jet-Wet Spinning

In a typical dry-jet-wet spinning (Figure 8.10), the anisotropic polymer dope of ~20 wt% concentration (in ~80 wt% of concentrated sulfuric acid) is extruded through spinnerets maintained at 100 °C through an air gap of about 1 cm into a cold extrusion water bath kept at 0–4 °C. The fiber precipitates and undergoes strain, and the solvent (acid) gets eliminated in the coagulation bath. The spinneret capillary and air gap causes orientation and alignment of crystal domains, resulting in highly oriented and crystalline as-spun fibers. When the anisotropic solution passes through the capillary hole, the shear due to the capillary causes some of the liquid crystal domains to orient along the direction of shear; however, at the capillary exit, some disorientation of liquid crystal domain occurs because of solution viscoelasticity. The disorientation is quickly overcome by sudden quenching of the filament in cooling bath. This orientation in filament is particularly important as it results in highly crystalline, high strength, and high modulus fiber. The fibers produced by this process show tenacity and initial modulus of two to four times that of a fiber prepared by a conventional wet spinning process.

If the same process is used to produce Kevlar filaments of large diameter, then the core of the filament might lose its orientation because the time required to quench the core will increase with the square of the filament radius. However, the outer part of the filament, i.e. the skin, will have a high degree of orientation due to quick quenching. This creates a "skin-core" effect, because the overall properties of the filaments, such as tensile strength per unit cross-sectional

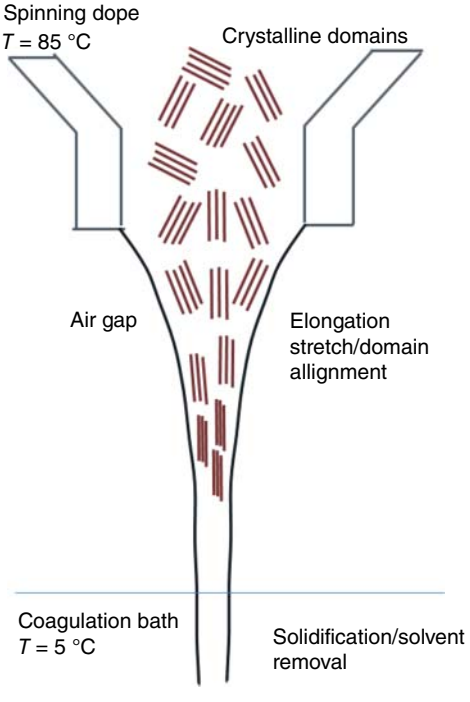


Figure 8.10 Schematic diagram showing dry-jet-wet spinning of lyotropic solution.

area, will diminish owing to a decrease in average orientation. The dry-jet-wet spinning process allows using a low temperature coagulant without concern for freezing the spinning dope. The extruded solution experiences more strain in the air gap and get fully stretched, thereby developing a higher degree of molecular orientation.

8.4.4 Aramid Nanofibers

Traditional methods of synthesizing aramid fibers constitute bottom-up approach where macrofibers are produced from monomers. In recent times, aramid macroscopic yarns are broken down into stable nanofiber dispersion by a top-down approach where deprotonation and dissolution in strong solvents such as dimethyl sulfoxide (DMSO) and potassium hydroxide (KOH) have been employed to produce nanoscale fibers of Kevlar [33, 34]. This could be a result of equilibrium between the antagonistic forces, namely, electrostatic repulsion, $\pi-\pi$ stacking, and van der Waals attraction. The other method of synthesizing nanoscale fibers of N-substituted Kevlar by electrospinning was demonstrated by Yeager et al. [35]. The N-substituted Kevlar showed better dissolution that leads to uniform aramid nanofibers (ANFs) as compared with nonuniform nanofibers of unsubstituted Kevlar dispersions in strong sulfuric acid [36]. However, electrospun substituted Kevlar nanofibers showed unoriented crystalline domains and lacked microvoids generally present in amorphous regions. Similarly, *m*-aramid nanofibers have been synthesized simply by dissolving pristine *m*-aramid polymer in DMAc at 80 °C followed by electrospinning [37]. The mechanical and chemical stability of ANFs has been improved by various methods such as post-treatment by microwave irradiation [37], washing, and heat treatment [38]. Schematic of different approaches of producing ANFs has been shown in Figure 8.11.

Nanoscale aramid fibers could be expected to possess high or better strength, rigidity, toughness, and many other properties. Further, fibers in nano-dimension would facilitate proper distribution of stress over multiple polymer chains and bonds. ANFs can be useful for nanoscale reinforcement for better mechanical properties [39], composite epoxy adhesives [37], ultrafiltration of water and hemodialysis [40], separation of oil and water [41], and battery separators [42]. Detailed applications of ANFs have been given in Section 8.6.

8.4.5 Fiber Heat Treatment

The physical and tensile properties of as-spun aramid fibers can be further enhanced by heat treatment under tension. In wet-spun yarns both tenacity and modulus increase exponentially with increasing temperature (and draw ratio). The effective increase begins at about 360 °C (T_g of polymer), and the properties attain a maximum at nearly 550 °C (T_m of polymer). During the process of heat treatment, wet-spun fibers show maximum increase in crystallinity, orientation, and structure perfection. In dry-jet-wet spun yarns, a jump in the modulus is observed, which becomes independent of temperature greater than 200 °C. The final modulus is a function of precursor modulus (or orientation), with tenacity

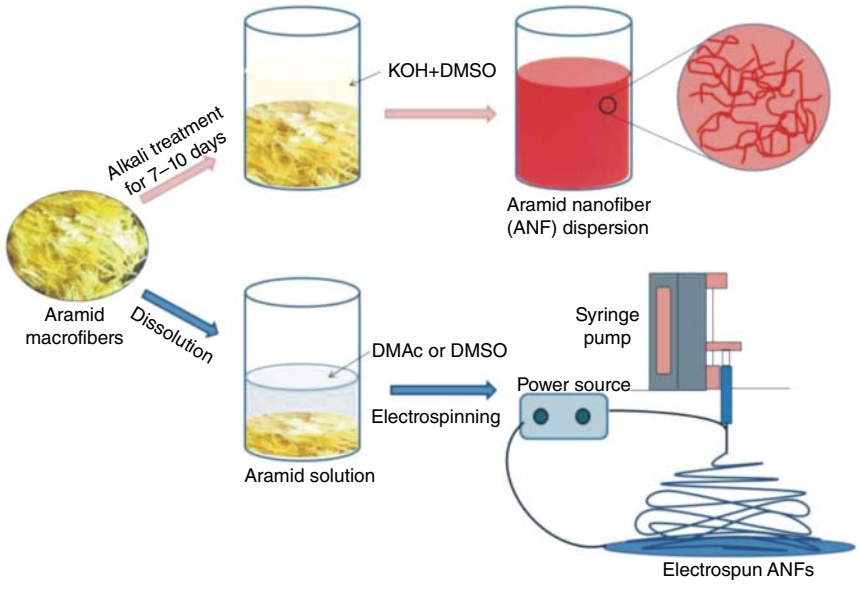


Figure 8.11 Schematic representation of various methods for the preparation of ANFs.

remaining constant. Structural perfections also occur that is indicated by density increase.

8.5 Influence of Structure on Properties

The important properties of aramids, particularly tensile properties, are associated with the fiber structure at molecular level. As mentioned earlier, when the solution is subjected to shear or elongational flow, the liquid crystalline domains tend to align in the direction of shear or flow and achieve a high molecular orientation. Fiber formation from a nematic lyotropic solution is best achieved at a critical concentration showing minimum viscosity and at a temperature close to its anisotropic transition temperature. These conditions are important as they facilitate solution orientation prior to spinning.

8.5.1 Fiber Structure

Different types of Kevlar fibers such as Kevlar 119, Kevlar 29, Kevlar 49, and Kevlar 149 show slight systematic variations in structure. PPTA is essentially a highly crystalline polymer. Morphologically, Kevlar 29 has a single-phase crystalline structure with imperfections in the lattice and a crystallinity of about 68%. The lattice arrangement of pseudo-orthorhombic crystals of PPTA (Figure 8.12a) has been given by Northolt and Aartsen [43]. Unit cell dimensions determined by Northolt are $a = 7.85$, $b = 5.15$, and $c = 12.8$. Panar and coworkers [44] proposed a paracrystalline distorted crystal structure. Intermolecular hydrogen bonds between the C=O and the N–H groups of the amide unit lead

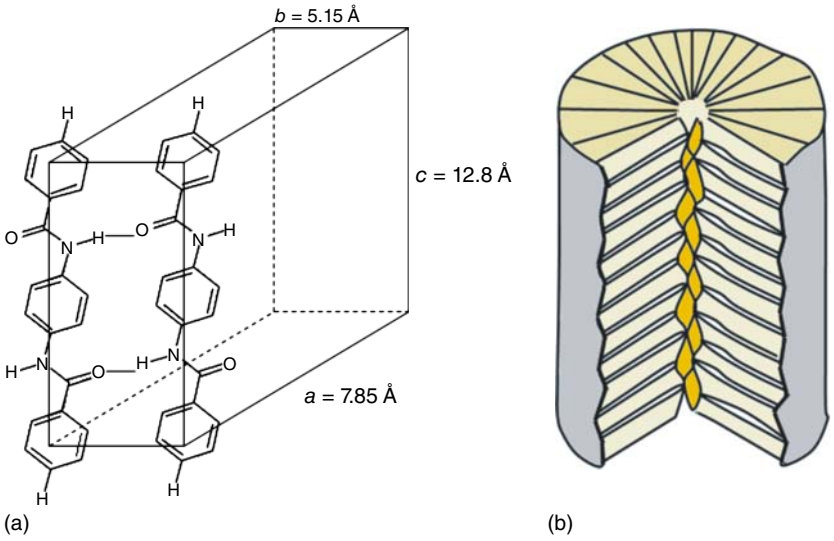


Figure 8.12 (a) Pleated sheet structure in Kevlar 49 fibers. (b) Unit cell of PPTA crystal.

to the formation of sheets linked with hydrogen bonds within the *b*–*c* plane. Using polarized optical microscopy, it has been shown that these imperfect crystals pack to form pleated sheets (Figure 8.12b) and the pleats are in a direction perpendicular to the fiber axis. Transmission electron microscopy and micro-X-ray diffraction measurements have shown that pleated sheets are formed in the plane of hydrogen bond and are arranged radially, forming a fibrillar structure.

The highly oriented polymer chains in the direction of fiber axis impart the necessary high longitudinal modulus of elasticity to the aramid fiber. The presence of aromatic rings and the conjugation of the electrons give the aramids their chemical stability and stiffness toward mechanical strain. The transverse hydrogen bonds and the covalent bonds in the direction of fiber axis lead to a unique mechanical property, anisotropy. Hydrogen bonds are important for the stability of the amide groups; however, they are much weaker than the existing covalent bonds along the fiber direction. Also, there is absence of any bonding between stacked sheets of polymer or pleats. The differential nature of bonding in each direction results in a high longitudinal strength and a low transverse strength, which is an important property for applications such as ballistics. The anisotropy of mechanical properties suggests that such materials should be used meticulously in engineering design and product development.

A skin-core morphology is also very common due to the processing of fibers as mentioned earlier. According to Li et al. [45], the high strength of PPTA fibers may be attributed to their fibrillar structure, the intertwining arrangement of the fibrils, and the presence of a highly oriented skin layer. On the other hand, appearance of defects that may be due to disorientation, at the ends of molecular crystallites in the core of the fiber, may lead to overall mechanical vulnerability.

Emergence of different morphological patterns from liquid crystalline solutions, due to various spinning processes, has been shown by Dayal et al. [46]. The liquid crystal polymer system in the isotropic state undergoes slow evaporation and exhibits a rough surface with no internal texture at the core. In the isotropic metastable region where the solvent evaporation is at a fast rate, the fiber develops a smooth skin within which isolated domains of microfibrillar structures are formed. These types of microfibrils are normally seen during the spinning process. In the unstable nematic region, the spinodal decomposition is dominant, generating the broken spiral or concentric ring patterns that proliferate toward the core of the fiber. Thus, the evolved morphology depends strongly on the initial thermodynamic states governed by the phase diagram, kinetics of phase separation, and the rate of solvent evaporation.

8.5.2 Fiber Properties

Aramid fibers possess medium to ultra-high tensile strength, medium to low extension, and moderate to ultra-high modulus. The densities for these crystalline fibers range from 1.35 g/cm^3 in the case of low oriented *m*-DPI (e.g. Nomex) to 1.45 g/cm^3 for fibers from PPTA (e.g. Kevlar). Meta-oriented phenylene rings are the major constituents of heat- and flame-resistant aramid fibers, whereas para-oriented phenylene rings are mainly present in ultra-high strength high modulus aramid fibers.

8.5.2.1 Chemical Properties

The PPTA fibers are resistant to many organic solvents and salts, but there can be a considerable loss of strength on using strong acids. Due to high crystallinity, aramid fibers have high glass transition temperature (T_g) and therefore are difficult to dye. By using recommended cationic dyes [47, 48] and pyridine for solvent dyeing, deep shades and excellent color fastness have been reported for Nomex and polyisophthalamides of both 4,4′-diaminodiphenylmethane and 2,2-bis(4-aminophenyl)propane.

The aromatic nature (i.e. electron conjugation) of *p*-aramids is responsible for oxidative reactions in the presence of ultraviolet (UV) light. This leads to change in color and loss of some mechanical strength. Kevlar 49 has a major drawback in that it strongly absorbs radiation in UV region around 250 nm and a low broad absorption is observed around 330 nm. As a consequence these fibers cannot be directly exposed to sunlight and should not be used for applications where there is presence of UV light. Light from the sun has wavelength in the range of 300–400 nm, and Kevlar, after absorption of this radiation in air, shows severe degradation of its mechanical properties.

Further, the amide linkages in aramids render these fibers hydrophilic, and they absorb moisture reversibly. Water molecules get absorbed by the amide linkages present at the chain ends, intramicrofibrillar spaces, crystal defects, and microvoids, which tend to reduce the mechanical properties [49].

Table 8.2 Properties of some aramids.

Fiber	Characteristics	Crystalline modulus, GPa	Tensile modulus, GPa (gpd)	Tensile strength, GPa (gpd)	Extension to break (%)	Moisture regain (%)
Nomex			17 (140)	0.6 (5)	22	4.5
Fiber B			128 (1000)	— (22)	5	—
Kevlar 29	Regular	153	70 (550)	2.9 (23)	4	5–7
Kevlar 49	High modulus	156	135 (950)	2.9 (23)	2.8	3–4
Kevlar 100	Colored	156	60 (475)	— (23)	3.9	—
Kevlar 119	High durability	156	55 (430)	3.1 (24)	4.4	5–7
Kevlar 129	High strength	156	99 (780)	3.4 (26.5)	3.3	4–6
Kevlar 149	Ultrahigh modulus	156	143 (1100)	2.3 (18)	1.5	1–1.2
Twaron	Regular	156	79 (622)	3	3.3	7
Twaron HM	High modulus	156	123 (960)	(22.1)	2	3.5
Technora	Regular	91	70 (570)	3.3 (27)	4.3	3.5–5
Trevar V106			77 (657)	—	3.7	—
Ekonol			136 (1100)	3.8 (31)	2.6	—
Vectran			91 (700)	3.2 (25)	—	<0.1
Armos			140–145	4.5	3	—

Source: With prior permission from Indian Journal of Fibre & Textile Research.

8.5.2.2 Mechanical Properties

Mechanical or tensile properties of the aramid fibers are controlled by the fiber structure as discussed earlier. The fiber modulus is governed by overall molecular orientation, crystallinity, formation of H-bonds between the polar amide groups on adjacent chain, and highly symmetrical internal fiber structure. Orientation of polymer chains promotes efficient load sharing between molecular chains. The properties of various aramids are summarized in Table 8.2.

Young et al. [50] have shown that fibers produced by different processing conditions develop different molecular structures, thereby imparting different mechanical properties. According to Dobb and Johnson [51], high molecular orientation, low skin-to-core ratio (more chains per unit cross-sectional area), and large crystallite size promote the development of high modulus in Kevlar. Fiber strength is critically affected by morphological defects, such as microvoids and the presence of cracks in the high modulus variant Kevlar 149. Typical stress–strain curve of Kevlar aramid yarn as compared with other high-performance fibers is shown in Figure 8.13. The figure shows that Kevlar yarn has a break tenacity of 18–26 gpd, which is twice as that of nylon or E-glass fibers and more than five times that of steel wire. Kevlar exhibits an unusually high initial modulus of 475–1100 gpd, which is two times that of steel wire and fiberglass and elongation of only 1.5–4.4%. As a spun fiber, Kevlar 29 has a modulus of 62 GPa. Crystalline orientation can be increased by heat treatment under tension as described in Section 8.4.4. The resulting Kevlar 29 fiber has a modulus of 131 GPa. Kevlar fibers, being thermally stable at high temperature,

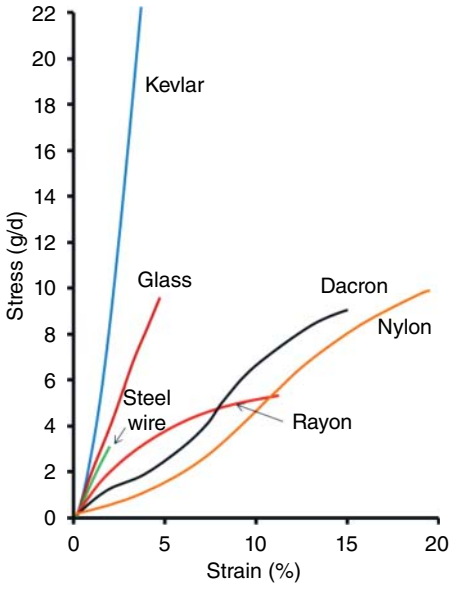


Figure 8.13 Stress–strain behavior of Kevlar compared with other high-performance fibers.

retain their strength and modulus even at temperatures as high as 300 °C. Kevlar shows creep at low load due to high crystallinity, but under high strain it significantly creeps.

8.5.2.3 Thermal Properties

There is no melting point of aramid fibers; however decomposition occurs at temperature as high as 550 °C. Aramids very easily take up moisture, reversibly. The differential scanning calorimetry studies of PPTA reveal moisture evolution at about 100 °C and a second-order transition at 360 °C, followed by melting and decomposition at 500–575 °C in nitrogen and until about 362 °C in air. Glass transition temperature (T_g) ranges from 250 °C to >400 °C. Some aramid fibers such as Nomex show shrinkage in a high heat source or a flame. Aramid fibers typically burn only with difficulty because of high limiting oxygen index (LOI) values. Burning produces a thick char covering the surface and acts as a thermal barrier. Pyrolysis of PPTA fiber produces *p*-phenylenediamine, aniline, benzonitrile, etc., indicating a homolytic cleavage of amide bond.

Such high thermal stability of aramids can be attributed to higher bond dissociation energies of C—C and C—N bonds in the main polymer chain in aromatic compounds than those in aliphatic ones. Excellent thermostability of poly(*p*-phenylene benzobisthiazole) is due to its fully aromatic character and highly rigid molecule. Introduction of flexible groups such as –O– into main polymer chain (e.g. Technora by Tenjin) leads to more flexible chains, thereby lowering the thermal stability.

Aramids show excellent retention of mechanical properties at elevated temperatures. This is due to the presence of C–N linkage of the amide group in PPTA and the electron conjugation between the amide groups and the aromatic ring in *p*-aramids. This results in the yellow color of these fibers and increased chain

rigidity. At 300 °C Kevlar retains about 50% of its strength of that at room temperature, while 70% of the modulus remains of this level. Aramids have a slight negative longitudinal coefficient of thermal expansion of about -2 to -4×10^{-6}/K and a positive transverse expansion of 60×10^{-6}/K. Its high crystallinity results in negligible shrinkage both at high temperature in air (<0.1% at 177 °C) and in hot water (<0.1% at 100 °C). They also have a low thermal conductivity that varies by about an order of magnitude in the longitudinal vs. transverse direction.

8.6 Applications

Due to their characteristic properties such as high strength, low density, compressive strength, low flammability, no melting point (direct degradation above 500 °C), and good resistance to impact, abrasion, and chemical and thermal degradation, aramids show a wide range of applications in the field of reinforcement as well as apparel-related applications [52]. Various applications of aramids are summarized in Table 8.3.

However, due to the difference in the properties of *m*-aramid and *p*-aramid, they find specific applications as per their properties. The *m*-aramid (Nomex) has excellent thermal resistance and good textile properties but inferior mechanical properties for high-performance fiber. Thus, it is generally used for protective clothing, hot gas filters, industrial-coated fabrics, felt scrims, and reinforcement of rubberized belts and hoses. The *p*-aramid (Kevlar), on the other hand, shows unique combinations of toughness, extra high tenacity and modulus, and exceptional thermal stability. Thus, *p*-aramid covers diverse end uses in areas such as industrial, aerospace, military, and civilian applications for various purposes such as cut, heat and bullet/fragment resistant (ballistic) apparel, hard armors, brake and transmission friction parts, reinforced tires and rubber goods, ropes and cables, various forms of composites, industrial gloves, circuit board reinforcements, etc. Various other copolymers containing combination of meta- and para-substituted monomers have also been developed for optimum properties. Various applications of aramids are discussed below in detail.

8.6.1 Composites with Soft Materials

Applications of high-performance composite entail reinforcement by fibrous materials with superior mechanical properties. Especially, PPTA fibers, i.e. Kevlar, are well suited for high-performance composite applications, as they possess a high tensile strength and modulus with a high thermal resistance and chemical inertness, and moreover, they exhibit low electrical conductivity compared with metallic or carbon fibers.

Since the advent of Kevlar in 1972, the availability of these aramid fibers has advanced in materials science, particularly in the areas of fiber-reinforced composites. Kevlar fibers have been readily composited with materials like epoxy matrix [53], nylon [54], carbon fibers, and glass fibers for improved mechanical properties and impact resistance.

Table 8.3 Various applications of aramids.

Contributing properties		Application area	Typical end uses	Aramids
Reinforcement applications				
High specific strength and stiffness	Good adhesion to rubber, axial compressive strain below ~0.8%	Composites with soft materials	Tyres, automotive products (belt, hose), conveyor belts	p-Aramid
	High fatigue resistance, weight reduction, and impact damage tolerance	Advanced composites	Air craft structural components, wound pressure vessel	
	No creep and outstanding dimensional stability, nonrusting	Ropes and cables	Telecommunication cables, civil engineering construction	
	—	Short fiber application	Friction products (brakes and clutches), gaskets and thixotropes and additives	Kevlar
	—	Communication	Reinforcement of delicate glass fiber for optical fiber	
	—	Other leisure industry, transport industry	Sailing boat hulls, tennis rackets, light containers, air ducting in aircraft industry, moisture wicking fiber	
Apparel-related applications				
High specific strength and stiffness, excellent thermal resistance, good textile properties	Excellent cut and puncture resistance	Protective application	For workers, furnishing, fire proof doors, protective gloves	*m*-aramid (Nomex)
	Dynamic energy absorption characteristics	Ballistic protection	Aramid sewing threads, soft and hard body armor	
	—	Perm-selective use	Hollow fiber permeation separation membranes	*m*-Aramid (Nomex)
	High volume resistivities and high dielectric strengths	Electrical application	Motors and transformers	

8.6.2 Advanced Composites

Composites reinforced with macroscopic aramid fibers are significantly useful in areas where their stiffness-to-weight and strength-to-weight ratios render them more desirable than conventional materials such as steel. Structural components of aircrafts have been imparted with high properties using such types of engineered materials. High impact resistance of these advanced composites ensures effective endurance of stresses and strains incurred in flight, which remain structurally intact and withstand catastrophic impact. On the contrary, carbon fibers, which exhibit good stiffness and compressive strength, are unsuitable as they undergo brittle fracture because of their rigid coplanar ring structure.

Recently, composites of aramid-boehmite have been prepared via sol–gel technique, which are transparent and yellow in color. Due to the presence of chemical bonding between the inorganic and organic phases, there is a significant enhancement in the mechanical strength and a thermal stability up to 450 °C. Such composites can be suitable as matrix for advanced applications [55].

As mentioned earlier, nanoscale reinforcement in composite materials is desired as it provides greater interfacial area leading to excellent stress transfer amid the matrix and filler [56]. Due to their higher surface-to-volume ratio, ANFs offer better interaction between fibers and the matrix and hence improved reinforcement as compared with conventional fibers. Guan et al. [57] prepared PVA/ANF nanocomposite films by solution casting technique. The presence of 5 wt% ANF-3 in PVA matrix resulted in significant enhancement of strength and toughness due to formation of multiple hydrogen bonds between the two components. Lin et al. [39] integrated ANFs in epoxy resin resulting in nanocomposites with enhanced elastic modulus, fracture toughness, and strength comparable to that of CNT-reinforced composites.

8.6.3 Ultrafiltration and Hemodialysis

ANFs are insoluble in water but impart hydrophilicity as they possess high susceptibility to moisture. Because of this property, Nie et al. [40] have shown that ANF-modified polysulfone membranes can suitably be used for ultrafiltration of water, separation of proteins, and adsorption of small molecules like creatinine toxins during dialysis. ANF-modified polymeric membranes show improved antifouling properties. ANFs have also been shown to improve the filtration efficiency of glass fiber filter media used for separation of water from water-in-oil emulsion [41].

8.6.4 Ropes and Cables

Ropes and cables made of aramid fibers are employed in a wide range of applications such as crane pendants, boom suspension ropes in mining machine, deep sea mooring, offshore and marine applications, heavy lifting, bridge stay cables, guyed towers, and antennas. Properties such as high specific strength and specific modulus, lack of creep, and outstanding dimensional stability render aramid fibers used as ropes and cables that are stronger and lighter than steel or other

materials. Unlike iron, cables prepared from Kevlar 29 do not rust and can be used in oil rigs to probe large depths because in air, the specific strength of Kevlar is 7 times that of steel, while in sea water, the strength increases to more than 20 times that of steel.

8.6.5 Industrial Protective Apparel

In industries, superior materials are required that facilitate protection against flame and fire [58], electric arc flash, cut hazards, chemicals, dry particles of lead and asbestos, and hazardous aerosols. The blends of Nomex and Kevlar ensure insulating protection by the material due to very low shrinkage of Kevlar in flames. The excellent mechanical and chemical properties of Kevlar result in protective clothing being cut, aberration, and chemical resistance with comfortable fit.

Breathable, waterproof, and thermally resistant materials have been prepared by Park et al. [59] by electrospinning of *m*-aramid in DMAc/LiCl solution. As compared with commercial polytetrafluoroethylene membranes, *m*-aramid nanofibrous membrane showed better water vapor permeability with good thermal (stable up to 450 °C) and mechanical resistance. Such materials can potentially be used for breathable, waterproof, and thermal-resistant clothing.

8.6.6 Ballistics

Ballistic protection is a category of protective clothing that function to protect individual from the bullets and metal fragments of handheld weapons and explosives [60, 61]. The basic requirements of body armor fit for such application should be that it must be lightweight, allow sufficient movement, be cost effective, and give maximum protection against trauma/impact. Technically, it is important that the material used for such application should absorb energy in a given time frame, accumulate strain energy, and dissipate energy in the form of heat. Kevlar has replaced nylon in ballistic applications. This is because it has high T_g and thermal stability that can withstand high temperatures due to ballistic collision. Their extremely crystalline and ordered nature gives rise to high dynamic modulus, which assists in rapid wave propagation and fast response to longitudinal deformation. Kevlar provides high toughness that is effective in assimilation of longitudinal strain energy and transverse kinetic energy [62]. A lightweight composite from Kevlar reinforcing fiber for anti-ballistic application having polybenzoxazine (PBA)/urethane prepolymer (PU) alloys as a matrix was investigated by Rimdusit et al. [63]. The appropriate thickness of Kevlar reinforced 80/20 PBA/PU composite panel was 30 plies and 50 plies to resist the penetration from the ballistic impact equivalent to levels II-A and III-A of NIJ standard.

8.6.7 Permselective Use

Due to their outstanding chemical, thermal, mechanical, and hydrolytic stability and permselective properties, especially in reverse osmosis, aramids find

application as membrane polymers. Hollow fibers of Nomex, being excellent semipermeable membranes, are used commercially for desalination of seawater or brackish water. Carrera-Figueiras and Aguilar-Vega [64] studied the gas barrier properties of aramids such as poly(benzophenone isophthalamide) (DBF/ISO) and poly(benzophenone-5-*tert*-butylisophthalamide) (DBF/TERT) homopolymers and their copolyamides with different DBF/TERT ratios. The copolymerization was observed to control their gas barrier properties. The presence of bulky groups increases fractional free volume and interchain spacing, thus increasing the diffusion coefficients and gas permeability. Similarly, resin-coated aramid papers (both Nomex and Kevlar) have also been used to study the helium permeability [65]. Nomex, being dense in nature, was observed to show lesser permeability, while Kevlar, being porous in nature, showed higher permeability. Due to their high abrasion resistance and good dimensional stability, *m*-aramids are also used for filter bags in baghouses for the purpose of air cleaning [66, 67]. These *m*-aramid bags remain dimensionally stable at high temperature (200 °C) with growth and shrinkage of approximately 1% only.

8.6.8 Electrical Application

Aramids possess high Young's modulus and excellent heat resistance due to which they are used for electrical insulation in generators, motors, transformers, and other electrical equipments. Their characteristic dielectric strength, thermal stability, cryogenic capability, chemical compatibility, moisture insensitivity, mechanical toughness, and radiation resistance make *m*-aramid papers suitable for such applications. These *m*-aramid papers are prepared using two physically distinct forms, floc and fibrids [68]. Floc is yarn cut to short lengths that provide mechanical strength. Fibrids are thin microscopic filmlike particles that provide dielectric strength and maintain the sheet integrity by binding the floc. A sheet is formed by combining these two forms and is kept under temperature and pressure. These components and the processing conditions of the sheets impart mechanical strength and impermeability, making them suitable for high temperature insulation. The electrical and mechanical properties of *m*-aramid papers are unaffected at temperatures up to 200 °C and show high sustainability for at least 10 years of continuous exposure at 220 °C. By varying the thickness, degree of densification, and floc-to-fibrid ratio, these electrical properties could be varied to a large extent. Two different commercially available poly-*p*-substituted phenylene terephthalamide-based aramid films with biaxial orientation, i.e. Micron and Aramica, have also been explored for their electrical properties [69]. Biaxial orientation imparts very high Young's modulus, and high heat resistance is owed to the *p*-aromatic polyamide linkages, making these films suitable for electrical insulation. The presence of aramids on electrical cables minimizes cable sagging and prevents the cables from coming into close contact with neighboring electrical cables.

8.6.9 Communication

p-Aramids, due to their high modulus and strength, low density, and resistance to creep, find important application in communication cables. They provide

lightweight flexible support structures for fiber-optic cables and ductile power conductors from excessive loading or axial strain. Untwisted aramid yarn that is present along the length of the cable provides very high modulus to resist stretching. Twisted aramid yarns, on the other hand, inserted as a ripcord, provide maximum strength for tearing the protective sheathing when installing or repairing the cable. Mower [70] reported low modulus aramid fibers with braided construction to be more tolerant of bending fatigue in communication cables. It was observed that bending-induced damage increased and residual strength decreased with increase in the modulus of aramid fiber.

8.7 Future Trends

Due to their characteristic properties such as low density, high strength, compressive strength, low flammability, no melting point (direct degradation before their melting), and good resistance to impact, abrasion, and chemical and thermal degradation, aramids have highly been explored for high-performance technical textiles and composites for aircraft, aerospace, automobile, marine, and other industries. *p*-Aramid fibers possess high tensile strength and modulus, low breakage elongation, and good resistance to chemicals but have poor compression strength and lack in fatigue strength. So, *p*-aramids are more suitable for various high-performance applications. *m*-Aramid fibers, on the other hand, show excellent thermal resistance properties and thus more suitable for electrical and flame-retardant applications. Aramid fibers also can be tailor-made to use for reinforcement of glass fibers for fiber optics and telecommunication, permselective application (hollow fiber), asbestos replacement in gaskets (Kevlar pulp), and various other new applications that are continuously being explored.

References

1 Jassal, M. and Ghosh, S. (2002). Aramid fibres: an overview. *Indian Journal of Fibre & Textile Research* 27: 290–306.
2 Ward, I.M. (1987). *Developments in Oriented Polymers-2*. London and New York: Elsevier Applied Science.
3 Lewin, M. and Preston, J. (eds.) (1985). *Handbook of Fiber Science and Technology Vol III: High technology fibers Part B*. New York and Basel: Marcel Dekker, Inc.
4 Jassal, M. (2000). Aramid fibers. In: *Man made Fibers-II: Solution Spun Fibers*, *1*e (eds. A.K. Agrawal and M. Jassal). India: Nodal Centre for Upgradation of Textile Education.
5 Lewin, M. (2007). *Handbook of Fiber Chemistry*. Boca Raton, FL: Taylor & Francis.
6 Hearle, J.W.S. (2001). *High Performance Fibres*. Cambridge, England: Woodhead Publishing Ltd.
7 Salem, D.R. (2001). *Structure Formation in Polymeric Fibers*. Munich: Hanser Verlag.

8 Akato, K. and Bhat, G. (2017). High performance fibers from aramid polymers. In: *Structure and Properties of High-Performance Fibers* (ed. G. Bhat), 245–266. Cambridge, England: Woodhead Publishing.

9 Deopura, B.L. and Padaki, N.V. (2015). *Synthetic Textile Fibres: Polyamide, Polyester and Aramid Fibres in Textiles and Fashion*, 1e (ed. R. Sinclair), 97–114. Cambridge, England: Woodhead Publishing.

10 Li, G. (2017). High-performance rigid-rod polymer fibers. In: *Structure and Properties of High-Performance Fibers* (ed. G. Bhat), 141, 166. Oxford: Woodhead Publishing.

11 Mittal, V. (2015). Advances in synthesis and properties of engineering polymers. In: *Manufacturing of Nanocomposites with Engineering Plastics*, 1–13. Cambridge, England: Woodhead Publishing.

12 Wypych, G. (2016). PPTA poly(p-phenylene terephthalamide). In: *Handbook of Polymers*, 2e (ed. G. Wypych), 542–545. Toronto, Canada: ChemTec Publishing.

13 Silver, F.M. and Dobinson, F. (1978). Aromatic polyamides. II. Synthesis, wet-spinning, and fiber thermal characterization of poly (4,4′-oxanilideterephthalamide) and copolymers with 4,4′-oxydianiline or isophthalic acid. *Journal of Polymer Science Part A* 16 (9): 2141–2149.

14 Afshari, M., Sikkema, D.J., Lee, K., and Bogle, M. (2008). High performance fibers based on rigid and flexible polymers. *Polymer Reviews* 48 (2): 230–274.

15 Zulfiqar, S., Lieberwirth, I., and Sarwar, M.I. (2008). Soluble aramid containing ether linkages: synthesis, static and dynamic light scattering studies. *Chemical Physics* 344 (1): 202–208.

16 Spiliopoulos, I.K., Mikroyannidis, J.A., and Tsivgoulis, G.M. (1998). Rigid-rod polyamides and polyimides derived from 4,3-diamino-2,6-diphenyl or di(4-biphenylyl)-p-terphenyl and 4-Amino-4-carboxy-2,6-diphenyl-p-terphenyl. *Macromolecules* 31 (2): 522–529.

17 Liaw, D.J., Liaw, B.Y., and Tseng, J.M. (1999). Synthesis and characterization of novel poly (amide-imide)s containing hexafluoroisopropylidene linkage. *Journal of Polymer Science Part A* 37 (14): 2629–2635.

18 Shi, H., Zhao, Y., Zhang, X. et al. (2004). Packing mode and conformational transition of alkyl side chains in *N*-alkylated poly (*p*-benzamide) comb-like polymer. *Polymer* 45 (18): 6299–6307.

19 Abe, A., Saito, Y., Imaizumi, M. et al. (2005). Surface derivatization of poly (*p*-phenylene terephthalamide) fiber designed for novel separation and extraction media. *Journal of Separation Science* 28 (17): 2413–2418.

20 More, A.S., Pasale, S.K., and Wadgaonkar, P.P. (2010). Synthesis and characterization of polyamides containing pendant pentadecyl chains. *European Polymer Journal* 46 (3): 557–567.

21 Spiliopoulos, I.K. and Mikroyannidis, J.A. (1996). Soluble, rigid-rod polyamide, polyimides, and polyazomethine with phenyl pendent groups derived from 4,4-diamino-3,5,3,5-tetraphenyl-p-terphenyl. *Macromolecules* 29 (16): 5313–5319.

22 Liu, Y.L. and Tsai, S.H. (2002). Synthesis and properties of new organosoluble aromatic polyamides with cyclic bulky groups containing phosphorus. *Polymer* 43 (21): 5757–5762.

23 Zhou, S., Zhang, M., Wang, R. et al. (2017). Synthesis and characterization of new aramids based on *o*-(*m*-triphenyl)-terephthaloyl chloride and *m*-(*m*-triphenyl)-isophthaloyl chloride. *Polymer* 109: 49–57.

24 García, J.M., García, F.C., Serna, F., and José, L. (2010). High-performance aromatic polyamides. *Progress in Polymer Science* 35 (5): 623–686.

25 Silver, F.M. (1979). Aromatic polyamides. IV. A novel synthesis of sulfonated poly (para-phenyleneterephthalamide): polymerization of terephthalic acid and para-phenylenediamine in sulfur trioxide. *Journal of Polymer Science, Polymer Chemistry Edition* 17 (11): 3519–3533.

26 Silver, F.M. (1979). Aromatic polyamides. V. A general synthesis of polyamides from aromatic diacids and aromatic diamines in sulfur trioxide. *Journal of Polymer Science, Polymer Chemistry Edition* 17 (11): 3535–3542.

27 Mallakpour, S. and Kolahdoozan, M. (2008). Synthesis and properties of novel soluble aromatic polyamides derived from 5-(2-phthalimidyl-3-methyl butanoylamino) isophthalic acid and aromatic diamines. *Reactive and Functional Polymers* 68 (1): 91–96.

28 Shoji, Y., Mizoguchi, K., and Ueda, M. (2008). Synthesis of aramids by polycondensation of aromatic dicarboxylic acids with aromatic diamines containing ether linkages. *Polymer Journal* 40 (8): 680–681.

29 Silver, F.M., Dobinson, F., and Ridgway, J.S. (1978). Aromatic polyamides. III. Copoly (4, 4′-oxanilideterephthalamide-4, 4′-phenyleneterephthalamide): Synthesis, wet-spinning, fiber thermal characterization, and stability in sulfuric acid. *Journal of Polymer Science* 16 (9): 2151–2157.

30 Boivin, J. and Brisson, J. (2004). Synthesis of rod copolyaramids with short flexible spacers. *Journal of Polymer Science Part A* 42 (20): 5098–5112.

31 Springer, H., Abu Obaid, A., Prabawa, A., and Hinrichsen, G. (1998). Influence of hydrolytic and chemical treatment on the mechanical properties of aramid and copolyaramid fibers. *Textile Research Journal* 68 (8): 588–594.

32 Chae, H.G. and Kumar, S. (2006). Rigid-rod polymeric fibers. *Journal of Applied Polymer Science* 100 (1): 791–802.

33 Yang, M., Cao, K., Lang Sui, Y.Q. et al. (2011). Dispersions of aramid nanofibers: a new nanoscale building block. *ACS Nano* 5 (9): 6945.

34 Li, J., Fan, J., Liao, K. et al. (2016). Facile fabrication of a multifunctional aramid nanofiber-based composite paper. *RSC Advances* 6 (93): 90263–90272.

35 Yeager, M.P., Hoffman, C.M., Xia, Z., and Trexler, M.M. (2016). Method for the synthesis of para-aramid nanofibers. *Journal of Applied Polymer Science* 133 (42): 1–8.

36 Srinivasan, G. and Reneker, D.H. (1995). Structure and morphology of small diameter electrospun aramid fibers. *Polymer International* 36 (2): 195–201.

37 On, S.Y., Kim, M.S., and Kim, S.S. (2017). Effects of post-treatment of meta-aramid nanofiber mats on the adhesion strength of epoxy adhesive joints. *Composite Structures* 159: 636–645.

38 Ryu, S.Y., Chung, J.W., and Kwak, S.Y. (2017). Amphiphobic meta-aramid nanofiber mat with improved chemical stability and mechanical properties. *European Polymer Journal* 91: 111–120.

39 Lin, J., Bang, S.H., Malakooti, M.H., and Sodano, H.A. (2017). Isolation of aramid nanofibers for high strength and toughness polymer nanocomposites. *ACS Applied Materials & Interfaces* 9 (12): 11167–11175.

40 Nie, C., Yang, Y., Peng, Z. et al. (2017). Aramid nanofiber as an emerging nanofibrous modifier to enhance ultrafiltration and biological performances of polymeric membranes. *Journal of Membrane Science* 528: 251–263.

41 Shin, C. and Chase, G. (2006). Separation of water-in-oil emulsions using glass fiber media augmented with polymer nanofibers. *Journal of Dispersion Science and Technology* 27 (4): 517–522.

42 Jeon, K.S., Nirmala, R., Navamathavan, R. et al. (2014). The study of efficiency of Al_2O_3 drop coated electrospun meta-aramid nanofibers as separating membrane in lithium-ion secondary batteries. *Materials Letters* 132: 384–388.

43 Northolt, M.G. and van Aartsen, J.J. (1973). On the crystal and molecular structure of poly-(*p*-phenylene terephthalamide). *Journal of Polymer Science, Polymer Letters Edition* 11 (5): 333–337.

44 Panar, M., Avakian, P., Blume, R.C. et al. (1983). Morphology of poly(p-phenylene terephthalamide) fibers. *Journal of Polymer Science, Polymer Physics Edition* 21 (10): 1955–1969.

45 Li, S., McGhie, A., and Tang, S. (1993). Internal structure of Kevlar® fibres by atomic force microscopy. *Polymer* 34 (21): 4573–4575.

46 Dayal, P., Guenthner, A.J., and Kyu, T. (2007). Morphology development of main-chain liquid crystalline polymer fibers during solvent evaporation. *Journal of Polymer Science Part B* 45 (4): 429–435.

47 Silver, F.M. and Dobinson, F. (1977). Aromatic polyamides. I. Poly-p-xylyleneterephthalamide: synthesis, fiber spinning, and characterization. *Journal of Polymer Science* 15 (10): 2535–2538.

48 Higashi, F., Goto, M., and Kakinoki, H. (1980). Synthesis of polyamides by a new direct polycondensation reaction using triphenyl phosphite and lithium chloride. *Journal of Polymer Science* 18 (6): 1711–1717.

49 Yahaya, R., Sapuan, S., Jawaid, M., Leman, Z., Zainudin, E. (2015) Effect of moisture absorption on mechanical properties of natural fibre hybrid composite. *Proceedings of the 13th International Conference on Environment, Ecosystems and Development (EED '15)* (1–2 April 2015). Kuala Lumpur, Malaysia.

50 Young, R.J., Lu, D., Day, R.J. et al. (1992). Relationship between structure and mechanical properties for aramid fibres. *Journal of Materials Science* 27 (20): 5431–5440.

51 Dobb, M., Johnson, D., and Saville, B. (1977). Supramolecular structure of a high-modulus polyaromatic fiber (Kevlar 49). *Journal of Polymer Science* 15 (12): 2201–2211.

52 Hahn, C. (2000). Characteristics of p-aramid fibers in friction and sealing materials. *Journal of Industrial Textiles* 30 (2): 146–165.

53 Reis, P., Ferreira, J., Santos, P. et al. (2012). Impact response of Kevlar composites with filled epoxy matrix. *Composite Structures* 94 (12): 3520–3528.

54 Yu, Z., Ait-Kadi, A., and Brisson, J. (1991). Nylon/Kevlar composites. I: mechanical properties. *Polymer Engineering & Science* 31 (16): 1222–1227.

55 Ahmad, Z., Sarwar, M.I., Krug, H., and Schmidt, H. (1997). Preparation and properties of composites of Kevlar-Nomex copolymer and boehmite. *Die Angewandte Makromolekulare Chemie* 248: 139–151.

56 Wagner, H.D. (2007). Nanocomposites: paving the way to stronger materials. *Nature Nanotechnology* 2 (12): 742–744.

57 Guan, Y., Li, W., Zhang, Y. et al. (2017). Aramid nanofibers and poly(vinyl alcohol) nanocomposites for ideal combination of strength and toughness via hydrogen bonding interactions. *Composites Science and Technology* 144: 193–201.

58 Horrocks, A.R. (2016). Technical fibres for heat and flame protection. In: *Handbook of Technical Textiles*, 2e (eds. A.R. Horrocks and S.C. Anand), 237–270. Cambridge, UK: Woodhead Publishing.

59 Park, Y.S., Lee, J.W., Nam, Y.S., and Park, W.H. (2015). Breathable properties of m-Aramid nanofibrous membrane with high thermal resistance. *Journal of Applied Polymer Science* 132 (8): 1–6.

60 Rebouillat, S. (2016). ARAMIDS: 'Disruptive', open andcontinuous innovation. In: *Advanced Fibrous Composite Materials for Ballistic Protection*, 2e (ed. X. Chen), 11–70. Cambridge, England: Woodhead Publishing.

61 Chen, X. and Zhou, Y. (2016). Technical textiles for ballistic protection. In: *Handbook of Technical Textiles*, 2e (ed. X. Chen), 169–192. Cambridge, UK: Woodhead Publishing.

62 Bajaj, P. (1997). Ballistic protective clothing: an overview. *Indian Journal of Fibre & Textile Research* 22 (4): 274–291.

63 Rimdusit, S., Pathomsap, S., Kasemsiri, P. et al. (2011). Kevlar™ fiber-reinforced polybenzoxazine alloys for ballistic impact application. *Engineering Journal* 15 (4): 23–40.

64 Carrera-Figueiras, C. and Aguilar-Vega, M. (2007). Gas permeability and selectivity of benzophenone aromatic isophthalic copolyamides. *Journal of Polymer Science Part B* 45 (15): 2083–2096.

65 Bubacz, M., Beyle, A., Hui, D., and Ibeh, C.C. (2008). Helium permeability of coated aramid papers. *Composites Part B Engineering* 39 (1): 50–56.

66 Kohli, A., Forsten, H. H., and Wyss, K. H. (2008) Bag filter comprising meta-aramid and acrylic fiber. US Patent 7,456,120, filed 13 Septembre 2006 and issued 25 November 2008.

67 Greatorex, A. T. (1998) Filter unit and process for manufacturing a filter unit. US Patent 5,753,001, filed 2 August 1995 and issued 19 May 1998.

68 Bhatia, A. (1995) Aramid papers with improved dimensional stability. *Proceedings: Electrical Electronics Insulation Conference and Electrical Manufacturing & Coil Winding Conference,* (18–21 Sepember 1995). Rosemont, USA: IEEE.

69 Yasufuku, S. (1995). Application of aramid film to electrical and electronic uses in Japan. *IEEE Electrical Insulation Magazine* 11 (6): 27–33.

70 Mower, T.M. (2000). Sheave-bending and tensile fatigue of aramid-fiber strength members for communications cables. *International Journal of Fatigue* 22 (2): 121–135.

9

Conductive Fibers

Tung Pham and Thomas Bechtold

University Innsbruck, Research Institute of Textile Chemistry and Textile Physics, Hoechsterstrasse 73, Dornbirn 6850, Austria

9.1 Introduction

Future smart textiles will exhibit a high level of integration of electronic components; thus miniaturization and appropriate strategies for integration of electric functionalities are essential.

The realization of conductive textiles is the basic requirement for the integration of miniaturized (e.g. nanosized) sensors in a textile structure, e.g. humidity, temperature, pressure, gas sensors, etc., as well as for connection concepts of sensors in large-area textile sensor networks. Instead of separated manufacturing of electronic devices, which then are mounted on a textile product, the buildup of a device is integrated into the different steps of the textile production. Functional elements are formed during yarn formation, mounted through weaving or knitting, and placed through embroidery and printing. Standardized textile processed products will be replaced by combination of individually designed steps. Thus, in the near future, integrated electronic devices will be produced through an appropriate combination of materials and specialized textile techniques. Finding the balance between electrical conductivity, flexibility, and comfort of the textile is a challenge.

9.2 Production of Conductive Fibers: Principles and Technologies

9.2.1 Conductivity

Fibers and their wide variety can be used for many purposes from insulation to conducting applications. Early examples in textiles consisting of fibers with electrical conductivity could be found not only in antistatic and shielding but also heating elements.

The conductivity is defined by Ohm's law as follows:

$$U = R \times I$$

Handbook of Fibrous Materials, First Edition. Edited by Jinlian Hu, Bipin Kumar, and Jing Lu.
© 2020 Wiley-VCH Verlag GmbH & Co. KGaA. Published 2020 by Wiley-VCH Verlag GmbH & Co. KGaA.

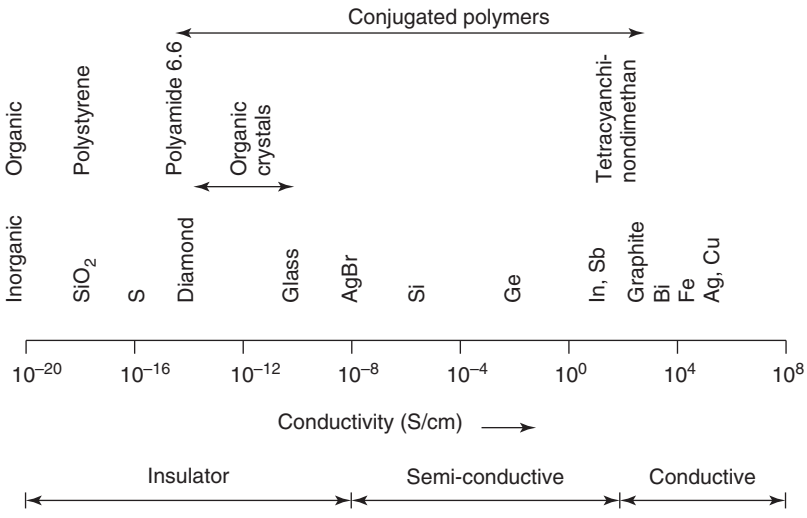


Figure 9.1 Conductivity range of typical material classes (according to [1]).

where I is the current through a resistor and U is the drop in potential across it.

The constant R is called the resistance and is proportional to the length l of the sample and inversely proportional to the sample cross section A:

$$R = \rho \frac{l}{A}$$

where ρ is defined as the bulk resistivity (Ω cm). Its inverse $\sigma = 1/\rho$ is the conductivity (S/cm).

Depending on the conductivity range, materials can be divided in three different classes, namely, insulator, semiconductive, and conductive materials (Figure 9.1) [1].

The typical values of resistivity and/or conductivity of some common materials are summarized in Table 9.1.

Depending on applications, different materials and approaches and materials are selected in order to fit the application-specific requirements. Examples on conductive fibers are given in Table 9.2. However, the values of the resistivity in different original publications are often given as linear resistance in Ω/cm, which indicates resistance per length unit.

9.2.2 Metal Fibers: Coating and Deposition

In very early stages of the development of conductive networks and/or connection in textile structures, insulated wires were fixed on a fabric with a very low degree of integration. While the problem of insulation could be handled, the electrical connection to the functional element required manual welding. The cables were stiff and did not exhibit sufficient textile character. Earlier works in producing metal yarns from metal filaments were dated back to the 1930s where the use of iron, nickel, chromium, or stainless metal wires is reported [7–9].

Table 9.1 Conductivity of different materials from conductive to insulation.

Material	Strength (cN/dtex)	Resistivity (Ω cm)	Conductivity (S/cm)	References
Ag	—	—	6.8×10^5	[2]
Cu	—	—	6.5×10^5	[2]
Stainless steel	—	—	1.8×10^4	[2]
Al	—	—	4.0×10^5	[2]
Graphite	—	—	5.0×10^2	[2]
PPy	—	—	1–10	[3]
PAn	—	—	1–5	[4]
Cellulose (Lyocell)	45–50	10^{14}–10^{16}	—	[5]
Cellulose (Viscose)	25–45	10^6–10^9	—	[1]
Cellulose (Cotton)	35–70	10^6–10^8	—	[1]
PA6,6	40–100	10^9–10^{12}	4×10^{-12}	[6]
PET	35–130	10^{11}–10^{14}	—	[1]
PP	22–55	$>10^{13}$	—	[1]
Carbon	200–300	10^{-3}	—	[1]
Glass	100–350	10^{12}–10^{15}	—	[1]

Today's approaches to integrating cables and wires during weaving or knitting already have reached technical scale. Full-scale prototypes with integration of different conductive materials such as wires and stainless steel yarn in knitted fabric were produced. A wide range of conductive metallic materials can be positioned on textile structures by embroidery techniques, which successfully could be used to manufacture conductive structures from stainless steel yarn, aluminum, or copper wires [10, 11].

Due to the nature of metals having lower elasticity, spinning techniques have been investigated to produce conductive polymer/metal wire composite yarns [12]. Wires of different types and diameters were obtained using core spinning and wrap spinning techniques to form a complex yarn. In order to introduce and/or to improve yarn elasticity, the concept of hybrid yarn was developed, where a conductive yarn (Bekinox BK50) winds around an elastic core yarn (Polyamide/Lycra) in a direct twisting device used in knitted fabrics as strain sensors [13]. Test results show that the hybrid yarns can effectively enhance the electromechanical properties of the knitted strain sensors without compromising processability and comfortability [13]. Another approach is to coat textile fibers with metals [14–16]. For example, Kalanyan et al. demonstrated that the deposition of wolfram on polyamide 6 fiber nonwoven mats using low temperature atomic layer deposition (ALD) leads to a conductivity of about 1000 S/cm [16]. The same technique was also applied to form platinum conductive layer via (methylcyclopentadienyl)trimethyl platinum and ozone on polyamide 6 nonwoven, having effective conductivities as high as ∼5500–6000 S/cm [17]. Also metals like gold can be deposited as coating on yarns [14, 15].

Table 9.2 Examples on conductive fibers/yarns/fabrics with best achieved conductivity.

Composition	Fineness	Tensile strength/tenacity/ modulus/elongation	Resistivity[a]	Conductivity (S/cm)	References
Metal based					
Stainless steel/polyester yarn	200 tex	5.97 cN 0.3 cN/tex — 57.6%	100 Ω/cm	—	[13]
Stainless steel/polyester yarn	400 tex	10.87 cN 0.27 cN/tex — 63.2%	50 Ω/cm	—	[13]
Nonwoven polyamide/tungsten deposition	—	—	—	1000	[16]
Nonwoven polyamide/platinum deposition	—	—		5700	[17]
Poly(*p*-phenylene terephthalamide)/ Poly(styrene-butadiene-styrene) nanosilver coating	—	—	0.15 Ω/cm	—	[25]
Polyurethane/silver nanowire ink coating	—	—	7.3×10^{-5} Ω/cm	—	[27]
Stainless steel	130–820 tex	—	<75–10 Ω/m	—	[66]
polyamide/silver plated	4–125 tex	—	<2000–5 Ω/m	—	[65]
Ag-coated monofilament	2.2 tex	—	68 Ω/cm	—	[67]
Ag-coated multifilament	47 tex		1 Ω/cm	—	[67]
Ag-coated Cu/polyester	61 tex	—	0.0925 Ω/cm	—	[68]
Intrinsically conductive polymer based					
Cotton/poly(3-hexylthiophene) coating	—	—	5.9×10^{7} Ω/cm	—	[49]
Polypyrrole nano fibers	4–5 μm			0.5	[69]

Polyaniline/gelatin blend	100–650 nm	6.56–10.49 MPa — — 0.49–0.09%		0.021	[70]
Polyaniline	200–1000 nm	—	—	10^{-3}–10^{2}	[71]
Polyaniline/polyamide blend	150–500 nm	—	—	6.2×10^{-7}	[72]
Polyaniline/polyamide coat	800–2000 nm	—	—	0.4–2	[73]
Polyaniline/silica	1–5 µm	—	—	5×10^{-7}–1.07	[74]
Polyaniline/Poly(D,L-lactide)	0.94 µm	—	—	0.044	[75]
Poly-3-hexylthiophene/polyethylene blend	380–1200 nm	—	—	0.16–0.3	[76]
Cotton/polypyrrole coating	—	—	—	5.8	[77]
Carbon based					
Cotton/graphene coating	—	—	374 Ω/cm	—	[52]
Polyurethane/carbon black coating	—	—	—	140	[55]
Polypropylene/carbon black/graphite melt spinning	—	—	—	0.32	[59]
Polyester/polypropylene/MWCNT coating	—	—	—	0.52	[60]
Cotton/MWCNT coating	—	—	20 Ω/cm	—	[78]
Carbon/polyethylene	26 dtex	— 24 cN/tex 126 cN/tex 105%	—	0.18–1.39	[79]
Cellulose/carbon	—	— 8–14 cN/tex 300–700 cN/tex 4–12%	—	0.0024–0.18	[80]

a) The values of the resistivity in different original publications are often given as linear resistance in Ω/cm, which indicates resistance per length unit.

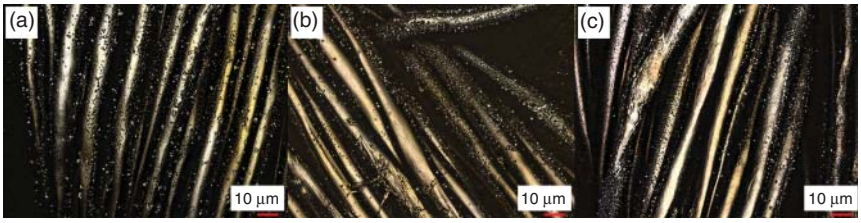


Figure 9.2 Laser scanning image of a cellulose knitted fabric coated with nanosized silver particles by reduction from silver salt $AgNO_3$ (a) 0.004 mol, (b) 0.005 mol, and (c) 0.009 mol.

Printing techniques such as screen printing and ink-jet printing can be used to form conductive layers from metals on textile fabrics with the distinct advantage of being able to build conductive areas independent of fabric structure and to position the conductive areas [18–22]. Techniques for making inks conductive include the use of silver flakes in polyurethane (PU) [19] or acrylic binder [22]. In Ref. [23], a three functional layer design was used to fabricate the durable conductive tracks consisting of an interface layer providing a smooth surface followed by a conductive silver layer and finally an encapsulation layer, which was screen-printed on top to provide upper-side protection and electrical insulation [23].

Also the in situ synthesis of nanosized silver particles to form conductive tracks was reported [24–26]. The improvement of the conductivity was achieved by a further sintering step at 200 °C for 30 minutes of the formed silver particles on the textile surfaces [24]. Additional elastic performance was achieved, along with electrical conductivity, by coating elastic rubber fibers with silver nanoparticles [25]. The conductive fibers exhibited outstanding stability against repeated external deformations with the help of the elastic rubber materials that act as elastic scaffolds and can be used to fabricate highly sensitive textile-based pressure sensor [25]. In Ref. [26], the polyamide 6 fabric was first treated with potassium permanganate to oxidize fabric surface and thus to increase number of assembled particles on the fabric surface. In another study, core–shell conductive fibers with high stretchability are developed by writing silver nanowires ink on pre-strained polyurethane fibers. The core–shell elastic fibers are twisted, forming flexible piezo-resistive fiber construction that shows desirable sensitivity to pressure and bending deformations [27].

Another approach to forming nanosized silver particles on fibers is the reduction from silver salt, e.g. $AgNO_3$. Using different $AgNO_3$ concentrations, different surface topology, and resistance could be achieved. Examples are given for 0.004, 0.005, and 0.009 mol $AgNO_3$ (Figure 9.2a–c).

By initiating the radical graft polymerization of glycidyl methacrylate monomer on plain woven cotton fabric using 10 kGy dose of electron beam irradiation, followed by the hydrazination of the epoxy ring to introduce reducing agents into the fiber structure, the electroless deposition of silver from silver salt solution could also be realized. The deposited silver nanoparticles make a conductive pathway through contact network in the cotton fabric [28].

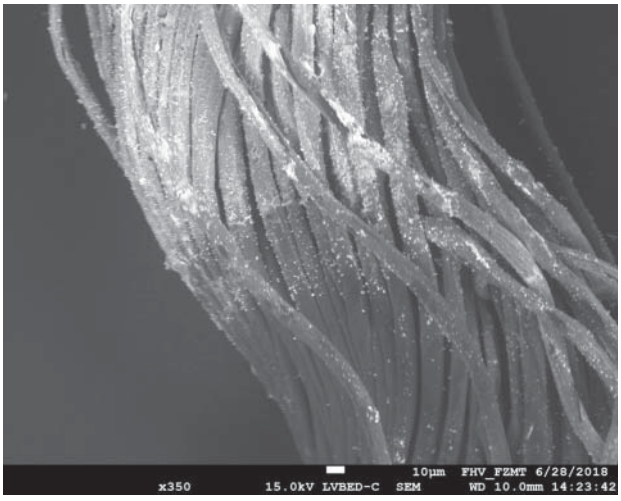


Figure 9.3 Scanning Electron Microscopy image of copper-deposited cellulose fiber by electroless copper deposition using nanosized silver seeds (bright areas: copper layers).

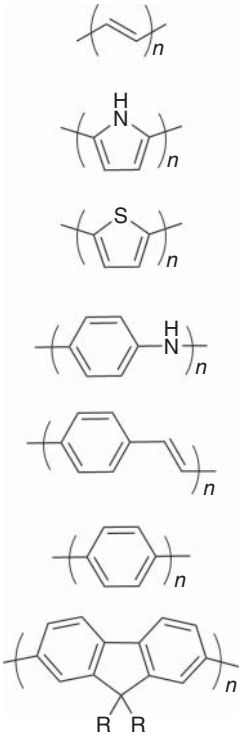
In our own work, further electroless deposition was initiated using nanosized silver seeds as catalysts. The techniques enable the localized formation of a thin copper layer on cellulose fibers (Figure 9.3).

Another approach was developed by Liu et al. to coat cotton fabric with copper through reduction using immobilized silver ions as catalyst [29].

9.2.3 Intrinsically Conductive Polymers and Coating

As described according to IUPAC Compendium of Chemical Terminology, intrinsically conducting polymer (ICP) composed of macromolecules having fully conjugated sequences of double bonds along the chains. The bulk electrical conductivity of an ICP is comparable to that of some metals and results from its macromolecules acquiring positive or negative charges through oxidation or reduction by an electron acceptor or electron donor (charge transfer agent), termed a dopant. Examples of ICPs are polyacetylene (PA), polypyrrole (PPy), polyaniline (PAn or PANI), polythiophene (PT or PTh), poly(*p*-phenylene vinylene) (PPV), poly(*p*-phenylene) (PPP), and polyfluorene (PF) (Figure 9.4) [30].

Unlike polymeric electrolytes, in which charge is transported by dissolved ions, charge in ICPs is transported along and between polymer molecules via generated charge carriers, e.g. holes and electrons [31]. The unique characteristic of conducting polymers is given by backbones of contiguous sp^2-hybridized carbon centers where the π-electrons delocalize over the whole polymer chain. The conductive characteristic of conducting polymers is transformed from insulating to conducting through a doping process. In the p-doped state (electron accepting), the main chain of the conducting polymer is oxidized with counteranion doping for keeping the electron neutrality of the whole molecule. There are holes in the main chains (lost electrons) that make the conducting polymer p-type conducting. In the n-doped state (electron donating), the main chain of the conducting



Polyacetylene (PA)

Polypyrrole (PPy)

Polythiphene (PTh)

Polyaniline (PAn)

Poly(*p*-phenylene vinylene)

Poly(*p*-phenylene) (PPP)

Polyfluorene (PF)

Figure 9.4 Main chain structures of several representative conjugated polymers (according to [30]).

polymer is reduced with counteraction doping for keeping the electron neutrality of the whole molecule. There are electrons in the main chains that make the conducting polymer n-type conductive [30]. In its oxidized form, the conductivity of PANI, for example, increases about 10 orders of magnitude.

Similar to the fiber coating approach with metals, synthetic fibers can also be functionalized through chemical oxidative deposition, in which conducting electroactive polymers such as PANI, PPy, and PT are used to coat textiles for improving tensile strength and thermal stability [32–37, 77]. PPy has high mechanical strength and is electroactive in organic and aqueous solutions. PT and its derivatives in p- or n-type forms can be used for application in field-effect transistors in flexible logic circuits. Furthermore, surface deposition of electroactive polymers increases conductivity of the fibers by 1 order of magnitude [38–40]. Cotton fabric coated with fibrillary PPy reached conductivity of 5.8 S/cm and can be used for electromagnetic interference shielding [77]. Application of PPy in electrically triggered color-changing fabric was realized by selective deposition of PPy on the cotton side of a polyester-covered cotton fabric, while the thermochromic ink was painted on the polyester side. The fabric showed remarkable resistive heating and color-changing properties under an applied current [34]. Also coating of three-dimensional fibrous scaffolds of polylactide

(PLA) with PPy in combination of chondroitin sulfate (CS) was investigated with respect to deliver electrical stimulation to cells in PLA scaffolds [41].

For application as biosensor, polypropylene (PP) fibers were coated with conductive PPy coating using iron(III) chloride as an oxidant, water as a solvent, and 5-sulfosalicylic acid as a dopant. The biological attachment of avidin onto the fiber surface was achieved through the inclusion of a carboxyl functional group via 3-thiopheneacetic acid in the monomer. The immobilized avidin was then successfully used to capture biotin [42].

In order to improve the adhesion between the coating layer and fiber surface, low temperature (oxygen and argon) plasma treatments were applied for polyester fabrics leading to the activation of the fiber surface and generation of a microscopically rough surface, prior to the deposition of PPy by in situ polymerization. The enhanced adhesion was confirmed by abrasion tests and subsequent surface resistivity measurements [43].

In another work, oxidative in situ polymerization of poly(3,4-ethylenedioxythiophene)–*p*-toluenesulfonic acid (PEDOT:PTSA) directly on a textile polyester fleece was realized. The finished textiles can be used as high-performance textile heating elements, e.g. in carpets, electric blankets, or automotive seat heaters [44]. A combined approach of coating of gold nanoparticles and deposition of thin layers of the conductive polymer poly(3,4-ethylenedioxithiophene) (PEDOT) was applied to increase the conductivity of plain cotton yarns. The application of the modified cotton yarns ranged from passive devices such as resistors to active devices, e.g. organic electrochemical transistors (OECTs) and organic field-effect transistors (OFETs) [45]. Oxidative chemical vapor deposition (OCVD) of PEDOT was also used to coat viscose fibers, leading to conductivity of 14.2 S/cm [46].

Using a direct coating method, a polyurethane-based formulation with poly(3,4-ethylenedioxythiophene)–polystyrene sulfonate (PEDOT:PSS) dispersion and ethylene glycol was applied to poly(ethylene terephthalate) (PET) substrates, and resistivity drop by a factor of 10 was registered [47]. With similar system, however, in poly(styrene-*r*-Bu acrylate) P(St-BA) aqueous solution, Wu et al. [48] created a conductive composite with outstanding stretchability. The elastic conductive composite is then formed on the PET nonwoven fabric substrate by dip coating, leading to conductive soft fabric structure.

Dip coating technique was also applied to coat poly(3-methylthiophene) (P3MT) polyester fabric [56] and poly(3-hexylthiophene) (P3HT) on cotton fabric. In the case of P3HT-coated cotton, a decrease by several orders of magnitude in both surface and volume resistivity was observed compared with untreated cotton [49].

Another approach in utilizing intrinsically conductive polymers in synthetic fibers was melt blending. In Ref. [50], a melt processable PANI complex was blended with polypropylene under different mixing conditions and melt-spun into fiber filaments under different draw ratios. The continuous conductive pathways (interpenetrating network [IPN]) of PANI depended strongly on two factors: the size of the initial dispersed conductive phase, which depended on the melt blending conditions, and the stress applied to orient this phase to a fibril-like morphology, which was controlled by the draw ratio of the fiber [50].

9.2.4 Carbon-Based Fibers (Carbon Black, Carbon Nanotubes, Graphene)

Graphene woven fabrics were synthesized through chemical vapor deposition (CVD) using Cu meshes consisting of wires with ~60 μm in diameter as substrates. The fabrication of the textiles involved growing graphene on the substrate, removing the Cu mesh wires, and subsequently collapsing the graphene to form double-layer microribbons. Such polymers could be also embedded in polydimethylsiloxane (PDMS) or PET films [51]. Conductive textiles could also be produced by immobilizing graphene via reduction from graphene oxide on cotton fabric by using a conventional dip and dry method. The electrical conductivity of the fabric is enhanced 3 orders of magnitude as the number of coating cycles was increased from 1 to 20. The surface conductivity of the resulting graphene depended on the reducing agent type and concentration [52]. Also infusion of pristine few-layer graphene (FLG) from natural bulk graphite onto fabrics using an interfacial trapping method led to higher electrical conductivities [53].

Conductive fibers can be realized by spinning carbon nanotubes (CNTs) containing polymers, for example, by coating techniques using functionalized multi-walled carbon nanotubes (MWCNTs). However the conductivity of these yarns and fibers is decreased by the drawing process during fiber fabrication [60, 78]. Another approach involved spray coating technique to coat electrospun polyurethane nanofiber webs with MWCNT [54].

Wet spinning technique has been investigated by different research groups to generate conductive fibers with carbon black (CB) and CNT. Seyedin et al. [55] reported on wet-spun PU fibers a range of conducting fillers including CB, single-walled carbon nanotubes (SWCNTs), and chemically converted graphene. They found that the electrical and mechanical properties of the conductive fibers were strongly dependent on the aspect ratio of the filler and the interaction between the filler and the elastomer. The high aspect ratio SWCNT filler resulted in fibers with the highest electrical properties and reinforcement, while fibers produced from the low aspect ratio CB had the highest stretchability. Furthermore, PU/SWCNT fibers presented the largest sensing range (up to 60% applied strain) and the most consistent and stable cyclic sensing behavior [55]. In another work [56], alkali hydrolyzed polyester fabric was treated with SWCNT, MWCNT, and CB in combination with nanosized TiO_2 and citric acid as a cross-linking agent through exhaustion method and post-curing. Alternatively, Jin et al. developed a new dissolving coating method to impregnate CB into the polyester fiber surface to enhance the fiber conductivity [57].

To produce sheath–core structured fibers, a CNT solution was used to form the core portion of the fibers, while the sheath was made from polymer such as polyvinyl alcohol (PVA) in a wet spinning process. It was found that stretching fibers in the coagulation bath was a significant step in the formation of a structured core. The drawn flexible fibers could be woven into a fabric for potential use as a pressure sensor [58].

Another approach to preparing conductive polypropylene composite is to mix CB and graphite nanoplatelets (GNP)into a polypropylene matrix during a melt mixing process [45]. Conductive fibers with a sheath–core structure were then

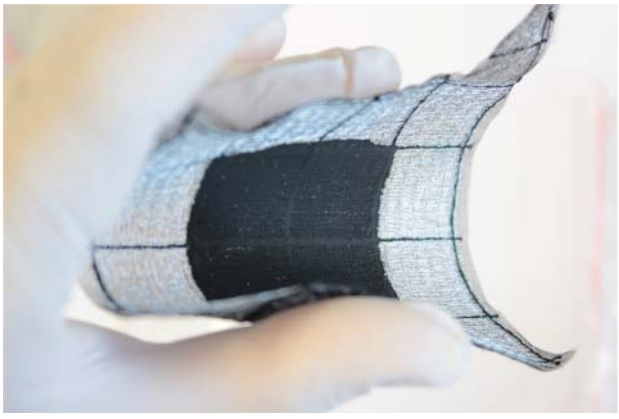


Figure 9.5 Coated textile electrode using active carbon black conductive paste.

produced on a bicomponent melt spinning line with the core materials from hybridized GNP/CB/PP composite and the sheath from polyamide [59]. Very similar concept was investigated by Lin et al. [60], however with the PP/MWCNT as conductive coating layer on PET yarns. The test results indicate that tensile strength of the conductive yarns increases with an increase in the coiling speed that contributes to a more orientated MWCNT arrangement in the yarn direction as well as a higher adhesion between PP/MWCNT and PET yarns [60]. Melt mixing technique was also applied for polycarbonate/MWCNT, subsequently melt-spun to monofilament fiber [61].

Another possibility to obtaining flexible conductive yarns is demonstrated by laser structuring [62], but these materials seem to be challenging regarding their cost efficiency for the use in large-area textile applications. Metal sputtering and CVD techniques are currently studied in basic research approaches; however at present the technology is still far from being on a cost level for commercialization.

Utilizing the conductive nature of active CB, conductive paste can be used to coat fabrics to form conductive areas and pattern in textiles (Figure 9.5) as alternatives to conductive polymers.

Another example is the use of carbon fibers as electrode in redox flow batteries, whereas the carbon fiber rowing is placed on a textile substrate using tailored fiber placement (technical embroidery) technique (Figure 9.6).

9.2.5 Combination of Different Techniques

Some research groups combined different concepts in producing conductive textile fibers. Hu et al. [63] applied the technique of dip coating for highly transparent polyethylene terephthalate mesh fabrics with CNT, followed by ink-jet printing with PEDOT:PSS to develop textile-based CNT/PEDOT:PSS composite conductors. These coated fabrics show a combination of conductivity transparency and flexibility suitable for use in flexible displays [63]. Similar approach was also developed in Ref. [64], where polyethylene terephthalate fabric was first dip-coated with reduced graphene oxide (RGO) sheets and



Figure 9.6 Embroidered carbon fibers as electrode in redox flow batteries.

then coated with PPy by in situ polymerization. The RGO–PPy coated samples exhibited much lower surface resistivity values than samples coated only with PPy and RGO, respectively [64].

Table 9.2 gives some examples on conductive fibers, yarns, or fabrics, with their typical material parameters such as fiber fineness, fiber strength, tenacity, Young's modulus, and best achieved electrical conductivity. Please note that the values and units are taken as published in the original publications.

9.3 Integration of Conductivity into Textile Structures

In the traditional concept of smart textiles, these were textile structures (garment, protective clothes, interior) that were able to carry electronic devices. The electronic devices were manufactured separately and integrated into the textile product during the procedures of assembly. Such concepts required complex manufacturing operations and often considerable amounts of manual work, e.g. for positioning and welding. The final products often could be defined as textile-coated electronic device [81]. The possible miniaturization of devices to the structural dimensions of textiles, e.g. the diameter of a thread, offers new strategies for integration of electronic functionality into textile products [82].

The integration of electronics, switches, actuators, displays, control elements, and panels has to occur on the level of the textile structure. Instead of an assembly of electronic components and a textile product as two components, which are merged at a late stage of production, the installation of an electronic device will be integrated into the textile production step.

The desired functionality is provided by the garment/textile while the electronics disappear and function as part of the textile structure. The integration of such *smart* textile sensors are a key component of a future suitable Internet of Everything.

Table 9.3 Stages of integration of conductivity in textile material and their characteristics.

Production stage	Product	Examples	Production volume required	Characteristics	Flexibility in design
Spinning	Yarn, ply	Conductive yarn	High	—	High
Weaving	Fabric	Fabric with electrical lines as weft	High	Rectangular crossing of threads	Medium
Knitting	Fabric, garment	Heating textiles using Ag-coated yarn	Medium	Loops in direction of production	—
Embroidery	Motifs	Sensor elements on fabric	Low	Free from	—
Printing	Print	Heating elements	Low	Free form	—
Garment production	Garment	Cloths for monitoring vital parameters in sports	Low	Flexible	—

As a result of a high level of integration, the borders between textile manufacturing and production of electronic devices disappear.

The textile processes have to be adapted with regard to their ability to process conductive materials and to form conductive structures; at the same time the performance of conductive elements and the production of a device have to be developed with consideration of the processing requirements of a certain textile technique. The overall concept of a textile product, both garment and technical product, thus will determine fiber material, processing techniques, and final performance, which at the same time also will limit the degree of freedom in choice of conductive material and concepts of integration (Table 9.3).

9.3.1 Fiber Material Selection/Yarn Production

Natural fibers such as cotton, flax, hemp, wool, and silk are staple fibers that exhibit limited length and require a spinning process to form threads. Man-made fibers, e.g. polyester, polyamide, and cellulosics, are initially produced and also available in form of endless fibers and filaments.

The selection of a fiber material follows the planned application; thus the development of conductive structures on the level of yarn formation has to follow the requirements defined by the product and by the manufacturing techniques. The conductive elements have to be processed on machinery that has been designed to handle textile threads, which are flexible, bendable, and elastic. Relevant strategies to integrating conductive elements include the following.

Production of threads with conductive properties can be achieved through a number of different techniques:

- Electroless deposition and electrochemical coating [83].
- CVD and sputtering [46].

- Coating with conductive polymers [84–86].
- Integration of metal wires (core–shell yarns).
- Spinning of metal staple fibers or conductive fibers to yarn.
- Wrapping of yarns with metal fillets.
- Ply formation with conductive threads.

Each of the techniques offers specific advantages and weaknesses. Using deposition and coating techniques, a layer of conductive material is formed on a fibrous substrate. For example, a very thin copper layer can be formed on a polyester fabric using electroless deposition technique (Figure 9.7). As a result a bendable conductive yarn structure is obtained, which exhibits textile characteristics, as long as thickness and mechanical properties of the conductive layer do not alter the yarn properties negatively. The adhesion between conductive layer and basic yarn fibers must be sufficient in height to withstand the mechanical and abrasive wear during formation of textile fabrics.

For technical applications and functional products, e.g. sensors that are built in a product technical aspect, e.g. corrosion resistance, mechanical stability, and overall lifetime, are of relevance, and the optical appearance of the elements is of lower. A substantial drawback for use of coated threads in garment applications results from the color of the coating or metal fibers used, which has to be considered at an early stage of the design.

Independent of the used coating and deposition technique, the layer formation will lead to interlinkages between neighboring fibers and filaments, which alter the mechanical properties of the threads to increased stiffness, lowered elasticity, and reduced flexibility. The overall conductivity of the structure will be dependent on the presence of a sufficient number of interlinkages between the fibers; thus tension and bending will influence conductivity negatively. The use of knitted fabric with strain-dependent electrical resistance allows production of textile-based electromechanical elongation sensors [13].

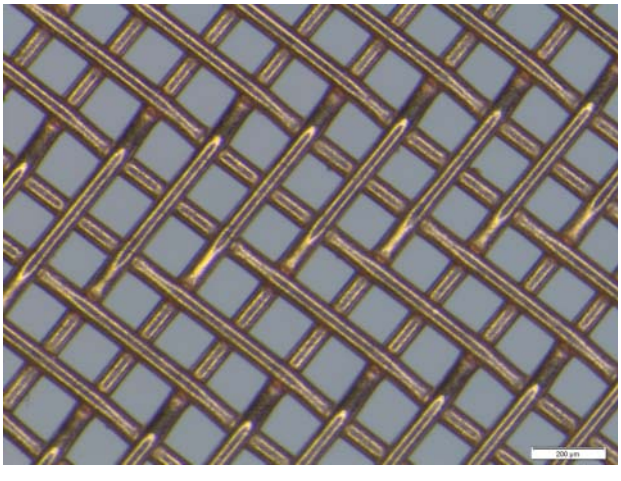


Figure 9.7 Polyester fabric after electroless coating with copper.

Use of conductive fibers, e.g. conductive polymers and metal fibers, allows direct production of conductive yarn; thus the mechanical properties and the optical appearance of the structures will be dependent on the material used. Electrical current is transferred between individual fibers through direct physical contact, which remains intact during bending, stretching, and compression, while individual fibers still can move in the yarn to adapt for length changes during bending. Through use of conductive polymer fibers or metal fibers with diameters in the range of 10–20 µm, the ratio between diameter and bending radius can be kept at low level; thus higher durability in bending tests can be achieved in comparison to metal wire-based concepts.

Another technique to form threads with conductive elements is based on the production of core–shell yarns, e.g. through friction spinning, which however limits the fineness of thread structures to rather coarse yarns. Such a technique allows production of conductive yarns with textile appearance as the yarn surface is built from conventional textile fibers, which can be dyed and finished with the basic textile material, which makes the conductive structure invisible. In many cases the textile characteristics of the core–shell yarns permit processing on standard textile machinery.

A drawback can result from the different strength elongation behavior of the conductive metal core compared with the more flexible and elastic fiber-based shell. Under mechanical stress, breakage of the conductive core will cause risk of interruption and loss of function. This property will require more attention in the case of woven structures and fabrics where the conductive element has been positioned in straight form, while the loops in knitted structures will permit higher deformation without development of high loads in the direction of the yarns. An improvement of yarn flexibility can be realized through use of ply yarns, which combine a textile fiber-based yarn with a metal fillet or wire (Figure 9.8). The screwed structure of the threads permits better adaptation on stress during



Figure 9.8 Synthetic filament yarn wrapped with copper fillet.

bending and elongation in yarn direction, which positively influences mechanical resistance.

As an important difference between core–shell structures and the other concepts mentioned above, the conductive structure in core–shell yarns is covered by an insulated coating of nonconductive standard textile fibers. This leads to an inherent protection against short circuits; however similar to the use of plastic insulated wires, later contacting requires local access through the fiber shell wound around the electrical line. Reversely the use of uncoated electrical lines permits simple connection to external devices; however dependent on the planned application, attention has to be paid to prevention of short circuits through direct contact between the open lines in the fabric.

9.3.2 Fabric Production

The integration of conductive elements by means of threads allows generation of well-defined pattern, and the design of an electrical circuit however is dependent on the manufacturing technique used.

Weaving technologies form fabric through defined crossings of threads. The direction and position of a conductive element thus has to follow the direction of the threads either in weft or warp direction. When conductive yarns are used as weft, in the weaving step the conductive element is integrated over the full width of the fabric. Mechanical stress and abrasive wear for weft yarns are substantially lower when compared with warp yarn, where abrasive forces result from the repetitive and rapid movement of the reed.

Special weaving techniques also allow the formation of localized patterns, however on the cost of substantial losses in conductive material, which have to be removed at the end of the weaving process.

Knitting processes including warp knitting can form a conductive structure in direction longitudinal and cross direction. The fabric production is based on conjunction of loops and highly elastic as well as rigid structures being formed, which contain the conductive elements. The process of loop formation requires flexible and bendable threads with appropriate frictional behavior to be processed by a series of needles working the needle bed of the knitting machine. Such concepts already are widely in use for heating textiles, e.g. by integration of silver-coated threads. The integration as weft or warp can be achieved more easily; however elastic properties have to be considered with care as the elongation of a loop-based structure is different compared with a straight laid weft.

9.3.3 Embroidery/Sewing

Originally designed as technique to form decorative textile motifs on a basic fabric, embroidery techniques have been adapted to process a wide range of materials including wires, carbon rovings, and coated yarns. The principle of embroidery technique is based on the formation of patterns through crossing of two yarns, one or both of which can be made from conductive fibers. The major advantage of embroidery techniques lies in the high flexibility of patterns

available as no specific direction is determined by the technology. Localized circuits can be formed, with high geometric accuracy (<0.1 mm).

Restrictions with regard to yarn diameter and yarn properties result from the principle used in embroidery machines, where the front yarn is pushed through the basic fabric by means of a needle and then has to form a loop on the backside of the fabric. The backing yarn has to be transported through this loop, which thus is an essential requirement to form the embroidery. Limitations also arise from limited textile characteristics of wires and stiff material, which exhibit low tendency to build the required loop at the backside of the fabric, which requires adaptations of the equipment used. Soutache techniques allow positioning of thick yarns and fiber rovings as well as stiff non-textile elements on one side of the fabric.

In a special technique the basic fabric is removed, e.g. through dissolution of PVA fleece in hot water or through organic acid hydrolysis of cellulose fabric, thus releasing the embroidered structure as motif. The chemical stability of the conductive fibers used in such an application thus has to be selected with regard to the later processing conditions to avoid corrosion or destruction of the conductive fibers or films.

A distinct advantage of embroidery lies in the possibility to apply such a technique at a final stage of the manufacturing, e.g. to form localized connections to the conductive structures in the fabric. This allows to build up electrical lines to external devices as well as to form position sensors and circuits at the appropriate position.

Similar requirements have to be considered when sewing techniques are applied to process conductive structures and to connect external devices to circuits inside the fabric.

9.3.4 Printing

Printing techniques permit formation of localized patterns of conductive structures on textile fibers. Through repeated printing, multilayered structures can be implemented and combined with conductive elements already present in the fabric; similarly to production of integrated circuits, contacting of printed structures also can be achieved by embroidery techniques, which allows mechanical contact formation without welding.

As a general disadvantage the formation of the circuits will always be on the surface of the material, which is of lower relevance for technical products that are designed to operate inside a device.

At present two major printing techniques are in use: screen printing and ink-jet printing. Both techniques have been used to form conductive structures on textile material.

In screen printing the conductive structure is placed on the textile in the form of a printing paste, which consists of conductive polymers, finely divided metal powders (e.g. silver), or finely dispersed carbon. To achieve conductivity a critical minimal content of conductive solids has to be achieved to permit sufficient probability for direct contact formation between individual particles. At the same a binder system is applied in the paste, which forms the elastic matrix

between the particles and binds the printing to the fibrous textile structure. Printing of pastes containing conductive polymers with positive temperature coefficient can be used to from flexible heating elements, which protect against overheating through increase of electrical resistance with temperature.

Ink-jet printing is more sensitive with regard to the presence of particulate material, which deposits inside the printing head or leads to abrasive effects during operation. Techniques to using ink-jet printing to form conductive patterns based on silver thus use solution of silver salts or silver complexes, which are printed on the fabric and then transferred to release silver upon heating.

Printing techniques allow formation of complex multilayered architectures and insulating layer can be printed as separator.

When polymer pastes, e.g. silicon-based pastes, are deposited on the conductive structures, protective layers can be applied locally and thus be useful to protect integrated electronic structures against corrosive environmental conditions during use (sweat, rain) and maintenance (washing).

9.4 Applications/Examples

Traditionally textile and garment production were organized as a more or less independent series of production steps that finally deliver the product, e.g. fiber production, yarn production, fabric production, textile chemical treatments (dyeing, finishing), and assembly of different components to obtain the final product, e.g. garment, home textile, and technical product.

The integration of wearable electronics requires a reconsideration of a product with regard to the desired functionality.

9.4.1 Material Selection

Selection and combination of conductive material is dependent on the conditions applied during use and maintenance, e.g. mechanical stress, bending cycles, elongation, compression, and abrasive effects. The selection of conductive materials has to consider the conditions applied during washing, e.g. temperature, mechanics, and chemical present during laundry and tumbler drying. Even when individual components are resistant to the conditions in use, corrosion can appear through galvanic element formation when incompatible materials have been connected, e.g. copper/steel/aluminum.

The final position of sensor elements in the garment defines the presence and position of integrated electrical lines in the fabric, which has to be produced and positioned during cutting of pieces in such an order that the lines will appear in right form at the appropriate part of the garment only. In the same way application of embroidery techniques and printing techniques has to be arranged into the production steps to form the final functional element through localized processing.

The overall concept of a smart textile depends on the function to be delivered. Relevant aspects that define the design are:

- *Energy consumption*: Devices that consume low amounts of energy, e.g. sensors, or switches or identification devices can be designed to operate with minimum energy consumption, which permits power generation through energy harvesting using textile-based antennas or piezoelectric effects. In applications where larger amounts of power have to be transferred in textile structures, e.g. electrical heat generation, the flexible connections have to be powerful and mechanically resistant to avoid interrupts, which could cause the risk of hot spots and short circuits. Devices for high power application usually will use metal wires or metal fiber-based yarns for energy transfer, while low energy applications permit use of coatings, conductive films, and prints.
- *Dimension of electronic components*: The functionality defines the dimension of the electronic elements, which can be fully integrated and cased or has to be built as separated unit that is disconnected before laundry. RFID devices that harvest sufficient energy to deliver a signal for identification can be built in the form of a fully coated tag that is integrated as washable device into the textile. Devices that contain sensors or switches connected to microcomputer often are built as separable units, which contain the electronic device as removable component, which are disconnected before use. As an example miniaturized electronic elements were placed on narrow stripes, which then were integrated into textile structures, e.g. through wrapping, weaving, or embroidery [87].
- *Functionality and transfer*: While Radio Frequency Identification (RFID) tags can be miniaturized and operated with minimal energy requirements, other devices, e.g. monitoring of electrocardiogram (ECG), will require conductive elements that form connections to the skin as well as to the evaluating electronic device. Thus combinations of conductive materials will be assembled to build the final product, e.g. skin electrodes, conductive lines inside the textile structure, and connections to the data acquisition unit [88].

The examples given must be understood as representatives to demonstrate the wide range of material concepts as well as applications.

9.4.2 Washable Sensors (Example: Moisture Bed Sensor)

For support of caregivers in care homes, a washable incontinence detector has been built up for detection of conductive liquids (urine) during sleep. For corrosion resistance and to achieve washability at 80–90 °C, the sensor textile was produced from stainless steel yarns using embroidery techniques (Figure 9.9). The connection to the electronic device is achieved through press buttons, which allow disconnection of the sensor textile for washing, while the electronic remains fixed to the bed of a patient.

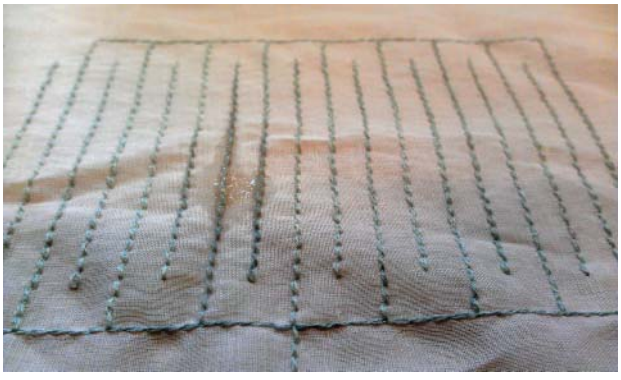


Figure 9.9 Washable wetness sensor for bedding (embroidered stainless steel).

9.4.3 Textile Electrodes

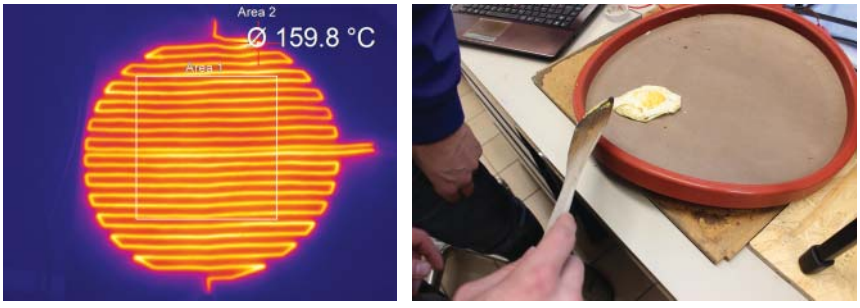
3D structures can replace metal film electrodes in batteries, which allows production of thicker coatings on electrodes. Figure 9.10 shows a current collector made of copper wires, coated with carbon, designed to serve as cathode for lithium-iron phosphate batteries.

The application of carbon felt and other nonwoven structures for application as current collectors in energy storage has been studied in detail. The use of such devices for flexible batteries and also in supercapacitors has been investigated in detail [89–94].

Another example on textile based conductive structure is demonstrated by the round-shaped flexible heating element which is produced by embedding an embroidered metal yarn heating structure into a silicone layer. As a result a flexible pan was obtained, which could reach temperatures above 150 °C (Figure 9.11).



Figure 9.10 Embroidered textile current collector (copper wire) coated with carbon for Li-$FePO_4$ batteries.



(a) (b)

Figure 9.11 Thermographic photo of a flexible heating pan (a) and in use for frying and egg (b).

9.4.4 Flexible Devices

An example for combination of several technological approaches is given by Dias and Monaragla, who could prepare electroluminescent threads by a combination of several approaches. A core–shell construction of a yarn was coated with a dielectric paste and a phosphor ink and finally wrapped with a thin copper wire. The system is operated with alternating current and permits integration of luminescent devices, e.g. into car interior. Through its complex structure the material will exhibit sensitivity to strain and abrasion; thus coverage through coating will be required to improve mechanical stability [95].

9.4.5 Wearable Electronics

Medical applications and therapy form a central field of application for wearable electronics as the added value of such devices can be demonstrated directly. Representative examples are integration of ECG electrodes in clothing in long-term observation [96, 97] and integrated stimulation electrodes for rehabilitation and therapy [98, 99].

9.4.6 Summary and Future Trends

During the last 20 years, a lot of different concepts for conductive materials has been developed by scientists and partly scaled up to commercial application. Technicians today may choose from organic polymers, semiconductors, and metal-based material. Dependent on the production scheme, the implementation of a conductive element can be undertaken during the production of a textile fabric, e.g. in the form of conductive yarns or metal wires, or applied at a late stage, e.g. in the form of prints with conductive inks or embroidery elements. This allows deep integration of smart electronic devices in textiles through combination of different techniques and materials. As a result important textile characteristics such as flexibility and elasticity can be maintained.

The toolkit of conductive fibers available can be understood as the first and highly relevant step for the future production of smart textiles for a wide range of applications.

Future trends in the development of conductive fibers for smart textiles will include the following aspects:

- Miniaturization of conductive lines to the dimension of fibers will be important to reducing dimensions of devices further.
- At present many functional elements, sensors, actuators, and other devices are still understood as technically designed functional element, which offers limited potential for miniaturization or integration. Size reduction to the dimension of threads and formation of flexible structures will facilitate the placement of devices during fabric production.
- Devices with minimum energy consumption and elements of energy harvesting will reduce dimensions of conductive elements, e.g. for local power supply and wireless signal transfer. Wireless communication and data reading further will contribute to the miniaturization of smart electronic elements in textiles.
- Conductive fibers will play a significant role in all applications that include transfer of electrical current and line-based information transfer.

In any case the further development of smart textile products will require the formation of development consortia including expertise from electronics, information technology, textiles, and materials sciences. Isolated developments will be rare, and successful concepts will require consortia built with complementary expertise. From the point of textile production, the formation of a functional electronic element will be based on a series of organized steps placed along the value added chain, e.g. spinning, fabric formation, printing, embroidery, and garment technology, which finally will lead to an electronic device with maximum level of integration.

References

1 Bobeth, W. (1993). *Textile Faserstoffe: Beschaffenheit und Eigenschaften*. Berlin, Heidelberg: Springer-Verlag.
2 Geetha, S., Satheesh Kumar, K.K., Rao, C.R.K. et al. (2009). EMI shielding: methods and materials—A review. *Journal of Applied Polymer Science* 112: 2073–2086. https://doi.org/10.1002/app.29812.
3 Nakata, M., Taga, M., and Kise, H. (1992). Synthesis of electrical conductive polypyrrole films by interphase oxidative polymerization—effects of polymerization temperature and oxidizing agents. *Polymer Journal* 24 (5): 437–441.
4 Stejskal, J., Riede, A., Hlavatá, D. et al. (1998). The effect of polymerization temperature on molecular weight, crystallinity, and electrical conductivity of polyaniline. *Synthetic Metals* 96 (1): 55–61. https://doi.org/10.1016/S0379-6779(98)00064-2.
5 Lenz, J., Schurz, J., and Eichinger, D. (1994). Properties and structure of Lyocell and viscose type fibres in the swollen state. *Lenzinger Berichte* 7: 19–25.

6 Zhang, K. and Ge, M. (2016). Preparation and characterization of PA6/titania conductive fibres. *Indian Journal of Fibre and Textile Research* 41 (2): 150–155.

7 James, E.S. (1936). Metal reducing method. US Patent 2, 050, 298.

8 Grisley, F. (1936). Improvements in blankets, pads, quilts, clothing, fabric, or the like, embodying electrical conductors. UK Patent GB445195.

9 Costanzo, R.J. (1936). Electrically heated socks. UK Patent GB1128224.

10 Aguiló-Aguayo, N. and Bechtold, T. (2014). Characterisation of embroidered 3D electrodes by use of anthraquinone-1,5-disulfonic acid as probe system. *Journal of Power Sources* 254C: 224–231.

11 Lenninger, M., Froeis, T., Scheiderbauer, M. et al. (2013). High current density 3D-electrodes manufactured by technical embroidery. *Journal of Solid State Electrochemistry* 17 (8): 2303–2309.

12 Celik Bedeloglu, A. and Sunter, N. (2013). Investigation of polyacrylic/metal wire composite yarn characteristics manufactured on fancy yarn machine. *Materials and Manufacturing Processes* 28 (6): 650–656. https://doi.org/10.1080/10426914.2012.727118.

13 Guo, L., Berglin, L., and Mattila, H. (2012). Improvement of electro-mechanical properties of strain sensors made of elastic-conductive hybrid yarns. *Textile Research Journal* 82 (19): 1937–1947. https://doi.org/10.1177/0040517512452931.

14 Schwarz, A., Hakuzimana, J., Gasana, E. et al. (2008). Gold coated polyester yarn. *Advances in Science and Technology* 60: 47–51.

15 Schwarz, A., Hukazimana, J., Kaczynska, A. et al. (2010). Gold coated yarns through electroless deposition. *Surface and Coatings Technology* 204: 1214–1418.

16 Kalanyan, B., Oldham, C.J., Sweet, W.J. III,, and Parsons, G.N. (2013). Highly conductive and flexible nylon-6 nonwoven fiber mats formed using tungsten atomic layer deposition. *ACS Applied Materials & Interfaces* 5 (11): 5253–5259. https://doi.org/10.1021/am401095r.

17 Mundy, J.Z., Shafiefarhood, A., Li, F. et al. (2016). Low temperature platinum atomic layer deposition on nylon-6 for highly conductive and catalytic fiber mats. *Journal of Vacuum Science an Technology, A: Vacuum, Surfaces, and Films* 34 (1): 01A152/1–01A152/6. https://doi.org/10.1116/1.4935448.

18 Karaguzel, B., Merritt, C.R., Kang, T. et al. (2008). Utility of nonwovens in the production of integrated electrical circuits via printing conductive inks. *Journal of The Textile Institute* 99: 37–45.

19 Araki, T., Nogi, M., Suganuma, K. et al. (2011). Printable and stretchable conductive wirings comprising silver flakes and elastomers. *IEEE Electron Device Letters* 32: 1424–1426.

20 Romaguera, V.S., Madec, M.B., and Yeates, S.G. (2009). Inkjet printing of conductive polymers for smart textiles and flexible electronics. *Materials Research Society Symposium Proceedings* 1192: 26–31.

21 Rai, P., Lee, J., Mathur, G.N., and Varadan, V.K. (2012). Carbon nanotubes polymer nanoparticle inks for healthcare textile. *Proceedings of SPIE* 8548 https://doi.org/10.1117/12.946253.

22 Rai, P., Kumar, P.S., Oh, S. et al. (2012). Smart healthcare textile sensor system for unhindered-pervasive health monitoring. *Proceedings of SPIE* 8344 https://doi.org/10.1117/12.921253.

23 Yang, K., Torah, R., Wei, Y. et al. (2013). Waterproof and durable screen printed silver conductive tracks on textiles. *Textile Research Journal* 83 (19): 2023–2031. https://doi.org/10.1177/0040517513490063.

24 Kardarian, K., Busani, T., Osorio, I. et al. (2014). Sintering of nanoscale silver coated textiles, a new approach to attain conductive fabrics for electromagnetic shielding. *Materials Chemistry and Physics* 147 (3): 815–822. https://doi.org/10.1016/j.matchemphys.2014.06.025.

25 Lee, J., Kwon, H., Seo, J. et al. (2015). Conductive fiber-based ultrasensitive textile pressure sensor for wearable electronics. *Advanced Materials (Weinheim, Germany)* 27 (15): 2433–2439. https://doi.org/10.1002/adma.201500009.

26 Montazer, M. and Komeily Nia, Z. (2015). Conductive nylon fabric through in situ synthesis of nano-silver: preparation and characterization. *Materials Science and Engineering, C: Materials for Biological Applications* 56: 341–347. https://doi.org/10.1016/j.msec.2015.06.044.

27 Wei, Y., Chen, S., Yuan, X. et al. (2016). Multiscale wrinkled microstructures for piezoresistive fibers. *Advanced Functional Materials* 26 (28): 5078–5085. https://doi.org/10.1002/adfm.201600580.

28 Krishnanand, K., Thite, A., and Mukhopadhyay, A.K. (2016). Electro-conductive cotton fabric prepared by electron beam induced graft polymerization and electroless deposition technology. *Journal of Applied Polymer Science* 133: 44576. https://doi.org/10.1002/app.44576.

29 Liu, S., Hu, M., and Yang, J. (2016). A facile way of fabricating a flexible and conductive cotton fabric. *Journal of Materials Chemistry C* 4: 1320–1325. https://doi.org/10.1039/C5TC03679H.

30 Li, Y. (ed.) (2015). *Organic Optoelectronic Materials*. Springer. ISBN: 978-3-319-16861-6.

31 IUPAC Gold Book. *Compendium of Chemical Terminology*. International Union of Pure and Applied Chemistry. http://publications.iupac.org/compendium/index.html.

32 Malinauskas, A. (2001). Chemical deposition of conducting polymers. *Polymer* 42: 3957–3972.

33 Li, H., Shi, G., Ye, W. et al. (1997). Polypyrrole-carbon fibre composite film prepared by chemical oxidative polymerization of pyrrole. *Journal of Applied Polymer Science* 64: 2149–2154.

34 Huang, G., Liu, L., Wang, R. et al. (2016). Smart color-changing textile with high contrast based on a single-sided conductive fabric. *Journal of Materials Chemistry C: Materials for Optical and Electronic Devices* 4 (32): 7589–7594. https://doi.org/10.1039/C6TC02051H.

35 Kim, B.C., Innis, P.C., Wallace, G.G. et al. (2013). Electrically conductive coatings of nickel and polypyrrole/poly(2-methoxyaniline-5-sulfonic acid) on nylon Lycra textiles. *Progress in Organic Coatings* 76 (10): 1296–1301. https://doi.org/10.1016/j.porgcoat.2013.04.004.

36 Firoz Babu, K., Siva Subramanian, S.P., and Anbu Kulandainathan, M. (2013). Functionalisation of fabrics with conducting polymer for tuning capacitance and fabrication of supercapacitor. *Carbohydrate Polymers* 94 (1): 487–495. https://doi.org/10.1016/j.carbpol.2013.01.021.

37 Molina, J., Esteves, M.F., Fernandez, J. et al. (2011). Polyaniline coated conducting fabrics. Chemical and electrochemical characterization. *European Polymer Journal* 47 (10): 2003–2015. https://doi.org/10.1016/j.eurpolymj.2011.07.021.

38 Anbarasan, R., Vasudevan, T., Kalaignan, G.P., and Gopalan, A. (1999). Chemical grafting of aniline and o-toluidine onto poly(ethylene terephthalate) fibre. *Journal of Applied Polymer Science* 73: 121–128.

39 Yin, X., Kobayashi, K., Yoshino, K. et al. (1995). Percolation conduction in polymer composites containing polypyrrole coated insulating polymer fibre and conducting polymer. *Synthetic Metals* 69: 367–368.

40 Bhadani, S.N., Sen Gupta, S.K., Sahu, G.C., and Kumari, M. (1996). Electrochemical formation of some conducting fibres. *Journal of Applied Polymer Science* 61: 207–212.

41 Hiltunen, M., Pelto, J., Ellae, V., and Kellomaeki, M. (2016). Uniform and electrically conductive biopolymer-doped polypyrrole coating for fibrous PLA. *Journal of Biomedical Materials Research, Part B: Applied Biomaterials* 104 (8): 1721–1729. https://doi.org/10.1002/jbm.b.33514.

42 McGraw, S.K., Alocilja, E., Senecal, A., and Senecal, K. (2012). Synthesis of a functionalized polypyrrole coated electrotextile for use in biosensors. *Biosensors* 2: 465–478. https://doi.org/10.3390/bios2040465.

43 Montarsolo, A., Varesano, A., Mossotti, R. et al. (2012). Enhanced adhesion of conductive coating on plasma-treated polyester fabric: a study on the ageing effect. *Journal of Applied Polymer Science* 126 (4): 1385–1393. https://doi.org/10.1002/app.36762.

44 Opwis, K., Knittel, D., and Gutmann, J.S. (2012). Oxidative in situ deposition of conductive PEDOT:PTSA on textile substrates and their application as textile heating element. *Synthetic Metals* 162 (21–22): 1912–1918. https://doi.org/10.1016/j.synthmet.2012.08.007.

45 Mattana, G., Cosseddu, P., Fraboni, B. et al. (2011). Organic electronics on natural cotton fibres. *Organic Electronics* 12 (12): 2033–2039. https://doi.org/10.1016/j.orgel.2011.09.001.

46 Bashir, T., Skrifvars, M., and Persson, N.-K. (2011). Production of highly conductive textile viscose yarns by chemical vapor deposition technique: a route to continuous process. *Polymers for Advanced Technologies* 22 (12): 2214–2221. https://doi.org/10.1002/pat.1748.

47 Aakerfeldt, M., Straaaat, M., and Walkenstroem, P. (2013). Electrically conductive textile coating with a PEDOT-PSS dispersion and a polyurethane binder. *Textile Research Journal* 83 (6): 618–627. https://doi.org/10.1177/0040517512444330.

48 Wu, C.-H., Shen, H.-P., Don, T.-M., and Chiu, W.-Y. (2013). Fabrication of flexible conductive films derived from poly(3,4-ethylenedioxythiophene)-poly(styrenesulfonic acid) (PEDOT:PSS) on the nonwoven fabrics substrate. *Materials Chemistry and Physics* 143 (1): 143–148. https://doi.org/10.1016/j.matchemphys.2013.08.037.

49 Cohen David, N., David, Y., Katz, N. et al. (2016). Electro-conductive fabrics based on dip coating of cotton in poly(3-hexylthiophene). *Polymers for Advanced Technologies* https://doi.org/10.1002/pat.3857.

50 Soroudi, A., Skrifvars, M., and Liu, H. (2011). Polyaniline-polypropylene melt-spun fiber filaments: the collaborative effects of blending conditions and fiber draw ratios on the electrical properties of fiber filaments. *Journal of Applied Polymer Science* 119 (1): 558–564. https://doi.org/10.1002/app.32655.

51 Li, X., Sun, P., Fan, L. et al. (2012). Multifunctional graphene woven fabrics. *Scientific Reports* 2: 395.

52 Shateri-Khalilabad, M. and Yazdanshenas, M.E. (2013). Fabricating electroconductive cotton textiles using graphene. *Carbohydrate Polymers* 96: 190–195.

53 Woltornist, S.J., Alamer, F.A., McDannald, A. et al. (2015). Preparation of conductive graphene/graphite infused fabrics using an interface trapping method. *Carbon* 81: 38–42. https://doi.org/10.1016/j.carbon.2014.09.020.

54 Yoo, H.J., Kim, H.H., Cho, J.W., and Kim, Y.H. (2012). Surface morphology and electrical properties of polyurethane nanofiber webs spray-coated with carbon nanotubes. *Surface and Interface Analysis* 44 (4): 405–411. https://doi.org/10.1002/sia.3817.

55 Seyedin, S., Razal, J.M., Innis, P.C., and Wallace, G.G. (2016). A facile approach to spinning multifunctional conductive elastomer fibres with nanocarbon fillers. *Smart Materials and Structures* 25 (3): 035015/1–035015/9. https://doi.org/10.1088/0964-1726/25/3/035015.

56 Ebrahimbeiki Chimeh, A. and Montazer, M. (2016). Fabrication of nano-TiO_2/carbon nanotubes and nano-TiO_2/nanocarbon black on alkali hydrolyzed polyester producing photoactive conductive fabric. *Journal of the Textile Institute* 107 (1): 95–106. https://doi.org/10.1080/00405000.2015.1012881.

57 Jin, X., Xiao, C., An, S. et al. (2006). Preparation and properties of a new coating method for preparing conductive polyester fibers with permanent conductivity. *Journal of Applied Polymer Science* 102: 2685–2691. https://doi.org/10.1002/app.24095.

58 Park, G., Jung, Y., Lee, G.-W. et al. (2012). Carbon nanotube/poly(vinyl alcohol) fibers with a sheath-core structure prepared by wet spinning. *Fibers and Polymers* 13 (7): 874–879. https://doi.org/10.1007/s12221-012-0874-5.

59 Nilsson, E., Oxfall, H., Wandelt, W. et al. (2013). Melt spinning of conductive textile fibers with hybridized graphite nanoplatelets and carbon black filler. *Journal of Applied Polymer Science* 130 (4): 2579–2587. https://doi.org/10.1002/app.39480.

60 Lin, J.-H., Lin, Z.-I., Pan, Y.-J. et al. (2016). Manufacturing techniques and property evaluations of conductive composite yarns coated with polypropylene and multi-walled carbon nanotubes. *Composites Part A: Applied Science*

and Manufacturing 84: 354–363. https://doi.org/10.1016/j.compositesa.2016.02.004.

61 Bautista-Quijano, J.R., Poetschke, P., Bruenig, H., and Heinrich, G. (2016). Strain sensing, electrical and mechanical properties of polycarbonate/multiwall carbon nanotube monofilament fibers fabricated by melt spinning. *Polymer* 82: 181–189. https://doi.org/10.1016/j.polymer.2015.11.030.

62 Thüringen-GreenTec (2012). Project-Nr. 2012 FE 9001., Verbund-Nr.: 2012 VF 0001: Erzeugung hochelastischer metallisierter Fasern als Grundbaustein für textilbasierte elektronische Komponenten durch kontinuierliche Laser- und elektrochemische Strukturierung von metallisierten Monofilamenten. Teilprojekt: Technologieentwicklung zur Erzeugung von metallisierten Monofilamenten auf der Basis von Spezialpolymeren – Lasertex.

63 Hu, B., Li, D., Manandharm, P. et al. (2012). CNT/conducting polymer composite conductors impart high flexibility to textile electroluminescent devices. *Journal of Materials Chemistry* 22 (4): 1598–1605. https://doi.org/10.1039/C1JM14121J.

64 Berendjchi, A., Khajavi, R., Yousefi, A.A., and Yazdanshenas, M.E. (2016). Improved continuity of reduced graphene oxide on polyester fabric by use of polypyrrole to achieve a highly electro-conductive and flexible substrate. *Applied Surface Science* 363: 264–272. https://doi.org/10.1016/j.apsusc.2015.12.030.

65 Bae, J. and Hong, K.H. (2012). Electrical properties of conductive fabrics for operating capacitive touch screen displays. *Textile Research Journal* 83 (4): 329–336. https://doi.org/10.1177/0040517512464298.

66 Kursun Bahadir, S. and Jevšnik, S. (2016). Optimization of hot air welding process parameters for manufacturing textile transmission lines for e-textiles applications: Part I: Electro-conductive properties. *Textile Research Journal* 87 (2): 232–243. https://doi.org/10.1177/0040517516629140.

67 Ding, J.T.F., Tao, X., Au, W.M., and Li, L. (2014). Temperature effect on the conductivity of knitted fabrics embedded with conducting yarns. *Textile Research Journal* 84 (17): 1849–1857. https://doi.org/10.1177/0040517514530026.

68 Jeong, M.J., Yun, T.-I., Baek, J.J., and Kim, Y.T. (2015). Wireless power transmission using a resonant coil consisting of conductive yarn for wearable devices. *Textile Research Journal* 86 (14): 1543–1548. https://doi.org/10.1177/0040517515586163.

69 Kang, T.S., Lee, S.W., and Joo, J. (2005). Electrically conducting polypyrrole fibers spun by electrospinning. *Synthetic Metals* 153: 61–64.

70 Li, M., Guo, Y., and Wei, Y. (2006). Electrospinning polyaniline-contained gelatin nanofibers for tissue engineering applications. *Biomaterials* 27: 2705–2715.

71 Cardenas, J.R., Franca, M.G.O., and Vasconcelos, E.A. (2007). Growth of sub-micron fibres of pure polyaniline using the electrospinning technique. *Journal of Physics D: Applied Physics* 40: 1068–1071.

72 Hong, K.H. and Kang, T.J. (2006). Polyaniline–nylon 6 composite nanowires prepared by emulsion polymerization and electrospinning process. *Journal of Applied Polymer Science* 99: 1277–1286.

73 Hong, K.H., Oh, K.W., and Kang, T.J. (2005). Preparation of conducting nylon-6 electrospun fiber webs by the in situ polymerization of polyaniline. *Journal of Applied Polymer Science* 96: 983–991.

74 Choi, S.S., Chu, B.Y., and Hwang, D.S. (2005). Preparation and characterization of polyaniline nanofiber webs by template reaction with electrospun silica nanofibers. *Thin Solid Films* 477: 233–239.

75 McKeon, K.D., Lewis, A., and Freeman, J.W. (2010). Electrospun poly(D,L-lactide) and polyaniline scaffold characterization. *Journal of Applied Polymer Science* 115: 1566–1572.

76 Laforgue, A. and Robitaille, L. (2008). Fabrication of poly-3-hexylthiophene/polyethylene oxide nanofibers using electrospinning. *Synthetic Metals* 158: 577–584.

77 Lu, M., Xie, R., Liu, Z. et al. (2016). Enhancement in electrical conductive property of polypyrrole-coated cotton fabrics using cationic surfactant. *Journal of Applied Polymer Science* 133 (32) https://doi.org/10.1002/app.43601.

78 Shim, B.S., Chen, W., Doty, C. et al. (2008). Smart electronic yarns and wearable fabrics for human biomonitoring made by carbon nanotube coating with polyelectrolytes. *Nano Letters* 8: 4151–4157.

79 Nilsson, E., Rigdahl, M., and Hagström, B. (2015). Electrically conductive polymeric bi-component fibers containing a high load of low-structured carbon black. *Journal of Applied Polymer Science* 132: 42255. https://doi.org/10.1002/app.42255.

80 Härdelin, L. and Hagström, B. (2015). Wet spun fibers from solutions of cellulose in an ionic liquid with suspended carbon nanoparticles. *Journal of Applied Polymer Science* 132: 41417. https://doi.org/10.1002/app.41417.

81 Maiellaro, G., Ragonese, E., Gwoziecki, R. et al. (2013). Ambient light organic sensor in a printed complementary organic TFT technology on flexible plastic foil. *IEEE Transactions on Circuits and Systems I* 61: 1036–1043.

82 Lee, J. (2015). Conductive fiber-bases ultrasensitive textile pressure for wearable electonics. *Advanced Materials* 27: 2433–2439.

83 Kim, S.M., Kim, I.Y., and Kim, H.R. (2017). Production of electromagnetic shielding fabrics by optimization of electroless silver plating conditions for PET fabrics. *Journal of the Textile Institute* 108 (6): 1065–1073. https://doi.org/10.1080/00405000.2016.1219449.

84 Schwarz, A., Hakuzimana, J., Westbroek, P. et al. (2012). A study on the morphology of thin copper films on para-aramid yarns and their influence on the yarn's electro-conductive and mechanical properties. *Textile Research Journal* 82 (15): 1587–1596, 10 pp. DOI:https://doi.org/10.1177/0040517511431291.

85 Mohammadian, M., Afzali, A., Mottaghitalab, V., and Haghi, A.K. (2012). Washing and rubbing fastness of electroless plated polyester conductive fabric. *Materiale Plastice (Bucharest, Romania)* 49 (3): 182–185.

86 Lee, H.M., Choi, S., Jung, A., and Ko, S. (2013). Highly conductive aluminum textile and paper for flexible and wearable electronics. *Angewandte Chemie International Edition* 52 (30): 7718–7723. https://doi.org/10.1002/anie.201301941.

87 Zysset, C., Kinkeldei, T., Muenzenrieder, N. et al. (2013). Combining electronics on flexible plastic strips with textiles. *Textile Research Journal* 83 (11): 1130–1142. https://doi.org/10.1177/0040517512468813.

88 Kannaian, T., Neelaveni, R., and Thilagavathi, G. (2013). Design and development of embroidered textile electrodes for continuous measurement of electrocardiogram signals. *Textile Research Journal* 42 (3): 303–318. https://doi.org/10.1177/1528083712438069.

89 Fan, T., Zhao, C., Xiao, Z. et al. (2016). Fabricating of high-performance functional graphene fibers for micro-capacitive energy storage. *Scientific Reports* 6: 29534. https://doi.org/10.1038/srep29534.

90 Xie, K., Zhang, K., Han, Y. et al. (2016). A novel TiO_2-wrapped activated carbon fiber/sulfur hybrid cathode for high performance lithium sulfur batteries. *Electrochimica Acta* 210: 415–421. https://doi.org/10.1016/j.electacta.2016.05.172.

91 Cheng, X., Zhang, J., Ren, J. et al. (2016). Design of a hierarchical ternary hybrid for a fiber-shaped asymmetric supercapacitor with high volumetric energy density. *Journal of Physical Chemistry C* 120 (18): 9685–9691. https://doi.org/10.1021/acs.jpcc.6b02794.

92 Ma, K., Cheng, J.P., Liu, F., and Zhang, X. (2016). Co-Fe layered double hydroxides nanosheets vertically grown on carbon fiber cloth for electrochemical capacitors. *Journal of Alloys and Compounds* 679: 277–284. https://doi.org/10.1016/j.jallcom.2016.04.059.

93 Zhang, Y., Hu, Z., An, Y. et al. (2016). High-performance symmetric supercapacitor based on manganese oxyhydroxide nanosheets on carbon cloth as binder-free electrodes. *Journal of Power Sources* 311: 121–129. https://doi.org/10.1016/j.jpowsour.2016.02.017.

94 Dong, L., Xu, C., Li, Y. et al. (2016). Simultaneous production of high-performance flexible textile electrodes and fiber electrodes for wearable energy storage. *Advanced Materials (Weinheim, Germany)* 28 (8): 1675–1681. https://doi.org/10.1002/adma.201504747.

95 Dias, T. and Monaragla, R. (2012). Development and analysis of novel electroluminescent yarns and fabrics for localized automotive interior illumination. *Textile Research Journal* 82 (11): 1164–1176. https://doi.org/10.1177/0040517511420763.

96 Cho, H., Lim, H., Cho, S., and Lee, J. (2015). Development of textile electrode for electrocardiogram measurement based on conductive electrode configuration. *Fibers and Polymers* 16 (10): 2148–2157. https://doi.org/10.1007/s12221-015-5317-7.

97 Trindade, I.G., Martins, F., and Baptista, P. (2015). High electrical conductance poly(3,4-ethylenedioxythiophene) coatings on textile for electrocardiogram monitoring. *Synthetic Metals* 210 (Part_B): 179–185. https://doi.org/10.1016/j.synthmet.2015.09.024.

98 Aakerfeldt, M., Lund, A., and Walkenstroem, P. (2015). Textile sensing glove with piezoelectric PVDF fibers and printed electrodes of PEDOT:PSS. *Textile Research Journal* 85 (17): 1789–1799. https://doi.org/10.1177/0040517515578333.

99 Zieba, J., Frydrysiak, M., and Tokarska, M. (2011). Research of textile electrodes for electrotherapy. *Fibres & Textiles in Eastern Europe* 19 (5): 70–74.

10

Phase Change Fibers

Subrata Mondal

National Institute of Technical Teachers' Training and Research, Department of Mechanical Engineering, FC Block, Sector III, Salt Lake City, Kolkata, 700106, West Bengal, India

10.1 Introduction

In the last few decades, there are tremendous research activities to search efficient systems for the energy storage. Among the various energy storage systems (ESS), thermal energy storage (TES) is an attractive way to reduce the imbalance between energy supply and demand. Thermal ESS could be based on latent heat storage (LHS), sensible heat storage (SHS), and thermochemical heat storage processes. In the SHS materials, storage of energy is associated with the rise in temperature of TES materials either in liquid or solid form. Thermal energy would store/release in the LHS system, when it undergoes phase change from solid to liquid and vice versa. However, energy would store after reversible chemical reaction between the substances in the thermochemical ESS [1–4]. Phase change materials (PCMs) based on LHS system is an attractive way of storing thermal energy. PCM based on LHS system has two major advantages, viz. high energy storage density and isothermal nature of the storage process [5].

Nowadays, consumers are not only looking for the aesthetic look for their garments, but they are also looking for the added functionality to their garments specially comfort and ergonomic. Functional textiles are end users' requirement specific and can be tailored to achieve performance requirement of users' specific purposes. These textiles are specially tailored to perform a predefined functionality above its normal functions. Functional or interactive textiles induce shift from the passive to the active functionality [6].

The recent advances of various smart materials have opened up opportunities for many areas in the advanced material fields. PCM is one such type of smart materials gaining momentum for the applications in temperature regulating and thermal balance of advanced material applications [6]. This chapter aims to provide an overview for the principle of PCMs, various types of PCMs, PCMs for thermal management, and various techniques to prepare phase change fibrous structures and their applications in advanced material fields with a special focus on thermoregulating textiles.

Handbook of Fibrous Materials, First Edition. Edited by Jinlian Hu, Bipin Kumar, and Jing Lu.
© 2020 Wiley-VCH Verlag GmbH & Co. KGaA. Published 2020 by Wiley-VCH Verlag GmbH & Co. KGaA.

10.2 Phase Change Materials (PCMs)

PCMs are high heat of fusion and heat of solidification substances which melt or solidify at a certain temperature range. Therefore, PCMs are capable of storing and releasing large amounts of heat energy upon its phase changes. When the material changes from solid to liquid and vice versa, the heat is absorbed or released. Therefore, PCMs are classified as LHS materials. LHS can be achieved through (i) liquid–solid, (ii) solid–liquid, (iii) solid–gas, (iv) liquid–gas, and (v) solid–solid phase changes. However, only solid–liquid and vice versa phase changes of PCMs are suitable for practical applications [6].

10.2.1 Principle of Phase Change Materials

Solid to liquid or vice versa PCMs are used practically for the development of smart materials. Liquid to gas PCMs are not used for practical applications due to the large volume changes or high pressure required to store the materials in gas phase. However, solid to solid PCMs are not practical due to too low heat storage or release during the phase change processes. PCMs can absorb (and store) and release heat while the materials change from solid to liquid or vice versa. The amount of energy absorbed or released depends on the value of heat of fusion (ΔH_f) or heat of solidification (or heat of crystallization) (ΔH_c), respectively. Heat of fusion and heat of solidification or heat of crystallization can be measured by using differential scanning calorimetry (DSC) in heating and cooling cycles, respectively (Figure 10.1). The temperature of a PCM remains constant during the phase change processes (Figure 10.2) [6].

PCMs have enormous potential for the development of thermoregulating textiles. The heat exchange of textiles with the human body parts and the environment plays a major role for the thermal state of the human body. In general, thermal comfort is defined as the perception of mind that expresses satisfaction with the thermal environment, whereas dissatisfaction may be caused by warm/cold discomfort for the body [3, 7]. However, thermal dissatisfaction may

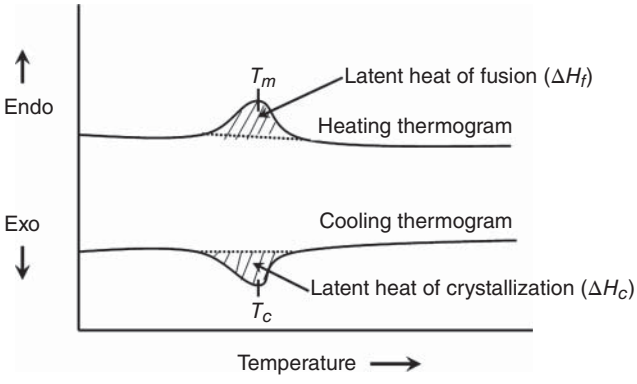


Figure 10.1 Schematic of DSC heating and cooling thermograms for PCMs (T_m, crystal melting temperature; T_c, crystallization temperature).

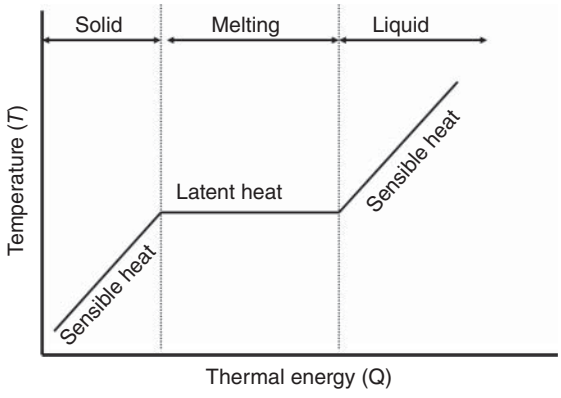


Figure 10.2 Thermal energy vs. temperature of solid–liquid phase changes.

also be caused by an unwanted heating or cooling of particular part of the body (local discomfort). Transfer of dry heat from a textile is complex process, which involves conduction, convection, and radiation mode of heat transfer [8]:

$$H_{\text{dry}} = M - W - C_{\text{res}} - E_{\text{res}} - E - S$$

where H_{dry} is the dry heat loss, M is the metabolic rate, W is the external work, C_{res} is the convective respiratory heat loss, E_{res} is the evaporative respiratory heat loss, E is the evaporative heat loss from the skin, and S is the change in body heat content, in which all values are expressed in W/m^2.

The movement of thermal energy through a textile is an important factor for the comfort. The human body would attempt to maintain a core body temperature around 37 °C. The balance between heat productions by the body and heat loss to the environment is the comfort factor. The body would be in a state of comfort when the body temperature is slightly below the core body temperature, and there is no moisture on the skin [9]. The loss of heat through perspiration and heat flux through fabrics are very important for the comfort of the wearer [10, 11].

TES is a process for high or low temperature ESS for later use; hence, TES bridges the time gap between energy requirements and energy use. Therefore, apart from the advanced textile fields, PCM could also be applicable in other advanced materials applications. Thermoregulating effect of PCM incorporated material would result from either heat absorption or release of the PCMs, which could be incorporated into the fibrous structure. An active thermal barrier effect may result from either heat absorption or heat emission of the PCMs of PCM incorporated materials, which regulates with the surrounding environment and, subsequently, adopts it to the thermal needs (i.e. activity level and ambient temperature) [12].

10.2.2 Various Types of Phase Change Materials

Simple and classical example of a PCM is water, and its various phases are ice (solid), liquid water (liquid), and steam (gas). PCMs could be classified into three categories such as (i) organic PCMs, (ii) inorganic PCMs, and (iii) eutectic PCMs of organic–organic, organic–inorganic, and inorganic–inorganic mixtures.

Table 10.1 Melting point temperature and latent heat of absorption for various PCMs.

Materials	Melting point (°C)	Latent heat of absorption, ΔH (J/g)	References
Organic PCMs			
n-Octadecane	35.6	233.8	[3]
n-Hexadecane	22.0	185.3	[3]
Capric acid	30.2	142.7	[13]
Tetradecanol	37.0	207.3	[13]
Lauric acid	43.2	177.7	[13]
Butyl stearate	19	200	[14]
Inorganic PCMs			
Glauber salt	32.4	254	[15]
$CaCl_2 \cdot 6H_2O$	29	190.8	[16]
Eutectic PCMs			
Lauric and stearic acid (75.5 : 24.5%)	37	182.7	[17]
Tetradecanol and capric acid (38 : 62%)	22.74	153.4	[13]
Tetradecanol and lauric acid (53.6 : 46.4%)	26.59	162.7	[13]
Tetradecanol and myristic acid (71.84 : 28.16%)	36.46	208	[13]

10.2.2.1 Organic PCMs

Organic PCMs commonly belong to two groups, viz. paraffin and fatty acids. Some of the organic PCMs with their melting point temperature and heat of absorption are presented in Table 10.1. Paraffin is linear alkanes with chemical formula of C_nH_{2n+2}. PCM based on paraffin has good TES capability per unit mass with little or no subcooling. Paraffinic PCMs are widely used to prepare the thermoregulated advanced materials due to their several outstanding properties such as noncorrosiveness, chemical and thermal stability, and low subcooling [18]. Polyethylene glycol (PEG) with appropriate molecular weight could also be used as PCMs for manufacturing thermoregulated fibrous structures for advanced material applications [6]. By selecting appropriate carbon atoms of hydrocarbons, the phase transition temperature of PCMs could be tailored for specific applications [6]. Various fatty acids, viz. capric, lauric, palmitic, and stearic acids (SAs), and their binary mixture are widely used as PCMs for thermal balance. Organic PCMs are relatively expensive; however, they have high latent heat per unit volume and low density. Key advantages and disadvantages of organic PCMs are tabulated in Table 10.2.

10.2.2.2 Inorganic PCMs

Inorganic PCMs generally belong to the hydrated salts that have number of hydrate molecules [6]. For specific applications, heat absorbing, and releasing temperature interval of PCMs should be in the specific range, for example, for textile purpose it should be around 10–35 °C. Couple of inorganic PCMs with their melting point temperature and heat of absorption are tabulated in

Table 10.2 Key advantages and disadvantages of organic PCMs.

Advantages	Disadvantages
○ Organic PCMs are generally noncorrosive ○ Chemically stable on repeated phase change cycles ○ High specific latent heat of fusion and solidification ○ Low vapor pressure	○ Low thermal conductivity ○ High change in volume as compared with inorganic PCMs on phase change ○ Organic PCMs are flammable

Source: Farid et al. 2004 [15].

Table 10.3 Major advantages and disadvantages of inorganic PCMs.

Advantages	Disadvantages
○ High specific heat ○ High thermal conductivity ○ Nonflammable ○ Cheap as compared with the organic PCMs	○ Corrosive to metals ○ Suffer from decomposition on repeated uses

Source: Farid et al. 2004 [15].

Table 10.1. Hydrated salts absorb high energy at its melting point while release energy when it solidifies [19]:

$$Na_2SO_4 \cdot 10H_2O \rightarrow Na_2SO_4 + 10H_2O + \Delta H$$

$$Na_2SO_4 + 10H_2O \rightarrow Na_2SO_4 \cdot 10H_2O - \Delta H$$

Inorganic PCMs have several major advantages and disadvantages as tabulated in Table 10.3.

10.2.2.3 Eutectic PCMs

Eutectic PCMs are mixture of two or more components in such a proportion that their combined melting point and solidification point temperature is single, and lower than the individual component. Eutectic mixture of PCMs could be classified as organic–organic, organic–inorganic, and inorganic–inorganic types. Some of the eutectic PCMs with their melting point temperature and latent heat of fusion are tabulated in Table 10.1.

10.3 Phase Change Fibers

10.3.1 How PCM Works with Fibrous Structures

Here author explains the working principles of PCM in fibrous structure, taking an example of specific filed such as advanced textile applications. The PCMs that change phases from 10 to 35 °C would be suitable for the development of fibrous structures for smart textiles. Textile with PCM-containing fibrous structure will

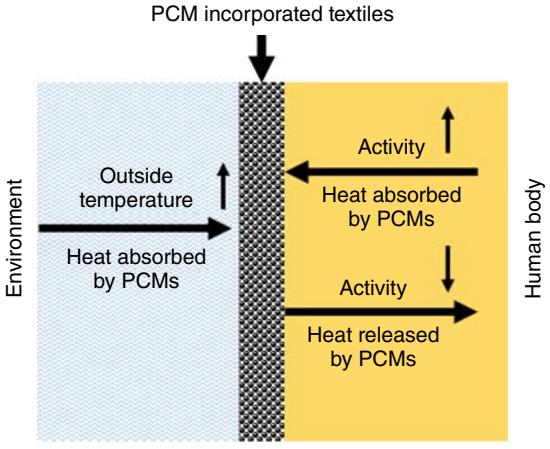


Figure 10.3 Schematic representation of interactions for the PCM incorporated textiles with environment and human body.

react with the changes of environmental temperature and the temperatures in different areas of body. PCM in fibrous structure absorbs body heat when the body temperature increases and PCM melts. However, melted or semi-melted PCM gives off heat when body temperature decreases. In this way, PCM incorporated textiles could keep the body in a comfortable state and are used for the thermal management of garments [3, 6, 20]. The process of phase change is a dynamic; hence, the PCMs inside the fibrous structures are constantly changing from solid to liquid and vice versa depending upon the physical activity of person and external environmental temperature (Figure 10.3).

10.3.2 Microencapsulation of PCMs

Though PCMs are used for the absorption, storage, or release of thermal energy, however, to effectively use the PCMs, they need to be packed in an inert and durable micro-container. Microencapsulation is a process of incorporating micro-sized solid or liquid droplet or gases inside the compatible thin solid wall structure. Tiny particles or droplets of PCMs are surrounded by a coating with a uniform wall, which is generally made with polymer. Therefore, microencapsulated PCM consists of two major parts, such as the PCM inside microcapsules known as core and the surrounding wall known as shell. The diameter of microcapsules varies from 100 µm to 1 mm. Scanning electron microscopic image for the microcapsule of paraffin core and polystyrene shell is shown in Figure 10.4 [21]. Microencapsulation of solid, liquid, or gases can be prepared by using various techniques such as interfacial polymerization, in situ polymerization, chemical coacervation, solvent evaporation, spray drying, fluidized bed methods, etc. [3, 22]. The core–shell structure of microencapsulated PCM structure formation process by single-stage emulsion technique is schematically illustrated in Figure 10.5. The selection of microencapsulation methods depends on desired characteristics and end applications in the fibrous structure. The properties of microcapsules, their size, shapes, shell materials, method of applications, and compatibility with the formulation of polymer depend on the type of applications. To preserve the functional properties of microencapsulated

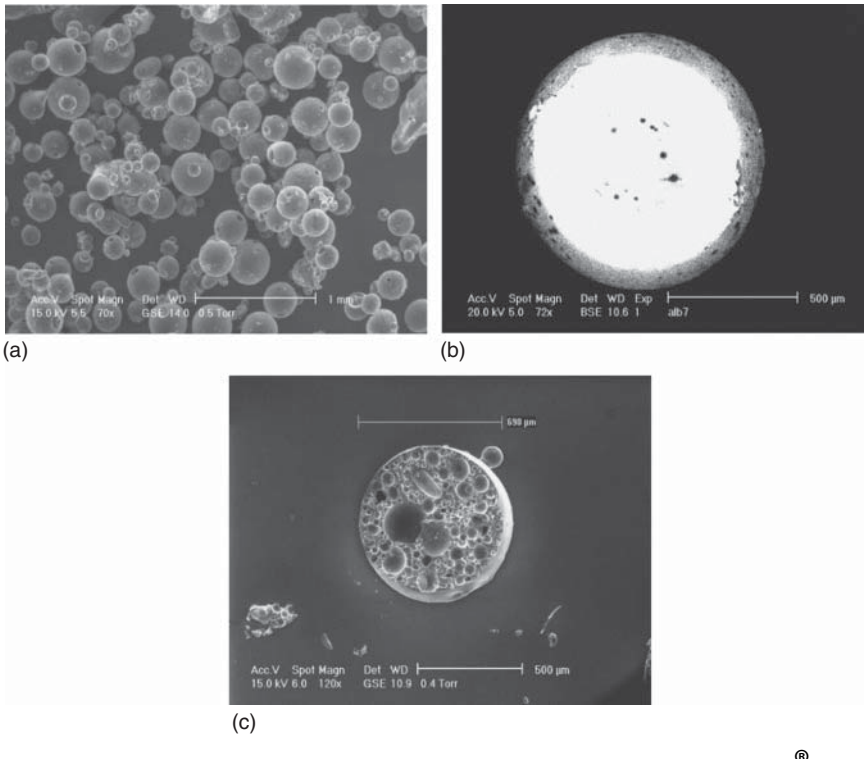


Figure 10.4 Scanning electron microscopic images of microcapsules containing PRS® paraffin wax as core materials and polystyrene as shell material. (a): Overall view of a batch of micro particles. (b) and (c) Cross sections of single microparticles. Source: Sanchez et al. 2007 [21]. Reproduced with permission of Springer Nature.

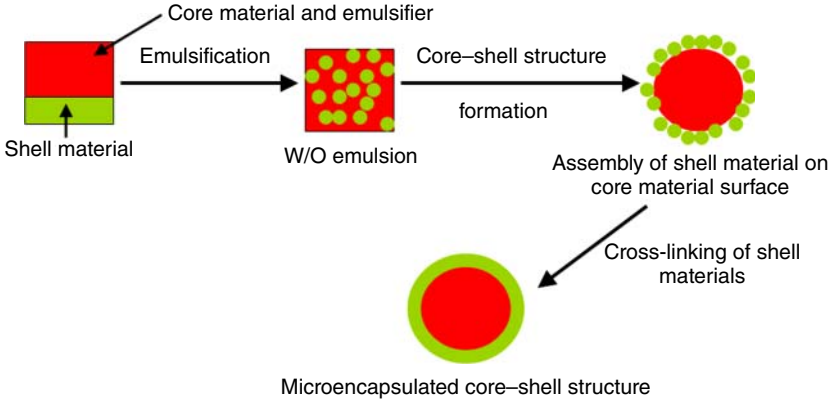


Figure 10.5 Schematic of process flow for the core–shell structure formation of microencapsulated PCMs by single-stage emulsion technique.

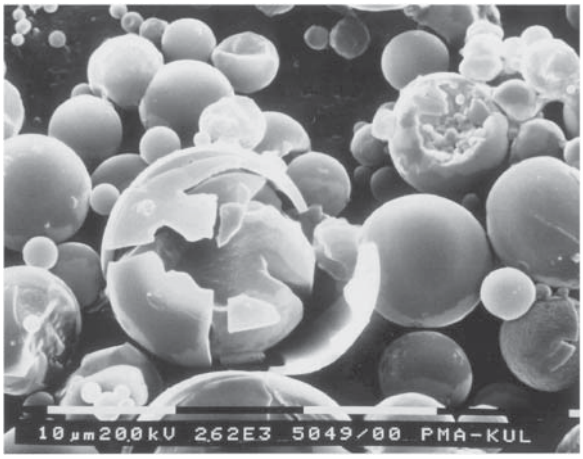


Figure 10.6 Scanning electron microscope image showing the thickness of urethane shell material. PCMs were cryogenically fractured. Source: Stappers et al. 2005 [24]. Reproduced with permission of Electrochemical Society.

PCMs over repeated phase transition cycles, PCM should remain within the shell over the entire product life cycles and should increase heat transfer area. Further, PCM microcapsules should be resistant to mechanical and thermal stress [15, 23]. Therefore, durability and thickness of shell (Figure 10.6) materials in core–shell structure is very important for the thermal balance and mechanical property of microencapsulated PCMs.

If PCMs are applied directly on the fibrous structure without microencapsulation, following problems may arises [25]:

(a) Leaking of PCM from the surface in its liquid or semi liquid forms.
(b) Changes for the numbers of hydrates in the salts specially in humid condition.
(c) Diffusion of low viscous melted PCMs from the textile substrate.

10.3.3 Techniques to Prepare Phase Change Fibrous Structures

Principally, PCM incorporated fibers could be made through two different approaches: (i) PCM microcapsules can be dispersed into the polymer solution or melt prior to the extrusion of fiber, and (ii) PCM microcapsules could be attached on the fiber surface by coating, finishing, etc. [6]. Various proposed PCM incorporated fibrous structures are schematically shown in Figure 10.7.

10.3.3.1 Coating of Encapsulated PCM on Fibrous Structure

Microencapsulated PCMs could be attached on the surface of fibrous structure of synthetic fiber during fiber finishing process, while for natural fiber during the preparation stage prior to the weaving or during the fabric finishing process by using a suitable binder (Figure 10.7a). In a typical coating process of encapsulated PCM on fiber, the microsphere PCMs are dispersed in a water solution, which contains a surfactant, dispersant, antifoaming agent, a thickener, and polymer binder [6]. Durability of microencapsulated PCM on the fiber surface depends on the interaction of microencapsulated PCM with the fiber surface. In general, softness and smoothness of the fibers are decreases after coating of PCMs on the fiber surfaces.

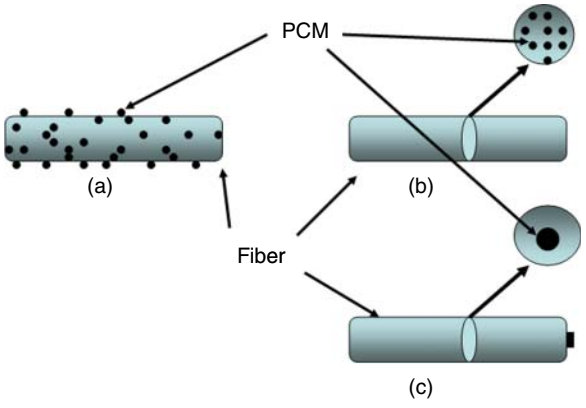


Figure 10.7 Schematic of PCM incorporated fibrous structures. (a) Encapsulated PCM-coated fiber. (b) Encapsulated PCM-entrapped fiber. (c) Core–sheath structure of PCM/polymer hollow fibers.

10.3.3.2 PCM Incorporated Fibrous Structure by Conventional Spinning

In this method, microencapsulated PCMs are added in the polymer solution or melt, and then PCM incorporated fibers are spun according to the methods of conventional melt spinning, dry or wet spinning, etc. Microencapsulated PCM incorporated fibers store or release heat energy with the changes of surrounding environment or human body temperature [6, 26]. Polypropylene monofilament fibers incorporated with PCM can be prepared by melt spinning with a PCM loading up to 12% [27]. Li et al. reported melt-spun polyethylene fibers embedded with microencapsulated PCMs and alginate fiber that contained PCM microcapsules spun by using wet spinning method [28]. Form-stable polyacrylonitrile (PAN) and SA fiber can be prepared by solution blending. Phase change transition temperature and phase transition enthalpy of PCM incorporated fiber increase with increasing stearic acid (SA) content in the fiber matrix [29]. SA could be attached with PAN matrix by intermolecular forces that ensure homogeneous distribution of PCMs in the PAN matrix [29, 30]. PCM incorporated composite fibre can be prepared by electrospinning technique [31–33]. Heat storage capacity for some of the phase change fibers has been tabulated in Table 10.4. However,

Table 10.4 Heat storage capacity of PCM incorporated fibers.

Material	PCMs	Enthalpy of melting (J/g)	Fiber preparation method	References
Polyacrylonitrile (PAN)	Eutactic mixture of fatty acids[a)]	120.1	Electrospinning	[32]
Carbon fibre mats	Capric acid	110.3	Electrospinning of PAN followed by carbonization	[32]
Polyethylene terephthalate	Lauric acid	70.76	Electrospinning	[31]
Polyacrylonitrile	Capric acid	165.4	Electrospinning	[32]
Polyethylene terephthalate	Adipic acid dioctadecyl esters (75%)	66.5	Electrospinning	[33]

a) Capric acid and lauric acid.

Table 10.5 Some of the key advantages and disadvantages of melt spinning and solution spinning of phase change fiber.

Spinning methods	Advantages	Disadvantages
Melt spinning	(i) PCMs are permanently locked within the fiber matrix. Therefore, durable phase change fiber as compared with coating or finishing of microencapsulated PCM on fiber surface (ii) Thermal properties of polymer of the fiber matrix will affect the resultant thermoregulating properties of phase change fiber (iii) Environmental friendly method due to the elimination of toxic solvent (as compared with solution spinning)	(i) Shell materials of microcapsules of PCM should be resistant to temperature of polymer melt (ii) Particle size and size distribution of microsphere of PCM affects the spin ability and mechanical properties of fibers (iii) Uniform distribution and dispersion of microencapsulated PCM in fiber matrix is difficult to achieve. (iv) Poor process ability and poor properties of fibers with high concentration of microencapsulated PCMs (v) Microcapsules of PCMs may not have the structural integrity to withstand the force exerted on the microcapsule during extrusion of fibers
Solution spinning (wet/dry spinning)	(i) PCMs are permanently incorporated locked within the fiber matrix. Therefore, durable phase change fiber as compared with coating or finishing of microencapsulated PCM on fiber surface (ii) Thermal properties of polymer of the fiber matrix will affect the resultant thermoregulating properties of phase change fiber (iii) Better mechanical properties of fiber in the case of wet solution spinning (as compared with melt spinning)	(i) Shell materials of microcapsules should be resistant to the dope solution (ii) Particle size and size distribution of microsphere of PCM affects the spin ability and mechanical properties of fibers (iii) In the case of wet spinning, PCM should not leach out from the microencapsulated PCM by solution of wet spinning bath (iv) Uniform distribution and dispersion of microencapsulated PCM in fiber matrix may be difficult to achieve (v) Poor process ability and poor properties of fibers with high concentration of microencapsulated PCMs (vi) Microcapsules of PCMs do not have the structural integrity to withstand the force exerted on the microcapsule during extrusion of fibers

advantages and disadvantages of conventional spinning processes for the preparation of phase change fibers have been summarized in Table 10.5.

10.3.3.3 Phase Change Fibers by Electrospinning

Electrospinning is an efficient technique to prepare ultrafine nanofibers and produces continuous nanofibers from submicron diameters down to nanometer diameters in a high potential electric field by using a conductive polymer solution. Application of high voltage creates electrically charged jet of polymer solution or melt. Before reaching the jet to the target surface, solvent evaporates,

and liquid polymer solidifies, and electrospun nanofibrous mats are collected on the conductive plate connected with ground. Electrospun fibers of lauric acid and polyethylene terephthalate (PET) show smooth cylindrical surface with a latent heat of fusion around 70.76 J/g while the diameter of the fiber ranges from several tens to several hundred nanometers [31]. Sheath–core structure of polymer and PCM nanofiber can be prepared by coaxial electrospinning technique. Wan et al. reported nanofiber of PAN as sheath and isopropyl palmitate and paraffin oil as PCM in the core material [34]. PCMs are well encapsulated in the hollow PAN fiber to ensure thermal balance with the sudden environmental temperature changes due to the homothermal effect of PCM incorporate fiber [34]. Zdraveva et al. reported poly(vinyl alcohol) nanofiber incorporated with PCM by using emulsion electrospinning technique. Nanofibers maintained morphological integrity during the phase change and heat-regulating performances over the cyclic phase changes [35]. Phase change electrospun fibers based on PEG as PCM and cellulose acetate as matrix have been reported by Chen et al. Morphology of composite fibers shows cylindrical and smooth surface (Figure 10.8). PCM such as PEG has been distributed both on the surface and in the core of the fiber matrix [36]. Mechanical properties

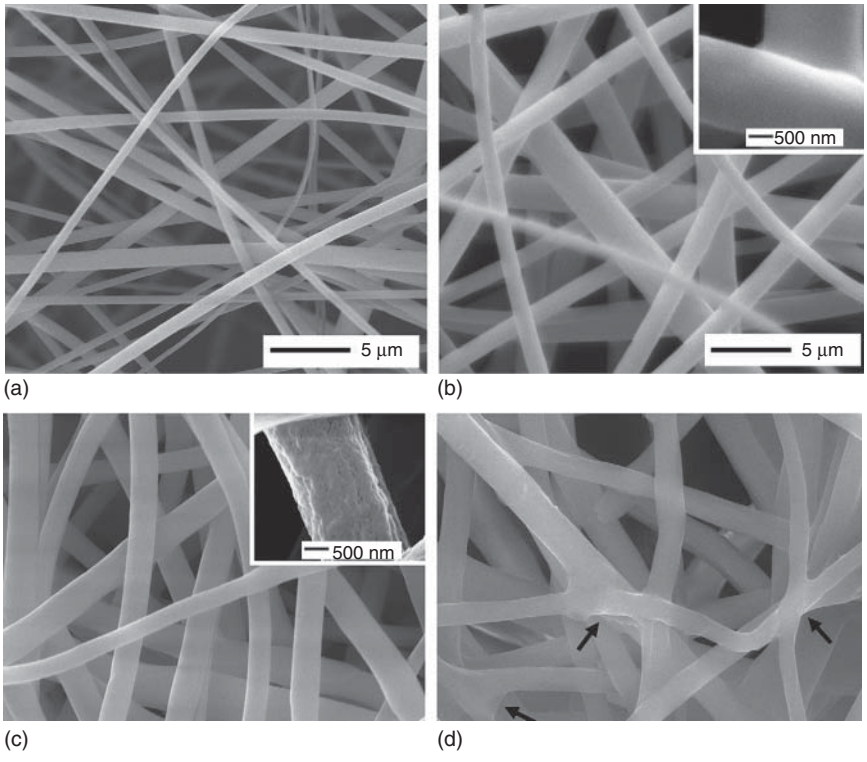


Figure 10.8 Scanning electron microscopy images of (a) electrospun cellulosic acetate (CA) fibers, (b) electrospun phase change fiber of polyethylene glycol (PEG)/CA, (c) washed phase change fiber of PEG/CA, and (d) electrospun PEG/CA composite fibers after 100 heating/cooling cycles treated. Source: Chen et al. 2007 [36]. Reproduced with permission of Elsevier.

of the PCM incorporated fibers generally decrease. The extent of decrease for tensile properties depends on the distribution and/or dispersion of PCM phases in the matrix phase and the intermolecular forces between the two phases of PCM and the matrix of fiber. Chen et al. shows that the tensile properties of the electrospun composite phase change PET fibers were lower than that of the electrospun pure PET fibers [31].

10.4 Phase Change Fibers for Advanced Material Applications

PCMs could adapt to the thermal regulating functional performance of the materials made with PCM incorporated fibrous structures [37, 38] by altering their state phases in a defined temperature range. Applications of phase change fibrous materials include smart textile, shoes/accessories, automotive, electrical, civil engineering, and many other advanced material applications. The following is a brief summary for the application of PCM incorporated fibers for the advanced material applications.

10.4.1 Phase Change Fibers for Advanced Textile Applications

10.4.1.1 Sportswear

Active wear required a thermal balance between the heat generated by the body and the heat released into the environment while engaged in physical activity to reduce thermal stress situation. For the normal garment, heat generated by the human body during physical activity is often not released into the environment in the required amount and thus increases the thermal stress to the wearer. When sportswear was prepared by using PCM incorporated fibers, during physical activity, the wearer's body temperature increases, and the excess heat is absorbed by the encapsulated PCMs and released when necessary (for example, during the rest time) [6].

PCM incorporated fibrous materials could be used to manufacture garments for the sportswear in order to control the sport persons' body temperature dynamically [3]. PCM in the fibrous structure will absorb the body heat during the sporting activity, whereas absorbed heat by PCM will be released and keep the body warm during the resting. Varieties of sports apparel with PCM incorporated fibrous structure can be realized such as skiwear, hunting cloth, other outdoor and indoor sportswear, etc. [39]. Cold winter sports such as alpine climbing, ice climbing, and recreational skiing have further stimulated the demand of PCM incorporated fibrous textiles, which can keep the outdoor sport individuals dry, warm, and comfortable. Snowboard gloves, garments for ice climbing, and underwear for cycling and running are few more examples for the applications of PCM incorporated fibrous structures in sportswear [6].

10.4.1.2 Hospital Applications

PCM interacts with the microclimate around the human body and could respond to the fluctuations in surrounding temperature due to the changes in patient

activity levels and external environment changes. Therefore, surgical apparel, bedding materials for patients, bandages, and other medical textile products prepared by using PCM incorporated fibrous structure could be applicable to the hospital applications. Microencapsulated PCM incorporated textiles could also be used for medical applications for hot and cold therapies [21].

10.4.1.3 Beddings and Accessories

PCM incorporated fibrous materials could be applicable in quilts, bed sheet, pillow cover, mattress, etc. to ensure dynamic temperature control in bed. Additional heat energy will be absorbed by PCM incorporated textiles when body temperature rises in order to absorb the body heat. However, in the case of drop of the body temperature, stored energy will be released and the body will keep warm [6].

10.4.1.4 Other Applications in Advanced Textiles

Textiles prepared with phase change fibers could be useful for the space suits, gloves, etc. to keep the astronauts in a comfortable state. Further, phase change fibers can be used for the manufacturing of thermal underwear, jackets, sports garments, skiwear, etc. Some of the other applications of phase change fibers in textile fields include textiles for the interior decorations, curtain, mattress, blankets, home furnishings, firefighter suits, etc.

10.4.2 Automotive Industries

Microencapsulated PCM incorporated fibrous structure can be applicable in automobile textiles, for example, seat covers. Paraffin-based PCM has several advantages such as high capacity of its heat storage capability, low toxicity, lack of hygroscopic properties, and low cost and obtains the targeted temperature range by blending, and all these excellent properties make paraffinic incorporated phase change fibers suitable for the automotive applications. Application of PCM incorporated fibrous structure in car interior and seat cover can provide superior thermal control to the passengers [6]. During the summer, temperature inside the automobile can increase significantly; in order to regulate the temperature inside, many cars are equipped with air conditioning systems, which is quite energy-intensive process. In order to regulate the interior temperature of car, the phase change fiber could be used in automotive interior, which could offer energy saving as well as improve the thermal comfort of car interior.

10.4.3 Electrical Applications

Phase change fibers can be used in electrical engineering as optical sensor fibers [40]. Phase change fibers act as passive elements and do not required any additional energy source; therefore, application of phase change fibers in electronic and computer is promising. Phase change fibers in thermal diode can be used to improve the effectiveness of heat sink [41]. Management of generated heat from the electronic devices is a very important issue as the size of electronic

component decreases while its speed increases. Inappropriate thermal management of electronic components can reduce its performance, and it could damage the electronic components. Electrospun nanofiber mat can be used to protect electronic devices by dissipation of heat from the electronic devices, computers, circuit board, etc. [42].

10.4.4 Other Applications

Phase change fibers can also be used for shoes and accessories. Phase change fibers can regulate the temperature by absorbing, storing, redistributing, and releasing of heat to prevent dramatic change of wearer head and feet temperatures. Therefore, the liner textiles made with phase change fibers could be applicable for helmet and shoes in order to regulate the wearer temperature. In civil engineering, it can be used as pipe wrap, building insulation, wallpapers, tiles, etc. Some of the other applications of PCM fibers include containers to regulate the temperature of food and drinks, household appliance insulation, etc. [43, 44].

10.5 Summary

LSH PCMs are suitable to develop thermoregulated advanced fibrous materials because these materials are efficient to store thermal energy and provide higher TES density with smaller temperature difference between storing and releasing of heat. In this chapter author provided an overview of PCM incorporated fibrous materials for advanced material applications with an emphasis on thermoregulating textiles. Generally, microencapsulated PCMs are applied on the substrates, for example, garment by finishing, coating, lamination, etc., and coating/lamination would affect the other properties of garments such as moisture permeability, fabric aesthetic look, garment hand, etc. The textile substrate prepared by using PCM incorporated fibers would be more effective to prepare thermoregulating textiles. Apart from the advanced textile applications of phase change fibers, this chapter also summarized the applications in electrical and automotive industries and other areas of advanced material applications. Uniform dispersion and distribution of microencapsulated PCMs throughout the fibrous structure is a major challenge, and this subsequently would affect the thermoregulating properties of PCM incorporated fibrous materials. Other challenges for manufacturing fibrous structure with PCMs include incorporation of PCMs in a single fibrous matrix or surface, cost, etc. Future research and developments in these areas are required for the further development.

References

1 Gasia, J., Miró, L., de Gracia, A. et al. (2016). Experimental evaluation of a paraffin as phase change material for thermal energy storage in laboratory equipment and in a shell-and-tube heat exchanger. *Applied Sciences* 6 (4): 112.

2 He, B. and Setterwall, F. (2002). Technical grade paraffin waxes as phase change materials for cool thermal storage and cool storage systems capital cost estimation. *Energy Conversion and Management* 43 (13): 1709–1723.

3 Sarier, N. and Onder, E. (2007). The manufacture of microencapsulated phase change materials suitable for the design of thermally enhanced fabrics. *Thermochimica Acta* 452 (2): 149–160.

4 Hasnain, S.M. (1998). Review on sustainable thermal energy storage technologies, Part I: Heat storage materials and techniques. *Energy Conversion and Management* 39 (11): 1127–1138.

5 Sharma, A., Tyagi, V.V., Chen, C.R., and Buddhi, D. (2009). Review on thermal energy storage with phase change materials and applications. *Renewable and Sustainable Energy Reviews* 13 (2): 318–345.

6 Mondal, S. (2008). Phase change materials for smart textiles – an overview. *Applied Thermal Engineering* 28 (11–12): 1536–1550.

7 Budd, G.M. (1989). Ergonomic aspects of cold stress and cold adaptation. *Scandinavian Journal of Work, Environment & Health* 15 (Suppl 1): 15–26.

8 Nielsen, R., Olesen, B.W., and Fanger, P.O. (1985). Effect of physical-activity and air velocity on the thermal insulation of clothing. *Ergonomics* 28 (12): 1617–1631.

9 Shishoo, R.L. (1998). Technology for comfort. *Textile Asia* 19 (6): 93–110.

10 Sen, A.K. (2001). *Coated Textiles: Principle and Applications* (Tech ed. Damewood J), 133–154. Technomic Publishing Co.

11 Ying, B.-A., Kwok, Y.-L., Li, Y. et al. (2004). Assessing the performance of textiles incorporating phase change materials. *Polymer Testing* 23 (5): 541–549.

12 Lennox-Kerr, P. (1998). Comfort in clothing through thermal control. *Textile Month* (November), pp. 8–9.

13 Huang, J.Y., Lu, S.L., Kong, X.F. et al. (2013). Form-stable phase change materials based on eutectic mixture of tetradecanol and fatty acids for building energy storage: preparation and performance analysis. *Materials* 6: 4758–4775.

14 Feldman, D., Shapiro, M.M., and Banu, D. (1986). Organic phase change materials for thermal energy storage. *Solar Energy Materials* 13 (1): 1–10.

15 Farid, M.M., Khudhair, A.M., Razack, S.A.K., and Al-Hallaj, S. (2004). A review on phase change energy storage: materials and applications. *Energy Conversion and Management* 45 (9–10): 1597–1615.

16 Lane, G.A. (1980). Low temperature heat storage with phase change materials. *International Journal of Ambient Energy* 1: 155–168.

17 Sari, A. and Kaygusuz, K. (2002). Thermal performance of a eutectic mixture of lauric and stearic acids as PCM encapsulated in the annulus of two concentric pipes. *Solar Energy* 72 (6): 493–504.

18 Arjun, D. and Hayavadana, J. (2014). Thermal energy storage materials (PCMs) for textile applications. *Journal of Textile and Apparel, Technology and Management* 8 (4): 1–11.

19 Saito, A., Okawa, S., Shintani, T., and Iwamoto, R. (2001). On the heat removal characteristics and the analytical model of a thermal energy storage capsule using gelled Glauber's salt as the PCM. *International Journal of Heat and Mass Transfer* 44 (24): 4693–4701.

20 Wang, S.X., Li, Y., Hu, J.Y. et al. (2006). Effect of phase-change material on energy consumption of intelligent thermal-protective clothing. *Polymer Testing* 25 (5): 580–587.

21 Sanchez, L., Sanchez, P., de Lucas, A. et al. (2007). Micro encapsulation of PCMs with a polystyrene shell. *Colloid and Polymer Science* 285 (12): 1377–1385.

22 Onder, E., Sarier, N., and Cimen, E. (2008). Encapsulation of phase change materials by complex coacervation to improve thermal performances of woven fabrics. *Thermochimica Acta* 467 (1–2): 63–72.

23 Boh, B. and Knez, E. (2006). Microencapsulation of essential oils and phase change materials for applications in textile products. *Indian Journal of Fibre and Textile Research* 31: 72–82.

24 Stappers, L., Yuan, Y., and Fransaer, J. (2005). Novel composite coatings for heat sink applications. *Journal of the Electrochemical Society* 152 (7): C457–C461.

25 Mondal, S. (2011). Thermo-regulating textiles with phase-change materials. In: *Functional Textiles for Improved Performance, Protection and Health*, (eds. Pan, N. and Sun. G.) 163–183. Woodhead Publishing.

26 Tjonnas, M.S., Faerevik, H., Sandsund, M., and Reinertsen, R.E. (2015). The dry-heat loss effect of melt-spun phase change material fibres. *Ergonomics* 58 (3): 535–542.

27 Iqbal, K. and Sun, D.M. (2014). Development of thermo-regulating polypropylene fibre containing microencapsulated phase change materials. *Renewable Energy* 71: 473–479.

28 Li, W., Ma, Y.-J., Tang, X.-F. et al. (2014). Composition and characterization of thermoregulated fiber containing acrylic-based copolymer microencapsulated phase-change materials (MicroPCMs). *Industrial and Engineering Chemistry Research* 53 (13): 5413–5420.

29 Guo, J., Xiang, H.X., and Wang, Q.Q. (2011). Preparation and properties of form-stable phase change materials polyacrylonitrile fiber/stearic acid blends. In: *New and Advanced Materials, Parts 1 and 2*, Advanced Materials Research, vol. 197–198 (eds. H.Y. Zhou, T.L. Gu, D.G. Yang, et al.), 584–588. Stafa-Zurich: Trans Tech Publications Ltd.

30 Guo, J., Xiang, H.X., Wang, Q.Q., and Xu, D.Z. (2013). Preparation and properties of polyacrylonitrile fiber/binary of fatty acids composites as phase change materials. *Energy Sources, Part A: Recovery, Utilization, and Environmental Effects* 35 (11): 1064–1072.

31 Chen, C., Wang, L., and Huang, Y. (2008). A novel shape-stabilized PCM: electrospun ultrafine fibers based on lauric acid/polyethylene terephthalate composite. *Materials Letters* 62 (20): 3515–3517.

32 Cai, Y.B., Zong, X., Zhang, J.J. et al. (2013). Electrospun nanofibrous mats absorbed with fatty acid eutectics as an innovative type of form-stable phase change materials for storage and retrieval of thermal energy. *Solar Energy Materials and Solar Cells* 109: 160–168.

33 Chen, C.Z., Liu, S.S., Liu, W.M. et al. (2012). Synthesis of novel solid-liquid phase change materials and electrospinning of ultrafine phase change fibers. *Solar Energy Materials and Solar Cells* 96 (1): 202–209.

34 Wan, Y.F., Zhou, P.C., Liu, Y.D., and Chen, H.X. (2016). Novel wearable polyacrylonitrile/phase-change material sheath/core nano-fibers fabricated by coaxial electro-spinning. *RSC Advances* 6 (25): 21204–21209.

35 Zdraveva, E., Fang, J., Mijovic, B., and Lin, T. (2015). Electrospun poly(vinyl alcohol)/phase change material fibers: morphology, heat properties, and stability. *Industrial and Engineering Chemistry Research* 54 (35): 8706–8712.

36 Chen, C.Z., Wang, L., and Huang, Y. (2007). Electrospinning of thermo-regulating ultrafine fibers based on polyethylene glycol/cellulose acetate composite. *Polymer* 48 (18): 5202–5207.

37 Bendkowska, W., Tysiak, J., Grabowski, L., and Blejzyk, A. (2005). Determining temperature regulating factor for apparel fabrics containing phase change material. *International Journal of Clothing Science and Technology* 17 (3–4): 209–214.

38 Ying, Y.L.K., Li, Y., Yeung, C.-Y., and Song, Q.-W. (2004). Thermal regulating functional performance of PCM garments. *International Journal of Clothing Science and Technology* 16 (1/2): 84–96.

39 Shin, Y., Yoo, D.-I., and Son, K. (2005). Development of thermoregulating textile materials with microencapsulated phase change materials (PCM). II. Preparation and application of PCM microcapsules. *Journal of Applied Polymer Science* 96 (6): 2005–2010.

40 Priest, R. and Hughes, R. (1980). Thermally induced optical phase effects in fiber optic sensors. *Applied Optics* 19 (9): 1477–1483.

41 Janarthanan, B. and Sagadevan, S. (2015). Thermal energy storage using phase change materials and their applications: a review. *International Journal of ChemTech Research* 8 (6): 250–256.

42 Li, Y., Li, X.-W., He, J.-H., and Wang, P. (2014). Thermal protection of electronic devices with the Nylon 6/66-PEG nanofiber membranes. *Thermal Science* 18 (5): 1441–1446.

43 Chalco-Sandoval, W., Fabra, M.J., Lopez-Rubio, A., and Lagaron, J.M. (2017). Use of phase change materials to develop electrospun coatings of interest in food packaging applications. *Journal of Food Engineering* 192: 122–128.

44 Dugan, J. and Kuckhoff, E. (2007). Multicomponent fiber comprising a phase change material. US Patent WO 2007035483 A1.

11

Bicomponent Fibers

Rudolf Hufenus[1], Yurong Yan[2], Martin Dauner[3], Donggang Yao[4], and Takeshi Kikutani[5]

[1] Empa, Swiss Federal Laboratories for Materials Testing and Research, Laboratory for Advanced Fibers, Department of Functional Materials, Lerchenfeldstrasse 5, 9014 St. Gallen, Switzerland
[2] South China University of Technology, Department of Polymer Materials and Engineering, No. 381 Wushan Road, Tianhe, Guangzhou 510640, China
[3] Institute of Textile Technology and Process Engineering, German Institutes of Textile and Fiber Research, Department of Filament and Nonwoven Technologies, Körschtalstraße 26, 73770 Denkendorf, Germany
[4] Georgia Institute of Technology, School of Materials Science & Engineering, Atlanta, GA 30332-0295, USA
[5] Tokyo Institute of Technology, School of Materials and Chemical Technology, Department of Materials Science and Engineering, 2-12-1-S8-32, O-okayama, Meguro-ku, Tokyo 152-8550, Japan

11.1 Introduction

Melt spinning is the most commonly used method for manufacturing commercial synthetic fibers. A trend in polymer melt spinning is variation of fiber morphology by bicomponent (conjugated) spinning [1, 2], one of the most interesting developments in the field of synthetic fibers [3–6]. A bicomponent fiber is made from two or more polymers of different chemical (e.g. composition, additives) and/or physical (e.g. average molecular weight, crystallinity) nature, extruded from one spinneret to form a single fiber [7]. The polymer flows are kept separate up to the spin pack, where they meet and exit together through the spinneret. When the filament leaves the spinneret, it consists of non-mixed components that touch at the interface. It is worth noting that the dynamics at the interface play a significant role in affecting the behavior and performance of the process.

Bicomponent fibers pass through common melt-drawing processes similar to conventional synthetic fibers [4]. In consequence, both thermoplastic polymers have to withstand extrusion temperature and shear stress without degradation (thermal stability), the average molecular weight has to be high (melt strength), and the molecular weight distribution narrow (constant flow) for the fiber not to break under draw-off strain, and the mobility of the molecular chains has to be high enough to disentangle and unfold under stress and to orient in fiber direction under strain [7, 8]. In addition, coextrusion of different polymers into bicomponent fibers with special cross sections requires that design of spin pack and spinneret is well understood, that respective processing temperatures and viscosities are well balanced, and that adhesion/bonding between the two components is well controlled.

Handbook of Fibrous Materials, First Edition. Edited by Jinlian Hu, Bipin Kumar, and Jing Lu.
© 2020 Wiley-VCH Verlag GmbH & Co. KGaA. Published 2020 by Wiley-VCH Verlag GmbH & Co. KGaA.

The main objective of bicomponent melt spinning is to exploit capabilities not existing in either polymer alone, as advantageous mechanical, physical, or chemical properties of two materials can be combined in one fiber, expanding the range of possible applications [9–11]. Depending on the characteristics of the different polymers, bicomponent fibers are predominately commercialized as bonding elements in thermobonded nonwoven fabrics, as self-crimping fibers to achieve textured yarn, or as fibers with the surface functionality of special polymers and additives at reduced cost [5, 6, 12]. In addition, the two components can mutually influence their thinning and solidification behavior along the spinline during melt spinning, which can be utilized to influence the molecular structure formation of both components in a desired way [13–15].

The first commercial bicomponent fiber was a PA66 – random copolymer side-by-side hosiery yarn produced by DuPont in the mid-1960s, which on retraction formed a highly coiled elastic fiber [16]. The first commercial core–sheath application was a binding fiber manufactured by ICI for carpets and upholstery, consisting of a higher melting temperature core (PA66) and a lower melting temperature sheath (PA6) [11]. Since then bicomponent technology progressed significantly, especially by combining commodity and engineering polymers and diverse additives to achieve tailored characteristics.

11.2 Bicomponent Fiber Spinning Technologies

11.2.1 Spin Pack Design

In bicomponent fiber spinning, one can differentiate between single die and multiple die spinneret, depending on the position where the molten polymers meet (Figure 11.1). In the first, by far most common type, two pressurized polymer

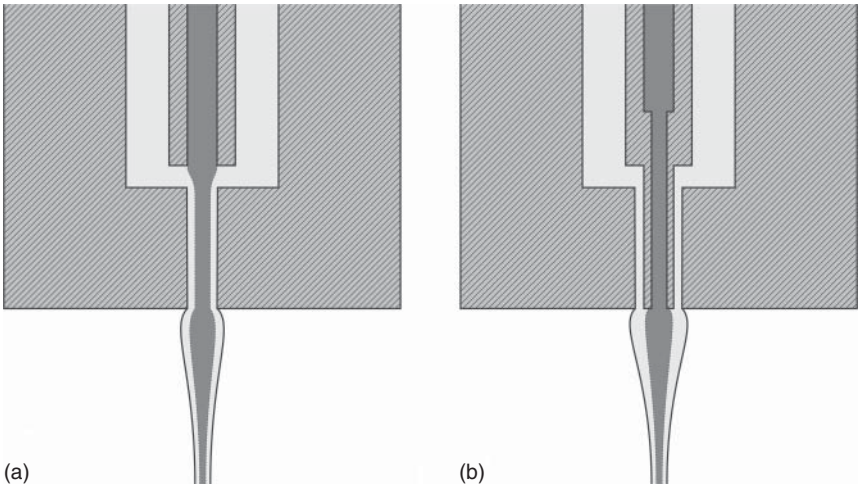


Figure 11.1 Two schematic examples of bicomponent spinnerets: (a) single die and (b) multiple die.

melts meet within the spinneret. Ensuring a laminar flow prevents mixing of the two phases. The development of etched stacked plates to create polymer channels in the spin pack led to smaller packs with higher hole densities and shorter residence times, as well as larger number of segments or islands in the fibers [17]. In the second, less prominent type, each polymer is extruder separately, and the melts meet just at the capillary exit. This geometry is complex to realize but can lessen rheological disparities between the components and enable an exact position of the core within the sheath polymer.

Central elements of bicomponent spinning equipment are the melt distribution plates. The polymer melts conveyed by the two spin pumps are fed to the respective filter packs. In the case of multifilament spinning, the two polymer melts have to be evenly distributed to each die in the required bicomponent configuration. Configurations like core–sheath and side by side can be served from simple geometries like concentric or alternating parallel melt channels from where boreholes guide the melt to the spinning capillaries. The higher the number of sectors in the cross section of each single filament, the more complicated the distribution design is. For drilled holes 16 segments are already a reasonable limit. Figure 11.2 shows a die for producing single islands-in-the-sea filaments. Even for this type of die, a spinneret for multiple filaments can be designed, but the number of filaments will be limited.

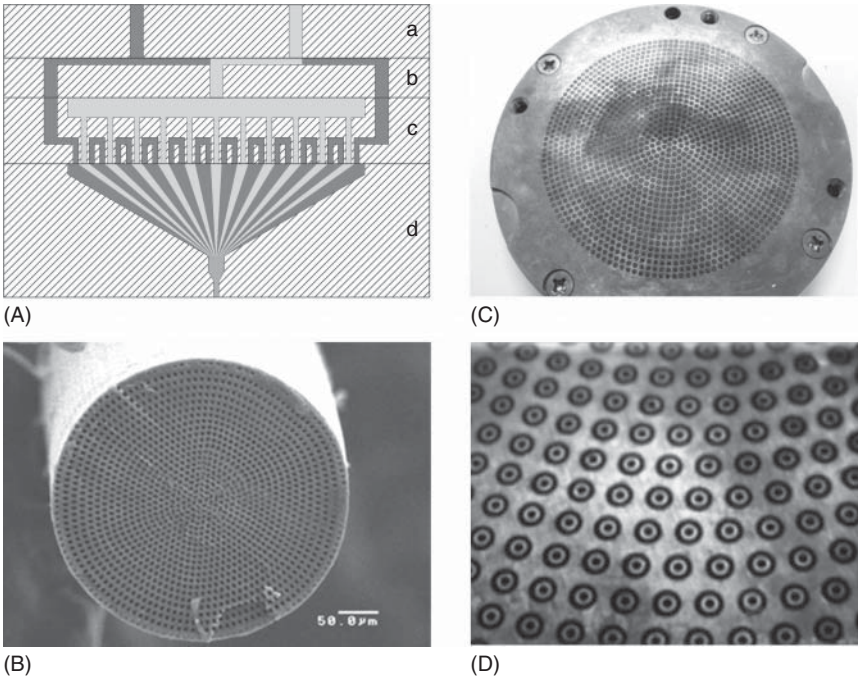


Figure 11.2 Die for producing islands-in-the-sea filament with 1519 islands: (A) schematic of die design, where a, b and c are melt distribution plates, and d is the spinneret plate, (B) cross section of fiber produced with respective die, (C) bottom side of plate c, and (D) magnified image of bottom side of plate c.

Islands-in-the-sea filaments with a large number (up to 10 000) islands need other solutions, like the Hills technology. The melt flow channels in thin distribution plates (0.1–1.5 mm) are produced by a proprietary etching process [18, 19]. This not only allows a comparably cheap production, almost optimal flow ducts, but also a high density of melt flow channels, which are required for high number of islands, resulting in sub-microstructures in the drawn filament.

11.2.2 Cross-Sectional Geometries

The three main geometries of multicomponent fibers are side-by-side, core–sheath, and multiple core configurations (Figure 11.3).

The core–sheath approach enables a variety of surfaces while maintaining major fiber and textile properties, because most thermoplastic polymers can be applied as a sheath over a core that provides the requested tensile strength [20]. Core–sheath types are predominately used as binder fibers for nonwovens, with a standard polymer as core and a low softening-point polymer as sheath [11, 21–24]. When applied in nonwoven production, the core–sheath fibers are heated to a temperature high enough to cause the sheath to soften, and consequently they will adhere to one another and stabilize the fabric [25, 26].

Side-by-side and eccentric core–sheath bicomponent fibers are most commonly used to produce self-crimping yarns applied in voluminous products. By combining two polymers that undergo differential shrinkage, the yarn curls up after thermal treatment or relaxation and develops crimp contraction [27, 28].

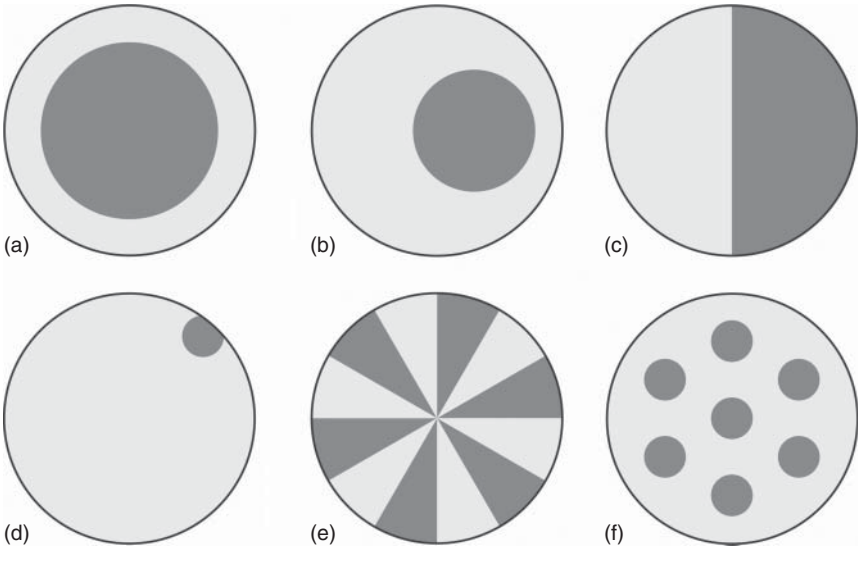


Figure 11.3 Typical cross sections of bicomponent fibers: (a) concentric core–sheath, (b) eccentric core–sheath, (c) 50/50 side by side, (d) unequal side by side, (e) segmented pie, and (f) islands in the sea.

Multiple core configurations, like islands-in-the-sea and segmented pie, are mainly applied to produce microfibers with diameters, smaller than those obtained via conventional melt spinning [29]. Kamiyama et al. [30] reported the production of nanofibers through the bicomponent spinning of islands-in-the-sea fibers with about 1000 islands. Islands-in-the-sea fibers comprise fibrils dispersed in a dissolvable matrix polymer that will be removed in a follow-up process [20]. In the segmented-pie technique, a bicomponent fiber is spun from two incompatible polymers that adhere poorly and split into microfibers when subjected to mechanical stress [12]. Prahsarn et al. [31] describe the splitting behavior of segmented-pie bicomponent fibers of polypropylene (PP)/polyethylene (PE). Fabrics made from microfibers are very flexible, and the high density of fibers makes them inherently windproof, while water vapor from perspiration can evaporate easily.

Hollow fibers can be considered as a type of core–sheath fibers in which the core is composed of a gaseous fluid (e.g. air). They have specialized uses in medical devices [32], but the largest volume market of melt-spun hollow fibers is in thermal insulation products [20]. Hollow fibers can be melt-spun using two different types of spinneret geometries. Most commonly used are "segmented arc" spinnerets, where the polymer melt flows through three or more separated arc slits, and subsequently fuses together below the spinneret to form a tubular shape [33–35]. Here, the fusing mechanism is driven by die swell and controlled by deflection of the melt streams, and it depends on the interplay of inertial and viscous forces [36]. In a "tube in orifice" spinneret, the polymer melt is spun through an annular opening, while inside the annulus a "lumen fluid," usually nitrogen or CO_2, is injected through a coaxial conduit [37, 38]. The second, less common case, indeed involves a bicomponent spinning process.

11.2.3 Melt Spinning Equipment

A typical bicomponent melt spinning plant comprises two screw extruders, a spin pack with discrete polymer conduits, and a set of spinnerets allowing for elaborate fiber cross sections. A schematic drawing of such a melt spinning plant is shown in Figure 11.4.

The polymers are melted using two single screw extruders (1, 2); for instance, one extruder is used for the core component and the other for the sheath component of a bicomponent fiber. Two separate spin pumps (3) and a special spin pack (4) combining the polymers in the spinneret (5) enable a well-balanced polymer flow. Leaving the spinneret the further run of the filaments is equal to conventional melt spinning. For safety reasons, evaporating monomers and oligomers are sucked in by an exhaust (6). The extrudate is spun into the quenching chamber (7) with adjustable air flow and quenching temperature (8). After cooling and application of a spin finish (9), the filaments (10) are drawn (online or offline) by several heated godets (11) with variable revolving speeds. The draw ratio, i.e. the ratio of speeds of draw and feed godets, can be chosen accordingly. Finally a winder (12) is used to spool the filaments on a bobbin.

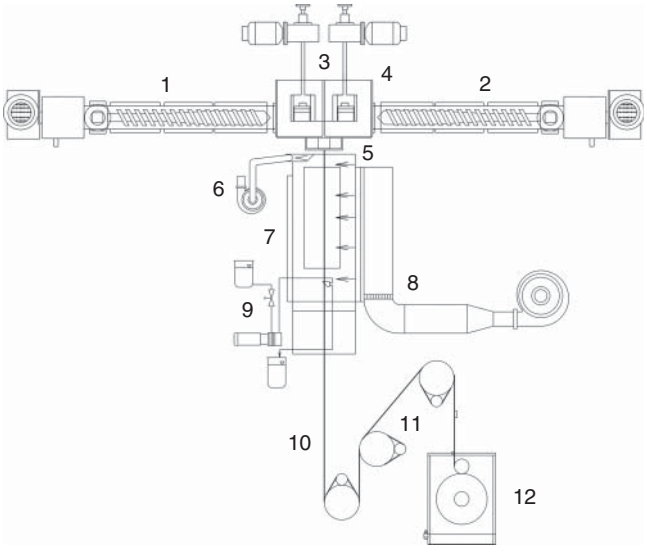


Figure 11.4 Schematic assembly of a bicomponent melt spinning plant (see text for an explanation of the numbered parts).

11.2.4 Special Spin Pack Designs

As nonlinear and elastic flow properties of polymer melts would lead to flow instabilities in coextrusion of a molten polymer and a liquid core [39], a special spin pack was designed that enabled the stable melt spinning of a bicomponent fiber with a liquid core. Figure 11.5 shows a 3D cross section of the customized spin pack [40]. The polymer is supplied from the gear pump through the inlet on the right-hand side; it flows into a conical chamber before entering an annular co-flow channel. The well-sealed inner injection capillary conveys the core liquid, injected by an attached high-pressure pump that prevents polymer backflow into the liquid-filled capillary. A suitable liquid has to meet several elementary requirements: It must exhibit a relatively low vapor pressure (e.g. $<10^5$ Pa) at the processing temperature to prevent exit spraying, the thermal stability of the liquid should be high enough, the liquid has to be noncorrosive to the extrusion equipment, and the liquid must not act as solvent for the polymer component.

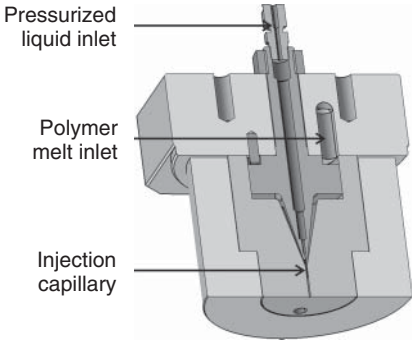


Figure 11.5 Cross section of the liquid-polymer coextrusion spin pack with concentric co-flow region. Source: Hufenus et al. 2016 [40]. Reproduced with permission of Elsevier.

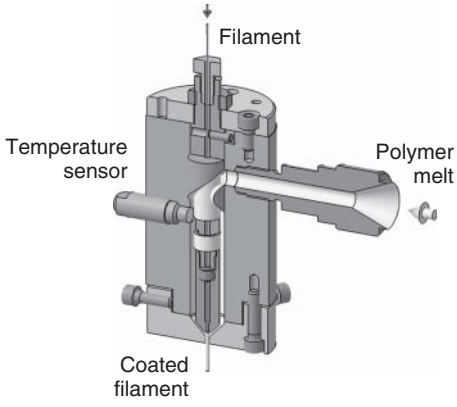


Figure 11.6 Schematic of wire coating die used for overjacketing high tenacity filaments with a thermoplastic polymer. Source: Leal et al. 2016 [41]. Reproduced with permission of Elsevier.

In order to produce bicomponent thermoplastic core–sheath fibers with a high tenacity core, a wire-coating spin pack (Figure 11.6) was modified to enable coating a high tenacity thermoplastic filament with a polymeric sheath [41]. The two materials are allowed to come in contact inside the die, mimicking a pressure-type die in which the pressure exerted by the polymer mass is used as an aid to enhance the adhesion between the two materials. Given that a filament lacks the rigidity of a metallic wire used in the conventional wire coating process, a steel capillary tube threaded vertically into the wire coating die serves as a guide.

The other important part in bicomponent spinning is to maintain and control the polymers as long as possible at their optimal temperatures during extrusion. One of the well-known technologies for bicomponent fiber extrusion with the concept of temperature separation is patented by Hills Inc. [42]. With the same goal, a highly integrated spin pack allowing the separate heating or cooling of up to three polymer channels was developed [43]. It comprises a separate oil cooling and heating system for each channel to keep the polymer melt flows at different temperatures down to the spinneret plate. Each of the three channel sections is thermally isolated toward the other two sections by an internal narrow grid of convection channels [44–46] (Figure 11.7). The spin pack was produced by

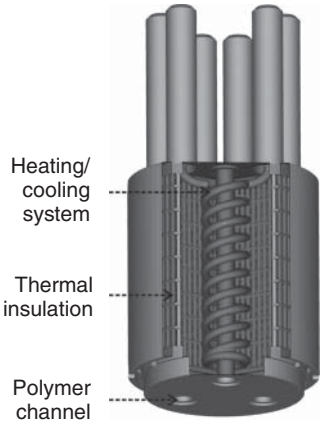


Figure 11.7 Schematic of a highly integrated spin pack for three different polymers with double helix heating/cooling channels and thermal insulation grid. Source: Hufenus et al. 2012 [43]. Reproduced with permission of John Wiley & Sons.

selective laser melting (SLM), an additive manufacturing process used for the fabrication of three dimensional metal parts [47].

11.3 Principles and Theories of Bicomponent Spinning

11.3.1 Structure Formation During Spinning and Drawing

In general, flexible-chain polymers can only be partially oriented in the fluid state during the melt spinning step. Their orientation has to be completed in the solid state, i.e. in the post-spinning drawing step, and for such fibers, drawing is the principal mean of building up their tensile properties. The orientation is a function of the actual strain, and a high degree of orientation can be produced without application of high stress if the strain rate is low. During the drawing process, the as-spun filament is irreversibly stretched up to several times its original length. The elongation is accompanied by extension and parallelization of macromolecules and crystallites along the fiber axis [48]. Increasing both the orientation and the degree of crystallinity through the drawing process finally leads to a fiber with greatly improved tenacity and modulus [49–51].

Significant fiber structure development also can be achieved in the melt spinning process if spinning speed is extremely high, where molecular orientation can develop in the molten state. In this case, tensile stress that originates from the strain rate and not from strain itself is the principal reason for the imposed orientation. Since viscosity increases with the decrease of temperature in cooling, the development of orientation in the spinline completes at the moment of solidification. High tensile stress can be achieved simply by applying high spinning speed, because the stresses originating from inertia and air-friction forces are the key factors. It also needs to be noted that crystallization can be accelerated significantly under the effect of molecular orientation.

In order to develop bicomponent fibers with good mechanical properties, it is essential to have information about crystallinity and orientation of both polymers. Wide-angle X-ray diffraction (WAXD) using a two-dimensional detector can provide such data [52]. Raman spectroscopy provides alternative yet supplemental information about fiber structure and morphology [53]. By comparison of the spectroscopic pattern of the orientated fiber with that of the bulk polymer, one can perform quantitative analysis of the fiber structure, e.g. to calculate the Herman's orientation factor. Coaxial distribution of molecular orientation and crystallinity in the cross section of circular fibers can be analyzed using an interference microscope [34, 54]. This technique can also be applied for the analysis of the structure of core and sheath polymers in bicomponent fibers [15].

11.3.2 Mutual Influence of Components on Orientation and Crystallinity

In addition to the high controllability of cross-sectional configuration of fibers, utilization of bicomponent melt spinning for the control of the structure development of individual polymers also attracts much attention [15]. In the

melt spinning process, the polymers mutually modify their thinning behaviors along the spinline and therefore alter the tensile stress development, leading to different structure (orientation and crystallization) and properties when compared with the respective single-component fibers [55].

This mutual influence can be very well demonstrated in the case of core–sheath bicomponent fibers composed of polymers that do not crystallize in the melt spinning process. In poly(ethylene terephthalate) (PET)/polystyrene (PS) bicomponent spinning, orientation development of the polymer with higher glass transition temperature (T_g), PS, is enhanced, while that of the polymer with lower T_g, PET, is suppressed. When the spinline cools down to the T_g of PS, where the molecular chain movement of PS stops, there can be an enhancement of deformation, because the coexistence of PET in the fiber cross section leads to stress concentration on PS. When the spinline temperature further cools down to the T_g of PET, the orientation of PET can be suppressed because thinning of the spinline is already completed at T_g of PS. This mechanism of mutual influence can be found irrespective of where the two components are situated within the fiber. The same principle is applicable to the high-speed spinning of poly(methyl methacrylate) (PMMA)/PET, where enhancement and suppression of orientation of PMMA and PET, respectively, were observed [56].

Even when one of the polymers in the bicomponent spinning possesses good crystallizability, in many cases, the same mechanism can be applied. Examples are the combinations of poly(butylene terephthalate) (PBT)/poly(butylene adipate-*co*-terephthalate) (PBAT) [1], PET/PE [57, 58], PET/PP [15], and thermotropic liquid crystalline polymer (TLCP)/PP [59]. In these cases, when PBT, PET, or TLCP loose fluidity in the spinline, the counterparts are considered to be still in a molten state. Therefore, structure formation of the former was enhanced, while that of the latter was suppressed.

For PBT/PBAT core–sheath fibers, the mutual interaction in the bicomponent melt spinning process also improved the high-speed processability (in terms of highest take-up speed) of both polymers, when compared with the corresponding monocomponent spinning [1]. For PET/PE bicomponent fibers, structural formation of the PET component was promoted both when acting as the core [57] and when positioned in the sheath [58], whereas the structure development of PE was suppressed in both cases. Enhanced structure formation of the PET core can be noticed with PP sheath [15]. For TLCP/PP bicomponent fibers, enhancement and suppression of structure development of TLCP and PP, respectively, as well as improvement of spinnability, were also reported [59].

When solidification of the spinline starts to occur at high speed because of the orientation-induced crystallization of one component, structure development becomes much more complicated. Even for the combination of polymers with similar T_g, when one component starts to crystallize earlier than the other component, orientation development of one part can be significantly suppressed by its counterpart. Suppression of orientation becomes more prominent when crystallization of the counterpart proceeds at higher temperatures, which generally occurs at higher take-up speed. In the case of the combination of the amorphous atactic polystyrene (a-PS), and crystalline syndiotactic polystyrenes (s-PSs), orientation of a-PS was significantly suppressed at high take-up speed

because of the starting of crystallization of s-PS. The spinnability of both s-PS and a-PS was improved by core–sheath bicomponent spinning [60]. On the other hand, in case of the combination of high and low molecular weight PETs, orientation and crystallization of low molecular weight PET was suppressed when orientation-induced crystallization of high molecular weight PET started to occur at high speed [13].

When both polymers have the capability of crystallization in the bicomponent melt spinning process, the structure formation behavior can reverse at a certain take-up speed. In the case of PP/PE, orientation development of PE was promoted while that of PP was suppressed at low speed [31]. This is because of the higher crystallization rate of PE compared with PP. When the take-up speed exceeds a certain level, however, orientation-induced crystallization of PP starts to occur at a temperature above the crystallization temperature of PE. In this case, orientation of PE can be significantly suppressed. The reversed structure development behavior occurs because the melting temperature of PP is higher than that of PE, while the crystallization rate of PE in the quiescent state is faster than that of PP.

In bicomponent spinning of PET with biodegradable aliphatic polyesters, i.e. PET/poly(butylene succinate/L-lactate) (PBSL) and PET/poly(L-lactic acid) (PLLA), enhanced structure formation of PET was observed even after applying high draw ratios of 5 or 7 [61]. When take-up speed in the melt spinning process is relatively high, such effect can be more intense.

When drawing is applied after solidification of the bicomponent spinline, structure development of both polymers can essentially be controlled by the drawing conditions. However, mechanisms for the mutual interaction of components in the melt spinning process stated above may still influence the structure of the final product. Accordingly, the structures of individual polymers in a bicomponent fiber are different from those of melt-spun and drawn monocomponent fibers.

In PET/poly(phenylene sulfide) (PPS) bicomponent fibers [14], structure formation of the polymer that solidifies first, i.e. PPS, is enhanced in the as-spun fibers due to higher tensile stress applied in the melt spinning process, whereas stress relaxation of PET after the solidification of PPS, which corresponds to the cessation of thinning of the spinline, suppressed the orientation development in PET. Such structural difference may lead to highly developed fiber structure for PPS and a more uniform crystal growth in the PET component after applying the drawing process. Similar tendency was found for the PET/polyamide 6 (PA6) bicomponent fibers with spinning speed of 3200 m/min and draw ratio of 1.53. Side-by-side, segmented-pie, and islands-in-the-sea configuration showed that the crystallinity of the PET component was enhanced, whereas the crystallinity of the PA6 component was suppressed. The total (weight percent) crystallinity of the fibers was a function of the interfacial area: the side-by-side type with the smallest interfacial area between the two polymers showed the highest crystallinity [62].

11.3.3 Interfacial Adhesion

For the combination of different polymers in bicomponent fibers, the melting temperatures and viscosities of the materials have to be considered, as well as the bonding strength of boundary surfaces [5, 6]. In the melt state, interdiffusion

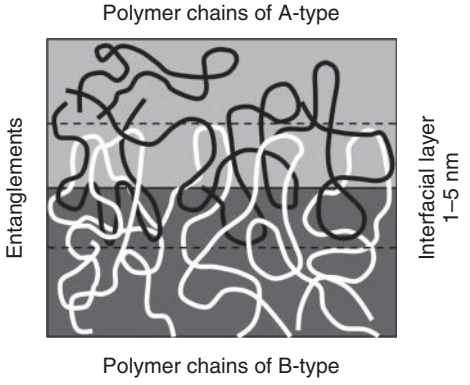


Figure 11.8 Example of interaction of nonmiscible polymers with local segmental diffusion (interdiffusion) of macromolecules across the interface of two polymers [63, 64].

occurs at the interface between the two polymers. For two nonmiscible polymers, the diffusion coefficient is fairly small, and it is unlikely for a chain to migrate completely from one side to the other side of the interface. However, due to local segmental diffusion [63], an interfacial adhesion layer between two incompatible polymers can develop in bicomponent fibers (Figure 11.8). Interdiffusion at polymer interfaces depends on a number of parameters including, but not limited to, temperature, composition of the interface, molecular weight, polydispersity, chain orientation, and molecular structure of the polymers [65]. The interfacial adhesion strength (adhesive bond strength) increases with compatibility, molecular weight, and chain flexibility of the polymers, as well as contact time, temperature, and pressure of the co-flowing melts [64, 66].

To further increase the adhesion between the two polymers of a bicomponent fiber, and thus prevent drawing and service wear, compatibilizers can be applied. In the case of bonding a polyolefin with a polyamide (PA), a maleic anhydride-grafted polyolefin is commonly added to induce compatibilization in situ during the spinning process [9, 67, 68]. Other methods have also been reported for improvement of interfacial adhesion in bicomponent spinning. For example, interfacial reaction such as transesterification between different polyester components, e.g. PET and poly(trimethylene terephthalate) (PTT), can be used to boost the interfacial adhesion [69]. Additionally, mechanical interlocking at the interface, e.g. by employment of a contoured interface, can be used to improve bonding between the two components [70, 71].

Segmented-pie fibers are intended to split. Thus the interfacial adhesion should be limited to allow easy splitting yet being high enough to ensure safe spinning and consecutive drawing, crimping, and textile processing.

11.3.4 Coextrusion Instabilities

In melt spinning, flow instabilities can hinder the production of filaments with uniform cross section [72]. The typical melt instability that affects the flow of a polymer melt in a capillary is melt fracture: entangled polymer melts extruded through a spin pack at high shear rates can exhibit a wavy or spiral distortion of the extrudate [73–75], which can become worse with an inappropriate spinneret design. The occurrence of this instability depends on many factors including

polymer chemistry, molecular weight and distribution, and surface interaction between polymer and die [76, 77].

Another unwanted spinning instability is the so-called draw resonance [78, 79], which is a finite-amplitude periodic fluctuation of the cross-sectional area [73] that starts at a critical drawdown ratio (ratio between take-up speed and extrusion velocity at the exit of the spin pack) [74, 80]. Draw resonance occurs when the mass flow rate is not constant between spinneret and take-up godet. To accommodate the variation, small fluctuations in the fiber cross-sectional area occur and produce oscillations in the fiber tension that amplify the fluctuations [81]. Once started, this resonance may not correct itself, requiring a complete shutdown of the extrusion line. For example, PP is particularly susceptible to draw resonance when quenched in a water bath [80]; usually draw resonance does not occur with polymers like PP, PET, or PA when quenched by air [82]. The critical drawdown ratio is known to be affected by polymer properties, extrusion temperature, filament nominal diameter, and distance between spinneret and water bath [83].

In the coextrusion process, two or more fluids meet in a die and flow with a common interface. This type of flow can quite easily generate all sorts of interface instabilities [84], which occur because of differences between the fluids in some property such as density, viscosity, or elasticity [81]. The viscosity difference is considered more important in driving interface deformation than elasticity effects [85, 86].

The melt viscosities of the two polymers at the die must be similar in order to avoid buckling in the fiber. Otherwise the high-viscosity polymer will lose more momentum than the low-viscosity polymer, and the latter will bend toward the former [87]. Extrudate bending occurs when the bicomponent stratified system is in a side-by-side configuration when it emerges from the die, the exit angle decreases as encapsulation progresses, and no extrudate bending occurs when the flow is in a core–sheath configuration [86]. Suggested mechanisms for instabilities in coextrusion include a jump in viscosity and/or first normal stress difference across a flat interface and a coupling of normal stresses with streamline curvature in the region where the two streams merge [88]. When the fluid with higher viscoelasticity is the minority component, i.e. occupies less than half of the channel, a jump in the normal stress difference at the interface is destabilizing; otherwise it is stabilizing (elastic stratification); this stabilizing effect of elasticity can be used to stabilize flow that would otherwise be unstable because of density or viscosity stratification [81].

11.3.5 Encapsulation

Coextrusion experiments [89–97] show that the less viscous melt tends to wrap around the higher viscosity polymer (Figure 11.9). The degree of this interfacial distortion depends primarily on the extent of the viscosity difference and the residence time, with an increasing length-to-diameter (L/D) ratio of the extrusion capillary amplifying the effect [98]. When the less viscous component migrates toward the die wall, the flow minimizes its viscous dissipation (promoted by thermodynamics) [99]. This can be significant for extruding highly viscous

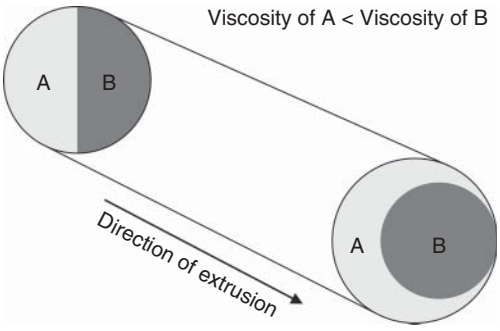


Figure 11.9 Two polymer melts introduced side by side into a capillary experience interfacial distortion during flow of the melts, if the viscosities are mismatched: the lower viscosity polymer tends to encapsulate the higher viscosity polymer [85].

polymers, where the exceedingly high pressure drop in a die is a bottleneck to production [93]. Viscosities of polymers are dependent on extrusion temperature and shear rate, both of which may vary within the coextrusion die [85].

11.3.6 Volatiles

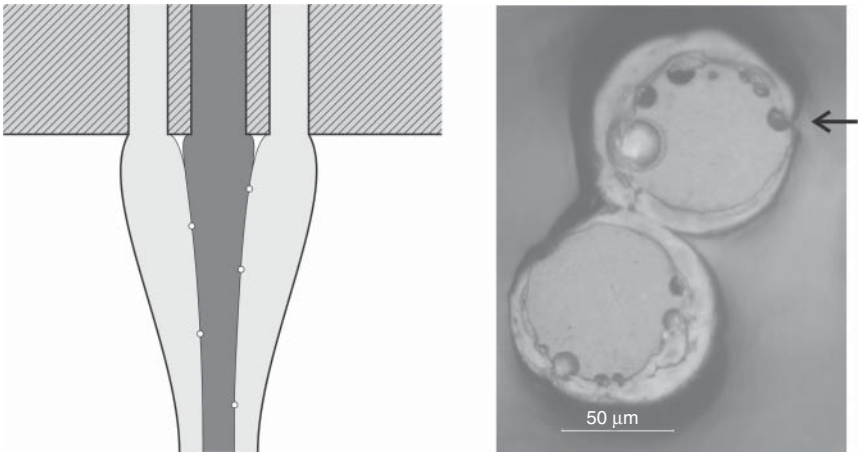
Polymers for man-made fibers can contain dissolved and dispersed gases, as well as volatile liquids and solids (e.g. monomers, water) [100]. When the polymer melt exits the die, respective gas-phase bubbles can evolve, which impair the quality of the fiber [101]. In the case of a bicomponent fiber with a liquid-crystalline-polymer (LCP) core and a PET sheath, a disruption of the core–sheath interface by bubble-like craters was found. The craters could be explained by expanding gas bubbles – degassing products of LCP – trapped in the interface between core and sheath (Figure 11.10). Significant mechanical deformation of the interface was observed, and in some cases the bubbles appeared to push through the sheath interface as the force of the expanding gas overcame the elastic resistance of the sheath layer (indicated by arrow in Figure 11.10b).

11.3.7 Simulation and Modeling

Simulation and modeling of co-flow behavior of polymers and fluids with different rheological properties are discussed in several reports. Mainly surface tension, viscosity, and elastic normal stresses influence the structure of a melt-spun bicomponent fiber, where the viscosity ratio of the two polymers has the most important effect on the final structure of the fiber [51, 102].

Park and coworker [103, 104] simulated bicomponent melt spinning processes and identified the Deborah number as an important parameter regarding the flow behavior of two co-spun polymers of different viscosities. In a follow-up study by Ramos [105–107], the co-flowing behavior of two polymer phases was investigated to predict velocity and radius distribution, assuming Newtonian liquids.

Kikutani et al. [13, 15] developed a one-dimensional model for the spinline dynamics of the bicomponent melt spinning process and discussed the effects of the activation energy for temperature dependence of viscosity, the effects of spinline solidification through glass transition and crystallization, and the effect of molecular weight (absolute value of viscosity) difference for the mutual



(a) (b)

Figure 11.10 (a) In a multiple die core–sheath spinneret, the polymer flow produces a vacuum between core and sheath at the die exit. This vacuum is filled by dissolved/dispersed gases and volatile liquids/solids evaporating from the polymers. As a result, bubbles can accumulate between core and sheath. The bubbles remain when the polymers solidify before the content dissolves or condensates. (b) Optical microscopy images of the cross sections of bicomponent fibers – LCP (core) and PET (sheath) – with bubble-like craters disrupting the core–sheath interface.

interaction of two components for orientation development and relaxation behaviors in the spinning line. Ji et al. [108] investigated different parameters influencing viscosity and flowing instability and developed a one-dimensional model by ignoring surface tension and gravity forces.

Simulation and modeling of two-phase flows is of particular importance when it comes to semicrystalline polymers [109]. Fiber spinning from such polymers is often accompanied by the flow-induced crystallization, which necessitates a model capable to represent both the crystalline and amorphous phases. A pioneering study on the coexistence of these phases was carried out by Kulkarni and Beris [110] who followed the onset and development of crystals by mixing a viscoelastic fluid (representing the amorphous phase) and an anelastic solid (representing the crystalline phase) in a model. A macroscopic continuum model was developed by Doufas et al. [111] who also utilized the Avrami model. In their work, a Giesekus model was incorporated for the amorphous phase, while the crystalline phase was represented by a collection of beads forming rigid rods that could grow and orient in the flow field. The stress and momentum balance as well as the relation of the crystallinity with the relaxation time of the system were later used to couple the descriptions of the two phases in a general mathematical model [112, 113]. The resulting model was shown to be capable to correctly predict the experimental spinline data [114–117]. The latest updates on such approaches can be found in the works of Francisco et al. [118, 119] who developed a two-dimensional model to estimate the temperature distribution, crystallinity, and orientation. Moreover, Zhu and coworkers [120] have studied

the dynamics of spinline formation during bicomponent fiber spinning using a log-additive model for elongational viscosity.

The flow inside a bicomponent die is typically a high Weissenberg number and high Deborah number flow. Therefore, nonlinear viscoelastic effects can significantly affect the evolution of the interface. Existing work in modeling and simulation of bicomponent spinning, however, mostly focused on viscous constitutive models. It is prudent to investigate more realistic viscoelastic constitutive models in prediction of the spinline development. In addition, the elastic membrane stress of the interface can significantly alter the flow development. Such elastic stress should also be incorporated into flow modeling and simulation.

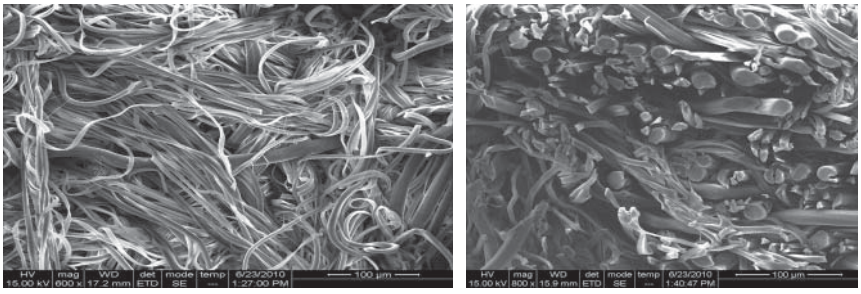
11.4 Post-treatment of Bicomponent Fibers

Usually fibers undergo diverse processing steps to increase the strength, to texturize yarns, or to crimp and cut fibers for a staple fiber or wet-laid process. Heat setting is often applied to crystallize the fibers in order to avoid shrinkage. There are standard processes available, which in most cases can be applied for bicomponent fibers as well. Limitations may occur, for example, when the core polymer needs a certain temperature for heat setting (e.g. PET: 180 °C) and the polymer in the sheath is a PE (melting temperature about 135 °C) for easy bonding. It is obvious that the heat setting must be achieved without a hot contacting surface, but by hot air flow at reduced temperature and low speed.

In the very most cases, splittable fibers are produced by segmented-pie technology (Figure 11.3e). Easy splitting is desired, which may be achieved by hollow segmented-pie fibers [121]. Yet during fiber melt spinning, drawing, crimping, and carding, the fibers must not split, as this would significantly impair these processes. To avoid splitting during processing, but enabling it in posttreatment, the polymer melts should be compatible, but show almost no interdiffusion of macromolecules across the interface, and the polymers should have similar drawing behavior and extensibility to allow deformation during the crimping process at low force. Steam supports the crimping process but can lead to shrinkage and thereby to splitting.

Splittable fibers are processed into knits, woven fabrics, or nonwovens. For splitting, woven and knitted materials are brushed, needled, or treated by water jet, where the mechanical force separates the segments. The filaments are bound in the fabric, which allows a harsh procedure yet limits a spreading of the mechanically induced splitting. In the case of nonwovens, the fibers are being split and entangled by needling or water jets (Figure 11.11). At first the fibers are loose and able to move; they will draw aside the force, thus limiting the effect of splitting. The more the fibers are entangled, the more power each stroke applies to the fibers. Apart from the desired fiber splitting, also fiber break may happen in the needling process. Yet the split fiber bundles are immobilized due to the entanglement.

Other mechanisms to split are heat treatment through air or infrared heating if both of the fiber components have different shrinkage behavior. Chemical



(a) (b)

Figure 11.11 Segmented-pie (PET/PA6) spun-laid, moderately needle punched, and finally hydroentangled nonwovens. (a) Nonwoven surface with completely split fibers. (b) Cross section of the inner part of the nonwoven (200 g/m^2) with only partially split fibers.

splitting is realized by hot water, sodium hydroxide, caustic soda, and benzyl alcohol solutions, eventually supported by ultrasonic force [122].

Hot drawing and heat setting for bicomponent fibers are more complex than single-component fiber. In addition to the increased number of process parameters due to the introduction of a second polymer, the interaction between the two components during drawing and heat setting can greatly limit the process window. Unfortunately, there has relatively been little work about drawing and heat setting of bicomponent fibers. However, some simple rules can be derived from existing work. In the case of core–sheath fibers, one in general can use the core as the stronger component and therefore can select drawing conditions to promote strengthening of the core. When an amorphous component is combined with a semicrystalline component, one can draw the fiber above the glass temperature of the amorphous component and optimize the process condition to promote orientation and crystallization of the crystalline component.

11.5 Applications of Bicomponent Fibers

11.5.1 Fibers as Bonding Elements in Nonwovens

In the through-air thermal bonding of bicomponent fibers for the production of nonwoven fabrics [123, 124], a fiber web mixed with thermo-bondable core–sheath bicomponent fibers is treated by blowing hot air through the web. The temperature of the air needs to be higher than the melting temperature of the sheath component but lower than that of the core component, so that the shape of the fiber can be maintained. With this technique, nonwovens of excellent flexibility, high bulkiness, and good absorbency can be produced. In addition, the product safety is ensured because the use of adhesives can be avoided. Further advancement of thermo-bondable fibers is accomplished through the development of a PP/PE bicomponent fiber with the potential of spontaneous elongation. This fiber is utilized for the production of nonwoven fabrics with soft touch, which are applicable for diapers and hygiene products [125].

11.5.2 Microfibers

One of the first and best-known microfiber products is the artificial leather called Alcantara®. Here, islands-in-the-sea fibers with polyester islands and polystyrene sea are processed to a felt. The sea (matrix) can be dissolved by trichloroethylene [126]. But from an ecological point of view, this process is not acceptable, but could be replaced by water-soluble matrix polymers (e.g. polyvinyl alcohol (PVA), EastOne). The most successful technical application was the combination of PET as islands and EastOne as matrix [127]. Starting from a 1.3 dtex filament, the resulting island fiber diameter after removal of the matrix was 1.8 µm (Figure 11.12). Meanwhile EastOne is replaced by Cyphrex™, shortcut PET fibers (1.5 mm) with diameters of 2.5–4.5 µm, or ribbon shapes of 2.5 × 18 µm. The best-known fabric produced from these fibers is the wet-laid filter Captimax™ from Ahlstrom.

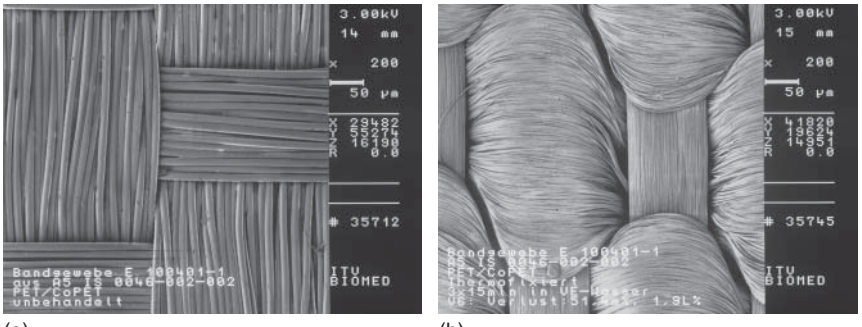
The islands-in-the-sea and segmented-pie approaches have been applied to produce canals for water transportation parallel to the fiber axis. For islands in the sea, the common approach is to use an insoluble polymer as islands and a soluble polymer as matrix and then extract the islands (in the case of islands in the sea through the matrix). Aiming at an environmentally friendly approach, a water-soluble polymer as islands with a water-insoluble polymer as the sea (matrix) polymer can be considered [128].

Under the brand Nanofront™, Teijin produces islands-in-the-sea filaments and staple fibers with PET as islands and modified polyester as matrix. The matrix is dissolved by an alkali solution, which is less economic and ecologic. Teijin even offers such fibers with diameters down to 0.7 µm, with possible applications in functional sportswear, inner wear, skin care products, filters, and precision grinding cloths [129].

A solvent-free alternative to produce microfibers is the application of mechanical stress to separate the different parts of segmented-pie fibers (see Section 11.4).

11.5.3 Fibers with Special Cross Sections

A special feature of the islands-in-the-sea technology is the logotype fiber, where the islands polymer has a different color (Figure 11.13) or has different dyeability



(a) (b)

Figure 11.12 Woven textile of PET/EastOne islands-in-the-sea fibers; (a) before and (b) after removal of the water-soluble matrix.



Figure 11.13 Logotype of ITV; islands-in-the-sea fiber by Hills.

compared with the matrix (e.g. PA vs. PET). The picture quality depends on the number of islands, i.e. the pixel count. On the one hand, a fiber with respective cross section can be used as marketing tool, and on the other hand, it can provide an effective copy protection.

One of the most fascinating fibers is Morphotex® by Teijin. The fiber is a biomimetic example copied from a morpho butterfly, which get the colorful shine of their wings not as a result of pigmentation, but of light diffraction by submicrometer structures inside the fiber [130]. A PET sheath is filled by interpenetrated lamellae from PET and PA, or concentric rings of alternating polymers or winged lamellae close to the natural archetype (Figure 11.14).

11.5.4 Fibers with High-Performance Core

The reinforcement of concrete with fibers can be an economical alternative to conventional steel bar reinforcement. Polyolefin-based bicomponent fibers, with high tensile strength and elastic modulus in the core, nanoparticles and other additives in the sheath, and a structured fiber surface were successfully applied to enhance the mechanical properties of concrete [131]. The superior performance of such fiber-reinforced concrete was shown regarding pullout characteristics of the fiber and bending behavior of the concrete, making these fibers interesting for applications in precast elements, industrial floors, and earthquake protecting systems [131].

Artificial turf is a lower maintenance all-weather alternative to natural turf [132]. While PA carpets have excellent resilience but provoke abrasion injuries (friction burn), PE monofilaments are skin friendly but prone to permanent

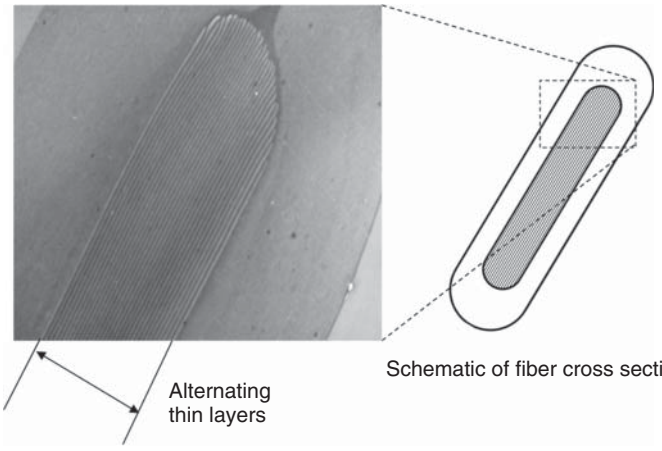


Figure 11.14 Cross section of Morphotex® fiber by Teijin, consisting of 61 alternating thin layers of polyamide and polyester. The interference color of the fiber can be defined by choosing the thickness of each layer between 70 and 100 nm [130].

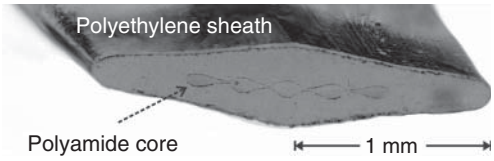


Figure 11.15 Cross section of a PA/PE bicomponent monofilament applied in skin-friendly artificial turf with good resilience [133].

deformation. With the development of PA/PE core–sheath fibers with optimized cross section (Figure 11.15), an artificial turf that shows a better resilience than up-to-date synthetic grass, without cutback in skin friendliness, could be produced [9].

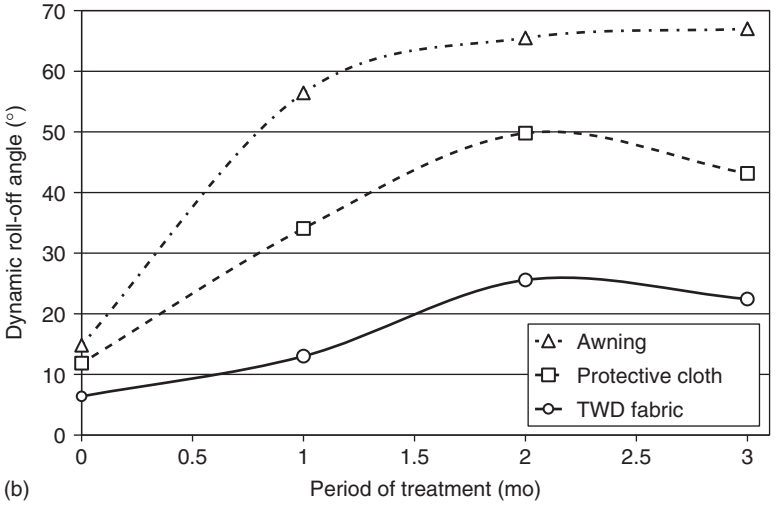
11.5.5 Fibers with Functional Surface

Core–sheath fibers offer the chance to modify the surface while leaving the bulk unchanged. The majority of commercialized bicomponent fibers are binder fibers with a low melting temperature sheath. Typically such fibers are treated in a through-air oven where the binder melts, concentrates at fiber crossings, and glues the fibers together, which finally form a stable network. Another common application is antimicrobial fibers, where the effect of the expensive active substance is required on the fiber surface, i.e. in the sheath only.

Usually easy-to-clean surfaces are achieved by coating of textiles. The so-called lotus effect requires a structured hydrophobic surface. The conventional coating is prone to wear and limits breathability. An alternative approach is to structure the fiber surface, which can be realized by a high filling of the sheath polymer by particles [134]. Again, the function is required on the surface only (Figure 11.16a); the unfilled bulk provides strength and required textile properties. For the required easy-to-clean function, the fibers require an additional hydrophobic treatment. It was shown that a breathable woven textile produced



(a)



(b)

Figure 11.16 Easy-to-clean fiber. (a) Fiber structure and (b) diagram of environmental aging, contact angle vs. aging time [135].

from this novel fiber was superior to a selection of easy-to-clean coated textiles suitable for awnings and protective textiles, respectively (Figure 11.16b).

11.5.6 Biodegradable Fibers

For temporary textile implants, fibers from biocompatible and biodegradable polymers are preferable [52]. The commercially available aliphatic polyesters polylactide (PLA) and polyhydroxyalkanoate (PHA) combine these aspects. PHA/PLA core–sheath fibers were produced, where the PLA component alone was responsible for the tensile strength [43]. In vitro biocompatibility studies with human dermal fibroblasts showed that cells adhered on the fibers, making them good candidates for medical therapeutic approaches. By adjusting

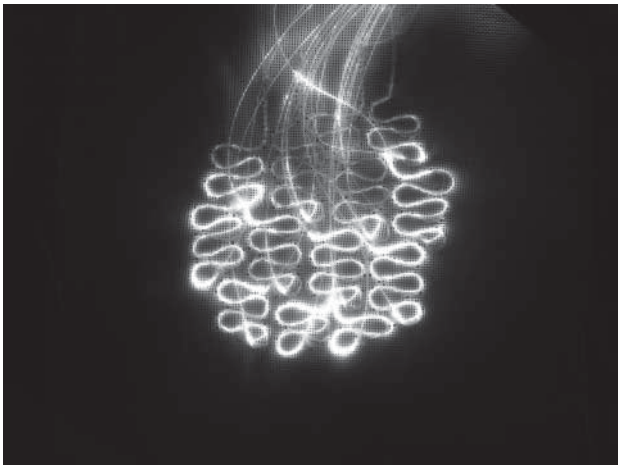


Figure 11.17 Embroidery produced from flexible bicomponent polymer optical fibers.

core–sheath ratio of the bicomponent fiber, a better controlled degradation process could be achieved.

11.5.7 Polymer Optical Fibers

To obtain thin and flexible polymer optical fibers (POFs) for textile applications, bicomponent melt-spun fibers with a cyclic olefin polymer (COP) as the core and a tetrafluoroethylene-hexafluoropropylene-vinylidene fluoride (THV) terpolymer as the sheath have been coextruded on the pilot scale [136, 137]. The bicomponent arrangement could promote the formation of a regular core surface in POFs, because thermal shielding by the sheath component could prevent unevenness at the core–sheath interface. Light propagation and tensile properties of the fibers turned out to be adequate to enable their use in industrially produced luminous textiles (Figure 11.17).

There are some papers and patents on the fabrication of graded-index (GI) POFs utilizing the diffusion of a low molecular weight polymer with high refractive index in the extrusion process of bicomponent fibers. In this process, PMMA blended with diphenyl sulfide (DPS) and virgin PMMA are used as core and sheath components, respectively. With the help of a long capillary die, diffusion of DPS is promoted to produce fibers with a refractive index variation over their cross section [138].

11.5.8 Electrically Conductive Fibers

In order to make fibers antistatic or conductive, electrically conducting materials like carbon black, carbon nanotubes (CNTs), graphene, or metal powders are used as additives. Depending on the type of additive, a polymer compound with 10–30 wt% of conductive additive is generally required to achieve conductivity [139]. As a fiber melt-spun from a respective compound would have a very low

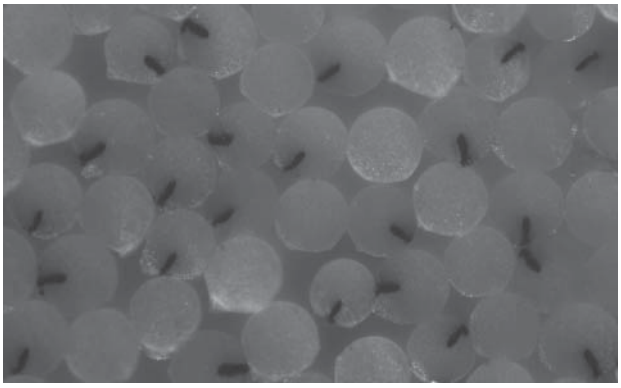


Figure 11.18 Yarn with 50% antistatic side-by-side filaments melt-spun on the pilot-scale (filament diameter approx. 50 µm). The main component is pure polyamide; the side component is a polyamide mixed with carbon black.

tenacity, bicomponent fibers with an antistatic compound as minor element have been introduced, e.g. "Belltron" (side by side) by Kanebo or "Antistat" (core–sheath) by Perlon Nextrusion. Side-by-side bicomponent fibers with the conductive element buried partially inside the filament can attenuate the unrequested dark color coming from carbon black (Figure 11.18).

Lund and Hagström, Nilsson et al., and Glauß et al. [140–143] reported about bicomponent fibers developed for piezoelectric applications, with carbon-black or CNT-filled polyolefin core and a polyvinylidene fluoride (PVDF) sheath. Straat et al. [144] developed an electrically conducting fiber with carbon-black and MWNT-filled PE core and PA sheath. They developed a solution for a common problem: as-spun fibers with reasonable conductive properties loose the conductivity at drawing. So one has to choose between acceptable strength or conductivity, respectively. The reason for the loss of conductivity is the orientation of the fillers and especially of CNT at the drawing. Straat et al. [144] produced the bicomponent fibers and drew them. After a heat treatment at 190 °C, far above its melting point, the molecules of the PE core relax and coil back resolving the orientation of the carbonaceous fillers. This gains the conductivity back by up to factor 2. Conductivity after heat treatment reached values $>200 \times 10^{-3}$ S/cm. Strength up to 36 cN/tex was reported only before heat treatment. From other data one can conclude that heat treatment leads to a decrease in tensile strength of about 20%. Convincing data of fibers were reported for both conductivity (24×10^{-3} S/cm) and strength (31.1 ± 4.2 cN/tex) after heat treatment.

11.5.9 Liquid-Core Fibers

Hufenus et al. [40] demonstrated the continuous production of liquid-filled polymeric fibers in a stable melt spinning process at the pilot plant scale (Figure 11.19). The ability to produce a continuous liquid-core fiber (LCF) is attractive since post-filling of a hollow fiber with similar dimensions is not practical [145]. As a

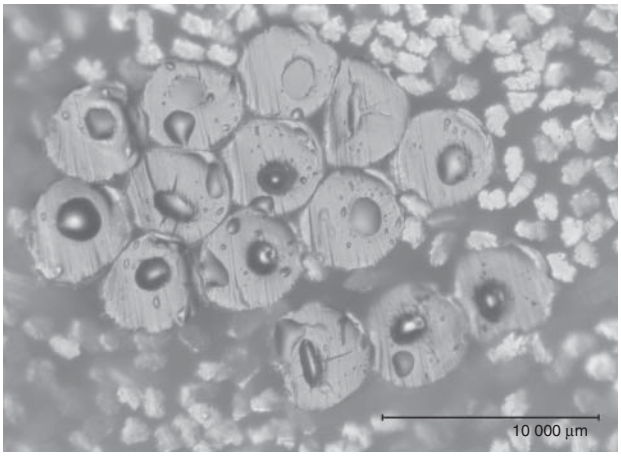


Figure 11.19 Cross sections of liquid-core fibers (LCFs) with 18% liquid content, recorded by optical microscopy (the bright viscose fibers are fillers for supporting sample preparation).

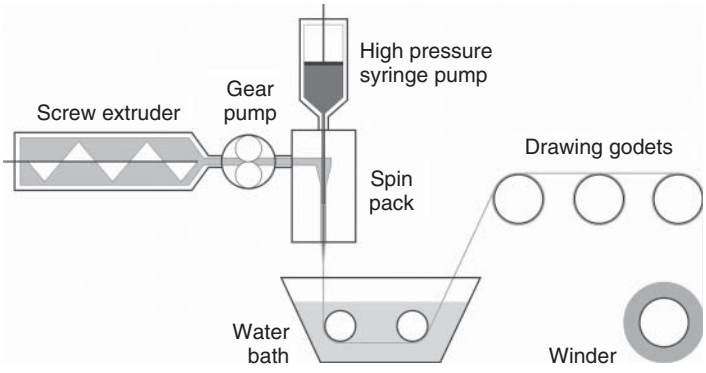


Figure 11.20 Scheme of the LCF coextrusion equipment. Design of spin pack (see Figure 11.5).

result of model experiments [39], a special extrusion line including a quenching, drawing, and winding unit was built (Figure 11.20). A LCF can exhibit significantly enhanced damping properties compared with plain polymeric filaments of same dimensions. This new type of fiber could find future applications in the enhancement of the damping factor of fiber-reinforced lightweight structures, as a fiber can precisely and seamlessly be blended into a composite material, without compromising its structural integrity. Such bicomponent fibers also have potential applications in self-healing composites [146, 147].

11.5.10 Fibers for Fully Thermoplastic Fiber-Reinforced Composites

Core–sheath and islands-in-the-sea bicomponent fibers can be utilized for the production of fully thermoplastic fiber-reinforced composites. In this case, the core or island component, which is designed to become the reinforcing fiber, must have a higher melting temperature than the sheath or sea component, which

is the designated matrix material. Such a fiber-reinforced composite can be fabricated by compression molding of aligned bicomponent fibers at a temperature in between the melting temperatures of both components. The fabrication of respective composites with a structural gradient mimicking the structure of bamboo was also proposed [59].

More recently, the fabrication of fiber-reinforced composites through the compression molding of fabrics from core sheath bicomponent fibers of high and low molecular weight PET was proposed. In this case, a high-speed bicomponent spinning process was utilized to fabricate fibers with highly oriented and crystallized core and low oriented amorphous sheath (see Section 11.3.1). These fibers can be compression-molded at a temperature higher than the glass transition temperature but lower than the melting temperature of PET [148].

Leal et al. [41] introduced a novel approach for the development of ultralight, fully thermoplastic fiber-reinforced composites, based on hybrid yarn produced with a modified wire coating (overjacketing) process (see Figure 11.6). The composite material consisted of a polyolefin plastomer (POP) matrix reinforced with ultrahigh molecular weight polyethylene (UHMWPE) fibers. The interfacial affinity of both polyolefins was enhanced by the deposition of a nanometer-scale polar functional plasma polymer film on the surface of the filaments within a reel-to-reel continuous process. The activated UHMWPE yarn was subsequently coated (overjacketed) with a layer of the matrix material. Alternate layers of woven hybrid yarn and woven pure UHMWPE yarn were then stacked, and the layup was consolidated by hot compaction, resulting in a composite laminate with a fiber volume fraction of 0.54 and a density of 0.93 g/cm^3.

11.5.11 Shape Memory Fibers

Two polymers with different phase transition temperature can be combined to form a composite material with a shape memory character [149]. Bicomponent spinning provides a useful platform for engineering shape memory composites or blends. Spontak and coworkers recently demonstrated a bicomponent core–sheath fiber with a shape memory character [150]. The core is made of a thermoplastic elastomer (TPE), poly[styrene-*block*-(ethylene-*co*-butylene)-*block*-styrene], and the sheath PE. A new shape can be programmed by deforming the fiber above the soften temperature of PE and quenching to preserve the shape. Upon reheating above PE's softening temperature, the original shape can be recovered.

References

1 Shi, X.Q., Ito, H., and Kikutani, T. (2006). Structure development and properties of high-speed melt spun poly(butylene terephthalate)/poly(butylene adipate-*co*-terephthalate) bicomponent fibers. *Polymer* 47 (2): 611–616.

2 Huang, J., Baird, D.G., Loos, A.C. et al. (2001). Filament winding of bicomponent fibers consisting of polypropylene and a liquid crystalline polymer. *Composites Part A: Applied Science and Manufacturing* 32 (8): 1013–1020.

3 Kathiervelu, S.S. (2002). Bicomponent fibers. *Synthetic Fibres* 31 (3): 11–16.
4 Koslowski, H.J. (2009). Bicomponent fibers: processes, products, markets. *Technical Textiles* 52 (5): E202–E204.
5 Houis, S., Schreiber, F., and Gries, T. (2008). Fiber table: bicomponent fibers (Part 1). *Chemical Fibers International* 58 (1): 38–45.
6 Houis, S., Schreiber, F., and Gries, T. (2008). Fibers-fiber table: bicomponent fibers (Part 2). *Chemical Fibers International* 58 (3): 158–165.
7 Fourné, F. (1999). Synthetic Fibers. Munich: Hanser Publishers.
8 Walczak, Z.K. (2002). *Processes of Fiber Formation*, 1e. Amsterdam: Elsevier Science Ltd.
9 Hufenus, R., Affolter, C., Camenzind, M., and Reifler, F.A. (2013). Design and characterization of a bicomponent melt-spun fiber optimized for artificial turf applications. *Macromolecular Materials and Engineering* 298 (6): 653–663.
10 Mukhopadhyay, S. (2014). Bi-component and bi-constituent spinning of synthetic polymer fibres. In: *Advances in Filament Yarn Spinning of Textiles and Polymers* (ed. Dong Zhanged), p. 113. Cambridge, UK: Woodland Publishing.
11 Mochizuki, M. and Matsunaga, N. (2016). Bicomponent polyester fibers for nonwovens. In: *High-Performance and Specialty Fibers* (The Society of Fiber Science and Technology), pp. 395–408. Tokyo: Springer Japan.
12 Yang, H.H. (2007). Polyamide fibers. In: *Handbook of Fiber Chemistry* (ed. M. Lewin), 31–137. CRC Press.
13 Radhakrishnan, J., Kikutani, T., and Okui, N. (1997). High-speed melt spinning of sheath-core bicomponent polyester fibers: high and low molecular weight poly(ethylene terephthalate) systems. *Textile Research Journal* 67 (9): 684–694.
14 Perret, E., Reifler, F.A., Hufenus, R. et al. (2013). Modified crystallization in PET/PPS bicomponent fibers revealed by small-angle and wide-angle X-ray scattering. *Macromolecules* 46 (2): 440–448.
15 Kikutani, T., Radhakrishnan, J., Arikawa, S. et al. (1996). High-speed melt spinning of bicomponent fibers: mechanism of fiber structure development in poly(ethylene terephthalate)/polypropylene system. *Journal of Applied Polymer Science* 62 (11): 1913–1924.
16 Tippetts, E.A. (1967). Fiber engineering to meet end use requirements. *Textile Research Journal* 37 (6): 524–533.
17 Hagewood, J. (2014). 3 – Technologies for the manufacture of synthetic polymer fibers A2. In: *Advances in Filament Yarn Spinning of Textiles and Polymers* (ed. Z. Dong), 48–71. Woodhead Publishing.
18 Hills, W.H. (1996). Distribution plate for spin pack assembly. USPTO, US 5562930 A, USA.
19 Robson, T. (2013). *Multicomponent Fiber Extrusion Technology Applied to Precursors*. Buffalo, NY: Carbon Fiber R&D Workshop.
20 Jaffe, M. and East, A.J. (2007). Polyester fibers. In: *Handbook of Fiber Chemistry* (ed. M. Lewin), 1–29. CRC Press.
21 Purane, S.V. and Panigrahi, N.R. (2007). Microfibers microfilaments and their applications. *Autex Research Journal* 7 (3): 148–158.
22 Jeffries, R. (1971). *Bicomponent Fibres*. Merrow Publication.

23 Zhao, R.R., Wadsworth, L.C., Sun, C., and Zhang, D. (2003). Properties of PP/PET bicomponent melt blown microfiber nonwovens after heat-treatment. *Polymer International* 52 (1): 133–137.

24 Tomasino, C. (1992). *Chemistry & Technology of Fabric Preparation & Finishing*. North Carolina State University NC.

25 Baker, B. (1998). Bicomponent fibers: a personal perspective. *International Fiber Journal* 13: 26–42.

26 Yaida, O. (2016). Current status and future outlook for nonwovens in Japan. In: *High-Performance and Specialty Fibers* (The Society of Fiber Science and Technology), pp. 375–393. Tokyo: Springer Japan.

27 Oh, T.H. (2006). Melt spinning and drawing process of PET side-by-side bicomponent fibers. *Journal of Applied Polymer Science* 101 (3): 1362–1367.

28 Prahsarn, C., Klinsukhon, W., Roungpaisan, N., and Srisawat, N. (2013). Self-crimped bicomponent fibers containing polypropylene/ethylene octene copolymer. *Materials Letters* 91: 232–234.

29 Robeson, L.M., Axelrod, R.J., Vratsanos, M.S., and Kittek, M.R. (1994). Microfiber formation: immiscible polymer blends involving thermoplastic poly(vinyl alcohol) as an extractable matrix. *Journal of Applied Polymer Science* 52 (13): 1837–1846.

30 Kamiyama, M., Soeda, T., Nagajima, S., and Tanaka, K. (2012). Development and application of high-strength polyester nanofibers. *Polymer Journal* 44 (10): 987–994.

31 Prahsarn, C., Matsubara, A., Motomura, S., and Kikutani, T. (2008). Development of bicomponent spunbond nonwoven webs consisting of ultra-fine splitted fibers. *International Polymer Processing* 23 (2): 178–182.

32 Sonnenschein, M.F. (1999). Hollow fiber microfiltration membranes from poly(ether ether ketone) (PEEK). *Journal of Applied Polymer Science* 72 (2): 175–181.

33 Oh, T.H., Lee, M.S., Kim, S.Y., and Shim, H.J. (1998). Studies on melt-spinning process of hollow fibers. *Journal of Applied Polymer Science* 68 (8): 1209–1217.

34 Takarada, W., Ito, H., Kikutani, T., and Okui, N. (2001). Studies on high-speed melt spinning of noncircular cross-section fibers. I. Structural analysis of As-spun fibers. *Journal of Applied Polymer Science* 80 (9): 1575–1581.

35 Rwei, S.P. (2001). Formation of hollow fibers in the melt-spinning process. *Journal of Applied Polymer Science* 82 (12): 2896–2902.

36 Su, Y.Y., Rwei, S.P., Wu, L.Y. et al. (2011). Shaping conjugated hollow fibers using a four-segmented arc spinneret. *Polymer Engineering and Science* 51 (4): 704–711.

37 Huang, Q., Seibig, B., and Paul, D. (1999). Polycarbonate hollow fiber membranes by melt extrusion. *Journal of Membrane Science* 161 (1–2): 287–291.

38 De Rovère, A. and Shambaugh, R.L. (2001). Melt-spun hollow fibers: modeling and experiments. *Polymer Engineering and Science* 41 (7): 1206–1219.

39 Heuberger, M., Gottardo, L., Dressler, M., and Hufenus, R. (2015). Biphasic fluid oscillator with coaxial injection and upstream mass and momentum transfer. *Microfluidics and Nanofluidics* 19 (3): 653–663.

40 Hufenus, R., Gottardo, L., Leal, A.A. et al. (2016). Melt-spun polymer fibers with liquid core exhibit enhanced mechanical damping. *Materials and Design* 110: 685–692.

41 Leal, A.A., Veeramachaneni, J.C., Reifler, F.A. et al. (2016). Novel approach for the development of ultra-light, fully-thermoplastic composites. *Materials and Design* 93: 334–342.

42 Johnston, B., Haggard, J., Wilkie, A. et al. (2007). Temperature control system to independently maintain separate molten polymer streams at selected temperatures during fiber extrusion. USPTO, US 7252493 B1. USA: Google Patents.

43 Hufenus, R., Reifler, F.A., Maniura-Weber, K. et al. (2012). Biodegradable bicomponent fibers from renewable sources: melt-spinning of poly(lactic acid) and poly[(3-hydroxybutyrate)-co-(3-hydroxyvalerate)]. *Macromolecular Materials and Engineering* 297 (1): 75–84.

44 Dimla, D.E., Camilotto, M., and Miani, F. (2005). Design and optimisation of conformal cooling channels in injection moulding tools. *Journal of Materials Processing Technology* 164: 1294–1300.

45 Dormal, T. (2008). Rapid manufacturing of mould inserts for tooling improvements. *International Conference on Additive Technologies*, Ptuj, Slovenia.

46 Villalon, A.V. (2005). Electron beam fabrication of injection mold tooling with conformal cooling channels. MSc. Raleigh: North Carolina State University, p. 68.

47 Levy, G.N., Schindel, R., and Kruth, J.P. (2003). Rapid manufacturing and rapid tooling with layer manufacturing (LM) technologies, state of the art and future perspectives. *CIRP Annals – Manufacturing Technology* 52 (2): 589–609.

48 Kikutani, T. (2009). Structure development in synthetic fiber production. In: *Handbook of Textile Fibre Structure – Fundamentals and Manufactured Polymer Fibres* (eds. S. Eichhorn, J.W.S. Hearle, M. Jaffe and T. Kikutani). Elsevier.

49 Smith, K.J. Jr., (1990). The breaking strength of perfect polymer fibers. *Polymer Engineering and Science* 30 (8): 437–443.

50 Spruiell, J.E. (Munich, 2001). Structure formation during melt spinning. In: *Structure Formation in Polymeric Fibers* (ed. D.R. Salem), 5–93. Carl Hanser Verlag.

51 Ziabicki, A. (1976). *Fundamentals of Fibre Formation*. London: Wiley.

52 Hearle, J.W.S. (2008). Fibers, Structure. In: *Ullmann's Fibers: Fiber Classes, Production and Characterization*, vol. 1, 39–79. Weinheim: Wiley-VCH.

53 Lewis, I.R. and Edwards, H.G.M. (2001). *Handbook of Raman Spectroscopy – From the Research Laboratory to the Process Line*. New York: Marcel Dekker.

54 Shimizu, J., Okui, N., and Kikutani, T. (1981). High-speed melt spinning of poly(ethylene terephthalate): radial variation across fibers. *Sen'i Gakkaishi* 47 (4): T135–T142.

55 Kikutani, T., Arikawa, S., Takaku, A., and Okui, N. (1995). Fiber structure formation in high-speed melt spinning of sheath-core type bicomponent fibers. *Sen'i Gakkaishi* 51 (9): 408–415.

56 Yoshimura, M., Iohara, K., Nagai, H. et al. (2003). Structure formation of blend and sheath/core conjugated fibers in high-speed spinning of PET, including a small amount of PMMA. *Journal of Macromolecular Science, Part B Physics* 42 (2): 325–339.

57 Cho, H.H., Kim, K.H., Kang, Y.A. et al. (2000). Fine structure and physical properties of polyethylene/poly(ethylene terephthalate) bicomponent fibers in high-speed spinning. I. Polyethylene sheath/poly(ethylene terephthalate) core fibers. *Journal of Applied Polymer Science* 77 (10): 2254–2266.

58 Cho, H.H., Kim, K.H., Kang, Y.A. et al. (2000). Fine structure and physical properties of poly(ethylene terephthalate)/polyethylene bicomponent fibers in high-speed spinning. II. Poly(ethylene terephthalate) sheath/polyethylene core fibers. *Journal of Applied Polymer Science* 77 (10): 2267–2277.

59 Furuta, T., Radhakrishnan, J., Ito, H. et al. (1999). Fabrication of continuous fiber-reinforced thermoplastic composites with structural gradient from sheath-core type bicomponent fibers. *Composite Interfaces* 6 (5): 451–466.

60 Hada, Y., Shikuma, H., Ito, H., and Kikutani, T. (2005). High-speed melt spinning of syndiotactic-polystyrene; improvement of spinnability and fiber structure development via bicomponent spinning with atactic-polystyrene. *Journal of Macromolecular Science, Part B Physics* 44 (4): 549–571.

61 El-Salmawy, A. and Kimura, Y. (2001). Structure and properties of bicomponent core-sheath fibers from poly(ethylene terephthalate) and biodegradable aliphatic polyesters. *Textile Research Journal* 71 (2): 145–152.

62 Choi, Y.B. and Kim, S.Y. (1999). Effects of interface on the dynamic mechanical properties of PET/nylon 6 bicomponent fibers. *Journal of Applied Polymer Science* 74 (8): 2083–2093.

63 Paul, D.R. (1978). Fibers from Polymer Blends. In: *Polymer Blends* (eds. D.R. Paul and S. Newman), 167–217. New York: Academic Press.

64 Sun, C., Zhang, D., Liu, Y., and Xiao, R. (2004). Preliminary study on fiber splitting of bicomponent meltblown fibers. *Journal of Applied Polymer Science* 93 (5): 2090–2094.

65 Jablonski, E.L. (2002). Interdiffusion phenomena at partially miscible polymer interfaces. PhD thesis. Retrospective Theses and Dissertations: Iowa State University.

66 Cassidy, P.E., Johnson, J.M., and Locke, C.E. (1972). The relationship of glass transition temperature to adhesive strength. *The Journal of Adhesion* 4 (3): 183–191.

67 Ide, F. and Hasegawa, A. (1974). Studies on polymer blend of nylon 6 and polypropylene or nylon 6 and polystyrene using the reaction of polymer. *Journal of Applied Polymer Science* 18 (4): 963–974.

68 Godshall, D., White, C., and Wilkes, G.L. (2001). Effect of compatibilizer molecular weight and maleic anhydride content on interfacial adhesion of polypropylene-PA6 bicomponent fibers. *Journal of Applied Polymer Science* 80 (2): 130–141.

69 Yang, Z., Wang, F., and Xu, B. (2016). Key factors affecting binding tightness between two components of PTT/PET side-by-side filaments. *Industria Textila* 67 (4): 226–232.

70 Ando, S., Tanaka, Y., and Ogata, F. (1969). Specific conjugate composite filament. USPTO, US 3, 458, 390.

71 Levine, M., O'Connor, J., DiTaranto, F. et al. (2005). Durable highly conductive synthetic fabric construction. USPTO, US 20050095935 A1.

72 Gupta, V.B. and Bhuvanesh, Y.C. (1997). Basic principles of flow during fibre spinning. In: *Manufactured Fibre Technology* (eds. V.B. Gupta and V.K. Kothari), 31–66. London: Chapman & Hall.

73 Hatzikiriakos, S.G. and Migler, K.B. (2005). Overview of processing instabilities. In: *Polymer Processing Instabilities* (eds. S.G. Hatzikiriakos and K.B. Migler), 1–12. New York: Marcel Dekker.

74 Denn, M.M. (2004). Fifty years of non-Newtonian fluid dynamics. *AIChE Journal* 50 (10): 2335–2345.

75 Baird, D.G. and Collias, D.I. (1998). *Polymer Processing: Principles and Design*. Wiley.

76 Denn, M.M. (2001). Extrusion instabilities and wall slip. *Annual Review of Fluid Mechanics* 33: 265–287.

77 Migler, K.B., Son, Y., Qiao, F., and Flynn, K. (2002). Extensional deformation, cohesive failure, and boundary conditions during sharkskin melt fracture. *Journal of Rheology* 46 (2): 383–400.

78 Petrie, C.J.S. and Denn, M.M. (1976). Instabilities in polymer processing. *AIChE Journal* 22 (2): 209–236.

79 Jung, H.W. and Hyun, J.C. (2004). Fiber spinning and film blowing instabilities. In: *Polymer Processing Instabilities: Control and Understanding*, Marcel Dekker Series, vol. 102 (eds. S.G. Hatzikiriakos and K.B. Migler), 321–382.

80 Yoo, H.J. (1987). Draw resonance in polypropylene melt spinning. *Polymer Engineering and Science* 27 (3): 192–201.

81 Larson, R.G. (1992). Instabilities in viscoelastic flows. *Rheologica Acta* 31 (3): 213–263.

82 Kase, S. (1974). Studies on melt spinning. IV. On the stability of melt spinning. *Journal of Applied Polymer Science* 18 (11): 3279–3304.

83 Mei-Fang, Z. and Yang, H.H. (2006). *Polypropylene Fibers. Handbook of Fiber Chemistry*, 3e, vol. 8. CRC Press.

84 Mitsoulis, E. (2005). Secondary flow instabilities. In: *Polymer Processing Instabilities* (eds. S.G. Hatzikiriakos and K.B. Migler), 43–71. New York: Marcel Dekker.

85 Dooley, J. (2005). Coextrusion instabilities. In: *Polymer Processing Instabilities* (eds. S.G. Hatzikiriakos and K.B. Migler), 383–426. New York: Marcel Dekker.

86 Karagiannis, A., Hrymak, A.N., Vlachopoulos, J., and Vlcek, J. (1995). Coextrusion of polymer melts. In: *Rheological Fundamentals of Polymer Processing* (eds. J.A. Covas, J.F. Agassant, A.C. Diogo, et al.), 113–137. Kluwer Academic Publishers.

87 Yu, J.-P. (1998). Producing bicomponent Fibers: spinneret design is crucial. *International Fiber Journal* 13: 49–53.

88 Reis, T., Sahin, M., and Wilson, H. (2008). Co-extrusion instabilities modeled with a single fluid. In: *XV International Congress on Rheology: Society of Rheology* (eds. A. Co, L.G. Leal, R.H. Colby and A.J. Giacomm), 150–152.
89 Karami, A. and Balke, S.T. (2000). Polymer blend de-mixing and morphology development of immiscible polymer blends during tube flow. *Polymer Engineering and Science* 40 (11): 2342–2355.
90 Lee, B.L. and White, J.L. (1975). Notes: experimental studies of disperse two-phase flow of molten polymers through dies. *Journal of Rheology* 19 (3): 481–492.
91 Utracki, L.A., Dumoulin, M.M., and Toma, P. (1986). Melt rheology of high density polyethylene/polyamide-6 blends. *Polymer Engineering and Science* 26: 34–44.
92 Lohfink, G.W. and Kamal, M.R. (1993). Morphology and permeability in extruded polypropylene/ethylene vinyl-alcohol copolymer blends. *Polymer Engineering and Science* 33 (21): 1404–1420.
93 Han, C.D. (1975). A study of coextrusion in a circular die. *Journal of Applied Polymer Science* 19: 1875–1883.
94 Stone, H.A., Stroock, A.D., and Ajdari, A. (2004). Engineering flows in small devices: microfluidics toward a lab-on-a-chip. *Annual Review of Fluid Mechanics* 36: 381–411.
95 Minagawa, N. and White, J.L. (1975). Co-extrusion of unfilled and TiO_2-filled polyethylene: influence of viscosity and die cross-section on interface shape. *Polymer Engineering and Science* 15 (12): 825–830.
96 Kerswell, R. (2011). Exchange flow of two immiscible fluids and the principle of maximum flux. *Journal of Fluid Mechanics* 682: 132–159.
97 Ayad, E., Cayla, A., Rault, F. et al. (2016). Influence of rheological and thermal properties of polymers during melt spinning on bicomponent fiber morphology. *Journal of Materials Engineering and Performance* 25 (8): 3296–3302.
98 Southern, J.H. and Ballman, R.L. (1975). Additional observations on stratified bicomponent flow of polymer melts in a tube. *Journal of Polymer Science* 13: 863–869.
99 Borzacchiello, D., Leriche, E., Blottière, B., and Guillet, J. (2014). On the mechanism of viscoelastic encapsulation of fluid layers in polymer coextrusion. *Journal of Rheology* 58 (2): 493–512.
100 Rosato, D.V., Schott, N.R., Rosato, D.V., and Rosato, M.G. (2001). *Plastics Engineering, Manufacturing and Data Handbook*. Kluwer Academic Publishers.
101 Perepelkin, K.E. (1972). The effect of the liquid and gas phase transitions on the extrusion stability in man-made fibre and film processes. *Fibre Chemistry* 3 (2): 115–123.
102 Ward, I.M. and Sweeney, J. (2005). *An Introduction to the Mechanical Properties of Solid Polymers*. Wiley Publication.
103 Lee, W.S. and Park, C.W. (1995). Stability of a bicomponent fiber spinning flow. *ASME Journal of Applied Mechanics* 62: 511–516.
104 Park, C.W. (1990). Extensional flow of a two-phase fiber. *AIChE Journal* 36 (2): 197–206.

105 Ramos, J. (1999). Asymptotic analysis of compound liquid jets at low Reynolds numbers. *Applied Mathematics and Computation* 100 (2): 223–240.

106 Ramos, J. (2001). Drawing of annular liquid jets at low Reynolds numbers. *Computational and Theoretical Polymer Science* 11 (6): 429–443.

107 Ramos, J. (2002). Compound liquid jets at low Reynolds numbers. *Polymer* 43 (9): 2889–2896.

108 Ji, C.C., Yang, J.C., and Lee, W.S. (1996). Stability of Newtonian-PTT coextrusion fiber spinning. *Polymer Engineering and Science* 36 (22): 2685–2693.

109 Ramos, J.I. (2016). Models of liquid crystalline polymer fibers. In: *Liquid Crystalline Polymers* (eds. V.K. Thakur and M.R. Kessler), 411–451. Springer International Publishing.

110 Kulkarni, J.A. and Beris, A.N. (1998). A model for the necking phenomenon in high-speed fiber spinning based on flow-induced crystallization. *Journal of Rheology* 42 (4): 971–994.

111 Doufas, A.K., Dairanieh, I.S., and McHugh, A.J. (1999). A continuum model for flow-induced crystallization of polymer melts. *Journal of Rheology* 43 (1): 85–109.

112 Doufas, A.K., McHugh, A.J., and Miller, C. (2000). Simulation of melt spinning including flow-induced crystallization: Part I. Model development and predictions. *Journal of Non-Newtonian Fluid Mechanics* 92 (1): 27–66.

113 Doufas, A.K. and McHugh, A.J. (2001). Two-dimensional simulation of melt spinning with a microstructural model for flow-induced crystallization. *Journal of Rheology* 45 (4): 855–879.

114 Doufas, A.K., McHugh, A.J., Miller, C., and Immaneni, A. (2000). Simulation of melt spinning including flow-induced crystallization: Part II. Quantitative comparisons with industrial spinline data. *Journal of Non-Newtonian Fluid Mechanics* 92 (1): 81–103.

115 Doufas, A.K. and McHugh, A.J. (2001). Simulation of melt spinning including flow-induced crystallization. Part III. Quantitative comparisons with PET spinline data. *Journal of Rheology* 45 (2): 403–420.

116 Kohler, W.H. and McHugh, A.J. (2007). Sensitivity analysis of low-speed melt spinning of isotactic polypropylene. *Chemical Engineering Science* 62 (10): 2690–2697.

117 Kohler, W.H. and McHugh, A.J. (2008). Prediction of the influence of flow-enhanced crystallization on the dynamics of fiber spinning. *Polymer Engineering and Science* 48 (1): 88–96.

118 Francisco, J., Rodríguez, B., and Ramos, J. (2011). Melt spinning of semi-crystalline compound fibers. *Polymer* 52 (24): 5573–5586.

119 Ramos, J. (2005). Modelling of liquid crystalline compound fibres. *Polymer* 46 (26): 12612–12625.

120 Chen, L., He, H.K., Zhang, Y. et al. (2015). Studies on melt spinning of sea-island fibers. *Fibers and Polymers* 16 (2): 449–462.

121 Prahsarn, C., Klinsukhon, W., Padee, S. et al. (2016). Hollow segmented-pie PLA/PBS and PLA/PP bicomponent fibers: an investigation on fiber properties and splittability. *Journal of Materials Science* 51 (24): 10910–10916.

122 Wang, X., Yao, J., and Pan, X. (2009). Fiber splitting of bicomponent melt-blown nonwovens by ultrasonic wave. *International Journal of Chemistry* 1 (2): 26–33.
123 Kim, H.S., Ito, H., Kikutani, T., and Okui, N. (1997). The thermal-bonding behaviour of polyethylene/poly(ethylene terephthalate) bicomponent fibres. *Journal of the Textile Institute* 88 (1): 37–51.
124 Kim, H.S., Ito, H., Kikutani, T., and Okui, N. (1999). Computational analysis on the thermal bonding behaviour of bicomponent fibres. *Journal of the Textile Institute* 90 (1 Part IV): 508–525.
125 Nakano, Y. (2011). Development of nonwovens for sanitary products. *Sen'i Gakkaishi* 67 (10): P288–P292.
126 DOW. Trichloroethylene: Industrial Use as Process Chemical in Alcantara Material Production. Socio-Economic Analysis. https://echa.europa.eu/documents/10162/18584504/afa_tce-0024-02-sea_en.pdf.
127 Funk, A., Dauner, M., Hoss, M., Rieger, C., Planck, H. (2011). Entwicklung von 1 Mikrometer-Supermikrofilamenten mit der Bikomponenten-Spinntechnik, International Techtextil-Symposium, Frankfurt am Main: 1-28. https://www.tib.eu/de/suchen/id/tema%3ATEMA20110600625/Entwicklung-von-1-Mikrometer-Supermikrofilamenten.
128 Rieger, C., Funk, A., Hoss, M. et al. (2010). Special fiber structures through bicomponent technology. *Chemical Fibers International* 3: 162–163.
129 Kamiyama, M. (2012). Industrial application of polyester nanofiber. *51st Man-Made Fibers Congress*. Dornbirn.
130 Asano, M., Kuroda, T., Shimizu, S. et al. (2001). Fiber structure and textile using same. USPTO, US 6326094 B1.
131 Kaufmann, J., Lübben, J.F., and Schwitter, E. (2007). Mechanical reinforcement of concrete with bi-component fibers. *Composites Part A: Applied Science and Manufacturing* 38: 1975–1984.
132 McLeod, A. (2008). The management and maintenance of second generation sand-filled synthetic sports pitches. National Resources Department, Doctor of Engineering. Cranfield: Cranfield University, p. 351.
133 Hufenus, R., Halbeisen, M., Camenzind, M. et al. (2014). Kunststofffaser für einen Kunstrasenbelag. Europäische Patentschrift, EP 2520696 B1, p. 9.
134 Dauner, M., Hundt, W., Stegmaier, T. et al. (2011). Textile product and production thereof. EP 2061926 B1, TWD Fibres Gmbh.
135 Dauner, M., Hundt, W., Funk, A. et al. (2012). Fibers with easy to clean surfaces. *51th Man-made Fibers Congress*, Dornbirn.
136 Reifler, F.A., Hufenus, R., Krehel, M. et al. (2014). Polymer optical fibers for textile applications: Bicomponent melt spinning from cyclic olefin polymer and structural characteristics revealed by wide angle X-ray diffraction. *Polymer* 55 (22): 5509–5846.
137 Quandt, B.M., Ferrario, D., Rossi, R.M. et al. (2017). Body-monitoring with photonic textiles: a reflective heartbeat sensor based on polymer optical fibers. *Journal of the Royal Society Interface* 14 (128): 20170060.
138 Sohn, I.-S. and Park, C.-W. (2001). Diffusion-assisted coextrusion process for the fabrication of graded-index plastic optical fibers. *Industrial and Engineering Chemistry Research* 40 (17): 3740–3748.

139 Manabe, T. (1997). Speciality polyamide and polyester yarns: an industrial approach to their production and rheology. In: *Manufactured Fibre Technology* (eds. V.B. Gupta and V.K. Kothari), 360–405. Chapman & Hall.

140 Lund, A. and Hagström, B. (2011). Melt spinning of β-phase poly(vinylidene fluoride) yarns with and without a conductive core. *Journal of Applied Polymer Science* 120 (2): 1080–1089.

141 Lund, A., Jonasson, C., Johansson, C. et al. (2012). Piezoelectric polymeric bicomponent fibers produced by melt spinning. *Journal of Applied Polymer Science* 126 (2): 490–500.

142 Glauß, B., Steinmann, W., Walter, S. et al. (2013). Spinnability and characteristics of polyvinylidene fluoride (PVDF)-based bicomponent fibers with a carbon nanotube (CNT) modified polypropylene core for piezoelectric applications. *Materials* 6 (7): 2642–2661.

143 Nilsson, E., Lund, A., Jonasson, C. et al. (2013). Poling and characterization of piezoelectric polymer fibers for use in textile sensors. *Sensors and Actuators A: Physical* 201: 477–486.

144 Stråat, M., Rigdahl, M., and Hagström, B. (2012). Conducting bicomponent fibers obtained by melt spinning of PA6 and polyolefins containing high amounts of carbonaceous fillers. *Journal of Applied Polymer Science* 123 (2): 936–943.

145 Leal, A.A., Naeimirad, M., Gottardo, L. et al. (2016). Microfluidic behavior in melt-spun hollow and liquid core fibers. *International Journal of Polymeric Materials* 65 (9): 451–456.

146 Blaiszik, B., Kramer, S., Olugebefola, S. et al. (2010). Self-healing polymers and composites. *Annual Review of Materials Research* 40: 179–211.

147 Thakur, V.K. and Kessler, M.R. (2015). Self-healing polymer nanocomposite materials: a review. *Polymer* 69: 369–383.

148 Zhang, Y.J., Takarada, W., and Kikutani, T. (2015). Fabrication of fiber-reinforced single-polymer composites through compression molding of bicomponent fibers prepared by high-speed melt spinning process. *Sen'i Gakkaishi* 71 (5): 172–179.

149 Meng, Q. and Hu, J. (2009). A review of shape memory polymer composites and blends. *Composites Part A: Applied Science and Manufacturing* 40 (1): 1661–1672.

150 Tallury, S.S., Pourdeyhimi, B., Pasquinelli, M.A., and Spontak, R.J. (2016). Physical microfabrication of shape-memory polymer systems via bicomponent fiber spinning. *Macromolecular Rapid Communications* 37: 1837–1184.

12

Superabsorbent Fibers

Nuray Ucar and Burçak K. Kayaoğlu

Istanbul Technical University, Faculty of Textile Technologies and Design, Department of Textile Engineering, Inonu Caddesi, No: 65, Gumussuyu, Beyoglu, Istanbul, 34437, Turkey

12.1 Introduction

Superabsorbent polymer (SAP) is a commodity product used in a variety of industries over the last 30 years, from hygiene to filtration and from agriculture to sportswear and food packaging [1]. These materials have added great value to their product applications and improved the lives of millions of people every day. They serve for holding and retaining extremely large volumes of water and aqueous solutions inside, relative to its own mass [1–3]. Highly absorbing polyelectrolyte polymer-based materials are able to absorb up to 50 g of fluid per gram of dry mass; on the other hand, superabsorbent fibers can absorb 100 times its own weight in water [4].

As the population grows, the global demand for absorbent products increases that triggers the growth in global SAPs market. According to Future Market Insights' report [5], by 2020, the value of global SAP market is projected to be slightly over US$9 billion and reach 2,892,400 tons by volume. Another report addresses the expected growth of global SAPs market to reach US$11.03 billion by 2022. BASF SE, Nippon Shokubai, and Evonik Industries are the key manufacturers of SAPs employing 51% of the production [6].

There are many ways to use SAPs such as SAP powder, SAP granule, and SAP fiber. Among these, superabsorbent fiber can be handled easily during processing and may have higher absorption speed than SAP powder/granule, due to their fibrous shape. Thus, superabsorbent fiber can be transformed into yarn to be knitted or woven in single or blended form with other fiber types in order to meet end use expectations. Superabsorbent fiber can also be produced in micro- or nanoscale that provides higher surface area, leading to improvement in absorption and vapor transmission properties.

Handbook of Fibrous Materials, First Edition. Edited by Jinlian Hu, Bipin Kumar, and Jing Lu.
© 2020 Wiley-VCH Verlag GmbH & Co. KGaA. Published 2020 by Wiley-VCH Verlag GmbH & Co. KGaA.

12.2 Overview of Superabsorbent Fibers

12.2.1 History of Superabsorbent Fibers

The first water-absorbent polymer was synthesized in 1938 by the thermal polymerization of acrylic acid and divinylbenzene. In the 1950s, the hydroxyalkyl methacrylate-based hydrogels were manufactured, finding application in contact lenses. In the 1970s, hydrolyzed starch-*graft*-polyacrylonitrile product was produced as the first commercial SAP. Commercial production and utilization of SAP in feminine napkins and baby diapers started in 1978 in Japan and in 1980 in Germany and France, which was followed by Asian countries, United States, and Europe. The worldwide production of SAP reached more than 1 million tons in the late 1990s [7].

Besides the granular SAP, in the early of 1990s, ARCO Chemical developed a superabsorbent fiber [8, 9]. In the 1993, Technical Absorbents in the United Kingdom that was a joint venture between Allied Colloids and Courtaulds has also been one of the manufacturers of Super Absorbent Fibre (OASIS SAF®) [8, 10–13]. Today, Technical Absorbents (TAL) is a subsidiary company of China National BlueStar (Group) Company Limited, who in turn are wholly owned by ChemChina [14].

12.2.2 Main Principle of Superabsorbency

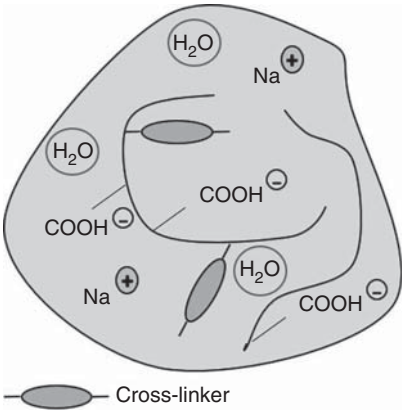
SAPs are natural or synthetic cross-linked polyelectrolytes, comprising an insoluble polymer matrix with about 96% water content, starting to swell upon contact with water or aqueous solutions, resulting in a rubbery hydrogel formation [15–17]. They can also be tailored to be soluble in water and other solvents [14].

SAPs are able to absorb up to several hundred times water per gram of SAP [16, 18]. They are able to swell or shrink in aqueous solutions due to the association, dissociation, and binding of various ions to polymer chains. SAPs may swell in water until an equilibrium state is reached and retain their original shape [15, 16]. The cross-linking degree of SAP directly affects its mechanical strength, total absorbency, and swelling degree. Low density cross-linked SAP has a soft and cohesive gel formation with high absorbent capacity, whereas high density cross-linked polymer shows a firmer gel formation with lower absorbent capacity [1, 8].

Figure 12.1 shows a commercial cross-linked polyacrylic acid (PAA)-based SAP, where negative carboxylate groups are partially neutralized with hydroxides of alkali metals, usually sodium [3, 16, 17]. The main driving force responsible for swelling of SAPs includes hydration due to the presence of hydrophilic chemical groups such as –OH, –COOH, $–CONH_2$, –CONH–, and $–SO_3H$ and capillary areas and differences in osmotic pressure inside and outside the gel [15–17].

When a superabsorbent material comes in contact with water, hydration of sodium ions reduce their attraction to the carboxylate ions and allow them to move freely within the network, which increases the osmotic pressure within the

Figure 12.1 SAP based on polyacrylic acid.



gel [1, 17]. The osmotic pressure is proportional to the concentration of ions in SAPs [16].

The forces that make hydrogel dissolution impossible and help to maintain superabsorbent material's integrity or control the extent of swelling when wet are the presence of cross-links between polymer chains forming a three-dimensional network and hydrophobic and electrostatic interactions [15, 17, 19].

Hydrophilic sodium polyacrylate powder is able to absorb up to 800 times its weight in distilled water and takes the form of a coiled chain (Figure 12.2). When the polymer interacts with water, the sodium (Na) on its polymer chains detaches from the carbonyl (COOH) group creating water-attracting carboxyl (COO^-) and sodium (Na^+) ions. In the presence of water, due to repulsion between the negatively charged carboxyl groups, the sodium polyacrylate chain uncoils and generates a gel substance. The dry coiled SAP molecules form hydrogen bonding during interaction with water, which leads to unfolding and extension of their chains (Figure 12.2) [20].

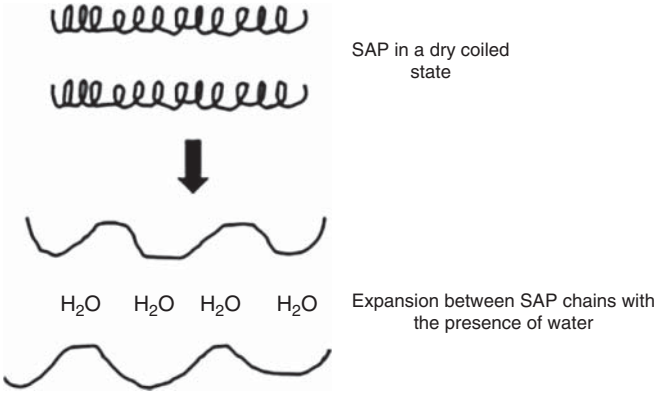


Figure 12.2 Schematic representation of the interaction of a dry superabsorbent polymer with water.

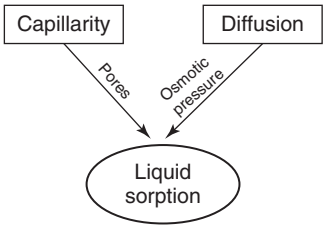


Figure 12.3 Liquid sorption mechanism of a superabsorbent textile-based product.

The liquid sorption capacity of superabsorbent textile-based products is controlled not only by the diffusion of liquid into the superabsorbent fibers but also transport to the pores between the fibers by capillary action [1, 21] (Figure 12.3).

When the solvent is water, hydrophilic interactions between water molecules and hydrophilic groups of the superabsorbent material and electrostatic interactions between ionic groups of an aqueous liquid and superabsorbent material take place [1]. Nevertheless oil superabsorbent materials, based on polyolefins, are oleophilic (oil attracting) and hydrophobic (water repellent). A high oil absorption (up to 45 times of its weight) was reported for a polyolefin-based oil SAP (oil-SAP) [22]. Since the superabsorbent material has affinity to oil, during absorption, hydrophobic interactions occur between oil and fatty liquid and the material [1].

Superabsorbent fibers are superior to conventional wood pulp and cotton linter since they can absorb up to 50 times their mass in water; in turn, wood pulp and cotton linter absorbents absorb approximately six times their mass in water. Their small diameter, around 30 μm, and high surface areas allow these superabsorbent fibers to typically absorb 95% of the ultimate capacity within 15 seconds [23, 24].

The textile-based superabsorbent products are commonly designed to absorb and retain bodily fluids and exudates [1, 25, 26]. Under 0.5–7 kPa load, representing real-use conditions, swollen SAP particles in absorbent products were reported to hold 20–50 g of body liquid per gram of SAP dry mass [19]. When the absorbent products are worn next to the skin, superabsorbent materials help to keep the skin dry, which is a necessity for comfort [3].

Das et al. [21] reported that useful combination of normal plus superabsorbent materials is necessary to achieve enhanced liquid sorption property. Because as the liquid diffuses into the superabsorbent fibers, since pore space is reduced due to gel blocking [19] and extensive swelling of the fibers, the rate of liquid absorption is reduced, preventing further transport of liquid. Therefore Das et al. [21] developed liquid-absorbent composite nonwoven media by combining superabsorbent fibers made from acrylic acid, methylacrylate, and a small quantity of special acrylate/methylacrylate monomer, with normal polypropylene (PP) and polyester fibers. It was reported that nonwovens produced by random mixing of equal proportion of superabsorbent fibers and fine denier circular PP fibers yielded highest sorption capacity and highest sorption rate [21]. Combination of equal proportion of superabsorbent fibers and fine denier (2.5 den) PP fibers compared to the combination of superabsorbent fibers and higher denier (6 den) PP fibers resulted in higher liquid sorption capacity and rate [21]. As a result, better sorption properties can be achieved by the use of finer fibers in the absorbent

structure. It was also reported that the noncircular (trilobal and deep-grooved) fibers displayed poorer sorption characteristics than the circular fibers [21].

12.2.3 Polymer Materials

SAPs are produced by free radical polymerization of partially neutralized acrylic acid and/or other comonomers such as methacrylic acid, blended with sodium hydroxide, in the presence of a suitable cross-linking agent such as *N,N′*-methylene bisacrylamide and 1,1,1-trimethylol-propane triacrylate or ethylene glycol diacrylate [27]. Polyacrylamide copolymer, ethylene maleic anhydride copolymer, and polyvinyl alcohol (PVA) copolymers are among different examples of these polymers [20].

There are different polymerization techniques such as bulk polymerization, solution polymerization, and inverse suspension polymerization. Among the mentioned techniques, a high molecular weight polymer with high purity may be obtained by bulk polymerization [27].

For the production of SAP, solution-based polymerization is most commonly used, which is an efficient and low-cost method. In this method, a mass of reactant polymerized gel is obtained from a water-based monomer solution. Then the final granule size is obtained after chopping and drying processes. The suspension process provides a good production control during polymerization step where a water-based reactant is suspended in a hydrocarbon-based solvent [20].

Research groups have currently focused on producing SAPs from natural polymers such as cellulose and starch by converting them into carboxymethyl derivatives followed by structural cross-linking [4].

Among natural polymers, cotton, rayon, wood pulp are superabsorbent by nature [1, 28]. These fibers may be chemically modified to render them superabsorbent. Cotton fibers can be chemically modified, i.e. grafting with acrylonitrite, to produce superabsorbent grafted cellulosic fibers. Absorbency of rayon fiber was enhanced by introducing additives such as polyacrylic salt and cellulose sulfates to spinning solution [4]. A superabsorbent material was produced from pretreated flax yarn waste by grafting acrylic acid and acrylamide (AM) by free radical graft copolymerization [29].

12.2.4 Production Methods

Besides in the form of powder, foil, or foam, superabsorbent materials are produced in the form of fibers. Superabsorbent fibers are commonly cross-linked acrylic copolymers neutralized by a sodium salt [28].

Because of its fibrous shape, superabsorbent fiber can be mixed with other fibers and can be easily processed through spinning, weaving, and nonwoven technology, leading to better and easier processability compared with conventional SAP powder and granules [30]. In some structures, it is also possible to get 8–10 times higher absorption speed than the SAP powder/granules [31]. OASIS superabsorbent yarn (polyacrylate (copolymer superabsorbent)) which is a type of superabsorbent fiber yarn has a specific gravity of 1.4 g/cm^3, a tenacity

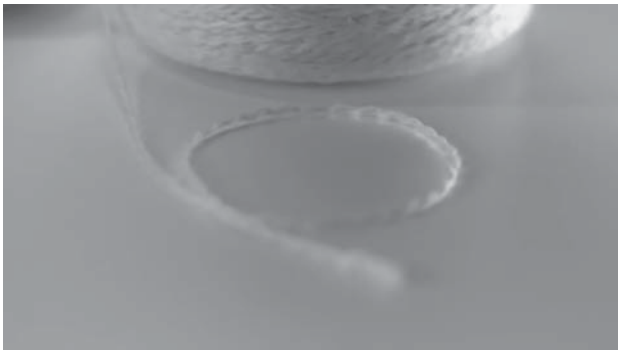


Figure 12.4 Superabsorbent yarn (containing SAF) [14] (having a permission from Technical Absorbents dated May 5, 2017). Source: Reproduced with permission from http://techabsorbents.com/.



Figure 12.5 Swollen superabsorbent yarn (containing SAF) [14] (having a permission from Technical Absorbents dated May 5, 2017). Source: Reproduced with permission from http://techabsorbents.com/.

of 0.6–0.7 g/denier, and an elongation at break of 15–30% [32]. In Figures 12.4 and 12.5, superabsorbent yarn can be seen [14].

Superabsorbent fiber is mainly produced by two different ways, i.e. mixing the superabsorbent material with hydrophobic/hydrophilic material or directly using a SAP [33].

12.2.4.1 Mixing the Superabsorbent Material with Hydrophobic/Hydrophilic Material

Some superabsorbent fibers could be obtained by mixing an SAP with any other material. For example, Lanseal® F has an outer layer with SAP and an inner layer of acrylic fiber itself. Whet it contacts with water, outer surface (SAP) absorbs water and swells (Figure 12.6) [34].

Beskisiz et al. [35] blended polyester staple fiber (PES) with superabsorbent fiber to produce a knitted fabric. They have concluded that water absorption performance of knitted fabric produced by blended yarn (superabsorbent fiber and PES) changes slightly during repeated water absorption test. Although dry cleaning treatment applied on the knitted fabric results in slight change on water absorption performance, washing and drying treatments applied to knitted fabric result in very dramatic change and decrease of water absorbance performance.

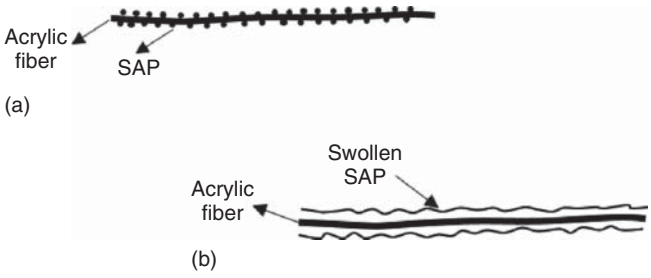
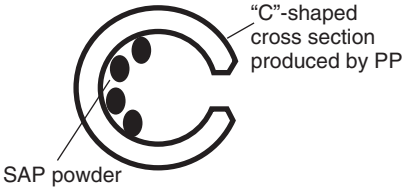


Figure 12.6 (a) Schematic representation of SAP-coated acrylic fiber. (b) After contact with liquid.

Figure 12.7 "C" cross-sectional shape in which the outer surface is polypropylene (PP) and inner cavity is filled by superabsorbent powder.



In one study, it has also been pointed out that as the percentage of SAP fiber in the blend of PES and SAP fiber increases, the absorbent capacity (cm^3/g) increases while the absorbency rate (cm^3/g-sec) decreases because of the transverse diffusion of fluid in the fibers that leads to a reduction in forward velocity and the swelling of fibers, resulting in a decrease of pore size in the structure. However, an increase of saline concentration from 0% to 2% has an opposite effect, i.e. the presence of saline causes a decrease of capacity and increase of rate. The decrease of capacity has been explained by the reduction in the coulombic repulsion in the polymer network, which limits the swelling and penetration of fluid into the fiber [36].

Ucar et al. [37] produced a filament with "C" cross-sectional shape in which the outer surface is PP and inner cavity is filled by superabsorbent powder (Figure 12.7). It has been pointed out that the filament with SAP could absorb water vapor due to the SAP filled into the cavity of C-shaped filament, while PP at the outer surface provides dry feeling.

Eskin et al. [38] also studied on the "C"-shaped filament yarn whose outer layer is consisted of a nonpolar polymer such as PP and maleic anhydride PP (MAPP) and inner cavity is filled by a hydrophilic polymer such as superabsorbent powder. Authors reported that the filament can absorb water (approximately 23%) because of SAP powder without creating any feeling of wetness due to the hydrophobic polymer at the outer layer and completely dries in 20 minutes. The water absorbance performance after washing and drying treatment could be improved because of MAPP.

In these studies [37, 38], the theory was to absorb moisture and liquid into SAP powder placed into cavity of C-cross-sectional-shaped filament that outer surface of filament is hydrophobic polymer (Figure 12.8). Thus, while filament absorbs liquid such as sweat, the skin that contacts with filament will not feel any wetness.

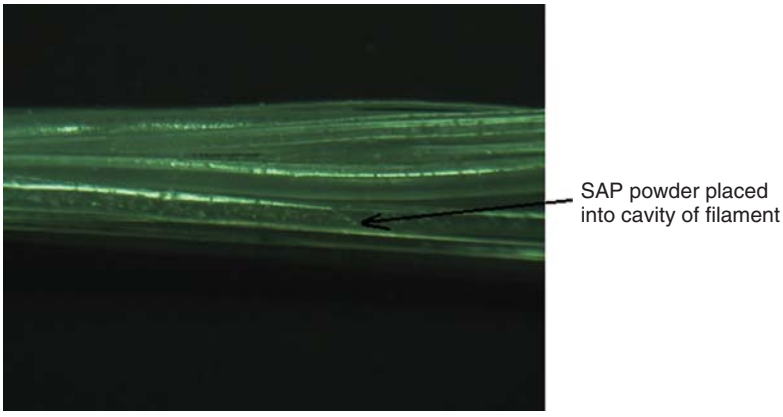


Figure 12.8 C-cross-sectional-shaped filament bundle where cavity of filament was filled by SAP powder.

12.2.4.2 Directly Using a Superabsorbent Polymer for Superabsorbent Fiber Production

In textile industry, there are many ways to produce synthetic fiber such as melt spinning, wet spinning, dry spinning, dry–wet spinning, etc. For micro-superabsorbent fiber, dry spinning and wet spinning methods have been widely used, while it is also possible to produce nano-superabsorbent fiber by the use of an electrospinning technique.

In dry spinning that can have faster production rate than wet or melt spinning, the polymer is dissolved in a volatile solvent, and after many times of filtering, spinning solution is injected through spinneret holes into hot area/drying tower where hot air or other hot gases can be used (Figure 12.9). Hot air evaporates the solvent, leading to the solidification of filament (fiber). Before winding on a take-up cylinder (drawing roller), filaments are drawn for improvement of orientation and crystallization. Evaporated solvent is absorbed or condensed and then recycled that can be costly. Solvent selection is very important with respect to boiling point, toxicity, inertness, vaporization, and thermal stability. Nonpolar

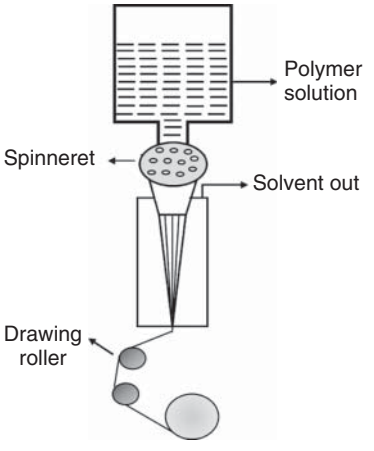


Figure 12.9 Schematic representation of dry spinning.

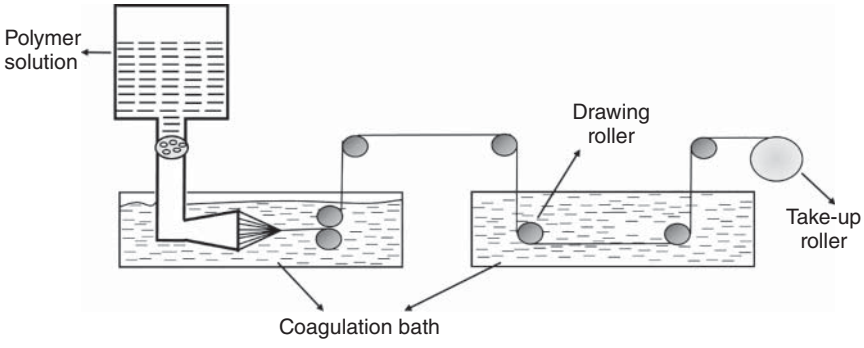


Figure 12.10 Schematic representation of wet spinning.

solvent can be preferred for their low boiling point; however its use can be risky due to building up of electrostatic charges [39, 40].

In wet spinning, the polymer that is dissolved in a nonvolatile solvent is injected into a coagulation bath for solidification of filament/fiber (Figure 12.10). During solidification steps, filament/fiber is also drawn in order to improve the orientation and crystallization. The solvent can then be recovered from wastewater in coagulation bath; however this process can be costly [40].

One of the commercial Super Absorbent Fibre that belongs to Technical Absorbents, UK, is called SAF™ and is produced by solution spinning technique (Figure 12.11). It has been announced that SAF, which is a cross-linked



Figure 12.11 SAF by Technical Absorbents [14] (having a permission from Technical Absorbents dated May 5, 2017). Source: Reproduced with permission from http://techabsorbents.com/.

polyacrylate polymer, is produced by solution spinning through the water evaporation. It has an ability to absorb up to 200 times its own weight in water. SAF with approximately 1.4 g/ml density and 10 cN/tex tenacity with 5% extensibility has a length range of 6–80 mm, a linear density range of 2–20 dtex, 15 minutes free swelling capacity of 60 $g \cdot g^{-1}$ in saline, and 200 $g \cdot g^{-1}$ in distilled water and does not melt and decompose at a temperature higher than 200 °C [10, 14, 41].

There are several studies on superabsorbent fiber produced by wet spinning or dry spinning technique. For example, Kim et al. [42] prepared superabsorbent fiber based on sodium alginate using glutaraldehyde as a cross-linking agent. Alginate that is dissolved in water and aged for 24 hours was extruded into hydrochloric acid (HCl, 35%) coagulation bath in order to produce alginic acid gel filament by wet spinning technique. The gel fiber was then placed in dioxane solution containing glutaraldehyde and 0.1% HCl (35%) in order to cross-link, decreasing the solubility. Then, it has been neutralized to increase an absorbency. It has been pointed out that decrease of glutaraldehyde concentration up to a certain concentration results to an increase of absorbency of alginate fibers in synthetic urine solution and in saline solution.

Liu et al. [30] studied on acrylic-based superabsorbent fiber manufactured by solvent spinning. It was observed that water absorbency of superabsorbent fiber is affected by ionic valence, ion concentration, and pH values of saline solution. Maximum absorbency of superabsorbent fiber is about 117 $g \cdot g^{-1}$. An increase of concentration of saline solution results to a decrease of absorbency, and maximum absorbency could be obtained in neutral solution.

Fei-Ming et al. [43] studied the absorption ability of PVA/PAA-AM-based superabsorbent fibers. It has been reported that AM content affects the absorption ability and a moderate amount of AM can improve the absorption ability.

In addition to conventional micro-superabsorbent fiber production, it is possible to produce nano-superabsorbent fiber by electrospinning. Because of nanostructure with higher surface area leading to improvement in absorption and vapor transmission properties, they can be used in various applications such as food preservation, filtration, personal hygiene products, etc. [44].

At the electrospinning system (Figure 12.12), a polymer solution is subjected to an electric field so that a charged jet of solution is ejected from the nozzle of electrospinning system. The solvent evaporates during traveling of jets through the air, resulting in solidified nanofibers (Figure 12.13) collected onto a collector [44].

There are several studies on nano-superabsorbent fiber produced by electrospinning system [44, 45]. For example, Islam et al. [45] produced nano-superabsorbent fibrous web by using the natural polysaccharide pullulan (PULL), PVA, and montmorillonite (MMT) clay and double distilled water as a solvent. They have reported that these materials have greater environmental and commercial values and low production cost together with better biodegradability. During electrospinning, applied voltage was set to 15 kV, and the distance between nozzle and aluminum foil collector was set to 15 cm. Then, nanofiber web was heated for four minutes at 150 °C without direct contact with

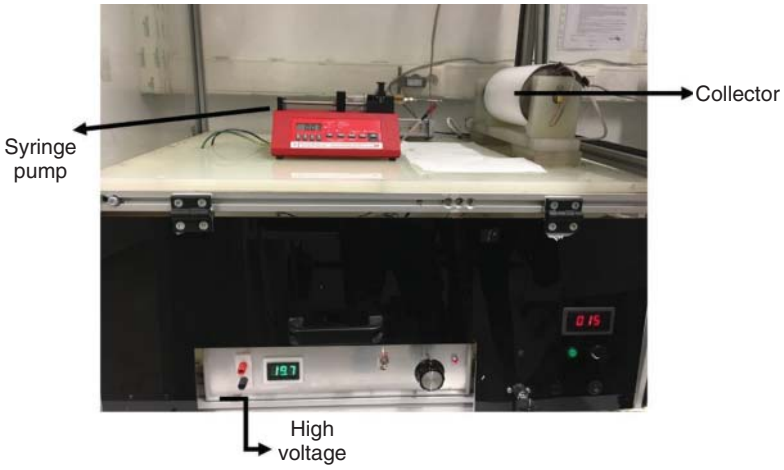


Figure 12.12 Photographic image of an electrospinning system.

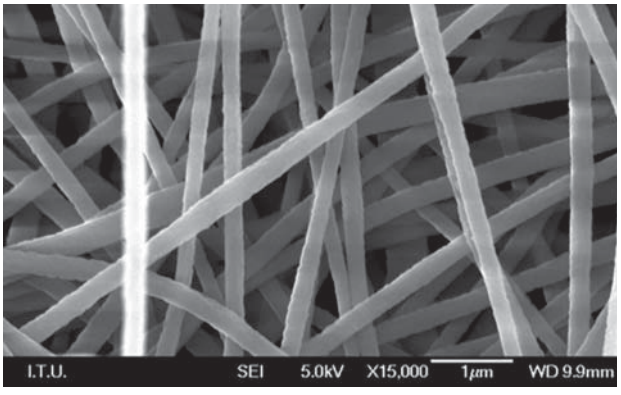


Figure 12.13 Scanning electron micrograph of electrospun nanofibers.

hot plate. Researchers have pointed out that the heat-treated nanocomposite superabsorbent fiber showed water absorbency of 143.42 $g \cdot g^{-1}$ and 39.75 $g \cdot g^{-1}$ in distilled water and a 0.9 wt% NaCl solution. They have pointed out that the heat treatment improved the stability by improvement of the crystallinity in addition to an improvement in water absorbency due to MMT. It has been concluded that an increase of MMT results in an increase of water absorbency.

12.2.5 Test Methods

The performance of superabsorbent textiles is determined by liquid absorption rate and retention measurements. The water/liquid absorption capacity can be measured by gravimetric, dynamic wetting, and topographic measurements. Liquid absorption capacity is expressed in grams of liquid retained per gram of dry superabsorbent sample ($g \cdot g^{-1}$). Another parameter related to superabsorbent material's ability to absorb liquid at a certain temperature is the

absorbency under load (AUL), where there is predetermined load acting on the superabsorbent material. This parameter is important to prevent the leakage of liquid from the absorbent core of a hygiene product under body loads and provide improved surface dryness [1, 4, 46].

Liu et al. [30] used the following equation to calculate water absorbency (Q) of acrylic-based superabsorbent fibers, where U_d and U_s are the weight of the dry and swollen superabsorbent fibers, respectively:

$$Q\,(\mathrm{g/g}) = \frac{U_{S\_}U_d}{U_d} \tag{12.1}$$

The liquid retention measurement involves entire wetting and swelling of the superabsorbent material, which is followed by centrifugation at a fixed rotation speed for a given period of time. This parameter is expressed with the following equation [1, 29], where U_c and D are the weights of the sample after centrifuging and when dry:

$$R\,(\mathrm{g/g}) = \frac{U_c - D}{D} \tag{12.2}$$

Higher wicking values imply higher liquid transport capability of a superabsorbent textile. Wicking parameter may be determined gravimetrically by measuring the amount of liquid drawn into capillaries of a superabsorbent product (in percentage) after a certain period of time or the vertical height (in cm) that the liquid reaches above the level of the reservoir during a certain period of time [47].

High absorbency, protection against leakage, and low rewet are required for absorbent hygiene products. Therefore retention, rewet and absorption time under load are measured for these products. In absorption time under load test, the absorbent product, i.e. a diaper, is placed on a polyurethane foam base onto which a cover plate and weights are placed. The foam base helps to divide the pressure equally across the diaper. Synthetic urine is pumped into an application tube through a hole on the cover plate. An electrode on the application tube connected to a computer measures the time required for the absorption of all the liquid of the tube by the diaper. Absorption rates are reported as ml/s [3].

Rewet property is related to keeping the wearer's skin dry, which shows the amount of absorbed liquid forced out again through the facing under pressure. A weight is applied on a liquid loaded diaper onto which an absorbent material such as filter paper is placed. After the removal of the weight, the amount of liquid absorbed by the absorbent material in grams or milligrams is calculated from the change in material's weight. Besides the abovementioned tests, the time in seconds for liquid to penetrate the top sheet of the diaper is measured that is known as strikethrough [3].

For ionic sensitivity of SAP materials, a dimensionless swelling factor, f, is measured with the following formula [7]:

$$f = 1 - (\text{Absorption in a given fluid/absorption in distilled water}) \tag{12.3}$$

SAP materials with lower swelling factor are desired since it implies lower absorbency loss of the sample swollen in salt solutions.

Free swell capacity of SAP material implies absorption capacity of SAP without pressure. For this test, pure SAP is placed in a tea bag and submerged in 0.9% saline. Then excess solution is removed by letting the bag drip off for 10 minutes. Then swelling capacity is calculated from the difference between the weights of tea bag and initial weight of SAP sample. In centrifuge retention capacity test, the solution between particles is removed by centrifugation of the tea bag. The swelling capacity is calculated by the following formula:

$$S = (W_2 - W_0 - W_1)/W_1 \tag{12.4}$$

where W_1 is the weight of SAP material, W_2 is the weight of the tea bag, and W_0 is the weight of an empty bag [7, 48].

12.3 Application

Superabsorbents may be placed in the product as layers or enclosed in between textile layers in the form of compressed particulate powder [1]. Absorbent structures comprise an absorbent core in which SAPs and/or mixtures of fibrous absorbents from cellulose or fluffed wood pulp and SAPs have been incorporated [2, 3]. Superabsorbent textiles including superabsorbent fibers and their blends with other natural and synthetic fibers can be produced by spinning, weaving, or nonwoven manufacturing techniques [30]. It is also possible to bond or laminate superabsorbent fiber-based fabrics to spunbond fabrics or films for special product applications such as food packaging and filtration. In Figure 12.14, several application areas done by SAF can be seen [14].

Superabsorbent fibers have been utilized mainly in liquid absorbent products such as disposable infant diaper, feminine sanitary napkin, underpad, adult incontinence pad, wound dressing, and absorbent wipes for hygiene and health-care industries [3, 21, 26, 49]. These products can be very thin yet absorbent due to the existence of SAPs [46]. For instance, Mextra® superabsorbent dressing, produced as a wound care product, has a four-layered structure comprising polyacrylate superabsorbent particles [50]. Xtrasorb® is a superabsorbent



Figure 12.14 Application of SAF nonwoven. (a) Packaging, (b) medical, and (c) agriculture [14] (having a permission from Technical Absorbents dated May 5, 2017). Source: Reproduced with permission from http://techabsorbents.com/.

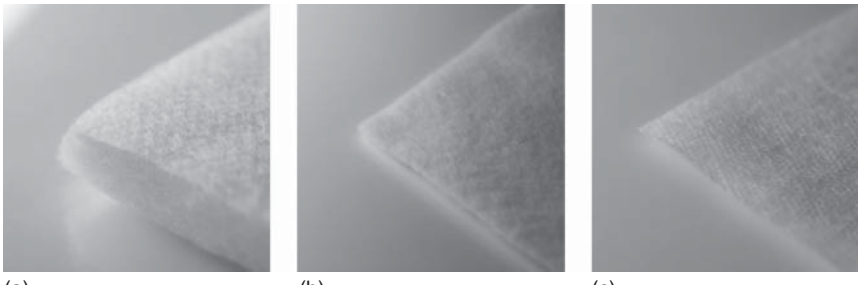


Figure 12.15 Nonwoven structures. (a) Airlaid fabric, (b) needlefelt fabric, and (c) carded fabric [14] (having a permission from Technical Absorbents dated May 5, 2017). Source: Reproduced with permission from http://techabsorbents.com/.

wound dressing that comes in the form of pad and foam and helps to take the wound fluid away from the wound and turn it into gel [51].

Superabsorbent textiles also find application in sportswear and footwear for heat and moisture management [1]. SAF [52] has been converted into 2.0 m wide, 150–1000 gsm fabrics through needle punching technology (Figure 12.15). Airlaid nonwoven fabrics, 50–1000 gsm, have also been produced by blending short staple SAF with wood pulp and low melt fibers [52].

SAF is also blended with man-made fibers such as polyester and nylon to produce spun yarns using traditional yarn spinning technologies, i.e. open end and ring. These yarns may also be used to produce woven, knitted, and net structures.

Swellcoat™ from Fiberline [53] is a water-blocking finish comprising a SAP. It may be applied on fibers, yarns, and textile substrates and generates a stable gel and can absorb up to 10 times its own weight. Universal Carbon Fibres Ltd. [54] produced staple yarns from OASIS Super Absorbent Fibre (SAF), which can absorb high volumes of moisture rapidly and have been used by cable manufacturers.

Baby diapers were reported to have 85% share among hygiene products that depend on superabsorbent materials, while adult incontinence products followed with 10% share [28]. In Figure 12.16, swollen structures of superabsorbent fibers can be seen [14].

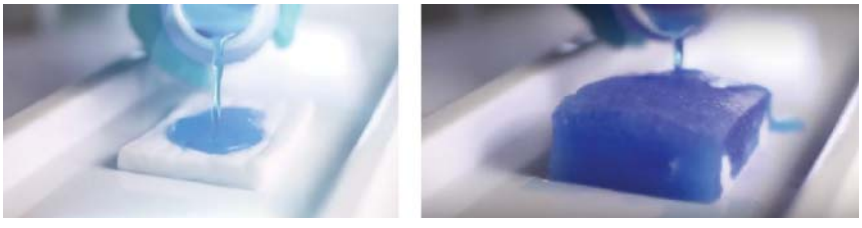


Figure 12.16 Nonwoven. (a) Before swollen and (b) after swollen [14] (having a permission from Technical Absorbents dated May 5, 2017). Source: Reproduced with permission from http://techabsorbents.com/.

According to Future Market Insights' report, the highest global demand for SAP was in disposable diaper industry with more than 74% share in 2014, and the adult incontinence products accounted for almost 12%, while it was over 9% for feminine hygiene products [5]. Commercial brand names like Pampers® and Huggies® use tiny SAP crystals scattered inside the layers of the absorbent core of a baby diaper in order to absorb and trap fluids such as urine and wet poopy [55].

In biomedical applications such as wound dressings, hydrogels present water to the wound site and maintain a moist environment, absorb a degree of wound exudate, and help in the wound healing process [15]. Aquaform, Intrasite, Granugel, Nu-Gel, Purilon, and Sterigel are some of the examples of hydrogels used in biomedical applications [15].

Superabsorbent materials have also been used in technical applications such as oil recovery and air and water purification [56, 57] to absorb other types of fluids such as organic liquids and gases, heavy metal ions, and dyes [1, 4]. Arkema and SNF Floerger are the manufacturers of AM and acrylic acid-based technical SAPs used for cable isolation [58], landscaping, and food packaging [24, 59].

In food pads, superabsorbent materials are used to keep the meat or vegetables fresher for a longer period of time by absorbing their liquids. Dry SAP particles have been reported to be used in concrete mixture as well, serving for absorbing water and finally forming empty pores in the cement paste [16].

Different applications for SAF include filter fabrics, used to remove contaminants and separate water from fuel and oil and also in active sportswear garments, which cools down the user with the evaporation of water [52]. Another field of application for superabsorbent materials is protective clothing, for instance, for fire protection [60]. Bartkowiak [23] developed needled nonwoven materials with high liquid sorption capacity, containing superabsorbent fibers, designed for sweat-absorbing inlays inside protective clothing. They combined "Oasis 102" superabsorbent fibers [61] with cotton, polyester, and PP fibers. These fibers were reported to have high salt water absorption under pressure, which is important for absorption of sweat and human liquids [28].

Superabsorbent textiles were used to enhance the release of agrochemicals and water in agriculture application while they serve for drainage or soil reinforcement in geotextiles application [1]. Aquasorb [62] is a SAP, based on an anionic polyacrylamide, used to increase the water holding capacity of the soil, which is beneficial in growing trees, shrubs, and plants. Another commercial SAP containing potassium, phosphorus, and nitrogen was developed by Ma's Group for agriculture application [63]. Table 12.1 summarizes the common application fields of SAPs.

12.4 Future Scope and Challenges Ahead

There is a growing global demand for improved superabsorbent materials as they find applications in medical, food, and personal care articles representing a multibillion-dollar market [19].

Table 12.1 Main applications of superabsorbent materials.

Superabsorbent powders
Disposable infant diaper
Underpad
Adult incontinence pad
Oil recovery
Air and water purification
Cable isolation
Landscaping
Food packaging
Superabsorbent fibers
Sportswear
Footwear
Protective clothing
Agrotextiles
Geotextiles
Disposable infant diaper
Wound and surgical dressing
Feminine sanitary napkin
Absorbent wipes for hygiene and healthcare industries
Food packaging
Cable isolation
Automotive filter cartridges
Filtration

The introduction of inorganic fillers and nanocomposites such as antiseptic and healing agents to the superabsorbent systems to have added value and functionalities and the use of natural polymers with lower environmental impact and higher biocompatibility are currently the subjects of interest [1]. Research and development efforts on efficient absorbent materials for medical and personal care purposes have shifted toward the development of new absorbent materials with biodegradability and an ability to decompose in landfills [4, 19, 29]. With respect to superabsorbent fibers, research efforts have been carried out to reduce the fiber size to submicron and nanoscales in order to enhance the absorption properties.

12.5 Summary

High volumes of superabsorbent materials have been manufactured worldwide as they have a variety of consumer and industrial product applications such as wound dressings, hydrogels, biomedical applications, hygienic products, oil recovery, air and water purification, cable isolation, landscaping, food packaging, protective clothing, agriculture, etc.

Superabsorbent materials that are commonly cross-linked acrylic copolymers are produced in the form of fibers in addition to powder form, foil, or foam. Superabsorbent fibers can be mixed with other natural and synthetic fibers or polymers. They can be easily processed in the fiber form through spinning, weaving, and nonwoven technology.

Superabsorbent materials, either natural or synthetic based, will continue to expand their application areas by the modification of their morphological, surface, and chemical characteristics and the introduction of new additives to build composite structures and develop new functionalities.

References

1 Glampedaki, P. and Dutschk, V. (2015). Superabsorbent finishes for textiles. In: *Functional Finishes for Textiles: Improving Comfort, Performance and Protection*, 1e (ed. R. Paul), 283–302. Woodhead Publishing.

2 Gupta, B.S. and Smith, D.K. (2002). Nonwovens in absorbent materials. In: *Absorbent Technology*, 1e (eds. P.K. Chatterjee and B.S. Gupta), 372–384. Elsevier Science B.V.

3 Wiesemann, F. and Adam, R. (2011). Absorbent products for personal health care and hygiene. In: *Handbook of Medical Textiles*, 1e (ed. V.T. Bartels), 316–328. Woodhead Publishing.

4 Chinta, S.K., Mhetre, S.B., and Daberao, A.M. (2014). Superabsorbent fibers and antimicrobial activity: a textile review. *Man-Made Textiles in India* 42 (1): 13–17.

5 http://www.futuremarketinsights.com/reports/super-absorbent-polymer-market (accessed 28 April 2017).

6 Global SAP Market Expected to Grow (2015). Nonwovens Industry.

7 Zohuriaan-Mehr, M.J. and Kabiri, K. (2008). Superabsorbent polymer materials: a review. *Iranian Polymer Journal* 17 (6): 451–477.

8 Gooch, J.W. (2010). *Biocompatible Polymeric Materials and Tourniquets for Wounds*, Topics in Applied Chemistry Series, 1e, 34. New York: Springer-Verlag.

9 http://www.m2polymer.com/html/history_of_superabsorbents.html (accessed 28 April 2017).

10 Technical Absorbents Ltd (2015). Super absorbent fibres provide greater flexibility. *Filtration & Separation* 52 (6): 32–34.

11 http://pdfs.findtheneedle.co.uk/9098-21018827-MSDS-International.pdf (accessed 28 April 2017).

12 http://www.innovationintextiles.com/super-absorbent-fibre-technology-well-received-at-cinte-techtextil/ (accessed 28 April 2017).

13 http://www.technicaltextile.net/featureproduct/super-absorbent-fibre-saf (accessed 28 April 2017).

14 http://techabsorbents.com/ (accessed 28 April 2017).

15 Gupta, B., Agarwal, R., and Alam, M.S. (2011). Hydrogels for wound healing applications. In: *Biomedical Hydrogels: Biochemistry, Manufacture and Medical Applications*, 1e (ed. S. Rimmer), 184–227. Woodhead Publishing.

16 Friedrich, S. (2012). Superabsorbent polymers (SAP). In: *Application of Superabsorbent Polymers (SAP) in Concrete Construction*, 1e (eds. V. Mechtcherine and H.-W. Reinhardt), 13–20. Springer.
17 Elliott, M. (2004). *Superabsorbent Polymers*, 1–13. BASF.
18 http://www.venturecenter.co.in/techrx/pdfs/TechShowcase_SAP.pdf (accessed 28 April 2017).
19 Dutkiewicz, J.K. (2002). Superabsorbent materials from shellfish waste - a review. *Journal of Biomedical Materials Research* 63 (3): 373–381.
20 Gooch, J.W. (2011). Super absorbent fibers. In: *Encyclopedic Dictionary of Polymers* (ed. J. W. Gooch), 2e, pp. 712–714. Springer.
21 Das, D., Rengasamy, R.S., and Kumar, M. (2013). Liquid sorption behavior of superabsorbent fiber based nonwoven media. *Fibers and Polymers* 14 (7): 1165–1171.
22 Chung, M. (2015). Polyolefin from commodity to specialty. *Journal of Material Science & Engineering* 4 (2): 1–2.
23 Bartkowiak, G. (2006). Liquid sorption by nonwovens containing superabsorbent fibres. *Fibres & Textiles in Eastern Europe* 14 (1): 57–61.
24 Wiesemann, F. and Adam, R. (2016). An overview of medical textile products. In: *Medical Textile Materials*, 1e (ed. Y. Quin), 14–15. Woodhead Publishing.
25 Tijing, L.D., Ruelo, M.T.G., Amarjargal, A. et al. (2012). Antibacterial and superhydrophilic electrospun polyurethane nanocomposite fibers containing tourmaline nanoparticles. *Chemical Engineering Journal* 197: 41–48.
26 Watson, D.E. (2012). Compositions comprising honey and a super-absorbent material. US Patent 9180219 B2, filed 12 September 2013.
27 http://nptel.ac.in/courses/116102006/17 (accessed 28 April 2017).
28 Bartkowiak, G. and Frydrych, I. (2011). Superabsorbents and their medical applications. In: *Handbook of Medical Textiles*, 1e (ed. V.T. Bartels), 505–546. Woodhead Publishing.
29 Liu, H., Zhang, Y., and Yao, J. (2014). Preparation and properties of an eco-friendly superabsorbent based on flax yarn waste for sanitary napkin applications. *Fibers and Polymers* 15 (1): 145–152.
30 Liu, Q., Ding, Z., and Dong, Z. (2012). Swelling behaviors of acrylic-based superabsorbent fibers. *Advances in Materials Research* 476–478: 1331–1335.
31 Nantong Jiangchao Fiber Products Co., Ltd., China. http://www.jcxw.cn/en.asp (accessed 28 April 2017).
32 http://www.patrickyarns.com/files/687b1d39-8af3-4331-95e7-29cc47823af0--6f55a7f1-820b-400d-bfee-e8f10915a42a/fiber-fact-sheet-2013-lettersize.pdf (accessed 28 April 2017).
33 Kavitha, A., Arjun, D., and Farheen, M.N. (2013). Super absorbent fibre-overview. *International Journal of Advanced Research in Engineering and Technology* 4 (7): 85–91.
34 http://www.toyobo-global.com/seihin/ap/lanseal_f/lanseal_f.html (accessed 28 April 2017).
35 Beskisiz, E., Ucar, N., and Demir, A. (2009). The effects of super absorbent fibers on the washing, dry cleaning and drying behavior of knitted fabrics. *Textile Research Journal* 79 (16): 1459–1466.

36 Chatterjee, P.K. and Gupta, B.S. (2002). *Textile Science and Technology, Absorbent Technology*, 115–117. Elsevier Science B.V.

37 Ucar, N., Beskisiz, E., and Demir, A. (2009). Design of a novel filament with vapor absorption capacity without creating any feeling of wetness. *Textile Research Journal* 79 (17): 1539–1546.

38 Eskin, B., Ucar, N., and Demir, A. (2011). Water vapor absorption properties of a novel filament composed of maleic anhydride polypropylene, polypropylene and super absorbent polymer. *Textile Research Journal* 81 (14): 1503–1509.

39 http://www.polymerprocessing.com/operations/dspin/ (accessed 28 April 2017).

40 http://encyclopedia.che.engin.umich.edu/Pages/PolymerProcessing/FiberSpinning/FiberSpinning.html (accessed 28 April 2017).

41 http://www.packplus.in/images/Technical-Absorbents.pdf (accessed 28 April 2017).

42 Kim, Y.-J., Yoon, K.-J., and Ko, S.-W. (2000). Preparation and properties of alginate superabsorbent filament fibers crosslinked with glutaraldehyde. *Journal of Applied Polymer Science* 78 (10): 1797–1804.

43 Fei-Ming, C., Xian-Zhong, Z., and Hui-Xia, Y. (2013). Effect of the pore fractal dimensions on absorption ability in superabsorbent fibers. *Applied Mechanics and Materials* 345: 205–208.

44 Ali, A.A. (2008). New generation of super absorber nano-fibroses hybrid fabric by electro-spinning. *Journal of Materials Processing Technology* 199: 193–198.

45 Islam, M.S., Rahaman, M.S., and Yeum, J.H. (2015). Electrospun novel super-absorbent based on polysaccharide–polyvinyl alcohol–montmorillonite clay nanocomposites. *Carbohydrate Polymers* 115: 69–77.

46 Buchholz, F.L., Pesce, S.R., and Powell, C.L. (2005). Deswelling stresses and reduced swelling of superabsorbent polymer in composites of fiber and superabsorbent polymers. *Journal of Applied Polymer Science* 98: 2493–2507.

47 Fangueiro, R., Filgueiras, A., Soutinho, F., and Meidi, X. (2010). Wicking behavior and drying capability of functional knitted fabrics. *Textile Research Journal* 80: 1522–1530.

48 Brown, P. (2012). Superabsorbent principles & properties, *VISION Consumer Products Conference*, New Orleans, Louisiana (23–26 January 2012), pp. 1–25.

49 Yu, C., Yu, L., Yiguli, A. et al. (2012). Structure and drug release of superabsorbent sponge prepared by polyelectrolyte complexation and freezing-induced phase separation. *Journal of Applied Polymer Science* 126: 1307–1315.

50 http://www.molnlycke.com.au/wound-care-dressings/absorbent-dressings/mextra-superabsorbent/#confirm (accessed 28 April 2017).

51 http://www.dermasciences.com/xtrasorb (accessed 28 April 2017).

52 https://www.environmental-expert.com/companies/technical-absorbents-42860/products (accessed 28 April 2017).

53 http://www.fiber-line.com/en/products/water-blocking-yarn (accessed 28 April 2017).

54 http://ucfltd.co.uk/water-absorption/ (accessed 28 April 2017).

55 http://www.babygearlab.com/a/11113/What-Is-Inside-Those-Disposable-Diapers (accessed 28 April 2017).
56 Kalayci, V.E., Doyle, J., Jones, D.O. et al. (2011). Superabsorbent-containing web that can act as a filter, absorbent, reactive layer or fuel fuse. US Patent 7, 988, 860 B2, filed 13 March 2008.
57 Yuan, X. and Chung, T.C.M. (2012). Novel solution to oil spill recovery: using thermodegradable 19. Polyolefin oil superabsorbent polymer (Oil–SAP). *Energy Fuels* 26: 4896–4902.
58 Flautt, M.C., Priest, J.R., Stotler, D.V., and Hager, T.P. (2012). Superabsorbent water-resistant coatings. US patent 8, 313, 833 B2, filed 13 February 2009.
59 Mango, P. (2011). The future of superabsorbents in food packaging: nonwovens powders or fibers? Nonwovens Industry, October.
60 Rogers, M.E., Phillips, J.P., and Koene, B. (2008). Flame retardant synthetic textile articles and methods of making the same. US Patent 7, 423, 079 B2, filed 17 May 2005.
61 http://www.m2polymer.com/pdf/Tech%20Sheet_Oasis%20SAF%2052mm_M2PT.pdf (accessed 28 April 2017).
62 http://www.kntp.ru/en/produkty/reagenty/vodouderzhivajushhie-polimery-aquasorb.html (accessed 28 April 2017).
63 http://www.socochem.com/super-absorbent-polymer-for-agriculture.html (accessed 28 April 2017).

13

Elastic Fibers

Lu Jing

The Hong Kong Polytechnic University, Institute of Textiles and Clothing, QT807a, Hung Hom, Kowloon, Hong Kong, China

13.1 Introduction

13.1.1 Definition

Elastic fiber can deform to a relative large elongation in proportion to the load applied and recover its original length after removal of the applied stress. Elastic fiber is an important class of polymer fiber with elastic and recovery performance, which can be achieved by wet spinning, dry spinning, or melt spinning of elastomers or other polymers with specific molecular structures, which can provide high elongation and recovery after post-treatment. The stretch and recovery property of elastic fiber can be controlled by adjusting the polymer structures and post-treatment like heat setting, drawing, or cross-linking. Besides the stretch and recovery performance such as elongation, recovery percentage, and recovery force, other physical properties have also been studied including modulus, strength, heat resistance and anti-chloride, dye ability and UV resistance, etc.

As the idea of most thinking, larger elasticity and recovery is better for elastic fibers. However, diversity and controllable combination of the elasticity and recovery performance is just what the elastic fiber is.

13.1.2 Classification

Naturally, the elastic fiber is commonly classified according to the elastic elongation, that is, high elastic fiber with elongation of 400–800%, medium elastic fiber with elongation of 150–390%, low elastic fiber with elongation of 20–150%, and micro-elastic fibers with elastic elongation below 20% [1].

Based on the polymer structures, elastic fibers consist of polyurethane (PU) elastic fiber, polyester-ether elastic fiber, polyester elastic fibers, olefin-based elastic fiber like XLA, and others such as hard elastic fibers and bicomponent elastic fiber. Shape memory fiber also exhibits elasticity property to some extent, but it will not be included in this chapter.

The most well-known and most widely used elastic fiber is PU elastic fiber, and spandex is the representative, which has been commercialized for many years.

Handbook of Fibrous Materials, First Edition. Edited by Jinlian Hu, Bipin Kumar, and Jing Lu.
© 2020 Wiley-VCH Verlag GmbH & Co. KGaA. Published 2020 by Wiley-VCH Verlag GmbH & Co. KGaA.

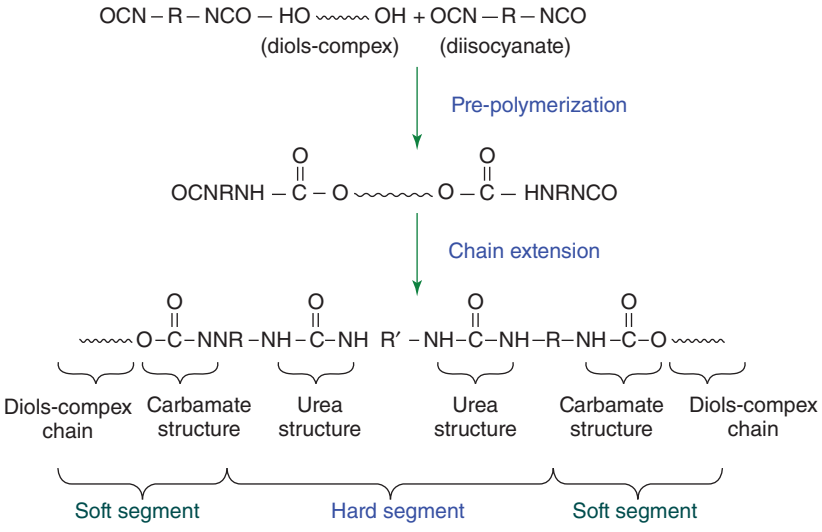


Figure 13.1 Reaction process and structure of PU fibers.

By definition, these fibers have an elongation to break more than 200%, usually 400–800%, and, on release of the deforming stress, return quickly and almost completely to their original length [1, 2]. A major advantage of PU fibers over rubber yarns is that they are easily spinnable into thin fibers, making them suitable for textile applications. PU elastic fiber can be developed by wet spinning, dry spinning, reactive spinning, and melt spinning process from the PU solution or PU polymer with the structure shown in Figure 13.1. The basis for PU elastic fibers in commercial production was the diisocyanate polyaddition technology, which has been discovered in 1937 by Fabricius and Wulfhorst [2].

H. Rinke firstly succeeded in spinning fibers from the high molecular weight PU resulting from the reaction of butylene glycol and hexamethylene diisocyanate. In 1939, P. Schlack obtained high molecular PU by diisocyanate polyaddition process, which has been used since 1941 to synthesize high value elastomers having higher tenacities and better end-use properties than the previously known diene polymers. Reaction spinning was first investigated by H. A. Pohl in 1942 [3]. Windemuth developed a chemical spinning process in which the chemical synthesis of high molecular weight PU occurred simultaneously with extrusion and fiber formation. W. Brenschede succeeded in solution spinning PU elastomers in 1951. Based on earlier work by M. D. Snyder, J. C. Shivers achieved the first large-scale technical production of PU fibers by the dry spinning. The final development of the fibers was worked out by scientists at DuPont and the US Rubber Company. DuPont used the brand name Lycra and began full-scale manufacture in 1962. All large producers attempted to find a melt spinning route for elastane yarns. In 1967 Nisshinbo Industries introduced a melt-spun elastane into the Japanese market. This was followed by Kanebo Ltd. in 1977 and Kuraray Co. Ltd. in 1991. A single-stage synthesis was next sought, in which the PU raw materials are obtained in the form of granulate and are subsequently melt-spun as

Table 13.1 Comparison of four spinning processes of polyurethane fiber.

Item	Dry spinning	Wet spinning	Reactive spinning	Melt spinning
Spinning speed (m/min)	200–900	50–150	50–150	400–1000
Spinning temperature (°C)	200–230	<90	—	160–220
Liner density (tex)	2.22–124.4	4.4–44.0	4.4–38.0	2.2–110
Fiber quality	Excellent	Common	Common	Good
Capacity factor (%)	~70	~1	<5	~20
Pollution	High	High	High	Low

reacted PU. A two-stage reaction process is more modern and provides filaments of improved properties. Despite these developments, dry spinning remains the most widely used production process with high production and better fiber quality [4]. Table 13.1 compares the four spinning methods of PU fibers. Melt spinning of PU fiber has been developed rapidly recently because of the low cost and less pollution.

The polyester elastic fibers of polytrimethylene terephthalate (PTT) fiber and polybutylene terephthalate (PBT) are discovered in the 1940s [5]. PBT fiber production for textiles first started between the end of the 1970s and the mid-1980s in the company of Toray, Teijin, Kuraray, and Unitika in Japan and the company of Celanese in the United States. PTT fiber [5] was first patented in 1941, but until the 1990s, Shell Chemicals developed a low-cost production method. The polyester elastic fibers also show a very good recovery rate under low loads and create a wearing comfort. The fibers can recover 100% from 120% strain. Melt spinning is the main production method for this kind of elastic fiber [6].

Polyether-ester (PEE) fiber was developed early as a thermoplastic elastomer in the 1970s and industrialized in plastic trade. Recently some research center and factories have done some research about the PEE, but do not produce volume. PEE elastic fiber was obtained by melt spinning technology from the polyester and polyether block copolymer [6]. It shows good elastic recovery rate under the elongation of 100%. It has good dye ability and anti-chemical properties. The polyester-ether elastic fibers are promising fibers with wide range uses and lower cost than PU elastic fibers. By controlling the molecular structure, different functional polyester-ether fibers will be developed. The advantages of PEE fiber are the cheap raw materials and nontoxicity and spinning on conventional melt spinning machines for polyester fiber. So the PEE fiber may replace PU elastic fiber in some applications.

Olefin-based stretch fiber is naturally resistant to harsh chemicals, high heat, and UV light. It is a good replacement to PU fiber in some end-use conditions of chloride or high temperature processing. The most well-known olefin-based elastic fiber is XLA fiber developed by Dow Company. Dow XLA elastic fiber can withstand temperature of more than 220 °C. Because of the inherent properties of olefins, it can be bleached, mercerized, stone-washed, or thermosol-dyed using standard processes without special care.

Bicomponent elastic fibers will produce twisting curl effects like natural wool with a textured appearance. The curl effects are formed from the fiber with two parallel components of differing shrinkage or expansion properties. This kind of elastic fiber shows more durable elasticity and recovery than the fibers made of elastomers.

The hard elastic fiber is a small part of elastic fiber family from the production or application view. It shows a low elasticity around less than 50–100%. But the recovery is very good under the lower elongation [6] but deteriorates when the elongation exceeds 200–300%. It was discovered in the 1960s that polypropylene (PP), as well as other highly crystalline polymers, can be produced as elastic fibers. Because of the higher modulus, this kind of fibers was termed as "hard" elastic fiber to distinguish from common elastomer fibers. Hard elastic PP fiber is made by melt spinning and processed by annealing under tension to form lamellar crystallization structure. Between the lamellae, microfibrils are oriented parallel to the draw direction. Under stress, the lamellae tend to separate and voids bridged by fibrils appear [7].

13.2 Structure, Principles, and Characteristics

13.2.1 Structure and Principle in Elasticity

The unique stretch and recovery characteristics of elastic fibers are based on the polymer structure and fiber morphology.

For most kinds of elastic fibers such as PU fiber, PEE elastic fiber, and olefin-based stretch fibers, the elasticity performance comes from the combination of soft segments and the hard segments of the polymer structure (Table 13.2). As shown in Figure 13.2, the soft segments are commonly the long, soft amorphous regions with random molecular structures in natural state, which can be stretched easily under low force and recover to the original coil morphology state due to the elastic entropy. The hard segments are the short, rigid crystalline regions or cross-linking points, which keep the fiber structure stable when stretching, heating, and so forth.

The soft segments of polyether type PU include the polyether as shown in Figure 13.3, such as polyoxyethylene, PP oxide, or polytetrahydrofuran. The interaction between them is mainly the van der Waals force, which is too weak to form hydrogen bonds. The soft segments of polyester-type PU (Figure 13.4) comprise

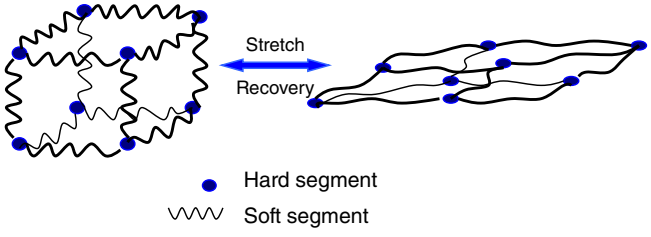


Figure 13.2 Scheme of principles of elasticity with hard and soft segments.

Table 13.2 Elasticity principle of the fibers with hard and soft segments.

Type	Crystalline (%)	Hard segments	Soft segments	Elongation (%)	Recovery at 100% elongation (%)	Fiber examples
Polyurethane elastic fiber	~40	Hydrogen bonds/crystals	Amorphous polyol chains	Maximum ~800	>95	Spandex; Lycra
Polyolefin elastic fiber	~14	Crosskicking and crystals	Amorphous polyolefin chains	Maximum ~500	>90	XLA
Polyether-ester elastic fiber	25–35	Polyester segments	Polyether segments	Maximum ~600	>85	Polybutylene terephthalate–polytetramethylene glycol (PBT–PTMG) fiber; polytrimethylene terephthalate (PTT) fiber; polybutylene terephthalate (PBT) fiber

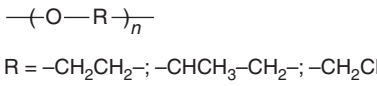


Figure 13.3 Molecular structure of polyether type PU.

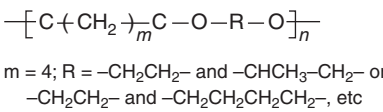


Figure 13.4 Molecular structure of polyester type PU fiber.

polyadipate of mixed dihydric alcohol, which forms the polyester chains. For PU fibers, when the external force is applied to stretch the fibers, the amorphous segments straighten out. This makes the amorphous segments longer, thereby increasing the length of the fiber. When the fiber is stretched to its maximum length, the rigid segments still keep the crystalline states and resist the slippage of amorphous segment chains. After the force is removed, the amorphous segments recoil, and the fiber returns to its original relaxed state [2, 6, 8]. The formation of soft segments and hard segments in PU fibers is due to the thermodynamic incompatibility between the two segments, and PU s undergo micro-phase separation, resulting in the phase-separated heterogeneous structure consisting of hard and soft domains and interphases between them. Better phase separation leads to higher stretch and recovery performance [9, 10]. The hard segments of PU fibers include the main chains of carbamin acid ester and diisocyanate, which have the high cohesive energy and form large amount of hydrogen bonds with each other and give the fiber structure.

Fiber of polyether ester was obtained by melt spinning from the polyester and polyether block copolymer [4, 11]. As shown in Figure 13.5, the PEE fiber is composed by crystalline aliphatic polyester as hard segment A and amorphous aliphatic polyether as soft segment B. Among them, Ar is aryl group of aromatic bi-carboxylic acid, D is the alkyl group of dihydric alcohol, n is the degree of polymerization of polyether, and x is the average polymerization degree of hard segment. The hard segment A and soft segment B are alternated and linked by chemical bonds to form a copolymer. At present, industrialized PEE polymer mainly use polytetramethylene oxide (PTMO) as soft segment and PBT as hard segment. Besides PTMO, polyethylene oxide (PEO), nylon, and polydimethylsiloxane (PDMS) are also used as soft segments. The hard segment can adopt polyethylene (PE) glycol terephthalate or PBT.

The polyester part forms crystalline regions as hard segments. Larger crystal size and polymerization degree of hard segments are helpful to the recovery. To achieve the elasticity property, the contents of polyglycol will be at least 60% or 70–80%, and the polyester contents are only 20–30%. It was a high elastic fiber with breaking elongation of 500%, and the elastic recovery is above 85% at the

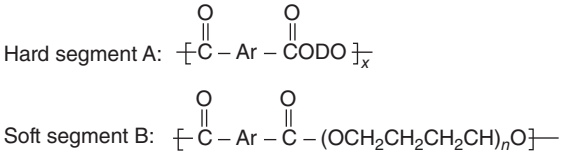


Figure 13.5 Structure of hard segment and soft segment of polyether-ester fiber.

elongation of 100%. It has good dye ability and anti-chemical properties. With the increase of hard segments, under the same spinning parameters, the crystallinity will increase, but the crystal size becomes smaller, which leads to the higher tenacity but less elasticity and recovery. For a kind of PEE fiber with PBT as hard segments and polytetramethylene glycol (PTMG) 2000 as soft segments, when the PBT weight fraction increasing from 40% to 60%, the elastic recovery decreases from 80% to 50%. Heat drawing and heat setting will improve the crystal size and molecular orientation and accordingly increase the elasticity and elastic recovery. After heat setting, the elastic recovery will increase from 80% to 90% [12].

Polyolefin elastic fiber consists of at least 95% polyethylene by mass and a little other olefins. The polyethylene macromolecules partially cross-link and partially crystallize, which make the hard segments. The soft, long amorphous polyethylene macromolecules form the soft segments, which is easily stretched. XLA is a representative polyolefin fiber. The special microstructure of XLA combines long, flexible chains with crystallites, and covalent bonds or cross-links, forming an intricate network. The length of the chains and number of crystallites are specifically controlled to give XLA fiber a unique elastic profile. High stretch is achieved with low levels of force, allowing garments to stretch and flex effortlessly and still return to their original shape.

The polyester elastic fiber mainly includes PTT fiber and PBT fiber. Comparing with PU fibers, the polyester elastic fiber displays lower elongation. The elasticity of this fiber is due to the configuration changing of the molecular chains. As shown in Figures 13.6 and 13.7, molecule chains of polyester fiber are fully extended with two carboxyl groups of each terephthaloyl group in opposite directions, and all open-chained bonds are trans with successive phenylene groups at the same inclination along the chain. PTT has a conformation with bonds of the $–OO(CH_2)_3OO–$ unit having the sequence of trans–gauche–gauche–trans, leading to a concentration of the repeating unit. The opposite inclinations of successive phenylene groups along the chain force the molecular chains to take on an extended zigzag shape, which can be extended and recover easily [6].

Hard elastic fibers exhibit 50–95% recovery from 100% extension. They are generally produced by spinning at relatively high spinline stress levels, and the elastic effect is enhanced significantly by annealing. Traditionally, the recovery of elastic fibers has been explained by the entropic mechanisms of elasticity network theory. The elasticity of the hard elastic fibers, on the other hand, is primarily contributed by energetic rather than entropic mechanisms. Hard elastic fibers may be

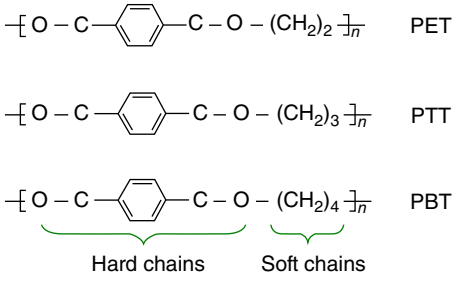


Figure 13.6 Molecular structure comparison of PET, PTT, and PBT fiber.

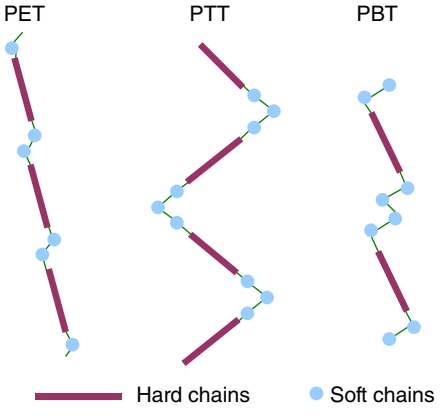


Figure 13.7 Macromolecular structure diagram of PET, PTT, and PBT fiber.

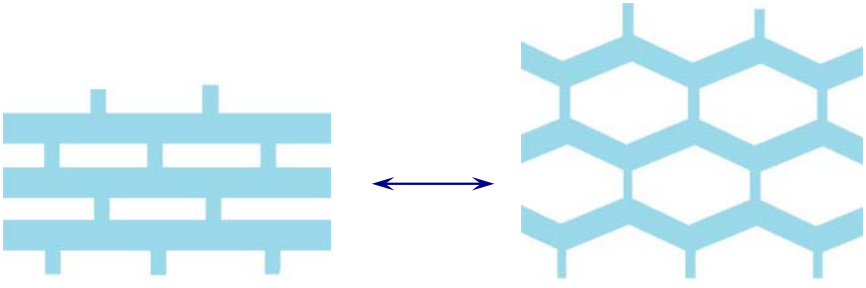


Figure 13.8 Model of lamella structure and microvoids created of hard elastic fiber.

produced from many polymers, including polypivalotactone, acetal copolymer, polybutene-1, poly-4-methyl pentene, polyethylene, and PP [13].

Some structural models have been proposed to explain the elastic properties of these fibers. Clark [13] has given a reasonable model for the mechanism of energy-driven elasticity. The feature of this model is the existence of short tie molecules connecting adjacent lamellae normal to the fiber direction. The short tie molecules comprise the load-bearing elements, transferring stress from one lamella to the next. Figure 13.8 proposed a weblike system that is created by large numbers of lamellae to form a row structure. The interconnecting fibrils will distribute an applied strain in a cooperative action to deform each lamella slightly. Small deformations of the folded-chain lamellae are reversible. If an assembly of lamellae and fibril links is highly oriented, as in a row structure, this effect is additive and produces elasticity in the macroscopic fiber. Figure 13.8 also predicts that a large number of microvoids will develop during fiber extension. The diameter of a fiber with this type of structure should remain constant for a considerable elongation. A plot of relative specific volume versus extension for elastic PP and a classical elastomer confirm the same. The PP volume increases, and the diameter remains constant up to an extension of nearly 100%.

The fibers annealed above 135–140 °C showed complete reversibility for extension as large as 100%. The annealing results in additional ordering of the initial

row-nucleated materials. This ordering also gives higher recoveries after repeated cycles [12].

Because of a higher modulus, the time effects, and the limited extensibility and recovery in comparison to classical elastomers, energy-driven elastic fibers have not been applied widely in textiles.

Although the elastic fiber with soft segment and hard segment shows extraordinary elongation property and good recovery performance, with the cycling use or stretch, the recovery rate will decrease gradually. This is inevitable because of the polymer macromolecule fatigue. The elasticity of bicomponent fibers is with the self-crimp-textured appearance, which is formed from a composition of two parallel but attached fibers with differing shrinkage or expansion properties made by melt spinning method. Since the crimp is naturally formed by heating and not mechanically induced, the fiber gives greater, more durable stretch and recovery than textured yarns that are used for stretch.

13.2.2 Structure and Principle in Other Performances

The thermal behavior of PU fibers at use and processing temperatures are governed by the soft segments. PU with polyester-type soft segments has worse heat resistance property than that of polyester PU fiber. For the polyester-type PU fiber, it will become yellow at 150 °C, and strength will decrease at 170 °C. For polyester-type PU fiber, the strength decreases at about 190 °C. The anti-chemical property of PU fiber is good. PU fibers are soluble in highly polar solvents, such as dimethylacetamide. While PU fibers containing polyether soft segment are less subject to hydrolysis, polyester elastanes are more resistant to oxidation. But the polyester-type PU fiber is poor in alkali resistance. All the traditional PU fibers are with worse anti-chloride performance. Elastane fibers have good resistance to oxygen and ozone. Nitrogen oxides cause a color change to yellow or yellow brown, the intensity depending on the concentration, ambient temperature, and relative humidity. PU fibers are more resistant to aging and abrasion than rubber yarns. Long exposure, particularly to UV radiation, leads to a change in color of the fiber and to photochemical degradation. Polyester urethane has higher resistance to photooxidation than polyether urethane [10].

The polyester elastic fibers have the similar physical properties to the common polyester fibers. However, they also shows some specific performances besides the large elongation and recovery. PTT fiber is a typical polyester elastic fiber. The diacid group affects the mechanical property, and its process ability depends on the type of the diol group. In particular, PTT is a highly crystalline polymer. Its melting temperature is lower than that of polyethylene terephthalate (PET) by 20–30 °C. Therefore, the process ability of PTT is superior to that of PET. The highly flexible PTT fibers are obtained as a result of its low initial modulus. The elasticity and dye ability of PTT are better than those of PET or PBT. It is well-known that the number of methylene unit influences the physical properties of many polycondensation polymers such as polyamides (PAs) and polyesters, which is called the odd–even effect. PTT have the best soft hand of all, as PBT will be close to PET. PTT can be dyeable at low temperature (100 °C) with the same or slightly deeper shades than PET at 130 °C. Disperse-dyed PTT shows

excellent colorfastness to laundering, crocking test, and UV light and ozone. It also has the better abrasion resistance and dimensional stability.

There are many similar properties of PEE fiber and PU fiber. In chemical structure, both fibers have long-chain polyether and the elasticity root from the entropy change. It has good dye ability and anti-chemical properties. But there are many ether bonds, which lead to the poor thermal stability of the PEE fiber. Therefore the temperature in the dry and melt spinning process should be controlled reasonably. The water and oil resistance properties can be enhanced by the larger hard segment concentration in the copolymer. The hot water shrinkage of PEE fiber is large. Heat setting is a useful method to decrease the hot water shrinkage. Under 60 °C relax heat setting, the shrinkage in boiling water decreases from 12% to 2.5% and after heat setting at 100 °C, the shrinkage will decrease to 1%. From the Small-angle X-ray (SAX) data, after relax heat setting, the crystal size of 010 lattice increases from 5.5 to 8.5 nm, and the size of 100 lattice increases from 4.7 to 6.0 nm [9, 10].

The olefin-based elastic fiber is with superior heat resistance because of the cross-links formed in the fiber's molecular structure. The olefin elastic fiber can maintain its integrity at 220 °C for three minutes; however PU fiber comes apart. The fibers are inherently resistant to strong acid or alkali or chloride. But olefins have an affinity to hydrocarbon solvents and mineral oils; the fiber should not be exposed to these classes of chemicals for extended periods of time. UV/xenon resistance makes the fibers to deliver stretch in outdoor applications.

Polymers that can be used for producing hard elastic fibers include semicrystalline polymers as polyoxymethylene (POM), PP, poly-(4-methyl-1-pentene) (PMP) (TPX™), PE, etc. [14, 15]. All the above hard elastic fibers have the higher modulus than PU fibers. The physical properties are based on the chemical structures. For PP hard elastic fibers, the physical properties depend on the chemical structure. The PP hard elastic fiber has high strength and initial modulus and worse moisture absorption and dye ability. It can resist acid and alkali. But it is with worse light resistance and heat resistance. The poly(vinylidene fluoride) (PVDF) hard elastic fiber shows higher initial modulus, and it decreases with the increasing stretching rates when spinning.

According to the above description, Table 13.3 summarizes the physical properties of these elastic fibers.

13.3 New Development of Elastic Fibers

13.3.1 Polyurethane Elastic Fiber

PU elastic fibers are superior in elasticity and elastic recovery. Due to these advantages, PU elastic fibers are widely used as materials for stockings, women's underwear, and flexible fabrics, and their applications continue to be extended to aerobic clothing and swimming suits. However, PU fibers have worse heat and chemical resistance, which are the enduring conditions during the textiles process. Some techniques have been recently developed for increasing the performance of PU fibers.

Table 13.3 Physical properties of elastic fibers.

Fiber type	Tenacity (cN/dtex)	Modulus (cN/dtex)	Melting point (°C)	Heat shrinkage (%) (100 °C water)	Chemical resistance	Atmosphere resistance
PU, polyester type	0.4–0.6	~0.45	~250	~10	Cool and dilute acid resistance; hot alkali and chloride labile	Tenacity loss color change
PU, polyether type	0.6–1.0	~0.11	200–290	~10	Acid resistance; yellowing in H_2SO_4 or HCl; chloride labile	Tenacity loss under light
Polyester ether	0.4–4.0	0.2–0.5	200–230	~20	Good anti-oils; hydrolysis under hot water	Degradation under UV light
PTT	~3.0	~1.0	220–230	~12	Good chemical resistance	Good anti-light aging
XLA	~1.0	<0.1	Decomposition at 300	~20	Chloride and acid and alkali resistance	UV resistance
Hard elastic fiber (PP)	0.4–0.8	~4.5	160–180	~2.5	Good acid and alkali resistance	Tenacity loss under light
PTT/PET bicomponent elastic fiber	~2.0	~0.5	~225	N/A	Good anti-chemical	Good anti-light

PU fibers have alkali resistance property to some extent but are likely to easily degrade in caustic soda solution at a high concentration of about 25% to about 30% and applied at a temperature as high as 150 °C. For some fabric treatments such as burning-out and printing process should be conducted under high temperature and alkali solutions. Accordingly, it should separate these processes for the fabric containing PU fibers, and there is still no technique established that simultaneously proceed to both. Thus, there is a need for PU elastic fibers having superior resistance to heat and alkali and without any problem associated with nonuniform physical properties.

A patent [16] has found that when adding a cellulose acetate (diacetate or triacetate) in PU polymer solution for spinning, the final PU fiber will have a high modulus and superior resistance to heat without changing polymerization viscosity or physical properties of the fibrous product. This kind of PU fiber can resist 25% aqueous NaOH solution and be heated to 150 °C. This PU fiber increases the heat resistance of about 25% and extends the alkali resistance time to 20 minutes than the common PU elastic fiber.

PU elastic fiber is known to display heavy tackiness as compared with conventional, nonelastic fibers. Because of the tackiness, PU fiber may cohere to each other or alternatively adhere to various surfaces. High tackiness becomes a problem in unwinding during weaving. The pressure caused by elasticity leads to the adjacent fibers to cohere to each other, particularly near the core of the cone. It is difficult to remove the fiber from the cone package without breaking. Unusable fiber commonly occurs at the core and is referred to as "core waste." After winding and packaging, fiber tackiness may become even worse during storage depending on time and temperature. Longer storage time and higher temperatures lead to higher tackiness and more core waste than freshly spun and packaged PU fibers. Accordingly, a reduction in PU fiber tackiness would reduce core waste and increase cost-effectiveness.

To increase the anti-tackiness property of PU fiber, an embodiment including cellulose ester (CE), calcium stearate, magnesium stearate, organic stearates, silicon oil, mineral oil, and mixtures thereof can be added into the PU polymer before spinning or during spinning. The soluble anti-tack CE may be a specific cellulose acetate butyrate (CAB) or cellulose acetate propionate (CAP). The PU fiber with 1% of CE embodiment by weight shows a significant reductions in yarn tackiness by about 20% or more and improvements in spinning performance such as fewer breaks [17].

PU elastic fiber is usually used together with other natural or synthetic fibers for weaving or knitting. However PU fibers are with worse color fastness, especially some dark color like black. After several washing with hot water or prolonged use, the fading of PU fibers may occur due to the "grin" phenomenon. This is mainly because of the dyeing process; most of the dye is only attached to the surface of the PU fibers and cannot penetrate the interior of the fibers. Using colored PU fiber itself can effectively solve this problem. Black spandex is most commonly used as a colored spandex, which is mainly used in black underwear, stockings, and swimwear.

The black PU fiber is typically made of adding black fillers such as carbon black into polymers or spinning solutions directly. The key issues include how to

achieve uniform dispersion of black fillers, thus ensuring stable spinning process and uniform product quality, and how to strengthen the interaction between black filler and PU urea, thereby enhancing the coloring effect and color fastness. A China patent [18] mentioned the use of surfactants to improve the carbon black dispersion, but it did not establish an effective chemical bond between the carbon black and the polymer to increase the force between the two phases. Therefore, the carbon black particles and the polymer molecule chains rely only on intermolecular physical force or a mechanical combination lock, which also cause discoloration of PU fabric after long uses. Another China patent [19] mentioned the use of carbon black particles with active surface hydroxyl groups with the isocyanate groups to form chemical bonds to increase the color fastness of PU fiber and mechanical strength. But carbon black itself is with limited reactive sites on surface; therefore it is still difficult to build enough chemical bonds between the carbon black and the polymer chains. Both of these patents are not good solutions to how to improve the binding between carbon black and PU urea.

The invention [20] adopts single-walled or multiwalled carbon nanotubes with diameter of 10–50 nm and a length of 1–10 μm as fillers to increase the bindings between two phases and solves the dispersion problems. The present invention deals with the surface modification of carbon nanotubes by carboxylic acid and then dispersion of carbon nanotubes in black PU urea for improved adhesion. Only 0.01% by mass of carbon nanotubes can effectively increase the chemical binding.

Besides the black PU fiber made by this method has a good color fastness. They also have high mechanical strength, elongation, and low volume resistivity and at same time excellent antistatic effect and excellent heat temperature resistance, which can withstand prolonged high temperature boiling and still maintain good performance.

Besides the improvement of physical property and chemical resistance property of PU fibers, some studies also have developed other high performance PU fibers, for example, anion PU fibers. Anion is beneficial to health and can facilitate body growth and prevent disease. Anion can also improve sleep quality and ease pain and tension. Anion can improve reflex system and endothelial system and enhances body's anti-disease ability. CN 205501464 U [21] reported a hollow PU fibers with anion core structures, which has high elasticity and a good anion effect.

PU fibers are with poor moisture absorption property due to lack of hydrophilic groups, which maybe limit the textile applications requiring high hygroscopicity. The patent CN 104153037 [22] published a PU fiber with higher moisture absorption through adding natural silk fibroin in the PU polymers. Natural silk fibroin is made from silk, and it is a natural polymer and nontoxic and non-irritating and has good biocompatibility and biodegradability. Silk fibroin has the forms of solution, fiber, powder, or film. A patent of CN 1560136A [23] published a method of making silk fibroin from silk, which can produce nanoscaled silk fibroin with average particle size of 30–60 nm. In terms of chemical structure, silk fibroin as a natural polymer contains carboxyl, amino, hydroxyl, and other polar groups, which have good water absorption property.

At present, the commonly used hydrophilic modification methods include surface modification, graft, copolymer, and blends. Among these methods, blending is relatively easy to implement in the industry. In this patent, the silk fibroin powder is blended with PU urea polymer and then for dry spinning. When the silk fibroin content is 20% by weight, the moisture absorption rate of the fibers increases from 0.8% to 4.6%, and breaking elongation just decreases to 7% compared with the fiber without silk fibroin.

As we know textiles are excellent substrate for bacterial growth. The fabric provides a good base for attachment, and sweat provides nutrients necessary for bacterial growth. The bacteria do not lead to some diseases but break down sweat into fatty and acids and accordingly cause smelly odor. Some mildew will damage the fabric and the body health. Particularly, women's underwear, such as girdles and braziers, are commonly made of PU elastic fibers; therefore some attempts to impart antimicrobial properties to PU elastic fibers have been proposed.

For example, A US patent [24] discloses a process for imparting antimicrobial properties to PU fiber by using poly(pentane-1,5-carbonate)diol or poly(hexane-1,6-carbonate)diol, which is a polycarbonate diol selected among aliphatic diols, or a copolymer thereof, as a soft segment. This method has the advantage that the antimicrobial property is achieved by inherent physical properties of the raw materials and without adding additional antimicrobial agent, but it has the poor antimicrobial effect.

Further, Korean Patent Publication No. 93-5099 [24] teaches a method with a porous inorganic antimicrobial agent of porous crystalline aluminosilicate zeolite to impart antimicrobial properties to a PU elastic fiber. However, the zeolite has strong water absorption property, which will cause too much cross-linking during the preparation of PU. This cross-linking increases the viscosity of the polymer and causes the formation of a gel, which results in high spinning pressure and frequent occurrence of fiber breakage during the spinning.

Another Korean Patent No. 103406 describes the use of a nonporous inorganic ceramic containing silver or zirconium as antimicrobial components in order to impart antimicrobial properties to PU fiber. However, the silver causes undesirable yellowing of the elastic fiber during spinning at a high temperature of 200 °C or more.

Further, Korean Patent No. 445313 describes the use of a glass metal compound as an antimicrobial agent, containing ZnO, SiO_2, and an alkali metal oxide in order to impart antimicrobial properties to PU elastic fiber. Although no yellowing of the fiber occurs during spinning at a high temperature of 200 °C or more, the antimicrobial agent tends to agglomerate in dimethylacetamide or dimethylformamide, which is a polar solvent for PU. As a consequence of the agglomeration, the pressure of spinning head increases, and fiber breakage frequently occurs during spinning, which make it difficult to maintain stable spinning of the antimicrobial fiber for a long period of time. So the particle size of antimicrobial agent must be suitable for addition to the PU. To this end, extending the milling time of the antimicrobial agent is required. At this step, the antimicrobial agent will be discolored to gray, which also renders the final antimicrobial elastic fiber gray [24].

Therefore, there is a need to develop a process for preparing an antimicrobial elastic fiber without affecting the spinnability or the color of the fiber while maintaining superior antimicrobial properties. US 20070292684 A1 [24] describes a method for antimicrobial PU fiber producing with a glass metal compound containing ZnO, SiO_2, and an alkali metal oxide and having an average particle size of 0.1–5 μm.

It is preferred that the antimicrobial agent is nonporous and preferably contains 50–78 mol% of ZnO. When the ZnO content exceeds 78 mol%, it is difficult to form the antimicrobial agent into a glass compound. On the other hand, when the ZnO content is below 50 mol%, the antimicrobial properties of the antimicrobial agent are insufficient. The antimicrobial agent preferably contains 21–49 mol% of SiO_2, which is a component for glass formation. When the SiO_2 content exceeds 49 mol%, the water solubility of the antimicrobial agent is high, thus causing poor antimicrobial properties. Meanwhile, when the SiO_2 content is less than 21 mol%, it is difficult to obtain a stable glass compound. SiO_2 is used as an essential component for glass formation in the antimicrobial agent, but a portion of SiO_2 may be replaced with other components for glass formation, such as P_2O_5, Al_2O_3, TiO_2, and ZrO_2. The preferred amounts of the components range from 0.1 to 19 mol%.

The antimicrobial agent preferably contains 1–10 mol% of an alkali metal oxide. When the content of the alkali metal oxide is less than 1 mol%, the antimicrobial properties of the antimicrobial agent are degraded. On the other hand, when the content of the alkali metal oxide exceeds 10 mol%, the water solubility of the antimicrobial agent is high, and thus poor antimicrobial properties are caused with impairing the discoloration resistance of the antimicrobial agent. In the process of the present invention, the antimicrobial agent is preferably added in an amount of 0.2–5% by weight, relative to the weight of yarn. If the antimicrobial agent is added in an amount of less than 0.2% by weight, the antimicrobial effects cannot be ensured. If the antimicrobial agent is added in an amount exceeding 5% by weight, the physical properties of the antimicrobial elastic fiber may be deteriorated. According to the process of the present invention, a dispersant, such as a fatty acid, a fatty acid salt, a fatty acid ester, or an aliphatic alcohol, is added to improve the dispersibility of the antimicrobial agent in the polar solvent, thereby shortening the milling time and preventing the discoloration of the antimicrobial agent. The antimicrobial PU fibers prepared by the process of this invention exhibit excellent spinnability while maintaining superior antimicrobial properties and remaining color whiteness.

Electronic, stretchable, and flexible PU fiber also has been studied for wearable electronics or smart textile applications. A novel and environment-friendly method was presented for fabricating silver plating PU fiber, which exhibits high conductivity and excellent elasticity. An adherent polydopamine film was coated on the surface of PU filaments by in situ polymerization reaction of dopamine. The silver particles and silver plating were reduced on the surface of PU fibers by in situ reduction of polydopamine and glucose in turn. The silver particles could be combined on the surface of fiber by the catechol groups of polydopamine. The testing results show the electrical resistivity of silver plating PU fiber can reach the minimum value of $4.5 \pm 0.1\ \Omega$/cm, when the concentration of silver

nitrate and dopamine are, respectively, 55 and 3 g/l. The loss of the breaking strength and breaking elongation are, respectively, 5% and 11.9%. The nonlinearity error and the hysteresis of this PU fiber strain sensor are, respectively, less than 29.3% and 34.3% [25].

13.3.2 Bicomponent Elastic Fiber

Elasticity, comfort, and durability make polyester bicomponent elastic fibers have broader applications. But the study of this kind of fiber still focuses on a single function. The diversity development is still in a blank state. The present inventions address the deficiencies of the prior words and develop some multifunctional polyester bicomponent elastic fibers.

The bicomponent parallel fiber technology began in the late 1980s, but the progress has been slow. The parallel bicomponent fiber has a permanent self-crimping performance, which provides bulkiness, flexibility, and resilience and feel good of the textile products. The two components for this kind of elastic fibers should have different heat shrinkage, or different relative viscosity, which will lead to the three-dimensional crimps of fiber after heat treatment.

The stretch and recovery property of bicomponent elastic fibers comes from the three-dimensional spiral crimps due to the different shrinkage rate of two polymers. Patent CN 1962968A [26] discloses a preparation method and application of a PBT/PET three-dimensional crimped fibers, using PBT chips with an intrinsic viscosity of 1.0 dl/g and PET chips with intrinsic viscosity of 0.64 dl/g as raw materials. Because of the small intrinsic viscosity of two components, the final curl fibers show small elongation and elastic recovery. In addition, patent CN101126180A [27] discloses a bicomponent elastic fibers with peanut cross section but not the common circular cross section. Because the distance between the centers of two components is larger than that of the round fiber, this leads to less number of crimps per unit and large crimp radius and accordingly the lower elastic and recovery.

The objective of the CN104342802A [28] is to provide a flexible and elastic recovery bicomponent elastic fiber with high rate of production. The invention is as follows: a melt-spun two-component composite elastic fibers, which are made of PET and PBT under the ratio of 70 : 30 to 30 : 70. The intrinsic viscosity of two components is controlled between 0.5 and 1.0 dl/g. The cross section is oval, and the boundary between two components is along the long axis of the oval. The center distance of two components is smaller than the common round cross section or other shapes, which is beneficial to the crimp formation and elasticity. In the final bicomponent the fibers have a crimp of 55–75/25 mm, the elastic elongation is about 100%, and recovery rate is above 95%.

CN104726946A [29] reported a thermal insulation bicomponent elastic fiber, which comprises two parallel components with hollow structure, and the far-infrared powders are added in at least one component. The elastic or cured spiral structure of fiber is formed through the different shrinkage rate of two different polyester ingredients, which are selected form PET, PBT, PTT, etc. This far-infrared bicomponent elastic fiber has excellent heat retention effect and is widely applied to underwear, sportswear, and warm clothing, which

have the advantages of elasticity, comfort, lightness, and thermal insulation performance. With addition of 2–4% by weight, the final fiber will increase the thermal insulation of 30% than common bicomponent elastic fiber, and the elastic elongation is 35% or more, and elastic recovery rate is more than 70%.

The fabric sheerness directly affects the garment appearance, especially for some thin, light color fabrics for summer or swimwear. If the fabric has poor shading property, the unwanted see-through effect will occur, which is very ungraceful. The bicomponent elastic fiber as a widely used material in garment also needs the excellent shading property. CN 102534861 B [30] reported a high-resistance parallel shading bicomponent elastic fiber, which comprises two different parallel components selected from PET, PTT, PA, and PBT. TiO_2 powder, with particle size below 200 nm and refractivity index of 2.6–2.9, will be added into the two components 5–10% by weight. The white fabric made of these fibers shows a good shading effect than common white fabric.

13.3.3 Polyolefin Elastic Fiber

The common polyolefin elastic fiber made of PE and Polyolefin Elastomers (POE) has less elastic recovery and lack of flexibility. The high-performance polyolefin elastic fiber has good stretch and recovery property but with a high cost. CN 103276584 B [31] describes a technology, which provides a way to improve the elastic recovery property of polyolefin fibers, and the process is simple and low cost.

The method of the this invention includes the following steps: a radiation-sensitive agent such as vinyl-terminated PDMS or octamethylcyclotetrasiloxane siloxane of 0.1–5.0% by mass is added in the polyolefin polymer for melt spinning to obtain a polyolefin-spun filament; radiate the polyolefin filament under the radiation dose of 10–100 kGy to prepare elastic polyolefin fibers. After radiation, the polyolefin macromolecular can be cross-linked to form a three-dimensional network structure, which increases the elastic recovery property of the fiber, to avoid additional residual shrinkage force, resulting in better flexibility polyolefin elastic fiber and improve the weathering resistance, aging resistance, UV resistance, and toughness.

CN 105088403 A [32] publishes a core–shell melt-spun polyolefin elastic fiber, which does not need radiation cross-linking process but still has excellent elasticity and recovery. The core layer is made of a kind of polyolefin with melt temperature at most 160 °C, and the core layer is made of another polyolefin with melt temperature at most 120 °C. The elongation will be above 600%, and the recovery rate after five cycles under 300% elongation will be more than 90%. Other advantages of this core–shell polyolefin elastic fiber comprise antiaging, acid and alkali resistance, anti-oxygen, and heat setting under low temperature (100–140 °C). It has a wide application in wrinkle-free shirt, swimwear, underwears, socks, denim fabrics, etc.

A China patent [33] publishes a simple preparation process and low-cost method for preparing polyolefin composite elastic fibers with good elastic recovery. It comprises a polyolefin elastomer, a thermoplastic resin, silicone rubber, radiation-sensitive agent, and an antioxidant, which are mixed and fed to

a twin screw extruder to obtain a polyolefin mixer master batch. The amount of polyolefin elastomer is 60–80% of the total mass; the amount of the thermoplastic resin makes up the total mass of 5–25%; the amount of the silicone rubber is 10–20% of the total mass; the amount of the radiation-sensitive agent shares 0.1–0.5% in the total mass. The polyolefin mixer master batch is processed by melt spinning to get as spun fiber and then placed under irradiation treatment at 50–500 kGy to obtain the polyolefin composite elastic fiber, which has a elongation about 900% and the recovery rate above 95% under 100% elongation and a breaking strength above 1.0 cN/dtex. CA 2642462 A1 [34] describes a method to produce cross-linked polyethylene elastic fibers with higher tenacity to further reduce the fiber breaking during downstream process. It has been discovered that a polyolefin composite comprises two or more polyolefin components, in which one imparts the elasticity and cross-linking to meet the stretch and recovery performance and other component with higher molecular weight improves the tenacity.

13.3.4 Polyether-Ester Elastic Fiber

PEE elastic fibers contain a high crystalline polyester such as a polyalkylene terephthalate as a hard segment and a polyalkylene glycol as a soft segment and are capable of being melt-spun. It has some advantages such as high productivity, excellent heat resistance, and excellent heat setting property. Furthermore, the future development of the PEE elastic fibers has been expected as elastic fibers suitable for the multifunctional applications.

The present [34] invention relates to a PEE elastic that has a good moisture absorbing or releasing property and reversibly expanded or contracted by the absorption or release of water. It especially gives a comfort for sportswear and intimates applications. This patent discloses the PEE elastomer, which uses PBT as a hard segment and polyoxyethylene glycol as a soft segment, characterized by having a coefficient of moisture absorption of not less than 5% at 35 °C and not less than 10% at a relative humidity of 95%. The PEE elastomer is copolymerized with a metal organic sulfonate, which consists of an aromatic hydrocarbon group or an aliphatic hydrocarbon group, an ester-forming functional group, and an alkali metal or an alkaline earth metal. In the present invention, the weight ratio of the hard segment and soft segment is preferably in a range of 70 : 30 to 30 : 70, more preferably in a range of 60 : 40 to 40 : 60. When the weight ratio of the hard segment exceeds 70%, the elongation is lowered, and it becomes difficult to use it for high stretch textiles. The moisture absorption property is liable to be lowered. When the weight ratio of the hard segment is less than 30%, the strength is liable to be lowered, because the rate of the crystal portion of the polyester is small. It is difficult to copolymerize other added polyoxyethylene glycol, and the colorfastness is to be deteriorated in post-processing such as scoring and dyeing.

PEE elastic fiber has better chemical resistance property than PU fiber, but the elastic recovery is worse than it. So improvement of the elastic recovery is also a development direction of the PEE elastic fiber. The common ways to improve the elastic recovery rate of the PEE elastomer fibers generally include changing the spinning parameters and processing conditions, such as spinneret draw ratio,

after-stretching ratio and temperature, and heat setting time and temperature, increasing more hard segment crystalline regions to prevent the slipping between macromolecules of the soft segments such as blended spinning with PBT, or adding nucleating agents. These methods are good attempts to enforce physical cross-linking of the hard segment to improve elastic recovery; however, they cannot solve the problem well.

CN 101100768 A [35] discloses a method to improve the elastic recovery rate by adding nano-TiO_2 particles, which has high surface energy. When dispersed in polymer, it can absorb the macromolecular chains to reduce its surface energy as physical cross-linking points, which can form a network structures between macromolecular chains, thereby improving the elastic recovery performance of the fibers. The preferable ratio of nano-TiO_2 is 0.3–1.0% by mass in the polymer. Among this range, the TiO_2 can be dispersed evenly and stably, and the elastic recovery rate will be 97% under 100% elongation and 88% under 300% elongation.

Method for preparing glycerol micro-cross-linking PEE elastic fiber has been published by CN 101100769 A [36], which is another method to improve the micro-cross-link and elastic recovery rate of PEE elastic fiber. The final PEE elastic fiber will be with 90% elastic recovery rate at 100% elongation and 88% recovery rate at 300% elongation.

13.3.5 Polyester Elastic Fiber

Polyester elastic fibers have excellent physical and chemical properties, in particular chemical, heat stability, high melting points, and high strength. Fabrics made of polyester elastic fibers exhibit softness hand feeling, resiliency, and stretch recovery, among other desirable properties.

PTT has recently received much attention as a polymer for use in textiles, flooring, packaging, and other end uses. There are also some special demands on this fiber such as in automotive interiors textiles, outdoor uses including housing, garden and patio furniture, or personnel protective equipment, which demand the PTT fiber to have a good UV resistance property. US 7196125 B2 [37] provides the colored PTT fibers suitable for use in transportation areas, in which fibers can be subjected to high UV exposures and stringent heat conditions. The processes include the use of a dye bath consisting of 3.0% benzotriazine derivative UV absorber by weight, 0.5% disperse dye, 0.25% sequestering agent, 0.5% alcohol ethoxylate surfactant, and water. The dyeing temperature is 132–145 °C for 30 minutes. The final dyed PTT fiber shows at least grade 4 light fastness after exposure to 488 kJ of UV radiation.

13.4 Evaluation and Application

Elastic fibers have been widely used in different areas from apparel, home textiles, personal protective equipment, furniture, automobiles, outdoor textiles, medical textiles, etc. Among these, textile applications are the main market. In textiles, elastic fibers are usually applied in woven fabrics to increase the stretchable and

comfortable property such as in two-way or four-way stretchable denim. Elastic fibers also are used in knitted fabrics to achieve a more large elasticity for applications of underwear, sportswear, and yoga garments. Elastic fibers with high recovery force are often adopted in medical socks for the prevention and treatment of varicose vein and sports pants for prevention of sports injury and fatigue recovery. Due to the excellent resilience of some elastic fiber, it is a preferable choice for floor rugs, packaging, and furniture covers.

As most consideration, the most import performances of elastic fibers are elongation and recovery rate index; however the elastic force at specified elongation also plays an important role in applications. The most common method for elastic properties of elastic fibers is ASTM D 2731-2015 [38], which is applicable to elastic fibers having a range of 40–3200 dtex. The elastic properties include force at specified elongations, permanent deformation, and stress decay, and the hysteresis-related properties can be calculated. The specimen is mounted in a constant rate of extension (CRE)-type machine, and a series of five loading/unloading cycles is subjected in which the specimen is extended and relaxed between 0% and 75% of the elongation at first fiber break. During the fifth cycle, the specimen is held at the maximum extension point for 30 seconds and then unloaded to allow a return to its original gauge length position. The specimen is then subjected to a sixth load/unload cycle. Forces at specified elongations are calculated form the force–elongation curve for the first and fifty loadings and for the fifth unloading. Stress decay is calculated on the fifty cycle. Extension at a specified force is determined on the sixth loading and is used to calculate the permanent deformation. In the previous, elongation rate and permanent deformation are the main concerns. With the developing of varied products and endues, the force at specified extension and stress decay attract more and more attentions.

As shown in Figure 13.9, fibers 1 and 2 have almost the same elongations and excellent recovery rate. However, considering the elastic forces, these two kinds of fibers have different application areas. Fiber 1 displays higher extension force and recovery force than that of fiber 1. The large force is beneficial to some textiles need high pressure such as compression socks or compression sportswear wears.

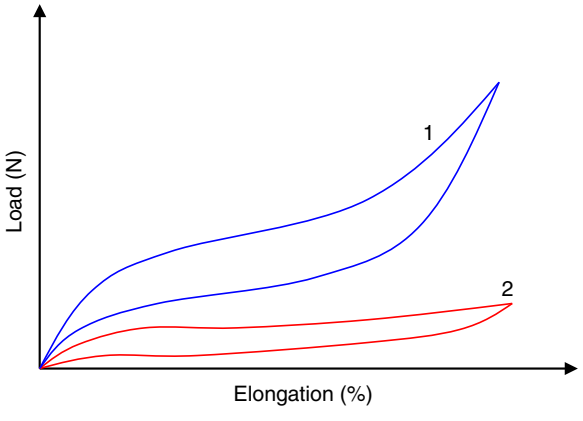


Figure 13.9 Load–elongation curves of different elastic fibers.

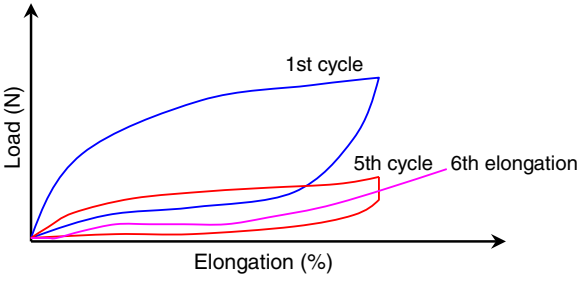


Figure 13.10 Elastic property test of elastic fiber.

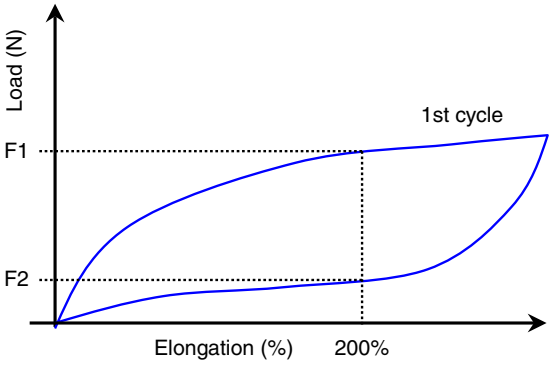


Figure 13.11 Force at specified elongation of elastic fiber.

Fiber 2 shows a relative flat load and elongation/recovery curves, which is more suitable for comfortable textiles with large elongation but low pressure such as intimate, sock welts, etc.

Figure 13.10 displays the elongation and load curves of the first cycle, the fifth cycle, and the sixth elongation based on ASTM D 2731. From the curves, the first cycle shows a higher elongation and recovery force than that of the fifth cycle. From Figure 13.11 the force at specified elongation can be determined as F1 and F2. The stress decay of the elastic fibers can be calculated based on the force f1 at maximum extension and the force f2 after holding at maximum extension for 30 seconds (Figure 13.12) on the fifth loading cycle. Higher stress decay rate means the elastic fiber easily to relax, and the elastic force cannot maintain, which is not good for high elastic stress applications such as compression

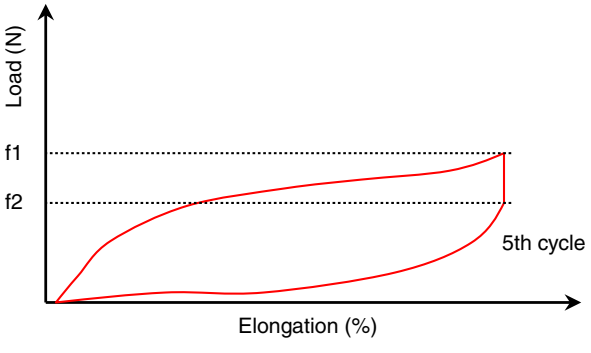


Figure 13.12 Stress decay of elastic fiber.

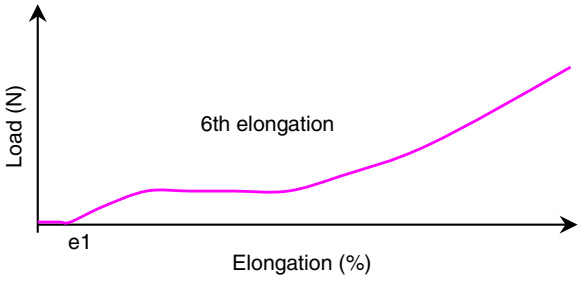


Figure 13.13 Permanent elongation of elastic fiber below e1.

socks. No matter what kind of elastic fibers, the elasticity fatigue exists. After several cycles of extension, the elastic recovery rate will decrease, and accordingly the permanent deformation occurs. Figure 13.13 shows the determination of the permanent deformation from the sixth extension curve. The force before e1 elongation is almost zero on the sixth cycle that means the fiber can be elongated before the elongation of e1. The permanent deformation is calculated by the e1 divided by the gauge length. Higher permanent deformation means worse elasticity recovery property.

The applications of elastic fibers mainly depend on the elastic property of fibers. The fiber with large elongation, high stress, and low stress decay is suitable to compression socks, pressure pants, or shape wears. The fiber with small elongation but higher stress and low stress decay is suitable to some carpets. The underwears need the elastic fiber with large elongation and low stress, which supplies comfort elasticity on human body. As we know, the stress will increase with the extension. But for comfortable textiles, the customers want it easily extended but without large compression. Therefore, this kind of elastic fiber shows a relative flat load–elongation curves compared to others.

Besides the elastic property, other physical or chemical properties also determine the application areas of elastic fibers. The chloride resistance elastic fibers such as XLA or polyester elastic fibers are good choice for swimwear. The low temperature heat setting PU elastic fiber is suitable to anti-laddering hosiery or fabrics containing wool fibers, which are sensitive to heat. The UV resistance elastic fibers are suitable for some outdoor textiles like outdoor car coverage or awning. Hard elastic fiber shows excellent stretch and recovery property under cold environment than other elastic fibers, so it can be used in some industry or engineering areas in outdoor. Because of the microvoids when stretching, the hard elastic fiber can be processed to make filtration hollow fibers for water or blood filtration and separation.

13.5 Future Trends

The principles of difference types of elastic fibers have been studied thoroughly. So the future works for elastic fibers mainly focus on the fiber modifications to achieve functional performances or overcome the present shortcomings and improve the production efficiency.

The PU fiber will continue to improve the chemical or chlorine resistance, heat setting efficiency, and easy dyeing properties and develop comfortable fiber with lower elongation force, high tenacity, and stress fibers or other functional fibers.

The bicomponent elastic fibers will aim to multifunctional development such as thermal and elasticity property, temperature controlled, and elasticity property for high-performance textile applications.

The polyolefin fibers will enhance the elastic durability and focus on the advantage of lower elongation stress than PU fibers.

The PEE elastic fibers are promising fibers with a wide range of uses and lower cost than PU elastic fiber. By controlling their molecular structure, different functional polyester-ether fibers will be developed.

The developments of hard elastic fiber will emphasize on the production of hollow fiber and filter materials in medical applications and the fibers with excellent resilience for furniture endues.

References

1 Xin-yuan, S. (2006). Structure and elasticity of elastic fiber and its dyeing and finishing (I). *Printing and Dyeing* 8: 44–46.

2 Fabricius, M. and Wulfhorst, B. (1995). Elastane fibers (spandex). *Chemical Fibres International* 45 (10): 400.

3 Hicks, E.M. (1963). Lycra spandex fiber I structure and properties. *American Dyestuff Reporter* 7: 33–35.

4 Ibrahim, S.M. (1967). Fibers, elastomeric. In: *Encyclopedia of Polymer Science and Technology* (eds. Herman Francis Mark, Norman Grant Gaylord and Norbert M. Bikales), vol. 6, pp. 573–593. Interscience Publishers.

5 Hoe, H.C. (1998). A new polyester fibre. *Textile Magazine* 2 (1): 12–14.

6 Hu, J., Lu, J., and Zhu, Y. (2008). New developments in Elastic fibers. *Polymer Reviews* 48: 275–301.

7 Chodák, I. (1999). Hard-elastic or 'springy' polypropylene. In: *Polymer Science and Technology* (ed. Karger-Kocsis, J.), vol. 2, 291–294. Dordrecht: Springer Science+Businessmedia.

8 Bonart, H. (1968). X-ray investigations concerning the physical structure of cross-linking in segmented urethane elastomers. *Journal of Macromolecular Science, Part B Physics* 2 (1): 115–138.

9 Lee, H.S., Ko, J.H., Song, K.S., and Choi, K.H. (1997). Segmental and chain orientational behavior of spandex fibers. *Journal of Polymer Science Part B: Polymer Physics*: 1882–1832.

10 Liang, Z., Wenke, W., and Dongyan, S. (2001). Development of high performance polyurethane elastic fiber. *Polyester Industry* 14 (2): 12–16.

11 Zhao, Q. and Xia, H. (1994). Polyether ester elastic fibers. *Textile Science Research* 1: 18–22.

12 Yan, T. (2016). Relationship between structure, properties and processing technology of copolyester-ether fiber. Marter dissertation. China: Donghua University.

13 Lewin, M. and Pearce, E.M. (1998). *Handbook of Fiber Chemistry*, 2e, 258.

14 Sprague, B.S. (1973). Relationship of structure and morphology to properties of "hard" elastic fibers and films. *Journal of Macromolecular Science, Part B: Physics*, 8 (1–2): 157–187.
15 Youyi, X., Changhui, X., and Baiming, X. (1996). Research development of crystalline hard elastic polymer material. *Functional Material* 27 (1): 12–31.
16 Kang, Y.S., Jin, J.S., Seo, S.W., and Kwon, I.H. (2005). Process for preparing elastic fiber having high modulus, alkali-resistance and heat-resistance. WO 2005021847 A1, published 10 March 2005.
17 Pardini, S.P., Bing-Wo, R.D., and Teerlink, T.W. (2016). Methods of making and using elastic fiber containing an anti-tack additive. US 9315924 B2, published 19 April 2016.
18 Liu, G., Zhou, Z., and Zheng, Y. (2012). Method for producing polyether black spandex fibers. CN 101984158B, published 4 July 2012.
19 Xue, S., Liu, Y., Wen, Z. et al. (2014). Method for preparing black polyurethane elastic fiber via in situ polymerization. CN 102899739 A, 20130130.
20 Xu, T., Liang, H., Feng, Y. et al. (2015). A kind of black polyurethane urea elastomer adding CNT and preparation method thereof. CN103726127B, published 12 August 2015.
21 Shen, J., Shen, D., and Shen, X. (2016). High elastic anion fibre. CN 205501464 U, published 24 August 2016.
22 Xue, S., Fei, C., Wang, X. et al. There is the preparation method of the polyurethane elastomeric fiber of humidity absorption and release performance. CN 104153037 A, published 19 November 2014.
23 Zhang, Y. (2005). Manufacture process of nano fibroin particle. CN 1560136 A, published 5 January 2005.
24 Song, B., Seo, S., Kim, J., and Kwon, I. (2007). Process for preparing antimicrobial elastic fiber. US 20070292684 A1, published 20 December 2007.
25 Liu, H., Zhu, L., He, Y., and Cheng, B. (2017). A novel method for fabricating elastic conductive polyurethane filaments by in-situ reduction of polydopamine and electroless silver plating. *Materials and Design* 113: 254–263.
26 Gong, J. (2007). A method of making PBT/PET fibers and its applications. CN 1962968A, published 16 May 2007.
27 Cui, H., Zhang, S., Wang, G. et al. (2008). Elastic polyester fibre and preparation method thereof. CN 101126180 A, published 20 February 2008.
28 Cao, H. and Fujimori, A. et al. (2015). A kind of bi-component elastic fiber. CN 104342802 A, published 11 February 2015.
29 Zhao, M., Chen, L., Qian, J. et al. (2015). A thermal insulation bi-component elastic fiber. CN 104726946 A, published 24 June 2015.
30 Shi, M., Gan, G., Qiu, Y. et al. (2014). A high sheerness bi-component elastic fiber. CN 102534861 B, published 2 April 2014.
31 Wang, X., Zhang, H., Huang, N. et al. (2015). A method of making polyolefin elastic fiber by radiation. CN 103276584 B, published 22 April 2015.
32 Xiang, H. (2015). Two-component polyolefin elastic fiber. CN 105088403 A, published 25 November 2015.

33 Wang, X., Zhang, H., Huang, N. et al. (2016). A component elastic fiber. CN 103668550 B, published 17 August 2016.
34 Mizohata, S., Makino, S., Morioka, S. et al. (2006). Polyether ester elastic fiber and fabric, clothes made by using the same. US 20060177655 A1, published 10 August 2006.
35 Song, X., Li, G., Jiang, J. et al. (2008). Method for preparing nano TiO_2 polyester ether elastic fiber. CN 101100768 A, published 9 October 2008.
36 Song, X., Li, G., Yang, S. et al. (2008). Method for preparing glycerol crosslinked polyether ester elastic fiber. CN 101100769 A, published 9 January 2008.
37 Chang, J.C. and Nolan, D.P. (2007). Poly(trimethylene terephthalate) fibers useful in high-UV exposure end uses. US 7196125 B2, published 27 March 2007.
38 ASTM D 2731-2015 (2015). *Elastic properties of elastomeric yarns (CRE type tensile testing machines).*

14

Smart Fibers

Dong Wang[1,2], Weibing Zhong[2], Wen Wang[2], Qing Zhu[2], and Mu Fang Li[1]

[1] *Hubei Key Laboratory of Advanced Textile Materials & Application, Wuhan Textile University, 1st Yangguang Road, Wuhan 430200, China*
[2] *Donghua University, College of Chemistry, Chemical Engineering and Biotechnology, 2999 North Renmin Road, Shanghai 201620, China*

14.1 Introduction

14.1.1 Definition

Smart fibers, as well as intelligent fibers, are special designed fibers or fiber-based materials that could realize the biomimetic response to stimulus with dynamic property changes [1, 2]. For more intelligent fibers, judgment and self-control abilities to vary stimulus are also necessary [3]. Generally, sensing and responding are typical features of smart fibers [3, 4]. Sensor systems provide a perception to the stimulus, such as thermal [5, 6], mechanical [7, 8], chemical [9], optical [10], electromagnetic [11], and humidity changes [12, 13], while the response systems exhibit the appropriate responses that can be measured in mild method [14]. It is the perfect cooperation between the two systems that the whole response process completes spontaneously. On the other words, smart fibers can implement functions of stimulus-controlled switching or self-adjustment and self-healing. Figure 14.1 presents the distinguish features of stimuli-responsive fibers, intelligent fibers, and smart fibers. Smart fiber exhibits dynamic response including perception and response ability, while the stimuli-responsive fiber can only present discriminative characteristic. Additionally, intelligent fiber possesses central processor to deal with varies of stimulus.

14.1.2 Research Status

Smart fiber is a kind of developed fiber variety derived from the smart materials or intelligent materials that was proposed in the 1990s. After that, smart fiber is gradually investigated due to their potential applications in smart textiles [15–18] due to its flexibility, spinnability, and wearability. The earliest smart fiber that was considered as the shape memory silk was studied in 1979. During the latest decades, intensive investigations about smart fibers were carried out because amounts of high quality and multifunctional materials and the preparation

Handbook of Fibrous Materials, First Edition. Edited by Jinlian Hu, Bipin Kumar, and Jing Lu.
© 2020 Wiley-VCH Verlag GmbH & Co. KGaA. Published 2020 by Wiley-VCH Verlag GmbH & Co. KGaA.

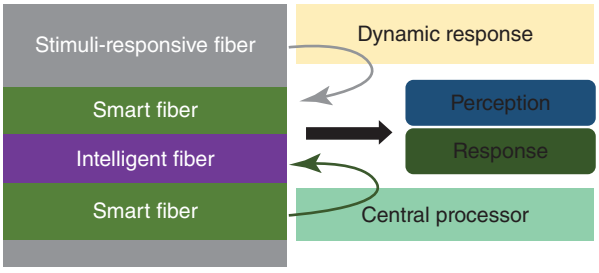


Figure 14.1 Factors of smart fibers differ from stimuli-responsive fibers with presenting dynamic response and from intelligent fibers with unnecessarily possessing of central processor.

methods were discovered [11, 19–26]. Cultivars of smart fibers were extremely expanded with the gradually progressing theories of preparation methods. For example, Cheng et al. [12] prepared a fiber-based motor by rotary processing of freshly spun GO fiber hydrogel. Chen et al. [27] reported a hierarchically arranged helical fibrous actuators fabricated by dry-spun from multi-wall carbon nanotube (MWCNT) arrays. Consequently nonnegligible effects of microstructure on the performance of smart fibers were perceived gradually, and plenty efforts were taken place on the researching of micromorphologies. For example, Jiang et al. [5] utilized electrospinning method to prepare a rapid thermo-responsive actuator with nanofibrous structure. So far, quantities of investigations are still devoting to develop high-performance smart fibers.

14.1.3 Classification

With more and more novel researches about the smart fibers have been raised up, different kinds of mechanisms and applications make it complicated and difficult to classify. Conventional classifications were mostly based on the materials composition that was summarized into metal related species [28, 29], inorganic nonmetallic species [30–32], and polymers species [33, 34]. Here we would like to give a division according to their response behaviors.

The response behaviors vary according to different stimulus source such as thermal, mechanical, chemical, optical, electromagnetical, and humidity changes. In details, smart fibers can be divided into shape memory fibers, piezoelectric fibers, fiber-shaped actuators, color-changed fibers, thermoregulated fibers, smart antibacterial fiber, etc. Figure 14.2a shows the variable responsive behaviors, and rest of Figure 14.2 exhibit several reports of representative smart fibers.

14.2 Raw Materials and Preparation

14.2.1 Raw Materials

Smart fibers set extreme requirements to raw materials and preparation procedure due to the unique response mechanism [2, 39]. Intelligent unit is necessary

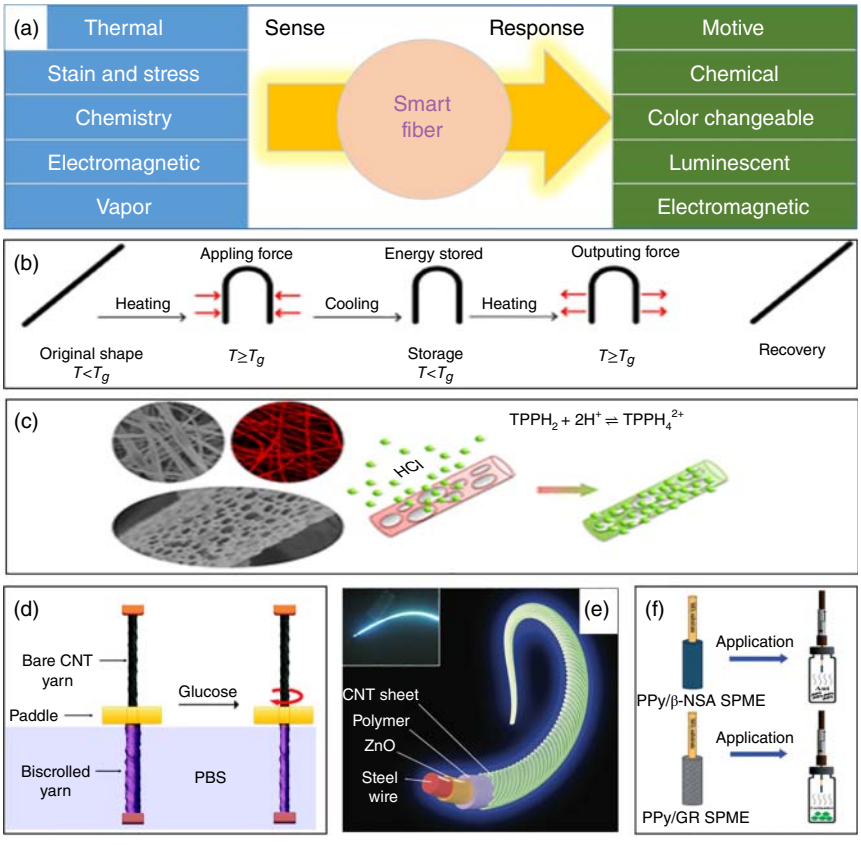


Figure 14.2 (a) Typical components of smart fiber and conventional stimulus and response. (b) Schematic diagram of thermal induced shape memory. Source: AIAA 2009 [35]. Reproduced with permission of Institute of Physics. (c) Sensitive and fast HCl sensor with porous structure. Source: Hu et al. 2016 [36]. Reproduced with permission of Springer Nature. (d) Biothermal sensitive torsional artificial muscle. Source: Lee et al. 2016 [37]. Reproduced with permission of Royal Society of Chemistry. (e) Fiber-shaped color turnable electroluminescence. Source: Zhang et al. 2015 [28]. Reproduced with permission of Springer Nature. (f) Polypyrrole composite solid-phase microextracted fiber for the trace analysis of volatile organic. Source: Zhang et al. 2013 [38]. Reproduced with permission of Royal Society of Chemistry.

for raw materials, which can quickly sense and response to the external stimulus. Otherwise, the materials should be easy to be intelligentized [4]. Generally, the raw materials can be concluded in metal related [40–42], inorganic nonmetallic materials [12, 23, 43, 44], and functionalized polymers [45–47]. They will be demonstrated, respectively, below. Figure 14.3 presents the classifications.

14.2.1.1 Metal Related

Metal-related smart fibers usually use metal, alloy, and metallic compounds as the functional elements to functionalize fibers with stimuli responsibility. Pure metal, alloy, and partial metallic compounds are expected to be ideal materials with high electrical and thermal conductivity, so they are frequently utilized

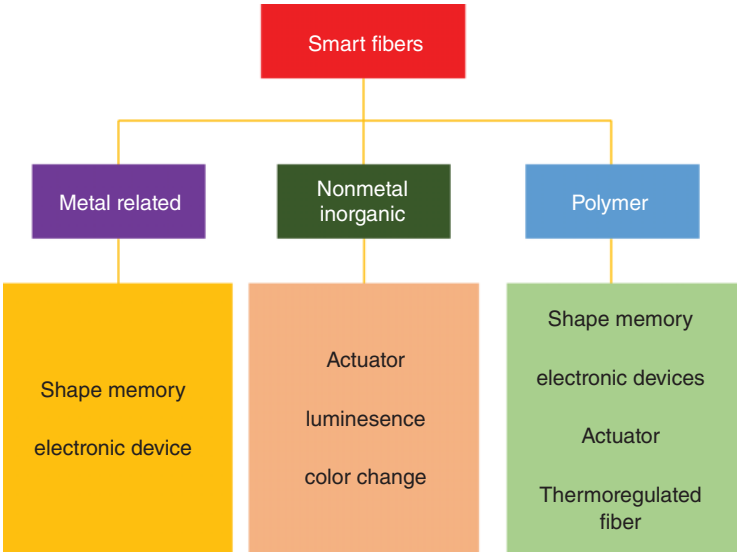


Figure 14.3 Raw materials of smart fibers and their main application.

as the main materials or smart ingredients in thermal- and electricity-induced smart fibers. For example, Seung Hwan Ko group [48] reported a transparent and highly stretchable Ag nanowire (NW)-based heater used for flexible and wearable instrument, which could produce and transfer heat sufficiently. Besides, stimulus induces complex crystal transitions that exist in alloys extensively and may lead to series of motions subsequently. So they were successfully applied in shape memory fiber and actuators. For instance, Choi et al. [49] used NiTi alloy to make a superelastic shape memory alloy (SMA) fiber with different anchorages. Li et al. [50] applied Cu/Ni/Al for main parts to get a shape memory fiber that have temperature-induced martensitic transformation.

Except that, many kinds of metallic compounds are recommended for the excellent stimulus responsibility. For example, ZnS and 8-tris-hydroxyquinoline aluminum (Alq_3) were discovered to be good candidates for high-efficiency electroluminescence. Highly designed ZnO nanowire arrays were constructed to the implementation of smart nanogenerator, which sufficiently convert mechanical energy into electricity [51].

14.2.1.2 Inorganic Nonmetallic and Polymer Related

Inorganic nonmetallic materials mainly include certain elements of oxide, nitride, carbide, halogen compounds, boride, silicate, aluminum acid salt, phosphate and boric acid salt, etc. Single-crystal silicon fibers and silicon oxide fibers are frequently used for their wondrous optical performance, which contributes to hold the crucial position in high-performance communication optical fibers. What's more, crystalline silicon (c-Si) is preferred for electronic devices because of its superior thermal and electronic properties compares with amorphous counterpart [52]. Lagonigro et al. [53] reported a kind of silicon fibers used for photonics field with low loss. Besides, carbon materials were intensively studied

for their superb chemical and physical properties [54, 55]. Graphene fibers and oriented carbon nanotube (CNT) fibers with the superior electric conductive rate (10^5 S/cm), thermal conductive rate (3500 W/m·K), and mechanical strength (0.9 TPa) were adopted to fabricate high-performance smart fibers [56–59].

Polymer is one of the top drawer candidates to manufacture smart fibers for their flexibility and easy processing [60, 61]. A plenty of smart fibers can be fabricated with different kinds of polymers or modified polymers directly [14, 62]. In addition polymeric fibers can also be selected to be fiber-shaped substrates for some smart fibers. Usually, the manufacture procedure of being smart fibers is easily to achieve. Firstly, functional modification can be implemented easily due to the abundant reaction sites on the backbone of polymers. After that, responsive agents can be embedded homogeneously for the proper viscoelasticity of polymer melt and solution. For example, microcapsule and sea-island fibers were two typical formations, which were obtained for controllable release, temperature regulation, and self-heal. Lastly, polymer-based fibers can be designed and controlled, manufactured into varies of micromorphologies that enable them to combine with responsive agents in special way [5, 14, 63].

14.2.2 Preparations

Preparations of smart fibers can be summarized into two processes, which refer to spinning and intelligentization [4]. The order of the two processes can be adjusted according to the featured structure of target product. In other words, the intelligentization process can be brought into effect by the master batches or spinning solution so that smart fibers can be straight acquired after spinning. And the intelligentization can also be carried out on manufactured fiber products [4]. Obviously, spinning after intelligentization is a prior choice for the commercial production due to its simple technology and the predominance of nonpollution additional. However, simplified preparation method leads to univocal structure, which eventually results in response limitation. Naturally, many reports rise up a novel scheme to get smart fibers by intelligentizing primary fibers. With this method, the implementation of smart fibers is the combination of common fiber and responsive agent. Respectively, the spinning method and intelligentization method will be introduced in detail below.

14.2.2.1 Spinning Methods

As we all know, conventional spinning processes are melt spinning and solution spinning.

Melt spinning method is a straightforward process for fiber acquisition by cooling and drawing the melts. Most of the alloy fibers are prepared with melt blending method. Smart fibers can also be obtained by inputting responsive agents during the melt spinning process. Some kind of piezoelectric fibers were obtained by melt blending with piezoelectric ceramic ultrafine powder, which is an ideal material with excellent piezoelectric performance. However, if the responsive agents are added that could not bear the melting temperature, it will lead to degradation and result in dysfunction eventually. Moreover, extra efforts such as adding compatibilizers or subtle controlling should be taken to improve the

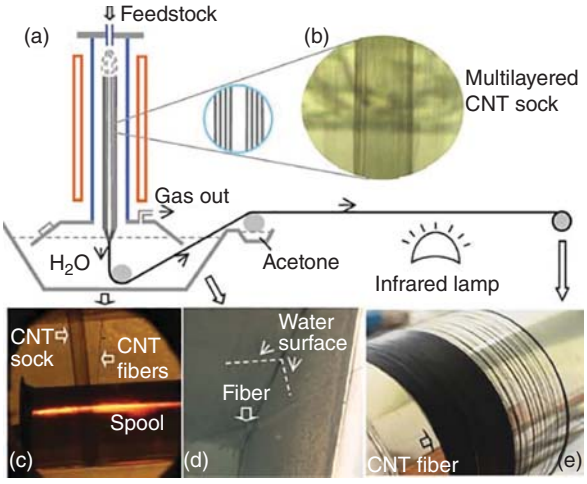


Figure 14.4 Schematic diagram of wet-spun method to prepare multilayered CNT sock. (a) Schematic diagram of the synthesis and spinning for CNT fiber, (b) photograph of CNT aerogel formed in the gas flow, (c) transformation of the CNT aerogel into a fiber, (d) followed by water densification, and (e) spinning of the resultant CNT fiber on a spool.

uniformity of melt blends, which is also critical to smart performance. Although every process was perfectly manifested, performance of responsive agents cannot work perfectly due to the wrapping and isolation effect of substrate melts. Solution spinning can largely ignore the disadvantages because the porous structure is built by solvent evaporation (dry spun) or double diffusion process (wet spun). Figure 14.4 shows schematic diagram of wet-spun method to prepare multilayered CNT sock. What's more, high temperature induced degradation of responsive agents, and it is no longer the limitation of mixture. Wet spinning, which manufactures fiber products by flocculation effect in poor solvent, can be the optimal method to acquire high quality CNTs and graphene fibers.

Electrospinning is a developed preparation method, which shares similar principle with dry spun. The fibers are drawn by extra high voltage electricity field, and the diameter of fiber decreases to micrometer or even nanometer [64, 65]. The scale effect entrusts the fibers with new properties. However, electrospinning is not suit for mass production due to the difficulties in fabrication facilities and production speed, so the melt extrusion or solution spinning method may be the best choice in the case of mass production. For example, polyolefin and cellulose acetate butyrate nanofibers, which share the same principle of sea-island fibers, are usually fabricated by melt extrusion.

14.2.2.2 Intelligentization Method

Treatments on primary fibers were selected as a mild fabrication of smart fibers. Abundant treatment methods lead to the diversity of smart fibers. Taking the chemical structure of the primary fibers into consideration, conventional treatment methods can be divided into chemical modification, coating, self-assembling, absorption, etc.

Chemical modification is a common method that uses the chemical reaction to alter the physical or chemical properties of materials. For example, Zhu and Sun [66] reported a method that organic photocatalyst anthraquinone-2-carbon acid was grafted onto the nanofibers to get the antibacterial nanofibrous membrane.

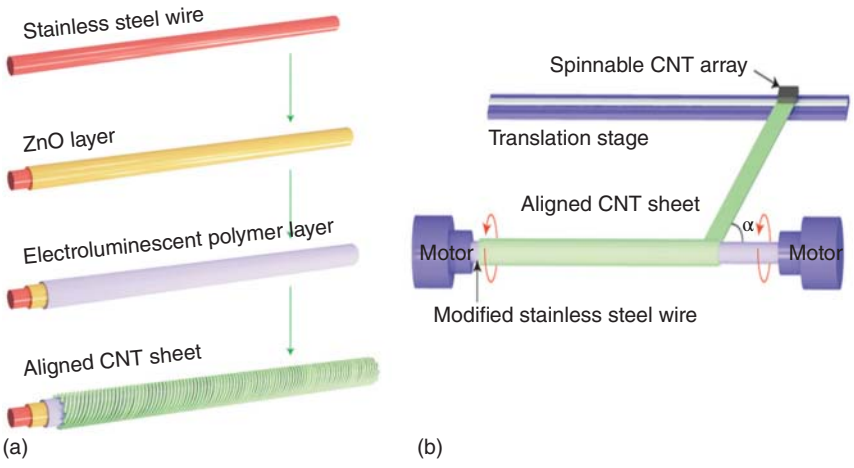


Figure 14.5 (a) Schematic illustration of the fabrication of a fiber-based light-emitting electrochemical cells (PLEC). (b) Schematic of wrapping an aligned CNT sheet around a modified stainless steel wire. Source: Zhang et al. 2015 [28]. Reproduced with permission of Springer Nature.

Coating is a frequently used method to obtain hierarchical-structured smart fibers. For example, electricity-induced responsive behaviors usually need electrodes, which were fabricated by adding conductive materials on the basic fiber substrate [23, 28, 67]. Commonly used methods include vacuum evaporation, chemical vapor deposition, and in situ polymerization [63, 68–70]. Figure 14.5a shows schematic illustration of the fabrication of fiber-based devices with coating method.

Self-assembling is an easy-operating method to acquire featured structure by utilizing unique chemical or physical properties. It would be an excellent candidate to prepare gel-based smart fibers. Typical process can be applied on particular materials, which can provide Coulomb force, hydrogen bond, coordinate bond, and even steric effect.

14.3 Structure and Properties

Structure design is crucial to smart fibers by determination of the responsive properties. Therefore, the structures of smart fibers diverse kind to kind by using the different preparation methods introduced above. Currently, diverse micromorphologies of smart fibers were designed so that they can response to different kinds of stimulus [24, 71, 72]. So the diameters of fibers are usually diminished to microscale or even nanoscale, and porous structured fibers are put forward. Majority of smart fibers are composite fibers comprising functional agents and substrates [73]. Totally, structures of smart fibers can be classified into primary fiber structure, multilayered structure, and three-dimensional fiber-based structure.

14.3.1 Primary Fiber Structure

As already introduced in paragraph of Section 14.2.2, if the melts or spinning solution has been functionalized, the smart fibers will be obtained directly after spinning. With this method, the structures can be manifested by changing the formula of raw materials and the shape of spinneret plate. As whole, primary fiber structures include conventional fibers, profiled fibers, skin-core structure, hollow fibers, and sea-island fibers. Among them, secondary structure of multi-holes is usually a method to construct smart fibers with higher performance.

14.3.1.1 Conventional Fiber Structure

Conventional fiber structure merges in fibers that are obtained from smart raw materials or chemical-intelligentized fibers. Alloys always use such a structure with secondary structure of densification for the excellent ductility of metal melts. However, solution-spun fibers are often porous so that they can be applied in actuators [12, 30] and artificial muscles [31, 74, 75]. Figure 14.6 demonstrates the schematic diagram of CNT-PDDA artificial muscles. Porous structure brings higher specific surface area, which could be helpful for reacting to external stimulus. For example, Cheng et al. [12] managed to prepare a humidity-driven graphene oxide actuators, which achieved rotary speed of 5190 revolutions/minute. Gu et al. [31] reported a twisting hybrid CNT fiber artificial muscle; also, fiber-shaped devices were usually prepared into primary monofilament structure with an easy way.

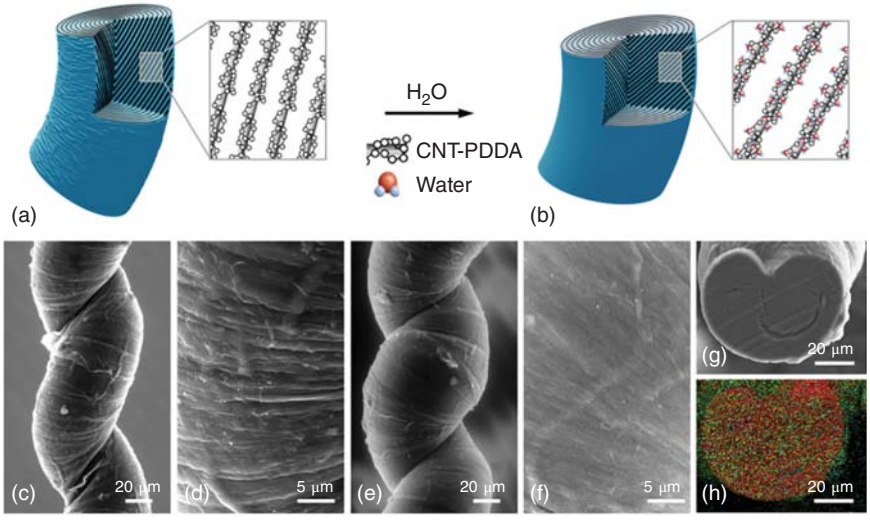


Figure 14.6 Schematic diagram of moisture-driven actuator (a) before and (b) after water absorption. (c, d) Morphology of yarns at 10% RH. (e, f) Morphology of yarns at 90% RH. (g) Cross-sectional SEM image. (h) Elemental mapping by EDAX over the image. Source: Kim et al. 2016 [74]. https://www.nature.com/articles/srep23016#rightslink. http://creativecommons.org/licenses/by/4.0/. Licensed under CCBY 4.0.

14.3.1.2 Skin-Core Structure

Skin-core fibers, which present some unique performance than conventional fibers, are a kind of differential fibers with at least two components incompatibly aligned into concentric or eccentric shape along the radial direction of the fiber. From the view of designer, skin-core fibers can be a desirable candidate for thermal regulating fibers, because the skin can prevent the phase change material from leakage. Moreover, if external stimulus activates the skin as a switch, the core would be spontaneous response against the stimulus. For instance, Shi et al. [76] prepared electrospinning skin-core nanofiber with temperature-responsive poly(*N*-isopropylacrylamide) (PNIPAM) as skin and polycaprolactone (PCL)-loaded nattokinase (NK) as the core; as Figure 14.7 demonstrated, the switchable skin would be turned on, and the anti-thrombus agent NK would be released and worked.

14.3.2 Multilayered Structure

Compared with primary fiber structure, multilayered structure is more adopted for the whole intelligenize process, which is accomplished only by finishing. The multilayered structure is constructed owing to the different properties between coatings and substrates such as electronic parameters and mechanical strength. Besides, for fiber-shaped electronics, several layers such as electrodes layers, carrier transmission layers, and functional layers are needed. Common methods to get multilayered structures are by means of chemical vapor deposition (CVD) [29], in situ polymerization [33], layer-by-layer self-assembling [77] and core spun [78]. For example, Huang et al. [79] reported yarn-based resistance sensors prepared with single and double wrapping method. Shim et al. [81] designed

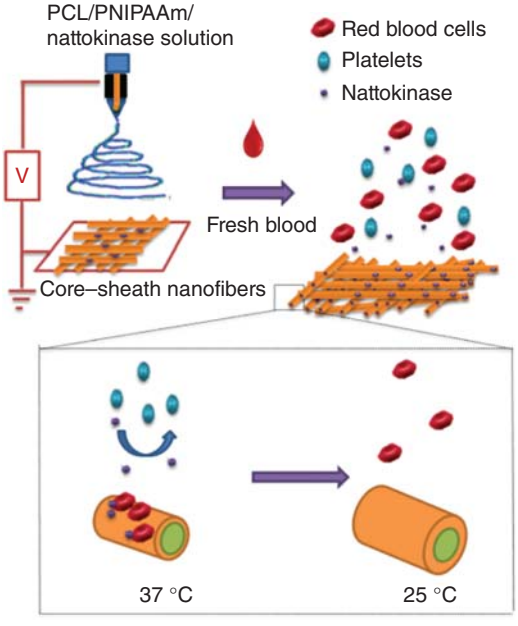


Figure 14.7 Schematic procedure for fabrication of PCL/PNIPAAm core–sheath nanofibers containing nattokinase (NK) to capture and release red blood cells (RBCs) from the blood. Source: Shi et al. 2016 [76]. Reproduced with permission of Royal Society of Chemistry.

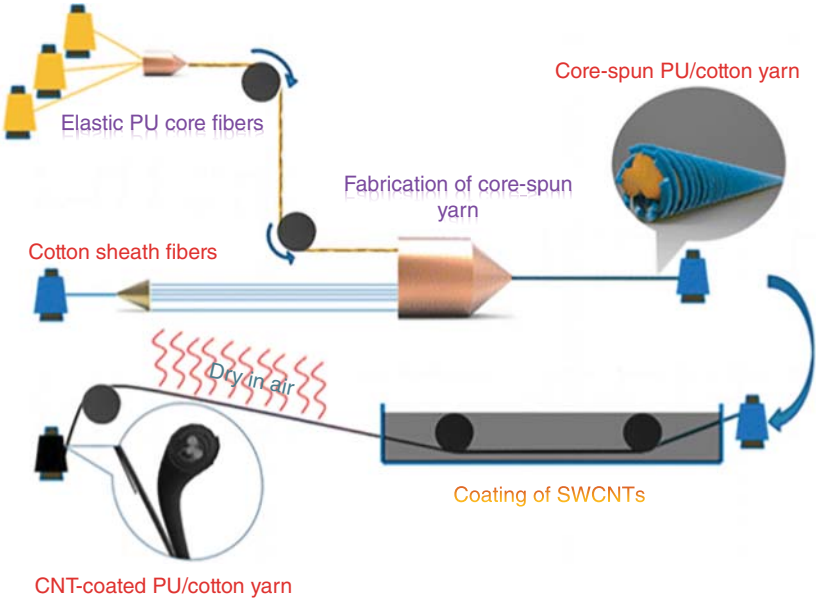


Figure 14.8 Schematic diagram of preparation of core-spun CNT-coated PU/cotton fiber. Source: Wang et al. 2016 [78]. Reproduced with permission of American Chemical Society.

a CNT/electrolyte-coated cotton yarn to fabric e-textiles. Correspondingly, the diversity of preparation leads to wide applications. Figure 14.8 gives the preparation process of single-walled carbon nanotube (SWCNT)-modified core-spun PU/cotton yarn.

14.3.2.1 Coating with Single Layer

Single coating is sufficient for most smart fibers, which is applied in sensors and primitive electronics. There are two kinds of situations. One is that the responsive agents are attached to the fiber-shaped substrates and the responsive agents accomplish the whole procedures of perception and response. For example, fiber-shaped photoluminescence [80] could be the representations. The other one is comprehensive utilization of substrates and coating. Stimulus will lead to the change of unique property of coating (substrate), which affects the structure of substrate (coating); as a result, the changed substrate (coating) delivers measurable functional changes. For instance, ultrathin conductive layer wrapped polyurethane yarns were fabricated though layer-by-layer assembling to monitoring tiny human motions [14]. Figure 14.9 shows the SWNT-coated cotton yarn.

14.3.2.2 Coating with No Less Than Double Layers

Coating with no less than double layers is a typical structure for electricity-induced devices such as electroluminescence and electrochromic fibers. Usually, layers of electrodes such as anodes and cathodes, layers of electron transmitting and carrier transmitting, and layers of electroluminescence or electrochromic

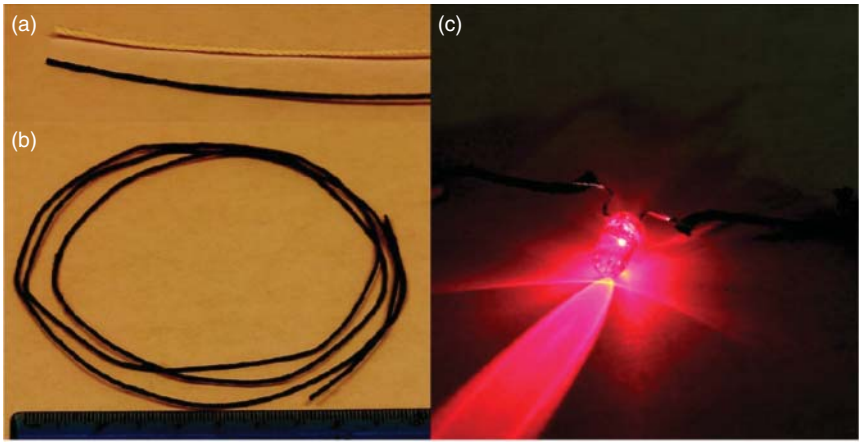


Figure 14.9 Photographs of SWNT-cotton yarn. (a) Comparison of the original and surface modified yarn. (b) 1 m long piece as made. (c) Demonstration of LED emission with the current passing through the yarn. Source: Shim et al. 2008 [81]. Reproduced with permission of American Chemical Society.

chemicals are required for archetypal smart devices, which are simplified later. The first fiber-shaped electroluminescence device was considered to be constructed in 2007 by vacuum thermal evaporation of organic active materials onto swiveling polyimide-coated silica fiber [82]. In this application, the conductivity and flatness may heavily influent the performance of devices [28]. Peng et al. [83] prepared an electrochromic fiber with multilayer structure. Zhang et al. [28] constructed a fiber-based polymer light-emitting cell of which the luminescence changed no more than 6% with different observation angles. Figure 14.10 exhibits typical structure of fiber-shaped organic light-emitting device (OLED).

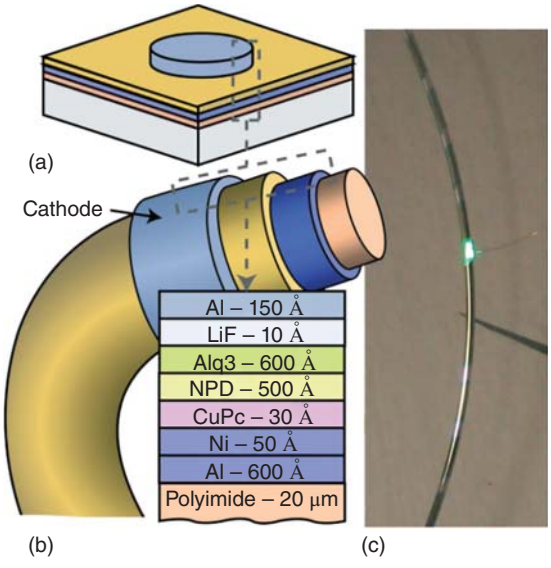


Figure 14.10 (a) An illustration of a typical organic light-emitting device (OLED) structure, along with (b) an illustration of a fiber-based OLED structure analyzed in this report. (c) A photograph of a flexed fiber having a 1 mm green light-emitting "pixel" turned on. Source: O'Connor et al. 2007 [82]. Reproduced with permission of John Wiley & Sons.

14.3.3 Three-Dimensional Fiber-Based Structures

Since the high-speed development of nanotechnology, sub-microfibers, and nanofibers are intensively investigated because of the amazing high specific surface area and additional properties. Currently, these fibers with superfine diameters are designed into membranes and aerogels to construct novel fiber-based smart material.

14.3.3.1 Fabrics and Fiber-Based Membrane

Smart fabrics and fiber-based membranes are typical fiber-based structures, which are fabricated by weaving or stacking of smart fibers or direct treatment to conventional fabrics and fiber-based membranes. Generally, smart fabrics show spiffy softness and wearability, which have promising applications like color-changed textiles [84], smart antibacterial textiles [85], smart robots [86], and oil/water separation [87]. For example, Zhong et al. [63] constructed ultrasensitive pressure sensor by using patterned hybrid nanofiber membrane. Figure 14.11 shows the fiber-based functional fabrics.

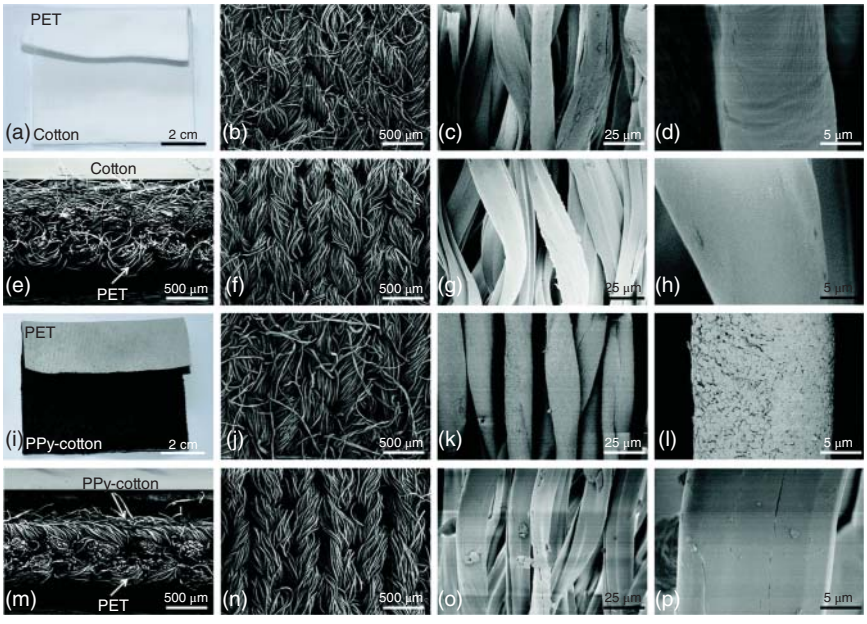


Figure 14.11 (a) Photograph of a blank fabric. (b–d) SEM images of the cotton side of the blank fabric with increasing magnification. (e) Cross-sectional SEM image of the blank fabric. (f–h) Polyester side of the blank fabric with increasing magnification. (i) Photograph of a single-sided conductive fabric. (j–l) SEM images of the cotton side of the single-sided conductive fabric with increasing magnification. (m) Cross-sectional SEM image of the single-sided conductive fabric. (n–p) Polyester side of the single-sided conductive fabric with increasing magnification. Source: Huang et al. 2016 [84]. Reproduced with permission of Royal Society of Chemistry.

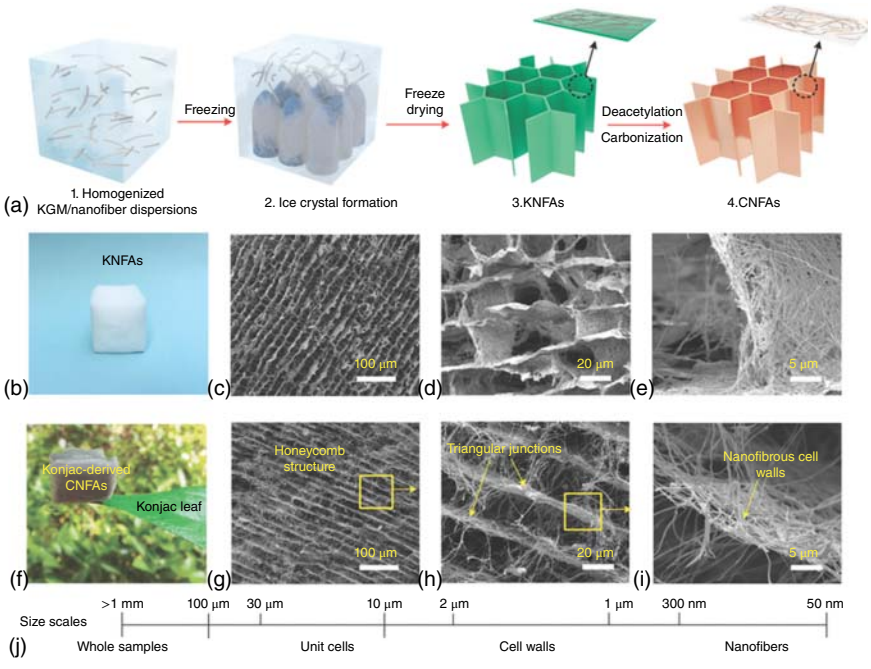


Figure 14.12 (a) Schematic showing the synthetic steps: (1) Homogenized nanofiber dispersions are prepared through high-speed homogenization. (2) Frozen dispersions are prepared by freezing in liquid nitrogen. (3) KNFAs are fabricated via freeze-drying the frozen dispersions. (4) The resultant CNFAs are fabricated by the deacetylation and carbonization of KNFAs. (b) An optical photograph of a KNFA. (c–e) Microscopic structure of KNFAs at different magnifications. (f) An optical photograph showing a 20 cm^3 CNFA ($\rho = 0.14$ mg/cm^3) standing on the tip of a konjac leaf. (g–i) Microscopic structure of CNFAs at various magnifications, demonstrating the biomimetic honeycomb cellular fibrous architecture. (j) Schematic showing the four levels of hierarchy at three distinct length scales. Source: Si et al. 2016 [88]. Reproduced with permission of John Wiley & Sons.

14.3.3.2 Aerogel

Aerogels are well known for their high porosity up to 95–99% and outstanding mechanical property. Si et al. [88] demonstrated a creating of ordered honeycomb-like structure aerogel with konjac glucomannan and silicon dioxide nanofiber to establish high sensitive pressure sensor of which are demonstrated in Figure 14.12.

14.4 Principles and Theories

14.4.1 Shape Memory Fiber

Shape memory fibers are smart and intelligent fibers, which can realize the cycle from other shape to memorized shape under the control of stimulus such as temperature, pH, and light [89, 90]. There are many different types of shape

memory fibers. However, the most common types among them are SMAs and shape memory polymers (SMPs) [91–93]. Typically, shape memory materials include fixed phase and revisable phase. The fixed phase is the provider of recovery force that contributes to avoidance of unacceptable damage and memory of the original shape, while the shape of revisable phase can be changed and locked in another status. For alloys, the fixed phase is the crystal transformation of thermal elastic martensitic, which would balance the thermal effect and elastic behaviors [90, 94], while for polymers, the fixed phase would be chemical cross-linking or supermolecular entanglements; the undefined structure can be transformed into glass state by cooling. Beyond the softening temperature, the recovery force provided by fixed segments contributes to the shape recovery. Besides, a new kind of shape memory fibers, which is made from at least two polymers that share the same mechanism as the polymers, was reported and named with shape memory hybrids (SMHs) [91, 95].

Except that the differences of expansion coefficient can also lead to shape memory effect (SME) [96]. The expansion extent of one phase can be revisable controllable; with stretch or extrusion, the shape of the fiber will change.

14.4.2 Fiber-Based Actuator

Fiber-based actuator is a kind of materials that possess the dynamic motor behaviors in response to environmental stimulus including temperature, humidity, pH, electricity, magnetic field, and so on [13, 97]. Among these different kinds of stimulus, the responsive mechanism can be roughly summarized as the following two categories: one is discriminative expansion/contraction effect that is very common in hydrogels, and the other is deformation that includes structure reformation and crystal transformation induced by microstructure.

Discriminative expansion/contraction effect can be induced by variety of stimulus such as temperature, humidity, pH, and solvent [98, 99]. Generally, the fiber-based actuators are manufactured with more than two different materials, and the different swell and deswell performances between different materials could cause the actuate behavior. Among them, the thermo-responsive hydrogel is widely used for thermo-responsive actuator. For example, Jiang et al. [5] reported a fiber-based superfast thermo-triggered actuator with a double-layer structure including thermo-responsive hydrogel layer and hydrophobic PU layer. The hydrogel phase (PNIPAM) could transform from hydrophilicity to hydrophobicity above the critical temperature, which resulted in actuate behavior because of the unbalanced swell/deswell in water. Besides, hydrogels with weak acid or alkaline groups, such as carbonyls or amino, can also be used to fabricate pH-active actuator [100, 101]. Mahdavinia et al. [102] reported a pH-responsive hydrogel with a polyacrylic acid system.

There are also some fiber-based actuators with one phase that show up obvious expansion under the featured environment. For example, Cheng et al. [12] reported a method to prepare moisture-activated graphene fiber-shaped actuator; the pre-twisting graphene oxide fiber would expanse/contract due to the absorption/desorption of water molecular from the rich oxygen groups. Besides, Chen et al. [27] demonstrated a method to create solvent- and vapor-responsive MWCNT-wrapped primary fiber with large actuation (Figure 14.13).

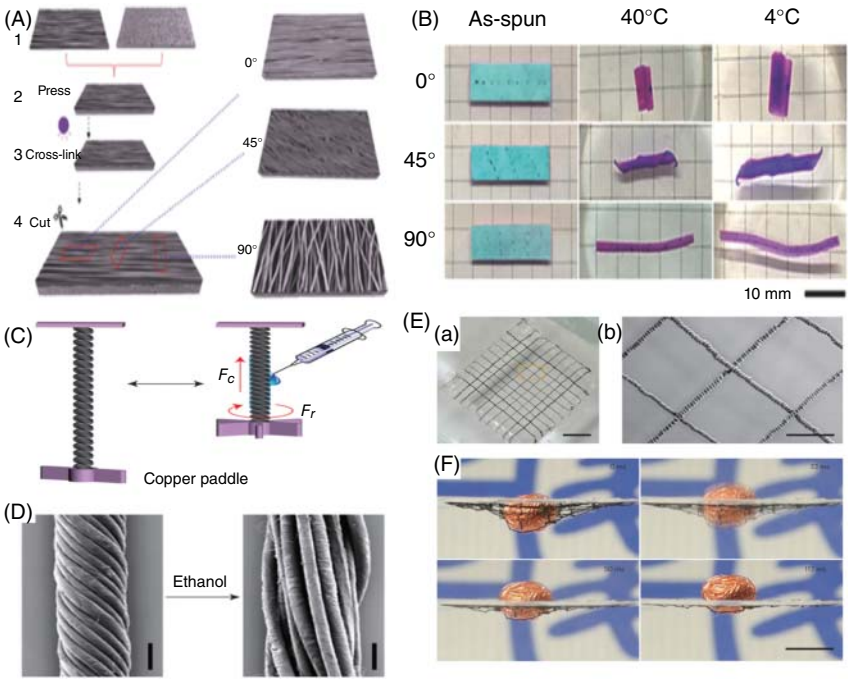


Figure 14.13 (A) Schematic of formation of parallel-arranged PNIPAM fiber actuator along different directions of PNIPAM-0°, PNIPAM-45°, and PNIPAM-90° by electrospinning. (B) The fiber-based actuator was actuated under different temperatures (0, 40, 4 °C). Source: Niu et al. 2016 [47]. Reproduced with permission of Elsevier. (C) Schematic illustration of the contractive and rotary actuations of a hierarchically arranged helical fibers. (D) SEM images of twisted primary fibers before and after ethanol infiltration. The helical structure broke down due to excessive untwisting. (E) Photograph of an actuating textile woven ((a) actuating textile woven fabricated by 18 hierarchically arranged helical fibers (HHF) and (b) the HHF was twisted from 20 primary fibers)). (F) Photographs of the smart textile lifting a copper ball (240 mg) at 0, 33, 50, and 117 ms after being sprayed with ethanol. Source: Chen et al. 2015 [27]. Reproduced with permission of Springer Nature.

The field-induced deformation of the microstructure is the typical mechanism of electric actuator and magnetic actuator. Under the influence of electric field or magnetic field, the microstructures of the materials are forced to adjust along the featured direction with mechanism of crystal transition and the rearrangement of the dipoles and spontaneous magnetization of the magnetic domain. For example, Gu et al. reported a liner actuator of polymeric nanofibrous bundle that can produce a high strain under electric stimuli [26]. Figure 14.13 gives several kinds of specially designed actuators.

14.4.3 Luminescence Fiber

Luminescence fibers are highly functionalized fiber-shaped devices that possess the ability of light emitting. Photoluminescence and electroluminescence are the most investigated branches.

Photoluminescence is a phenomenon of photo-induced light emitting after stock shift or anti-stock shift, which is determined by inner dipole moment.

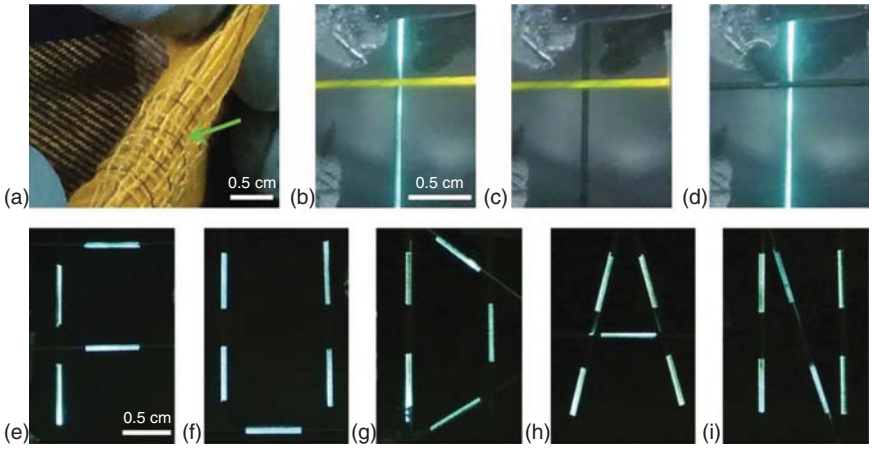


Figure 14.14 (a) Electroluminescent fiber was fabricated into textile under bending and twisting. (b–d) Two fiber-based light-emitting electrochemical cells (PLECs) with different colors (biased at 10 V). (e–i) Fiber-shaped light-emitting electrochemical cells (PLECs) were woven into letter shapes (biased at 9 V). Source: Zhang et al. 2015 [28]. Reproduced with permission of Springer Nature.

From the view of energy, excited electrons spent extra energy on overcoming the barrier and return to ground state meanwhile, and during this process, energy is released by emitting visible lights. Besides, the electrons can be trapped in unique designed chemical structure before their journey back, and only stimulated by temperature the trapped electrons can be reactivated to transited back and luminescent. This phenomenon is named lasting phosphorescence. Lasting phosphorescence phenomenon is often applied in environmental friendly lighting fixture.

Electroluminescence is one of the energy conversion forms. The electrons from cathode and carriers from anode are forced to overcome the interfacial potential barrier by the electricity field. After passing the transporting layer, electroluminescence layer was the final site of incoming electrons and carriers. They will combine in very near distance to form excitons, which can release energy by luminescence. Typically, the electrodes, transporting layer, and the light-emitting layer are critical factors to the efficiency of luminescence. To obtain the high-performance electroluminescence, the work function of the electrodes and the interfacial potential barrier should be concerned and dedicatedly designed. Figure 14.14 shows the electroluminescence fiber with woven ability.

14.4.4 Color-Changed Fiber

Color-changed fibers are unique structured fibers that can rapidly change their color or transparency under the thermal, electrical, and optical impact [103–105]. Generally, the mechanism of color-changed fibers can be roughly summarized as redox reaction, crystal transformation, and geometric configuration changes of ligand [1, 106].

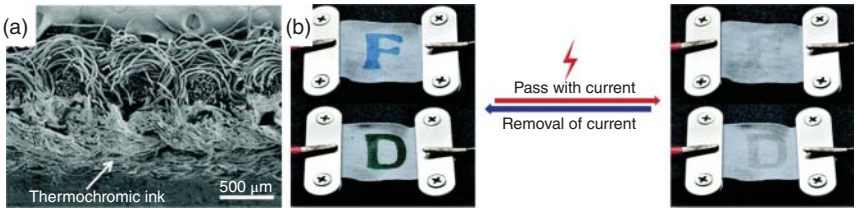


Figure 14.15 (a) Cross-sectional SEM image of color-changed smart textile. (b) The smart textile shows color-changed phenomenon under currents. Source: Huang et al. 2016 [84]. Reproduced with permission of Royal Society of Chemistry.

Redox reaction mechanism often takes place in electrochromic and photochromic [104]. It requires different colors between reduction state and oxidation state. The electrons are obtained or lost in order to alter the oxidation–reduction state results in the change of absorption spectrum with visible behavior of color change. Amounts of chemicals can expose the property; so far, the most popular candidates are metal ions, dyes, and conductive polymers.

Crystal transformation mechanism often exerts in thermal-induced color-changed phenomenon [107]. Amounts of iodine–iodides change their color due to the crystal transformation. For example, α crystal form of Cu_2HgI_4 appears a red color, while the β form gives purple color. Additionally, α form can transform into β form under a higher temperature beyond 68 °C.

The geometric configuration changes of ligand are often used in titration. The fiber can give a similar color-changed performance when the ligand compound is immobilized on. Figure 14.15 exhibits a sample of color-changed textile.

14.4.5 Thermoregulated Fiber

Thermoregulated fiber is microstructure-designed fiber with the function to store heat and adjust temperature. The thermal behaviors are controlled by phase change, which can store or release plenty of energy. In detail, the material will absorb energy and store by means of phase change to prevent the temperature from increasing; on the contrary, it inverses phase change causing heat release to prevent the temperature from decreasing. The often used phase change material were polyethylene glycol (PEG) and wax.

14.5 Applications

With the further research of the smart fibers, multifunctional, and high intelligent fibers have been developed, and its applications have been extended to all walks of life.

14.5.1 Smart Fibers Used in Textiles

14.5.1.1 Smart Clothing

Smart fibers have the properties such as flexibility, spinnability, and knittability, as well as the perception and responsiveness to the external environment, and

can be easily fabricated to different kinds of fabrics and apparels with special functions. Thermoregulated fibers with reversible temperature adjustable ability can be used in different temperature conditions. These textiles can adjust the temperature without changing the conditions or loadings to protect the body. For example, the thermoregulated fibers or fiber-based materials can be used in space suits and gloves as developed products to protect the astronauts from the hard conditions [108]. And with the dramatically development, they will gradually appears in our common garments, such as sportswear, shoes, some special kinds of bedding, and accessories [108, 109].

In recently years, photochromic and thermochromic fibers have also aroused great interests among people, for they can change their colors under different radiations or temperatures. These outstanding performances have been applied in clothing and decorative textiles, such as cap, jacket, skirt, bedspread, chimney, curtain cloth, etc. [110].

14.5.1.2 Wearable Electronics

Recently, wearable electronics have attracted lots of interests due to the potential applications on human physical signal monitoring, human robot interface, and wearable energy collector.

Artificial electronic skin consisted of fiber-based pressure sensor is the representative branch of wearable electronics. By mimicking the natural human skins, artificial e-skins can realize the real-time monitoring for the human physical signals, which can be the judgment indexes of health condition. For example, the resistance sensor prepared by patterned nanofibrous membrane could collect human pulse with high accuracy [63]. In addition, the human physiological signals, such as blood pressure, heartbeat, breathing, etc., can also be detected by wearable electronics [14, 111].

The wearable energy collector can capture and store energy from the movement behavior, which realize the effective use of energy. Wang Zhong Lin group [112] reported a self-charging power system with a fabric-hybridized system. The system could harvest the solar energy from the natural source and gather the mechanical energy from the human motion. This system realized the energy storage and conversion in wearable device. Besides, his group also reported a whole textile-based energy harvesting system that could convert low-frequency human motion energy into high-frequency current outputs [113] (see in Figure 14.16).

Besides, wearable electronics with special optical performance also show prior advantages than traditional flat devices. Peng Huisheng group has taken much effort to promote the fiber-shaped electroluminescence and electrochromic devices into practical uses.

14.5.2 Smart Fibers Used in Industrial

14.5.2.1 Medical Supplies

The smart fibers also show great potential in applications of medical care. Among them, the most common applications are controllable drug delivery. Figure 14.17 shows application for physical signal diagnose with smart textile. Smart materials used for drug delivery have been studied since the last couple of



Figure 14.16 (a) Scheme of a self-charging power textile. (SC, supercapacitor yarns; TENG, triboelectric nanogenerator cloth). Source: Pu et al. 2016 [114]. Reproduced with permission of John Wiley & Sons. A self-charging power textile woven with F-TENGs, F-DSSCs, and F-SCs under outdoor (b), indoor (c), and movement (d) conditions. Source: Wen et al. 2016 [112]. Reproduced with permission of AAAS. (e) Scheme of a self-charging power system, among them being a fiber-based dye-sensitized solar cell (F-DSSC) and a fiber-based tribolectric nanogenerator (F-TENG) act as energy harvesting devices and a fiber-shaped supercapacitor (F-SC) act as an energy-storing device.

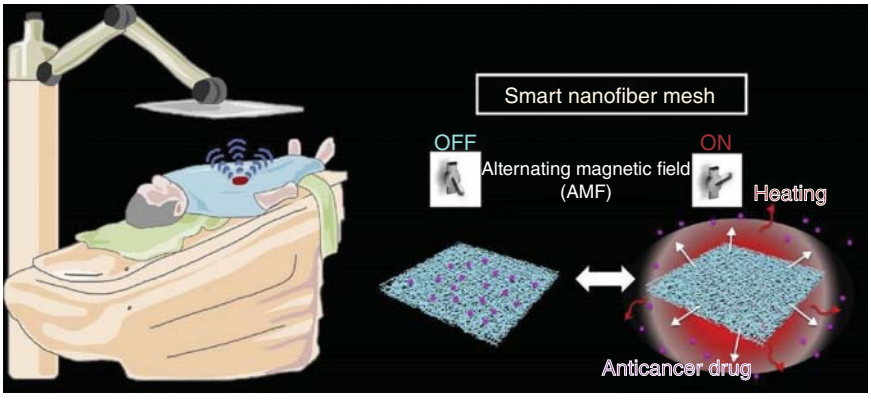


Figure 14.17 A scheme of a smart hyperthermia nanofiber system that utilizes magnetic hyperthermia and temperature-responsive polymers.

decades and substantive progress had been made in recent years especially on the automated drug delivery systems with automaticity and targeted [68, 115]. For example, the thermo-responsive hydrogel of PNIPAM and its copolymers are widely designed as automatic switch in temperature-controllable drug delivery systems. Furthermore, the biologically available phase change temperature of PNIPAM about 32 °C is the fundamental insurance of this application [5, 115]. Except this, in the field of engineering and cell engineering, smart fibers have been further developed and succeeded in using as scaffolds with required dimensions and sizes [116–118]. For example, the nonwoven biodegradable nanofiber scaffolds fabricated by electrospinning were used in bone tissue engineering. The nanofiber-based scaffolds with highly porous structure and large surface area can promote the tissue ingrowth [118, 119]. Besides artificial muscles, smart bandages also arouse great interests in medical field. Gu et al. [26] reported an artificial muscle fibers that had the function to imitate natural muscles. The smart bandage integrated with a variety of sensors could detect bacteria, humidity, and oxygen concentration that can better cure diseases [120].

14.5.2.2 Sensors

Sensors have played a significant role in promoting the automatic production that tremendously improves the industrial production efficiency. Smart fibers are good candidate to fabricate sensors especially some microsensors, since they have small size and volume that can be easily encapsulate into different kinds of devices [110]. Figure 14.18 shows the nanofiber-based pressure sensor used as large area pressure-sensitive device and human pulse detection.

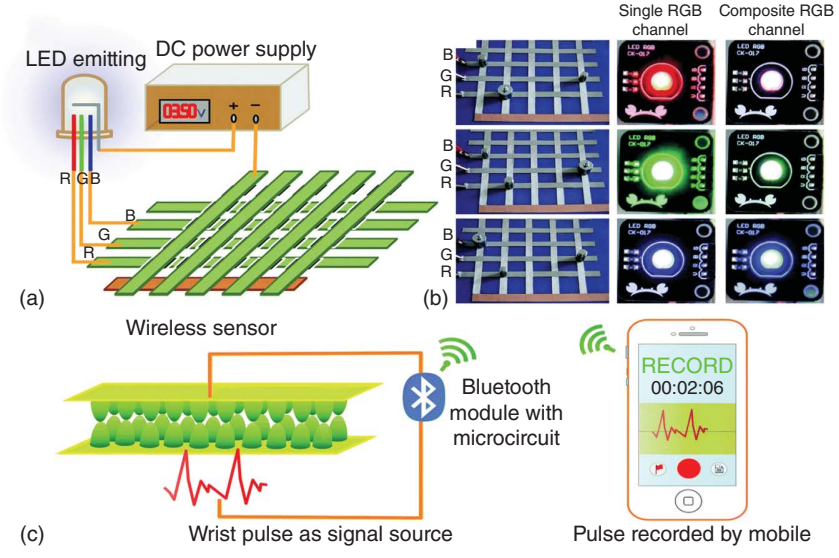


Figure 14.18 (a) A schematic illustration of the fiber-based stress sensor network with a connecting RGB-LED module. (b) When three different weights (20, 10, and 5 g) stand the distinguished stress were placed on the pixels, different color lights (red, ~2.2 V; green, ~3.0 V; and blue, ~3.1 V) will be lighted up (from individual and composite channels). (c) A schematic illustration of the wireless sensor with a Bluetooth module. The weak signals can be converted into wireless electromagnetic waves and simultaneously recorded by a smartphone.

Liu et al. prepared a nanofiber-based sensor based on conductive nickel-deposited PET membrane intertwined with PVA-*co*-PE nanofibers for alcohol concentration detection and healthcare-related industries [121]. In this sensor, the alcohol concentration detection property could be reflected by capacitance values, which had great sensitivity and efficiency.

In addition, smart fibers have also spread to the humidity sensing field. High sensitive humidity sensor based on single SnO_2 nanowire [122], oxidation of graphene (GO) [12], and NW films [123, 124] have been reported.

14.5.2.3 Energy Conversion

Energy conversion is a very important part in smart materials. Recently, with the further research of the fibrous materials, more and more fiber-based energy conversion devices are developed.

Fiber-based piezoelectric materials especially the nanogenerator is widely studied for converting low-frequency vibration and biomechanical energy into electrical energy. For example, Chen et al. [125] reported a nanogenerator using lead zirconate titanate (PZT) nanofiber for energy harvesting. Besides, Yang et al. [126] used a piezoelectric fine wire and fabricated a flexible generator with cyclic stretching–releasing properties. This generator could create an oscillating output voltage up to approximately 50 mV under a strain of 0.05–0.1%. Li and coworkers [127] reported a single-wire generator by ZnO nanowire, which can convert the biomechanical energy to electric.

CNTs and graphene oxide are popular in scientific since their emergence. They are always the good candidates to make various energy conversion devices for their excellent conductivity, moisture absorption, photothermal hearting effect, etc. [59]. For example, the twist GO hydrogel fibers act as a generator under humidity condition can reverse the kinetic energy into electrical energy [12] (Figure 14.19).

14.5.3 Other Uses

Smart fibers can also be used in the defense industry, semiconductor/electronic industry, nuclear power plant, automobile industry, sports equipment, etc. At present, the research of smart fibers has not yet reached a wide range of applications. The true sense of intelligence still needs unremitting efforts of scientific research workers.

14.6 Future Trends

Although the research of smart fiber has made great progress, there are still some challenges that restrict its further development. To realize the real intelligence, there is still a long way to go:

(1) *Sensitivity*: Sensitivity is the most important part of the smart fiber. At present, most smart fibers have the stimuli-responsive property, but the sensitivity still needs to be improved. For example, in order to improve the response speed, the temperature-triggered actuator made by hydrogel should be made into very small form, which greatly restricted its application in large-scale equipment. Besides, some wearable pressure sensing devices

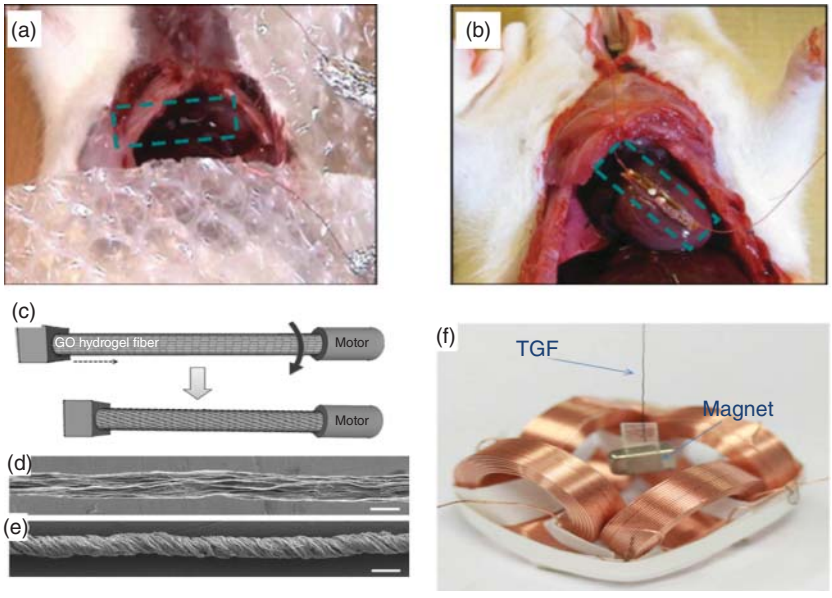


Figure 14.19 Energy harvesting from the breath (a) and heartbeat (b) of a live rat using a single-wire generator (SWG). Source: Li et al. 2010 [8]. Reproduced with permission of John Wiley & Sons. (c) Scheme of the fabrication of a twisted GO fiber; SEM images of a nontwist-dried GO fiber (d) and a twist one (e) with an applied 5000 turns/m. (f) A twisted GO fiber (TGF) used as an humidity alternating current generator. Source: Cheng et al. 2014 [12]. Reproduced with permission of John Wiley & Sons.

can detect very weak signal from human body only if they reach a high sensitivity. Therefore, continued molecular analogs and mechanics modeling are needed to optimize the molecular structure and improve the smart fiber sensitivity.

(2) *Multiple responsive*: Multiple responsive smart fibers mean to respond to multiple stimuli at the same time. At present, most smart fibers are unilateral intelligence. For fabricating multiple-stimulus-active smart fibers or fiber-based smart materials, we should combine the different stimuli-responsive structures into one single fiber. While in many cases, the incompatibility of the structure performance and processing method will make the smart process hard to continue further. For example, a sort of raw materials cannot withstand high temperature treatment or incompatible with the main solvent that causes the process hard to continue. Therefore, the material composition, size, processing method, shape design, macroscopic, or microcosmic configuration also should be optimized to obtain the optimum performance.

(3) *Stability*: Stability is one of the most important factors; it must be considered for practical application. Compared with the common fibers, smart fibers have a more complex and difficult production process. A bad stability will affect the accuracy, which finally limits the applications.

(4) *Large-scale production*: Large-scale production is the biggest challenge of fibrous intelligent materials for the future development. To achieve large-scale production, the fiber must possess the following characteristics: firstly, the technological process should be simple and easy to operate. Secondly, there are no toxic and harmful substances or gas releasing during the whole progress. Thirdly, low production cost and mass production ability should be achieved. Lastly, products should be safe and stable. The existing smart fibers have a relatively complicated manufacturing process, and the conversion cost is high. Therefore, the further exploration should be carried to optimize technique process. Besides, single fibrous energy storage devices can only transfer or store small amounts of energy. In order to improve the energy conversion rate, the fibers should be further processed into fibrous energy device. This progress still has many difficulties that need to be solved.

Last, smart fibers play an increasingly important role in our daily life. Therefore, the research and development of smart fiber and materials should be valued and make contributes to the textile industry and other fields.

References

1 Hu, J., Meng, H., Li, G. et al. (2012). A review of stimuli-responsive polymers for smart textile applications. *Smart Materials and Structures* 21 (5): 053001.

2 Pelipenko, J., Kocbek, P., and Kristl, J. (2015). Critical attributes of nanofibers: preparation, drug loading, and tissue regeneration. *International Journal of Pharmaceutics* 484 (1): 57–74.

3 Schwarz, A., Van Langenhove, L., Guermonprez, P. et al. (2010). A roadmap on smart textiles. *Textile Progress* 42 (2): 99–180.

4 Castano, L.M. and Flatau, A.B. (2014). Smart fabric sensors and e-textile technologies: a review. *Smart Materials and Structures* 23 (5): 053001.

5 Jiang, S., Liu, F., Lerch, A. et al. (2015). Unusual and superfast temperature-triggered actuators. *Advanced Materials* 27 (33): 4865–4870.

6 Yang, B., Huang, W., Li, C. et al. (2006). Effects of moisture on the thermomechanical properties of a polyurethane shape memory polymer. *Polymer* 47 (4): 1348–1356.

7 Zhang, M., Tao, J., Wang, J. et al. (2015). Single $BaTiO_3$ nanowires-polymer fiber based nanogenerator. *Nano Energy* 11: 510–517.

8 Li, Z., Zhu, G., Yang, R. et al. (2010). Muscle-driven in vivo nanogenerator. *Advanced Materials* 22 (23): 2534–2537.

9 Feil, H., Bae, Y., Feijen, J. et al. (1992). Mutual influence of pH and temperature on the swelling of ionizable and thermosensitive hydrogels. *Macromolecules* 25 (20): 5528–5530.

10 Lee, E., Kim, D., Kim, H. et al. (2015). Photothermally driven fast responding photo-actuators fabricated with comb-type hydrogels and magnetite nanoparticles. *Scientific Reports* 5: 15124.

11 Sendoh, M., Ishiyama, K., and Arai, K.I. (2003). Fabrication of magnetic actuator for use in a capsule endoscope. *IEEE Transactions on Magnetics* 39 (5): 3232–3234.

12 Cheng, H., Hu, Y., Zhao, F. et al. (2014). Moisture-activated torsional graphene-fiber motor. *Advanced Materials* 26 (18): 2909–2913.

13 Mu, J. et al. (2015). A multi-responsive water-driven actuator with instant and powerful performance for versatile applications. *Scientific Reports* 5: 9503.

14 Wu, X. et al. (2016). Highly sensitive, stretchable, and wash-durable strain sensor based on ultrathin conductive layer@polyurethane yarn for tiny motion monitoring. *ACS Applied Materials & Interfaces* 8 (15): 9936–9945.

15 Wang, Z. et al. (2007). Voltage generation from individual $BaTiO_3$ nanowires under periodic tensile mechanical load. *Nano Letters* 7 (10): 2966–2969.

16 Karlsson, J.O. and Gatenholm, P. (1999). Cellulose fibre-supported pH-sensitive hydrogels. *Polymer* 40 (2): 379–387.

17 Casper, C.L. et al. (2005). Functionalizing electrospun fibers with biologically relevant macromolecules. *Biomacromolecules* 6 (4): 1998–2007.

18 Lendlein, A. and Langer, R. (2002). Biodegradable, elastic shape-memory polymers for potential biomedical applications. *Science* 296 (5573): 1673–1676.

19 Koncherry, V., Potluri, P., and Fernando, A. (2016). Multifunctional carbon fibre tapes for automotive composites. *Applied Composite Materials* 24 (2): 477–493.

20 Descloux, A., Amitonova, L.V., and Pinkse, P.W. (2016). Aberrations of the point spread function of a multimode fiber due to partial mode excitation. *Optics Express* 24 (16): 18501–18512.

21 Wang, D., Sun, G., and Chiou, B.S. (2007). A high-throughput, controllable, and environmentally benign fabrication process of thermoplastic nanofibers. *Macromolecular Materials and Engineering* 292 (4): 407–414.

22 Li, M. et al. (2015). Highly hydrophilic and anti-fouling cellulose thin film composite membrane based on the hierarchical poly(vinyl alcohol-co-ethylene) nanofiber substrate. *Cellulose* 22 (4): 2717–2727.

23 Zhang, Z. et al. (2015). Flexible electroluminescent fiber fabricated from coaxially wound carbon nanotube sheets. *Journal of Materials Chemistry C* 3 (22): 5621–5624.

24 Di, J. et al. (2016). Carbon-nanotube fibers for wearable devices and smart textiles. *Advanced Materials* 28 (47): 10529–10538.

25 Daghash, S.M. and Ozbulut, O.E. (2016). Characterization of superelastic shape memory alloy fiber-reinforced polymer composites under tensile cyclic loading. *Materials and Design* 111: 504–512.

26 Gu, B.K. et al. (2009). A linear actuation of polymeric nanofibrous bundle for artificial muscles. *Chemistry of Materials* 21 (3): 511–515.

27 Chen, P. et al. (2015). Hierarchically arranged helical fibre actuators driven by solvents and vapours. *Nature Nanotechnology* 10 (12): 1077–1083.

28 Zhang, Z. et al. (2015). A colour-tunable, weavable fibre-shaped polymer light-emitting electrochemical cell. *Nature Photonics* 9 (4): 233–238.

29 Mandia, D.J. et al. (2015). The effect of ALD-grown Al_2O_3 on the refractive index sensitivity of CVD gold-coated optical fiber sensors. *Nanotechnology* 26 (43): 434002.

30 Kim, H. et al. (2016). Temperature-responsive tensile actuator based on multi-walled carbon nanotube yarn. *Nano-Micro Letters* 8 (3): 254–259.

31 Gu, X. et al. (2016). Hydro-actuation of hybrid carbon nanotube yarn muscles. *Nanoscale* 8 (41): 17881–17886.

32 Li, B. et al. (2008). Simultaneous growth of SiC nanowires, SiC nanotubes, and SiC/SiO_2 core–shell nanocables. *Journal of Alloys and Compounds* 462 (1–2): 446–451.

33 Wang, Y. et al. (2016). Polypyrrole/poly(vinyl alcohol-co-ethylene) nanofiber composites on polyethylene terephthalate substrate as flexible electric heating elements. *Composites Part A Applied Science and Manufacturing* 81: 234–242.

34 Guo, H. et al. (2014). Ultrafast and reversible thermochromism of a conjugated polymer material based on the assembly of peptide amphiphiles. *Chemical Science* 5 (11): 4189–4195.

35 AIAA (2009). Fiber reinforced shape-memory polymer composite and its application in deployable hinge in space. *Smart Materials and Structures* 18 (2): 1282–1294.

36 Hu, M. et al. (2016). Sensitive and fast optical HCl gas sensor using a nanoporous fiber membrane consisting of poly(lactic acid) doped with tetraphenylporphyrin. *Microchimica Acta* 183 (5): 1713–1720.

37 Lee, S.H. et al. (2016). Biothermal sensing of a torsional artificial muscle. *Nanoscale* 8 (6): 3248–3253.

38 Zhang, Z. et al. (2013). Preparation of polypyrrole composite solid-phase microextraction fiber coatings by sol-gel technique for the trace analysis of polar biological volatile organic compounds. *Analyst* 138 (4): 1156–1166.

39 Sridhar, R. et al. (2015). Electrosprayed nanoparticles and electrospun nanofibers based on natural materials: applications in tissue regeneration, drug delivery and pharmaceuticals. *Chemical Society Reviews* 44 (3): 790–814.

40 Daghia, F. et al. (2008). Shape memory alloy hybrid composite plates for shape and stiffness control. *Journal of Intelligent Material Systems and Structures* 19 (5): 609–619.

41 An, S. et al. (2016). Self-junctioned copper nanofiber transparent flexible conducting film via electrospinning and electroplating. *Advanced Materials* 28 (33): 7149–7154.

42 Sohn, J.W. et al. (2009). Vibration and position tracking control of a flexible beam using SMA wire actuators. *Journal of Vibration and Control* 15 (2): 263–281.

43 Lusiola, T. et al. (2015). Ferroelectric KNNT fibers by thermoplastic extrusion process: microstructure and electromechanical characterization. *Actuators* 4 (2): 99–113.

44 Bortolani, F. et al. (2014). High strain in $(K,Na)NbO_3$-based lead-free piezoelectric fibers. *Chemistry of Materials* 26 (12): 3838–3848.

45 Tallury, S.S. et al. (2016). Physical microfabrication of shape-memory polymer systems via bicomponent fiber spinning. *Macromolecular Rapid Communications* 37 (22): 1837–1843.

46 Nunes-Pereira, J. et al. (2013). Energy harvesting performance of piezoelectric electrospun polymer fibers and polymer/ceramic composites. *Sensors and Actuators A: Physical* 196 (7): 55–62.

47 Niu, W. et al. (2016). Photoresponse enhancement of Cu_2O solar cell with sulfur-doped ZnO buffer layer to mediate the interfacial band alignment. *Solar Energy Materials and Solar Cells* 144: 717–723.

48 Hong, S. et al. (2015). Highly stretchable and transparent metal nanowire heater for wearable electronics applications. *Advanced Materials* 27 (32): 4744–4751.

49 Choi, E. et al. (2017). Monotonic and hysteretic pullout behavior of superelastic SMA fibers with different anchorages. *Composites Part B Engineering* 108: 232–242.

50 Li, D.Y. et al. (2016). Superelasticity of Cu–Ni–Al shape-memory fibers prepared by melt extraction technique. *Journal of Minerals, Metallurgy and Materials* 23 (8): 928–933.

51 Wang, X. et al. (2007). Direct-current nanogenerator driven by ultrasonic waves. *Science* 316 (5821): 102–105.

52 Sazio, P.J. et al. (2006). Microstructured optical fibers as high-pressure microfluidic reactors. *Science* 311 (5767): 1583–1586.

53 Lagonigro, L. et al. (2010). Low loss silicon fibers for photonics applications. *Applied Physics Letters* 96 (4): 041105.

54 Zhang, W. et al. (2011). Synergistic effect of chemo-photothermal therapy using PEGylated graphene oxide. *Biomaterials* 32 (33): 8555–8561.

55 Cao, X. et al. (2013). Ambient fabrication of large-area graphene films via a synchronous reduction and assembly strategy. *Advanced Materials* 25 (21): 2957–2962.

56 Dong, Z. et al. (2012). Facile fabrication of light, flexible and multifunctional graphene fibers. *Advanced Materials* 24 (14): 1856–1861.

57 Chen, J. et al. (2010). Preparation and evaluation of graphene-coated solid-phase microextraction fiber. *Analytica Chimica Acta* 678 (1): 44–49.

58 Zhang, Q. et al. (2009). Hierarchical composites of carbon nanotubes on carbon fiber: influence of growth condition on fiber tensile properties. *Composites Science and Technology* 69 (5): 594–601.

59 Koziol, K. et al. (2007). High-performance carbon nanotube fiber. *Science* 318 (5858): 1892–1895.

60 Saheb, D.N. and Jog, J.P. (1999). Natural fiber polymer composites: a review. *Advances in Polymer Technology* 18 (4): 351–363.

61 Huang, Z.M. et al. (2003). A review on polymer nanofibers by electrospinning and their applications in nanocomposites. *Composites Science and Technology* 63 (15): 2223–2253.

62 Li, R. et al. (2008). Polyamide 11/poly(vinylidene fluoride) blends as novel flexible materials for capacitors. *Macromolecular Rapid Communications* 29 (17): 1449–1454.

63 Zhong, W. et al. (2016). A nanofiber based artificial electronic skin with high pressure sensitivity and 3D conformability. *Nanoscale* 8 (24): 12105–12112.

64 El-Hadi, A.M. et al. (2014). Enhancing the crystallization and orientation of electrospinning poly(lactic acid) (PLLA) by combining with additives. *Journal of Polymer Research* 21 (12): 1–12.

65 Matabola, K.P. and Moutloali, R.M. (2013). The influence of electrospinning parameters on the morphology and diameter of poly(vinylidene fluoride) nanofibers- effect of sodium chloride. *Journal of Materials Science* 48 (16): 5475–5482.

66 Zhu, J. and Sun, G. (2014). Fabrication and evaluation of nanofibrous membranes with photo-induced chemical and biological decontamination functions. *RSC Advances* 4 (92): 50858–50865.

67 Xin, Y. et al. (2015). Full-fiber piezoelectric sensor by straight PVDF/nanoclay nanofibers. *Materials Letters* 164: 136–139.

68 Caldoreramoore, M.E., Liechty, W.B., and Peppas, N.A. (2011). Responsive theranostic systems: integration of diagnostic imaging agents and responsive controlled release drug delivery carriers. *Accounts of Chemical Research* 44 (10): 1061–1070.

69 Reina, A. et al. (2009). Large area, few-layer graphene films on arbitrary substrates by chemical vapor deposition. *Nano Letters* 9 (8): 655–663.

70 Yang, X. et al. (2009). Anti-oxidation behavior of chemical vapor reaction SiC coatings on different carbon materials at high temperatures. *The Chinese Journal of Nonferrous Metal* 19 (5): 1044–1050.

71 Sonnenfeld, C. et al. (2011). Microstructured optical fiber sensors embedded in a laminate composite for smart material applications. *Sensors (Basel)* 11 (3): 2566–2579.

72 Bhuvana, T. et al. (2010). Contiguous petal-like carbon nanosheet outgrowths from graphite fibers by plasma CVD. *ACS Applied Materials & Interfaces* 2 (3): 644–648.

73 Muller, D. et al. (2015). Synthesis of conductive PPy/SiO_2 aerogels nanocomposites by in situ polymerization of pyrrole. *Journal of Nanomaterials* 2015: 1–6.

74 Kim, S.H. et al. (2016). Bio-inspired, moisture-powered hybrid carbon nanotube yarn muscles. *Scientific Reports* 6: 23016.

75 Lee, J. et al. (2016). Carbon nanotube yarn-based glucose sensing artificial muscle. *Small* 12 (15): 2085–2091.

76 Shi, Q. et al. (2016). A smart core-sheath nanofiber that captures and releases red blood cells from the blood. *Nanoscale* 8 (4): 2022–2029.

77 Bhattacharjee, Y. et al. (2016). Construction of a carbon fiber based layer-by-layer (LbL) assembly – a smart approach towards effective EMI shielding. *RSC Advances* 6 (113): 112614–112619.

78 Wang, Z. et al. (2016). Polyurethane/cotton/carbon nanotubes core-spun yarn as high reliability stretchable strain sensor for human motion detection. *ACS Applied Materials & Interfaces* 8 (37): 24837–24843.

79 Huang, C.-T. et al. (2008). A wearable yarn-based piezo-resistive sensor. *Sensors and Actuators A: Physical* 141 (2): 396–403.

80 Duval, Y. et al. (1992). Correlation between ultraviolet-induced refractive index change and photoluminescence in Ge-doped fiber. *Applied Physics Letters* 61 (25): 2955.

81 Shim, B.S. et al. (2008). Smart electronic yarns and wearable fabrics for human biomonitoring made by carbon nanotube coating with polyelectrolytes. *Nano Letters* 8 (12): 4151–4157.

82 O'Connor, B. et al. (2007). Fiber shaped light emitting device. *Advanced Materials* 19 (22): 3897–3900.

83 Peng, H. et al. (2009). Electrochromatic carbon nanotube|[sol]| polydiacetylene nanocomposite fibres. *Nature Nanotechnology* 4 (11): 738–741.

84 Huang, G. et al. (2016). Smart color-changing textile with high contrast based on a single-sided conductive fabric. *Journal of Materials Chemistry C* 4 (32): 7589–7594.

85 Davoudi, Z.M. et al. (2014). Hybrid antibacterial fabrics with extremely high aspect ratio Ag/AgTCNQ nanowires. *Advanced Functional Materials* 24 (8): 1047–1053.

86 Tajitsu, Y. (2016). Smart piezoelectric fabric and its application to control of humanoid robot. *Ferroelectrics* 499 (1): 36–46.

87 Li, J.J., Zhou, Y.N., and Luo, Z.H. (2015). Smart fiber membrane for pH-induced oil/water separation. *ACS Applied Materials & Interfaces* 7 (35): 19643–19650.

88 Si, Y. et al. (2016). Ultralight biomass-derived carbonaceous nanofibrous aerogels with superelasticity and high pressure-sensitivity. *Advanced Materials* 28 (43): 9512–9518.

89 Wagermaier, W. et al. (2010). Shape-memory polymers: characterization methods for shape-memory polymers. *Advances in Polymer Science* 226 (1): 97–145.

90 Sun, L. et al. (2012). Stimulus-responsive shape memory materials: a review. *Materials and Design* 33 (1): 577–640.

91 Huang, W.M. et al. (2010). Shape memory materials. *Materials Today* 13 (7): 54–61.

92 Wei, Z.G., Sandstrom, R., and Miyazaki, S. (1998). Shape memory materials and hybrid composites for smart systems: Part II Shape-memory hybrid composites. *Journal of Materials Science* 33 (15): 3763–3783.

93 Janke, L. et al. (2005). Applications of shape memory alloys in civil engineering structures—overview, limits and new ideas. *Materials and Structures* 38 (5): 578–592.

94 Fan, K. et al. (2011). Water-responsive shape memory hybrid: design concept and demonstration. *Express Polymer Letters* 5: 409–416.

95 Wei, Z., Sandstroröm, R., and Miyazaki, S. (1998). Shape-memory materials and hybrid composites for smart systems: Part I Shape-memory materials. *Journal of Materials Science* 33 (15): 3743–3762.

96 Lv, H. et al. (2008). Shape-memory polymer in response to solution. *Advanced Engineering Materials* 10 (6): 592–595.

97 Bauer, S. et al. (2014). 25th anniversary article: a soft future: from robots and sensor skin to energy harvesters. *Advanced Materials* 26 (1): 149–162.

98 Wang, C. et al. (2016). A solution-processed high-temperature, flexible, thin-film actuator. *Advanced Materials* 28 (39): 8618–8624.

99 Meng, H. and Hu, J. (2010). A brief review of stimulus-active polymers responsive to thermal, light, magnetic, electric, and water/solvent stimuli. *Journal of Intelligent Material Systems and Structures* 21 (9): 859–885.

100 Hoffman, A.S. (2000). Bioconjugates of intelligent polymers and recognition proteins for use in diagnostics and affinity separations. *Clinical Chemistry* 46 (9): 1478–1486.

101 Jocic, D. (2008). Smart textile materials by surface modification with biopolymeric systems. *Research Journal of Textile and Apparel* 12 (2): 58–65.

102 Mahdavinia, G. et al. (2004). Modified chitosan 4. Superabsorbent hydrogels from poly(acrylic acid-co-acrylamide) grafted chitosan with salt-and pH-responsiveness properties. *European Polymer Journal* 40 (7): 1399–1407.

103 Monk, P.M.S., R.J. Mortimer, and D.R. Rosseinsky (2007). *Electrochromism: Fundamentals and Applications*. John Wiley & Sons.

104 Irie, M. (2000). Photochromism: memories and switches-introduction. *Chemical Reviews* 100 (5): 1683–1684.

105 Hadjoudis, E. and Mavridis, I.M. (2005). Photochromism and thermochromism of Schiff bases in the solid state: structural aspects. *ChemInform* 33 (14): 579–588.

106 Zhao, X.Y., Wang, M.Z., and Liu, H.J. (2008). Structure dependence of photochromism of azobenzene-functionalized polythiophene derivatives. *Journal of Applied Polymer Science* 108 (2): 863–869.

107 Chance, R.R. et al. (1977). Thermochromism in a polydiacetylene crystal. *Journal of Chemical Physics* 67 (8): 3616–3618.

108 Mondal, S. (2008). Phase change materials for smart textiles – an overview. *Applied Thermal Engineering* 28 (11): 1536–1550.

109 Zhang, X. (2001). Heat-storage and thermo-regulated textiles and clothing. *Smart Fibres, Fabrics and Clothing* 2001: 34–57.

110 Shen, X. and Shen, Y. (2001). Present situation and development of intelligent fiber. *China Synthetic Fiber Industry* 24 (1): 1–5.

111 He, Z., Zhang, X., and Batchelor, W. (2016). Cellulose nanofibre aerogel filter with tuneable pore structure for oil/water separation and recovery. *RSC Advances* 6 (26): 21435–21438.

112 Wen, Z. et al. (2016). Self-powered textile for wearable electronics by hybridizing fiber-shaped nanogenerators, solar cells, and supercapacitors. *Science Advances* 2 (10): e1600097.

113 Pu, X. et al. (2016). Wearable power-textiles by integrating fabric triboelectric nanogenerators and fiber-shaped dye-sensitized solar cells. *Advanced Energy Materials* 6 (20): 1601048.

114 Pu, X. et al. (2016). Wearable self-charging power textile based on flexible yarn supercapacitors and fabric nanogenerators. *Advanced Materials* 28 (1): 98–105.

115 Stoychev, G., Puretskiy, N., and Ionov, L. (2011). Self-folding all-polymer thermoresponsive microcapsules. *Soft Matter* 7 (7): 3277–3279.

116 Xu, C. et al. (2004). In vitro study of human vascular endothelial cell function on materials with various surface roughness. *Journal of Biomedical Materials Research Part A* 71 (1): 154–161.

117 Yang, F. et al. (2005). Electrospinning of nano/micro scale poly(L-lactic acid) aligned fibers and their potential in neural tissue engineering. *Biomaterials* 26 (15): 2603–2610.

118 Yoshimoto, H. et al. (2003). A biodegradable nanofiber scaffold by electrospinning and its potential for bone tissue engineering. *Biomaterials* 24 (12): 2077–2082.

119 Hu, Y. et al. (2002). Fabrication of poly(α-hydroxy acid) foam scaffolds using multiple solvent systems. *Journal of Biomedical Materials Research* 59 (3): 563–572.

120 Hua, Z. (2007). The preparation of intelligent fiber and its application in biomedicine domanial. *New Chemical Materials* 9: 015.

121 Liu, X. et al. (2014). Surface tailoring of nanoparticles via mixed-charge monolayers and their biomedical applications. *Small* 10 (21): 4230–4242.

122 Kuang, Q. et al. (2007). High-sensitivity humidity sensor based on a single SnO_2 nanowire. *Journal of the American Chemical Society* 129 (19): 6070–6071.

123 Zhang, Y. et al. (2005). Zinc oxide nanorod and nanowire for humidity sensor. *Applied Surface Science* 242 (1–2): 212–217.

124 Wu, R.J. et al. (2006). Composite of TiO_2 nanowires and Nafion as humidity sensor material. *Sensors and Actuators B: Chemical* 115 (1): 198–204.

125 Chen, X. et al. (2010). 1.6 V nanogenerator for mechanical energy harvesting using PZT nanofibers. *Nano Letters* 10 (6): 2133–2137.

126 Wang, Z.L. (2007). The new field of nanopiezotronics. *Materials Today* 10 (5): 20–28.

127 Yang, R. et al. (2009). Converting biomechanical energy into electricity by a muscle-movement-driven nanogenerator. *Nano Letters* 9 (3): 1201–1205.

15

Optical Fibers

Hiroaki Ishizawa

Shinshu University, Institute for Fiber Engineering, Interdisciplinary Cluster for Cutting Edge Research, Ueda, 386-8567, Japan

15.1 Introduction

When we survey some database by using the keyword "optical material," we could find out a huge number of research articles. From the electrical and electronic engineering view point, over 50 thousands of them could be found nowadays [1]. Furthermore, in the case of "fibers" and "optical material," we could find thousands of them as well. Therefore, optical system based on fibers is now one of the most active research areas. For example, there have been published over 200 papers in the transactions of *IEEE,* which comprises over 170 journals, during this year. They are composed mainly by photonics, light wave technologies, electronics, and sensors. Their percentages are approximately 40%, 25%, 20%, and 10%, respectively. In turn, it is well known that optical fibers have been applied to the telecommunication technology and its related technologies. As the fiber-optic telecommunication industry has matured, the costs of its related devices have decreased. Based on these backgrounds, the new application technologies appeared for sensing. The initial application was the fiber-optic gyroscope, which are used on a various vehicles, airplanes, cars, and so on. After that, technologies have been developed for fiber Bragg grating (FBG) sensing method. It could detect multipoint strain along with the fiber length continuously. Therefore, FBG has been applied to remote sensing of the soundness of infrastructures [2]. Recently, it is assumed that technologies for FBG sensors have also matured in its fabrication and application, resulting in very wide diversity. For example, single-mode polymer optical fiber (POF) has been proposed for FBG-based materials end up to obtaining high sensitivity and high reflectivity sensors [3]. Multimode polymer waveguides are also an attractive technology for onboard optical interconnects, as they can be cost-effectively integrated onto standard printed circuit boards (PCBs) [4]. In the electronic field, the ultrasonic welding of POFs onto carbon fiber-reinforced polymers for advanced fiber-optic sensing is demonstrated [5]. Regarding with the optical fiber application to textiles, it is conceivable that sensing system on textile such as the "smart textiles" has been developed during these years [6].

Handbook of Fibrous Materials, First Edition. Edited by Jinlian Hu, Bipin Kumar, and Jing Lu.
© 2020 Wiley-VCH Verlag GmbH & Co. KGaA. Published 2020 by Wiley-VCH Verlag GmbH & Co. KGaA.

In this chapter, optical fiber sensing technologies as the textile material would be introduced. At first, this would glance at the manufacturing process of fiber optics. And secondly, fiber-optic sensing applications would be overviewed. Temperature measurement, oxygen concentration sensing, strain measurement, and biomedical measurement would be introduced mainly on these 20 years. And this chapter focuses the structures and properties of FBG sensor. After that sensing principles in order to detect human vital signs and their application would be introduced before having a view of the future based on the healthcare textile circumstances.

15.2 Fundamentals of Fiber Optics

15.2.1 Fiber Optics Classification

Basic principles of optical fibers such as guided ray, guided waves, attenuation, and dispersion could be reviewed in many references [7]. Furthermore, the engineering of fiber optics has been reviewed in outstanding books [8]. This section would glance at fiber optics from the material viewpoint. It could be categorized basically into two groups by the materials, such as silica glass and plastics.

Table 15.1 shows this classification and their typical properties. Today, glass optical fibers are well known of their types and properties, since they have been applied to the telecommunication technology and its related technologies [8]. However, they are so fragile that glass fiber devices are not easy to fabricate and end up to being quite expensive. Polymeric materials permit the mass production of low-cost high-port-count photonic circuits in parallel on a planar substrate [9]. Commercially available polymer optical fibers have been emerged now as well as the active and effective manufacturing process developments. Furthermore, plastic fiber-optic applications to telecommunication or data communication are now developed worldwide.

15.2.2 Manufacturing Process

Figure 15.1 illustrates the manufacturing process of silica fiber optics. The preform rod making is the first process. In this process mainly three kinds

Table 15.1 Classification of fiber optics.

Materials	Type/index distribution	Dimensions (μm) core/cladding	Properties (band μm)
Silica glass	Multimode/step	50/125	Hard/brittle/stable
	Multimode/graded		Mode dispersion
	Single mode	8/125	Low loss (1.55)
Plastics	Core: PMMA Cladding: fluoride acrylic	Core: 500	High loss (0.6) Flexible/stable

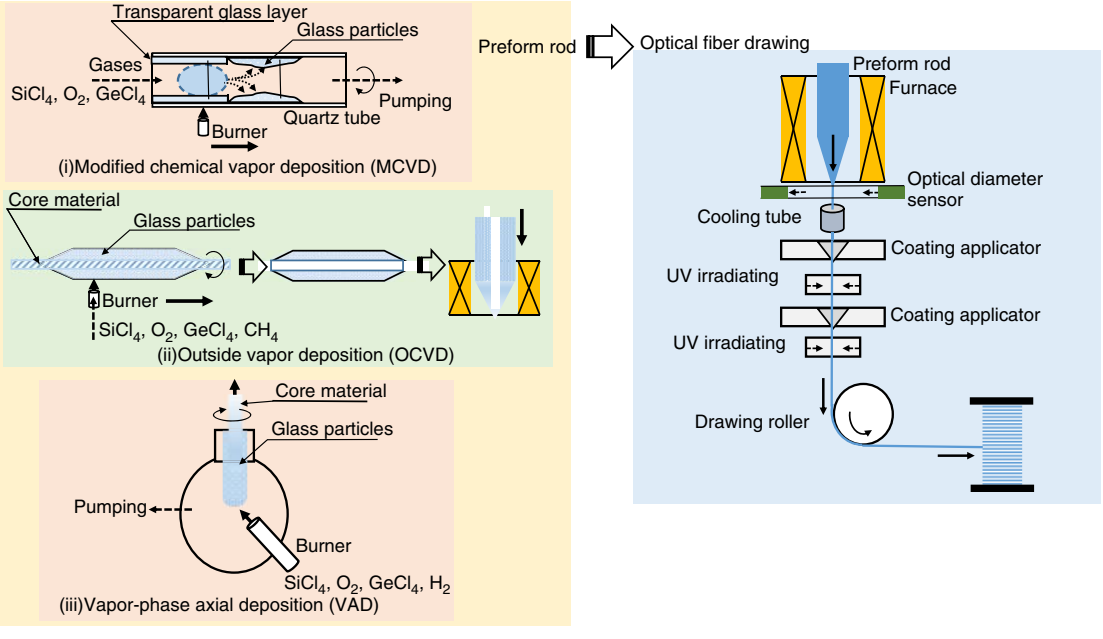


Figure 15.1 Typical fiber optics manufacturing process.

of deposition process have been developed and applied in those industries. Modified vapor deposition method (MCVD) [10], outside vapor deposition method (OVD) [11], or vapor-phase axial deposition method (VAD) [12] has been developed to make preform of glass optical fiber as in Figure 15.1. The second process is the drawing process as in right part of Figure 15.1. The preform rod is inserted into a furnace and heated over 2100 °C. This process is controlled by the diameter of fiber (125 μm), the cleanliness of the atmosphere (100 class), temperature, and rotation speed of the roller. The drawing speed depends on the conditions above mentioned, which is around 10–100 km/h.

15.2.3 General Characteristics of Fiber Optics

The compositions of silica glass remained chemically stable for a long time. Therefore, silica glass optical fiber has the same stability as the glass basically. Highly pure silica is characterized by extremely low optical loss. In most commercially available silica fibers, the optical intensity loss is about 0.2 dB/km. The intrinsic strength of glass is about 1.5×10^5 kg/cm^2, so that a typical glass fiber optics of diameter 125 μm can support a load of 18 kg. Broken off probability of a typical silica glass fiber optics is low enough that it keeps the reliability at 1% strain. It is well known that silica glass optical fiber has such robustness against electromagnetic field, since its dielectric constant is low.

POF are fibers made from polymethyl methacrylate (PMMA), polystyrene, polycarbonates, and fluorinated polymers. Optical losses in the fibers are higher than silica glass, with 100–500 dB/km. The losses are due to such factors as Rayleigh scattering and intrinsic absorption of the material itself and of the impurities [8]. POFs are generally environmental stable, and some of them are thermally stable [9].

15.3 Optical Fiber Sensor

15.3.1 Advantages of Optical Fiber Sensors

Fiber-optic sensors have shown a growth since the 1970s. Recently, they have been studied so actively, because they have various merits, which could never expected by using the electrical sensors. These have the outstanding properties of silica glass. Furthermore, their application is now on the practical phase. Generally, fiber-optic sensors have such advantages as follows;

(1) Compact lightweight
(2) No need to electrical energy supply
(3) Robust against electromagnetic noises
(4) Signal transmittable for length of kilometers
(5) Stable and high environmental durability

This section overviews the properties of fiber sensors.

15.3.2 Principles and Applications of Optical Fiber Sensors

15.3.2.1 Temperature Measurement

Fiber-optic fluorescence thermometer has been proposed by Aizawa et al. [13, 14]. Temperature dependence of emission spectra from both Tb : SiO_2 and Tb : YAG sensor head was studied for the fiber-optic thermometer application. They proposed fiber-optic thermometer equipment using Tb-doped phosphor sensor head connected with silica fiber. They found out that Tb : SiO_2 glass is suitable sensor head for an intensity-based fiber-optic thermometer at the temperature range from 300 to 1200 K. Until now, the design and development of a plastic optical fiber temperature sensor is recently proposed by Wildner and Drummer [15]. In their study, the design and development of POF temperature sensor is presented. By combining two different thermo-optic coefficients a transparent oil or polymer and glass particles, a temperature-dependent transmission can be achieved. FBG has been also applied to the temperature sensing by using metal coating FBG [16]. By the continuous chemical electroplating process of nickel layer, the temperature sensitivity of FBG sensor could be enhanced. It could be used as a temperature sensor from 0 to 300 °C.

15.3.2.2 Oxygen Concentration Measurement

Oxygen measurement could be propose by using fiber-optic fluorosensor [17]. Toba and coworkers fabricated luminous probe by using solvent green 5 as the fluorescence material. The construction of the measurement system was similar with one of temperature measurements by Aizawa et al. [13]. Fluorescent light (514 nm) could be excited by the light of which wavelength is 468 nm. Fluorescent light intensity decreases according to the concentration of oxygen. They found out that it could measure oxygen concentration from 5% to 50% in vapor and from 1 to 10 ppm in liquid. Furthermore, they also found out that a linear relation exists in vitro between oxygen concentration and optical intensity in human blood, and the fluorosensor probe could be used for in vivo measurement of oxygen partial pressure in blood.

15.3.2.3 Strain Measurement by Brillouin Optical Time Domain Reflectometry (B-OTDR) and Fiber Bragg Grating Sensors (FBG)

Table 15.2 compares Brillouin optical time domain reflectometry (B-OTDR) and FBG sensor as the strain sensor. In the case of a strain measurement by B-OTDR method, it is possible to use a commercial-based optical fibers without any additional processing to the fibers. Furthermore, it could detect the strain distribution through a long distance by detecting the Brillouin scattering in the optical fiber core. Therefore, B-OTDR has been applied to measure and monitor the strains of the large infrastructures such as railroads, bridges, and so on [18]. However, the spatial resolution of B-OTDR is several tens of centimeters long. And it is difficult to detect the spatial dynamic measurement because it is time-consuming method. As a result, it is not adequate to apply B-OTDR method to detect the human-caused strain, such as pulse wave, or chest movement.

On the other hand, FBG sensors have the grating in its core along with long axis direction as was shown in Table 15.2. This grating functions as the strain sensor.

Table 15.2 Comparison of FBG and B-OTDR as a strain sensor.

	FBG	B-OTDR
Spatial resolution	<10 mm	~1 m
Sampling period	100 ns–100 ms	~Minutes
Sensor element	Grating	Optical fiber
Advantage	Real-time measurement High wavelength precision	Low cost
Demerits	Finite measuring points	Low spatial resolution
Application	Dynamic or static analysis	Wide area measurement

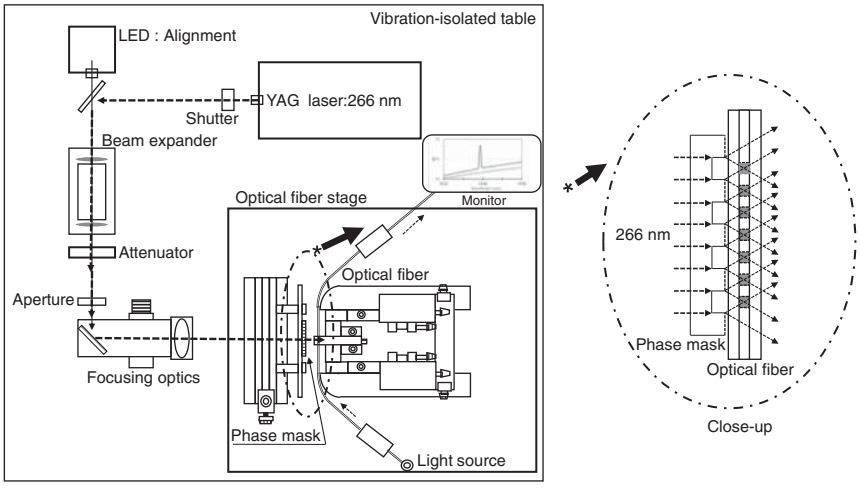


Figure 15.2 FBG making apparatus by using YAG 4th harmonic (266 nm).

As a result, FBG has gotten a very small spatial resolution as small as 10 mm or less [19].

Figure 15.2 introduces the outlook of FBG making apparatus based on phase-mask method equipped at author's laboratory in Institute for Fiber Engineering, Interdisciplinary Cluster for Cutting Edge Research, Shinshu University. Laser light (Spectra-Physics, Model HIPPO prime 266-2, 2W) is used as the drawing light source for grating formation in the fiber core. The wavelength is 266 nm that is the fourth harmonic of YAG laser. Optical fiber stage is made of low thermal expansion cast iron. It also has a set of monitoring optics to confirm the constant distance between optical fiber and phase mask. It also checks the power of laser beam by a laser power meter and monitors the grating formation process by a spectrum analyzer. This figure shows the close-up of phase mask and optical fiber. Diffraction pattern from the phase mask makes the periodic variation of optical index in the core of the optical fiber. This part works as the grating of the FBG sensor. The Bragg wavelength can be selected by

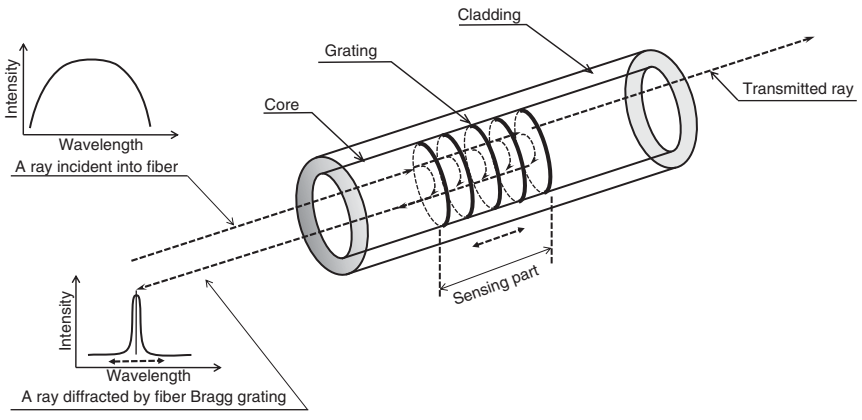


Figure 15.3 Geometry and Bragg wave diffraction of FBG sensor.

setting the optimal phase mask. It takes several minutes to make one grating in a single-mode silica optical fiber.

Figure 15.3 shows the construction and the strain detection principle of a typical FBG sensor. FBG is a sort of optical fiber that reflects the specified light wave. It is called Bragg wavelength, and it shifts according to the grating period of FBG. If some pressure changes the grating period, or as the result some strain changes, the reflected Bragg wavelength of the FBG sensor on the sample surface changes. In other words, the Bragg wavelength shift is linear to the strain caused by the pressure. It is the strain measurement principle of the FBG sensor. In order to detect the wavelength shift, the rapid optical wavelength interrogator has been used [20, 21].

15.3.2.4 Biomedical Measurement

The characteristics of optical fibers abovementioned in this section are very adequate for the biomedical sensing applications. The size of typical optical fibers makes it possible to insert it into the hypodermic needles. They could offer the minimum invasive operations, or the position-sensitive monitoring.

Physical measurement such as temperature, oxygen concentration, pressure, and so on could be possible even in vivo by applying technologies in this section. Regarding with the vital sign detection, Toba et al. proposed a new vital sign by using fiber optics [22]. They had shown that pulse waves could be detected base on the reflectometry through optical fiber bundle as in Figure 15.4. And the heart rates as well as the respiratory rates could be measured simultaneously at high accuracy. It would be one of the earliest works on this issue.

Optical fiber itself has been applied to detect the respiratory monitoring by Krehel et al. [6]. Highly flexible POF reacts to applied pressure. Throughput light intensity of POFs changes in accordance with the pressure between the human torso and the wearable sensor-embedded textiles. Continuous respiratory monitoring could be possible within ± 3/min. Its ranges from 5 to 50 min^{-1}, which covers human respiratory rate in daily life [6].

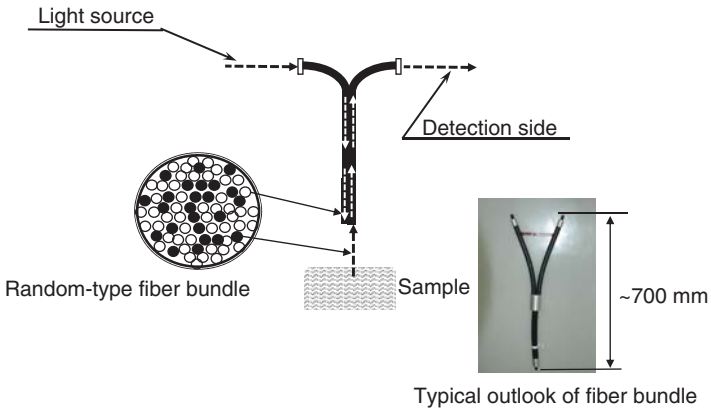


Figure 15.4 An arrangement for vital sign measurement by using fiber-optics.

15.3.3 Principles and Application of the Vital Sign Measurement by FBG Sensor

This section describes the principles of vital sign measurement by FBG sensor. FBG sensor is a fiber whose diameter is submillimeter and is flexible. These characteristics are suitable ones in order to make "a sensor on textiles" for realizing a healthcare circumstances.

15.3.3.1 FBG Sensor Interrogator to Measure Human Vital Signs

In the case of application of FBG sensor to detect human vital signs, high sensitive interrogator has to be used, because the target human pulse wave is very weak. The resultant strain is estimated as small as submicrometer. It is known that typical strain of pulse wave at wrist is sometimes less than 0.1 μm. Therefore, Mach–Zehnder interferometry is suitable [15, 23].

Table 15.3 lists the specifications of the typical interrogator (PF25-S01: Nagano Keiki, Inc.). Wideband light of which wavelength range is from 1525 to 1575 nm

Table 15.3 Specification of FBG sensor system of Mach–Zehnder interrogator.

Light source	Type	Amplified spontaneous emission
	Power	30 mW
	Wavelength range	1525–1575 nm
FBG sensor	Grating length	10 mm
	Bragg wavelength	1550 ± 0.5 nm
	Wavelength resolution	0.1 pm
	Strain resolution	0.08 μm
Optical fiber	Material	Quartz glass
	Cladding diameter	145 μm
	Core diameter	10.5 μm
Detector	Type	InGaAs PIN
	Wavelength range	900–1650 nm

from amplified spontaneous emission (ASE) is connected with the optical fiber. Through the optical circulator, light reaches to the FBG sensor and to reflecting the light of Bragg wavelength. The reflection light is interfered by a Mach–Zehnder interferometer. The optical path difference of the interferometer is set at 3.3 mm. Beam splitter makes three phase of which phase shifts were every $2\pi/3$ radian. Three phases were detected by the wavelength division multiplexing. The wavelength shift is calculated by Eq. (15.1):

$$\Delta\phi = (2\pi nd/\lambda^2)\Delta\lambda \tag{15.1}$$

where $\Delta\phi$ is the phase shift obtained, n is the optical constant of the fiber, and d is the grating period that is 500 nm in this setup. The phase resolution depends on the sampling frequency that is 10 kHz. As a result, the wavelength resolution of this measuring system is 0.1 pm as in Table 15.3, which corresponds to equivalent the resolution of strain, which is 0.08 μm [20].

15.3.3.2 Pulse Wave Measurement

In order to measure the pulse waves, FBG sensor was attached on subject's skin by a medical adhesive tape.

Figure 15.5 shows the look of typical pulse wave measurement. Subject is in supine position, and his wrist was kept as high as his heart. The radial artery exists beneath the measuring point. Sampling rate of the system setting was 10 kHz. Measurement was carried out for 20 seconds that is as long as the one cycle time of the automatic sphygmomanometer to measure the subject's blood pressure as in Figure 15.5.

Each raw pulse wave was filtered by a band-pass filter, of which passband is 0.5–5 Hz. This bandwidth covers the ordinal human heart rate. Figure 15.6 shows the typical raw signals and corresponding pulse waves filtered by band-pass filter. It is clear that FBG-detected waveforms seem to show the heartbeats.

By the comparison of typical acceleration of pulse waveform obtained by photo-plethysmograph and the waveforms measured by FBG sensor, FBG-sensed waveform resembles the acceleration of pulse waveform closely. Therefore, it is conceivable that filtered FBG-detected waves (Figure 15.6 lower) are ones of pulses of heartbeats.

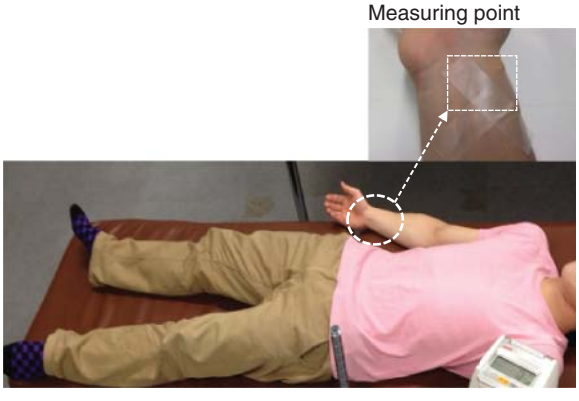


Figure 15.5 Pulse wave measurement at subject's wrist on the radial artery.

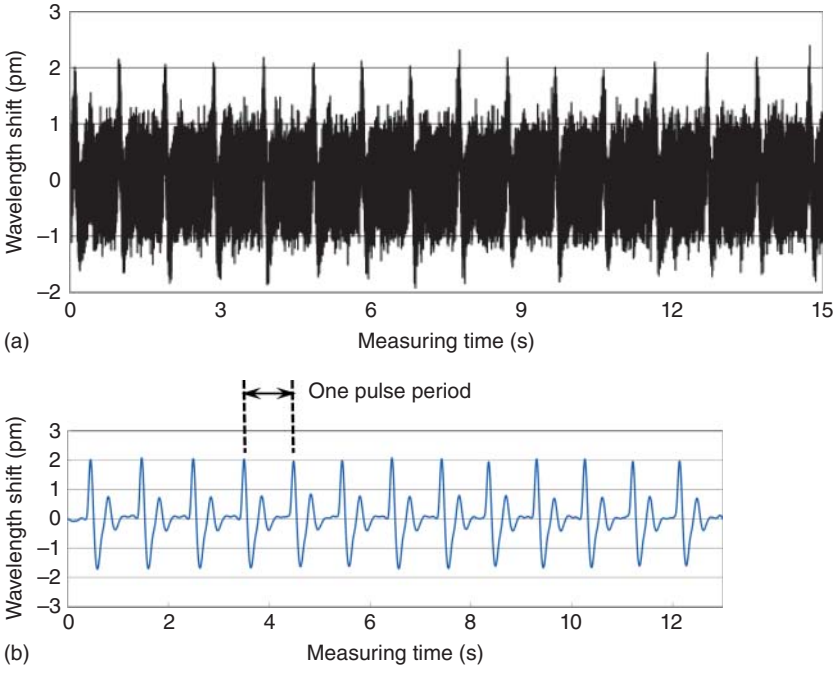


Figure 15.6 Detected raw signals of FBG (upper) and filtered waves. (a) Typical raw signal measured by FBG. (b) Corresponding waves processed by the band pass filter.

15.3.3.3 Pulse Rate Measurement

Base on the consideration above mentioned in Section 15.3.3.2, after obtaining the filtered pulse waves, mean pulse period during 20 seconds could be estimated [23]. Pulse rate per minute (beat per minute, bpm) at this measurement timing (20 seconds) could be easily obtained. Miyauchi et al. showed the typical correlation of reference values and predicted heart rates by using three subjects [23]. The correlation coefficients for subject A, B, and C are 0.83, 0.67, and 0.60, respectively. The corresponding standard errors are 3, 2, and 2 bpm, respectively [23]. Additionally, total correlation coefficient and standard error over these three subjects are 0.89 and 2 bpm. Based on these results, this method is proved to be significant ($p < 0.01$). This method takes about eight seconds to detect [23].

15.3.3.4 Respiratory Rate Measurement

Respiratory pulse (respiratory arrhythmia) is observed normally for human [24]. In breathing in, the pulse rate increases, and conversely when we breathe out, it decreases. Therefore, by monitoring the pulse waves and detecting the pulse periods simultaneously, the real-time respiratory could be easily measured.

Miyauchi et al. showed the relationship between the pulse period fluctuations and corresponding temperature fluctuations of subject's expiration breathing measured by a face mask equipped with a temperature sensor [23]. The pulse period fluctuation is synchronous with the respiration temperature fluctuation. Therefore, respiratory rate could be measured by detecting the frequency of pulse

period fluctuation [23]. They reported a typical correlation of reference values and predicted respiratory rates [23]. The correlation coefficients for subject A, B, and C are reported to be 0.99, 0.99, and 0.99, respectively. The corresponding standard errors are 0.6, 0.4, and 0.4 bpm, respectively. Additionally, overall correlation coefficient and standard error of three subjects are 0.99 and 0.5 bpm. Based on these results, this method is proved to be significant ($p < 0.01$) as well.

Miyauchi et al. also reported that the signal to noise ratio in these measurement can be estimated to be 26 dB based on the wavelength shift and its resolution. The conventional pulse measurement systems have relative error of ±5%, which corresponds ±3 bpm at 60 bpm [23].

Therefore, by attaching FBG sensor on the human skin, it was found out that pulse rate can measured accurately. In the case of respiratory measurement, it is proved to be very accurate without any individual differences. As a consequence, FBG sensor could be expected to monitor heart rates and respiratory rates simultaneously.

15.3.3.5 Blood Pressure Measurement by Pulse Transit Time Detection

The arrival time lag of pulse wave between the different places of skin is called pulse transit time (PTT). PTT could be obtained by calculating the measuring points distance to pulse wave velocity (PWV) ratio. PWV is the velocity of the pulse waves from a point to the other point through the artery. It has been expressed by Eq. (15.2) by Moens and Kortberg since 1878, assuming that the artery wall is isotropic and experiences isovolumetric change with pulse pressure [24]:

$$\mathrm{PWV} = \sqrt{\frac{E \cdot h}{2r \cdot \rho}} \tag{15.2}$$

E, h, r, and ρ are Young's modulus of the blood vessel, blood vessel wall thickness, radius of the blood vessel, and viscosity of blood, respectively. PWV is proportional to the square root of the Young's modulus. Therefore, it correlates with the blood pressure [25]. In this method, two gratings are set in one fiber as is seen in Figure 15.7 [26], so that this could measure the pulse wave at two points.

The Bragg wavelength of FBG1 and FBG2 is 1550 ± 0.5 nm and 1560 ± 0.5 nm. The length (L) between FBG1 and FBG2 is 250 mm (constant). As a result, time difference of the pulse wave (PTT) could be detected by means of this system as in Figure 15.7. As a result, if some relationship between PTT and blood pressure could be obtained, this method could be applicable to measure blood pressure without any machetes of the conventional methods.

Takagi et al. reported that by using PTT, blood pressure could be measured.

Figure 15.8 shows a typical relationship between PTT and systolic blood pressure in the experimental set of them [26]. This shows that PTT decreases according to the increase of systolic blood pressure. Takagi et al. reported that the correlation coefficients of the calibration curves obtained were around 0.70 and had high significances ($p < 0.01$) [26]. However, in this method, multipoint's measurement is inevitable. Subjects can never neglect the restraint feeling.

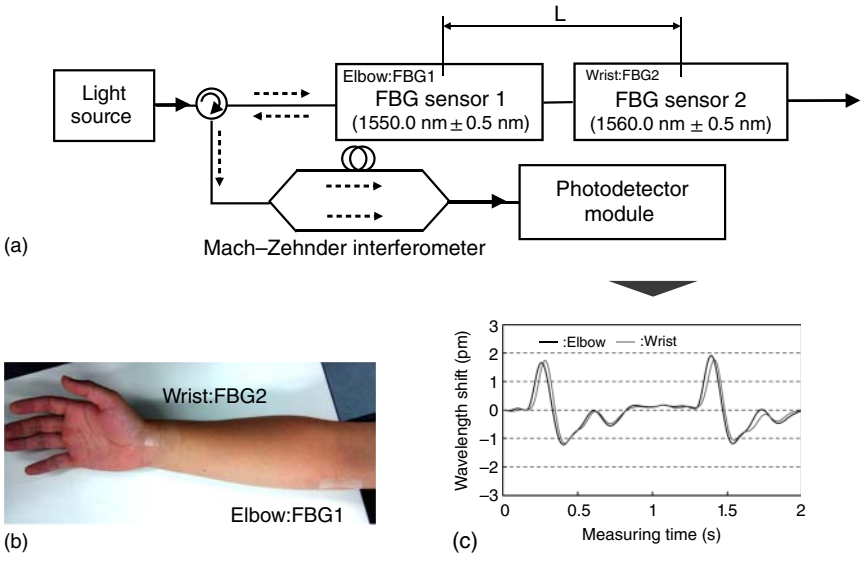


Figure 15.7 Pulse transit time measurement by FBG sensors. (a) Block diagram of PTT measurement. (b) FBG method: radial artery (L-250 mm). (c) Typical pulse waves at two points with time lag.

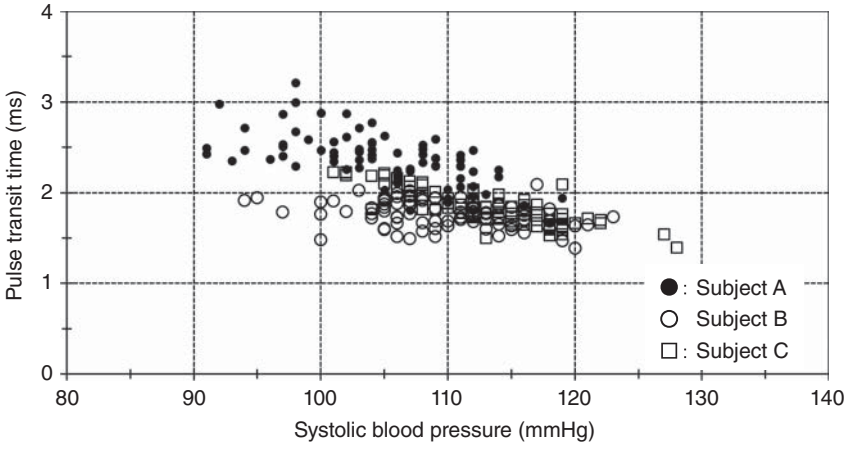


Figure 15.8 Relationship between pulse transit time and systolic blood pressure of three subject.

15.3.3.6 Partial Least Squares Regression Calibration for Blood Pressure Measurement

In order to calibrate the blood pressure level by using the pulse waves measured by FBG sensor, partial least squares regression (PLSR) could be applied to obtain the calibration curve. PLSR is a multivariate analysis that combines feature extraction by principal component analysis and multiple regression [27]. In PLSR, the elements are obtained by successive extraction of the feature values

both from the objective variables and the explanatory variables. As a result, it gives feature vectors from the explanatory variables, and variances minimize the explanatory variables for explaining the objective variables. It finds for a set of latent PLS vectors. In this case, one-point measurement by FBG sensor is enough. Therefore, if PLSR is successful, FBG sensor system would be more practical than multipoint method in Section 15.3.3.5.

Pulse waves at wrist, for example, as in Figure 15.4, could be used as the explanatory variables, and the blood pressure levels measured by the automatic sphygmomanometer were used as the objective variables. In this case pulse waves were normalized, setting the first peak value one and the first valley value zero. Principle component analysis is carried out for the pulse waves, which is a vector having 10^4 elements in the case of 10 kHz sampling frequency. And the feature vector called PLS factor was extracted successively, such as factor 1, factor 2, and so on. In this process, the objective variables (blood pressure levels) were explained by a linear combination of the latent PLS factor. The residuals of this linear combination were the new set for next extraction step until the predicted residues of the objective values reach minimum [27]. In this calibration, the cross-validation of the model is carried out by the leave-one-out method. The optimal numbers of the PLS factors were tested statistically with an adequate significant level, such as 5%. In the validation of the PLSR calibration model, pulse waves that had not used in the calibration process were used to have the predicted values of blood pressure levels [28, 29].

Figure 15.9 shows the typical PLSR calibrated results of systolic blood pressure obtained by authors. They could be easily detected by a FBG sensor on human wrist. Table 15.4 shows the typical result of PLSR calibration and validation for systolic blood pressure measurement by FBG sensor at wrist. In this case, systolic blood pressure can be measured by a PLSR calibration model that has four factors. In the calibration, the mean absolute difference is within 3 mmHg. Furthermore, in the validation, it is 4 mmHg. This model has significant number of four PLS factors as in Figure 15.9b.

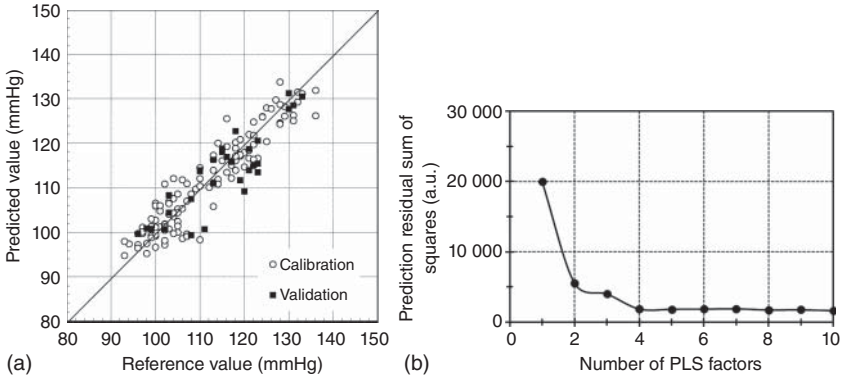


Figure 15.9 Typical PLSR model for systolic blood pressure calibration and validation. (a) PLS models for systolic blood pressure. (b) Relation between the predicted residual sum of squares and extracted PLS factors.

Table 15.4 Calibration and validation of PLS models for systolic blood pressure measurement.

Measuring point	PLS factor	Correlation coefficient	Calibration MAD (mmHg)[a)]	Validation
Wrist	4	0.93	3	4

a) MAD: mean absolute difference (IEEE 1708).

Once the PLSR calibration model is obtained, it is possible to measure systolic blood pressure only by detecting pulse wave. Katsuragawa and Ishizawa presented that it can measure not only systolic blood pressure but also diastolic blood pressure [28]. They also presented that by using FBG sensor, blood pressure could be measured continuously and noninvasively. S. Koyama et al. have shown that the influence of the individual differences on the calculated blood pressure model by using FBG sensor method was very low. Therefore, this measurement method has been found to be suitable for use by many people [29].

15.4 Healthcare Monitoring by Using FBG Sensor

Multi-vital sign measurement is possible by using FBG sensor. This section introduces experimental results of vital sign measurement by using subjects. This section also views the multi-vital sign smart textiles for healthcare monitoring system.

15.4.1 FBG Sensor Application to Multi-vital Sign Measurement

Pulse rate, respiratory rate, and systolic blood pressure could be measured simultaneously by using FBG sensor. Until now, it is well known that a single function measuring system has been proposed and used for monitoring each vital sign such as pulse rate, respiratory rate, and blood pressure. Recently, POFs have applied to respiratory rate detection based on the optical intensity measurement on human torso [6]. However, FBG sensing system could measure multiple vital signs at the same time. FBG is highly flexible and reacts to the pressure waves in the blood vessel caused by the heartbeat.

On the other hand, it has been suggested by the authors that pulse wave contains the information of the blood contents such as blood glucose concentration [30, 31]. The pulse wave depends on the viscoelasticity of blood vessel as in Eq. (15.2). So, it seems to be possible to detect arteriosclerosis base on the pulse wave pattern [29].

The pulse wave intervals synchronize with the R-R intervals of electrocardiogram. Based on this discovery, pulse waves measured by FBG sensor could show the state variables of human psychological stress [32].

As mentioned in Section 15.3.2.1, FBG could be used as a temperature sensor from 0 to 300 °C [16]. It means that it also could measure body temperatures.

Therefore, FBG sensor could offer most practical healthcare monitoring smart textiles that inform users their vital signs such as body temperature, heart rate, respiratory rate, blood pressure, blood glucose levels, and/or level of psychological stress.

15.4.2 Fabrication of Smart Textiles

One of the next tasks should be introducing the FBG sensor on textiles. From the practical point of view, wearable textiles with embedded sensors are the main problem. One of the most important projects is EU FP6 project OFSETH [33]. In this project, medical textiles with embedded FBG sensors have been proposed for monitoring respiratory movement [34]. By this development, non-intrusive system for continuous measurement of abdominal and thoracic respiratory movement was proposed. In this system FBG was applied. They wrote the gratings in a silica optical fiber and stitched it on an elastic fabrics for measurement of thoracic respiratory movement. As a result, the system on textiles enables the continuous measurement of respiratory movement.

In order to embed FBG sensor on textiles, covering FBG by silk yarns has been developed by Sakaguchi et al. [35, 36] Silica optical fiber is not suitable to embed directly. They covered optical fiber by silk yarn, of which diameter was approximately 200 μm. The covering was carried out by a braiding machine. This method and covered optical fiber are illustrated in Figure 15.10. Based on this technology, FBG sensor could be easily embedded on knitted fabrics. Figure 15.11 shows the knitted fabrics embedded covered FBG sensor [35]. The covered FBG was implemented halfway round of tubular knitted fabrics. It is easily implemented by a connection of covered FBG every nine wales. Base on this breakthrough, there is some possibility of realizing wearable healthcare smart textiles [37].

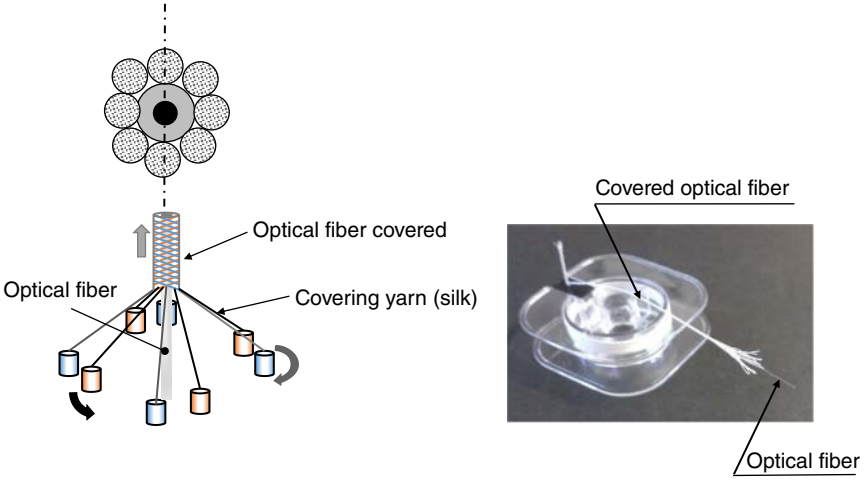


Figure 15.10 Covering method (braiding) and look of covered optical fiber(right).

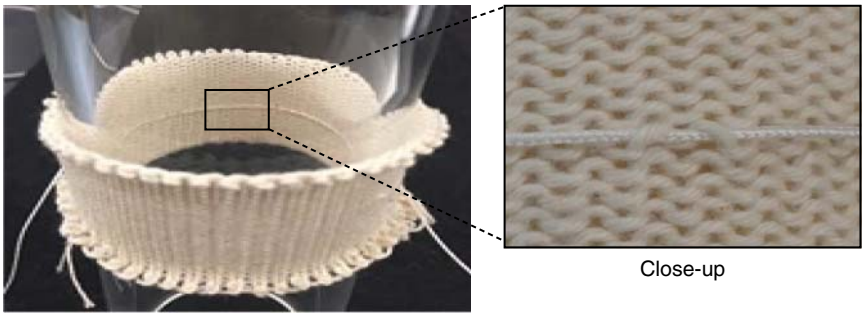


Figure 15.11 Covered FBG embedded knitted fabric.

15.5 Future Trends: As the Summary

Javier Andreu-Perez et al. categorized the evolution of health monitoring application of wearable system [38]. According to them, in the first generation, "a single sensing modality with wireless connectivity" had been realized. After that, "continuous monitoring with multiple sensors" has been proposed in the second generation. In the final generation until now, "combining continuous health monitoring with other sources of medical knowledge" has been studied. Healthcare monitoring devices are tending to smart implants from wearable sensors on these 10 years. FBG sensor applications to health monitoring are now in the second generation. As aforementioned, FBG can measure almost all the vital signs continuously. Therefore, FBG and its embedded smart textiles aim to combine with other sources of medical knowledge. It also should integrate the information technologies. Furthermore, FBG sensor could work as the nervous system for controlling the human states. FBG sensor could be implanted, because it does not change in quality in vivo. Also, it could be some practical wearable devices such as fabrics, caps, glasses, pillows, and beds as for monitoring and communicating the health indicators.

Figure 15.12 proposes the applications of FBG sensor-embedded smart textiles to health monitoring and the development of FBG sensor system on textiles in order to summarize this chapter. In the personal healthcare information space, smart sensors on textiles would play the most important role and meet the human needs all over the world. FBG sensor would be one of the successful solutions, because it is a flexible, easy to embed, stable, and robust material.

In this chapter, the author has focused on the newly developed applications of FBG sensor to human vital sign sensing. It is needless to say that optical fibers and/or optical fiber sensors have a great potential. Many outstanding reviews have been published as the author mentioned above [7, 8]. The author does not have enough experience or academic standing to describe the whole potential of fiber optics. Fiber-optic communication system would get the highest speed and largest capacity according to optical fiber progresses [39]. In relation to the instrumentation and measurement, POFs and/or silica glass optical fiber would play an

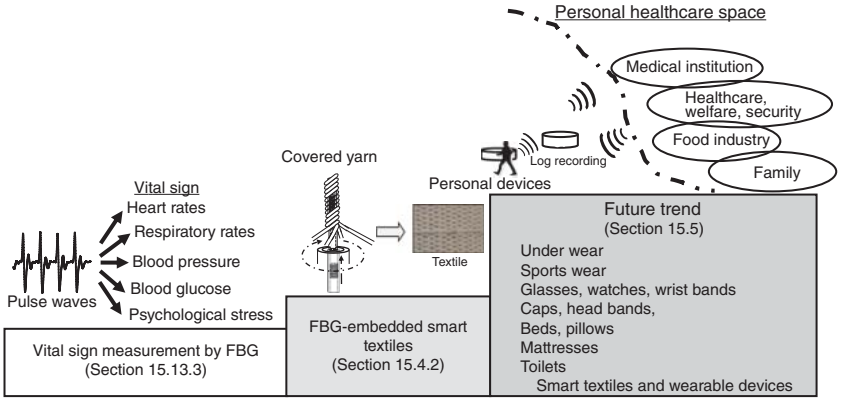


Figure 15.12 Development of smart textiles embedded FBG sensor.

important role in the process control, health monitoring of the infrastructures, and other industrial sensing systems. These should be ceded to the author of qualified somewhere. Finally, this chapter would wrap up to describing that FBG sensor and its system could curve out future of humankinds, since it could not only sense our health condition but also contribute to medical care environment.

Fiber Bragg Grating sensing (FGB) application developments to human vital sign sensing in this chapter are supported by JSPS KAKENHI Grant 16H01805 that is ongoing from 2016 to 2020.

These research results in this chapter are partially supported by the creation of a development platform for implantable/wearable medical devices by a novel physiological data integration system of the Program on Open Innovation Platform with Enterprises, Research Institute and Academia (OPERA) from the Japan Science, and Technology Agency (JST).

References

1 For example, IEEE Xplore®, Digital Library. http://ieeexplore.ieee.org/Xplore/cookiedetectresponse.jsp (accessed 16 October 2016).
2 Yau, M.H., Chan, T.H.T., Thambiratnam, D.P., and Tam, H.Y. (2013). Static vertical displacement measurement of bridges using fiber Bragg grating (FBG) sensors. *Special Issues of Advances in Structural Engineering* 16 (1): 165–176.
3 Bhowmik, K., Peng, G.D., Luo, Y. et al. (2016). Etching process related changes and effects on solid–core single-mode polymer optical fiber grating. *IEEE Photonics Journal* 8 (1): 1–9.
4 Liu, W., Romeira, B., Li, M. et al. (2016). A wavelength tunable optical buffer based on self-pulsation in an active microring resonator. *Journal of Lightwave Technology* 34 (14): 3466–3472.
5 Shimada, S., Tanaka, H., Hasebe, K. et al. (2016). Ultrasonic welding of polymer optical fibres onto composite materials. *Electronics Letters* 52 (17): 1474–1474.

6 Krehel, M., Schmid, M., Rossi, R.M. et al. (2014). An optical fibre-based sensor for respiratory monitoring. *Sensors* 2014 (14): 13088–13101.

7 For example, Kao, C. and John Russel, P.S. (2009). *Fiber Optics, Fundamentals of Photonics*, Chapter 9, 2e (eds. B.E.A. Saleh and M.C. Teich), 325–364. Wiley.

8 For example, Thyagarajan, K. and Ghatak, A. (2007). *Fiber Optic Essentials*. Wiley.

9 Eldada, L. and Shacklette, L.W. (2000). Advances in polymer integrated optics. *IEEE Journal of Selected Topics in Quantum Electronics* 6 (1): 54–67.

10 Reed, W.A., Yan, M.F., and Schnitzer, M.J. (2002). Gradient-index fiber-optic microprobes for minimally invasive in vivo low-coherence interferometry. *Optics Letters* 27 (20): 1794–1796.

11 For example, Blankenship, M. and Deneka, C. (1982). The outside vapor deposition method of fabricating optical waveguide fibers. *IEEE Journal of Quantum Electronics* 18 (10): 1418–1423.

12 For example, Takahashi, H. and Sugimoto, I. (1983). Preparation of germanate glass by vapor-phase axial deposition.

13 Aizawa, H., Takei, K., Katsumata, T. et al. (2005). Development of erbium-doped silica sensor probe for fiber-optic fluorescence thermometer. *Review of Scientific Instruments* 76: 094902.

14 Aizawa, H., Takei, K., Katsumata, T. et al. (2006). Fluorescence thermometer based on the photoluminescence intensity ratio in Tb doped phosphor materials. *Sensors and Actuators A: Physical* 126: 78–82.

15 Wildner, W. and Drummer, D. (2016). A fiber optic temperature sensor based on the combination of two materials with different thermo-optic coefficients. *IEEE Sensors Journal* 16 (3): 688–692.

16 Li, Y., Hua, Z., Yan, F., and Gang, P. (2009). Metal coating fiber Bragg grating and the temperature sensing after metallization. *Optical Fiber Technology* 15: 391–397.

17 Toba, E., Kazama, J., Tanaka, H. et al. (2000). Fiber optical fluorosensor for oxygen measurement. *IEICE Transactions on Electronics* E83-C (3): 366–370.

18 Izumita, H., Sato, T., Tateda, M., and Koyamada, Y. (1996). Brillouin OTDR employing optical frequency shifter using side-band generation technique with high-speed LN phase-modulator. *IEEE Photonics Technology Letters* 8 (12): 1674–1676.

19 Li, K., Yau, M.H., Chan, T. et al. (2013). Fiber Bragg grating strain modulation based on nonlinear string transverse force amplifier. *Optics Letters* 38: 311–313.

20 Sano, Y. and Yoshino, T. (2003). Fast optical wavelength interrogator employing arrayed waveguide grating for distributed fiber Bragg grating sensors. *Journal of Lightwave Technology* 21 (1): 132–139.

21 Todd, M.D., Johnson, G.A., and Chang, C.C. (1999). Passive, light intensity-independent interferometric method for fiber Bragg grating interrogation. *Electron Letters* 35 (22): 1970–1971.

22 Toba, E., Shimada, T., Kamoto, T. et al. (2000). Development of vital sign sensor by using fiber-optics. *Journal of Robotics and Mechatronics* 12 (3): 286–291.

23 Miyauchi, Y., Ishizawa, H., and Niimura, M. (2013). Measurement of pulse rate and respiration rate using Fiber Bragg grating sensor. *Transactions of SICE* 49 (12): 1101–1105.

24 de Boer, R.W., Karmaker, J.M., and Strackee, J. (1985). Relationship between short-term blood-pressure fluctuations and heart-rate variability in resting subjects II. *Medical and Biological Engineering and Computing* 23 (4): 359–364.

25 Scisence Pressure Technical Note. Pulse wave velocity (PWV) basics. http://www.transonic.com/resources/research/pulse-wave-velocity/. (Accessed 11 March 2017).

26 Takagi, T., Ishizawa, H., Koyama, S., and Niimura, M. (2015). Fundamental study on blood pressure measurement by FBG sensor. *Transaction of SICE* 51 (4): 274–279.

27 Martens, H. and Neas, T. (1993). *Partial Least Squares Regression (PLSR), in Multivariate Calibration*, 116–125. Wiley.

28 Katsuragawa, Y. and Ishizawa, H. (2015). Non-invasive blood pressure measurement by pulse wave analysis using FBG sensor. In: *Proceedings IEEE IIMTC 2015* (11–14 May 2015), 511–515.

29 Koyama, S., Ishizawa, H., Fujimoto, K. et al. (2017). Influence of individual differences on the calculation method for FBG-type blood pressure sensors. *Sensors* 2017 (17): 48. https://doi.org/10.3390/s17010048.

30 Ishizawa, H. and Koyama, S. (2016). Non-invasive blood glucose level measurement method and non-invasive blood glucose level measurement device. Japanese patent pending No. N15067, USA Patent Pending 15/544,677, EU Patent Pending 16 764 625.6. Chinese Patent Pending 201680006291.2, Korean Patent Pending 10-2017-7023639.

31 Kurasawa, S., Koyama, S., Ishizawa, H. et al. (2017). Verification of non-invasive blood glucose measurement method based on pulse wave signal detected by FBG sensor system. *MDPI-Sensors* 17: 2702. https://doi.org/10.3390/s17122702.

32 Koyama, S., Ishizawa, H., Hosoya, S. et al. (2017). Stress loading detection method using the FBG sensor for smart textile. *Journal of Fiber Science and Technology* 73 (11): 276–283.

33 European Commission Six framework programe 2002–2006. https://ec.europa.eu/research/fp6/index_en.cfm. (Accessed 17 March 2017).

34 Witt, J., Narbonneau, F., Schukar, M. et al. (2012). Medical textile with embedded fiber optic sensors for monitoring of respiratory movement. *IEEE Sensors Journal* 12 (1): 246–254.

35 Sakaguchi, A. and Kato, M. Japanese Patent Pending No. P151033.

36 Sakaguchi, A., Kato, M., Ishizawa, H. et al. (2016). Optical fiber embedded knitted fabrics for smart textiles. *Journal of Textile Engineering* 62 (6): 129–134.

37 Koyama, S., Sakaguchi, A., Ishizawa, H. et al. (2017). Vital sign measurement using covered FBG sensor embedded into knitted fabric for smart textile. *Journal of Fiber Science and Technology* 73 (11): 300–308.
38 Andreu-Perez, J. et al. (2015). From wearable sensors to smart implants–toward pervasive and personalized healthcare. *IEEE Transactions on Biomedical Engineering* 62 (12): 2750–2762.
39 Thyagarajan, K. and Ghatak, A. (2007). *Fiber Optic Essentials*, Chapter 8, 100–124. Wiley.

16

Memory Fibers

Harishkumar Narayana[1], Jinlian Hu[1], and Bipin Kumar[2]

[1] The Hong Kong Polytechnic University, Institute of Textiles and Clothing, R403 Hung Hom, Kowloon, Hong Kong, China
[2] Indian Institute of Technology Delhi, Department of Textile and Fibre Engineering, TX135, Hauz Khas, New Delhi 110016, India

16.1 Introduction

Fibers are fine substances with a high ratio of length to its thickness. The heritage of fibers is quite long, and they have traditionally been used in vivid cultures on Earth to meet the fundamental requirements of clothing and utilitarian products such as fishing nets and ropes. In general, fibers are obtained from natural resources, regenerated or man-made. Shape memory polymers (SMPs) are exciting class of smart materials and have been considered as an important milestone in the revolutionary path toward impactful transformation from active to smart era. SMPs have been gained a significant research interest from both academic and industries due to their fascinating behaviors leading profound applications in multidisciplinary arenas to mankind over the past few decades [1–4]. The word "shape memory" was first proposed by Vernon in the year 1941 [5]. SMPs comes under the shape memory materials (SMMs) including shape memory alloys (SMAs) and shape memory ceramics (SMCs). SMPs can undergo a significant macroscopic deformation or a temporary shape and recover spontaneously to its original conformation upon an external heat stimulus such as heat, light, solvent, water, and magnetic field [2, 6–8]. SMPs are not only able to store the shapes, but also other physical parameters could be stored and retrieved reversibly such as stress (stress memory) [9], temperature (temperature memory) [10], chrome (chromic memory) [11], and electricity (electric memory) [12]. Hence this polymeric system could also be termed as memory polymers (MPs). MPs are composed of thermodynamically immiscible fixed (hard) and reversible (soft) segments. The transition temperature of these polymers is very critical and can be tailor-made to deploy them into suitable applications. Transition is the temperature range in which a significant change of modulus and shape could occur caused by temperature change. There are two types of transition states in MPs, and they are glassy (T_g) and melting (T_m) transition type. This critical temperature range can be fine-tuned to custom needs by controlling the two phases in

Handbook of Fibrous Materials, First Edition. Edited by Jinlian Hu, Bipin Kumar, and Jing Lu.
© 2020 Wiley-VCH Verlag GmbH & Co. KGaA. Published 2020 by Wiley-VCH Verlag GmbH & Co. KGaA.

a heterogeneous structure. MPs have been developed for numerous applications such as aerospace, construction, transportation, textiles, and biomedical [2, 3].

Memory polyurethanes can be synthesized practically via bulk or solution polymerization technique. In general, MPs can be processed and utilized into several applications via different forms such as fibers, films, coating solution, gels, and foams. MPs could be spun into fibrous structure via almost all spinning methods such as melt spinning, dry spinning, wet spinning, reaction spinning, and electrospinning [13]. MPs can be easily spun into macro-, micro-, and nanofibers via aforementioned spinning methods. The mechanical and thermal properties of MP fibers can be controlled or tailor-made via controlled synthesis, chemical composition, and ratio between soft and hard segments. In addition, shape memory behavior, mechanical, thermomechanical, and thermal properties, can be further enhanced by post-spinning operations such as heat setting and drawing process. MP fibers could possess other unique behaviors apart from shape memory characteristics such as stress memory phenomenon, which is recently discovered by Hu et al. in a semicrystalline polyurethane material [9]. In this chapter, fundamentals of MPs, processing of fibers, effect of chemical composition and post-spinning operations, stress memory behavior, and their implications in medical compression and textiles are broadly discussed. The organization of contents is to let the reader comprehend the background and impactful potentials of MP fibrous materials. Fibers could be scientifically applied into multidisciplinary areas such as artificial muscles, tissue engineering, pressure or massage garments, drug-controlled release, and energy storage devices.

16.2 Morphology and Molecular Mechanism of Memory Polymers

MPs are stimulus-responsive materials that can be easily deformed above the T_{trans} (transition temperature) and fixed to a temporary shape upon cooling below the T_{trans}. This temporary shape can be spontaneously recovered back to the original conformation by reheating above the T_{trans}. This effect is generally denoted as shape memory effect (SME). The thermomechanical properties such as shape fixity and shape recovery can be easily tailored by blending MP using different types of fillers. The notable advantage of MPs is their switching, or transition temperature can be fine-tuned to a wide range from −20 to +150 °C, and they are responsive to multiple stimulus. They possess very good chemical stability, biodegradability, and biocompatibility. MPs are inherently sensitive to ambient temperature and do respond within a narrow range of temperature as shown in Figure 16.1a.

An overall 3D architecture of MPs was proposed by Hu and coworkers based on the molecular mechanisms, and it is shown in Figure 16.1b. The SME in MPs is basically induced by the conformational changes that occur in polymeric molecular chains and segmental bonds [14, 15]. Herein, Figure 16.1b shows switch and netpoint that basically represent the soft (reversible phase) and hard (fixed phase) segments. The entropic elasticity of molecular chains enables the shape recovery in the soft segment switch, whereas netpoint decides the overall structural integrity and permanent shape of MPs during the thermomechanical

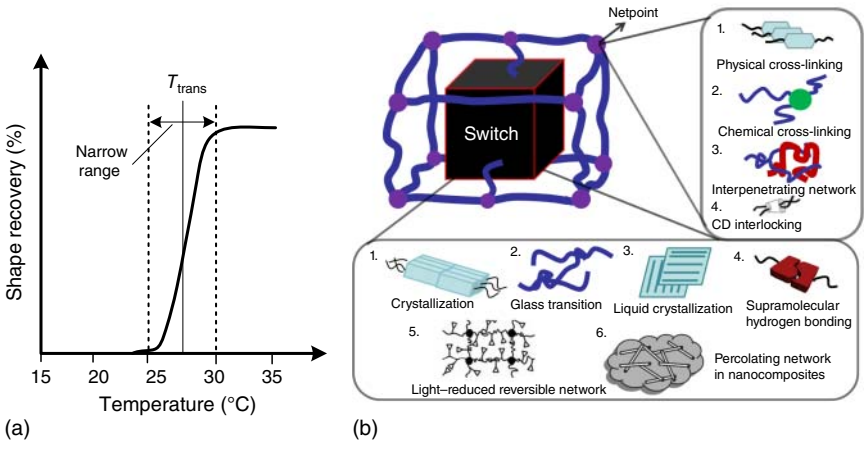


Figure 16.1 Molecular structure and mechanism of MPs. (a) Responsiveness trend of MPs in an ambient temperature; (b) the overall 3D architecture of MPs.

deformation. Netpoint or hard segments connect with molecular chains via cross-linkage such as physical, chemical, interpenetrating, or interlocked supramolecular network. The type of transition in MPs and controlling SME is decided by the soft segment switch, and it could be of amorphous, crystalline, liquid crystalline, supramolecular hydrogen bonding, light-reversible network, and percolating nanocomposite whiskers [2].

16.2.1 Nature of Transitions in MPs

As mentioned in the previous section, polyurethane-based MPs are segmental type, and the nature of the soft or reversible phase decides the transition type. A temperature range where a significant change occurs in the modulus and shape is known as transition, and this could be either a glass (T_g) or melting type (T_m) for the reversible phase. If molecular chains in the soft segment is semicrystalline type, the T_{trans} is T_m, and if it is amorphous, the T_{trans} is T_g type [15–17]. If the transition is T_m type, crystallites melt during heating with deformation and further lead to strain-induced crystallization [18] upon cooling below the T_m range. The presence of crystallites in the molecular network below the $T_{\text{trans}} = T_m$ prevents the shape recovery until it is reheated above T_m [16]. Tobushi et al. [19] and Takahashi et al. [20] mentioned that the micro-brown motions of the molecular chains will be set into glassy region and frozen when the MP is cooled below $T_{\text{trans}} = T_g$. The network will be in nonequilibrium state until it is reheated above $T_{\text{trans}} = T_g$ to activate the micro-brown motions. The transition type of MPs decides by the compositions of hard and soft segments [1, 21–30].

16.3 Evaluation of Shape Memory Properties

Before the discussion of memory fibers, the reader should know the evaluation of shape memory properties by thermomechanical cyclic testing [15, 16, 19, 31].

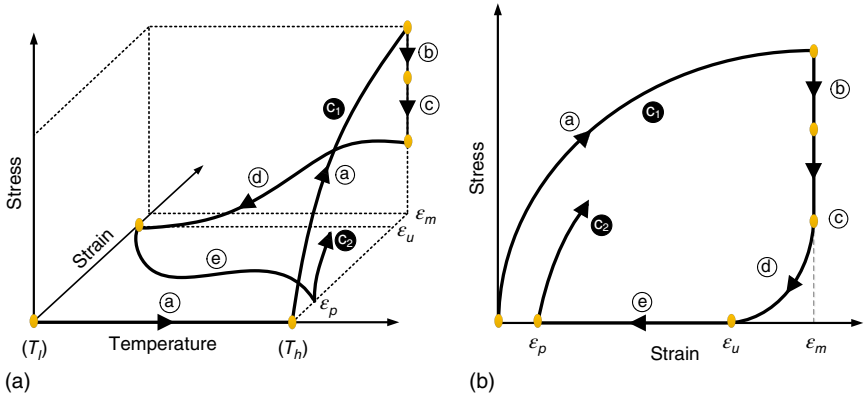


Figure 16.2 Scheme of thermomechanical cyclic test. (a) Plot of stress with strain and temperature. (b) Typical curve of stress vs strain. (T_l), low temperature ($T < T_{trans}$); (T_h), high temperature; (ε_p), plastic strain; (ε_u), fixed strain; (ε_m), programming strain; ($\varepsilon_m - \varepsilon_u$), elastic strain; $\varepsilon_r = (\varepsilon_m - \varepsilon_p)$.

So that this would assist in comprehending the further sections easily, Figure 16.2 shows the detailed steps involved in a typical thermomechanical cyclic test, and this helps to determine the shape fixity and shape recovery properties. Description for the steps are as follows:

Step a: Heating the specimen above the T_{trans} under zero strain condition and programming to a desired strain level (ε_m) under constant strain rate (e.g. 10 mm/min) at elevated temperature.

Step b: Holding the specimen under same temperature and constant strain for about 10 minutes.

Steps c and d: Cooling ($T < T_{trans}$) and unloading the specimen under a constant rate to a strain level ε_u (ε_u can be achieved due to presence of elastic strain and hinders the complete shape fixation).

Step e: Heating ($T > T_{trans}$) to achieve the shape recovery and to release the stored strain to ε_p.

Step C_2: Repeating another cycle from steps a to e.

Shape fixity and recovery ratios are calculated from Eqs. (16.1) and (16.2).

$$\% \text{ Shape fixity} = \frac{\varepsilon_u}{\varepsilon_m} \times 100 \tag{16.1}$$

$$\% \text{ Shape recovery} = \frac{\varepsilon_r}{\varepsilon_m} \times 100 \tag{16.2}$$

16.4 Memory Polymers As Fibers (MPFs)

Polyurethane-based MPs are segmented structure in which soft and hard segments are present in the same polymeric chain. Usually soft segment contains long-chain macroglycol, and hard segment possesses low molecular weight chain extenders. Segmented polyurethanes are generally synthesized by

pre-polymerization techniques, in which macroglycol reacts with diisocyanate to form soft segment and chain extender reacts with diisocyanate to provide hard segment. MPs possess versatility in processing them into fibers via different spinning methods; melt spinning, dry spinning, wet spinning, reaction spinning, and electrospinning. There are several polymeric systems available for making the fibers; however polyurethane-based memory fibers are discussed in this chapter.

MPs have been investigated for few decades, and spinning them into fibers and utilizing in the textile applications were first achieved by Hu et al. [32]. Their research team have developed MPU filaments (MPFs) via different spinning methods; dry spinning, wet spinning, melt spinning, reaction spinning, and electrospinning, using polyol as soft segment and small-size polydiols/MDI as hard segment [13, 33]. For the first time, Hu and coworkers have developed memory fibers via wet spinning in 2006 and investigated their mechanical, thermal, and shape memory properties. In addition, they have compared the difference between memory fibers and other man-made fibers (Figure 16.3a). Varying the ratio of hard segment content to soft segment could change the behavior of fibers. Zhu et al. achieved complete shape recoverability in wet-spun fibers (Figure 16.3b) [25]. Investigation of dynamic analysis revealed the difference between memory fibers and other man-made fibers in terms of decrease in the elastic modulus (E') in the normal apparel using temperature range. It can be seen from Figure 16.3a that the decreased elastic modulus in memory fibers PU56-120 and PU66-120 is very much significant in the normal using temperature range. Increasing the temperature above T_g transforms glassy state into rubbery region, and this enabled to decrease the modulus. Lycra showed the decrease at −40 °C, whereas other fibers showed between 100 and 105 °C. Hence, memory fibers show the switch temperature in the normal using temperature to tune their memory behaviors, and it is advantageous to implicate for several applications.

The plastic deformation or irreversible strain is most common in the film substrates, whereas thermal shrinkage occurs in the case of fibers. Zhu et al. [25] claim that counteraction effect of two opposite factors irreversible strain and thermal shrinkage induces MP fibers to achieve complete shape recoverability as shown in Figure 16.3b.

16.4.1 Which Fibers Do Have Better Performance, Wet or Melt Spun?

Method of fiber spinning is very much crucial, which thus decides the properties of fibers for adopting them into several applications. In line with this, Meng et al. [34] have investigated a comprehensive and extensive research to reveal the relationship between phase separation, thermal, and mechanical properties and fibers spun with different spinning methods to unveil the underlying physics and property differences. Table 16.1 shows the thermal and mechanical properties of MP fibers spun by melt and wet spinning methods as a comparison. Melt spinning induces fibers to have higher crystallinity and melting transition of soft segment compared with wet spinning method (Table 16.1). It can also be seen that melt-spun fibers have significant transition peaks for both soft

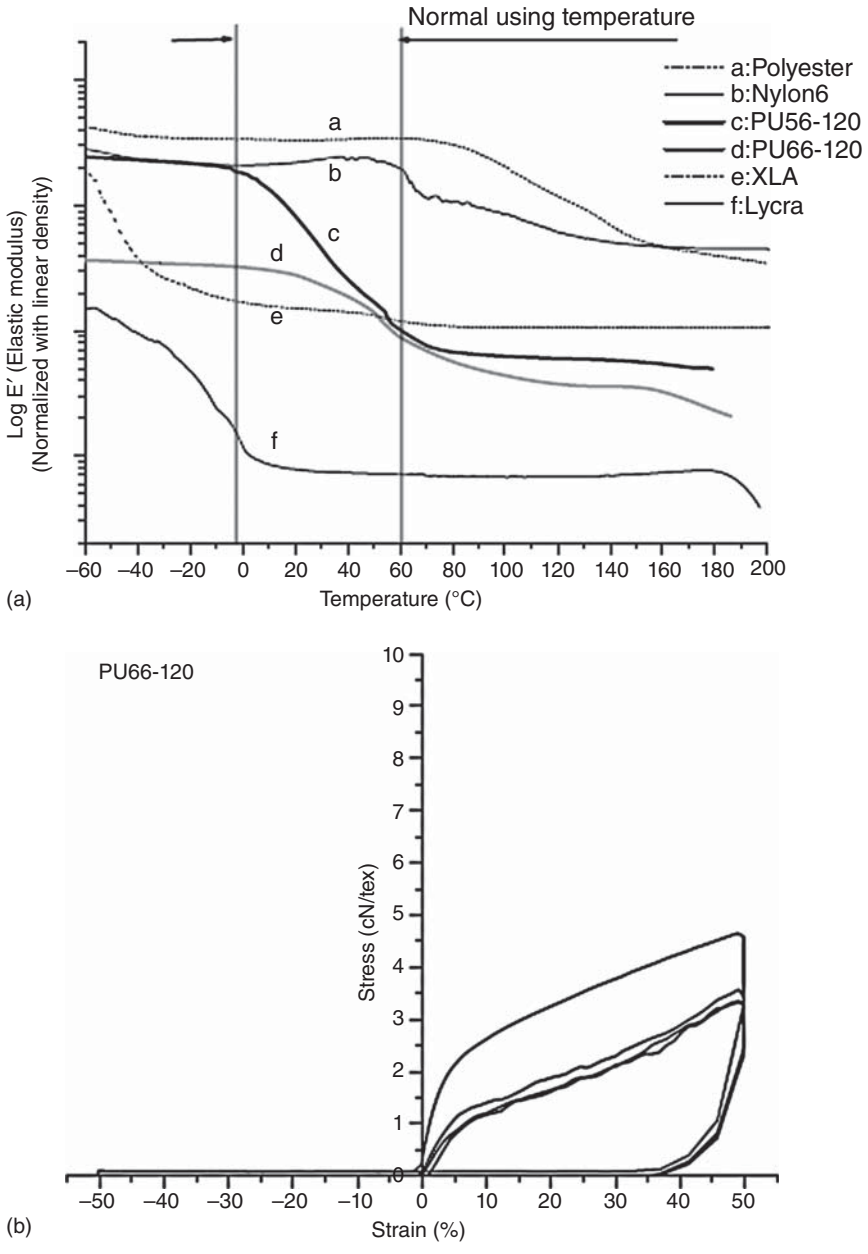


Figure 16.3 Properties of wet-spun memory fibers. (a) Comparison of elastic modulus (*E′*) in MP fibers and other man-made fibers. (b) MP fibers showing complete shape recoverability.

segment (36–47 °C) and hard segment (214 °C) compared with no peaks in hard segment for wet-spun fibers (Figure 16.4a). Higher crystallinity and larger melting enthalpy of melt-spun fibers suggest that melt spinning induces perfect crystallinity and more ordered polymer packaging, a significant rich hard

Table 16.1 Thermal properties of melt- and wet-spun MP fibers.

	Soft segment			Hard segment	
	T_m (°C)	ΔH (J/g)	Crystallinity (%)	T_m (°C)	ΔH (J/g)
1Melt spun	48.73	27.89	19.93	214.33	1.294
2Melt spun	47.67	28.46	20.17	214.94	1.305
3Melt spun	46.82	27.94	19.96	214.64	1.286
1Wet spun	36.23	22.8	16.29		
2Wet spun	36.62	22.82	16.3		
3Wet spun	36.98	22.78	16.27		

Source: Meng et al. 2007 [34]. Reproduced with permission of Springer Nature.

segment phase in the fibers. The results of X-ray diffraction (XRD) profiles for fibers also show that the crystalline peaks are significant and higher for melt spun fibers and this is in accordance with the differential scanning calorimetry (DSC) traces (Figure 16.4b).

In addition, thermomechanical cyclic test results also have proven that melt-spun fibers (shape fixity, 86%; shape recovery, 98%) could provide higher shape fixity and recovery ratios compared with wet-spun (shape fixity, 82%; shape recovery, 95%) fibers (Figure 16.4c,d). The physical properties of MP fibers are shown and tabulated in Table 16.2. Preparation of fibers using melt spinning does not include any type of solvent, and it is also advantageous in terms of environmental and economy concerns. Henceforth, it is imperative to note that melt spinning could be chosen to produce MP fibers to have better performance to implicate them into vivid applications.

16.4.2 Effect of Post-spinning Operations on MP Fiber Properties

Now, we know that MP fibers can be spun using different spinning methods. Spinning may induce some internal stress and structure deficiency in the fiber along its axis, and this has to be removed or nullified to enhance their performance properties. Post-spinning operations such as heat treatment and drawing could help fiber to rearrange their molecular orientation and polymer packaging at temperature above the transition of soft segment. The influence of post-spinning operations on thermal, mechanical, and thermomechanical cyclic properties are discussed in this section.

16.4.2.1 Effect of Thermal Setting or Heat Treatment

Thermal setting or heat setting process is carried out at high temperature above the transition of soft segment in the fibers. A schematic of filament passage for roller heat setting is shown in Figure 16.5. Meng et al. have experimentally investigated and stated that thermal setting has a significant influence on the soft segment and thermal and mechanical properties [35]. In general, the transition temperature of soft segment ranges from 40 to 50 °C and hard segment with 200–240 °C. Heating the fibers above the soft segment transition helps to

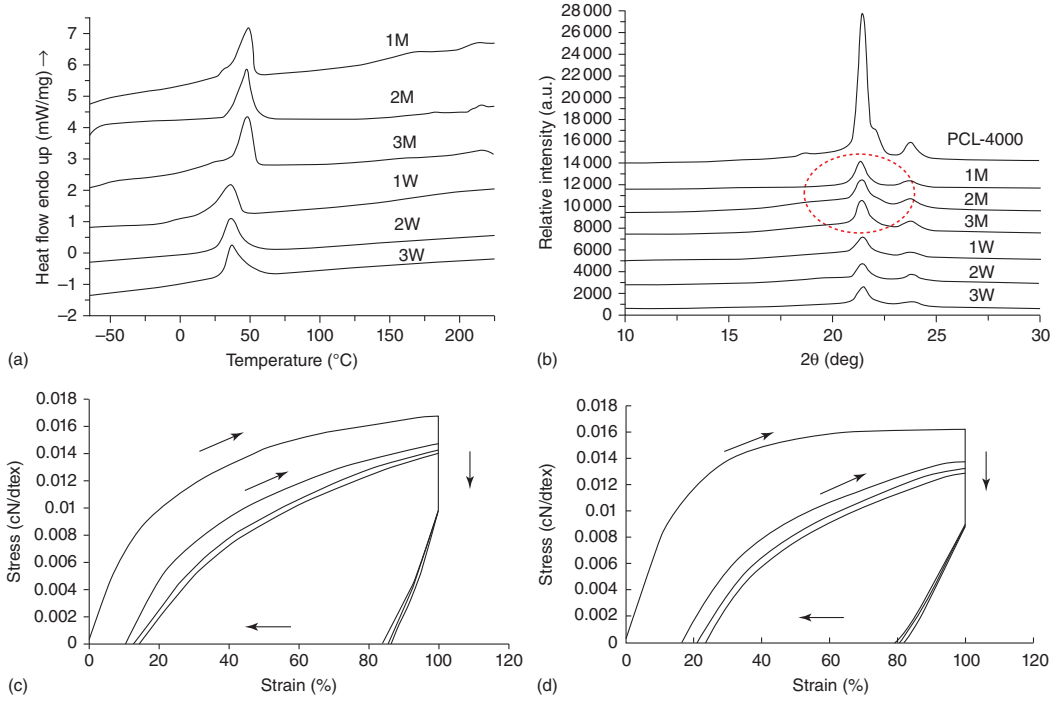


Figure 16.4 Thermal and mechanical properties of melt- and wet-spun MP fibers. (a) DSc thermographs. (b) XRD profiles. (c) Stress–strain plot of melt-spun fibers. (d) Stress–strain plot of wet spun fibers.

Table 16.2 Physical properties of MP fibers.

Si no.	Particulars	
1	Tensile strength	> 0.9 cN/dtex
2	Elongation at break	350–500%
3	Initial modulus	0.08–0.3 cN/dtex
4	Shape fixity ratio	80–100%
5	Shape recovery ratio	90–100%
6	Tunable switch temperature range	0–100 °C
7	Diameter of electrospun fibers	50–700 nm

dtex: weight in grams of 10 km of fiber.

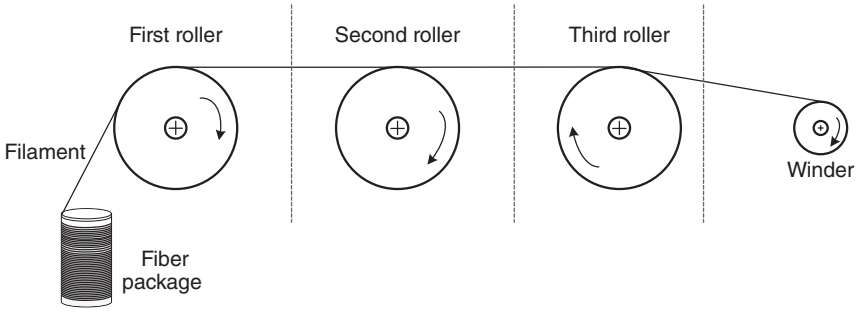


Figure 16.5 Schematic passage of MP filament through thermal setting process.

increase the crystallinity and melting enthalpy by molecular reorientation with reduced entanglement in the molecular chains. It can be seen from Figure 16.6a that transition peak of soft segment is increasing with heat setting temperature and there is a significant peak for hard segment in the fiber treated at 125 °C. This suggests that the crystallinity of soft segment increases, which is enabled by rotation of polymeric chains and ordered packaging. Heat treatment may repair the destroyed crystals during the spinning process to increase the crystallinity. Figure 16.6b shows the effect of heat treatment on the fiber tenacity; it can be noticed that at low temperature above the transition, molecular disorientation occurs, thus yielding lower tenacity. Heat treatment at higher temperature improves the phase separation and hard segment stability that is visible in Figure 16.6b. Partial molecular disorientation at low temperature can also influence the linear density by decreasing it; increasing the temperature can make the stable network and thus avoid further decrease in the linear density (Figure 16.6c).

Apart from molecular disorientation, releasing the internal stress at high temperature can also increase the breaking elongation of the fiber (Figure 16.6d). If a fiber needs to be employed in an application that needs a long-time response, stress relaxation is the most important criteria to be considered. Increasing the heat treatment would cause the fiber to improve the phase separation and strong hydrogen bond with well-ordered hard segment network. High

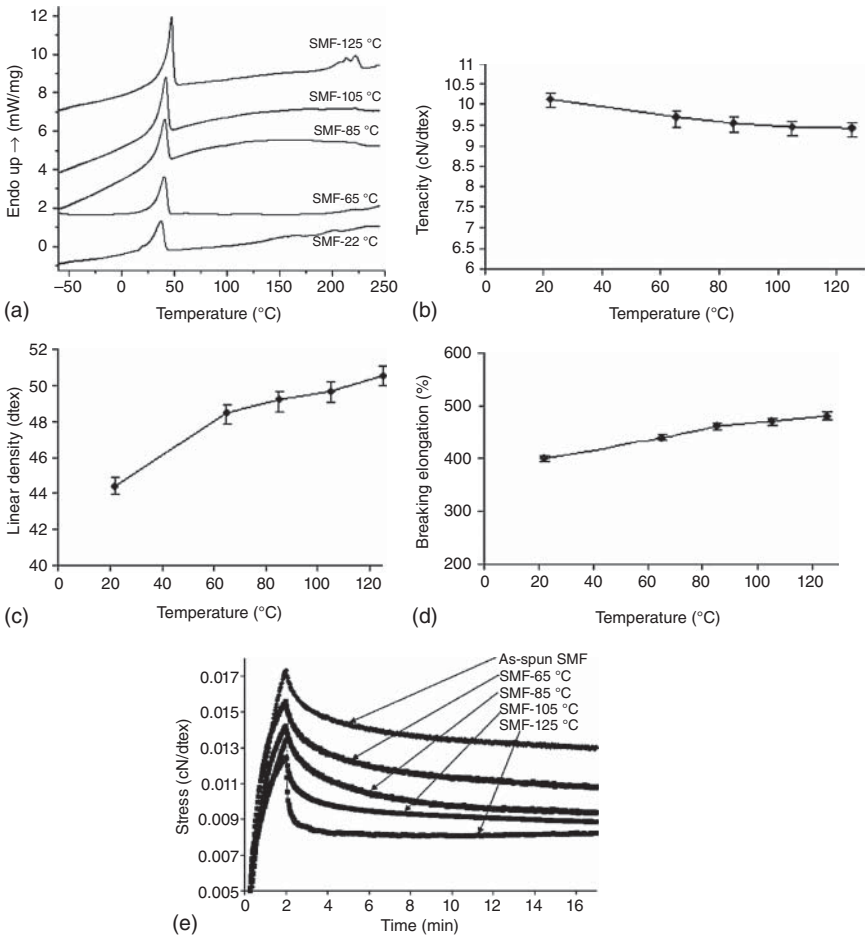


Figure 16.6 Influence of heat treatment on fiber properties. (a) DSC thermograms. (b) Effect on tenacity. (c) Effect on linear density. (d) Effect on breaking elongation. (e) Effect on stress relaxation.

temperature-treated fibers could show less decay in the stress and great stability over time (Figure 16.6e). Increasing the crystallinity, phase separation, and hydrogen bonding of hard segment would improve the shape fixity and shape recovery ratios as well. As we know, soft segment is responsible for shape fixation and hard segment stability for shape recovery during thermomechanical cyclic process [35].

16.4.2.2 Influence of Drawing Process

Drawing here refers to stretching or tensile deformation during the thermomechanical cyclic testing. Meng et al. have studied the effect of both cold and thermal drawing on the SMEs for the wet-spun fibers in comparison with commercial polyurethane fibers. Their experimental investigation reported that thermal drawn fibers could improve the shape fixation and shape recovery ratios

as the soft segment crystallinity increases with hard segment stability and phase separation [36].

16.4.3 Other Type of MPU Fibers

16.4.3.1 Smart Hollow Fibers

Memory fibers can be spun into different shapes of cross section depending on the type of spinnerets being used. Hu and coworkers have developed a thermal-responsive hollow polyurethane fiber via melt spinning, which can change and recover their diameter upon thermal stimulation. The cross-sectional image is shown in Figure 16.7a and thermally adjustable internal holes in Figure 16.7b–d. The hollow fiber showed tenacity of 1.14 cN/dtex, breaking elongation of 682%, and shape fixity of 87% with 89% recovery ratio. These could be used for the applications such as smart filtration and drug-controlled release and in other suitable fields [37].

16.4.3.2 Electro-responsive Fibers

Electro-responsive MPU fibers were developed by Hu and coworkers and could recover their shapes under electrical stimulation. The shape memory

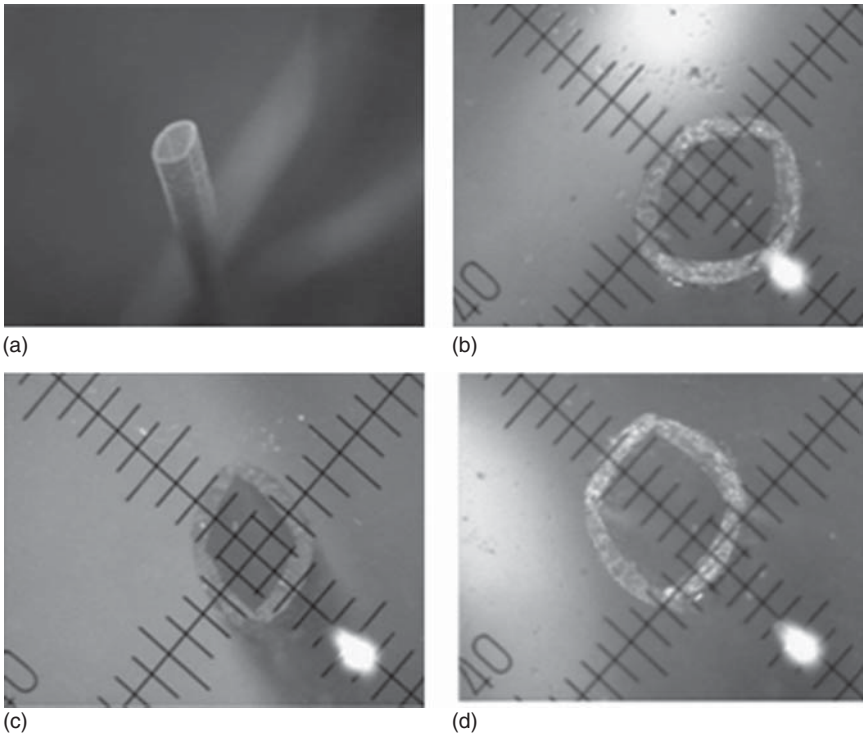


Figure 16.7 Melt-spun smart MPU hollow fiber. (a) Cross-sectional image. (b–d) Thermally adjustable internal holes.

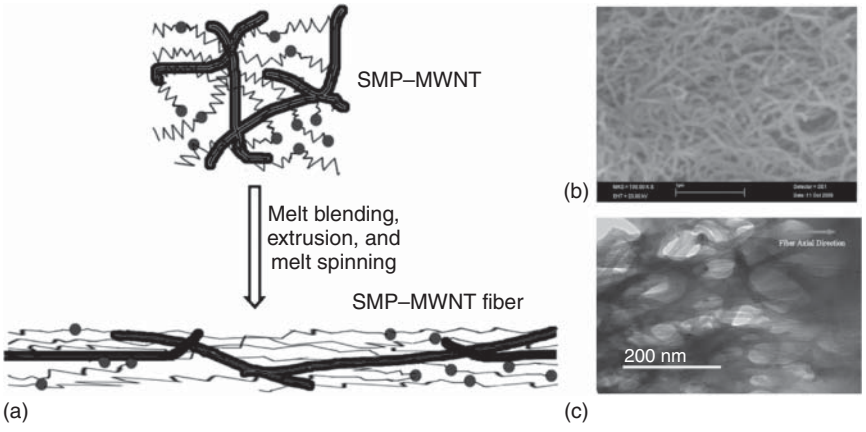


Figure 16.8 Electro-active memory fiber reinforced with MWNTs. (a) Schematic of composite fiber and MWNTs alignment. (b) SEM image. (c) TEM image.

polyurethane (SMP–MWNT) composite was prepared by in situ polymerization, and the MPU–MWNT fiber was prepared by melt spinning. Carbon nanotubes were incorporated into the MPU fibers and are charged at both ends (Figure 16.8). Voltage required to generate the heat to trigger the shape recovery was still high. Scanning electron microscopy and transmission electron microscopy (TEM) observations of the morphology revealed that the MWNTs are axially aligned and homogenously distributed in the MPU matrix, which is helpful for the fiber's electrical conductivity improvement and for the electro-active SME [38].

16.4.3.3 Electrospun Fibers

Electrospinning is used to produce ultrafine nanofibers using MP solution or melt with an external electric field. The main advantage of these fibers is they provide a large surface area to volume ratio, smaller fiber diameter, potential to carry active chemicals, filtration abilities, low weight, and high permeability. As the memory fibers have the ability to change and recover the shapes, it would allow nanofibers to some unique functions such as controlled water vapor permeability and hydro-absorbency upon an external heat stimulus [39]. Hu and coworkers have achieved shape fixity and recovery ratios of up to 80% and 98% respectively [40]. Core–shell structured nanofibers containing pyridine moieties could offer antibacterial properties [41].

16.5 Novel Stress Memory Behavior in MPs

16.5.1 What Is Stress Memory?

Stress memory is a novel phenomenon that was recently discovered by Hu et al. in a thermal-sensitive memory polyurethane material [9]. Like shape

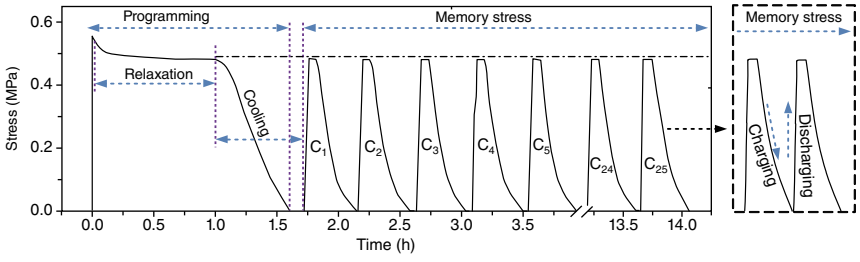


Figure 16.9 Stress memory profile of a thermal-sensitive memory polymer.

memory, stress in MPs can also be stored and retrieved reversibly upon an external heat stimulus. Figure 16.9 shows the profile of stress memory cycles in a thermal-induced memory polyurethane film substrate. When the material is stretched with a known deformation strain level, corresponding stress will be generated. In Figure 16.9, the MP is heated above the transition of soft segment and given a particular level of strain, and further it is continued to hold under the same constraint strain and temperature level to carry out the stress relaxation process. After obtaining a plateau of stress level, it is further cooled down to room temperature below the transition point of soft segment to fix the strain, and this process is called charging. During this cooling process, the generated amount of stress is being stored completely and reached zero stress level. This entire step is denoted as "stress memory programming" process, where the required amount of stress is programmed and stored. In the next step, the MP film is heated above the transition level under the same constraint strain level to trigger the stored stress, and this element is called as "memory stress," and the process is denoted as discharging. These charging and discharging cycles can be continued for several cycles without any significant loss of stress, and this is known as "stress memory" cycle.

16.5.2 Mechanism of Stress Memory

The molecular mechanism involved in stress memory process can be explained using the switch-spring-frame model as shown in Figure 16.10. Thermal-sensitive memory polyurethane used in this study comprises physically cross-linkable hard segment (fixed phase) and semicrystalline soft segment. Crystalline phase represents the switch, and amorphous region represents the spring in the model. When the MP is heated above the transition temperature, crystals in the soft segment melt and enable the modulus to decrease to assist easy deformation. Switches are open, assisting to increase the entropy elasticity of springs above the transition. Detailed steps are depicted in Figure 16.10, and step 2 shows the stretched molecular chains with amorphous network having no more crystals. After deforming above the transition, the next step is cooling the network in stretched constraint strain (step 3). During cooling process, the entropy elasticity of springs is stored in the network by closing the switches (OFF state). Crystallization or vitrification

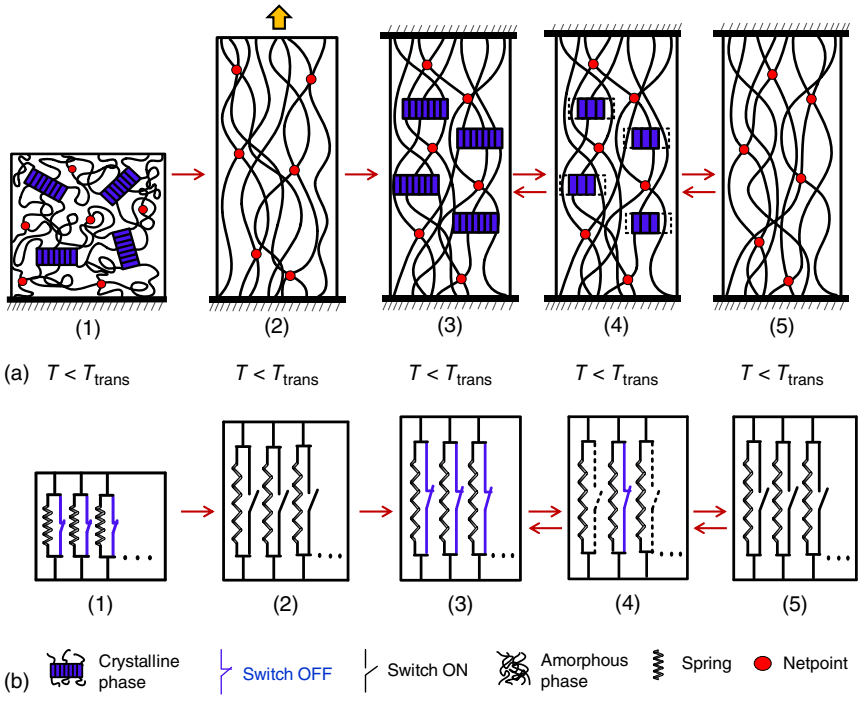


Figure 16.10 Mechanism of stress memory process. (a) Crystal-coil-cross-link model. (b) Switch-spring-frame model.

process occurs during cooling to form new crystals in the network and to close the switch to store the stress.

In step 5, MP is heated above the transition to melt the newly formed crystals and open the switch (ON state) to release the stored entropy elasticity. This results in breaking of strong internal bonds and enables conformational motion of polymeric chains in soft segment. During this step, the spring tries to recoil back, but it is kept under the constant strain, thus enabling to increase the stress upon thermal stimulus. Step 4 is shown as an intermediate step between step 3 and step 5. The more the number of switch opens, the more the recovery of memory stress will be.

16.5.3 Components of Stress Memory

Stress memory programming mentioned in this chapter is based on a tensile stretch programming method. When MPs are deformed under constant rate of strain and temperature, it induces five major components in a polymer matrix [42]. These components are plasticity (ε_p), viscoelasticity (ε_v), memory (ε_m), elasticity (ε_e), and thermal strain (ε_e) as shown in the Eq. (16.3), whereas total stress components are viscous stress (σ_v), memory stress (σ_m), elastic stress (σ_e), and thermal stress (σ_t). To obtain a pure memory stress, it is imperative to eliminate all other impeditive components in the molecular network. Plasticity is

also referred as irreversible strain occurs due to permanent slippage of molecular chains in the network. As mentioned in Figure 16.2, thermomechanical process should be carried out at higher strain than the stress memory programming strain to eliminate both plasticity and elasticity. Viscoelasticity and viscous stress are nullified during the stress relaxation process at above the transition with constant strain over time. Thermal strain and thermal stress are caused by thermal expansion coefficient, which is unavoidable and in a negligible amount. The thermal stress and thermal strain components are negative or impeditive in tensile stretch programming and positive in the compression-type programming method. Narayana et al. [42] have analytically investigated to predict pure memory stress and total stress components using constitutive model via phase transition approach [43, 44].

$$\varepsilon_{\text{Total}} = \varepsilon_p + \varepsilon_v + \varepsilon_m + \varepsilon_e \pm \varepsilon_t \tag{16.3}$$

$$\sigma_{\text{Total}} = \sigma_v + \sigma_m + \sigma_e \pm \sigma_t \tag{16.4}$$

16.6 Stress Memory Behavior in Memory Fibers

Evaluation of mechanical, thermal, and shape memory properties in MPs is extensively studied by several researchers and industrial technocrats. However, revelation of other novel behavior such as stress memory is not reported anywhere till date. Stress memory behavior may differ from material to material such as film, fibers, and foam. For the first time, Narayana et al. [45] have unveiled the novel stress memory behavior in a thermal-sensitive memory fiber made of semicrystalline polyurethane. The soft segment is composed of poly(1,6-hexanediol adipate), 4,4′-diphenylmethane diisocyanate, and chain extender 1,4-butanediol as hard segment. The as-resulted semicrystalline MP is used and prepared fibers via melt spinning method. The response of memory stress in MP film and filament is slightly different.

Figure 16.11 shows the two plots of stress memory response in both film and filament. It can be noticed that the amount of memory stress generated or recovered in the filament/fiber is greater than the film. MP film is able to freeze the complete stress in the soft segment molecular chains upon cooling. Whereas filament shows some residual stress upon cooling, this could be of two reasons: First, the crystallization peak is below the room temperature; second is the incapability of filament to store huge amount of memory stress upon cooling at room temperature. This residual stress is also very much useful in the potential application such as compression stockings, which will be discussed in detail in the next section.

Figure 16.12 shows the evolution of memory stress and their relationships with thermal and X-ray properties. The response of memory stress is higher in the filaments compared with film, and it increases with temperature and strain level (Figure 16.12b). The reason for stress escalation could be well explained by the switch-spring-frame model (Figure 16.10) as discussed earlier. As the temperature increases, more number of switches actuates and

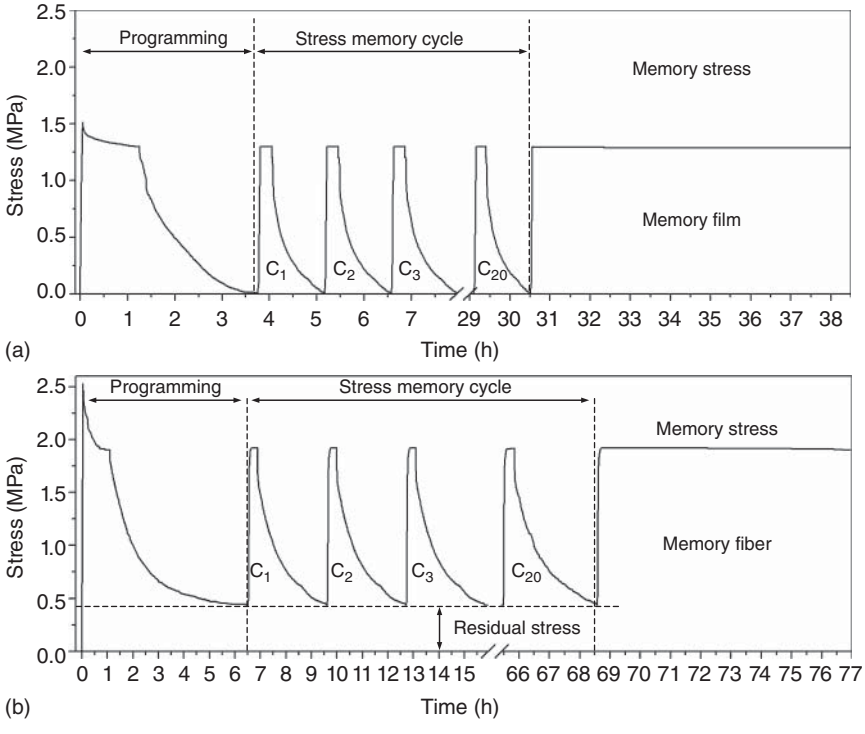


Figure 16.11 Comparison of stress memory behavior in MPs. (a) Stress memory in MP film. (b) Stress memory in MP fiber/filament.

releases the stored memory stress from the strained amorphous springs with gradual melting of crystals. The elevation of stress with strain at constant temperature level is in linear trend with correlation coefficient almost nearly 1 (Figure 16.12b). Crystallization in the soft segment is the main criteria to store memory stress upon cooling. Filament shows higher memory stress than the film, and the reason could be ascribed to higher melting enthalpy and increased crystallization. As discussed in previous section somewhere, melt spinning induces perfect crystallinity, orientation of molecular chains, and compact packaging of polymer. Figure 16.12c shows that the melting enthalpy of MP filament is higher than the film with more prominent crystallization peak obtained from the DSC analysis of stress memory programmed specimens. In addition, evidence for increased crystallinity in MP filament/fiber can be seen from wide-angle X-ray diffraction peaks (WAXD) of stress memory programmed specimens in Figure 16.12d. The difference in the evolution of memory stress in film and filaments are known, which is caused by melt spinning, and the structural changes are schematically depicted in Figure 16.13.

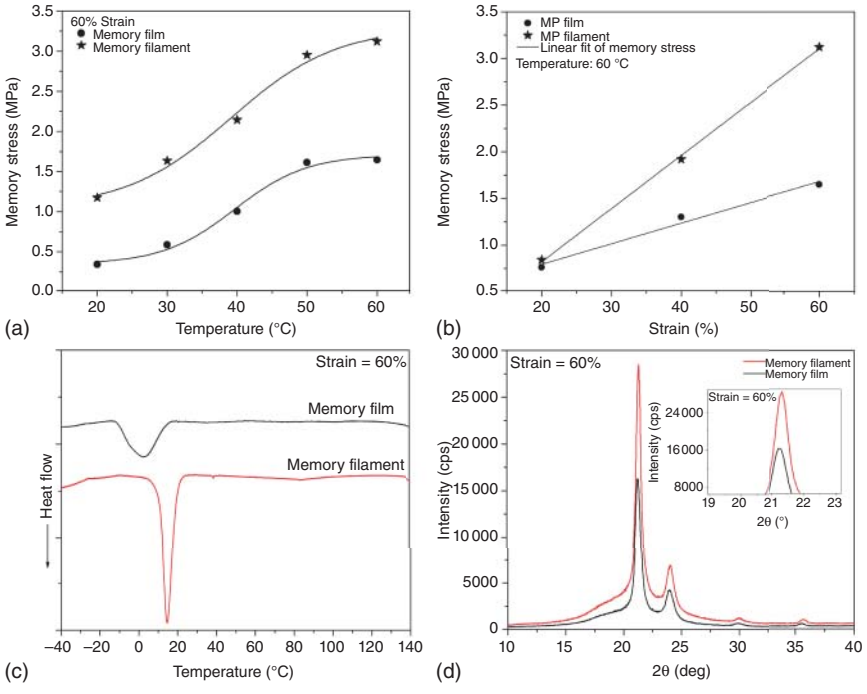


Figure 16.12 Memory stress and their relationships in MP film and filaments. (a) Evolution of memory stress with temperature. (b) Response of memory stress with strain at constant temperature. (c) DSC thermograms of stress memory programmed specimens. (d) WAXD profiles of stress memory programmed specimens.

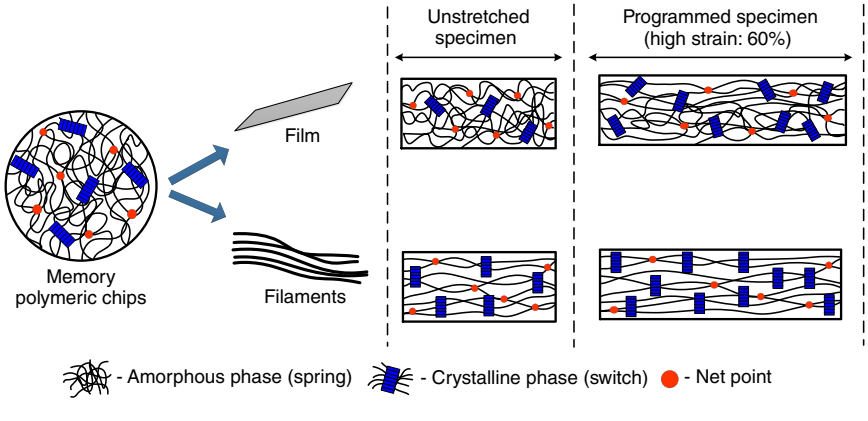


Figure 16.13 Schematic scheme showing structural changes in MP film and filaments.

16.7 Techniques of Characterization for Memory Fibers

Choosing the right method and equipment for characterization of memory polymeric fiber properties is very much important. Figure 16.14 shows the various structural property characterization methods and equipment to be chosen in one chart.

16.8 Potential Application of Stress Memory Fiber/Filaments

Novel stress memory behavior was first discovered in the memory polymeric film [9, 42], and then it is revealed in fiber or filament [45, 46]. As discussed in the previous section, memory fibers could memorize and retrieve maximum amount of stress reversibly upon an external heat stimulus. Memory stress can be controlled with strain and temperature. If the stress control is possible in the fibers, it would help to control the stress in other smart structures such as textile fabrics for numerous application. Narayana et al. [45] have utilized the stress memory filament potential to implicate them into textile knitted fabric structure for smart compression stockings. The memory polymeric composition can be tailor-made to obtain a residual stress upon cooling, and this is very much helpful in compression stockings. Compression stocking is considered as a gold standard for compression therapy to treat phlebological and lymphological deceases such as venous ulcers, varicose veins, venous stasis, and deep vein thrombosis (DVT) [47–50]. It has been a great challenge to maintain the constant interfacial pressure in the stockings due to various attributes such as material

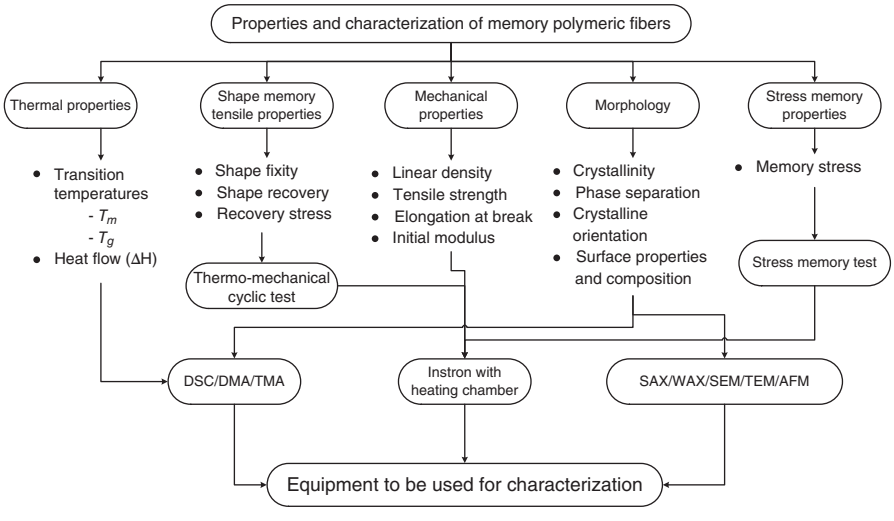


Figure 16.14 Method of characterization for memory polymeric fibers.

characteristics (stress relaxation), different size of legs, and pressure loss over time. Usage of memory polymeric filaments in the compression stockings could solve the current real problems by maintaining the stable memory stress over time. Stockings with smart stress memory filaments could provide a pressure gradient [9], massage effect, and selective pressure control just by triggering the memory stress. Compression stockings should not reach to zero pressure upon application on human leg and must retain with some base pressure around 20 mmHg; this could be achieved using the residual stress present in the stress memory filaments. The experimental investigation of massage effect in the compression stockings is shown in Figure 16.15. The potential of stress memory filaments could bring the groundbreaking revolutionary changes in the field of smart compression management.

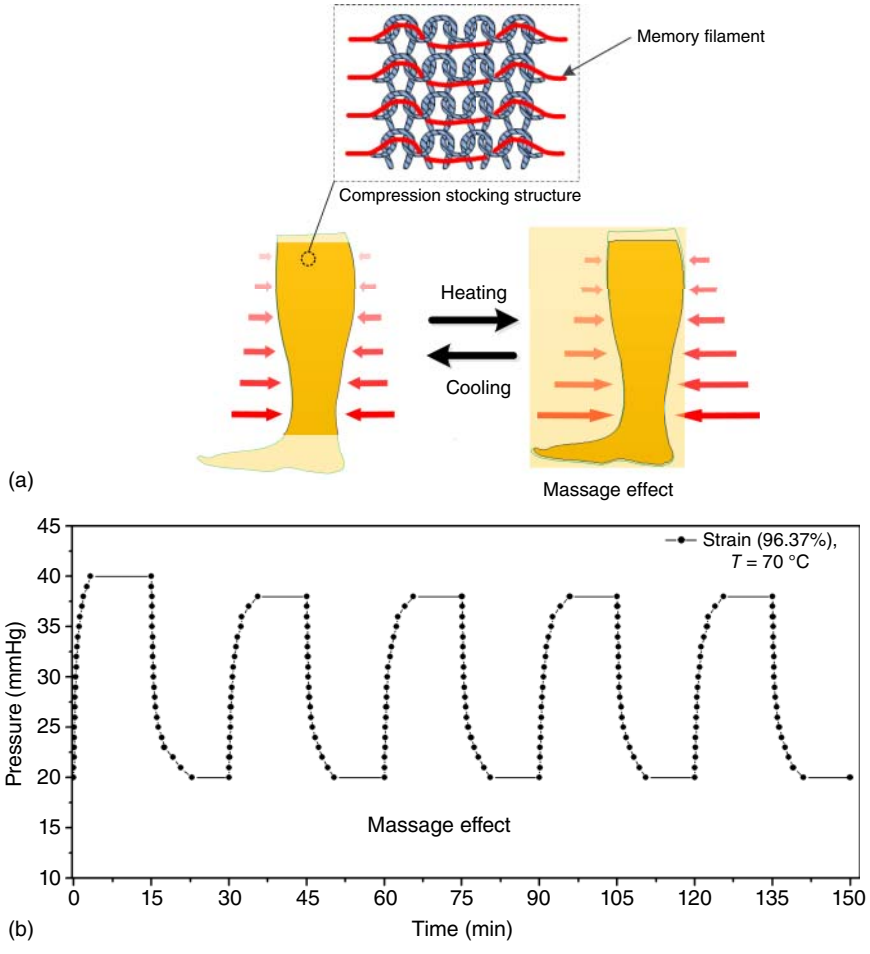


Figure 16.15 Stress memory filaments integrative smart compression stocking. (a) Schematic of smart compression stockings. (b) Massage effect in smart stockings with heat stimulus.

16.9 Recent Advances in MP Fibers

Researchers and industrial technocrats have been continuously working in the arena of MP fibers to scientifically apply them into vivid applications in multidisciplinary areas such as fiber supercapacitors, vibration damping structures, biomimetic fibrous scaffolds, fiber assembly for artificial muscles, and self-healing composites. Zhang and coworkers have fabricated a biodegradable nanofibrous scaffolds with shape memory properties and implied into bone tissue engineering offering shape fixity and recovery ratios more than 90% [51]. Electrochemical performance of MP fiber-based supercapacitors could offer an excellent stability suitable for shape programming and recovery [52, 53]. MP fibers possess higher toughness (276–289 MJ/m^3) compared with spider dragline silks (160 MJ/m^3) due to their excellent stretchability and have higher vibration damping capability [54, 55]. Two-way shape memory behavior-based MP fibers can be utilized in making hierarchically chiral structured artificial muscles [56]. The negative coefficient of thermal expansion of MP fibers is one order higher than those made of polyethylene fibers [57]. The great potential of memory fibers would further enable unveiling of untapped novel behaviors to prepare them as a futuristic smart material for broad horizon of applications to the mankind.

16.10 Future Trends

Undoubtedly, memory fibers could be a futuristic material for broad applications in multidisciplinary areas. MPs offers great advantages such as less density, cheaper price, and easily available. Memory fibers can be processed via spinning methods such as melt spinning, dry spinning, wet spinning, and electrospinning into different diameters from nano- to macrosize. They possess excellent platform to fine-tune their transition temperature range suitable for vivid specific applications. The revelation of novel stress memory behavior in smart MP fibers could inspire researchers to unveil other untapped unique behaviors to prepare for the future. Controlling the stress via stress memory programming in MP fibers could help them integrate into other novel structures for versatile applications. MP fiber integrative smart compression stockings would bring the revolutionary changes in the field of compression management for chronic disorders. At present, nowhere we could see commercially manufacturing plants of memory fibers except research institutes or universities. Commercialization of memory fiber manufacturing and adopting them into different end uses may uncover their great potentials by solving many real problems such as compression stockings.

References

1 Lendlein, A. and Langer, R. (2002). Biodegradable, elastic shape-memory polymers for potential biomedical applications. *Science* 296 (5573): 1673–1676.

2 Hu, J.L., Zhu, Y., Huang, H.H., and Lu, J. (2012). Recent advances in shape-memory polymers: structure, mechanism, functionality, modeling and applications. *Progress in Polymer Science* 37 (12): 1720–1763.
3 Leng, J.S., Lan, X., Liu, Y.J., and Du, S.Y. (2011). Shape-memory polymers and their composites: stimulus methods and applications. *Progress in Materials Science* 56 (7): 1077–1135.
4 Sun, L., Huang, W.M., Ding, Z. et al. (2012). Stimulus-responsive shape memory materials: a review. *Materials and Design* 33: 577–640.
5 Lester, B.V.B. and Vernon, H.M. (1941). Process of manufacturing articles of thermoplastic synthetic resins. Patent No. US2234994A.
6 Weigel, T., Mohr, R., and Lendlein, A. (2009). Investigation of parameters to achieve temperatures required to initiate the shape-memory effect of magnetic nanocomposites by inductive heating. *Smart Materials and Structures* 18 (2): 1–21.
7 Choi, W., Lahiri, I., Seelaboyina, R., and Kang, Y.S. (2010). Synthesis of graphene and its applications: a review. *Critical Reviews in Solid State and Materials Sciences* 35 (1): 52–71.
8 Kim, H., Abdala, A.A., and Macosko, C.W. (2010). Graphene/polymer nanocomposites. *Macromolecules* 43 (16): 6515–6530.
9 Hu, J.L., Kumar, B., and Narayana, H. (2015). Stress memory polymers. *Journal of Polymer Science Part B: Polymer Physics* 53 (13): 893–898.
10 Kratz, K., Madbouly, S.A., Wagermaier, W., and Lendlein, A. (2011). Temperature-memory polymer networks with crystallizable controlling units. *Advanced Materials* 23 (35): 4058–4062.
11 Wu, Y., Hu, J.L., Huang, H.H. et al. (2014). Memory chromic polyurethane with tetraphenylethylene. *Journal of Polymer Science Part B: Polymer Physics* 52 (2): 104–110.
12 Yuan, J.K., Zakri, C., Grillard, F. et al. (2014). Temperature and electrical memory of polymer fibers. *Times of Polymers (Top) and Composites*, Volume 1599, pp. 198–201.
13 Hu, J.L, Lu, J., Meng, Q. et al. (2007). Shape memory fibers prepared via wet, reaction, dry, melt, and electro spinning. US Patent US20090093606 A1, filed 7 October 2007 and issued 9 April 2009.
14 Ji, F.L., Hu, J.L., Li, T.C., and Wong, Y.W. (2007). Morphology and shape memory effect of segmented polyurethanes. Part I: With crystalline reversible phase. *Polymer* 48 (17): 5133–5145.
15 Lendlein, A. and Kelch, S. (2002). Shape-memory polymers. *Angewandte Chemie International Edition* 41 (12): 2034–2057.
16 Kim, B.K., Lee, S.Y., and Xu, M. (1996). Polyurethanes having shape memory effects. *Polymer* 37 (26): 5781–5793.
17 Liu, C.D., Chun, S.B., Mather, P.T. et al. (2002). Chemically cross-linked polycyclooctene: synthesis, characterization, and shape memory behavior. *Macromolecules* 35 (27): 9868–9874.
18 Voit, W., Ware, T., Dasari, R.R. et al. (2010). High-strain shape-memory polymers. *Advanced Functional Materials* 20 (1): 162–171.

19 Tobushi, H., Hara, H., Yamada, E., and Hayashi, S. (1996). Thermomechanical properties in a thin film of shape memory polymer of polyurethane series. *Smart Materials and Structures* 5 (4): 483–491.

20 Takahashi, T., Hayashi, N., and Hayashi, S. (1996). Structure and properties of shape-memory polyurethane block copolymers. *Journal of Applied Polymer Science* 60 (7): 1061–1069.

21 Hu, J.L. (2014). *Shape Memory Polymers: Fundamentals, Advances and Applications*. Shropshire, United Kingdom: Smithers Rapra.

22 Lin, J.R. and Chen, L.W. (1998). Study on shape-memory behavior of polyether-based polyurethanes. I. Influence of the hard-segment content. *Journal of Applied Polymer Science* 69 (8): 1563–1574.

23 Chun, B.C., Cho, T.K., and Chung, Y.C. (2006). Enhanced mechanical and shape memory properties of polyurethane block copolymers chain-extended by ethylene diamine. *European Polymer Journal* 42 (12): 3367–3373.

24 Ji, F.L., Zhu, Y., Hu, J.L. et al. (2006). Smart polymer fibers with shape memory effect. *Smart Materials and Structures* 15 (6): 1547–1554.

25 Zhu, Y., Hu, J.L., Yeung, L.Y. et al. (2006). Development of shape memory polyurethane fiber with complete shape recoverability. *Smart Materials and Structures* 15 (5): 1385–1394.

26 Wang, W.S., Ping, P., Chen, X.S., and Jing, X.B. (2007). Biodegradable polyurethane based on random copolymer of L-lactide and epsilon-caprolactone and its shape-memory property. *Journal of Applied Polymer Science* 104 (6): 4182–4187.

27 Min, C.C., Cui, W.J., Bei, J.Z., and Wang, S.G. (2005). Biodegradable shape-memory polymer-polylactideco-poly(glycolide-co-caprolactone) multiblock copolymer. *Polymers for Advanced Technologies* 16 (8): 608–615.

28 Li, F.K., Zhang, X., Hou, J.N. et al. (1997). Studies on thermally stimulated shape memory effect of segmented polyurethanes. *Journal of Applied Polymer Science* 64 (8): 1511–1516.

29 Zhu, Y., Hu, J., Yeung, K.W. et al. (2007). Effect of cationic group content on shape memory effect in segmented polyurethane cationomer. *Journal of Applied Polymer Science* 103 (1): 545–556.

30 Jeong, H.M., Kim, B.K., and Choi, Y.J. (2000). Synthesis and properties of thermotropic liquid crystalline polyurethane elastomers. *Polymer* 41 (5): 1849–1855.

31 Anthamatten, M., Roddecha, S., and Li, J.H. (2013). Energy storage capacity of shape-memory polymers. *Macromolecules* 46 (10): 4230–4234.

32 Hu, J.L, Han, J., Lu, J. et al. (2010). Items of clothing having shape memory. US Patent US20120000251 A1, filed 30 June 2010 and issued 5 January 2012.

33 Meng, Q.H. and Hu, J.L. (2008). Study on poly(epsilon-caprolactone)-based shape memory copolymer fiber prepared by bulk polymerization and melt spinning. *Polymers for Advanced Technologies* 19 (2): 131–136.

34 Meng, Q.H., Hu, J.L., Zhu, Y. et al. (2007). Morphology, phase separation, thermal and mechanical property differences of shape memory fibers prepared by different spinning methods. *Smart Materials and Structures* 16 (4): 1192–1197.

35 Meng, Q.H., Hu, J.L., Yeung, L.Y., and Hu, Y. (2009). The influence of heat treatment on the properties of shape memory fibers. II. Tensile properties, dimensional stability, recovery force relaxation, and thermomechanical cyclic properties. *Journal of Applied Polymer Science* 111 (3): 1156–1164.

36 Meng, Q.H., Hu, J.L., Zhu, Y. et al. (2007). Polycaprolactone-based shape memory segmented polyurethane fiber. *Journal of Applied Polymer Science* 106 (4): 2515–2523.

37 Meng, Q.H., Liu, J.L., Shen, L.M. et al. (2009). A smart hollow filament with thermal sensitive internal diameter. *Journal of Applied Polymer Science* 113 (4): 2440–2449.

38 Meng, Q.H., Hu, J.L., and Yeung, L. (2007). An electro-active shape memory fiber by incorporating multi-walled carbon nanotubes. *Smart Materials and Structures* 16 (3): 830–836.

39 Zhuo, H.T., Hu, J.L., and Chen, S.J. (2011). Study of water vapor permeability of shape memory polyurethane nanofibrous nonwovens. *Textile Research Journal* 81 (9): 883–891.

40 Zhuo, H.T., Hu, J.L., and Chen, S.J. (2008). Electrospun polyurethane nanofibers having shape memory effect. *Materials Letters* 62 (14): 2074–2076.

41 Zhuo, H.T., Hu, J.L., and Chen, S.J. (2011). Coaxial electrospun polyurethane core-shell nanofibers for shape memory and antibacterial nanomaterials. *Express Polymer Letters* 5 (2): 182–187.

42 Narayana, H., Hu, J.L., Kumar, B., and Shang, S.M. (2016). Constituent analysis of stress memory in semicrystalline polyurethane. *Journal of Polymer Science Part B: Polymer Physics* 54 (10): 941–947.

43 Wang, A.Q. and Li, G.Q. (2015). Stress memory of a thermoset shape memory polymer. *Journal of Applied Polymer Science* 132 (24): 1–11.

44 Liu, Y.P., Gall, K., Dunn, M.L. et al. (2006). Thermomechanics of shape memory polymers: uniaxial experiments and constitutive modeling. *International Journal of Plasticity* 22 (2): 279–313.

45 Narayana, H., Hu, J.L., Kumar, B. et al. (2017). Stress-memory polymeric filaments for advanced compression therapy. *Journal of Materials Chemistry B* 5 (10): 1905–1916.

46 Hu, J.L. and Narayana, H. (2016). Review of memory polymeric fibers and its potential applications. *Advance Research in Textile Engineering* 1 (2): 1–7.

47 Sue, J. (2002). Compression hosiery in the prevention and treatment of venous leg ulcers. *Journal of Tissue Viability* 12 (2): 67–74.

48 Labropoulos, N., Gasparis, A.P., Caprini, J.A., and Partsch, H. (2014). Compression stockings to prevent post-thrombotic syndrome. *Lancet* 384 (9938): 129–130.

49 Partsch, H. (2013). Compression therapy in leg ulcers. *Reviews in Vascular Medicine* 1 (1): 9–14.

50 Partsch, H. (2014). Compression for the management of venous leg ulcers: which material do we have? *Phlebology: The Journal of Venous Disease* 29: 140–145.

51 Bao, M., Lou, X.X., Zhou, Q.H. et al. (2014). Electrospun biomimetic fibrous scaffold from shape memory polymer of PDLLA-co-TMC for bone tissue engineering. *ACS Applied Materials & Interfaces* 6 (4): 2611–2621.

52 Deng, J.E., Zhang, Y., Zhao, Y. et al. (2015). A shape-memory supercapacitor fiber. *Angewandte Chemie International Edition* 54 (51): 15419–15423.
53 Zhong, J., Meng, J., Yang, Z.Y. et al. (2015). Shape memory fiber supercapacitors. *Nano Energy* 17: 330–338.
54 Yang, Q.X. and Li, G.Q. (2014). Spider-silk-like shape memory polymer fiber for vibration damping. *Smart Materials and Structures* 23 (10): 1–14.
55 Sharafi, S. and Li, G.Q. (2016). Multiscale modeling of vibration damping response of shape memory polymer fibers. *Composites Part B: Engineering* 91: 306–314.
56 Fan, J. and Li, G. (2017). High performance and tunable artificial muscle based on two-way shape memory polymer. *RSC Advances* 7 (2): 1127–1136.
57 Yang, Q.X., Fan, J.Z., and Li, G.Q. (2016). Artificial muscles made of chiral two-way shape memory polymer fibers. *Applied Physics Letters* 109 (18).

17

Textile Mechanics: Fibers and Yarns

Zubair Khaliq[1] *and Adeel Zulifqar*[2]

[1] *National Textile University, Faculty of Engineering and Technology, Faisalabad, Pakistan*
[2] *The Hong Kong Polytechnic University, Institute of Textile and Clothing, Hung Hom, Kowloon, Hong Kong, China*

17.1 Introduction

The yarn is a long and fine structure that consists of very fine fibers. The yarns are usually intermediate products that are further used to make ropes, braids, cords, and fabrics (knitted and woven). The fiber is the building block of these products, so the physical properties of these textile products are highly dependent on the physical properties of the fiber. Practically, the mechanical properties of textile products are important to meet certain standards. The structure of textile products contributes to these properties. However, fiber and yarn mechanical properties remain a fundamental element. Since fabrics can be used in multiple end products like carpets, towels, sheets, apparel, and woven clothing, the requirement of fiber and yarn mechanical properties can be varied with its requirement. This results in desired fiber and yarn properties instead of general requirements. Indeed, if we consider yarn, the required yarn properties are different according to the end user. The requirements of a spinner can be uniformity, low level of imperfections, optimum hairiness, and high strength. A knitter might not be sensitive about high strength but bulkiness, flexibility, and softness of yarn, so the yarn can bend easily during the knitting process. However, a weaver might require the high strength of yarn to withstand the larger stresses during the weaving process to make fabric. Better pilling resistance, lower fluff, lower hairiness, higher abrasion resistance, least contamination, and higher evenness are the general requirements of yarn. Conclusively, it becomes very difficult to quantify general yarn standards. The variable requirements of end users lead to different yarn structures to meet their specific needs. This becomes important to understand these yarn structures to study the textile product scientifically. This chapter describes the general properties of fibers along with the yarn structure to give a better understanding of mechanical properties of the final textile product.

Handbook of Fibrous Materials, First Edition. Edited by Jinlian Hu, Bipin Kumar, and Jing Lu.
© 2020 Wiley-VCH Verlag GmbH & Co. KGaA. Published 2020 by Wiley-VCH Verlag GmbH & Co. KGaA.

17.2 Fiber

Fiber is the smallest and fundamental element of yarn and a textile product. A significant factor of the mechanical properties of a textile product originated from the mechanical properties of a fiber. However, the fibers are very small. The length of a textile fiber should be at least 1000 times longer than its width. If the length of the fiber is too short, then it will be difficult to process and to make a textile product. Also, the fibers should be flexible, which is a prerequisite to process and make a textile product. Otherwise, the stiffer fibers are difficult to process and uncomfortable to wear. In the past, the natural fibers were the first to be used as textile fibers. The mechanical properties of textile fibers are largely dependent on their building polymer molecules. The nature of covalent bonding along with the physical interactions between fiber molecules contribute to the mechanical behavior of the fiber. The physical interaction includes van der Waals forces, polar interaction, and hydrogen bonding between polymer molecules. These interactions define the amorphous and crystalline structure of a fiber and eventually the mechanical behavior.

17.2.1 Fiber Consumption

Figure 17.1 shows the classification of textile fibers. Yarn spinning consumes the largest share (90%) of total fiber volume produced. Nonwovens have a share of 7%, and the remaining share of 3% is being used as fillings and cigarette filters. According to science from the 1960s, the world's population is increasing leading to the increased demand of fibers for clothing. This demand was satisfied by synthetic fibers. As the production of synthetic fibers is time saving, people moved

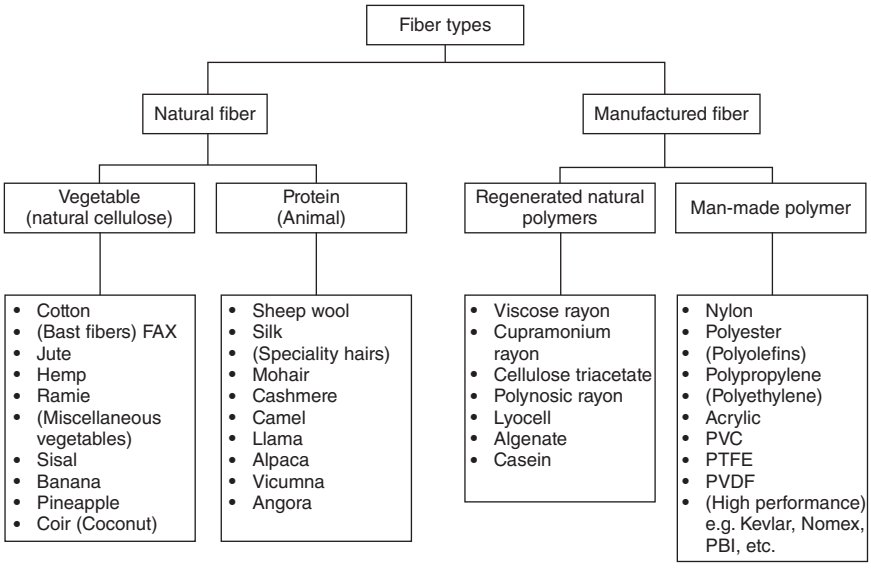


Figure 17.1 Flow chart of different textile fibers.

toward it, and its share rose up to 57%. The natural fibers have the share of only 43% of total fiber production. Among synthetic fibers, polyester has the highest share of 59.3%, then followed polyolefin fibers (polypropylene + polyethylene) having a share of 18.4% and polyamide (Nylon) fiber having a share of 13.1%. The acrylic has the least share of 8.5%. The manufactured cellulosic fibers may also be included into the class of synthetic fibers, which have a share of about 8% in the global production of synthetic fibers.

Cotton is being used in textiles from the beginning. It has been used in history for over 5000 years. Almost every human on earth was using it to cover his body. Cotton is still very important fiber till now because it is largely used to produce fabric, apparel, and composites. It occupies the second largest share of 33% after polyester, followed by jute that is most widely used in the production of sacks for vegetable or other food item storage and transportation. It is also widely used in composite manufacturing as cheap and environment-friendly reinforcement. Wool is also an important client for fashion and textile design, having a share of 2.3% of total fiber production. Other natural fibers have relatively less share in the market.

Spun yarn spinning technique may be used to produce yarn from these remaining organic natural fibers (except bast fibers). These techniques include spun on short-staple, worsted, woolen, or the exceptional spinning techniques. The bast fibers, on the other hand, cannot be spun by conventional spinning techniques but with special techniques [1].

Asbestos is also a natural fiber from the mineral origin, but it is not widely used in textiles due to its carcinogenic effects and environmental hazards. However, scientists are developing its environment-friendly formulation with concrete to produce heat-resistant building structures. Other mineral fibers like glass fiber, bast fibers, and metal fibers are largely used as a filament to produce yarn. Nonwoven fabrics may also be produced from these yarns. Metal staple fibers may also be spun into yarn to produce conductive clothing. It was used to produce protective clothing for soldiers in traditional wars.

The inorganic fibers have a very low application that's why they are not being produced in large quantity. So, they are quite significant in yarn spinning and textile clothing. But on the other hand synthetic fibers like polyester, acrylic, and regenerated cellulosic fibers and natural fibers like cotton, jute, wool, etc. are quite significant for spinning and clothing. Many of them are very useful for medical applications. Cotton is used as a wound dressing from the beginning. Many other fibers are also discovered to be inherently antimicrobial and also cure the wound more quickly. Silk and hairs are used to produce luxury clothing, which is very expensive and exotic. But theses fibers have highest potential growth in the field of textiles.

Fiber growth rate strongly depends upon population, fiber cost, and the ability of personnel to buy them. The world's population is about 6 billion peoples, which is increasing by a ratio of 1.7% every year. Sixteen percent of world's population consumes more than 10 kg fibers per capita. And the remaining 84% of world's population is using 3–10 kg of fibers per capita. It is supposed that the average annual fiber consumption will increase up 12 kg/capita, up to the middle of the twenty-first century, in which natural fibers will have their share of

40% and synthetic fibers will occupy a huge share of 60% in the global market. Sixty-two percent of total fibers produced will be converted into spun yarn, and the volume of filament yarn will 30%. The remaining 8% will be used to nonwoven fabrics, filters, and cigarettes.

17.3 Strength Contributing Fiber Parameters

The components of a textile fiber that are observable to the human eye are its diameter, length, and crimp. The diameter of a fiber is the average width of the fiber along the fiber's length. The diameter and length of a fiber determine its size, which is one of the most important quality parameters of fiber. It is described as the linear density of fiber. The linear density of fiber can be described in different ways like the weight of fiber per unit length (direct system) or length per unit weight of fiber (indirect system). A direct system is usually used to define the fineness of fiber and filament yarns, while the indirect system is used for the staple spun yarns. Depending on the fineness of the fibers, linear density can be measured in denier or tex. Denier is the weight of fiber in grams per 9000 m of fiber length, while tex is the weight in grams of 1000 m of fiber length. One denier is equal to nine times of tex. Fiber size has an important impact on fiber stiffness, which then influences the stiffness of the yarn and fabric made from that fiber. Also, it significantly influences the drape of the fabric. In addition, fiber stiffness is an important factor of how comfortable or uncomfortable the fabric feels when it is worn next to the skin. Fiber length is another most significant property of fiber. Fiber length is analytical in the processing of fibers and yarns and the transformation of fiber strength to yarn strength. Usually, a longer fiber length is favored. Textile fibers are either staple or filament length. The length of staple fibers can be from 2 to 46 cm, and that of filament fibers is the infinite length. Except silk all natural fibers are of staple length. The manufactured fibers may be staple or filament fibers. Fiber crimp indicates waves, bends, twists, or curls along the fiber length. It is measured as crimps per unit length. Synthetic fibers have a smooth surface, which increases its slippage during fiber spinning. A desired and controlled crimp is introduced in synthetic fibers to attain the desired properties of yarns and fabrics. Crimped fibers contribute to having higher elongation than linear fibers.

17.4 Mechanical Properties of Fiber

17.4.1 Stress–Strain Curve

Owing to the linear shape of the fiber, the tensile properties are the most significant and are the most studied parameter. This is because of the reason that most forces and deformations occur along the fiber length. A gradually increasing force is applied along the fiber axis until the fiber breaks. Stress–strain curve is shown in Figure 17.2, which shows many important mechanical characteristics of the fiber. Specific stress is often used in textile industry instead of the general

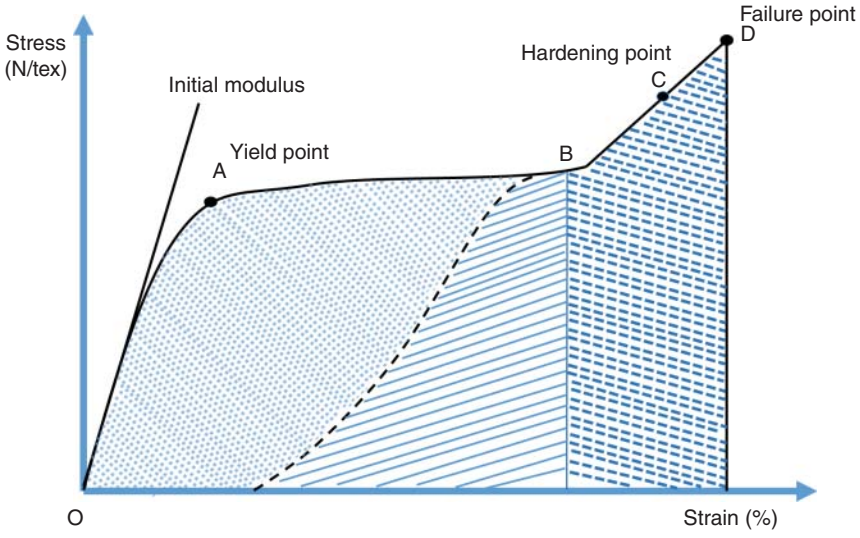


Figure 17.2 Schematic of the stress–strain curve of a fiber under tensile loading.

stress. The specific stress describes the general stress regarding linear density of the fiber.

In general engineering,

Tensile stress = Force/Area

$$s = F/A$$

Tensile strain = Change in length/Original length

$$e = \Delta l/l$$

Specific stress = Force/Linear density

$$\text{ss} = F/dl$$

Figure 17.2 shows schematic stress–strain curve. The curve begins with a straight line segment that rises as stress is increased (OA) and then suddenly flattens and rises at a slower rate (AB). Close to the failure point, the curve rises steeply (BC). The details of each of the regions are addressed as follows:

In region OA, the deformation occurs due to the bond stretching and flexing. It is reversible as long as Hooke's law is obeyed: $s = Ee$, where E is the slope of the line and called Young's modulus. In this region, it is elastic, and the deformation is recoverable. After the yield point, it is usually a plastic region, and the deformation becomes nonlinear. The deformation, results of the polymers skidding by each other, is partially recoverable. In region AB, the fiber can extend easily. The intra-fiber bonding is represented by the slope of the segment AB. When the polymers become more compact, the fiber reaches a deformation limit, harden

point. Following the hardening point, the internal structure of the fiber begins to give way, and the failure point is reached. The stress and strain at this point give the tenacity and the elongation at break, respectively.

17.4.2 Elastic Recovery, Work of Rupture, and Resilience

In the initial segment of the stress–strain curve (BC), the fiber behaves like an elastic spring. When the load is applied, the polymer chains are being uncurled, perhaps becoming more oriented to the fiber direction. The fibers will retain their original length when the load is removed at any point from O to A. The elastic recovery is 100% in this case. The fiber will not recover 100% when they are stretched beyond the yield point before its hardening point. At this stage, if the load is removed, then the polymer chains will partially recover.

Work of rupture or toughness is a measure of the ability of a fiber to withstand sudden shocks of energy. The area under the stress–strain curve determined the total amount of work required to deform a fiber up to the failure point, the sum of dotted, lined, and a dashed area in Figure 17.2. The work of recovery is also known as resilience. It is the ratio of energy returned to energy absorbed when a fiber is under load or the applied load is removed. It may be extensional, flexural, compressional, or torsional. In Figure 17.2, the fiber resilience of extension is the ratio of lined area to the sum of the lined and dotted area.

17.4.3 Effects of Time, Temperature, and Moisture

The stress–strain curve behavior of a textile fiber also depends on some other factors. One of the important factors is the earlier mechanical history of the fiber. Another important factor is temperature. Also, the mechanical characteristics of the fiber depend on the aging time with temperature. It is usually called viscoelastic (combined viscous and elastic) behavior. This is because of the reason that polymers contain elastic as well as viscous nature. The mechanical history along with aging time and temperature affects this viscoelastic behavior [2–5]. Fiber may perform poorly if it suffers from these conditions. Creep and stress relaxation are the tests developed to probe their time-dependent behavior. These characteristics are measured by other mechanical factors like creep and stress relaxation. In the creep test, the sample is under constant load, and the strain increases with time. In the stress relaxation test, the stress reduces with time after the sample is given an instantaneous strain. The mechanical behavior of fibers can also be affected due to moisture. The moisture camps in the noncrystalline regions and plasticizes them results in reducing the modulus.

17.5 Yarn Classification

Figure 17.3 shows that yarn is usually expressed in the form of fiber strand made of either intertwine staple fibers or consistent parallel filaments that are proficient to interweave into a woven structure or intermeshed into a knit structure.

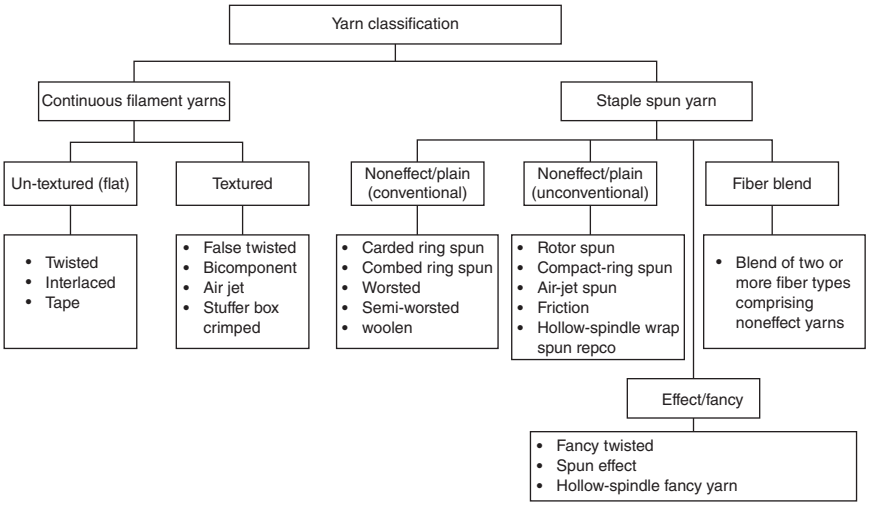


Figure 17.3 Flow chart of different yarn types.

The yarn can be intertwisted into non-fabric materials like braids and ropes. Figure 17.3 indicates that there are two important types of yarn. One is continuous filament yarns, and second is spun yarns. A continuous filament yarn is usually obtained by using extruding polymer liquid to form liquid filaments through a spinneret that are solidified into a continuous fiber strand. As shown in Figure 17.4, when a continuous filament yarn consists of single filament, then it is called a monofilament yarn, and when it consist of many filaments, then it is called multifilament yarn. The texturizing process can be used for the purpose of generating bulky yarn. The continuous filaments can also be converted into another structural form via deliberate entanglement or geometrical reconfiguration. The spun yarn can be generated from staple fibers after using many connective processes like the opening, blending, cleaning, drawing, and spinning. These fibers are stabilized into a yarn structure via twisting. These processes are summarized in Figure 17.5. These yarns can be produced with fibers, which are obtained from natural or synthetic sources. In addition, the staple spun yarn structure depends on the method that is used for fiber preparation like carded, combed, or worsted yarns. Also, it depends on spinning methods like ring-spun, rotor-spun, air-jet, and friction spun yarn.

17.6 Yarn Construction

Yarn structure had been discussed in multiple research work, and it is difficult to add further strength contributing factors. However, an understanding of the strength contributing factors should be considered. These factors include (a) fiber arrangement in the yarn, (b) the binding force of fibers (twist), and (c) fiber compactness in the yarn. Different yarn spinning methods are used to convert fibers into yarn. We will discuss the most commonly used techniques in the industry.

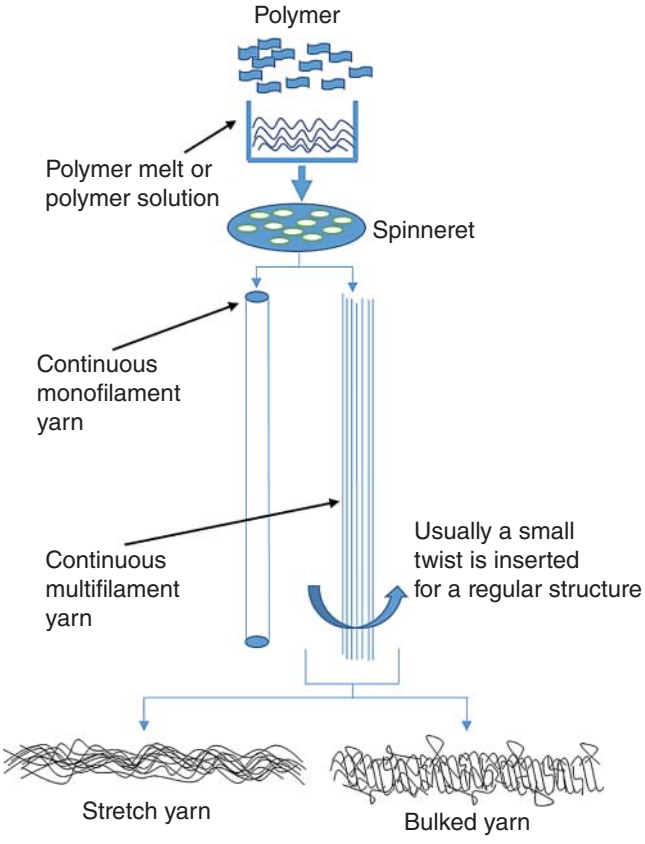


Figure 17.4 Schematic of a continuous filament yarn.

17.6.1 Ring-Spun Yarn

This yarn is produced on a ring frame, and this technology is known as "ring spinning." Ring spinning was first discovered by an American scientist John Thorp. Then another American scientist introduced the rotating traveler on the ring. Ring-spun yarn is used in all types of fabrics from knitting to woven with the most diverse yarn type. Ring spinning is relatively an expensive process due to its slower speed of production. Roving and winding are needed additionally in the process. In ring spinning, the yarn linear density ranges from fine to medium count range. Also, it has some small production range in the coarser count. In this process, the final yarn fineness is led by the process of blow room, carding, drawing and then winding the yarn on a bobbin after inserting the twist to the fibers with the rotating traveler. These stages take place continuously. In ring-spun yarn, the twist is inserted uniformly on all the yarn structure up to a certain limit. As the thickness of the yarn is uneven, the thinner section has the concentrated twisting. Comparatively a loose twisting comes at the thicker section, which results in the hairiness of yarn. Ring-spun yarn has different types depending upon the

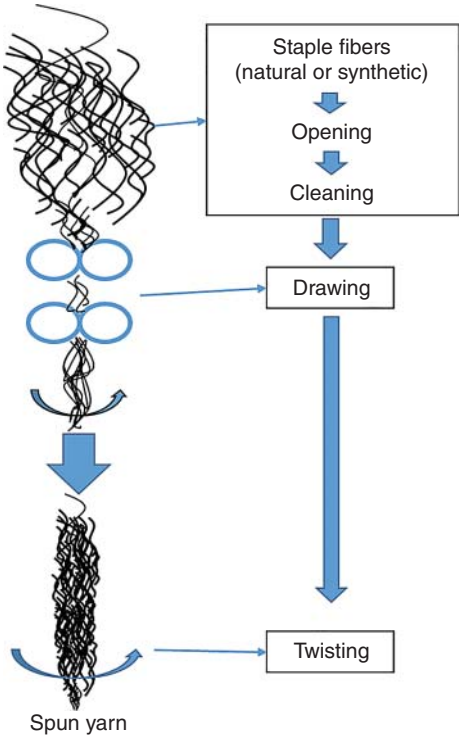


Figure 17.5 Schematic of a spinning process for a staple spun yarn.

requirement of the final product. These types include carded yarn, combed yarn, and compact yarn.

17.6.2 Yarn Structure

17.6.2.1 Carded and Combed Yarns

Carded yarn is relatively cheaper than combed yarn due to its smooth and simplest structure. It can be manufactured by ordinary spinning tools, after opening, cleaning, carding, and drawing of fibers. Cheap tooling and easy manufacturing make carded yarn very economical. Carded yarn, especially when made up of cotton, may have a high level of trash due to poor fiber alignment and may have a high number of neps. This leads the carded yarn poor in mechanical properties. However, a wide range of courser counts may be produced and applied to make a wide range of apparel from heavy denim to shirts and blouses. Both weaving and knitting techniques may be used for fabrication. A schematic diagram of carded yarn is shown in Figure 17.6a.

Combed yarn, on the other hand, is also a single yarn. The simple tools used to make carded yarn may also be used to manufacture combed yarn, but the process of combing is to be performed additionally. Combing process usually eliminates the neps and short fibers, which results in the reduction of overall trash in yarn and improvement in physical properties of the yarn. It improves the fiber mechanical properties, and hence higher quality yarns are produced.

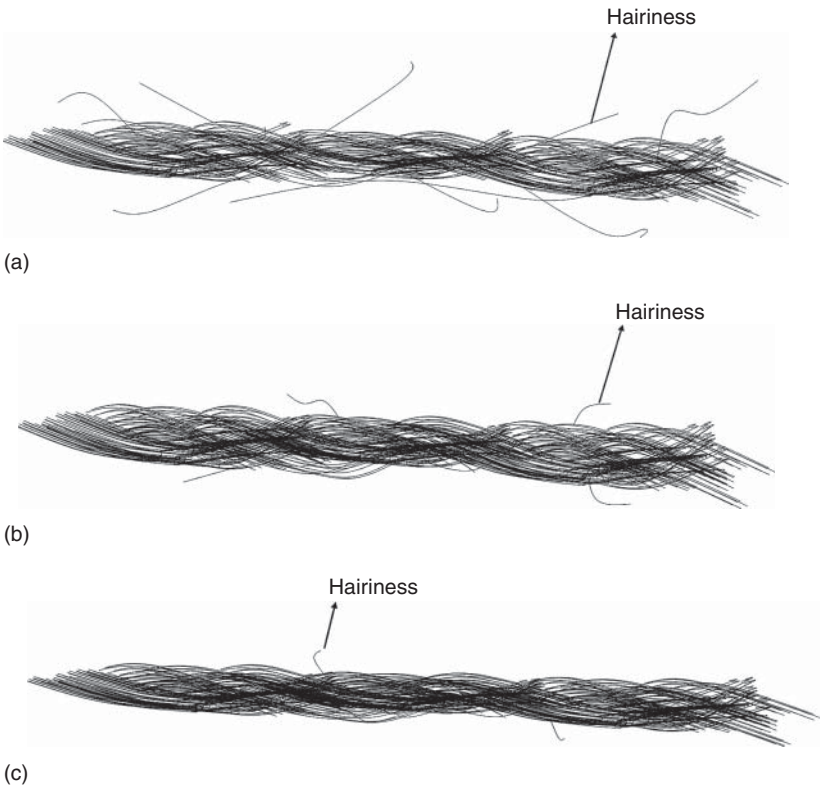


Figure 17.6 Different types of ring-spun yarn. (a) Carded yarn. (b) Combed yarn. (c) Compact yarn.

As many of raw material is wasted in the form of short fibers and neps, cost rises. That is why combed yarns are relatively expensive then carded yarns. A schematic diagram of combed yarn is shown in Figure 17.6b. After the combing process, upper medium counts, as well as very fine counts, may be produced, which have superior properties along with smooth fiber orientation and high comfort. These combed yarns have great potential to be used for highly attractive and fashionable textiles with excellent comfort and durability on behalf of exclusive performance amalgamation.

17.6.2.2 Compact Yarn

Yarn strength may also be improved by fiber condensation. A modified ring spinning technique so-called compact spinning is used to condense fibers aerodynamically. This process not only improves yarn strength but also reduces hairiness. Very fine count yarns of high strength may be produced through this technique. High-quality fabrics and apparels may be produced. A schematic diagram of compact yarn is shown in Figure 17.6c.

Prominent features:

- The ring yarn has better parallelization and orientation than other yarn types.



Figure 17.7 Modern ring spinning machines.

- It has larger hairiness, pilling, and unevenness.
- It has better strength, surface smoothness, and core fibers as compared with the other yarn types.
- It has a high breaking strength.
- The elongation at break of ring-spun yarn is lower than other yarn.
- Ring-spun yarn has a high imperfection index.
- Ring-spun yarn has lower abrasion resistance and stiffness.

Figure 17.7 indicates a modern ring spinning frame.

17.6.3 Rotor-Spun Yarn

Rotor spinning is a technique that is used for creating yarn without the use of a spindle. It is also known as open-end (OE) spinning, break spinning, or free fiber spinning. It was invented and developed in Czechoslovakia. Unlike the ring spinning, rotor spinning combines two process stages of spinning and winding in a single machine. Usually, the coarser counts are spun on the rotor. Mostly the count is below 20s, but it may as high as 40s. Rotor spinning is more successful method than many other open-end spinning methods. The fiber bundle that can be obtained from the sliver feedstock are separated into individual fibers by using the opening roller in an air stream, and the fibers that are separated are recollected using rotor groove. In rotor spun the yarn needs more twisting than ring-spun yarn. It has much application in knitwear and woven cloth, but

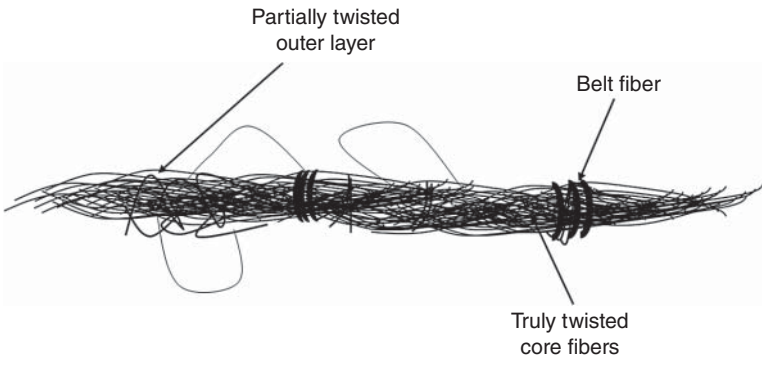


Figure 17.8 Schematic structure of a rotor yarn.

mostly its use remains in denim. It is also used in medical and industrial fabrics. The fabric is absorbent and contains a longer lifetime that is made by using open-end yarn.

17.6.3.1 Yarn Structure

The rotor yarn can adopt a carded or a combed process before it is fed to the rotor spinning system. The rotor yarn contains three-layer structures, which include truly twisted core fibers, partially twisted outer layer, and belt fibers. The schematic illustration of a rotor-spun yarn is shown in Figure 17.8. Usually coarser yarns are made on rotor spinning, which requires higher twist than ring spun. Comparatively the rotor yarn is weaker than ring-spun yarns. However, it has a lower mass variation as compared with ring spun. In addition, unlike the ring-spun yarn, the twist is inserted from center to outer side and in some cases in opposite direction. Figure 17.8 shows the schematic of a rotor yarn structure, and Figure 17.9 indicates a modern rotor machine.

Prominent features:

- The rotor yarn is more extensible as compared with ring yarn.
- Rotor spinning system takes less power than ring spinning system.
- The imperfection index of rotor yarn is lower than ring yarn.
- Rotor spinning requires more maintenance than ring machine.

17.6.4 Air Vortex Spun Yarn

This technology was developed in 1997 in Japan by Murata Company. In this process, the yarn spinning is carried out through a stream of the air jet. After its invention, a lot of improvement and modification had been introduced with the latest improvement in 2008. Murata Vortex Spinning technology is used for a wider range of fiber lengths.

17.6.4.1 Yarn Structure

In this spinning system, the drafted fibers are introduced in a spindle through an air vortex. The twist is inserted through a swirling air when the fibers are entering



Figure 17.9 Rotor machine.

and passing through the orifice. Also the lengthier fiber moves to the core, and the smaller fiber departs to the outer layer with the application of air. This procedure divides the vortex yarn into two parts in which one is twisted and other is untwisted as shown in Figure 17.10. The air vortex spinning requires less maintenance than other spinning systems due to the lesser moving parts. The yarn production can be delivered up to 400 m/min. Also, the roving formation stage is eliminated with the addition of fully automatic piecing system. Air vortex yarn has lesser hairiness than the ring-spun yarn. This is due to the air singed and air combed process, which results in reduced fabric pilling.

Prominent features:

- Vortex yarn has more abrasion resistance than other yarns.
- Vortex yarn is stiffer than other yarns, which indicate that it has a high value of tenacity.

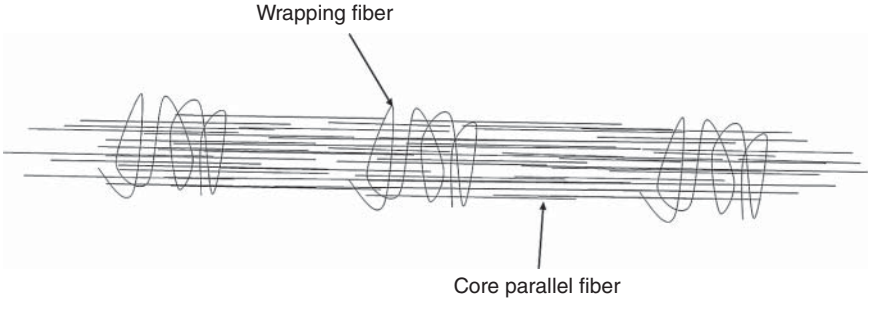


Figure 17.10 The schematic diagram of an air vortex yarn.

- Vortex yarn has minimum lint shedding and can hold its bulk as compared with ring-spun yarn, which makes a potential use as high-quality towels.
- It is used in fancy or high-fashioned fabrics due to lesser hairiness, which enhances its appearance.

The yarn structure of ring, rotor, and vortex differs significantly in terms of twist imparted. The twist insertion in the yarn structure is different in these techniques. Figure 17.11 shows this difference graphically. Ring-spun yarn has a uniform twist from core to outer layer. Rotor-spun yarn has twisted fibers in the core along with the belt fibers on the outer layer of yarn. The abrupt change in the twist level indicates the belt fibers for OE yarn in Figure 17.11b. Vortex yarn has a minimum twist in the core parallel fibers. However, this twist increases abruptly for the wrapping fibers at the outer layer of the yarn structure.

17.6.5 Frictional Spun Yarn

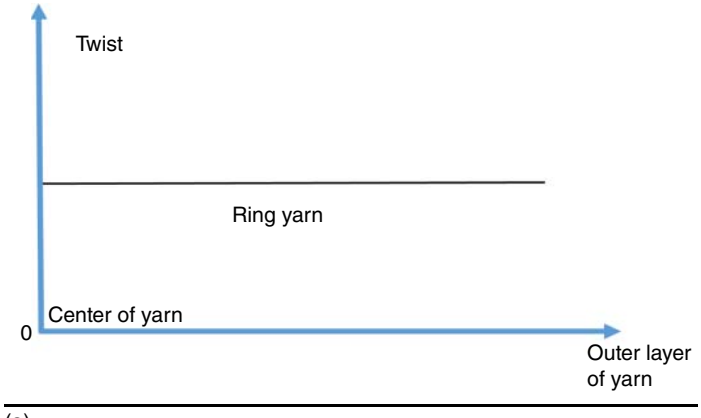
Frictional spun yarns are made using friction spinning. The yarn illustrates truly twisted fibers, but a great several fiber loops are present. It can be made only in very coarse yarn for the use of industrial applications. It is largely used for making industrial yarns of various structures including core/sheath yarns. Blends of raw fiber and waste fiber can also be used for its preparation. Figure 17.12 shows a schematic diagram of a frictional spun yarn.

17.6.6 Mechanical Properties of the Yarn

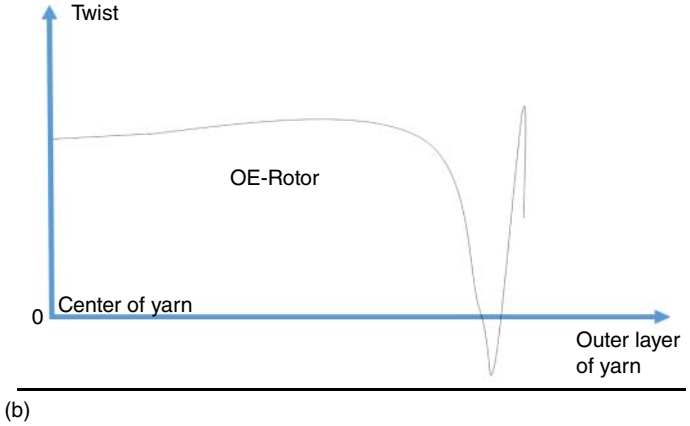
The mechanical properties of yarn include its behavior under the application of forces along with its recovery behavior when the forces are removed. As mentioned before, the yarn mechanical behavior depends on the fiber mechanics and yarn structure. We have discussed the yarn structure in different processing techniques. Almost all of these types include twist as a binding force of fibers. However, the level of twist in yarn varies on the final desired characteristics in the fabric.

17.6.7 Important Parameters of Yarn Tensile Strength

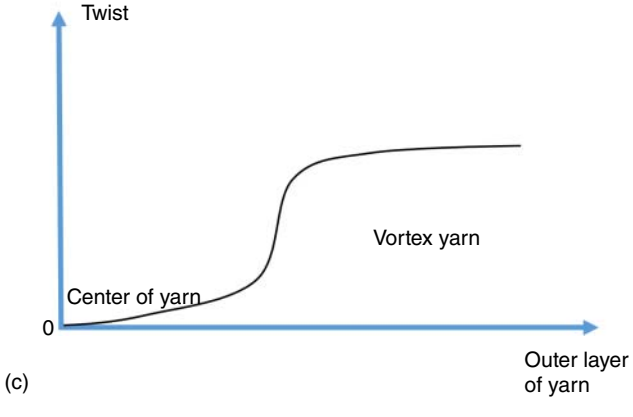
Mechanical properties of yarn are of core interest in the field of textile research. The scientists have discovered so many relations that relate mechanical properties of yarn with structural features. Yarn mechanics may also be addressed greatly by using computer simulating software. Many softwares are now available in the market. Studies reveal that an ideal model of twisted yarn is that which bear a resemblance to filament yarn. This means the greater the resemblance with a filament yarn, the better the twisted yarn. Ring-spun yarn provides great resemblance due to its structure. Fibers are uniformly distributed and combined in yarn under tension. This structure made the behavior of fibers easily foreseeable and understandable. Hearle et al. [6] discovered a theoretical relationship for determining the mechanical properties of continuous filament yarn. Spun yarns are more complex to understand because they have less tension in the surface layer as



(a)



(b)



(c)

Figure 17.11 A comparison of twist in (a) ring-spun yarn, (b) rotor yarn, and (c) vortex yarn.

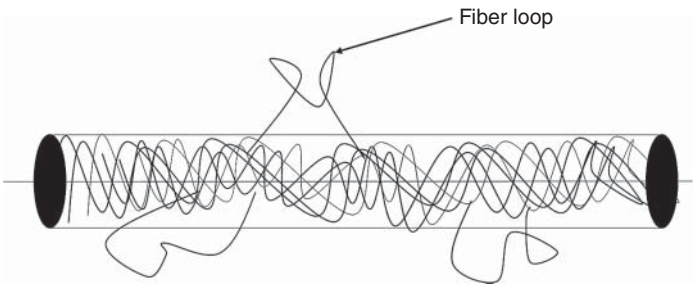


Figure 17.12 Schematic structure of friction spun yarn.

compared with inner layers due to discontinuous fiber segments or staple fibers. So, some empirical and analytical amendments were made to accommodate such complex yarns. This discovered relationship is written below:

$$\frac{\text{Yarn strength (or modulus)}}{\text{Fiber strength (or modulus)}} = \frac{E_y}{E_f} = \cos^2 \alpha \, [1 - K \operatorname{cosec} \alpha]$$

where

E_y	yarn modulus
E_f	fiber modulus
α	twist angle

and "K" may be defined by the following expression:

$$K = \frac{\sqrt{2}}{3L_f}\left(\frac{aQ}{\mu}\right)^{1/2}$$

where

L	fiber length
a	fiber radius
Q	margin period
μ	coefficient of friction

The above relationship relates to the strength of yarn on twist by two basic parameters; first is "$\cos^2 \alpha$," and second is "$1 - K$ cosec α."

"$\text{Cos}^2\ \alpha$" can only be used when studying the continuous filament yarn, and it cannot be used for staple fiber spun yarn, whereas "$1 - K$ cosec α" is the parameter used to measure twist angle of fibers in spun or staple yarn. The previous parameter shows a trend of yarn strength with a twist angle. In the beginning, the yarn strength is inversely related to twist angle, but after it shows a linear relationship with a twist angle. The yarn strength may also have a great dependence on "K" value; the lower the K value, the higher the strength of yarn. K value increases as the length of fiber contracts, which means long fibers will impart more strength into yarn as compared with short fibers.

Fiber diameter also has an impact on yarn strength. As the diameter increases, the K value also increases, which leads to lower strength of overall yarn. The above expression also relates the yarn strength with fiber friction. Yarn strength may also be improved by using fibers having high friction. The greater the friction between fibers, the lesser the value of "K," and hence, the higher the strength.

Scientists have revealed that the above expression is based on estimation. However, the key parameters of yarn structure like fiber length, fiber diameter, twist angle, friction, and consolidation may be easily addressed through it. That's why it may be proved very beneficial while predicting the properties of newly developed yarn or developing a new yarn of specified properties.

17.6.8 Strength–Comfort–Twist Relationship

While designing the yarn strength, other parameters, which may have an impact on yarn integrity, should not be ignored. For example, yarn strength increases as a number of twists per unit length increase. However, this effect may not be true after a certain level says optimum twist. After this point, an increase in the number of twists per unit length will decrease the strength of yarn. That's why some twists must be optimized. A trend of yarn strength on twist factor is shown in Figure 17.13. The reason behind twist–strength relationship is "friction." For example, when there is no twist in yarn, fibers are oriented parallel to the axis of yarn, but due to lack of cohesive force, slippage of fibers may reduce the overall strength of yarn. A small twist may provide the necessary cohesive forces in terms of friction and consolidation. Whenever somebody is going to stretch the yarn, the transverse pressure will build up, causing the frictional forces to increase.

Further increase in twist may cause more friction between fibers, which will provide more intertwining and cross-linking points to facilitate fiber to fiber attraction by joining fibers at their ends with other fibers on the same axis. Another important factor is fiber strength. The overall strength of yarn is distributed on fiber level. The greater the fiber strength, the higher the load bearing property of yarn, and hence the higher the overall strength of yarn. Both

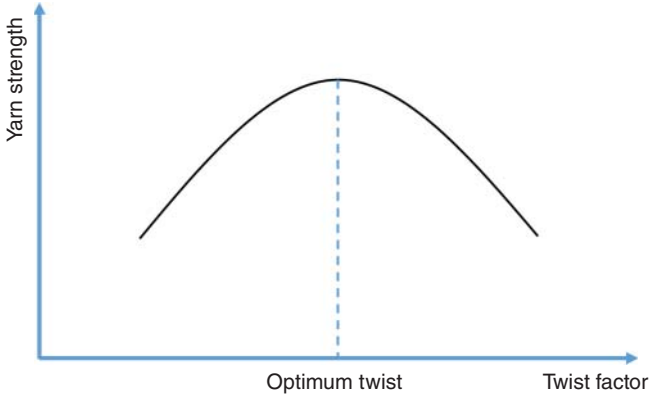


Figure 17.13 Schematic of a yarn strength with increasing twist.

the frictional forces (the number of twists per unit length) and fiber strength play their integral role in the overall strength of yarn. Most of the time, the role of fiber strength is more significant than frictional forces while determining tensile resistance. However, the role of frictional forces due to twist is also very important to bind the fibers together. The frictional force is a key parameter for spun yarn to bind short, discrete fibers together and to strengthen the yarn. As discussed before, yarn strength can only be increased by twisting up to a certain level, which is called an optimum twist. After that optimum value, any further increase in twist will cause inclination of fiber to the yarn axis. That will obviously reduce the influence of fiber strength to overall yarn strength. Therefore, after a critical value, any further increase in twist will cause in the reduction of yarn strength. From the above discussion, it is concluded that there are two leading possessions, overriding the strength–twist relationship. The first procession is the "binding force between fibers," and the second procession is "angle of inclination." Yarn strength will increase as a binding force between fibers increase, which is the result of twist before critical (optimum) value. The angle of inclination of fibers to the yarn axis also plays a vital role in terms of contribution of fiber strength to overall yarn strength.

This phenomenon happens after a critical point. As twist increases, the angle of inclination increases, causing a decrease in the contribution of fiber strength to overall yarn strength. An interpretation of strength–twist relationship is shown in Figure 17.14. The red curve shows the increasing trend for the binding force between fibers as the result of a twist. In the beginning, all fibers will slip as there is no binding force. As the number of twists per unit length increases, the fiber slippage decreases. The blue curve shows the contribution of fiber strength to overall yarn strength. The contribution decreases as a number of twists per unit length increase. The point at which two curves coincide is the critical value of twists per unit length at which maximum yarn strength is obtained. The value of twist below this point is called an optimum twist. The twist level may also affect the properties of fabric like fabric hand and skew. Yarns that have a high level of twist are dynamic, and they have the potential to untwist. In the case of spun yarn,

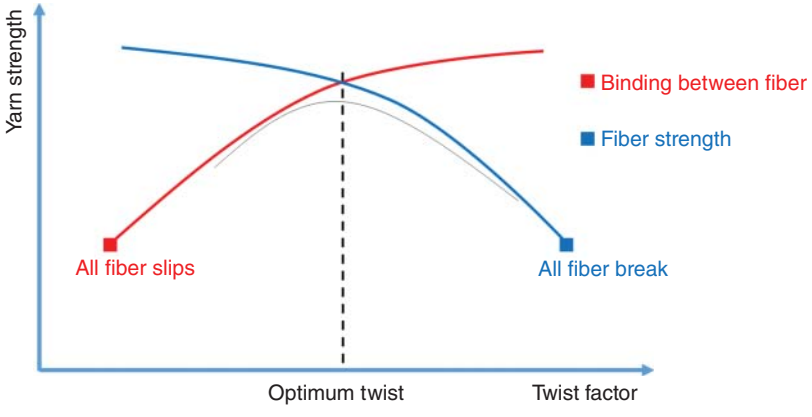


Figure 17.14 Schematic of an interpretation of strength–twist relationship.

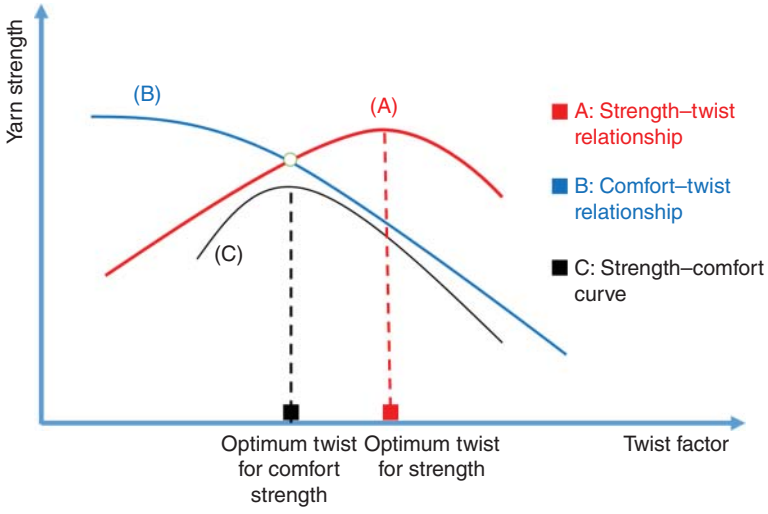


Figure 17.15 Schematic of a comfort–strength–twist relationship.

strength may be increased by the high level of twist (up to critical value), but it will reduce the softness, which is highly undesirable in fabrics [7, 8]. Fabric should not be too hard to wear. That's why not only strength but also the comfort of yarn and fabric should also be addressed properly. Y. EL Moghzy et al. examined the effect of twist on the harshness of yarn and ultimately on the discomfort of fabric [7].

They concluded that both yarn softness and yarn strength should be made under consideration to knit (or weave) wearable fabric. The twist–strength relationship was overlaid by a third parameter, which is "comfort index," which also depends on twist index. In other words, the greater the twist index, the higher the yarn strength, but adversely the lower the comfort (or softness) of yarn. As shown in Figure 17.15, the optimum twist is the point on the x-axis at which two curves (A and B) coincides. The curve A is the strength–twist relationship, which shows the increasing trend of yarn strength with twist index. The curve B is a twist–comfort relationship, which shows that comfort will decrease as twist index increases. So, an optimum level of twist was suggested. For the sake of convenience, comfort index may be denoted by numbers from zero to one. Zero indicates discomfort, and one indicate maximum possible comfort. The strength index may be described as the ratio of actual strength obtained at a certain level of twist to the maximum possible strength. The curve C is the optimization of these two active parameters. Both parameters are twist dependent. So, both strength and comfort are optimized by the twist. That's why this curve is called a strength–comfort characteristic curve. Estimation of yarn strength and prediction of yarn strength are two key factors that are addressed by yarn mechanics. Empirical methods may be employed to optimize yarn strength regarding processing parameters. But these empirical models are very limited to specific processing conditions. However, they may be modified by other processing methods. But still, they cannot be employed in generalized form to address all the processing conditions and methods.

References

1 Stout, H. and Harrison, P. (1988). *Fibre and Yarn Quality in Jute Spinning*. Textile Institute.
2 Kumar, S. and Gupta, V. (1978). A nonlinear viscoelastic model for textile fibers. *Textile Research Journal* 48 (7): 429–431.
3 Cai, Z. (1995). A nonlinear viscoelastic model for describing the deformation behavior of braided fiber seals. *Textile Research Journal* 65 (8): 461–470.
4 Jianchun, Z. (1999). The model of viscoplastoelastic behavior of tencel fibre. *Journal-Northwest Institute of Textile Science and Technology* 13 (4): 399–402.
5 Baltussen, J. and Northolt, M. (2004). The Eyring reduced time model for viscoelastic and yield deformation of polymer fibres. *Polymer* 45 (5): 1717–1728.
6 Hearle, J.W., P. Grosberg, and Backer, S. (1969). *Structural Mechanics of Fibers, Yarns, and Fabrics*. USA: Wiley-Interscience.
7 El Mogahzy, Y., Kilinc, F.S., and Hassan, M. (2005). Developments in measurement and evaluation of fabric hand. In: *Effect of Mechanical and Physical Properties on Fabric Hand* (ed. H. Behery), p. 45. Elsevier.
8 El-Mogahzy, Y. (2008). Structure and mechanics of yarns. In: *Structure and Mechanics of Textile Fibre Assemblies* (ed. Peter Schwartz), pp. 190–212. Cambridge: Woodhead Publishing Limited.

18

Textile Mechanics: Woven Fabrics

Adeel Zulifqar[1], *Zubair Khaliq*[2], *and Hong Hu*[1]

[1] *The Hong Kong Polytechnic University, Institute of Textile and clothing, Hung Hom, Kowloon, Hong Kong, China*
[2] *National Textile University, Faculty of Engineering and Technology, Faisalabad, Pakistan*

18.1 Introduction

Woven fabric is a textile material that is fabricated by interlacement of two sets of constituent orthogonal yarns called the warp (along length of fabric) and the weft (along width of fabric). The interlacement of warp and weft with each other results in an integrated and firm structure. The inter-yarn friction is responsible for holding the constituent yarns in place. The properties of the woven fabric depend greatly on the fabric structural constraints like weave, thread density per unit area, crimp, and linear densities of warp and weft yarns. The basic components of woven fabric are weave, yarns, and fibers. All these components together with post-fabrication treatments influence the ultimate fabric properties and mechanical behavior in real use. Therefore, in woven fabric (with desired mechanical behavior) manufacturing, selection of fibers with individual properties, arrangement of fibers in the yarn structure, and shaping the interlacements of warp and weft yarns in different fashions within the fabric are some vital factors to be considered. This gives the woven fabric engineer a great liberty to control and modify the woven fabric structure for desired mechanical behavior.

This section aims to describe woven fabric mechanics and factors in relation to the constituent yarns and fabric structure, which may affect the ultimate mechanical properties of woven fabrics. Factors including weave, crimp, weave factor, and structural geometry are discussed. The importance of woven fabric geometry in terms of mechanical behavior cannot be ignored; therefore, the geometries of woven fabric proposed by various fabric scientists are discussed. In order to develop a better understanding of woven fabric mechanics, different modeling approaches including Pierce's geometric model of woven fabric, numerical models, constitutive laws, energy methods, and modern modeling methodologies like computational mechanics are also included in the scope of this section.

Handbook of Fibrous Materials, First Edition. Edited by Jinlian Hu, Bipin Kumar, and Jing Lu.
© 2020 Wiley-VCH Verlag GmbH & Co. KGaA. Published 2020 by Wiley-VCH Verlag GmbH & Co. KGaA.

18.1.1 Woven Fabric Structures

The structural unit or weave of a fabric is termed as repeating unit, and it is the interlacement of warp and weft in a predefined regular or irregular configuration. The repeating unit contains the smallest number of different interlacements between warp and weft, which, when repeated in either direction, gives the fabric structure. It is usually presented by a grid of squares in which horizontal and vertical lines depict the weft and warp yarns, respectively. Each square shows the interlacement point of warp and weft. The filled square means that the warp yarn is over the weft yarn, while blank means that weft is over the warp at the corresponding place in the fabric. The weave of the fabric influences greatly the properties of fabric including its mechanical behavior in response to tensile loads [1].

18.1.1.1 Regular Woven Structures (Basic Weaves)

The warp and weft yarns intersect/interlace in same manner, and the interlacement pattern of consecutive warp and weft yarns relative to each other is displaced in equal steps in one repeat. The basic regular weaves including plain, twill, satin, and sateen are explained briefly in the following sections [2].

Plain Weave The most frequently used and simplest weave is the plain weave. It is the most rigid and stronger network of warp and weft yarns owing to the fact that it has maximum number of possible interlacements of warp and weft. It is usually written as 1/1, which means that warp yarn runs over and under the weft yarn in alternate fashion. The numerator represents number of weft yarn under warp yarn, while the denominator represents number of weft yarns over warp yarns. The repeat is the sum of two numbers ($1 + 1 = 2$), which states that after every two warp yarns or weft yarns, the interlacement pattern is repeated as shown in Figure 18.1a.

Twill Weaves Twill weaves are described by continuous diagonal lines created by the interlacements of warp and weft yarns. Twill weaves are less rigid than plain weaves with same thread density per unit area owing to the fact that they have less number of interlacements per repeating unit. The smallest number of threads that can be used to construct twill is three. It is written as 2/1 (which means that the warp yarn runs over two weft yarns and under one weft yarn in diagonal fashion and that it is warp-faced twill) or 1/2 (which means that the warp yarn runs over one weft yarn and under two weft yarns in diagonal fashion and that it is weft

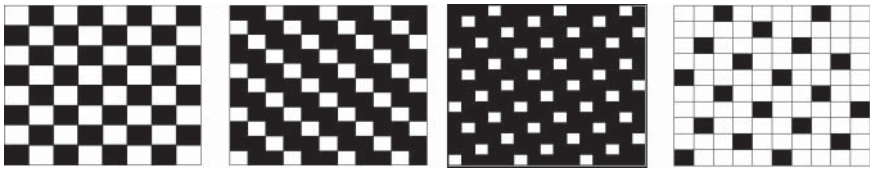


Figure 18.1 Unit cells of regular weaves. (a) Plain, (b) twill, (c) satin, and (d) sateen.

faced twill). The repeat is $1 + 2 = 2 + 1 = 3$. Therefore, after every three warp yarn or weft yarns, the interlacement patterns are repeated. The direction of diagonal can be up to the right (Z twill) or up to the left (S twill) depending upon the starting point of twill as shown in Figure 18.1b.

Warp and Weft Satins In satin or sateen weaves, the interlacement points of warp and weft yarns are distributed such as they are never adjacent. The smallest number of threads that can be used to create a satin or sateen is five. A warp satin is warp faced written as 4/1 as shown in Figure 18.1c, while a weft satin (also termed as sateen) is weft faced written as 1/4 as shown in Figure 18.1d. Warp satins are usually created by higher number of warp yarns than weft yarns. Although an infinite number of interlacements are possible, but five 4/1 and eight 7/1, end satin weaves are most common.

18.1.1.2 Irregular Woven Structures

Unlike regular or basic weaves, the warp and weft yarns interlacements in irregular weaves are not in same manner, and the interlacement pattern of consecutive warp and weft yarns relative to each other is not displaced in equal steps in one repeat as shown in Figure 18.2 [3].

18.1.2 Weave Factor

Weave factor is a number that accounts for the number of interlacements of warp and weft in a given repeat [3, 4]. It is also equal to average float and is expressed as in Eq. (18.1):

$$M = \frac{E}{I} \tag{18.1}$$

where M is the weave factor, E is number of threads per repeat, and I is number of intersections per repeat. The weave interlacing patterns of warp and weft yarns may be different. In such cases, weave factors are calculated separately with suffix 1 and 2 for warp and weft, respectively. Therefore,

$M_1 = \frac{E_1}{I_2} E_1$ and I_2 can be found by observing individual weft pick in a repeat, and

$M_2 = \frac{E_2}{I_1} E_2$ and I_1 can be found by observing individual warp end in a repeat.

As in the case of irregular weaves, the number of intersections of each thread in the weave repeat is not equal. In such cases the weave factor is obtained as in



Figure 18.2 Unit cell of some irregular weaves. Source: Behera et al. 2012 [3]. https://www.intechopen.com/books/woven-fabrics/modeling-of-woven-fabrics-geometry-and-properties. Licensed under CCBY 3.0.

Eq. (18.2):

$$M = \frac{\sum E}{\sum I} \tag{18.2}$$

18.1.3 The Myth of Crimp

Crimp is the waviness in the yarn produced due to the interlacement of warp and weft yarns. The amount of crimp is a result of various factors that include the tension in the warp yarn, linear densities of warp and weft yarns, type of fibers in warp and weft yarn, twist level in both yarns, and the weave. The crimp is calculated by Eq. (18.3):

$$C = ((L_e - L_s)/L_s) \times 100 \tag{18.3}$$

where L_s is the length of yarn removed from the fabric sample and L_e is the extended length of the removed yarn. The crimp is expressed as percentage of sample length of yarn [4], generally, the warp faced.

18.2 Woven Fabrics Geometrical Models

The geometric structure of a woven fabric is extremely complicated and differentiates greatly from a continuum structure such as a metal sheet. The yarns in a woven fabric are crimped at the interlacement point with irregular cross-sectional shapes and having frictional contact with each other. The porosity of fabric depends upon the distance between two parallel adjacent yarns. The simplest theoretical model of yarn configuration is developed by Peirce in 1937, but in actual scenario the model contradicts with reality because in the theoretical study, the cross-sectional shape and physical properties of a yarn are always simplified and idealized. Peirce studied the shape taken up by the warp and weft yarn in a woven fabric and proposed a geometrical model [5]. The mathematical relations derived from the Peirce's geometrical model and physical characteristics of yarn can be used to understand woven fabric behavior under various conditions. The Peirce's geometrical model is shown in Figure 18.3. It exemplifies a unit cell of a plain woven fabric and satisfies to some degree loom state of the fabric. Peirce considered that the yarns as inextensible and flexible

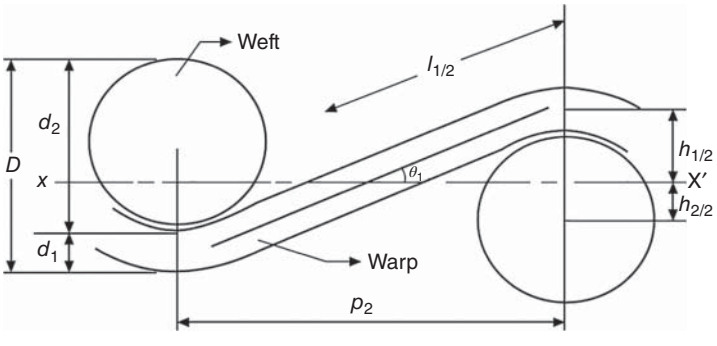


Figure 18.3 Geometrical model of plain woven fabric. Source: Peirce 1937 [5]. Reproduced with permission from Taylor & Francis.

having a circular cross section consisting of straight and curved segments. This simple geometrical model helps to study the relationship between various geometrical parameters. The parameters that can be studied by using Peirce's geometrical model of a plain woven fabric includes resistance of the fabric to mechanical deformation (initial extension, bending, and shear in terms of the resistance to deformation of individual fibers), relative resistance of the fabric to the passage of air, water or light, and maximum yarn packing density possible in the fabric. The geometrical parameters of a unit cell of plain woven fabric Peirce studied are as follows:

c = crimp
h = crimp height (maximum displacement of thread axis normal to the plane of fabric)
q = weave angle in radians (angle of thread axis to the plane of fabric)
d = diameter of thread, fabric thickness, and
p = thread spacing and derived a set of equations
l = modular length (length of thread axis between the planes through the axes of consecutive cross-threads)

$$D = d_1 + d_2$$

The suffixes 1 and 2 represent warp and weft threads, respectively. The estimation of yarn axis parallel and normal to the fabric plane provides the following equations:

$$c_1 - \frac{l_1}{p_2} - 1 \tag{18.4}$$

$$p_2 = (l_1 - Dq_1)\cos\ q_1 + D\sin\ q_1 \tag{18.5}$$

$$h_1 = (l_1 - Dq_1)\sin\ q_1 + D(1 - \cos\ q_1) \tag{18.6}$$

Three similar equations are obtained for the weft direction by interchanging suffixes 1 and 2 or vice versa as follows:

$$c_2 - \frac{l_2}{p_1} - 1 \tag{18.7}$$

$$p_1 = (l_2 - Dq_2)\cos\ q_2 + D\sin\ q_2 \tag{18.8}$$

$$h_2 = (l_2 - Dq_2)\sin\ q_2 + D(1 - \cos\ q_2) \tag{18.9}$$

$$d_1 + d_2 = h_1 + h_2 = D \tag{18.10}$$

The above equations provide relationship between eleven variables. If any four variables are known, then the equations can be solved for unknown variables [5].

Whereas the assumption of a circular thread cross section is mostly valid in the case of very open structures, due to the inter-yarn pressures that are set up during weaving process especially in the case of tightly woven fabrics, there might be yarn flattening normal to the plane of the fabric. Peirce took this into consideration and assumed the possibility of fabric geometry based on elliptical sections as shown in Figure 18.4, by replacing the circular thread diameter by the minor diameter of the appropriate elliptical section. This approximate treatment was

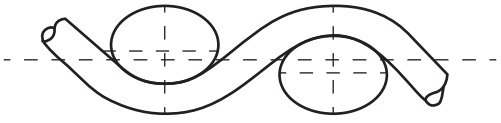


Figure 18.4 Elliptical cross section. Source: Peirce 1937 [5]. Reproduced with permission from Taylor & Francis.

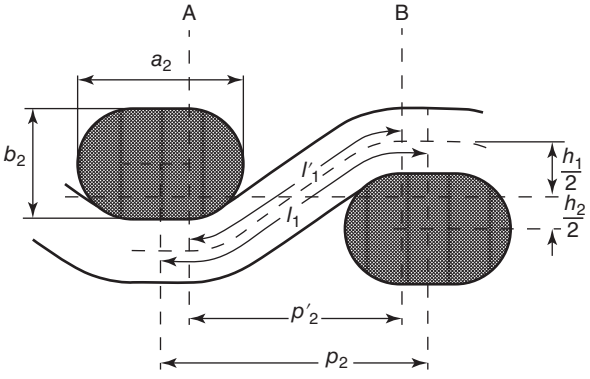


Figure 18.5 Kemp's racetrack cross section. Source: Kemp 1958 [6]. Reproduced with permission from Taylor & Francis.

still invalid for tightly woven fabrics, but this model is practically valid for fabrics after dry and wet relaxation treatments. To overcome this difficulty, Kemp proposed new fabric geometry by considering yarn cross-sectional shape as racetrack section [6], which encloses a rectangle between semicircular ends as shown in Figure 18.5. This allowed the application of simple relations of circular thread geometry for the treatment of flattened thread. Generally speaking, the racetrack model is reasonably valid for pressed and calendared fabrics. Further, Hamilton used Kemp's racetrack approach of the plain woven fabrics for other weaves [7]. Olofsson and Grosberg considered yarn geometry as a function of external and reaction forces in the fabric and assumed a relation between the curvature of the yarn in the fabric and in the released state [8, 9]. Dorkin et al. developed a simpler model by assuming that the path of the yarn is made up of two equal circular arcs [10]. It has been found that the yarn shapes within the woven fabric is influenced by the weaving force, the warp and weft setts, and the finishing conditions [11–13].

According to the study of woven fabric geometrical models, it can be concluded that Peirce's flexible model, Peirce's elliptical model, and Kemp's racetrack model are true representative of the actual fabric structure.

18.3 Woven Fabric Mechanics, Theories, and Methodologies

Woven fabric mechanics gained interest of researchers in 1912 when development of airships was under focus of engineers and scientists. In 1937, Peirce first established the geometrical model of plain weave structure [5]. Other researchers contributed toward the further advancement in the area [8, 9, 14–21]. Up till today, the researchers adopted three different approaches to carry out studies in this area. Firstly, the component-oriented approach to

predict the mechanical behavior of woven fabrics directed by Hearle, Grosberg, and Postle. They have studied the physical theories together with yarn properties, inter-yarn interactions, and fabric structures on the basis of Newton's third law, minimum energy principles, and mathematical analysis of construction. Secondly, the phenomenon-oriented approach that involves the behavior of woven fabrics in response to external loads including elastic, plastic, viscoelastic, and frictional aspects. Thirdly, the result-oriented approach that involves a hypothesis, a function, and a statement to describe the results and then finding a relationship of the function with fabric behavior. Theoretically, this approach involves pure mathematics and statistics; therefore, the wrong assumptions can be avoided. Woven fabrics possess complexity in terms of geometrical configuration of interlaced constituent yarns; this is the major difficulty of computational modeling of woven fabrics. The tensile deformation of a woven fabric is obviously related to that of constituent yarns, which is the combination of bending, tensile, compression, and also the intrafiber frictional sliding. In order to simplify the modeling, some assumptions must be made, for example, it is assumed that the yarn is an elastic homogeneous material and would exhibit a viscoelastic behavior. Therefore, the elastic property of homogeneous yarn could be either linear or nonlinear. To study the mechanics of woven fabric structure, it is essential to include the contacts of warp and weft yarns with each other in the modeling because the frictional contact of both at cross over point greatly influences the stress and strain relationship for a woven fabric, and during frictional contact the force would be transferred from one yarn to the contacting and adjacent yarn [22].

18.3.1 Tensile Deformation of Woven Fabrics

Unlike traditional engineering materials (TEMs), woven fabrics are inhomogeneous, discrete, and anisotropic. They can undergo large strains even at low stresses and can easily be deformed into shapes with double curvatures through buckling [14, 15]. The study of woven fabric tensile behavior reveals that small tensile forces produce fairly large membrane strain as shown in Figure 18.6a. The reason for this large deformability might be the straightening of the crimped constituent yarns within the fabric. The initial tensile modulus of a typical woven fabric is observed to be of the order of 10 MPa, compared with elastic modulus of steel, i.e. of 2×10^5 MPa. The woven fabrics under transverse loading are more prone to bending deformations in contrast to tensile deformation as sown by Figure 18.6b. Unlike stiff materials, the large deformations cannot be neglected in the engineering of woven fabrics. Woven fabrics are prone to move through these large deformations and buckle even at very small compressive stresses within fabric plane under its own weight and/or external forces. TEMs undergoes small strains at low stresses, and the stress and strain relationship is linear, but for woven fabrics this relationship is nonlinear at low stresses and becomes almost linear beyond a critical value of stress. This critical value is higher in the case of tensile loading and almost zero in other modes of loading like shear and bending. This behavior of woven fabrics could be explained by the fact that under tensile loading or tension, the crimped yarns get straight at

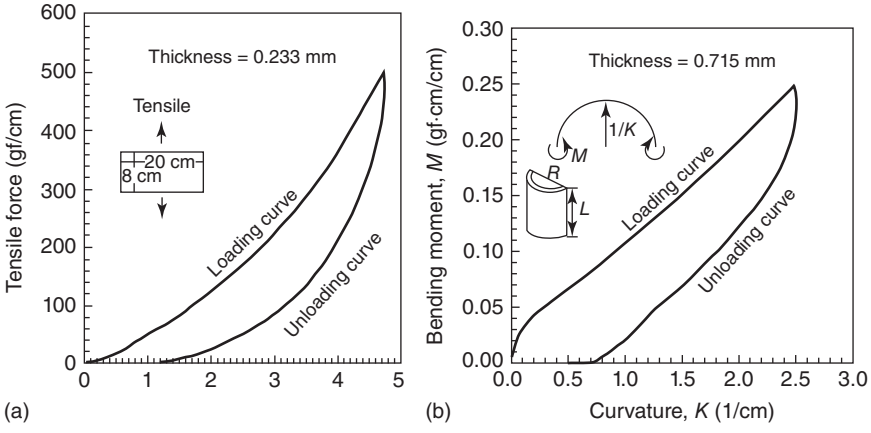


Figure 18.6 (a) Tensile stress–strain curve of a woven fabric. (b) Moment–curvature curve of a woven fabric. Source: Hu 2004 [22]. Reproduced with permission from Elsevier.

low stresses, and when they became fully straight at high stresses, the interfiber friction is increased.

At this stage, the fabric is more consolidated, and the fibers are in better orientation than before resulting in a linear relationship of stress and strain. The nonlinearity occurs at intermediary stage of fabric consolidation. An interesting observation from this explanation for tensile behavior of woven fabrics can be made in the case of TEMs when the applied stress increases the microstructure moves toward disorder. Conversely, in the case of woven fabrics, the applied stresses bring about order in the microstructure as the fiber orientation is improved [22].

18.3.1.1 Woven Fabric Behavior When Extended in Principal Directions

When a plain woven fabric is extended in principal direction (either along warp or weft direction), the crimped yarns will get straight along the direction of applied force. At this stage, the yarn amplitude and the weave angle will decrease as the contact between warp and weft yarn increases, and they tend to become more circular [19]. Furthermore, the crimp interchange will take place at the interlacement point, increasing the crimp in one set of yarns while decreasing in the other. Further extension of fabric is followed by yarn extension with decrimping and fiber extension within the yarn at the interlacement point, but the yarn extension is relatively small as compared with total extension. The movement of fiber restricts the development of high strains. During this process some energy loss will also occur due to interfiber friction. De Jong and Postle reported that the following six independent dimensionless parameters must be considered in order to study uniaxial tensile properties for a balanced plain woven fabric produced from identical warp and weft yarns [16]. The parameters include (i) the ratio of warp to weft yarn length per crossing yarn, (ii) the ratio of yarn diameter to yarn modular length, (iii) the ratio of yarn compression rigidity to bending rigidity, (iv) the yarn compression index, (v) the ratio of yarn extension rigidity to bending rigidity, and (vi) the degree of set. They also stated that the fabric extension can be explained by yarn extension when the ratio of yarn compression rigidity to bending rigidity is

lower. Furthermore, the Poisson's ratios can also be explained; during extension the inter-yarn distance will increase, and yarns tend to become more circular. Conversely, a higher magnitude of tensile properties will result when fabric is extended in the bias directions than in the warp and weft directions.

18.3.1.2 Woven Fabric Behavior When Extended in Bias Direction

When a woven fabric is extended in a bias direction as shown in Figure 18.7, the maximum elongation will occur along the direction of applied force and with a deviation in the direction ($\theta_1 > \theta_2$). The magnitude of strain will be associated with the deviation of the angle to the warp direction. The maximum change in length will be associated with the diagonal direction, i.e. ($\pm 45°$) resulting in maximum elongation along one diagonal direction with maximum contraction along other diagonal direction. When extended in bias direction, there will be very little tension in the yarns, and due to frictional forces at interlacement points, some tension will also exist between two adjacent interlacements and a bending couple, which is responsible for deforming the interlaced yarns. When a fabric is extended in bias direction, it must be taken into account whether both ends of the warp or weft yarns are clamped for extension in respective directions or only one end is clamped from $\pm 15°$ to $\pm 75°$ bias direction to the warp direction or both ends of the yarn are free for extension [23].

18.3.1.3 Effect of Yarn Crimp and Yarn Friction Coefficient on Fabric Mechanical Properties

The crimp in warp and weft yarns greatly influences the fabric behavior under tensile loads. As higher crimp is usually obtained in the warp yarns, the values of tensile properties in the warp direction are comparatively higher than those in the weft direction. In the fabrics with warp-faced plain weave, the weft yarn lies near to straight, and warp is bent resulting in high warp crimp and ultimately higher shrinkage in warp direction. On the other hand, in the fabrics with weft-faced plain weave, the weft yarns have higher crimp than the warp. Therefore, it is evident that increasing crimp in one direction of the fabric reduces it in the direction. This phenomenon is known as crimp imbalance [12]. When a woven fabric is

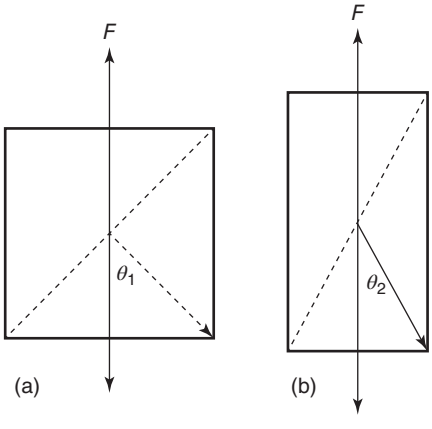


Figure 18.7 Extension in bias direction arrows inside square indicates warp direction. (a) Initial position before extension. (b) Final position after extension. Source: Hu 2004 [22]. Reproduced with permission from Elsevier.

subjected to uniaxial tensile load, the crimp decreases in the direction of applied load while increases in the cross direction. This phenomenon can be explained as when the applied load in the tensile direction is increased, the yarns in the loading direction get more straight, and the diameter of the yarns decreases (consolidation), resulting in more circular cross section. Conversely, the yarns in the cross direction gets more flatten, and the amount of crimp increases to maximum. This phenomenon is responsible for the initial low-resistance portion of the stress strain curve of a woven fabric. Therefore, fabric elongation at break depends on the amount of crimp in the constituent yarns. When the load is applied biaxially, the load buildup will occur in one direction before the other. The yarns in two directions undergo consolidation, i.e. they tend to move toward more circular cross section and take the position of maximum crimp [19]. Realff, with the help of series of fabric cross-sectional images taken at various strain levels, reported [24] that yarn consolidation (diameter decrease), yarn flattening, yarn bending, and fabric shearing are potentially important factors that influence the fabric deformation and failure. It was further reported that the shearing behavior of the fabric depends on the yarn frictional properties and normal forces at the yarn interlacement points, and the yarns with higher friction coefficient will undergo less shearing.

18.3.1.4 Anisotropy of Woven Fabric Tensile Properties

Hearle et al. reported that the tensile performance of a woven fabric is an integration of a multidirectional effect, which means that the woven fabric tensile properties are influenced by loading direction [25, 26]. For example, when a woven fabric is subjected to bias extension, shear deformation will occur and influence the tensile behavior of the fabric, and the tensile behavior of the fabric will be different from the behavior of the fabric, when it is extended in the warp and weft directions. They named this phenomenon the "anisotropy" of tensile properties of woven fabrics. They have studied all the four parameters measured on Kawabata Evaluation System of Fabric (KES-F), including tensile work (WT), tensile elongation (EMT), tensile linearity (LT), and tensile resilience (RT) based on Kilby's Young's Modulus model [27].

Tensile Work (WT) In order to describe the stress strain curve of a woven fabric, an exponential function with two parameters can be written as

$$f = \frac{e^{\alpha\varepsilon} - 1}{\beta} + e_r \tag{18.11}$$

where f is stress, ε is strain, α and β are unknown parameters, and e_r is the error term. The f and ε can be obtained from tensile stress strain curves of the fabric tested on the KES system. The unknown parameters α and β can be estimated by using a nonlinear regression technique using data obtained from the curves of woven fabrics. WT is a parameter to calculate the amount of work done during tensile loading process. It is also termed as tensile energy and can be from Eq. (18.12)

$$\mathrm{WT} = \frac{E}{\alpha^2} - \left[\frac{\ln(\beta F_m + 1) + 1}{\alpha\beta}\right] \tag{18.12}$$

WT depends upon several factors that contribute to the amount of energy loss, including the ratio of the yarn counts in the warp and weft yarns, the ratio of the yarn spacing, the average yarn spacing, the type of weaves, the direction of force applied to the fabrics, and frictional force between the interlacement points of the warp and weft yarns. The experimental data of WT indicates that for plain woven fabrics, the WT is higher than twill and satin woven fabrics. As the ratio of yarn spacing and the average yarn spacing of plain woven fabrics is comparatively smaller than those of twill and satin woven fabrics, also greater energy is needed to overcome the frictional forces at the interlacement points of the warp and weft yarns. Therefore, higher energy intake occurs in the extension of plain woven fabric in bias directions. In contrast with this, lower yarn crimp is exhibited in the looser weave construction of twill and satin woven fabrics, especially in the weft direction This also explains why the tensile work in the weft direction is found to be higher than that in the warp direction [22].

Tensile Elongation (EMT) EMT is the measure of the extensibility of a fabric. It explains a fabric's ability to be stretched under tensile load. The higher EMT value means the fabric is more extensible. Kilby [27] established the model for the prediction of Young's modulus in any direction other than the warp and weft directions. EMT can be obtained by following Eq. (18.13) [22]:

$$\mathrm{EMT}_{\theta} = \mathrm{EMT}_1 \cos^4\theta + \frac{\cos^2\theta \sin^2\theta}{G'} + \mathrm{EMT}_2 \ \sin^4\theta \tag{18.13}$$

Linearity (LT) LT is the measure of the degree of nonlinearity of the tensile stress–strain curve. It depends on the ratio between WT and EMT from the stress–strain curve. The model of LT can thus be given as follows [22]:

$$\mathrm{LT}_{\theta} = \frac{\mathrm{WT}_{\theta}}{\text{Constant } t^* \mathrm{EMT}_{\theta}} \tag{18.14}$$

Tensile Resilience (RT) RT is the ratio of work recovered to the work done in tensile deformation, and it is expressed as a percentage. Work recovered is the tensile force at the recovery process, while tensile deformation is obtained by the area under the stress–strain curve during loading process. Therefore RT of woven fabrics can be obtained by Eq. (18.15) [22]:

$$\mathrm{RT} = \frac{\mathrm{WT}'}{\mathrm{WT}} \times 100\% \tag{18.15}$$

18.3.2 Compression Deformation of Woven Fabrics

The response of a woven fabric to applied forces normal to its plane is known as fabric compressional behavior. A change in cross-sectional area of yarn occurs when a fabric is under compressive load. This change affects the void ratio, which has a profound effect on the mechanical properties of the fabric. Pierce's geometrical model assumes that yarn cross section in a woven fabric is circular or elliptical. The yarn cross-sectional areas under different loading conditions can be calculated by assuming a lenticular model. The Kemp's racetrack model or

lenticular cross-sectional model is more suitable for fabrics made up of filament yarns under compressive loading.

When a woven fabric is under compression, two major changes occur: (i) Warp and weft yarns are compressed, and (ii) the less crimped yarn system increases its crimp and vice versa due to additional bending forces resulting from interaction of more crimped parts of the yarn with compression surface. This change of crimp in the yarn systems results in reduction of fabric thickness. Figure 18.8 shows a typical compression curve recorded on the KES system. It can be observed from the curve that relationship between pressure and thickness under a pressure larger than 20 gf/cm^2 is very close to linear.

This part of curve also has a very steep slope, which shows that woven fabrics are really incompressible. Therefore, the shape of the curve is largely governed by pressure in the range from 0 to 20 gf/cm^2. The values of t_m and WC provided by the KES system are not very reliable for predicting the whole curve because they do not usually match the data read off the curves. In order to examine the mechanics of woven fabric compression, De Jong et al. [35] considered the woven fabric as a three-layer structure as shown in Figure 18.9. They considered that there is an incompressible core layer in contact with more compressible surface layers that consists of protruding fibers on both sides of the fabric as shown in Figure 18.9. These two compressible surface layers follow Van Wyk's law that is actually the relationship of applied compressive load and thickness of the fabric. They developed the equation as the following:

$$P = \frac{\lambda}{(t - t')^3}$$

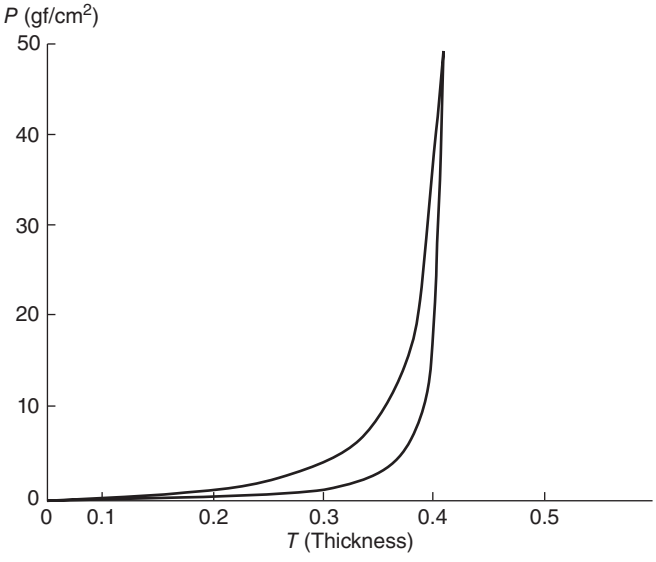


Figure 18.8 Typical compression (pressure–thickness) curve of woven fabrics.

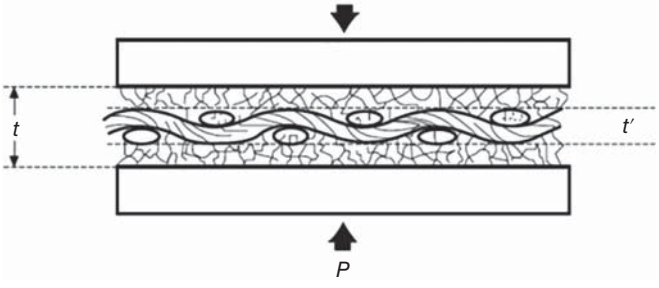


Figure 18.9 The proposed model of a woven fabric under lateral compression.

where P = compressive load, λ = a constant of proportionality, t = thickness of fabric at zero load, and t' = thickness of the incompressible core or limiting thickness. The value of t' and λ can be obtained by the following equations:

$$t' = t_m \frac{2E}{P}, \lambda = \frac{8E^3}{P^2}$$

where E = energy absorbed by the fabric with pressure between 0 and 50 gf/cm^2 and equals to WC that can be obtained by KES system.

They have applied this equation to wool fabrics. Wool fabric is very different from cotton fabric in structure, and cotton fabrics have very few protruding fibers on their surface than wool. The applicability of the above equation to cotton fabric was tested by Jinlian Hu [22]. Nonlinear regression method was used to improve the fitting of the compression curve of cotton fabric obtained by KES; also a five-layer structure is suggested as shown in Figure 18.10. The thickness of fabric t at zero compressive load can also be regarded as the geometrical thickness and can be calculated from measured geometrical parameters, i.e. crimp height and minor diameter of yarn. The mechanical thicknesses of fabric T_0 at 0.5 gf/cm^2 pressure and T_m at 50 gf/cm^2 can be obtained from the KES system. The limiting thickness t' can be obtained from above equation.

The geometrical thickness of all woven fabrics lies between T_0 and T_m, or T_0 and t'. The geometrical thickness is actually much smaller than T_0. This is beyond expectation because the geometrical thickness was measured principally under zero pressure, but T_0 was measured under a pressure of 0.5 gf/cm^2. Therefore,

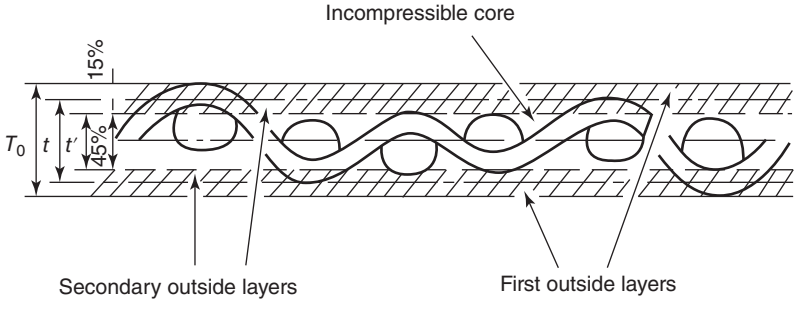


Figure 18.10 Five-layer structure of woven fabrics.

theoretically, T_0 should be smaller than the geometrical thickness t. This phenomenon can possibly be explained by the fact that during the measurement of the geometrical parameters, crimp height h, and minor diameter b, the protruding fibers of the yarn surface were ignored. Therefore, the geometrical thickness ignores hairs on the yarn surface and the crimp crowns above the average thickness. Conversely, the KES compression tester cannot ignore it and can sense anything including the hairs and the crimp crowns above the average height of woven fabrics. Therefore, the actual structure of woven fabrics can be considered as a five-layer structure. The outer layers on both sides of the fabric contain hairy fibers and crowns above the average geometrical thickness and retain about 40% of the whole fabric thickness. The secondary layers on both sides of the fabric represent another two compressible layers that form the firm structure of the fabric and retain about 20% of the whole fabric thickness. The t' represents the incompressible core of a fabric and retains about 40% of the whole fabric thickness, which confirms that fabrics are highly incompressible. The outer layers and secondary layers of this structure obey Van Wyk's law [22].

18.3.3 Shearing Deformation of Woven Fabrics

When a woven fabric is subjected to shear deformed at lower strains, the initial shear stiffness is large as shown in the OA region of the typical shear stress–strain curve in Figure 18.11. Initially, the frictional forces at the interlacement points are higher, and the incremental stiffness is decreased due to the progressive movement of the frictional elements. When the stress overcomes the smallest frictional forces at the crossover points of warp and weft, the yarns start to slip at crossover points, and incremental shear stiffness decreases as shown in the AB region of the curve. The point B in the curve represents the minimum value of incremental stiffness corresponding to a particular value of stress. Beyond this point, the incremental stiffness is linear and controlled by the deformation of the purported

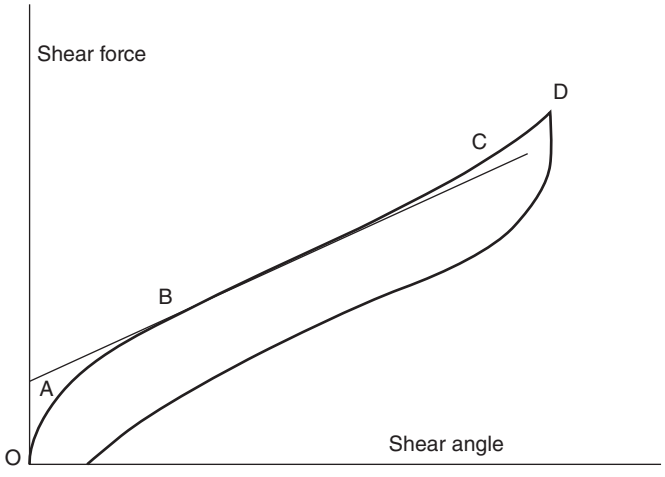


Figure 18.11 Stress–strain curve of woven fabrics during shear deformation.

elastic elements in the fabric. The increase in shear stiffness is observed above a low level of shear strains (5–10°). At stress levels higher than a certain amount, the incremental stiffness again increases, and the closed curve becomes wider as the shear angle increases. This is caused by the steric hindrance between the warp and weft yarns, which results in transverse distortion of yarns or dislocation of the crossover. Two important parameters are responsible for controlling the extent of nonlinear region of the curve. One is the point where the slope reaches its minimum value, which is attributed by the elastic elements in the fabric structure, and at this point it is assumed that the frictional contact points are in motion or dislocated, and the other is the region where stiffness decreases, which can be used to determine the hysteresis loss. The shear stiffness is also influenced by the direction of shearing force and fabric cover factor. In the case of square fabrics, those with similar yarns in warp and weft direction and similar cover factor, the shear stiffness is higher in the warp direction and also higher for the large cover factor. The hardening in the warp direction has little influence on the fabric shear properties but more on bending properties. This can be explained by the fact of jamming due to friction at crossover points in warp direction in the case of fabrics with high cover factor, but the jamming effect is less influential in the case of fabrics with low cover factor or similar cover factor in both warp and weft directions. The friction in the case of shear deformation exists mainly at the crossover of the two yarns, but interfiber friction within a yarn occurs in the case of bending deformation. The interfiber friction in the case of shear deformation is less important than in the case of bending deformation. Therefore, the hardening of warp yarns of woven fabrics, which affects the internal friction, has less effect on shear behavior [22].

18.4 Mathematical Modeling of Woven Fabric Constitutive Laws

A mathematical model is based on a large number of assumptions. However, remarkable work is done in this area, but most of the work is of theoretical nature and not sufficient to deal with problems of real fabric. Up till today three kinds of modeling techniques including predictive, descriptive, and fitting or numerical models are established by textile scientists [22]. The predictive models developed by Hearle et al. [19], Postle et al. [28] are based on consideration of the most important factors, and the effect of others is shown by some assumptions. The number of assumption for this kind of modeling is high, and it involves too much mathematics. A detailed study of the mechanisms of fabric deformation is therefore possible, yielding relationships between the structural parameters of a woven fabric and its important mechanical properties. The descriptive models developed by Paipetis [29] on the other hand are largely empirical and reflect the need for simple mathematical relations, expressing the phenomenological behavior of a fabric from the point of view of a particular property. However, such models completely ignore the physics of the material, need adjustment to reality through a number of experimental values, and operate within a specific range of the relevant parameters only. Still, they are undoubtedly useful, if no rigorous models

are available. The fitting or numerical models are based on statistical considerations. Such models emphasize on numerical relationship of two variables such as stress and strain relation, ignoring the exact mechanism. This method needs fewer assumptions and provides an approach that is more relevant to real situations. There exist various methods for fitting a curve in many industrial or science fields. Constitutive laws are often estimated by using a polynomial, which contains the appropriate variables and approximates to the true function over some limited range of the variables involved. Spline, especially the cubic spline interpolation method, is also widely used for this purpose [22].

18.4.1 Constitutive Laws of Woven Fabric

The complex mechanical behavior of a woven fabric can be explored by basic frame of the infinitesimal elastic theory of a sheet. In the most general case, the stress–strain relationships, or constitutive laws, of a linearly elastic plate (an initially flat) sheet are as follows in Eqs. (18.16) and (18.17), where T_1 and T_2 are the tensile stresses, ε_1 and ε_2 are the tensile strains, T_{12} and ε_{12} are the shear stress and shear strain in the fabric plane, M_1 and M_2 are the bending stresses, K_1 and K_2 are the bending curvatures, M_{12} and K_{12} are twisting stress and strain, and the submatrices A_{ij} and D_{ij} represent the membrane and bending (and twisting) stiffness, respectively:

$$\begin{Bmatrix} T_1 \\ T_2 \\ T_{12} \\ M_1 \\ M_2 \\ M_{12} \end{Bmatrix} = \begin{bmatrix} A_{11} & A_{12} & A_{13} & B_{14} & B_{15} & B_{16} \\ & A_{22} & A_{23} & B_{24} & B_{25} & B_{26} \\ & & A_{33} & B_{34} & B_{35} & B_{36} \\ & & & D_{44} & D_{45} & D_{46} \\ & & & & D_{55} & D_{56} \\ & & & & & D_{66} \end{bmatrix} \begin{Bmatrix} \varepsilon_1 \\ \varepsilon_2 \\ \varepsilon_{12} \\ K_1 \\ K_2 \\ K_{12} \end{Bmatrix} \tag{18.16}$$

Total elements = 21

$$[\sigma] = [S][\varepsilon] \tag{18.17}$$

The B_{ij} is coupling stiffness that connects the membrane and bending modes of deformation. $[\sigma]$ is the stress matrix, $[S]$ the stiffness matrix, and $[\varepsilon]$ the strain matrix. Therefore, in order to specify the elastic behavior of an originally flat sheet, a total of 21 stiffnesses (6 for membrane deformations, 6 for bending and twisting, and 9 for coupling between the two modes) are required. For orthotropic fabric where directions 1 and 2 are assumed to coincide with the principal directions of orthotropy, i.e. the warp and weft directions, 13 stiffnesses are required. When the coupling matrix is symmetric, 12 stiffnesses are required. For symmetric fabric 8 stiffnesses, for square fabric (with the same yarns in each direction) 6 stiffnesses, for an isotropic sheet with bending behavior unrelated to planar behavior 4 stiffnesses, and for an isotropic solid sheet 2 stiffnesses plus the thickness are required. If the relationship is nonlinear, many of the interaction terms would reappear. The tangential elasticity matrix given in Eq. (18.18) can be used

in continuum analysis for nonlinear material properties, provided that the form of nonlinear stress–strain laws is already known. If the initial stresses are 0 at zero displacement, then the nonlinearities can be contained in $[\sigma_0]$ and used to apply the necessary corrections. This is known as the initial stress method in such analysis as finite element methods [22]:

$$[S_T] = \frac{d[\sigma]}{d[\varepsilon]} \tag{18.18}$$

18.4.2 Computational Woven Fabric Mechanics

Computational fabric mechanics deals with the challenging numerical problems with the help of an intelligent CAD system. Hearle et al. initiated the use of computer programs to approach woven fabric mechanics problems [30]. One of the significant algorithms used in computational techniques is the finite element method to predict the behavior of a fabric under certain loading conditions.

18.4.2.1 Continuum Models

Continuum models assume woven fabric as a continuum regardless of its discrete microstructure. Previously developed mathematical methods (numerical solutions) of continuum mechanics are applied to the fabric deformation problem. Finite element method is one such example of continuum technique; in this method the fabric is divided into numerous small areas called the finite elements. The fabric is then modeled using flat or curved shell elements in order to consider both bending and stretching. So far this method has only been able to study simple draping behavior of fabric by nonlinear finite element analysis considering the fabric as two-dimensional orthotropic sheets with both bending and membrane stiffnesses. The nonlinear stress–strain relationships on fabric deformations are an area that is still unaddressed by this method due to absence of unambiguous nonlinear constitutive equations of woven fabrics. Recently, Hu and Newton established a whole set of nonlinear constitutive equations for woven fabrics under tension, bending, shear, and lateral compression [31, 32]. Use of these equations in finite element method will further improve predictability of nonlinear stress–strain relationships during fabric deformations [22].

18.4.2.2 Discontinuum Models

Unlike continuum models, the discontinuum models consider fabric as discrete assembly of their constituent yarns. The mechanical responses of fabrics are predicted by combining yarn properties, inter-yarn interactions, and fabric structures. By considering the yarns as curved or straight rod elements with frictional connections at the interlacement points between the warp and weft yarns, the finite element method can be further extended to study fabrics using discontinuum models. A discontinuum model is useful in predicting fabric mechanical properties from yarn properties, because only a small patch of cloth needs to be modeled. Therefore, a discontinuum model is useful for modeling of fabric deformations before they are actually manufactured but has limitations in predicting complex fabric deformations due to the prohibitive number of yarns present [22].

18.4.3 Energy Methods for Woven Fabric Mechanics

Hearle et al. described an energy-based approach for development of CAD in order to deal with fabric mechanics [33]. They have introduced appropriate energy terms to deal with yarn extension, bending, flattening, and frictional forces at interlacement points in a woven fabric:

$$U = -(F_1 x_1 + F_2 x_2) \tag{18.19}$$

where F_1 *and* F_2 are the forces in the warp and weft directions and x_1 *and* x_2 are the lengths of the unit cell in corresponding directions. The principle of energy minimization will lead to Eq. (18.20) [34]:

$$\frac{F_1}{F_2} = -\frac{dx_2}{dx_1} \tag{18.20}$$

This equation can be applied to any fabric model; in some suitable circumstances it may be useful to study the state of crimp interchange in the fabric. They not only have studied the elastic response of plain woven fabrics but also suggested the methods to deal with other weaves. According to their study, when fabric is under deformation, interfiber and intrafiber energy changes may occur and are associated with yarn deformations and displacements and can be expressed as

$$U = -\sum(F_x) + \sum(U_y) \tag{18.21}$$

where F *and* x may include other directions like shear and bending or biaxial directions and the sign convention shows the reduction in potential energy of the applied forces due to increase in strain energy. If the fabric is perfectly elastic, the state of the fabric can be given by minimum value of U. They have reported that in the case of biaxial deformation, the energies involved are yarn extension U_e, yarn bending U_b, and energy associated with change in yarn cross section U_x:

$$\sum(U_y) = \sum_{1,2}(U_e) + \sum_{1,2}(U_b) + \sum_{1,2}(U_x) \tag{18.22}$$

The energy associated to yarn extension can easily be stated for linear elasticity. It can be expressed as

$$U_e = \sum\left(\frac{1}{2}\right)(tEe^2)l \tag{18.23}$$

where t is the linear density, E is the specific modulus, e is the strain, and l is an increment of the yarn length. $\left(\frac{1}{2}\right)(Ee^2)$ can be replaced by the area under the stress–strain curve, which is conveniently expressed by a polynomial function. The other two energy terms can be expressed as

$$U_b = \sum\frac{1}{2}(Mc)\delta l = \sum\frac{1}{2}(Bc^2)\delta l \tag{18.24}$$

where M is the bending moment, c is the yarn curvature (reciprocal of radius of curvature), and B is the bending stiffness. For a nonlinear response, $(1/2)(Mc)$ could be replaced by the area under a plot of bending moment against curvature. In order to describe the energy term associated with change in yarn cross section,

two effects must be taken into account: change in yarn volume and change in yarn shape; therefore it can be expressed as

$$U_x = U_v + U_s \tag{18.25}$$

where U_v and U_S are the energies related to volume and shape, respectively, and can be formulated as shown in Eqs. (18.26) and (18.27):

$$U_v = \frac{1}{2}K_2[(V - v)/V]^2 \tag{18.26}$$

$$U_s = \frac{1}{2}K_3[(D_v - d)/D_v]^2 \tag{18.27}$$

where K_2 is the bulk modulus related to the reduction in yarn volume from V to v, K_3 is the shape change modulus, and D_v is the diameter of the circle for the volume v. For weaves other than a plain weave, two additional features need to be taken into account in formulating the energy terms:

(1) The contact zones will include straight yarn sections as well as curved sections at the edge of crossovers. This will influence the bending energy terms.
(2) When the yarns are in contact, the change of shape due to flattening will be different, and this will influence the flattening energy terms.

By taking these two features into account, energy terms for other weaves like twill and satin can also be formulated. The energy methods will make it possible to develop CAD programs in order to predict the mechanical properties of fabric in terms of structure and yarn properties.

18.5 Conclusion

From the above study it can be concluded that the mechanical response of woven fabrics in the case of tensile deformation depends greatly on certain factors including the constituent yarn properties, the amount of crimp, the weave of the fabric, or the number of interlacements per unit area and density of yarns (warp and weft). The mechanical response is also influenced greatly by the direction of loading like in the case of tensile stress in principle direction or biased direction. When a woven fabric is subjected to uniaxial tensile load, the crimp imbalance will occur, i.e. crimp decreases in the direction of applied load while increases in the cross direction. When a woven fabric is subjected to bias extension, shear deformation will occur and influence the tensile behavior of the fabric, and anisotropy will increase. Additionally, in the case of biased extension, the maximum change in length will be associated with the diagonal direction, i.e. ($\pm 45°$) resulting in maximum elongation along one diagonal direction with maximum contraction along other diagonal direction. From the study of modeling techniques, it can be concluded that in the case of continuum analysis of woven fabric, if the forms of nonlinear stress–strain laws are already known, the tangential elasticity matrix given in Eq. (18.18) can be used in continuum nonlinear material properties. A discontinuum can be used for

modeling of fabric deformations before they are actually manufactured by using yarn properties, but not useful in the case of complex fabric deformations. Set of nonlinear constitutive equations for woven fabrics under tension, bending, shear, and lateral compression formulated by Hu and Newton [31, 32] can be used in finite element method to improve predictability of nonlinear stress–strain relationships during fabric deformations. Energy methods can be successfully applied for the development of CAD to deal yarn extension, bending, flattening, and frictional forces at interlacement points in a plain woven fabric. By taking into account the straight yarn section and curved sections at the edges of interlacement point together with the change of shape due to flattening when yarns are in contact, energy terms can also be described for weaves other than plain like twill and satin. The energy methods are capable of developing CAD programs in order to predict the mechanical properties of fabric in terms of structure and yarn properties.

References

1 Gandhi, K. (2012). *Woven Textiles: Principles, Technologies and Applications*. Elsevier.
2 Robinson, A. T. C., & Marks, R. (1967). *Woven Cloth Construction*. New York: Plenum Press.
3 Behera, B., Kremenakova, D., Militky, J., and Mishra, R. (2012). *Modeling of Woven Fabrics Geometry and Properties*. INTECH Open Access Publisher.
4 Behera, B.K. and Hari, P. (2010). *Woven Textile Structure: Theory and Applications*. Elsevier.
5 Peirce, F.T. (1937). 5—The geometry of cloth structure. *Journal of the Textile Institute Transactions* 28 (3): T45–T96.
6 Kemp, A. (1958). An extension of Peirce's cloth geometry to the treatment of non-circular threads. *Journal of Textile Institute Transactions* 49 (1): T44–T48.
7 Hamilton, J. (1964). 7—A general system of woven-fabric geometry. *Journal of the Textile Institute Transactions* 55 (1): T66–T82.
8 Grosberg, P. and Park, B. (1966). The mechanical properties of woven fabrics Part V: the initial modulus and the frictional restraint in shearing of plain weave fabrics. *Textile Research Journal* 36 (5): 420–431.
9 Olofsson, B. (1964). 49—A general model of a fabric as a geometric-mechanical structure. *Journal of the Textile Institute Transactions* 55 (11): T541–T557.
10 Dorkin, C., Munden, D., and Whewell, C. (1973). The rôle of science in a modern clothing industry. *Journal of the Royal Society of Arts* 121 (5208): 799–812.
11 Ellis, P. and Munden, D. (1973). 52—A theoretical analysis and experimental study of the plain square weave. Part III: The geometry of the plain square weave. *Journal of the Textile Institute* 64 (10): 565–571.
12 Liao, T. and Adanur, S. (1998). A novel approach to three-dimensional modeling of interlaced fabric structures. *Textile Research Journal* 68 (11): 841–847.

13 Liao, T. and Chen, W. (1990). An investigation of wool worsted yarn relaxation shrinkage and its effect on fabric structure and performance. In: *Proceedings of the 8th International Wool Textile Research Conference* (7–14 February 1990), 128. Christchurch, New Zealand: Fibre Assemblies and Product Properties.

14 Amirbayat, J. (1991). The buckling of flexible sheets under tension part I: Theoretical analysis. *Journal of the Textile Institute* 82 (1): 61–70.

15 Amirbayat, J. and Hearle, J. (1989). The anatomy of buckling of textile fabrics: drape and conformability. *Journal of the Textile Institute* 80 (1): 51–70.

16 De Jong, S. and Postle, R. (1978). A general energy analysis of fabric mechanics using optimal control theory. *Textile Research Journal* 48 (3): 127–135.

17 Hearle, J.W. (1980). *Mechanics of Flexible Fibre Assemblies*. Kluwer Academic Publishers.

18 Hearle, J. (1980). The mechanics of dense fibre assemblies. In: *The Mechanics of Flexible Fibre Assemblies* (eds. J.W. Hearle, J.J. Thwaites, and J. Amirbayat), pp. 51–86. UK: Springer.

19 Hearle, J., Grosberg, P., and Backer, S. (1969). *Structural Mechanics of Yarns and Fabrics*, vol. 1. USA: Wiley-Interscience.

20 Hu, J. and Teng, J. (1996). Computational fabric mechanics: present status and future trends. *Finite Elements in Analysis and Design* 21 (4): 225–237.

21 Moghe, S., Hearle, J., Thwaites, J., and Amirbayat, J. (1980). From fibers to woven fabrics. In: *Mechanics of Flexible Fiber Assemblies* (eds. J.W. Hearle, J.J. Thwaites, and J. Amirbayat). Sijthoff and Noordhoff.

22 Hu, J. (2004). *Structure and Mechanics of Woven Fabrics*. Elsevier.

23 Spivak, S. and Treloar, L. (1968). The behavior of fabrics in shear part III: the relation between bias extension and simple shear. *Textile Research Journal* 38 (9): 963–971.

24 Realff, M.L. (1994). Identifying local deformation phenomena during woven fabric uniaxial tensile loading. *Textile Research Journal* 64 (3): 135–141.

25 Amirbayat, J. and Hearle, J. (1986). The complex buckling of flexible sheet materials—Part I. Theoretical approach. *International Journal of Mechanical Sciences* 28 (6): 339–358.

26 Hearle, J. and Amirbayat, J. (1986). Analysis of drape by means of dimensionless groups. *Textile Research Journal* 56 (12): 727–733.

27 Kilby, W. (1963). 2—Planar stress–strain relationships in woven fabrics. *Journal of the Textile Institute Transactions* 54 (1): T9–T27.

28 Postle, R., Carnaby, G., and De Jong, S. (1987). Woven-fabric structure and tensile properties. In: *Mechanics of Wool Structures* (eds. R. Postle, G.A. Carnaby, and S. de Jong). Wiley.

29 Paipetis, S. (1981). Mathematical modelling of composites. In: *Developments in Composite Materials- 2: Stress Analysis (A 82-28568 13-39)*, 1–37. London: Applied Science Publishers.

30 Hearle, J., Konopasek, M., and Newton, A. (1972). On some general features of a computer-based system for calculation of the mechanics of textile structures. *Textile Research Journal* 42 (10): 613–626.

31 Hu, J. (1994). Structure and low-stress mechanics of woven fabrics-a comprehensive study based on the KES system. Ph.D.

32 Hu, J. and Newton, A. (1993). Modelling of tensile stress-strain curve of woven fabrics. *Journal-China Textile University-English Edition* 10: 49–49.
33 Hearle, J., Potluri, P., and Thammandra, V. (2001). Modelling fabric mechanics. *Journal of the Textile Institute* 92 (3): 53–69.
34 Hearle, J. and Shanahan, W. (1978). 11—An energy method for calculations in fabric mechanics part I: principles of the method. *Journal of the Textile Institute* 69 (4): 81–91.
35 De Jong, S., Snaith, J.W., and Michie, N.A. (1986). A mechanical model for the lateral compression of woven fabrics. *Textile Research Journal* 56 (12): 759–767.

19

Fabric Making Technologies

Tao Hua

The Hong Kong Polytechnic University, Institute of Textiles and Clothing, ST 703, Hung Hom, Kowloon, Hong Kong, China

19.1 Introduction

Fabric can be defined as the manufactured assembly of fibers and/or yarns. A wide variety of textile materials are used to produce fabrics including advanced materials. In the conversion of materials such as fibers and yarns to fabric, the fabric making technology that involves the processing machine, procedures, and parameters for fabric formation has significant influence on the properties and appearance of the resulting fabrics. There are many ways to make fabrics. The most commonly used techniques include weaving, knitting, nonwoven manufacturing, and braiding. Each fabric making method constructs a unique fabric structure that partially determines the fabric properties and appearance. Figure 19.1 shows the schematic of fabric structures formed by these methods.

Weaving is a traditional method used for fabric production wherein the resultant woven fabrics are manufactured by interlacing at least two sets of thread systems – warp and weft threads at right angles to each other. In a simple woven structure, the warp threads, which are called the warp ends in weaving terms, always run along the length of the fabric or up and down, while the weft threads, also known as picks or filling yarn in weaving terms, run in the horizontal direction or left to right and vice versa. The warp and weft threads are perpendicular to each other. More thread systems can be inserted into weaving machines to produce woven fabrics with different structures. In the past, they were mostly in one layer. With time, double-layer, triaxial, and three-dimensional (3D) woven fabrics have been developed for the textile market. They have various properties and applications for daily use.

Knitting is the second most popular technique of fabric making in the textile industry. In the knitting process, knitted fabrics are produced by interlooping yarns. There are two ways of knitting based on the direction of the yarn movement, which are known as weft and warp knitting. In weft knitting, the loops are constructed in the horizontal direction, while in warp knitting, the yarns are knitted along the vertical or diagonal direction. Compared with woven fabrics, knitted fabrics have better extensibility and formability due to their loop

Handbook of Fibrous Materials, First Edition. Edited by Jinlian Hu, Bipin Kumar, and Jing Lu.
© 2020 Wiley-VCH Verlag GmbH & Co. KGaA. Published 2020 by Wiley-VCH Verlag GmbH & Co. KGaA.

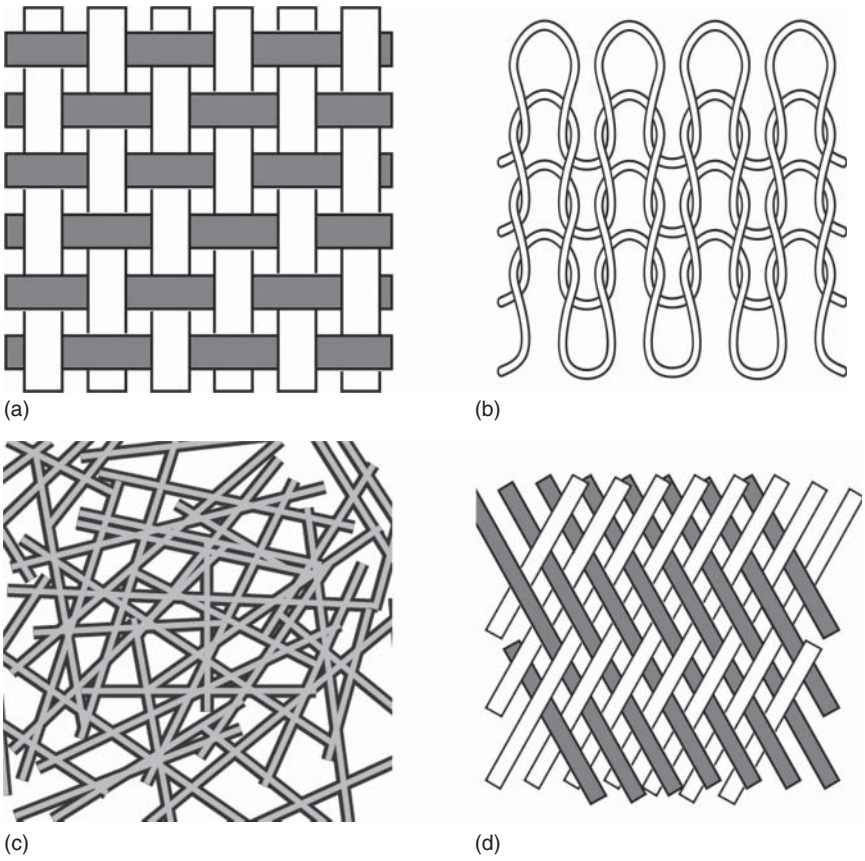


Figure 19.1 Schematic of structures of main fabric types. (a) Woven. (b) Knit. (c) Nonwoven. (d) Braided.

structure. Nowadays, knitted fabrics are widely used in apparel, home furnishings, and technical textiles.

Nonwoven fabric technology is one of the major technologies for the manufacture of fabric. Nonwoven fabrics are a manufactured sheet of web, sheet, or batt, which are produced with staple fibers or filaments through various bonding techniques that hold them together. In terms of processing by machinery, nonwovens do not need to be prepared through the yarn spinning process and can be directly made from fibers or even polymers. One of the greatest benefits of the production of nonwoven fabrics is that the production rate is much higher than that of fabrics produced by weaving or knitting technologies since there are fewer yarn procedures and the process can be more automated. A wide range of raw materials can be applied, regardless if they are natural or synthetic fibers. Nowadays, most synthetic or bicomponent fibers, or even special fibers such as nanofibers, glass fibers, and biodegradable materials, can be used to produce nonwoven fabrics since they have unique characteristics, uniformity, and consistency. These textiles can be applied toward different end uses, especially for hygiene, civil engineering, and building materials.

Braiding is a common process for constructing narrow fabrics or products, which are known as braided or plaited textiles. Braided fabrics are produced by interlacing three or more separate threads in such a way that they can cross one another in a diagonally overlapping direction. Based on the unique constructed structures through braiding, the resultant fabrics exhibit good strength in the primary loading direction and shear resistance as well as complex-shaped parts. Moreover, by varying the braided structures, different types of braided fabrics can be fabricated with different properties and shapes, including two-dimensional (2D) and 3D braids, biaxial and triaxial braids, and flat and circular braids. Traditionally, braiding was used to produce ropes and cords with a simple structure. Braids with complicated structures were normally thicker and stronger with high physical strength. Nowadays, braided fabrics are used for various industrial applications since they have good extension and are very pliable with nicely curved edges.

19.2 Weaving

19.2.1 Weaving Machines

Woven fabrics are manufactured by interlacing lengthwise warps and crosswise wefts into designed patterns on weaving machines. There are many different types of weaving machines that have been developed for the production of woven fabrics in the textile industry. Weaving machines are divided into shuttle and shuttleless based on how the weft yarns are inserted. Shuttle looms are the oldest and most simple type of weaving machines, where the weft yarn is inserted with a shuttle. Nowadays, shuttle looms are not commonly used for the production of woven fabric except for some of the specialty markets. They have been replaced by shuttleless looms, which started from the mid-twentieth century and include rapier, projectile, air-jet, and water-jet looms [1–6]. Compared with shuttle looms, shuttleless looms have a much higher production rate and are more flexible for manufacturing different types of woven fabrics.

Rapier weaving machines are a primary type of shuttleless weaving machine used for making woven fabric with a versatile insertion system and excellent control of the filling yarn in the process. In rapier looms, flexible or rigid rapiers are used to insert the weft yarn across the shed. There are two types of rapier weaving machines: single or double rapier looms. In the former, only one long and rigid rapier, which is made of metal or a composite material, is used to feed the filling yarn and then retracted, while there are two rapiers in the latter: a giver, which picks up and carries the filling yarn to the shed center, and a taker, which takes the yarn from the giver and transports the yarn to the end of the shed. The advantage of a two-rapier system is increased efficiency as opposed to the use of a single rapier loom. In addition, there are rigid and flexible double rapier machines. Nowadays, flexible double rapier looms are preferred over single or rigid rapier looms due to their advantages, such as space saving and a higher machine speed.

Projectile weaving machines involve a small bullet-like gripper that holds and then brings the weft yarn through the shed without the use of a heavy shuttle. During the insertion of the weft yarn, a picking lever beats the gripper with the yarn to slide through a channel composed of the thin prongs of a rake. When the gripper arrives the other side of the machine, it is braked in the receiving unit. Several grippers are usually used in projectile looms. After one gripper reaches the other side of the loom with the weft yarn and then returns to the starting position by the conveyor system, the other grippers are ready for the next picking. Compared with the shuttle loom, the grippers of the projectile loom can move faster and farther because of the reduced dimensions and the mass of the carrier. Therefore, projectile weaving machines are more suitable for producing wider woven fabrics and thus commonly used for the production of technical fabrics.

Jet looms take the weft yarn across the loom by using the force of air or water at high pressure. Thus, jet looms can be operated at higher speeds as opposed to projectile or rapier looms. However, they cannot accommodate heavy or bulky yarns, nor can they produce fabric with wider dimensions as they have less yarn-carrying power. In air-jet weaving machines, the filling yarn is propelled by compressed air that come from several nozzles to weave fabric. The main and tandem nozzles provide weft yarns with an initial propulsion force, while the relay nozzles found in the entire shed offer additional high-velocity air to assist with conveying the yarn through the warp shed. Another main feature of air-jet looms is that a specially designed profiled reed is used for the weft yarn insertion wherein the profiled reed builds a channel to guide the air, which prevents the abrasion of the inserted wefts with the warps. They are one of the most popular types of weaving machines since the weft insertion rate is very high with low production requirements and thus offers high productivity for mass production, relative to other shuttleless machines. Many standard types of fabrics or fabrics with a variety of styles can be produced through air-jet weaving, such as denim, glass, or terry fabric.

The operation principle of water-jet looms is similar to that of air-jet looms. During the weaving process, the nozzle provides highly pressurized water to insert the weft yarn. A small amount of water is required for the fabric production, and the weaving process is carried out at extremely high speed. Therefore, water-jet looms are very efficient. However, efficient drying units need to be equipped on the water-jet looms to dry the wet fabric. The main disadvantage of the water-jet weaving machine is that it is more suitable for weaving hydrophobic filament yarns such as polyester and nylon [1, 4–9].

In addition to these different weaving machines with weft yarn insertion systems, there are three types of shedding systems, namely, the cam, dobby, and jacquard machines. Their function is to separate the warp sheet into at least two layers for weft yarn insertion. For producing common types of fabrics, weaving machines are normally equipped with a dobby shedding system, which include negative, positive, and rotary dobbies. The latest manufactured weaving machines use rotary dobbies as they are suitable for the high speed of these machines and offer flexibility for changing patterns. Weaving machines equipped with a dobby shedding system control the movement of the warp yarn by using the harnesses, which means warps on the same harness have

the same movement. In order to vary the movement of the warp yarn for weaving a pattern, more harnesses are used, but the number of harnesses that can be accommodated in a dobby system is limited. Therefore, when the patterning capacity of dobbies fails to meet the requirements of the weaving design, a jacquard shedding system must be used. The main feature of jacquard shedding is that this mechanism can control the movement of the warp yarn individually. In recent years, jacquard shedding machines are becoming more and more ubiquitous for manufacturing woven fabric since they can produce extraordinary and intricate patterns or figures, such as brocades, tapestry, and damask. There are mechanical and electronic jacquard looms with single or double lift mechanisms [10, 11].

There are also special types of weaving machines that have been developed for high productivity or creating special woven fabrics, including multiphase, circular, and triaxial weaving machines. The multiphase weaving machine can insert several weft yarns simultaneously so that more than one shed can be formed at a time. Thus, this machine offers high productivity. In circular weaving machines, the shuttles run continuously and circularly around the periphery in a ripple or wave shed. The produced fabrics are in a tubular form and mainly used for sacks and tubes. In triaxial weaving machines, two sets of warp threads and one set of weft threads are interlaced to form a multitude of equilateral triangles. The constructed fabric structures are unique and endow the resultant fabrics with good tear, burst, and abrasion resistance. Triaxial fabrics are largely used for industrial purposes, such as conveyor belts, reinforcements for plastics, and aerospace accessories.

19.2.2 Woven Structures

A woven fabric is formed by the interlacement of the warp and weft threads. This interlacing pattern is called the weave of a woven fabric. The final fabric properties and appearance depend on the weave and other structural parameters such as the fabric density and yarn count. Weaves are planned on point paper wherein each vertical column and horizontal row means a warp end and a weft pick, respectively. In a weave diagram, each square represents an intersection point between a warp and a weft yarn, and if the warp yarn crosses over the weft yarn at this point, the square is filled or shaded with a mark. On the other hand, if the weft yarn is above the warp yarn in the point of intersection, the square will be left blank. An unlimited variety of weaves can be designed for woven fabrics. The most commonly used weaves in the production of woven fabric include fundamental weaves and their derivatives, combined weaves as well as compound weaves. Each has their own characteristics.

Plain, twill, and satin/sateen weaves are three types of fundamental weaves, as shown in Figure 19.2. They have a simple structure but form the basis of even the most complex weaves where every warp and weft thread within a repeat is interlaced by only one thread of the opposite system. Plain weaves are the simplest and most commonly used weave of all woven fabrics. In this structure, weft filling yarn is alternately passed through the warp yarn, which follows the order of one up and one down. If the plain weave is extended in the warpwise or weftwise or



Figure 19.2 Fundamental weaves. (a) Plain. (b) Twill. (c) Sateen.

both directions, new structures with rib or basket effects are further created, such as warp rib, weft rib, and basket weaves in a regular or an irregular form.

Twill weaves also have a simple structure but can generate pronounced diagonal lines along the fabric width. Twill lines are created by the stepwise progression of yarn interlacing patterns that appear on both sides of the fabric, and the fabric constructed with a twill weave is usually strong and durable. In terms of the direction of the twill lines, there are two types: right-hand and left-hand twill. In the former, the twill lines run from lower left to upper right, while the twill lines run from lower right to upper left in the latter. There are several factors that affect the prominence of twill weaves, including the nature of the yarn, yarn floats, fabric density, and relative direction of the twill and yarn twist. By extending the floats and changing the move number and direction of the diagonal lines on the twill weaves, various twill weave derivatives can be created in woven fabrics. Commonly used twill derivatives are pointed, herringbone, curved, broken, and elongated twills as well as diamond and diaper weaves.

Sateen/satin weaves have a higher luster on one side of the fabric since there are many long floats on the fabric surface that reflect light. Sateen is a weft-faced weave wherein the long weft float is on the top surface of the fabric while the satin weave consists of long warp float on the fabric surface, thus a warp-faced weave. During the weave design, both repeat and move numbers are important parameters. The satin/sateen weaves may be modified by subtracting or adding marks or changing move number or both [12–14]. Consequently, a series of satin/sateen weave derivatives can be produced such as reinforced and rearranged sateen/satin.

Combined weaves are constructed on the basis of two or more fundamental weaves and their derivatives, which results in irregular or uneven fabric surface or small woven figures on the fabric. Commonly used combined weaves include crepe, honeycomb, and mock leno weaves, Bedford cords, simple spot figure designs, and stripe and check weave combinations. Crepe weaves give fabric the appearance of being covered by minute spots or seeds through several construction methods. Honeycomb weaves are a very special type of weave that can create a 3D cell-like structure for the fabric with excellent moisture and water absorbent properties. Mock leno weaves endow fabrics with an open structure and small holes or gaps similar to leno weave fabrics. By floating the ordinary weft or warp threads on the surface of the fabric in an order, spots or small figure

designs can be created for decorative purposes. By combining two, three, or more weaves or weave variations in the warpwise or both the warp and weft directions, stripe and check effects form on the fabric surface.

Compound weaves are often referred to as a group of weaves that feature more than one layered structure to make multilayered, 3D, and other specialized types of woven fabrics. These fabrics are constructed with more than one system of warp and weft threads that are often arranged in different planes by forming two or more layers. Common types of woven fabrics fabricated with compound weaves are warp and weft backed, double, treble, gauze and leno, warp pile and weft pile fabrics, carpets, and other types of 3D fabrics. Figure 19.3 illustrates several compound weaves and structures for woven fabrics. Backing fabric is based on backed weaves, in which a second series of either weft or warp threads back single layer fabric in order to increase fabric weight and enhance warmth while maintaining a smooth surface. When double weaves are constructed, two layers of threads in which one is woven above the other and stitched together form double fabrics. There are three common types of double fabrics based on the stitching methods: self-stitched, center-stitched, and interchanging double fabrics. By using conventional or specialized weaving machines, different types of 3D woven fabrics can be manufactured. In general, 3D fabrics are produced in several layers. Solid, hollow, and shell structures have been developed in 3D woven fabrics. 3D solid woven fabrics are classified as having multilayer, orthogonal, and angle interlock architectures. They feature compound construction with different fabric thicknesses so as to provide better mechanical properties, such as fabric strength. A 3D hollow structure can be created with multiple layers of woven fabrics with even and uneven surfaces. The hollows can be triangular, rectangular, or cell shaped, which can improve the air permeability and thermal conductivity of fabrics. 3D shell woven fabrics are manufactured with a curved shell structure, which can maintain fiber continuity. Moreover, they can also feature spherical or cubic shells [15, 16].

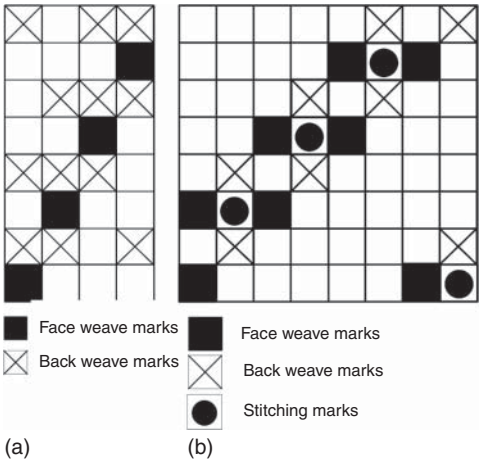


Figure 19.3 Compound weaves and structures. (a) Weft-backed weave. (b) Self-stitched double weave.

In addition to the fabric weave, there are other important structural parameters that have great impacts on the properties and appearance of woven fabrics. The main parameters are yarn linear density (count), fabric sett (density), cover factor, yarn crimp, and fabric weight (area density). The term "sett" is normally expressed as the number of threads per unit length (inches or cm) including the warp and weft densities, which are used to indicate the spacing of threads in a fabric. The cover factor is the fraction of the fabric area that is covered by the component warp or weft yarns. It shows the relative closeness of the yarns within the fabric by considering both the yarn count and fabric density. In a woven fabric, yarns are not straight, but in a wavy shape due to the interlacing of the warps with the wefts. This waviness of the yarn is called yarn crimp. The yarn crimp is an important parameter because it affects the property and appearance of fabric as well as the yarn length required for an intended fabric. Fabric weight is expressed in mass per square area, e.g. g/m^2 or oz/yd^2, which can be calculated based on the yarn linear density, fabric density, and yarn crimp.

19.2.3 Properties

The properties and appearance of woven fabrics depend on the fiber and yarn and their structure, which are commonly evaluated in terms of tensile strength and elongation, tearing strength, abrasion resistance, air permeability, fabric bow and skew, and fabric dimensional changes in accordance with ASTM, AATCC, or other testing method standards. Fabric tensile strength and tearing strength are crucial for the durability of garments, especially for finished woven fabrics such as denim fabric. Fabrics with a plain weave and its derivatives normally have maximum binding points with short yarn floats, which result in their high tensile strength but low tearing strength. Fabrics with a twill weave and its derivatives can be fabricated with more warps and wefts per unit area than those with a plain weave, so they have a higher thickness and density. There are many prominent diagonal wale lines on twill fabrics. Twill fabrics are usually durable with adequate tensile and tearing strength. Fabrics fabricated with a satin or sateen weave structure have fewer binding points and longer floating lengths, which can provide a smooth and luster surface. However, such a structure causes the yarns to more easily ravel and fray. In addition, satin/sateen fabrics have good ability to resist tearing but have low tensile strength [1, 7, 12, 16, 17].

19.2.4 Applications

As a primary type of fabric, wovens are widely used in daily life. Their applications include the three main areas of apparel, home furnishing, and technical products. Compared with knitted fabrics, woven fabrics have high stability and a tighter structure due to yarn interlacing that makes woven fabrics suitable for more formal garments. Plain weave fabrics can be made thick or thin and are widely used for shirts, blankets, canvases, and organza and chiffon fabric. Twill weave fabrics are mainly for the production of suits and jeans. Sateen or satin fabrics are usually found in evening and wedding dresses and for decorations. Besides, in order to meet the growing demand of customers for comfort and function in terms

of fabric for home furnishing, more and more woven fabrics are applied in this area. Woven products include bedspreads, floor coverings, cushion covers, curtains, towels, sheets, pillowcases, etc. More complex structures are commonly employed in these types of textiles for the required thickness, color, and pattern.

Woven technical textiles are becoming universal today, which include those for medical use, sportswear, filtration, industrial use, protection, civil engineering applications, transport, and packaging and in geotextiles [1, 2, 12, 17]. Woven fabrics can be used as medical and biological textiles for hygienic and clinical purposes. The construction of such fabrics needs to be extremely stable and durable. For hygiene purposes, woven fabrics are commonly used in nappies, incontinence pads, or tampons. Besides, woven fabrics can be applied for protective and healthcare textiles, such as operation dresses and staff uniforms for doctors and nurses. Moreover, woven fabrics can be used as implantable materials, which are utilized as vascular grafts, sutures, and artificial limbs. In the latest developments, they are applied in extracorporeal devices that include artificial livers, kidneys, and lungs. Woven fabrics are the primary textile product used for automobiles since they have a highly stable structure and high mechanical resistance. They are usually applied in seat covers, headrests, door panels, and reinforcements. Woven fabrics are also commonly found in airbags with or without a coating. The purpose of airbags is to reduce the forward motion of passengers when an accident takes place in a split second. Therefore, the fabric used for airbags should be able to resist the force of the movement and have substantial strength. Woven technical textiles are usually used in sports applications. Waterproof and breathable fabrics are some of the popular fabrics in sportswear, which are mainly applied in outdoor apparel, especially for winter coats because not only can this prevent liquid penetration but also allow water vapor transfer to the outside environment and provide a comfortable temperature for the human body. This type of fabric is manufactured with a high fabric density or application of coating and laminating. Another important application of woven fabrics is as 3D fabrics, which are widely used as reinforcements and preforms for advanced textile composites due to their properties and shapes.

19.3 Knitting

19.3.1 Knitting Machines

Weft and warp knitting machines are two types of knitting machines used in the textile industry. The former is the most commonly used knitting machine due to the advantages of versatility, ability to quickly change patterns, requirement of little floor space, and low investment. The key components of weft knitting machines include knitting needles, needle bed, cam box, sinker, and yarn feeder. The needles are the main knitting element that is responsible for loop formation and subsequent interlooping with the help of the sinker. The sinker that is positioned in between the needles performs functions such as loop formation, holding down, and knocking over. The needle bed is a metal plate with a slot for needle insertion and movement. Cams provide the needles and other

elements with a suitable reciprocating action for the knitting action. Weft knitting machines can be generally grouped into flat bed or circular bed machines in accordance with the needle bed arrangement. There are typically two types of flat needle beds that are organized in an inverted V formation. Latch needles are commonly used and placed in the grooves on the machine, which are also known as needle tricks. The machine gauge is normally 3–18 needles per inch. The yarn can change direction with each course on a flat bed machine, while the yarn runs continuously and horizontally in the same direction on a circular machine. In the circular machine, two sets of needles are arranged in a circular form at right angles to each other wherein one set is in the vertical and the other is in the horizontal. Latch, bearded, and occasionally compound needles can be used. By using the multiple yarn feeds, hundreds of yarns can be knitted in one rotation, so weft knitted fabric can be quickly produced. Single jersey, rib, interlock, and purl fabrics can be manufactured by using circular machines [18–23].

In terms of warp knitting, the yarns from the warp beam in the form of a parallel sheet are used to form fabric through loop formation. Each yarn is fed to an individual needle. During the same knitting cycle, every needle in the needle bar conducts the action of yarn feeding and loop forming simultaneously. A typical warp knitting machine consists of several functional elements, including needles and needle bar, presser bar, sinkers and sinker bar, guides and guide bars and warp beams. With regard to the production of warp knitted fabrics, there are two popular classes of warp knitting machines with one or two needle bars employed, which are called tricot and Raschel machines. In the tricot machine, bearded or compound needles and sinkers are normally used. Warp beams are positioned at the back of machine, and also, the guide bars are moved from the back to the front of machine in fabric knitting. Moreover, the machine gauge used in a tricot machine is high, which ranges from 28 to 40 needles per inch, and the machine speed can be up to 3500 courses per minute or even higher. Continuous filament yarns are commonly used in fabric production. Latch needles are generally used in Raschel machines, and sometimes, compound needles are now common for the production of warp knitted fabric. The warp beams are placed on the top of the machine, and the guide bars run from the front side toward the back side to knit warp knitted fabrics in overlapping and underlapping arrangements. Furthermore, the machine gauge is coarser from 12 to 32 needles per inch. The machine speed is lower compared with that of the tricot. More yarn guide bars need to be mounted on the machine. Besides, a wide range of yarns can be used, and various products can be manufactured [18–22].

19.3.2 Knitted Fabric Structures

By controlling the motion of the needle on a knitting machine, different types of knitted fabrics can be produced with different fabric structures. There are three fundamental knitting stitches for the production of weft knitted fabric: knit, tuck, and miss stitches. The majority of knitted fabrics are produced with the knit stitch. Knit stitches are a normal loop formed when a needle knocks over the old loop and receives a new yarn. Then, the loop formation is carried out by the old loop. The function of the needles is to rise to the clearing position, carry the

yarn down, and then form the loop. In the formation of a tuck stitch, a needle receives the new loop but still grips the old loop, so there are two stitches on the needle. To form a tuck loop, a needle is only raised to the tuck position where the old loop is still on the latch of the needle. A miss stitch is also known as a float stitch, which is created when a needle that is holding the old loop fails to receive the new yarn and then feeds the yarn into the two nearest needle loops. The purpose of miss stitches is to reduce space widthwise and increase fabric stability [18].

Depending on whether a single knit stitch or a combination with other stitches is used, weft knitted structures can be created with different effects. Weft knitted structures can be mainly categorized as single or double jersey structures. Single jerseys are produced by using one set of needles of the machine, while double jerseys are made by using two sets of needles. Single plain jersey knitting is the simplest knitting construction in that all the loops can be knitted by using V-bed, circular, or fully fashion machines. Each loop has the same shape, which is formed on the face side of the fabric because only one set of needles is applied. The "technical face" of the fabric has a V-shape appearance while the Ω-shape appearance forms on the "technical back" of the fabric.

In the case where two set of needles are used for double jersey production, each set can produce their own loops on one side of fabric. Therefore, complicated structures with special effects can be easily constructed on double jersey machines. There are three basic structures and their derivatives, including rib, interlock, and purl. Rib structures are one of the common knitted structures in which loops are constructed in the opposite directions by using two sets of needles. The 1×1 rib is the simplest rib fabric wherein one wale of face loops is alternated with two wales of back loops. In the same way, more rib structures such as 2×2, 3×3, and 3×2 can be constructed. No curling problem may occur on the edge of fabric and fabric with a rib structure can acquire good elastic recovery. Furthermore, there are a variety of rib derivatives, such as tubular, cable, half Milano, and full Milano. Interlocking is fabricated by using both long and short needles. The row of interlocks comprises joining the two half gauge 1×1 ribs by interloping sinker loops. It has a perfectly balanced structure and the same appearance on both sides of the fabric, like the face of a single jersey. Moreover, it can be elongated to 30–40% in the crosswise direction. The interlock of 2×2, 3×3, and 4×4 can also be fabricated according to its basis.

In weft knitted jacquard fabrics, a diversity of colors and designs can be found on the fabric surface by selecting needles and colored yarns to knit for desired colors and figures. Jacquard fabric can be classified into two types: single jersey jacquard and double jacquard. In single jersey jacquard, a tie-in technique called "accordion" is used wherein specific needles are cleared to tuck the height. Consequently, the length of the floats can be minimized at the fabric back. By using one more set of needles to knit the back loop, the double jacquard can overcome the floats in a single jacquard. Moreover, it is commonly used to produce different types of backings, such as birdseye and twill backings [18, 22, 25].

Basic warp knitted structures are constructed by using warp knitting machines with only one yarn guide bar and one set of needle bar, including pillar stitches,

half-tricot and variation, atlas, and double loop stitches. Pillar stitches are produced by feeding the same yarn on the same needle. They are usually used with other types of structures to produce fabric with particular effects. Half-tricot is the structure formed by alternatively feeding the same yarn on two adjacent needles. The basic half-tricot is in 1×1 lapping movement, and the loops are easily inclined because of the production with the single guide bar. The structures in the 2×1 and 3×1 lapping movement are common structures in half-tricot variation, which have a longer underlap space. The atlas structure is constructed where the yarn guide bar laps increasingly in the same direction for a minimum of two consecutive courses. In addition, double loop stitches are constructed by overlapping two needles for the mixing of the weft and warp loops [18, 25, 26].

Nowadays, warp knitting machines with two yarns guide bars are universal. Through the use of two guide bars, advanced fabric structures can be developed by combining two or more basic structures. The simplest structure of the advanced fabrics is the full tricot, which can be constructed with two half-tricots in symmetrical lapping movements. Besides, locknit and reverse locknit are the most commonly used structures for warp knitted fabrics, which are developed based on the half-tricot in 1×1 and 2×1 lapping movements, but the movement of the guide bars is reversed. Satin is the reverse structure with sharkskin that can be constructed by half-tricot and its variation in a 3×1 or 4×1 lapping movement. For queenscord, it is also composed of pillar stitches and half-tricot variation in a 3×1 or 4×1 lapping movement.

19.3.3 Properties

Modern knitted fabrics can be produced in a wide range of structures that endow the resultant fabrics with different properties. In general, knitted fabrics have high resilience and wrinkle resistance and are light in weight, better form fitting, soft, and comfortable. However, they may shrink easily after washing and pill after rubbing. Compared with weft knitted fabric, warp knitted fabric has less stretchability but better dimensional stability.

Usually, knitted fabrics have the distinct property of high stretchability and recovery. The 1×1 rib and 2×2 rib structures can provide substantial stretch. However, the stretch can be reduced by introducing horizontal linear yarns into the fabric structure. The recovery property means that when the fabric is stretched to a considerable length and then released, it will gradually return to its original form, which allows the fabric to extend in different directions – diagonal, vertical, and horizontal at the same time – and then the fabric recovers. Rib fabrics normally exhibit a much better recovery property than plain fabrics. In order to further enhance the fabric stretchability and recover property, elastomeric yarn elements under tension can be incorporated into the structure for elastic knitted fabrics.

Similar to the property of elastic recovery, wrinkle resistance is one of the characteristics of knitted fabrics. Generally, knitted fabrics are thicker, the yarns are more mobile in the fabric structure, and the yarn twist is lower compared to woven fabrics, which results in better wrinkle resistance of the knitted fabrics. It is also beneficial for garment production since it leads to ease-of-care garments.

In general, knitted fabrics offer good wear comfort that result from their high stretch properties for better conformability, good insulation property, and sweat transportation property.

The dimensional stability of fabric is its ability to resist permanent changes in its dimensions. Common knitted fabrics do not have a good performance in dimensional stability if they do not have any aftertreatment. Mostly, the dimensional changes of fabrics occur after the first laundering and drying cycle wherein the fabrics shrink or grow at different percentages lengthwise or widthwise. After several washing cycles, the knitted fabrics finally become steady. The dimensional stability of knitted fabric depends on the materials as well as the knitting structures. Interlock, double knit, and other fabrics with weft or warp inserted yarns are unusually more stable and exhibit less shrinkage. The dimensional stability of knitted fabric can be evaluated in accordance with ASTM and AATCC standards.

19.3.4 Applications

Knitted fabrics are widely applied for apparel and domestic products, such as T-shirts, sweaters, socks, stockings, panty hose, lingerie, sportswear, swimwear, sheets, and towels. In garment manufacturing, knitted fabrics are the second largest fabric type used for garments. In addition to traditional knitted fabrics, more specialized knitted fabrics are also developed for garments, including fleecy, raised, highly elastic, and plated fabrics. Nowadays, there is the rapid development of knitted fabrics applied in the technical textiles and composites. Based on the certain properties of knitted fabrics such as extensibility, moldability, openwork, and lightness, not only warp knitted fabrics but also weft knitted fabrics find more applications in these areas. With these two fabrics in different structures, many technical products can be manufactured by advanced knitting machines and techniques [18–21, 24–27].

Spacer fabrics have been developed for technical applications by using both warp and weft knitting technologies. Concerning the structure of space fabrics, two surface layers are interconnected by relatively thick monofilaments, which makes the fabric 3D, elastic, and compressible in the thickness direction. The main features of space knitted fabric include excellent compression elasticity and cushioning, high air permeability and thermal insulation, and good flexibility in surface design. The properties of the space fabric can be adjusted by varying three components: yarn material, fabric construction, and finishing. The space fabric can replace foam in shoes, bras, beds, and seats. The spacer fabrics also can be used for the manufacturing of mattresses for beds and tables.

Knitted fabric structures have the role of reinforcement in polymer composites. That is, warp and weft knitted fabrics with inlay yarns enhance the stiffness and strength of these composites. When inserted and warp stitch yarns are used to reinforce in-plane and through-thickness, this multiaxial warp knit increases the ability of fabric to conform to complex shapes and increases its tolerance to damage. Applications of these kinds of knitted fabric composites include bumper bars and door members for automobiles, rudder-tip fairings for passenger aircrafts, and aircraft radomes, helmets, and body armors.

With regard to medical applications, knitting technology is very flexible and versatile so that medical textile products and tubular fabrics for medical devices can be easily developed and produced through warp knitting. Also, the apparel worn by doctors and nurses in hospitals and clinics are normally produced by using knitting technology, such as their undershirts and socks. Most medical appliances such as artificial blood vessels, surgical meshes, and coverings of artificial heart valves are also made with weft and warp knitted fabrics in recent years. Moreover, the various types of bandages, surgical stockings, and certain parts of orthopedic equipment are produced with knitted fabrics as they have high extensibility. In addition, knitted fabrics can serve as important components of functional clothes. For example, spacer fabric is constructed as two layers – a top and a bottom layer that are kept apart by a pile layer, which has pile threads that allow elasticity. Thus the flexible structure of spacer fabrics means that they can be used as electric switches or pressure sensors when electrically conductive yarns are used to form the layers. These sensors can also be applied onto undershirts, trousers, and socks to fabricate functional clothing.

19.4 Nonwovens

19.4.1 Manufacture of Nonwovens

The basic steps for making a nonwoven fabric are first to form fibers into a web, which are then bonded and finally undergo the processes of drying, curing, and finishing, as shown in Figure 19.4. There are a variety of techniques that can be applied in the formation and bonding of a fiber web, which thus result in different fabric structures and properties. Web formation is the creation of a loosely joined sheet structure by laying down fibers through four basic techniques: drylaying, wetlaying, polymer laying, and other specialized techniques. Drylaying involves carding or airlaying of staple fibers. Carding blends and combs fibers into a web or batt, which can be parallel laid, that is, formed by feeding carded fiber layers parallel into a conveyor belt through carding machines, or random/cross laid, in which each fiber layer after carding is mounted at right angles to the main conveyor. The former results in a web with high strength and orientation in the machine direction but not in the cross direction. The latter results in a web with high strength in the cross direction but not oriented to the machine.

Airlaying allows isotropic web properties and is the aerodynamic formation of a fiber web, which involves feeding fibers into an airstream and then transported to a conveyor belt where the fibers are randomly deposited in the form of a web; thus the web is randomly oriented.

Wetlaying involves the use of a slurry of water and fibers or an aqueous suspension of fibers that are deposited into a perforated drum or a screen belt and then

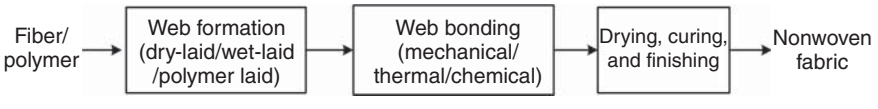


Figure 19.4 Basic steps for making a nonwoven fabric.

dewatered, dried, and cured with heat, much like the papermaking process. The fibers in the web are also randomly oriented. Wetlaying is appropriate for mass production at high speeds [28–34].

Direct or polymer laying means that nonwoven webs are produced from thermoplastic polymers in which they are spunlaid, meltblown, and electrospun. These are also known as direct laid webs, which are produced directly from filaments or short fibers during an extrusion spinning process. This method is one of the most cost-efficient ways of producing fabrics. In spunbonding, molten polymer is extruded through a spinneret, and the filament extruded is drawn into a specially designed aerodynamic device. The filaments formed are deposited onto a moving conveyor or screen drum, and then the web structure is formed. Following that is the web bonding and winding for making the fabrics. Polymers with high and broad molecular weight distribution are commonly applied for producing uniform spunbond webs, such as polypropylene, polyester, and polyamide. During the meltblowing process, molten polymer is extruded through a linear die, and then the extruded polymer streams are rapidly attenuated into extremely fine diameter fibers by using a high-velocity hot airstream. The attenuated fibers are subsequently transported toward a collector conveyor by high-velocity air blowing, thus creating a self-bonded meltblown web that consists of fine fibers. In electrospinning, the molten polymer or polymer solution is drawn from the tip of a capillary to a collector by using an electric field wherein the jet emerges from the charged surface and then electrical forces increases the polymer liquid to stretch the jet. This method is mainly used to produce nanofibers with diameters in the range of 40–2000 nm and their webs with appropriate polymer and solvent systems [30–32].

After the fiber web is formed, the bonding between fibers must be strengthened and stabilized by applying different bonding techniques [27]. These include chemical, mechanical, and thermal bonding, which are commonly used web bonding techniques with adhesives or application of heat and pressure. Mechanical bonding interlocks or entangles fibers in the web through needle punching or water jets, that is, through needle punching or hydroentangling, which are the most commonly used methods. During the needle punching process, the fiber web is fed into a space between a bottom bed plate and a top stripper plate. The barbed needles on a needle board punch the fed fiber web through the plates. Consequently, the fibers in the web are mechanically interlocked or bonded. The geometry and density of the needles are important because they greatly affect the properties of the final nonwoven fabric. In hydroentangling, the needles in needle punching are replaced with high-velocity water jets that entangle the fibers. In the production process, the fibrous web is fed onto a moving conveyor in the form of a flat bed or cylindrical surface. Then high-velocity water jets entangle the fiber web with turbulent water and fully bond the fibers. The de-energized water is then drawn through the permeable conveyor sleeve into the vacuum box for recycling and reuse [30, 33–35].

In chemical bonding, also known as adhesive bonding, adhesive binders are applied onto the fiber webs to hold and bond the fibers together through various techniques such as saturating, spraying, printing, and foaming. Following that, the water in the web is evaporated through drying, and the binders thus bond the

fibers. There are a variety of binders available that not only bond the fibers but also affect the properties of the resultant nonwoven fabrics. For example, spray bonding adhesives can provide some strength but high bulk, while saturation bonding provides high rigidity and stiffness. Latex polymers have now become the most commonly used binder for the chemical bonding of nonwoven fabrics due to the widely available different varieties, their good versatility, ease of application, and cost effectiveness.

The thermal bonding process fuses thermoplastic components in the form of homofil fibers, powder, film, web, etc. by using a heat supply on fiber to fiber crossover points with calender rollers and oven and ultrasonic bonding machines. The function of heat is to cause the thermoplastic component to become viscous or to melt. Consequently, the polymer flows to the fiber-to-fiber crossover points to form bonding regions followed by cooling. Hot calender bonding applies heat energy to the fiber web by passing the web through the nip of a pair of heated rollers. During this process, area bonding or point bonding can be formed by varying the surface pattern of the rollers. The ultrasonic bonding process generates thermal energy and transfers this to well-defined, restricted areas in the web through a mechanical hammering action onto the web surface by using an ultrasonic horn.

19.4.2 Properties

Nonwoven fabrics can have a wide diversity of properties, which depend on the composition and fabric structure. The latter is determined by the methods used to produce the nonwoven fabrics, including web formation, bonding, and finishing. Moreover, these properties can instill and realize specific functions, such as absorbency, liquid repellence, resilience, stretchability, softness, or flame retardancy. These properties are usually combined for specific applications.

Needle punching that uses barbed needles to entangle fibers can produce very thick textiles for various applications. Thin fabrics that are lint-free and have an excellent soft hand feel and high in quality can be produced for medical textiles with hydroentanglement. Products made by thermal bonding can be relatively soft and textile-like, while chemical-bonded nonwoven fabrics can be used for low-cost carpets, scraps, and highly stiff products [30, 31, 35].

Spunbond fabrics are very popular nonwoven fabrics because they can provide particular properties that act somewhere like between paper and woven fabric. The diameter ranges between 15 and 35 μm, whereas the weight ranges typically between 10 and 200 g/m^2, which means such fabrics range from very light with a flexible structure to heavy with a stiff structure. They have planar isotropic properties due to a random web structure. These fabrics offer excellent chemical and physical stability, such as good tearing strength, shear resistance, fray and crease resistance, and high liquid retention capacity. Furthermore, they have a high strength-to-weight and strength-to-cost ratios. Meltblown fabrics have a random fibrous structure and are constructed by using microfibers with a fiber diameter that ranges between 2 and 7 μm. Their structure and constituted fibers endow meltblown fabrics with a high surface area and smooth surface texture that result in good insulation and filtering characteristics [30, 33].

19.4.3 Applications

Nonwoven fabrics can be endowed with a variety of chemical and physical properties and thus can be used to produce a spectrum of products that fit a wide range of applications. They can be used alone or as components of apparel, home furnishings, and healthcare and engineering products as disposable or durable products, depending on the application. Disposable nonwovens can only be used once or reused a few times, whereas durable nonwovens are made to be used for a longer period of time. General applications of disposable nonwovens include personal hygiene products, such as diapers and feminine hygiene products, or medical products, such as surgical gowns and drapes. The main applications of durable nonwovens cover a wide range of areas including hygiene products, wipes, medical and surgical products, protective clothing, interlinings and garments, upholstery, furniture and bedding, floor coverings, buildings and roofings, civil engineering products and geosynthetics, filters (gas and liquids), and automotive items. According to a report from the European Disposables and Nonwovens Association (EDANA), nonwovens are mostly used for hygiene products, followed by civil engineering products and building materials and then wipes [30, 35–37].

Around 33% of nonwoven textiles are used for hygiene products including diapers and feminine hygiene and adult incontinence products. There are two major characteristics of nonwovens that make them exceptional as absorbent hygiene material, which are their high bulk for absorbing and retaining a large amount of fluid at a low product cost and their lightness in weight prior to use. Spunbonded and thermal-bonded nonwovens are also widely used for hygiene products due to their favorable structural characteristics and comfort. They are also low in cost as well as environmentally friendly. Chemically bonded nonwovens are still used for sanitary napkins but have the disadvantages of causing discomfort and environmental problems.

In the nonwoven industry, nearly 15% of nonwovens are found in the wipes market due to their absorbency, versatility, uniformity, and durability that traditional wiping materials cannot compete. Some of the nonwoven wipes are developed for consumers, including those for personal care, babies, and household cleaning. They are convenient to use and dispose, provide exceptional performance, and are low in price, which are the key demands of customers. Then there are wipes for industry applications, such as food services and medical applications. Their disposability and low cost are key for their popularity. They are therefore found in different industry segments, including food services, factories and shops, automotive industry, and hospitals.

19.5 Braiding

19.5.1 Braiding Processes and Machines

Different kinds of braiding machines have been developed to produce different kinds of braids including 2D and 3D structurally braided fabrics. Maypole braiding machines are popular 2D braiding machines that consist of a carrier motion

system, track plate, take-off, and other additional components. In carrier motion systems, the most important part is the carriers with bobbins that move following the track driven by horn gears. Bobbins are installed in the carrier, and the yarn length is adjusted by the carrier during the production process. The track that determines the path of the carriers can define the type and structure of the braid. A classical braiding machine has a base and a track plate wherein one, two, or more tracks can be used for producing flat, tubular, or other types of braids. The take-off mechanism is also important in a braiding machine because this determines the braided angle of the product, one of the most important parameters of braided structures, and thus significantly influence the properties of braids. In the Maypole braiding machines, there are two sets of yarn carriers that interlace and rotate yarn on a circular track at different preset angles. One set travels in the clockwise direction and the other set rotates in the anticlockwise direction. Consequently, two sets of yarns on the carriers are interlaced together at a biased angle to the machine axis to form braided fabrics. Then the produced braid is continuously moved forward by a take-up mechanism [38–40].

In the fabrication of 3D braids, the production principle is similar to that of 2D braiding, but the standing end yarns, also known as the core end, are an addition to the movable braiding threads. With the use of static yarns, they can be interlaced to the braids. There are four types of machines for producing 3D braids: circular, four-step, two-step, and 3D rotary braiding machines.

In the braiding process on circular braiding machine, the carriers with yarn bobbins move in two concentric orbits in the opposite directions. The braided yarns are intersected at a certain angle, and then the carriers change at the crossing point after one cycle of interlacing. Concerned on the machine in two-step process, the threads can move on the base plate only in two movement directions that move through the cross section formed by stationary standing ends. The productivity is high and efficient. Besides, 3D rotary braiding machines are universal and user friendly. There are mobile carriers on the base plate with horn gears in a square form. In the operation, each horn gear and carrier with bobbins can be shifted in different directions or stopped individually. Therefore, carriers with bobbins are free to move to any braiding point in the braiding area and also easy to move in a diagonal path. Thus, variable cross sections and scale over the length of the braid can be achieved [38–42].

19.5.2 Braided Structures and Properties

Braided structures can be classified as 2D or 3D. The former include two types of yarn intertwining configurations: biaxial and triaxial constructions. Biaxial constructions are the most commonly used braided structure wherein only two sets of yarns are interlaced together in a diagonal formation. In order to enhance the tensile and compression strength as well as modulus of the braid for its applications in fiber-reinforced composites, a third set of longitudinal yarns can be introduced to form the braid in a triaxial configuration, together with the biaxial interlaced yarns. The latter have multilayered interconnected structures and have been mainly developed through composite structures. Three dimensional braided structures can be produced by using the newly developed

braiding machines that are computer controlled. Since they have thicker and 3D architectures, they can be fabricated with different cross sections. Commonly, 3D braids can be categorized as tubular or rectangular-shaped structures. In 3D tubular braids, the yarns not only move in helical clockwise and anticlockwise directions but also pass under and over each other in the tube wall thickness direction. Braided fabrics with rectangular-shaped structures are produced by using a rectangular loom [39, 40, 42, 43]. Compared with 2D braids, 3D braiding can produce complex near-net-shape preforms, and the resultant composites have better impact damage tolerance and delamination resistance.

The properties of braided fabrics depend on the interlacing patterns of the braided yarns. Commonly used patterns include diamond, regular, and Hercules stitches, which are similar to the 1/1 plain, 2/2 twill, and 3/3 twill weaves of woven fabrics, respectively. Depending on how the carriers and horn gear are arranged, various patterns can be created. Besides, the geometry of the braided structure is also important for the resultant braid properties, including the line, stitch, and braiding angle. When interlacing the yarns in the diagonal direction, there is a braiding angle, which is usually in the range of 30–80°. The braiding angle is the most critical geometrical parameter for the production of braided architectures.

The characteristics of braided fabrics rely on the type of braiding yarns and architecture of the braid. Normally, braids have good dimensional flexibility since they can be controlled shapewise. In addition, braids have good porosity, ability to resist shear, and strength. Braided composites exhibit good impact resistance, efficient reinforcement for parts where torsional loads are applied, improved interlaminar shear properties, and reduced manufacturing cost of composite structures.

19.5.3 Applications

Braided fabrics have mainly been applied in the fields of engineering, medicine, and automotive in the previous century. Braided fabrics feature greater burst strength and flex fatigue and appropriate for use as hydraulic and fuel hoses in cars, trucks, earth-moving equipment, marine engines, and aeroplanes. In recent years, they are widely employed for technical purposes, such as fiber-reinforced composites, medical implants, and sports applications [42, 43].

Compared with other composites, braided structure composites have a more stable structure with isotropic properties, outstanding strength, and crack resistance. Therefore, braids can be applied to reinforce composites. In aerospace applications, braided composites have been used as rocket nozzles, rotor blades for helicopters, helicopter drive shafts, missile casing, stator vanes, and composite ducting, Braided structures are also applied in the transportation and civil engineering field, including as ropes, cables, drive shafts, belts, hoses, and concrete and wall reinforcements. In recreation, braided composites are used in hockey sticks, baseball bats, tennis racquets, and sports bicycle frames.

Medical applications of braids include sutures, stents, scaffolds, braided pillar implants, artificial limbs, and cartilage. Since braided textile has excellent agility, pliability, and surgical ease of use, high tensile strength, and a silky smooth feel, it

is very suitable for polyethylene sutures. The braiding technique can also be used for the fabrication of stents because this technique provides a versatile design for different applications. Moreover, braided fibrous scaffolds can serve as a base for tissue regeneration, so it is appropriately used as ligament scaffolds. In addition, the fracture resistance and longevity of braided structures mean that they can be used in dental posts for tooth restoration and repair [44].

In terms of sports, braided products can be used for lines in fishing since their structure can provide adequate toughness and abrasion resistance. Besides, polyester or polyethylene braided cords can be applied as archery strings for reinforcement. Furthermore, braided ropes can be manufactured for sail masts, which can maintain its stiffness and retain a constant diameter.

19.6 Future Trends

In the conversion of different materials to fabrics, various fabric making technologies including weaving, knitting, nonwoven manufacturing, and braiding are widely used in the production of fabrics for applications in apparel, furnishing, and technical textiles. With the advancement of materials, high-performance and functional fibers are now being realized and used to make fabrics that meet the demands for comfort, health, and safety as well as create aesthetics in fashion and domestic textiles and endow particular properties and functionalities in technical products. Fabric making technologies are continuously progressing, targeting to enhance fabric quality, advance production flexibility, increase productivity and automation, and enable environment-friendly processing as well as improving responses to consumer demands through innovations in machinery and optimization of the manufacturing process. It is clear that complex and functional fabrics will need to be further explored for technical applications since technical textiles are the fastest-growing sector in the textile and clothing industries. In order to accommodate this rapidly growing demand, advanced fabric making technologies and their produced fabrics will be further developed with advanced materials, machinery, and processes, such as manufacturing technologies for 3D woven, knitted, nonwoven, and braided fabrics, technologies for integrating different functions into fabrics, multiaxial warp knitting machines, and large braiding machines.

References

1 Adanur, S. (2001). *Handbook of Weaving*. Lancaster, PA: Technomic Publishing Co. Inc.
2 Gries, T., Veit, D., Wulfhorst, B., and Lenz, C. (2006). Principles and machinery for production of woven fabrics. In: *Textile Technology* (ed. Wulfhorst, B.), 124–151. Munich: Hanser Publishers.
3 Fannin, A. (1998). *Handloom Weaving Technology*. New York: Design Books.
4 Fox, T.W. (2010). *The Mechanism of Weaving*. Charleston, SC: Nabu Press.

5 Hua, T. (2016). Weaving machines. *Textile Asia* 47 (1): 17–19.
6 Hua, T. (2011). Weaving machines. *Textile Asia* 42 (11): 4–7.
7 Seyam, A.M. (2016). Weaving. *Textile World* 166 (3): 38–42.
8 Seyam, A.M. (2004). Weaving technology. *Textile World*: 34–39.
9 Choogin, V., Bandara, P., and Chepelyuk, E. (2013). *Mechanisms of Flat Weaving Technology*. Cambridge: Woodhead Publishing Ltd.
10 Seyam, A.M. (2011). *Developments in Jacquard Woven Fabrics*. Cambridge: Woodhead Publishing Ltd.
11 Jiang, S.Q. and Hua, T. (eds.) (2013). *Digital Jacquard: Mythologies*. The Hong Kong Polytechnic University.
12 Sondhelm, W.S. (2016). Technical fabric structures - 1. Woven fabrics. In: *Handbook of Technical Textiles* (ed. Horrocks, A.R. and Anand, S.C.), 63–106. Cambridge: Woodhead Publishing Ltd.
13 Naik, N.K. (1994). *Woven Fabric Composites*. Lancaster, PA: Technomic Publishing.
14 Selby, M. (2011). *Contemporary Weaving Patterns*. London: A&C Black.
15 Chen, X., Taylor, L.W., and Tsai, L.J. (2016). Three dimensional fabric structures. Part 1 an overview on fabrication of three dimensional woven textile preforms for composites. In: *Handbook of Technical Textiles* (ed. Horrocks, A.R. and Anand, S.C.), 107–162. Cambridge: Woodhead Publishing Ltd.
16 Hu, J.L. (2004). *Structure and Mechanics of Woven Fabrics*. Cambridge: Woodhead Publishing Ltd.
17 Behera, B.K. and Hari, P.K. (2010). *Woven Textile Structure Theory and Applications*. Cambridge: Woodhead Publishing Ltd.
18 Anand, S.C. (2016). Technical fabric structures – 2. knitted fabrics. In: *Handbook of Technical Textiles* (ed. Horrocks, A.R. and Anand, S.C.), 107–162. Cambridge: Woodhead Publishing Ltd.
19 Gligorijevic, V. (2016). *Technology of Knitting: Theoretical and Experimental Analysis*. Saarbrucken: Lambert Academic Publishing.
20 Au, K.F. (ed.) (2011). *Advances in Knitting Technology*. Cambridge: Woodhead Publishing Ltd.
21 Kadolph, S. (2010). *Textiles*. Upper Saddle River, NJ: Prentice Hall.
22 Raz, S. (1993). *Flat Knitting Technology*. Westhausen: Universal Maschinenfabrik.
23 Gries, T., Veit, D., Wulfhorst, B., Schrank, V., Hehl, A., and Weber, K.P. (2006). Processes and machines for knitwear production. In: *Textile Technology* (ed. Wulfhorst, B.), 152–166. Munich: Hanser Publishers.
24 Brackenbury, T. (1992). *Knitted Clothing Technology*. Oxford: Blackwell Scientific Publications.
25 Spencer, D.J. (2001). *Knitting Technology*, 3e. Cambridge: Woodhead Publishing Limited.
26 Yu, W. (ed.) (2016). *Advances in Women's Intimate Apparel Technology*. Duxford: Woodhead Publishing Ltd.
27 Hale, D. (2001). New developments in the manufacture of circular knitting machines for the production of medical textiles. In: *Medical Textiles* (ed. Anand, S.), 3–11. Cambridge: Woodhead Publishing Ltd.

28 Batra, S.K. (2012). *Introduction to Nonwovens Technology*. Lancaster, PA: Destech Publications.

29 Gries, T., Veit, D., Wulfhorst, B., and Gräber, A. (2006). Processes and machines for nonwoven production. In: *Textile Technology* (ed. Wulfhorst, B.), 167–187. Munich: Hanser Publishers.

30 Russell, S.J. (ed.) (2007). *Handbook of Nonwovens*. Cambridge: Textile Institute.

31 Banerjee, P.K. (2015). *Principles of Fabric Formation*. Boca Raton, FL: CRC Press.

32 Thompson, R. (2014). *Manufacturing Processes for Textile and Fashion Design Professionals*. New York: Thames & Hudson.

33 Das, D. and Pourdeyhimi, B. (2014). *Composite Nonwoven Materials: Structure, Properties and Applications*. Cambridge: Woodhead Publishing Ltd.

34 Turbak, A.F. (ed.) (1993). *Nonwovens—Theory, Process, Performance and Testing*. Atlanta, GA: TAPPI Press.

35 Anand, S.C. (2016). Technical fabric structures – 2. Knitted fabrics. In: *Handbook of Technical Textiles* (ed. Horrocks, A.R. and Anand, S.C.), pp. 163–188. Cambridge: Woodhead Publishing Ltd.

36 Walker, I.V. (2001). Nonwovens - the choice for the medical industry into the next millennium. In: *Medical Textiles* (ed. Anand, S.), 12–19. Cambridge: Woodhead Publishing.

37 Chapman, R. (ed.) (2010). *Applications of Nonwovens in Technical Textiles*. Cambridge: Woodhead Publishing Ltd.

38 Gries, T., Veit, D., and Wulfhorst, B. (2006). Braiding processes and machines. In: *Textile Technology* (ed. Wulfhorst, B.), 188–204. Munich: Hanser Publishers.

39 Kyosev, Y. (2015). *Braiding Technology for Textiles*. Cambridge: Woodhead Publishing Ltd.

40 Kyosev, Y. (2016). *Advances in Braiding Technology*. Cambridge: Woodhead Publishing Ltd.

41 Kyosev, Y. (2012). Simulation of wound packages, woven, braided and knitted structures. In: *Simulation in Textile Technology* (ed. Veit, D.), pp. 266–309. Cambridge: Woodhead Publishing Ltd.

42 Carey, J.P. (2016). *Handbook of Advances in Braided Composite Materials: Theory, Production, Testing and Applications*. Duxford: Woodhead Publishing.

43 Rana, S. (2016). *Composite Materials: Braided Structures and Composites: Reduction, Properties, Mechanics, and Technical Applications*, vol. 3. Boca Raton, FL: CRC Press.

44 Potluri, P. and Nawaz, S. (2011). Developments in braided fabrics. In: *Specialist Yarn and Fabric Structures: Developments and Applications* (ed. Gong, R.H.). Cambridge: Woodhead Publishing Ltd.

20

Chemical Characterization of Fibrous Materials

Chi-wai Kan and Ka-po Maggie Tang

The Hong Kong Polytechnic University, Institute of Textiles and Clothing, Hung Hom, Kowloon, Hong Kong, China

20.1 Introduction

New research trends focus on enhancing the functionality of fibrous materials. In the past, fibrous materials were mainly used for clothing to give warmth to the wearer, filter paper for household or industrial purposes, or hygiene products. Nowadays, the development of fibrous materials is rapid, and many advanced applications are found in the market, such as electronic textiles, medical textiles, and self-cleaning textiles.

Electronic textiles refer to a textile substrate with electrical functioning similar to electronics, which physically functions as a textile product [1]. Functional electronic textiles should be lightweight, should be comfortable to wear, and should have easy care properties [2, 3]. Conducting polymers, because of their lightweight, processability, relatively high conductivity, stability, and flexibility, are well suited for fabrication of conductive textiles [4].

Medical textiles usually have antimicrobial properties that inhibit the growth of microorganisms and can minimize a range of undesirable effects not only on the textile itself but also on the wearer. These effects include unpleasant odors, color degradation, allergic responses, deterioration of the textiles, and even potential health risks [5, 6]. A number of antimicrobial agents have been developed to impart antimicrobial properties to textile goods. These include silver, inorganic salts, organometallics, iodophors (substance that slowly releases iodine), phenols and thiophenols, onium salts, antibiotics, heterocyclics with anionic groups, nitro compounds, urea and related compounds, formaldehyde derivatives, and amines [5]. Chitosan [7], natural dyes [8], and other natural herbal products such as aloe vera, tea tree oil, eucalyptus oil, and tulsi leaf extracts can also provide antimicrobial effects.

Self-cleaning material is water, oil, and soil repellent. The superhydrophobicity is achieved by chemical and geometrical modification of the surface. By creating micro- and nanoscale roughness accompanied by a hydrophobic coating, water, and dirt on the surface can be removed easily, thus keeping the surface clean [9]. On the other hand, photocatalytic self-cleaning is based on chemical breakdown

Handbook of Fibrous Materials, First Edition. Edited by Jinlian Hu, Bipin Kumar, and Jing Lu.
© 2020 Wiley-VCH Verlag GmbH & Co. KGaA. Published 2020 by Wiley-VCH Verlag GmbH & Co. KGaA.

of dirt through photooxidation and photoreduction reactions in the presence of light. Titanium dioxide or titania is the most frequently used substance in this field [10]. Surfaces exhibit superhydrophobicity when the contact angle is greater than 150°, and contact angle hysteresis and sliding angle are low [11]. Self-cleaning materials have attracted tremendous attention in academic research and industrial areas [12].

The three advanced applications mentioned above suggest that nowadays more sophisticated treatment are being used to achieve these advanced features. The following sections describe the chemical finishing applied for these advanced applications, followed by discussion of the chemical characterization methods including Fourier transform infrared (FTIR) spectroscopy, X-ray diffraction (XRD), X-ray photoelectron spectroscopy (XPS), X-ray fluorescence, chromatographic methods, and energy-dispersive X-ray analysis (EDX). Apart from that, the performance of the treated samples and their applications are also described.

20.2 Chemical Finishing of Fibrous Materials for Advanced Applications

20.2.1 Electronic Textiles

Electronic textiles can be produced with conductive fibers, conductive yarns, or conductive inks. Properties of electronic textiles depend on the type of conductive materials used and the manufacturing method. Metallic coatings, sputtering, vacuum deposition, and filling fibers are used commonly. Applying carbon black, carbon nanotubes (CNTs), and intrinsically conducting polymers (ICPs) to a fiber surface through solution casting, inkjet printing, chemical vapor deposition, or vapor-phase polymerization methods can improve the quality of conductive fibers [13].

20.2.1.1 Conductive Fibers

Depending on the manufacturing processes adopted, conductive fibers can be divided into *intrinsic* or *extrinsic* [14], as shown in Table 20.1.

20.2.1.2 Conductive Fabrics

Apart from conductive fibers, another method of achieving conductivity is coating yarns or fabrics with a metal layer. A fine metal layer such as copper (Cu), silver (Ag), or gold (Au) can be deposited on the surface of the fibers by an electrochemical process [21]. The electrical conductivity of Cu, 99% Ag, and bronze is 58.5, 62.5, and 7.5 $S \cdot m/mm^2$, respectively [22].

20.2.1.3 Conductive Inks

Conductive ink is usually applied to fibrous materials through a coating process. It must contain a highly conductive metal precursor such as Ag, Cu, or Au nanoparticles, specific metal alloys, core–shell systems, and a carrier vehicle. Most of them are water based and can be printed onto various materials to

Table 20.1 List of conductive fibers.

Intrinsic	– Metallic and metallic alloy fibers are very thin metal filaments. They are brittle, and it is difficult to incorporate them into clothing, and they are not comfortable to wear. Also, they can damage the spinning machinery easily [15]. – Carbon fibers have a graphite-like structure [16]. – Intrinsically conducting polymers (ICPs) are organic conductive materials based on polyaniline (PANI), poly(3,4-ethylenedioxithiophene):polystyrene sulfonate (PEDOT:PSS), or polypyrrole (PPy) [17, 18]. PEDOT is a well-known and well-studied intrinsically conductive polymer (ICP). When coupled with acidic PSS, it forms a conductive, solution processable ionomer.
Extrinsic	– Conductive filled fibers, these are made by adding conductive fillers (e.g. metallic powder, metallic nanowires, carbon nanotubes (CNTs), or ICPs into nonconductive polymers such as polypropylene, polystyrene, or polyethylene [19]. These fibers are commonly made by melt spinning and solution spinning. – Conductive coated fibers are produced by coating insulating materials with conductive ones (e.g. carbon black, metals, CNTs, or ICPs) [20].

create electrically active patterns [22]. However, printing on the rough, uneven, and porous surface of the fabric can be an issue [23].

The chemical structure of conductive polymer is shown in Figures 20.1 and 20.2. Table 20.2 summarizes literature about chemicals used and treatment methods for electronic textiles.

20.2.2 Medical Textiles

For medical textiles, an active agent can be added to the fabric during different processing stages.

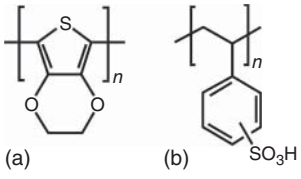


Figure 20.1 Chemical structure of (a) PEDOT and (b) PSS. Source: Irwin et al. 2011 [24]. Reproduced with permission of Springer Nature.

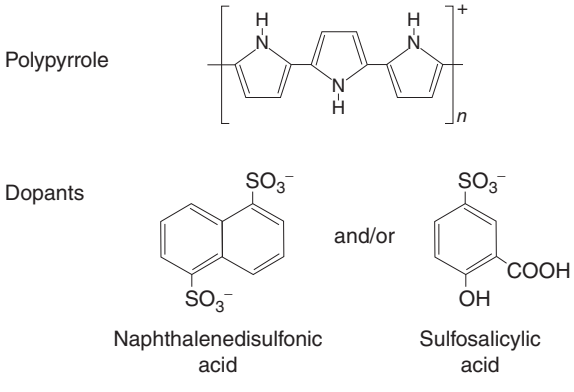


Figure 20.2 Chemical composition of electrically conductive polymer coating on Contex textiles. Source: Heisey et al. 1993 [25]. Reproduced with permission of SAGE.

Table 20.2 Literatures about chemicals used and treatment method for electronic textiles.

	Authors	Chemical used	Treatment
1	Irwin et al. [24]	The ionomer mixture of poly(3,4-ethylenedioxythiophene) and poly(styrenesulfonate) (PEDOT:PSS; 1 : 2.5, w:w) was cast onto silk fibers from a 50 : 50 (v:v) ethylene glycol solution	Dip coating
2	Yamashita et al. [26]	(1) Coating polyethylene terephthalate (PET) ribbon cable with hydrophilic poly(3,4-ethylenedioxythiophene): poly(4-styrenesulfonate) (PEDOT:PSS) followed by hydrophobic PEDOT:PSS using die-coating method (2) The PEDOT:PSS is thermally cured (3) A 10 µl drop of silicone emulsion is dropped on the hydrophobic PEDOT:PSS-coated cable, and it is then annealed	Coating
3	Rehnby and coworkers [27]	Conductive polymers (polyaniline, polythiophene, and polypyrrole) were mixed with an acrylic binder polymer and coated on a polyester fabric	Coating
4	Wu et al. [28]	Nylon Lycra fabric was soaked in an aqueous solution containing both monomer and dopant. Then an oxidant solution was added into the container to trigger polymerization on the fabric surface, followed by washing	—
5	Ding et al. [17]	(1) Soaking Spandex fabric in a conductive polymer aqueous dispersion, PEDOT–PSS (2) Secondary doping with D-sorbitol enhances the conductivity of the fabric	—
6	Kazani et al. [29]	Electrodag PF 410 conductive ink (consist of PES resin with silver particles) and 5025 conductive ink by Du-Pont (Epoxy resin with silver particles)	Screen printing
7	Karaguzel et al. [30]	(1) Different conductive silver inks of different viscosities and percentages of silver (2) The printed nonwoven fabrics were laminated using thermoplastic urethane (TPU) meltblown layer in order to secure the printed ink traces in place	Screen printing
8	Heisey et al. [25]	Polypyrrole-coated nylon	Coating
9	Lee et al. [31]	Nanosized silver colloids, synthesized by chemical reduction with formaldehyde, were dispersed by a cosolvent system made of diethylene glycol and water to get a 25 wt% silver ink	Ink-jet printing
10	Lin et al. [32]	– The polyester textile was initially immersed in either pyrrole/anthraquinone-2-sulfonic acid sodium salt (AQSA) (monomer/dopant) or a ferric chloride (oxidant) aqueous solution for a specified period of time before the polymerization reaction took place – Mixing the reactant solutions initialized the polymerization reaction – Two competitive processes occurred simultaneously in the reaction: polymerization on the surface of the substrate and in the solution.	—
11	Garg et al. [33]	Polymerization was carried out in an aqueous solution that contained pyrrole, AQSA monohydrate 97% (Sigma–Aldrich), ferric chloride hexahydrate, and Albegal FFA (Ciba Specialty Chemicals), resulting in a black PPy coating on the fabric surface	Coating

20.2.2.1 Add into the Initial Polymer Solution or Chemical Chain Prior to Fiber Extrusion

Numerous natural polymers, such as collagen, chitosan (Figure 20.3), and alginate (Figure 20.4), can be used for medical applications, including wound dressings, nonwoven felts, and meshes and sutures. These are bioabsorbable materials composed of cross-linked polymer chains and are degraded through hydrolysis of bonds, for example, peptide, hemiacetal, ester, and phosphate in the main chain into the water-soluble low molecular weight compounds. These are then absorbed by the surrounding body fluids. Similarly, anhydride, carbonate, ester, and orthoester hydrolysable units containing synthetic polymers are also bioabsorbable into the body tissues [35]. Chitosan (Figure 20.3), a major component of crustacean shells, is an effective natural antimicrobial agent derived from chitin. Burnett-Boothroyd and McCarthy [34] reported that combining these with kelp (seaweed) can increase the likelihood that the wound will heal more rapidly (Figures 20.5–20.7).

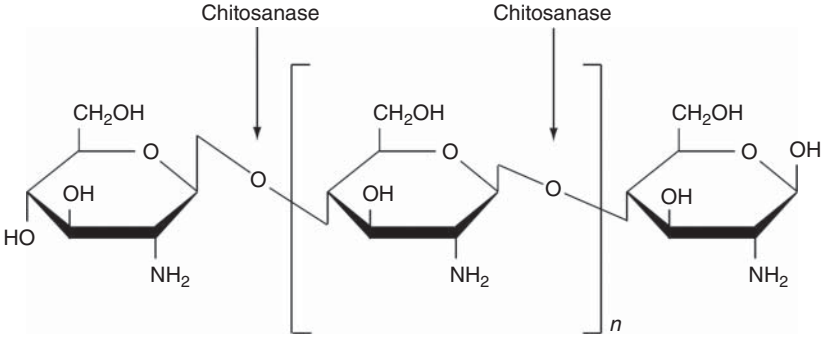


Figure 20.3 Chemical structure of chitosan polymer of β-(1-4)-D-glucosamine units. Source: Burnett-Boothroyd and McCarthy 2011 [34]. Reproduced with permission of Elsevier.

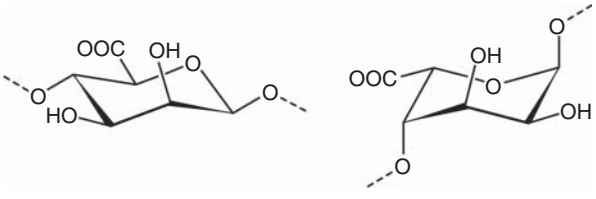
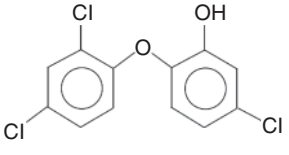


Figure 20.4 Chemical structure of alginate. Source: Rajendran et al. 2016 [35]. Reproduced with permission of Taylor & Francis.

Figure 20.5 Triclosan. Source: Burnett-Boothroyd and McCarthy 2011 [34]. Reproduced with permission of Elsevier.



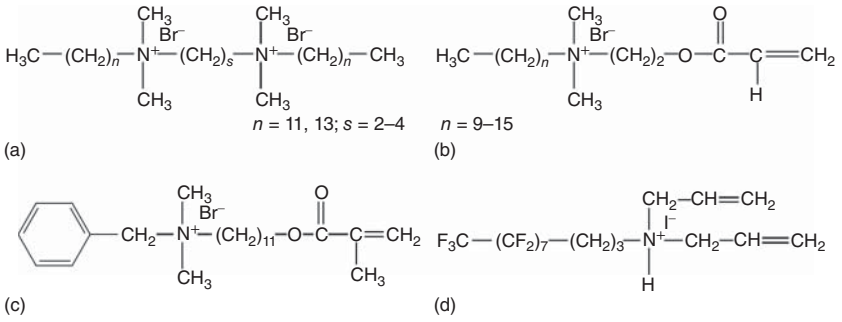


Figure 20.6 Chemical structure of quaternary ammonium compounds (QACs) used for textile applications: (a) diquaternary ammonium salt (alkanediyl-α, ω-bis(dimethylalkyl ammonium bromide)), (b) alkyl(2-(acryloyloxy)ethyl)dimethyl ammonium bromide, (c) benzyl(11-(acryloyloxy)undecyl) dimethyl ammonium bromide, and (d) *N*-(4,4,5,5,6,6,7,7,8,8,9,9,10,10,11,11-heptadecafluoroundecyl)-*N*,*N*-diallylmethylammonium iodide. Source: Nayak and Padhye 2015 [36]. Reproduced with permission of Elsevier.

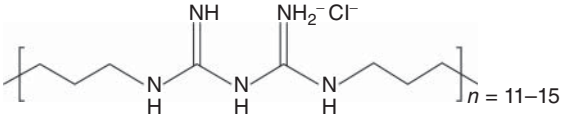


Figure 20.7 Structure of polyhexamethylene biguanide (PHMB). Source: Nayak and Padhye 2015 [36]. Reproduced with permission of Elsevier.

20.2.2.2 During Textile Finishing

The finishing agent can be applied to the textile substrate by pad-dry-cure, coating, spraying, and foam techniques and by exhaust application via a dyebath. Pad-dry-cure technique is the most commonly used. These techniques in most cases result in nondurable finishes. There are generally three mechanisms to treat fibers and fabrics for antimicrobial properties: (i) a controlled release mechanism, (ii) a regeneration principle, or (iii) a barrier or blocking action [37].

With a view to develop antimicrobial textile materials, considerable research has been carried out by making use of organic and inorganic compounds [38]. The chemicals used to achieve antibacterial function are summarized in Table 20.3. A variety of metals and metal oxides have been explored for antimicrobial finishing of textiles, including silver, titanium dioxide, zinc, copper, and cobalt. Research has also showed that metal nanoparticles are more effective than the corresponding bulk materials due to the smaller particle size, which provides larger surface area, leading to greater interaction with microorganisms [39]. A proposed scheme for silver nanoparticles attachment with 3-mercaptopropyltrimethoxysilane (3-MPTMS) on the glycidyltrimethylammonium chloride (GTAC)-treated cotton fiber is shown in Figure 20.8 [40]. Literatures about chemicals used and treatment methods for medical textiles are shown in Table 20.4.

Common polymers are used as hydrogels as scaffolds in tissue engineering, biosensors, disposable diapers, sanitary towels, and medical electrodes (Figure 20.9), including chitosan, poly(ethylene oxide) (PEO), poly(vinyl alcohol) (PVA), and poly(*N*-vinyl pyrrolidone) (PVP).

Table 20.3 Antimicrobial agents used for finishing of textiles.

Antimicrobial agents	Details
Chitosan (extracted from shrimps and crustacean shells)	Bactericidal mechanism: electrostatic interaction
Silk sericin (protein from silk worm)	Natural compounds based on animals
Triclosan (see Figure 20.5)	Inhibit growth of microorganisms using an electrochemical mode of action to penetrate and disrupt their cell walls
Quaternary ammonium compounds (see Figure 20.6)	Bind microorganisms to their cell membrane and disrupt the structure resulting in breakdown of the cell
Polybiguanides (see Figure 20.7)	– Polymeric polycationic amines that include cationic biguanide repeat units separated by hydrocarbon chain linkers of identical or dissimilar lengths [36] – One of the most used polybiguanides is a heterodisperse mixture of polyhexamethylene biguanides (PHMBs) (Figure 20.7)
Metallic compounds	– Metal-based, including cadmium, silver, copper, and mercury – Several heavy metals in the free state or in compounds are toxic to microbes at very low concentrations [36] – Cause inhibition of the active enzyme centers (inhibition of metabolism)
Silver	– The most used antibacterial agent [5] – A high degree of biocompatibility – An excellent resistance to sterilization conditions (usually temperatures in excess of 82 °C) – Antibacterial properties with respect to different bacteria with a long-term efficiency – Nanosilver can destruct the disease-causing microorganisms without any adverse effect on the human skin [5] – Low toxicity to humans
Dyes	– Mainly metal-based dyes. Chromium (Cr)- and copper (Cu)-based dyes on silk have shown effective antimicrobial efficacy [37] – Based on their respective molecular structures

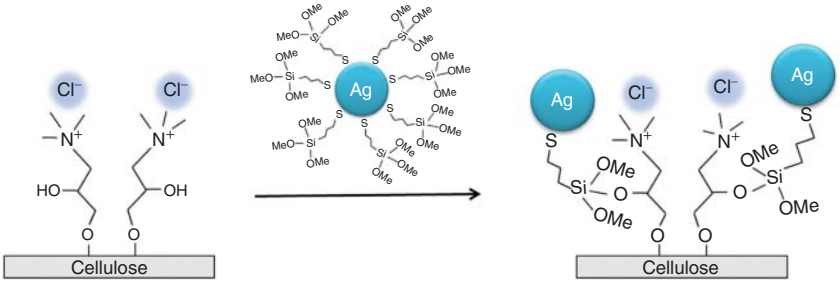


Figure 20.8 Proposed reaction scheme between silver nanoparticles/3-MPTMS and GTAC-treated cotton. Source: Kang et al. 2016 [40]. Reproduced with permission of Elsevier.

Table 20.4 Literatures about chemicals used and treatment methods for medical textiles.

	Author	Chemical used	Treatment
1	Kang et al. [40]	Cotton fibers were treated chemically with glycidyltrimethylammonium chloride (GTAC), a quaternary ammonium salt, and coated with silver nanoparticles/3-mercaptopropyltrimethoxysilane (3-MPTMS)	Coating
2	Shafei and Abou-Okeil [41]	ZnO/carboxymethyl chitosan bionano-composite	Pad-dry-cure method
3	Petkova et al. [42]	Cotton with zinc oxide nanoparticles (ZnO NPs)	Coating

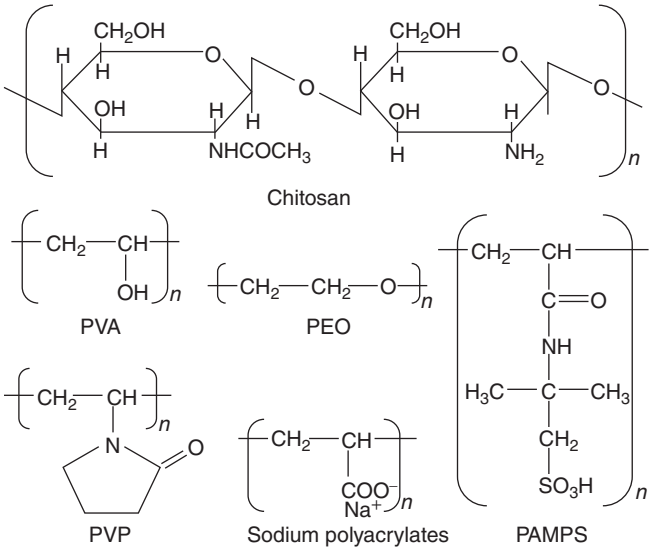


Figure 20.9 Chemical structure of polymers used as hydrogel. Source: Adapted from Gupta et al. 2010 [43].

20.2.3 Self-Cleaning Textiles

Superhydrophobic surface can be achieved by two techniques: making a rough surface from a low surface energy material or modifying a rough surface using a material of low surface energy.

The conventional padding, coating, and layer by layer (LbL) assembly technique have been used to deposit nano-coatings on textiles. Researchers have also tried to apply different materials onto the fibrous materials, including particles, rod arrays or pores, CNTs, silica particles, ZnO nanorods, and silver nanoparticles. Some examples are shown in Table 20.5.

Schematic illustration of the preparation of superhydrophobic cotton fabric in one-step treatment using EDTA and HDTMS (Figure 20.10).

Table 20.5 Literatures about chemicals used and treatment methods for self-cleaning textiles.

	Author	Chemical used	Treatment
1	Xue et al. [44]	– Coating silica nanoparticles with functional groups onto cotton textiles to generate a dual-size surface roughness – Followed by hydrophobization with stearic acid, 1H, 1H, 2H, 2H-perfluorodecyltrichlorosilane or their combination	Coating
2	Lee and Michielsen [45]	– Coating of nylon 6,6 fibers on polyester fabric – Grafted poly(acrylic acid) chains onto nylon-6,6 surfaces followed by grafting of 1H,1H-perfluorooctylamine to create a SH surface	Flock coating
3	Xu and Cai [46]	– Apply ZnO nanocrystals to cotton – Followed by fabrication of oriented ZnO nanorod arrays to develop nanoscale roughness – Fabrics were coated with dodecyltrimethoxysilane to impart surface hydrophobicity	Hydrothermal method
4	Hoefnagels et al. [47]	– Silica particles coated with amine groups were generated in situ and covalently bonded to cotton by a one or two step reaction – The amine groups were reacted with mono-epoxy functionalized polydimethylsiloxane to hydrophobize the surface	Silane-based sol–gel treatment
5	Zhao et al. [48]	Assembly of polyelectrolyte/silica nanoparticle multilayers on cotton fibers, followed by a fluoroalkylsilane treatment	Electrostatic layer by layer (LbL) assembly

A new class of self-cleaning textiles, which is superhydrophobic and photocatalytic simultaneously under visible light irradiation, is shown in Figure 20.11. Self-assembled monolayers of meso-tetra(4-carboxyphenyl)porphyrin (TCPP) were formed on TiO_2-coated cotton by a simple post-adsorption method, followed by hydrophobization with trimethoxy-(octadecyl)silane (OTMS) [50].

20.3 Principles and Methods in Chemical Characterization of Fibrous Materials

20.3.1 Fourier Transform Infrared (FTIR) Spectroscopy

Infrared spectroscopy can be used to identify compounds or investigate sample compositions. The infrared spectrum of a sample is collected by passing a beam of infrared light, in the 600–4000 cm^{-1} range, through the sample. The chemical bonds in the sample absorb specific wavelengths of the incident radiation. The amount of the transmitted light reveals how much energy is absorbed at each wavelength. A transmittance or absorbance spectrum can be produced, showing at which infrared wavelengths the sample absorbs. It depends on the nature of each molecule's vibrations or rotations. The molecular structure of the sample

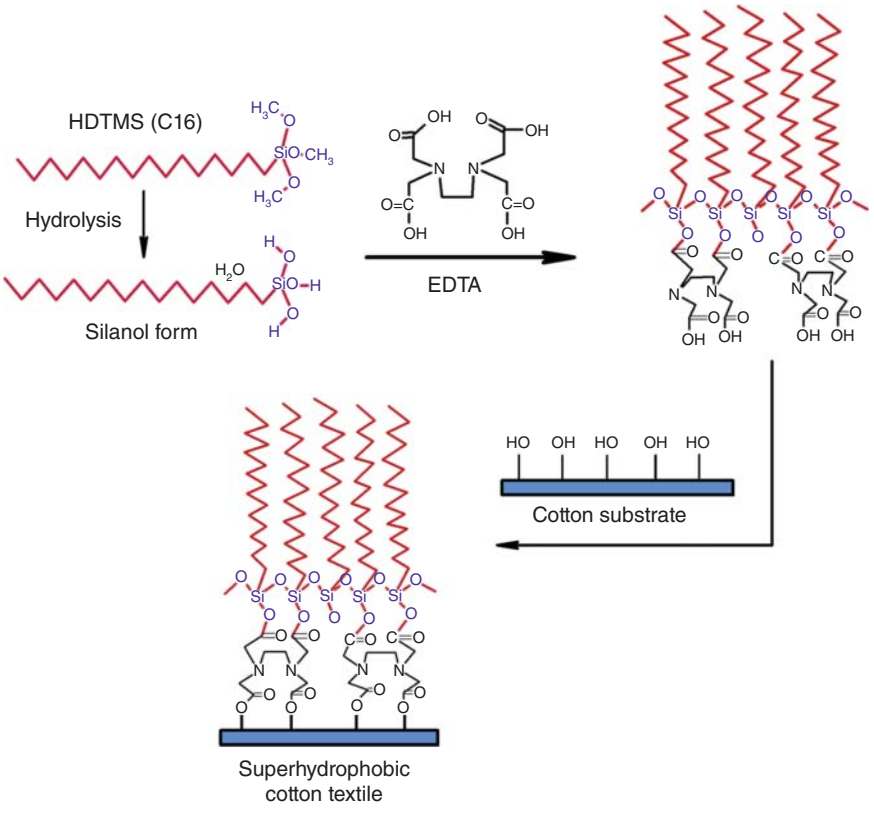


Figure 20.10 Schematic illustration of one step process for the preparation of superhydrophobic cotton textile. Source: Abbas et al. 2015 [49]. Reproduced with permission of Springer Nature.

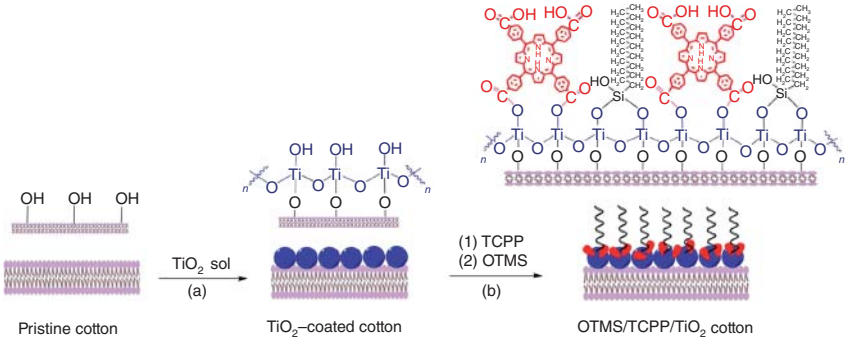


Figure 20.11 Formation of hydrophobized OTMS/TCPP/TiO_2-coated cotton. Source: Afzal et al. 2014 [50]. Reproduced with permission of Royal Society of Chemistry.

Table 20.6 Infrared frequencies associated with chemical finishes.

Absorption frequency (cm^{-1})	Chemical bond
3700–3300	O—H
3500–3200	N—H
2967–2857	C—H
2252–2062	C≡N
1750–1735	C=O (esters)
1725–1700	C=O (saturated aliphatic acids)
1725–1705	C=O (saturated aliphatic ketones)
1680–1630	C=O (amides)
1600–1500	C=C (aromatic)
1570–1515	N—H (secondary amides)
1250–1150	C—O (esters)
~1250	P=O
720–730	C—H

Source: Hauser 2005 [52]. Reproduced with permission of Elsevier.

and the presence of specific functional groups can be inferred in the transmittance or absorbance spectrum [51].

Table 20.6 lists some of the frequencies associated with chemical finishes used with textiles [52].

Krishnaveni and Thambidurai [53] confirmed the presence of chitosan by FTIR spectroscopic analysis (Figure 20.12a and b). FTIR spectra of cross-linked cotton fabric treated with chitosan (AN–CS) and chitosan–ZnO composite (AN–CZO) are shown in Figure 20.12c and d, respectively. Compared with chitosan and cotton cellulose, the new peak at 2372 cm^{-1} (Figure 20.12c) can be attributed to the C–N asymmetric band stretching [54]. The peak that appeared at 2252 cm^{-1} for AN–CZO (Figure 20.12d) is due to the stretching vibration of C≡N of the beta-cyanoethyl group resulting from the addition of acrylonitrile. The presence of ZnO in the cross-linked fabric was also confirmed from the peak that appeared at 470 cm^{-1} in Figure 20.12c [55]. This example demonstrates the use of FTIR to identify compounds or investigate sample compositions.

20.3.2 X-Ray Diffraction (XRD)

XRD is a powerful nondestructive technique for characterizing (identification/quantification) crystalline materials. It provides information on crystal structure, phase, preferred crystal orientation (texture), and other structural parameters, such as average grain size, crystallinity, strain, and crystal defects. Figure 20.13 shows the XRD pattern of bacterial cellulose (BC), polypyrrole (PPy), and a composite. The XRD spectrum of PPy exhibits no diffraction peaks, indicating its amorphous structure. Three main peaks can be identified in spectra of BC and BC/PPy, which can be assigned to the $(1\bar{1}0)$, (110), and (200) diffraction planes, which is typical for cellulose I [57, 58]. The estimated degree

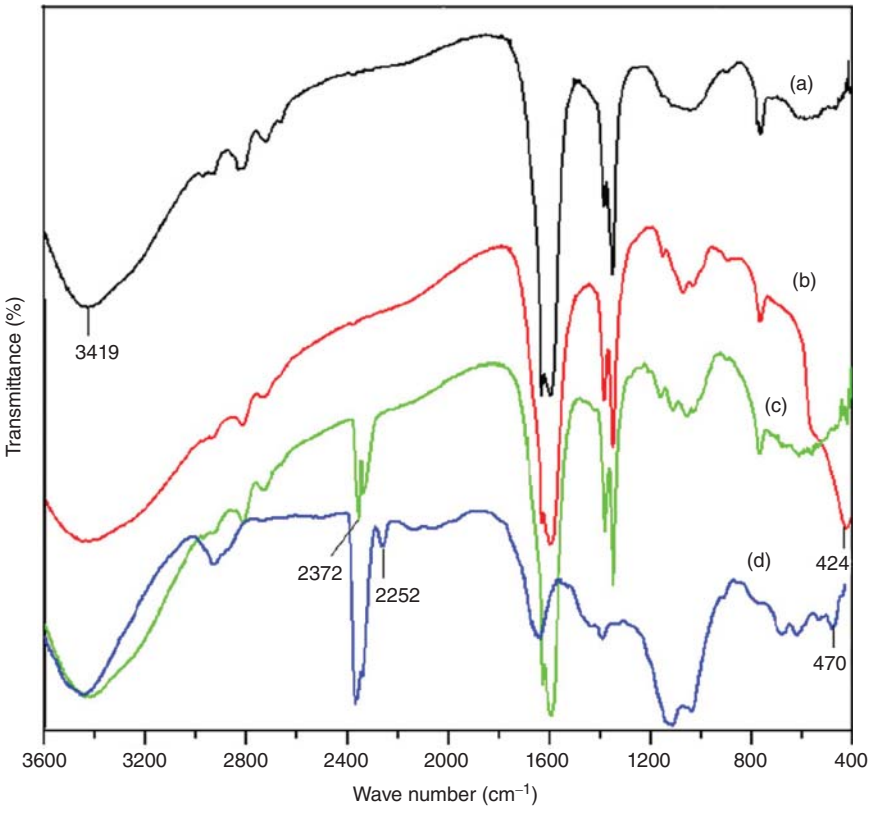


Figure 20.12 The FTIR spectrum of (a) chitosan, (b) CZO, (c) AN–CS, and (d) AN–CZO. Source: Krishnaveni and Thambidurai [53]. Reproduced with permission of Elsevier.

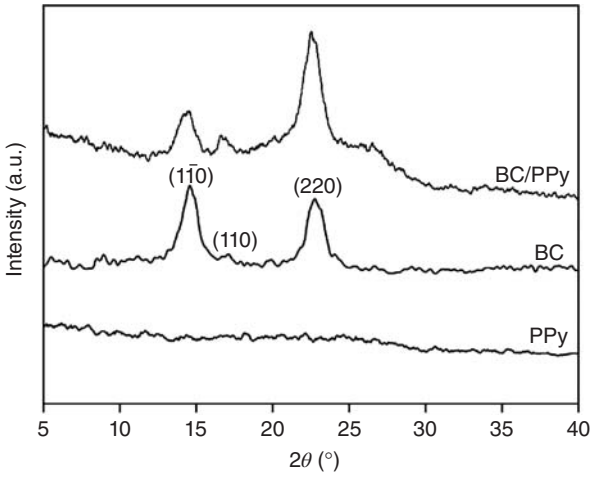


Figure 20.13 XRD spectra of pure BC, pure PPy, and a BC/PPy composite. Source: Müller et al. 2011 [56]. Reproduced with permission of Elsevier.

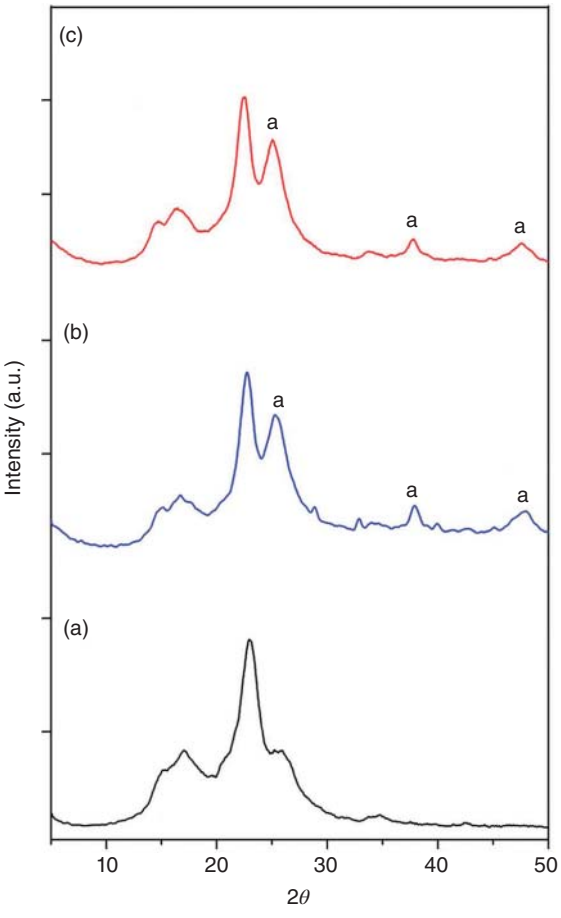


Figure 20.14 XRD spectra of cotton: (a) pristine, (b) TiO_2-coated cotton, (c) OTMS/TCPP/TiO_2-coated cotton (a = peaks associated with anatase). Source: Afzal et al. 2014 [50]. Reproduced with permission of Royal Society of Chemistry.

of crystallinity was $56 \pm 5\%$ for BC membrane and $51 \pm 5\%$ for the BC/PPy composite. This demonstrates that the crystalline structure of cellulose matrix was not significantly modified in the BC/PPy composites.

Another research work used XRD to determine crystallinity of TiO_2 films on cotton. Figure 20.14a shows that there is no anatase-associated peak for the pristine cotton while cotton samples coated with TiO_2 show the characteristic diffraction peaks for anatase at $2\theta = 25.4°$, 38.0°, and 48.0° (Figure 20.14b). After deposition of TCPP and OTMS, the same anatase peaks can still be observed (Figure 20.14c). Hence, TiO_2 retains its crystallinity even after modification with TCPP and OTMS [50].

20.3.3 X-Ray Photoelectron Spectroscopy (XPS)

XPS is also known as electron spectroscopy for chemical analysis (ESCA). Photoelectron spectroscopy uses photo-ionization and energy-dispersive analysis of the emitted photoelectrons to study the composition and electronic state of the surface region of a sample. The ejected electron energies are characteristic of

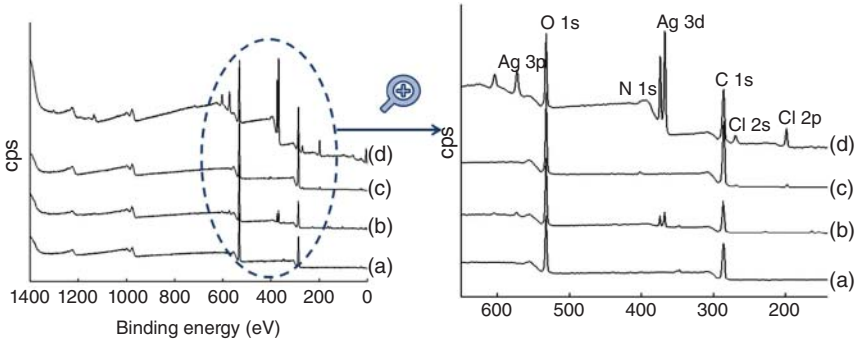


Figure 20.15 XPS spectra of (a) naïve cotton, (b) cotton treated with silver nanoparticles/0.1% (v/v) of 3-MPTMS, (c) cotton treated with 50% (v/v) of GTAC, (d) treated cotton with 50% (v/v) of GTAC and silver nanoparticles/0.1% (v/v) of 3-MPTMS. Source: Kang et al. 2016 [40]. Reproduced with permission of Elsevier.

binding energies of the atoms on the material's surface. The shapes of the peaks in the electron energy spectrum are influenced by chemical bonding, so XPS can provide both elemental and chemical bond information [51]. This can be used to characterize some treatments that are restricted to the surface of the material, such as plasma treatment and conductive polymer coating [25].

Kang et al. [40] used XPS to confirm the presence of silver in cotton fibers treated with 3-MPTMS/silver nanoparticles (Figure 20.15); the binding energy of the silver nanoparticles was 368 and 374 eV, which were assigned to Ag [59].

Figure 20.16 shows XPS results of various cotton samples. Ordinary cotton exhibits distinctive signals at 285.0, 532.0, and 400 eV indicating the presence of carbon, oxygen, and nitrogen, respectively. With Ar and H_2 plasma treatment, XPS results show an increase in carbon (C) and a decrease in oxygen (O) content, whereas the signal for oxygen plasma-pretreated cotton shows values comparable with pristine cotton [60].

20.3.4 X-Ray Fluorescence

When a material is exposed to a beam of high-energy X-ray radiation, the electrons emit characteristic fluorescence. The intensity of each individual fluorescence is proportional to the amount of that element present. The elements with atomic number 12 (magnesium) and higher are most suitable to be studied by X-ray fluorescence [52].

A study has shown that the amount of TiO_2 loaded on the cotton samples can be determined by X-ray fluorescence measurements. TiO_2 loaded on the cotton was found to be 1.5–2 wt% approximately, while pristine cotton was used as a reference [50].

20.3.5 Chromatographic Methods

The finishing must be separated from the fibrous materials and solubilized prior to chromatographic analysis. For pyrolysis chromatography, the samples should

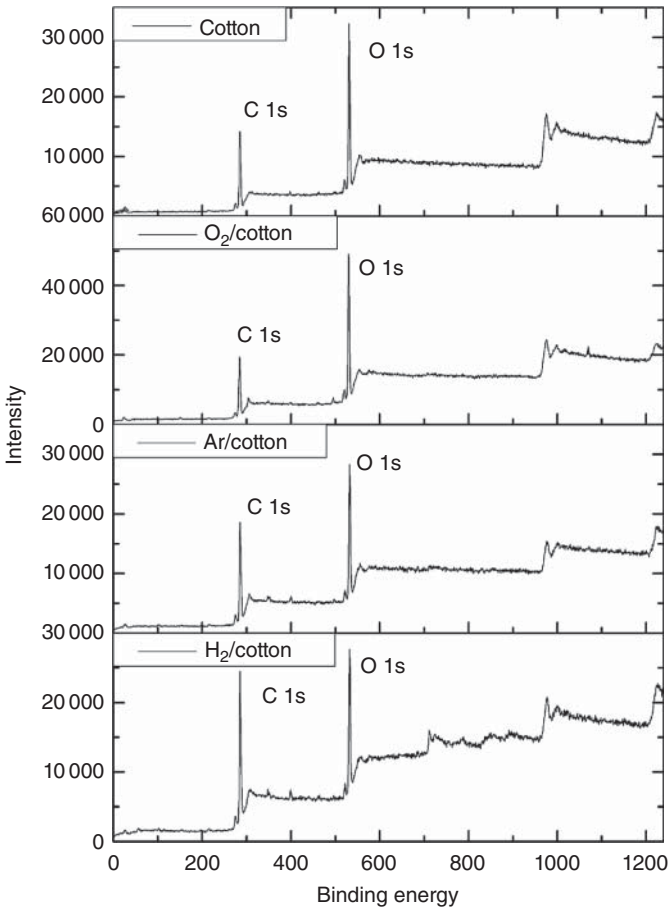


Figure 20.16 XPS survey scan analysis of pristine cotton compared with the cotton that has undergone various plasma pretreatments. Source: Caschera et al. 2013 [60]. Reproduced with permission of American Chemical Society.

be heated to very high temperature (600–1000 °C) for a very short period of time. The volatile products of this pyrolysis can then be analyzed by gas chromatography (PY–GC), mass spectrometry (PY–MS), or a combination of the two (PY–GC–MS) [52].

20.3.6 Energy-Dispersive X-Ray Analysis (EDX)

EDX analysis is an analytical technique commonly used for analysis of chemical compositions. It analyzes X-rays emitted by a material when it is hit with electromagnetic radiation [51]. Figure 20.17 shows the EDX spectrum of a treated sample confirming the existence of silver element on the surface of the fabric treated with 100 ppm of nanosilver particles. As a tiny peak of silver was observed, it suggests that there was only a small amount of nanosilver particles on the surface of the treated fabrics. Also the presence of sodium element in the EDX

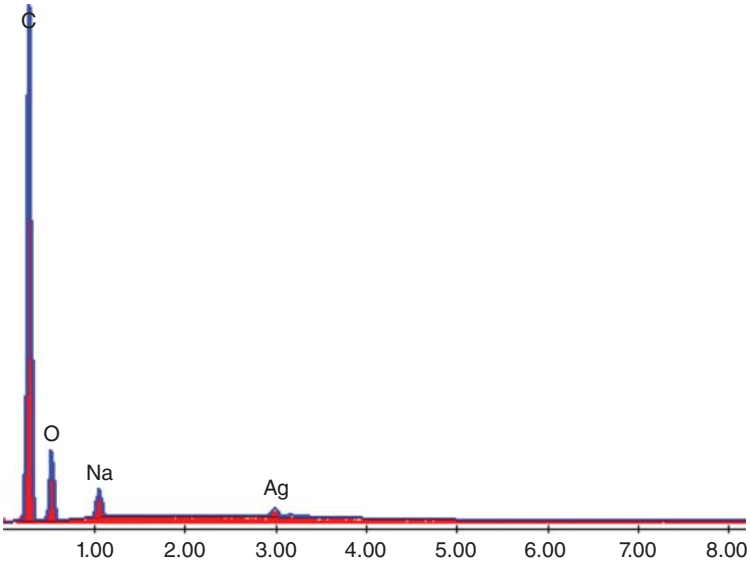


Figure 20.17 EDX image for cotton-coated fabric with 100 ppm AgNPs. Source: El-Rafie et al. 2014 [61]. Reproduced with permission of American Chemical Society.

spectrum is related to the alkaline solution of nanosilver particles that contains sodium hydroxide [61].

In another study, energy-dispersive spectroscopy analysis was conducted to examine chemical composition of the surface of the fabric. As shown in Figure 20.18a, only peaks of C and O were detected on the pristine fabric. After the polyvinylidene fluoride (PVDF)/polydimethylsiloxane (PDMS) treatment, new peaks for F and Si were observed (Figure 20.18b). F is mainly from PVDF, while Si is from PDMS. It suggests that the fabric was successfully coated with PVDF and PDMS [12].

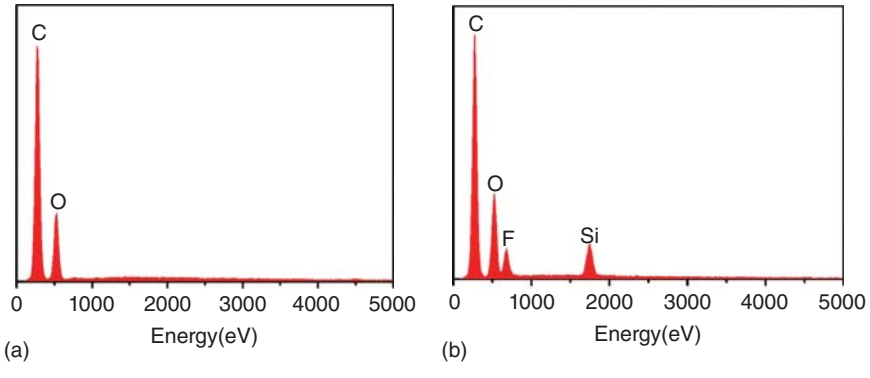


Figure 20.18 EDX of the samples (a) pristine fabric and (b) PVDF/PDMS-coated fabric. Source: Xue et al. 2016 [12]. Reproduced with permission of Royal Society of Chemistry.

20.3.7 Scanning Electron Microscope (SEM)

The scanning electron microscope (SEM) has the benefit of providing a great depth of field and extremely high resolution images at magnification levels in excess of 10 000× of a surface [62]. With the help of SEM, the fibrous surface characteristics can be analyzed extensively. The information obtained from SEM is normally qualitative, but with the use of software, surface properties of average roughness (R_a), rms roughness (R_{rms}), and fractal parameters can be obtained [62].

20.3.8 Atomic Force Microscopy (AFM)

The atomic force microscopy (AFM) comprises a scanning probe, with a tip at the end of a cantilever. The probe is made to scan in the very near surface region (in the van der Waals' forces) of a surface, and an intricate control system enables the tip to follow the contours of the surface in great details [62]. Imaging of individual atoms has been possible with the use of AFM for analyzing the fibrous surface [62]. The surface properties of fibrous materials for advanced application would play a fundamental role in affecting some key technical properties, which may closely be related to the processing condition [62]. With the understanding of the atomic changes in the surface of fibrous materials after different treatments, the processing parameters can be changed and optimized for achieving better final properties. The AFM can serve this purpose to obtain important topographical information of a fibrous material [62].

20.4 Performance, Evaluations, and Applications of Chemical Treatment on Fibrous Materials

20.4.1 Electronic Textiles

Electrically conducting fibers can be used for antistatic, antimicrobial, anti-odor, shielding, and other applications. In electronic textiles, the conducting elements can provide power, deliver input and output signals, or act as a transducer. E-textiles, depending on the purpose of usage, can be classified into two basic categories [62]: (i) fashion and (ii) utility. Table 20.7 summarizes some helpful literature on evaluations, performances, and applications of electronic textiles.

20.4.1.1 Fashion Statements

Electronic textiles can be used for costumes, catwalks, and consumer entertainment.

20.4.1.2 Utility Functions

Military This is highly desirable in applications such as uniform for warfighters where they integrate solar energy, optics, communication, and global positioning systems into clothing or an accessory [24].

Table 20.7 Literatures on evaluations, performance, and applications of electronic textiles.

Author	Evaluations	Performance	Applications
Irwin et al. [24]	– Dynamic mechanical analysis (DMA) – Electrical conductivity – SEM imaging	– Young's modulus and mechanical strength are maintained – The electrical conductivity of PEDOT:PSS-coated samples is 8.5 S/cm, which is only 10× less than sample made by Ag-coated thread	Electrical interconnects used in flexible, fully functional 555 timer circuits stitched into fabric substrates
Yamashita et al. [26]	– SEM imaging – Bending radius – Electrical resistance – Durability (cycle load test)	– Functions as the electrical contact between weft and warp (interlaced) fiber ribbons – Enhances the durability, flexibility, and stability of electrical contact in the woven e-textile better than those of the ribbons without it	Electrical contact structure in flexible device technology
Rehnby and coworkers [27]	– SEM imaging – Surface resistivity – Fastness to rubbing and shear	– The concentration of the conductive polymer and the number of coated layers should be further investigated	Conductive surfaces for smart textile applications
Wu et al. [28]	– Scanning electron microscopy – Thermogravimetric analysis (TGA) – Surface resistivity versus aging time – Force versus stretching	– Conductive polypyrrole-coated nylon Lycra fabric was found less stable in air due to its reactivity with a variety of atmospheric chemicals, especially oxygen – PPy-coated nylon Lycra is suitable to apply as a strain gauge when stretched up to 50–60%	Functional wearable textile sensing systems can monitor human motion and provide immediate, individual, and objective biofeedback. This innovative technique can be widely used for injury prevention, rehabilitation, sport techniques modification, and medical treatment
Ding et al. [17]	– Hydrophilicity – SEM imaging	– Fabrics with higher water uptake resulted in higher conductivity – Allowing for perception of the electrochromic color change on the surface of the fabric	Wearable displays and truly integrated fabric electronics

Kazani et al. [29]	Square resistance at different stages (i.e. after printing, abrading, and washing)	– Exhibit good electrical properties after printing and abrading	Produce flexible, conductive, lightweight, practical and comfortable "smart textiles"
Karaguzel et al. [30]	– Surface tension – Viscosity – Fastness to washing – Time domain reflectometry (TDR) measurement	Coating of the printed lines with a meltblown layer could improve the durability of the finishing	Fabric biomedical sensors
Heisey et al. [25]	– X-ray photoelectron spectroscopy – SEM imaging – Dynamic contact angle measurements – TGA	– Using TGA–MS, the 4.5% weight loss from the polypyrrole-coated nylon fiber by 298 °C was due to evolution of water and carbon dioxide – The adhesion of epoxy to the control nylon fiber was better than to the polypyrrole-coated nylon fiber	—
Lee et al. [31]	– Electrical resistivity	The electrical resistivity of the printed line is close to the bulk resistivity of silver	Serve as conducting lines for electronic applications
Lin et al. [32]	– FTIR – SEM imaging – Optical fibre diameter analyser (OFDA) – coating thickness – Transmission electron microscopy (TEM) – identifying the conducting polymer layer – Surface resistance – AATCC 76 – Abrasion resistance	Surface resistance changed as the thickness of the coating layer varied from 0.1–0.6 μm	Electromagnetic shielding, chemical sensors, and heating fabrics
Garg et al. [33]	– Surface contact angle – Wettability – Surface energy change – Abrasion resistance – Surface resistivity – Reflectance	– Treated fabrics exhibited better hydrophilicity and increased surface energy – Surface treatment by an APGD gas mixture of 95% helium/5% nitrogen yielded the best results with respect to coating uniformity, abrasion resistance, and conductivity	Sensors, actuators, electromagnetic shields, and absorbers and heating

Medical The electrocardiogram (ECG) is a skin surface measurement of the electrical activity of the heart muscle. The electrical potential on the body surface at different locations varies, generating different ECG vectors. These vectors are known as leads. The ECG leads are formed from three different electrodes placed on the body. Silver-coated yarns are commonly used to make the electrodes [63]. An electromyogram (EMG) records measurements of a muscle's electrical activity that occurs during muscle contraction and relaxation cycles [64]. Finni et al. [65] use textile electron embedded into shorts to measure EMG activity. An electroencephalogram (EEG) records voltage differences between points on the scalp generated by brain structures. The electrodes are often fixed onto a cap, made of elastic fabric, to guarantee a proper configuration [66].

Electrically conducting fibers can be used directly to measure strain. A strain sensor can measure a variation in length of an object. Most commonly the sensing mechanism is resistive, meaning that stretching the sensor causes a measurable change in resistance [67]. Cochrane et al. [68] made a flexible textile compatible strain sensor, which is based on conductive polymer composites. Xue et al. [69] studied a PPy-coated XLA elastic fiber as a textile strain sensor. These textile-based strain sensors can be used to measure breathing rate, posture, or body motion. It is reported that PPy-coated Lycra compares well with sensitive strain gauge materials and inorganic thermistors [70].

Electrically conducting fibers can also be used as pressure sensors. A pressure sensor can measure the change in resistance or in capacitance with the change in pressure. This can be used to evaluate the comfort when wearing some tight-fitting garment such as intimate apparel. Pressure sensors can be made by coating a composite of PDMS [71]. Apart from that, electronic fibers can also be used as temperature sensor, heat flux sensor, and sweat/humidity sensor.

Safety Gas sensors are used to detect volatile compounds, such as odor of urine, armpit sweat, or exhaled breath. The fibers used are able to change their electrical properties when a particular chemical agent is presented near the sensor [72]. Using a polymer coating such as PPy or polyaniline (PANI) onto polyethylene terephthalate (PET) can fabricate toxic gas sensors [73]. Poly(3,4-ethylenedioxithiophene) (PEDOT) nanotubes are suitable for monitoring concentration levels of nitric oxide (NO) [74].

Pragmatic Applications These include charging and controlling digital devices, caller ID and other smart phone applications, and visual feedback transferred to wearable displays.

Figure 20.19 depicts an example showing the application of electronic textiles. An intelligent knee sleeve is composed of a strip of Lycra coated with a thin layer of conducting PPy. When the coated fabric is stretched, resistance of the textile changes, resulting in changes of the output of an electronic circuit, so different sounds are emitted according to the strain from the coated fabrics.

20.4.2 Medical Textiles

An antimicrobial agent is defined as a natural or synthetic substance that kills or inhibits the growth of microorganisms such as bacteria, fungi, and algae.

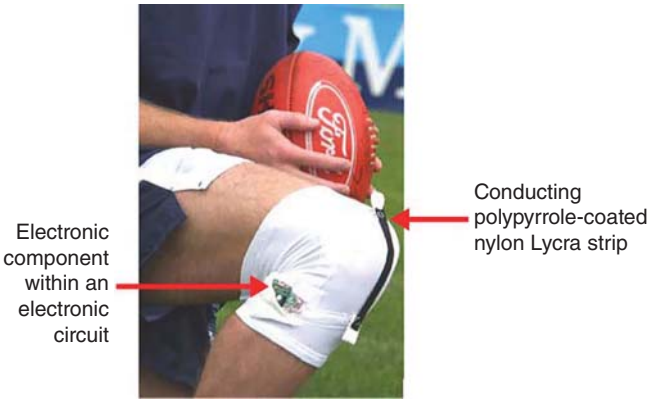


Figure 20.19 The knee sleeve . Source: Wu et al. 2005 [28]. Reproduced with permission of Elsevier. Photo: Courtesy of CSIRO TFT.

The application of this agent not only helps to protect the user of a textile material against microbes related to aesthetic, hygienic, or medical problems but also to protect the textile material itself. Some of the specific applications in medical and hygiene textiles include sutures, surgical gowns, face masks, bandages, drapes, bedding or blankets, surgical hosiery, and incontinence diapers [37].

Antimicrobial treatments for textiles materials are necessary [34]: (i) to avoid cross-contamination by pathogenic microorganisms, (ii) to control infestation by microorganisms, (iii) to reduce the formation of odor caused by metabolism in bacteria, and (iv) to prevent deterioration of the quality of a textile product. Therefore, the antimicrobial property, anti-odor property, and mechanical property of the medical textiles should be evaluated.

Antibacterial tests are used to determine the survival, growth, or inhibition of the isolate. Generally, testing involves using bacteria such as *Staphylococcus aureus* or *Klebsiella pneumoniae* (common isolates that can be replicated easily). The usual test methods for testing the antimicrobial efficacy of textiles are JIS 1907, AATCC 147, and AATCC 100. Table 20.8 summarizes some helpful literature on evaluations, performance, and applications of medical textiles.

20.4.3 Self-Cleaning Textiles

The most important method for evaluation of self-cleaning textiles is water and soil repellency, which can be measured using the contact angle method. Both static and sliding contact angles should be measured. Tablecloths, men's suits, awnings, tents, and other architectural structures can stay spotlessly clean without requiring any washing or cleaning [9] if they are self-cleaned. Apart from being water and soil repellent, self-cleaning textiles should not absorb any body tobacco odors. Table 20.9 summarizes some helpful literatures on evaluations, performance, and applications of self-cleaning textiles.

Table 20.8 Literatures on evaluations, performance, and applications of medical textiles.

Author	Evaluations	Performance	Applications
Kang et al. [40]	– Scanning electron microscopy – X-ray photoelectron spectroscopy (XPS) – Thermogravimetric analysis – Antibacterial property	The cotton fibers treated with both GTAC and silver nanoparticles showed synergistic antibacterial properties against *Pseudomonas aeruginosa*	A new approach to prepare hybrid antibacterial cotton fibers with a synergistic antibacterial efficacy in the medical and biomaterial industry
Shafei and Abou-Okeil [41]	– UV spectroscopy – FTIR – Transmission electron microscope (TEM) – X-ray diffraction (XRD) – UPF rating – Antibacterial property	Finished cotton fabric exhibits very good antibacterial properties against Gram-positive and Gram-negative bacteria, which increased with increasing the composite concentration, and also has a good UV protection, which increased with increasing the temperature of curing	Protection of the body against solar radiation, bacterial action, and for other technological applications
Cho (2009) [70]	– SEM imaging – Antibacterial property	The NP-coated cotton fabrics inhibited the growth of the medically relevant *Staphylococcus aureus* and *Escherichia coli*, respectively, by 67 and 100%	Diminish the risk of hospital-acquired infections

Table 20.9 Literatures on evaluations, performance, and applications of self-cleaning textiles.

Author	Evaluations	Performance	Applications
Xue et al. [44]	– Contact angle measurement – SEM imaging – Transmission electron microscopy – Fourier transformation infrared spectroscopy – Thermal gravimetric analysis	The incorporation of functionalized SiO_2 particles not only generates a dual-size surface roughness but also facilitates further hydrophobization of the surfaces to achieve a superhydrophobic property	Simple fabrication, easy availability of raw materials, and production of large superhydrophobic surfaces
Lai et al. [75]	– SEM imaging – TEM – XPS – XRD – UV–vis transmittance – AFM – Water contact angle	Upon heat treatment, samples with three very different wetting states can be obtained, viz. highly hydrophobic with strong adhesion, superhydrophobic with weak adhesion, and superhydrophilic with rapid water spreading	A wide range of applications such as microdroplet transportation, self-cleaning, antifogging, ultrafast spreading for biomolecules analysis, ultrafast absorption in printing

20.5 Performance Tests

In this chapter, we reviewed the development of fibrous materials with advanced applications such as electronic textiles, medical textiles, and self-cleaning textiles and discussed their specific performances. Although the development of each type of fibrous materials has its specific use, if they are applied for wearable use, they should meet certain wearable performance like general apparel. Despite their own applications, the functionality of fibrous materials with advanced application should be improved to meet the increasing expectations of the customers.

Table 20.10 lists various fabric performance tests, including easy care, flame retardancy, water and soil repellency, UV protection property, and anti-insect

Table 20.10 Summary of various performance tests.

Finishing	Test method
Durable press testing	AATCC 66 Wrinkle recovery of woven fabrics: Recovery Angle
	AATCC 88C Retention of creases in fabrics after repeated home laundering
	AATCC 124 Appearance of fabric after repeated home launderings
	AATCC 128 Wrinkle recovery of fabrics: Appearance method
	AATCC 135 Dimensional changes in automatic home laundering
Flame retardancy testing	Test 16 CFR 1610 Standard for the Flammability of Clothing Textiles
	ASTM D2863 Standard Test Method for Measuring the Minimum Oxygen Concentration to Support Candle-Like Combustion of Plastics (Oxygen Index)
Soil release testing	AATCC 130 Soil release: Oily stain release method
Repellency testing	AATCC 22 Water repellency: Spray test
	AATCC 35 Water resistance: Rain test AATCC 118 Oil repellency: Hydrocarbon resistance test
	ISO 9865 Textiles: Determination of water repellency of fabrics by the Bundesmann rain-shower test
UV Protective testing	AATCC 183 Transmittance or blocking of erythemally weighted ultraviolet radiation through fabrics
Anti-insect and mite testing	AATCC 24 Insects, resistance of textiles to AATCC 28 Insect pest deterrents on textiles
Strength	ASTM D6797 Standard Test Method for Bursting Strength of Fabrics Constant-Rate-of-Extension (CRE) Ball Burst Test
	ASTM D3787 Standard Test Method for Bursting Strength of Textiles—Constant-Rate-of-Traverse (CRT) Ball Burst Test
	ASTM D3786 Standard Test Method for Bursting Strength of Textile Fabrics—Diaphragm Bursting Strength Tester Method
	ASTM D5034 Standard Test Method for Breaking Strength and Elongation of Textile Fabrics (Grab Test)
	ASTM D1424 Standard Test Method for Tearing Strength of Fabrics by Falling-Pendulum
	(Elmendorf-Type) Apparatus

and mite testing, which should be considered when developing fibrous materials with advanced applications.

20.6 Conclusion

In this chapter, we have reviewed the performance and applications of electronic textiles, medical textiles, and self-cleaning textiles briefly. These textile applications are growing rapidly in textile and fashion product markets. Being comfortable, functional, and safe textile and fashion products, they should meet different criteria from the customers, and therefore, different existing evaluation methods are discussed. Due to the huge research on these products, it is not surprising that new technology and international standards will develop in the future for characterizing these products effectively.

Acknowledgment

The authors would like to thank the financial support from the Hong Kong Polytechnic University for this work.

References

1 Stoppa, M. and Chiolerio, A. (2016). 4 – Testing and evaluation of wearable electronic textiles and assessment thereof. In: *Performance Testing of Textiles* (ed. Lijing Wang), 65–101. Woodhead Publishing.
2 Mattila, H.R. (2006). *Intelligent Textiles and Clothing*. Cambridge, Boca Raton, FL: Woodhead Publishing.
3 Tao, X. and Textile, I. (2005). *Wearable Electronics and Photonics*. Boca Raton, FL; Cambridge: Woodhead Publishing.
4 Malinauskas, A. (2001). Chemical deposition of conducting polymers. *Polymer* 42: 3957–3972.
5 Murugesh Babu, K. and Ravindra, K. (2015). Bioactive antimicrobial agents for finishing of textiles for health care products. *Journal of the Textile Institute* 106: 706–717.
6 Zhang, Y., Xu, Q., Fu, F., and Liu, X. (2016). Durable antimicrobial cotton textiles modified with inorganic nanoparticles. *Cellulose* 23: 2791–2808.
7 Lim, S.-H. and Hudson, S.M. (2003). Review of chitosan and its derivatives as antimicrobial agents and their uses as textile chemicals. *Journal of Macromolecular Science, Part C: Polymer Reviews* 43: 223–269.
8 Gupta, D., Khare, S.K., and Laha, A. (2004). Antimicrobial properties of natural dyes against Gram-negative bacteria. *Coloration Technology* 120: 167–171.
9 Gupta, D. and Gulrajani, M.L. (2015). 8 – Self cleaning finishes for textiles. In: *Functional Finishes for Textiles* (ed. Roshan Paul), 257–281. Woodhead Publishing.

10 Fujishima, A. and Zhang, X. (2006). Titanium dioxide photocatalysis: present situation and future approaches. *Comptes Rendus Chimie* 9: 750–760.
11 Zhang, X., Shi, F., Niu, J. et al. (2008). Superhydrophobic surfaces: from structural control to functional application. *Journal of Materials Chemistry* 18: 621–633.
12 Xue, C.-H., Li, X., Jia, S.-T. et al. (2016). Fabrication of robust superhydrophobic fabrics based on coating with PVDF/PDMS. *RSC Advances* 6: 84887–84892.
13 Im, S.G. and Gleason, K.K. (2007). Systematic control of the electrical conductivity of poly (3,4-ethylenedioxythiophene) via oxidative chemical vapor deposition. *Macromolecules* 40: 6552–6556.
14 Bashir, T. (2013). Conjugated polymer-based conductive fibers for smart textile applications. Chalmers University of Technology. Ph.D.
15 Araki, T., Makikawa, M., and Hirai, S. (2012). Experimental investigation of surface identification ability of a low-profile fabric tactile sensor. In: *2012 IEEE/RSJ International Conference on Intelligent Robots and Systems (IROS)*, 4497–4504. IEEE.
16 Dalmas, F., Dendievel, R., Chazeau, L. et al. (2006). Carbon nanotube-filled polymer composites. Numerical simulation of electrical conductivity in three-dimensional entangled fibrous networks. *Acta Materialia* 54: 2923–2931.
17 Ding, Y., Invernale, M.A., and Sotzing, G.A. (2010). Conductivity trends of PEDOT-PSS impregnated fabric and the effect of conductivity on electrochromic textile. *ACS Applied Materials & Interfaces* 2: 1588–1593.
18 Bocchini, S., Chiolerio, A., Porro, S. et al. (2013). Synthesis of polyaniline-based inks, doping thereof and test device printing towards electronic applications. *Journal of Materials Chemistry C* 1: 5101–5109.
19 Thongruang, W., Spontak, R.J., and Balik, C.M. (2002). Correlated electrical conductivity and mechanical property analysis of high-density polyethylene filled with graphite and carbon fiber. *Polymer* 43: 2279–2286.
20 Xue, P., Tao, X., Kwok, K.W. et al. (2004). Electromechanical behavior of fibers coated with an electrically conductive polymer. *Textile Research Journal* 74: 929–936.
21 Schwarz, A., Hakuzimana, J., Westbroek, P., and Van Langenhove, L. (2009). How to equip para-aramide yarns with electro-conductive properties. In: *2009 6th International Workshop on Wearable and Implantable Body Sensor Networks. BSN 2009*, 278–281. IEEE.
22 Stoppa, M. and Chiolerio, A. (2014). Wearable electronics and smart textiles: a critical review. *Sensors* 14: 11957–11992.
23 Merilampi, S., Björninen, T., Haukka, V. et al. (2010). Analysis of electrically conductive silver ink on stretchable substrates under tensile load. *Microelectronics Reliability* 50: 2001–2011.
24 Irwin, M.D., Roberson, D.A., Olivas, R.I. et al. (2011). Conductive polymer-coated threads as electrical interconnects in e-textiles. *Fibers and Polymers* 12: 904.
25 Heisey, C., Wightman, J., Pittman, E., and Kuhn, H. (1993). Surface and adhesion properties of polypyrrole-coated textiles. *Textile Research Journal* 63: 247–256.

26 Yamashita, T., Miyake, K., and Itoh, T. (2012). Conductive polymer coated elastomer contact structure for woven electronic textile. In: *2012 IEEE 25th International Conference on Micro Electro Mechanical Systems (MEMS)*, 408–411. IEEE.

27 Skrifvars, M., Rehnby, W., and Gustafsson, M. (2008). Coating of textile fabrics with conductive polymers for smart textile applications. Ambience'08, Borås, Sweden.

28 Wu, J., Zhou, D., Too, C.O., and Wallace, G.G. (2005). Conducting polymer coated lycra. *Synthetic Metals* 155: 698–701.

29 Kazani, I., Hertleer, C., De Mey, G. et al. (2012). Electrical conductive textiles obtained by screen printing. *Fibres & Textiles in Eastern Europe* 20: 57–63.

30 Karaguzel, B., Merritt, C., Kang, T. et al. (2009). Flexible, durable printed electrical circuits. *Journal of the Textile Institute* 100: 1–9.

31 Lee, H.-H., Chou, K.-S., and Huang, K.-C. (2005). Inkjet printing of nanosized silver colloids. *Nanotechnology* 16: 2436.

32 Lin, T., Wang, L., Wang, X., and Kaynak, A. (2005). Polymerising pyrrole on polyester textiles and controlling the conductivity through coating thickness. *Thin Solid Films* 479: 77–82.

33 Garg, S., Hurren, C., and Kaynak, A. (2007). Improvement of adhesion of conductive polypyrrole coating on wool and polyester fabrics using atmospheric plasma treatment. *Synthetic Metals* 157: 41–47.

34 Burnett-Boothroyd, S.C. and McCarthy, B.J. (2011). 13 – Antimicrobial treatments of textiles for hygiene and infection control applications: an industrial perspective. In: *Textiles for Hygiene and Infection Control* (ed. McCarthy, B.J.), 196–209. Woodhead Publishing.

35 Rajendran, S., Anand, S.C., and Rigby, A.J. (2016). 5- Textiles for healthcare and medical applications. In: *Handbook of Technical Textiles* (eds. A. Richard Horrocks and Subhash C. Anand), 2e, 135–168. Woodhead Publishing.

36 Nayak, R. and Padhye, R. (2015). 12 – Antimicrobial finishes for textiles. In: *Functional Finishes for Textiles* (ed. Roshan Paul), 361–385. Woodhead Publishing.

37 Dhende, V.P., Hardin, I.R., and Locklin, J. (2012). 8 – Durable antimicrobial textiles: types, finishes and applications. In: *Understanding and Improving the Durability of Textiles* (ed. Patricia Annis), 145–173. Woodhead Publishing.

38 Montazer, M. and Afjeh, M.G. (2007). Simultaneous X-linking and antimicrobial finishing of cotton fabric. *Journal of Applied Polymer Science* 103: 178–185.

39 Morones, J.R., Elechiguerra, J.L., Camacho, A. et al. (2005). The bactericidal effect of silver nanoparticles. *Nanotechnology* 16: 2346.

40 Kang, C.K., Kim, S.S., Kim, S. et al. (2016). Antibacterial cotton fibers treated with silver nanoparticles and quaternary ammonium salts. *Carbohydrate Polymers* 151: 1012–1018.

41 Shafei, A.E. and Abou-Okeil, A. (2011). ZnO/carboxymethyl chitosan bionano-composite to impart antibacterial and UV protection for cotton fabric. *Carbohydrate Polymers* 83: 920–925.

42 Petkova, P., Francesko, A., Perelshtein, I. et al. (2016). Simultaneous sonochemical-enzymatic coating of medical textiles with antibacterial ZnO nanoparticles. *Ultrasonics Sonochemistry* 29: 244–250.

43 Gupta, B., Agarwal, R., and Alam, M. (2010). Textile-based smart wound dressings. *Indian Journal of Fibre and Textile Research* 35: 174–187.

44 Xue, C.-H., Jia, S.-T., Zhang, J. et al. (2008). Preparation of superhydrophobic surfaces on cotton textiles. *Science and Technology of Advanced Materials* 9: 035008.

45 Lee, H.J. and Michielsen, S. (2007). Preparation of a superhydrophobic rough surface. *Journal of Polymer Science Part B: Polymer Physics* 45: 253–261.

46 Xu, B. and Cai, Z. (2008). Fabrication of a superhydrophobic ZnO nanorod array film on cotton fabrics via a wet chemical route and hydrophobic modification. *Applied Surface Science* 254: 5899–5904.

47 Hoefnagels, H., Wu, D., De With, G., and Ming, W. (2007). Biomimetic superhydrophobic and highly oleophobic cotton textiles. *Langmuir* 23: 13158–13163.

48 Zhao, Y., Tang, Y., Wang, X., and Lin, T. (2010). Superhydrophobic cotton fabric fabricated by electrostatic assembly of silica nanoparticles and its remarkable buoyancy. *Applied Surface Science* 256: 6736–6742.

49 Abbas, R., Khereby, M.A., Sadik, W.A., and El Demerdash, A.G.M. (2015). Fabrication of durable and cost effective superhydrophobic cotton textiles via simple one step process. *Cellulose* 22: 887–896.

50 Afzal, S., Daoud, W.A., and Langford, S.J. (2014). Superhydrophobic and photocatalytic self-cleaning cotton. *Journal of Materials Chemistry A* 2: 18005–18011.

51 Wei, Q., Huang, F., and Cai, Y. (2009). 2 – Textile surface characterization methods. In: *Surface Modification of Textiles* (ed. Wei, Q.), 26–57. Woodhead Publishing.

52 Hauser, P.J. (2005). 6 – Chemical analysis of fabric finishes and performance-related tests. In: *Chemical Testing of Textiles* (ed. Fan, Q.), 107–125. Woodhead Publishing.

53 Krishnaveni, R. and Thambidurai, S. (2013). Industrial method of cotton fabric finishing with chitosan–ZnO composite for anti-bacterial and thermal stability. *Industrial Crops and Products* 47: 160–167.

54 Singh, J. and Dutta, P. (2010). Preparation, antibacterial and physicochemical behavior of chitosan/ofloxacin complexes. *International Journal of Polymeric Materials* 59: 793–807.

55 Al-Gaashani, R., Radiman, S., Tabet, N., and Daud, A.R. (2011). Effect of microwave power on the morphology and optical property of zinc oxide nano-structures prepared via a microwave-assisted aqueous solution method. *Materials Chemistry and Physics* 125: 846–852.

56 Müller, D., Rambo, C., Recouvreux, D. et al. (2011). Chemical in situ polymerization of polypyrrole on bacterial cellulose nanofibers. *Synthetic Metals* 161: 106–111.

57 Watanabe, K., Tabuchi, M., Morinaga, Y., and Yoshinaga, F. (1998). Structural features and properties of bacterial cellulose produced in agitated culture. *Cellulose* 5: 187–200.

58 Czaja, W., Krystynowicz, A., Bielecki, S., and Brown, R.M. (2006). Microbial cellulose—the natural power to heal wounds. *Biomaterials* 27: 145–151.

59 Scaini, M.J., Bancroft, G.M., Lorimer, J.W., and Maddox, L.M. (1995). The interaction of aqueous silver species with sulphur-containing minerals as studied by XPS, AES, SEM, and electrochemistry. *Geochimica et Cosmochimica Acta* 59: 2733–2747.

60 Caschera, D., Cortese, B., Mezzi, A. et al. (2013). Ultra hydrophobic/superhydrophilic modified cotton textiles through functionalized diamond-like carbon coatings for self-cleaning applications. *Langmuir* 29: 2775–2783.

61 El-Rafie, M., Ahmed, H.B., and Zahran, M. (2014). Characterization of nanosilver coated cotton fabrics and evaluation of its antibacterial efficacy. *Carbohydrate Polymers* 107: 174–181.

62 Wainwright, H.L. (2016). 9 – Design, evaluation, and applications of electronic textiles. In: *Performance Testing of Textiles* (ed. Lijing Wang), 193–213. Woodhead Publishing.

63 Alzaidi, A., Zhang, L., and Bajwa, H. (2012). Smart textiles based wireless ECG system, systems, applications and technology conference (LISAT). In: *2012 IEEE Long Island*, 1–5. IEEE.

64 Benatti, S., Farella, E., and Benini, L. (2014). Towards EMG control interface for smart garments. In: *Proceedings of the 2014 ACM International Symposium on Wearable Computers: Adjunct Program*, 163–170. Seattle, WA: ACM.

65 Finni, T., Hu, M., Kettunen, P. et al. (2007). Measurement of EMG activity with textile electrodes embedded into clothing. *Physiological Measurement* 28: 1405.

66 Löfhede, J., Seoane, F., and Thordstein, M. (2012). Textile electrodes for EEG recording—a pilot study. *Sensors* 12: 16907.

67 Cochrane, C., Hertleer, C., and Schwarz-Pfeiffer, A. (2016). 2 – Smart textiles in health: an overview. In: *Smart Textiles and their Applications* (ed. Vladan Koncar), 9–32. Oxford: Woodhead Publishing.

68 Cochrane, C., Koncar, V., Lewandowski, M., and Dufour, C. (2007). Design and development of a flexible strain sensor for textile structures based on a conductive polymer composite. *Sensors* 7: 473–492.

69 Xue, P., Wang, J., and Tao, X. (2014). Flexible textile strain sensors from polypyrrole-coated XLA™ elastic fibers. *High Performance Polymers* 26: 364–370.

70 Cho, G. (2009). *Smart Clothing: Technology and Applications*. CRC Press.

71 Wang, F., Zhu, B., Shu, L., and Tao, X. (2013). Flexible pressure sensors for smart protective clothing against impact loading. *Smart Materials and Structures* 23: 015001.

72 Windmiller, J.R. and Wang, J. (2013). Wearable electrochemical sensors and biosensors: a review. *Electroanalysis* 25: 29–46.

73 Hong, K.H., Oh, K.W., and Kang, T.J. (2004). Polyaniline–nylon 6 composite fabric for ammonia gas sensor. *Journal of Applied Polymer Science* 92: 37–42.

74 Lu, H.-H., Lin, C.-Y., Fang, Y.-Y. et al. (2008). NO gas sensor of PEDOT: PSS nanowires by using direct patterning DPN. In: *2008 30th Annual International Conference of the IEEE Engineering in Medicine and Biology Society. EMBS 2008*, 3208–3211. IEEE.

75 Lai, Y., Tang, Y., Gong, J. et al. (2012). Transparent superhydrophobic/superhydrophilic TiO_2-based coatings for self-cleaning and anti-fogging. *Journal of Materials Chemistry* 22: 7420–7426.

21

Soft Computing in Fibrous Materials

Abhijit Majumdar[1], Piyali Hatua[2], and Mirela Blaga[3]

[1] *Indian Institute of Technology, Department of Textile and Fibre Engineering, Hauz Khas, New Delhi 110016, Delhi, India*
[2] *Veermata Jijabai Technological Institute, Department of Textile Technology, Mumbai 400019, India*
[3] *University of Iaşi, Faculty of Textiles-Leather and Industrial Management, Iaşi 700050, Romania*

21.1 Introduction

Soft computing (SC) is a new breed of computing systems. Prof. Zadeh introduced the concept of soft computing in 1990. According to him "soft computing is a collection of methodologies that aim to exploit the tolerance for imprecision and uncertainty to achieve tractability, robustness, and low solution cost" [1]. Its principal constituents are fuzzy logic (FL), artificial neural networks (ANN), and genetic algorithms (GA). Hard computing is based on precise and accurate mathematical models. In contrast, the major advantage of soft computing lies in its tolerance to imprecision, uncertainty, and partial truth. It can produce effective solutions to difficult problems, which cannot be solved with the conventional analytical approach or other computational tools. Moreover, the potential of fusing soft computing with conventional hard computing techniques increases its acceptance in scientific community. Soft computing techniques have also been successfully applied in engineering design area, which increased their popularity in industrial applications. Soft computing techniques mimic the functioning of biological systems and get advantage over other hard computing techniques in imprecision handling and decision-making. ANN mimics the working of biological neurons, FL gets motivation from the highly imprecise nature of human speech, and GA follows nothing but the Darwinian evolution theory. Furthermore, soft computing systems are complementary to each other and therefore present more potent solutions when combined together.

For centuries, the main use of the textile materials has remained confined to clothing and interior applications. However, last few decades have witnessed a sharp increase in technical applications of textile materials and structures in various sectors like in agriculture, horticulture, construction, automobiles, protection, aeronautics, medicine, sports, etc. Technical textiles are mainly manufactured keeping focus on their functional and technical performances rather than on their aesthetic or decorative characteristics. Technical woven

Handbook of Fibrous Materials, First Edition. Edited by Jinlian Hu, Bipin Kumar, and Jing Lu.
© 2020 Wiley-VCH Verlag GmbH & Co. KGaA. Published 2020 by Wiley-VCH Verlag GmbH & Co. KGaA.

fabrics found various diversified application such as sports, protective clothing, filtration, belting, packaging, and in many other areas. Technical fabrics are also used as reinforcement material in composites [2]. Now these technical applications need a paradigm shift in designing principles of textile materials: from aesthetic design to engineering design so that a textile structure can meet certain functional properties according to its end use requirement. Textile structures are highly complex, flexible, and porous in nature. Structure-property modeling, process modeling, and process optimization should be carried out before making any attempt for engineering design of textile structures. However, these are highly complex tasks. In general, a woven textile material consists of yarns, and yarns consist of fibers. Thus the mechanical properties of fabrics are dependent on the structural complexity and nonlinearity. Furthermore, complexity amplifies when the inherent nonlinearities of the materials are added to the problem. This double nonlinear behavior of the textile fabric increases the difficulty in the fabric design and engineering processes. Conventional and precise analytical models often fail or perform poorly due to the intricacy induced by the complex structure and the nonlinearity in the behavior of raw materials. In many areas, models based on soft computing have been adapted to overcome these problems. Till date, soft computing techniques have been applied in almost every domain of textile such as fiber, yarn, woven and knitted fabrics, nonwovens, clothing and garment, textile quality control, etc. [3, 4]. In the subsequent sections of this chapter, soft computing techniques, namely, ANN, FL, GA, etc., have been described followed by their applications in fibrous materials.

21.2 Soft Computing Techniques

The following sections describe some of the soft computing techniques, namely, ANN, FL, GA, and adaptive network-based fuzzy inference system (FIS). These techniques have been widely used in textile research for modeling, prediction, and optimization.

21.2.1 Artificial Neural Network (ANN)

ANN is a powerful data modeling tool that can effectively capture and represent any kind of input–output relationship using historical or experimental data. It uses simple mathematical functions to represent highly complex functional relationships. Each mathematical function used in ANN mimics a specific operation of biological neurons. It can exhibit characteristics such as mapping or pattern recognition, generalization, robustness, fault tolerance, parallel and high-speed information processing, etc. [5].

ANN, in general, is a multilayered network consisting of a large number of structurally interconnected artificial neurons or nodes, which are the computing elements (Figure 21.1). The input parameters and output parameters are positioned at the input and output layer, respectively. One or more hidden layers are placed between the input and output layers.

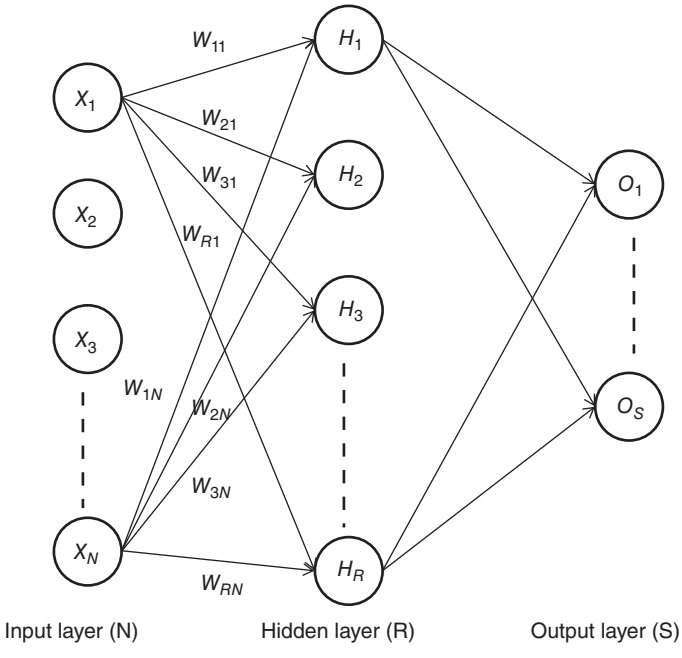


Figure 21.1 Multilayered artificial neural network structure.

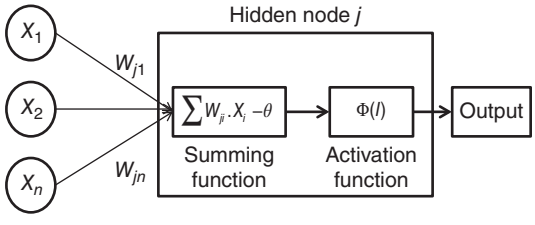


Figure 21.2 Simple model of an artificial neuron. Source: Majumdar 2011 [4].

The functioning of an ANN is explained by the simple model of an artificial neuron as shown in Figure 21.2. Here X_1, X_2, X_3, …, X_n are the n input parameters to the artificial neuron, and W_{j1}, W_{j2}, W_{j3}, …, W_{jn} are n weights by which inputs are connected to the hidden layer. W_{ji} is the synaptic weight connecting the hidden neuron j of hidden layer to the input neuron i. It acts as a multiplying factor for the signals coming out from the neurons of the previous layer and thus accelerates or retards the input signal. The weighted inputs are summed up to get the weighted sum of inputs received by an artificial neuron. The weighted sum of inputs is then compared with a threshold value called bias weight, which represents the membrane potential of a biological neuron. For neuron j, the net input (I) can be expressed as follows:

$$I = (W_{j1}X_1 + W_{j2}X_2 + \cdots + W_{jn}X_n) - \theta = \sum_{i=1}^{n} W_{ji}X_i - \theta \tag{21.1}$$

where θ is the bias weight.

The net input is then passed through a transfer function, which converts the output to a fixed range of values (either between 0 and 1 or between −1 and +1) as shown below:

$$Z = \phi(I) \tag{21.2}$$

Several kinds of transfer functions such as threshold or hard limit, saturating linear, log-sigmoid, tan-sigmoid, etc. can be used depending on the nature of problem [4]. The output of the transfer function is transmitted to the nodes of the next layer, and similar kind of computations is done again. Finally, the output is produced and is compared with the expected output, and an error signal is generated. The prediction accuracy of ANN depends on finding the optimum set of weights connecting various nodes. The weights are optimized by a process termed as "training." There are three types of training algorithm for ANN, namely, supervised learning, unsupervised learning, and reinforced learning [6]. Back-propagation and Levenberg–Marquardt training algorithms are popularly used for training of ANN.

21.2.1.1 Back-Propagation Algorithm

Back-propagation is a supervised training algorithm developed by Rumelhart et al. [7]. The details of this algorithm can be found in many standard textbooks of ANN authored by Haykin [8], Zurada [9], and Bose and Liang [10]. According to this algorithm, training occurs in two phases, namely, forward pass and backward pass. In the forward pass, a set of data is presented to ANN as input, and finally, a set of outputs is produced. The error vector is calculated according to the following equation:

$$E = \sum_{j=1}^{p} E_j \tag{21.3}$$

where E is the error vector, E_j is the error associated with the jth pattern, and p is the total number of training patterns.

The expression of E_j is given in the following equation:

$$E_j = \frac{1}{2} \sum_{k=1}^{s} (T_k - \text{out}_k)^2 \tag{21.4}$$

where T_k and out_k are the target output and predicted output, respectively, at output neuron k and s is the total number of output neurons.

In the backward pass, this error signal is propagated backward, and the synaptic weights are adjusted so that the error signal reduces in each iteration. The corrections necessary in synaptic weights between hidden and output layer are carried out by a delta rule. At the start of the training, ANN uses random combinations of synaptic weights, which cause very high error signal. Therefore, the gradient (slope) of the error function (surface) is determined with respect to the weights. Once the training converges to the point of minimum error, the gradient of the error surface becomes zero, and no further update of

the weights takes place. Mathematically this process is represented as shown below.

$$\Delta W_{jk} = W_{jk(\text{new})} - W_{jk(\text{old})} = -\eta[\partial E/\partial W_{jk}] = -\eta\left[\frac{\partial E}{\partial \text{out}_k} \times \frac{\partial \text{out}_k}{\partial \text{net}_k} \times \frac{\partial \text{net}_k}{\partial W_{jk}}\right] \tag{21.5}$$

$$\text{Now, } \frac{\partial E}{\partial \text{out}_k} = \frac{\partial}{\partial \text{out}_k}\left[\frac{1}{2}\sum_k (T_k - \text{out}_k)^2\right] = -(T_k - \text{out}_k) \tag{21.6}$$

$$\frac{\partial \text{out}_k}{\partial \text{net}_k} = f_0'(\text{net}_k) = \text{out}_k\,(1 - \text{out}_k) \text{ for log sigmoid transfer function} \tag{21.7}$$

$$\frac{\partial \text{net}_k}{\partial W_{jk}} = \frac{\partial}{\partial W_{jk}}\sum_k w_{jk}\text{out}_j = \text{out}_j \tag{21.8}$$

$$\text{Therefore, } \Delta W_{jk} = \eta[(T_k - \text{out}_k)\text{out}_k(1 - \text{out}_k)]\text{out}_j = \eta\delta_k\text{out}_j \tag{21.9}$$

where W_{jk} is the weight connecting the neurons j of hidden layer and neuron k of the output layer, ΔW_{jk} is the correction applied to W_{jk} at a particular iteration, η is a constant known as learning rate, and out_j is the output of neuron j.

The weight change between hidden layer and input layer is calculated as shown below.

$$\Delta W_{ij} = \eta f_H'(\text{net}_j)X_i \sum_k \delta_k W_{jk} \tag{21.10}$$

where ΔW_{ij} is the correction applied to the weight connecting input neuron i and hidden neuron j and X_i is the input received by the neuron i.

21.2.1.2 Levenberg–Marquardt Algorithm

Back-propagation training algorithm has poor convergence rate. Levenberg–Marquardt is another training algorithm that updates weight and bias values according to Levenberg–Marquardt optimization [11, 12]. Levenberg–Marquardt algorithm can be considered as a combination of steepest descent and the Gauss–Newton method. It can be expressed by Eq. (21.11):

$$(J^tJ + \lambda I)\delta = J^tE \tag{21.11}$$

where J is the Jacobian matrix for the system, λ is the Levenberg's damping factor, I is the identity matrix, δ is the weight update vector, and E is the error vector containing the output errors for each input vector used on training the network. The Jacobian is a matrix containing all first-order partial derivatives of a vector-valued function. It is a $N \times W$ matrix, where N is the number of entries in training set and W is the total number of parameters (weights and biases) of the network. It can be created by taking the partial derivatives of each output with respect to

each weight as given below:

$$J = \begin{bmatrix} \frac{\partial F(x_1, w)}{\partial w_1} & \cdots & \frac{\partial F(x_1, w)}{\partial w_w} \\ \vdots & \ddots & \vdots \\ \frac{\partial F(x_N, w)}{\partial w_1} & \cdots & \frac{\partial F(x_N, w)}{\partial w_w} \end{bmatrix} \tag{21.12}$$

where $F(x_i, w)$ is the network function evaluated for the ith input vector of the training set using the weight vector w and w_j is the jth element of the weight vector w of the network.

The δ quantifies the change in network weights to achieve an improved solution. The J^tJ matrix is also known as the approximated Hessian. The damping factor (λ) is adjusted at each iteration, and it guides the weight optimization process. If reduction of error E is rapid, a smaller value of λ can be used, making the algorithm closer to the Gauss–Newton algorithm. On the other hand, if an iteration gives insufficient reduction in the residual, λ can be increased, making the algorithm closer to the gradient descent direction.

21.2.1.3 Important Parameters of Artificial Neural Network

The structure of ANN and training parameters play important roles in determining the performance of ANN model. The important parameters are as follows.

Number of Hidden Layers and Nodes in Each Hidden Layer The number of hidden layers and number of nodes in each hidden layer depends on the complexity of the function that is being modeled by ANN. In most of the cases, one hidden layer can capture the nonlinear relationship between the input and output variables. However, for very complex functions, more than one hidden layer may be needed.

The number of nodes in the input layer and output layer is equal to the number of input and output variables, respectively. There is no exact rule to determine the optimum number of nodes in the hidden layers as it is dependent on the type of problem. Therefore, the number of nodes in the hidden layers is often determined by trial-and-error approach. If the number of nodes is too less, then ANN will fail to capture the input–output relationship. On the other hand, if the number of nodes is too high, then ANN may capture even the noise present in data. This will also cause poor prediction performance in the unseen testing data.

Learning Rate and Momentum Learning rate (η) determines the magnitude of weight adjustment during ANN training, and hence it influences the rate of convergence. If the learning rate is too small, then the training advances in small steps and training time may become very large. On the other hand, if the learning rate is too large, then the search path may oscillate, and "global minima" may not be attained as depicted in Figure 21.3. The learning rate has to be chosen as large as possible without inducing oscillations during ANN training. The value of learning rate ranges from 0 to 1.

The error function, in most of the practical problems, is not smooth. There can be several "local minima" in the error function, as depicted in

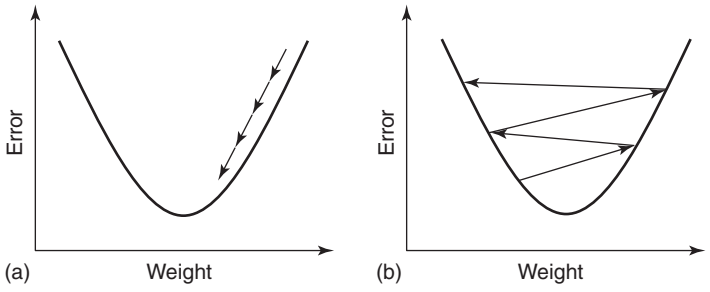


Figure 21.3 Effect of (a) very small and (b) very large learning rate on convergence.

Figure 21.4 Global and local minima of error surface.

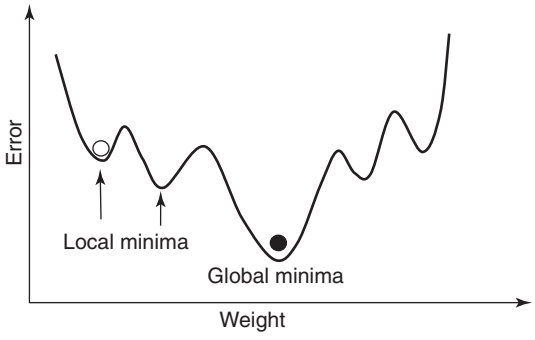


Figure 21.4. The back-propagation training algorithm may stuck as the slope of the error surface is zero at these local minima. To overcome this problem, back-propagation algorithm is often modified by adding a momentum term. The momentum is a constant that determines the effect of past weight changes on current direction of movement in weight space. If a pith ball is allowed to fall from the left side of error surface shown in Figure 21.4, then it will be caught in the local minima. However, if a marble is allowed to fall from the same position, it will be able to overcome curvatures of local minima due to its momentum, and finally it will rest at the global minima. This concept is used while adding the momentum term in the back-propagation algorithm.

The modified rule of weight adjustment with momentum term is shown below:

$$\Delta W_{jk}(t+1) = \eta \delta_k \text{out}_j + \mu \cdot \Delta W_{jk}(t) \tag{21.13}$$

where $\Delta W_{jk}(t+1)$ and $\Delta W_{jk}(t)$ are the weight changes in $(t+1)$ th and tth iteration, respectively, and μ is the momentum term and it ranges from 0 to 1.

The addition of momentum helps to smooth out the descent path by preventing extreme changes in the gradient due to local minima or potholes. If the momentum is 0, the smoothing is the least, and the weight adjustments are done solely by the newly calculated gradient. If the momentum is between 0 and 1, the weight adjustment is smoothed by an amount proportional to the momentum factor.

21.2.2 Fuzzy Logic

FL was propounded by Prof. Zadeh at the University of California, Berkeley, USA, in 1965 [1]. The concept of FL originated from the way human brain represents

and reasons with real-world knowledge in spite of uncertainty, vagueness, and incomplete knowledge. Fuzzy set theory and approximate reasoning have been used to deal with imprecision and ambiguity in decision-making [5].

FL has its foundation built on fuzzy sets. Fuzzy sets, an extension of their crisp counterpart, do not have clearly defined boundaries. A crisp set is defined by the characteristic function that can assume only two values, for example, 0 or 1, true or false, black or white. If A is a crisp set and x is an element in A, then testing of the element x using the characteristic function χ can be expressed as follows [13]:

$$\chi_A(x) = \begin{cases} 1, & \text{if } x \in A \\ 0, & \text{if } x \in A \end{cases} \tag{21.14}$$

On the other hand, in fuzzy set theory, the concept of membership function is introduced to handle uncertainty of classes, which is having unclear or overlapping boundaries [14, 15]. Thus a membership function is associated with a fuzzy set A, and this function maps every element of the universe of discourse X to the interval [0, 1]. If X is the universe of discourse and its elements are denoted by x, then a fuzzy set A in X is defined as a set of ordered pairs as shown below:

$$\chi_A(x) = \{x, \mu_A(x) | x \in X\} \tag{21.15}$$

where $\mu_A(x)$ is the membership function of x in fuzzy set A.

Membership function always takes values between 0 and 1. It may be in discrete form as well as in continuous function. Membership function can have various forms, such as triangle, trapezoid, sigmoid, and Gaussian as depicted in Figure 21.5. Dubois and Prade [16] defined the triangular membership function as shown below:

$$\mu_A(x) = \begin{cases} \dfrac{x-L}{m-L}, & \text{for } L < x < m \\ \dfrac{R-x}{R-m}, & \text{for } m < x < R \\ 0, & \text{otherwise} \end{cases} \tag{21.16}$$

where m is the most promising or modal value and L and R are the left and right spread (the smallest and largest value, respectively, that m can take).

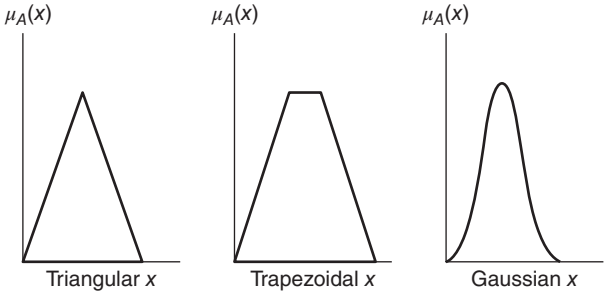


Figure 21.5 Different forms of membership function. Source: Majumdar 2011 [4].

The trapezoidal membership function is defined by four scalar parameters a, b, c, and d, as shown below:

$$f(x;a,b,c,d) = \begin{cases} 0, & \text{for } x \le a \text{ or } x \ge d \\ \dfrac{x-a}{b-a}, & \text{for } a \le x \le b \\ 1, & \text{for } b \le x \le c \\ \dfrac{d-x}{d-c}, & \text{for } c \le x \le d \end{cases} \tag{21.17}$$

The trapezoidal membership curve has a flat top. It is a truncated triangle producing $\mu_A(x) = 1$ over large regions of universe of discourse. The Gaussian membership function depends on two parameters, namely, standard deviation (σ) and mean (μ), and it is represented as shown below:

$$\mu_A(x) = e^{\frac{-(x-\mu)^2}{2\sigma^2}} \tag{21.18}$$

The general bell-shaped membership function is defined by three parameters (a, b, and c) as shown below:

$$\mu_A(x) = \frac{1}{1 + \left|\dfrac{x-c}{a}\right|^{2b}} \tag{21.19}$$

Membership function converts the crisp inputs to fuzzy membership values. This step is known as "fuzzification." Different linguistic terms such as high, medium, low, etc. are used to describe fuzzy sets. Then fuzzy if–then rules are established to relate input fuzzy sets with output fuzzy sets using linguistic terms. Fuzzy if–then rules are developed based on the experience and knowledge of experts. Fuzzy rules have two parts, namely, antecedent or if part and consequent or then part. The fuzzy sets in antecedent part are joined by "fuzzy AND" or "fuzzy OR" operators. For example, rules for predicting the yarn strength from cotton fiber properties can be as follows:

Rule 1: If fiber tenacity is *high* AND fiber length is *high*, then yarn strength is *very high*.
Rule 2: If fiber tenacity is *high* AND fiber length is *moderate*, then yarn strength is *high*.
Rule 3: If fiber tenacity is *moderate* AND fiber length is *high*, then yarn strength is *moderate*.
Rule 4: If fiber tenacity is *moderate* AND fiber length is *moderate*, then yarn strength is *low*.
Rule 5: If fiber tenacity is *low* AND fiber length is *low*, then yarn strength is *very low*.

The rule base shown above is nonexhaustive. It should be noted that there are two input variables, namely, fiber tenacity and fiber length, and only one output variable, i.e. yarn tenacity. Each of the input variables has three fuzzy sets, which are linguistically termed as high, moderate, and low. The output variable

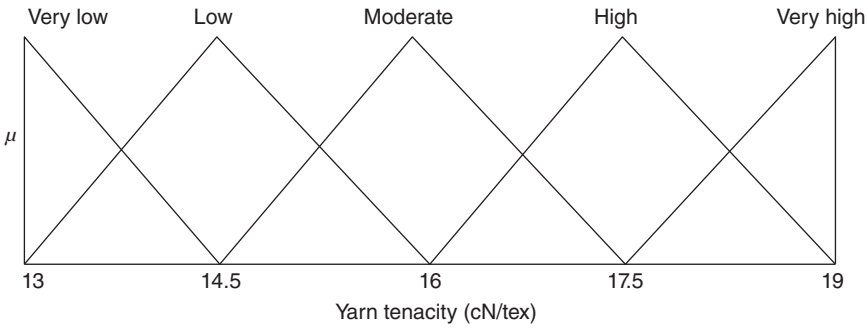


Figure 21.6 Membership functions of yarn tenacity.

has five fuzzy sets, which are linguistically termed as very high, high, moderate, low, and very low. As fuzzy sets do not have sharp boundaries, there will be overlaps between two neighboring fuzzy sets. Hypothetical fuzzy sets for yarn tenacity are shown in Figure 21.6.

The output of each rule is also a fuzzy set. Output fuzzy sets are aggregated into a single fuzzy set generally by the "MAX" operator. This step is known as "aggregation." Finally, the resulting fuzzy set is converted to a crisp output by the "defuzzification" method. There are many methods available for defuzzification as mentioned below.

- Centroid (center of gravity or center of area)
- Center of sums (COS)
- Mean of maxima (MOM)
- Smallest of maxima (SOM)
- Largest of maxima (LOM)

Centriod method is one of the most popular methods of defuzzification. In this method, the overlapped areas of output fuzzy sets are considered only once. According to this method, the defuzzified crisp value is calculated as follows:

$$x^* = \frac{\int \mu_A(x)x \ dx}{\int \mu_A(x) \ dx} \tag{21.20}$$

where x^* is the defuzzified output and $\mu_A(x)$ is the membership value in output fuzzy set after aggregation of individual implication results.

The steps involved in fuzzy modeling can be summarized as shown in Figure 21.7.

21.2.2.1 Types of Fuzzy Inference System

There are two types of FIS, namely, Mamdani type and Sugeno (Takagi, Sugeno, and Kang or TSK) type. In case of Mamdani FIS, the consequent membership functions are also fuzzy in nature. Mamdani FIS is more popularly used as it provides reasonably good results with a relatively simple structure. Besides, the intuitive and interpretable nature of the rule base makes it more appealing. Mamdani FIS can be used directly for multiple input single output (MISO) systems and multiple input multiple output (MIMO) systems. On the contrary, the consequent

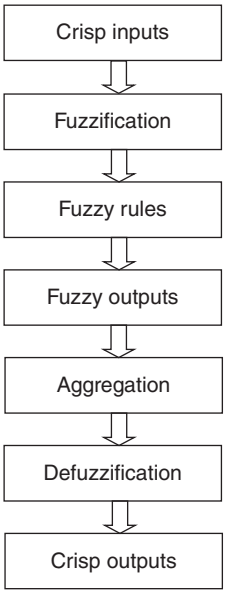


Figure 21.7 Steps involved in fuzzy modeling.

membership functions in a Sugeno FIS are non-fuzzy (either linear or constant), and thus they lack interpretability. However, in Sugeno FIS, the consequent membership functions can have as many parameters, per rule, as the number of input variables. This gives more degrees of freedom and flexibility in the design of Sugeno FIS as compared with Mamdani FIS. Sugeno FIS can only be used in the case of the MISO systems. Some advantages of Sugeno FIS over Mamdani FIS are listed below:

- Sugeno FIS is more apt for functional analysis than the Mamdani FIS.
- In computational terms, the Sugeno FIS is more effective because the complex defuzzification process of the Mamdani FIS is supplanted with weighted average method.
- Sugeno FIS is more flexible than the Mamdani FIS because the former allows more parameters in the output. Moreover, as the output is a function of the inputs Sugeno FIS expresses a more explicit relation among them.

21.2.3 Genetic Algorithm

GA was invented by John Holland in the early 1970s [17]. It is an unorthodox search and nondeterministic optimization algorithm inspired by Darwinian theory for the survival of the fittest. GA is very different from most of the other optimization methods. It can efficiently find optimal solutions to complicated optimization problem, which cannot be solved by conventional optimization techniques [18]. GA randomly searches for the best solution with respect to the given criterion of goodness expressed in terms of an objective function or fitness function. The fitness function is either to be maximized or minimized. Unlike

traditional optimization methods, it works on a population of solution points at a time instead of one solution point approach.

In GA, first a population of solutions is randomly generated. GA requires design space to be converted into genetic space. So each probable solution point, called "individuals," are converted to form a string using binary (0, 1) or real numbers (0, 9) coding. These strings are called "chromosomes," and each variable within a solution point (chromosome) is called "gene." Different genetic inheritance operators are used to create new and improved solution points called "offspring," which will in turn form the next generation population. The genetic inheritance operators are reproduction, crossover, mutation, inversion, deletion, duplication, etc. However, reproduction, crossover, and mutation are the most common operators used in optimization problems. Reproduction operator is generally the first operator applied to a population. It selects good individuals or chromosomes from the present population to form mating pool. It utilizes the fitness score of the individuals for selection. "Roulette wheel selection" and "tournament selection" are the two popular methods of selection in GA. The next operator is the crossover operator. It recombines the genes of two parents hoping to create better offspring, i.e. solution point. First, two parents are randomly chosen from mating pool, then a cross-site is selected along the length of the strings, and then their position values are swapped between each other to generate two new offspring as depicted in Figure 21.8. "Single-point crossover," "two-point crossover," and "matrix crossover" are some of the commonly used crossover operators. Mutation operator diversifies the population. It changes from 1 to 0 and vice versa in a point along the length of the chromosome. The probability of mutation should be very low; otherwise it can spoil the good individuals. The typical range of crossover probability is 0.6–0.8, whereas mutation probability is in the range of 0.001–0.01. Finally, the GA program stops searching when one of the termination criteria is achieved.

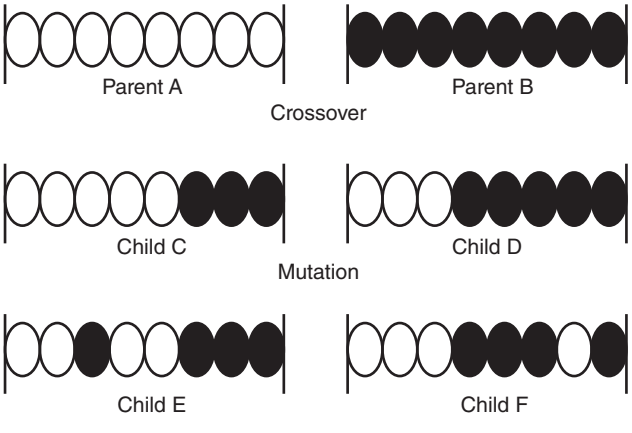


Figure 21.8 Schematic representation of single-point crossover and mutation. Source: Majumdar 2011 [4].

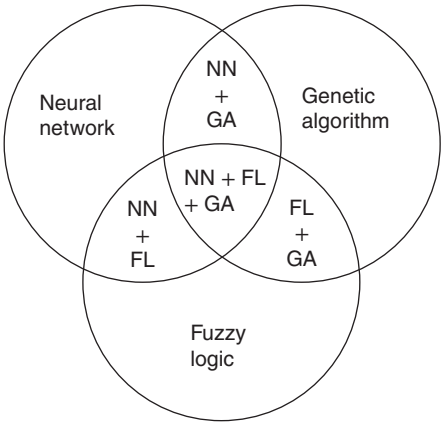


Figure 21.9 Possible hybrid combinations of three soft computing techniques.

21.2.4 Hybrid Systems

Hybrid systems employ more than one technology or system to solve a given problem. Hybridization is generally performed when an individual technology or system fails to obtain an acceptable solution. It overcomes the drawbacks of individual technologies while synergizing the strengths of each other [5]. Soft computing methods give efficient solutions to a wide range of problems. However, hybrid systems combining two or three of these methods have a tremendous potential to solve complex problems. The possible combinations are neuro-fuzzy, neuro-genetic, fuzzy-genetic, and neuro-fuzzy-genetic hybrids as shown in Figure 21.9. GA-based back propagation, ANN, and adaptive network-based fuzzy inference system (ANFIS) are some of the popular hybrid soft computing systems, which have been used to solve textile problems.

21.2.4.1 Adaptive Network-Based Fuzzy Inference System (ANFIS)

ANFIS is a multilayered adaptive network in which each node performs a particular function, often called node function, on incoming signals. The formula for the node functions varies from node to node. Mainly two types of nodes, namely, circle and square, are used in a network to reflect different adaptive capabilities (Figure 21.10). A square node is an adaptive node having parameters, while a circle node is a fixed node having no parameter. These parameters are updated according to given training data to achieve a desired input–output mapping [19]. The learning capability of ANN is used to tune the fuzzy membership function parameters using given input–output data sets. Generally two learning methods, namely, back-propagation learning and hybrid learning, are used for training of ANFIS model. In hybrid learning, ANFIS uses back-propagation learning (gradient descent method) to determine premise parameters (related to the input fuzzy sets) and least mean squares estimation to determine the consequent parameters (related to the output fuzzy sets). A step in the hybrid learning procedure is composed of two passes. In the forward pass, functional signals go forward, and the consequent parameters are estimated by an iterative least mean square procedure, while the premise parameters remain fixed. In the backward pass, the error is propagated backward to update the premise parameters by gradient descent

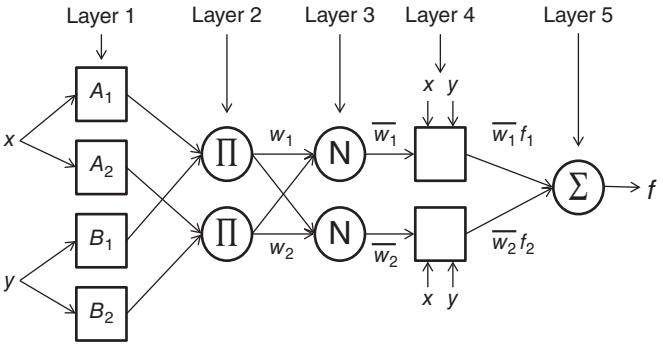


Figure 21.10 ANFIS architecture.

method, while the consequent parameters remain fixed. This procedure is then iterated until the error criterion is satisfied or preset number of cycles is reached.

ANFIS Architecture Figure 21.10 depicts the ANFIS architecture having five layers assuming two inputs x and y and one output z. A common first-order Sugeno fuzzy model with only two rules can be represented as follows:

Rule 1: If x is A_1 and y is B_1, then $f_1 = p_1x + q_1y + r_1$
Rule 2: If x is A_2 and y is B_2, then $f_2 = p_2x + q_2y + r_2$
Layer 1: Every node in this layer is an adaptive node with a node function as shown below:

$$O_{1,i} = \mu_{A_i}(x) \text{ for } i = 1, 2 \text{ or} \tag{21.21}$$

$$O_{1,i} = \mu_{B_{i-2}}(y) \text{ for } i = 3, 4 \tag{21.22}$$

where x and y are the input to node i; A_i and B_{i-2} are fuzzy sets associated with inputs x and y, respectively; and $\mu_{A_i}(x)$ is the membership of x in fuzzy set $A_i(A_1, A_2)$. $O_{1,i}$ is the output at layer 1 for the ith node. Here, the membership function for A can be any appropriate parameterized membership function, such as the generalized Gaussian function as shown in Eq. (21.24):

$$\mu_A(x) = e^{\frac{-(x-\mu)^2}{2\sigma^2}} \tag{21.23}$$

where $\{\mu, \sigma\}$ is the parameter set containing mean and standard deviation of the distribution, respectively. As the values of these parameters change, the Gaussian function varies accordingly, thus exhibiting various shapes of membership functions for fuzzy set A. Parameters in this layer are referred to as premise parameters.

Layer 2: Every node in this layer is a fixed node labeled Π, whose output is the product of all the incoming signals as shown in Eq. (21.24):

$$O_{2,i} = \mu_{A_i}(x)\mu_{B_i}(y) = w_i, \text{for } i = 1, 2 \tag{21.24}$$

Each node output represents the firing strengths of a fuzzy rule. In general, any T-norm operator that performs fuzzy AND operation can be used as the node function in this layer.

Layer 3: Every node in this layer is a fixed node labeled N. The ith node calculates the ratio of the ith rule's firing strength to the sum of all rules' firing strengths as shown in Eq. (21.25). Outputs of this layer represent normalized firing strength of rules:

$$O_{3,i} = \frac{w_i}{w_1 + w_2} = \overline{w}_i \tag{21.25}$$

Layer 4: Every node i in this layer is an adaptive node with a node function as shown in Eq. (21.26):

$$O_{4,i} = \overline{w}_i f_i = \overline{w}_i (p_i x + q_i y + r_i) \tag{21.26}$$

where $\overline{w}_i$ is a normalized firing strength from layer 3 and $\{p_i, q_i, r_i\}$ is the parameter set for this node. Parameters in this layer are referred to as consequent parameters.

Layer 5: The single node in this layer is a fixed node labeled Σ, which calculates the overall output as the summation of all incoming signals.

$$O_{5,i} = \sum \overline{w}_i f_i = \frac{\sum w_i f_i}{\sum w_i} \tag{21.27}$$

ANFIS Parameters Selection of input variables and determining the number of fuzzy sets for each of the inputs is very important for ANFIS modeling since they determine the number of rules to be trained. If p is the number of membership function for each input and q is the number of inputs, then there are p^q rules to be trained. Table 21.1 shows the number of nodes and number of parameters in various layers of ANFIS considering two parameter membership functions for the input variables.

The learning scheme for ANFIS is represented in Table 21.2. In the forward pass, the consequent parameters (p, q, and r) are optimized by least square method. In the backward pass, the premise parameters are optimized by gradient descent algorithm.

Table 21.1 Number of ANFIS parameters.

Layer number	Layer type	Number of nodes	Number of parameters
0	Inputs	q	0
1	Fuzzification	$p \times q$	$2 \times p \times q$
2	Rules	p^q	0
3	Normalization	p^q	0
4	Linear functions	p^q	$(q+1)\, p^q$
5	Summation	1	0

Table 21.2 Hybrid learning for ANFIS.

Parameters and signals	Forward pass	Backward pass
Premise parameters (nonlinear)	Fixed	Gradient descent
Consequent parameters (linear)	Least square	Fixed
Signals	Node outputs	Error signals

21.3 Applications of Soft Computing in Fibrous Materials

21.3.1 Applications in Yarn Manufacturing

Prediction of yarn properties from fiber properties and process parameters are one of the most favorite topics in yarn manufacturing research. Majority of these researches focuses on the prediction of yarn strength, elongation, unevenness, and hairiness. The advent of soft computing techniques has provided a new impetus in yarn modeling research. A glimpse of soft computing aided researches in yarn manufacturing is chronologically presented in Table 21.3.

21.3.1.1 Yarn Engineering and Process Optimization

Soft computing models have performed extremely well for the prediction of yarn properties from the cotton fiber properties or process parameters. However, reverse modeling that can predict the fiber properties or process parameters from the given yarn properties has been seldom attempted. Majumdar et al. [32] attempted to engineer ring spun yarn properties using ANN model and linear programming. Four yarn properties, namely, tenacity, elongation, unevenness, and hairiness, were considered for the yarn engineering and were used as input parameters to the ANN model. The outputs of the ANN model were spinning consistency index (SCI) and micronaire. The ANN model was able to predict the values of SCI and micronaire with mean absolute percentage error (MAPE) of 4.38% and 1.92%, respectively. From the five testing samples, three were finally chosen for the engineering. Linear programming problems were formulated with the objective of minimization of cotton mixing cost. Constraint equations were formed to ensure that the ANN predicted combinations of SCI and micronaire are fulfilled. A typical linear programming problem for the 40^s yarn is shown below:

$$\begin{aligned}
&\text{Minimize } Z = P_A \cdot 65 + P_B \cdot 52 \\
&P_A \cdot 160 + P_B \cdot 126 \geq 139 \\
&P_A \cdot \frac{1}{4.01} + P_B \cdot \frac{1}{4.35} \geq \frac{1}{4.19} \\
&P_A + P_B = 1, P_A \geq 0, P_B \geq 0
\end{aligned} \tag{21.28}$$

where Z is the overall cost of the mixing; P_A and P_B are the proportions of two cottons A and B, respectively; cotton cost per kilogram, SCI, and micronaire values of cotton A and B are 65 and 52, 160 and 126, and 4.01 and 4.35, respectively.

Table 21.3 Glimpse of soft computing applications in yarn technology.

Name of researchers	Predicted properties/application	System used	Accuracy of prediction
Pynckels et al. [20]	Spinnability	ANN	Accuracy 90–95%.
Cheng and Adams [21]	CSP	ANN	$R = 0.85$
Ethridge and Zhu [22]	CSP, tenacity, elongation, and unevenness	ANN	$R^2 = 0.80$, 0.78, 0.87, and 0.95, respectively
Zhu and Ethridge [23]	Unevenness	ANN	$R^2 = 0.88$
Sette et al. [24]	Tenacity and elongation	ANN and GA	Normalized error of 0.01 and 0.03, respectively
Rajamanickam et al. [25]	Tenacity	ANN	Error up to 8.5%
Zhu and Ethridge [26]	Hairiness	ANN	$R^2 = 0.84$ and 0.77, respectively
Pynckels et al. [27]	Tenacity and elongation	ANN	Error less than 5% in 90% data
Guha et al. [28]	Tenacity	ANN	Error = 6.9%
Chattopadhyay et al. [29]	Tenacity, CSP, U%, and imperfections	ANN	Error = 7.1% and 14.7%, respectively
Majumdar and Majumdar [30]	Elongation	ANN	Error = 4.536%
Majumdar et al. [31]	Tenacity	ANFIS	Error = 4.72% (ring) and 2.03% (rotor)
Majumdar et al. [32]	Yarn engineering	ANN	Error = 1.617–6.242%
Majumdar et al. [33]	Unevenness	ANFIS	Error = 2.367% in testing data
Majumdar and Ghosh [34]	Tenacity	FL	Error = 4.04%
Ghosh and Chatterjee [35]	Tenacity, elongation, unevenness, and hairiness	SVM	Accuracy > 95%
Ghosh et al. [36]	Stress–strain behavior	GA	$R^2 = 0.99$
Mishra [37]	Yarn strength utilization	ANN	$R^2 = 0.97$, error = 2.6%

Source: Majumdar 2011 [4]. Reproduced with permission of Taylor & Francis.

The linear programming problems were solved, and the solutions obtained in terms of proportion of fiber mix (P_A and P_B) were actually used for spinning of engineered yarns. Finally, the targeted and the experimentally achieved yarn properties were compared to evaluate the efficacy of yarn engineering. The results are shown in Table 21.4. It is observed that the yarn properties can be engineered with overall average error of less than 7%.

21.3.2 Applications in Fabric Property Prediction

In the field of fabrics, researchers have successfully applied various soft computing techniques for modeling and prediction of different properties such as tensile,

Table 21.4 The accuracy of yarn engineering system.

Test sample number	Yarn count (Ne)	Mean absolute error (%)				Overall % error
		Tenacity	Elongation	Unevenness	Hairiness	
1	40	2.727	1.515	3.924	11.777	4.986
3	50	3.510	0.549	0.197	2.210	1.617
5	60	2.982	13.871	2.661	5.455	6.242

shear, bending, comfort, drape, air permeability, thermal conductivity, etc. Apart from this, soft computing techniques have also been attempted for fabric defect detection both in static and dynamic conditions, fabric classification, and fabric engineering.

21.3.2.1 Prediction of Mechanical Properties of Fabrics

A plentiful of research works have been published on soft computing based modeling and prediction of fabric mechanical properties. Tensile properties of fabrics have been predicted using ANN model by Majumdar et al. [38] and Hadizadeh et al. [39]. Fan and Hunter [40, 41] and Behera and Guruprasad [42] have used ANN model to predict bending and shear behavior of fabrics. FIS and ANFIS have also been used for predicting fabric properties and knitting machine parameters [42, 43]. Bilisik and Demiryurek [44], Zeydan [45], and Hadizadeh et al. [46] have compared the efficacy of mathematical, statistical, and ANN models for the prediction of tensile and bending properties of fabrics. All of them reported lowest prediction error in case of ANN model.

21.3.2.2 Prediction of Transmission Properties of Fabrics

Comfort is a very important aspect of apparel fabric. A number of research studies have been reported in this area using soft computing techniques. Bhattacharjee and Kothari [47] developed two different types of ANN model to predict thermal resistance and instantaneous heat flow (Q_{max}) of woven fabrics. One model was having two parallel ANNs working in tandem, while another had a single network with two outputs. They used weave, yarn count and spacing of warp and weft, fabric thickness, and areal density as inputs to the ANN model. The first model with two networks working in tandem gave better result.

Fayala et al. [48] used ANN model to predict the thermal conductivity of knitted fabrics. The input parameters were yarn thermal conductivity, fabric areal density, porosity, and air permeability. They reported good prediction ($R^2 = 0.913$) in the training data set. In a similar study, Majumdar [49] predicted thermal conductivity of cotton–bamboo viscose blended knitted fabrics. Knitted fabric structure along with yarn count (tex), bamboo viscose fiber %, thickness, and areal density were considered as ANN inputs. Very good prediction accuracy was obtained in training and testing data set. The trend analysis given by ANN model revealed that thermal conductivity increases with increasing yarn count (tex), areal density and decreasing fabric thickness, and bamboo viscose %.

ANN has been utilized in predicting air permeability of woven fabrics. Tokarska [50] predicted impact air permeability using a simple ANN model. The author focused on the real pressure impulse $p(t)$ generated on fabrics. Therefore, an integral of actual pressure impulse $p(t)$ was considered as output, whereas fabric density (kg/m^3), warp twist, and weft twist were input parameters. A very low average error of prediction (0.00241 Pa) was obtained in this study. Brasquet and Le Cloirec [51] studied pressure drops across the fabric structure. They tried different classical pressure drop models and ANN model for predicting pressure drop. Apart from the fabric parameters (type, thickness, number of openings, and opening specific surface area), fluid parameters (viscosity, density, and Reynolds number) were also included as input parameters to the ANN model. It was revealed from the input variable analysis that characteristics of macroscopic interstices of fabric have significant influence on pressure drop. In another study, Brasquet and Le Cloirec [52] modeled pressure drop of activated carbon cloth with the help of ANN. Ten different weaves were used for this investigation. Six input parameters related to fabric and fluid characteristics were selected on the basis of knowledge of the experimental flow behavior of activated carbon cloth and cross-correlation analysis. The high R^2 value (0.992) confirmed high generalization ability of the ANN model. Analysis of importance of input variables was performed to figure out significant fabric and fluid characteristics influencing pressure drop.

21.3.2.3 Modeling of Fabric UV Protection

Hatua et al. [53, 54] have modeled the UV protection factor (UPF) of plain woven fabrics using nonlinear regression, ANN, and ANFIS models. Ring spun yarns made of 100% cotton, 100% polyester, and polyester–cotton blends (50 : 50 and 65 : 35) were used in this research. The yarn counts were 20, 30, and 40 Ne for each of the four blends making a total of 12 yarn samples. Fabrics were produced by varying the pick density at three levels (16, 20, and 24 cm^{-1}) for each of these 12 yarns, which were used in weft. So a total of 36 (3×12) fabric samples, differing in proportion of polyester (%), weft count (Ne), and pick density (cm^{-1}), were produced. Cotton warp (100%) with 40 Ne count and end density of 40 cm^{-1} was used for all the fabrics. Out of 36 data set, 27 data set were used for the model (nonlinear regression, ANN, and ANFIS) development. These are termed as training data set. Prediction accuracy of the models was evaluated by using the remaining nine data set (65:35 polyester–cotton blend), which are termed as testing data set.

Model Development The nonlinear regression model, as shown in Eq. (21.29), was developed using the experimental data. Here X_1, X_2, and X_3 are proportion of polyester (%), weft count (Ne), and pick density (cm^{-1}), respectively. Coded values were used to develop the regression model.

$$\begin{aligned}\text{UPF} = {} & 8.26 + 2.56X_1 - 1.88X_2 + 1.91X_3 - 1.04X_1X_2 + 1.28X_1X_3 \\ & - 0.91X_2X_3 - 1.58X_1^2 + 0.76X_2^2 \end{aligned} \tag{21.29}$$

$[R^2 = 0.973]$

Table 21.5 ANFIS parameters.

Layer number	Layer type	Number of nodes	Number of parameters
0	Inputs	Number of inputs = 3	0
1	Fuzzification	No. of fuzzy sets per input × No. of inputs = 2 × 3 = 6	No. of parameters per fuzzy set × No. of fuzzy sets = 2 × 6 = 12
2	Rules	(No. of fuzzy sets per input)$^{\text{No. of inputs}} = 2^3$	0
3	Normalization	(No. of fuzzy sets per input)$^{\text{No. of inputs}} = 2^3$	0
4	Constant function	(No. of fuzzy sets per input)$^{\text{No. of inputs}} = 2^3$	No. of fuzzy rules × No. of constants per rule = 8 × 1 = 8
5	Summation	1	0

An ANN model comprising three nodes in input layer, one hidden layer with four nodes, and one node in the output layer was also developed. Tan-sigmoid transfer function was used for both the hidden and output layers. Levenberg–Marquardt algorithm was used for training of ANN. The learning rate was kept at 0.3. Maximum iteration was set at 500, and mean squared error (MSE) was set at 0.01 as stopping criteria.

In ANFIS model, only two fuzzy sets (low and high) were used for each of the three input parameters so that the number of fuzzy rules becomes 8 (2^3). Gaussian membership function, which is defined by mean and standard deviation, was selected as the input membership function, and constant function was selected as output membership function. Hybrid optimization technique was employed for the training of ANFIS model. The number of nodes and parameters in different layers of ANFIS has been presented in Table 21.5.

Table 21.6 summarizes the UPF prediction accuracy of nonlinear, ANN, and ANFIS models. The nonlinear regression model can explain 97.3% variability of UPF for training data set. In the training data set, MAPE is 6.725, and MSE is 0.319 implying good prediction accuracy of the regression model. It is observed that R^2 value of nonlinear regression model has reduced marginally from 0.973 to 0.96 in testing data sets. The MAPE and MSE values are 4.748 and 0.704, respectively, which indicates quite good efficacy of the nonlinear regression model in unseen testing data set.

However, the prediction performance of both the soft computing models is found to be much better than that of nonlinear regression model. Coefficient of determination (R^2) of ANN model is very high (0.999), and prediction error is low (MAPE = 1.12 and MSE = 0.007) in training data set. The R^2, MAPE, and MSE values in the testing data set are 0.994, 2.590, and 0.007, respectively. The prediction accuracy is relatively poor in the case of testing data set as compared with that of training data set. For ANFIS model, coefficient of determination (R^2), in training and testing data set, is not only very high (0.988 and 0.992, respectively)

Table 21.6 Summary of UPF prediction accuracy of regression, ANN, and ANFIS models.

Model	Performance parameter	Data set	
		Training	Testing
Nonlinear regression	R^2	0.973	0.960
	MAPE	6.725	4.748
	MSE	0.319	0.704
	No. of samples with >5% error	11	2
ANN	R^2	0.999	0.994
	MAPE	1.120	2.590
	MSE	0.007	0.098
	No. of samples with >5% error	1	1
ANFIS	R^2	0.988	0.992
	MAPE	2.276	2.506
	MSE	0.047	0.173
	No. of samples with >5% error	3	1

but also very close to each other. The MAPE is 2.276 and 2.506 for training and testing data set, respectively. These results imply very good generalizing ability of ANFIS model.

Trend Analysis by ANN model Trend analysis was performed with the developed ANN model to check whether the model is able to decipher the effect of various input parameters on UPF of fabrics. Trend analysis results are depicted in Figures 21.11 and 21.12. Figure 21.11 shows the effect of proportion of polyester and weft yarn count on UPF keeping pick density constant at 20 cm^{-1}. It is observed that UPF improves with the increase in the proportion of polyester. However, the effect is very prominent when proportion of polyester is changed from 20% to 60%. Coarser weft yarn gives higher UPF, due to increased fabric cover, at same proportion of polyester. Figure 21.12 presents the effect of proportion of polyester and pick density keeping weft count constant at 30 Ne. It is observed that at low pick density (16 cm^{-1}), UPF increases marginally with the increase in the proportion of polyester as the fabric is very open. However, at high pick density (24 cm^{-1}), UPF continues to improve with the increase in the proportion of polyester. It is also observed that improvement in UPF with increasing pick density is negligible at low proportion of polyester. However, the difference amplifies continuously as the proportion of polyester increases. This implies the synergistic role of fiber material and fabric construction parameters on UPF.

Linguistic Rules of ANFIS Model Figure 21.13 shows eight fuzzy rules that are relating three input parameters (proportion of polyester, weft count, and pick density) with the output parameter (UPF). The fuzzy sets for each of the three input parameters have two levels, namely, high and low. The output variable (UPF) has

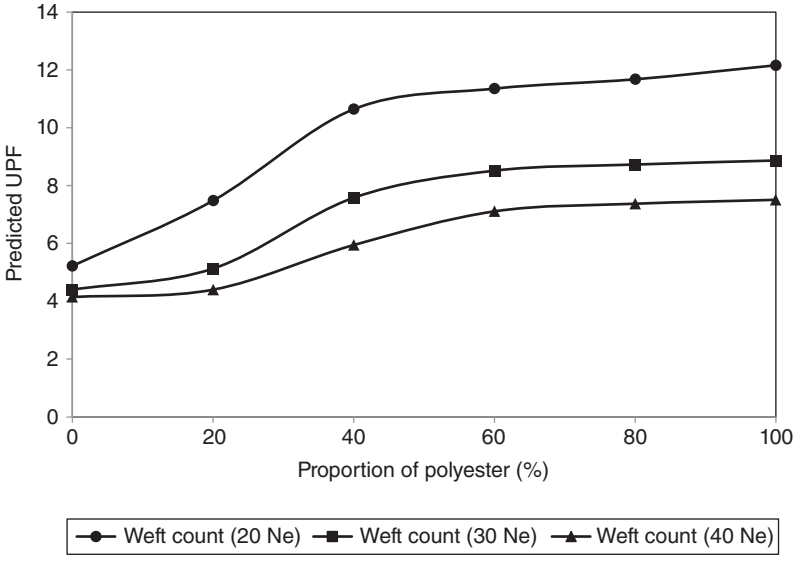


Figure 21.11 Effect of proportion of polyester and weft count on UPF. Source: Hatua et al. 2013 [53].

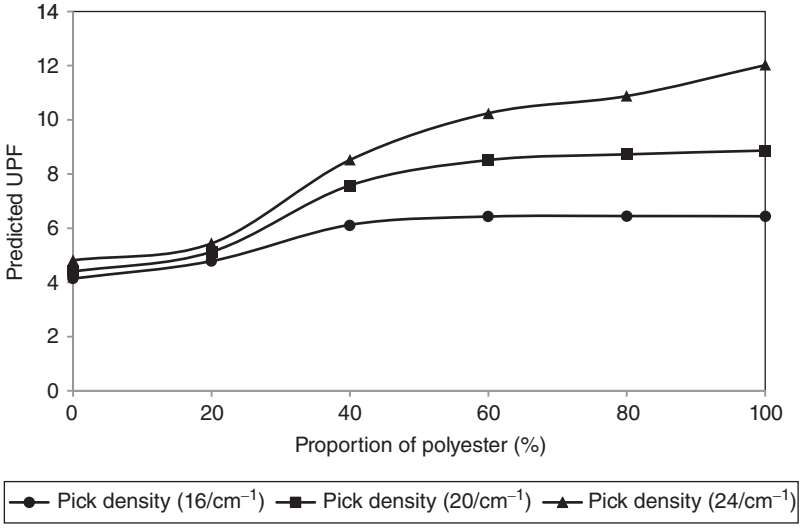


Figure 21.12 Effect of proportion of polyester and pick density on UPF. Source: Hatua et al. 2013 [53].

eight levels. From Figure 21.13, it is observed that when proportion of polyester, weft count, and pick density are 95%, 30 Ne, and 20 cm^{-1} respectively, four fuzzy rules (rules 5–8) are firing with different strength indicated by the heights of the blue pillars. Final output (UPF) of 8.87 is obtained by defuzzyfying, i.e. calculating the weighted average of these four fuzzy sets. It can be understood from rule 3 that the lowest UPF is obtained with the combination of the lowest proportion of

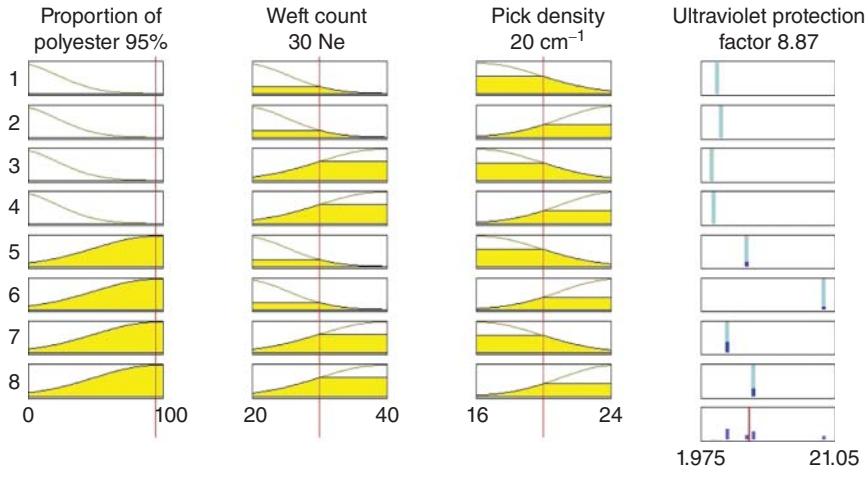


Figure 21.13 Fuzzy linguistic rules. Source: Hatua et al. 2014 [54].

polyester, the finest weft yarn, and the lowest pick density. Similarly, rule 6 implies that the highest UPF is obtained with the combination of the highest proportion of polyester, the coarsest weft yarn, and the highest pick density. Comparing rules 1 and 2, it can be inferred that UPF increases with increasing pick density keeping the proportion of polyester and weft count constant. Similarly, it can be said from rules 1 and 3 that UPF increases with coarser weft yarns if the other two input parameters are kept constant. Comparing rule 1 and 5, it can be inferred that UPF increases with the increasing proportion of polyester keeping the remaining two input parameters constant. These results are in agreement with the outcome of trend analysis of ANN model.

21.3.2.4 Applications in Nonwoven Fabrics

Rawal et al. [55] have used ANN modeling to predict the tensile properties of needlepunched nonwoven fabrics by relating them with the process parameters, namely, web area density, punch density, and depth of needle penetration. Out of 27 samples, 21 data sets were randomly chosen for training of ANN model, and remaining six data sets were for the testing purpose. Table 21.7 shows the summary of prediction performance of ANN models in training and testing data sets. Correlation coefficients between the experimental and predicted values were found to be excellent. The prediction error was also at acceptable level even in the testing or unseen data sets. Furthermore, the experimental and predicted values for individual test samples were reasonably close, as shown in Table 21.8.

21.4 Conclusions

Soft computing has opened a new horizon for fibrous material modeling and optimization research. These techniques have complementary strengths as ANN is good in modeling, FL is potent in imprecision handling, and GA is very powerful

Table 21.7 Prediction performance of ANN model.

	Bulk density		TMD		TXMD	
Statistical parameter	**Training**	**Testing**	**Training**	**Testing**	**Training**	**Testing**
Coefficient of correlation (R)	0.986	0.907	0.997	0.986	0.997	0.982
Mean absolute % error	5.40	6.70	3.17	9.21	3.69	6.71

Table 21.8 Comparison between experimental and predicted properties of needlepunched nonwoven fabrics.

	TXMD (kN/m)			TMD (kN/m)		
Sample	**Measured**	**Predicted**	**Absolute error (%)**	**Measured**	**Predicted**	**Absolute error (%)**
1	50.90	53.61	5.32	29.61	30.94	4.49
2	54.10	50.82	6.06	40.04	34.07	14.91
3	97.22	90.07	7.35	65.83	57.3	12.96
4	75.39	82.98	10.07	58.10	55.64	4.23
5	126.53	133.5	5.51	88.22	76.3	13.51
6	92.16	97.66	5.97	67.11	63.64	5.17

in solving optimization problems. These techniques in virgin or hybrid forms have been used to model gamut of yarn, fabric, and clothing properties with very good accuracy. However, soft computing tools are not panacea for modeling problems, and therefore they should be used with caution. These techniques should be used only in complex situations where simple modeling techniques like regression is not able to yield satisfactory prediction accuracy. It is also important to analyze whether soft computing tools are able to understand the underlying interactions among the input variables when the former is used as a modeling technique. It is envisaged that soft computing techniques will be used to solve complicated yarn, fabric, and clothing engineering related problems in future.

References

1 Zadeh, L.A. (1965). Fuzzy sets. *Information and Control* 8: 338–353.
2 Vassiliadis, S., Rangoussi, M., Cay, A., and Provatidis, C. (2010). Artificial neural networks and their applications in the engineering of fabrics. In: *Woven Fabric Engineering* (ed. P.D. Dubrovski), 111–134. Rijeka: Sciyo.
3 Chattopadhyay, R. and Guha, A. (2004). *Artificial Neural Networks: Applications to Textiles*. Manchester: The Textile Institute.
4 Majumdar, A. (2011). *Soft Computing in Fibrous Materials Engineering*. Manchester: The Textile Institute.
5 Rajasekaran, S. and Pai, G.A.V. (2003). *Neural Networks, Fuzzy Logic and Genetic Algorithms: Synthesis and Applications*. New Delhi: Prentice-Hall of India Pvt. Ltd.

6 Kartalopoulos, S.V. (2000). *Understanding Neural Networks and Fuzzy Logic: Basic Concepts and Applications*. New Delhi: Prentice-Hall of India Pvt. Ltd.

7 Rumelhart, D.E., Hinton, G.E., and Williams, R.J. (1986). Learning internal representations by error propagation. In: *Parallel Distributed Processing*, vol. 1, 318–362. Cambridge: MIT Press.

8 Haykin, S. (2004). *Neural Networks: A Comprehensive Foundation*, 2e. Singapore: Pearson Education.

9 Jurada, J.M. (1992). *Introduction to Artificial Neural Networks*. New York: West Publishing Company.

10 Bose, N.K. and Liang, P. (1998). *Neural Network Fundamentals with Graphs, Algorithms and Applications*. New Delhi: Tata McGraw Hill Publishing Company.

11 Hagan, M.T. and Menhaj, M.B. (1994). Training feed forward networks with the Marquardt algorithm. *IEEE Transactions on Neural Networks* 5 (6): 989–993.

12 Yu, H. and Wilamowski, B.M. (2010). Levenberg–Marquardt training. In: *Industrial Electronics Handbook* (eds. B.M. Wilamowski and J.D. Irwin), 12-1–12-16. Boca Raton, FL: CRC Press.

13 Zimmerman, H.J. (1996). *Fuzzy Set Theory and Its Applications*, 2e. New Delhi: Allied Publishers Limited.

14 Klir, G.J. and Yuan, B. (2000). *Fuzzy Sets and Fuzzy Logic: Theory and Applications*. New Delhi: Prentice-Hall of India Pvt. Ltd.

15 Berkan, R.C. and Trubatch, S.L. (2000). *Fuzzy Systems Design Principles*. New Delhi: Standard Publishers Distributors.

16 Dubois, D. and Prade, H. (1979). Fuzzy real algebra, some results. *Fuzzy Sets and Systems* 2: 327–348.

17 Holland, J.L. (1973). Genetic algorithms and their optimal allocation of trials. *SIAM Journal of Computing* 2 (2): 88–105.

18 Deb, K. (2001). *Multiobjective Optimization Using Evolutionary Algorithms*. Chichester: Wiley.

19 Jang, J.S.R. (1993). ANFIS: adaptive network based fuzzy inference system. *IEEE Transactions on Systems, Man, and Cybernetics* 23: 665–685.

20 Pynckels, F., Kiekens, P., Sette, S. et al. (1995). Use of neural nets for determining the spinnability of fibres. *Journal of the Textile Institute* 86: 425–437.

21 Cheng, L. and Adams, D.L. (1995). Yarn strength prediction using neural networks, Part I: Fibre properties and yarn strength relationship. *Textile Research Journal* 65: 495–500.

22 Ethridge, D. and Zhu, R. (1996). Prediction of rotor spun cotton yarn quality: a comparison of neural network and regression algorithms. In: *Proceedings of the Beltwide Cotton Conference*, Memphis TN, vol. 2, 1314–1317.

23 Zhu, R. and Ethridge, M.D. (1996). The prediction yarn irregularity based on the AFIS measurement. *Journal of the Textile Institute* 87: 509–512.

24 Sette, S., Boullart, L., and Van Langenhove, L. (1996). Optimizing a production process by a neural network/genetic algorithm approach. *Engineering Applications of Artificial Intelligence* 9: 681–689.

25 Rajamanickam, R., Hansen, S.M., and Jayaraman, S. (1997). Analysis of the modelling methodologies for predicting the strength of air-jet spun yarns. *Textile Research Journal* 67: 39–44.

26 Zhu, R. and Ethridge, M.D. (1997). Predicting hairiness for ring and rotor spun yarns and analyzing the impact of fibre properties. *Textile Research Journal* 67: 694–698.

27 Pynckels, F., Kiekens, P., Sette, S. et al. (1997). The use of neural nets to simulate the spinning process. *Journal of the Textile Institute* 88: 440–447.

28 Guha, A., Chattopadhyay, R., and Jayadeva (2001). Predicting yarn tenacity: a comparison of mechanistic, statistical and neural network models. *Journal of the Textile Institute* 92: 139–145.

29 Chattopadhyay, R., Guha, A., and Jayadeva (2004). Performance of neural networks for predicting yarn properties using principal component analysis. *Journal of Applied Polymer Science* 91: 1746–1751.

30 Majumdar, P.K. and Majumdar, A. (2004). Prediction of ring spun cotton yarn elongation using mathematical, statistical and artificial neural network models. *Textile Research Journal* 74: 652–655.

31 Majumdar, A., Majumdar, P.K., and Sarkar, B. (2005). Application of adaptive neuro-fuzzy system for the prediction of cotton yarn strength from HVI fibre properties. *Journal of the Textile Institute* 96: 55–60.

32 Majumdar, A., Sarkar, B., and Majumdar, P.K. (2006). An investigation on yarn engineering using artificial neural networks. *Journal of the Textile Institute* 97: 429–434.

33 Majumdar, A., Ciocoiu, M., and Blaga, M. (2008). Modelling of ring yarn unevenness by soft computing approach. *Fibers and Polymers* 9: 210–216.

34 Majumdar, A. and Ghosh, A. (2008). Yarn strength modelling by fuzzy expert systems. *Journal of Engineered Fibres and Fabrics* 3 (4): 61–68.

35 Ghosh, A. and Chatterjee, P. (2010). Prediction of cotton yarn properties using support vector machine. *Fibers and Polymers* 11: 84–88.

36 Ghosh, A., Das, S., and Saha, B. (2016). Simulation of stress–strain curves of polyester and viscose filaments. *Journal of Institution of Engineers India Series E* 96 (2): 139–143.

37 Mishra, S. (2016). Prediction of yarn strength utilization in cotton woven fabrics using artificial neural network. *Journal of Institution of Engineers India Series E* 96 (2): 151–157.

38 Majumdar, A., Ghosh, A., Saha, S.S. et al. (2008). Empirical modelling of tensile strength of woven fabrics. *Fibers and Polymers* 9 (2): 240–245.

39 Hadizadeh, M., Jeddi, A.A.A., and Tehran, M.A. (2009). The prediction of initial load extension behaviour of woven fabrics using artificial neural network. *Textile Research Journal* 79: 1599–1609.

40 Fan, J. and Hunter, L. (1998). A worsted fabric expert system: Part I: System development. *Textile Research Journal* 68 (9): 680–686.

41 Fan, J. and Hunter, L. (1998). A worsted fabric expert system, Part II: An artificial neural network model for predicting the properties of worsted fabrics. *Textile Research Journal* 68 (10): 763–771.

42 Behera, B.K. and Guruprasad, R. (2012). Predicting bending rigidity of woven fabrics using adaptive neuro-fuzzy inference system (ANFIS). *The Journal of the Textile Institute* 103 (11): 1205–1212.

43 Ucar, N. and Ertugrul, S. (2002). Predicting circular knitting machine parameters for cotton plain fabrics using conventional and neuro-fuzzy methods. *Textile Research Journal* 72 (4): 361–366.

44 Bilisik, K. and Demiryurek, O. (2011). Analysis and tensile-tear properties of abraded denim fabrics depending on pattern relations using statistical and artificial neural network models. *Fibers and Polymers* 12 (3): 422–430.

45 Zeydan, M. (2008). Modelling the woven fabric strength using artificial neural network and Taguchi methodologies. *International Journal of Clothing Science and Technology* 20 (2): 104–118.

46 Hadizadeh, M., Tehran, M.A., and Jeddi, A.A.A. (2010). Application of an adaptive neuro fuzzy system for prediction of initial load/extension behavior of plain-woven fabrics. *Textile Research Journal* 80 (10): 981–990.

47 Bhattacharjee, D. and Kothari, V.K. (2007). A neural network system for prediction of thermal resistance of textile fabrics. *Textile Research Journal* 77 (1): 4–12.

48 Fayala, F., Alibi, H., Benltoufa, S., and Jemni, A. (2008). Neural network for predicting thermal conductivity of knit materials. *Journal of Engineered Fibers and Fabrics* 3 (4): 53–60.

49 Majumdar, A. (2011). Modelling of thermal conductivity of knitted fabrics made of cotton–bamboo yarns using artificial neural network. *The Journal of the Textile Institute* 102 (9): 752–762.

50 Tokarska, M. (2004). Neural model of the permeability features of woven fabrics. *Textile Research Journal* 74 (12): 1045–1048.

51 Brasquet, C. and Le Cloirec, P. (2000). Pressure drop through textile fabrics-experimental data modeling using classical models and neural networks. *Chemical Engineering Science* 55: 2767–2778.

52 Brasquet, C.F. and Le Cloirec, P. (2003). Modelling of the flow behavior of activated carbon cloths using a neural network approach. *Chemical Engineering and Processing* 42: 645–652.

53 Hatua, P., Majumdar, A., and Das, A. (2013). Predicting the ultraviolet radiation protection by polyester-cotton blended woven fabrics using nonlinear regression and artificial neural network models. *Photodermatology, Photoimmunology and Photomedicine* 29: 182–189.

54 Hatua, P., Majumdar, A., and Das, A. (2014). Modeling ultraviolet protection factor of polyester-cotton blended woven fabrics using soft computing approaches. *Journal of Engineered Fibres and Fabrics* 9: 99–106.

55 Rawal, A., Majumdar, A., Anand, S., and Shah, T. (2009). Predicting the properties of needlepunched nonwovens using artificial neural network. *Journal of Applied Polymer Science* 112: 3375–3338.

22

Fiber-Shaped Electronic Devices

Yang Zhou, Jian Fang, Yan Zhao, and Tong Lin

Deakin University, Institute for Frontier Materials, Geelong Waurn Ponds Campus, Pigdons Road, Geelong, VIC 3216, Australia

22.1 Introduction

Wearable electronic devices are designed to be soft, flexible, and even stretchable, to adapt to bodies' shape and movement [1–4]. They are very useful for health monitoring, activity tracking, military garments, and energy conversion. Early wearable electronic devices were prepared by mounting electronic components on clothes or accessories. Some wearable electronics such as smart watches and wristbands have been commercialized for health monitoring. Since based on silicon electronics, they are rigid and unwashable, hence unsuitable for use in textiles. To improve device flexibility, great attention has been paid toward integrating functional components (e.g. integrated circuits, electrodes) into flexible plastic films. These flexible devices, however, still have poor wear comfort feature due to impermeable nature of the substrates to air and moisture. Meanwhile, these flexible devices are vulnerable to withstand twisting or wrapping [5, 6]. An alternative way to fabricate wearable electronics is to incorporate electronic functions into fibers and then weaving or knitting the electronic fibers into fabrics or textiles. Wearable electronic textiles prepared in this way possess high air permeability. They allow to prepare multifunctional devices simply by assembling fibers of different functions into the same fabric [7–9].

Considerable efforts have been made over recent decade to prepare fiber-shaped electronics, including energy generators [10, 11], energy storage devices [12–14], electrochromic fibers [15], and transistors [16]. The fiber-based energy generators can generate electricity from solar energy or mechanical vibration. They are expected to supply power to personal electronic devices and develop self-powered smart textiles. Electrochromic fibers, which can change color upon being charged with an electric potential, were reported with the purposes to prepare textiles with displaying feature [17]. Figure 22.1 shows an overview of fiber-shaped electronic devices.

Although the significant progress have been made in wearable fiber-based electronics, most of the existing fiber-shaped devices show inferior performance

Handbook of Fibrous Materials, First Edition. Edited by Jinlian Hu, Bipin Kumar, and Jing Lu.
© 2020 Wiley-VCH Verlag GmbH & Co. KGaA. Published 2020 by Wiley-VCH Verlag GmbH & Co. KGaA.

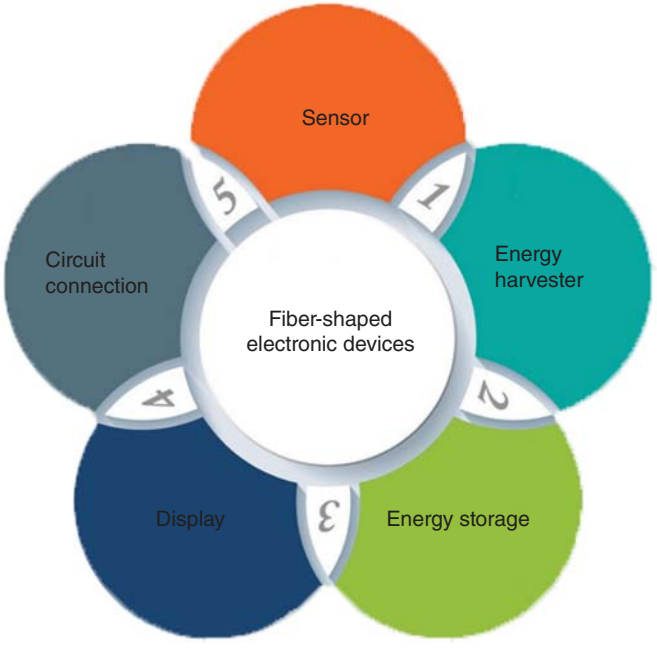


Figure 22.1 Overview of applications of fiber-based electronics.

when compared with their conventional counterparts. Challenges still exist in making flexible fiber-shaped devices. The small size and non-flat structure of fibers increase complicity during device fabrication. The working environment of wearable electronics requires the devices withstanding repeated squeezing or bending deformations caused by body movement. The durability against wearing and washing is critical.

In this chapter, we summarize typical device structures that have been employed in fiber-shaped electronics, along with an introduction of electrode materials and recent progresses in fiber electronics. The development trend of fibrous smart electronics is discussed as well.

22.2 Fiber-Shaped Electronic Devices

Four different structures of fiber-shaped electronic devices have been reported. They all consist of electrodes and functional layers (also called "active layers" in some papers). According to structure features, these devices are named as fiber electrode wrapped fiber devices (FEWFDs), twisted fiber devices (TFDs), sheath–core single fiber devices (SCSFDs), and parallel coil fiber devices (PCFDs). Figure 22.2 illustrates the typical structures of the devices, and the details about each devices are described below.

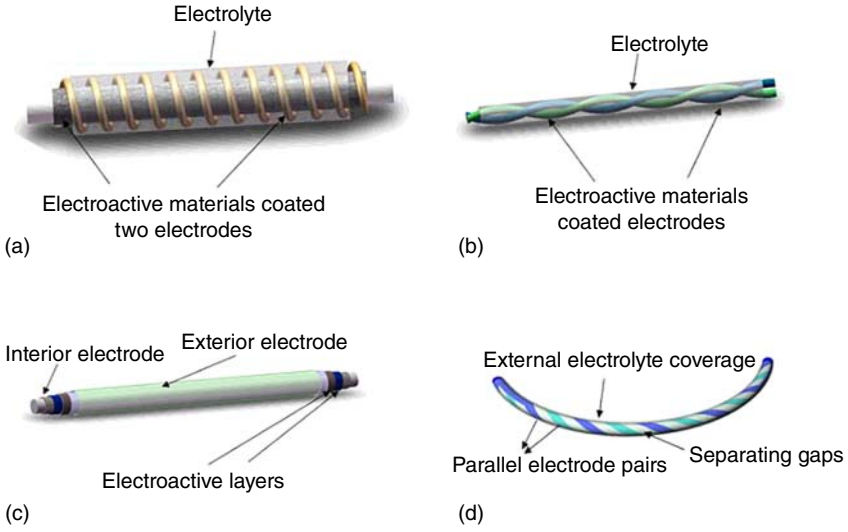


Figure 22.2 Typical structures of the fiber-shaped electronic devices: (a) FEWFDs, (b) TFDs, (c) SCSFDs, and (d) PCFDs.

22.2.1 Twisted Fiber Devices (TFDs)

TFDs are prepared by twisting two fibrous electrodes together. The fibrous electrodes can be made either by the electrode materials in bulk (e.g. carbon fiber or metal wire) or conducting coating on a polymer fiber. The active layer is loaded on either of the electrodes or the both. The twisting feature endows the TFD devices with sufficient specific surface area and contact points for occurrence of electrochemical reactions, which is beneficial for performance optimization. TFDs do not require an external substrate to hold electrodes. Hence, the fabrication process and dimension of TFDs can be simplified and minimized, respectively. The performance and stability of TFD devices are significantly affected by twisting parameters (e.g. twisting tightness, pitches), fiber diameters, and thickness of the active layers. Zhang et al. [18] reported the influence of twisting features on the performance of a TFD solar cell, where Ti wire and multiwalled carbon nanotube (MWCNT) fiber were used as two electrodes. It has been revealed that a TFD with an optimal pitch distance of 750 μm can provide the highest efficiency. Reducing pitch distance increases the possibility of blocking the incident light by MWCNT fibers, whereas increasing pitch distance will also reduce the contact area between two electrodes. It is mentioned as well that either over-twisted or under-twisted electrodes can affect device stability. A further investigation on tightness has been conducted by Chen et al. [19], where they reported that the twist tightness played a crucial role in deciding the performance of fiber-shaped solar cells. Increasing the tightness would increase the twisting stress and the possibility of short circuit within the device, whereas the efficiency will be reduced when the twists become

loosed due to the decreased intimate contact. The major concern of TFDs is the susceptibility to physical deformation when being used. For example, frequent fold, rub, or bending could result in loosing or untwisting the structure, or motion between two electrodes. To obtain better stability, fibrous electrodes for TFDs usually have similar diameters and mechanical properties.

22.2.2 Fiber Electrode Wrapped Fiber Devices (FEWFDs)

FEWFDs are prepared by wrapping a fibrous electrode on another central fibrous electrode. The two electrodes in FEWFDs are set asymmetrically, and the mechanical stretchability and elasticity of the devices can be turned through the central fiber. Electroactive materials are deposited onto either or both fibrous electrodes. For example, Wang et al. [20] deposited a layer of TiO_2 on Ti wire electrode to improve the power conversion efficiency (PCE) of a fiber solar cell. The TiO_2 layer provided the pathway for charge transport, and it served as a separator to avoid short circuit, which could be caused by the close contact between two electrodes. In most cases, electron and charge transport occurs within the effective area defined by two electrodes and the surrounded electrolyte. The effective area in the FEWFDs can be tuned by varying the angle and density of the wrapping fibers, which are key parameters to affect performance. Chen et al. [19] discussed the influence of various screw pitches on the performance of a FEWFD solar cell. The device with 0.8 mm pitch distance has the largest current density, whereas the device shows the lowest current density when the pitch distance was 1.4 mm. They explained that lower screw distance increased the number of contact point, which facilitates charge transport and increases the short circuit current density. In addition, increasing the coil density could block the incident light captured by the central electrode, resulting in decrease in light harvesting performance. Besides, exfoliation of coating layer might occur when high friction was introduced during wrapping the electrode.

Bending could lead to disconnection of the electrode. As shown in Figure 22.3, disconnection occurs between two electrodes after repeated bending. The PCE reduced from 0.48% to 0.14% after 50 cycles of bending the device.

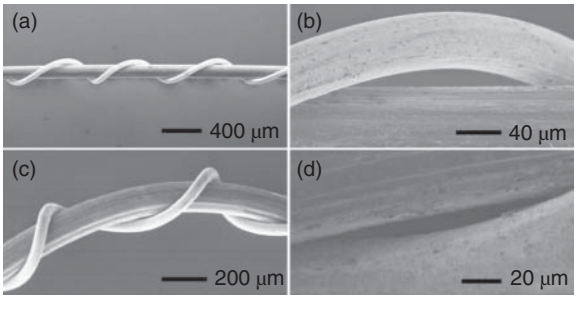


Figure 22.3 Fiber-shaped solar cell with FEWFD structure before bending at (a) low and (b) high magnifications, respectively. The twisted, wire-shaped polymer solar cell with the silver wire as the electrode after bending at (c) low and (d) high magnifications, respectively. Source: Zhang et al. 2014 [18]. Reprinted with permission of John Wiley & Sons.

The wrapping electrode offer a possibility to hold liquid electrolyte in the device. Liu et al. [21] reported a FEWFD solar cell using liquid electrolyte. The capillary effect originated from the gap between the two fiber-shaped electrode enables liquid to be stored in the space.

22.2.3 Sheath–Core Single Fiber Devices (SCSFDs)

SCSFDs have a multiple layer structure. They have a similar configuration to sandwich structured flat electronic device. In general, the two electrodes are separated by active layers in between. Unlike FEWFDs and TFDs where two fibers are used as electrodes, SCSFDs have a sheath–core structure that reduces device dimension because all components are integrated into a fibrous substrate. Because of the intimate contact among the materials, SCSFDs have higher utilization and better physical stability than FEWFDs and TFDs [22]. Zhang et al. [23] reported a SCSFD-structured DSSC with Ti wire and carbon nanotube (CNT) film electrodes. They indicated that the compact contact between two electrodes facilitated ion diffusion toward counter electrode. This allows electrons accumulated at the counter electrode to be captured timely by triiodide ions. Since the electrolyte is infiltrated between the two electrode layers, leakage of the electrolyte substance is eliminated. In addition, the compact electrode layers avoid potential physical disconnection between the electrode and the active layer. Peng [22] highlighted superior volume utilization in SCSFDs by suggesting that the cross-sectional area of a SCSFD ($2\pi r^2$) is two times larger than that of TFDs ($4\pi r^2$) when other parameters were controlled same (see the illustration in Figure 22.4).

Chen et al. [24] indicated that the SCSFD supercapacitor showed better performance than those with TFD structure. Based on Nyquist plot results, they concluded that the internal resistance of the SCSFD was lower than that of TFD. The galvanostatic charge–discharge plot also suggested that SCSFD required less time for a charging–discharging cycle.

A limitation for SCSFDs is the low transparency of the external electrode layer. This affects device performance when used for solar cells, touch screen, and display. Since incident light is blocked by multiple layers of active substances, SCSFD-structured solar cells allow less light to reach electroactive layer [25, 26].

22.2.4 Parallel Coil Fiber Devices (PCFDs)

PCFDs were later developed than other types of fiber devices. They combine the structure features of FEWFDs and SCSFDs. However, PCFDs differ to FEWFDs

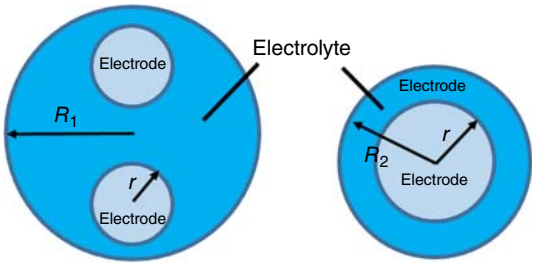


Figure 22.4 Cross-sectional comparison between fiber-shaped supercapacitor with twisting (left) and coaxial (right) structure with identical amount of electrode materials. Source: Peng 2015 [22]. Reproduced with permission of Springer.

and SCSFDs in that the fiber in PCFDs functions like a substrate. Two electrodes covered around the fiber substrate in the shape of parallel coils. The electrodes on the fiber substrate can be formed through a coating or deposition technology. This makes the parallel coils look like a structured sheath. Therefore, PCFDs have higher structure stability than FEWFDs and TFDs. Important structure parameters, features, and production techniques of abovementioned structures are summarized in Table 22.1.

22.3 Electrode Materials

Electrode materials play an essential role in deciding device properties. The electrode materials are often required to have the following features:

(1) Be electrically conductive to complete the circuit.
(2) Provide sufficient surfaces for connection with electroactive materials.
(3) Be able to form effective contact with active substances.
(4) Be stable in both physical and chemical properties.

The commonly used electrode materials for fibrous electronic devices include metal/metal oxides, carbon nanomaterials, and conducting polymers.

22.3.1 Metals and Metal Oxides

Metals are the mostly used electrode material because they are widely available and have high conductivity. For making fiber-shaped electronic devices, the metal electrode can be prepared either in the form of metallic wires or in a thin coating on a fiber substrate. The techniques to fabricate metal electrodes for fiber electronics include wrapping metal wires on the fibrous substrate or twisting with another fiber electrode. In some cases, the metallic wires are coated with a layer of electroactive materials on surface such as TiO_2 to enhance its light absorbing performance in DSSC [20].

For substrates that are intrinsically poor in conductivity, a wide range of coating techniques can be used, including sputter coating, thermal evaporation, electrodeposition, and dipcoating. Sputter coating and thermal evaporation are suitable mainly for flat surfaces, whereas wet chemical methods could suit both curve and flat surfaces.

Apart from metallic wires, indium tin oxide (ITO) is a widely employed owing to high transparency. Thermal evaporation, sputter coating, chemical vapor deposition (CVD), spray pyrolysis, and plating have been used to apply ITO on substrates. Most coating methods can be performed at room temperature, and they are cost effective and environment friendly as well [30, 31].

Metal and metal oxides in the form of nanowire possess both good transparency and conductivity. Lee et al. [32] reported the preparation of ITO nanowires, and the conductive coating has an optical transmittance up to 90% and sheet resistance of 89 Ω/sq. Kim et al. [33] prepared a transparent electrode based on Ag nanowires. The sheet resistance of the coating was less than 100 Ω/sq, and the optical transmittance was around 90%. By optimizing the

Table 22.1 Structure parameters and feature of the fiber-shaped electronic devices.

	Structure parameters	Preparation	Advantages	Disadvantages	References
TFDs	Twisting tightness Screw pitch	Twisting two fiber electrodes manually or via a twisting machine	High specific surface area Miniature in size Large incident area All-direction incident light received	Possibility of short circuit Ineffective contact Twisting stress	[18, 19, 27]
FEWFDs	Wrapping angle Screw pitch Wrapping tightness	Preparing central and sheath electrodes. Wrapping the sheath electrode onto the central electrode	More effective contact between electrodes Capillary effect	Wrapping may block incident light Gaps exist in both straight and bending states	[19, 28, 29]
SCSFDs	Coating thickness Substrate	Layer-by-layer covering the fiber substrate with the electrode electroactive materials and electrode	Intimate contact Compact size Structural stability	Exterior layer may block incident light Possibility of exfoliation	[22, 23, 25, 27]
PCFDs	Pattern design Coating thickness Substrate	Making pre-patterned on fiber substrate, then coating the patterned substrate with electrode materials, and finally removing the template	Parallel electrode Compact size Structural stability	Possibility of exfoliation	[17]

nanowire diameter and length, the nanowire coatings could be transparent in near-infrared region [34].

In addition, some transition metal oxides like zinc oxide (ZnO), manganese dioxide (MnO_2), and ruthenium dioxide (RuO_2) were used as electrode materials. They show great potential in making anode in lithium batteries and supercapacitors owing to the reversible redox reaction and high charge storage capacity [35]. When they are shaped into nanostructures, their electrical conductivity can be substantially improved. The synthesis of such transition metal oxides requires low working temperature and can be applied on a variety of surface especially on textiles and fabrics [36–38].

22.3.2 Carbon-Based Materials

Carbon-based materials such as CNTs, carbon nanofibers, and graphene have high carrier mobility, conductivity, and mechanical properties [39, 40]. Despite they have relatively lower electrical conductivity than metals, their chemical stability is much higher, and the conductivity can be improved by addition of conducting components [41].

The mechanical properties of CNTs were reported to have a tremendous effect on device performance. Liu et al. [28] reported that the PCE of a fibrous polymer solar cell can be improved from 0.8% to around 2% when silver wire electrode was replaced with CNT fiber. Firstly, high flexibility of CNTs led to superior performance by providing better-fitted contact area. The stability was improved since CNT films maintained their continuous morphology and adhered to substrate when the fiber substrate was under bending status. Secondly, the possibility of short circuit caused by the penetration of rigid metal wires on functional polymer layers can be reduced. The outstanding mechanical stability of CNTs allows them to be used to develop elastic electrodes. For example, a rubber fiber with a thin layer of CNTs sheet wrapped was used to prepare a fiber-shaped supercapacitor. Such a device can be stretched over 400% of its original length and still maintains the specific capacitance at 79.4 F/g [15].

CNT sheets are usually prepared by layer cross-stacking of aligned CNTs [42]. The number of layers and stack direction were used to modify the properties. When CNTs were doped with nitrogen, defects developed on the walls. The presence of the defects facilitates the diffusion of ions in batteries [43]. This improves battery performance where doped CNTs were used. It also enhances the capacitance when used as electrode material for supercapacitors [44].

Since electrode transparency is an important factor for wearable solar cell and organic light-emitting diodes (LEDs), the transparency of carbon-based materials has been improved by many methods. For example, optimization of rod coating or spin coating methods allowed to prepare an electrode with the transparency as high as 85% [45–47], and electrode from hybrid CNTs, fin-like Fe/CNTs, for instance, have an optical transmittance of 88% [48].

Graphene possesses high strength (0.1–0.5 GPa), excellent electrical conductivity (10^4 S/m), and wide potential window. Graphene has attracted intensive interest for making electrode [49–52]. Graphene-based materials can be used either in a conventional two-dimensional form or three-dimensional structures (e.g. aerogels and foams).

22.3.3 Conducting Polymers

Conducting polymers possess large conjugated structure. The electrical conductivity, solubility, optical properties, and stability of conducting polymers can be tailored by modifying the polymer structure. For example, the electrical conductivity and solubility of poly(3,4-ethylenedioxythiophene) (PEDOT) can be improved by doping the polymer with polystyrene sulfonate (PSS), which enables the easy applying of PEDOT on various substrates through dipcoating. Hou et al. [53] prepared dimethyl sulfoxide (DMSO)-doped PEDOT electrode, which had a high conductivity of 109 S/cm. Besides, the morphology of conducting polymers (e.g. nanofibers, nanotubes) also affects performance. Huang et al. [54] reported that polypyrrole (PPy) nanofibers with a diameter of 60–100 nm exhibited excellent conductivity (20–130 S/cm) at ambient temperature. Oh et al. [55] synthesized PPy nanowires via electrodeposition, and the PPy nanowires in aqueous dispersion had excellent electrochemical activities and strong emission. Table 22.2 summarizes typical electrode materials reported for wearable electronic devices.

Table 22.2 Summary of typical electrode materials used in wearable electronic devices.

Materials	Type	Features	References
Ti wire	Metal	Suitable for TiO_2 modification	[56–60]
Stainless wire	Metal	Anticorrosion	[61, 62]
Aligned CNTs sheet	Carbon-based	Good electrical and thermal conductivity High Young's modulus	[63–65]
Graphene/graphene oxide	Carbon-based	High specific surface area High theoretical specific capacitance Thermal conductivity	[66–68]
Carbon	Carbon-based	Good creep resistance Scalable production	[14, 69]
PANI/PEDOT	Conducting polymers	Redox reactions	[68, 70–72]
MnO_2	Metal oxide	High charge storage capacity for solar cell	[14]
ZnO	Metal oxide	Morphology can be precisely controlled Piezoelectricity	[73, 74]
$LiMn_2O_4/Li_4Ti_5O_{12}$	Metal oxide	High working voltage Little volume changes Excellent ion transport	[75, 76]

22.4 Applications

Fiber-shaped electronic devices have shown application potential in diverse fields, including energy generators, energy storage devices, electrochromic fibers, and transistors. The device structure and application performances of the fiber-shaped electronic devices are detailed below.

22.4.1 Energy Harvesters

22.4.1.1 Thermal Energy Harvesters

Thermoelectric devices convert temperature differences into electrical signal based on temperature gradient. Although the output voltage of thermoelectric devices remains small, the ability to convert heat energy, which is ubiquitous but usually cannot be effectively utilized, to electricity is favorable. Being as wearable electronics, thermoelectric devices can utilize the intrinsic temperature gradient from the human body, which is a promising feature over other electricity generator.

A thermoelectric device consists of thermoelectric material and two electrodes that used to conduct generated current. As early as 2008, Yadav et al. [77] reported a yarn-based thermoelectric generator as shown in Figure 22.5, where Bi_2Te_3 and Sb_2Te_3 served as n- and p-type semiconductors, respectively. Silicon fiber with a diameter of 710 μm was used as substrate. Silver and nickel were deposited via thermal deposition in an alternating pattern onto fiber substrates as metal hosts for heating. This fiber generator exhibited a maximum power of 2 nW for seven couples when ΔT was 6.6 K. Investigation on structure–performance relationship was conducted via finite element analysis (FEA), indicating that the power generated per couple increased firstly and then decreased along with the increase of segment length as depicted in Figure 22.5d. Before a maximum value was reached, the improvement of power output was

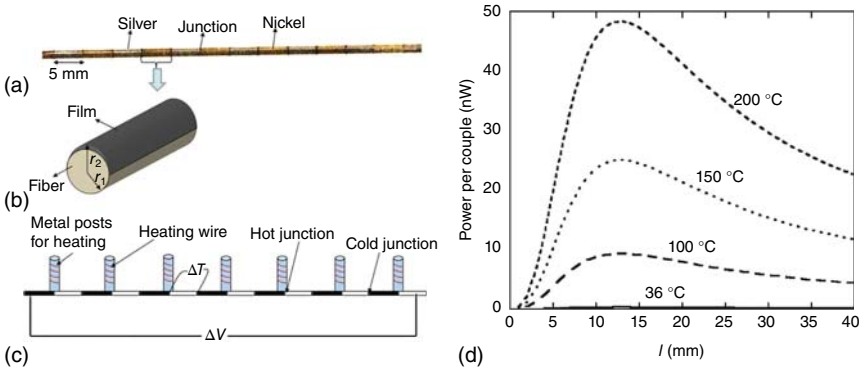


Figure 22.5 (a) Schematic of alternative coating of thermoelectric fibers. (b) Illustration of fiber with thin film deposited on one side. (c) Schematic of experimental setup for applying a temperature gradient and measuring the induced open-circuit voltage. (d) Power per couple vs. the segment length for different hot junction temperatures. Source: Yadav et al. 2008 [77]. Reprinted with permission of Elsevier.

attributed to the increase of temperature gradient caused by elongated segments. Afterward, the increasing resistance caused by excess length dominates, leading to a decline in final output.

It is known that the integration of electronics into textile will result in lower performance than theoretical value. To obtain an in-depth understanding of thermoelectric effects under practice scenario, Lee et al. [78] compared the output signals under various stitches, as shown in Figure 22.6. Flexible yarns were obtained by twisting basic n-type Bi_2Te_3 and p-type Sb_2Te_3 components. The yarns were then woven into zigzag stitch, garter stitch, and plain weave structures. The zigzag structure was easy to fabricate but had the lowest performance of 0.166 μW per couple since the requirement of insulating yarns reduced thermoelectric couples within a certain area. The garter stitch did not

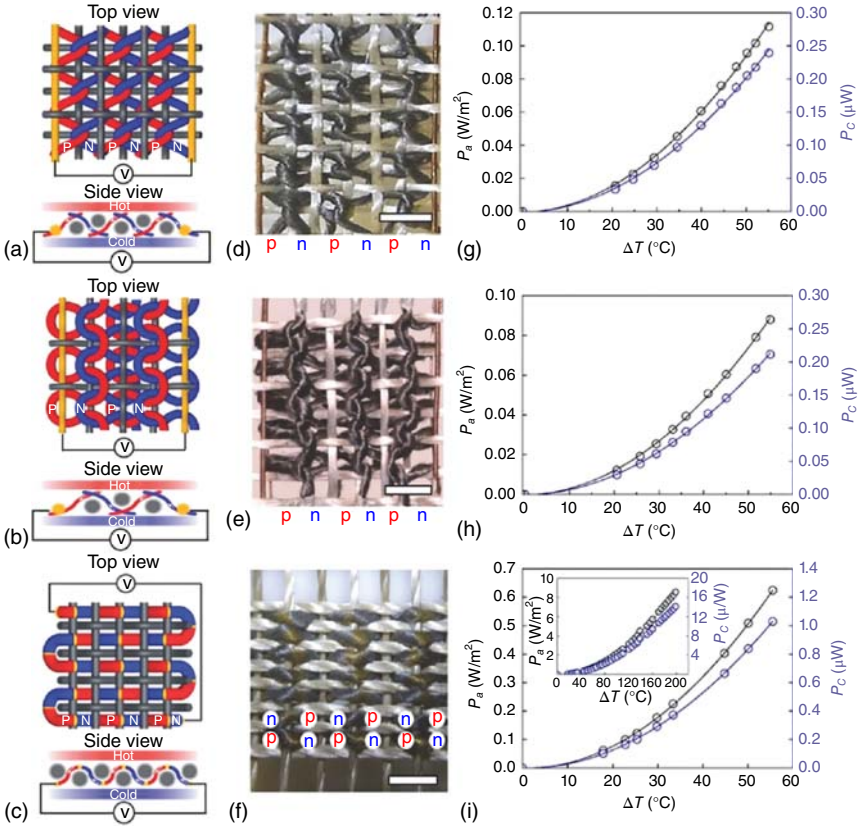


Figure 22.6 Structure and performance of TE textiles. (a–f) Schematic illustrations (a–c) and photographs (d–f) of realized zigzag stitch, garter stitch, and plain weave TE textiles, respectively. The scale bars are 2 mm long. (g–i) The output power per textile area (P_a) and per TE couple (P_c), measured as a function of the temperature difference (ΔT) for zigzag stitch, garter stitch, and plain weave TE textiles, respectively. The inset of (i) shows the output power of a plain weave TE textile for a ΔT of up to 200 °C. Source: Lee et al. 2016 [78]. Reprinted with permission of John Wiley & Sons.

need the presence of insulating yarn. The insulating yarns in garter stitch are used to control junction location during hand weaving process. The plain wave structure was used to provide thermoelectric materials connected in-series. The resulting thermoelectric textile has an outstanding output power up to 8.56 W/cm^2 when a temperature difference of 200 °C was applied toward textile thickness direction.

22.4.1.2 Solar Cells

The research on fiber-shaped solar cells focuses on three cell types: dye-sensitized solar cells, polymer solar cells, and perovskite solar cells. Although the exact mechanism varies from type to type, they all convert solar energy into electricity via photovoltaic effect. In general, dye-sensitized solar cells exhibit higher PCE than polymer cell while requiring the use of liquid electrolyte. Hence, most fiber-shaped dye-sensitized solar cells employ quasi-solid electrolyte or a tube infiltrated with electrolyte to protect the device. The key merit of polymer solar cell is the all-solid-state device feature where no liquid electrolyte is used. The all-solid-state feature is specifically suitable for wearable electronics. As an emerging type of solar cell, the possession of both solid state and high efficiency has made perovskite solar cells in the spotlight. As all of them are subgroups under solar cell, we do not intentionally distinct them in Section 22.4.1.2. In general, fiber-shaped solar cells consist of stainless steel or Ti wires coated with a layer of titanium dioxide (TiO_2) working electrode, and CNT sheet counter electrode [79]. Electroactive materials such as sensitizer and electrolyte surround the two electrodes in the form of gel or solid states. Table 22.3 lists recently reported fiber-shaped solar cells and their performance features.

In 2002, Baps et al. [81] reported a fiber-shaped solar cell with SCSFD structure where a TiO_2-coated stainless wire served as internal electrode and conducting polymer as external electrode. The device can generate a potential around 0.3 V. This prototype has inspired people to transform conventional planar device into a fiber. Later on, investigation on fiber-based solar cells has been burgeoning over the past decades. Liu et al. [82] reported a fiber-shaped polymer solar cell with a PCE of 0.6%. Fan et al. [83] reported a TFD-structured DSSC in 2008. The working electrode was made of TiO_2-coated stainless steel fiber, and the counter electrode was a polymer protective layer coated with Pt wire. The twisting structure enabled that incident light from all directions and angles can be captured by electrodes. Polymer protective layer was employed to release local stress between two electrodes via elastic deformation. Hence, the back-transfer of carrier can be reduced. The optimal thickness of protective layer was achieved at 3.5 μm. This device with 5 cm length exhibited 610 mV open circuit voltage and 0.06 mA short-circuit current. The emergence of fiber-shaped perovskite solar cell was in 2014. Qiu et al. reported a SCSFD-structured fibrous solar cell [25]. Stainless steel wire was adopted as internal electrode, followed by the deposition of perovskite electroactive material $CH_3NH_3PbI_3$. Aligned CNT sheet with high transparency was used as external electrode. The all-solid-states perovskite fiber showed promising future for wearable applications with a PCE of 3.3%, which was higher than fiber-shaped dye-sensitized solar cells and polymer cells reported on that time.

Table 22.3 Recent development on fiber-shaped solar cells.

Year	Structure	Electrode	PCE (%)	Feature	References
2013	SCSFD	Ti/TiO_2/CNT	4.10	Stability during deformation Ultrathin	[56]
2013	SCSFD	Ti/TiO_2/CNT	2.6	High thermal stability and flexibility Quasi-solid-state	[57]
2014	SCSFD	Ti/TiO_2/CNT	6.83	Core–sheath structured CNT/graphene nanoribbon fibrous electrode	[58]
2014	FEWFD	Ti/TiO_2/CNT	5.64	Investigation on a set of carbon-based materials	[59]
2014	FEWFD	Ti/TiO_2/CNT	7.13	Elastic and stretchable	[65]
2014	TFD	Ti/TiO_2/P3HT: PCBM/PEDOT: PSS/CNT	1.78	Sealing free Scalable production	[18]
2014	SCSFD	Stainless steel/ TiO_2/$MAPbI_3$/ OMeTAD/CNT	3.3	All solid flexible	[27]
2015	SCSFD	Stainless steel/ ZnO/$MAPbI_3$/ OMeTAD/CNT	3.8	Facile preparation Obelisk-like ZnO layer	[80]
2015	FEWFD	Ti/TiO_2/CNT	5.47	Stretchable Ultradurable	[11]
2015	FEWFD	Ti/TiO_2/CNT	5.22	Stable under both stretching and bending	[60]

Afterward, numerous efforts have been made to improve PCE and mechanical properties. The PCE of fiber-shaped solar cells can be improved by optimization of electrode in transparency and conductivity. For example, fiber-shaped solar cell with a PCE of 7.1% was produced recently [84]. The aligned CNTs electrode exhibited more than 80% transmittance and a conductivity of 500 S/cm. Low-dimensional metals such as Au, Ag, and Cu nanowires, which possess both high transparency and conductivity, have been incorporated into fiber substrate [85–87]. Based on scattering effect, Li et al. [88] reported a strategy to capture more light by controlling the thickness of TiO_2 layer.

Additionally, considerable efforts have been made to enhance electrode properties. For instance, the alignment of CNTs can enhanced both mechanical and electrical properties [89–91]. Alignment of CNTs leads to lower contact resistance, less defects, efficient load transfer, and larger surface area when compared with unaligned CNTs [92]. Additionally, aligned CNTs were condensed into thin films, serving as both effective hole extraction layers that eliminated the hole

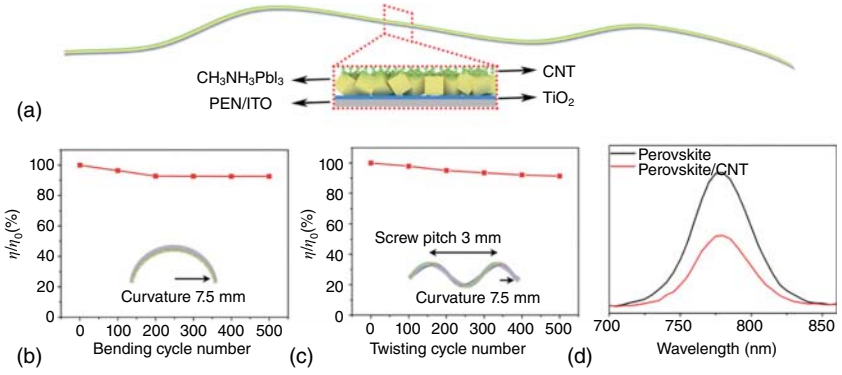


Figure 22.7 (a) Schematic of fiber perovskite solar cell, (b) performance decay under bending states, (c) performance decay under twisting states, and (d) fluorescence spectrum of devices with pristine perovskite and perovskite/CNT electrodes. Source: Qiu et al. 2016 [10]. Reprinted with permission of Royal Society of Chemistry.

transport layer. Benefited from aligned CNTs, Qiu et al. [10] reported a perovskite solar cell with high PCE up to 9.49% (Figure 22.7). It was stable under both bending and twisting operation modes. Significant decrease of fluorescence intensity in non-CNT contained perovskite indicated that CNTs facilitate the effective ion extraction process.

Apart from CNTs, silicon-based p-i-n photodiode junction fiber can be produced via high-pressure chemical vapor deposition (HPCVD) [93]. The fiber device possesses a coaxial p-i-n structure where amorphous silicon n^+, i, and p^+ layers were deposited, followed by crystallization process. The p-i-n photodiodes endowed the fibers with high quantum efficiency, which is desirable in solar cell. Zhang et al. [94] produced a SCSFD-structured solar cell based on $CuInSe_2$ (CIS) and Cds deposited Mo wire. The wire electrode was further coated by ZnO and ITO layers. The solar cell has a PCE of 2.31% under various working conditions. Due to the core–sheath structure where each layer was stacked firmly onto substrates, only 8% efficiency loss was observed when operating at 360° bending angle.

22.4.1.3 Mechanical Energy Harvesters

Mechanical energy harvesters can generate electricity from movement, which are particularly applicable for smart textiles because of the regular motion of wearers. Among many different types of mechanical energy harvesters, piezoelectric devices have attracted the majority of research interest. A piezoelectric device normally contains a layer of piezoelectric material and two electrodes on both sides. Piezoelectric outputs are generated under external force when the piezoelectric material experiences physical deformation. Qin et al. [74] reported a TFD-structured nanogenerator as elucidated in Figure 22.8a. Two fibers coated with ZnO and ZnO/Au were twisted together to form a piezoelectric device. Relative sliding and deflection of two fibers resulted in charge generation, where the uncoated ZnO produces potential across width direction and ZnO with gold coating is used for charge collection and transport. Figure 22.8b and c depicted

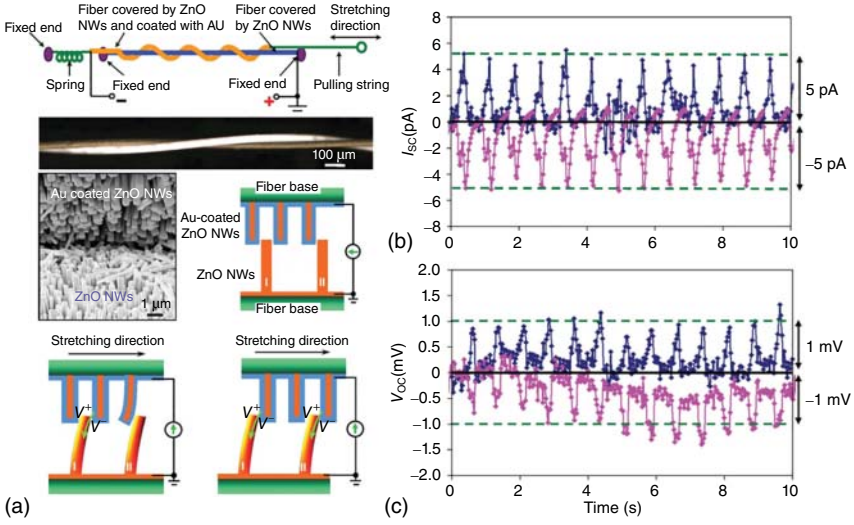


Figure 22.8 (a) Schematic of ZnO nanowires fiber-shaped piezoelectric device and electricity generating processes; (b) the short-circuit output current and (c) the open-circuit output voltage of a double-fiber nanogenerator measured by applying an external pulling force at a motor speed of 80 rpm. Source: Qin et al. 2008 [74]. Reprinted with permission of Springer Nature.

the short-circuit current and the open-circuit output voltage of the twisting nanogenerator. When as-prepared fiber generators were integrated into textile fabrics, an output density of 20–80 mW/m^2 was observed.

Liao et al. [95] reported a fiber-based piezoelectric device with the help of foldable ZnO paper (Figure 22.9). External force moved the Au-coated ZnO layer toward back and down direction, resulting in the formation of piezoelectric field. Flexible paper substrates can be folded at any angle and provide steady physical contact along with enlarged effective working area. The device showed an output voltage of 17 mV and current density of 0.09 $\mu A/cm^2$. Figure 22.9 can be further enhanced when operated under multifiber mode. A LED was lighten up by the power generated from a combination of 600 fibers.

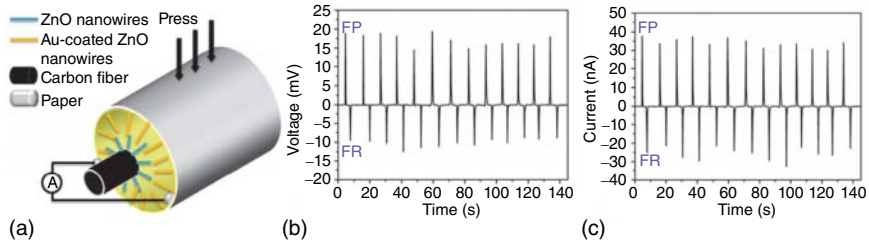


Figure 22.9 (a) Schematic of ZnO paper-based piezoelectric device, (b) output voltage, and (c) current of multifiber-based piezoelectric generator subjected to repeated cycles of FP and FR under forward-connected mode. Source: Liao et al. 2014 [95]. Reprinted with permission of Springer Nature.

Hybrid polyvinylidene fluoride (PVDF)/ZnO dual component device was prepared by incorporating both ZnO nanowires and PVDF polymer onto a fiber substrate. ZnO was considered as the main piezoelectric generator and served as semiconducting electrodes, which also improved piezoelectric coefficient of PVDF. PVDF was coated for multiple purposes. It served as a protective layer, piezoelectric generator, and surface contact enhancer. Hybrid feature endowed the device with better contact between two piezoelectric materials along with improvement of output signal and stability. It has been further demonstrated that electrical outputs could be generated by the releasing and folding processes of human elbow after attaching fiber generator to a human arm. A 2 cm length fiber device was able to generate a voltage output of 0.1 V, current density of 10 nA/cm^2, and power density of 16 $\mu W/cm^3$ [96].

22.4.2 Energy Storage

22.4.2.1 Supercapacitors

Fiber-shaped supercapacitors are more portable and ready to be woven into textiles when compared with their planar counterparts. A typical fiber-shaped supercapacitor consists of two electrodes and electrolyte, which acted as a separator and an ion transport domain. Recent studies on fiber-shaped supercapacitors are summarized in Table 22.4.

Single fiber-shaped supercapacitor was reported by Bae et al. [73] in 2011. They prepared a SCSFD that could convert energy and store it simultaneously. ZnO nanowires and graphene were deposited on the central plastic wire and copper mesh, respectively, as two electrodes, followed by the infiltration of PVA/H_3PO_4 gel electrolyte. The calculated specific capacitance reached to 0.4 mF/cm^2 and 0.025 mF/cm. Since then, giant leaps have been made toward two directions: improvement of capacitance and enhancement of mechanical properties. Electrode optimization is the mostly used method to improve specific capacitance. CNTs and their combination with metal, conducting polymer, or other carbon-based materials were reported to improve the capacitance of the devices. For example, graphene and CNT hybrid electrode have shown promising properties in making wire-shaped electronic devices, where graphene sheets served as conducting bridges and decreased contact resistance [99]. CNT sheets were drawn out from CVD-synthesized CNT arrays and stacked together with the addition of graphene oxide solution. The resulting CNTs exhibited multiwalled feature with a diameter of 10 μm. After reduction, strong interconnection between CNTs and graphene was established owing to π—π bonds. As-prepared energy device exhibited specific capacitance of 31.50 F/g, which is superior to bare CNT electrode.

Conducting polymers such as polyaniline (PANI) and PEDOT can provide extra specific surface area, effective pathway for charge transport, and pseudocapacitance when introduced into CNTs, leading to a significant increase in specific capacitance. Cai et al. [64] reported a PANI/CNT fiber supercapacitor with specific capacitance of 274 F/g. Figure 22.10 shows the influence of PANI on electrochemical properties. Two redox peaks were observed in the interval between 0.3 and 0.4 V, indicating pseudocapacitance feature. Symmetrical

Table 22.4 Recent progress on fiber-shaped supercapacitors.

Year	Structure	Electrode	Maximum performance	Features	References
2013	TFD	CNT/PANI	Specific capacitance of 274 F/g	Stable under bending Good weavability	[64]
2013	SCSFD	Ti/P3HT: PCBM/ PEDOT:PSS/ CNT	Energy density of 1.61×10^{-7} Wh/cm^2	Integration of solar cell and supercapacitor	[65]
2014	FEWFD	CNT/PANI	Energy density of 12.75 Wh/kg and power density of 1494 W/kg	Color indication	[15]
2014	SCSFD	CNT/PANI	Specific capacitance of 79.4 F/g after stretching at a strain of 300% and 100.8 F/g after bending	High stretchability over 400%	[70]
2015	FEWFD	CNT/PEDOT: PSS	Specific capacitance of 30.7 F/g at 0.5 A/g	Working at up to 350% strain	[71]
2016	SCSFD	MWCNT/ PANI	Specific capacitance of 11 F/g	High output voltages up to 1000 V In-series feature	[72]
2016	SCSFD	Thermoplastic polyurethane/ CNT	Specific capacitance of 24 F/g	Shape-memory features	[97]
2016	PCFD	GO/PEDOT: PSS/Vitamin C	Energy density of 27.1 μWh/cm^2 and power density of 66.5 μW/cm^2	Hollow fiber electrodes	[68]
2016	Hybrid	Rubber/CNT	Specific capacitance of 2.38 mF/cm	Against deformation Twistable sandwich structure	[98]
2016	TFD	Microporous carbon/CNT CNT/PEDOT: PSS/MnO_2	Energy density of 11.3 mWh/cm^3 and power density of 2.1 W/cm^3	High performance	[14]

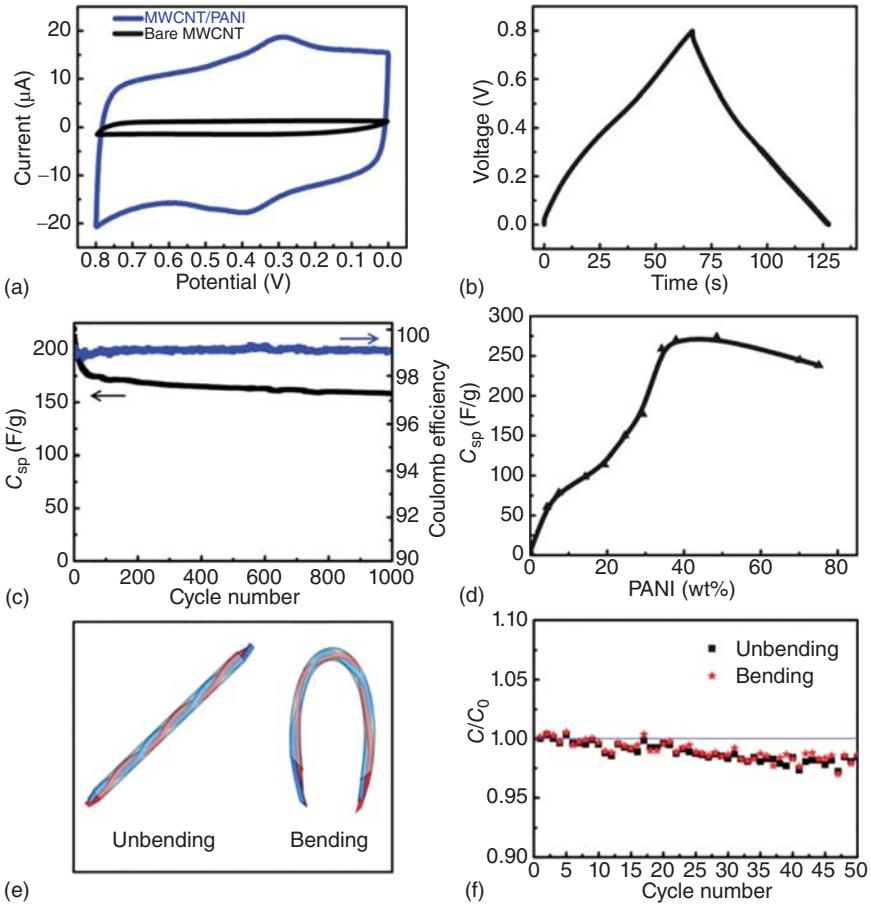


Figure 22.10 Electrochemical properties of supercapacitor wires. (a) Cyclic voltammogram of a supercapacitor with 24% PANI weight. (b) Galvanostatic charge–discharge curves of a supercapacitor with 24% PANI weight. (c) Dependence of specific capacitance and Coulomb efficiency on cycle number of a supercapacitor with 34% PANI weight. (d) Dependence of specific capacitance on the PANI weight percentage. (e) Schematic of the unbending and bending morphologies. (f) Dependence of the specific capacitance of a supercapacitor with 34% PANI weight on bending cycle number. Source: Cai et al. 2013 [64]. Reprinted with permission of Royal Society of Chemistry.

galvanostatic charge–discharge curves and stability test proved that the device exhibited improved stability. This significant improvement was attributed to the synergy of CNTs and PANI, where CNTs provided physical stability and effective contact and PANI afforded charge transfer pathway and high specific surface area. The weight percentage of PANI plays a crucial role in specific capacitance. Specific capacitance was increased along with the increase of PANI weight until a turning point was reached. The reverse trend after the turning point can be explained as excess PANI covered the surface of aligned CNTs and deteriorate electrical properties of CNTs. Meanwhile, stable mechanical properties of CNTs ensured the device can be operated under bending conditions.

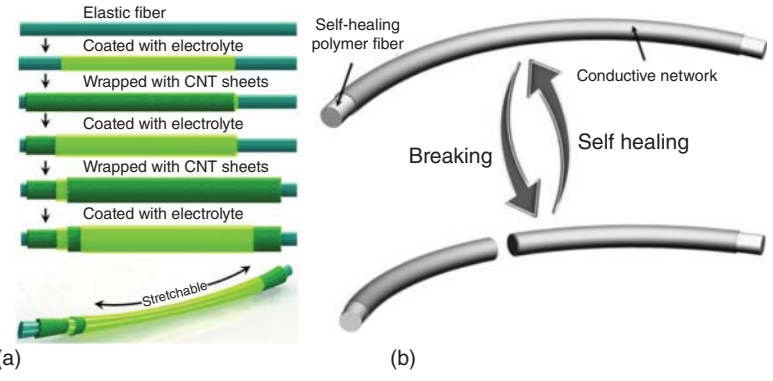


Figure 22.11 (a) Schematic of preparation process of a stretchable supercapacitor. Source: Reprinted with permission from Yang et al. 2013 [100]. (b) Schematic of self-healing supercapacitors. Source: Sun et al. 2014 [101]. Reprinted with permission of John Wiley & Sons.

Apart from specific capacitance, supercapacitors also require robust mechanical properties, which ensure devices can withstand various physical deformation. To date, most fiber-shaped supercapacitors have achieved the ability to work under bending states with little performance loss. However, other features such as stretchability are still highly desired. Yang et al. [100] have prepared SCSFD-structured supercapacitor with high stretchability based on an elastic fiber (Figure 22.11a). As-prepared device managed to achieve 18 F/g specific capacitance after being stretched by 75% for 100 cycles. Other features, such as self-healing and long lifetime fibrous devices, have been investigated as well [101]. As shown in Figure 22.11b, a self-healing polymer was used as a substrate, which was wrapped by CNTs and Ag nanowires. As-prepared device showed excellent performance (specific capacitance of 140.0 F/g) and could recover up to 92% of its original specific capacitance after repeated breaking–healing cycles.

22.4.2.2 Fiber-Shaped Li-Ion Battery

Fiber-shaped lithium-ion batteries are formed by two electrode and electrolyte. The development of fibrous Li-ion battery follows similar directions with fiber supercapacitors. Current fiber-shaped Li-ion batteries originated from a prototype reported by Kwon et al. [102] in 2012. A cable-shaped Li-ion battery was produced by employing a hollow Ni–Sn anode with multi-helix structure and $LiCoO_2$ cathode. Hollow structure reduced cell resistance and enlarged specific surface area, resulting better electrolyte permeability and electrical conductivity. A comparison between non-hollow and hollow structured devices was depicted in Figure 22.12. Device with hollow electrode can be charged and discharged repeatedly with less capacity loss.

Ren et al. [103] fabricated a wire-shaped battery with FEWFD structure that achieved a specific capacitance of 13.31 F/g, where lithium wire and MWCNTs were adopted as two electrodes. Later, they made a further improvement by coating silicon onto the exterior of MWCNTs as a composite anode [104]. When the weight percentage of Si increased from 0% to 38.1%, the specific capacities increased from 82 to 1670 mAh/g owing to remarkable specific capacity of Si

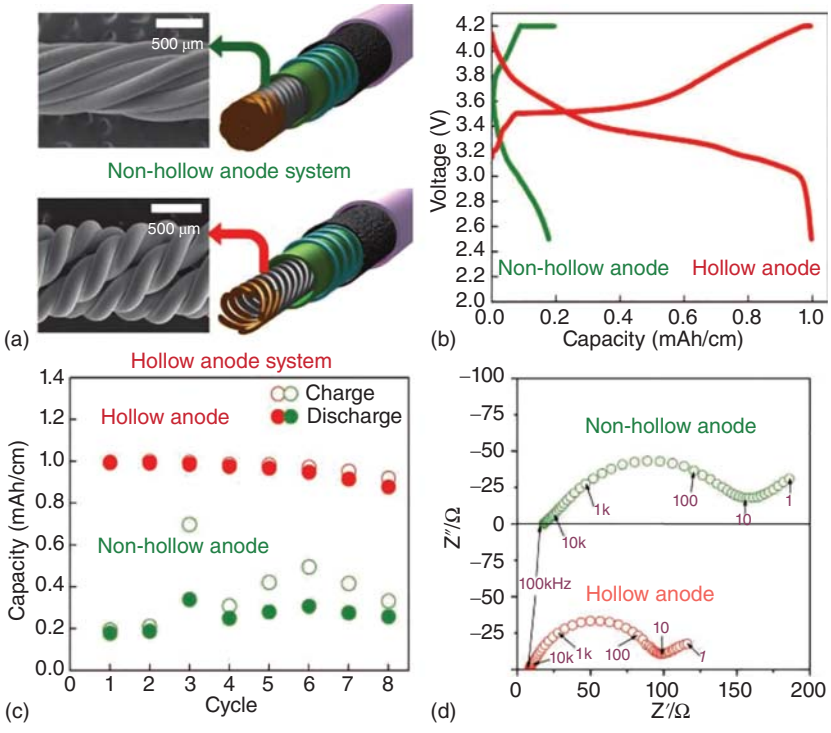


Figure 22.12 Electrochemical properties of the cable battery with hollow anode compared with a device with a dense anode. (a) Images of the cable batteries with dense and hollow anode system. (b) First charge and discharge profiles of cable batteries. (c) Capacity retention of cable batteries. (d) AC impedance spectra of cable battery after one cycle in the frequency range from 100 kHz to 1 Hz. Source: Kwon et al. 2012 [102]. Reprinted with permission of John Wiley & Sons.

[105]. The power density was further improved to 10 217.74 W/kg by employing $LiMn_2O_4$ (LMO)/CNT and polyimide (PI)/CNT hybrid fibers as cathode and anode, respectively, which was the highest reported value in this area and comparable with planar thin-film lithium-ion batteries (Figure 22.13) [75].

A typical method to improve the mechanical properties of fiber batteries is to use a core–sheath structure with a strong substrate. For example, self-healing devices have been produced by applying self-healing polymers to reconstruct their morphology after deformation [106–108]. Zhao et al. [106] produced a self-healing Li-ion battery with an energy density of 32.04 Wh/kg. The discharge voltage decreased from 1.58 to 1.45 V after three times cutting and self-healing processes. Specific capacity decreased from 28.2 to 17.2 mAh/g after the fifth self-healing process. Aside from self-healing features, lithium-ion batteries with high stretchability have also been fabricated. A conventional solution to enhance stretchability is to introduce elastomeric polymers into the device as a substrate [100, 109, 110]. However, the addition of elastic substrates will increase both size and weight of devices. A new solution to this issue is to use spring-like CNT fibers with coiled loops as electrodes instead of elastic polymers, as shown in

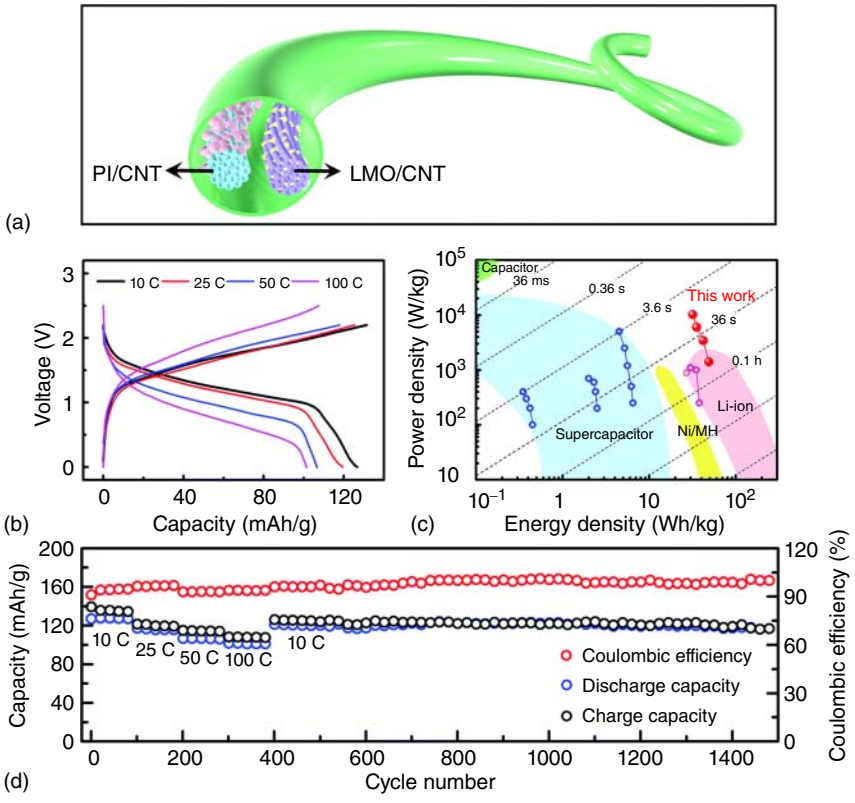


Figure 22.13 Schematic and electrochemical performance. (a) Schematic of a simplified structure showing only the two hybrid electrodes. (b) Charge and discharge curves under increasing current rates (1 C = 183 mA/g). (c) Energy and power densities compared with previous energy storage systems. (d) Rate performance at increasing current rates from 10 to 100 C and long-term stability test at a current rate of 10 C. Source: Zhang et al. 2016 [75]. Reprinted with permission of Royal Society of Chemistry.

Figure 22.14 [111]. By twisting CNT fibers into springs, an elongation of 305% and tensile stress of 82.7 MPa were attained. The volume and weight of this device can be reduced by 400% and 300%, respectively, when compared with devices that contain traditional polydimethylsiloxane (PDMS) or rubber. At a 100% strain level, the capacity of devices remained 85% of its original capacity.

22.4.3 Electrochromic Fibers

Electrochromic materials can change their optical properties by switching among various redox states that present different colors under an applied voltage. Electrochromic fibers are expected to be used for fashionable clothing, safety, and communication purposes. Early electrochromic fiber was made of polydiacetylene (PDA) and CNTs. It could switch color between blue and red by electrical stimulation [112]. The fiber turned from blue to red when an electric potential was applied, and the blue color restored once the applied voltage was

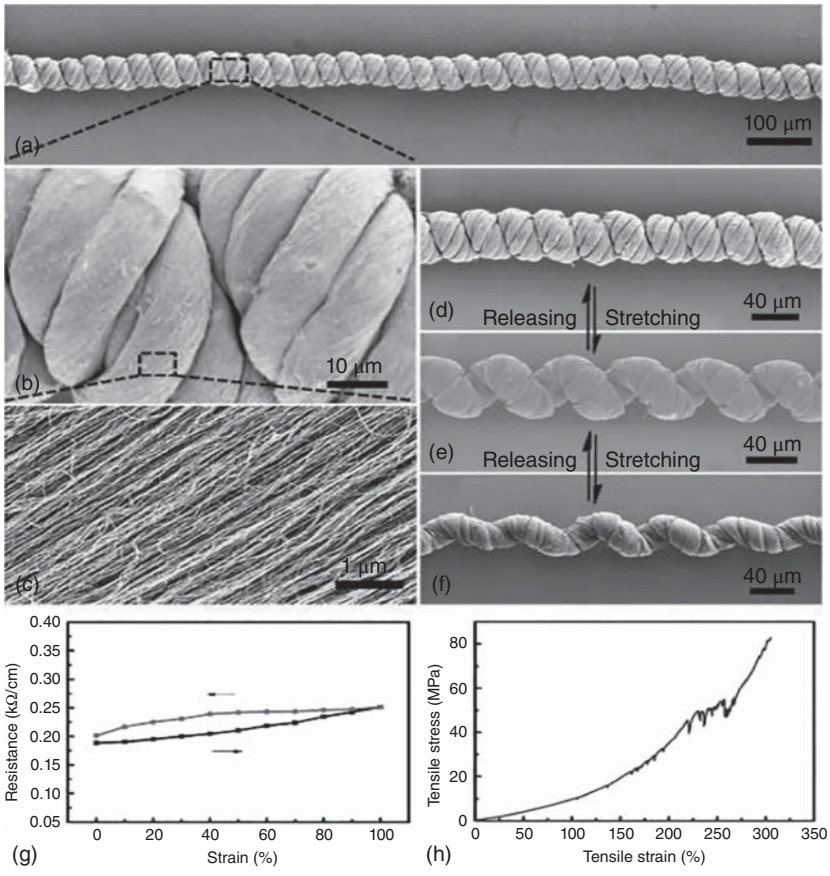


Figure 22.14 (a–c) Scanning electron microscopy (SEM) images of a spring-like fiber at different magnifications; (d–f) SEM images of a fiber at different strains 0% (d), 50% (e), and 100% (f). (g) Evolution of resistances of the fiber during a stretching and releasing process with a strain of 100%. (h) Tensile stress–strain curve of a fiber. Source: Zhang et al. 2014 [111]. Reprinted with permission of John Wiley & Sons.

removed. The CNT/PDA fibers possess high electrical conductivity and fast switching rate of 1×10^3 S/cm and one second, respectively. Color changing was attributed to the interaction between CNTs and PDA. Current induced electrons hopped among nanotubes within a fiber and led to the polarization of –COOH groups and PDA backbones. As a result, delocalization of π-electrons was decreased by above polarization, which corresponded to color changes.

Electrochromic fibers where color variation originated from switch among multiple redox states were later reported. Such electrochromic fibers were prepared by electrodepositing electrochromic materials onto fiber substrates. Li et al. [61] reported a set of electrochromic fibers with multiple colors when woven into clothes (Figure 22.15). A thinner stainless steel wire electrode was wrapped onto a coarse stainless steel wire, followed by electrodeposition of PEDOT, poly(3-methylthiophene) (P3MT), and poly(2,5-dimethoxyaniline)

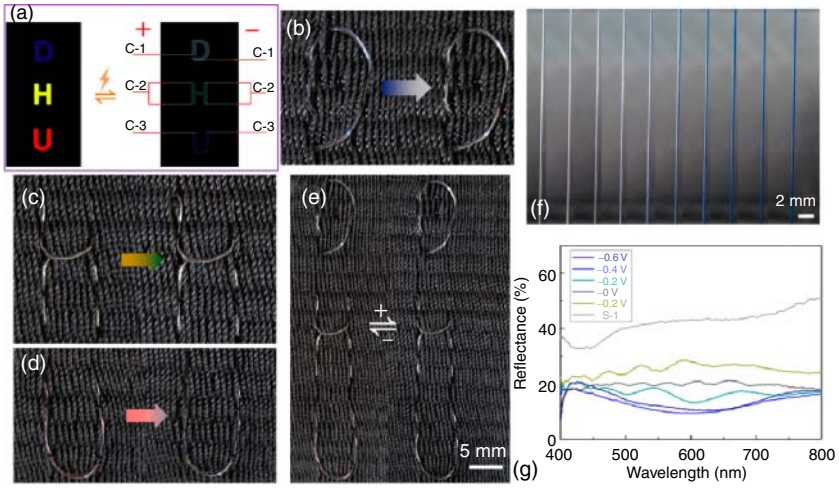


Figure 22.15 Illustration of electrochromic application of composite fibers: (a–e) digital photographs of electrochromic performance of fibers in various forms, (f) color gradient of electrochromic fiber, and (g) reflectance of composite fibers at different working potential. Source: Li et al. 2014 [61]. Reprinted with permission of American Chemical Society.

(PDMA). Multiple colors can be observed due to intrinsic optical properties of deposited polymers. Color response in millisecond at a relatively low voltage was observed. By manipulating the operating potential, color gradient ranging from gray to blue occurred, which was caused by the different intercalation level of dopant.

Aside from aesthetic enhancement, electrochromic fibers can be utilized as a potential monitor since electrochromic behavior is dependent on the potential applied. In addition, electrochromic polymer has pseudocapacitance features intrinsically and can be made as dual functional fiber. PEDOT-based dual functional fiber was reported as shown in Figure 22.16A [17]. Au was selectively coated onto fibrous substrate with the help of a helix-shaped mask, followed by electrodeposition of PEDOT. Uncoated blank space separated the continuous Au layer, resulting two electrodes integrated onto a single fiber substrate. Electrochromic performance can be observed on helix electrodes directly

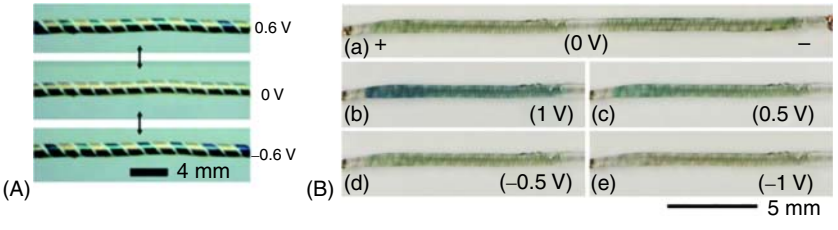


Figure 22.16 (A) Chromatic transitions during the charge–discharge process. Source: Zhou et al. 2016 [17]. Reprinted with permission of American Chemical Society. (B) An electrochromic fiber-shaped supercapacitor at various potential. Source: Chen et al. 2014 [15]. Reprinted with permission of John Wiley & Sons.

without color overlap, which occurred in a traditional core–sheath structure, and supercapacitor worked well without interference. Chen et al. [15] utilized this feature to monitor the working statues of a fiber-shaped supercapacitor. PANI-coated CNT electrodes were deposited onto elastic substrate, and the resulting substrate was further woven into a supercapacitor network, where PANI acted as both monitor and pseudocapacitor. The fiber exhibited various colors depending upon the potential of supercapacitor (Figure 22.16B). The direction and working potential can be known through different colors.

22.4.4 Transistors

Transistors are semiconductor components that amplify or switch electronic signals. Fiber-shaped organic field-effect transistors (OFETs) and organic electrochemical transistor (OECT) have become the mainstream of research interest among various types of transistors. Figure 22.17 presented a comparison between OFET and OECT [113]. For an OFET, the conductivity of polymer is subjected to the potential applied on gate electrode. More charges are accumulated within the polymer channel with increased conductivity when the device is under "ON"

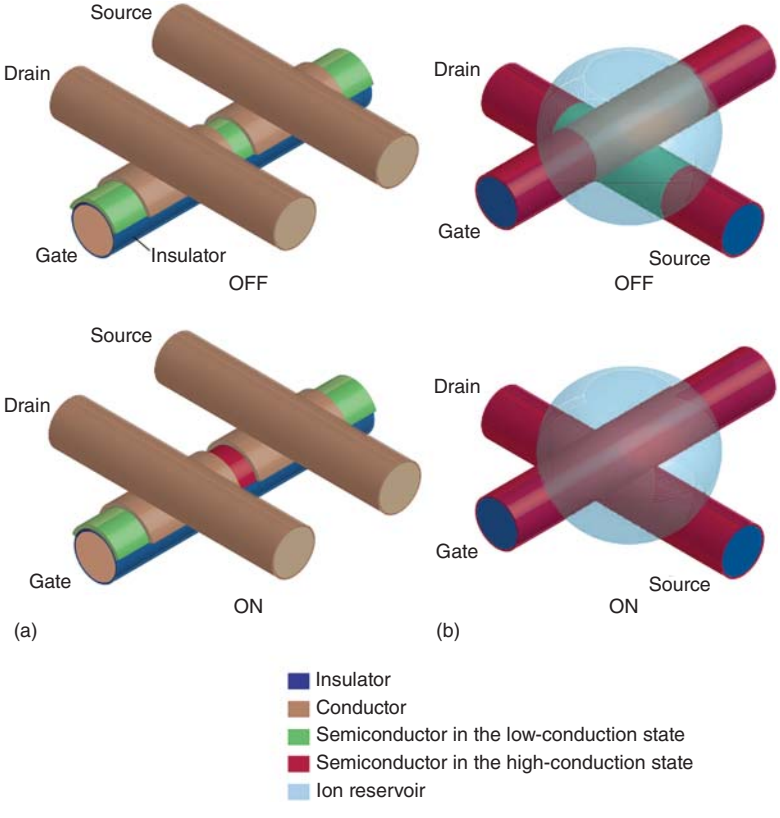


Figure 22.17 Working schematic of (a) OFET and (b) OECT with respect to their "ON" and "OFF" states. Source: De Rossi 2007 [113]. Reprinted with permission of Springer Nature.

mode. When it is switched to "OFF" mode, the number of accumulated charges reduces, leading to a decline in conductivity. In an OECT, the control of gate electrode results in conductivity change via the injection/extraction of ions from electrolyte.

Advantages of OECT include high current in channel and low cost. Additionally, an OECT does not require smooth substrate surface, making it more practical to be applied in wearable applications. However, restricted by the working mechanism, which is originated from the doping/de-doping features of conducting polymers, this type of transistor can only be operated in depletion mode. Meanwhile, the response time of OECT is longer than OFET since ion transport processes in ionic liquid are slower. Hamedi et al. [16] combined OECT and OFET by adopting poly(3-hexylthiophene) (P3HT) and imidazolium ionic liquid as electroactive materials. Conducting channel was established by the field-effect current at the interface of P3HT/electrolyte, followed by a significant response made by doping/de-doping process of P3HT. It possessed advantages of both OFET and OECT and can be operated at a low potential with large current density.

22.4.5 Fiber-Shaped Electroluminescent Device

Electroluminescent materials can emit light in response to the potential applied or current passed through. Fiber-shaped electroluminescent device can be woven into clothes for better information conveying functions. For example, Zhang et al. [114] prepared a fiber-shaped polymer light-emitting device by constructing a CNT/electroluminescent polymer (EP)/CNT core–sheath fiber. When the potential applied reached to a threshold, the EP switched to n-doped and p-doped states at cathode and anode, respectively, exhibiting a uniform electroluminescent effect (Figure 22.18).

The minimum working potential of resulting light-emitting device was 8.8 V, and the maximum light intensity reached at 505 cd/m^2, respectively. As-prepared device also exhibited remarkable performance under bending states where 91.2% of brightness was retained after 100 bending cycles.

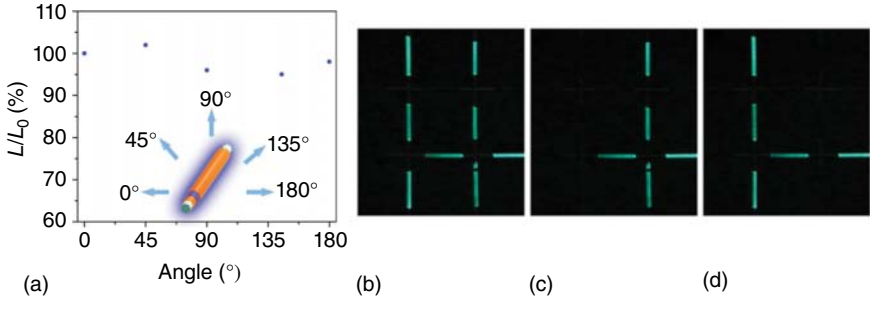


Figure 22.18 (a) The dependence of luminance on the observation angle for a "luminescent fiber." Here L_0 and L correspond to the luminance measured at 0 and at other observation angles, respectively. (b–d) Images of woven "luminescent fibers" being selectively lightened. Source: Zhang et al. 2015 [114]. Reprinted with permission of Royal Society of Chemistry.

22.4.6 Fiber-Shaped Sensors

Sensors are another typical application area of fiber-shaped electronic device. Ge et al. [115] produced a multifunctional sensor fabric, which could response to normal pressure, lateral strain, and flexion. A polyurethane fiber was used as substrate, followed by the wrapping of a nylon fiber. This basic fiber component was further treated with 3-triethoxysilylpropylamine in order to form hydrogen bonds between the interface. Ag nanowires and piezoresistive rubber were used afterward to construct a core–sheath structure. Figure 22.19 illustrated the working principle and performance of the mechanical sensor. The resistance of sensor

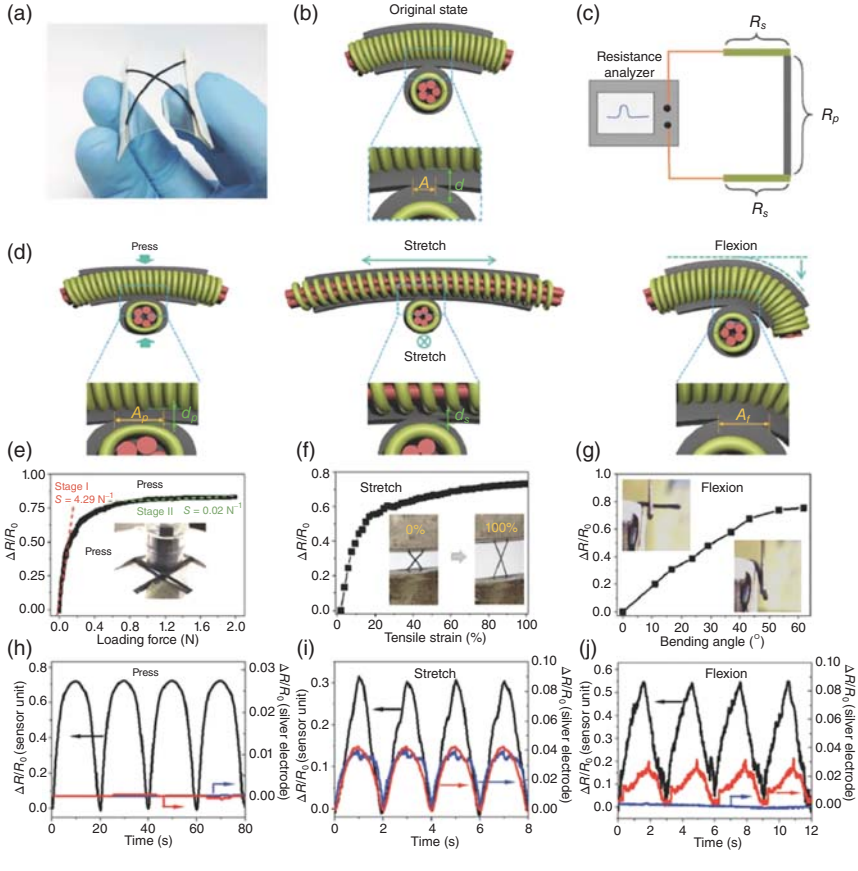


Figure 22.19 Mechanical–electric properties of the sensor unit. (a) Optical image of a typical sensor unit. (b) Schematic illustration of the cross contact point of the sensor unit. *A* is the contact area, and *d* is the thickness of the piezoresistive rubber layers between the silver electrodes. (c) The equivalent circuit of the sensor unit. (d) Schematic illustration of the shape deformation at the contact point of the sensor unit under press, stretch, and flexion. A_p and d_p are the contact area and thickness under press, d_s is the thickness under stretch, and A_f is the contact area under flexion. (e–g) The plots of relative resistance change ($\Delta R/R_0$) of the sensor unit as a function of loading force, tensile strain, and bending angle, respectively. Source: Reprinted with permission from Ge et al. 2016 [115].

will be changed under various operation modes and can be viewed as a function of input signal (e.g. loading force, tensile strain, and bending angle). They have further achieved force mapping by weaving a number of fiber sensors into a fabric, which can detect the position of the object placed on the fabric and quantify mechanical stress through pressure, strain, and flexion changes.

22.4.7 Characterization Techniques and Key Parameter

It is crucial to be aware of characterization techniques and corresponding parameters when describing fiber-shaped electronic devices that applied in various area. These parameters will be used to evaluate and compare the performance of a fiber-shaped electronic device with peers. Hence, a summary of characterization methods and evaluation parameters based on application types is presented as shown in Table 22.5.

Table 22.5 Summary of characterization techniques and key parameters.

Application	Characterization techniques	Evaluation parameters
Thermal energy harvesters	Voltage–temperature and current–temperature curves	Power density, figure-of-merit, net thermal voltage
Solar cells	Photoluminescence spectra, voltage–current curve	Fill factor, power conversion efficiency, open circuit voltage, short circuit current
Mechanical energy harvesters	Voltage–strain and current–strain curves, open-circuit voltage responses, short-circuit current plots	Power density, open-circuit voltage, short-circuit current
Supercapacitors	Cyclic voltammetry curves, galvanostatic charge–discharge curves, impedance spectroscopy	Energy density, power density, specific capacitance
Li-ion batteries	Cyclic voltammetry curves, charge–discharge curves, impedance spectroscopy	Energy density, power density, specific capacity, impedance
Electrochromic fibers	UV–vis spectrum, chromaticity	Contrast ratio, coloration efficiency, color chromaticity, response time
Transistors	Current–voltage plot, impedance spectroscopy	Capacitance, response time, driving voltage, current density
Electroluminescent fibers	Current–voltage plot, chromaticity	Light intensity, color chromaticity, illumination efficiency
Sensors	Strain–current plot, impedance spectroscopy	Sensitivity

22.5 Conclusions

During the past decade, the performance of fiber-based electronic devices has been significantly improved through material innovation and novel structure design. Meanwhile, the functionality of devices has evolved from single function to multiple functions. However, with great challenges in this area, continuous efforts are needed to make breakthrough innovation in the near future, especially in the following directions:

Improve performance through new materials and structures: The development of new materials and structures is a major driving force to facilitate the realization of wearable electronics, including optimization of microstructure, electrolyte, dopants, and modification of molecular chains, etc. For example, previous studies have demonstrated that aligned CNT sheets have remarkable electrical properties compared with CNTs without treatment.

Enhance interface for better stability and durability: Good stability and durability are mainly originated from structure optimization. Devices with high integration level will intrinsically have better stability. Future trends are high-level integration of electronic components within a fiber device and miniature of device dimensions. Single fiber-based electronics that can replace existing multifiber structures are desired. Making fiber electronics in micro- or nanoscales will improve the specific area and let people assemble as much as possible fiber components given certain surface areas.

Produce fibrous devices on large scale: To achieve commercialization of wearable devices, scalable fabrication and device assembly must be developed. High temperature and voltage should be avoided during manufacturing processes. The development of large-scale production of carbon-based materials might become a promising topic in terms of electrode fabrication.

Integration with normal textiles, washing, and ironing: The ultimate aim of wearable electronics is to integrate electronic components into textiles unperceivably, which requires extensive studies on woven ability, post treatment, and safety issues such as electrolyte leakage. Hence, scientists must seek balance between comfortability, performance, and safety. Some fiber-shaped devices are based on stainless steel wires or hard materials, which are not suitable to be worn. Taking a step further, we should treat wearable electronics as same as normal textiles, which means launderability, and the ability to undergo ironing and folding cannot be omitted.

In summary, we are still far from the truly realization of wearable electronics. More systematic awareness of wearable electronics, including materials, structures, fabrications, etc., should be established. However, given the joint efforts that have been made so far, it is believed that the ideal wearable electronics are at the corner.

References

1 He, X. et al. (2016). A highly stretchable fiber-based triboelectric nanogenerator for self-powered wearable electronics. *Advanced Functional Materials* 27 (4): 1604378.

2 Yu, N. et al. (2016). High-performance fiber-shaped all-solid-state asymmetric supercapacitors based on ultrathin MnO_2 nanosheet/carbon fiber cathodes for wearable electronics. *Advanced Energy Materials* 6 (2): 1501458.

3 Jung, Y.H. et al. (2016). Stretchable twisted-pair transmission lines for microwave frequency wearable electronics. *Advanced Functional Materials* 26 (26): 4635–4642.

4 Wang, J. et al. (2016). Sustainably powering wearable electronics solely by biomechanical energy. *Nature Communications* 7: 12744.

5 Yun, M.J. et al. (2015). Insertion of dye-sensitized solar cells in textiles using a conventional weaving process. *Scientific Reports* 5: 11022.

6 Zou, D.C. et al. (2010). Fiber-shaped flexible solar cells. *Coordination Chemistry Reviews* 254 (9–10): 1169–1178.

7 Xu, Y. et al. (2016). An all-solid-state fiber-shaped aluminum–air battery with flexibility, stretchability, and high electrochemical performance. *Angewandte Chemie* 128 (28): 8111–8114.

8 Fan, F.R., Tang, W., and Wang, Z.L. (2016). Flexible nanogenerators for energy harvesting and self-powered electronics. *Advanced Materials* 28 (22): 4283–4305.

9 Stoppa, M. and Chiolerio, A. (2014). Wearable electronics and smart textiles: a critical review. *Sensors* 14 (7): 11957–11992.

10 Qiu, L.B. et al. (2016). An all-solid-state fiber-type solar cell achieving 9.49% efficiency. *Journal of Materials Chemistry A* 4 (26): 10105–10109.

11 Li, H.P. et al. (2015). Stable hydrophobic ionic liquid gel electrolyte for stretchable fiber-shaped dye-sensitized solar cell. *ChemNanoMat* 1 (6): 399–402.

12 Zhang, Z.T. et al. (2015). A colour-tunable, weavable fibre-shaped polymer light-emitting electrochemical cell. *Nature Photonics* 9 (4): 233–238.

13 Xu, Y.F. et al. (2015). Flexible, stretchable, and rechargeable fiber-shaped zinc-air battery based on cross-stacked carbon nanotube sheets. *Angewandte Chemie International Edition* 54 (51): 15390–15394.

14 Cheng, X.L. et al. (2016). Design of a hierarchical ternary hybrid for a fiber-shaped asymmetric supercapacitor with high volumetric energy density. *Journal of Physical Chemistry C* 120 (18): 9685–9691.

15 Chen, X. et al. (2014). Electrochromic fiber-shaped supercapacitors. *Advanced Materials* 26 (48): 8126–8132.

16 Hamedi, M. et al. (2009). Fiber-embedded electrolyte-gated field-effect transistors for e-textiles. *Advanced Materials* 21 (5): 573–577.

17 Zhou, Y. et al. (2016). Electrochromic/supercapacitive dual functional fibres. *RSC Advances* 6 (111): 110164–110170.

18 Zhang, Z.T. et al. (2014). Weaving efficient polymer solar cell wires into flexible power textiles. *Advanced Energy Materials* 4 (11): 1301750.

19 Chen, T. et al. (2012). Designing aligned inorganic nanotubes at the electrode interface: towards highly efficient photovoltaic wires. *Advanced Materials* 24 (34): 4623–4628.

20 Wang, H. et al. (2009). Hydrothermal growth of large-scale macroporous TiO_2 nanowires and its application in 3D dye-sensitized solar cells. *Applied Physics A: Materials Science and Processing* 97 (1): 25–29.

21 Liu, Y. et al. (2010). Synthesis of TiO_2 nanotube arrays and its application in mini-3D dye-sensitized solar cells. *Journal of Physics D: Applied Physics* 43 (20): 205103.

22 Peng, H. (2015). *Fiber-Shaped Energy Harvesting and Storage Devices*. Springer.

23 Zhang, S. et al. (2011). Single-wire dye-sensitized solar cells wrapped by carbon nanotube film electrodes. *Nano Letters* 11 (8): 3383–3387.

24 Chen, X. et al. (2013). Novel electric double-layer capacitor with a coaxial fiber structure. *Advanced Materials* 25 (44): 6436–6441.

25 Qiu, L. et al. (2014). Integrating perovskite solar cells into a flexible fiber. *Angewandte Chemie International Edition* 53 (39): 10425–10428.

26 Chen, T. et al. (2012). An integrated "energy wire" for both photoelectric conversion and energy storage. *Angewandte Chemie International Edition* 51 (48): 11977–11980.

27 Chen, T. et al. (2012). Polymer photovoltaic wires based on aligned carbon nanotube fibers. *Journal of Materials Chemistry* 22 (44): 23655–23658.

28 Liu, D. et al. (2012). Solid-state, polymer-based fiber solar cells with carbon nanotube electrodes. *ACS Nano* 6 (12): 11027–11034.

29 Yang, Z.B. et al. (2014). Stretchable, wearable dye-sensitized solar cells. *Advanced Materials* 26 (17): 2643–2647.

30 Marikkannan, M. et al. (2015). Effect of ambient combinations of argon, oxygen, and hydrogen on the properties of DC magnetron sputtered indium tin oxide films. *AIP Advances* 5 (1): 017128.

31 Kudryashov, D., Gudovskikh, A., and Zelentsov, K. (2013). Low temperature growth of ITO transparent conductive oxide layers in oxygen-free environment by RF magnetron sputtering. *Journal of Physics: Conference Series*. 012021.

32 Lee, J.Y. et al. (2008). Solution-processed metal nanowire mesh transparent electrodes. *Nano Letters* 8 (2): 689–692.

33 Kim, T. et al. (2014). Highly transparent Au-coated Ag nanowire transparent electrode with reduction in haze. *ACS Applied Materials & Interfaces* 6 (16): 13527–13534.

34 Hu, L.B. et al. (2010). Scalable coating and properties of transparent, flexible, silver nanowire electrodes. *ACS Nano* 4 (5): 2955–2963.

35 Wang, R.R. et al. (2014). A novel method to enhance the conductance of transitional metal oxide electrodes. *Nanoscale* 6 (7): 3791–3795.

36 Bae, J. et al. (2011). Fiber supercapacitors made of nanowire-fiber hybrid structures for wearable/flexible energy storage. *Angewandte Chemie International Edition* 50 (7): 1683–1687.

37 Wei, Z. et al. (2013). Facile synthesis of Sn/TiO_2 nanowire array composites as superior lithium-ion battery anodes. *Journal of Power Sources* 223: 50–55.

38 Ren, J. et al. (2013). Twisting carbon nanotube fibers for both wire-shaped micro-supercapacitor and micro-battery. *Advanced Materials* 25 (8): 1155–1159.

39 Sun, D.M. et al. (2013). A review of carbon nanotube- and graphene-based flexible thin-film transistors. *Small* 9 (8): 1188–1205.

40 Zeng, W. et al. (2014). Fiber-based wearable electronics: a review of materials, fabrication, devices, and applications. *Advanced Materials* 26 (31): 5310–5336.

41 Hou, S. et al. (2011). Transparent conductive oxide-less, flexible, and highly efficient dye-sensitized solar cells with commercialized carbon fiber as the counter electrode. *Journal of Materials Chemistry* 21 (36): 13776–13779.

42 Zhang, M., Atkinson, K.R., and Baughman, R.H. (2004). Multifunctional carbon nanotube yarns by downsizing an ancient technology. *Science* 306 (5700): 1358–1361.

43 Reddy, A.L.M. et al. (2010). Synthesis of nitrogen-doped graphene films for lithium battery application. *ACS Nano* 4 (11): 6337–6342.

44 Zhang, Z. et al. (2016). Nitrogen-doped core-sheath carbon nanotube array for highly stretchable supercapacitor. *Advanced Energy Materials* 27 (4): 1604378.

45 Zhang, D.H. et al. (2006). Transparent, conductive, and flexible carbon nanotube films and their application in organic light-emitting diodes. *Nano Letters* 6 (9): 1880–1886.

46 Wang, X. et al. (2008). Transparent carbon films as electrodes in organic solar cells. *Angewandte Chemie International Edition* 47 (16): 2990–2992.

47 Dan, B., Irvin, G.C., and Pasquali, M. (2009). Continuous and scalable fabrication of transparent conducting carbon nanotube films. *ACS Nano* 3 (4): 835–843.

48 Jiang, D. et al. (2016). Embedded fin-like metal/CNT hybrid structures for flexible and transparent conductors. *Small* 12 (11): 1521–1526.

49 Hu, Y. et al. (2014). All-in-one graphene fiber supercapacitor. *Nanoscale* 6 (12): 6448–6451.

50 Cong, H.P. et al. (2012). Wet-spinning assembly of continuous, neat, and macroscopic graphene fibers. *Scientific Reports* 2: 613.

51 Kim, K.M. et al. (2016). Shape-engineerable composite fibers and their supercapacitor application. *Nanoscale* 8 (4): 1910–1914.

52 Chen, D., Tang, L.H., and Li, J.H. (2010). Graphene-based materials in electrochemistry. *Chemical Society Reviews* 39 (8): 3157–3180.

53 Hou, S.C. et al. (2012). Flexible conductive threads for wearable dye-sensitized solar cells. *Journal of Materials Chemistry* 22 (14): 6549–6552.

54 Huang, K. et al. (2005). Multi-functional polypyrrole nanofibers via a functional dopant-introduced process. *Synthetic Metals* 155 (3): 495–500.

55 Oh, J.H. et al. (2009). Solution-processed, high-performance n-channel organic microwire transistors. *Proceedings of the National Academy of Sciences of the United States of America* 106 (15): 6065–6070.

56 Sun, H. et al. (2013). Winding ultrathin, transparent, and electrically conductive carbon nanotube sheets into high-performance fiber-shaped dye-sensitized solar cells. *Journal of Materials Chemistry A* 1 (40): 12422–12425.

57 Sun, H. et al. (2014). Quasi-solid-state, coaxial, fiber-shaped dye-sensitized solar cells. *Journal of Materials Chemistry A* 2 (2): 345–349.

58 Fang, X. et al. (2014). Core-sheath carbon nanostructured fibers for efficient wire-shaped dye-sensitized solar cells. *Advanced Materials* 26 (11): 1694–1698.

59 Pan, S.W. et al. (2014). Carbon nanostructured fibers as counter electrodes in wire-shaped dye-sensitized solar cells. *Journal of Physical Chemistry C* 118 (30): 16419–16425.

60 Deng, J. et al. (2015). Elastic perovskite solar cells. *Journal of Materials Chemistry A* 3 (42): 21070–21076.

61 Li, K.R. et al. (2014). Red, green, blue (RGB) electrochromic fibers for the new smart color change fabrics. *ACS Applied Materials & Interfaces* 6 (15): 13043–13050.

62 Lee, M.R. et al. (2009). Solar power wires based on organic photovoltaic materials. *Science* 324 (5924): 232–235.

63 Liu, L., Ma, W., and Zhang, Z. (2011). Macroscopic carbon nanotube assemblies: preparation, properties, and potential applications. *Small* 7 (11): 1504–1520.

64 Cai, Z.B. et al. (2013). Flexible, weavable and efficient microsupercapacitor wires based on polyaniline composite fibers incorporated with aligned carbon nanotubes. *Journal of Materials Chemistry A* 1 (2): 258–261.

65 Zhang, Z.T. et al. (2014). Integrated polymer solar cell and electrochemical supercapacitor in a flexible and stable fiber format. *Advanced Materials* 26 (3): 466–470.

66 Li, X. et al. (2013). Large-area flexible core–shell graphene/porous carbon woven fabric films for fiber supercapacitor electrodes. *Advanced Functional Materials* 23 (38): 4862–4869.

67 Meng, Y. et al. (2013). All-graphene core-sheath microfibers for all-solid-state, stretchable fibriform supercapacitors and wearable electronic textiles. *Advanced Materials* 25 (16): 2326–2331.

68 Qu, G.X. et al. (2016). A fiber supercapacitor with high energy density based on hollow graphene/conducting polymer fiber electrode. *Advanced Materials* 28 (19): 3646–3652.

69 Hou, S.C. et al. (2012). Flexible, metal-free composite counter electrodes for efficient fiber-shaped dye-sensitized solar cells. *Journal of Power Sources* 215: 164–169.

70 Zhang, Z.T. et al. (2015). Superelastic supercapacitors with high performances during stretching. *Advanced Materials* 27 (2): 356–362.

71 Chen, T. et al. (2015). High-performance, stretchable, wire-shaped supercapacitors. *Angewandte Chemie International Edition* 54 (2): 618–622.

72 Sun, H. et al. (2016). Electrochemical capacitors with high output voltages that mimic electric eels. *Advanced Materials* 28 (10): 2070–2076.

73 Bae, J. et al. (2011). Single-fiber-based hybridization of energy converters and storage units using graphene as electrodes. *Advanced Materials* 23 (30): 3446–3449.

74 Qin, Y., Wang, X.D., and Wang, Z.L. (2008). Microfibre-nanowire hybrid structure for energy scavenging. *Nature* 451 (7180): 809–813.

75 Zhang, Y. et al. (2016). A fiber-shaped aqueous lithium ion battery with high power density. *Journal of Materials Chemistry A* 4 (23): 9002–9008.

76 Ren, J. et al. (2014). Elastic and wearable wire-shaped lithium-ion battery with high electrochemical performance. *Angewandte Chemie* 126 (30): 7998–8003.

77 Yadav, A., Pipe, K.P., and Shtein, M. (2008). Fiber-based flexible thermoelectric power generator. *Journal of Power Sources* 175 (2): 909–913.

78 Lee, J.A. et al. (2016). Woven-yarn thermoelectric textiles. *Advanced Materials* 28 (25): 5038–5044.

79 Zou, D.C. et al. (2012). Macro/microfiber-shaped electronic devices. *Nano Energy* 1 (2): 273–281.

80 He, S.S. et al. (2015). Radically grown obelisk-like ZnO arrays for perovskite solar cell fibers and fabrics through a mild solution process. *Journal of Materials Chemistry A* 3 (18): 9406–9410.

81 Baps, B., Eber-Koyuncu, M., and Koyuncu, M. (2002). Ceramic based solar cells in fiber form. *Key Engineering Materials* 937–940.

82 Liu, J., Namboothiry, M.A.G., and Carroll, D.L. (2007). Fiber-based architectures for organic photovoltaics. *Applied Physics Letters* 90 (6): 063501.

83 Fan, X. et al. (2008). Wire-shaped flexible dye-sensitized solar cells. *Advanced Materials* 20 (3): 592–595.

84 Qiu, L.B. et al. (2016). Fiber-shaped perovskite solar cells with high power conversion efficiency. *Small* 12 (18): 2419–2424.

85 Rathmell, A.R. et al. (2010). The growth mechanism of copper nanowires and their properties in flexible, transparent conducting films. *Advanced Materials* 22 (32): 3558–3563.

86 Yang, Y. et al. (2016). Facile fabrication of stretchable Ag nanowire/polyurethane electrodes using high intensity pulsed light. *Nano Research* 9 (2): 401–414.

87 Maurer, J.H.M. et al. (2016). Templated self-assembly of ultrathin gold nanowires by nanoimprinting for transparent flexible electronics. *Nano Letters* 16 (5): 2921–2925.

88 Li, Z.D. et al. (2016). Electrophoretic deposition of graphene-TiO_2 hierarchical spheres onto Ti thread for flexible fiber-shaped dye-sensitized solar cells. *Materials and Design* 105: 352–358.

89 Craddock, J.D. and Weisenberger, M.C. (2015). Harvesting of large, substrate-free sheets of vertically aligned multiwall carbon nanotube arrays. *Carbon* 81: 839–841.

90 Zhai, H.Y. et al. (2015). A sensitive electrochemical sensor with sulfonated graphene sheets/oxygen-functionalized multi-walled carbon nanotubes modified electrode for the detection of clenbuterol. *Sensors and Actuators B: Chemical* 210: 483–490.

91 Ternon, C. et al. (2015). Carbon nanotube sheet as top contact electrode for nanowires: highly versatile and simple process. *Journal of Nanoscience and Nanotechnology* 15 (2): 1669–1673.

92 Chen, H. et al. (2010). Controlled growth and modification of vertically-aligned carbon nanotubes for multifunctional applications. *Materials Science and Engineering R: Reports* 70 (3–6): 63–91.

93 He, R.R. et al. (2013). Silicon p-i-n junction fibers. *Advanced Materials* 25 (10): 1461–1467.

94 Zhang, L. et al. (2012). Flexible fiber-shaped $CuInSe_2$ solar cells with single-wire-structure: design, construction and performance. *Nano Energy* 1 (6): 769–776.

95 Liao, Q. et al. (2014). Flexible piezoelectric nanogenerators based on a fiber/ZnO nanowires/paper hybrid structure for energy harvesting. *Nano Research* 7 (6): 917–928.

96 Lee, M. et al. (2012). A hybrid piezoelectric structure for wearable nanogenerators. *Advanced Materials* 24 (13): 1759–1764.

97 Deng, J.E. et al. (2015). A shape-memory supercapacitor fiber. *Angewandte Chemie International Edition* 54 (51): 15419–15423.

98 Choi, C. et al. (2016). Twistable and stretchable sandwich structured fiber for wearable sensors and supercapacitors. *Nano Letters* 16 (12): 7677–7684.

99 Sun, H. et al. (2014). Novel graphene/carbon nanotube composite fibers for efficient wire-shaped miniature energy devices. *Advanced Materials* 26 (18): 2868–2873.

100 Yang, Z.B. et al. (2013). A highly stretchable, fiber-shaped supercapacitor. *Angewandte Chemie International Edition* 52 (50): 13453–13457.

101 Sun, H. et al. (2014). Self-healable electrically conducting wires for wearable microelectronics. *Angewandte Chemie International Edition* 53 (36): 9526–9531.

102 Kwon, Y.H. et al. (2012). Cable-type flexible lithium ion battery based on hollow multi-helix electrodes. *Advanced Materials* 24 (38): 5192–5197.

103 Ren, J. et al. (2013). Batteries: twisting carbon nanotube fibers for both wire-shaped micro-supercapacitor and micro-battery (Adv. Mater. 8/2013). *Advanced Materials* 25 (8): 1224–1224.

104 Lin, H.J. et al. (2014). Twisted aligned carbon nanotube/silicon composite fiber anode for flexible wire-shaped lithium-ion battery. *Advanced Materials* 26 (8): 1217–1222.

105 Weng, W. et al. (2014). Winding aligned carbon nanotube composite yarns into coaxial fiber full batteries with high performances. *Nano Letters* 14 (6): 3432–3438.

106 Zhao, Y. et al. (2016). A self-healing aqueous lithium-ion battery. *Angewandte Chemie International Edition* 55 (46): 14382–14386.

107 Borre, E. et al. (2016). Light-powered self-healable metallosupramolecular soft actuators. *Angewandte Chemie International Edition* 55 (4): 1313–1317.

108 Huang, Y. et al. (2015). Magnetic-assisted, self-healable, yarn-based supercapacitor. *ACS Nano* 9 (6): 6242–6251.

109 Li, X., Gu, T.L., and Wei, B.Q. (2012). Dynamic and galvanic stability of stretchable supercapacitors. *Nano Letters* 12 (12): 6366–6371.

110 Zhao, C. et al. (2013). Intrinsically stretchable supercapacitors composed of polypyrrole electrodes and highly stretchable gel electrolyte. *ACS Applied Materials & Interfaces* 5 (18): 9008–9014.

111 Zhang, Y. et al. (2014). Flexible and stretchable lithium-ion batteries and supercapacitors based on electrically conducting carbon nanotube fiber springs. *Angewandte Chemie International Edition* 53 (52): 14564–14568.

112 Peng, H.S. et al. (2009). Electrochromatic carbon nanotube/polydiacetylene nanocomposite fibres. *Nature Nanotechnology* 4 (11): 738–741.

113 De Rossi, D. (2007). Electronic textiles: a logical step. *Nature Materials* 6 (5): 328–329.
114 Zhang, Z.T. et al. (2015). Flexible electroluminescent fiber fabricated from coaxially wound carbon nanotube sheets. *Journal of Materials Chemistry C* 3 (22): 5621–5624.
115 Ge, J. et al. (2016). A stretchable electronic fabric artificial skin with pressure-, lateral strain-, and flexion-sensitive properties. *Advanced Materials* 28 (4): 722–728.

23

Fibers for Optical Textiles

Dana Křemenáková, Jiri Militky, and Rajesh Mishra

Technical University of Liberec, Faculty of Textile Engineering, Department of Material Engineering (KMI), Building B, 2nd Floor, 46117 Liberec, Czech Republic

23.1 Introduction

Optical fibers are one category of specialty fibers originally developed for light transmission (fiber optic) and information (optical cables). Guiding of light through water stream was shown by John Tyndall (1870). History of classic optical fiber development and their basic functions are described, e.g. in the book [27].

Conventional end-emitting inorganic or polymeric optical fiber (POF) is a dielectric wave guide that transmits light or infrared radiation along its axis by total internal reflection at the interface between two media with different refractive index. The fiber consists of a core surrounded by a cladding. In order to transmit the optical signal, the refractive index of the core should be higher than the cladding (see Figure 23.1).

Inorganic optical fibers are mainly used to transmit data over long distances at very high bit rates. The advantage of using optical fibers in telecommunications is their flexibility, no electromagnetic interference, and low attenuation rate. In data networks, the multimode optical fibers with a diameter of 50/125 μm and in the United States 62.5/125 μm are most commonly used. In telecommunications single-mode fibers with a diameter of 9/125 μm are used. The advantages of optical fibers over metal conductors are as follows: low attenuation (less amps on the optical path), resistance to electromagnetic interference and cross-talk, electrical insulation, transmission security, and high bandwidth.

The well-known POF with polymethylmethacrylate (PMMA) core were introduced in the 1960s of last century by Du Pont. The commercial product was first marketed by Mitsubishi Rayon.

In the past several decades, concurrent with the successive improvements in glass fibers, POF have become increasingly popular, owing to their growing utility [2–7]. The classical POF are made of polycarbonate (PC), PMMA, or polystyrene (PS). Modern POF based on "perfluorinated" polymers are used to replace conventional inorganic optical fibers in particular for the transmission of information. For the production of simple "light pipes," extrusion of polymers

Handbook of Fibrous Materials, First Edition. Edited by Jinlian Hu, Bipin Kumar, and Jing Lu.
© 2020 Wiley-VCH Verlag GmbH & Co. KGaA. Published 2020 by Wiley-VCH Verlag GmbH & Co. KGaA.

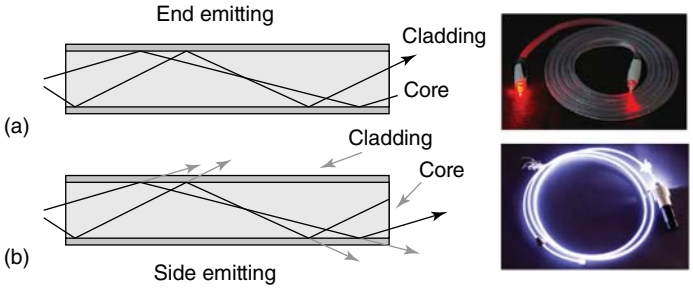


Figure 23.1 Light passing through (a) end-emitting POF and (b) side emitting optical fibers (SEPOF).

and for transmitting data subsequent drawing is used. Classic "light pipes" have a core–jacket structure. The core consists of a polymer with higher refractive index, and the cladding is formed by a polymeric layer having a lower refractive index, thereby ensuring conduction of light inside the fiber and minimal loss of radiation from the side.

In addition, POF serves as a complement for glass fibers in short-haul communication links because they are easy to handle, flexible, and economical, although they are not used for very long distances because of their relatively high attenuation. These characteristics make them especially suitable as a means of connection between a large net of glass optical fiber and a residential area, where distances to cover are generally less than 1 km. Nowadays, with the PMMA core optical fibers, transmissions at 156 Mbit/s over distances up to 100 m can be carried out [8], and transmission speeds of 500 Mbit/s over 50 m can be reached [9]. To achieve higher transmission speeds, graded-index POF can be used [10].

The large diameter of POF (typically 0.25–1 mm) allows low precision plastic connectors to be used, which reduces the total cost of the system. In addition, POFs stand out for their greater flexibility and resistance to impacts and vibrations, as well as for the greater coupling of light from the light source to the fiber. Because of these merits, varied applications with POF have been developed and commercialized, from their use as a simple light transmission guide in displays to their utilization as sensors and telecommunication cables. Because of their large diameter, POF are easier to install and align than their glass counterparts [2–7]. POF found its use as a high-capacity transmission medium only recently, thanks to their improved transparency and bandwidth [6, 7].

However, still it is difficult to draw conclusions whether the POF can replace the silica fiber to be the main transmission medium in communication networks; it depends on the further development of production technology in the future. From the current situation, there is still a big gap in attenuation, bandwidth, and working wavelength for POF compared with silica fiber, and silica fiber is also not less than POF in flexibility, connection performance, and cost. For example, silica fiber can be wound even knotted on the fingers; the assembly of site connector is quick and easy. As for cost, the price of POF is higher than silica fiber.

In the field of sensors, numerous types of products based on POF have been commercialized [11], for example, scanning heads, shape-defect detectors used

in bottling plants, and liquid-level detectors. In addition, by using conventional POF, it is possible to make sensors measure distance, position, shape, color, brightness, opacity, density, turbidity, etc. [11, 12]. These sensors can serve to control the various manufacturing parameters in automated production processes with robots.

Gradually, the use of optical fibers was extended to the special textiles (displays, safety fabrics, special effects for apparel fabrics, etc.). For these applications, either by a suitable arrangement (micro-bends) or structures (side-emitting plastic optical fiber [SEPOF]), the side emission from surface of the fibers was obtained (see Figure 23.1).

POF integrated in weaving patterns can be described by a sequence of locally bent and straight sections. For this case the transmission loss is based on the distance between threads, thickness of threads, and weaves. Local bends are unwanted in the cases of using SEPOF for achieving active visibility at higher distances from light source. It is therefore necessary to prepare line illumination hybrid structure (LIHS) combining SEPOF in the core wrapped by the special textile-based outer layer, e.g. in form of tube from textile yarns.

Comprehensive information about properties and applications of POF in the textile field are presented in the book [1] and special chapter [28]. In this chapter the basic types of POF and their potential use in textile structures are discussed. One of main aims here is description of basic properties of SEPOF and their not so known applications in LIHS enabling them to be used in textile structures and enhancing side illumination intensity. Applications of LIHS for safety textiles, fashion purposes, and for special line illumination purposes are shown.

23.2 Principles of Fibers Optics

Standard, i.e. *end-emitting optical fiber*, is a special form of a relatively long distance (hundreds meters to some kilometers) optical wave guide and consists typically of a cylindrical core and a cladding (see Figure 23.2), both made from highly transparent materials. The core refractive index n_1 should be slightly higher than that of the cladding n_2 to avoid loss of illumination power due to side emission. Depending on ultimate applications, on the surface, there is additional protective layer called as jacket.

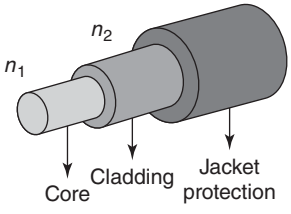


Figure 23.2 Typical structure of optical fiber.

For purposes of line lighting in short distances (few meters), the so-called SEPOF are used. The simple way how to obtain side emission is to change magnitude of refractive indexes, i.e. using slightly smaller core refractive index n_1 than that of the cladding n_2. Still there are a limited number of companies only producing SEPOF based on this simple idea. Second possibility is to use the end-emitting optical fiber with modification enabling side emission. There are in fact possibilities to promote scattering of core by adding particles or changing

super molecular structure; creating imperfections (grooves) in cladding; and using structures with sharp bends (as in woven fabrics). In fact all these modifications are a little bit against aims of producers to suppress attenuation, i.e. side emission. The SEPOF will be probably in future produced according to their main goal, i.e. side emission, with more even and approximately constant decay of illumination power along their working length.

The properties and functionality of optical fibers are dependent on the refractive indexes of core and cladding. The refractive index $n = n(\lambda)$ of medium can be expressed as ratio of the velocity of a light wave having wavelength λ in vacuum C_v and velocity of a light wave in a medium $C_m(\lambda)$

$$n(\lambda) = \frac{C_v}{C_m(\lambda)} \tag{23.1}$$

The speed of light in vacuum is about 300 000 000 m/s. Typical refractive index of optical fiber cladding is $n_2 = 1.46$, and typical value for the core is $n_1 = 1.48$ [1]. The higher the refractive index, the slower rate of light travels in the given environment.

For transparent and clear substances, refractive index can be regarded as constant in the whole range of visible light. In this case, the refractive index is always greater than 1. The higher the refractive index of a material, the slower the speed of light, and the lower the refractive index, the higher the speed of light (see Figure 23.3).

Factors that affect the amount of light that is transmitted through a medium are absorption and scattering of the light. The absorption of radiation results in heat generation in a material. Sum of absorption and scattering is known as attenuation.

When light passes from a medium with a lower refractive index to a medium with a higher index, it is bent toward the normal plane between media. Otherwise light bends in the opposite direction (away from the normal plane, see Figure 23.4).

If the angle of incidence in this case is greater than the critical angle N_c, all the light energy is reflected back into the medium with a higher refractive index. This phenomenon known as total internal reflection is used to guide the light in optical fibers (Figure 23.4).

The reflection and refraction of incident ray in optical fibers vary accordingly with the material refractive index. For instance, higher refractive index would result in higher reflection than refraction of the incident light ray. The fraction of the incident light ray power R (reflectance) at direction normal to interface z

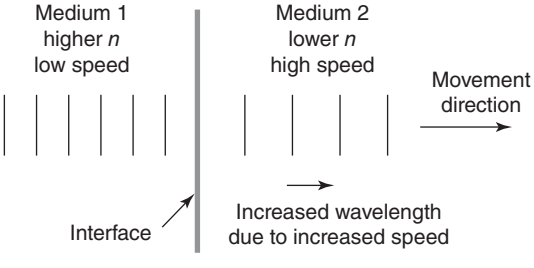


Figure 23.3 Effect of refractive index on speed of light rays. Source: Adapted from Crisp 2001 [42].

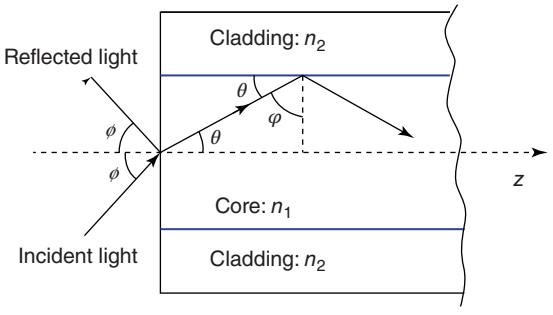


Figure 23.4 Internal reflection in optical fibers. Source: Azadeh 2009 [84]. Reproduced with permission of Springer.

($\varphi = 0°$ in Figure 23.4) reflected from the interface can be described by Fresnel's law [60]:

$$R = \left(\frac{n_1 - n_2}{n_1 + n_2}\right)^2 \tag{23.2}$$

In the standard end-emitting optical fibers, refractive index of core n_1 is always higher than refractive index of cladding n_2, i.e. $n_1 > n_2$. Below a certain angle N_c, the total reflection then takes place at the boundary between the core and the cladding. If light enters under higher angle, the partial refraction (side emission) occurs, and only part of the total light energy is reflected back to core. Figure 23.4 shows that total internal reflection (generally electromagnetic wave) occurs in the optical fibers at the boundary between the core and the sheath. The minimum angle φ_m (see Figure 23.4) when there is total internal reflection of light is equal to

$$\varphi_m = \arcsin\left(\frac{n_2}{n_1}\right) \quad \text{or} \theta_m = \arccos\left(\frac{n_2}{n_1}\right) \quad \text{or}$$
$$\left(\frac{n_2}{n_1}\right) = \sqrt{(1 - \sin^2(\varphi_m))} \tag{23.3}$$

From Figure 23.4 it is obvious that $\theta = 90 - \varphi$ and $\sin(\theta) = \cos(\varphi)$. According to Snell's law, the upper critical angle $\phi = N_c$ at input into the optical fiber is equal to [60]

$$N_c = \arcsin\left(\frac{\sqrt{n_1^2 - n_2^2}}{n_0}\right) \tag{23.4}$$

Here n_0 is refractive index of surroundings (for air $n_0 = 1$). The acceptance angle ($2N_c$) corresponds to the vertex angle of the largest cone of rays that can enter the core of the fiber.

Assuming that there is a total internal reflection (i.e. input angle ϕ is below the critical angle N_c), the whole electromagnetic radiation is captured in core and propagates along the fiber axis. If the angle of incidence on the optical fiber is higher, the part of the light is refracted, and there appears so-called leakage or partial side emission. Side emission occurs if the input angle of light incidence ϕ

is higher than critical angle N_c. This effect can be obtained by the increase of n_2 or decrease of n_1 or by the change of input angle of incident light ϕ.

The angle φ of the reflected light at the boundary between the core and the cladding at given incidence angle ϕ is given by Snell's law:

$$\phi = \arccos\left(\frac{n_0 \sin(\varphi)}{n_1}\right) \tag{23.5}$$

The number of reflections of light beam in the optical fiber is related to its length L and a core diameter d according to the equation [3]:

$$K = \frac{L}{d}\sqrt{\frac{n_2^2}{n_1^2} - 1} \tag{23.6}$$

The sine of the maximum incident angle N_c is defined as the *numerical aperture* $\mathrm{NA} = n_0 \sin(N_c)$. The angle N_c is often denoted to as the acceptance angle, and twice the acceptance angle is denoted as the aperture angle. The NA is defined by relation

$$\mathrm{NA} = \sqrt{n_1^2 - n_2^2} \tag{23.7}$$

The NA is a very important parameter of optical fibers, since it indicates their capacity for accepting and guiding light. The size of the NA is solely dependent on the difference in the refractive indexes of the core and cladding material. For standard PMMA fiber $n_1 = 1.49$ and $n_2 = 1.40$; thus NA = 0.50 and $N_c = 30°$.

Compared with other fiber types [6], POF has the largest numerical aperture and the largest core diameter. This is one of the most important advantages of POF, since the connection technology that can be used for POF fibers is more economical to apply than that used for glass fibers.

The behavior of light rays in optical fiber is influenced by the profile of the refractive index of the core and cladding. In a step-index profile fiber (see Figure 23.5), the refractive index is constant across the entire cross section of the core and cladding, while the light rays propagate along straight lines in the core and are completely reflected at the core/cladding boundary [6].

It is visible that the individual light rays are passing by different trajectories and have different transit times. Graded-index profile optical fibers can minimize these differences. These fibers have cladding with a constant refractive index, and core follows the parabolic refractive index profile (see Figure 23.5). The mathematical expression of this profile has the following form [6]:

$$n^2(r) = \begin{cases} n_{1\max}^2 \left[1 - 2\Delta\left(\frac{r}{r_c}\right)^2\right]; & 0 < r < r_c \\ n_{1\max}^2[1 - 2\Delta] = n_2^2; & r > r_c \end{cases} \tag{23.8}$$

where $n_{1\max}$ is maximum refractive index of core, r_c is core radius, and $\Delta = \frac{n_1^2 - n_2^2}{2n_1^2}$.

The numerical aperture of the step-index profile fiber remains constant over the entire core; the graded-index profile fiber exhibits a decreasing acceptance angle from the center of the core to the cladding.

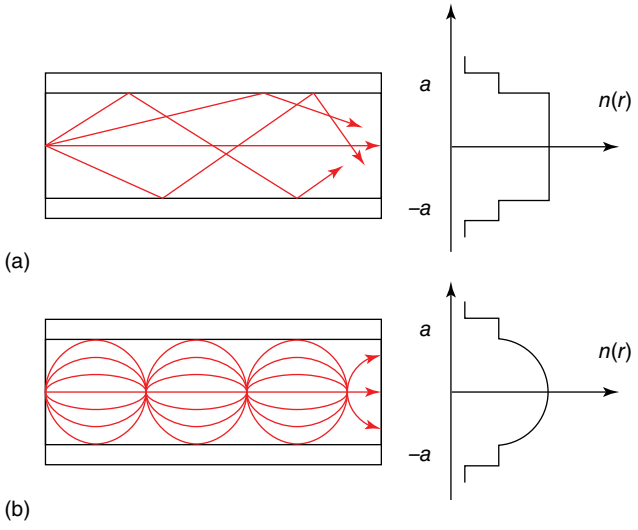


Figure 23.5 (a) Step-index and (b) graded-index profile optical fiber.

Figure 23.6 Light passing through single-mode optical fibers.



According to the mode of light propagation (the number of transmitted light rays), the optical fibers are divided into single mode (see Figure 23.6) and multimode (see Figure 23.7) [1–6].

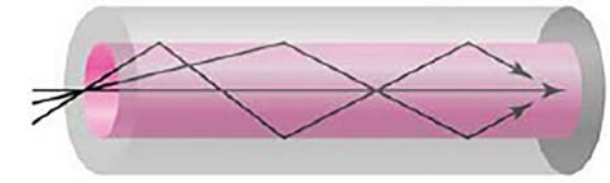
Single-mode optical fibers have a comparatively small core diameter, typically around 8–10 μm, ensuring to guide light by direct way only. They can be analyzed by using the wave model of light (see Figure 23.8).

This type of fibers allows only the lowest order or the fundamental mode and is suitable for the applications preferably at 1300 nm wavelength. Single-mode optical fibers have lower signal loss and higher information capacity (i.e. bandwidth) than multimode optical fibers. These fibers are capable of transferring higher amounts of optical data due to lower fiber dispersion [13].

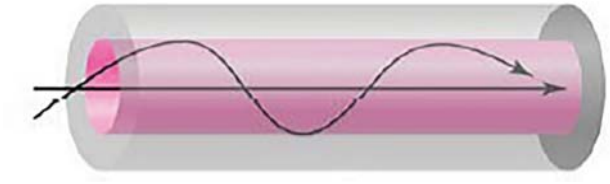
Single-mode fiber has low transmitted light loss about 0.25 dB/km. They are relatively cheaper. Electromagnetic radiation is ideally emitted from only one end, which is also used for the data transmission. The disadvantage of single-mode optical fiber is just keeping only one light ray.

Multimode optical fibers have a large core (see Figure 23.7). They can be analyzed by geometric ray-tracing model (see Figure 23.8).

Step-index multimode optical fiber guides light rays by more modes simultaneously. The individual light rays enter the fiber at different angles, thereby each

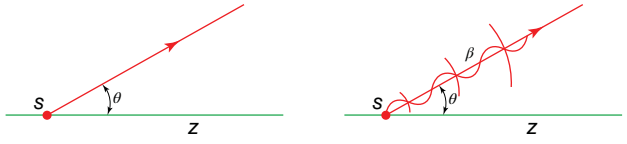


(a)



(b)

Figure 23.7 Light passing through multimode optical fibers. (a) Step index and (b) graded index.



(a) (b)

Figure 23.8 Different models of light propagation. (a) Geometric model of light propagation and (b) wave model of light propagation.

reflected along a different path. They are used primarily for short connections due to the scattering of light rays.

Graded multimode optical fibers guide light rays by more modes simultaneously, but the light is refracted in them gradually, thereby forming a coil circumscribing the interior of the fiber.

Optical fibers for special purposes have noncircular core or sheath. Typically the elliptical or rectangular cross section is used. Multimode optical fibers are generally suitable for illumination purposes, because their larger diameter allows obtaining higher light flux intensity.

In dependence on core diameter, the aperture of glass and POFs differ (see Figure 23.9).

The boundary between single-mode and multimode optical fiber types are determined by the structural parameter V, which is given by

$$V = \frac{2\pi\rho}{\lambda}\sqrt{(n_1^2 - n_2^2)} \tag{23.9}$$

where ρ is fiber density and λ is wavelength of rays passing through optical fiber. Typical wavelength is 650 nm for PMMA and 850 or 1310 nm for perfluorinated polymer core.

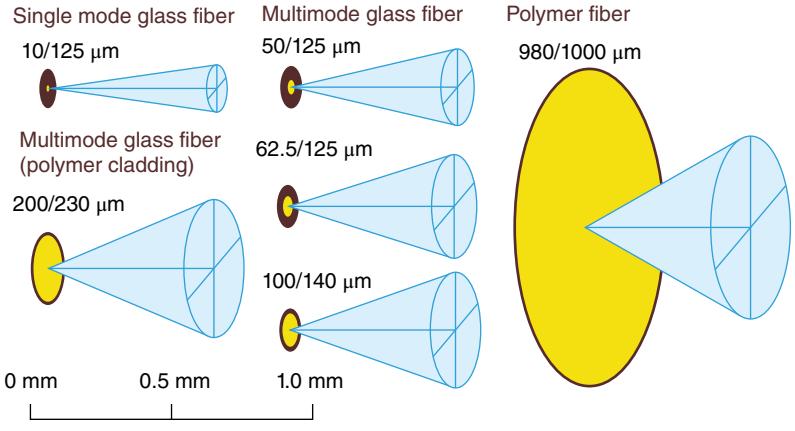


Figure 23.9 Aperture angle and core diameter of single and multimode glass fibers and polymer optical fibers. Source: Daum et al. 2002 [6]. Reproduced with permission of Springer.

When the size of the parameter V is higher than 2.405, it can be proved that for silica core the optical fiber is multimode [14, 15]. For larger values of V is a number of modes equal to

$$N = V^2/2 \tag{23.10}$$

Each mode represents one solution of Maxwell's equations. For typical plastic optical fibers, the number of modes is of the order of 10^4–10^6.

Single-mode plastic optical fibers exhibit much higher attenuation than glass single-mode optical fibers [14, 15].

Due to the transmission loss, the power of radiation P (W) emitted in any direction decays exponentially along the fiber axis with increasing distance from the light source of the fiber as observed by Zajkowski [16, 17], while the percentage of light emitted per unit length is uniform over the entire fiber length.

The simple exponential model for prediction of this attenuation is proposed. Illumination power $P(L)$ for straight optical fiber is decreasing with increasing distance from source L according to relation [18]:

$$P(L) = P(0)10^{-\alpha L/10} \tag{23.11}$$

where $P(0)$ is illumination intensity of source and α is attenuation coefficient of optical fiber. Coefficient α describes attenuation dependent on fiber length:

$$\alpha = \frac{-10}{L} \log\left(\frac{P(L)}{P(0)}\right) \tag{23.12}$$

Unit of attenuation coefficient α is dB/m. Decibel (dB) is logarithm of ratio between two illuminating powers P_1 and P_2:

$$\text{dB} = 10 \log\left(\frac{P_2}{P_1}\right)$$

i.e. if $P_2 = 10P_1$, then P_2 is higher by about 10 dB. Illuminating power is dependent on the fiber radius and on the bending radius. High level of illumination loss should be due to light transmission through bent fiber [18].

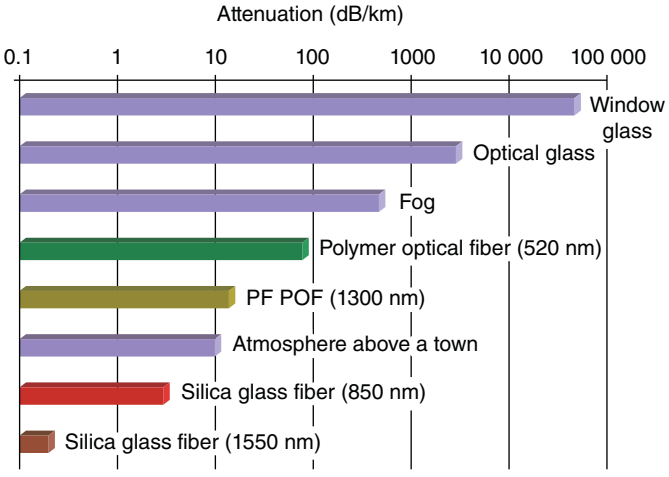


Figure 23.10 Attenuation of various media. Source: Daum et al. 2002 [6]. Reproduced with permission of Springer.

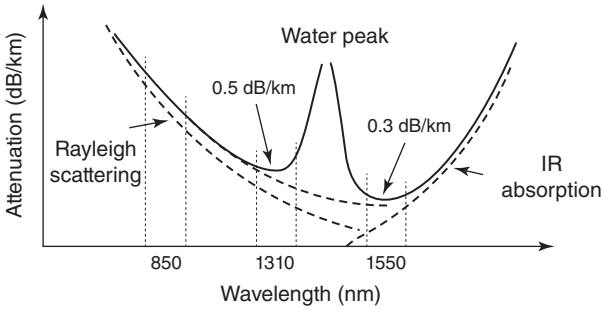


Figure 23.11 Attenuation profile of silica optical fiber.

The attenuation coefficient in the different media is shown in Figure 23.10.

Due to their high level of attenuation, POFs are suitable for short distances (approx. 100 m).

Attenuation profile of silica optical fiber is shown in Figure 23.11.

For the purpose of optical communication, the silica optical fiber uses three bands around the wavelengths of 850, 1310, and 1550 nm, which lies in the infrared region.

Attenuation profile of PMMA optical fiber is shown in Figure 23.12.

The attenuation profile of PMMA step-index fiber has three attenuation minima at 520, 570, and 650 nm [6]. Due to the molecular vibrations, attenuation increases considerably with the wavelength. If a light-emitting diode (LED) is used at 650 nm, a level of attenuation substantially higher than 130 dB/km is obtained [6].

The attenuation of POF is caused by intrinsic and extrinsic losses (see Table 23.1).

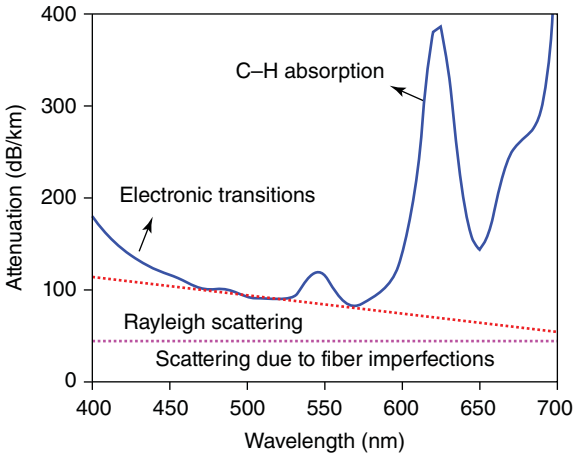


Figure 23.12 Attenuation profile of PMMA optical fiber.

Table 23.1 The attenuation of POF.

Type	Mechanism	Origin
Intrinsic	Absorption	• Molecular vibrations of C–H • Electronic transitions (UV, IR range)
	Rayleigh scattering	• Density or refractive index fluctuations • Orientation fluctuations • Composition fluctuations
Extrinsic	Absorption	• Transition metals • Organic contaminants • Absorbed water
	Scattering	• Dust, micro-voids, and fractures • Fluctuations in core diameter • Orientation birefringence • Core–cladding boundary • Micro- and macro-voids

The intrinsic sources of attenuation are caused by the material mainly. Rayleigh scattering caused particularly by fluctuations in density, composition, and molecular orientation of the polymer material changes is proportional to λ^{-4}.

The primary sources of absorption are vibrations and electronic transitions of molecular groups.

Vibrations of molecular groups such as carbon–hydrogen (C—H), carbon–deuterium (C—D), carbon–fluorine (C—F), carbon–chlorine (C—Cl), carbon–bromine (C—Br), oxygen–hydrogen (O—H), carbon double-bond oxygen (C=O), carbon–oxygen (C—O), and carbon–carbon (C—C) are responsible for the absorption loss. Molecular groups such as carbon double-bond carbon (C=C) and C=O are responsible for the optical loss by light absorption owing to electronic transitions [1–6].

The extrinsic sources of attenuation are caused by external contamination in the fiber core and physical imperfections in the fiber. The presence of impurities such as polymerization initiators, additives, and polymerization by-products are the most likely organic contaminants in POFs, which can cause

a significant increase of the attenuation by light absorption or scattering. The water absorption by POF core can induce an increase in its attenuation due to OH group vibration absorption and a minor scattering loss due to agglomeration of water molecules. During the fiber drawing process, many imperfections such as dusts, micro-voids, micro-cracks, core diameter fluctuation, orientation birefringence, and core–cladding boundary imperfections appeared in the fiber. These imperfections can increase the optical loss by light scattering, independent of wavelength. The extrinsic sources of attenuation can be suppressed by proper manufacturing of POF. In the case of SEPOF, scattering of light rays that are wanted and targeted adding of particles into core is often used to enhance this.

Special class of optical fibers is microstructured optical fibers (photonic crystals). In contrast to the standard optical fibers, the microstructured optical fibers are made from one material, and light guidance is achieved by introducing microscopic air holes running along the entire fiber length [48]. These fibers can have a cladding formed from microstructural elements, usually holes. Basic preference of microstructured optical fibers is the dependence of optical characteristics on the geometry of the microstructure. The size of the microstructural elements is of the same order as the wavelength of the radiation passing through them. Other types of special POF are described in the book [1].

23.3 Materials of POF

The fundamental requirements for selecting materials for POF fabrication are that the polymers should be (i) nearly completely transparent, (ii) resistant to high temperatures, (iii) able to be drawn into a fiber, and (iv) sufficiently flexible. Although the temperature requirement depends on utilization of POF, in most cases, it is preferred that POF glass transition T_g should be above 80 °C.

Polymeric optical fibers can be produced from the preform, like silica optical fibers, only at a much lower temperature (e.g. 200 °C). Preforms can be produced by using a hollow tube of sheath material, which is filled with the liquid mixture of monomer and suitable reactive substance enabling polymerization of the core. Alternatively, a dopant dispersed in a tube or within tubes can be used. These processes can be tuned with respect to the acquisition of different refractive index profiles. An alternative to preforms is extrusion processes. These techniques were originally used for PMMA optical fiber, but there are also variants for perfluorinated materials. In the extruder the two distinct polymer materials can be inserted only. By the control of the diffusion process, the nonconstant refractive index profiles can be produced. Typical operation is hot drawing changing super molecular structure and optical properties [1–6].

23.3.1 Core

The most widely used polymers for optical fibers core include *PMMA* (Figure 23.13), which has a high transmission rate and low attenuation. Amorphous homopolymer of PMMA has a refractive index of $n = 1.492$ measured at wavelength of 589.2 nm. Refractive index is systematically decreasing with increasing of wavelength especially in infrared region.

This index can be changed using special dopants. PMMA has a relatively high T_g of around 105 °C. It can be drawn in the temperature range from 175 to 220 °C. The polymer is stable in air at temperatures of 85 °C. At higher temperatures, the presence of moisture leads to rapid degradation and durability constraints.

Contact angle of water for PMMA is 80° and bandwidth 0.003 GHz km. Typical core diameter is 250–1000 µm, and numerical aperture is NA = 0.47.

The PMMA core has two attenuation, absolute low value of 70 dB/km at 522 and 570 nm (green region) and the relative minimum around 650 nm (red region) [41]. Each methyl methacrylate unit has a total of eight C—H bonds. The vibrations of these bonds or precisely their harmonic waves are a main cause for the losses in PMMA fibers.

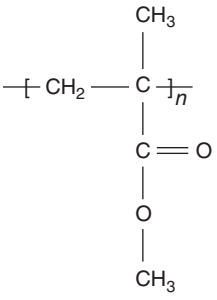


Figure 23.13 Structure of PMMA.

PMMA is thermoplastic polymer and can be spun from melt. Solvents for PMMA are aromatic or chlorinated hydrocarbons, esters and ketones as benzene, toluene, dichloromethane, chloroform, tetrahydrofuran, dimethylformamide, ethyl acetate, and acetone.

Selected properties of PMMA are summarized in Table 23.2.

Over a greater temperature range up to 120 °C *PC* (Figure 23.14), core may be used, which is also mechanically more robust and less sensitive to moisture and has a larger ductility (10.8% compared with 6.3% for PMMA).

Table 23.2 Selected properties of PMMA [19, 20, 28, 32].

Property	Typical value	Unit	Test
Refractive index	1.491	—	DIN 53291
Density	1180	kg/m^3	DIN 53479
Tensile strength	80 (72)	MPa	DIN 53455
Impact strength	15	kJ/m^2	ISO 179/1D
Bending strength	115 (105)	MPa	DIN 53452
Initial modulus	3300	MPa	DIN 53457
Glass temperature, T_g	105	°C	[55]
Thermal expansion		K^{-1}	DIN 53752-A
• Linear	7.0×10^{-5} (0–50 °C)		
• Volume	2.72×10^{-4} ($<T_g$)		[20]
	5.80×10^{-4} ($>T_g$)		
Starting temperature of shrinkage	>80	°C	[20]
Water absorption	30	mg	DIN 53495

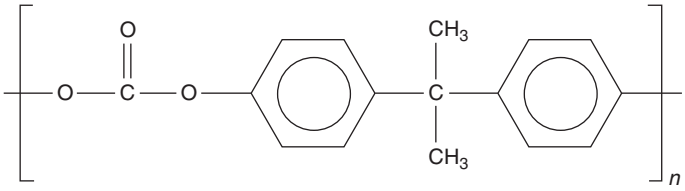


Figure 23.14 Structure of polycarbonate (PC).

PC has a refractive index of $n = 1.582$, and bandwidth is 0.0015 GHz km. Typical core diameter is 500–1000 μm, and numerical aperture is NA = 0.78. The PC core has minimal attenuation of 600 dB/km at 670 nm, density 1200 kg/m^3, and glass transition temperature $T_g = 145\,^{\circ}$C [1]. The bisphenol A type PC POF core can be used in industrial applications where the temperature is an important parameter. PC core POF can be used for creation of textile integrated illumination elements [21]. A problem with PC is that it has large birefringence.

More hydrophobic *PS* (Figure 23.15) core has a minimum attenuation 330 dB/km at 580 nm, i.e. in the red region.

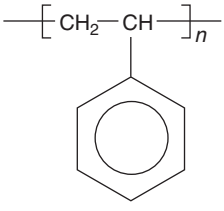


Figure 23.15 Structure of polystyrene (PS).

PS is soluble in aromatic and halogenated hydrocarbons and in aliphatic ethers, esters, and ketones. From the mechanical standpoint, the PS fibers are superior to fibers of PMMA, although they have higher attenuation [41]. PS has a refractive index of $n = 1.592$, and bandwidth is 0.0015 GHz km. Typical core diameter is 500–1000 μm, and numerical aperture is NA = 0.73 [41]. The glass transition temperature of PS is around 100 °C. This material is now not of any practical significance [6].

One of the lowest attenuation 16 dB/km at 1310 nm has amorphous *fluorinated polymer* cyclic transparent optical polymer (*CYTOP*) (Figure 23.16) [39–41]. This material poly(perfluorobutenyl vinyl ether) no longer contains hydrogen.

CYTOP has similar excellent chemical, thermal, electrical, and surface properties as conventional fluoropolymers. This material obeys high optical transparency and good solubility in specific fluorinated solvent due to amorphous morphology. CYTOP has a refractive index of $n = 1.353$, bandwidth 0.0005 GHz km, density 2030 kg/m^3, $T_g = 108\,^{\circ}$C, and contact angle with water 110°. Typical core diameter is 110–1000 μm, and numerical aperture is NA = 0.40 [41].

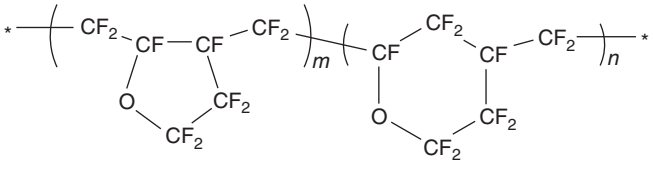


Figure 23.16 Structure of CYTOP.

Core attenuation generally increases with the decrease of its diameter. Attenuation of PMMA core at 570 nm is 70 dB/km for a diameter of 0.5 mm and 130 dB/km for a diameter of 0.25 mm. Production process is difficult to be controlled for smaller diameters of POF. The temperature gradient is greater, resulting in a high number of defects.

Attenuation can be induced by bending and tensile or torsion deformation [35, 36]. The initial tensile modulus for POF is almost 2 orders of magnitude lower than that of silica optical fibers (2.1 GPa for PMMA [37], 1.55 GPa for PS, and 2.55 GPa for PC [35]). Therefore, the POF of diameter 1 mm are still sufficiently flexible and the minimum bend radius for POF is smaller than for conventional glass optical fibers.

POF light transfer rate also depends on the degree of elongation (drawing). When stretched by 10% the attenuation increases by less than 0.1 dB [37]. Also cyclic bending causes changes in attenuation (for 1 mm thick PMMA, it is 0.15 dB after 1000 bends around bending radius of 50 mm [38]).

The maximum operating temperature of the POF is 80–100 °C. Above this threshold, there is a loss of rigidity and transparency. The operating temperature can be increased up to 125 °C or even to 135 °C using a cladding of cross-linked polyethylene or polyolefin elastomers.

Resistance to high temperatures strongly depends on the humidity. For example, if the POF is maintained at 85 °C with 85% RH (air relative humidity) for 1000 hours, it is increasing attenuation of 0.02 dB/km. If the relative humidity is around 90%, it increases the attenuation of more than about 0.03 dB/m. Fluorinated POF cores do not absorb water, so that their attenuation is virtually unchanged with the increase of the moisture.

Standard core materials (PMMA, PS, and PC) generally have a high attenuation, which limits their applicability for information transfer.

It is possible to reduce the absorption losses of POF by using different materials in which less or no C—H bonds are present. A heavier atom X replacing hydrogen atoms H leads to lowering of stretch and bending fundamental vibrations of C–X and moving the attenuation bands to a larger wavelength. The selected atoms X are deuterium (heavy hydrogen with the atomic mass 2), fluorine (atomic mass 19), and chlorine (atomic mass 35 or 37). Generally, the materials for POF can be compounds containing hydrogen, compounds with partial substitution of hydrogen, and compounds with complete substitution of hydrogen [6].

One way to suppress attenuation was to use deuterated polymers [6]. In deuterated polymer, hydrogen is substituted by heavier deuterium. This isotope has two times higher atomic mass than hydrogen. Behavior of deuterium is the same as hydrogen so that it is simple to use so-called heavy water (D_2O) instead of water H_2O for synthesis. It was possible to prepare deuterated material with a minimum attenuation of 20 dB/km at 680 nm. Disadvantages of deuterated polymers are a gradual increase of attenuation due to replacement of deuterium by hydrogen as a result of atmospheric water vapor absorption and a high price.

Problems with the attenuation and wetting ability of the core can be solved by using halogenated polymers. Fully halogenated polymers, e.g. polytetrafluoroethylene (PTFE), are highly crystalline, which increases optical attenuation. Usually the partially halogenated polymers blended with PMMA or amorphous

fluorinated polymers of CYTOP type can be used for avoiding unwanted wetting and lowering of attenuation.

For producing core of step-index POF, *bulk polymerization* technique is preferred because of the purity of an obtainable polymer. Continuous or batch extrusion and melt spinning followed by hot drawing are mostly widely used for POF preparation [1–6]. Production of graded-index POF mainly uses the preform hot drawing technology [1–6].

23.3.2 Cladding

Two of the main requirements for cladding materials are low refractive index (but close to the index of the core) and good film forming ability. In addition, the application of cladding can provide a good mechanical and thermal resistance to the core. A variety of cladding polymers have been developed since the invention of glass and POFs. Majority of perfluoropolymers and partially fluorinated polymers alone are unsuitable for the POF core but are good cladding materials. Actually, there are two classes of fluoropolymers, which are widely used as cladding materials: copolymers of fluoroolefins and poly(fluoroalkyl acrylates) (PFA). The PFA are preferred because of their amorphous nature, high transparency, good adhesion properties, etc. As a result durable optical properties can be obtained. Another main advantage of PFA is their monomers easily coating (by solution) on the core and can be easily photopolymerized.

In general, there are already a number of monomers of PFA mainly for fiber-optic applications especially as cladding materials available in the market. Some monomers of poly(fluoroalkyl methacrylates) are listed in Table 23.3.

However, the formulation of cladding materials depends on individual optical fiber producers. Copolymers of fluorinated methyl and ethyl esters of acrylic and methacrylic acids are usually used as cladding materials for the PMMA core.

23.3.3 Jacket

Selection of jacket depends on the intended field of POF use. The basic mechanical and thermal characteristics of jacket affect the overall life of the POF. Selected suitable types of jackets and their properties are listed in Table 23.4 [6].

Table 23.3 Monomers of poly(fluoroalkyl methacrylates).

Monomer	Alkyl group in methacrylate	T_g (°C)	n
Methyl methacrylate	$—CH_3$	105	1.489
2,2,2-Trifluoroethyl methacrylate	$—CH_2—CF_3$	69	1.418
2,2,3,3-Tetrafluoropropyl methacrylate	$—CH_2—CF_2—CHF_2$	68	1.417–1.422
2,2,3,3,3-Pentafluoropropyl methacrylate	$—CH_2—CF_2—CF_3$	70–77	1.1395
2,2,3,3,4,4,4-Heptafluorobutyl methacrylate	$—CH_2—CF_2—CF_2—CF_3$	65	1.383

Table 23.4 Polymers suitable for jackets.

Polymer	Maximum working temperature (°C)	Density (kg/m^3)
Polyvinylchloride (PVC)	70	1200–1500
Polyethylene (PE)		
• Low density	70	1300–1600
• High density	80	950–980
Polypropylene	90	910
Polyamide 6 (PA 6)	80–90	1100–1150
Polyurethane (PU)	90–100	1150–1200
Copolymer ethylene-vinyl acetate (EVA)	120	1300–1500
Perfluoroethylenepropylene (PFEP)	180	2000–2300
Polytetrafluoroethylene (PTFE)	260	2000–2300

Polyethylene (PE) jacket also serves to protect the POF, to liquids such as water, NaOH, sulfuric acid (34.6%), or motor oil. Attenuation remains constant if the POF having POE jacket is immersed in these fluids at 50 °C for 1000 hours [6].

23.4 Side-Emitting POF

For a variety of textile applications (e.g. the so-called active safety textiles) the side emission should be ensured. In side-emitting POF, i.e. *SEPOF*, the light leaks out from their surface. For illumination purposes, light emission along the fiber is necessary. In this case, multimodal fibers are most likely to be used, since their larger diameter allows higher emission intensities to be obtained. Side emission occurs if the light incidence angle is higher than critical angle N_c. This effect can be obtained by the increasing of cladding refractive index, decreasing of core refractive index, or changing of incident light angle. For optical characterization of SEPOF, it is favorable to use so-called *attenuation profile* (see Section 5.1). The *attenuation profile* is the dependence of light intensity of omnidirectional rays passing from optical fibers through their sides measured as function of distance from light source. Higher level and smaller decay (slope) of attenuation profile is better for more even side emission. Detailed discussion about attenuation profile characterization and shapes for different types of side-emitting fibers is presented by Křemenáková et al. [29].

There are some possibilities on how to obtain side emission by using standard or modified end-emitting POF. Various types of patented side-emitting fibers

and wave guides including methods of their preparation are discussed in Ref. [26]. In all cases the aim is to avoid total internal reflection by using multiple micro-bending of the fiber, dispersion of fluorescent additives or particles into the core or cladding material, creating asymmetries in the core/cladding geometry, partial destruction or grooving of cladding, etc. [22–26]. Emission from side-emitting optical fibers referring to a fiber design with scattering cladding is described in work [22, 23]. Various commercial side emission optical fibers and light guides and methods for their manufacture were developed and patented [21–26].

23.4.1 SEPOF Based on Difference Between Refractive Indexes

There exist a lot of producers of SEPOF, e.g. from China, England, the United States, and Australia offering wide range of diameters, different types of cladding, different composition of core, and different flexibility. Majority of these fibers are based on changing relation between refractive indexes of core n_1 and cladding n_2, i.e. following inequality $n_1 < n_2$. For specific applications it is necessary to select proper diameter mainly because the illumination intensity and height of attenuation profile (see Figure 23.19) depends critically on this parameter.

As example, the two typical SEPOF fibers, *standard* and *flexi* (Grace POF Co., Ltd. China), are compared. The fiber Grace standard is composed from PMMA core and PC cladding of low irregular thickness below 10 μm (see Figure 23.17). These fibers are relatively stiff and brittle. Offered diameters of these fibers are from 0.25 to 1 mm.

Fibers of type Grace flexi are formed of a PMMA core and polytetrafluorethylene cladding of thickness about 0.2 mm, which can be easily detached (see Figure 23.18). Grace flexi fibers are produced in diameters of 2–14 mm or more. These fibers have lower stiffness and higher flexibility in spite of higher diameter, which is advantageous for their incorporation into textiles.

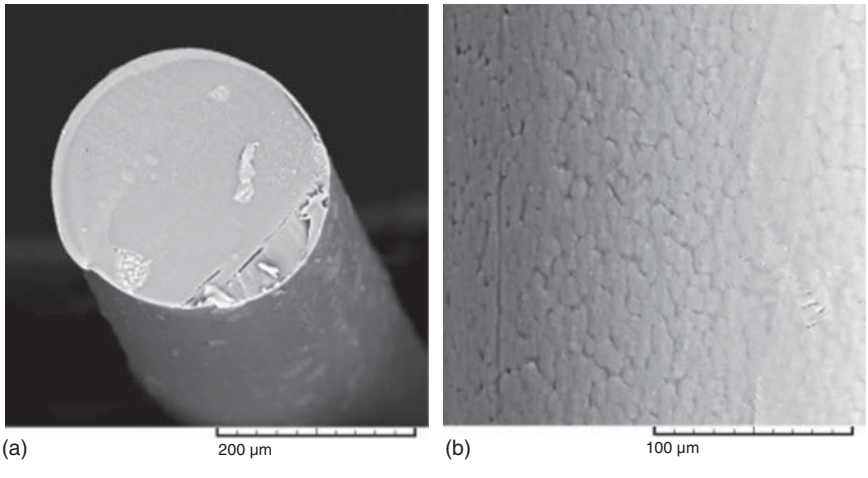


Figure 23.17 SEPOF Grace standard. (a) Cross section – magnification 350× and (b) surface – magnification 700×.

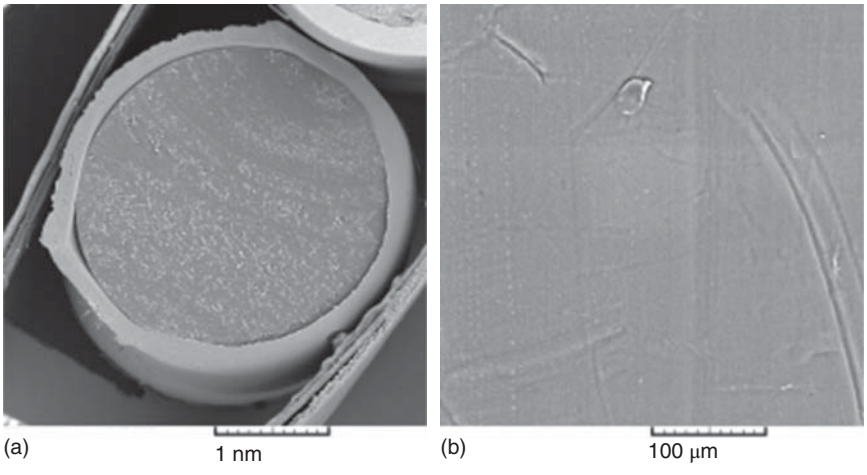


Figure 23.18 SEPOF Grace flexi. (a) Cross section – magnification 40× and (b) surface – magnification 400×.

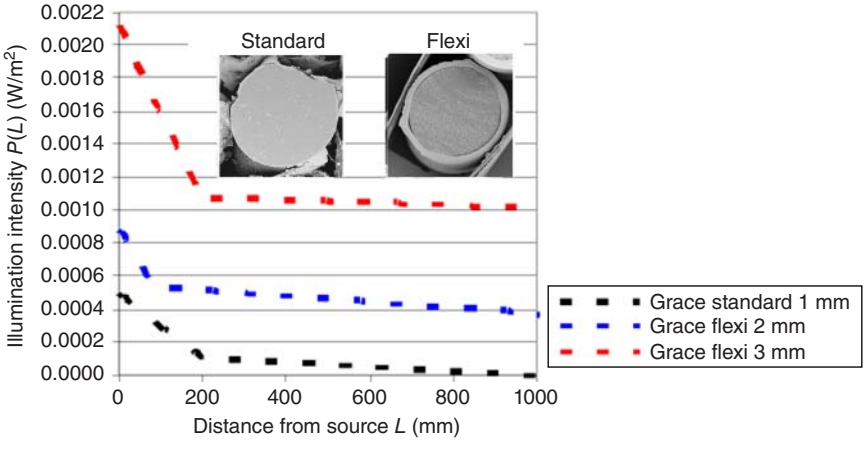


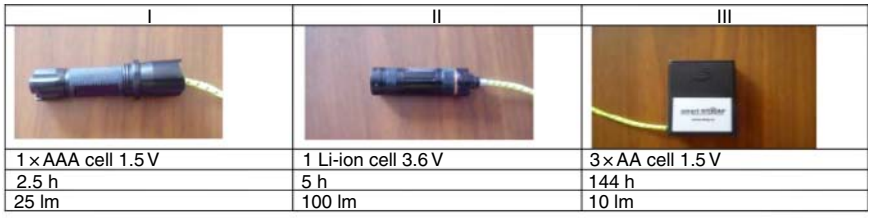
Figure 23.19 Influence of type and diameter of SEPOF on their illumination intensity.

The attenuation profiles of these fibers (see Section 5.1) for different diameters are compared in Figure 23.19.

It is clearly visible that the illumination intensity, i.e. height of attenuation profile, can be simply enhanced by increasing of SEPOF diameter.

Second important parameter is applied voltage, i.e. electric power necessary for light generation. In Figure 23.20, attenuation profiles of three portable power sources are compared for the same LED. Here the light intensity is expressed in lux (lm) units.

It is clear that the proper voltage is very important to obtain required illumination intensity and therefore lighting efficiency.



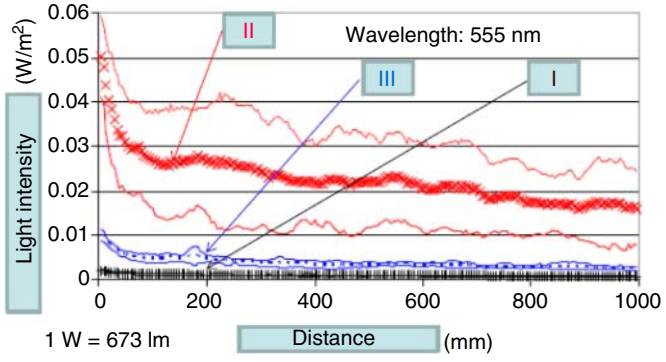


Figure 23.20 Influence power source voltage on SEPOF illumination intensity.

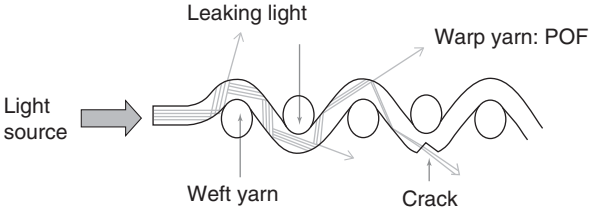


Figure 23.21 Local side emitting due to creating of woven fabric. Source: Adapted from Masuda et al. 2006 [43].

23.4.2 SEPOF Based on Multiple Micro-bending

For end-emitting optical fibers, micro-bending is usually unwanted phenomenon causing increase of attenuation. Micro-bending is here commonly described as a random variable with a distribution of spacing and amplitude; radius of bent is typically less than 1 mm [74, 75]. Micro-bending due to the incorporation of POF fibers into woven or knitted fabrics, respectively, will induce their side emission. Incorporation of end-emitting POF into textile structures thus can cause local side illumination (see Figure 23.21). When creating micro-bending due to weaving of end-emitting POF to fabrics, the bend angle exceeds over critical angle N_c, and the light is reflected out.

By the creation of woven/knitted structures, optical fibers are subjected to bending, and the angle of incidence of light rays at the interface between the core and the cladding is locally changed so that there may be appearing local side emission (instead of internal reflections in end-emitting optical fibers). It is known that the intensity of the transmitted light generally decreases with increasing bending angle of optical fibers. Transmission loss increases exponentially with increase in the ratio between the bending radius and the radius of the

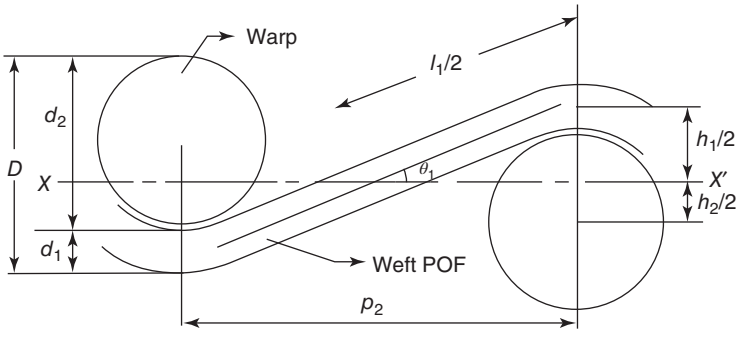


Figure 23.22 Peirce geometrical model of cloth. Source: Adapted from Peirce 1937 [64] and Behera et al. 2012 [70].

fiber [62]. For optical fibers inserted into textile structures, the influence of the bending on the macroscale is relatively small. On the other hand, the bending caused by the integration of fibers into the fabric structure, i.e. a local bending in binding points between warps and wefts (mesoscale), can lead to significant losses in light transmission or provide side emission.

Usually at least the local side radiation is required, so the incorporation of end-emitting optical fiber as part of the fabric structure is advantageous (local side radiation due mesoscale bends at crimps ensuring the high curvature). For SEPOF this local increase of side radiation in areas of highest curvature is usually not so beneficial. That is why the side-emitting fibers are inserted into the textile structures with the smallest deviations from the straight state (textile structure is serving as wrapping).

A separate problem is that flexibility and elasticity of optical fibers is limited, and at higher crimps due to weave, some damage may occur. The incorporation of optical fibers into the fabric so that at least part of them are on surface (as part of the structure) is protected by a patent [69]. Patent pending [68] protects the use of LIHS, wherein no part of SEPOF is on the fabric surface.

For characterization of POF shape and meso-bending in the fabric, the various geometric models can be used. Most common Peirce geometric model [64, 70] is shown in Figure 23.22. This model defines the arrangement of threads (yarns) in the woven fabric elementary unit (cell) for the case of direct inextensible but flexible materials. Threads have a circular cross section and consist of straight and bent segments.

The basic parameters of this model are as follows: the diameter of the warp threads d_2; the diameter of the weft thread d_1 warp sett $S_o = 1/p_2$, where p_2 is the distance between warp yarns; weft sett $S_u = 1/p_1$, where p_1 is the distance between the weft threads; and the fabrics thickness D and h_1, h_2, i.e. maximum displacement of thread axis normal to the plane of cloth (crimp height) of warp (2) and weft (1) in Figure 23.22.

Based on this two-dimensional model of the unit cell of fabric, a number of geometric parameters of fabrics, such as the angle of inclination of the thread, the thickness of the fabric, etc., can be calculated [70]. For a radius of curvature

of the weft threads r_c, it can be then derived

$$r_c = \frac{1/S_o}{2 \operatorname{arc} t_g \left(\frac{D-d_2}{1/S_u} \right)} + \frac{D}{2} \tag{23.13}$$

The fabric thickness is equal to $D = h_2 + d_1 \cong d_1 + d_2$. Trajectory of optical fiber integrated in weaving patterns can be simply described by Novikov waviness (see Ref. [73]). Warp weaves amplitude h_o and weft weave amplitude h_u are distance between fabric axis and yarn warp/weft axis (see Figure 23.10). Novikov relative warp waviness e_o and relative weft waviness e_u are ratio between warp/weft weave amplitude h_o/h_u and mean warp/weft diameter D_{str} [73]:

$$e_1 = h_1/d_{\text{str}} \quad e_2 = h_2/d_{\text{str}} \quad e_1 + e_2 = 1 \quad d_{\text{str}} = (d_1 + d_2)/2 \tag{23.14}$$

Value of this ratio for the case of POF in the warp can be varied from 0 (Phase 1 – straight) to 1 (Phase 9 – maximum bending of warp thread, axis of weft thread is lying on the straight line).

The radius of curvature of the optical fiber built in warp can be determined by using Eq. (23.13). It is only necessary to replace the parameter of warp by parameters of weft and vice versa. The physical simulation system of fabrics created from metal wires replacing the wefts and putting optical fibers as warps was proposed in Ref. [65]. The bending radius r_b of locally bent optical fiber in this simulated system is equal to

$$r_b = \frac{D}{4} + \frac{p_2^2}{16D} \tag{23.15}$$

Numerical aperture NA_b of bent POF can be calculated from relation [66]:

$$\text{NA}_b = \sqrt{\text{NA}^2 - \frac{n_2^2 r_c}{r_b} \left(2 + \frac{r_c}{r_b} \right)} \tag{23.16}$$

where NA is numerical aperture of straight POF, n_2 is refractive index of cladding, and r_c is core radius. The ratio of transmitted light energies is equal to the square of the ratio of NA, and therefore the light transmission efficiency E_t of bent POF is equal to

$$E_t = \left(\frac{\text{NA}_b}{\text{NA}} \right)^2 \tag{23.17}$$

The light emission efficiency E_e of bent POF without including intrinsic losses can be calculated from relation $E_t + E_e = 1$ [67]. For the same POF, light emission efficiency is then determined by the core radius and bending radius of POF only [65]. Based on the results of simulation experiments, it was found that the side-emitting intensity is directly proportional to the diameter of POF and indirectly proportional to the bending radius of POF. In accordance with Eqs. (23.15) and (23.16), the following model for prediction of side-emitting intensity I_e was proposed [65]:

$$I_e = \frac{A(r_c)}{r_b^2} + \frac{B(r_c)}{r_b} + C \tag{23.18}$$

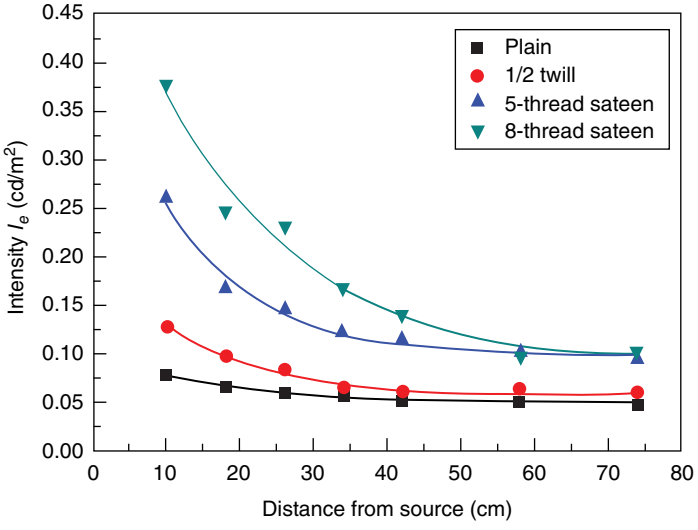


Figure 23.23 Side-emitting intensity of woven structures with POF fibers in weft. Source: Adapted from Wang et al. 2013 [65].

where constants $A(r_c)$ and $B(r_c)$ depend on the radius of core and constant C is connected with light source quality and POF diameter. The minimum bending radius r_{bm} of the POF before the break can be calculated from knowledge of deformation at yield point ε_y according to the relation [66]:

$$r_{\mathrm{bm}} = \frac{r_c}{\varepsilon_y} \tag{23.19}$$

It was found that for PMMA core POF having diameters 250 and 500 µm, minimum bending radius r_{bm} were equal to 2.6 and 4.46 mm. Side-emitting intensity I_e of different woven structures having POF from PMMA with diameter 250 mm in weft is shown in Figure 23.23.

It is obvious that looser weaves provide higher side emission intensity. In the case of sateen weaves, there was a significant improvement in the side emission intensity of radiation at small radii of curvature (see Figure 23.24).

Generally, it is therefore necessary to appropriately select the bending radius (dependent on weave type) and the radius of the POF with respect to initial modulus, strength, and parameters at the yield point, respectively. Light transmission losses of bent optical fiber may be unacceptably high for a SEPOF as well [44].

The most significant loss of illumination intensity of about 55% are in the area where POF passes from straight shape to bent form. Since the weft yarns in the fabric are relatively more bent than the warp yarn, the fabrics with POF in the warp obey more side emission for the same weave.

Increased lateral emissions can be achieved also by using fluorescent dye stuffs in the cladding of the POF [31]. During textile processing of POF, their plastic elongation occurs frequently, which negatively affects transmission of light. For weaving of POF, the rapier weaving machines are particularly suitable.

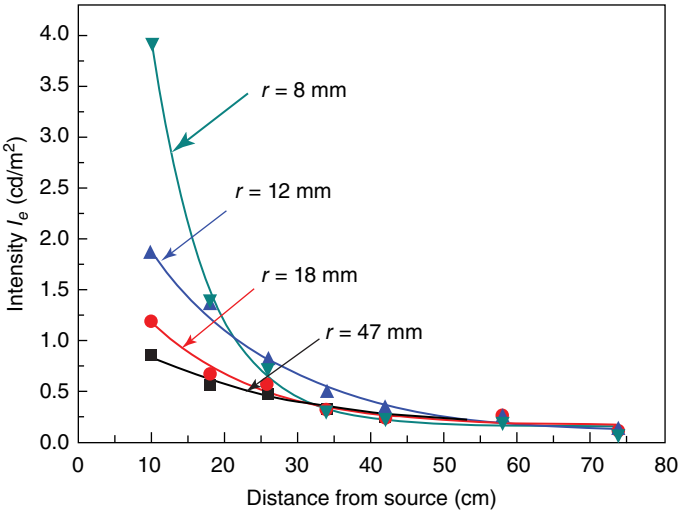


Figure 23.24 Influence of radii of curvature *r* on the side-emitting intensity of sateen weaves. Source: Adapted from Wang et al. 2013 [65].

23.4.3 Modifications of POF Structure

To provide or enhance side emission, it is possible to use the following techniques modifying standard end-emitting POF:

1) During the manufacture of fibers, appropriate "micro" particles (ZnO, Al_2O_3, etc.) are placed into the polymer core or cladding (see Figures 23.26 and 23.27).
2) The cladding of the POF is chemically or mechanically damaged (see Figures 23.31, 23.33 and 23.34).
3) The micro-cuts or notches are added in the cladding layer (see Figures 23.28 and 23.29).

For industrial purposes these techniques can be combined with the selection of materials of core and cladding according to principles of side emission, i.e. $n_2 > n_1$.

For some textile applications, the special polymers comprising alternating layers of material having a high refractive index difference (2D photonic crystals) are proposed [49]. In their cross section these fibers contain a periodic sequence of micron-sized layers of different materials. The so-called Bragg fibers combining PMMA core, multilayered PPMA/PC Bragg reflector, and PMMA cladding are shown in Figure 23.25 [49].

Photonic bandgap (PBG) fibers guide light using PBG effect rather than total internal reflection. Intensity of side-emitted light can be controlled by choosing the number of layers in the microstructured region surrounding the optical fiber core. Such fibers always emit a certain color sideways without necessity of surface corrugation or micro-bending.

Hollow core Bragg fiber consists of an air-filled core surrounded by a periodic sequence of high and low refractive index layers forming a so-called Bragg reflector [50]. Typical feature of reflector is the presence of regions of high reflector

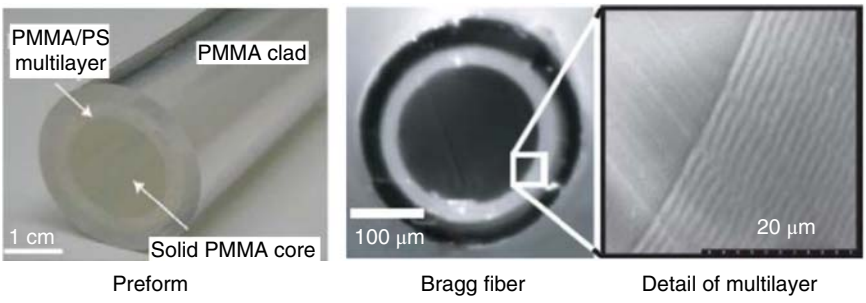


Figure 23.25 Solid core Bragg photonic fiber.

efficiency caused by the interference effects inside a periodic multilayer. Light with frequency inside of a reflector bandgap can be confined in the fiber hollow core through reflections from a surrounding periodic reflector. By changing the number of reflector layers, it is possible to control the rate of potential side emission. For light transmission the number of reflector layers should be sufficiently high to suppress radiation loss. For illumination purposes a relatively small number of reflector layers should be used.

The SEPOF containing particles of Al_2O_3 in core are schematically illustrated in Figure 23.26, and SEPOF containing particles of ZnO in cladding are in Figure 23.27.

Diffusing jacket on SEPOF (Figure 23.26) is usually used as a protection against humidity and mechanical damage. Metallic particles such as iron, copper, cobalt, nickel, manganese, and chromium have the effect of absorbing the radiation,

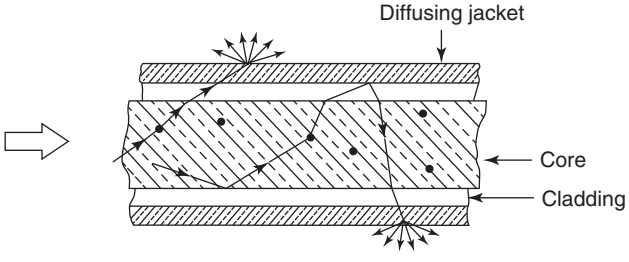


Figure 23.26 SEPOF with particles in core [25].

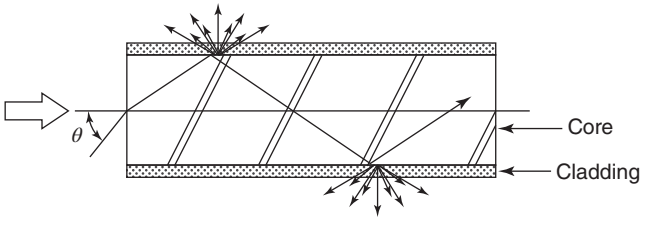


Figure 23.27 SEPOF with particles in cladding [47].

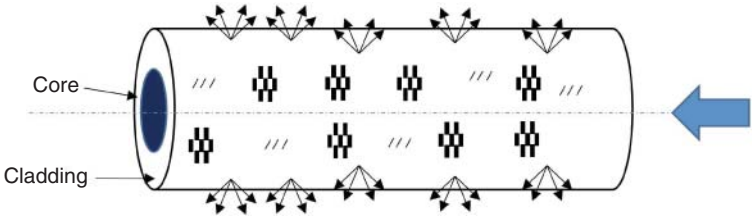


Figure 23.28 SEPOF with micro-cuts or notches in the cladding. Source: Spigulis et al. 1996 [22]. Reproduced with permission of Society of Photo-Optical Instrumentation Engineers (SPIE).

increasing attenuation, and, consequently, decreasing the overall radiation intensity in the fiber [33, 51, 52].

SEPOF with micro-cuts or notches in the cladding is shown in Figure 23.28.

Notches can be created by local surface melting by using CO_2 infrared laser micromachining [71]. The size of one notch created on POF having the PMMA core (diameter 240 mm) and fluorinated PMMA cladding (diameter 10 mm) was as follows: height $h = 98.3$ mm, angle $2\delta = 148.2°$.

Structure of typical notch created by local laser surface melting is shown in Figure 23.29.

Combination of surface notches created by laser and micro-bending in woven structure for creation of light side-emitting fabrics was investigated in work [71].

Enhanced side illumination of SEPOF having PMMA core and PTFE cladding by combination of TiO_2 particles (diameter of 0.5 mm) attached on cladding surface and subsequent CO_2 laser treatment was investigated in work [72].

It is visible (see Figure 23.30) that surface of cladding is damaged especially in places where agglomerates of TiO_2 particles are present.

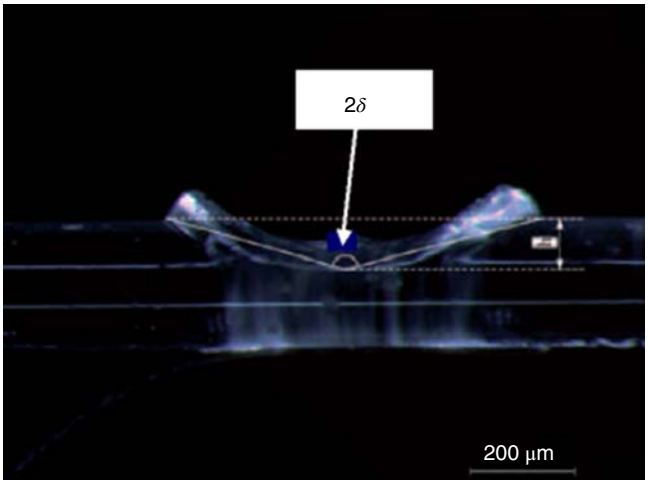


Figure 23.29 Micrograph of polymer optical fiber with one notch. Source: Shen et al. 2013 [71]. Reproduced with permission of SAGE.

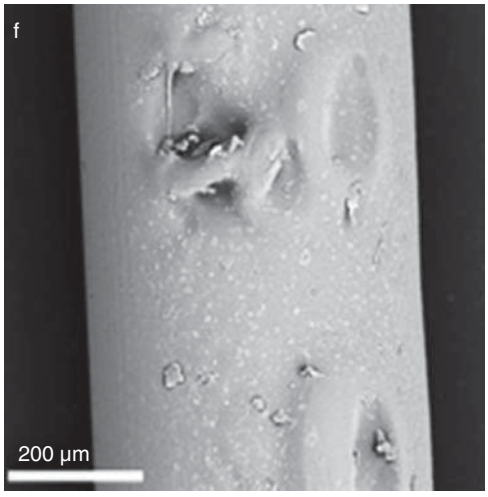


Figure 23.30 Surface scanning electron microscopy (SEM) images of SEPOF with TiO_2 particles after CO_2 laser treatment (intensity 150 µs pixel time). Source: Huang et al. 2015 [72]. Reproduced with permission of De Gruyter.

The formation of micro-mirrors inside a POF with PMMA core through cutting, masking, metallic coating, and polymer redeposition is described in work [51]. It was found that power loss at a single micro-mirror is about 0.7 dB, and approximately 16 mirrors are uniformly embedded along a 20 mm.

Zajkowski [15, 16] experimentally studied the intensity of side-emitting optical fibers for materials with different values of refractive index of core and cladding. The intensity of the total side emission was strongly decreased along the direction of fiber axis.

Spigulis et al. [22] described the side emission of optical fiber containing additives causing scattering in the cladding. Zarian et al. [54] described an optical fiber that was manufactured using the notches in claddings extended to the core. Suitably defined nonconstant changes in the distance between the notches permitted to obtain a constant intensity of the side emission along the fiber.

Sillyman et al. [53] used paraboloid reflector system to control the numerical aperture for delivery of light to ensure a constant intensity of the lateral radiation along the fiber.

Harlin et al. [21] reported that the main area of side-emitting optical fiber utilization is illumination in the visible spectrum. There are also more advanced applications, e.g. photochemical reactions induced by a side-emitting optical fiber, a photomedical therapy [56], the disinfection of waste water [57] and the photocuring of the polymers. In these applications the UV radiation is generally used. UV radiation obeys stronger attenuation during transmission through the fibers than visible light.

Various types of commercial SEPOF were compared according to their emission spectrum and their suitability for applications in the spectral range from UV-A to the visible blue [55]. The SEPOF based on particles in core and notches in cladding were compared. The higher levels of intensity obey SEPOF fibers with micro-notches, but intensity distribution is more uneven. PMMA core SEPOF with micro-notches has significantly greater loss in emission at longer distances

from the light source compared with fibers containing silicon core. The higher uniformity of side emission can be achieved also by appropriate surface treatment [55].

23.4.4 Local Side Emission

The local side emission of end-emitting POF and enhancement of side emission intensity can be obtained by partial damage of cladding layer. Simple method is mechanical damage by abrasion. The extent of damage to SEPOF by abrasion on Zweigle yarn abrasion device covered by emery paper 80 after 20 cycles is shown in Figure 23.31.

The changes of attenuation profiles due to abrasion are shown in Figure 23.32. For comparison, the end-emitting POF of the same diameters subjected to the same abrasion degree is presented as well.

It is visible that improvement of side illumination intensity in the case of end-emitting POF is relatively small and far from intensity of SEPOF. In the case of SEPOF, abrasion is effective, and local illumination is much higher (see Figure 23.32).

The visual changes of side emission of end-emitting POF with fluoropolymer cladding due to abrasion, etching in ethyl acetate (20 minutes) and combined etching abrasion were published in work [26]. The best results, i.e. maximum of side emission, were obtained by abrasion followed by solvent etching (see Figure 23.33).

The repeated bending is in fact responsible for local mechanical damage of cladding as well. The changes of SEPOF Grace standard attenuation profile due to repeated bending on Flexometer device to prescribed percentage of cycles till fracture (25%, 50%, and 75%) are shown in Figure 23.34.

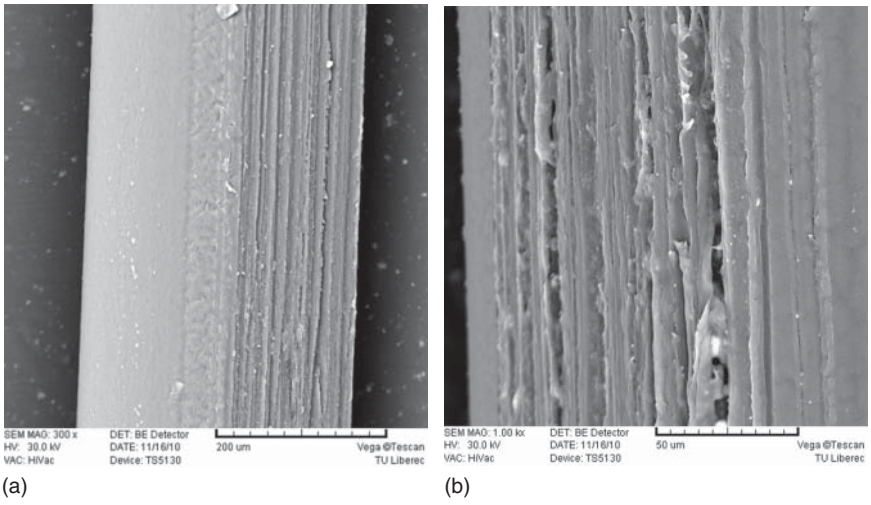


Figure 23.31 Abrasion of SEPOF type Hypo by using of emery paper graininess 80 (after 20 cycles) at different magnifications.

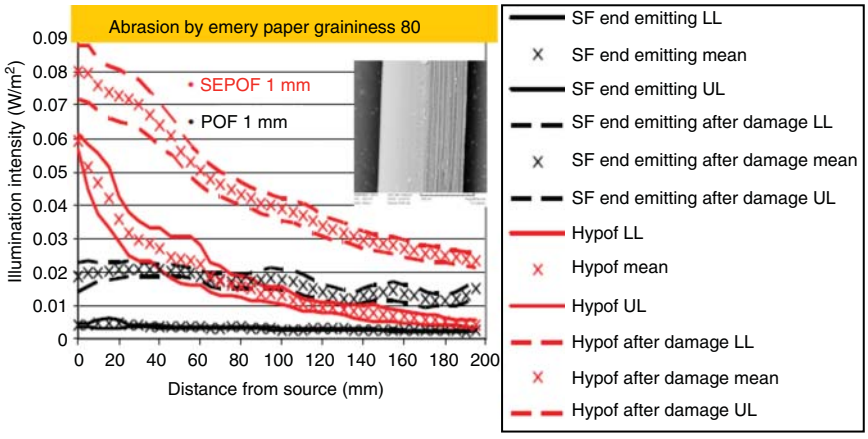


Figure 23.32 Changes of attenuation profiles of end-emitting POF and SEPOF before and after abrasion.

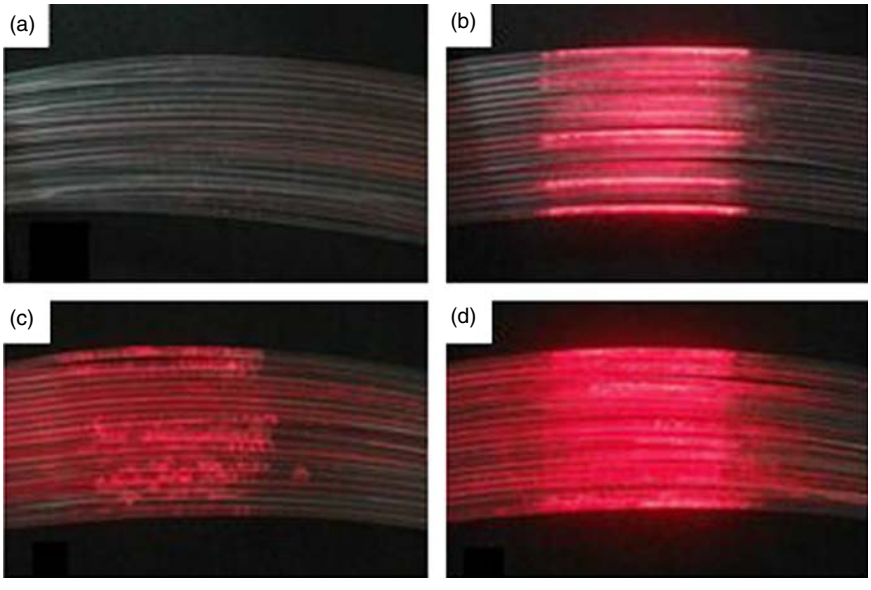


Figure 23.33 Side light emission effect on end-emitting POF: (a) without treatment; (b) abraded by sandpaper; (c) etched with solvent; (d) abraded and then solvent-etched. Source: Im 2007 [26]. Reproduced with permission of Springer.

For comparative purposes the SEPOF Grace standard with a diameter of 0.75 mm was subjected to mechanical and chemical damage and influence of UV radiation under the following conditions:

1) Twenty cycles of abrasion on Zweigle yarn abrasion device covered by emery paper 80
2) Treatment in tetrachloroethylene for one hour

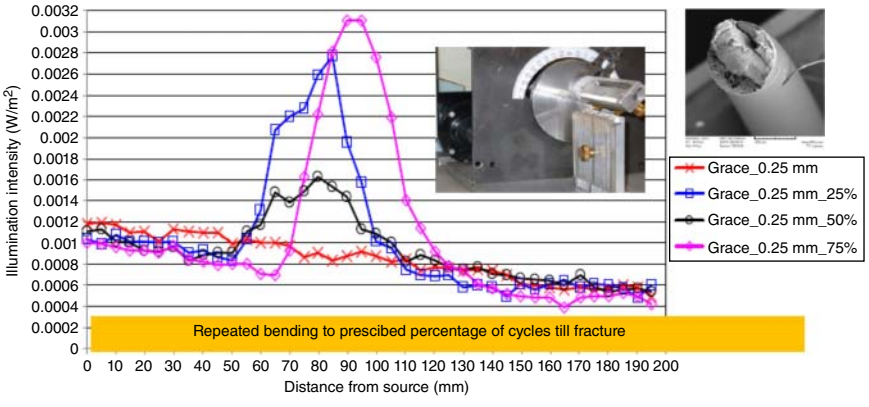


Figure 23.34 Attenuation profiles of fibers damaged by repeated bending.

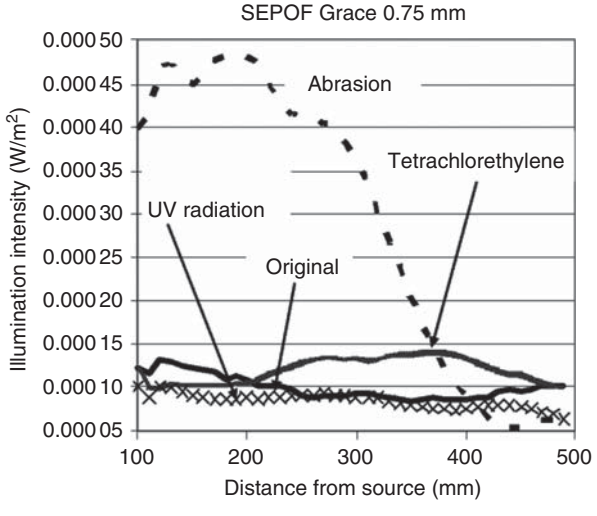


Figure 23.35 Attenuation profiles of fibers damaged by various manner.

3) UV exposure for seven days on the instrument ATLAS UV 340th

Comparison of attenuation profiles for original and damaged samples is shown in Figure 23.35.

The abrasion looks as very simple and in practice can be combined with increasing of temperature. Few cycles only have visible effect. Very simple method for local enhancement of POF emission is the combination of pressure and temperature, i.e. pressing at elevated temperatures (see Figure 23.36).

23.5 Properties of POF

Like glass fibers, POF is characterized by a wide range of different parameters. The properties characterizing the quality of light propagation as attenuation and

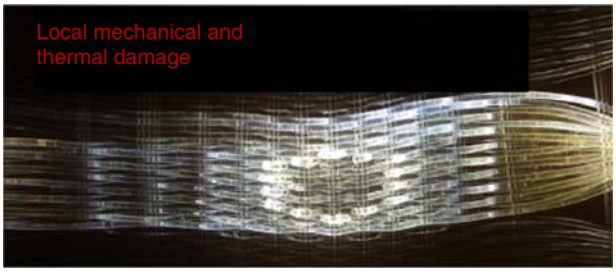


Figure 23.36 Local enhancement of POF side emission by combination of pressure and temperature.

bandwidth are essential for applications of POF. For the practical use, it is necessary to have POF with other characteristics such as the following:

- Durability of the fiber in conditions of use
- Thermal resistance
- Resistance to bending and repeated flexing
- Mechanical stability (flexibility, stress limits for tensile and compressive stress, etc.)
- UV radiation resistance
- Resistance against chemicals, water vapor, etc.

Some of these characteristics are dependent critically on the jacket and can be tuned in connection with areas of application. Some properties, e.g. repeated flexing, are important for SEPOF mainly, and some are necessary for all kind of POF. General properties of POF including measurements and characterization are comprehensively described in many books [1–6]. Here we are focused on optical, mechanical, and thermal properties of POF and mainly SEPOF.

23.5.1 Optical Attenuation

Since the development of POFs, the primary importance has been given to understand and to reduce their optical transmission loss.

Loss of light intensity generally depends on the following: light wavelength, fiber type, fiber structure (i.e. crystallinity and orientation), impurities and accompanying substances (dopants), outer geometric shape (micro-bends, macro-bends, surface damage), and mainly on distance from the source. For classical end-emitting optical fibers, the goal is to suppress attenuation because it is the source of information loss or loss of transferred illumination power. For SEPOF side emission is wanted and can be supported. The standard approach to characterize attenuation, dispersion, and bandwidth of end-emitting optical fibers is comprehensively described in books [1–6], and therefore it is not discussed here.

Special measurement and evaluation system was constructed for evaluation of SEPOF attenuation in straight state and creation of the *attenuation profile* $P(L)$, i.e. dependence of illumination intensity on distance from light source L till maximum length in the range of 1–10 m [44]. Main principle is the measurement

of illumination intensity by using integrating cylinder. The light emitted by the POF falls on the inner surface of the cylinder, which has a high reflectivity and is opaque; thus incident rays are scattered randomly in all directions (into the interior of the cylinder). For sufficiently big dimensions of this cylinder, the random light scattering extends substantially to the statistically uniform illumination of its internal surface.

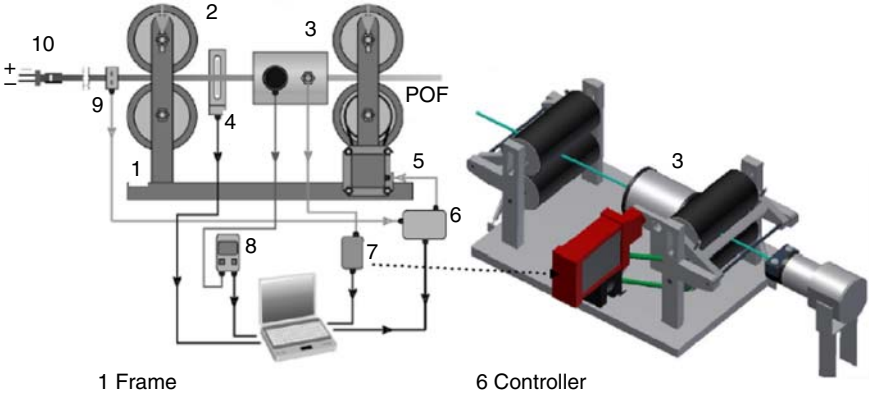
Irradiation of inner surface $E(A)$ (W/m^2) depends on the light power (illumination intensity) $P(L)$ (W/m^2) escaping from measured surface area A of the POF to the inner surface of the cylinder at distance L from light source:

$$E(A) = \eta P(L)\left(\frac{\pi d^2}{4} l\right)^{-1} \tag{23.20}$$

where η (–) is efficiency coefficient, l is length, and d is inner diameter of integrating cylinder. The sensor of light power has active area S_s. Then the illumination intensity $P(L)$ is calculated from measured radiant flux Φ_V (W) by using the following equation:

$$P(L) = \frac{\pi d^2}{4} \frac{\Phi_V}{\eta S_s} l \tag{23.21}$$

This principle was used for construction of online computer-controlled measurement and evaluation system for creation of the *attenuation profile* (Figure 23.37). System is composed of radiant flux light sensor (THORLABS PM 1000 SB), step driver, control unit, measuring channel, input/output rolls, and illumination unit based on LED.



1 Frame
2 Rubber roller
3 Optical integration cylinder
4 Raster camera
5 Stepping motor
6 Controller
7 Spectrophotometer
8 Power measuring unit
9 End of fiber detector
10 Illumination unit

Figure 23.37 Device for measurement of POF light intensity in straight state. Source: Adapted from Lédl and Václavík 2009 [45].

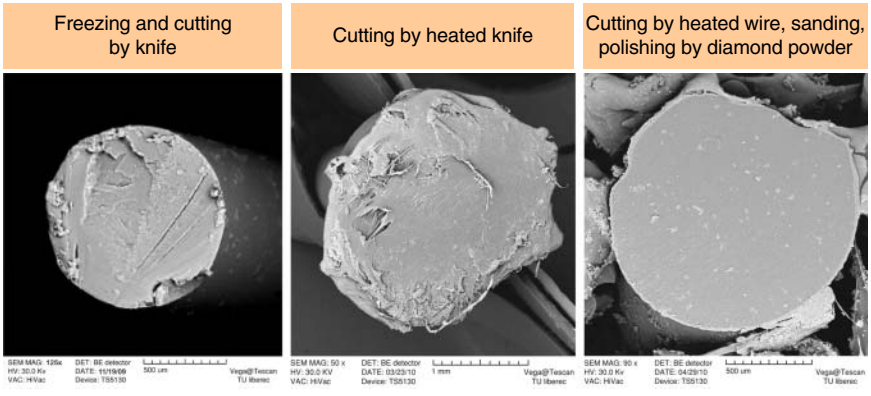


Figure 23.38 Preparation of POF ends. Source: Adapted from Křemenáková et al. 2013 [29].

The illumination of POF is realized by illumination unit composed of LED connected with power source. Electric power supply is 3 W (3 V voltage and current of 1 A). At 10% conversion efficiency, the light output power is of 300 mW. Moreover, about 30% radiates outward from the fiber, so that the radiant flux at the input into the fiber is 100 mW.

The POF or tubular textile structure is located between the feed rollers, which guide them to the integrating cylinder. The tow rollers are driven by step motor. The actual measurement is performed in predefined step lengths. Step lengths are processed by a step motor that drives the two rollers. The measurement process is controlled by a computer program created in MATLAB.

The computer unit is used also for the calculation of *attenuation profile* including statistical analysis.

The POF end connected with illumination unit was prepared by cutting with heated wire or freeze knife and then by polishing with diamond powder (Figure 23.38).

Typical mean attenuation profile of SEPOF Grace standard having diameter 0.25 mm is shown in Figure 23.39 [29]. Due to relative high variability of results,

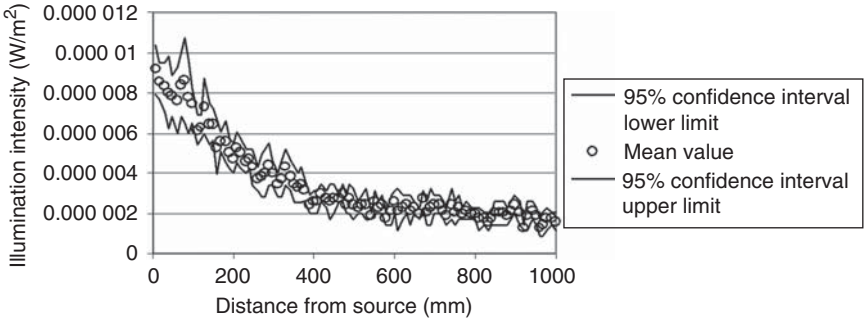


Figure 23.39 Mean attenuation profile and lines of 95% confidence interval for SEPOF Grace standard.

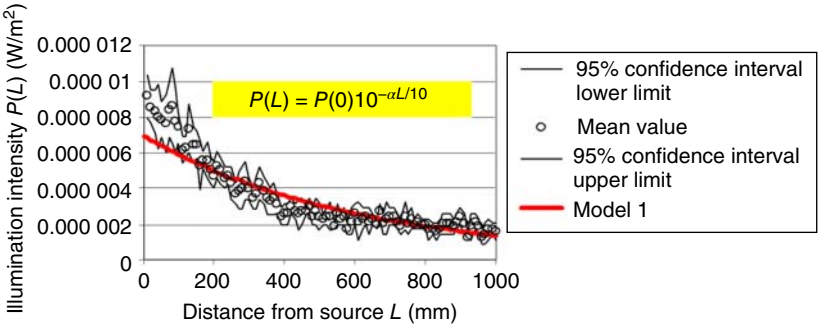


Figure 23.40 Mean attenuation profile for SEPOF Grace standard with added line of $P(L)$ from Eq. (23.11).

20 attenuation profiles are usually measured. Robust estimator of mean illumination intensity (points in Figure 23.4) and corresponding 95% confidence intervals (lines in Figure 23.39) is then calculated by robust Horn procedure suitable for small sample sizes [46].

Experimental mean attenuation profiles can be used for obtaining parameters of exponential model describing the $P(L)$ function (see Eq. (23.11)) by the standard nonlinear or linearized regression using least-squares criterion [46]. By logarithmic transformation of Eq. (23.11), the straight line type dependence $\log P(L) = -\alpha L/10 + \log P(0)$ results. Slope of this straight line k can be used for calculation of mean attenuation rate $\alpha = -10k$, and intercept q can be used for calculation of illumination intensity on the fiber input $P(0) = 10^q$. By using regression straight line parameters k and q, coefficient of determination R^2 and parameters $P(0)$ and α can be calculated [46]. The experimental variances of $P(L)$ can be used as weights in regression analysis. For refining the estimators of α and $P(0)$, the nonlinear regression should be used. The $P(L)$ curve based on Eq. (23.11) is added into experimental attenuation profile in Figure 23.40.

It is clearly visible that the model from Eq. (23.11) is not sufficient for mean intensity profile experimental course approximation. It was found that at short distances from light source, illumination intensity *is* strongly decreasing especially for POF with higher diameter (higher than 1 mm). For better expression of $P(L)$ behavior, the so-called LLF2 model was proposed. LLF2 is in fact linear spline, i.e. linear piece-wise function composed from two different straight sections [46]. This model is based on the assumption that in short distances from light source, there are some nonuniformities in side emission due to accommodation to aperture and critical angle. In second phase the illumination intensity is slowly decreasing with distance L from light source (system is accommodated). Local slopes of LLF2 are in fact sensitivity coefficients a_1, a_2. Corrected illumination intensity on the fiber input is $P_{cor}(0)$. LLF2 model is described by the following equation (linear regression spline with one knot):

$$\mathrm{LLF2} = P_{cor}(0) + a_1 L + a_2 (L - L_c)_+ \tag{23.22}$$

where function $(x)_+ = 0$ if x is negative and if x is positive, function $(x)_+ = x$. L_c is the distance of transition between first and second phase. By using modified

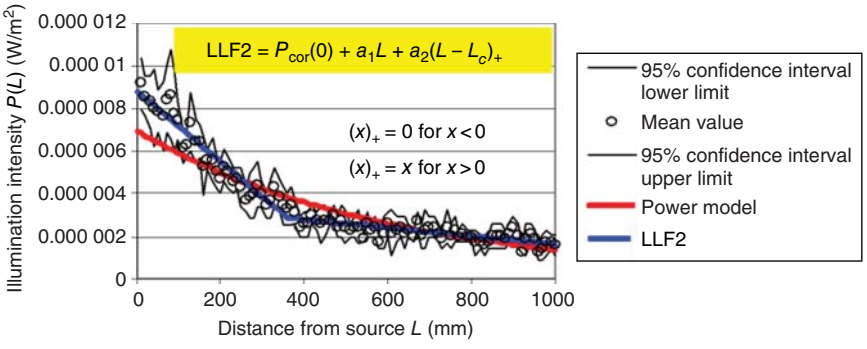


Figure 23.41 Mean attenuation profile for SEPOF Grace standard with added line of $P(L)$ from Eq. (23.11) and line corresponding to LLF2.

linear regression [46], parameters of LLF2 for experimental mean attenuation profiles can be calculated. The *LLF2* curve from Eq. (23.22) is added into experimental attenuation profile in Figure 23.41.

As attenuation profile characteristics of POF, the sensitivity coefficients a_1, a_2, corrected illumination intensity on the fiber input $P_{\text{cor}}(0)$, and distance of transition between first and second phase L_c can be used. Based on comprehensive tests, it was found that the main factor influencing the intensity of the side emission of SEPOF is their diameter. For straight SEPOF, 20–40% of illumination intensity is lost at short distances from light source. The intensity of radiation is here falling sharply. After a certain length L_c the illumination intensity decreases slowly.

The intensity of radiation at the entrance to the fiber $P_{\text{cor}}(0)$ and slope a_2 of model (23.22) obey power law dependence on SEPOF diameter [29].

For expression of acceptable working length L_p of POF, illuminating power P_{L_p} must be on the end of this length corresponding to sufficient value of attenuation coefficient α_{L_p}:

$$P_{L_p} = P(0)10^{-\alpha_{L_p} L_p/10} \tag{23.23}$$

Illuminating power P_{L_p} can replace $P(L)$ in Eq. (23.23), and then working length of optical fiber L_p can be calculated:

$$L_p = \frac{10}{\alpha_{L_p}} \log(P(0)/P_{L_p}) \tag{23.24}$$

Working length of optical fiber are typically calculated for attenuation coefficient α_{L_p} from 10 to 20 dB.

23.5.2 Mechanical Properties

Several authors have studied the mechanical properties of POF. Most of these studies have been focused on the attenuation induced by bends and tensile or torsion stresses and fiber fatigue [35, 36, 58, 59]. In contrast to silica optical fibers,

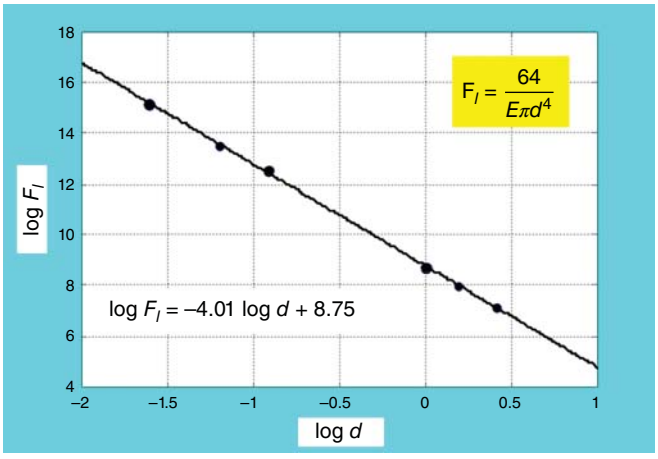


Figure 23.42 Dependence of SEPOF flexibility on their diameter d.

POFs are made of polymeric materials. One of main difference is that initial modulus E for a POF (about 3 GPa) is nearly 2 orders of magnitude lower than that of a silica optical fiber (about 73 GPa).

The flexibility F_l of optical fibers with diameter d can be calculated as characterization of their usefulness:

$$F_l = \frac{64}{E\pi d^4} \tag{23.25}$$

For this reason, e.g. even a diameter of POF will be approximately two times higher than diameter of silica fibers, it will have the same flexibility sufficient to be installed according to typical configurations. For the same reason, the minimum bending radius for POF is smaller, since polymers are more ductile and much flexible than silica or glass. For SEPOF brand Hypof, dependence of flexibility on fiber diameter is approximately linear (see Figure 23.42).

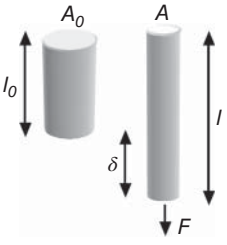


Figure 23.43 Ideal geometry o fiber extension.

Stress–strain curves of POF are created by using tensile testing machines (dynamometers), which are at disposal in every material testing laboratory. Initial undeformed straight fiber has cross-sectional area A_o (diameter d_o) and length l_o. After applying the load F, the fiber is extended to the length l and shortened to the area A or diameter d (see Figure 23.43).

The engineering stress σ, engineering strain ε, and draw ratio λ are defined by well-known equations:

$$\sigma = \frac{F}{A_o} \quad \varepsilon = \frac{l - l_o}{l_o} = \frac{\delta}{l_o} \quad \lambda = \frac{l}{l_o} = 1 + \varepsilon \tag{23.26}$$

The differential of draw ratio is then defined as $d\lambda = dl/l$. After integration the so-called true strain ε_t can be obtained:

$$\varepsilon_t = \int_{l_o}^{l} \frac{dl^*}{l^*} = \ln(\lambda) = \ln(1+\varepsilon) \tag{23.27}$$

The important characteristics of material deformation is so-called Poisson ratio ν, defined as ratio of the relative transversal deformation ε_T and relative longitudinal extension ε:

$$\nu = -\frac{\varepsilon_T}{\varepsilon} \quad \text{where} \quad \varepsilon_T = \frac{d-d_o}{d_o} \tag{23.28}$$

For liquids and rubber the volume is not changed during deformation, i.e. $V/V_o = 1$ (incompressible material) and $\nu = 0.5$. For majority of fiber forming polymers, volume is increased due to extension (i.e. $V/V_o > 1$) and then $\nu < 0.5$ (obviously $0.2 \leq \nu \leq 0.45$). Poisson ratio of PS is 0.325–0.33, Poisson ratio of PC is 0.37, and Poisson ratio of PMMA is 0.34–0.4. For sufficiently small deformations, the values computed for constant ν are fully acceptable, and the true stress σ_t can be then expressed in the form

$$\sigma_t = \frac{F}{A} = \frac{\sigma}{(1-\nu\varepsilon)^2} \tag{23.29}$$

It is interesting that for linear true stress/true strain dependence $\sigma_t = E\varepsilon_t$, the engineering stress–strain diagram is a convex increasing curve defined as

$$\sigma = E(1-\nu\varepsilon)^2 \ln(1+\varepsilon) \approx \frac{E\varepsilon(1-\nu\varepsilon)^2}{1+\varepsilon} \tag{23.30}$$

Equation (23.30) can be used for small deformation range till yield point. The initial modulus for true stress/strain dependence is equal to initial modulus of the engineering stress–strain curve. It was experimentally proved that Poisson ratio decreased with increasing tensile elongation. It is interesting that the stress–strain relation of silica optical fibers was described by relation [76]:

$$\sigma = E\varepsilon\left(1 + \frac{0.75\alpha\varepsilon}{2}\right) \tag{23.31}$$

where value for the nonlinearity constant α is about 6. For small ε, it is Eq. (23.30) quadratic polynomial according to ε as Eq. (23.31).

There are big differences between mechanical characteristic of POF obtained by different authors [61]. One reason is that the mechanical properties of POF depend strongly upon the polymer molecular mass and structure of fiber influenced by drawing process parameters as the drawing ratio and temperature. For PMMA polymers the following typical mechanical parameters are tabulated: impact strength (Charpy) 20 kJ/m^2, shear modulus 1.7 GPa, initial modulus 3.3 GPa, and mechanical loss factor (tan δ) 0.08 at 25 °C and 10 Hz [20].

The mean initial modulus $\overline{E}$, mean deformation to break $\overline{D}_B$, and tensile strength $\overline{\sigma}_B$ with corresponding standard deviation CV_σ for SEPOF brand Hypof for different fiber diameters are given in Table 23.5 [30, 34].

It is interesting that the tensile strength is decreasing for the increasing of fiber diameter. It can be partially caused by different draw ratio. Preparation of

Table 23.5 Tensile characteristics of Hypof.

d (mm)	$\overline{E}$ (GPa)	$\overline{D}_B$ (%)	$\overline{\sigma}_B$ (MPa)	CV_σ (%)
0.2	3.3	21.80	107.6	7.4
0.3	3.4	42.1	91.5	2.4
0.4	2.8	22.4	78.6	9.3
1	3.4	4.8	88.2	8.6
1.2	3.3	5.8	84.7	4.5
1.5	3.1	8.7	82.9	1.2

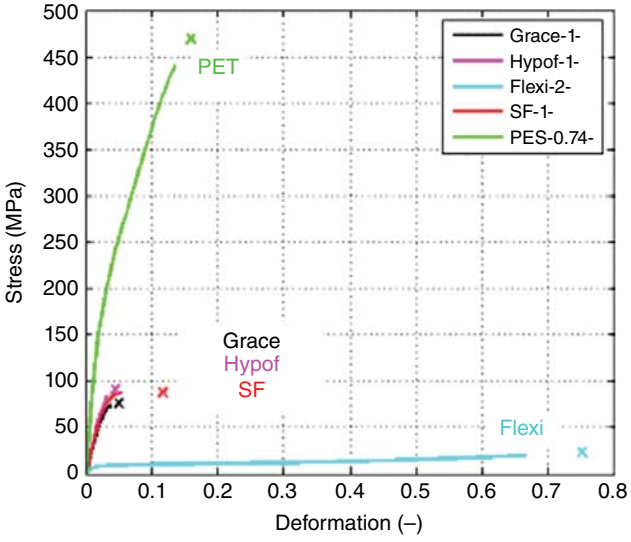


Figure 23.44 Stress–strain curves of SEPOF and polyester fibers.

thicker fiber requires generally lower draw ratio. The deformation to break is ideally increasing for increasing of fiber diameter.

The stress–strain tensile curves of different SEPOF (Grace, Hypof, SF, and Grace Flexi) and standard polyester fiber of the similar diameter are shown in Figure 23.44.

It is visible that SEPOF have very low tensile strength in comparison with standard textile fibers. SEPOF Flexi is characterized by lowest tensile strength but very high deformation to break. The breaking stress distribution of polymeric fibers follows often three-parameter Weibull distribution (see Eq. (23.34)).

For service lifetime predictions of optical fibers, the static fatigue measurements are commonly used. In the tensile tests the time to failure of a fiber due to axial constant applied stress σ_a is measured. The mandrel bending tests involve winding a portion of optical fiber around a precision ground mandrel, and the two-point bend technique involves bending short portions of fiber due

to insertion into a precision bore glass tube. Comparison of these techniques and statistical analysis of life time data is presented in the work [57]. The optical fiber lifetime t_f as a function of constant applied stress σ_a and fiber strength σ_b is expressed by empiric relation:

$$t_f = B\frac{\sigma_b^p}{\sigma_a^n} \tag{23.32}$$

where B is constant dependent on environment, n is considered as material property (stress corrosion parameter), and p depends on the nature of defects causing failure (for crack like flaws, $p = n - 2$). The n value for bulk silica is around 40 and around 20 and 25 for fibers (see Ref. [57]).

For evaluation of flex fatigue of POF, SEPOF, and LIHS, the special device was constructed [30, 34]. Basic principle is the evaluation of number of repeated flexing cycles till break FC of fibrous materials. Fiber is fixed in upper movable clamp and guided through slot of diameter 0.2 till 3 mm. Upper clamp should be adjusted to the selected maximum flexing angle from 0° to 140° (see Figure 23.45). On the free end of fiber (adjustable in range 8–27 mm), prescribed load is mounted. Upper clamp is driven by electrical drive with adjustable frequency of flexing per minute.

For analysis of FC data, it is necessary to know the suitable theoretical distribution. The computationally assisted exploratory data analysis methods including techniques used here are described in the book [63].

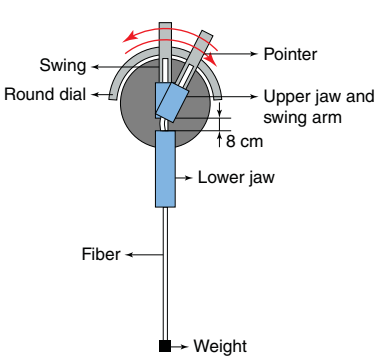
The estimation of proper distribution of FC can be realized by using so-called quantile–quantile (Q–Q) plot. Classical Q–Q plot is based on comparison of empirical quantile function $Q(P_i) \approx \mathrm{FC}_{(i)}$ with chosen theoretical quantile function $\mathrm{QT}(P_i)$. The probability estimator $P_i = i/(n+1)$ and so-called order statistics [63].

$$\mathrm{FC}_{(1)} < \mathrm{FC}_{(2)} < \cdots < \mathrm{FC}_{(N)}$$

The sample values arranged in the increasing order are used. It was found that for flex fatigue of polymeric fibers, three-parameter Weibull distribution is useful



(a)



(b)

Figure 23.45 Device for flex fatigue measurements.

[63]. Distribution function has simple form:

$$F(\mathrm{FC}) = 1 - \exp\left[-\left(\frac{\mathrm{FC} - A}{B}\right)^{C}\right] \tag{23.33}$$

Here A is threshold, i.e. lowest number of repeated flexing cycles till break, B is scale parameter, and C is shape parameter. For quick and rough parameter estimates of three-parameter Weibull models, the moment-based method can be used. The main idea of this method is very simple. Based on the selected three sample moments and corresponding theoretical moments for number of repeated flexing cycles till break, the three nonlinear equations can be created. Their complexity is based on the suitable selection of moments [63].

Moment method based on so-called Weibull moments is very simple (see Ref. [30]). The Weibull sample moments m_r are defined as

$$m_r = \sum_{i=0}^{N-1} (1 - i/N)^r [\mathrm{FC}_{(i+1)} - \mathrm{FC}_{(i)}] \tag{23.34}$$

For $i = 0$ is formally $\mathrm{FC}_{(0)} = 0$. Shape parameter C can be estimated from relation

$$C = \frac{\ln(2)}{\ln(m_1 - m_2) - \ln(m_2 - m_4)} \tag{23.35}$$

For estimation of the lower limiting number of repeated flexing A is valid

$$A = \frac{m_1 m_4 - m_2^2}{m_1 + m_4 - 2m_2} \tag{23.36}$$

and estimate of scale parameter B is in the form

$$B = \frac{m_1 - A}{\Gamma(1 + 1/C)} \tag{23.37}$$

where $\Gamma(x)$ is Gamma function.

This very simple technique can be used for the rough estimation of threshold A in three-parameter Weibull models.

Then Q–Q plot can be simply constructed for three-parameter Weibull distribution [63]. After rearrangements the linear dependence, $y = ax + b$ in Q–Q plot occurs. Here,

$$y = \ln[-\ln(1 - p_i)], \quad x = \ln(FC_{(i)}) - A$$

$$a = C \text{ and } b = -\ln(B)C$$

In this case it is necessary to know in advance the estimator of lowest number of repeated flexing cycles till break A calculated from Eq. (23.3).

The bending fatigue tests were realized on device shown in Figure 23.45 for SEPOF brand Hypof with different diameters. For bending fatigue measurements, the following conditions were selected:

- Frequency of flexing – 116 (min^{-1})
- Free-end load – 5 (g).
- Fiber length – 8 (mm)

Table 23.6 Standard characteristics of flex fatigue.

Fiber diameter d (mm)	FC_M (cycles)	S_{FC} (cycles)	CV_{FC} (%)
0.2	2454.3	1284.2	52.32
0.3	7904	7091.1	89.7
0.4	1034.8	554.1	53.5
1	89.0	37.7	42.4
1.2	41.7	14.2	34.1
1.5	6.2	2.5	40.6

Table 23.7 Calculated parameters of Weibull distribution.

Fiber diameter (mm)	A (cycles)	B (cycles)	C (–)
0.2	1028	3887.9	3.21
0.3	1377.3	6314.3	0.93
0.4	455.5	599.3	1.093
1	16.12	80.65	2.1
1.2	30.69	13.32	1.1
1.5	2.12	4.52	1.81

- Maximum bending angle – 140°

For comparative purposes the initial modulus, deformation to break and tensile strength was evaluated by Instron device at rate of deformation 0.5 min^{-1} (see Table 23.5).

In Table 23.6 the arithmetic means of numbers of repeated flexing cycles till break FC_M of Hypof fibers corresponding standard deviations S_{FC} and variation coefficients CV_{FC} calculated by standard manner (as moment estimators) are given.

The rough estimators of Weibull distribution parameters calculated from Eqs. (23.35), (23.36), and (23.37) are given in Table 23.7.

It is visible that the higher fiber diameter leads to the decrease of lowest number of repeated flexing cycles till break A and corresponding scale parameter B.

The mean number of repeated flexing cycles $E(\text{FC})$ and corresponding standard deviation SD(FC) can be now computed from the following equations:

$$E(\text{FC}) = A + B\,\Gamma\left(1 + \frac{1}{C}\right) \tag{23.38}$$

$$\text{SD(FC)} = E(\text{FC})\left(\frac{\Gamma\left(1 + \frac{2}{C}\right)}{\Gamma^2\left(1 + \frac{1}{C}\right)} - 1\right)^{\frac{1}{2}} \tag{23.39}$$

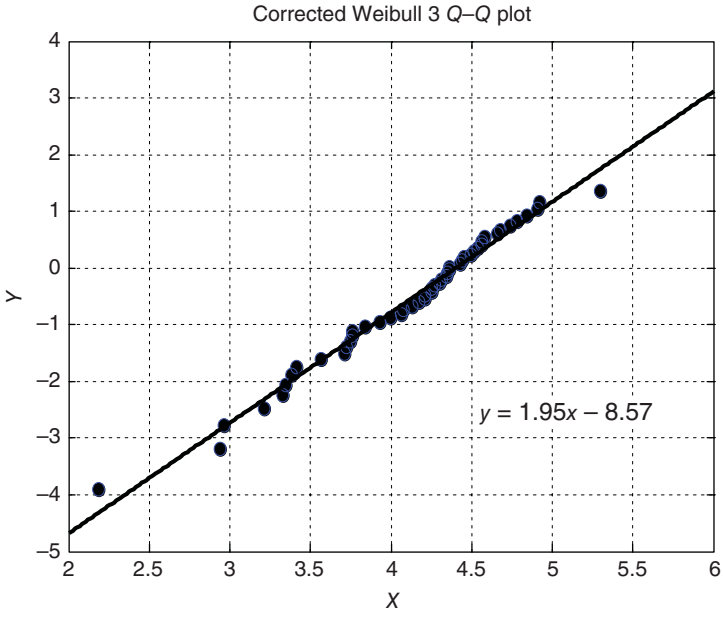


Figure 23.46 Weibull *Q*–*Q* plot for Hypof 1 mm.

The typical *Q*–*Q* plot for Hypof (diameter of 1 mm) is shown in Figure 23.46. It is visible that the linearity is relatively good. This plot for all investigated fibers was approximately linear, which is proving the usefulness of Weibull distribution.

It is interesting to compare mean number of repeated flexing cycles till break FC_M with fiber flexibility F_l (see Eq. (23.25)) calculated from measured initial modulus. The dependence of $\log(F_l)$ on $\log(FC_M)$ is shown in Figure 23.47.

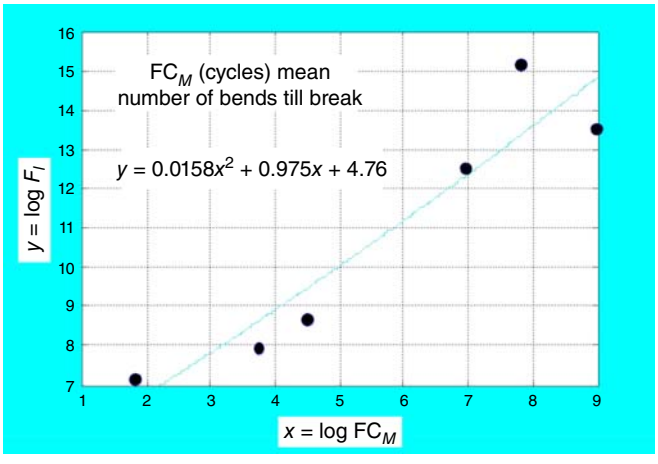


Figure 23.47 The dependence of $\log(F_l)$ on $\log(FC_M)$.

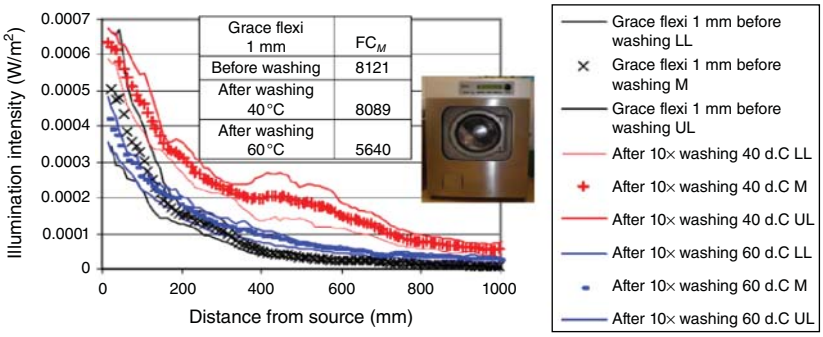


Figure 23.48 Change of attenuation and FC_M of SEPOF due to repeated washing.

It is visible that the flex fatigue characteristic FC_M is the increasing function of flexibility parameter. From corresponding quadratic fitting, the empiric equation

$$\ln(F_l) = 0.0158[\ln(FC_M)]^2 + 0.975\ \ln(FC_M) + 4.76$$

was found.

The fatigue characteristic FC_M can be used for characterization of changes of mechanical response to external influences. For SEPOF brand Grace flexi, this characteristic *is* used as indication of *changes* in mechanical characteristics due to repeated washing (see Figure 23.48).

It is clear that the washing is changing structure (loss of FC_M) and amount of illumination intensity as well (in details see Ref. [29]).

The transmission rate through a POF also depends on some mechanical properties [35]. For example, if the POF is elongated till 10% of its length, the attenuation increases about less than 0.1 dB. Regarding other factors that can change the POF optical properties, cyclic bending can also cause variations in the attenuation, up to a certain limit 0.15 dB for 1000 bending times with a bending radius of 50 mm, in the case of 1 mm PMMA POF [80].

23.5.3 Thermal Properties

Standard POF can be used in working conditions at temperatures up to 80–110 °C. At higher temperatures the POFs lose their transparency. The working temperature can be increased to 125 °C or to 135 °C by using jackets made from more temperature-resistant materials [2–6].

It is known that amorphous polymers including PMMA exhibit anisotropic thermal expansion dependent on the polymer processing history. The thermal expansion coefficient is lower in the direction of the fiber axis than in the perpendicular direction. Such anisotropic behavior of polymers can also be expected in the fiber core material PMMA. Changes of POF surface structure composed of PMMA core and fluoropolymer cladding are due to thermal exposition.

In connection with the absorption of humidity, the thermal aging that occurs at high temperatures is the essential mechanism influencing the durability of POFs.

Thermal aging leads to the decomposition effects as a consequence of the polymer chain splitting by the energy of heat.

With PMMA there is particular risk of depolymerization, i.e. splitting off of end groups and the loosening of monomer components from the end of the chain.

During the depolymerization, free radicals are formed. They can react with oxygen and promote degradation by thermooxidation. The consequence is brittleness and disintegration, with a direct effect on the mechanical and optical properties of the POF.

Takezewa et al. [78] have investigated the effects of high-temperature (150 °C) exposure of cross-linked PMMA-based POF and found that oxidative degradation products of the core polymer cause an increase of the optical loss by light absorption. Schartel et al. [79] have studied the thermooxidative degradation behavior of PMMA-based silica POF. They have found that the optical transmission stability of POF is most likely to be governed by the thermooxidative stability of the core.

The resistance of some POF to higher temperatures strongly depends on the air relative humidity RH as well. For example, if the PMMA core POF is maintained at 85 °C with 85% of relative humidity for 1000 hours, the attenuation will increase in 0.02 dB/km. If the relative humidity level is around 90%, the attenuation increases more than 0.03 dB/m [33].

Model for the deterioration of the optical transmission under high temperature and humidity was proposed in Ref. [6]. According to this model, the loss of optical transmission of silica POF (cables) occurs in four phases: first phase characterized by a definite loss of transmission within a short period (25–50 hours), second phase characterized by a very slow deterioration of transmission, third phase characterized by rapid decline in the transmission, and finally fourth phase characterized by increase of the transmission to a higher level when the humidity is varied while the temperature is kept constant. This behavior is due to the strong OH^- absorption band in the visible range. The anisotropic nature of PMMA core fibers due to the orientation of polymer chains was found [77]. Therefore the more expansion in the transversal direction than in the longitudinal direction of POF can be predicted. The anisotropic behavior of expansion of polymers can be visible when they are heated to their T_g and then cooled down.

Therefore the observed significant increase of the POF diameter and a contraction of their length should be due to plasticizing effects of water in the core of POF. It is known that water in POF reduced their T_g by increasing the chain mobility. As a result the expansion occurred in a faster rate than it would take place when exposing to dry conditions. The plasticizer effect is irreversible because the observed expansion (diameter and contraction of length) and brittle nature of the cooled POF are an indication of the occurrence of molecular disorder [32].

23.6 Illumination Systems Using POF

Direct application of POF for embedding into textiles or creation of line lighting systems is not so easy. POFs are created from polymeric materials that

are sensitive to surface damage, their mechanical properties are not as good as properties of synthetic fibers, durability in standard conditions of use is limited, they are degraded under UV radiation and sensitive to moisture, and their comfort properties including hand (touch) and drape are generally bad. Some negative characteristics of POF can be suppressed by proper selection of jacket, but it is not sufficient for their effective application especially for direct embedding into the textile structures.

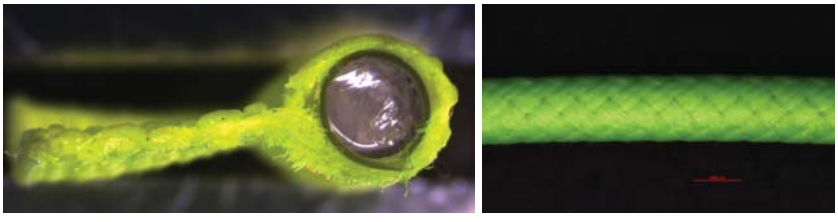
In bent state, POF structure is subjected to plastic deformations and repeated multiaxial deformation during use, which can deteriorated their properties. Each optical fiber should have delivery of light, which is serious limitation for using multiple fibers in wider areas.

For SEPOF it is possible to have sufficient side illumination in straight state, and all kinds of deformation appeared due to necessities to form textile products mainly. There is a continuous effort to increase the side emission by using dopants as fluorescent or luminescent dyestuffs. Direct dyeing of POF is complicated due to changes of their structure and negative influence on their properties. One solution on how to avoid these problems with SEPOF is to use so-called LIHS composed from SEPOF in core and cover (textile tube) from textile material [18, 29, 44]. This layer can be prepared by weaving, knitting, braiding, etc. [18, 29, 44]. Textile structures containing embedded side-emitting POF, i.e. LIHS, have the following benefits:

- Enhancing illumination intensity by selection of textile layer composition and surface dopants
- Protection of LIHS against weather including UV and combination of temperature/moisture
- Enabling LIHS standard maintenance during use as washing
- Suppression of mechanical damage as abrasion and sensitivity to repeated multiaxial deformation
- Simplification of attachment of LIHS into textiles by standard techniques as sewing

Typical structure of LIHS is shown in Figure 23.49.

It is visible that beside of the textile tube covering the SEPOF, the tape is created. This tape is enabling the simple attachments to supporting material in the case of side illumination or sewing into seems in the case of textile products. Comparison



(a) (b)

Figure 23.49 Device for flex fatigue measurements. (a) Picture and (b) schematic arrangement.

of SEPOF and LIHS containing the same SEPOF active illumination is shown in Figure 23.50.

For quantitative comparison of SEPOF and LIHT side illumination, the attenuation profiles were created. Illumination intensity as function of distance from source for POF and the same POF embedded into textile tube are shown in Figure 23.51.

It is visible that LIHS (SEPOF in textile cover) is producing higher side emission intensity in comparison with SEPOF only.

LIHS can be incorporated into a variety of textile structures as labels, strips and bands, cords, special patches, woven fabrics, and knitted structures.

Each structure containing LIHS needs to have lighting system and power supply. The resulting complex system can be constructed as easily attachable to various fabrics and easily removable. Components of side illumination system containing LIHS (SEPOF and textile cover) are shown in Figure 23.52.

The light source is critical for obtaining sufficient side emission for creation of safety textiles, fashion purposes, and line lighting.

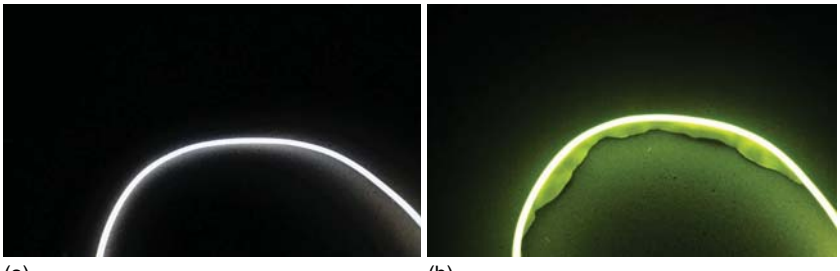


Figure 23.50 Active illumination by (a) SEPOF and (b) LIHS.

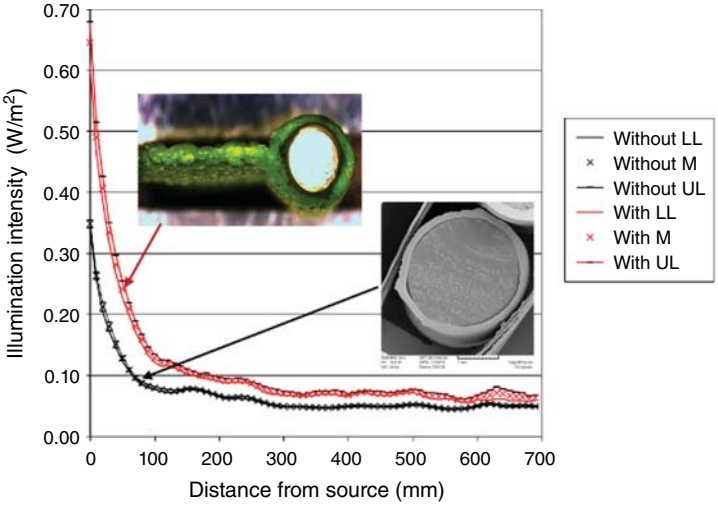


Figure 23.51 Side illumination intensity of SEPOF and LIHS.

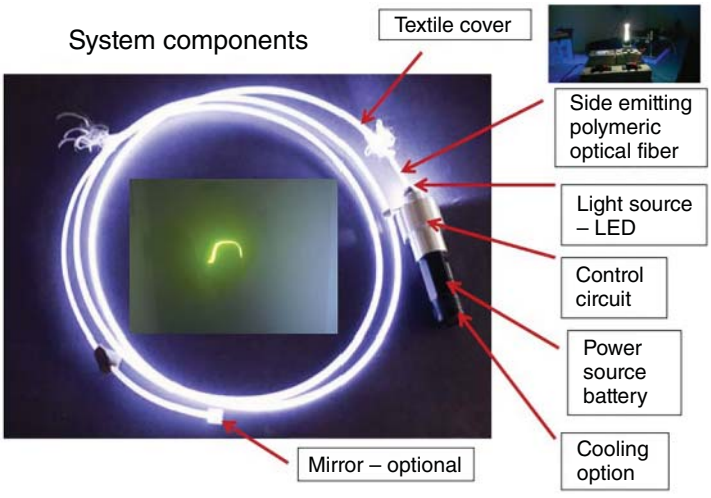


Figure 23.52 System components for side illumination.

As effective source of light with directional output, the LEDs are used for all kind of applications. The comparison of light outputs from incandescent bulb, compact fluorescent light bulb, and LED is shown in Figure 23.53.

The comparison of some characteristics of these sources of illumination is shown in Table 23.8.

The use of LED leads to considerable savings in the use of electrical power and, in addition, lowers maintenance costs. The LED lifetime is the time in which the brightness of 50% of a sampling of LEDs decreases by 30% of its incipient value,

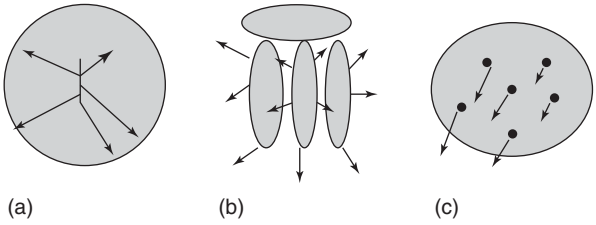


Figure 23.53 Light output from typical sources of illumination [81]. (a) Incandescent, (b) CFL, and (c) LED. Source: Held 2009 [81]. Reproduced with permission of Taylor & Francis.

Table 23.8 Selected characteristics of typical sources of illumination.

Characteristics	Incandescent bulb	CFL	LED
Life (h)	750	7 500	60 000
Equivalent number of bulbs	80	8	1
Electric power (W) for 1100 lm	100	20	9
Effectivity (lm/W)	11	55	122

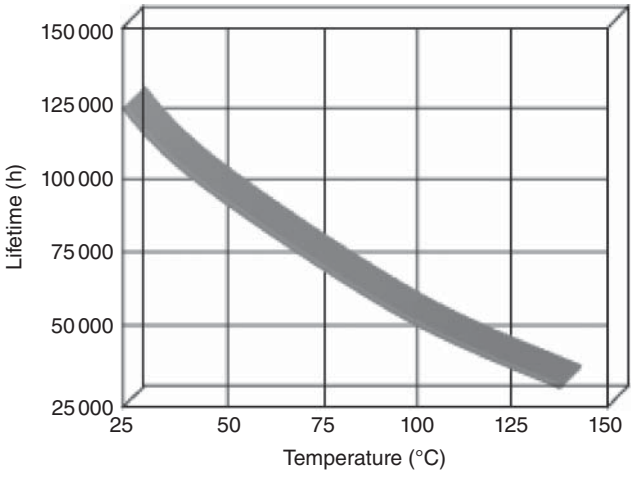


Figure 23.54 Influence of temperature on the lifetime of LED.

that is, drops down to 70% of the brightness in the beginning. The LED lifetime is approximately exponentially decreasing with increase of temperature as is shown in Figure 23.54.

During lighting by using LED, temperature is rising till 60–80 °C in two to three minutes, and after this, it is nearly constant. This temperature can be reduced by selection of cover of illumination unit and its construction. The best portable powering structures have maximum temperature due to lighting significantly lower than 50 °C.

Based on the comprehensive testing and refinements, one-chip LED with power in the range of 1–3 W was selected as light source. These LED delivers optical power in the range of 40–120 lx/m, which is sufficient to illumination by SEPOF till length of several meters. At the same time such LED have small size, and the heat generation is manageable despite the smaller size of the light source unit. The typical attachment of LED for two branches illumination purpose is shown in Figure 23.55.

Selection of energy source depends on the LED used and on the application area. Recent very quick development of portable energy sources based on hard or flexible miniature batteries for wearable electronics including sensing, heating, and lighting applications is promising for future. It will be interesting to try to check the energy harvesting from mechanical vibrations, thermoelectric effect, solar power, etc. Some of currently available portable powering structures for LIHS are shown in Figure 23.56.

There are plenty of different types of rechargeable batteries in current market suitable for use in powering structure for LIHS. Only few of them are here mentioned.

Lithium-ion (Li-ion) batteries were the good choice of battery for powering consumer electronics due to their high energy and power density and stable electrochemical performance. Batteries have high capacity (mAh) and energy density, but they are bulky and nonflexible. For the fabrication of flexible batteries,

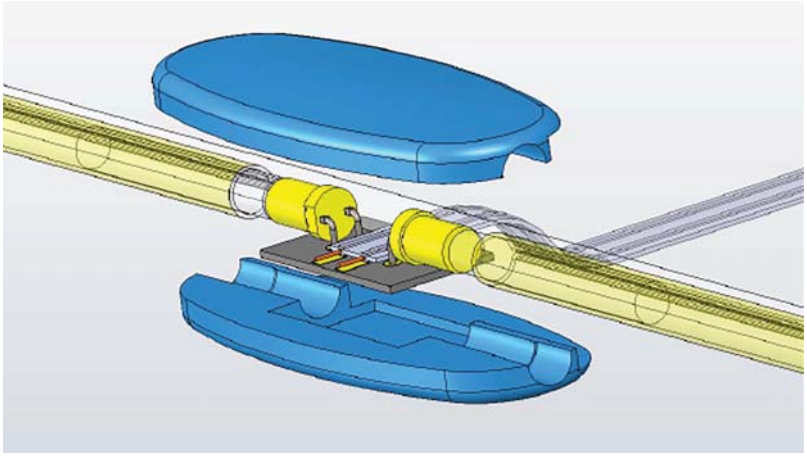


Figure 23.55 Attachment of LED for two branches of SEPOF.

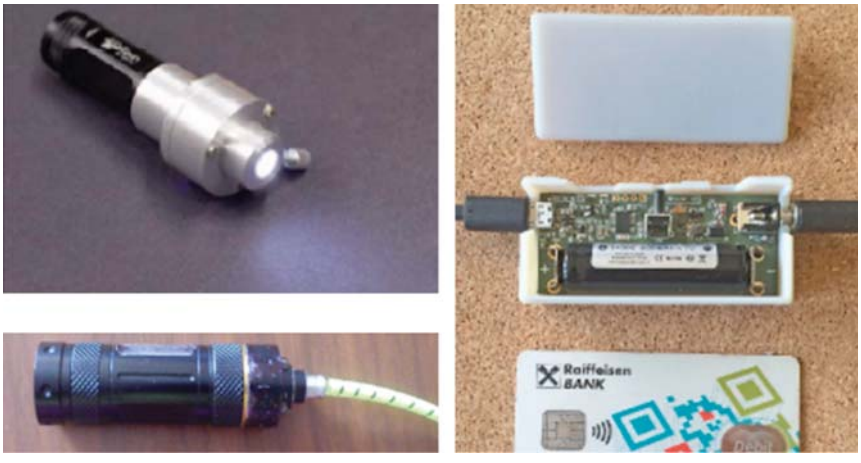


Figure 23.56 Some portable powering structure for LIHS.

a thin-film configuration is adopted where single layers of anode, separator, and cathode are stacked together and sealed within a flexible encapsulation.

Main limitations of these batteries are as follows:

- Requires protection circuit to maintain voltage and current within safe limits
- Subject to aging, even if not in use – storage in a cool place at 40% charge reduces aging effect
- Expensive to manufacture – about 40% higher in cost than nickel–cadmium
- Fire hazard because electrolyte is organic solvent

Alternates are LiPol batteries with high-energy density (20% more than classical Li-ion batteries). Their flexible cover causes high reduction of total mass.

Low self-discharge nickel–metal hydride (Ni–MH) rechargeable batteries Eneloop Plus have a thermistor built-in that cuts the power in case the batteries

are overheating. This makes them especially suitable for toys and devices, which generate an increased amount of heat. AA size has 1900 mAh minimum capacity. The discharge rate holds 90% up to one year and approx. 70% after five years. Number of recharge: 1800 times.

Lithium phosphorus oxynitride electrolyte (LiPON), deposited as amorphous thin (2 μm) film is used in all-solid-state micro-batteries. The capacity loss is negligible during 100 charge and discharge cycles [82].

23.7 LIHS Applications

LIHS can be used for creation of safety textiles, fashion purposes, and line lighting. Safety textiles containing LIHS have these main advantages:

- The object shape is highlighted directly, which significantly reduce the risk of incorrect interpretation of their size.
- Side emission is not dependent on the conditions of external exposure (typically vehicle headlights); these active lighting systems operate well in darkness.
- There is no glare disturbing, e.g. road users.

Due to full integration into the fabric, SEPOF are protected against environmental influences (moisture, UV radiation). It is simple to use reflective or fluorescence colors for dyeing or coating outer textile layer enhancing diffusion scattering.

The simple removal of power/light source enables treatment of textiles according to standard procedures. Based on the practical testing, the following care rules were specified:

- Gentle machine wash, moderate mechanical treatment, rinses, and spin drying
- Do not bleach with chlorine
- Do not iron
- Can be cleaned with perchlorethylene,
- Do not tumble dry

The examples of application of systems containing LIHS for clothing and accessories are shown in Figure 23.57.

Line lighting systems based on LIHS have the following advantages:

- Can be used for line illumination of complicated ways and significantly reduce the local variation of light intensity
- Low cost of lighting on the level of illumination standards
- Not local over lighting
- Intensity of light is controlled by voltage
- Simple connections to permanent or portable electricity sources
- Simple branching of line lighting
- Maintenance according to standard procedures

Line lighting systems based on LIHS can be used for

- setting of limits (parking barriers, end of carpets, stairs, etc.),



Figure 23.57 Systems using LIHS for accessories.

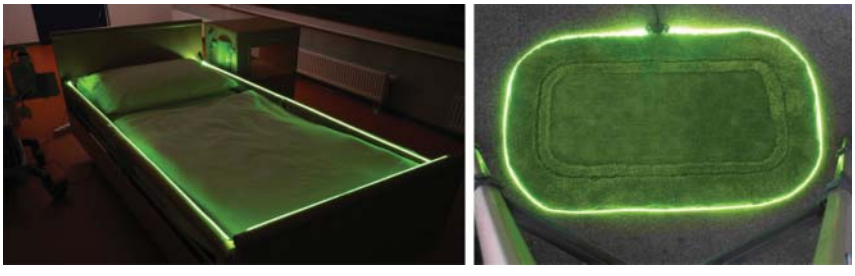


Figure 23.58 Systems using LIHS for line illumination.

- emergency lighting (hospitals, hotel, dormitories, supermarkets),
- lighting in corridors, lifts, edge visualization, etc.

The example of line lighting is in Figure 23.58.

23.8 Conclusion

The emphasis of POF is focused on reduction of attenuation coefficient and increase in thermal stability mainly. For example, PC, silicone resin, cross-linked acrylic acid, and copolymer can be used to increase the thermal stability up to 125–150 °C. Plastic optical fibers applied in illumination and decorations are as follows [83]:

- End-emitting optical fiber POF are mainly using the lighting effect of the end face of fibers to achieve decorative lighting. The fibers have many applications, such as, using endpoints to form various patterns and simulate star blinking effect – as if going into fairyland, making a variety of technological models to create an atmosphere for entertainment, and making Christmas tree more attractive and advertising signs graceful, in order to increase the noble mystery of artifacts and jewelry.
- Side-emitting optical fiber SEPOFs are easy to be used to set off the outline of patterns of objects and produce a variety of artistic design.

- Flash point optical fiber is used to make special effect. These fibers can be made into fiber-optic curtains, fiber-optic waterfall, and other fiber-optic craft products.

Recently, the POF and SEPOF technology has been developing quickly; the applications have been recognized in many branches. The LIHS are still in the first stage of industrial realization, and it will be necessary to optimize their composition and functionality for various targeted applications including surface effects, doping, and use of special dye stuffs. The system of creation of illumination intensity profiles (see Figure 23.45) will be simple tool for evaluation of new effects and optimization of LIHS-based systems. Probably the most important element for efficient low cost active illumination system creation is the battery. Limits are flexibility, power, size, weight, and price.

References

1 Bunge, C.A. et al. (eds.) (2017). *Polymer Optical Fibres Fibre Types, Materials, Fabrication, Characterisation and Applications*. Elsevier Amsterdam.
2 Koike, Y. (2015). *Fundamentals of Plastic Optical Fibers*. Weinheim: Wiley-VCH.
3 Bäumer, S. (ed.) (2010). *Handbook of Plastic Optics*. Weinheim: Wiley-VCH.
4 Harmon, J.P. and Noren, G.K. (eds.) (2001). *Optical Polymers Fibers and Waveguides*. Washington, DC: American Chemical Society.
5 Kuzyk, M.G. (2007). *Polymer Fiber Optics Materials, Physics, and Applications*. Boca Raton, FL: CRC Press.
6 Daum, W. et al. (2002). *POF - Polymer Optical Fibers for Data Communication*. Berlin: Springer-Verlag.
7 Thévenaz, L. (ed.) (2011). *Advanced Fiber Optics Concepts and Technology*. Lausanne: EPFL Press.
8 Nyu, T. et al. (1995). Experiments on 156 Mbps-100 m transmission using 650 nm LED and SI POF. In: *Proceedings of the 4th International Conference on Plastic Optical Fibres and Applications POF'95*, 119–121. Boston, MA.
9 Numata, K., Furusawa, S., and Mirikura, S. (1999). Transmission characteristics of 500 Mbs optical link using 650 nm RC-LED and POF. In: *Proceedings of the 8th International Conference on Plastic Optical Fibres and Applications POF'99*, 74–77. Chiba, Japan.
10 Koike, Y., Ishigure, T., and Nihei, E. (1995). High-bandwidth graded index polymer optical fiber. *Journal of Lightwave Technology* 13: 1475.
11 Matias, I.R. et al. (eds.) (2017). *Fiber Optic Sensors Current Status and Future Possibilities*. Springer International Publishing Switzerland.
12 Bartlett, R.J. et al. (1998). Plastic optical fibers sensors and devices. In: *Proceedings of the 7th International Conference on Plastic Optical Fibres and Applications POF'98*, 245–246. Berlin, Germany.
13 Schilk, A.J. and Bowyer, T.W. (1995). The use of scintillating plastic optical fibers for the detection of radioactive contamination. In: *Proceedings of*

the 4th International Conference on Plastic Optical Fibres and Applications POF'95, 171–176. Boston, MA.

14 Marcuse, D. (1974). *Theory of Dielectric Waveguides*, 75–80. San Diego, CA: Academic Press.

15 Snyder, A.W. and Love, J.D. (1983). *Optical Waveguide Theory*, 2e. London: Chapman and Hall.

16 Zajkowski, M. (2002). Emission of flux light in 'side light' fiber optic. *Proceedings of SPIE* 5125: 322–327.

17 Zajkowski, M. (2005). Luminous flux emission calculation analysis in side light illumination optical fibres. *Proceedings of SPIE* 5775: 440–445.

18 Křemenáková, D., Militký, J., Meryová, B., and Lédl, V. (2012). Testing and characterization of side emitting polymer optical fibers. In: *International Symposium TBIS*. Ueda, Japan: Shinshu University.

19 Stickler, M. and Rhein, T. (2005). Polymethacrylates. In: *Ullamann's Encyclopedia of Industrial Chemistry*, Weinheim: Wiley-VCH Verlag GmbH & Co. KGaA. 10.1002/14356007.a21 473.

20 Wunderlich, W. (1989). Physical constants of PMMA. In: *Polymer Handbook* (eds. J. Brandrup and E.H. Immergut). Wiley.

21 Harlin, A., Makinen, M., and Vuorivirta, A. (2003). Development of polymeric optical fiber fabrics as illumination elements and textile displays. *AUTEX Research Journal* 3: 1–8.

22 Spigulis, J. et al. (1996). The 'glowing' optical fiber designs and parameters. *Proceedings of SPIE* 2967: 231–236.

23 Koncar, V. (2005). Optical fiber fabric displays. *Optics & Photonics News* 16 (4): 40–44.

24 Franklin, J.B., Smith, G.B., and Joseph, K.J. (2004). Side-scattering polymer light guide and method of manufacture. US Patent No. 0196648.

25 Joseph, E.K., Franklin, J.B., and Smith, G.B. (2006). Side-scattering light guides. US Patent No. 2006140562.

26 Im, M.H. (2007). Modification of plastic optical fiber for side-illumination. In: *Human-Computer Interaction, Part II* (ed. J. Jacko), 1123–1129. Berlin, Heidelberg: Springer-Verlag.

27 Šesták, J. and Militký, J. (2013). Selected properties of functional materials. In: *Background of Fiber Optics*, Chapter 5 (eds. D. Křemenáková et al.). Pilzen: OPS Kanina Publ. House.

28 Huang, J. et al. (2013). Selected properties of functional materials. In: *Review on Polymeric Optical Fibers*, Chapter 6 (eds. D. Křemenáková et al.). Pilzen: OPS Kanina Publ. House.

29 Křemenáková, D. et al. (2013). Selected properties of functional materials. In: *Characterization of Side Emitting Polymeric Optical Fibres Illumination Intensity*, Chapter 7 (eds. D. Křemenáková et al.). Pilzen: OPS Kanina Publ. House.

30 Militký, J. and Křemenáková, D. (2013). Selected properties of functional materials. In: *Flex Fatigue of Side Emitting Polymeric Optical Fiber*, Chapter 8 (eds. D. Křemenáková et al.). Pilzen: OPS Kanina Publ. House.

31 Mishra, R. et al. (2013). Selected properties of functional materials. In: *Surface Modification of Polymer Optical Fibers for Enhanced Side Emission*

Behavior, Chapter 9 (eds. D. Křemenáková et al.). Pilzen: OPS Kanina Publ. House.

32 Appajaiah, A. (2005). Climatic stability of polymer optical fibers (POF). BAM-Dissertationsreihe Band 9 Berlin.

33 Zubia, J. and Arrue, J. (2001). Plastic optical fibers: an introduction to their technological processes and applications. *Optical Fiber Technology* 7: 101–140.

34 Militký, J. and Křemenáková, D. (2012). Flex fatigue of polymeric optical fibers. In: *41st TRS – Textile Research Symposium*. Guimarães, Portugal: University of Minho (12–14 September 2012).

35 Guerrero, H. et al. (1998). Mechanical properties of polycarbonate optical fibers. *Fiber and Integrated Optics* 17: 231.

36 Zubia, J. et al. (1997). Theoretical analysis of the torsion induced optical effect in plastic optical fibers. *Optical Fiber Technology* 3: 162.

37 Blyler, L. (1999). Material science and technology for POF. In: *Proceedings of the 8th Conference on Plastic Optical Fibers and Applications POF'99*, 196–200. Chiva, Japan.

38 Information Gatekeepers (1993). *Plastic Optical Fiber POF Data Book*, 47–49. Information Gatekeepers.

39 Anonym. *CYTOP™ Technical Information*. AGC Chemicals Europe http://www.agcce.com/cytop-technical-information/.

40 Liu, H.Y. et al. (2002). Thermal stability of gratings in PMMA and CYTOP polymer fibers. *Optics Communications* 204: 151–156.

41 De Torres, M.C.P. (2013). Dispositivos fotonicos de medida basados en fibra optica de polımero. Thesis Universidad de Alcala, Chapter 2.

42 Crisp, J. (2001). *Introduction to Fiber Optics*. Oxford: Butterworth-Heinemann.

43 Masuda, A. et al. (2006). Optical properties of woven fabrics by plastic optical fibers. *Journal of Textile Engineering* 52: 93–97.

44 Křemenáková, D. et al. (2012). Characterization of side emitting polymeric optical fibres. *Journal of Fiber Bioengineering & Informatics* 5 (4): 423–431.

45 Lédl, V. and Václavík, J. (2009). Device for Evaluating the Side Emitting Optical Fiber Illumination Intensity. Report TU Liberec December 2009.

46 Meloun, M. and Militky, J. (2012). *Statistical Data Analysis*. New Delhi: Woodhead.

47 Yokogawa, H. et al. (2000). Side face illuminating optical fiber. US Patent 6, 154, 595.

48 King, J.C. et al. (1996). All-silica single-mode optical fiber with photonic crystal cladding. *Optics Letters* 21: 1547–15489.

49 Gauvreau, B. et al. (2008). Color-changing and color-tunable photonic bandgap fiber textiles. *Optics Express* 16 (20): 15677–15693.

50 Johnson, S.G. et al. (2001). Low-loss asymptotically single-mode propagation in large core OmniGuide fibers. *Optics Express* 9: 748.

51 Appajaiah, A., Kretzschmar, H.J., and Daum, W. (2007). Aging behavior of polymer optical fibers: degradation characterization by FTIR. *Journal of Applied Polymer Science* 103: 860–870.

52 Takezawa, Y. et al. (1992). Empirial estimation method of intrinsic loss spectra in transparent amorphous polymers for plastic optical fibres. *Journal of Applied Polymer Science* 46: 1835–1841.

53 Sillyman, S. (2004). a kol.: Source numerical aperture control for efficient light emission from notched, side-lighting fiber optics. *Proceedings of SPIE* 5529: 70–78.

54 Zarian, J.R. et al. (1999). Side lighting optical conduit. US Patent 5, 987, 199, 16 December 1999.

55 Endruweit, A. et al. (2008). Spectroscopic experiments regarding the efficiency of side emission optical fibres in the UV-A and visible blue spectrum. *Optics and Lasers in Engineering* 46: 97–105.

56 Spigulis, J. and Pfafrods, D. (1997). Clinical potential of the side-glowing optical fibers. *Proceedings of SPIE* 2977: 84–88.

57 Matthewson, M.J. and Kurkjian, C.R. (1987). Static fatigue of optical fibers in bending. *Journal of the American Ceramic Society* 70: 662–668.

58 Arrue, J. et al. (1998). Light power behavior when bending plastic optical fibers. *IEEE Proceedings - Optoelectronics* 145 (6): 313.

59 Measures, R.M. (2001). *Structural Monitoring with Fiber Optic Technology*. San Diego, CA: Academic Press.

60 Hecht, E. (2017). *Optic*. Boston, MA: Pearson.

61 Peters, K. (2011). Polymer optical fiber sensors – a review. *Smart Materials and Structures* 20: 013002 (17 pp).

62 Endruweit, A., Long, A.C., and Johnson, M.S. (2006). Textile composites with embedded optical fibers. In: *8th International Conference on Textile Composites (TEXCOMP-8)*. Nottingham, UK.

63 Meloun, M. and Militký, J. (2011). *Experimental Data Treatment*. New Delhi: Woodhead Publishing.

64 Peirce, F.T. (1937). The geometry of cloth structure. *Journal of the Textile Institute* 28: T45–T196.

65 Wang, J. et al. (2013). Effect of weave structure on the side-emitting properties of polymer optical fiber jacquard fabrics. *Textile Research Journal* 83: 1170–1180.

66 Fu, H.J. and Chen, M.X. (1993). Effect of bending on optical fiber numerical aperture. *Opt. Commun.* 65: 59–61.

67 Yao, S. et al. (2011). Transmission efficiency of bending fiber with small radius. *Acta Optica Sinica* 31 (01): 06001.

68 Křemenáková, D. et al. Textile sheath containing side-emitting optical fibre. EP 2917391, pending.

69 Givoletti, M. (2001). Textile product containing optical fibres. EP 1307687B1.

70 Behera, B.K. et al. (2012). *Modeling of Woven Fabrics Geometry and Properties: Woven Fabrics*, Chapter 2 (ed. H.Y. Jeon). Rjeka: Intech.

71 Shen, J. et al. (2013). Light-emitting fabrics integrated with structured polymer optical fibers treated with an infrared CO_2 laser. *Textile Research Journal* 83 (7): 730–739.

72 Huang, J. et al. (2015). Evaluation of illumination intensity of plastic optical fibers with TiO_2 particles by laser treatment. *AUTEX Research Journal* 15 (1): 13–18.

73 Chepelyuk, E. et al. (2010). Geometric disposition of threads in single-layer woven structures. *International Journal of Clothing Science and Technology* 22: 35–48.

74 Barnoski, M.K. et al. (2001). *Fundamentals of Optical Fiber Communication*. Academic Press.

75 Jay, J.A. (2010). *An Overview of Macrobending and Microbending of Optical Fibers*. New York: Corning Inc.

76 Mallinder, F.P. and Proctor, B.A. (1964). Elastic constants of fused silica as a function of large tensile strain. *Physics and Chemistry of Glasses* 5 (4): 91–103.

77 Dugas, J. and Maurel, G. (1992). Mode-coupling processes in polymethyl methacrylate-core optical fibers. *Applied Optics* 31: 5069–5079.

78 Takezewa, Y. et al. (1991). Analysis of thermal degradation for plastic optical fibers. *Journal of Applied Polymer Science* 42: 2811–2817.

79 Schartel, B. et al. (1999). Chemiluminescence: a promising new testing method for plastic optical fibers. *Journal of Lightwave Technology* 17 (11): 2291–2296.

80 Boston Optical Fiber (2000). *Raytela Polymer Optical Fiber Cord, Toray Industries*. "OptiMega and OptiGiga".

81 Held, G. (2009). *Introduction to Light Emitting Diode Technology and Applications*. Boca Raton, FL: CRC Press.

82 Wang, X. et al. (2014). Flexible energy-storage devices. *Advanced Materials* 26 (28): 4763–4782.

83 Mao, Q. (2010). Plastic optical fiber and its application prospect, Communication technology and standards, Expert forum, 9 China.

84 Azadeh, M. (2009). *Fiber Optic Engineering*. Dordrecht: Springer.

24

Fibers as Energy Materials

Jiadeng Zhu, Esra Serife Pampal, Yeqian Ge, Jennifer D. Leary, and Xiangwu Zhang

North Carolina State University, College of Textiles, Department of Textile Engineering, Chemistry and Science, 1020 Main Campus Drive, Raleigh, NC 27695-8301, USA

24.1 Introduction to Fibers as Energy Materials

Renewable energy resources and their devices have received a lot of attention recently, caused by the limited availability and negative environmental impacts of fossil and nuclear fuels. It is also mandatory to develop an efficient storage system to retain all of the energy generated by renewable sources such as solar and wind power [1–3]. In contrast to those intermittent sources, rechargeable batteries and supercapacitors are increasing in importance, and they have become ubiquitous in our daily lives by powering numerous electronic devices, including cell phones, laptops, rechargeable vehicles, etc. [4–6].

Fibrous materials are considered promising candidates for fabricating energy-related systems due to their unique structure and excellent properties [7–9]. In particular, they can be employed as high-performance electrodes and separators in supercapacitors and secondary rechargeable batteries, transparent conductive electrodes or active materials in solar cells, and electrocatalysts for oxygen reduction in fuel cells, to name a few examples [10–15].

This chapter introduces the fundamental principles of energy storage and conversion systems and the applications of fibrous materials in rechargeable batteries and supercapacitors, followed by detailed discussion. It concludes with a comprehensive and up-to-date review of current and future trends for fibers as energy materials.

24.2 Fundamental Principles

Among the various dimensional energy materials, fiber-based 1D materials have attracted much attention due to the unique structure of those fibrous materials that can provide a continuous pathway for either electrons or ions and enhance the kinetic properties of the system [16, 17].

Handbook of Fibrous Materials, First Edition. Edited by Jinlian Hu, Bipin Kumar, and Jing Lu.
© 2020 Wiley-VCH Verlag GmbH & Co. KGaA. Published 2020 by Wiley-VCH Verlag GmbH & Co. KGaA.

24.2.1 Basic Terms Related to Energy

Several basic terms related to energy are explained here to give a basic understanding on the required properties of fibers for use as energy materials. Generally, energy density represents the amount of energy stored in a system (e.g. batteries, fuel cells, supercapacitors) per unit volume (volumetric energy density) or mass (gravimetric energy density). Power density is the amount of power per unit volume or mass. A measure of the density of an electric current is called current density, which is the amount of current per unit area or mass. Capacity and capacitance are the system's ability to store electric charge for batteries and supercapacitors, respectively. Gravimetric specific capacity or capacitance specifies the amount of capacity or capacitance per unit mass. Coulombic efficiency is generally considered as the efficiency of charge or electron transportation in a system promoting an electrochemical reaction.

24.2.2 Principles of Lithium-Ion Batteries

A lithium-ion battery (LIB) is an energy storage system that stores electrical energy based on lithium-ion chemistry. It involves a reversible intercalation/deintercalation of lithium ions during the discharge/charge process. In the first-generation LIBs (Figure 24.1), graphite (C) and layered lithium cobalt dioxide ($LiCoO_2$) have been used as anode and cathode, respectively [18]. The electrolyte, acting as a conductive medium to shuttle lithium ions between the active electrodes, is 1 M lithium hexafluorophosphate ($LiPF_6$) dissolved in a mixture of ethylene carbonate, dimethyl carbonate, and diethyl carbonate with a volume ratio of 1 : 1 : 1. Microporous polyolefin membranes are typically utilized as separators for lithium batteries of this type.

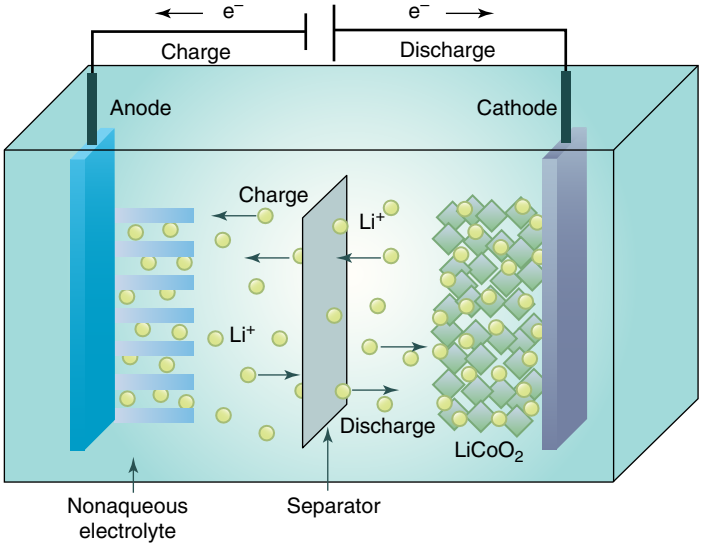


Figure 24.1 Schematic representation of a first-generation Li-ion cell. Source: Reproduced with permission from Roy and Srivastava [18]. Copyright 2014, Royal Society of Chemistry.

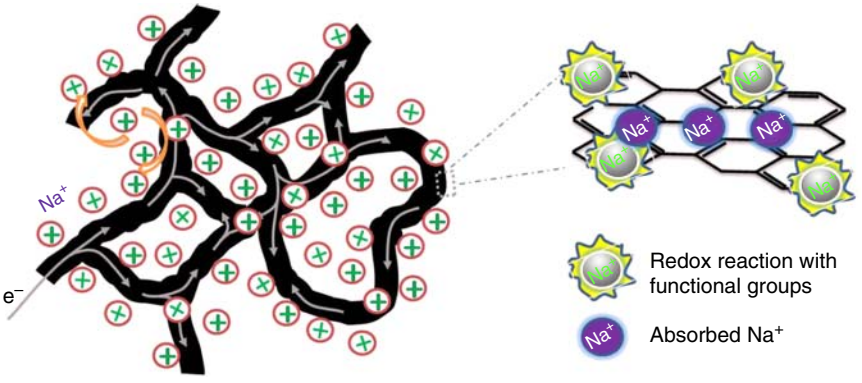


Figure 24.2 Schematic illustration of sodium storage in carbon nanofibers. Source: Reproduced with permission from Wang et al. [19]. Copyright 2013, Elsevier.

The lithium ions move from the anode (C) to the cathode ($LiCoO_2$) during discharge and return back while charging. The reversible reactions during the discharge process can be written as

$$\text{Cathode:} \quad Li_{1-x}CoO_2 + xLi^+ + xe^- \longrightarrow LiCoO_2 \tag{24.1}$$

$$\text{Anode:} \quad Li_xC_6 \longrightarrow xLi^+ + 6C + xe^- \tag{24.2}$$

It is important to note that fibrous electrode material can be beneficial to the electrochemical performance of the devices by shortening the diffusion distance of Li/Na ions and further improving the effective transfer pathway of electrons (Figure 24.2) [19].

24.2.3 Principles of Supercapacitors

Supercapacitors, also called ultracapacitors, are energy devices that store and release energy through charge separation at the electrochemical interface between electrodes and electrolytes. They exhibit high power density, longer cycle life, and rapid charge/discharge ability [20, 21].

There are two main types of supercapacitors. One type, called the double-layer capacitor, achieves energy storage by separation of charge in a Helmholtz double layer, as shown in Figure 24.3 [20]. Generally, the electrodes used for double-layer capacitor are porous carbon materials with high specific surface area. Compared with the infinite planar one, the behavior of electrical double-layer is more complicated since the ion transportation in a confined system can be influenced by many factors, such as the space constrain inside the pores, the tortuous mass transfer path, and the wettability of the pore surface by the electrolyte [20].

The second type is known as a pseudocapacitor, and its electrical energy is obtained by faradaic redox reactions with charge transfer. It can be seen from Figure 24.4 that fast and reversible faradaic reactions occur on the electrode materials when a potential is applied, producing charges and resulting in charge transfer [21]. Pseudocapacitors usually suffer from a severe capacitance decay/fading due to those redox reactions. It is, therefore, important to design a stable structure that can be maintained during cycling.

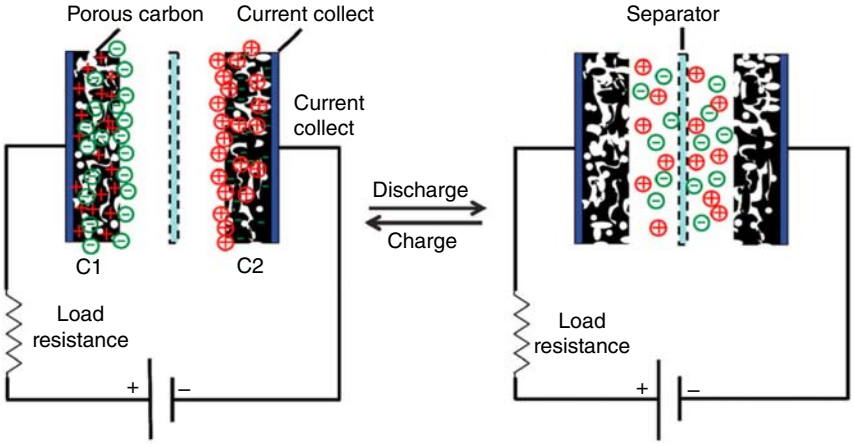


Figure 24.3 Schematic representation of a double-layer capacitor by using porous carbon electrodes. Source: Reproduced with permission from Wu and Xu [20]. Copyright 2014, Royal Society of Chemistry.

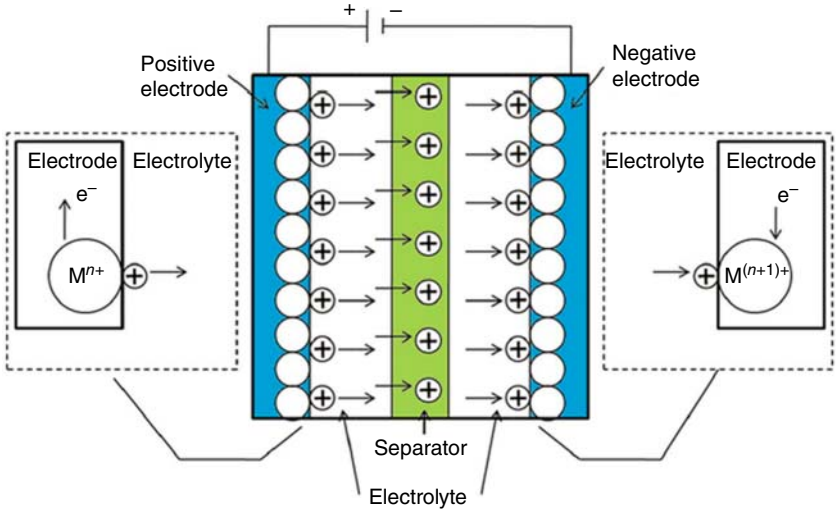


Figure 24.4 Schematic illustration of a pseudocapacitor (M: a metal atom). Source: Reproduced with permission from Shi et al. [21]. Copyright 2014, Royal Society of Chemistry.

24.3 Characterization, Structure, and Fabrication of Fibrous Energy Materials

Some common characterization techniques have been introduced to investigate the physical and chemical properties of energy materials with fibrous structures to pursue better properties. When incorporated into electrodes for electrochemical systems, materials are expected to possess good cycling life and high

energy/power density. In some cases, flexibility is also one of the important factors. One-dimensional fiber structure gives rise to high surface area, short ion diffusion distance, and electron transfer path in electronic devices, thus capturing many researchers' attention. Besides, as separators, membranes are desired to have excellent ion permeability, good wettability, and chemical stability. Meanwhile, they are also characterized as having large porosity, interconnected open pore structure, high electrolyte permeability, and excellent electrolyte uptake. Therefore, fibrous mats are quite promising in contrast to commercial polyolefin membranes [22, 23]. In short, the structure and fabrication of energy materials are extremely critical in this field.

24.3.1 Commonly Used Characterization Techniques for Fibrous Energy Materials

It is well known that both physical and chemical properties of fibrous materials play important roles in determining their final applications. The morphology and diameters of fibrous energy materials can be observed by using scanning electron microscopy (SEM) and transmission electron microscopy (TEM). Their crystal structure and surface areas can be investigated by X-ray diffraction (XRD) and Brunauer–Emmett–Teller (BET), respectively. Thermogravimetric analysis (TGA) and differential scanning calorimetry (DSSC) can be performed to acquire their thermal properties. The composition of fibers can be characterized by using X-ray photoelectron spectroscopy (XPS), elemental analysis (EA), and energy-dispersive X-ray spectroscopy (EDS). Raman spectroscopy is a useful tool for characterizing the carbonaceous structure in carbon-based fibers.

24.3.2 Fibrous Structures of Electrodes

A variety of fibrous structures have been explored in the pursuit of obtaining the perfect construction, including carbon fibers, fiber composites, core–shell and tubular structure fiber, and porous fibers [24–26]. Here, we introduce some typical fibrous structures.

24.3.2.1 Continuous Fibers

The continuous fiber network of carbon fiber possesses large surface area and good mechanical properties, extending the electron transfer pathway. Therefore, carbon fibers have great potential to be applied as electrodes for advanced energy storage systems [27]. Zhu et al. have produced continuous nitrogen-doped carbon nanofibers (N-CNFs) derived from polyacrylonitrile (PAN), which were subsequently used as anode materials for sodium-ion batteries by electrospinning and thermal treatment. The prepared N-CNFs have a diameter of 150–250 nm [24]. It provided an efficient and uninterrupted electron transport and enhanced ion transport and storage capability, shown in Figure 24.5.

24.3.2.2 Carbon Fibers Containing Nanoparticles

It is well known that the conventional method of electrode preparation by mixing active material with conductive agent and binder can reduce the mass loading

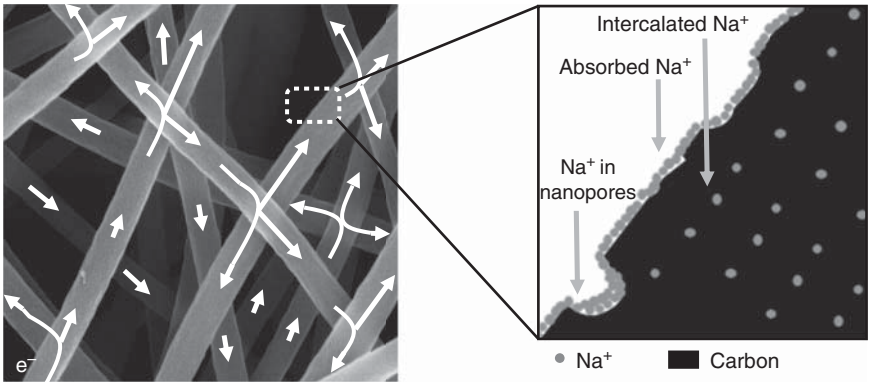


Figure 24.5 Schematic illustration of sodium storage mechanism in N-CNFs. Source: Reproduced with permission from Zhu et al. [24]. Copyright 2015, Elsevier.

and specific capacity of the electrode. On the other hand, by impregnating active material into carbon fiber matrix by electrospinning, the electrode can be used as flexible and binder free. Especially, while silicon is used as the anode, it has a large volume change during charge–discharge process, which is suppressed by using carbon fiber matrix as a buffer to confine the volume change [28]. Ji and Zhang have introduced a framework of Si/carbon nanofiber (Si/CNF), where Si nanoparticles were embedded in carbon nanofibers (CNFs). This composite was obtained by electrospinning from the mixture of Si nanoparticles and PAN solution with subsequent heating process. This anode material demonstrated the advantage of using carbon matrix in terms of its cycle life as well as the active Si (high lithium-storage capacity) [29].

What's more, some active materials such as metal oxides have low electrical conductivity, but when combined with CNF, the electrical conductivity can be significantly enhanced. Ge et al. have prepared copper-doped $Li_4Ti_5O_{12}$/CNF composite by electrospinning with subsequent process, where poly(vinylpyrrolidone) (PVP) was used as the carbon source. The prepared composite demonstrated consistent fibrous structure in the diameter of 200–600 nm (Figure 24.6). Within the carbon fiber matrix, copper-doped $Li_4Ti_5O_{12}$ particles with a grain size of 50 nm were uniformly distributed [30].

Core–shell structure is another approach to combine inorganic components with CNF. Li et al. designed Si/C–C core–shell nanofiber structure by dual nozzle coaxial electrospinning with carbonization process and used these as anode in LIBs. As shown in Figure 24.7, the core was filled with Si/C composite and covered with carbon as the shell. The carbon shell served as buffer to confine the large volume expansion of Si/C core during the lithiation process [31].

24.3.2.3 Porous and Tubular Fibers

Generally, porous fiber structure and tubular fiber structure are made by eliminating the sacrificial components in the fiber to create hollow space, which could provide high surface area and thus enhance the electrochemical properties of

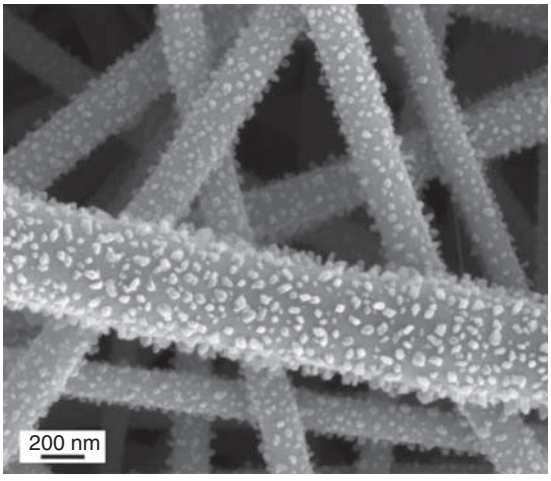


Figure 24.6 SEM image of $Li_{3.95}Cu_{0.05}Ti_5O_{12}$/CNFs. Source: Reproduced with permission from Ge et al. [30]. Copyright 2014, Elsevier.

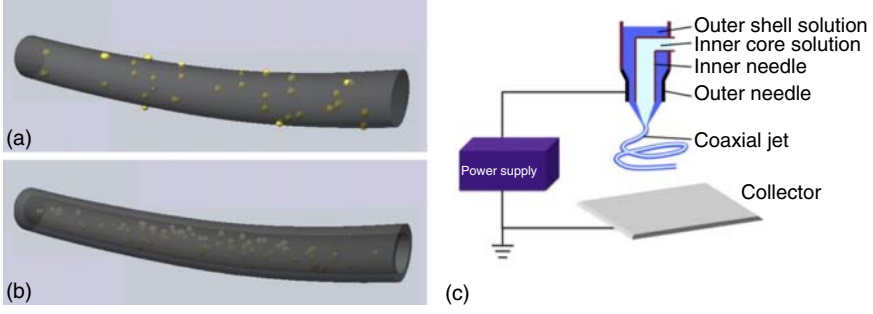


Figure 24.7 Schematic image of (a) Si/C composite nanofibers and (b) Si/C–C core–shell nanofiber, (c) dual nozzle coaxial electrospinning setup. Source: Reproduced with permission from Li et al. [31]. Copyright 2014, Elsevier.

energy materials. Basically, inorganic substances such as SiO_2 [32] and Ni particles as well as certain polymers such as poly(methyl methacrylate) (PMMA) [33] and poly-L-lactic acid [34] are favorable choices for designers. Sacrificial components are removed by dissolution in suitable solvents or decomposed during heat treatment.

Ji et al. generated porous CNF using SiO_2 nanoparticles as sacrificial template, which were etched by hydrofluoric (HF) acid in the as-produced carbon/SiO_2 composite. After etching, the surface area was increased from 26.1 to 91.8 m^2/g, as seen in Figure 24.8 [32]. Lu et al. prepared porous CNF via centrifugal spinning of PAN/PMMA solution and used these in electric double-layer capacitor (EDLC) electrodes. The result indicated that when the PAN/PMMA weight ratio was 7/3, the specific surface area increased from 405 to 444 m^2/g as the carbonization temperature increased from 700 to 900 °C. The total pore volume also increased from 0.171 to 0.310 cm^3/g [35].

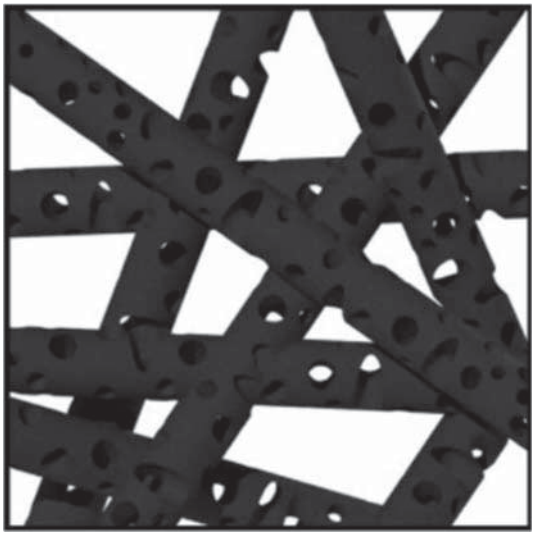


Figure 24.8 Schematic image of porous carbon nanofiber. Source: Reproduced with permission from Ji et al. [32]. Copyright 2009, Elsevier.

24.3.3 Fibrous Structures of Separators

It is well known that separators play an important role in the electrochemical devices [23]. They allow ions to be transported from one side to the other while preventing electrons from passing. Therefore, they should have good insulativity and penetrability.

The thickness and porosity of fiber membranes are two key factors for separators. Yanilmaz et al. prepared silica/PAN membranes as the separator for LIBs. The thickness of the prepared membranes was around 65 μm. In addition, it could reduce the pore size from 478 to 275 nm by adding 27 wt% SiO_2 in the fiber composite [36]. In Figure 24.9, Raghavan et al. designed sandwich structure of poly(vinylidene fluoride-*co*-hexafluoropropylene) and PAN and converted it into polymer electrolytes [37]. The obtained membranes had uniform morphology

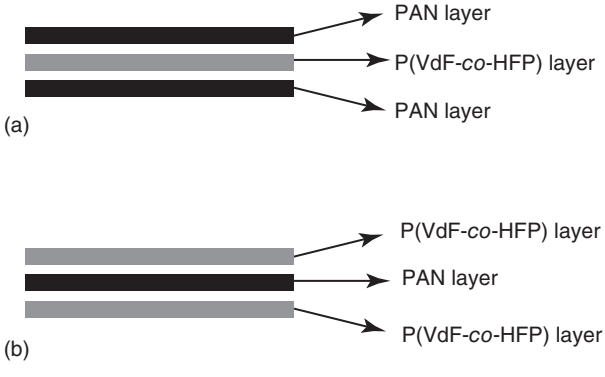


Figure 24.9 Schematic of electrospun trilayer nonwoven mats. (a) PAN/P(VdF-co-HFP)/PAN and (b) P(VdF-co-HFP)/PAN/ P(VdF-co-HFP). Source: Reproduced with permission from Raghavan et al. [37]. Copyright 2010, Elsevier.

with a diameter of 320–490 nm and a high porosity of 82–85%, demonstrating a high electrolyte uptake.

24.3.4 Fabrication Approaches

Several methodological approaches have been explored to produce fibrous materials in the nanoscale or microscale in order to achieve high surface area and high kinetic for energy storage applications. In fact, for the usage in energy storage systems, fibers have been achieved overwhelmingly by two main approaches: electrospinning and centrifugal spinning [25, 38, 39].

Electrospinning is a relatively mature and common technique to produce ultrafine fiber with diameter in the range of 40–2000 nm [40, 41]. The electrospinning setup revealed in Figure 24.10 consists of a high voltage supply, spinning nozzle, syringe, and collector. Polymer solution is stretched from the needle tip by electrostatic force to form a "Taylor cone" and then stacked on the collector [23]. This technique supplies many advantages. First of all, the process is simple and agile and can be used to tailor various one-dimensional structures, including structures of multicomponent nanofiber, core–shell nanofiber, and heterogeneous nanofiber [27]. Secondly, by using rotary collector, one can obtain an oriented and aligned nanofiber mat [42]. The method is widely adopted in the field of energy conversion and storage devices. Ji et al. prepared one-dimensional Ni/CNFs for lithium-ion storage by initially electrospinning the solution of $[Ni(OAc)_2]\cdot 4H_2O$ (30 wt%) and PAN (10 wt%) dissolved in dimethylformamide (DMF) and then carbonized the as-spun nanofiber mat. The final obtained CNFs showed that the Ni spherical nanoparticles could be uniformly distributed in CNFs and the prepared Ni/CNFs delivered favorable electrochemical performances [43].

Centrifugal spinning is an effective and high-speed route to create fibrous structures in the micro- or nanoscale at high throughput, deriving from cotton

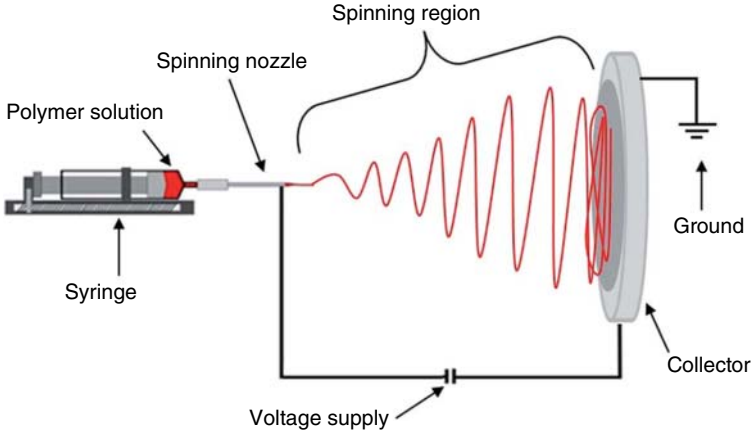


Figure 24.10 Schematic of a typical electrospinning setup. Source: Reproduced with permission from Lee et al. [23]. Copyright 2014, Royal Society of Chemistry.

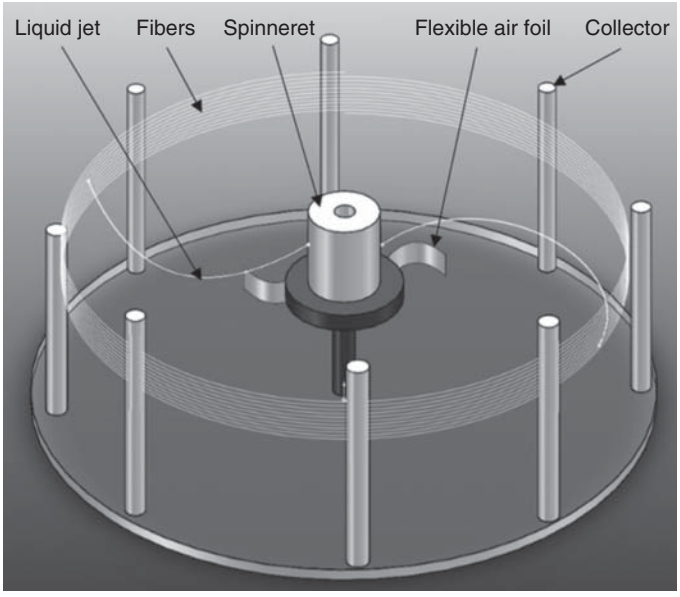


Figure 24.11 Schematic image of the centrifugal spinning system. Source: Reproduced with permission from Lu et al. [44]. Copyright 2013, Elsevier.

candy maker. In Figure 24.11, the centrifugal spinning setup shown is composed of a perforated Teflon spinneret fixed in the center of the spinning platform, with a motor underneath the spinneret to provide high-speed rotation, a speed controller connected to the motor to adjust the rotational speed, and a set of collectors in the outer perimeter of the spinning platform. During the processing, the polymer precursor is subjected to the action of centrifugal force and drawn to the collectors. The advantages of centrifugal spinning can be summarized as follows: (i) It is productive with high-speed rotation of 2000–13 000 rpm [45]; (ii) the fiber is generated by centrifugal force, which eliminates some safety issue from high voltage like electrospinning; (iii) the process has less impact on the environment, and it can produce environmentally sensitive or electrically sensitive polymers. There are an increasing number of publications about centrifugal spinning fibers for energy material preparation. Lu et al. produced PAN micro-/nanofiber by using centrifugal spinning approach. The resultant fiber was in the diameter of 407–1066 nm [44]. Dirican and Zhang fabricated porous carbon microfibers as anode materials for sodium-ion batteries by centrifugal spinning the solution of PAN/PMMA precursor and combining with thermal process. The prepared fiber was observed with many internal pores and surface roughness, which gave rise to greater sodium-ion storage ability [33].

Apart from the techniques mentioned above, self-assembly, chemical vapor deposition (CVD), and hydrothermal method or hybrid process are also adopted to produce fiber materials for energy storage use [46–48]. Fu et al. tailored aligned CNT–Si structure, which could be used as binder-free and flexible anodes for LIBs. Carbon nanotube (CNT) sheet was winded from CNT forests, which were

grown on a quartz substrate using iron chloride ($FeCl_2$) as the catalyst in a horizontal tube furnace. Then silicon-active material was deposited onto 10-layer CNT sheet (2 mg/cm^3) by CVD processing [49].

24.4 Applications to Batteries, Supercapacitors, and Energy Harvesting

The growing interest in renewable energy sources also increases the need for devices that will store the energy produced from them. Therefore, the investigation on energy harvesting and energy storage components occupies huge space of the academic and industrial R&D programs. In this regard, the development of electrodes for either energy storage or conversion takes the position in these programs as a core part that can overcome the shortcomings and significantly improve the performances of such devices. Various nanostructures made of different materials have been proposed for this purpose [50]. Among them, fibrous 1D structures attract attention due to their unique properties that allow improved and efficient energy harvesting and storage [51].

24.4.1 Batteries

Since the commercialization of LIBs, graphite has been used as the negative electrode. Due to its layered structure, which enables reversible Li-ion insertion and extraction, a high and stable energy efficiency is achieved despite its limited capacity (372 mAh/g) [52]. Soft carbons obtained from carbonization of an organic compound, usually resins, have been used as an alternative; however these showed a lower reversible capacity retention. CNFs obtained from different precursors and by different methods attract the attention due to their 1D structure, controllable diameter, enhanced surface area-to-volume ratio, low density, and the possibility to be produced in a feasible process in a variety of structures and in combination with other compounds. Neat, porous, or doped CNFs obtained from PAN by electrospinning and subsequent carbonization have been most widely investigated as anodes for LIBs [53, 54]. Electrospun PAN-based CNFs obtained after carbonization at 1000 °C provided a capacity of 450 mAh/g at a current density of 30 mA/g, or 350 mAh/g at 100 mA/g [53]. The high price and the limited processability of PAN forced researchers to investigate more environmentally friendly and cost-effective alternatives. Among them, lignin, as an abundant natural polymer with high carbon content and thermoplastic character, has great potential to replace PAN to produce carbon fiber-based electrodes for energy applications [55]. Polyvinyl alcohol (PVA), polyvinyl chloride (PVC), PVP, poly(amic acid) (PAA), polyimide (PI), and polybenzimidazole (PBI) are other alternatives toward lower-cost CNF production [56–58]. Although neat CNFs can provide higher capacity than graphite, it still cannot meet the required increased demand for high capacity and long-lasting batteries for larger applications, such as electrical vehicles, grid energy storage, etc. [59]. Therefore, the research in the last few decades has

focused on the development of 1D structures containing active materials that can store large amounts of Li ions.

With a theoretical capacity of 4212 mAh/g, silicon (Si) is the most investigated active material for anode application in LIBs in a wide range of structures and combinations [18]. Despite its high Li-ion storage capacity, it shows large capacity loss during cycling as a result of its volume expansion when alloying with Li ions. This volume change causes electrode disintegration and decrease of electrical contact between particles [59]. Thus, its combination with carbonaceous materials is most commonly used approach to suppress the volume expansion and to maintain the electrical conductivity during cycling. Among the structures proposed, fibrous 1D structures show promising electrochemical performances. Si/CNF composites obtained from electrospinning of Si/PAN solution and subsequent carbonization demonstrate an effective production method. They delivered an initial capacity of 1750 mAh/g that decreased to around 1000 mAh/g after 20 cycles [60]. However, optimization of the nanoparticle loading and other process parameters can improve the cycling stability of these electrodes. Si nanoparticles embedded within the holes of porous CNFs is one alternative approach to this goal [61]. Such structures covered with an additional carbon layer and used as freestanding anodes exhibited capacity of 600 mAh/g after 200 cycles at a current density of 100 mA/g. The stability of the composites can be further improved with the use of carbon-coated Si/CNF composite nanofibers. Such coating can be achieved by immersing the Si/CNF into sucrose solution followed by carbonization, as can be seen in Figure 24.12 [62]. Optimized carbon-layer thickness buffers the volume expansion of the Si nanoparticles maintaining the

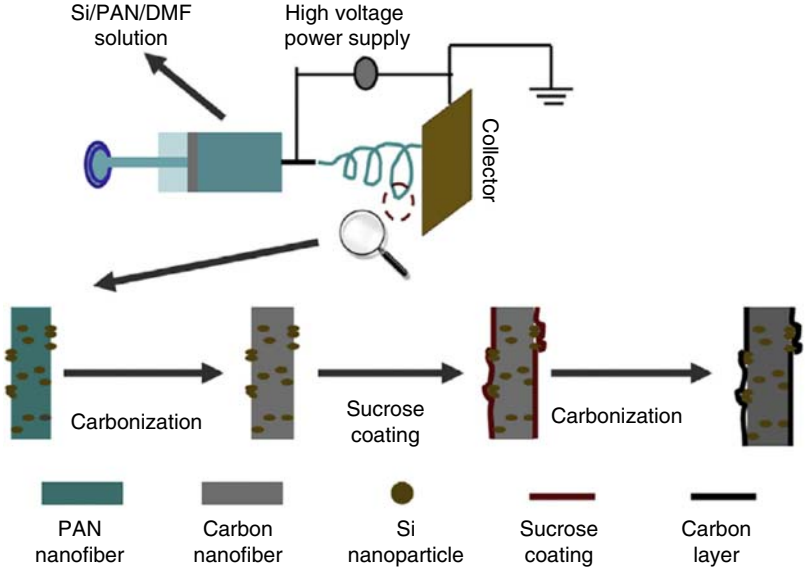


Figure 24.12 Schematic representation of Si/C/CNF nanofiber production and the way its structure changes during different production steps. Source: Reproduced with permission from Chen et al. [62]. Copyright 2015, Elsevier.

structural integrity of the electrode during cycling. These Si/C/CNF could give a capacity of 1215 mAh/g after 50 cycles at 6 A/g. SiO_2-coated Si/CNF composite could also improve the cycling stability and rate capability of the anodes [63]. Additionally, Lin et al. reported a study of twisted aligned multiwalled carbon nanotube (MWCNT) and MWCNT/Si fibers as the anode materials for LIBs, and the procedure is shown in Figure 24.13a [64]. The diameter of the twisted aligned MWCNT fiber was 30 μm, shown in Figure 24.13b,c. In contrast, the diameter of twisted aligned MWCNT/Si composite fiber increased to 60 μm due to the presence of a uniform Si coating (Figure 24.13d,e). The prepared aligned composite fiber could deliver a capacity of 1970 mAh/g with a current density of 1 A/g at the 50th cycle.

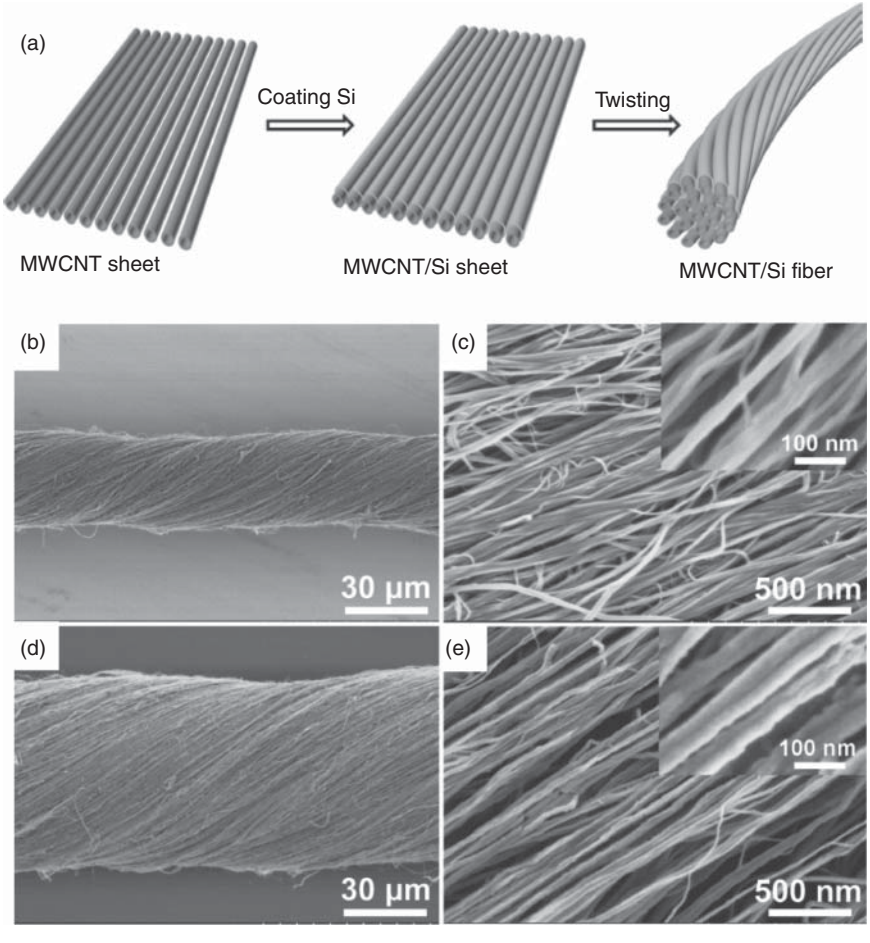


Figure 24.13 (a) Schematic image of the synthesis of aligned MWCNT/Si fiber; SEM images of the twisted aligned (b, c) pure MWCNT and (d, e) MWCNT/Si composite fibers with different magnifications. Source: Reproduced with permission from Lin et al. [64]. Copyright 2014, John Wiley & Sons.

Besides silicon, tin (Sn) has also attracted significant attention for LIB and NIB (sodium-ion battery) anodes application due to its low cost and high theoretical capacity for both chemistries, namely, 990 and 847 mAh/g for LIB and NIB, respectively. Similar to silicon, Sn also suffers from volume expansion due to the alloy formation with Li/Na ions during cycling, which further provokes electrode disintegration and shortens cycle life. Sn nanoparticles embedded into submicron carbon fibers could be produced via the cost-effective centrifugal spinning method [65]. Carbonized $SnCl_2$/PAN nanofibers obtained by this method exhibited a capacity of approximately 400 mAh/g after 100 cycles at 100 mA/g when used as anodes for LIBs. Notably, centrifugally spun SnO_2 microfibers, applied as anodes in NIBs, had a capacity of 150 mAh/g at 640 mA/g, which is three times higher the capacity of pure SnO_2 nanoparticles at the same current density [66]. Furthermore, SnO_2 microfibers show better rate performance with lower capacity decay at higher current densities. Sn/Cu/CNF core–shell structures with improved conductivity have been suggested as an alternate way to improve the cycling stability over prolonged cycling for both Li- and Na-ion chemistries [67]. Tin oxide with its rutile structure and theoretical capacity of 782 mAh/g can also be used as active material for energy storage, due to its lighter volume expansion compared with pure Sn [68]. Electrodeposited SnO_2 over porous CNFs as a freestanding anode in LIBs gave a capacity of 554 mAh/g after 100 cycles, and their cycling stability could be further improved by controlling carbon deposition [69]. Freestanding Sn/SnO_2/CNFs coated with carbon layer exhibited an excellent capacity of 712 mAh/g after 200 cycles at 800 mA/g in the LIB half-cell [70]. A similar structure used for a NIB anode also improved the capacity and the cycling stability of the cell, with 82.7% capacity retention at 50 mA/g (or 374 mAh/g) after 100 cycles [71]. Moreover, ZnO/SnO_2 heterostructures with optimized fiber diameter, particle size, and porosity showed excellent cycling stability of LIBs [72].

On the other hand, hematite iron oxide (α-Fe_2O_3) is a low-cost and non-toxic potential active material for LIB anodes with a theoretical capacity of 1007 mAh/g. Its composites with carbonaceous materials showed an improved electrochemical performance due to the increased electrical conductivity [73]. However, the electrochemical capacity of α-Fe_2O_3 nanoparticles cannot be fully utilized when embedded into CNF, due to the lack of space for Li-ion diffusion. Therefore, to facilitate the Li-ion transport to the pores of the active materials, 1D α-Fe_2O_3 nanofibers were coated with carbon as schematized in Figure 24.14 [74]. The space between the particles were covered with a carbon layer and embedded into 1D structure. This allowed facile and reversible insertion and

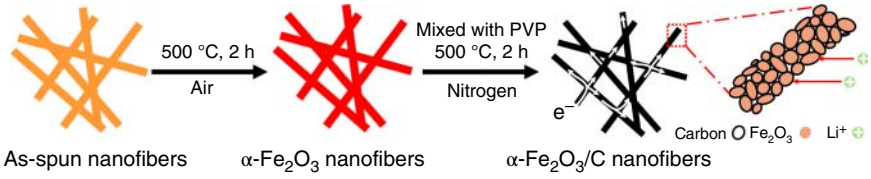


Figure 24.14 Schematic representation of porous 1D α-Fe_2O_3/CNF nanofiber production and its storage mechanism. Source: Reproduced with permission from Zhu et al. [74]. Copyright 2016, Elsevier.

de-insertion of Li ions during cycling, which enables full usage of the active material and enough space to buffer its volume expansion. This unique 1D structure showed capacity of 715 mAh/g (capacity retention of 91%) after 200 cycles at 100 mA/g, or almost double the capacity of α-Fe_2O_3 nanoparticles/CNF composite (400 mAh/g after 100 cycles at 100 mA/g).

The versatility of CNFs allows them to be used as conductive support for 3D structures. $Zn_xCo_{3-x}O_4$ (ZCO) nanocubes coated onto CNFs have been successfully applied as anodes for LIBs [75]. The combination of hydrothermal–thermal treatment of CNF mats with suitable chemicals and optimized process conditions allows formation of nanosized ternary metal oxide/CNF composites with enhanced electrochemical properties that can find application not only for energy storage but also for energy conversion devices.

Despite the extended research on fiber structures as anodes, which are usually carbon based, the versatile approaches for fiber/nanofiber production allow their application as cathodes as well [76]. Even though the structure of cathode materials is more complex, they do require high conductivity and reversible and stable reactivity with the ions [77]. In this regard, layered, spinel, and olivine single or multi-metal structures have been designed as fibrous structures and applied in either LIBs or NIBs [76–79].

$LiFePO_4$/CNF freestanding cathodes were obtained by electrospinning of PAN solution containing Li, Fe acetate, and phosphoric acid followed by carbonization [78]. This 1D structure enabled the formation of well-distributed $LiFePO_4$ particles throughout the CNF, which resulted in enhanced capacity and cycling stability of the cathode. The addition of CNT or graphene within the structure further improved the electrochemical performances due to the increased electrical conductivity between the particles [78, 79]. Zhang et al. prepared LiF/Fe/CNF cathodes from ferrocene/PAN solution via electrospinning [80]. Such cathodes, with a controllable fiber diameter and distribution of active particles, enable better contact between LiF and Fe, which provided high and stable capacity during cycling. On the other hand, the presence of carbon over the particles of the active material enables easy and fast Li-ion diffusion and electron transport. Embedding the multicomponent olivine of $Li_2Mn_{(1-x)}Cr_xSiO_4$ with controlled Mn-to-Cr ratio into a CNF matrix could significantly prevent its structural collapse during cycling [81]. Furthermore, the enhanced conductivity between the particles during cycling enables reaching capacity near the theoretical capacity of Li_2MnSiO_4 (330 mAh/g). The improved performances of Li_2MnSiO_4 cathode in LIB cells can be also obtained by Fe doping [82]. Recently, Lu et al. obtained Li-substituted Na-layered transition metal oxide fibers by centrifugal spinning of PAN/nitrile solutions with different content of Li and Na, as shown in Figure 24.15 [83]. The results indicated that the obtained materials had good cycling stability when performed as electrodes for NIBs.

Fiber cathodes for Li–S and Li–air batteries have also been widely investigated [84–87]. CNFs act as supports for sulfur or catalysts where carbon compensates for the low electrical conductivity of the active materials. This enables freestanding structures with high surface area and porosity. In the case of Li–S batteries, PAN-based CNFs can be doped with sulfur via a vapor deposition [88]. CNFs can act as interlayers between the cathode and the separator in Li–S batteries

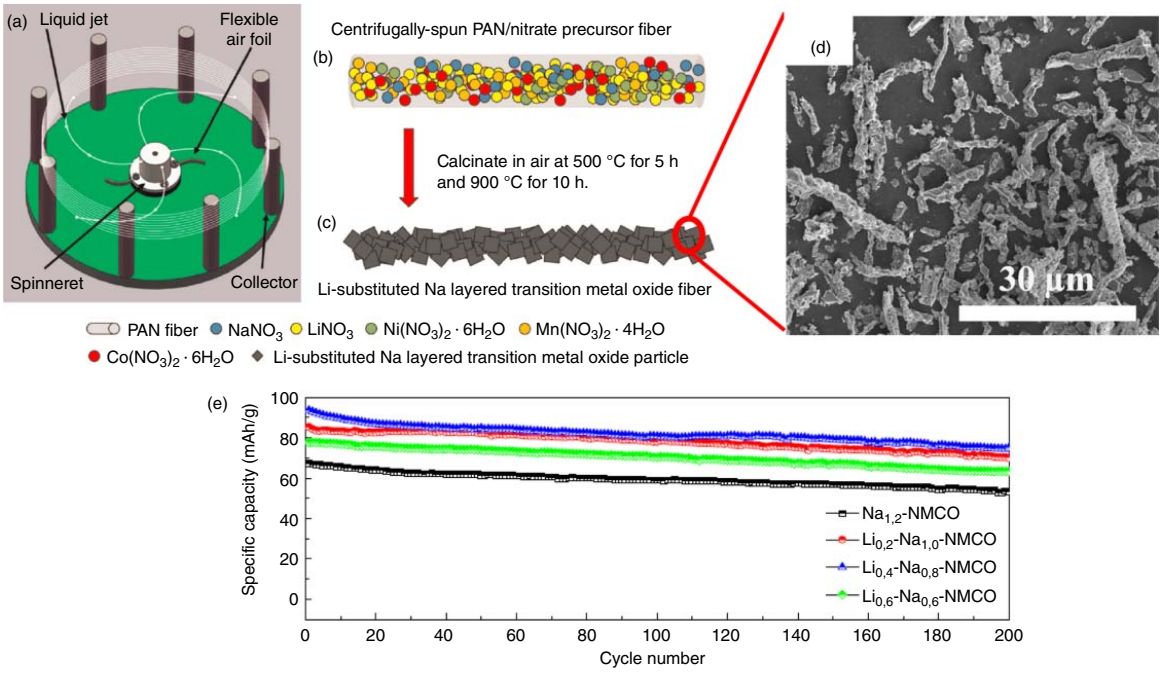


Figure 24.15 Schematic illustration of (a) centrifugal spinning device, (b) the fiber precursor, and (c) the fiber cathode, including its (d) SEM image and (e) cycling performances at 75 mA/g. Source: Reproduced with permission from Lu et al. [83]. Copyright 2015, Elsevier.

in order to prevent the shuttling effect by localizing the soluble polysulfides during cycling. That improves the electrical conductivity of the cathode and reduces the charge-transfer resistance [86]. The electrical conductivity of the cell can be enhanced by using CNFs deposited on polyvinylidene fluoride (PVDF) membrane [87], or CNF/rGO (reduced graphene oxide) membrane obtained by the filtration method. Different catalysts with high activity for oxygen reduction reaction (ORR) and the oxygen evolution reaction (OER) such as cobalt oxide (Co_2O_3), nickel–cobalt oxide ($NiCo_2O_4$), or MnO_2 can be in situ introduced into CNF [89, 90] or mixed with CNF in a suspension that gives a freestanding porous film after filtration method [91]. Well-distributed active particles in CNF showed lower overpotential and improved capacity and cyclic performance [91].

Polymer fibrous membranes with good thermal stability and chemical resistivity lead to facile migration of ions and decreased cell resistance [77]. In this regard, nanofiber membranes have been widely used as separators for energy storage systems [92, 93].

Silica nanopowder embedded in PVDF [93], PAN [36], or nylon 6,6 [94] nanofibers can be used as a separator with improved thermal stability, higher ionic conductivity, and lower interfacial resistance that results in an enhanced cycling performance of a LIB cell. As can be seen in Figure 24.16, when spun onto self-standing CNT sheets, the composite structure acted as both separator and interlayer for Li–S batteries, providing fast diffusion of both lithium ions and electrons, and reduced diffusion of polysulfides [95].

Centrifugally spun fibrous membranes either doped or from a blend of polymers can also be used as separators in energy storage devices [39, 96–98]. SiO_2/PAN membranes with optimized amount of SiO_2, obtained by centrifugal spinning, could significantly improve the ionic conductivity of the separator and consequently enhance the discharge capacity of LIBs (Figure 24.17) [39]. Furthermore, it offered low-cost fiber production due to much lower power consumption and high production rates.

24.4.2 Supercapacitors

Supercapacitors are energy storage devices that can provide high power density due to the highly porous electrode structure with controlled pore size distribution

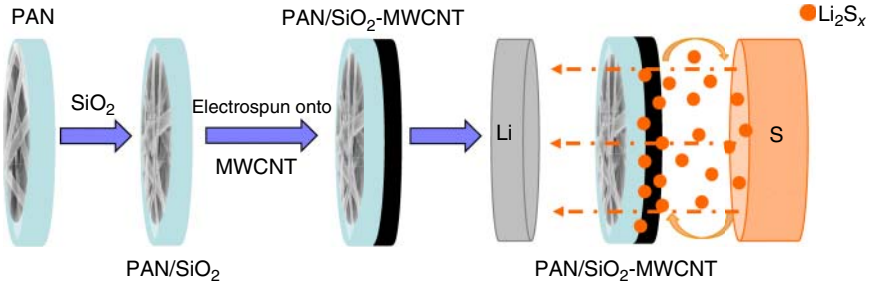


Figure 24.16 Schematic presentation of PAN/SiO_2-adapted separator for Li–S batteries. Source: Reproduced with permission from Zhu et al. [95]. Copyright 2016, Royal Society of Chemistry.

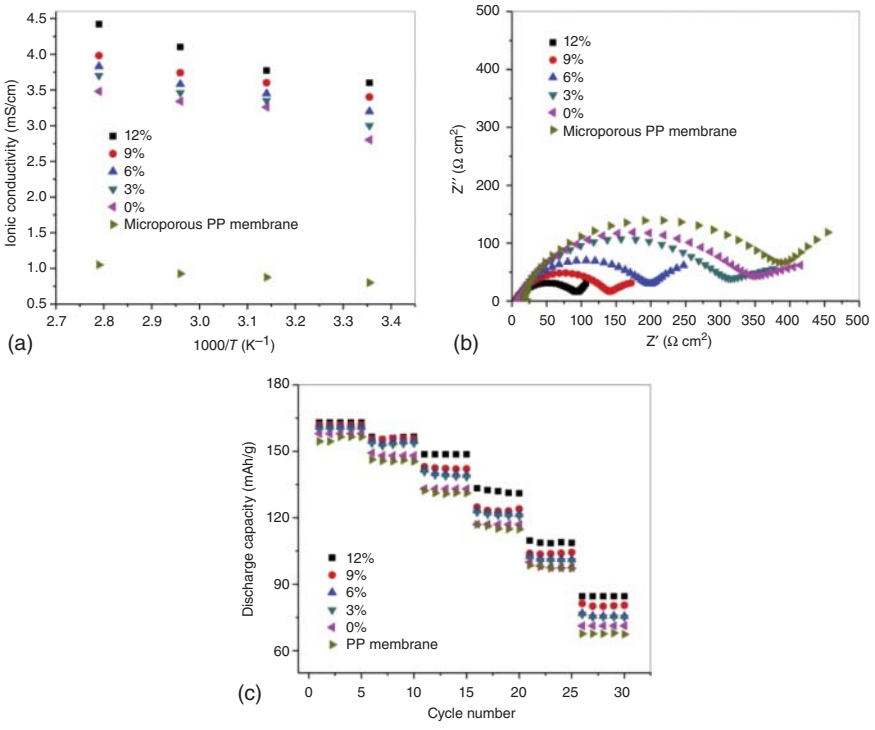


Figure 24.17 (a) Ionic conductivity, (b) electrochemical impedance spectra of SiO_2/PAN membranes, and (c) C-rate performance of Li/$LiFePO_4$ cells containing SiO_2/PAN membranes as separator. Source: Reproduced with permission from Yanilmaz et al. [39]. Copyright 2015, Elsevier.

via an electrostatic mechanism [99]. Thus, CNFs with increased surface area can be ideal for this application [100].

Lu et al. obtained CNFs with controlled porosity by centrifugal spinning of polymer blends and thermal treatment. The prepared CNFs that were carbonized at 900 °C could deliver a capacitance of approximately 100 F/g at 2 A/g. A high capacity retention of 74% could be achieved for the sample carbonized at 900 °C when current density increased from 0.1 to 2 A/g [35]. The production steps and the morphology of such CNFs are given in Figure 24.18. On the other hand, CNF doped with metal oxides such as RuO_2, Fe_2O_3, MnO_2, and NiO could serve as electrodes for hybrid capacitors with higher energy and power densities because of the synergetic effect between carbon's conductivity and metal oxide's pseudocapacitance [101, 102].

Conductive polymers can also give pseudocapacitance and can be deposited onto porous CNF or be used alone as electrodes for either symmetric or asymmetric supercapacitors [103, 104]. Studies showed that hollow fiber structures made of conductive polymers could be used as supercapacitor electrodes, which significantly improved the pseudocapacitance performance of the device. Electrodes were obtained from electrospun PAA fiber membrane as a template for in

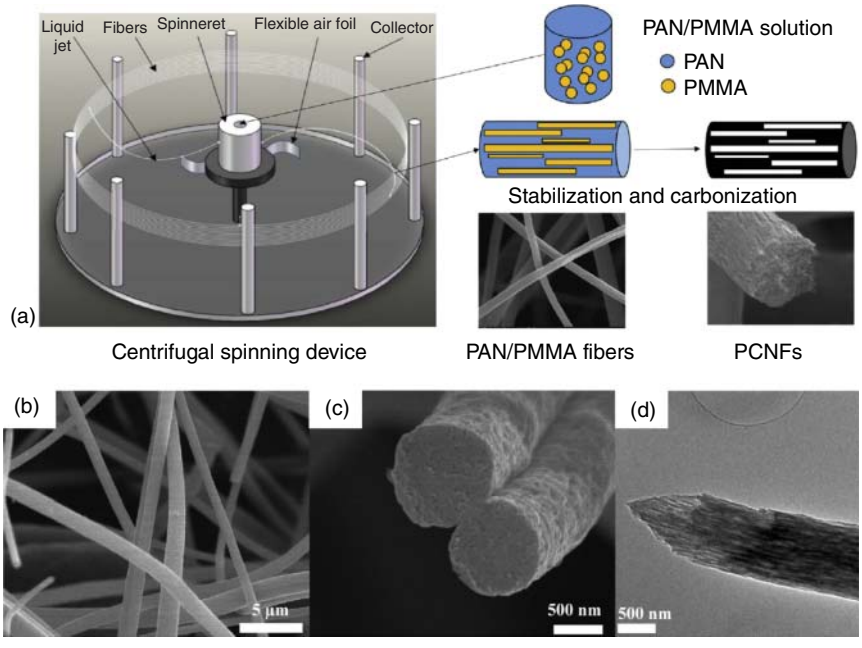


Figure 24.18 (a) Production method of porous CNFs and (b–d) their morphology: (b) plane-viewed SEM, (c) cross-sectional SEM, and (d) TEM images. Source: Reproduced with permission from Lu et al. [35]. Copyright 2015, Elsevier.

situ polymerization of polyaniline (PANI) (Figure 24.19) [103]. These electrodes delivered the capacitance of 500 F/g at 2 A/g using three-electrode system.

Pan et al. prepared a novel wearable energy device by using aligned CNT fiber textiles that were coated by PANI [104]. During the preparation, CNT fibers were first formed from a spinnable CNT array that were then woven into textiles (Figure 24.20a). The CV curves of pristine CNT and CNT/PANI composite textiles are shown in Figure 24.20b. It is obvious that the current density of CNT/PANI textiles was much higher than that of pristine CNT textiles. In Figure 24.20c, the composite textiles with 50 wt% PANI could deliver a specific capacitance of 272.7 F/g at a current density of 1 A/g.

24.4.3 Energy Harvesting Devices

Energy harvesting or the process of capturing and transforming the energy derived from an external force has attracted a great amount of attention in the last decade. Among the sources from which electrical energy can be obtained, photovoltaic, fuel cells, and nanogenerators give a chance for incorporation of fibrous structures as their constituents [105].

In dye-sensitized solar cells (DSSCs), the high specific surface area of nanofibrous structure enables improved absorption of photosensitizing dye and electrolyte uptake. Additionally, their improved interconnectivity lowers the grain boundaries that leads to enhanced charge conduction and

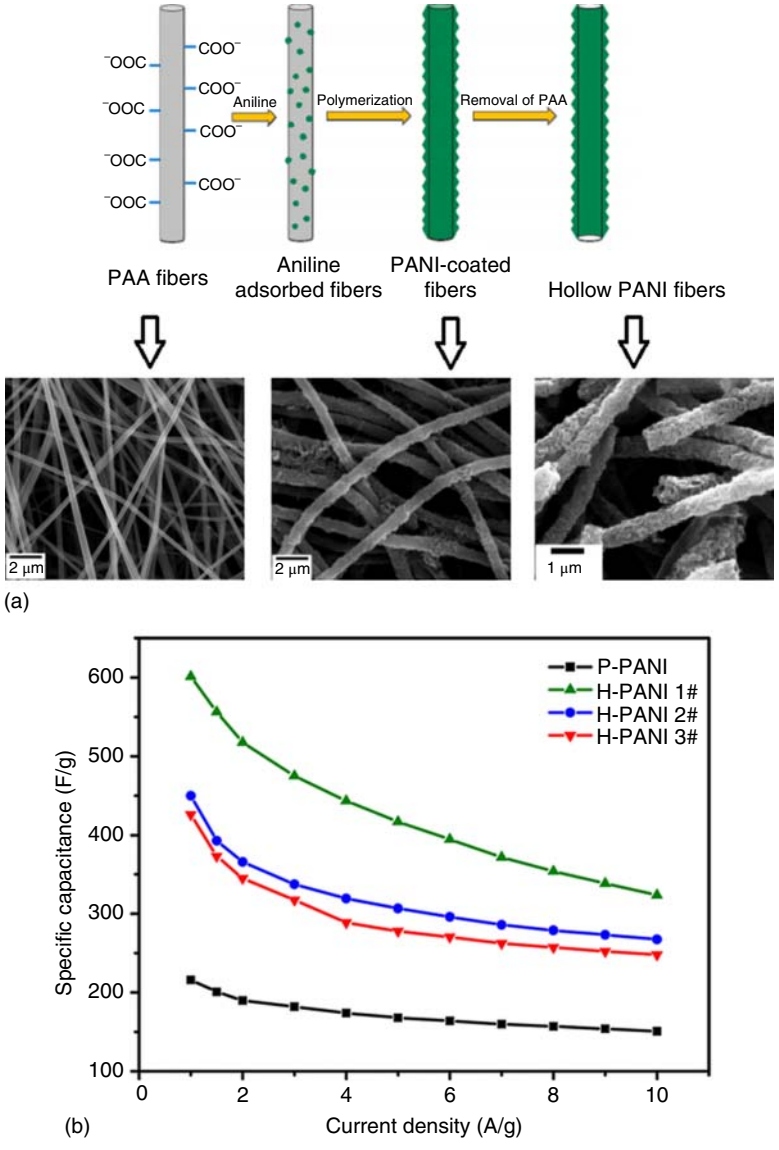


Figure 24.19 (a) Production method and (b) rate capability of a supercapacitor using hollow PANI electrode. Source: Reproduced with permission from Miao et al. [103]. Copyright 2013, American Chemical Society.

reduced charge–carrier recombination. For this purpose, inorganic titania and silica-based nanofibers have been used as photoanodes [106, 107]. Mohamed et al. synthesized one-dimensional SnO_2@TiO_2 nanofibers (NFs), which were developed into electrode for DSSCs [107]. The diameters of the prepared nanofibers cover a range from 160 to 360 nm (Figure 24.21a). The photocurrent–voltage curves (J–V) of the cells with SnO_2@TiO_2 NFs and pure

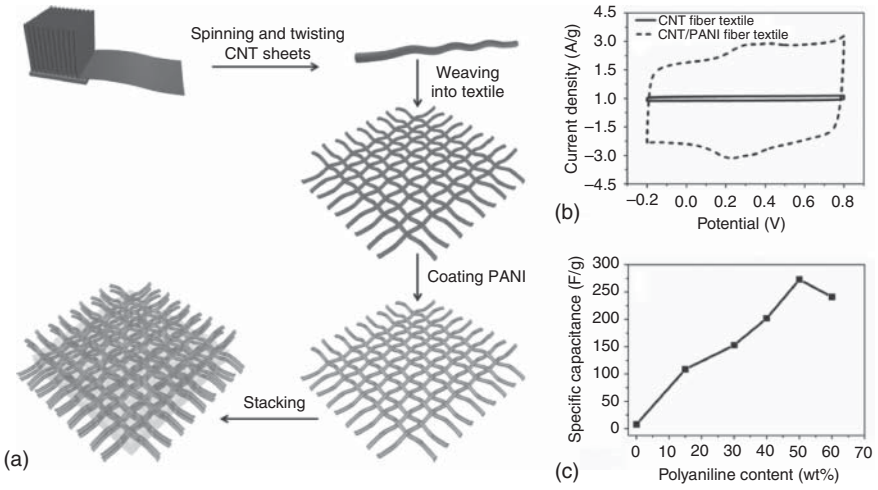


Figure 24.20 (a) Schematic image of preparation of CNT/PANI composite fiber-based textiles used for a supercapacitor; (b) CV curves of CNT fiber textile and CNT/PANI fiber textile; (c) Specific capacitances of CNT/PANI fiber textiles with various PANI weight percentages at a current density of 1 A/g. Source: Reproduced with permission from Pan et al. [104]. Copyright 2015, John Wiley & Sons.

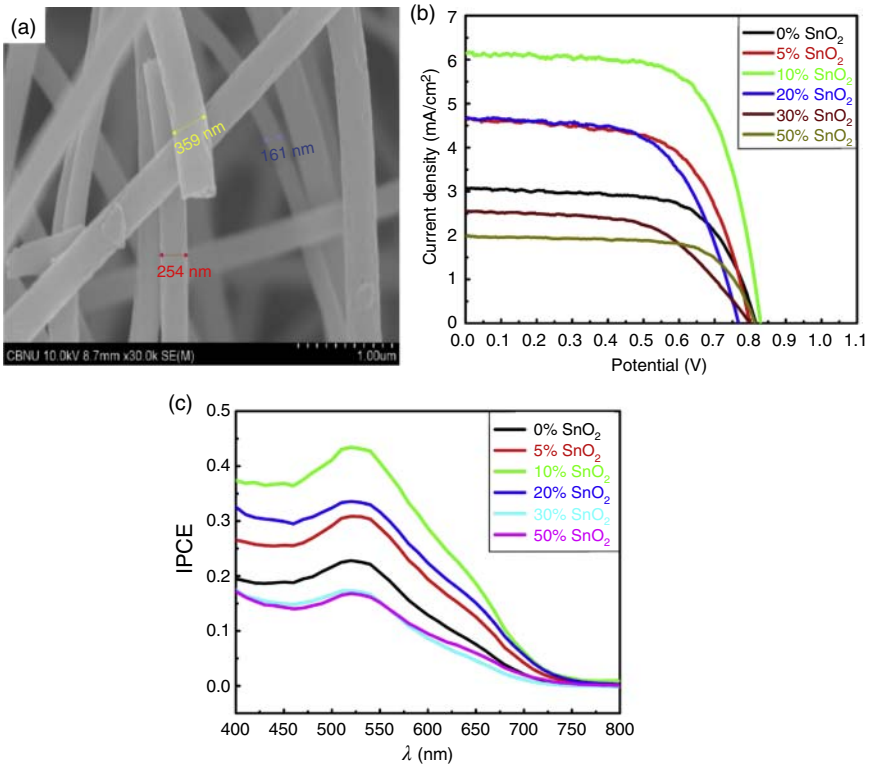


Figure 24.21 (a) SEM image of the SnO_2-TiO_2-NF photoanode containing 10% SnO_2 and comparison of performances of dye-sensitized SnO_2-TiO_2-NF composite photoanodes with different concentrations of SnO_2 (b) J–V curves and (c) IPCE spectra. Source: Reproduced with permission from Mohamed et al. [107]. Copyright 2016, Elsevier.

TiO_2 NFs in comparison are shown in Figure 24.21b. It can be seen that TiO_2 NFs with 10% SnO_2 have the highest current density (6.10 mA/cm^2) with a significant enhancement in the incident photon-to-current conversion efficiency (IPCE) (Figure 24.21c), which is probably because the existence of SnO_2 at a proper concentration (10%) can improve the electron transfer from the dye to the fluorine-tin-oxide (FTO) substrate by reducing the recombination between electrons and the excited dye molecules. Stable, ultrastrong, and flexible aligned CNT fibers were obtained by Chen et al. for DSSC [15]. During the preparation process, a highly aligned CNT fiber (Figure 24.22a,c) was first formed by using a CVD method. The obtained aligned CNT fiber was then dipped into a TiO_2 dispersion, followed by heating at 500 °C for 60 minutes. TiO_2 particles with size of ~25 nm were uniformly attached on the surface of the oriented CNT fiber (Figure 24.22b,d). A high-power conversion efficiency of 2.94% could be achieved by using this unique fiber-shaped DSSC.

In fuel cells, CNFs can serve as support for catalysts that enable ORR and OER. Nitrogen, Pt, Au, or Mn oxides are among the most widely used catalysts incorporated into CNF structures [108, 109]. As shown in Figure 24.23a, Pt-doped porous carbon nanofibers (Pt/N-PCNF) with an average diameter of 150 nm (Figure 24.23b) were successfully fabricated by the synthetic procedure [108]. It is obvious that the electrochemical surface area (ECSA) retention of Pt/N-PCNF is better compared with that of both the commercial one (JM20) and Pt-supported porous CNF (Pt/PCNF) (Figure 24.23c), which is due to the existence of functional anchoring groups as well as the enhanced Pt-orbital

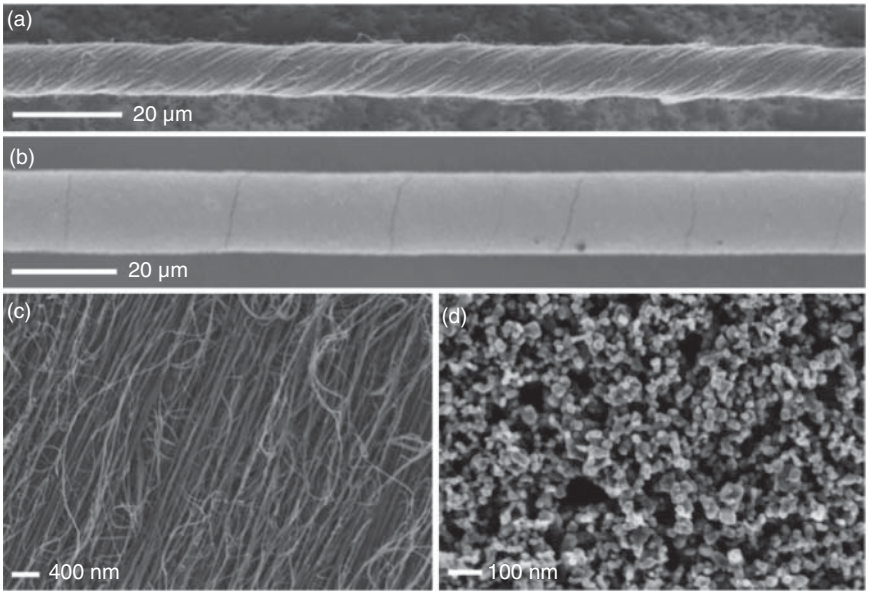


Figure 24.22 SEM images of twisted aligned (a, c) CNT and (b, d) CNT/TiO_2 fibers with different magnifications. Source: Reproduced with permission from Chen et al. [15]. Copyright 2012, American Chemical Society.

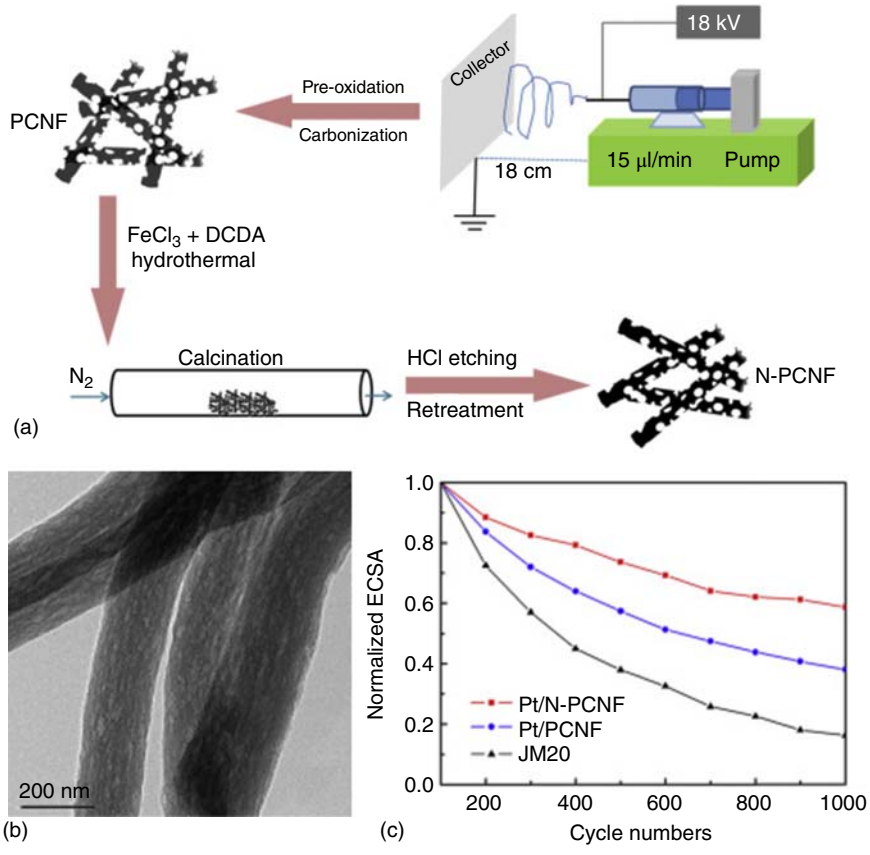


Figure 24.23 (a) Production method of Pt-supported N-doped porous CNF, (b) their morphology, and (c) their electrochemical surface area retention. Source: Reproduced with permission from Wang et al. [108]. Copyright 2016, Elsevier.

bonding strength. Bessel et al. used 5 wt% Pt supported on graphite nanofibers (Pt/GNF) as an electrode for fuel cell applications [109]. The results showed that the activities of the obtained Pt/GNF were comparable with that of about 25 wt% Pt on Vulcan carbon. This performance improvement is probably due to the metal particles, Pt, adopting specific crystallographic orientations when dispersed on the highly tailored GNF structures [109].

Nanogenerators are mechanical energy harvesting devices that use the piezoelectric effect to capture and convert energy [105]. In other words, the mechanical movement of a people or objects can be converted into an electric charge. These devices can use textile fibers, yarns, fabrics, or nanomembranes as electrodes due to their flexibility and mechanical stability [110–113]. A piezoelectric nanogenerator based on lead zirconate titanate (PZT) nanofibers with a diameter and length of about 60 nm and 500 μm was prepared by Chen et al. [114]. This nanogenerator provided a voltage of 1.63 V and a power of 0.03 μW, respectively. Meanwhile, the PZT nanofibers could be protected by embedding in soft polydimethylsiloxane (PDMS), prolonging the cycle life of this nanogenerator.

24.5 Future Trends

Fibers applied as energy materials have been intensively studied. Research interests mainly focus on (i) new materials' exploitation with fibrous structure, (ii) the combination of modification, and (iii) application developments.

Generally, electrode materials having fibrous structures are able to provide more active area and enhance the reaction kinetics. Additionally, if using CNFs as the matrix, it is possible to limit the volume change of the active materials during the cycling process, especially for Si, Sn, metal oxides, etc. To further improve the electrochemical properties in terms of cycling ability and rate capability, many additional modifications on fibrous energy materials have also been highlighted. For example, certain doping agents have been added into the substance that can increase the electrical conductivity and surface properties.

Moreover, some continuous fiber networks possess good mechanical property withstanding bending, stretching, compressing forces in a certain extent, and achieving freestanding electrodes, even flexible energy devices (flexible batteries and supercapacitors).

From another perspective, apart from randomly arranged fibers, they can also be fabricated into 1D aligned or even 2D woven textile architecture for energy use. For further developing, common textiles (such as cotton, polyester, nylon, carbon fiber, etc.) that incorporate activated materials (CNT, graphene, etc.) will be explored.

In summary, there has been great interest in flexible and wearable energy devices for applications in stretchable electronics by using fibrous materials. Enhancement of the performances and cost reduction of those energy storage systems should be achieved for future development.

References

1 Goldemberg, J. (2007). Ethanol for a sustainable energy future. *Science* 315 (5813): 808–810.
2 Zhu, J., Ge, Y., Kim, D. et al. (2016). A novel separator coated by carbon for achieving exceptional high performance lithium-sulfur batteries. *Nano Energy* 20: 176–184.
3 Nema, P., Nema, R.K., and Rangnekar, S. (2009). A current and future state of art development of hybrid energy system using wind and PV-solar: a review. *Renewable and Sustainable Energy Reviews* 13 (8): 2096–2103.
4 Lu, L., Han, X., Li, J. et al. (2013). A review on the key issues for lithium-ion battery management in electric vehicles. *Journal of Power Sources* 226: 272–288.
5 He, C., Wu, S., Zhao, N. et al. (2013). Carbon-encapsulated Fe_3O_4 nanoparticles as a high-rate lithium ion battery anode material. *ACS Nano* 7 (5): 4459–4469.
6 Jiang, H., Lee, P.S., and Li, C. (2013). 3D carbon based nanostructures for advanced supercapacitors. *Energy & Environmental Science* 6 (1): 41–53.

7 Fu, Y., Cai, X., Wu, H. et al. (2012). Fiber supercapacitors utilizing pen ink for flexible/wearable energy storage. *Advanced Materials* 24 (42): 5713–5718.
8 Zeng, W., Shu, L., Li, Q. et al. (2014). Fiber-based wearable electronics: a review of materials, fabrication, devices, and applications. *Advanced Materials* 26 (31): 5310–5336.
9 Wang, X., Liu, B., Liu, R. et al. (2014). Fiber-based flexible all-solid-state asymmetric supercapacitors for integrated photodetecting system. *Angewandte Chemie International Edition* 53 (7): 1849–1853.
10 Saetia, K., Schnorr, J.M., Mannarino, M.M. et al. (2014). Spray-layer-by-layer carbon nanotube/electrospun fiber electrodes for flexible chemiresistive sensor applications. *Advanced Functional Materials* 24 (4): 492–502.
11 Zhu, J., Yanilmaz, M., Fu, K. et al. (2016). Understanding glass fiber membrane used as a novel separator for lithium-sulfur batteries. *Journal of Membrane Science* 504: 89–96.
12 Zhu, J. (2016). Advanced Separator Selection and Design for High-performance Lithium-Sulfur Batteries. PhD Thesis, North Carolina State University, Raleigh, United States.
13 Lv, Z., Yu, J., Wu, H. et al. (2012). Highly efficient and completely flexible fiber-shaped dye-sensitized solar cell based on TiO_2 nanotube array. *Nanoscale* 4 (4): 1248–1253.
14 Liu, G., Peng, M., Song, W. et al. (2015). An 8.07% efficient fiber dye-sensitized solar cell based on a TiO_2 micron-core array and multilayer structure photoanode. *Nano Energy* 11: 341–347.
15 Chen, T., Qiu, L., Cai, Z. et al. (2012). Intertwined aligned carbon nanotube fiber based dye-sensitized solar cells. *Nano Letters* 12 (5): 2568–2572.
16 Wang, S.X., Yang, L., Stubbs, L.P. et al. (2013). Lignin-derived fused electrospun carbon fibrous mats as high performance anode materials for lithium ion batteries. *ACS Applied Materials & Interfaces* 5 (23): 12275–12282.
17 Wu, J., Qin, X., Miao, C. et al. (2016). A honeycomb-cobweb inspired hierarchical core–shell structure design for electrospun silicon/carbon fibers as lithium-ion battery anodes. *Carbon* 98: 582–591.
18 Roy, P. and Srivastava, S.K. (2015). Nanostructured anode materials for lithium ion batteries. *Journal of Materials Chemistry A* 3 (6): 2454–2484.
19 Wang, Z., Qie, L., Yuan, L. et al. (2013). Functionalized N-doped interconnected carbon nanofibers as an anode material for sodium-ion storage with excellent performance. *Carbon* 55: 328–334.
20 Wu, X.L. and Xu, A.W. (2014). Carbonaceous hydrogels and aerogels for supercapacitors. *Journal of Materials Chemistry A* 2 (14): 4852–4864.
21 Shi, F., Li, L., Wang, X.L. et al. (2014). Metal oxide/hydroxide-based materials for supercapacitors. *RSC Advances* 4 (79): 41910–41921.
22 Zhang, X., Ji, L., Toprakci, O. et al. (2011). Electrospun nanofiber-based anodes, cathodes, and separators for advanced lithium-ion batteries. *Polymer Reviews* 51 (3): 239–264.
23 Lee, H., Yanilmaz, M., Toprakci, O. et al. (2014). A review of recent developments in membrane separators for rechargeable lithium-ion batteries. *Energy & Environmental Science* 7: 3857–3886.

24 Zhu, J., Chen, C., Lu, Y. et al. (2015). Nitrogen-doped carbon nanofibers derived from polyacrylonitrile for use as anode material in sodium-ion batteries. *Carbon* 94: 189–195.

25 Ge, Y., Zhu, J., Lu, Y. et al. (2015). The study on structure and electrochemical sodiation of one-dimensional nanocrystalline TiO_2@C nanofiber composites. *Electrochimica Acta* 176: 989–996.

26 Dirican, M., Yildiz, O., Lu, Y. et al. (2015). Flexible binder-free silicon/silica/carbon nanofiber composites as anode for lithium-ion batteries. *Electrochimica Acta* 169: 52–60.

27 Peng, S., Li, L., Lee, J.K.Y. et al. (2016). Electrospun carbon nanofibers and their hybrid composites as advanced materials for energy conversion and storage. *Nano Energy* 22: 361–395.

28 Zhang, C.L. and Yu, S.H. (2014). Nanoparticles meet electrospinning: recent advances and future prospects. *Chemical Society Reviews* 43 (13): 4423–4448.

29 Ji, L. and Zhang, X. (2009). Electrospun carbon nanofibers containing silicon particles as an energy-storage medium. *Carbon* 47 (14): 3219–3226.

30 Ge, Y., Jiang, H., Fu, K. et al. (2014). Copper-doped $Li_4Ti_5O_{12}$/carbon nanofiber composites as anode for high-performance sodium-ion batteries. *Journal of Power Sources* 272: 860–865.

31 Li, Y., Xu, G., Yao, Y. et al. (2014). Coaxial electrospun Si/C-C core–shell composite nanofibers as binder-free anodes for lithium-ion batteries. *Solid State Ionics* 258: 67–73.

32 Ji, L., Lin, Z., Medford, A.J., and Zhang, X. (2009). Porous carbon nanofibers from electrospun polyacrylonitrile/SiO_2 composites as an energy storage material. *Carbon* 47 (14): 3346–3354.

33 Dirican, M. and Zhang, X. (2016). Centrifugally-spun carbon microfibers and porous carbon microfibers as anode materials for sodium-ion batteries. *Journal of Power Sources* 327: 333–339.

34 Ji, L. and Zhang, X. (2009). Fabrication of porous carbon/Si composite nanofibers as high-capacity battery electrodes. *Electrochemistry Communications* 11 (6): 1146–1149.

35 Lu, Y., Fu, K., Zhang, S. et al. (2015). Centrifugal spinning: a novel approach to fabricate porous carbon fibers as binder-free electrodes for electric double-layer capacitors. *Journal of Power Sources* 273: 502–510.

36 Yanilmaz, M., Lu, Y., Zhu, J., and Zhang, X. (2016). Silica/polyacrylonitrile hybrid nanofiber membrane separators via sol–gel and electrospinning techniques for lithium-ion batteries. *Journal of Power Sources* 313: 205–212.

37 Raghavan, P., Zhao, X., Shin, C. et al. (2010). Preparation and electrochemical characterization of polymer electrolytes based on electrospun poly(vinylidene fluoride-co-hexafluoropropylene)/polyacrylonitrile blend/composite membranes for lithium batteries. *Journal of Power Sources* 195 (18): 6088–6094.

38 Zhu, J., Chen, C., Lu, Y. et al. (2016). Highly porous polyacrylonitrile/graphene oxide membrane separator exhibiting excellent anti-self-discharge feature for high-performance lithium–sulfur batteries. *Carbon* 101: 272–280.

39 Yanilmaz, M., Lu, Y., Li, Y., and Zhang, X. (2015). SiO_2/polyacrylonitrile membranes via centrifugal spinning as a separator for Li-ion batteries. *Journal of Power Sources* 273: 1114–1119.

40 Du, J., Shintay, S., and Zhang, X. (2008). Diameter control of electrospun polyacrylonitrile/iron acetylacetonate ultrafine nanofibers. *Journal of Polymer Science Part B: Polymer Physics* 46 (15): 1611–1618.

41 Reneker, D.H. and Chun, I. (1996). Nanometre-diameter-fibres-of-polymer,-produced-by-electrospinning. *Nanotechnology* 7: 216–223.

42 Valizadeh, A. and Farkhani, S.M. (2014). Electrospinning and electrospun nanofibres. *IET Nanobiotechnology* 8 (2): 83–92.

43 Ji, L., Lin, Z., Medford, A.J., and Zhang, X. (2009). In-situ encapsulation of nickel particles in electrospun carbon nanofibers and the resultant electrochemical performance. *Chemistry A European Journal* 15 (41): 10718–10722.

44 Lu, Y., Li, Y., Zhang, S. et al. (2013). Parameter study and characterization for polyacrylonitrile nanofibers fabricated via centrifugal spinning process. *European Polymer Journal* 49 (12): 3834–3845.

45 Marano, S., Barker, S.A., Raimi-Abraham, B.T. et al. (2016). Development of micro-fibrous solid dispersions of poorly water-soluble drugs in sucrose using temperature-controlled centrifugal spinning. *European Journal of Pharmaceutics and Biopharmaceutics* 103: 84–94.

46 Li, Z., Liu, Z., Li, B. et al. (2014). MnO_2 nanosilks self-assembled micropowders: facile one-step hydrothermal synthesis and their application as supercapacitor electrodes. *Journal of the Taiwan Institute of Chemical Engineers* 45 (6): 2995–2999.

47 Zhang, R., Yang, X., Gao, Y. et al. (2016). In-situ preparation of $Li_3V_2(PO_4)_3$/C and carbon nanofibers hierarchical cathode by the chemical vapor deposition reaction. *Electrochimica Acta* 188: 254–261.

48 Waller, G.H., Lai, S.Y., Rainwater, B.H., and Liu, M. (2014). Hydrothermal synthesis of $LiMn_2O_4$ onto carbon fiber paper current collector for binder free lithium-ion battery positive electrodes. *Journal of Power Sources* 251: 411–416.

49 Fu, K., Yildiz, O., Bhanushali, H. et al. (2013). Aligned carbon nanotube-silicon sheets: a novel nano-architecture for flexible lithium ion battery electrodes. *Advanced Materials* 25 (36): 5109–5114.

50 Arico, A.S., Bruce, P., Scrosati, B. et al. (2005). Nanostructured materials for advanced energy conversion and storage devices. *Nature Materials* 4 (5): 366–377.

51 Lu, Y., Chen, C., and Zhang, X. (2015). Functional nanofibers for energy storage. In: *Handbook of Smart Textiles* (ed. X. Tao), 1–28. Springer Singapore.

52 Flandrois, S. and Simon, B. (1999). Carbon materials for lithium-ion rechargeable batteries. *Carbon* 37 (2): 165–180.

53 Kim, C., Yang, K.S., Kojima, M. et al. (2006). Fabrication of electrospinning-derived carbon nanofiber webs for the anode material of lithium-ion secondary batteries. *Advanced Functional Materials* 16 (18): 2393–2397.

54 Raza, A., Wang, J., Yang, S. et al. (2014). Hierarchical porous carbon nanofibers via electrospinning. *Carbon Letters* 15 (1): 1–14.

55 Chatterjee, S., Saito, T., Rios, O., and Johs, A. (2014). Lignin based carbon materials for energy storage applications. In: *Green Technologies for the Environment*, vol. 1186, 203–218. Washington, DC: American Chemical Society.

56 Bai, Y., Wang, Z., Wu, C. et al. (2015). Hard carbon originated from polyvinyl chloride nanofibers as high-performance anode material for na-ion battery. *ACS Applied Materials & Interfaces* 7 (9): 5598–5604.

57 Zou, L., Gan, L., Kang, F. et al. (2010). Sn/C non-woven film prepared by electrospinning as anode materials for lithium ion batteries. *Journal of Power Sources* 195 (4): 1216–1220.

58 Qie, L., Chen, W.-M., Wang, Z.-H. et al. (2012). Nitrogen-doped porous carbon nanofiber webs as anodes for lithium ion batteries with a superhigh capacity and rate capability. *Advanced Materials* 24 (15): 2047–2050.

59 Ji, L., Lin, Z., Alcoutlabi, M., and Zhang, X. (2011). Recent developments in nanostructured anode materials for rechargeable lithium-ion batteries. *Energy & Environmental Science* 4 (8): 2682–2699.

60 Li, S., Chen, C., Fu, K. et al. (2014). Comparison of Si/C, Ge/C and Sn/C composite nanofiber anodes used in advanced lithium-ion batteries. *Solid State Ionics* 254: 17–26.

61 Fu, K., Lu, Y., Dirican, M. et al. (2014). Chamber-confined silicon–carbon nanofiber composites for prolonged cycling life of Li-ion batteries. *Nanoscale* 6 (13): 7489–7495.

62 Chen, Y., Hu, Y., Shao, J. et al. (2015). Pyrolytic carbon-coated silicon/carbon nanofiber composite anodes for high-performance lithium-ion batteries. *Journal of Power Sources* 298: 130–137.

63 Dirican, M., Lu, Y., Fu, K. et al. (2015). SiO_2-confined silicon/carbon nanofiber composites as an anode for lithium-ion batteries. *RSC Advances* 5 (44): 34744–34751.

64 Lin, H., Weng, W., Ren, J. et al. (2014). Twisted aligned carbon nanotube/silicon composite fiber anode for flexible wire-shaped lithium-ion battery. *Advanced Materials* 26 (8): 1217–1222.

65 Jiang, H., Ge, Y., Fu, K. et al. (2014). Centrifugally-spun tin-containing carbon nanofibers as anode material for lithium-ion batteries. *Journal of Materials Science* 50 (3): 1094–1102.

66 Lu, Y., Yanilmaz, M., Chen, C. et al. (2015). Centrifugally spun SnO_2 microfibers composed of interconnected nanoparticles as the anode in sodium-ion batteries. *ChemElectroChem* 2 (12): 1947–1956.

67 Kim, J.-C. and Kim, D.-W. (2014). Electrospun Cu/Sn/C nanocomposite fiber anodes with superior usable lifetime for lithium- and sodium-ion batteries. *Chemistry - An Asian Journal* 9 (11): 3313–3318.

68 Nitta, N. and Yushin, G. (2014). High-capacity anode materials for lithium-ion batteries: choice of elements and structures for active particles. *Particle and Particle Systems Characterization* 31 (3): 317–336.

69 Dirican, M., Yanilmaz, M., Fu, K. et al. (2014). Carbon-enhanced electrodeposited SnO_2/carbon nanofiber composites as anode for lithium-ion batteries. *Journal of Power Sources* 264: 240–247.

70 Shen, Z., Hu, Y., Chen, Y. et al. (2016). Controllable synthesis of carbon-coated Sn–SnO_2–carbon-nanofiber membrane as advanced binder-free anode for lithium-ion batteries. *Electrochimica Acta* 188: 661–670.

71 Dirican, M., Lu, Y., Ge, Y. et al. (2015). Carbon-confined SnO_2-electrodeposited porous carbon nanofiber composite as high-capacity sodium-ion battery anode material. *ACS Applied Materials & Interfaces* 7 (33): 18387–18396.

72 Luo, L., Xu, W., Xia, Z. et al. (2016). Electrospun ZnO–SnO_2 composite nanofibers with enhanced electrochemical performance as lithium-ion anodes. *Ceramics International* 42 (9): 10826–10832.

73 Ji, L., Toprakci, O., Alcoutlabi, M. et al. (2012). α-Fe_2O_3 nanoparticle-loaded carbon nanofibers as stable and high-capacity anodes for rechargeable lithium-ion batteries. *ACS Applied Materials & Interfaces* 4 (5): 2672–2679.

74 Zhu, J., Lu, Y., Chen, C. et al. (2016). Porous one-dimensional carbon/iron oxide composite for rechargeable lithium-ion batteries with high and stable capacity. *Journal of Alloys and Compounds* 672: 79–85.

75 Chen, R., Hu, Y., Shen, Z. et al. (2016). Controlled synthesis of carbon nanofibers anchored with $Zn_xCo_{3-x}O_4$ nanocubes as binder-free anode materials for lithium-ion batteries. *ACS Applied Materials & Interfaces* 8 (4): 2591–2599.

76 Pampal, E.S., Stojanovska, E., Simon, B., and Kilic, A. (2015). A review of nanofibrous structures in lithium ion batteries. *Journal of Power Sources* 300: 199–215.

77 Whittingham, M.S. (2004). Lithium batteries and cathode materials. *Chemical Reviews* 104 (10): 4271–4302.

78 Toprakci, O., Toprakci, H.A.K., Ji, L. et al. (2012). Carbon nanotube-loaded electrospun $LiFePO_4$/carbon composite nanofibers as stable and binder-free cathodes for rechargeable lithium-ion batteries. *ACS Applied Materials & Interfaces* 4 (3): 1273–1280.

79 Toprakci, O., Toprakci, H.A.K., Ji, L. et al. (2012). $LiFePO_4$ nanoparticles encapsulated in graphene-containing carbon nanofibers for use as energy storage materials. *Journal of Renewable and Sustainable Energy* 4 (1): 013121.

80 Zhang, S., Lu, Y., Xu, G. et al. (2012). LiF/Fe/C nanofibres as a high-capacity cathode material for Li-ion batteries. *Journal of Physics D: Applied Physics* 45 (39): 395301.

81 Zhang, S., Lin, Z., Ji, L. et al. (2012). Cr-doped Li_2MnSiO_4/carbon composite nanofibers as high-energy cathodes for Li-ion batteries. *Journal of Materials Chemistry* 22 (29): 14661–14666.

82 Zhang, S., Li, Y., Xu, G. et al. (2012). High-capacity $Li_2Mn_{0.8}Fe_{0.2}SiO_4$/carbon composite nanofiber cathodes for lithium-ion batteries. *Journal of Power Sources* 213: 10–15.

83 Lu, Y., Yanilmaz, M., Chen, C. et al. (2015). Lithium-substituted sodium layered transition metal oxide fibers as cathodes for sodium-ion batteries. *Energy Storage Materials* 1: 74–81.

84 Zeng, L., Yao, Y., Shi, J. et al. (2016). A flexible $S_{1-x}Se_x$@porous carbon nanofibers ($x \leq 0.1$) thin film with high performance for Li-S batteries and room-temperature Na-S batteries. *Energy Storage Materials* 5: 50–57.

85 Liang, G., Wu, J., Qin, X. et al. (2016). Ultrafine TiO_2 decorated carbon nanofibers as multifunctional interlayer for high-performance lithium-sulfur battery. *ACS Applied Materials & Interfaces* 8 (35): 23105–23113.

86 Zhang, Z., Wang, G., Lai, Y., and Li, J. (2016). A freestanding hollow carbon nanofiber/reduced graphene oxide interlayer for high-performance lithium-sulfur batteries. *Journal of Alloys and Compounds* 663: 501–506.

87 Wang, Z., Zhang, J., Yang, Y. et al. (2016). Flexible carbon nanofiber/polyvinylidene fluoride composite membranes as interlayers in high-performance lithium sulfur batteries. *Journal of Power Sources* 329: 305–313.

88 Fu, K., Li, Y., Dirican, M. et al. (2014). Sulfur gradient-distributed CNF composite: a self-inhibiting cathode for binder-free lithium-sulfur batteries. *Chemical Communications* 50 (71): 10277–10280.

89 Kim, D.S. and Park, Y.J. (2014). Buckypaper electrode containing carbon nanofiber/Co_3O_4 composite for enhanced lithium air batteries. *Solid State Ionics* 268: 216–221.

90 Xue, H., Mu, X., Tang, J. et al. (2016). A nickel cobaltate nanoparticle-decorated hierarchical porous N-doped carbon nanofiber film as a binder-free self-supported cathode for nonaqueous Li–O_2 batteries. *Journal of Materials Chemistry A* 4 (23): 9106–9112.

91 Zhang, G.Q., Zheng, J.P., Liang, R. et al. (2011). α-MnO_2/carbon nanotube/carbon nanofiber composite catalytic air electrodes for rechargeable lithium-air batteries. *Journal of the Electrochemical Society* 158 (7): A822–A827.

92 Alcoutlabi, M., Lee, H., Watson, J.V., and Zhang, X. (2012). Preparation and properties of nanofiber-coated composite membranes as battery separators via electrospinning. *Journal of Materials Science* 48 (6): 2690–2700.

93 Yanilmaz, M., Lu, Y., Dirican, M. et al. (2014). Nanoparticle-on-nanofiber hybrid membrane separators for lithium-ion batteries via combining electrospraying and electrospinning techniques. *Journal of Membrane Science* 456: 57–65.

94 Yanilmaz, M., Dirican, M., and Zhang, X. (2014). Evaluation of electrospun SiO_2/nylon 6,6 nanofiber membranes as a thermally-stable separator for lithium-ion batteries. *Electrochimica Acta* 133: 501–508.

95 Zhu, J., Yildirim, E., Aly, K. et al. (2016). Hierarchical multi-component nanofiber separators for lithium polysulfide capture in lithium-sulfur batteries: an experimental and molecular modeling study. *Journal of Materials Chemistry A* 4 (35): 13572–13581.

96 Yanilmaz, M. and Zhang, X. (2015). Polymethylmethacrylate/polyacrylonitrile membranes via centrifugal spinning as separator in Li-ion batteries. *Polymers* 7 (4): 629–643.

97 Zhang, X. and Lu, Y. (2014). Centrifugal spinning: an alternative approach to fabricate nanofibers at high speed and low cost. *Polymer Reviews* 54 (4): 677–701.

98 Lv, R., Zhu, Y., Liu, H. et al. (2016). Poly(vinylidene fluoride)/poly(acrylonitrile) blend fibrous membranes by centrifugal spinning for high-performance lithium ion battery separators. *Journal of Applied Polymer Science* 134 (8): 4451511–7.

99 Luo, X., Wang, J., Dooner, M., and Clarke, J. (2015). Overview of current development in electrical energy storage technologies and the application potential in power system operation. *Applied Energy* 137: 511–536.

100 Wei, K. and Kim, I.S. (2014). Application of nanofibers in supercapacitors. In: *Electrospun Nanofibers for Energy and Environmental Applications* (eds. Ding, B. and Yu, J.), 163–181. Springer.

101 Lai, F., Miao, Y.-E., Huang, Y. et al. (2015). Flexible hybrid membranes of $NiCo_2O_4$-doped carbon nanofiber@MnO_2 core–sheath nanostructures for high-performance supercapacitors. *The Journal of Physical Chemistry C* 119 (24): 13442–13450.

102 Wang, J.-G., Yang, Y., Huang, Z.-H., and Kang, F. (2011). Coaxial carbon nanofibers/MnO_2 nanocomposites as freestanding electrodes for high-performance electrochemical capacitors. *Electrochimica Acta* 56 (25): 9240–9247.

103 Miao, Y.-E., Fan, W., Chen, D., and Liu, T. (2013). High-performance supercapacitors based on hollow polyaniline nanofibers by electrospinning. *ACS Applied Materials & Interfaces* 5 (10): 4423–4428.

104 Pan, S., Lin, H., Deng, J. et al. (2015). Novel wearable energy devices based on aligned carbon nanotube fiber textiles. *Advanced Energy Materials* 5 (4): 1401438.

105 Shi, X., Zhou, W., Ma, D. et al. (2015). Electrospinning of nanofibers and their applications for energy devices. *Journal of Nanomaterials* 16 (1): 122.

106 Macdonald, T.J., Tune, D.D., Dewi, M.R. et al. (2015). A TiO_2 nanofiber–carbon nanotube-composite photoanode for improved efficiency in dye-sensitized solar cells. *ChemSusChem* 8 (20): 3396–3400.

107 Mohamed, I.M.A., Dao, V.-D., Yasin, A.S. et al. (2016). Synthesis of novel SnO_2@TiO_2 nanofibers as an efficient photoanode of dye-sensitized solar cells. *International Journal of Hydrogen Energy* 41 (25): 10578–10589.

108 Wang, Y., Jin, J., Yang, S. et al. (2016). Nitrogen-doped porous carbon nanofiber based oxygen reduction reaction electrocatalysts with high activity and durability. *International Journal of Hydrogen Energy* 41 (26): 11174–11184.

109 Bessel, C.A., Laubernds, K., Rodriguez, N.M., and Baker, R.T.K. (2001). Graphite nanofibers as an electrode for fuel cell applications. *The Journal of Physical Chemistry B* 105 (6): 1115–1118.

110 Sung, M.-T., Chang, M.-H., and Ho, M.-H. (2014). Investigation of cathode electrocatalysts composed of electrospun Pt nanowires and Pt/C for proton exchange membrane fuel cells. *Journal of Power Sources* 249: 320–326.

111 Delmondo, L., Salvador, G.P., Muñoz-Tabares, J.A. et al. (2016). Nanostructured Mn_xO_y for oxygen reduction reaction (ORR) catalysts. *Applied Surface Science* 388: 631–639.
112 Pu, X., Li, L., Song, H. et al. (2015). A self-charging power unit by integration of a textile triboelectric nanogenerator and a flexible lithium-ion battery for wearable electronics. *Advanced Materials* 27 (15): 2472–2478.
113 Jost, K., Dion, G., and Gogotsi, Y. (2014). Textile energy storage in perspective. *Journal of Materials Chemistry A* 2 (28): 10776–10787.
114 Chen, X., Xu, S., Yao, N., and Shi, Y. (2010). 1.6 V nanogenerator for mechanical energy harvesting using PZT nanofibers. *Nano Letters* 10 (6): 2133–2137.

25

Fiber-Based Sensors and Actuators

Xiaomeng Fang, Kony Chatterjee, Ashish Kapoor, and Tushar Ghosh

Wilson College of Textiles, North Carolina State University, 1020 Main Campus Drive, Raleigh, NC 27606, USA

25.1 Introduction

Wearable electronic devices are increasingly becoming a part of our daily lives. Commercial wearable devices currently available range from smart glasses with audiovisual integration to athletic apparel for real-time biometric tracking. As the field of flexible electronics progresses, there is significant research underway to integrate wearable and other electronic capabilities into textiles. The motivation is obvious since textiles are deployed over a vast number of surfaces including the human body. The increasing use of textiles for clothing and beyond is due to its unique and desirable properties derived mostly from their hierarchical structure with fibers as building blocks. Fiber-based "wearables" are inherently advantageous because they combine breathability, conformability, strength, and stability of textiles with electrical functionalities. Arguably, the future seems to point toward a system with electronic capabilities integrated into fiber-based textile substrates, or electronic textiles. Sensors and actuators are likely to become integral part of this emerging system. A sensor detects a change in any stimulus into a measurable signal, similar to human sensory organs [1, 2]. Actuators are used to convert a form of input energy into mechanical motion. As an illustration, the concept of an autonomous closed loop system for human thermophysiological comfort with sensors and actuators is shown in Figure 25.1.

This chapter focuses particularly on the working principles, fabrication processes, and applications of fiber-based sensors and actuators reported in the literature. The operating principles, performance, and the remaining challenges associated with these technologies are described. While sensory and actuation properties could be built into a monolithic fiber, it can also be developed in an assembly of fibers. For this discussion, both types are included with a particular focus on sensors and actuators that have been designed in the form of fibers. Additionally, a less restrictive definition of a fiber being a flexible cylindrical body with a high aspect ratio and diameter in the range of hundreds of microns is used.

Handbook of Fibrous Materials, First Edition. Edited by Jinlian Hu, Bipin Kumar, and Jing Lu.
© 2020 Wiley-VCH Verlag GmbH & Co. KGaA. Published 2020 by Wiley-VCH Verlag GmbH & Co. KGaA.

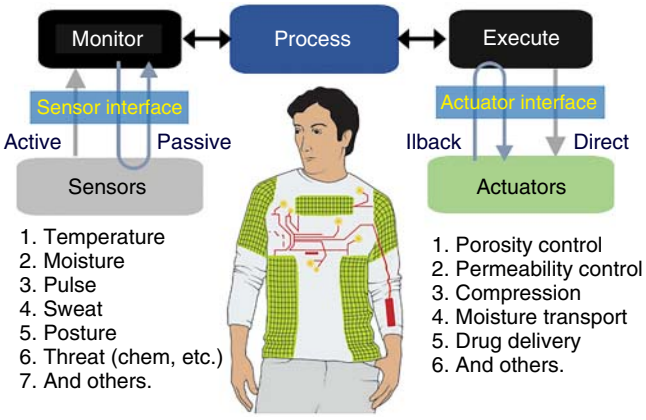


Figure 25.1 Illustration of a closed loop of system of integrated sensors and actuators.

25.2 Fibers as Actuators and Sensors

The traditional electromagnetic, pneumatic, and hydraulic actuators, currently used extensively in many applications, are not particularly suitable for wearable or flexible electronic applications. Material-based actuation technologies with high power to mass ratio such as piezoelectric ceramics, shape memory alloys (SMAs), and electroactive polymers (EAPs) seem to offer properties that are more attractive when flexibility and wearability are required. Biological muscles work for billions of cycles to generate about 150–300 kPa stress and 25% strain driven by complex mechanisms with a very short response time (milliseconds) [3, 4]. Hence, they have always been used as a benchmark to evaluate artificial material-based actuators. Interestingly, the natural muscle consists of hierarchical, aligned in parallel, robust, and resilient fibers [3, 5]. Hence, fiber-shaped actuators have the potential to mimic biological muscles. It is also important to note that some materials that are used as actuators are also capable of sensing modalities and hence can act as self-sensing actuators.

Sensors in the form of fibers in a textile substrate can be used in intimate contact with the human body via clothing or as sensors in large areas of deployment, for example, on tents, parachutes, etc. Fiber sensors are inherently advantageous because they can help retain the desirable properties of textiles – breathability, conformability, and strength – while simultaneously offering a sensory response. In the broadest sense, a sensor is a device that can detect changes in its environment and provide a usable output suitable for processing. In addition to the selective sensitivity toward a specific stimulus, important sensor characteristics include fast response, repeatability, reliability, and low hysteresis [6]. Apart from fiber-optic sensors, the concept of fiber sensors is relatively new. In this chapter, sensors are categorized based on their sensing modalities, i.e. strain sensing, humidity and temperature sensing, and chemical sensing. The discussion that follows covers the fiber-sensor concepts proposed in the literature mainly in the context of flexible electronics and electronic textiles. It is important to

remember that very few of these have resulted in the commercial production of devices except for fiber-optic gyroscopes, temperature, pressure, and vibration sensors.

25.3 Fundamental Principle and Types of Fiber Actuators

Fiber-based actuators convert input energy, in the form of thermal, electrical, magnetic, or others into mechanical motion. These actuators differ from traditional rigid actuators by exhibiting a high degree of conformability and offering flexibility in their material selection and synthesis [7].

To comprehensively summarize relevant technologies and developments, this chapter includes most of the fiber-shaped devices with a large aspect ratio as well as those in tubular structures with relatively large dimensions (beyond macro), different from traditional fibers. The information about actuators in this chapter is classified and organized based on the materials used in the device.

25.3.1 Shape Memory Materials

These constitute a class of smart materials that can remember their original shape/size after significant and seemingly inelastic deformation when subjected to a stimulus such as temperature or magnetic field. Shape memory materials include shape memory alloys (SMA) and shape memory polymers (SMP). The most investigated SMA is the nickel–titanium (NiTi) alloy known as Nitinol. Typical SMA fiber actuators are relatively larger than traditional textile fibers with diameters in the range of 100–400 μm. Elastic and flexible SMA filaments have been plied with commonly used textile fibers and subsequently woven and knitted into fabrics with controllable properties [8]. SMPs are generally considered more suitable for textiles because of their flexibility, lightweight, and better processability. SMPs have a much higher actuation strain of 400–800% with substantially low densities (0.9–1.25 g/cm^3 compared with 6–8 g/cm^3 for SMAs) [9].

SMPs can be actuated using thermal, chemical, and optical stimuli. Thermally activated SMPs are the most common and are generally designed to maintain a temporary shape below a transition temperature (T_{trans}) and actuate to their original shape as the temperature increases above T_{trans}. Polymer chains tend to stay in their random coiled status as long as they are constrained by cross-links or temporary bonding. In case of chemical cross-links, SMPs are phase separated into hard and soft segments that act as the frozen and reversible phases, respectively [10]. Many polymeric materials could be used as segments in SMPs, for example, the most commonly used is polyurethane (PU) based.

The fabrication processes for SMP fibers can be similar to those of traditional polymeric fibers, such as wet spinning [11, 12], melting spinning [13, 14], and electrospinning [15]. In addition to monofilaments, SMP fibers can also be processed into yarns and woven/knitted/nonwoven fabrics [16]. However, due to

Table 25.1 Summary of shape memory polymer-based fiber actuators.

Materials and dimension	Actuation stimuli	Maximum linear strain	Applications
PU[a]-based SMP Diameter: 200–500 μm [16–18]	Heat, 50 °C	N/A	• To improve textile aesthetics with "lively" effects • Breathable fabrics
PU-MWCNT[b] composite fiber Diameter: ~250 μm [13]	Heat, 70 °C	Fixed strain to 100% and shape recovery ratio up to 90%	• Smart textiles • Biomedical materials • High-performance actuators, e.g. microgrippers
Triblock liquid-crystal polymers Diameter: ~200 μm [19]	Heat	Strain up to 500%	• Smart textiles • Surgical technology • Artificial muscles
PU[a]-based SMP Diameter: N/A [15]	Heat	Fixed strain to 100% and shape recovery ratio up to 90%	• Smart textiles

a) Polyurethane.
b) Multiwalled carbon nanotube.

their unusual tactile properties, SMP fibers are generally incorporated with other types of fibers. In SMP-based textiles, the fabric structure also has a considerable influence on the shape memory effect [15].

Table 25.1 describes some SMP fiber actuators proposed in the literature. Typical SMP fiber diameters range from 200 to 500 μm. Nanoscale SMP fibers have also been fabricated with diameters ranging from 50 to 700 nm via electrospinning [20]. SMP fiber actuators offer a vast array of applications for textile- and clothing-related products, such as interactive shape changeable fabrics for windows or wall hangings, breathable fabrics, shoes, and crease- and shrink-resistant apparels. SMP fibers/fabrics are also used in biomedical application such as implants, scaffolds for tissue constructs, and sutures [10]. Shape memory material-based fiber actuators (refer Figure 25.2) offer new vistas for smart textiles, fashion garments, robotics, and biomedical product design [9].

25.3.2 Piezoelectric Materials

Piezoelectric effect is an electromechanical phenomenon wherein materials produce an electric voltage in response to a mechanical stimulation. The inverse piezoelectric effect, strain induced due to applied voltage, forms the principle of actuation of piezoelectric actuators. Piezoelectric effect is generated due to the reorientation or "poling" of randomly orientated neutral-state dipoles in the material to form an anisotropic structure as well as a dipole moment. When the

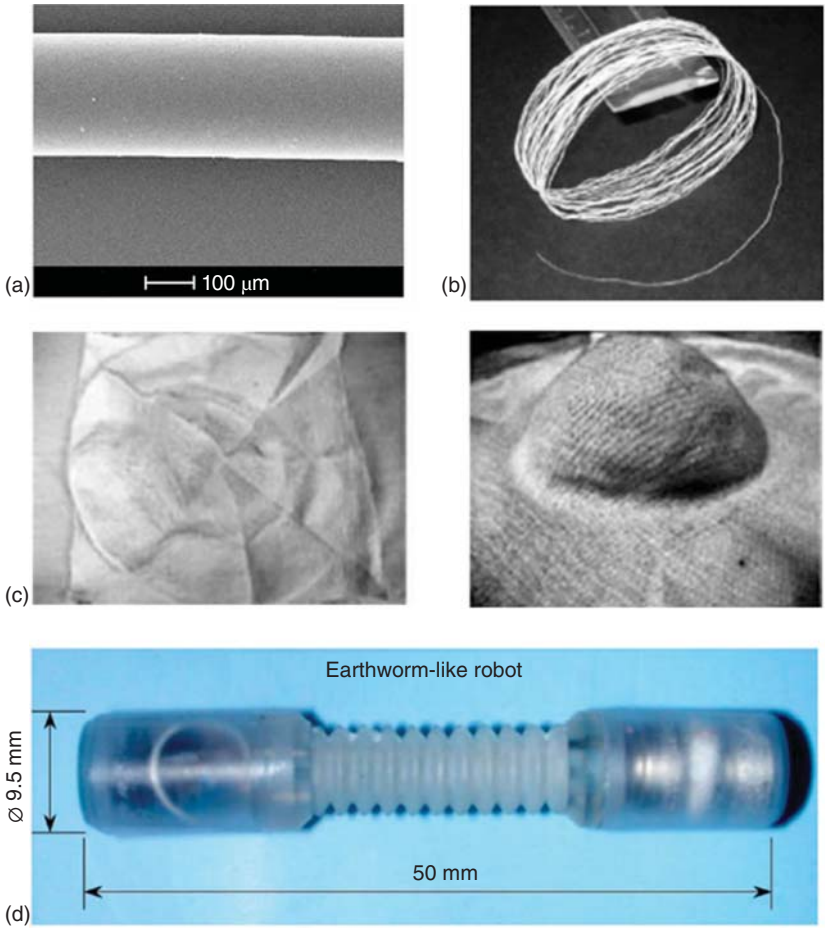


Figure 25.2 Shape memory material-based fiber actuators. (a) Scanning electron microscopy (SEM) image of fiber actuator based on polyurethane multiwalled carbon nanotube composites. Source: Meng and Hu 2008 [13]. Reproduced with permission of Elsevier. (b) Roll of triblock liquid-crystal polymer-based actuator. Source: Ahir et al. 2006 [19]. Reproduced with permission of John Wiley & Sons. (c) Creased shape and recovered smooth knitted SMP fabrics. Source: Hu and Chen 2010 [15]. Reproduced with permission of Royal Society of Chemistry. (d) SMA fiber muscles used in worm-like robot. Source: Kim et al. 2006 [21]. Reproduced with permission of Elsevier.

poled material is subjected to an electric voltage, it may show either contractional or elongational deformation due to reconfiguration of its dipoles [22]. Lead zirconate titanate (PZT) polycrystalline ceramic and polyvinylidene difluoride (PVDF) polymers are the most commonly used piezoelectric materials [22]. Piezoelectric actuators offer many benefits such as compact structures (usually multilayered), precision response, short response time, vacuum and clean room processabilities, and the possibility of operation at cryogenic temperatures [23]. However, they have fragile mechanical properties and very limited actuation strains especially for the ceramic actuators.

Piezoelectric fiber-based actuators (refer Figure 25.3) have been extensively used in various applications such as optical device control, reinforcements in composites, miniaturized rotary motors, controls for medical devices, and artificial muscles, see Table 25.2. Most piezoelectric fiber diameters are in the range of 100–200 μm, with some extremely wide fibers that can go up to 1000 μm. Typical driving electric voltages for actuation are in the order of hundreds of volts. Interestingly, piezoelectric fibers show extremely small linear actuation strains – substantially less than 1%. Piezoelectric fiber composites actuators have been developed [27, 41, 42] for applications in tunable Bragg gratings, helicopter motor blades, tail fins for fighter aircrafts, and inflatable spacecrafts.

Compared with their inorganic counterparts, piezoelectric polymers are lighter, less expensive, easiest to process, and offer better flexibility and deformability [43]. PVDF and its copolymers are well-known piezoelectric polymers with a high-energy conversion factor between its electrical and mechanical domains. Similar to piezoceramics, a poling process is required during fabrication of PVDF to achieve piezoelectricity. Electrospinning has been used to spin and pole PVDF fibers simultaneously to produce fibers of diameters in the range of hundreds of nanometers. Conventional electrospinning process normally produces randomly distributed fiber webs, and thus their piezoelectric response is not significant. Near-field electrospinning (NFES) has been developed to spin fiber in more ordered and controllable manner (also known as "direct-writing" method). Single or patterned PVDF fibers fabricated by NFES have been investigated and explored in actuator applications [26, 39]. The L-isomer of polylactic acid (PLA) and poly-L-lactic acid (PLLA) molecule with its asymmetric structure is a chiral polymer that requires no polling like PVDF to exhibit its piezoelectric behavior. Due to its chirality, deformation by shear in the drawing process is required to display piezoelectric behavior [44]. PLA fiber actuators have been investigated to work as bending actuator [37] and in tweezers for thrombosis sample exfoliation in blood vessel [25, 37].

25.3.3 Electrically Conducting Polymers

Electrically conducting polymers (CPs) can be used as actuators due to dimensional changes resulting from electromechanical ion insertion and removal. CP actuators offer many advantages, including being lightweight and low cost and having high-output stresses and relatively low operating voltages [45]. Among a wide range of available CPs, polypyrrole (PPy) and polyaniline (PANI) have been extensively investigated for their actuation properties. The strain generated by PPy and PANI actuators is usually small, and their performance is limited by a relatively slow response speed [46] and very low energy conversion efficiencies. Most CP actuators require a surrounding aqueous electrolyte, and hence solid or gel electrolytes have been developed to broaden the utility of CP actuators. Fabrication of CP filaments is usually via wet spinning wherein CP-based solution is extruded through the spinneret and the resultant as-spun fibers are kept in a liquid bath to remove the solvent [47–49]. Electrospinning has also been employed to spin CP fibers [50]. The obvious advantage of CPs over electronic EAPs is their low operating voltage.

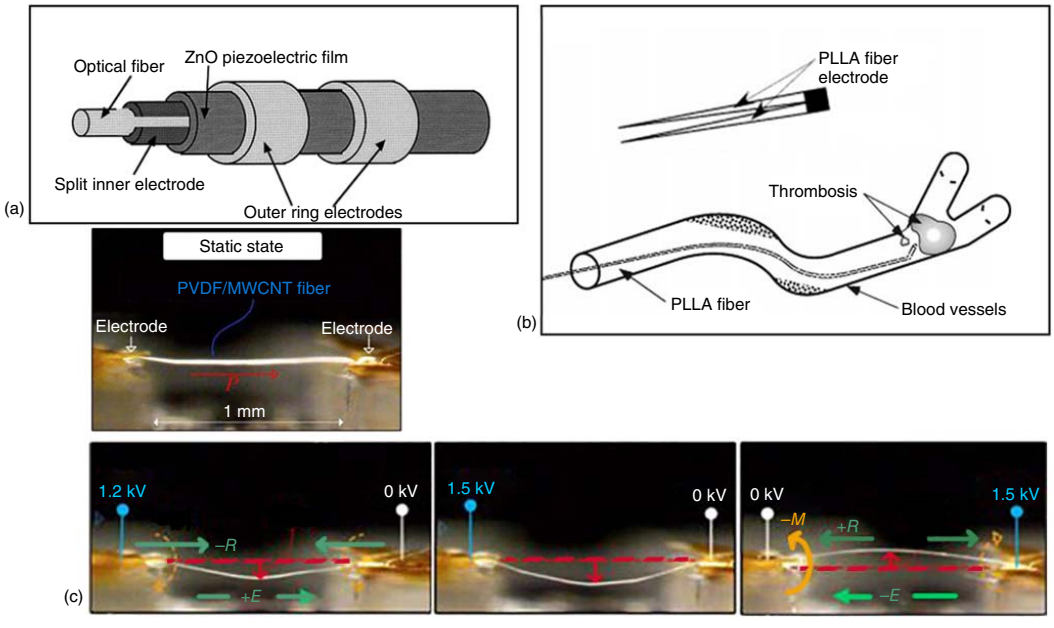


Figure 25.3 Piezoelectric material-based fiber actuators. (a) Hollow piezoelectric fibers actuator with optical fiber core. Source: Trolier-McKinstry et al. 1999 [24]. Reproduced with permission of Elsevier. (b) Piezoelectric poly(L-lactic acid) (PLLA) fiber tweezer and catheter. Source: Tajitsu 2006 [25]. Reproduced with permission of John Wiley & Sons. (c) PVDF/MWCNT composite fiber bending actuator. Source: Liu et al. 2013 [26]. Reproduced with permission of Elsevier.

Table 25.2 Summary of piezoelectric material-based fiber actuators.

Materials and dimension	Actuation stimuli	Maximum linear strain	Applications
PZT, PMN-PT[a] single-crystal fibers Diameter: 120–250 μm [27–31]	100 V–3 kV	1.5×10^{-4}% to 1.25×10^{-3}%	• Piezoelectric fiber reinforced composite actuator
Hollow ZnO fiber Diameter: ~140 μm [24]	AC: 0.5–5 V	4.5×10^{-6}%	• Control optical fiber located in the core of the hollow piezoelectric fiber actuator
PZT fiber Diameter: 1000 μm [32–36]	AC: −500 to 500 V	Torsion angle: 1.7°	• As rotary motor • To control miniature orthogonal optical scanning mirror
Chiral poly(L-lactic acid) (PLLA) polymer fiber Diameter: 20–100 μm [25, 37, 38]	AC/DC: −300 to 800 V	2.2×10^{-5}%	• To control catheter and tweezers for thrombosis sample exfoliation in blood vessels
PVDF or PVDF/CNT composite fibers Diameter: 2.6–35 μm [26, 39, 40]	DC: 1200–1500 V	1.9×10^{-3}% to 9.7×10^{-2}%	• Artificial muscles and switches

a) Lead magnesium niobate-lead titanate.

CP fiber actuators (refer Figure 25.4) reported in the literature are summarized in Table 25.3. Their main applications are in biomedical devices, such as microcatheters, and in robotic devices, such as artificial muscles. Their diameters range from 0.9 to 2000 μm. Fibers with very larger diameters are referred to as "dry" state actuators, which are assembled with a gel or solid electrolyte as the layer or core.

25.3.4 Dielectric Electroactive Polymers

Dielectric electroactive polymers (D-EAPs) constitute a class of electronic EAPs, which offer a tremendous potential as flexible actuators. They are lightweight and low cost and can generate large strains at high frequencies. In a typical actuator configuration, a layer of soft D-EAP is sandwiched between two layers of compliant electrodes. When an electric potential is applied across the electrodes, the attractive force between the opposite charges and the repulsive force between the like charges in the compliant electrode generates a compressive force on the D-EAP sandwich layer. This compressive force normalized over the area of the D-EAP is known as "Maxwell stress" [3]. Silicones [56, 57], acrylics [58, 59], and PU [60, 61] are the most commonly used D-EAP materials. Fiber-like D-EAP actuators were first developed by SRI International (SRI) [62], and subsequently

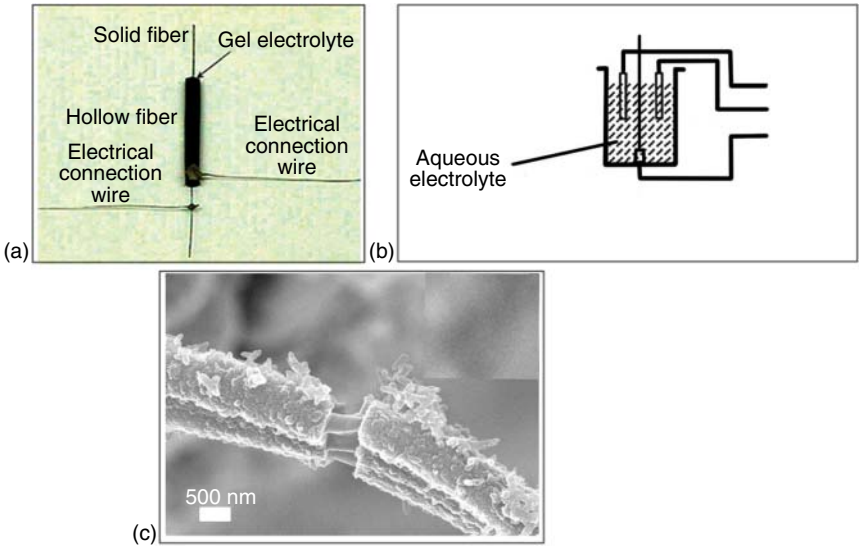


Figure 25.4 Electrically conductive polymer-based fiber actuators. (a) Solid-in-hollow fiber all polymer linear actuator. Source: Lu et al. 2004 [45]. Reproduced with permission of American Chemical Society. (b) Linear fiber actuator working in an aqueous electrolyte. Source: Qi et al. 2004 [47]. Reproduced with permission of American Chemical Society. (c) SEM image of electrospun PU/PANI hybrid fiber to assemble into bundles as artificial myofibril. Source: Gu et al. 2009 [50]. Reproduced with permission of American Chemical Society.

their many modifications have been demonstrated by Ghosh and coworkers [63], Carpi and De Rossi [64], and Cameron et al. [65]. D-EAP fiber actuators normally consist of an electrically conductive inner core, a middle elastomer layer, and an outer conductive layer. Technologies used to fabricate D-EAP fiber actuators include addition of conductive materials on the inside and outside walls of hollow tubes [64], repeatedly dipcoating a cylindrical core alternately into solutions of insulating and conducting precursors [66], and various co-extrusion methods [65].

D-EAP fiber actuators (refer Figure 25.5) reported in the literature generally have relatively larger diameters (~1000 μm) and moderate to high actuation strains in the range of 2–8%, see Table 25.4, although this strain range is promising for many applications and can be further improved by enhancing the material's dielectric properties or mechanical softness. However, the D-EAP actuator is limited by its requirement of high actuating voltages, usually of the magnitude of several kilovolts [67]. To some extent, this can be combatted by decreasing the thickness of the dielectric elastomer or by incorporating a voltage amplifier in the circuit. Miniaturization of D-EAP fiber actuators is another exciting, research-intensive challenge.

25.3.5 Carbon Nanotubes

Carbon nanotubes (CNTs) can be considered as graphene sheets rolled into cylinders with multiple layers and a nanoscale diameter (dubbed single-walled carbon nanotube [SWCNT] and multiwalled carbon nanotube [MWCNT] based on the number of layers) [68]. The actuation principle behind these

Table 25.3 Summary of electrical conductive polymer-based fiber actuators.

Materials and dimension	Actuation stimuli (V)	Maximum linear strain	Applications
PPy tube or PANI fiber Diameter: 10–400 μm [51–53]	AC: −0.5 to 0.8	0.2–0.95%	• To control a steerable microcatheter • Smart wearable garments
PPy tube infiltrated with liquid electrolyte Diameter: 1300–2200 μm [46]	AC: 3.6	Torsion angle: 0.034–0.017°	• Biomedical and biological devices
PANI doped with 2-acrylamido-2-methyl-1 -propanesulfonic acid (PANI·AMPSA) Diameter: ~1250 μm [4, 45, 54]	AC: −0.8 to 0.3	0.91%	• Lifelike robots • Artificial limbs • Biomimetic devices
PANI fiber working in aqueous electrolyte Diameter: ~90 μm [47]	AC: −0.2 to 0.6	~1.2%	• Linear actuator
20 PANI fibers twisted yarn, trade name PANION™ Filament diameter: ~60 μm Yarn diameter: ~300 μm [55]	AC: −1 to 1.75	0.82%	• To drive a cantilever device
PU/PANI hybrid fiber bundle working in aqueous methane sulfonic acid Filament diameter: 0.9 μm [50]	AC: −0.2 to 0.8	1.65%	• To mimic myofibrils

carbonaceous materials is complex. Many different independent mechanisms have been proposed, such as double-layer charge injection [69–71], electrostatic force, photothermal phenomenon, and "pneumatic mechanism" [72].

A CNT-based actuator that can generate large strains by melting and solidifying a "guest" or filler component such as paraffin has been reported. For example, CNT yarns infiltrated by paraffin wax form a hybrid yarn that undergoes torsional actuation upon a change in temperature. This has been attributed to the phase transition and thermal expansion of the paraffin wax. Other filler materials activated by pulsed light heating have also been used [73]. Another twisted CNT yarn actuator driven by internal pressure associated with ion insertion of CNTs was developed, behaving in a manner similar to the deformation finger trap stent [74]. Recently, a novel actuation mechanism involving an electromagnetic driving force applied onto spun CNT fibers has been introduced [75, 76]. Besides

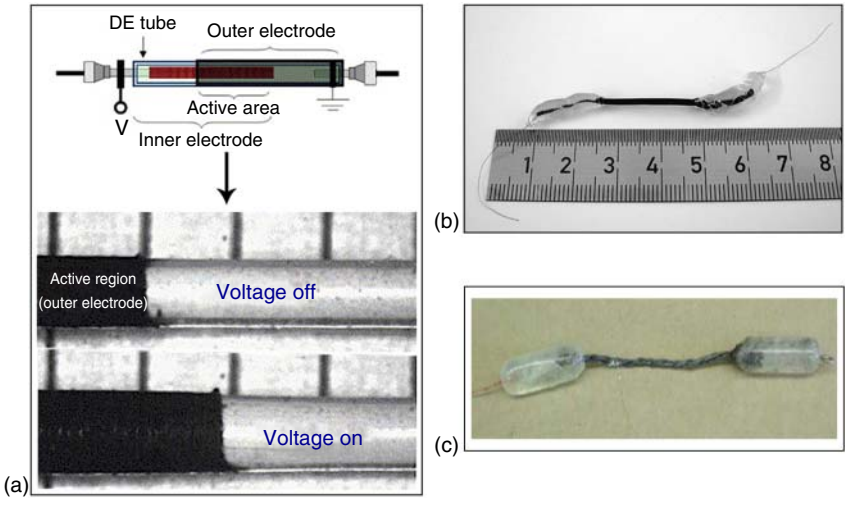


Figure 25.5 Dielectric elastomer (DE)-based fiber actuators. (a) Prototype of D-EAP fiber actuator made of silicone and PU tube. Source: Arora et al. 2007 [63]. Reproduced with permission of Elsevier. (b) Styrene-ethylene-butylene-styrene (SEBS) fiber actuator. Source: Kofod et al. 2010 [66]. Reproduced with permission of Springer. (c) Thermoplastic PU fiber actuator. Source: Cameron et al. 2008 [65]. Reproduced with permission of Elsevier.

Table 25.4 Summary of dielectric elastomer-based fiber actuators.

Materials and dimension	Actuation stimuli (kV)	Maximum linear strain (%)	Applications
Silicone and PU Diameter: 900 μm [63]	DC: ~3	7	• Fiber actuator used in conventional textiles or active, smart structures
Poly-(styrene-ethylene-butylene-styrene) (SEBS) Diameter: 1100 μm [66]	DC: 10	8	• Highly compact actuators
Thermoplastic polyurethane elastomer Diameter: ~1000 μm [65]	DC: 3.5	~2	• Linear actuator

electrical stimulation, solvent or vapor has also been explored as a viable actuation stimulus for CNT-based actuators [77, 78]. Table 25.5 lists various CNT or graphene fiber actuators.

Though the CNT-/graphene-based actuators (refer Figure 25.6) have diverse and complex actuation mechanisms, CNT fibers twisted into continuous strands of yarns offer the potential of forming into other textile structures.

Table 25.5 Summary of CNT-/graphene-based fiber actuators.

Material and dimension	Actuation stimuli	Maximum linear strain	Applications
Twisted CNT yarns working with guest matrix Yarn diameter: 10–200 μm; CNT diameter: 0.009 μm [73, 79]	Heat: 25–200°C DC: ~280 V Optical stimulus: 100 W lamp	Torsion: 11 500 revolutions/min Tensile: 3% contraction	• Carbon nanotube yarn muscles • To hurl a projectile
Electrolyte filled twisted CNT yarns Yarn diameter: 3.8 μm; CNT diameter: 0.012 μm [74]	AC: −2 to 2 V	Torsion: 590 revolution/min Tensile: 1% contraction	• Torsional carbon nanotube artificial muscles
Over-twisted CNT yarns Diameter: 280–530 μm [75, 80]	DC: <40 V	14%	• To create crawling motion in an electric walker robot
CNT yarn Diameter: 70–270 μm [78]	Ethanol, acetone, toluene, and dichloromethane	15%	• Hierarchically arranged helical fiber actuators • Smart textile woven lifting robot
Graphene fiber coated with electrolyte containing PPy Diameter: ~33 μm [81]	AC: −0.8 to 0.8 V	2.5%	• To fabricate multi-armed tweezers and net actuators
Graphene/graphene oxide fibers Diameter: ~30 μm [77]	Water vapor	5%	• Moisture-triggered actuators and application in smart textile robot and walking robot

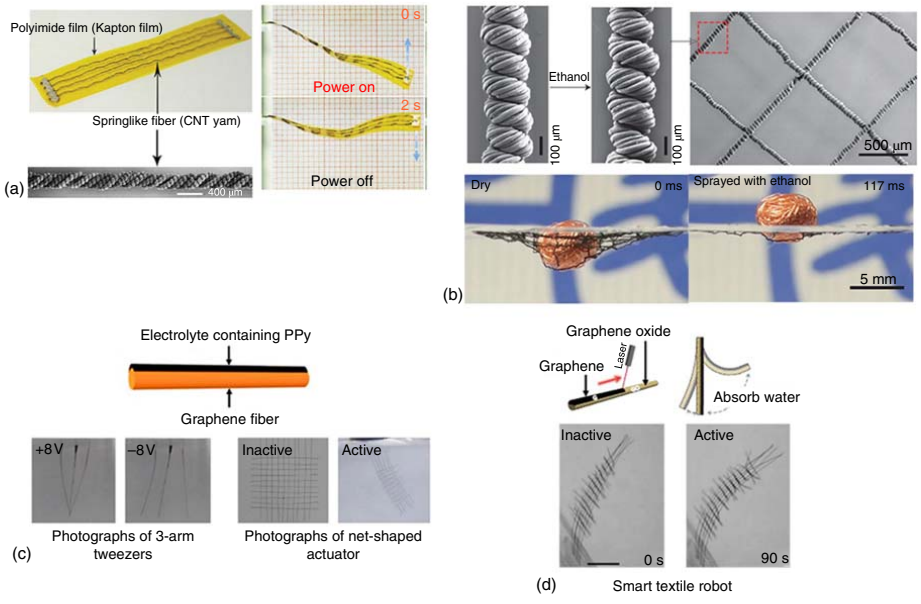


Figure 25.6 CNT-/graphene-based fiber actuators. (a) Kapton fabric ribbon woven from springlike CNT yarn actuators. Source: Chen et al. 2015 [80]. Reproduced with permission of John Wiley & Sons. (b) Woven textile-based lifting robot driven by CNT yarn muscles. Source: Chen et al. 2015 [78]. Reproduced with permission of Springer. (c) Multi-armed tweezers and net actuators made of graphene fiber actuators. Source: Wang et al. 2013 [81]. Reproduced with permission of Elsevier. (d) Moisture-triggered graphene fiber actuators and their application in smart textile robot and walking robot. Source: Cheng et al. 2013 [77]. Reproduced with permission of John Wiley & Sons.

25.3.6 Twisted/Coiled Fibers

Use of twist (or untwist) to produce linear and/or rotational actuation was proposed in the form of a strand-muscle actuator. The simple principle involved the use of length contraction (or extension) upon twisting (or untwisting) of two strands of polymeric fibers [82]. Thermally induced dimensional change in highly twisted and/or coiled polymeric fibers as a means of actuation forms this relatively new but innovative class fiber-based of actuators. Termed as fishing line and sewing thread muscles, these were first reported in 2014 [83]. Interestingly, these actuators made of commonly used polymeric (nylon, polyethylene, etc.) fibers with generally high levels of twist can generate fast, scalable, non-hysteretic tensile, and torsional actuations upon electrothermal or hydrothermal stimulation. Yarns with extreme twist can reach up to 49% contractile deformation and surprisingly lift loads over 100 times heavier than what a human muscle of the same dimension. The simple mechanism behind this actuator involves thermal expansion of the polymer filaments.

Various polymers such as nylon (nylon 6 and nylon 6,6), polyethylene, Kevlar, PVDF, polypropylene, and polyester have been used to fabricate twisted yarn muscles. In terms of applications, fishing line and sewing thread actuators not only work as muscles individually – for example, to electrothermally drive a window shutter or as a muscle to drive a robotic finger [84] – but also possess the capability to be woven or braided into novel textile structures as comfort-adjustable clothing with thermally or electrothermally driven porosity changes.

25.3.7 Other Types

In addition to the often-investigated fiber-based actuators described thus far, there are other types of fiber actuators, such as, pneumatic, electromagnetic, and photothermal. Some of these actuators offer potential future opportunities for development and have been summarized in Table 25.6.

25.4 Fundamental Principle and Types of Fiber Sensors

Fiber-based sensors integrated in a fabric are able to provide a measurable and quantifiable signal when there is a change in the input – referred to as the measurand. These sensors can detect changes in strain, pressure, humidity, temperature, or chemical composition among others and exhibit these changes in a variety of manners. Figure 25.7 explains the operating mechanism of sensors in a manner that makes their principle more apparent.

The information in this section is organized in terms of common measurand types and the transduction principle utilized to quantify the measurand.

Table 25.6 Summary of other types of fiber actuators.

Actuator type	Actuation mechanism	Fiber fabrication	Applications
Polymer gel-based fiber actuator [85–90]	Change in concentration of hydrogen ion or flow of solvated charges induced an asymmetric pressure	Electrospinning, wet spinning, and coagulation spinning	Analogous to muscles in living creatures
Liquid crystal elastomer (LCE) fiber actuator [89–91]	Electroclinic effect or the tilting angle of mesogens changes upon actuation or nematic–isotropic (NI) phase transition	Technology to fabricate LCE fibers has not yet been well developed	Artificial muscles
Magnetic microfibers used in textile actuators [92, 93]	Electromagnetic actuators	By introducing magnetic/ferromagnetic nanoparticle powders into the fiber matter during fiber production	Textile actuators
Photothermal actuator composed of optical fibers [94, 95]	Photothermal effect at the end of optical fiber causes stretching vibration at the end	One end of an optical fiber is cut as a bevel and painted black, and the incident light is along the length of the fiber	Novel optical robots
Pneumatic fiber actuator [96–99]	Pressurized air inflating or deflating a pneumatic bladder	An internal bladder surrounded by a braided structural shell made of threads	Artificial muscles

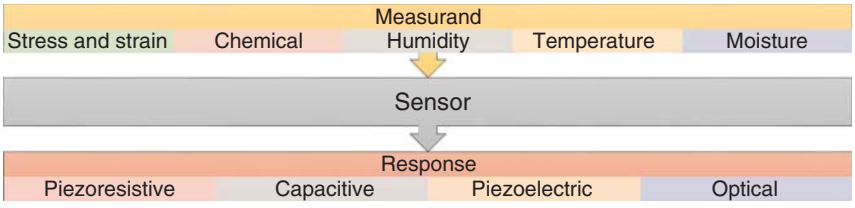


Figure 25.7 Basic working principle of a sensor with the various measurands and the sensor's sensing responses that will be discussed in this chapter.

25.4.1 Strain and Pressure Sensors

Most of the fiber-based sensors reported in the literature are designed to measure displacement or motion. Strain sensors are designed to measure relative displacement or motion and produce a measurable signal. The signal in turn is processed to calculate one or more of the very useful parameters such as strain, pressure (or stress), weight, and posture. This signal can be resistive, capacitive, optical, or piezoelectric. Pressure sensing involves the characterization of the force applied over a unit area of the component via generation of an electrical signal. Since application of pressure in many cases causes a relative displacement in the material, the characterization of such signals can be done again via a sensor capable of generating a resistive, capacitive, optical, or piezoelectric response.

25.4.1.1 Piezoresistive Type

The principle of piezoresistance is based on the simple concept that an electrical resistor may change its resistance upon experiencing a deformation. A *strain gauge* is one such piezoresistive sensor wherein the mechanical motion experienced by the sensor is directly translated to an electronic signal. The dependence of electrical resistance on the shape and material properties is straightforward. For a prismatic bar of length L and cross-sectional area A, it can be expressed as

$$R = \frac{\rho L}{A}$$

The electrical resistivity (ρ) is an intrinsic material property for homogeneous materials and is an invariant; therefore the piezoresistive behavior for homogeneous materials is derived from the changes in the shape parameters (A and L). However, in the case of a biphasic system, such as polymer particle composites, the change in electrical resistance cones from shape parameters as well as change in resistivity. At an atomic level, piezoresistance is due to a change in the energy gap between valence and conduction bands resulting in a change in the number of charge carriers, subsequently changing the resistance [2]. The most common morphology of a piezoresistive fiber includes a polymeric fiber with conductive particles dispersed throughout its volume or on the surface at or around its percolation threshold. Upon deformation, the relative movement of the conducting particles causes measurable change in its electrical resistance through breakage and reformation of conductive pathways. In the case of fiber assemblies, application of pressure on a network of conducting fibers (e.g. yarns/fabrics) results in a change in the contact resistance within the network, and this change can provide information about the location of the pressure being applied on the grid [100, 101]. Table 25.7 summarizes some piezoresistive sensors described in literature and their applications. Figure 25.8 illustrates the fabrication methods for some of these sensors.

Obviously, the research thrust has been toward integrating fiber-based sensors into continuous health monitoring systems. In general, piezoresistive fibers provide a large range of strain measurements in various configurations of bending, twisting, and stretching, enabling a strain sensitivities ranging from the measurement of heartbeats to giant deflections of up to 900% [105]. However, problems like unpredictable response, large hysteresis, and material choice limitations in

Table 25.7 Piezoresistive fiber-based sensors and their applications.

Sensor material [References]	Fabrication method	Sensing mechanism	Sensor performance	Applications
rGO[a]- and AgNW[b]-coated cotton fiber film [102, 103]	Dipcoating	Dynamic bridging effect of AgNW[b] with rGO[a] under external load	• 5.8 kPa^{-1} pressure sensitivity • 29.5 ms response time • 0.125 Pa detection limit • >10 000 cycles stability	• Measuring wrist hand pulses • Monitor motion of human body compression, bending, twisting sensor
rGO[a]-coated nylon fabric [104]	Dipcoating	Piezoresistivity of rGO[a] due to changes in its interlayers under pressure, fiber–fiber interactions, nylon's elastic strain	• 24 kPa^{-1} pressure sensitivity • 3 mm bend radius results in 213 ± 12 kΩ resistance change • At least 6000 cycles stability	• Low-cost forced touch trackpads for laptops • Wearable devices for health monitoring
CNT[c] wrapped on SEBS[d] fiber [105]	Benchtop melt drawing	Decrease in fiber diameter decreases CNT[c] sheath mass per unit length, increasing resistance with strain	• 14.1–65.1 Q_R depending on core diameter • 31.8–44.5 Q_R depending on CNT[c] layers • Up to 900% strain range	• Amperometric glucose sensing • Weaveable sensors in clothing
PU fiber coated with carbon ink and CNTs[c] [106]	Dipcoating	Piezoresistive strain response of CNTs[c] because of their higher deformability due to their fibrous structure	• Up to 100% strain measurement • Gauge factor ~ 3	• In microfluidic channels for delivering analytes • Multimodal physiological sensing
Hybrid Spandex-CNT[c] yarns [107]	CNT wrapped on outer surface of Spandex via interlocking knitting machine	Increase in resistance with increasing strain due to deformation of percolated networks	• Repeatable strain sensing from 0% to 100% strain for minimum 1000 cycles with low hysteresis • Gauge factor from 0.12 to 0.4	• Adjustable smart clothing, robotics, and medical devices • Smart actuating textiles

(Continued)

Table 25.7 (Continued)

Sensor material [References]	Fabrication method	Sensing mechanism	Sensor performance	Applications
CCF[e] integrated with polyester fiber and Lycra® [108]	Polyester and Lycra form composite core yarn with CCF[e] wrapped around it	CCF[e] yarn shows piezoresistive strain response due to elongational strain with increased resistance	• Can sustain 0.3–0.4 kg force under 23% strain compared with single CCF yarn, which only sustains 0.09 kg force • Measures bpm[f] accurately for humans (10–20 bpm)	• Sensitive strain sensor • Wearable respiration monitoring systems
Stainless steel threads and AgNW embedded into PDMS [109]	Patterning AgNW on PDMS surface, gluing it to cloth substrate, with stainless steel threads as electrodes	Transconductance causes pressure-sensitive current flow between the two electrodes at a fixed potential difference results in resistive pressure sensing	• 4/16 ms response time • 0.6 Pa detection limit • Stable for >5000 cycles • Works in <1 kPa pressure regime	• Ultrasensitive electronic skin • Flexible solar cells and optoelectronic devices • Disposable skin sensor
PPy[g] on SWCNT[h] coated cellulose yarns [110]	Cellulose yarn coated with SWCNT[h] via bobbin winding, PPy[g] electrodeposited on yarns	Conductive yarns act as piezoresistive strain sensors with differential strain sensing compared with no strain current and 100% strain current	• Up to 100% strain response stable after 4400 cycles	• Capable of energy storage and strain sensing • Self-powered sensory wearables • Possible large scale production

a) Reduced graphene oxide.
b) Silver nanowire.
c) Carbon nanotube(s).
d) Styrene-ethylene-butylene-styrene block copolymer.
e) Carbon-coated fibers.
f) Beats per minute.
g) Polypyrrole.
h) Single-walled carbon nanotube.

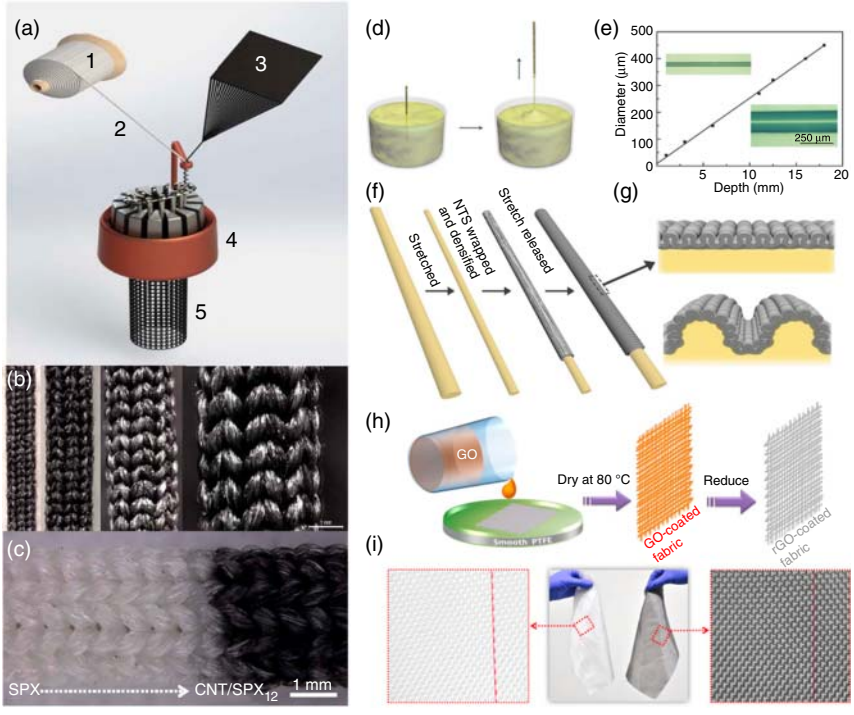


Figure 25.8 Fabrication methods of some piezoresistive sensors: (a) schematic for producing a knitted CNT/Spandex (SPX) textile. The different components are (1) a spool of SPX fibers, (2) an *n*-fiber SPX yarn, (3) a CNT forest, (4) a circular knitting machine, and (5) a knitted CNT/SPX textile. (b) Photograph of knitted CNT/SPX structures, containing 1, 4, 8, and 12 SPX fibers from left to right, respectively. (c) The transition between SPX_{12} yarns and CNT-wrapped SPX_{12} yarns in the knitted textile. Source: (Panels a–c) Foroughi et al. 2016 [107]. Reproduced with permission of American Chemical Society. (d) Schematic illustration of melt drawing used for fibers in Ref. [105]. (e) Influence of immersion depth of wooden rod on rubber fiber diameter with inset showing optical microscope images of rubber core fiber. (f) Detailed steps in fabrication. (g) Differences in buckling of the fibers depending on mass of CNT sheath to that of rubber core. Source: (Panels d–g) Wang et al. 2016 [105]. Reproduced with permission of John Wiley & Sons. (h) Coating nylon fabric with GO and subsequent reduction to rGO. Panel (i) shows the pristine nylon fabric (white) compared with coated nylon fabric. Source: (Panels h and i) Abdul Samad et al. 2017 [104]. Reproduced with permission of Elsevier.

the case of piezoresistive sensing belie the need for a better strain and pressure sensing mechanism explored in Sections 25.3.1.2–25.3.1.4.

25.4.1.2 Capacitive Type

Capacitive sensors convert a mechanical motion to an electrical signal via a change in their capacitance. A capacitor consists of a pair of electrodes separated by a dielectric medium, and a change in either the distance (d) between the electrodes, the area (A) of the electrodes, or the dielectric constant (ε) of the medium can cause a change in the capacitance (C_0), for parallel plate capacitors:

$$C_0 = \varepsilon \frac{A}{d}$$

For designing a highly sensitive capacitive pressure or strain sensor, it would be ideal to have a capacitor design with a large plate area and a narrow gap between the plates, without compromising the performance accuracy and fabrication reproducibility of the sensor [2]. Capacitive sensors provide the advantage of a linear relation between the mechanical deformation and the capacitance in certain sensor configurations, with lower hysteresis compared with piezoresistive sensors. More importantly, capacitive sensors can be formed in fibrous structures relatively easily. A summary of some of the capacitive fiber-based sensors proposed in the literature is provided in Table 25.8. Some capacitive fiber sensors may combine strain sensing mechanisms with capabilities of performing as energy storage or energy harvesting devices as supercapacitors [111, 112]. Various capacitor geometries (parallel plate, cylindrical, etc.) can be implemented in capacitive sensors making multimodal flexible sensors with the ability to sense pressure, axial strain, bending, and twisting. A large variety of materials can be used for capacitive fiber sensors, and the low hysteresis response of such sensors enables more accuracy in the measuring parameters. Figure 25.9 also summarizes the fabrication methods of some of the capacitive fiber-based sensors discussed in Table 25.8.

25.4.1.3 Piezoelectric Type

Piezoelectric materials exhibit an electric polarization when subjected to mechanical stresses, resulting in measurable potential difference. Conversely, they can act as actuators to generate displacement on application of an electric field. Therefore, these materials can be potentially used as self-sensing actuators [115, 116]. In the case of piezoelectric sensors, the mechanical stress applied on the sensor causes a differential potential difference between the two sides or faces of the sensor, and the resulting potential difference is measured as the sensor response. This differs from piezoresistive sensors in the manner that piezoelectric sensors generate a potential difference rather than a resistance change. It is important to remember that piezoelectric strain sensors generate an electrostatic charge only when force is applied to or removed from them and are generally not suitable for static force measurements because of charge leakage. They can be used effectively for transient or dynamic force measurements.

Polyvinylidene fluoride (PVDF) and its copolymers are the most widely used materials for flexible sensors including those in the form of fibers. PVDF consists of long chains of repeating monomer ($-CH_2-CF_2-$). The hydrogen atoms contain a net positive charge with respect to the carbon atom, and hence the monomer unit has an intrinsic dipole moment, causing it to show piezoelectric behavior. PVDF is pyroelectric, and hence its piezoelectric performance shows a strong dependence on temperature [117]. Table 25.9 summarizes some piezoelectric fiber sensors and their applications. Some of these piezoelectric sensors perform pressure sensing in an acoustic medium whereby acoustic waves are converted into electrical signals.

Table 25.8 Capacitive sensors and their applications.

Sensor material [References]	Fabrication method	Sensing mechanism	Sensor performance	Applications
CNT[a] buckled around silicone rubber core fibers [111]	CNT[a] aerogel sheets wrapped around silicone core fiber axially stretched by 300%	Capacitor structure made via buckled CNT[a]/dielectric rubber/buckled CNT[a] structure shows capacitive change in response to strain due to Poisson's ratio of rubber core ~ 0.49	• Strain sensing via 115.7% and 26% capacitive changes during stretching (200%) and twisting (1700 rad/m), respectively • 36.8 kPa pressure sensing range	• Highly deformable batteries, solar cells, wearable sensors, and energy harvesters
Silicone elastomer dielectric and encapsulating layers with ionically conductive ink as electrode [112]	Multicore–shell fiber printing process	Sensor arranged as a cylindrical resistor, a cylindrical capacitor, and a cylindrical ring resistor in series, which shows a resistive and capacitive response to strain	• Good agreement with theoretical model for capacitive and resistive response up to 250% strain • Gauge factor of 0.348 ± 0.11	• Can be integrated with wearable textiles for exo-suits, soft robotics, and health monitoring data
Primaloft® yarn (non-resistive) with carbon fiber yarn (sensing element) [113]	Weft knitting machine used to form knitted structure of carbon fiber trace	Measures differential voltage output and capacitance changes due to charging and discharging cause by finger	• Deviation RMS[b] error of 0.225 between simulation and experimental data for touch location via capacitance	• For robotics and smart garments • Gesture recognition
Pt deposited on cotton fibers and coated with PDMS[c] [114]	Thermal atomic layer deposition of metallic Pt	PDMS[c] acts as dielectric with conductive fiber as electrodes, showing capacitive response with pressure due to change in PDMS[c] thickness	• Stable capacitive response during loading and unloading of 0.4 N load for over 10 000 cycles • Capacitive response mapping for 56-pixel pressure sensors	• For advanced occupant classification system for vehicles • Wearable electronic sensors

a) Carbon nanotube.
b) Root mean square.
c) Polydimethylsiloxane.

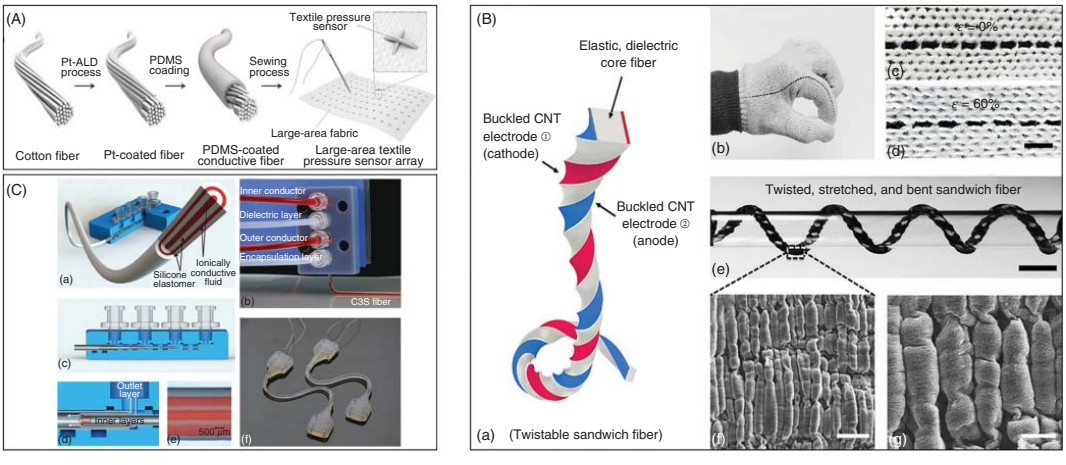


Figure 25.9 Fabrication processes of various capacitive fiber sensors. (A) Schematic illustration showing coating the cotton fiber with Pt via low-temperature atomic layer deposition (ALD) and a polydimethylsiloxane (PDMS) coating on the surface of the conductive fiber and subsequent integration of the pressure sensors into a fabric by sewing. Source: Lee et al. 2016 [114]. Reproduced with permission of Springer. (B) (a) Schematic illustration of twisted sandwich fibers with Ecoflex™ rubber core and two symmetric, buckled CNT electrodes and (b) 20 cm long fiber woven into a commercial glove and its magnified image in (c) before and (d) after applying 60% tensile strain with 8 mm scale bar. (e) Photograph of fiber wound around a glass tube (scale bar: 50 mm). SEM images of buckles formed in CNT due to straining and relaxation: (f) low (scale bar: 50 µm) and (g) high (scale bar: 20 µm) magnification. Source: Choi et al. 2016 [111]. Reproduced with permission of American Chemical Society. (C) (a) Schematic illustration and (b) image of multicore–shell printing process of fibers in Ref. [112]. Source: Frutiger et al. 2015 [112]. Reproduced with permission of John Wiley & Sons. (c, d) Schematic illustrations of the print-head design used for the process and higher magnification view of the printing outlet. (e) Optical image of a printed multicore–shell capacitive soft sensor filaments. (f) Two sensing filaments of different lengths. Source: Frutiger et al. 2015 [112]. Reproduced with permission of John Wiley & Sons.

Table 25.9 Piezoelectric sensors and their applications.

Sensor material [References]	Fabrication method	Sensing mechanism	Sensor performance	Applications
PVDF sheath with an HDPE[a]/CB[b] compound electrically conductive core [118]	Melt spinning bicomponent fibers	Piezoelectric response of the fiber with linear increase in output voltage with increasing strain	• 57 V/% voltage strain ratio • 0.313 (V/m)/(N m^2) piezoelectric coefficient	• Powering low power electronics • Heart rate and respiratory signal monitoring
CPC and PVDF-TrFE[c] with indium filaments and PC[d] cladding [119]	Thermal drawing of preform	Piezoelectric response via acoustic signal generation of the fibers on receiving pulsed excitations from an acoustic transducer	• Fibers generated audible sound between 7 and 15 kHz at 5 V driving voltage	• Active catheters for pressure and flow measurements in blood vessels • Acoustic microscopy
Aligned PVDF-TrFE[c] nanofibers [120]	Electrospinning	Generates a voltage across the effective contact length of the nanofibers in response to pressure Shows a positive and negative peak for current in response to bending cycles	• In 0.4–2 kPa pressure range shows sensitivity of 1.1 V/kPa • Current and voltage outputs for bending sensor were 6–40 nA and 0.5–1.5 V, respectively	• Skin conformal pressure sensor in small pressure regime • Accelerometers, vibrometers, orientational sensors
PVDF nanofiber web [121]	Electrospinning	PVDF sandwiched between gold-coated PET[d] films (electrodes), sound waves exert pressure on film to generate electric signals	• 266 mV/Pa sensitivity • Sensitivity to sound pressure level above 100 dB	• Acoustic sensor for detecting noise in a system

a) High-density polyethylene.
b) Carbon black.
c) Poly(vinylidene-fluoride-trifluoroethylene) copolymer.
d) Polyethylene terephthalate.

25.4.1.4 Optical Type

The use of optical fibers for sensing applications was first implemented in the early 1970s. An optical fiber is a high aspect ratio material that works on the principle of optical total internal reflection (TIR) for guiding light waves [122].

Optical fiber sensors can be described as a sensor wherein physical, chemical, or biological stimuli interact with light guided through an optical fiber to produce a quantifiable optical signal, which contains information about the stimulus being measured. Optical fiber sensors are classified as extrinsic types where the optical fiber acts as a carrier for transporting light to an external sensing system or intrinsic types wherein the entire sensing process is carried out within the optical fiber. In terms of materials, glass optical fibers (GOFs) have been traditionally used for optical fiber sensors, but they present problems in terms of being rigid and brittle. For something that is conformable and flexible, polymeric optical fibers (POFs) are preferred. POFs also have lower manufacturing costs, are lighter due to lower density, and have large core diameters, which make them less prone to breakage during handling. POFs also have a higher sensitivity to strain and temperature compared with GOFs. Some commonly used POF materials include polymethyl methacrylate (PMMA), polystyrene (PS), and amorphous fluorinated polymer (CYTOP) [123].

While it is not within the scope of this chapter to discuss all the different types of optical fiber sensors, in terms of strain and pressure sensing, optical fiber sensors can have various modes of operation – namely, fiber Bragg gratings (FBGs), interferometric sensing, and fiber bend sensing. Fiber-optic sensors used for strain and pressure sensing can have various modes of operation – namely, FBGs, interferometric sensing, and fiber bend sensing. In the case of FBGs, application of any local strain on the optical fiber sensor results in a change in the effective refractive index of the core in the optical fiber, resulting in a change in the wavelength of the reflected light. In interferometric sensing, the input light is split into a reference fiber and a sensory fiber (manipulated by the stimulus). On exposure to an external perturbation, such as longitudinal strain or pressure, a phase shift occurs. When these two recombine, they display an interference pattern at the output. Interferometric sensors for strain and pressure sensing provide high sensitivity and are used for applications such as monitoring structural health [124–127]. In microbend (or macro) sensing, when a fiber is subjected to small deformations, light rays in the core of the fiber exceed the critical angle causing small amounts of light escape the core. This results in a redistribution of energy in the core and the cladding. As the severity of microbending increases, the light intensity in the core decreases. The amount of received light is related to the amplitude of strain or deformation. Microbend sensors are useful for contact mode mechanical sensing applications such as tactile systems and strain detection. The difference between macro- and microbend sensors lies in the bending diameters and in the power loss mechanism; macrobend sensors have power loss due to the large bend causing changes in phase velocity of the light and transition loss due to light coupling in the leaky mode of the optical fiber [123] near the macrobend. Micro- and macrobend sensors are used for many shape and deformation sensing systems

[128–130]. Table 25.10 summarizes some POFs that operate on one of the abovementioned principles of sensing.

Optical fiber sensors offer the advantage of resilience to electromagnetic interference, a wide range of operating temperatures and conditions (such as high voltage or explosive environments), and chemical inertness. These have been under development for many years, and the technology is rather mature compared with all others. Commercial fiber-optic devices include gyroscopes, sensors for temperature, pressure, and vibration measurements [123, 135].

25.4.2 Humidity and Temperature Sensors

The principle of operation of humidity sensors can be same as that of pressure and strain sensors, i.e. capacitive, piezoresistive, optical [136], and mechanical [137] (swelling of the sensor due to moisture). Capacitive humidity sensors respond to changes in humidity levels via a change in the dielectric behavior of their dielectric medium. Resistive humidity sensors show a response via change in their resistance due to the presence of moisture, while optical humidity sensors respond via interferometric sensing wherein change in the relative humidity causes a change in the reflected optical power. Mechanical humidity sensors can detect changes in shape due to swelling in response to humidity changes. In terms of fiber-based sensors, interferometric, capacitive, and resistive responses to humidity changes have been extensively explored with CNTs being the most commonly used sensor material. The change in resistance of CNTs in response to humidity is due to reversible hygroscopic swelling [138]. Other materials such as polyvinyl alcohol (PVA), polyacrylic acid (PAA), hydroxyethyl cellulose (HEC), carbon black (CB), PANI have also been used as resistive humidity sensors. Such sensors are fabricated via simple dipcoating [139], electrospinning [140], and wet spinning [141]. Traditionally, metallic wires such as W, Ni, Cu, and Pt have been used as temperature sensors due to their intrinsic change in resistivity in response to temperature gradients. These metals can also be incorporated into fabric structures via knitting to form flexible temperature sensors [142, 143]. However, metallic fiber sensors in textiles add undesirable bulk and discomfort. Hence, polymeric temperature sensors with small amounts of temperature-sensitive additives such as CNTs, CB, carbon fibers, and metallic particles have been incorporated through fabrication methods such as dipcoating and wet and melt spinning, in an effort toward developing temperature sensing fibers [144–146]. Table 25.11 summarizes some humidity and temperature sensing fibers and their applications.

25.4.3 Chemical Sensors

When it comes to safety in hazardous environments, sensors play a vital role in saving human lives and protecting critical assets. Conformable chemical sensors in the form of fibers not only will be able to detect threats but also will be relatively comfortable to wear as a protective layer. Gas sensors in fibrous forms can provide enough porosity for the gas to penetrate the sensor system and change a key parameter of the sensor.

Table 25.10 Polymeric optical fiber sensors and their applications.

Sensor material [References]	Fabrication method	Sensing mechanism	Sensor performance	Applications
TOPAS COC[a] grade 5013 [131]	Drill and draw method: TOPAS drilled with hexagonal holes and then drawn to fiber	FBG mechanism causes shift in Bragg wavelength of sensor	• Sensitivity of 0.76, 0.80, 1.0 pm/$\mu\varepsilon$[b] at 50, 80, 110 °C, respectively, to small strains up to 0.3% • Sensitivity of 0.75 pm/$\mu\varepsilon$ at 98 °C for large strain up to 3%	• FBG POFs that can operate at temperatures up to 110 °C • In vivo biosensing applications
PMMA mPOF[c] [132]	Drill and draw technique	FBG mechanism wherein resonance wavelength depends linearly on applied force and strain up to 1%	• Strain sensitivity of 0.73 ± 0.02 pm/$\mu\varepsilon$ up to 1.53% strain • Temperature sensitivity of -77 ± 7 pm/°C • Linear resonance tunability of 7 nm	• In vivo biomedical applications for strain and temperature sensing
PMMA doped with <3% polystyrene [133]	N/A	Interferometric sensing causes change in phase of the light in response to elongation	• Elongation sensitivity of $131 \pm 3 \times 10^5$ rad/m • Temperature sensitivity of -212 ± 26 (rad/m)/K	• Structural health monitoring of bridges, highways, aircraft wings, and engineering structures
PMMA embedded into PDMS [134]	PMMA fabricated via preform-drawing method	FBG sensing mechanism enabling shear and pressure sensing due to change in Bragg wavelength shifts	• Pressure sensitivity of 0.8 pm/Pa in the range of 2.4 kPa • Shear stress sensitivity of 1.3 pm/Pa for a range of 0.06 kPa	• Measuring contact stress sensing for the human skin and tissues

a) Cyclic olefin copolymer.
b) Strain.
c) Microstructured polymer optical fiber.

Table 25.11 Humidity and temperature sensing fibers and their applications.

Sensor	Sensor material [References]	Fabrication method	Sensing mechanism	Sensor performance	Applications
Humidity	Cotton thread/CNTs dissolved in nafion or PSS water solutions [139]	Dipcoating	Resistance increases with humidity due to hygroscopic swelling of nafion and cotton, disrupting electron transport between CNTs	• Instantaneous and reversible change in resistance even at low humidity (20%)	• Human physiological sensing
	GO–silicon bilayer structure [137]	Spin coating GO thin films on silicon microbridge	Humidity-induced deformation of GO causes increased interlayer distance of GO sheets resulting in bending of silicon microbridge	• Sensitivity of 28.02 μV/%RH[a)] • Maximum humidity hysteresis ~3%	• Integration into MEMS[b)]/NEMS[c)] for multimodal sensing
	PVA/MWCNT [141]	CVD for preparing MWCNT and subsequent drawing in PVA solution	Sudden increase in electrical resistance of MWCNT/PVA due to swelling PVA matrix causes dispersed particles and interfaces in the composite matrix	• Sensitivity up to 1.89 at 100% RH[a)] • Adjustable switch point between 75 and 84% RH[a)] • High residual sensitivity of 0.63	• Monitoring real-time RH[a)] in electronic devices
Temperature	Copper, nickel, and tungsten wires embedded in knitted polyester fabric [142]	Flatbed knitting	Intrinsic resistance of the wire wrapped around an insulator changes with temperature	• Linear trend of temperature–resistance curve with coefficient of determination over 99.9%	• Garments to monitor skin temperature
	Nylon-6 functionalized with MWCNT/PPy [145]	Electrospun nylon-6 with vacuum-deposited MWCNT and polymerized PPy	Resistance linearly varies with temperature depending on temperature coefficient of resistance of the sensor	• Reliable detection in 25–45 °C range • Average temperature coefficient of resistance −0.204 ± 0.008%/°C	• Smart clothing and physiological monitoring in prosthetic sockets
	Double-helix SWCNT yarns [146]	SWCNT film twisted into double-helix structure	Double-helix structure acts as a thermocouple with the two CNT yarns as the electrodes Linear increase of resistance with temperature	• Sensitivity of 0.08–0.14 Ω/°C • Linear decrease of resistance upon cooling	• Lightweight and flexible thermocouple

a) Relative humidity.
b) Microelectromechanical systems.
c) Nanoelectromechanical systems.

Table 25.12 Chemical sensors and their applications.

Sensor material [References]	Fabrication method	Sensing mechanism	Detected gas	Detection limit
SWCNT[a]/cotton yarn/PEI[b] [149]	Dipcoating/immersion	NH_3 increases resistance of sensor due to charge transfer of electrons from NH_3 to SWCNT,[a] which increases distance between conductance and valence band in SWCNT[a]	NH_3	N/A
(PVC,[c] cumene-PSMA,[d] PSE,[e] and PVP[f]) Functionalized SWCNT on cotton fiber [150]	Dipcoating followed by embroidering	Percolation of gas molecules into the porous film, increasing resistance of sensor fiber	Body odors	50 ppm
PANI–nylon 6 composite fabric [153]	Immersion of nylon fabric in aniline and subsequent polymerization	PANI behaves as a p-type material, and NH_3 acts as a strong reducing agent to decrease conductivity	NH_3	1000 ppm
HCSA[g] doped-PANI nanofibers [154]	Directly via chemical synthesis or indirectly via electrospinning	Change in sensor resistance on exposure to gas is due to hygroscopic nature of the material and size of alkyl group of the alcohol, which affects the penetration of alcohol molecules into the polymer	Methanol, ethanol, 2-propanol	N/A

a) Single-walled CNT.
b) Polyethyleneimine.
c) Polyvinyl chloride.
d) Polystyrene-*co*-maleic anhydride.
e) Partial isobutyl/methyl mixed ester.
f) Polyvinylpyrrolidone.
g) Camphorsulfonic acid

Source: Seesaard et al. 2015 [150]. https://www.mdpi.com/1424-8220/15/1/1885. https://creativecommons.org/licenses/by/4.0/. Licensed under CCBY 4.0.

Chemical sensors in fiber form can be made of TiO_2- and CNT-incorporated porous carbon fibers [147], PANI-coated optical fibers [148], CNT coated onto polyethylenimine (PEI)/cotton yarns [149], functionalized CNT on cotton fibers [150], and pitch-based carbon fibers [151, 152].

Summary of some of the relevant chemical sensor concepts and their applications proposed in the literature is provided in Table 25.12. In all of these cases, the sensing response comes from relative change in the electrical resistance of the sensing fiber. Development of chemical sensors in the fiber form is an active area of scientific research.

25.5 Conclusions and Outlook

Flexible electronics is emerging as an important technology, critical in many applications including wearables, human–machine interfaces, healthcare, microrobotics, and electronic textiles. One of the earliest development in flexible electronics was thin silicon wafer solar cells assembled on polymer substrates for flexibility [155]. Many of the advances over the years have resulted in a wealth of demonstrators. The academic and commercial interest is driven primarily by the need for reduced cost, large area, roll to roll, and flexible systems that require conformal, distributed, and integrated functionality, which are unavailable from more traditional brittle material and device platforms.

Fiber-based sensing and actuation are a relatively new area of research and development within flexible electronics and mostly relevant to electronic textiles. In most cases, initial applications are being explored. The tremendous commercial interest in these technologies come from their potential to benefit many current applications as well as new applications that are beyond the abilities of current semiconductor-based sensors and actuators. In the case of actuators, many of the polymer-based materials and principles being employed feature a combination of high work density, large strain, and high stress, comparable or more than that of the natural muscles. Some of the electric field-driven EAP technologies demonstrate particularly high performance, but the requirement of high voltages may prove to be an obstacle. On the other hand, ionic EAPs often suffer from slow response and low electromechanical coupling. In all cases, life cycle issues such as creep deformation and fatigue life need further investigation.

Soft, polymer-based sensors have been under development for a long time and had resulted in the commercial production of various devices. Research and development in fiber sensors is relatively new with the exception of optical fiber sensors. Fiber-based sensors can be employed as part of clothing as a diagnostic and monitoring tool. For example, heat, moisture, salinity, or pressure sensor arrays can be used to monitor a patient in real time. The body heat and pressure distribution, sweat content, and posture can all reveal vital information on pathological symptoms. Textile-embedded electronics is becoming a reality, and textile-embedded sensors are likely to become ubiquitous. Electronic devices that can be seamlessly integrated to textiles require not only dimensional but also mechanical compatibility, such as flexibility, conformability, and

tolerance to stretch (10–20% strain). Fibrous structures offer not only high porosity and permeability but also large surface area for the measurement of biopotentials. Fiber-based devices open up a vast area of new possibilities for deployment of sensors, energy harvesting, etc. Current technologies to precisely manipulate fibers into useful structures may help in developing sensors that can combine multimodal functionalities into one and provide versatile sensing regimes. Another aspect in the development of fiber-based sensors that has not been touched upon here is the development of self-powered fiber sensors. Research in this area focuses on developing fiber sensors that act as supercapacitors for energy storage and conversion or thermoelectric materials (such as poly-(3,4-ethylenedioxythiophene):polystyrene sulfonate [PEDOT:PSS], PEI, Bi_2Te_3) that can harvest body heat into usable forms of energy. In this way, fiber-based sensors can transcend to form a complete system that can be self-powered and sensitive to various parameters at the same time.

The opportunities also come with challenges, such as dealing with material and geometric nonlinearities associated with large strains. Moreover, sensors that are typically designed to sense a specific measurand are most likely to respond to other stimuli that are not of interest. For example, a piezoresistive strain measurement sensor may respond to temperature. In the realm of fabrication or manufacturing of fiber-based devices, some of the common methods of fabricating sensors such as dipcoating might not be the most robust when it comes to multiple use and wash cycles. To overcome this, sensing capabilities must be integrated into the more fundamental fiber form – which can act as a building block for the entire textile.

Other problems such as biocompatibility of certain sensing materials also should be addressed especially when used in intimate skin applications. Another aspect that has a growing interest in the research community is the routing of signals from these fiber-based sensors to processors and transducers. Methods to interconnect the sensor and actuators to other electronic elements of a circuit need to be examined to allow development of flexible circuits that can transfer data in a facile, fast, and reliable manner. Finally, scaling up of fiber-based sensors in terms of a low-cost, high-output manufacture is an area that still needs significant research. Adapting existing fiber manufacturing techniques such as melt spinning so that fiber sensors can be manufactured on a large scale seems to be one way in which this problem can be tackled. Further work by the material community including fiber scientists should help make these technologies widely applicable in a range of applications where fiber-based electronic systems are desirable.

References

1 Trung, T.Q. and Lee, N. (2016). Flexible and stretchable physical sensor integrated platforms for wearable human-activity monitoring and personal healthcare. *Advanced Materials* 28: 4338–4372.

2 Kloeck, B. and De Rooij, N.F. (1994). Mechanical sensors. In: *Semiconductor Sensors* (ed. S.M. Sze), 153–204. New York: Wiley.

3 Bar-Cohen, Y. (2004). *Electroactive Polymer (EAP) Actuators as Artificial Muscles: Reality, Potential, and Challenges*, 2e. Bellingham, WA: SPIE.

4 Baughman, R.H. (2005). Playing nature's game with artificial muscles. *Science* 308: 63–65.

5 Gregorio, C.C., Granzier, H., Sorimachi, H., and Labeit, S. (1999). Muscle assembly: a titanic achievement? *Current Opinion in Cell Biology* 11: 18–25.

6 Fink, J.K. (2012). Sensor types and polymers. In: *Polymeric Sensors and Actuators* (ed. Pilla, Srikanth), 1–42. Wiley.

7 Peng, H., Sun, X., Weng, W., and Fang, X. *Polymer Materials for Energy and Electronic Applications*. London, United Kingdom: Academic Press.

8 Seelecke, S. and Muller, I. (2004). Shape memory alloy actuators in smart structures: modeling and simulation. *Applied Mechanics Reviews* 57: 23–46.

9 Lam Po Tang, S. and Stylios, G.K. (2006). An overview of smart technologies for clothing design and engineering. *International Journal of Clothing Science and Technology* 18: 108–128.

10 Hu, J. (2007). Development of shape memory polyurethane (SMPU) fiber. In: *Shape Memory Polymers and Textiles* (ed. Hu, Jinlian). pp. 305–337. Boca Raton, FL, USA: Woodhead Publishing.

11 Meng, Q., Hu, J., Zhu, Y. et al. (2007). Morphology, phase separation, thermal and mechanical property differences of shape memory fibres prepared by different spinning methods. *Smart Materials and Structures* 16: 1192.

12 Meng, Q., Hu, J., Zhu, Y. et al. (2007). Polycaprolactone-based shape memory segmented polyurethane fiber. *Journal of Applied Polymer Science* 106: 2515–2523.

13 Meng, Q. and Hu, J. (2008). Self-organizing alignment of carbon nanotube in shape memory segmented fiber prepared by in situ polymerization and melt spinning. *Composites Part A: Applied Science and Manufacturing* 39: 314–321.

14 Meng, Q. and Hu, J. (2008). Study on poly(Îµ-caprolactone)-based shape memory copolymer fiber prepared by bulk polymerization and melt spinning. *Polymers for Advanced Technologies* 19: 131–136.

15 Hu, J. and Chen, S. (2010). A review of actively moving polymers in textile applications. *Journal of Materials Chemistry* 20: 3346.

16 Chan Vili, Y.Y.F. (2007). Investigating smart textiles based on shape memory materials. *Textile Research Journal* 77: 290–300.

17 Gok, M.O., Bilir, M.Z., and Gurcum, B.H. (2015). Shape-memory applications in textile design. *Procedia Social and Behavioral Sciences* 195: 2160–2169.

18 Stylios, G.K. and Wan, T. (2007). Shape memory training for smart fabrics. *Transactions of the Institute of Measurement and Control* 29: 321–336.

19 Ahir, S.V., Tajbakhsh, A.R., and Terentjev, E.M. (2006). Self-assembled shape-memory fibers of triblock liquid-crystal polymers. *Advanced Functional Materials* 16: 556–560.

20 Zhuo, H., Hu, J., and Chen, S. (2008). Electrospun polyurethane nanofibres having shape memory effect. *Materials Letters* 62: 2074–2076.

21 Kim, B., Lee, M.G., Lee, Y.P. et al. (2006). An earthworm-like micro robot using shape memory alloy actuator. *Sensors and Actuators A: Physical* 125: 429–437.

22 Choi, S. and Han, Y. (2010). *Piezoelectric Actuators: Control Applications of Smart Materials (1)*. Boca Raton, FL: CRC Press.

23 Ballas, R.G. (2007). Piezoelectric materials. In: *Piezoelectric Multilayer Beam Bending Actuators*, 17–30. Berlin Heidelberg: Springer-Verlag.

24 Trolier-McKinstry, S., Fox, G.R., Kholkin, A. et al. (1999). Optical fibers with patterned ZnO/electrode coatings for flexural actuators. *Sensors and Actuators A: Physical* 73: 267–274.

25 Tajitsu, Y. (2006). Development of electric control catheter and tweezers for thrombosis sample in blood vessels using piezoelectric polymeric fibers. *Polymers for Advanced Technologies* 17: 907–913.

26 Liu, Z.H., Pan, C.T., Lin, L.W., and Lai, H.W. (2013). Piezoelectric properties of PVDF/MWCNT nanofiber using near-field electrospinning. *Sensors and Actuators A: Physical* 193: 13–24.

27 Wilkie, W.K., Inman, D.J., Lloyd, J.M., and High, J.W. (2006). Anisotropic laminar piezocomposite actuator incorporating machined PMN-PT single-crystal fibers. *Journal of Intelligent Material Systems and Structures* 17: 15–28.

28 NASA Technology Transfer Program (2006). Piezoelectric fiber composite actuator portfolio. https://technology.nasa.gov/patent/LAR-TOPS-17 (accessed 22 June 2017).

29 Bent, A.A., Hagood, N.W., and Rodgers, J.P. (1995). Anisotropic actuation with piezoelectric fiber composites. *Journal of Intelligent Material Systems and Structures* 6: 338–349.

30 Williams, R.B., Inman, D.J., Schultz, M.R. et al. (2004). Nonlinear tensile and shear behavior of macro fiber composite actuators. *Journal of Composite Materials* 38: 855–869.

31 Nguyen, C. and Kornmann, X. (2006). A comparison of dynamic piezoactuation of fiber-based actuators and conventional PZT patches. *Journal of Intelligent Material Systems and Structures* 17: 45–55.

32 Pan, C.L., Feng, Z.H., Ma, Y.T., and Liu, Y.B. (2008). Small torsional piezoelectric fiber actuators with helical electrodes. *Applied Physics Letters* 92: 012923.

33 Pan, C.L., Ma, Y.T., Liu, Y.B. et al. (2008). Torsional displacement of piezoelectric fiber actuators with helical electrodes. *Sensors and Actuators A: Physical* 148: 250–258.

34 Han, W.X., Zhang, Q., Ma, Y.T. et al. (2009). An impact rotary motor based on a fiber torsional piezoelectric actuator. *The Review of Scientific Instruments* 80: 014701.

35 Pan, C.L., Feng, Z.H., Ma, Y.T. et al. (2011). Coupled torsional and longitudinal vibrations of piezoelectric fiber actuator with helical electrodes. *IEEE Transactions on Ultrasonics, Ferroelectrics, and Frequency Control* 58: 829–837.

36 Pan, C.L., Ma, Y.T., Yin, J. et al. (2011). Miniature orthogonal optical scanning mirror excited by torsional piezoelectric fiber actuator. *Sensors and Actuators A: Physical* 165: 329–337.

37 Tajitsu, Y. (2008). Piezoelectricity of chiral polymeric fiber and its application in biomedical engineering. *IEEE Transactions on Ultrasonics, Ferroelectrics, and Frequency Control* 55: 1000–1008.

38 Itoh, S., Sawano, M., Hikawa, H. et al. (2010). Fundamental study of piezoelectric motion of chiral polymeric fibers for realizing tubular-type polymeric actuator for large macroscale physical object. *Japanese Journal of Applied Physics* 49: 09MD14.

39 Pu, J., Yan, X., Jiang, Y. et al. (2010). Piezoelectric actuation of direct-write electrospun fibers. *Sensors and Actuators A: Physical* 164: 131–136.

40 Chang, C., Tran, V.H., Wang, J. et al. (2010). Direct-write piezoelectric polymeric nanogenerator with high energy conversion efficiency. *Nano Letters* 10: 726–731.

41 French, J.D., Weitz, G.E., Luke, J.E. et al. (1996). Production of continuous piezoelectric fibers for sensor/actuator applications. In: *Proceedings of the 10th IEEE International Symposium on Applications of Ferroelectrics, 1996. ISAF'96*, vol. 2, 867–870.

42 Williams, R.B., Park, G., Inman, D.J., and Wilkie, W.K. (2002). An overview of composite actuators with piezoceramic fibers. In: *20th International Modal Analysis Conference*, 421–427. Los Angeles, CA.

43 Martins, P., Lopes, A.C., and Lanceros-Mendez, S. (2014). Electroactive phases of poly(vinylidene fluoride): determination, processing and applications. *Progress in Polymer Science* 39: 683–706.

44 Li, Z. and Cheng, Z. (2009). Piezoelectric and electrostrictive polymer actuators: fundamentals. In: *Biomedical Applications of Electroactive Polymer Actuators*, 317–334. Wiley.

45 Lu, W., Smela, E., Adams, P. et al. (2004). Development of solid-in-hollow electrochemical linear actuators using highly conductive polyaniline. *Chemistry of Materials* 16: 1615–1621.

46 Fang, Y., Pence, T.J., and Tan, X. (2011). Fiber-directed conjugated-polymer torsional actuator: nonlinear elasticity modeling and experimental validation. *IEEE/ASME Transactions on Mechatronics* 16: 656–664.

47 Qi, B., Lu, W., and Mattes, B.R. (2004). Strain and energy efficiency of polyaniline fiber electrochemical actuators in aqueous electrolytes. *The Journal of Physical Chemistry B* 108: 6222–6227.

48 Uh, K., Yoon, B., Lee, C.W., and Kim, J. (2016). An electrolyte-free conducting polymer actuator that displays electrothermal bending and flapping wing motions under a magnetic field. *ACS Applied Materials & Interfaces* 8: 1289–1296.

49 Spinks, G.M., Mottaghitalab, V., Bahrami-Samani, M. et al. (2006). Carbon-nanotube-reinforced polyaniline fibers for high-strength artificial muscles. *Advanced Materials* 18: 637–640.

50 Gu, B.K., Ismail, Y.A., Spinks, G.A. et al. (2009). A linear actuation of polymeric nanofibrous bundle for artificial muscles. *Chemistry of Materials* 21: 511–515.

51 De Rossi, D., Lorussi, F., Mazzoldi, A. et al. (2001). Active dressware: wearable proprioceptive systems based on electroactive polymers. In: *Proceedings of the 5th International Symposium on Wearable Computers*, 161–162.

52 Santa, A.D., Mazzoldi, A., and Rossi, D. (1996). Steerable microcatheters actuated by embedded conducting polymer structures. *Journal of Intelligent Material Systems and Structures* 7: 292–300.

53 De Rossi, D. and Mazzoldi, A. (1999). Linear fully dry polymer actuators. In: *Proceedings of SPIE 3669, Smart Structures and Materials 1999: Electroactive Polymer Actuators and Devices*, vol. 3669, 35–44.

54 Ding, J., Zhou, D., Spinks, G. et al. (2003). Use of ionic liquids as electrolytes in electromechanical actuator systems based on inherently conducting polymers. *Chemistry of Materials* 15: 2392–2398.

55 Lu, W., Norris, I.D., and Mattes, B.R. (2005). Electrochemical actuator devices based on polyaniline yarns and ionic liquid electrolytes. *Australian Journal of Chemistry* 58: 263–269.

56 Zhang, X., Wissler, M., Jaehne, B. et al. (2004). Effects of crosslinking, prestrain, and dielectric filler on the electromechanical response of a new silicone and comparison with acrylic elastomer. In: *Proceedings of SPIE 5385, Smart Structures and Materials 2004: Electroactive Polymer Actuators and Devices (EAPAD)*, vol. 5385, 78.

57 Kofod, G. and Sommer-Larsen, P. (2005). Silicone dielectric elastomer actuators: finite-elasticity model of actuation. *Sensors and Actuators A: Physical* 122: 273–283.

58 Kofod, G., Sommer-Larsen, P., Kornbluh, R., and Pelrine, R. (2003). Actuation response of polyacrylate dielectric elastomers. *Journal of Intelligent Material Systems and Structures* 14: 787–793.

59 Ma, W. and Cross, L.E. (2004). An experimental investigation of electromechanical response in a dielectric acrylic elastomer. *Applied Physics A* 78: 1201–1204.

60 Anonymous (1997). An experimental investigation of electromechanical responses in a polyurethane elastomer. *Journal of Applied Physics* 81: 2770–2776.

61 Su, J., Zhang, Q.M., Kim, C.H. et al. (1997). Effects of transitional phenomena on the electric field induced strain–electrostrictive response of a segmented polyurethane elastomer. *Journal of Applied Polymer Science* 65: 1363–1370.

62 Pelrine, R.E., Kornbluh, R.D., and Joseph, J.P. (1998). Electrostriction of polymer dielectrics with compliant electrodes as a means of actuation. *Sensors and Actuators A: Physical* 64: 77–85.

63 Arora, S., Ghosh, T., and Muth, J. (2007). Dielectric elastomer based prototype fiber actuators. *Sensors and Actuators A: Physical* 136: 321–328.

64 Carpi, F. and De Rossi, D. (2004). Dielectric elastomer cylindrical actuators: electromechanical modelling and experimental evaluation. *Materials Science and Engineering C* 24: 555–562.

65 Cameron, C.G., Szabo, J.P., Johnstone, S. et al. (2008). Linear actuation in coextruded dielectric elastomer tubes. *Sensors and Actuators A: Physical* 147: 286–291.

66 Kofod, G., Stoyanov, H., and Gerhard, R. (2010). Multilayer coaxial fiber dielectric elastomers for actuation and sensing. *Applied Physics A* 102: 577–581.

67 Ashley, S. (2003). Artificial muscles. *Scientific American* 289: 52–59.

68 Mirfakhrai, T., Madden, J.D.W., and Baughman, R.H. (2007). Polymer artificial muscles. *Materials Today* 10: 30–38.

69 Kosidlo, U., Omastova, M., Micusik, M. et al. (2013). Nanocarbon based ionic actuators: a review. *Smart Materials and Structures* 22: 104022.

70 Baughman, R.H., Cui, C., Zakhidov, A.A. et al. (1999). Carbon nanotube actuators. *Science* 284: 1340–1344.

71 Carpi, F., Kornbluh, R., Sommer-Larsen, P., and Alici, G. (2011). Electroactive polymer actuators as artificial muscles: are they ready for bioinspired applications? *Bioinspiration & Biomimetics* 6: 045006.

72 Spinks, G.M., Wallace, G.G., Fifield, L.S. et al. (2002). Pneumatic carbon nanotube actuators. *Advanced Materials* 14: 1728–1732.

73 Lima, M.D., Li, N., Andrade, M. et al. (2012). Electrically, chemically, and photonically powered torsional and tensile actuation of hybrid carbon nanotube yarn muscles. *Science* 338: 928–932.

74 Foroughi, J., Spinks, G.M., Wallace, G.G. et al. (2011). Torsional carbon nanotube artificial muscles. *Science* 334: 494–497.

75 Guo, W., Liu, C., Zhao, F. et al. (2012). A novel electromechanical actuation mechanism of a carbon nanotube fiber. *Advanced Materials* 24: 5379–5384.

76 Meng, F., Zhang, X., Li, R. et al. (2014). Electro-induced mechanical and thermal responses of carbon nanotube fibers. *Advanced Materials* 26: 2480–2485.

77 Cheng, H., Liu, J., Zhao, Y. et al. (2013). Graphene fibers with predetermined deformation as moisture-triggered actuators and robots. *Angewandte Chemie International Edition* 52: 10482–10486.

78 Chen, P., Xu, Y., He, S. et al. (2015). Hierarchically arranged helical fibre actuators driven by solvents and vapours. *Nature Nanotechnology* 10: 1077–1083.

79 Chun, K., Hyeong Kim, S., Kyoon Shin, M. et al. (2014). Hybrid carbon nanotube yarn artificial muscle inspired by spider dragline silk. *Nature Communications* 5: 3322.

80 Chen, P., He, S., Xu, Y. et al. (2015). Electromechanical actuator ribbons driven by electrically conducting spring-like fibers. *Advanced Materials* 27: 4982–4988.

81 Wang, Y., Bian, K., Hu, C. et al. (2013). Flexible and wearable graphene/polypyrrole fibers towards multifunctional actuator applications. *Electrochemistry Communications* 35: 49–52.

82 Suzuki, M. and Ichikawa, A. (2005). Toward springy robot walk using strand-muscle actuators. In: *Climbing and Walking Robots* (eds. Armada, M. A. and Santos, Pablo de Gonzalez), 479–486. Berlin Heidelberg: Springer-Verlag.

83 Haines, C.S., Lima, M.D., Li, N. et al. (2014). Artificial muscles from fishing line and sewing thread. *Science* 343: 868.

84 Wu, L., Jung, D.A., Rome, R.S. et al. (2015). Nylon-muscle-actuated robotic finger. In: *Proceedings of SPIE 9431, Active and Passive Smart Structures and Integrated Systems 2015*, vol. 9431, 94310I-12.

85 Lee, S.J., Lee, D.Y., Song, Y.S., and Cho, N.I. (2007). Chemically driven polyacrylonitrile fibers as a linear actuator. *Solid State Phenomena* 124–126: 1197–1200.

86 Samatham, R., Park, I.S., Kim, K.J. et al. (2006). Electrospun nanoscale polyacrylonitrile artificial muscle. *Smart Materials and Structures* 15: N152.

87 Shahinpoor, M., Norris, I.D., Mattes, B.R. et al. (2002). Electroactive polyacrylonitrile nanofibers as artificial nanomuscles. In: *Proceedings of SPIE 4695, Smart Structures and Materials 2002: Electroactive Polymer Actuators and Devices (EAPAD)*, vol. 4695, 351–358.

88 Gonzalez, M.A. and Walter, W.W. An investigation of electrochemomechanical actuation of conductive polyacrylonitrile (PAN) nanofiber composites. In: *Proceedings of SPIE 9056, Electroactive Polymer Actuators and Devices (EAPAD) 2014*, vol. 9056, 90563J-9.

89 Yu, L. and Gu, L. (2009). Effects of microstructure, crosslinking density, temperature and exterior load on dynamic pH-response of hydrolyzed polyacrylonitrile-blend-gelatin hydrogel fibers. *European Polymer Journal* 45: 1706–1715.

90 Michardiere, A., Mateo-Mateo, C., Derre, A. et al. (2016). Carbon nanotube microfiber actuators with reduced stress relaxation. *Journal of Physical Chemistry C* 120: 6851–6858.

91 Naciri, J., Srinivasan, A., Jeon, H. et al. (2003). Nematic elastomer fiber actuator. *Macromolecules* 36: 8499–8505.

92 Wiak, S., Firych-Nowacka, A., and Smolka, K. (2008). Computer model of 3-D magnetic micro fibres used in textile actuators. In: *2008 18th International Conference on Electrical Machines*, 1–6.

93 Rubacha, M. and Zieba, J. (2006). Magnetic textile elements. *Fibres & Textiles in Eastern Europe* 14: 49–53.

94 Otani, Y., Matsuba, Y., and Yoshizawa, T. (2002). Two-dimensional movement of photothermal actuator composed of optical fibers. In: *Proceedings of SPIE 4902, Optomechatronic Systems III*, vol. 4902, 78–82.

95 Otani, Y., Matsuba, Y., and Yoshizawa, T. (2001). Photothermal actuator composed of optical fibers. In: *Proceedings of SPIE 4564, Optomechatronic Systems II*, vol. 4564, 216–219.

96 Chou, C.-P. and Hannaford, B. (1994). Static and dynamic characteristics of McKibben pneumatic artificial muscles. In: *Proceedings of the 1994 IEEE International Conference on Robotics and Automation*, vol. 1, 281–286.

97 Yeh, T., Wu, M., Lu, T. et al. (2010). Control of McKibben pneumatic muscles for a power-assist, lower-limb orthosis. *Mechatronics* 20: 686–697.

98 Connolly, F., Polygerinos, P., Walsh, C.J., and Bertoldi, K. (2015). Mechanical programming of soft actuators by varying fiber angle. *Soft Robotics* 2: 26–32.

99 Tondu, B. (2012). Modelling of the McKibben artificial muscle: a review. *Journal of Intelligent Material Systems and Structures* 23: 225–253.

100 Shimojo, M., Namiki, A., Ishikawa, M. et al. (2004). A tactile sensor sheet using pressure conductive rubber with electrical-wires stitched method. *IEEE Sensors Journal* 4: 589–596.

101 Hui, Z., Ming, T.X., Xi, Y.T., and Sheng, L.X. (2006). Pressure sensing fabric. *Proceedings MRS* 001, 920.

102 Wei, Y., Chen, S., Dong, X. et al. (2017). Flexible piezoresistive sensors based on aerodynamic bridging effect of silver nanowires toward graphene. *Carbon* 113: 395–403.

103 Wei, Y., Chen, S., Lin, Y. et al. (2016). Silver nanowires coated on cotton for flexible pressure sensors. *Journal of Materials Chemistry C* 4: 935–943.

104 Abdul Samad, Y., Komatsu, K., Yamashita, D. et al. (2017). From sewing thread to sensor: Nylon® fiber strain and pressure sensors. *Sensors and Actuators B: Chemical* 240: 1083–1090.

105 Wang, H., Liu, Z., Ding, J. et al. (2016). Downsized sheath–core conducting fibers for weavable superelastic wires, biosensors, supercapacitors, and strain sensors. *Advanced Materials* 28: 4998–5007.

106 Mostafalu, P., Akbari, M., Alberti, K.A. et al. (2016). A toolkit of thread-based microfluidics, sensors, and electronics for 3D tissue embedding for medical diagnostics. *Microsystems & Nanoengineering* 2: 16039.

107 Foroughi, J., Spinks, G.M., Aziz, S. et al. (2016). Knitted carbon-nanotube-sheath/spandex-core elastomeric yarns for artificial muscles and strain sensing. *ACS Nano* 10: 9129–9135.

108 Huang, C., Shen, C., Tang, C., and Chang, S. (2008). A wearable yarn-based piezo-resistive sensor. *Sensors and Actuators A: Physical* 141: 396–403.

109 Lai, Y., Ye, B., Lu, C. et al. (2016). Extraordinarily sensitive and low-voltage operational cloth-based electronic skin for wearable sensing and multifunctional integration uses: a tactile-induced insulating-to-conducting transition. *Advanced Functional Materials* 26: 1286–1295.

110 Huang, Y., Kershaw, S.V., Wang, Z. et al. (2016). Highly integrated supercapacitor-sensor systems via material and geometry design. *Small* 12: 3393–3399.

111 Choi, C., Lee, J.M., Kim, S.H. et al. (2016). Twistable and stretchable sandwich structured fiber for wearable sensors and supercapacitors. *Nano Letters* 16: 7677–7684.

112 Frutiger, A., Muth, J.T., Vogt, D.M. et al. (2015). Capacitive soft strain sensors via multicore–shell fiber printing. *Advanced Materials* 27: 2440–2446.

113 Vallett, R., Young, R., Knittel, C. et al. (2016). Development of a carbon fiber knitted capacitive touch sensor. *MRS Advances* 1: 2641–2651.

114 Lee, J., Yoon, J., Kim, H.G. et al. (2016). Highly conductive and flexible fiber for textile electronics obtained by extremely low-temperature atomic layer deposition of Pt. *NPG Asia Materials* 8: e331.

115 Ikeda, H. and Morita, T. (2011). High-precision positioning using a self-sensing piezoelectric actuator control with a differential detection method. *Sensors and Actuators A: Physical* 170: 147–155.

116 Rakotondrabe, M., Ivan, I.A., Khadraoui, S. et al. (2014). Simultaneous displacement/force self-sensing in piezoelectric actuators and applications to robust control. *IEEE/ASME Transactions on Mechatronics* 20: 519–531.

117 Sirohi, J. and Chopra, I. (2000). Fundamental understanding of piezoelectric strain sensors. *Journal of Intelligent Material Systems and Structures* 11: 246–257.

118 Nilsson, E., Lund, A., Jonasson, C. et al. (2013). Poling and characterization of piezoelectric polymer fibers for use in textile sensors. *Sensors and Actuators A: Physical* 201: 477–486.

119 Egusa, S., Wang, Z., Chocat, N. et al. (2010). Multimaterial piezoelectric fibres. *Nature Materials* 9: 643–648.

120 Persano, L., Dagdeviren, C., Su, Y. et al. (2013). High performance piezoelectric devices based on aligned arrays of nanofibers of poly(vinylidenefluoride-co-trifluoroethylene). *Nature Communications* 4: 1633.

121 Lang, C., Fang, J., Shao, H. et al. (2016). High-sensitivity acoustic sensors from nanofibre webs. *Nature Communications* 7: 11108.

122 Chin, K., Fang, Z., and Qu, R. (2012). *Fundamentals of Optical Fiber Sensors (1)*, Wiley Series in Microwave and Optical Engineering. Somerset, NJ: Wiley.

123 Rajan, G. (2014). *Optical Fiber Sensors : Advanced Techniques and Applications*. Boca Raton, FL: CRC Press.

124 Her, S.C., and Yang, C.M. (2012). Dynamic strain measured by Mach-Zehnder interferometric optical fiber sensors. *Sensors* 12 (3): 3314–3326.

125 Xu, F., Ren, D., Shi, X. et al. (2012). High-sensitivity Fabry-Perot interferometric pressure sensor based on a nanothick silver diaphragm. *Optics Letters* 37: 133–135.

126 Zhang, Y., Yuan, L., Lan, X. et al. (2013). High-temperature fiber-optic Fabry-Perot interferometric pressure sensor fabricated by femtosecond laser. *Optics Letters* 38: 4609–4612.

127 Tian, Z. and Yam, S.S.H. (2009). In-Line abrupt taper optical fiber Mach-Zehnder interferometric strain sensor. *IEEE Photonics Technology Letters* 21: 161–163.

128 Chen, Y. and Liu, C. (2016). Radius and orientation measurement for cylindrical objects by a light section sensor. *Sensors* 16: 1981.

129 Bianchi, M., Haschke, R., Büscher, G., Ciotti, S., Carbonaro, N. and Tognetti, A., 2016. A multi-modal sensing glove for human manual-interaction studies. *Electronics* 5 (3): 42.

130 Noh, Y., Liu, H., Sareh, S. et al. (2016). Image-based optical miniaturized three-axis force sensor for cardiac catheterization. *IEEE Sensors Journal* 16: 7924–7932.

131 Markos, C., Stefani, A., Nielsen, K. et al. (2013). High-Tg TOPAS microstructured polymer optical fiber for fiber Bragg grating strain sensing at 110 degrees. *Optics Express* 21: 4758–4765.

132 Yuan, W., Stefani, A., and Bang, O. (2011). Tunable polymer fiber Bragg grating (FBG) inscription: fabrication of dual-FBG temperature compensated polymer optical fiber strain sensors. *IEEE Photonics Technology Letters* 24: 401–403.

133 Silva-Lopez, M., Fender, A., MacPherson, W.N. et al. (2005). Strain and temperature sensitivity of a single-mode polymer optical fiber. *Optics Letters* 30: 3129–3131.

134 Zhang, Z.F., Tao, X.M., Zhang, H.P., and Zhu, B. (2013). Soft fiber optic sensors for precision measurement of shear stress and pressure. *IEEE Sensors Journal* 13: 1478–1482.

135 Jha, A.R. (2007). *Fiber Optic Technology - Applications to Commercial, Industrial, Military, and Space Optical Systems* Raleigh, NC, USA: SciTech Publishing.

136 Arregui, F.J., Liu, Y., Matias, I.R., and Claus, R.O. (1999). Optical fiber humidity sensor using a nano Fabry-Perot cavity formed by the ionic self-assembly method. *Sensors and Actuators B: Chemical* 59: 54–59.

137 Yao, Y., Chen, X., Guo, H. et al. (2012). Humidity sensing behaviors of graphene oxide-silicon bi-layer flexible structure. *Sensors and Actuators B: Chemical* 161: 1053–1058.

138 Na, P.S. and Kim, H. (2005). Investigation of the humidity effect on the electrical properties of single-walled carbon nanotube transistors. *Applied Physics Letters* 87: 093101.

139 Shim, B.S., Chen, W., Doty, C. et al. (2008). Smart electronic yarns and wearable fabrics for human biomonitoring made by carbon nanotube coating with polyelectrolytes. *Nano Letters* 8: 4151–4157.

140 Lin, Q., Li, Y., and Yang, M. (2012). Investigations on the sensing mechanism of humidity sensors based on electrospun polymer nanofibers. *Sensors and Actuators B: Chemical* 171–172: 309–314.

141 Li, W., Xu, F., Sun, L. et al. (2016). A novel flexible humidity switch material based on multi-walled carbon nanotube/polyvinyl alcohol composite yarn. *Sensors and Actuators B: Chemical* 230: 528–535.

142 Husain, M.D., Kennon, R., and Dias, T. (2014). Design and fabrication of temperature sensing fabric. *Journal of Industrial Textiles* 44: 398–417.

143 Husain, M.D. and Kennon, R. (2013). Preliminary investigations into the development of textile based temperature sensor for healthcare applications. *Fibers* 1: 2–10.

144 Zhang, C., Ma, C., Wang, P., and Sumita, M. (2005). Temperature dependence of electrical resistivity for carbon black filled ultra-high molecular weight polyethylene composites prepared by hot compaction. *Carbon* 43: 2544–2553.

145 Blasdel, N.J., Wujcik, E.K., Carletta, J.E. et al. (2015). Nanocomposite resistance temperature detector. *IEEE Sensors Journal* 15: 300–306.

146 Shang, Y., Li, Y., He, X. et al. (2013). Highly twisted double-helix carbon nanotube yarns. *ACS Nano* 7: 1446–1453.

147 Yun, J., Kim, H., and Lee, Y. (2013). A hybrid gas-sensing material based on porous carbon fibers and a TiO_2 photocatalyst. *Journal of Materials Science* 48: 8320–8328.

148 Shao, S., Huang, Y., and Tao Simultaneous, S. (2014). Monitoring of ammonia and moisture using a single fiber optoelectrode as a transducer. *IEEE Sensors Journal* 14: 847–852.

149 Zhang, W., Tan, Y.Y., Wu, C., and Silva, S.R.P. (2012). Self-assembly of single walled carbon nanotubes onto cotton to make conductive yarn. *Particuology* 10: 517–521.

150 Seesaard, T., Lorwongtragool, P., and Kerdcharoen, T. (2015). Development of fabric-based chemical gas sensors for use as wearable electronic noses. *Sensors* 15 (1): 1885–1902.

151 Lee, S.K., Im, J.S., Kang, S.C. et al. (2012). Effects of improved porosity and electrical conductivity on pitch-based carbon nanofibers for high-performance gas sensors. *Journal of Porous Materials* 19: 989–994.

152 Kim, J., Lee, S.H., Park, S., and Lee, Y. (2014). Preparation and gas-sensing properties of pitch-based carbon fiber prepared using a melt-electrospinning method. *Research on Chemical Intermediates* 40: 2571–2581.

153 Hong, K.H., Oh, K.W., and Kang, T.J. (2004). Polyaniline–nylon 6 composite fabric for ammonia gas sensor. *Journal of Applied Polymer Science* 92: 37–42.

154 Pinto, N.J., Ramos, I., Rojas, R. et al. (2008). Electric response of isolated electrospun polyaniline nanofibers to vapors of aliphatic alcohols. *Sensors and Actuators B: Chemical* 129: 621–627.

155 Crabb, R.L. and Treble, F.C. (1967). Thin silicon solar cells for large flexible arrays. *Nature* 213: 1223–1224.

26

Textile-Based Electronics: Polymer-Assisted Metal Deposition (PAMD)

Casey Yan and Zijian Zheng

Laboratory for Advanced Interfacial Materials and Devices, Institute of Textiles and Clothing, The Hong Kong Polytechnic University, Hung Hom, Kowloon, Hong Kong SAR, China

26.1 Introduction

26.1.1 The Rise of Textile-Based Electronics

With many silicon-based technology breakthroughs demonstrated in the past few decades, lightweight electronic gadgets such as cell phones, GPS navigation, and MP3 had emerged and successfully dominated consumer's market. Today, semiconductor electronics get even more advanced, faster in clock speed, and physically smaller in size. With these technological advances and huge demand for mobile devices, recently, electronics evolutionarily transform from "portable" to even "wearable" with many thought-provoking worn-on-the-body applications targeting daily communication, entertainment, fitness tracking, etc. Well-known examples are Google Glass, Apple Watch, and other various fitness trackers developed by Jawbone, Nike, Fitbit, Garmin, etc. However, most of these wearable electronics are accessory-based devices that are still rigid and bulky. When it comes to what people define as "wearables" that can effortlessly accommodate the shape of human body and at the same time can provide electronic functions, flexibility and stretching ability of the device are the concerns. Apparently, conventional rigid silicon-based electronics cannot do this job well. Still, a flexible and stretchable platform for wearable electronics is highly demanded [1].

Among the many flexible and stretchable material substrates, the most familiar one is textile. Textile consisting of trillion thousands of fibers creates a versatile platform for the implementation of electronics because of not only its functional aspect, such as the large surface area of one fiber that make them desirable to be incorporated with plenty of electronic stuffs at micro- to nanoscale, but also their unique attributes such as commodity, comfort, wearing ability, and ultrahigh flexibility intrinsically inherited from the nature [2]. As textile is the most in dispensable necessity that we cannot live without, the implementation of electronics onto textile injects new research direction for the future development of electronics. In fact, such an idea to integrate electronics in textiles had already been demonstrated by Park and coworkers, who presented the first prototype of textile-based

Handbook of Fibrous Materials, First Edition. Edited by Jinlian Hu, Bipin Kumar, and Jing Lu.
© 2020 Wiley-VCH Verlag GmbH & Co. KGaA. Published 2020 by Wiley-VCH Verlag GmbH & Co. KGaA.

electronics, Georgia Tech Wearable Motherboard (GTWM), by directly attaching devices and computer chips onto textiles for monitoring human vital signs and wireless communications [3–5]. Recently, because of the increasing market demands especially from the medical and sports sectors, direct attachment of electronics onto textiles becomes technically viable. Some have already been well branded by many renowned sports companies, such as Adidas miCoach training shirt that detects one's heart rate during physical training and the North Face Hustle Audio Jacket that features an external joystick panel on sleeves to control iPod. Recently, Google and Samsung have also engaged in developing electronic garment prototypes, such as Project Jacquard and Smart Suit. Other than sports and entertainment, wearable electronic garments directly attached with small electronic components are also readily recognized in both medical and military sectors [6, 7].

To date, most of the wearable electronic garments still rely heavily on direct attachment or embedment of conventional off-the-shelf electronic devices and other bulky components. The wearing ability of these wearable electronics, however, has never been compromised due to the rigidness of the electronic devices that are conventionally constructed on the rigid silicon wafers. Besides, wearable electronic devices as tangible extras adding on clothing are bulky and bothersome to the wearers. Therefore, to truly develop textile-based electronics, the ultimate goal is to fully get rid of all the off-the-shell, rigid, and bulky silicon-based electronic devices and to construct all electronic devices from scratch on flexible and stretchable textile substrates such as fibers, yarns, and fabrics that can soon be seamlessly integrated into wearable forms via different textile technologies. The recent rise of textile-based electronics attracts many research efforts with many promising textile-based electronic devices demonstrated such as sensors [8], solar cells [9], energy storage devices [10–12], etc.

26.1.2 The Essential: High-Performance Conductive Textiles

As we all know, conductive traces are inevitable components in constructing electronic circuits to enable movements of electrons for driving all the electronic devices. There is no exception for textile-based electronics where high-performance flexible and stretchable textile conductors as interconnects, contacts, and electrodes are highly demanded. Considering the criteria for conductive textiles qualifying for electronic purposes, conductivity of the textile conductor is the first concern that should be taken into serious account. In particular, textile conductors should possess a high conductivity to ensure the performance of the device, and the conductivity should retain stable without significant performance drop throughout the devices' lifespan. Other than conductivity, concerns regarding the mechanical attributes and robustness of the textile conductors are also important. First, in order to allow electronics fully integrate into the textile structure, conductive textiles must be flexible enough in such an extent that a certain degree of stretching/bending is allowed. Second, a stable performance of the conductive textile must be maintained even under stretching/bending, as textiles are meant to be worn on the body and have to endure repeated cycles of bending, stretching, and release of these

actions because of daily human motions. Third, it is the washing durability of the conductive textiles. No wonder daily uses of textiles require hand to mild machine washing. Therefore, it is of particular importance whether the textile-based electronics can withstand such a vigorous mechanical abrasion underwater. Fourth, the fabrication process of these textile conductors must be compatible with the industry, so as to allow scale production of textile-based electronics.

Synthesizing high-performance, stable, and washable conductive textile is one biggest challenge that materials scientists have ever encountered. Addressing the needs of conductive textiles, many fabrication methods for high-performance conductive textiles have been reported in the past decades, such as yarns and fabrics directly drawn or incorporated with metal or metal oxide [13, 14], coated with intrinsically conducting polymers (ICPs) [15–17], spun using carbon nanotubes (CNTs) [18–20], etc. However, most of them fail in at least one or two abovementioned criteria to meet the needs. For example, textiles directly drawn or incorporated with metal or metal oxide impart extra rigidness on the final textile garments. Further, textiles coated with ICPs suffer majorly from chemical instability as conductivity of ICPs depends on different doping levels, which can be decreased dramatically during washing, so as the conductivity of the ICPs [16]. Even though CNTs can provide superior mechanical properties and electrical conductivity, the cost of the material is one of the major obstacles. Moreover, the potential hazard of CNTs to human body is not yet confirmed. Therefore, among all the conductive materials, only metals can beat to provide the best conductivity and stability at low cost for electronic purposes.

26.1.3 Fabrication of Metallic Textiles and the Challenges

Fabrication of metallic textiles once was a hot topic in the field of both academic research and industry. The simplest strategy is to directly deposit a layer of metal on the textile surface via electroplating [21]. Indeed, this strategy demands external electricity supply, which imparts high cost to the fabrication. Moreover, metallization by electroplating requires conductive substrates. As all textile fibers are intrinsically nonconductive, electroplating on textiles requires surface coating of conductive materials, which impart extra steps to the fabrication. Apparently electroplating is not a promising approach to yield metallic textiles. Other work involved to achieve metallic textiles is to incorporate metal wires into textiles [22, 23]. Even though high conductivity can be achieved, low flexibility and bending ability of these textiles remain big issues due to the rigidness of the metal wires. In addition, heavyweight brought by the metal wires is one major trouble during transport, not to mention the adoption in any worn-on-the-body applications.

Metal particles are later directly deposited onto textile surface by means of physical and chemical deposition techniques [24–29]. These techniques provide a great upscale potential in the textile industry to fabricate metallic textiles in bulk. However, a number of limitations still exit. First, these deposition techniques require high vacuum condition, which are still cost-ineffective. Second, the adhesion of the as-deposited metal particles on the textile surface is so poor that metal

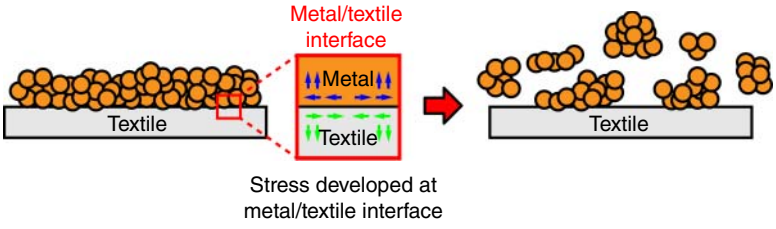


Figure 26.1 Schematic illustration showing stress developed at metal/textile interface when metal particles are barely attached onto the textile surface. Illustration is not drawn to scale.

particles are barely attached on the textile surface by weak physical interactions. Due to the mismatch between materials' physical properties, large amount of stress developed at the metal/textile interface can result in falling off of these metal particles from the textile surface (Figure 26.1). Third, the metal-deposited textile by these deposition techniques suffers majorly from the shadow effect. Those textile fibers on top shield the fibers underneath and block the passage of the sputtered or deposited metal particles. As a result, only outermost textile fibers can be coated with metal particles. With such a poor fiber contact, metallic textiles prepared by sputtering usually suffer from poor conductivity, which is not suitable for high-performance electronic applications.

In later development, electroless metal deposition (ELD) stands out as an alternative approach to depositing conformal metal particles on flexible polymeric substrates. Conventional ELD is an autocatalytic redox reaction, which involves the reduction of metal ions in the solution on the surface-catalyzed/activated substrate to form a conformal metal layer. Compared with other metal deposition techniques aforementioned, ELD is particularly attractive to achieve metal-deposited polymeric surface since ELD is an aqueous- and air-compatible process where external electricity, conductive substrates (required in electroplating), and vacuum condition (required in both physical and chemical vapor depositions) are eliminated. Thus, ELD is especially suitable for most of the intrinsically nonconductive textile materials that cannot withstand high temperatures and harsh environment. Demonstrations of ELD on textiles have been widely reported [30–34]. Notwithstanding, as the catalysts immobilized on the textile surface are physically attached via weak physisorption on the textile surface, adhesion of the as-deposited metal thin films on the polymeric substrates is still not assured owing to the metal/textile interfacial instability. Metal thin films can be easily delaminated from the textile surface.

26.1.4 Polymer Brushes Tackle Metal/Textile Interfacial Challenge

Metal/textile interfacial mismatch remains one significant challenge in the fabrication of robust and high-performance metallic textiles. To address this challenge, the metal/textile interface must be engineered in order to accommodate a stable metal/textile interfacial structure. To allow such a structure, one material must be present in between metal and textile for the establishment of a stable interface to ease material's mechanical mismatch. Recently, surface

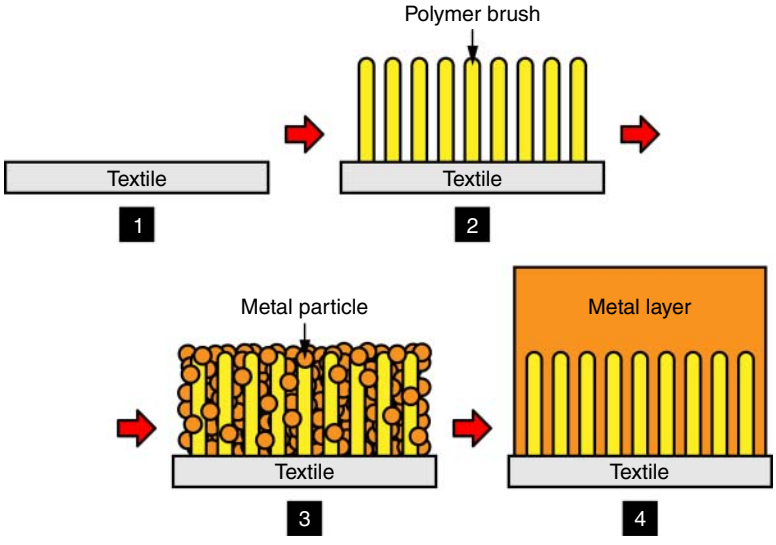


Figure 26.2 Polymer brush as an interfacial layer in between textiles and the deposited metal enables outstanding adhesion of metal on the textiles surface. Illustration is not drawn to scale.

modification of materials using polymer brushes emerges as one promising strategy to control surface architecture by changing the entire surface chemistry and topographical structures. In addition, polymer brushes possess large amount of functional groups along the polymer chains, which can be further utilized in subsequent chemical reactions. Taking both the advantages of polymer brushes as well as the aqueous- and air-compatible ELD process, an all-solution strategy, namely, PAMD, has been developed to fabricate highly durable, flexible, and stretchable metal conductors of various substrates including plastics, elastomers, papers, and textiles [35].

Literally, PAMD approach is a combined strategy of polymer brush grafting and ELD, involving (i) grafting of polymer brushes forming an interfacial layer on the textile surface and (ii) subsequent ELD of metals. The interfacial instability between the mechanically mismatched textiles and metal thin films can be tackled (Figure 26.2). Besides, outstanding adhesion of metal on the textiles surface is exhibited with robust metal coating to withstand repeated cycles of bending, stretching, and even washing. More importantly, unlike other conventional metal deposition strategies, PAMD is an all-solution process and is potentially favorable for scale production of flexible metallic textile conductors of both natural and synthetic substrates including cotton, wool, silk, polyester, nylon, Kevlar, spandex, etc. to suit different end purposes.

In this chapter, we specifically look into the PAMD process and briefly explore the underlying mechanism of PAMD. Also, we shall briefly explain the reaction chemistry behind PAMD, as well as the selection of polymer brush to enable PAMD. In Sections 26.3 and 26.4, we particularly focus on how PAMD realizes textile metal conductors and their applications in textile-based electronics.

Last but not least, the challenges of PAMD in realizing soft metal conductors in the foreseeable future will be discussed at the end of this chapter.

26.2 Polymer-Assisted Metal Deposition (PAMD)

26.2.1 What Are Polymer Brushes?

PAMD utilizes polymer brushes to assist ELD for strongly adhered metal thin films on substrate surface. The core part of the PAMD strategy is to combine polymer brush grafting and ELD to construct a thin layer of polymer brush in between the substrate and the as-deposited metal layer. Some basic understandings of polymer brushes will be introduced to readers in this section.

Polymer brushes are regarded as assemblies of macromolecular chains covalently tethered one end on a substrate surface. Once with sufficiently high grafting density, polymer chains are forced to induce significant stretch away from the tethered sites on the substrate surface to form a brushlike configuration [36, 37]. Polymer brushes grafted on a surface is commonly used to modify surface architecture of a substrate. Not only the surface chemistry is tailored by introducing new functional groups, but also the amount of functional groups can be dramatically increased for being further utilized in subsequent chemical reactions. Compared with self-assembled monolayer (SAM) [38], long-chain polymer brushes in a "brush-protruding" structure can accommodate many more functional groups along the polymer chains of repeated functional monomer units (Figure 26.3). With such a significant increase in the amount of functional groups on the surface, surface behavior of a brush-modified substrate can be controlled by the interaction of polymer brushes with the surrounding environment. The most well-known applications of polymer brushes are their switchable self-responsive behaviors to the surrounding solvent, ions, pH, temperature, etc. [39].

Grafting of polymer chains on one surface can be accomplished by either two brush grafting strategies. One is called the "grafting-to" strategy while another is called the "grafting-from" strategy. The "grafting-to" strategy involves the grafting of pre-synthesized long polymer chains on a substrate surface (Figure 26.4). These pre-synthesized polymer chains have functional binding sites for binding on the complementary sites on the substrate. "Grafting to" relies heavily on the diffusion of large polymer chains from the polymer solution to the substrate surface. Thus, it is very difficult to obtain polymer brushes with high grafting density, particularly due to steric hindrance of these long polymer chains that eventually prevent the surrounding polymer chains from approaching to the substrate surface and binding to the neighboring complementary sites. As the binding process proceeds with time, the substrate surface is getting more crowded and packed with bonded polymer chains. Those remaining polymer chains have to diffuse against the concentration gradient in order to reach the substrate surface, which is highly unfavorable for further binding. Thus, low grafting density will be resulted, leaving polymer chains in either "mushroom" or "pancake" configuration.

In order to achieve a "brush-protruding" configuration, materials scientists start manipulating the polymerization process in situ, and it is where the

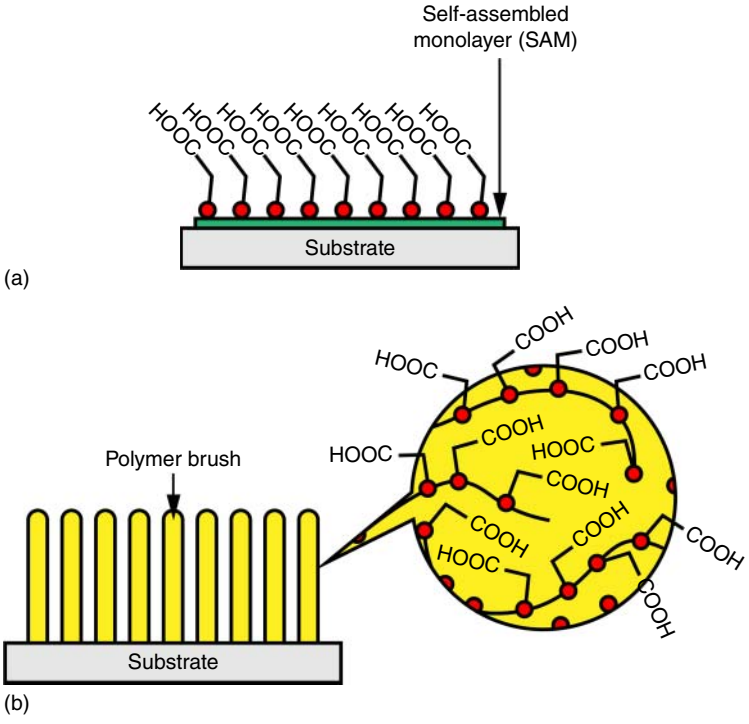


Figure 26.3 Schematic illustration comparing the amount of functional groups (–COOH as an example) on (a) SAM-modified and (b) polymer brush-modified substrate surfaces. Illustration is not drawn to scale.

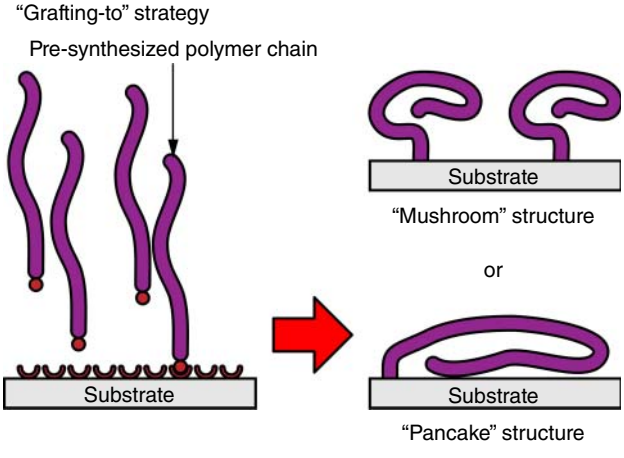


Figure 26.4 "Grafting-to" strategy only allows low brush grafting density, thus resulting in "mushroom" or "pancake" structure on the substrate surface, particularly due to the steric hindrance of the polymer chains as well as unfavorable diffusion against the concentration gradient. Illustration is not drawn to scale.

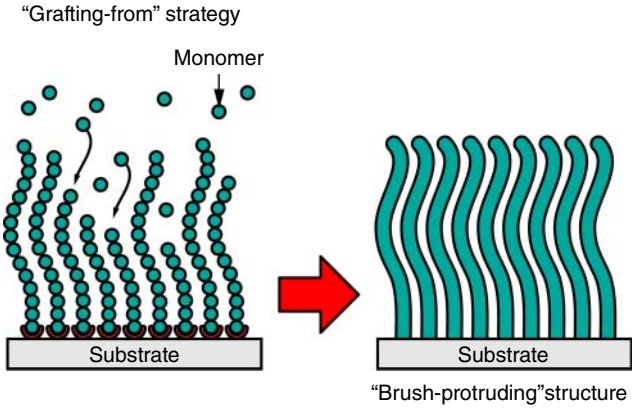


Figure 26.5 "Grafting-from" strategy allows high brush grafting density for a "brush-protruding" structure so as to maximize the amount of functional groups on the substrate surface for further chemical reaction. Illustration is not drawn to scale.

"grafting-from" strategy originates from. The "grafting-from" strategy involves in situ polymerization, i.e. polymerization of a polymer chain synthesis is initiated from a surface-immobilized initiator (Figure 26.5). To make in situ polymerization form a surface, a layer of initiator must first be deposited onto the substrate for the initiation of a polymerization process.

In PAMD, the "grafting-from" strategy is usually adopted to ensure a high grafting density of polymer brushes. There are mainly two polymerization strategies for the growth of polymer chains from the surface. First, it is the surface-initiated atom transfer radical polymerization (SI-ATRP) [40] that is the most commonly used strategy in PAMD. One supreme advantage of adopting SI-ATRP is that it is capable of preparing well-defined polymer brushes of desired molecular weight. However, it usually takes longer time to obtain a desired brush length. In addition, nitrogen protection is required throughout the entire polymerization process. Therefore, concerning the feasibility in upscaling the whole PAMD process, atom transfer radical polymerization (ATRP) is always not the first choice. On the contrary, conventional free radical polymerization (FRP) is always preferred in scale production as the whole process can be done under ambient conditions. However, as FRP is a kind of polymerization strategy that cannot be controlled, no well-defined polymer brushes of desired molecular weight can be obtained.

26.2.2 Mechanism of PAMD

PAMD is a universal strategy that takes both the advantages of polymer brushes and ELD to achieve conformal metal layer under aqueous- and air-compatible conditions [35]. Here, we particularly focus on the PAMD process on textiles, which consists of four steps: (i) surface modification of textiles with a functional organosilane layer, (ii) grafting of polymer brushes on the organosilane-modified textiles, (iii) immobilization of catalytic moieties onto the polymer brushes, and (iv) ELD of metal on the catalyst-loaded areas (Figure 26.6).

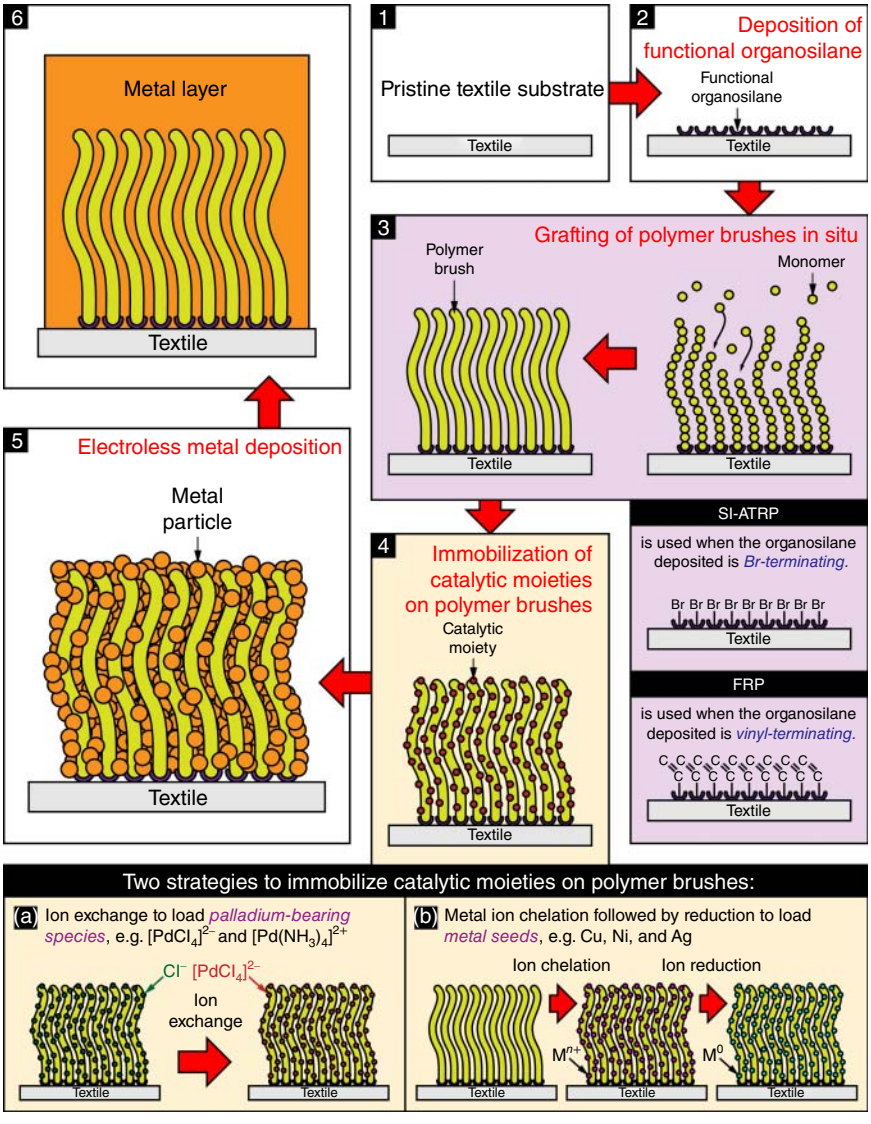


Figure 26.6 Typical PAMD process on a textile substrate. (1) A pristine textile substrate is first deposited with a layer of functional organosilane as shown in (2). (3) Surface modification of textiles with a functional organosilane can initiate grafting of polymer brushes in situ from the organosilane-modified textile surface. (4) Immobilization of catalytic moieties onto the polymer brushes either by (a) ion exchange to load palladium-bearing species or by (b) metal ion chelation and reduction to load metal seeds. (5) Electroless metal deposition (ELD) of metal on the catalyst-loaded areas. Panel (6) represents the typical metal layer on the brush-grafted textile substrate. Illustration is not drawn to scale.

In brief, one textiles surface intended to be coated with metal is first modified with a layer of functional organosilane. In general, any kinds of textile materials can be used as the substrates in PAMD. The function of such an organosilane layer is to provide initiation sites for the subsequent in situ grafting of polymer brushes.

In a typical silanization process on textile materials, organosilane is hydrolyzed under suitable pH where the hydrolyzed organosilanes are then condensed on the textile surface by self-assembly. This procedure is particularly critical for textile materials to proceed to subsequent brush grafting as most of the textiles lack functional groups for initiating polymer brush grafting. If the textile surface is not modified by organosilane, there will be no polymer brushes grafted on the textile surface.

Moreover, the use of organosilane to modify textile surface is highly favorable to many industries as it is rather common in materials surface engineering. The only requirement for organosilane deposition is the presence of hydroxyl groups on the substrate surface. Hydroxyl groups can be easily found in many textile natural fibers such as cotton. For man-made fibers such as polyester, hydroxyl groups can be rendered on the surface by just immersing the textiles into concentrated sodium hydroxide solution or by exposing the textile substrates with oxygen plasma to render the surface hydrophilic.

In the next step, polymer brushes are synthesized in situ from the organosilane initiators. Depending on the types of organosilanes deposited, suitable polymerization strategy is adopted. For example, SI-ATRP will be used to grow the polymer chains if the organosilane previously deposited is Br terminating; or FRP will be used to grow the polymer chains if the organosilane is deposited is vinyl terminating. It is also worth mentioning that polymer brush length varies upon the adoption of different polymerization strategies. For ATRP, well-defined brush length can vary from ~20 to ~50 nm, depending on the types of polymers as well as polymerization parameters such as ligand to transition metal ratio, types of counterion and solvent, etc. [40]. Conversely, in FRP, no well-defined molecular weight of polymer brush can be achieved. Instead, the brush length can only achieve in a broad range of ~5 to ~20 nm, depending on the polymerization parameters such as monomer concentration and polymerization temperature. Even so, FRP strategy eliminates the undesirable inert atmosphere required in ATRP, which is more suitable in scale production.

After grafting of polymer brushes on the textile surface, catalytic moieties are immobilized onto the polymer brushes for initiating subsequent metal ELD. In PAMD, the most commonly used catalysts to initiate metal ELD are either (i) palladium-bearing species or (ii) metal seeds. Their respective loading mechanisms on the brushes are quite different. To load the palladium-bearing species on the brushes, it is done via an ion exchange process. Examples of palladium-bearing catalyst for ELD include tetrachloropalladate(II) anion ($[PdCl_4]^{2-}$) and tetraamminepalladium(II) cation ($[Pd(NH_3)_4]^{2+}$). It is worth mentioning that in order to allow successful ion exchange, the selection of palladium-bearing species is highly specific in which the grafted polymer brushes must bear suitable functional groups for capturing these palladium-bearing species. For instance, $[PdCl_4]^{2-}$ is one of the most reported catalytic moieties to couple with poly[2-(methacryloyloxy)ethyl]trimethylammonium chloride (PMETAC) brushes, due to the high affinity of the quaternary ammonium groups (QA^+) in the PMETAC brushes toward $[PdCl_4]^{2-}$, while another catalytic moiety $[Pd(NH_3)_4]^{2+}$ can only couple with poly(methacryloyl ethyl phosphate) (PMEP) brushes, due to the high affinity of the phosphate groups in the PMEP brushes toward $[Pd(NH_3)_4]^{2+}$.

Another method to immobilize catalytic moieties onto the brushes is the absorption of metal seeds on the brushes as catalysts for the initiation and growth of metals. To do so, chelation of metal cations onto the grafted polymer brushes is first required, followed by subsequent reduction of these metal ions to form a thin layer of metal seeds on the brushes. Such an extra step of metal ion reduction is required that is usually accomplished by sodium borohydride solution. Chelation of metal ions on the brushes is specially suitable for those brushes that possess carboxylate groups, for instance, poly(acrylic acid) (PAA). Details will be provided in Section 26.2.3.2.

In the final step of PAMD, the catalytic moieties loaded substrates are immersed into the ELD plating bath for metal deposition, where the areas immobilized with catalytic moieties act as effective catalytic sites for metal ELD. It should be noted that the loading amount of catalytic moieties plays an important role in the ELD process, which affects the amount of metal deposited on the brushes. Azzaroni et al. evidenced the effect of the metal deposited by varying the amount of the catalytic moieties loaded on the brushes [41]. Scarce loading of the catalytic moieties can only result in thin metal deposited on the substrate. Other than the amount of catalytic moieties, thickness of the metal deposited is also affected by brush length, ELD time, and concentration of the ELD bath [42].

26.2.3 Brush Selection for ELD

The selection of polymer brush is highly critical and selective in PAMD and was systematically reviewed by Liu et al. [43]. It should be noted that only those polymer brushes that possess specific functional groups for the immobilization of catalytic moieties to initiate subsequent ELD are only applicable in PAMD. To help further understand the system, some polymer brushes used in PAMD for ELD will be introduced as follows according to their intrinsic charges that the brushes are carrying, i.e. cationic, anionic, and nonionic.

26.2.3.1 Cationic Polymer Brushes

Cationic polymer brushes, as its name suggests, are positively charged polyelectrolytes in an aqueous solution. Examples of cationic polymer brushes are the earlier mentioned PMETAC and poly[1,1′-bis(4-vinylbenzyl)-4,4′-bipyridinium dinitrate] (PVBVN), with chemical structures illustrated in Figure 26.7.

The mostly reported cationic polymer brush in PAMD is the PMETAC brush that possesses QA^+ groups for strong coupling with anionic catalytic moiety $[PdCl_4]^{2-}$ to initiate ELD. Azzaroni et al. first demonstrated the utilization

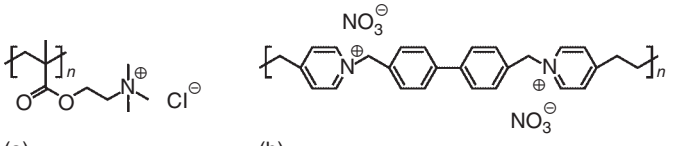


Figure 26.7 Chemical structures of two cationic polymer brushes: (a) PMETAC and (b) PVBVN that can be used in PAMD.

of PMETAC brushes that were grafted on wafer surface using SI-ATRP [41]. PMETAC brushes captured anionic catalytic moieties $[PdCl_4]^{2-}$ for subsequent ELD where a robust metal layer was selectively deposited with outstanding adhesion properties.

In 2009, Cui et al. demonstrated the fabrication of silver-coated polyimide (PI) film via ultraviolet (UV)-induced surface graft copolymerization of 1,1′-bis(4-vinylbenzyl)-4,4′-bipyridinium dinitrate (VBVN) to yield PVBVN bonded to the PI film surface [44]. Even though PVBVN is cationic, its chemical route for subsequent ELD is quite different from that of PMETAC as previously discussed. As mentioned, PMETAC requires the coupling of a catalytic moiety for subsequent ELD. On the contrary, PVBVN consists of viologen derivatives. Upon UV radiation, viologen derivatives on the brushes undergo redox reaction in which the metal ions in the solution can be readily reduced on the surface of the viologen-grafted substrate to form a very thin layer of metals. In their experiment, Cui et al. successfully grafted PVBVN brushes on the PI surface via a UV-induced polymerization, followed by exposure to UV irradiation in which silver nanoparticles were deposited on the surface of the PVBVN brushes through photo-induced reduction of silver ions in the silver salt solutions to obtain conformal and uniform silver layer on the PI surface.

26.2.3.2 Anionic Polymer Brushes

Anionic polymer brushes are negatively charged polyelectrolytes in an aqueous solution. Examples of anionic polymer brushes include PAA and PMEP with chemical structures respectively illustrated in Figure 26.8.

The chemical route for PAA enabling ELD is quite selective, thanks to the carboxylate groups present in the PAA brushes that allow chelation of metal cations. The mechanism is to first chelate metal cations on carboxylate groups in the PAA brushes, followed by a reduction of metal cations to obtain a thin layer of metal seeds for subsequent metal ELD. Garcia et al. reported the ELD of copper on different polymeric substrates by grafting PAA via a GraftFast technology [45, 46]. Taking the advantage of PAA brush that can complex with copper(II) ions, after grafting of PAA brushes, the PAA-grafted sample was immersed into copper(II) ion source to induce an chelation process, followed by a reduction of the copper(II) ions using sodium borohydride as a reducing agent. As a result, a thin layer of metal seeds is adsorbed on the bushes, which act as efficient catalysts for the subsequent ELD. Finally, the sample was put into a copper ELD bath for the subsequent growth of copper metals. This strategy can eliminate the use of costly palladium-bearing catalyst.

For another anionic brush PMEP, the mechanism in fact is quite similar to the cationic PMETAC brushes, which is capable of coupling with specific counterions as catalytic moiety due to the presence of specific functional groups. PMEP brush possesses phosphate groups for strong coupling with cationic catalytic moiety

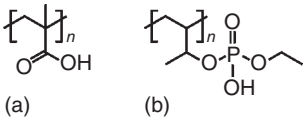


Figure 26.8 Chemical structures of two anionic polymer brushes: (a) PAA and (b) PMEP that can be used in PAMD.

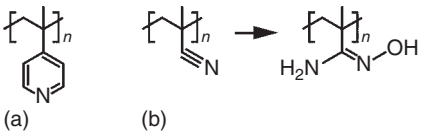


Figure 26.9 Chemical structures of two nonionic polymer brushes: (a) P4VP and (b) PAN that can be used in PAMD.

$[Pd(NH_3)_4]^{2+}$ to initiate ELD. Grafting of PMEP was demonstrated by Liu et al. [47]. They fabricated two oppositely charges polymer brushes that were cationic PMETAC and anionic PMEP via SI-ATRP on a substrate. Respective immobilization of catalytic anionic moieties $[PdCl_4]^{2-}$ for PMETAC and cationic moieties $[Pd(NH_3)_4]^{2+}$ for PMEP was then carried out. Subsequent copper and nickel ELD yielded bimetallic patterns on the substrate surface.

26.2.3.3 Nonionic Polymer Brushes

Nonionic polymer brushes are neutrally charged polyelectrolytes in an aqueous solution. Even though they are non-charge-bearing, they possess special functional groups with binding mechanism for the attachment of catalytic moieties for subsequent ELD. Examples of nonionic polymer brushes are poly(4-vinylpyridine) (P4VP) and polyacrylonitrile (PAN) with chemical structures illustrated in Figure 26.9.

Yang et al. first demonstrated the grafting of P4VP on poly(tetrafluoroethylene) (PTFE) and poly(vinylidene fluoride) (PVDF) films via UV-induced grafting [48]. After grafting of P4VP brushes, direct immobilization of the palladium catalyst was carried out for the subsequent ELD of nickel. Due to the presence of nitrogen-containing pyridine ring on the P4VP brushes, the palladium species complexed with the nitrogen moiety in the pyridine ring, therefore enabling a strong chemisorption of the palladium species on the grafted polymer brushes to initiate subsequent ELD.

Similarly, grafting of PAN brushes was demonstrated by Yu et al. via a UV-induced grafting on poly(tetrafluoroethylene-*co*-hexafluoropropylene) (FEP) films [49]. However, due to the lack of any functional groups on PAN brushes for the immobilization of the catalytic moieties for ELD, cyano groups on PAN brushes were firstly amidoximated using hydroxylamine hydrochloride to introduce amidoxime groups on the PAN brushes. Amidoxime groups are capable of complexing with palladium species. The amidoximated PAN brushes were then subjected to sensitization in the $SnCl_2$ solution, followed by activation in the $PdCl_2$ solution. Subsequent ELD was then carried out to yield a conformal copper layer on the substrate surface.

26.2.3.4 Advantages of Using Polymer Brushes as ELD Platform

The major innovation in PAMD strategy is the use of polymer brushes that act as a bridging layer in between the substrate and the as-deposited metal so as to ease the stress developed at the substrate/metal interface. As a result, outstanding metal adhesion on the substrates can be ensured. Theoretically, metal deposition can be assisted by adopting a layer of SAM once it possesses suitable functional groups for metal deposition [50, 51]. However, when comparing polymer brushes to SAM in assisting ELD, polymer brush has two major advantages that cannot be accomplished by SAM. First, polymer brush can numerously increase the number

of immobilization sites for catalytic moieties or metal seeds attachment for metal ELD. Polymer brushes can provide a "three-dimensional" functional layer, which accommodates much more functional binding sites or accommodation sites for the attachment of catalytic moieties. With an increased amount of catalysts or metal seeds loaded onto the polymer brushes, the rate of ELD can be significantly increased under the same ELD condition, due to the increased number of reactive sites for the growth of metal. Conversely, catalyst uptake in SAM is rather poor than in polymer brushes as SAM only have "one-dimensional" functional layer, which limits the number of surface binding sites for the attachment of catalytic moieties for metal ELD. Second, polymer brush allows an interpenetrating matrix structure to be established that enables a remarkable adhesion between the as-deposited metal and the substrate. In this context, polymer brush as an interfacial layer can be regarded as a layer of adhesive that bridges the deposited metal and the substrate surface. Outstanding robustness of metal layer against repeated cycles of mechanical actions is exhibited, and remarkable adhesion of metal on the substrate surface is therefore enabled.

26.2.3.5 Fabrication of Metallic Textiles via PAMD

Textiles inheritably of great flexibility and wearability are suitable platforms for electronics. One advantage of using textiles as the substrate for PAMD is that the metal-coated textiles can be flexibly integrated into many fabrics and even garments as conductive interconnects, contacts, and electrodes for many electronic purposes. In 2010, Liu et al. first reported on the preparation of highly durable conductive metal-coated cotton yarns via PAMD approach [52]. They first modified the cotton fiber surface with Br-terminating silane for the grafting of PMETAC brushes by SI-ATRP. Subsequent ELD of copper on the cotton fiber surface resulted in copper-coated cotton yarns with outstanding mechanical durability and electrical stability upon repeated cycles of bending, stretching, and washing (Figure 26.10a). Application of these metallic cotton textiles was also demonstrated as interconnects in textile electronics by connecting a 9 V battery and a light emitting diode (LED), showing great potential to be used as electrical wires in wearable and flexible electronic devices (Figure 26.10b,c).

However, concerning the feasibility in scale production, such demonstration by Liu and coworkers is not practical as ATRP requires long polymerization time as well as protection under inert nitrogen atmosphere. Therefore, further modification has been made in 2014 by Wang et al. for a more practical and scalable approach to yield metallic textiles, in which the polymerization of PMETAC was carried out via in situ FRP instead of SI-ATRP [42]. In the fabrication, vinyl-terminating silane was deposited on the cotton fibers to allow FRP to graft PMETAC brushes on the fiber surface. The polymerization time can be greatly reduced to ~30 minutes with comparable sheet resistance achieved under the same experimental conditions. Since the whole fabrication is aqueous and air compatible, the fabrication can be scaled up and incorporated with pad-dry-cure technology – a textile finishing technique commonly used in dyeing and finishing with special treatment on fabrics. Importantly, PAMD can be applied on wide varieties of natural and synthetic fibers such as nylon, polyester, Kevlar, and spandex (Figure 26.10d–g), showing a great versatility of

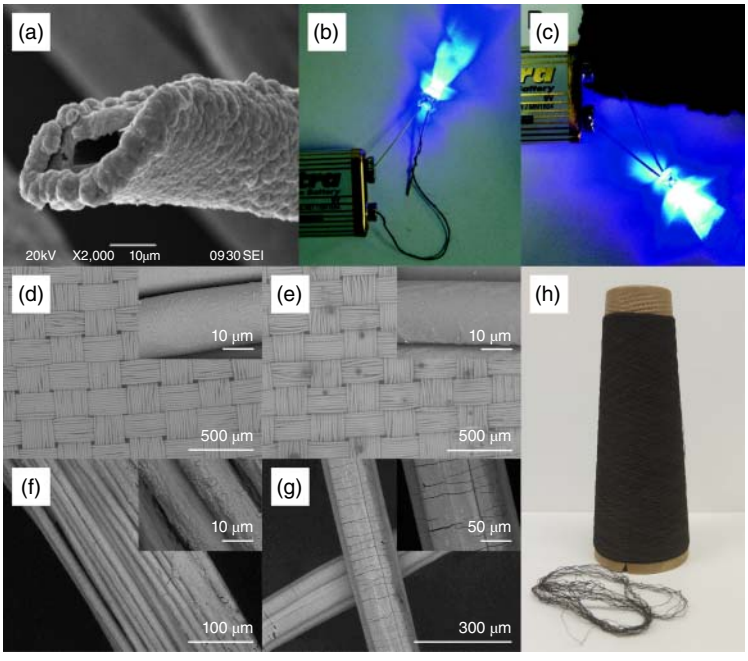


Figure 26.10 (a) Scanning electron microscopy (SEM) images of the cross-sectional morphologies of PMETAC-modified cotton fiber that was immersed in copper ELD plating bath for 30 minutes. (b) Conductive yarn or (c) fabric was used as electrical wire for powering a blue LED. The yarn or fabric was placed in contact with the battery and LED without using extra conductive glue or paste. Source: (Panel c) Reproduced with permission from Liu et al. [52]. Copyright 2010, American Chemical Society. SEM images of Cu-coated (d) nylon fabric, (e) polyester fabric, (f) Kevlar yarns, and (g) spandex monofilaments. Insets are SEM images of fibers in high magnification. Source: Reproduced with permission from Wang et al. [42]. Copyright 2014, John Wiley & Sons. (h) Digital image of a 500 m long nickel-coated cotton yarn wound on a spinning cone. Source: Reproduced with permission from Liu et al. [53]. Copyright 2015, Macmillan Publishers Limited.

PAMD on different textile substrates that well suit different end applications. With such a potential in scale-up fabrication, Liu et al. first demonstrated the feasibility of scale fabrication of 500 m long nickel-coated cotton yarn prepared on spinning cone in one batch (Figure 26.10h) [53]. These nickel-coated cotton yarns still possess both textile-like flexibility and an outstanding conductivity (~1.3 Ω/cm), which are highly suitable for flexible electronic applications.

As the performance of the as-fabricated metallic textiles is crucial to the fabrication of any electronic devices, Wang et al. analyzed the effect of different experimental parameters in PAMD on the electrical performance of the metallic textiles. It is found that critical parameters determining the performance of metallic textiles in PAMD are majorly threefold, including polymerization time, polymerization temperature, and ELD time [42]. It is also worth mentioning that the conductivity of the as-fabricated metallic textiles highly depends on the fibrous structure of the textile materials. For example, metal-coated spun yarns provide relatively lower conductivity when compared with those using filament yarns as

substrates due to more fiber-to-fiber contacts. Thus, the contact resistance will be higher when compared with metal-coated filament yarns. Even so, natural staple fibers are of more advantages in holding up more active materials in some device fabrication, thanks to the larger surface areas that the fibers can provide with, as well as the intrinsic ability to absorb foreign materials essential for boosting device performance.

26.3 Strategy to Fabricate Patterned Metallic Traces in PAMD

26.3.1 Why Patterning Is Required?

Theoretically, infinitely large metal-coated textiles can be prepared by PAMD for scale applications in large-area electromagnetic shielding, electrostatic discharge, etc. However, metal patterns are always demanded for the constructions of electronic circuitries. To pattern precise metal traces on textile surface, conventional resist-based lithographic techniques long been developed in the semiconductor industries should be borrowed, which involve multiple steps such as masking, resist patterning, etching, metal deposition, lift-off, annealing, etc. Nonetheless, these techniques are all incompatible with soft polymeric substrates especially textiles, particularly due to the harsh chemical environment where most textiles cannot withstand, as well as the high temperature required in the annealing step (~900 °C) that can almost damage all textile substrates. Concerning the incompatibility in transitional patterning methods with textile substrates, rather than adopting the old technologies, recently, the continuous roll-to-roll (R2R) printing to realize flexible electronics comes into the spotlights. The continuous manner and the high throughput enabled in the R2R printing technology have always been impressive to allow greater production capacity because it is ultrafast, accurate, and less facility-demanded (only common printing facilities are required). In the textile industry, the printing sectors are in fact very well developed, especially the fabrication of various prints and patterns using screen printing and ink-jet printing. PAMD is also applicable to the fabrication of patterned metal-coated textiles by printing strategies, which can be realized by either two strategies: (i) catalytic moiety ink patterning or (ii) copolymer ink patterning.

26.3.2 Catalytic Moiety Ink Patterning

The method of patterning metallic trace in PAMD on textile is to pattern the catalytic moieties that are responsible for the initiation of metal ELD. The schematic illustration of this approach is shown in Figure 26.11. Only the areas immobilized with catalytic moieties can result in metal deposition to yield patterned metal coatings on the textile surface. In 2013, Guo et al. first demonstrated the synthesis of well-defined metal traces on textile substrates via matrix-assisted catalytic printing (MACP) [54]. Such a printing strategy is in fact a modified PAMD process, where the catalytic moieties were first prepared as printable ink with suitable viscosity tuned for different printing techniques such

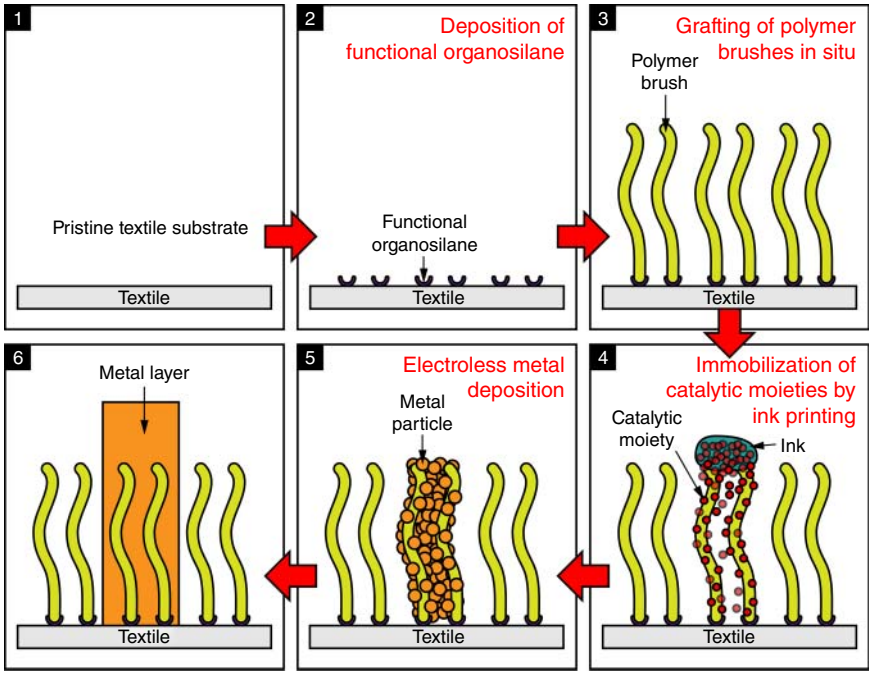


Figure 26.11 Schematic illustration showing the procedures to obtain metal patterns on textile surface by catalytic moiety ink patterning. (1) Pristine textile substrate is first deposited with a layer of functional organosilane as shown in (2). (3) Grafting of polymer brushes in situ from the organosilane initiators. (4) Printing of ink containing catalytic moieties with a delivering matrix polymer, poly(ethylene glycol) (PEG) as the moiety carrier and thickening agent. Catalytic moieties then diffuse from the ink to the polymer brushes. After diffusion, localized brush area is loaded with catalytic moieties. (5) Electroless metal deposition (ELD) to obtain patterned metal trace on the textile surface to obtain metal layer on textile surface in (6). Illustration is not drawn to scale.

as screen printing and ink-jet printing. To do so, the viscosity of the catalytic moiety solution must first be fine-tuned. Guo and coworkers used a delivering matrix polymer, poly(ethylene glycol) (PEG) serving as both the carrier of the catalytic moieties as well as the thickening agent for tuning the ink viscosity.

As a proof of concept, a layer of PMETAC brushes was first grafted on papers and fabrics via FRP. Subsequently, catalytic $[PdCl_4]^{2-}$ as ink was printed on the desired areas intended for metal deposition via screen printing or ink-jet printing. The catalytic moieties as a result diffused from the delivering matrix polymer PEG to the receiving matrix polymers, i.e. the grafted PMETAC brush layer. As the area immobilized with $[PdCl_4]^{2-}$ determines the area for the subsequent ELD of metal, patterned metal-coated paper and fabric can be resulted with feature size of the metal patterns ranging from micro- to millimeter scales. Importantly, such a patterning process is compatible with industrial printing facilities such as screen printing and ink-jet printing in the textile industry, which is of great importance in making patterned electronic circuits for textile-based electronic devices.

26.3.3 Copolymer Ink Patterning

Recently, PAMD strategy was further modified for an ultrafast fabrication of metallic patterned textiles. A first printable copolymer ink used for the rapid fabrication of metallic textiles in PAMD was proposed by Yu et al. [55]. The schematic illustration of this approach is shown in Figure 26.12. To achieve this,

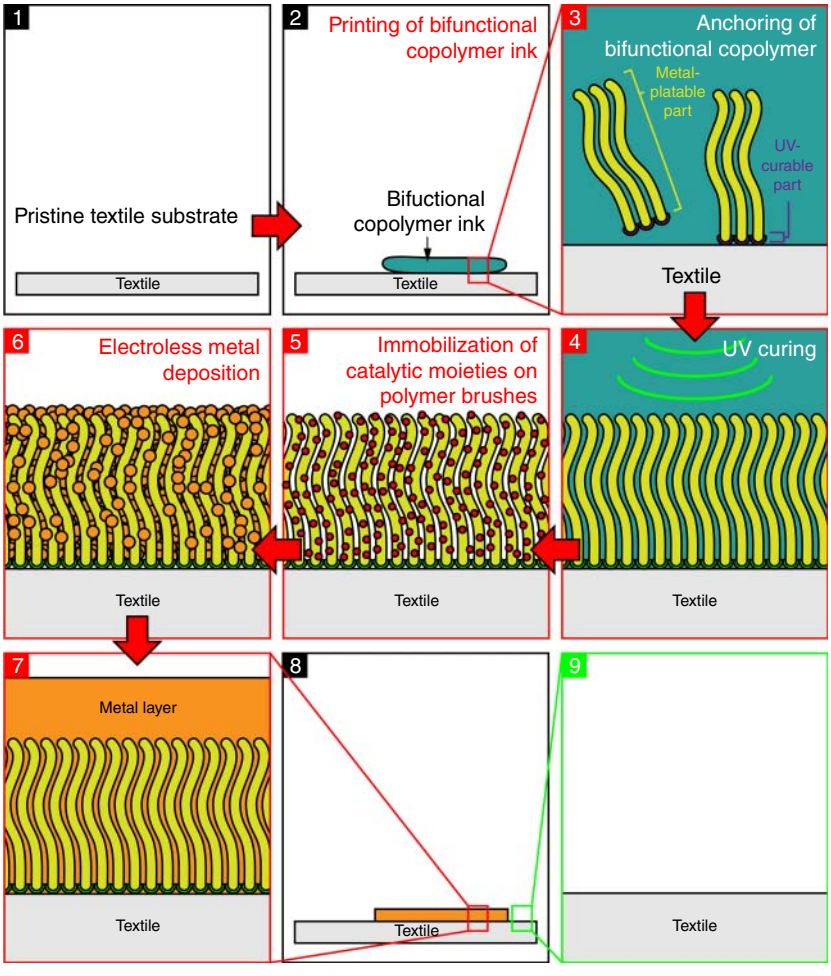


Figure 26.12 Schematic illustration showing the procedures to obtain metal patterns on textile surface via copolymer ink patterning. (1) Pristine textile substrate is first deposited with a layer of bifunctional copolymer ink as shown in (2) via screen printing or ink-jet printing. The bifunctional copolymer consists of two major components that are a metal-platable part and a UV-curable part as indicated in (3). (4) UV radiation simultaneously triggers the self-cross-linking and surface grafting of the copolymer under ambient conditions. (5) Localized brush area is loaded with catalytic moieties. (6) Electroless metal deposition (ELD) to obtain patterned metal trace on the textile surface as shown in (7) and (8). Areas without ink printing result in none of the metal deposited as shown in (8) and (9). Illustration is not drawn to scale.

a bifunctional UV-curable and metal-platable copolymer poly(4-methacryloyl benzophenone-*co*-2-methacryloyloxy ethyltrimethylammonium chloride) [P(MBP-*co*-METAC)] was first synthesized as ink. Instead of controlling the areas where the catalytic moieties immobilized onto like catalytic moiety ink patterning, this strategy takes a step forward to pattern the brushes on to the area where metal particle is intended to deposit onto. After printing of this copolymer on the textile surface via screen printing or ink-jet printing, a one-step curing procedure of the copolymer ink using UV radiation can yield metal-platable copolymers securely cross-linked on the textile surface. Subsequent loading of catalytic moieties and ELD can readily yield the textile surface with strongly surface-deposited metallic patterns. Importantly, the copolymer ink can be fabricated easily under ambient condition and is readily compatible with commercialized screen printing and ink-jet printing facilities. Such a fabrication can greatly reduce the fabrication time when compared with the conventional PAMD process.

26.4 Applications in Textile-Based Electronics

26.4.1 Supercapacitor

In 2015, Liu et al. first demonstrated a flexible and wearable yarn-based supercapacitor (SC) utilizing nickel-coated cotton yarns synthesized by PAMD [53]. The nickel-coated cotton yarns served as current collectors in the as-prepared SC, which processed high conductivity and robustness in repeated bending with only 2% increase in electrical resistance after 5000 bending cycles. With subsequent electrochemical deposition of reduced graphene oxide (RGO) on the nickel-coated cotton fiber surface and the deposition of electrolyte gel, a solid-state yarn SC was obtained (Figure 26.13a). Owing to the robustness of the nickel metal and also the hierarchical structures offered by the nickel-coated cotton fibers, the solid-state yarn SC not only achieved remarkable performance with efficient ionic and electronic transport (Figure 26.13b,c) but also maintained good cyclic stability (82%) even after 10 000 cycles of charging and discharging (Figure 26.13d). Moreover, the capacitance of the SC yarn increased proportionally in a first order as the device length increased. As indicated in Figure 26.13e, the capacitance of the SC yarn increased from 0.28 to 1.52 F with the length increased from 3 to 17 cm, showing a 20-fold increased performance when compared with other work reported in the literature [56, 57].

Later in 2016, Huang et al. successfully fabricated fabric-based SC using nickel-coated cotton fabrics (Ni cotton) synthesized by PAMD [58]. They eliminated any harsh processing conditions required in the conventional fabrication of fabric-based SC and reported a cost-effective and continuous approach for high-performance SC fabric via a one-step electrospinning of carbon nanowebs (C-web) on Ni cotton to first form C-web@Ni-cotton electrode. Then, two pieces of C-web@Ni-cotton electrodes were assembled together with a piece of pristine cotton fabric as the separator in between to form a symmetrical SC fabric device (Figure 26.14a). Fabric samples after deposition of nickel and

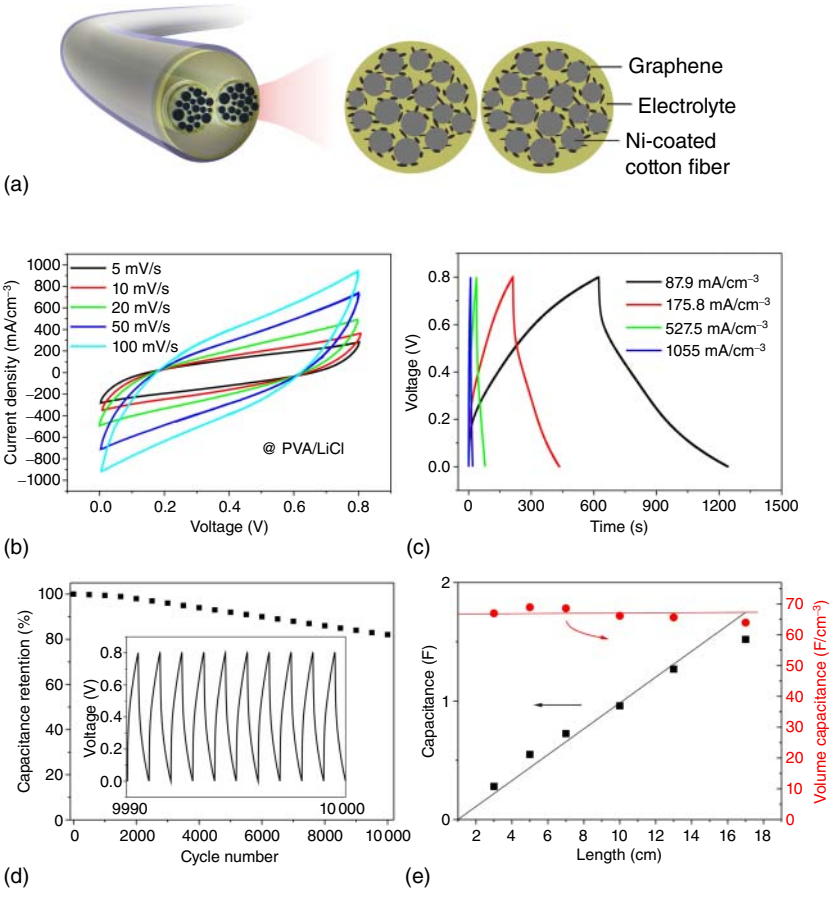


Figure 26.13 Performance of solid-state supercapacitor (SC) yarns. (a) Schematic illustration of the structure of one SC yarn. (b) Cyclic voltammetry (CV) curves of the device at scan rates ranging from 5 to 100 mV/s. (c) Galvanostatic charge/discharge (GCD) curves of the device at different current densities. (d) Cycle life of the device at a current density of 439.6 mA/cm^3. The inset is the GCD curve from the 9990th to the 10 000th cycle. (e) Device capacitance as a function of the device length. Source: Reproduced with permission from Liu et al. [53]. Copyright 2015, Macmillan Publishers Limited.

subsequently with C-web are shown in Figure 26.14b. Remarkably, Ni cotton retained its good flexibility (Figure 26.14c) even though nickel particles were densely deposited on the cotton fibers (Figure 26.14d,e). After the electrospinning process, a three-dimensional nanoweb was formed on the surface of Ni cotton (Figure 26.14f). To demonstrate the practical application of such C-web@Ni-cotton fabric electrode, solid-state SC fabric devices using a polyvinyl alcohol (PVA)/LiCl gel electrolyte was fabricated. As shown in Figure 26.14g,h, the solid-state device exhibits a high areal capacitance of 275.8 mF/cm^2 at 1 mA/cm^2 with a low internal resistance. Importantly, such SC fabrics can be further integrated into commercial textiles with any desirable forms, indicating application potentials in wearable electronics.

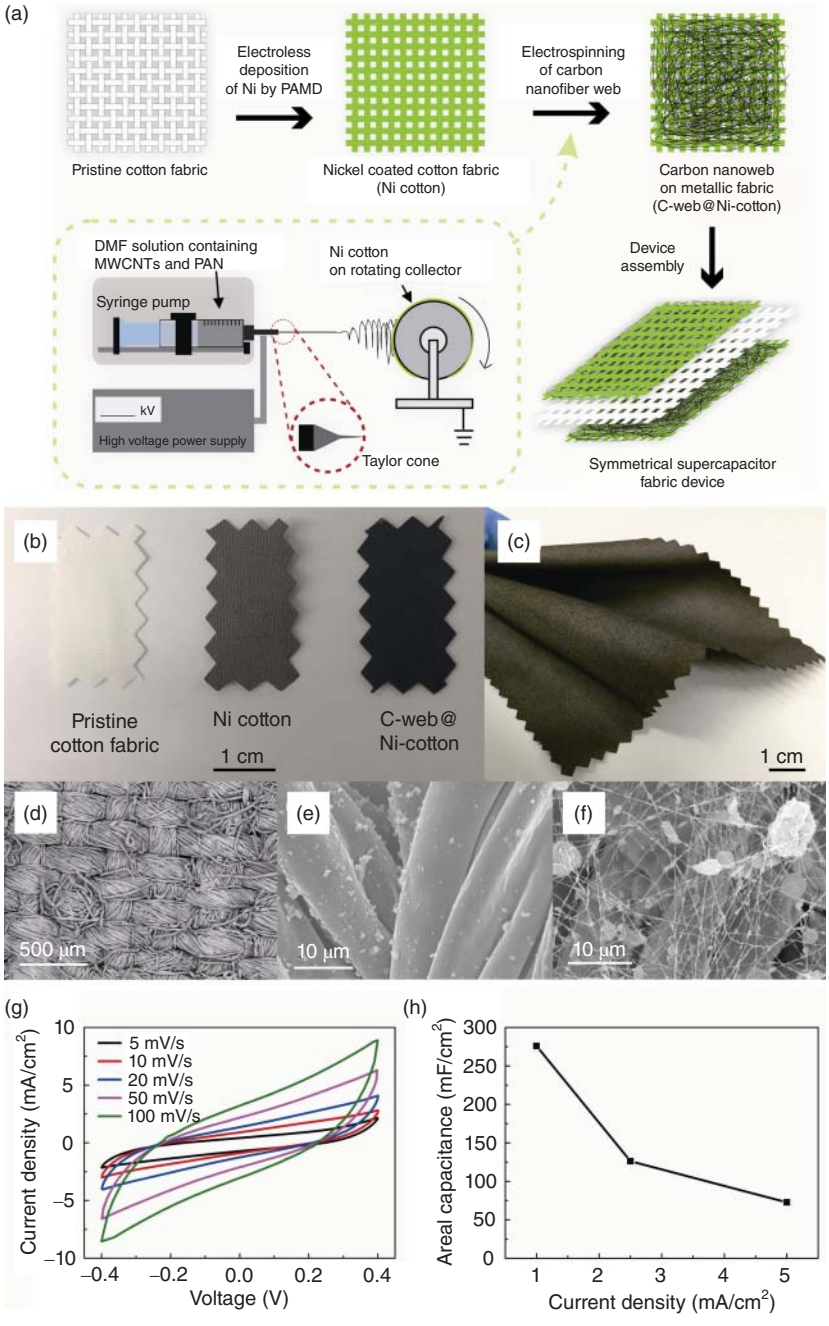


Figure 26.14 (a) Schematic illustration of the fabrication procedures of supercapacitor fabrics. The inset shows the details of the one-step electrospinning setup. (b) Photographs of the pristine cotton fabric, nickel-coated cotton fabric (Ni cotton), and carbon nanofiber web-coated Ni-cotton fabric (C-web@Ni-cotton). (c) Photograph of the Ni-cotton fabric with large dimension, showing good flexibility. (d, e) SEM images showing the surface morphology of the Ni-cotton fabric. (f) SEM image of the C-web@Ni-cotton fabric electrode. (g) CV curves of solid-state C-web@Ni-cotton supercapacitor fabric. (h) Summary of the areal capacitance of the supercapacitor at different current densities. Source: Reproduced with permission from Huang et al. [58]. Copyright 2016, Royal Society of Chemistry.

26.4.2 Triboelectric Nanogenerator

Zhao et al. fabricated the first machine-washable textile-based triboelectric nanogenerator (t-TENG) by adopting the metallic textile fabricated by PAMD [59]. Such a textile-based sensor was successfully demonstrated as an effective human respiratory monitor to detect human respiratory patterns. The whole fabrication of the device was based on plain weaving of copper-coated polyethylene terephthalate (PET) yarns (Cu-PET) as warp and PI-coated Cu-yarns (PI-Cu-PET) as weft to form a flexible fabric (Figure 26.15a). In the fabrication, 1-ply PET yarn was first coated with a thin layer of copper metal by PAMD technique to obtain Cu-PET yarn (Figure 26.15b). Subsequently, two 1-ply Cu-PET yarns were twisted together to obtain a 2-ply Cu-PET yarn to further decrease the linear resistance of the yarn (Figure 26.15c). After coating PI on the PI-Cu-PET yarn (Figure 26.15d,e), 2-ply Cu-PET yarns and PI-Cu-PET yarns were woven to form a flexible fabric. As a proof of concept, the metallic yarns were wound onto a cone for industrial automatic weaving (Figure 26.15f,g). The as-prepared woven fabric as t-TENG (Figure 26.15h) comprised 9 pieces of 2-ply Cu-PET as warp and 60 pieces of PI-Cu-PET as weft (Figure 26.15i). As copper and PI can serve as one effective triboelectric couple, every yarn crisscross intersection in the device is regarded as a triboelectric nanogenerator. As a result, upon even very subtle deformation of the device by tapping or bending, the contact area at each yarn crisscross intersection changes thus leads to an effective generation of triboelectric charges. Thus, such device is highly suitable for detecting human subtle motions such as human respiration to monitor the respiratory patterns. Besides, the device is remarkably durable that can withstand washing cycles in the washing machines, thanks to the robust metallic yarns fabricated by PAMD for the outstanding metal adhesion on the yarn surface. Upon machine washing up to 20 cycles in the standard washing machine, 2-ply Cu-PET yarns can maintain a linear resistance $<0.6\,\Omega/cm$ (Figure 26.15j), with copper particles still strongly adhered on the yarn surface (Figure 26.15k–o).

26.4.3 Solar Cell

In 2017, Zhen et al. successfully fabricated foldable polymer solar cells (PSCs) on woven fabrics by a freestanding wet transfer method [60]. Since the conventional method to fabricate solar cells by direct spin coating is not applicable to common textile fabrics due to their intrinsically nonplanar properties and rugged surface morphologies, a novel new fabrication concept is therefore proposed by Zhen and coworkers, in which a wet transfer method is utilized to laminate the PSC onto the woven fabric electrode. The fabrication procedure of the device is illustrated in Figure 26.16a. In this work, they first utilized PAMD technique to obtain patterned silver-coated PET (fabric A) and nylon (fabric B). PSC device fabrication was then carried out on the flat silicon substrates by successive spin coating a water-soluble sacrificial layer PSSNa, active layer, and doped PH1000 as the top electrode. The resulting silicon/PSSNa/active layer/PH1000 layer was then put into the water. As PSSNa layer is water soluble, the PSC can be easily detached from the silicon substrate and transferred onto patterned silver-coated

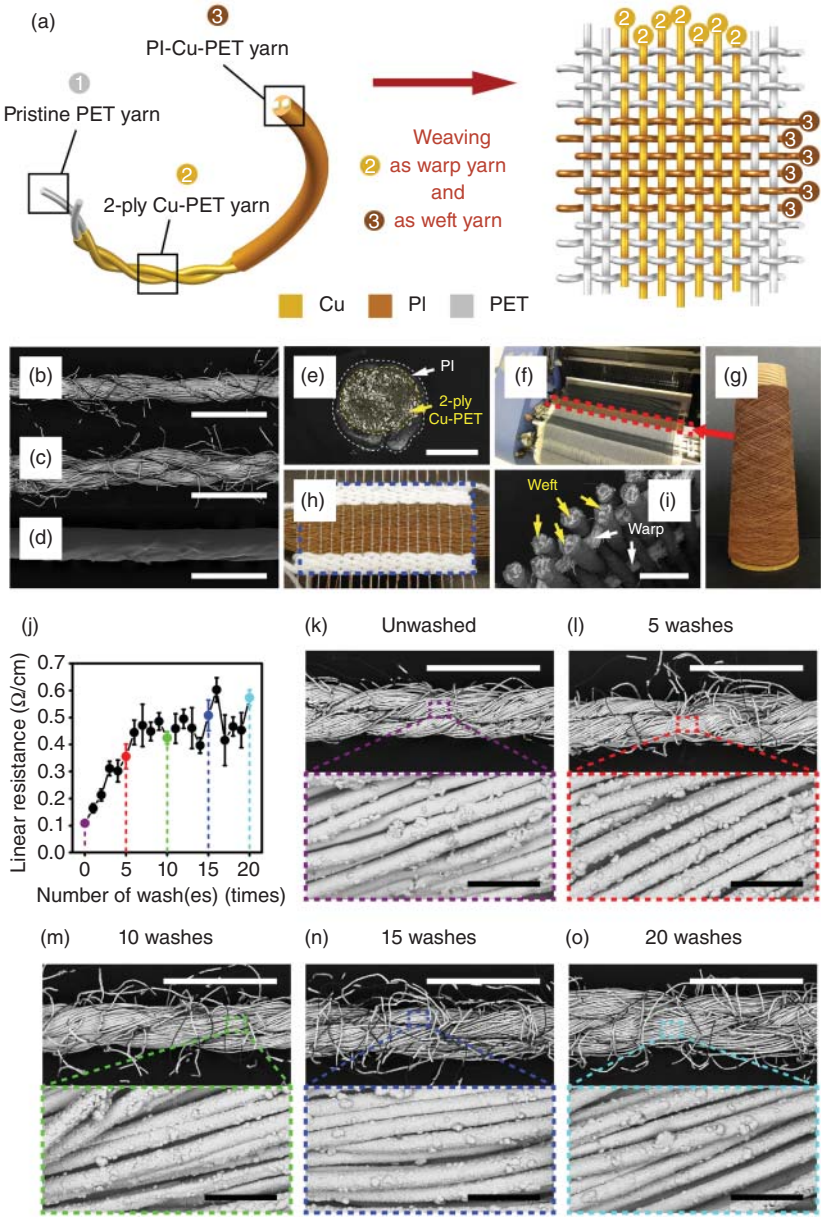


Figure 26.15 Fabrication and structure of the t-TENG. (a) Schematic illustration of the preparation of warp and weft yarns and structure of the woven t-TENG. SEM images of (b) 1-ply Cu-PET yarn, (c) 2-ply Cu-PET yarn, (d) PI-Cu-PET yarn (scale bar: 1 mm), and (e) cross section of PI-Cu-PET yarn (scale bar: 250 μm). Yellow dashed line outlines the cross section of the 2-ply Cu-PET yarn while the white dashed line outlines the cross section of PI wrapping around the 2-ply Cu-PET yarn. Digital image of (f) sample weaving loom carrying out automatic weaving of (g) metallic yarns wound on a cone. (h) As-woven t-TENG on the loom with a device area of ≈6 cm × 4 cm (blue dashed box). (i) SEM image of the cross section of the woven structure of the t-TENG, showing the up and down interlacement of the weft and warp yarns (scale bar: 1 mm). Washing durability tests. (j) Linear resistance and (k–o) SEM images of the unwashed 2-ply Cu-PET yarn and 2-ply Cu-PET yarn washed up to 20 cycles of standard washing (white scale bar, 1 mm; black scale bar, 50 μm). Source: Reproduced with permission from Zhao et al. [59]. Copyright 2016, John Wiley & Sons, Inc.

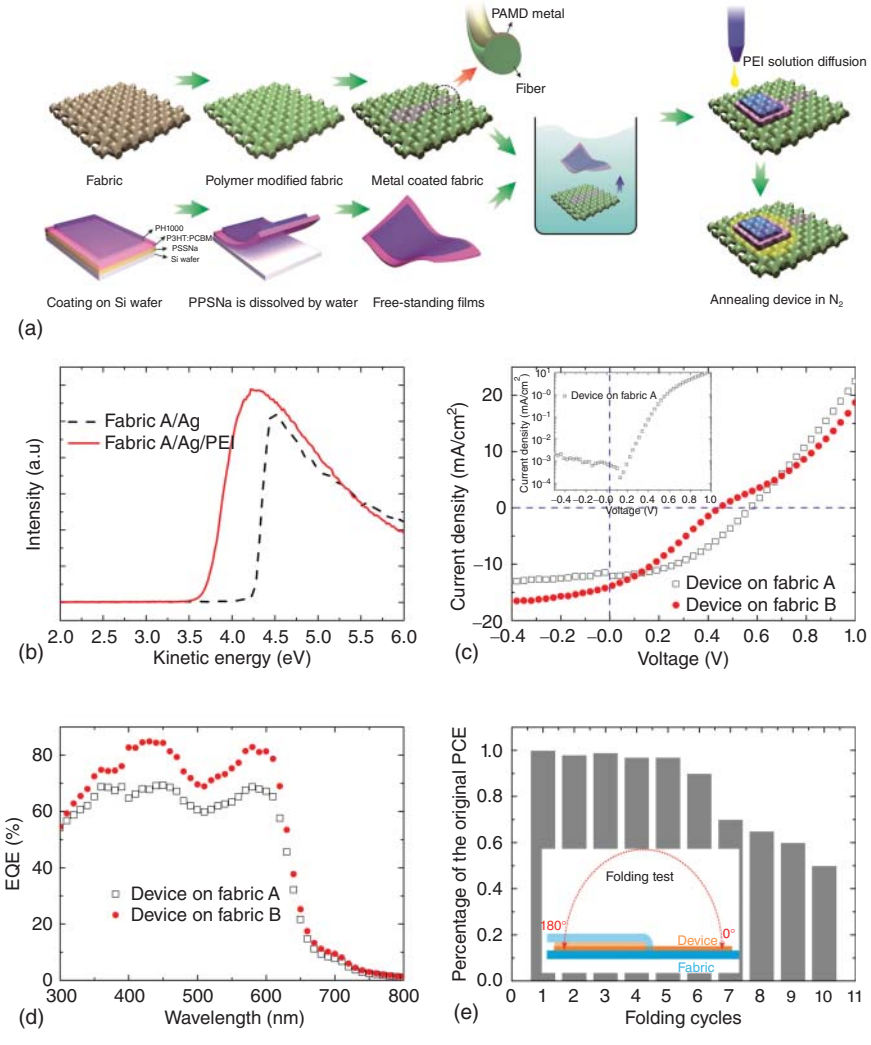


Figure 26.16 (a) Schematic illustration of the fabrication process of the PSCs on a woven fabric. (b) UPS spectra of a woven fabric electrode with/without PEI. (c) *J–V* characteristics of the PSCs on a woven fabric under AM 1.5 illumination (inset: dark *J–V* characteristics of the PSCs on fabric A). (d) EQE spectra of the PSCs on a woven fabric. (e) Performance degradation of the PSCs on fabric A in the folding test. Source: Reproduced with permission from Zhen et al. [60]. Copyright 2017, Royal Society of Chemistry.

fabric substrates. Finally, interface modification layer (IML) between the woven fabric electrode and active layer was obtained by the diffusion of the dilute solution of polyethylenimine (PEI) as the interface modification material. Such a PEI thin film is highly important in achieving high power conversion efficiency (PCE) performance by decreasing the work function of the fabric silver electrode to 3.6 ± 0.2 eV (Figure 26.16b). The performance of the PSC on fabric A exhibits a power conversion efficiency of 2.90% with a V_{OC} of 0.58 V, an fill factor (FF) of

0.41, and a J_{SC} of 12.10 mA/cm^2 (Figure 26.16c), which is close to the photovoltaic performance compared with those devices using the same active materials, while the performance on fabric B exhibits a power conversion efficiency of 1.85% with a V_{OC} of 0.46 V, an FF of 0.29, and a J_{SC} of 13.58 mA/cm^2. The external quantum efficiency (EQE) spectra of the PSCs based on fabric electrodes and also the performance degradation of the PSC sample up cycles of folding tests are, respectively, shown in Figure 26.16d,e. Still, the stability of the device upon folding requires further improvement in the future by proper encapsulation method.

26.5 Conclusion, Future Outlook, and Challenges

Wearable electronics are one of the most exciting technologies that attract considerable attention after the smart phone era. Meanwhile, advanced portable technology motivates and promotes further development of many textile-based electronic devices. With an urge to realize electronic devices based on textile fibers, yarns, and fabrics as the substrate materials, high-performance, durable, and washable textile metal conductors acting as interconnects, contacts, and electrodes are inevitably essential. In this chapter, a universal strategy, namely, PAMD, aiming to tackle the interfacial instability of metal/textile interface has been discussed. Remarkably, PAMD qualifies the as-deposited metal on textiles for excellent durability to withstand repeated cycles of bending and stretching without significant conductivity failure. In addition, PAMD is compatible with common printing technologies and textile dyeing and finishing technologies, providing a promising fabrication of high-performance, durable textile metal conductors for electronic purposes.

Although PAMD can solve critical challenges in the fabrication of metallic textiles such as metal adhesion on the textiles surface, durability, electrical conductivity, and compatibility in scale production, there are some limitations in the PAMD process. First, PAMD adopts ELD as the final step to deposit metal. Constrained by the ELD chemistry, limited choices of metal are only allowed such as copper, nickel, silver, and gold. Second, PAMD involves quite a lot of steps to go through. Its experimental design is based on a bottom-up approach, which means that the fabrication process consists of repetitive step-by-step immersion and drying procedures that must be done after one another. In the production point of view, the fabrication process is still tedious. Even though recently a printing approach has been proposed to reduce the steps taken in the PAMD process, printing can result in lateral diffusion in textile materials if the printing parameters are not well controlled.

Sooner or later, it is expected that more textile-based electronics such as flexible and wearable displays, energy harvesting devices, and robotic skins will be demonstrated by using the textile metal conductors fabricated by PAMD. Particularly, more focuses and efforts will be put in improving device's performance stability, reliability, washing durability, and compatibility of the manufacturing process with the current textile manufacturing industry. It is anticipated that different encapsulation methods of the devices will be demonstrated and optimized

in order to fully incorporate textile-based devices into garments. However, the integration of these textile-based electronic devices into garment wearables is still not an easy feat. First, it still takes a lot redesign and experiment works that require technology transfer of PAMD from a lab-scale fabrication to the bulk production in the industry. Second, fabrication of textile-based electronic devices is still tough and challenging as it involves all precise synthesis, construction, and alignment of electronic devices on flexible form of materials, which demands revolutionary development of all the compatible machineries. Third, the construction of microelectronics on textiles still requires many research efforts as it involves the incorporation of multiple-level electronic components such as conductive traces, construction of integrated circuits, packaging, cable connections, and the construction of the whole wearable systems that are still not yet established at such an early development stage. Most importantly, the safety issues still require the incorporation of multidisciplinary expertise to pave the way for mass production of washable textile-based electronics in the near future.

References

1 Service, R.F. (2003). *Science* 301: 909.
2 Park, S. and Jayaraman, S. (2003). *MRS Bulletin* 28: 585.
3 Park, S., Gopalsamy, C., Rajamanickam, R., and Jayaraman, S. (1999). *Studies in Health Technology and Informatics* 62: 252.
4 Firoozbakhsh, B., Jayant, N., Park, S., and Jayaraman, S. (2000). *Proceedings IEEE International Conference on Multimedia and Expo*, 1253. New York.
5 Park, S., Mackenzie, K., and Jayaraman, S. (2002). *Proceedings of the ACM/IEEE 39th Design Automation Conference*, 170. New Orleans.
6 Tao, X. (2005). *Wearable Electronics and Photonics*. Cambridge: Woodhead Publishing Ltd.
7 Langenhove, L.V. (2007). *Smart Textiles for Medicine and Healthcare: Materials, Systems and Applications*. Cambridge: Woodhead Publishing Ltd.
8 Lee, J., Kwon, H., Seo, J. et al. (2015). *Advanced Materials* 27: 2433.
9 Zhang, Z.T., Yang, Z.B., Wu, Z.W. et al. (2014). *Advanced Energy Materials* 4: 1301750.
10 Lee, Y.H., Kim, J.S., Noh, J. et al. (2013). *Nano Letters* 13: 5753.
11 Aboutalebi, S.H., Jalili, R., Esrafilzadeh, D. et al. (2014). *ACS Nano* 8: 2456.
12 Huang, Q.Y., Wang, D.R., and Zheng, Z.J. (2016). *Advanced Energy Materials* 6: 1600783.
13 Drew, C., Liu, X., Ziegler, D. et al. (2003). *Nano Letters* 3: 143.
14 Lotus, A.F., Bender, E.T., Evans, E.A. et al. (2008). *Journal of Applied Physics* 103: 024910.
15 Dall'Acqua, L., Tonin, C., Peila, R. et al. (2004). *Synthetic Metals* 146: 213.
16 Bhat, N.V., Seshadri, D.T., and Radhakrishnan, S. (2004). *Textile Research Journal* 74: 155.
17 Kim, B., Koncar, V., and Dufour, C. (2006). *Journal of Applied Polymer Science* 101: 1252.
18 Jiang, K.L., Li, Q.Q., and Fan, S.S. (2002). *Nature* 419: 801.

19 Zhang, M., Atkinson, K.R., and Baughman, R.H. (2004). *Science* 306: 1358.
20 Lima, M.D., Fang, S.L., Lepro, X. et al. (2011). *Science* 331: 51.
21 Little, B.K., Li, Y.F., Cammarata, V. et al. (2011). *ACS Applied Materials & Interfaces* 3: 1965.
22 Lou, C.W. (2005). *Textile Research Journal* 75: 466.
23 Chen, H.C., Lee, K.C., Lin, J.H., and Koch, A. (2007). *Journal of Materials Processing Technology* 184: 124.
24 Lai, K., Sun, R.J., Chen, M.Y. et al. (2007). *Textile Research Journal* 77: 242.
25 Wei, Q.F., Yu, L.Y., Wu, N., and Hong, S.J. (2008). *Journal of Industrial Textiles* 37: 275.
26 Depla, D., Segers, S., Leroy, W. et al. (2011). *Textile Research Journal* 81: 1808.
27 Jur, J.S., Sweet, W.J., Oldham, C.J., and Parsons, G.N. (2011). *Advanced Functional Materials* 21: 1993.
28 Kalanyan, B., Oldham, C.J., Sweet, W.J., and Parsons, G.N. (2013). *ACS Applied Materials & Interfaces* 5: 5253.
29 Sweet, W.J., Oldham, C.J., and Parsons, G.N. (2014). *ACS Applied Materials & Interfaces* 6: 9280.
30 Lu, Y.X., Liang, Q., and Xue, L.L. (2012). *Applied Surface Science* 258: 4782.
31 Zhang, H.R., Zou, X.G., Liang, J.J. et al. (2012). *Journal of Applied Polymer Science* 124: 3363.
32 Lee, H.M., Choi, S.Y., Jung, A., and Ko, S.H. (2013). *Angewandte Chemie International Edition* 52: 7718.
33 Montazer, M. and Allahyarzadeh, V. (2013). *Industrial and Engineering Chemistry Research* 52: 8436.
34 Wang, W.C., Li, R.Y., Tian, M. et al. (2013). *ACS Applied Materials & Interfaces* 5: 2062.
35 Yu, Y., Yan, C., and Zheng, Z.J. (2014). *Advanced Materials* 26: 5508.
36 Milner, S.T. (1991). *Science* 251: 905.
37 Brittain, W.J. and Minko, S. (2007). *Journal of Polymer Science Part A: Polymer Chemistry* 45: 3505.
38 Ulman, A. (1996). *Chemical Reviews* 96: 1533.
39 Azzaroni, O., Brown, A.A., and Huck, W.T.S. (2007). *Advanced Materials* 19: 151.
40 Barbey, R., Lavanant, L., Paripovic, D. et al. (2009). *Chemical Reviews* 109: 5437.
41 Azzaroni, O., Zheng, Z.J., Yang, Z.Q., and Huck, W.T.S. (2006). *Langmuir* 22: 6730.
42 Wang, X.L., Yan, C., Hu, H. et al. (2014). *Chemistry - An Asian Journal* 9: 2170.
43 Liu, X.Q., Zhou, X.C., Li, Y., and Zheng, Z.J. (2012). *Chemistry - An Asian Journal* 7: 862.
44 Cui, W.S., Wu, D.Z., Wang, W.C. et al. (2009). *Surface and Coatings Technology* 203: 1885.
45 Garcia, A., Berthelot, T., Viel, P. et al. (2010). *ACS Applied Materials & Interfaces* 2: 3043.
46 Garcia, A., Polesel-Maris, J., Viel, P. et al. (2011). *Advanced Functional Materials* 21: 2096.

47 Liu, Z.L., Hu, H.Y., Yu, B. et al. (2009). *Electrochemistry Communications* 11: 492.
48 Yang, G.H., Lim, C., Tan, Y.P. et al. (2002). *European Polymer Journal* 38: 2153.
49 Yu, Z.J., Kang, E.T., and Neoh, K.G. (2002). *Langmuir* 18: 10221.
50 Guo, R.H., Li, Y.N., Lan, J.W. et al. (2013). *Journal of Applied Polymer Science* 130: 3862.
51 Guo, R.H., Jiang, S.X., Zheng, Y.D., and Lan, J.W. (2013). *Journal of Applied Polymer Science* 127: 4186.
52 Liu, X.Q., Chang, H.X., Li, Y. et al. (2010). *ACS Applied Materials & Interfaces* 2: 529.
53 Liu, L.B., Yu, Y., Yan, C. et al. (2015). *Nature Communications* 6: 7260.
54 Guo, R.S., Yu, Y., Xie, Z. et al. (2013). *Advanced Materials* 25: 3343.
55 Yu, Y., Xiao, X., Zhang, Y.K. et al. (2016). *Advanced Materials* 28: 4926.
56 Le, V.T., Kim, H., Ghosh, A. et al. (2013). *ACS Nano* 7: 5940.
57 Kou, L., Huang, T.Q., Zheng, B.N. et al. (2014). *Nature Communications* 5: 3754.
58 Huang, Q.Y., Liu, L.B., Wang, D.R. et al. (2016). *Journal of Materials Chemistry A* 4: 6802.
59 Zhao, Z., Yan, C., Liu, Z. et al. (2016). *Advanced Materials* 28: 10267.
60 Zhen, H., Li, K., Chen, C. et al. (2017). *Journal of Materials Chemistry A* 5: 782.

27

Fibers for Medical Compression

Bipin Kumar[1], Harishkumar Narayana[2], and Jinlian Hu[2]

[1] *Indian Institute of Technology Delhi, Department of Textile Technology, TX135, Hauz Khas, New Delhi 110016, India*
[2] *The Hong Kong Polytechnic University, Institute of Textiles and Clothing, Hung Hom, Kowloon, Hong Kong, China*

27.1 Introduction

It has been estimated that 2% of the general population in the world (age group: 18–64) is suffering from chronic venous disorders such as venous ulcers, varicose veins, edema, deep vein thrombosis, etc. [1]. This rate is further increased to 4% in people over the age of 65. This has significant socioeconomic impact, costing 1% of total healthcare budgets in developed countries, for example, in the United States, this costs US$2.5 billion to treat 6 million patients every year [1]. This number is bound to increase with a growing aging population and changing lifestyle (sitting working culture with limited limb movements) that increases the risk of poor blood circulation [2, 3]. Thus there is a huge market in compression products for improving life quality of world population.

As an efficient and long-term medical intervention for chronic venous disorders, compression therapy is preferred so as to minimize the post-thrombotic syndrome, prevent ulcer recurrence, and alleviate the related symptoms, such as leg pain and swelling caused by damaged veins [4–6]. Herein, a textile bandage or stocking is used to apply certain level of pressure around the affected site on the limb. The objectives of compression therapy are to reduce the venous hypertension in the affected area, to reduce the swollen limb to minimum the size, and also to maintain a uniform pressure gradient in the leg from toe to knee to improve the venous return to the heart [7]. External compression is given to the affected leg portion during compression therapy using compression materials like bandage, stockings, or pressure garments [8]. The efficacy of the treatment is undoubtedly dependent on the pressure generated at the interface between the textiles (used for compression) and the skin [9]. This pressure is called interface pressure or sub-bandage pressure. The interface pressure exerted here depends on several factors like limb shape and size, application technique, physical and structural properties of the bandage, physical activities taken by the patient, etc. [10, 11]. It has been observed by several researchers that the interface pressure decreases

Handbook of Fibrous Materials, First Edition. Edited by Jinlian Hu, Bipin Kumar, and Jing Lu.
© 2020 Wiley-VCH Verlag GmbH & Co. KGaA. Published 2020 by Wiley-VCH Verlag GmbH & Co. KGaA.

over a period of time and hence reduces the effectiveness of the treatment of the compression system [5, 12–15]. Undoubtedly, the pressure drop or the success of the treatment entirely depends on the fiber and fabric construction used in the product; therefore, more understanding of the underlying interaction and performance of different fibrous materials and structures is needed. This could be useful for the academicians, R&D managers, product manufacturers, processing industries, doctors, health practitioners, researchers, nurses, and all others related to medical compression.

In this chapter, it is aimed to review several aspects of textile fibers used for compression therapy. Although the above subject demands the understanding of the fundamental nature of compression therapy, compression or pressure itself requires multidisciplinary approaches involving various concepts of physics, biological science, biomaterials, fabric engineering, structural dynamics, material science, technical textiles, and instrumentation to better deal the subject from different perspective. For simplification and meeting the desired requirements, this chapter introduces several multidisciplinary topics and describes the complex subject with very basic and simple discussions and gradually proceeds to list some of the recent developments in designing smart textiles for compression.

27.2 Compression Therapy

27.2.1 Pathophysiology and Implications of Chronic Venous Disorders

The cardiovascular system is a closed circulatory system in which blood flows in one direction only. It is organized around a central organ called the heart and is made up of three different types of blood vessels (arteries, veins, and capillaries; Figure 27.1). The arterial system is responsible to circulate blood from the heart to tissue and organs, and the venous system carries blood back to the heart. The venous system helps in the general circulation to send oxygen depleted blood rich in cell metabolism waste to the heart. The venous return toward the heart depends on the venous pressure that is developed in the veins. For a proper venous return, it is the combined action of the foot pump and calf muscle during movement and the efficacy of the venous valve system that ensures proper functioning and maintains the balance of blood flow in the body.

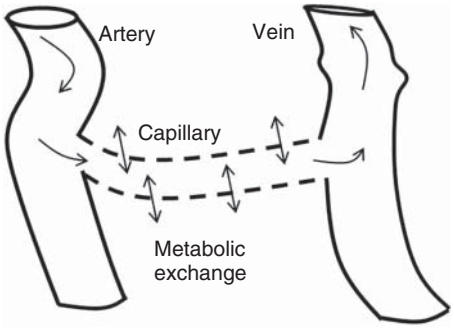
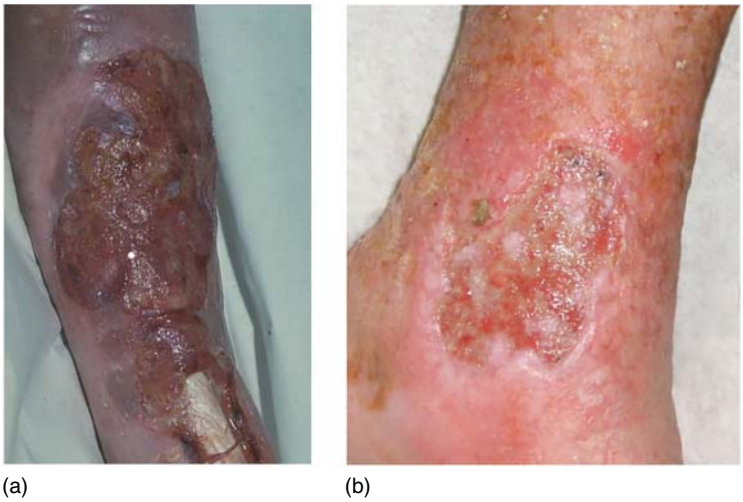


Figure 27.1 Schematic of the fluid transport of the human in the cardiovascular system.

Due to aging or limited movement, there exists high risk of imbalance in the cardiovascular function of the human body, and this results in loss of cutaneous substance, which might progresses over an indeterminate time period. This results in the development of chronic wounds, e.g. venous ulcer, leg ulcer, arterial ulcer, mixed ulcer, pressure ulcers, etc. Among these wounds, majority of cases are reported for venous hypertension (~80%), arterial insufficiency (~10%), or a combination of both [16]. One should be aware that chronic wounds may occur from venous or arterial disease, diabetes, arthritis, or malignancy. The basic characteristics of the venous and arterial ulcers are reviewed in Ref. [17]. The treatment for these etiologies will be different for each case. It has been advised that a comprehensive assessment of the patient, limb, vascular status, limb, and ulcer should be done to determine the underlying etiology and to formulate an appropriate compression management plan.

The level of chronic venous diseases in older patient is considerably higher in percentage, and their recurrence rate is also higher. Increase in venous pressure is obtained due to damage to the veins or venous valves. Also the action of foot and calf muscle movement does not function properly for older people due to their limited movement. The poor pump mechanism and the incompetent venous valve lead to venous hypertension due to increase in venous pressure. If the venous valves do not perform well or there is not enough pressure in the veins to push back the blood toward the heart, the pooling of blood occurs, and this causes edema (swelling of leg). If not managed, venous hypertension causes excessive pooling of fluid in the surrounding muscle that generates high pressure and lack of availability of oxygen and food. This causes skin deterioration and eventually the venous leg ulcers occur (Figure 27.2). Patients suffering from this experience a decreased quality of life because of continuous pain, discomfort, clinical depression, anxiety, social isolation, high cost for their treatment, lay beliefs, and also professional/patient conflict. Majority of patients (~68%)



(a) (b)

Figure 27.2 (a) Chronic venous deficiency (CVD). (b) Venous leg ulcer.

experience depression, anger, fear, depression, etc. These wounds have a high reoccurrence rate and are considered a major healthcare problem. It is also a difficult task for the healthcare practitioner to deal with these diseases because of their underlying implications associated with patient's life.

27.2.2 Need for External Pressure and Its Physiopathology

Compression therapy has been shown to improve the lives of patients by significantly reducing pain, reducing the swollen limb to minimum size, maintaining that size, increasing mobility, and allowing the patient to participate for the treatment of his limb whenever possible. The pressure is exerted to the affected limb part by some external means like medical compression bandage, stockings, pressure garments, etc. There are two pressure mechanisms acting within venous system: the hydrostatic pressure and the oncotic pressure [18]. The hydrostatic pressure is equal to the great saphenous vein pressure, while the oncotic pressure is the osmotic pressure created by protein colloid in plasma. The oncotic pressure difference causes reabsorption of fluid, while the hydrostatic pressure causes filtration. The amount of lymph formed depends upon the permeability of the capillary wall and the gradient of hydrostatic pressure and oncotic pressure between blood and tissue. Increasing venous or hydrostatic pressure in the vein leads to more depositions of venous fluid from the veins to surrounding tissues because of increasing filtration through venous tubes. Compression therapy aims to decrease the pressure difference across the venous tubes and increases the action of the venous pumps in order to restore venous blood flow. It is based on application of external pressure equal to the excess venous pressure in order to restore normal transmural pressure. The main effects of applying external pressure are as follows:

(i) It reduces the venous diameter and increases the interstitial pressure in the surrounding and hence leads to an increase in blood flow in the deep veins, a reduction in pathologic reflux, and a reduction of the hydrostatic pressure (Figure 27.3a).

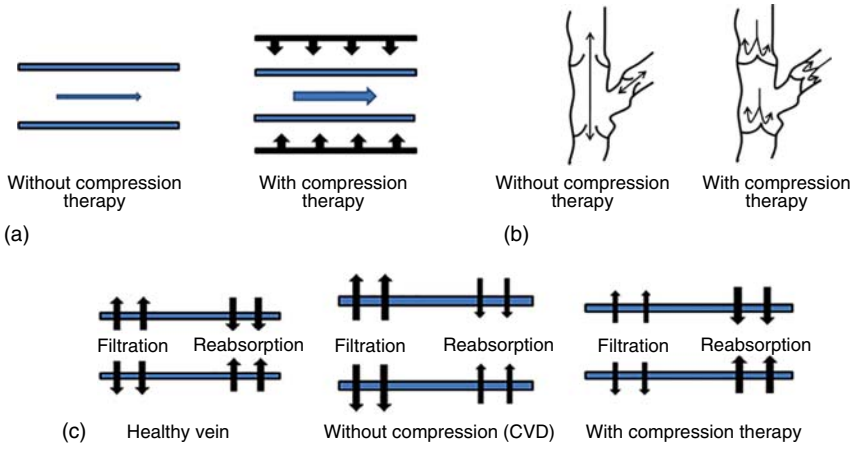


Figure 27.3 Effect of compression. (a) Increase in venous flow. (b) Restoration of venous valve function. (c) Increase in reabsorption of interstitial liquid.

(ii) It restores the valve function by bringing the walls of the veins closer together (Figure 27.3b).
(iii) It reduces blood pressure in the superficial venous system.
(iv) It reduces the pressure differences between the capillaries and the tissue to prevent back flow.
(v) It increases the cutaneous microcirculation, favors white cell detachment from the endothelium, and prevents further adhesion.
(vi) It reintegrates the interstitial liquids into the vessels (Figure 27.3c).

27.3 Role of Fibers in Compression Therapy

27.3.1 Fiber-Based Compression Modalities

Several compression methods and combinations are available for treatment of venous disorders. The fiber-based compression products can be categorized based on the elasticity, pressure, material, and structure (Figure 27.4). The pressure or compression is the ley to the treatment success, and the primary methods for applying compression are bandages, stockings, and intermittent pneumatic compression (IPC) [5, 16]. Bandages are preferred for the patients who require frequent dressing changes and recommended during the therapy phase of treatment for venous ulceration and also to control edema. Bandages are more practical for those incapable of applying compression stockings or for patients with fragile skin. Compression bandages are often more useful than the topical dressings for managing peripheral edema. The disadvantages of compression by bandages are the variability of pressure achieved even when applied by experienced professionals and patient compliance because of discomfort. Medical compression stockings are used to provide compression, which

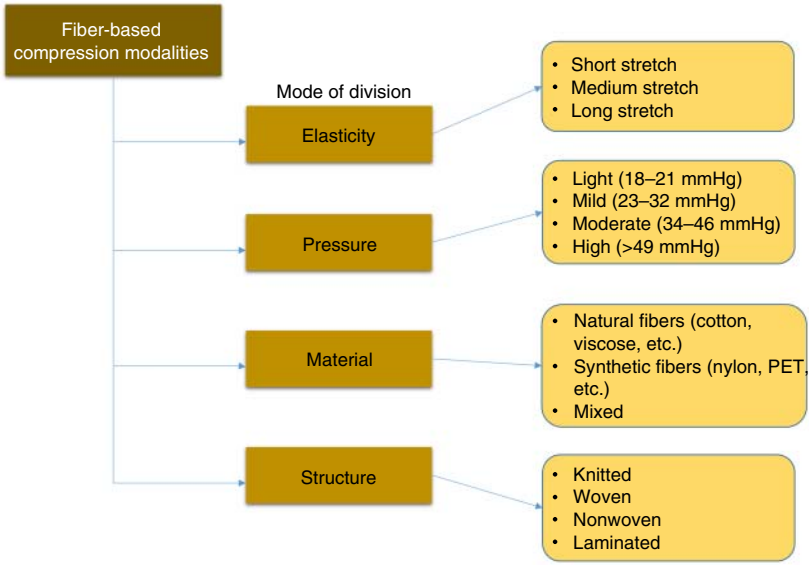


Figure 27.4 Fiber-based compression modalities.

is maximum at the ankle and gradual reduction in compression as the limb circumference increases. Unlike compression bandaging, the pressure generated with stockings is less dependent on the person applying it. It is imperative that the appropriate size and compression rating be prescribed for the condition and the patient being treated. IPC is useful for those who are not able to tolerate compression bandaging, who have reduced calf muscle function or limited ankle mobility, or who have peripheral arterial disease where other forms of compression are contradicted. In this technique, the limb is sequentially inflated and deflated, so as to simulate normal circulatory action and venous foot and calf muscle action. The disadvantages are that it is costly, can be bulky and noisy, and requires power supply.

27.3.2 Compression Requirements

Success of the compression therapy requires proper management plan designed to handle the underlying pathology and contributing factors. Several important factors need to be present for a health practitioner to use compression systems, like knowing how to use different compression systems, knowing the best available compression systems available for the treatment, being able to identify the etiology of the ulcer, and the willingness of the patient to agree to the commencement of compression treatment and for this to be sustained. Undoubtedly, the first step is to achieve the right amount of compression. A general guide to the amount of compression recommended for various indications is given in Table 27.1. It is likely that calf muscle function and variable ankle mobility may account for much of the variability in the success of compression therapy.

Although, the compression redistributes blood from the venous system into the central parts of the body in the case of the patients with poor blood flow. However, the product should also maintain a pressure gradient, which is paramount for such treatment. Figure 27.5a shows that the ankle pressure is different when the subject is lying, rising, standing, and walking for a normal and diseased person. So, when a normal person stands still, the pressure of venous blood in the leg increases from knee to foot because of gravity. Compression

Table 27.1 Recommended compression.

Degree of compression (kPa)	Indication
<2.6	Prevention of deep vein thrombosis (graduated compression stocking), mild edema, aching legs (occupational leg symptoms)
2.6–4	Mild varicose veins, mild to moderate edema, long-haul flights, varicose veins during and after pregnancy
4–5.3	Venous ulcers (including healed ulcers), deep vein thrombosis, superficial thrombophlebitis, varicose veins with severe edema, post-thrombotic syndrome, mild lymphedema
>5.3	Severe lymphedema, severe chronic venous insufficiency

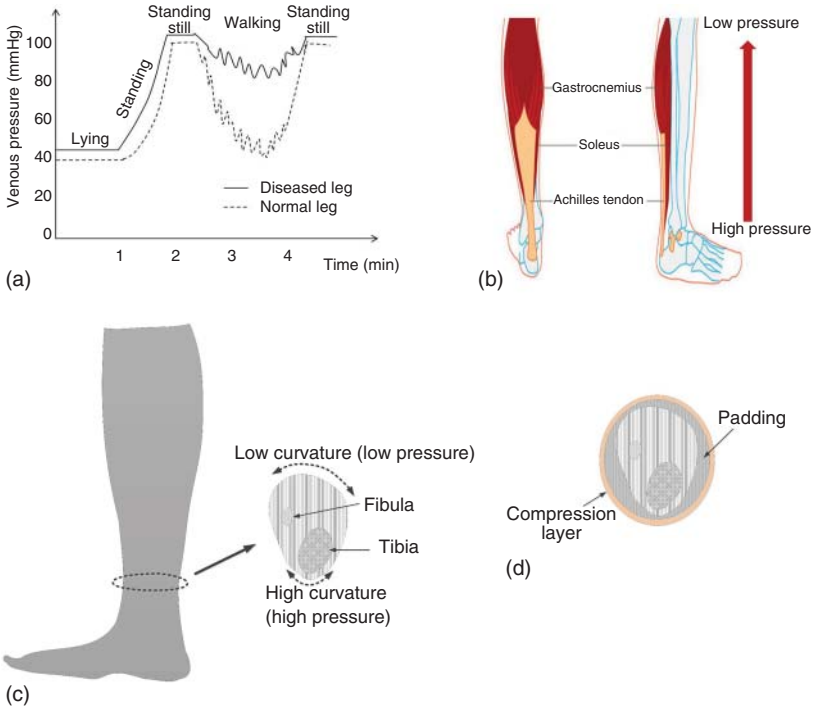


Figure 27.5 (a) Changes of ankle pressure. (b) Pressure gradient due to compression. (c) Irregular cross section of the leg causing high and low pressure around the (d) fibers as padding in pressure redistribution.

product should produce gradient pressure from foot to knee to propel blood toward heart (Figure 27.5b). Apart from the gradient requirement, the pressure should also be uniform around the circumference. In general, the cross section of the leg is not circular due to which the pressure around the circumference could vary significantly. The radius of curvature is small over bony prominences such as tibia or fibula due to which they can experience high pressure (Figure 27.5c). This all indicates the need for pressure management where it is aimed to prevent high pressure at critical regions such as the tibia or fibula and to ensure uniform distribution of pressure equally around the circumference at a particular height. In order to distribute pressure evenly around the limb, it is essential that high pressures created at the tibia and fibula regions should be absorbed. Fibers are therefore used as padding layer to reshape legs (Figure 27.5d), which are not narrower at the ankle than the calf. It helps to reshape the limb more like a cone shape so that the pressure gradient can be achieved with more pressure at the ankle and less at the calf.

27.3.3 Practical Challenges

Current compression products have the following shortcomings: (i) The application of a bandage needs trained personal to wrap the bandage on the patient's leg

with constant force or extension, hence raising the treatment cost to hospitals and patients [19]. For maximum treatment efficacy, a required pressure gradient from "toe to knee" is critical yet arduous to achieve during bandage mounting due to reasons including different leg attributes (shape or size) among patients and difference in bandage materials/designs. Even after proper training to a staff, it is difficult to ensure the uniform bandage extension on the limb of the patient. (ii) Maintenance of the initially set pressure over time is another major challenge, due to the time and temperature dependence of the material behaviors [20–22], leading to a diminished treatment efficacy. (iii) For some patients, a dynamic (massaging) compression is recommended, but the required equipment like the IPC is costly, noisy, bulky, and, once attached, severely constraining the patients [23]. (iv) Also, all of the existing devices are incapable of offering heating therapy, preferred especially for non-active patients to improve blood flow.

27.4 Theoretical Insights into Pressure Prediction

Prediction of interface pressure applied by a bandage to a wounded leg segment could facilitate the efficiency of compression products. The Laplace's law is used to predict the interface pressure generated by the bandage immediately after the application that is a function of the tension in the fabric, the number of layers wrapped, the bandage width, and the circumference of the limb. The derivation of Laplace's law is attributed to the French scientist Pierre Simon de Laplace (1749–1827). The Laplace's law states that the force in the walls of the container is dependent on both the pressure of the container's content and its radius. The derivation of Laplace's law can be easily described by simplistic models like spheres or cylinders that can serve as models for many organs (Figure 27.6). In the case of air-filled cylinder removed from a longer tube, the forces in the wall of the cylinder must counterbalance the outward tension of the trapped air. In other words, $F_{\text{wall}} = F_{\text{air}}$. The total downward force applied by the wall to contain the air for a half cylinder is expressed as

$$F_{\text{wall}} = 2 \times T \times (L \times w) \tag{27.1}$$

where T is the tension in the wall per unit area and L and w are the length and wall thickness of the cylindrical vessel, respectively.

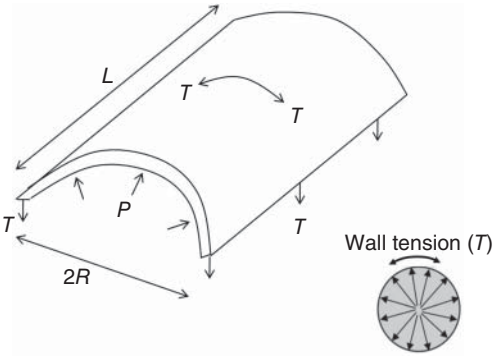


Figure 27.6 Derivation of Laplace's law for a cylinder.

The air inside the cylinder exerts pressure on the walls of the cylindrical vessel. The force exerted by the air pressure is equal to

$$F_{\text{air}} = P \times 2 \times R \times L \tag{27.2}$$

where P is the pressure difference across the wall and R is the radius of vessel. As the cylindrical container is neither expanding nor contracting, hence the tensions applied by the walls should be equal to those generated by its compressed contents. These simplify to

$$F_{\text{air}} = P \times 2 \times (R \times L) = F_{\text{wall}} = T \times 2 \times (L \times w)$$
$$\text{or } P = \frac{T \times w}{R} \tag{27.3}$$

This law is frequently used in medical science with an improved understanding of the functioning of the human body, the pathology of vascular wall, varicose vein, bladder rupture, the physics of respiratory physiology, and shape of the ventricles of the heart. This law is also used in compression therapy to predict interface pressure applied by a bandage on limb surface. To use Laplace's law in clinical practice, Thomas [24] modified Laplace's law to calculate pressure of compression system, which is described as

$$P = \frac{F \times n}{R \times W} \tag{27.4}$$

where P is the interface pressure (N/m^2), F is the longitudinal force applied to the bandage while wrapping (N), n is the number of layers of the bandage wrapped, R is the radius of the limb (m), and W is the bandage width (m).

The use of Laplace's law to determine interface pressure remains a controversial issue. Medical compression bandages are mostly applied in the form of multiple or overlapping layers, which results in the increase of the overall thickness of bandage fabric over the limb. Bandage application in spiral with 50% overlap results in two layers of bandage, while spiral with 33% overlap results in three layers of bandage. Four layers of bandage result from figure-of-eight bandage application with 50% overlap. Also multilayer multicomponent bandaging system involves the use of multiple layers of different medical bandages like padding, crepe bandage, compression bandage, adhesive bandage, etc. The modified equation of Laplace's law, described by Thomas [24], does not consider the increase in radius because of the preceding layers of the bandage. The reported model is based on the assumption that the bandage thickness has a negligible effect on the pressure. This may result in erred prediction of interface pressure for multiple layers. Schuren and Mohr [25] found that the interface pressure based on theoretical mathematical equations is not supported by experimental results. When compared between single layer and four-layer bandaging systems, it has been observed that the final pressure achieved by a multilayer bandaging system is not equal to the sum of the pressure exerted by each individual layer as predicted by Laplace's law [26, 27]. So, it is mandatory to use Laplace's law carefully to predict interface pressure as it could influence the selection of a particular bandage system according to a patient's condition and circumstances. The effect might be negligible or small for a few layers of bandage.

It is important to consider the bandage thickness to estimate interface pressure exerted by multilayer multicomponent bandaging system in order to avoid overestimating the pressure. The error can be 19% or even more at the ankle (circumference 25 cm) in the case of four-component multilayer bandaging systems. Al Khaburi et al. [28] have proposed a model based on thick wall cylinder theory to predict interface pressure by multiple layers of medical compression bandages:

$$P = \sum_{i=1}^{n} \frac{T[d + t + 2t(i-1)]}{((1/2)w[d + 2t(i-1)]^2) + (wt[d + t + 2t(i-1)])} \tag{27.5}$$

where P is the total pressure due to n layers of bandage (N/m^2), T is the tension in the bandage (N), d is the limb diameter (m), w is the bandage width when it is extended (m), t is the bandage thickness when it is extended (m), and n is the number of layers wrapped.

Interface pressure generated by the bandage varies significantly in the active patients as they walk due to the variation in limb size or shape as a result of calf muscle activity and the associated dynamic variation in the leg dimensions. The amount of variation in the interface pressure is dependent on the stiffness of the bandaging system. Al Khaburi et al. [29] have also developed mathematical models to predict the pressure change under dynamic conditions using Chord modulus, which can be calculated using force–elongation curve of bandage fabric. Chord modulus is defined as the slope of the straight line drawn between any two points on the force–elongation curve. Chord modulus indicates the change in force in dynamic conditions. The change in interface pressure due to change in limb shape is described as

$$\Delta P = \frac{2 \times \Delta d \times E \times w}{d^2} \quad \text{(using thin wall cylinder theory)} \tag{27.6a}$$

$$\Delta P = \frac{\Delta d \times E \times w}{2 \times r \times (r + w)} \quad \text{(using thick wall cylinder theory)} \tag{27.6b}$$

where ΔP is the change in the interface pressure that is caused by change in leg diameter (N/m^2), E is the chord modulus (N/m^2), w is the bandage thickness, d is the original leg diameter (m), Δd is the change in the leg diameter (m), and r is the leg radius (m).

27.5 Fibrous Material and Construction Used in Compression and Their Performance

Textile material, structure, and fabrication technology determines the product properties and performance and so decides the treatment outcomes and success. A textile fabric is defined as an assembly of fibers, yarns, or combinations of these. Different fabric construction has been frequently used for the preparation of compression product to apply pressure to the diseased limb. There are many ways to manufacture a textile fabric. Each manufacturing method is able to produce a wide range of fabric that depends on the raw materials used, the equipment, the machinery employed, and the manufacturing processes involved. The

commonly used structures in the medical compression are woven, knitted, nonwoven, and spacer fabrics. Woven construction consists of two sets of perpendicular yarns (also known as warp and weft yarns) that are interlaced together with the help of weaving process. Knitted construction consists of intersecting loops that are produced by a knitting process. It is characterized by courses and wales. Nonwovens are also used commonly for the preparation of padding material for the multilayer compression bandaging system. Nonwovens are defined as the manufactured sheet, web, or batt of directionally or randomly oriented fibers that are bonded by friction, cohesion, or adhesion. Spacer fabric is three-dimensional knitted fabrics that consist of two separate knitted substrates. These two separate substrates are kept apart by spacer yarn. Spacer fabrics are much like a sandwich and feature with two complementary slabs of fabrics with a third layer tucked in between.

Textile structures used in compression bandages or stockings are made from fibers or yarns. Fiber is the first building block of any textile structure, and the fiber has to be converted into yarn to finally weave or knit any structure. Yarn, used for compression, is a heterogeneous structure (consist two or more fiber type) that can be produced by different covering methods (e.g. single or double covering, core spinning, stitch covering, core twisting, and air jet covering) [11]. Core–sheath yarn is more popular as it contains the elastomeric filament covered by staple cotton, PET, or nylon fibers. Among them polyamide-based conventional covered spandex elastomeric yarns are more frequently used in making compression stockings or other pressure garments. Sometimes, the elastomeric yarn is directly used in the fabric structure in the form of inlay fabric structure with the help of tuck, float, and stiches in the construction (Figure 27.7). The construction (tuck, float, stitch, thread density) and material properties (fiber extensibility, denier, twist, type of covering) need to be optimized to achieve desired thickness, tension, and stiffness from a compression product.

During the compression treatment, it is expected from a textile to sustain a uniform interface pressure gradient over the limb for faster recovery. The efficiency of different textiles to provide sustained pressure varies because of the

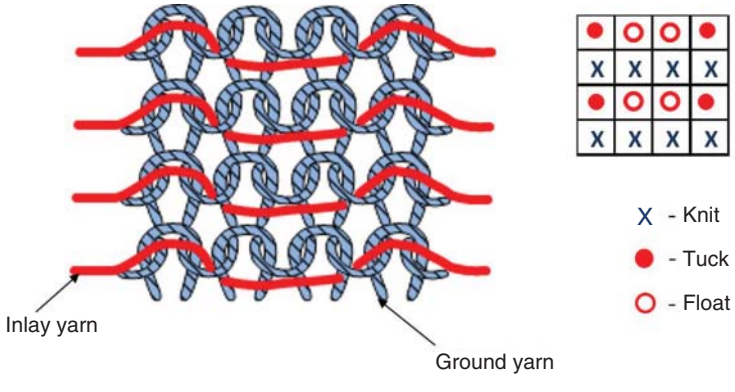


Figure 27.7 Inlay structure used for medical stocking for compression.

differences in their structure and constituent material type. A textile applies pressure over the limb because of the internal stress developed in the structure during its application over limb by applying external force. The capacity of a product to sustain pressure is greatly dependent on its ability to maintain this internal stress developed in the bandage under wrapped position. All textile fibers or structures are made from polymers that are viscoelastic in nature. Because of the viscoelasticity, the stress developed in the textile structure under constant extension decreases over time. This process is called stress relaxation that refers to the material behavior to relax the internal stress over time under a fixed level of elongation (Figure 27.8a). This can be experimentally measured by applying a constant elongation to the specimen and measuring the internal stress required to maintain that elongation as a function of time. Figure 27.8b,c shows the general relaxation behavior of textile fibers at different strains and temperatures, respectively.

The capacity of a bandage to sustain pressure is greatly dependent on its ability to maintain the internal stress developed in the bandage under wrapped position. Because of viscoelastic behavior of fiber or yarn, the stress developed in the bandage structure decreases over time. The reduction of the internal stress in the bandage over time could be an important factor for the interface pressure drop during course of compression treatment and hence could be a deciding factor to evaluate bandage performance [12, 13, 30]. Kumar et al. [14, 22] showed the pressure drop by compression bandages due to relaxation of stress in the fibers

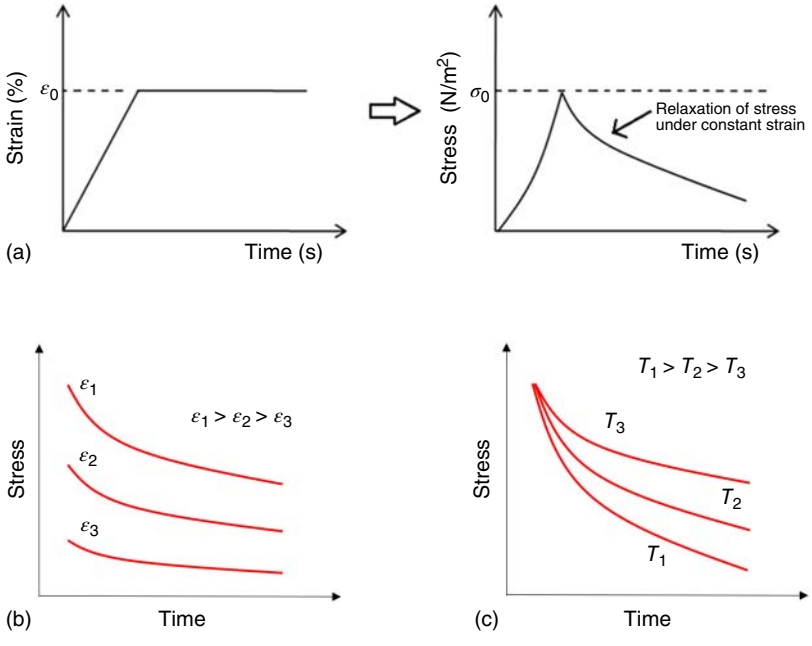


Figure 27.8 (a) Stress relaxation behavior of the material. (b) Generalized relaxation behavior of textile behaviors at different extensions. (c) Generalized relaxation behavior of textile behaviors at different temperatures.

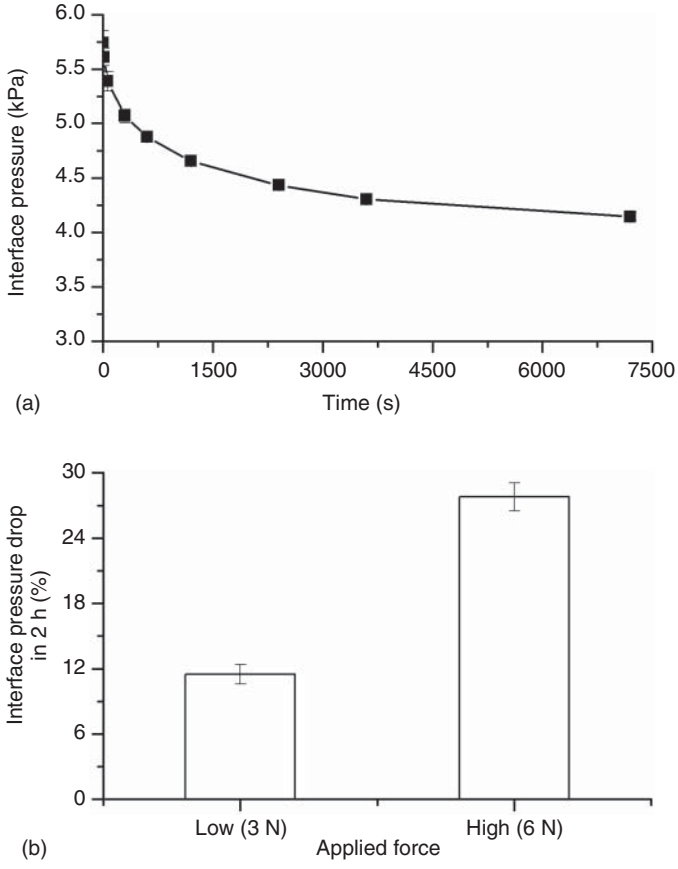


Figure 27.9 (a) Pressure profiles over time for a cotton bandage. (b) Pressure drop at different applied forces.

(Figure 27.9). Understanding viscoelastic behaviors of different fibrous materials present in the compression product is therefore critical and helps to design and evaluate long-term product performance.

Kumar et al. [12–14, 21, 22, 30–35] also conducted extensive study on different materials and other factors and obtain critical information on the product performance. Pressure relaxation by a bandage depends significantly on the relaxation behavior of fibers or yarns used in it. Relaxation time is commonly used to describe stress relaxation behavior of a viscoelastic material, which indicates the time required to reach from unrelaxed state to new relaxed state of the material. It has been found that cotton and viscose fibers have the lower relaxation time due to which the relaxation of stress is faster. Synthetic fibers (e.g. nylon, PET, elastase) have low stress relaxation as compared with cotton fiber because of their higher relaxation time. This could be the reason for different pressure profiles obtained for bandages developed from different fibers (Figure 27.10). Higher and faster pressure drop for 100% cotton and viscose samples were obtained because of their poor ability to sustain internal stress in the structure. Elastomeric yarns

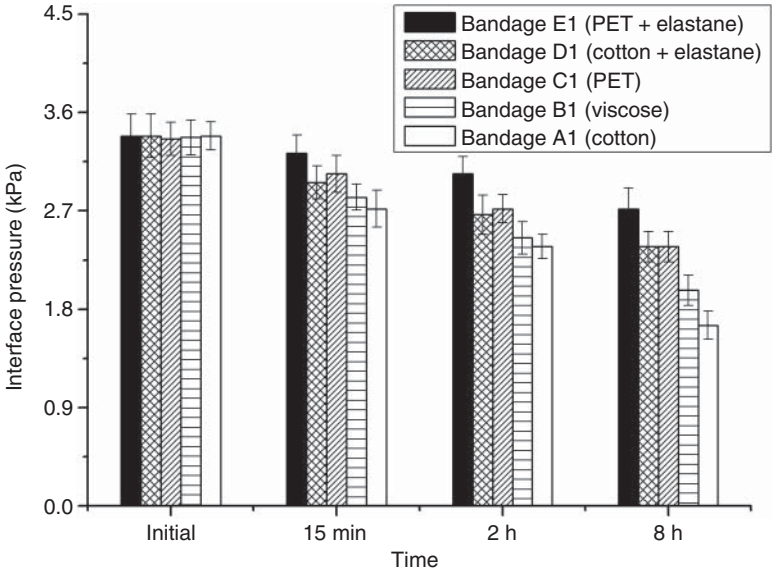


Figure 27.10 Effect of material type on interface pressure profile generated over time for different bandages.

have excellent elastic and rheological properties. They can maintain the internal stress for longer time because of their good elastic properties [36]. It has been also observed that fabrics containing elastomeric yarn tend to be tighter and have more number of threads per unit area. So, a compression product containing elastomeric yarn is best suited to maintain the pressure. Kumar et al. [14, 22] also observed that the pressure drop can be minimized by increasing the tightness of the structure (Figure 27.11). It has been observed that pressure drop is less for a structure having higher thread density compared with the structure having lower thread density. More pressure drop is expected at higher applied force in the bandage.

27.6 Innovation in Compression Products

A number of innovations have been noticed in the field of compression to use smart fabrics or structure with added benefits or functions for the treatment. Schafer and Jung [37] proposed the suitability of wide bandage fabric with more transverse stability and easy tearing capacity. Herein, the tearing capacity is obtained by utilizing the spun crape threads with *S* and *Z* twisting directions. In other innovation, the leno structure is used to provide high frictional resistance between warp and weft yarns particularly to improve the durability of the bandage, where frequent washing is necessary [38]. Application of bandage at a constant extension is always a challenge for unexperienced nurses or practitioners, and to ease the application process, an innovative design with visual pattern is used to assure uniform wrapping. In this, the

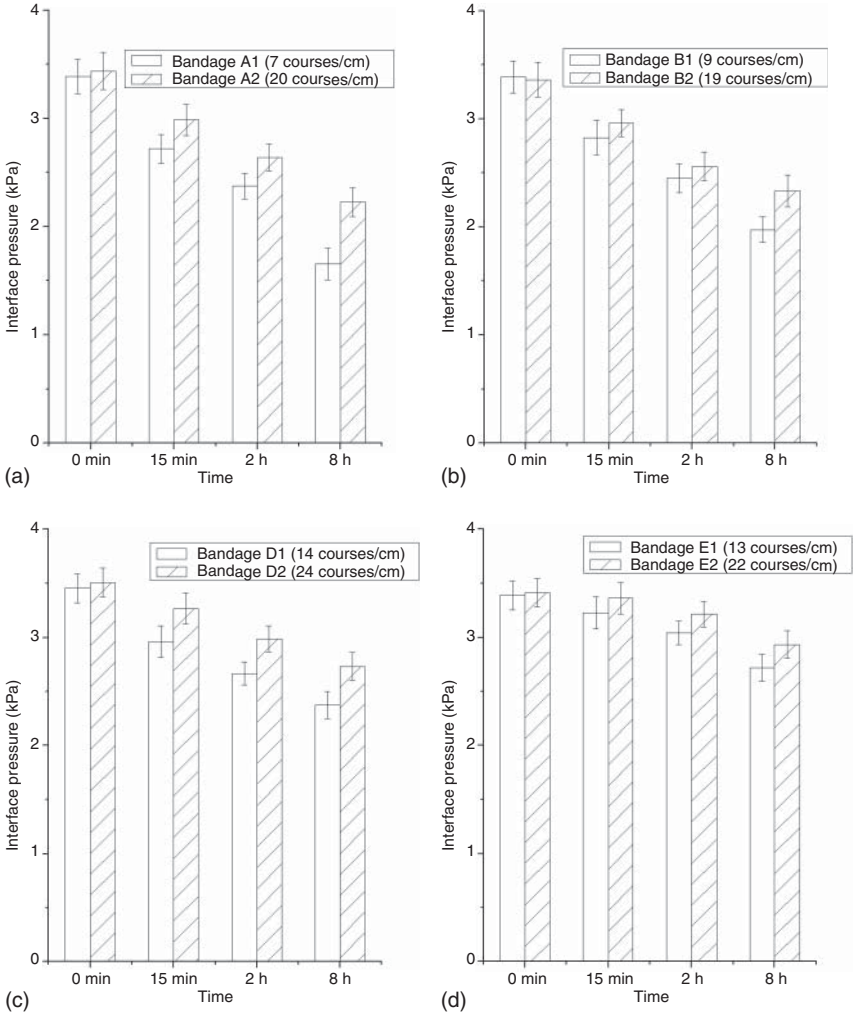


Figure 27.11 Effect of thread density on the pressure profile of different bandages. (a) Cotton, (b) viscose, (c) cotton + elastane, and (d) PET + elastane.

continuous pattern is formed across the length of bandage, so that the shape of each geometric shape is changed when tension is applied to the bandage and shape of the deformed pattern is indicative of compression force applied (Figure 27.12a). Another approach to maintain constant force is to use yarns made from synthetic elastomeric polymer containing triblock A-B-C copolymer (styrene–butadiene–styrene) [39]. In general, if a normal bandage is stretched too much during the application, the compressive force over the bandage may be overly great and cause damage, for example, by restriction of blood supply. But the bandage manufactured by block A-B-C copolymer achieves an effective compressive force at an extension of between 20% and 60% after which any further extension of the bandage is accompanied by only a small increase in compressive

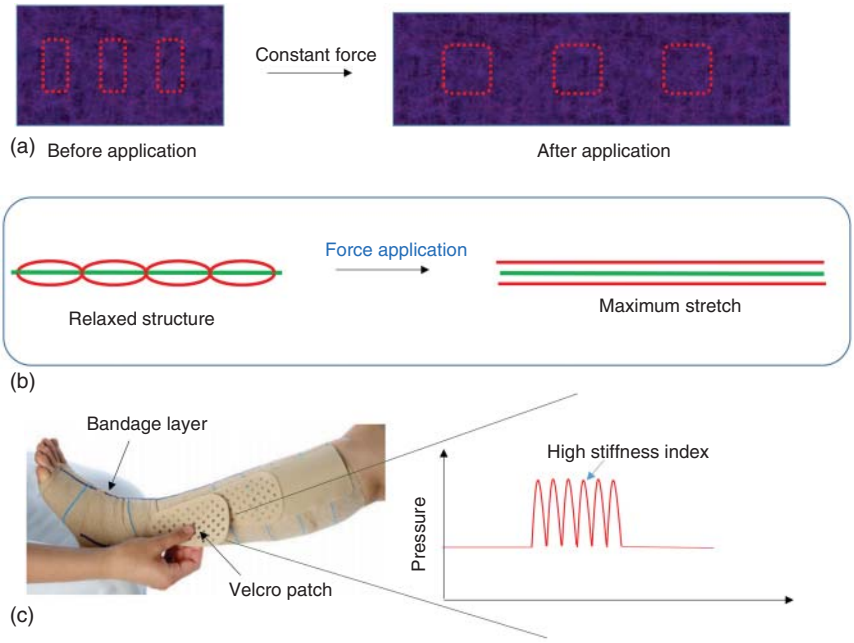


Figure 27.12 (a) Mechanism to obtain constant stretch. (b) Thonic bandage to apply at constant extension. (c) Velcro patch to control bandage stiffness.

force. This way it eliminates the risk of high force due to over stretching. More recently, the use of Thonic bandage (Figure 27.12b) is becoming popular, which helps the medical practitioners to apply bandage at a constant extension [40]. It suggests the use of leno structure for the cotton yarn to control the stretchability of the bandage. In addition to application at constant extension, the stiffness of compression product is also critical. The functioning of calf muscle pump helps in returning the blood to the heart; and the function of calf pump gets enhanced during compression therapy when an inelastic bandage (short-stretch bandage) is applied to the limb. More recently, an innovative method is proposed to provide a low, sustained resting pressure but high, efficient working pressure [41]. Herein, the Velcro patches (Figure 27.12c) are used above bandage layer to increase the stiffness of the underlying material and enhance the working pressure.

Multilayer compression bandaging system comprises crepe bandage, padding bandage, compression bandage, and adhesive bandage. The whole system is bulky and provides discomfort to the patient. With a view to replace both the compression and padding bandages, 3D knitted single-layer bandages have been introduced, which is produced by spacer technology [42]. The fabric sample contains two different layers of fabric that are combined with an inner spacer yarns. The construction allows using different materials for its layers and spacer yarns and hence could be engineered for a wide range of applications. It provides softness, good resilience, and a cushioning effect to the body. The need for health monitoring is becoming popular in the twenty-first century to get continuous feedback of the pressure results and access the efficacy of product remotely. In such product, a pressure sensor can be integrated for providing an indication of the compression

applied by a bandage to a human or animal body. Such pressure sensing device can be directly designed from the conductive yarns integrated in the fabric structure [43].

27.7 Shape Memory Fibers for Compression

There exist several limitations of conventional compression treatments in the current clinical practice. The level of pressure is difficult to achieve due to several influencing factors including the difference in limb size or shape, material properties, and application procedure [14]. Additionally, the pressure gradient achieved by the bandages or stockings varies over times due to changes in limb shape (i.e. reduction of edema over time), and there exists no external means to adjust the pressure gradient. Inevitably pressures drop during use, as for all compression bandages in the market. And there exists no current solution to control the pressure and its distribution by the bandage locally or as a whole. Clearly, controlling or readjusting pressure on the leg would serve many advantages to health practitioners and would make the treatment even more effective.

The aforementioned challenges in compression products (i.e. easy application at constant extension and external pressure control) could be resolved if there is a possibility of shape and stress control in the bandage materials. The stimulus-responsive polymers, such known as memory polymers (MPs), could be useful here as they demonstrate shape memory ability that permits programming or fixing of different deformed shapes from an original (permanent) shape (Figure 27.13a) and simultaneously allows the shape recovery to the original shape by external stimulus such as heat [44, 45]. Many applications of MPs have been demonstrated in aerospace, biomedical, transport, construction, electronic, textile, and consumer products [46–48]. This shape control ability of MP could be utilized in compression bandage to provide easy and alternative method of uniform wrapping; thus it will eliminate the need for a trained personal for bandage application. In the textile, the shape memory effect can be achieved by incorporating MP filaments in the fabric structure (Figure 27.13b). To achieve constant extension, the deformed shape (constant strain) of an MP-based bandage could be programmed first using shape fixity potential of the MP, and then the bandage could be wrapped over the limb with no further extension. The bandage could be then activated directly on the limb to initiate the recovery process that would result in the uniform shrinkage throughout the wrapping area, hence achieving nearly constant extension in the entire length. This process could be easily achieved using external stimulus such as heat.

More recently, another new phenomenon in MP, i.e. stress memory, is also discovered [49]. Similar to shape memory, stress memory is a phenomenon whereby the stress in a polymer can be programmed, stored at temperature below its thermal transition temperature T_{trans}, and then retrieved reversibly, when needed, with an external thermal stimulus at $T > T_{trans}$ (Figure 27.13c,d), thus to realize the in situ material stress control. In other words, the integration of MP fibers into bandage fabric structures could allow in situ stress control [50–52]. As the bandage interface pressure depends on the internal stress in the fabric, so the possibility of stress alteration could help in achieving recommended pressure level in the wrapped state of the bandage. Also, this will allow the bandage to provide

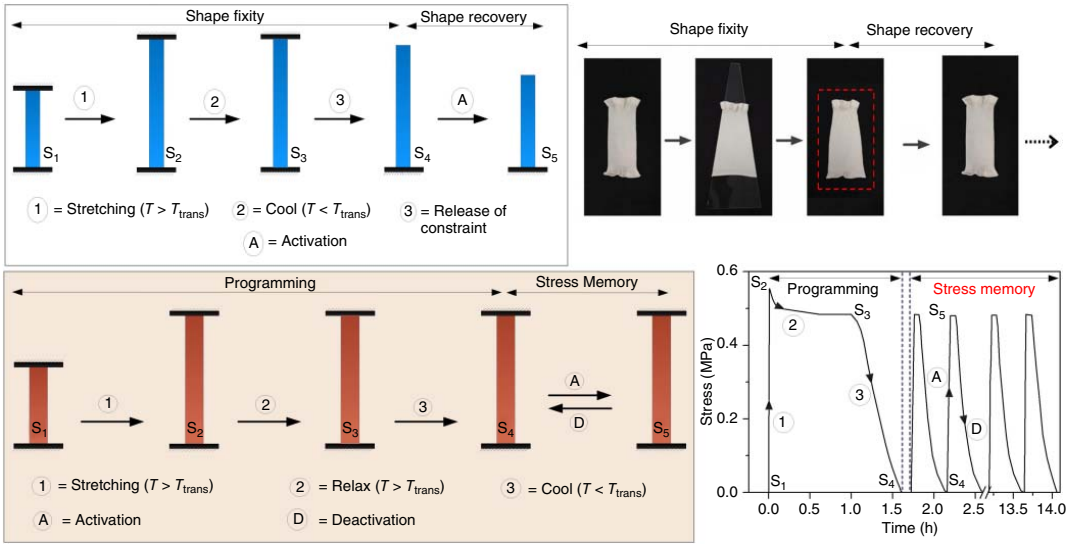


Figure 27.13 (a) Thermomechanical process to observe shape memory (fixity and recovery) in a memory polymer (MP). (b) Demonstration of shape memory using a memory fabric. (c) Stress memory programming in the MP. (d) Results of stress memory response of an MP.

dynamic massage effect via alternating stress modulation and so would eliminate the need for IPC.

More recently, Hu and coworkers [49–53] have designed and proposed stimulus responsive memory fibers for the smart compression management. The fibers were prepared from poly(1,6-hexanediol adipate) (PHA) (UBE Industries, Japan) having molecular weight of 3000 g/mol as a reversible phase (soft segment), 4,4′-diphenylmethanediisocyanate (MDI) (Aldrich Chemical Company, USA), and chain extender 1,4-butanediol (BDO) (Acros Organics, USA) as a fixed phase (hard segment). These filaments could be incorporated in the stocking fabric for external pressure control functions. The pressure testing of memory filaments integrative compression stocking allows to provide extra pressure (Figure 27.14a) and massage effect (Figure 27.14b) in the same deformation constraint just by change in an external heat stimulus to trigger the stocking. The

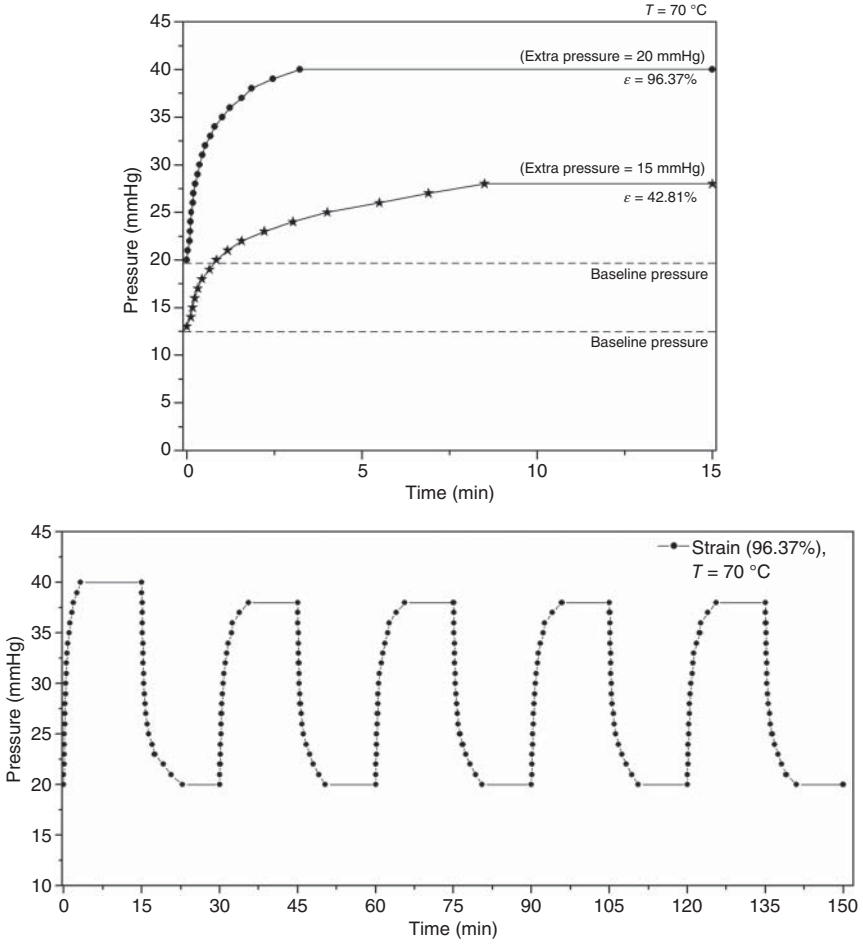


Figure 27.14 Experimental results of memory filaments integrative stocking fabric. (a) Pressure–time profile at different strains. (b) Pressure–time profile showing massage effect.

novel memory phenomenon could be further implemented scientifically with applied technology in multidisciplinary arenas such as massage devices, artificial muscles, and smart fabrics, where the stimuli-responsive stress is needed.

27.8 Conclusions

The present chapter introduces the principles of compassion therapy and the role of different textile material and structures. More emphasis is given on the interface pressure exerted by a compression product on the limb. The relaxation behavior of the fibers as well as related structures plays a critical role in maintaining the pressure over time. Elastomeric fiber in such product is a must if one has to maintain elasticity and eliminate the problem of pressure drop over time. At the end, the future potential of memory filaments in the field of compression is briefly introduced. The memory fabric allows to change the internal stress in its structure by external heating. It is possible to control or manage the pressure in wrapped position. This smart compression system could offer several advantages in compression management. First, it could give more freedom to nurses to control or readjust pressure to achieve an appropriate pressure whenever needed. Second, the advantage of memory compression system over other conventional compression products is that when the pressure drops below a targeted level, then it would be possible to readjust pressure level and therefore could provide sustained compression. Future work needs to be focused on designing and optimization of such filament and fabrics for smart compression management.

References

1 Pascarella, L. and Shortell, C.K. (2015). Medical management of venous ulcers. *Seminars in Vascular Surgery* 28 (1): 21–28.
2 Ruckley, C. (1997). Socioeconomic impact of chronic venous insufficiency and leg ulcers. *Angiology* 48 (1): 67–69.
3 Bergan, J.J., Schmid-Schönbein, G.W., Smith, P.D.C. et al. (2006). Chronic venous disease. *New England Journal of Medicine* 355 (5): 488–498.
4 Partsch, H. (2013). Compression therapy in leg ulcers. *Reviews in Vascular Medicine* 1 (1): 9–14.
5 Partsch, H. (2014). Compression for the management of venous leg ulcers: which material do we have? *Phlebology* 29 (1 Suppl): 140–145.
6 Mosti, G., Picerni, P., and Partsch, H. (2012). Compression stockings with moderate pressure are able to reduce chronic leg oedema. *Phlebology* 27 (6): 289–296.
7 Cullum, N.A., Nelson, E.A., Fletcher, A., and Sheldon, T. (2001). *Compression for Venous Leg Ulcers*. The Cochrane Library, 2.
8 Kumar, B., Das, A., and Alagirusamy, R. (2014). *Science of Compression Bandages*. WPI Publishing.

9 Partsch, H., Clark, M., Bassez, S., et al. (2006). Measurement of lower leg compression in vivo: recommendations for the performance of measurements of interface pressure and stiffness. *Dermatologic Surgery* 32 (2): 224–233.

10 Hirai, M. (1998). Changes in interface pressure under elastic and short-stretch bandages during posture changes and exercise. *Phlebology* 13 (1): 25–28.

11 Liu, R., Guo, X., Lao, T.T., and Little, T. (2016). A critical review on compression textiles for compression therapy: textile-based compression interventions for chronic venous insufficiency. *Textile Research Journal* 87 (9): 1121–1141.

12 Kumar, B., Das, A., and Alagirusamy, R. (2012). Prediction of internal pressure profile of compression bandages using stress relaxation parameters. *Biorheology* 49 (1): 1–13.

13 Kumar, B., Das, A., and Alagirusamy, R. (2013). An approach to examine dynamic behavior of medical compression bandage. *Journal of the Textile Institute* 104 (5): 521–529.

14 Kumar, B., Das, A., and Alagirusamy, R. (2013). Effect of material and structure of compression bandage on interface pressure variation over time. *Phlebology* 29 (6): 376–385.

15 Mosti, G. and Partsch, H. (2010). Inelastic bandages maintain their hemodynamic effectiveness over time despite significant pressure loss. *Journal of Vascular Surgery* 52 (4): 925–931.

16 Farah, R.S. and Davis, M.D. (2010). Venous leg ulcerations: a treatment update. *Current Treatment Options in Cardiovascular Medicine* 12 (2): 101–116.

17 Schmidt, K., Debus, E.S., St, J., et al. (2000). Bacterial population of chronic crural ulcers: is there a difference between the diabetic, the venous, and the arterial ulcer? *VASA, Zeitschrift fur Gefasskrankheiten* 29 (1): 62–70.

18 Partsch, H. (2003). Understanding the pathophysiological effects of compression. In: *EWMA Position Document. Understanding Compression Therapy* (ed. Suzie Calne), 2–4. London: Medical Education Partnership Ltd.

19 Partsch, H. (2014). Compression therapy for deep vein thrombosis. *VASA* 43 (5): 305–307.

20 Kumar, B., Das, A., and Alagirusamy, R. (2014). Effect of material and structure of compression bandage on interface pressure variation over time. *Phlebology* 29 (6): 376–385.

21 Kumar, B., Das, A., and Alagirusamy, R. (2012). An approach to determine pressure profile generated by compression bandage using quasi-linear viscoelastic model. *Journal of Biomechanical Engineering-Transactions of the ASME* 134 (9).

22 Kumar, B., Das, A., and Alagirusamy, R. (2013). Study of the effect of composition and construction of material on sub-bandage pressure during dynamic loading of a limb in vitro. *Biorheology* 50 (1–2): 83–94.

23 Feldman, J.F., Stout, N.L., Wanchai, A., et al. (2012). Intermittent pneumatic compression therapy: a systematic review. *Lymphology* 45 (1): 13–25.

24 Thomas, S. (2003). The use of the Laplace equation in the calculation of sub-bandage pressure. *EWMA Journal* 3 (1): 21–23.

25 Schuren, J. and Mohr, K. (2008). The efficacy of Laplace's equation in calculating bandage pressure in venous leg ulcers. *Wounds Uk* 4 (2): 38.

26 Dale, J.J., Ruckley, C.V., Gibson, B., et al. (2004). Multi-layer compression: comparison of four different four-layer bandage systems applied to the leg. *European Journal of Vascular and Endovascular Surgery* 27 (1): 94–99.

27 Ruckley, C.V., Dale, J.J., Gibson, B., et al. (2003). Multi-layer compression: comparison of four different four-layer bandage systems applied to the leg. *Phlebology* 18 (3): 123–129.

28 Al Khaburi, J., Nelson, E.A., Hutchinson, J., and Dehghani-Sanij, A.A. (2011). Impact of multilayered compression bandages on sub-bandage interface pressure: a model. *Phlebology* 26 (2): 75–83.

29 Al Khaburi, J., Nelson, E.A., Hutchinson, J., and Dehghani-Sanij, A.A. (2011). Impact of variation in limb shape on sub-bandage interface pressure. *Phlebology* 26 (1): 20–28.

30 Das, A., Kumar, B., Mittal, T., et al. (2012). Pressure profiling of compression bandages by a computerized instrument. *Indian Journal of Fibre and Textile Research* 37 (2): 114–119.

31 Kumar, B. and Das, A. (2014). Design and development of a Computerized Wicking Tester for longitudinal wicking in fibrous assemblies. *Journal of the Textile Institute* 105 (8): 850–859.

32 Kumar, B., Das, A., and Alagirusamy, R. (2012). Analysis of sub-bandage pressure of compression bandages during exercise. *Journal of Tissue Viability* 21 (4): 115–124.

33 Kumar, B., Das, A., and Alagirusamy, R. (2012). Analysis of factors governing dynamic stiffness index of medical compression bandages. *Biorheology* 49 (5-6): 375–384.

34 Kumar, B., Das, A., and Alagirusamy, R. (2013). Study on interface pressure generated by a bandage using in vitro pressure measurement system. *Journal of the Textile Institute* 104 (12): 1374–1383.

35 Kumar, B., Das, A., and Alagirusamy, R. (2013). *Science of Compression Bandages*. Woodhead Publishing India Pvt. Ltd. ISBN: 9781782422686.

36 Senthilkumar, M., Anbumani, N., and Hayavadana, J. (2011). *Elastane Fabrics–A Tool for Stretch Applications in Sports*. India: NISCAIR-CSIR.

37 Schafer, E. and Jung, H. (1984). Wide bandage fabric. Google Patents.

38 Hampton, R. and Hanes, P.F. Jr., (1980). Woven elastic compression bandage. Google Patents.

39 Miller, N.D. (1998). Woven or knitted elastic bandages having controlled compressive forces. Google Patents.

40 Gonon, P. (2014). Elastic bandage for bandaging and methods for manufacturing such a bandage. Google Patents.

41 Damm, J., Lundh, T., Partsch, H., and Mosti, G. (2017). An innovative compression system providing low, sustained resting pressure and high, efficient working pressure. *Veins and Lymphatics* 6 (1): 10–11.

42 Lee, G., Rajendran, S., and Anand, S. (2009). New single-layer compression bandage system for chronic venous leg ulcers. *British Journal of Nursing* 18 (15): S4–S18.

43 Seitz, P. (2013). Textile pressure sensor. Google Patents.

44 Leng, J., Lan, X., Liu, Y., and Du, S. (2011). Shape-memory polymers and their composites: stimulus methods and applications. *Progress in Materials Science* 56 (7): 1077–1135.

45 Xie, T. (2010). Tunable polymer multi-shape memory effect. *Nature* 464 (7286): 267–270.
46 Mather, P.T., Luo, X., and Rousseau, I.A. (2009). Shape memory polymer research. *Annual Review of Materials Research* 39: 445–471.
47 Hu, J., Zhu, Y., Huang, H., and Lu, J. (2012). Recent advances in shape-memory polymers: structure, mechanism, functionality, modeling and applications. *Progress in Polymer Science* 37 (12): 1720–1763.
48 Zhao, Q., Qi, H.J., and Xie, T. (2015). Recent progress in shape memory polymer: new behavior, enabling materials, and mechanistic understanding. *Progress in Polymer Science* 49–50: 79–120.
49 Hu, J.L., Kumar, B., and Narayan, H.K. (2015). Stress memory polymers. *Journal of Polymer Science Part B: Polymer Physics* 53 (13): 893–898.
50 Kumar, B., Hu, J.L., and Pan, N. (2016). Smart medical stocking using memory polymer for chronic venous disorders. *Biomaterials* 75: 174–181.
51 Kumar, B., Hu, J., Pan, N., and Narayana, H. (2016). A smart orthopedic compression device based on a polymeric stress memory actuator. *Materials and Design* 97: 222–229.
52 Kumar, B., Hu, J., and Pan, N. (2016). Memory bandage for functional compression management for venous ulcers. *Fibers* 4 (1): 1–10.
53 Narayana, H., Hu, J., Kumar, B., and Shang, S. (2016). Constituent analysis of stress memory in semicrystalline polyurethane. *Journal of Polymer Science Part B: Polymer Physics* https://doi.org/10.1002/polb.24000.

28

Electrospun Nanofibers for Environmental Protection: Water Purification

Hongyang Ma[1,2], Christian Burger[2], Benjamin Chu[2], and Benjamin S. Hsiao[2]

[1] *Beijing University of Chemical Technology, State Key Laboratory of Organic-Inorganic Composites, College of Materials Science and Engineering, 15 North Third Ring Road, Beijing 100029, China*
[2] *Stony Brook University, Department of Chemistry, 100 Nicolls Road, Stony Brook, NY 11794-3400, USA*

28.1 Introduction

The water crisis in the twenty-first century not only brings pressing challenges to humanity but also creates tremendous opportunities for the membrane community to tackle these challenges. Great efforts have already been made for research and development of membranes with new structures and properties using new nanomaterials for water purification [1–3]. In this endeavor, nanofibrous composite membranes are a novel class of new membrane, consisting of multiple fibrous layers with different fiber diameters, serving as support layer, barrier layer, or additive to the barrier layer [4–7]. The unique features of these membranes include high porosity and functionalizability, which can lead to high permeability, high rejection, low fouling, low energy consumption, and low environmental impact for water purification applications.

Nanofibers with diameters in the nanoscale range can be fabricated from a variety of natural or synthetic, inorganic, organic, or polymeric materials by using a variety of technologies, including template synthesis, self-assembly, electrospinning, and chemical/mechanical separation [8–12]. Although many nanofiber systems produced by different methods have been demonstrated, only a few are really practical to use in water purification when considering factors of safety, stability, and cost. Among these fabrication technologies, electrospinning is one of the scalable methods that can produce useful membranes and meet the considerations [13–15].

The principle of electrospinning is simple but the description of the process is complex. Electrospinning is based on the interplay between the surface tension of a polymer solution and an external electrostatic field that pulls this solution [16–20]. A droplet of polymer solution can be formed at the tip of a spinneret because of the surface tension. But when this droplet is charged and placed in an external electrical field, the electrospinning process can take place. In specific, with increasing applied voltage, the surface tension of polymer solution can be overcome by the electrical force. At that point, the tip of the droplet will

Handbook of Fibrous Materials, First Edition. Edited by Jinlian Hu, Bipin Kumar, and Jing Lu.
© 2020 Wiley-VCH Verlag GmbH & Co. KGaA. Published 2020 by Wiley-VCH Verlag GmbH & Co. KGaA.

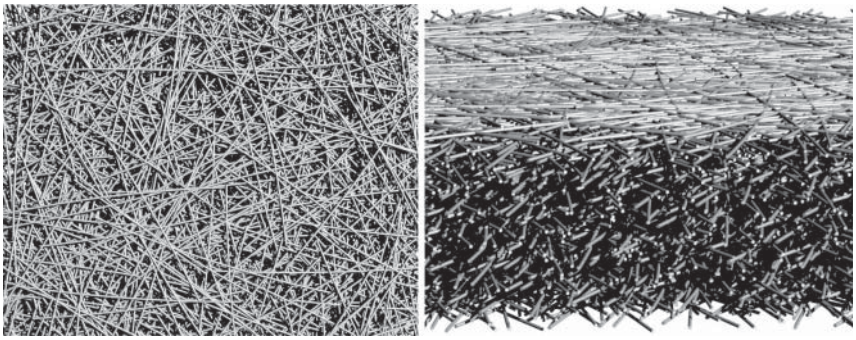


Figure 28.1 Simulations of electrospun nanofibrous composite membrane with top view (a) and cross-sectional view (b). Source: Adapted from Ma et al. 2013 [21]. Reproduced with permission from Bentham Science Publishers.

deform into a Taylor cone and eject a fine jet of polymer solution. While the jet stream is traveling between the spinneret and the collector, the solvent evaporates and the traveling jet becomes unstable due to the combined effects of increasing viscoelasticity and enhanced charge repulsion as a result of increasing polymer concentration. This process leads to significant stretching of the jet with final velocity near a fraction of sound speed and results in a fine fiber with diameters of submicrons on the surface of the collector. As the nanofiber is created without guided direction, the resulting scaffold has a nonwoven structure with high porosity (Figure 28.1) [21].

The fabrication and morphology of electrospun nanofiber scaffold can be affected by several parameters of the polymer solutions, such as concentration, viscosity, conductivity, polymer nature, and solvent, as well as by processing parameters, such as applied voltage, flow rate, jet traveling distance, temperature, and humidity. The morphology and properties of electrospun scaffolds such as fiber uniformity, fiber diameter, pore size, pore size distribution, porosity, and mechanical strength can be controlled by adjusting these parameters [13]. With increasing interests in commercialization of the electrospinning process [22], more and more researchers have engaged in research and development of scalable methods, resulting in flourishing activities not only in fabrication but also in application. The primary attractive feature of electrospun nanofiber scaffolds is the high surface-to-volume ratio and high porosity as a result of the very small fiber diameters (submicron to nanometer). Combined with their functionality, electrospun fibrous scaffolds can be used in a broad range of applications, including tissue engineering [23, 24], drug delivery [24–26], air and water purification [2, 27–29], gas storage [30], sensors, and electrodes [31–34]. A few comprehensive reviews and book chapters regarding these applications have already been published [35].

In this chapter, we will focus on the application of electrospun nanofiber scaffolds for water purification, where these nanofiber scaffolds can function either as a barrier layer or as a supporting layer in the assembly of composite fibrous membranes having unique properties such as high porosity, high surface area,

and interconnected water channels created by the fibrous network. The hierarchical structure of these nanofibrous composite membranes are highly permeable; thus it will provide high flux, high rejection, and low fouling properties, which is essential to meet the increasing performance demand of the water industry today [2, 6, 7].

28.2 Characters of Electrospun Nanofiber Scaffold

The filtration performance of nanofibrous composite membranes, including flux, rejection, and serviceable life span are highly affected by the electrospun nanofiber component, either as a barrier or as a support [7, 36]. Therefore, the understanding of the nanofiber scaffold properties will be essential for the design and fabrication of nanofibrous composite membranes with high filtration efficiency.

28.2.1 Porosity

The permeation flux of a membrane intimately depends on the porosity of the scaffold, if used as a barrier layer [37–39]. In general, the higher the porosity, the higher the permeation flux. Depending on the fabricate technique, its pore distribution can be inhomogeneous, resulting in a surface porosity that differs from the bulk porosity with both of them having an effect on the permeation flux. The surface porosity can be estimated based on scanning electron microscopy (SEM) measurements and software analysis, while the bulky porosity, defined as the volume ratio of cavity to mat, can usually be estimated by the following equation [40]:

$$\varepsilon = 1 - \frac{V_b}{V_f} = 1 - \frac{m_f}{A_f \times z_f \times \rho_b} \tag{28.1}$$

where ε is the bulky porosity and V_b, V_f, and ρ_b are the bulk volume, fiber mat volume, and bulk density, respectively. By measuring the mass (m_f), area (A_f), and thickness (z_f) of the fiber mat, the porosity of the electrospun nanofiber scaffold can be estimated. It is worthwhile to note that the thickness of a fibrous mat can simply be measured with a micrometer [41], but the compaction of the membrane under pressure during filtration can create significant deviation. For this purpose, a solvent gravimetric method has been reported that can improve the accuracy of the measurement [42].

The typical membrane produced by the phase inversion method usually has an anisotropic pore structure [43]. As a result, the surface porosity and the bulk porosity are quite different in the membrane produced by phase inversion, with the surface porosity being lower. The surface porosity controlled by the solvent extraction route is typically 10–30 vol%, while the bulk porosity is 50–80 vol% [44–46]. It should be noted that some commercially available membranes made by this method using cellulose nitrate/ester can also have a relatively similar porosity (60–80 vol%) on the surface as well as in bulk [47]. Electrospun nanofiber scaffold, however, always display a similar porosity for both surface and bulk, which is often above 80 vol% and could be up to 95 vol% [48, 49].

The porosity of the barrier layer directly affects the permeation flux of the filtration membrane. Empirically, the permeation flux is proportional to the porosity of the media in a linear manner [50]. For a filtration media with tubular pores, the relationship between the flux and porosity can be expressed by the Hagen–Poiseuille equation [49, 51]:

$$J = \frac{r_p^2 \Delta P \varepsilon}{8\mu z} \tag{28.2}$$

where J is the permeation flux (m/s), r_p represents the effective pore radius (m), $\Delta P/z$ is the differential pressure per unit thickness (Pa/m), μ is the solution viscosity (Pa s), and ε is the porosity of the filtration media, respectively.

It is clear that the flux increases with increasing porosity when the pore geometry is kept constant. For an electrospun nanofiber scaffold with tortuous and interconnected pores, the tortuosity (τ) needs to be considered. The correlation of tortuosity and porosity (ε) is empirically suggested by Eq. (28.3) [52]:

$$\tau = \frac{(2-\varepsilon)^2}{\varepsilon} \tag{28.3}$$

Thus, the relationship between the flux and porosity becomes more complex when the tortuosity is considered. Nevertheless, Eq. (28.2) provides a simple correlation of the permeation flux and porosity, which implies that an electrospun nanofiber scaffold with its high porosity of 80–95 vol% will consistently provide a high permeation flux [44, 53, 54]. This property can be visually understood by a simulation. Figure 28.2 represents the morphology of nonwoven nanofiber scaffolds with different porosities. All fiber diameters remain the same, the fibers are

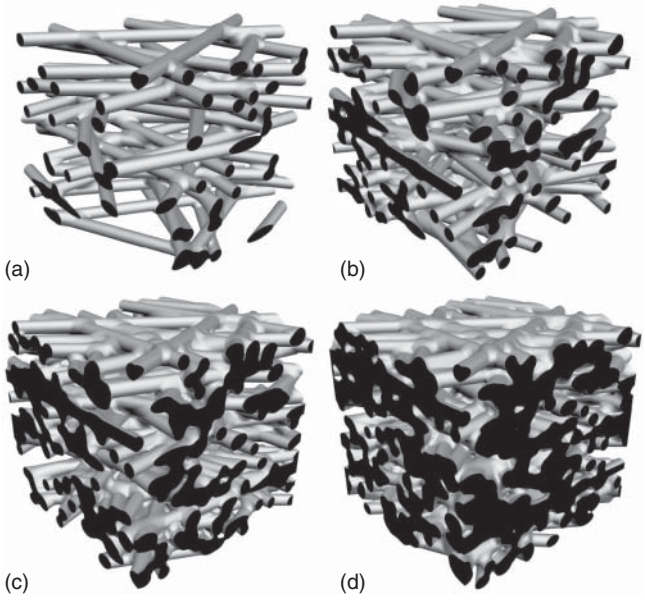


Figure 28.2 Representative electrospun nanofiber scaffolds with porosity of (a) 80 vol%, (b) 60 vol%, (c) 40 vol%, and (d) 20 vol%, respectively.

randomly deposited together, and fiber-crossing points can be "soldered" to form pseudo-nanotrusses [36]. The pore space-to-material volume ratio varied from 4 : 1 to 1 : 4.

It is evident that high porosity can reduce hydraulic resistance and increase the volume of the water paths and therefore can contribute a high permeation flux to the membrane.

28.2.2 Pore Size

The pore size and pore size distribution of a nanofibrous scaffold can also affect the permeation flux and rejection capability [44, 55]. Larger pore sizes will increase the flux but lower the rejection, when the porosity is kept constant. From Eq. (28.2), it is clear that the permeation flux (J) is proportional to the square of the effective pore radius (r_p), as shown in Eq. (28.4):

$$J \sim r_p^2 \tag{28.4}$$

For a nonwoven electrospun nanofiber scaffold, when the fibers were deposited and collected randomly and the porosity of the fibrous mat was kept constant at 80 vol%, the pore geometry and size distribution can be correlated with the fiber diameter. This relationship is illustrated in Figure 28.3 [7].

Empirically, the maximum and average pore size was found to scale linearly with the fiber diameter at the optimal flux performance [56]. The mean pore size (d_{avp}) was found to be about 3 ± 1 times the average fiber diameter (d_{avf}), and the maximum pore size (d_{mxp}) was about 10 ± 2 times the mean fiber diameter, as shown in Eqs. (28.5) and (28.6):

$$d_{\text{avp}} = (3 \pm 1) d_{\text{avf}} \tag{28.5}$$

$$d_{\text{mxp}} = (10 \pm 2) d_{\text{avf}} \tag{28.6}$$

Thus, the pore sizes can be adjusted by controlling the fiber diameter of the electrospun membrane, allowing them to satisfy the requirements for different applications [56, 57]. It is clear that the large pore size decreases the hydraulic resistance in a filtration process and therefore increases the permeation flux, but this may reduce the rejection capability (or selectivity).

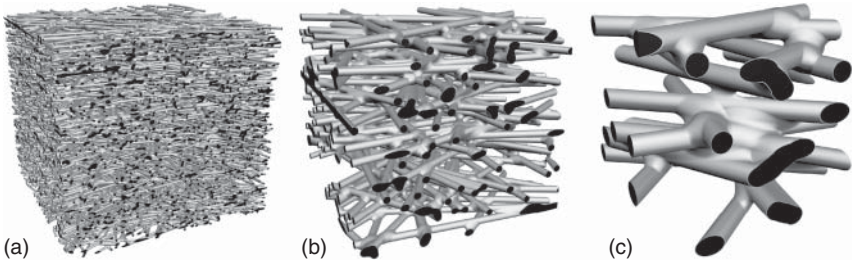


Figure 28.3 Illustration of the correlations between pore size and fiber diameter at a constant porosity of 80 vol% in a fixed volume. The relative fiber diameter ratio of panels (a), (b), and (c) is 1 : 3 : 10. Source: Ma et al. 2011 [7]. Reproduced with permission of Royal Society of Chemistry.

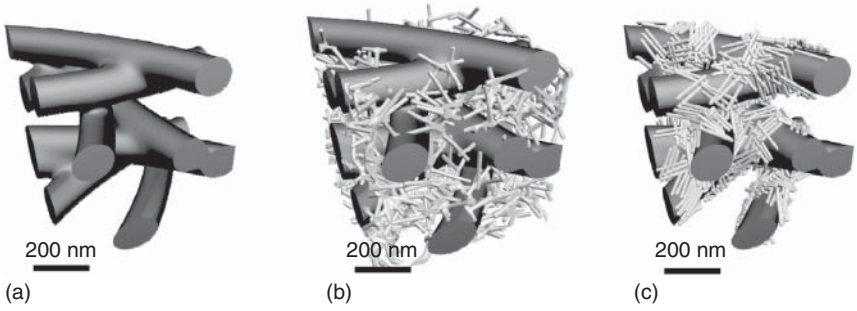


Figure 28.4 Schematic representations of electrospun nanofiber scaffolds: (a) scaffold before nanowhisker infusion, (b) infused nanowhiskers forming loose cross-linked mesh, and (c) nanowhiskers collapsed onto the scaffold, forming bundles. Source: Ma et al. 2012 [60]. Reproduced with permission of American Chemical Society.

The pore size uniformity in the barrier layer can greatly affect the selectivity of the membranes for separation [58, 59]. In general, the narrower pore size distribution (more uniform pore sizes) will lead to higher rejection and better selectivity [39, 60]. Membranes with narrow pore size distribution often need to be fabricated by special methods, such as templating [61, 62], self-assembly [63], track etching [64], and microfabrication [65]. The membranes prepared by these methods can have high permeation flux and rejection capability but often suffer from fouling [66] and cost issues. Nonwoven nanofiber scaffolds prepared by electrospinning typically have a relatively broad pore size distribution in 1–2 orders of magnitude range [40]. It is worthy to mention that the impregnation of ultrafine nanofibers (e.g. cellulose nanowhiskers or cellulose nanofibers [CNs]) into the electrospun nanofiber scaffolds can decrease the pore size and narrow down the pore size distribution, as shown in Figure 28.4 [60].

The above behavior is probably due to the "leveling effect." That is, the ultrafine nanofibers can penetrate into the large pores in the electrospun scaffold and subdivide them into smaller pores while leaving the small pores empty. It should be noted that for a membrane produced by the phase inversion method, the pores mentioned above are referring to the surface pores, while bulk pores located in the interior of the membrane affect the rejection to a lesser degree [67].

28.2.3 Surface Area

In a fibrous scaffold, the specific surface area is inversely proportional to the radius of the fiber. Therefore, the thinner the fiber diameter (d_f, m), the higher the specific surface area (S, m^2/g), where the two have the following relationship [68]:

$$S = \frac{4}{d_f \times 10^6} \tag{28.7}$$

Based on this equation, the diameter of electrospun nanofiber is in submicrons, so the specific surface area is typically 10–40 m^2/g [69]. The high surface area of nanofibrous composite membranes offers high retention of contaminant through adsorption (or depth filtration). A high adsorption capacity can be achieved

when a large number of functional adsorption sites located on the surface of the scaffold are reachable by the targeted contaminants [70, 71]. Common fibrous scaffolds [72], such as polyester nonwoven substrate, glass fiber, or cellulose paper, have larger fiber diameters of a few microns to a few tens of microns. Based on Eq. (28.7), their surface area will be 10–100 times lower than that of an electrospun nanofiber scaffold of the same mass, i.e. 10–100 times lower retention capability in an adsorption process. Thus, reducing the diameter of the electrospun nanofiber scaffold can efficiently increase the adsorption capacity in water purification [73]. However, the reduction of the fiber diameter can also lead to a decrease in pore size and increase the pressure drop across the membrane. This situation becomes more critical when the targeted contaminants are adsorbed on the surface of the fiber, thereby further decreasing both porosity and average pore size, reducing the permeation flux, and increasing the pressure drop [74].

The increase in surface roughness of the electrospun nanofiber can also enhance the surface area [75–77]. There are numerous strategies, mostly using the phase separation behavior during the formation of nanofiber in electrospinning, to create a rough surface (Figure 28.5). These strategies including the incorporation of nanoparticles (e.g. polyhedral oligomeric silsesquioxane (POSS), silica/titanium dioxide particles) into the spinning solution [78, 79], spinning of a bicomponents system followed by leaching out one component [80], or using a special volatile solvent to induce porous nanofibers [81]. In addition, some posttreatment approaches, such as post-coating [82] or etching [83] of electrospun nanofiber scaffolds, have also been demonstrated to create a rough fiber surface to increase the surface area.

28.2.4 Pore Geometry

The pore geometry in the barrier layer of a membrane can have an either interconnected (e.g. tubular or tortuous paths with interconnectivity) or dead-end nature (e.g. closed voids) [47, 84–86]. In general, tubular or tortuous interconnected pores, regarded as fluid paths, are beneficial to achieve a high permeation flux. This is because the interconnected pores can reduce the hydraulic resistance when the fluid is traveling in the membrane [87]. In addition, the interconnected pores can reduce the fouling problem of the membrane in the filtration process [85]. However, the typical tubular and gyroidal pores, as shown in Figure 28.6a,b, are difficult to achieve with conventional methods, where a special fabrication process is necessary [39].

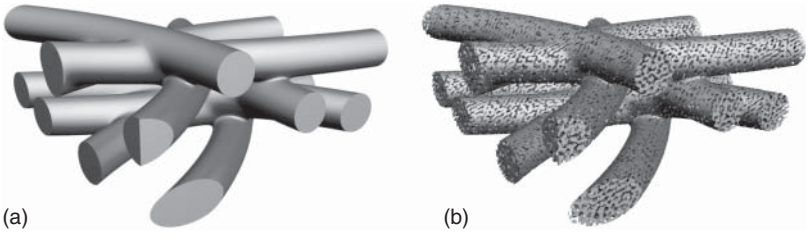


Figure 28.5 Illustration of the nonwoven electrospun nanofibers (a) and porous nanofibers (b).

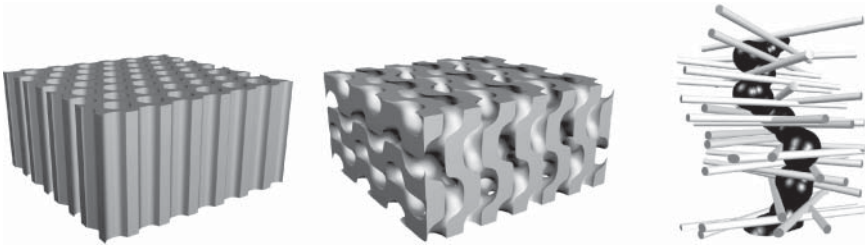


Figure 28.6 Schematic representative of (a) straight tubular pores, (b) tortuous gyroidal pores, and (c) tortuous interconnected pores in an electrospun nanofiber scaffold, where water can go through the water path easily.

It is interesting to note that the pores in an electrospun scaffold are interconnected and spontaneously created in the spinning process, as shown in Figure 28.6c. This indicates that the nature of the electrospun nanofiber scaffolds will lead to higher flux and lower fouling performance than conventional membranes. These advantages have been verified experimentally. The tortuosity in the electrospun nanofiber scaffold has been proven to be relatively low when compared with those of the conventional membranes containing some dead-end cavities [49, 89]. As a result, membranes containing electrospun nanofibers as the barrier layer always have a higher permeation flux than membranes made by the phase inversion method.

Furthermore, the interconnected pores in electrospun nanofiber scaffolds that can reduce the fouling tendency have also been seen experimentally [47]. Although the fouling problem of the membrane is closely related to the chemical and physical interactions between the membrane and the feed solution, the pore geometry, especially the interconnections among the pores, also plays an important role to affect the membrane fouling property. There are two fouling mechanisms that can be reduced by using an electrospun nanofibrous composite membrane. One is the internal concentration polarization, for example, in the forward osmosis (FO) process. The concern of internal concentration polarization may be reduced significantly due to the rapid equilibrium of the permeate water and draw solution in the interconnected pores of the electrospun scaffold as a result of the higher water flux [90]. Another fouling improvement is due to the following consideration. When the foulants in the feed solution enter the membrane and adhere to the surface of the pores, the irreversible fouling occurs. As a result, the pore size will decrease as the pores are blocked [88]. If the pores are of the dead-end type, as in conventional membranes, the tendency of blocking the pores by the foulants is high. In contrast, electrospun nanofiber scaffolds contain interconnected pores, which are more difficult to block completely and are relatively easier to be cleaned by flushing or back-flushing than conventional membranes [91]. Therefore, the usable lifetime of the membrane based on electrospun nanofiber scaffolds could be longer, and a higher recovery of the flux could be achieved.

28.2.5 Mechanical Properties

The mechanical properties of electrospun nanofiber scaffolds in filtration are mainly associated with the capability to resist compression or deformation [92, 93]. The compaction of the membrane is inevitable in a pressure-driving filtration process, which can significantly reduce the permeation flux [94–96]. The irreversible deformation of the pores in the barrier layer can also lead to notable reduction of permeation flux as a result of the decrease in porosity, pore size, and pore geometry change. Therefore, a membrane with a good compaction resistance will exhibit high durability, which means that the permeation flux can be retained at the high initial level. Membranes produced by the phase inversion method usually have good mechanical properties as some cavities are disconnected and the solid portion forms a strong support. However, after a long-term operation under pressure, the structure of the phase inversion membrane can also change and be stabilized at a certain status [97]. For electrospun nanofiber scaffolds with very high porosity (e.g. 80–95%), adhesion between the nanofibers will be relatively weak [49]. Thus, an electrospun nanofiber scaffold can easily be compacted when compared with a phase inversion membrane. The effective porosity of the electrospun nanofiber scaffold does not depend on the initial porosity of the membrane, but is a function of the applied pressure [50, 98]. Figure 28.7 shows the compaction effect on a nonwoven nanofiber scaffold, where the porosity is changed from 80 to 5 vol%, respectively. It is seen that as the scaffold becomes denser, pore size, pore size distribution, and pore geometry all change correspondingly. In most cases, the deformation of the nanofiber scaffold is irreversible, whereas the permeation flux could only be partially recovered after the pressure release. This implies that the electrospun nanofiber scaffold is more suitable for low-pressure filtration, where a high energy-saving benefit can be obtained. However, if the electrospun nanofiber layer does not account for the major volume component in the filtration membrane, as to be described in the design of thin-film nanofibrous composite (TFNC) membranes, the system can stand high-pressure operations and still yield significant energy-saving benefits.

By adjusting the electrospinning parameters, such as a special solvent, suitable humidity and temperature, or post-heating treatment, the adhesion between the nanofibers could be significantly improved [99, 100]. For example, when polyethersulfone (PES) electrospun nanofiber scaffolds are fabricated from a mixed solvent of *N*,*N*-dimethylformamide (DMF)/*N*-methylpyrrolidone (NMP)

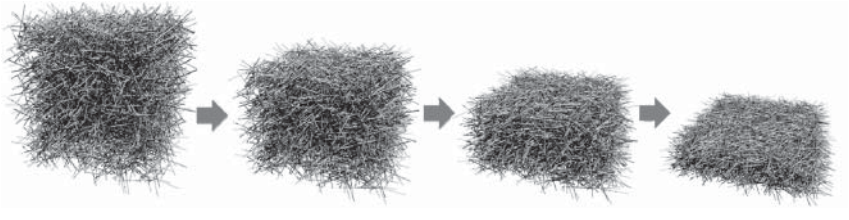


Figure 28.7 Compaction effect of electrospun nanofiber scaffold from 80 to 55 vol% and 30 to 5 vol%.

at different ratios, the mechanical properties can be greatly enhanced [101]. With increasing NMP content (from 0 to 50 wt%) at the fixed PES concentration of 26 wt%, the diameter of electrospun nanofibers was found to increase from 550 to 760 nm, while the corresponding modulus and ultimate tensile strength were found to improve by 570% and 360%, respectively. The increase in mechanical properties was not just due to the increased fiber diameter, but was mostly due to the enhanced junction points between the interconnected nanofibers by partial fusion as a result of the residual solvent in nanofibers. Similarly, chemical cross-linking at the crossover points between the nanofibers is an efficient method to improve the mechanical properties [74]. It is interesting to note that cross-linked polyvinyl alcohol (PVA) nanofiber scaffolds using glutaraldehyde (GA) exhibited a consistent flow rate without the sign of compaction. This is because the cross-linking reaction resulted in the formation of a rigid fibrous network structure, where the crossover points between the fibers were "soldered" together [36, 57]. The concept of cross-linking the nanofiber scaffold to overcome the compaction problem has led us to design the TFNC membranes, which will later be further elaborated on. In this new membrane design, a coating of dense barrier layer (e.g. cellulose nanofibers) is applied on the surface of electrospun nanofibrous composite membrane (e.g. polyacrylonitrile [PAN]), where the barrier matrix can induce a nanocomposite layer below the barrier layer. The nanocomposite layer containing electrospun nanofiber scaffold and the matrix component of barrier layer significantly increased the Young modulus of the final composite membrane, where no yielding point could be observed during the tensile stretching process [60]. Similarly, bi-vinyl and tri-vinyl monomers were polymerized on the surface of the PAN electrospun nanofibers, which significantly improved the mechanical properties of the membranes due to the formation of a nanocomposite structure. The resulting membranes showed an excellent ultrafiltration (UF) performance that could simultaneously remove bacteria and viruses from contaminated water but still retain their high permeation flux [74, 92].

28.2.6 Materials

The electrospun nanofibers can be fabricated from a variety of natural or synthetic, inorganic, organic, or polymeric materials. Typically, polymer materials such as PAN, PVA, polysulfone (PSU), PES, and polyvinylidene fluoride (PVDF) are employed to fabricate electrospun nanofibers for water purification [2, 13]. Common solvents used to dissolve abovementioned polymers in electrospinning are DMF, dimethyl sulfone (DMSO), and NMP, which has a relative high boiling point. It is clearly that the surface properties of the electrospun nanofibers depend on the chosen materials, where PVDF, PSU, PES, and polystyrene (PS) nanofibrous membranes exhibit hydrophobic property, while PVA and PAN membranes possess relative hydrophilic property. The filtration performance of electrospun nanofibers, functioning either as a barrier layer or as a substrate, is intimately dependent on the material properties, aside from the structural characteristics.

28.3 Applications of Electrospun Nanofibrous Composite Membranes

Highly permeable nanofibrous composite membranes with multilayered hierarchical structures, where an electrospun nanofiber scaffold acts as a barrier layer and/or a support, can be obtained [2, 6, 7, 38]. This new membrane structure offers high permeation flux and high rejection rate. One-, two-, three-, and even four-layered structures can be constructed, depending on the demands of rejection vs. mechanical stability of the membranes. Some examples of these membranes are as follows.

28.3.1 As a Barrier Layer

Typically, microfiltration membranes have a pore size in the range of 0.1–10 μm, which is ideal to remove micron- or submicron-size contaminants, such as waterborne bacteria, for drinking water application. The purification process is through size exclusion separation. However, if smaller charged contaminants such as dyes, viruses, proteins, and heavy metal ions are involved, the size exclusion mechanism will not work. To remove these contaminants, the adsorption process has to be utilized [102–105]. For this purpose, electrospun nanofiber scaffolds, having pore sizes in the range of 0.1–10 μm, are good candidates for a barrier layer for both filtration and adsorption purposes. This indicates that we can design a microfiltration membrane that also behaves as a good adsorbent medium.

28.3.1.1 Size Exclusion

Waterborne bacteria typically have diameters above 0.2 μm. For example, the dimension of *Escherichia coli* is 0.5 × 2.0 μm and that of *Brevundimonas diminuta* is 0.3 × 0.9 μm [7, 106, 107]. Therefore, a membrane designed with a mean pore size of 0.2 μm can be expected to successfully remove waterborne bacteria from contaminated water (Figure 28.8) [2].

For microfiltration, the electrospun nanofibrous composite membrane can have either one layer (i.e. self-standing nanofiber scaffold) [49] or a two-layered structure involving an electrospun nanofiber scaffold and a nonwoven substrate (e.g. polyethylene terephthalate [PET] nonwoven) [2]. The nanofiber scaffold is

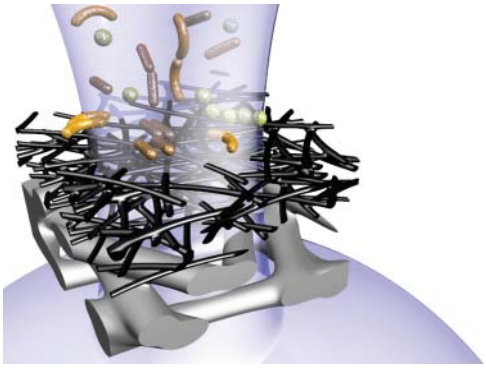


Figure 28.8 Microfiltration membrane for removal of bacteria from contaminated water. Source: Ma et al. 2012 [2]. Reproduced with permission of Springer.

used as the barrier or selective barrier, where the nonwoven substrate functions as the mechanical support. In the case of self-standing electrospun nanofibrous microfiltration membranes, both PVDF and PSU have been demonstrated to remove micron-size particles from water [91, 98]. In specific, the electrospun nanofibrous membranes having mean fiber diameters ranging from 380 to 470 nm exhibited a fairly high flux (>100 l/(m^2 h)/psi) and good rejection (>91%) of 1.0 μm particles. However, these membranes failed to retain 0.5 and 0.1 μm particles through size exclusion (the rejection ratio was only 47% and 14%, respectively). However, when the mean fiber diameter was reduced to about 100 nm, the two-layered electrospun PAN nanofibrous composite membranes and cross-linked PVA nanofibrous composite membranes (both use a PET nonwoven substrate) could retain 0.2 μm particles with a very high rejection (>93%). When challenged with 10^6 colony-forming unit (cfu)/ml of *E. coli* aqueous suspension, these membranes showed an impressive rejection ratio of 99.9999%. The typical SEM cross-sectional images of electrospun nanofibrous composite membranes after filtration of 0.2 μm particles and *E. coli* are shown in Figure 28.9, respectively [57, 58]. The unique characteristics of these membranes were that they exhibited two to three times higher flux than that of commercially available microfiltration membranes (e.g. GS9035).

Alternatively, the electrospun PAN nanofiber scaffold can be modified with nano-absorbents, such as cellulose nanofibers (fibers with 5 nm diameter [108, 109]) that can be derived from natural cellulose resources, forming a nanoweb within the electrospun nanofiber scaffold. The nanoweb structure not only improved the mechanical properties of electrospun nanofiber scaffolds but also minimized the pore size and narrowed the pore size distribution [60, 110]. As a result, the rejection of 0.2 μm particles was larger than 98%, and the rejection of both of *E. coli* and *B. diminuta* were over 99.9999%. Figure 28.10 represents the structure of cellulose nanofibers infused into electrospun PAN nanofibrous composite membranes.

Similarly, the surface of PAN electrospun nanofibers could be modified with a polymer network formed by in situ polymerization of bi-vinyl and tri-vinyl monomers [92]. These membranes also exhibited 99.9999% rejection to *E. coli* while retaining a high permeation flux. The surface modification of an electrospun nanofiber scaffold could also introduce adsorption functionality into the

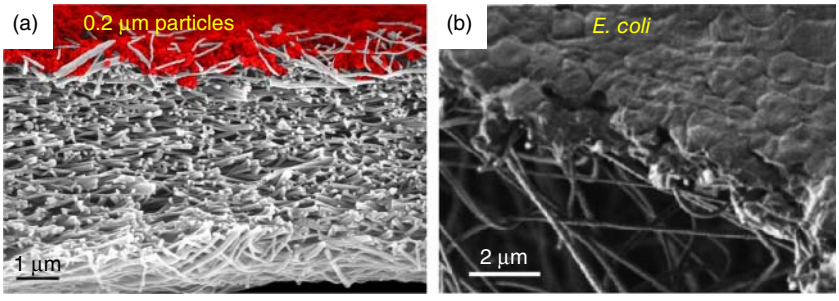


Figure 28.9 Electrospun nanofibrous composite membranes after filtration of 0.2 μm particles (a) and *E. coli* (b). Source: Adapted from Liu et al. 2013 [57] and Wang et al. 2012 [58].

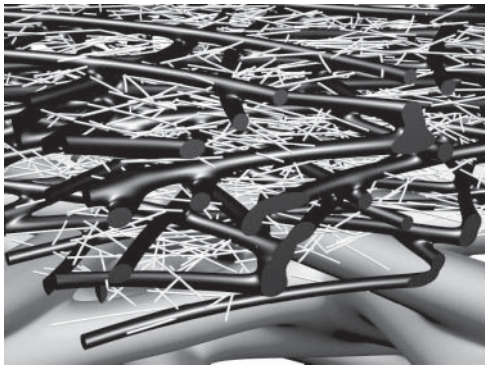


Figure 28.10 Depiction of a two-layered fibrous structure with a top electrospun nanofibrous layer infused with cellulose nanofibers [73].

membrane and remove charged species, such as viruses, dyes, proteins, and heavy metal ions [74]. This can be elaborated as follows.

28.3.1.2 Adsorption

The separation mechanism through adsorption, also known as depth filtration, is based on electrostatic interactions, hydrophobic interactions, or ligand coordination between the functional groups on the surface of nanofibers and the targeted contaminants [21, 111–113]. Therefore, the adsorption capacity mainly depends on the surface area of the membrane and the density of functional groups. It should be noted that the adsorption capacity is limited by the separation mechanism, where the theoretical maximum rejection (or retention) ratio depends on the amount of functional groups on the surface of the scaffold in depth filtration. There are trade-offs among the flux, retention, pressure drop, and thickness of the membrane associated with the membrane usage. Nonwoven fibrous membranes with large fiber diameters usually led to large pore sizes when the porosity was fixed [7]. These membranes could exhibit a high permeation flux and low pressure drop. In this scenario, the larger the fiber diameter, the higher the permeation flux. However, the retention of the contaminants is associated with the total amount of the functional groups, which depend on the surface-to-volume ratio of the scaffold. In this case, the membranes with smaller fiber diameters will provide a larger surface-to-volume ratio and, therefore, the higher retention capability. Obviously, the permeation flux decreases when the average pore size of the membrane defined by the fiber diameter becomes small, and the pressure drop will increase correspondingly. Moreover, during the actual filtration process, as the contaminants are adsorbed on the fiber surface, the pore sizes will be further decreased, therefore reducing the flux and increasing the pressure drop [74]. The service life span of the membrane is also related to the thickness of the membrane. The thicker the membrane, the higher the usage life. However, the increase of the membrane thickness will lead to a decline in permeation flux and an increase in pressure drop, which has to be taken into account. Furthermore, the surface chemistry of the fibrous membrane is another key factor in the adsorption process. Generally, the adsorption equilibrium should be achieved as fast as possible in order to capture the contaminant molecules under the given pressure or flow rate [21]. Based on electrostatic interactions, commercially available nonwoven

microfibrous mats, such as PET, polypropylene (PP), or glass fiber mats, have been used for the adsorption of Metanil Yellow (dye), *Klebsiella terrigena*, *E. coli*, *B. diminuta* (bacteria), and *MS2* (bacteriophage) after surface modification with amino-based chemicals [72, 114]. With the proper treatment, high flux and high adsorption capacity could be achieved. However, the surface area of these fibrous mats was limited due to the large fiber diameters (typically a few tens of microns). Nanofibrous composite membranes could be used to significantly increase the adsorption capacity since typical diameters of electrospun nanofibers are in the range of a 100 nm [73, 74]. In this case, an electrospun nanofibrous composite membrane with a properly functionalized surface could also be used as an adsorption medium [21].

Some example surface modification schemes of electrospun nanofiber scaffolds are as follows. A regenerated cellulose nanofibrous membrane has been prepared by hydrolysis of electrospun cellulose acetate (CA) nanofibers. After surface grafting with special ligands, the membranes could be used either for adsorption of proteins (e.g. bovine serum albumin [BSA]) or for filtration purification of antibody IgG [115, 116]. In another study, the electrospun PSU nanofibrous membrane covalently bonded with ligand could be used for BSA adsorption [117]. In yet another study, a facile method involving the surface wrapping of electrospun PAN nanofibers with a positively charged polymer through in situ polymerization of bi-vinyl monomers has been demonstrated [92]. This membrane system exhibited very high retention of BSA in static adsorption as well as dynamic adsorption separation (or depth filtration) with high permeation flux. This positively charged membrane can work as an effective microfiltration membrane but also simultaneously removed 99.99% of bacteriophage, *MS2*, a virus model.

The fiber diameter of an electrospun nanofibrous composite membrane is typically higher than 100 nm, whereas a further decrease in fiber diameter is usually limited by practical electrospinning conditions [118]. To further increase the active surface area, a novel hierarchical structure of a nanofibrous composite membrane has been demonstrated. In this system, the electrospun nanofiber scaffold is used as a network, where much smaller nanofibers (diameters in the range of a few nanometers) are infused into the gaps between the electrospun fibers. As a result, the pore size can be decreased, offering both high rejection of large contaminants due to size exclusion and high retention of small contaminants due to the increase in surface area for adsorption. For example, two strategies to form such a membrane structure have been demonstrated. One is through the infusion of cellulose nanofibers (having ~5 nm fiber diameter) into electrospun PAN mats having diameters in the range of 100–500 nm, forming a very fine nanoweb immersed in the electrospun nanofiber scaffold (Figure 28.11a–d) [60, 119].

This membrane system exhibits 16 times higher adsorption capacity against the positively charged crystal violet dye molecules than that of a commercially available membrane. Meanwhile, in dynamic adsorption of *MS2* (the virus model), the retention ratio could reach 99%, which is also better than that of the commercial system. This is because commercially available microfiltration membranes are

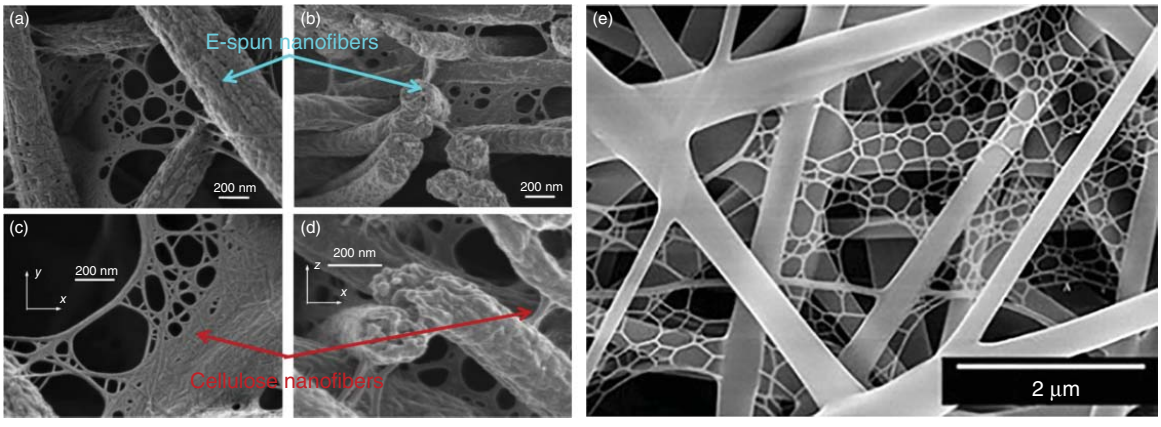


Figure 28.11 Top view (a, b) and cross-sectional view (c, d) of SEM image of the nanostructure of the electrospun PAN scaffold infused with cellulose nanofibers. Source: Ma et al. 2012 [60]. Reproduced with permission of American Chemical Society. (e) Electrospun nylon 6 nanofibers containing nanowebs. Source: Ding et al. 2006 [119]. Reproduced with permission of Elsevier.

often produced by the phase inversion method, where the resulting porous structure has a lower porosity (60–80%) [43]. For example, the commercially available porous membranes, made of nitrocellulose-based cellulose ester, has exhibited good adsorption and is commonly used for protein binding in the field of microbiology [120]. However, this membrane is not as good as the composite nanofibrous microfiltration membranes containing both electrospun PAN nanofiber scaffolds and infused webs of ultrathin cellulose nanofibers. The composite nanofibrous microfiltration membranes can be made by techniques, thus possessing different configurations. For example, they can be fabricated by the "electronetting" method. With this approach, both scaffolds containing electrospun nanofibers with a mean diameter of 100–500 nm and a web of finer nanofibers with a mean diameter of 10–40 nm could be simultaneously produced in a co-mingled manner. The average pore size of the nanoweb could be about 16 nm, as shown in Figure 28.11e [32, 119, 121]. The formation of nanowebs (or nanonets) has been attributed to the phase separation of charged droplets generated during electrospinning. Such a membrane system showed excellent retention to *E. coli* and viruses, such as *H1N1* (diameter: 80–120 nm) and *SARS* (diameter: ~100 nm) in air filtration, but they have not been tested in water filtration.

It should be noted that direct electrospinning of polymers with suitable functional groups, such as chitosan [122, 123] or PVA/polyethylenimine (PEI) polymer blend [124], could produce positively charged nanofiber scaffolds to adsorb negatively charged macromolecules or microorganisms such as viruses. These scaffolds do not require further surface functionalization. However, the mechanical strengths of these electrospun scaffolds are usually weak, which should be supported on a strong substrate. In this case, a post-cross-linking step is usually necessary in order to immobilize the functional nanofibrous scaffold in the composite membrane.

Recently, a composite nanofibrous membrane system containing carbon nanotubes (CNTs) has been demonstrated for bacteria/virus removal [125, 126]. In this system, single-walled or multiwalled CNTs were deposited onto a commercially available microfiltration membrane, where the resulting membranes could remove bacteria (e.g. *E. coli*) by screen filtration with very high retention ratio. In addition, these membranes could also remove viruses (e.g. *MS2*) by depth filtration (adsorption) with 99.9% retention ratio. Unfortunately, this membrane system exhibited a relatively short lifetime, high cost, and the need to be stored in the wet state to preserve permeation flux. However, even though one can overcome these hurdles, the intrinsic risk of using potentially toxic CNTs for drinking water applications may outweigh any benefits in performance improvement. We thus believe the electrospinning technique is a more versatile and safer technique to produce nanofibrous membranes for drinking water applications.

28.3.2 As a Support Layer

Electrospun nanofiber scaffolds deposited onto nonwoven microfibrous substrates have also been used as a mid-layer to support another denser barrier layer, thus forming high-performance membranes for varying filtration applications including ultrafiltration (UF), nanofiltration (NF), reverse osmosis (RO),

forward osmosis (FO), pervaporation, and membrane distillation (MD) [2]. In this section, we will review the structure and properties relations of these membranes containing electrospun nanofiber scaffolds as a support layer for selective applications (i.e. UF, NF/RO, and pervaporation).

28.3.2.1 Ultrafiltration

Ultrafiltration (UF) membranes with typical pore sizes between 2 and 100 nm are typically used for separation of proteins, emulsified oily droplets, macromolecules, and suspended solids (in that size range) with water [127]. Ultrafiltration is not fundamentally different from microfiltration, except that the sizes of the targeted contaminant particles are smaller. The major problems in ultrafiltration are the relatively low filtration efficiency and membrane fouling [128]. For example, conventional ultrafiltration membranes are typically prepared by the phase inversion method, resulting in a low surface porosity (10–30 vol%) that would severely limit the membrane permeation flux [129]. The low porosity, dead-end pore structure, compounding with the use of relatively hydrophobic materials, such as PSU, PES, PAN, and PVDF, can drastically increase the fouling tendency, even though the membranes usually exhibit excellent chemical and mechanical stability [130]. It turns out that the new structure in TFNC membrane (as shown in Figure 28.12) [93], containing the electrospun nanofiber scaffold as a mid-layer support, can overcome these challenges.

In TFNC membranes, the bottom layer is a nonwoven substrate (e.g. PET nonwoven) containing microfibers with a typical thickness of ~100 μm, providing mechanical stability for the system. The mid-layer is an electrospun nanofiber scaffold (thickness ~ 50 μm) with high porosity (above 80 vol%) and interconnected pores, which replaces the conventional porous support produced by the phase inversion method. The materials used in the electrospun nanofiber middle layer can be the same as conventional filter materials, such as PAN

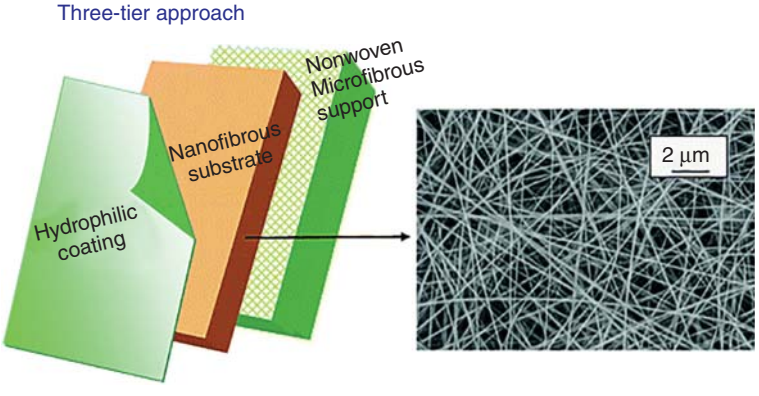


Figure 28.12 Schematic representation of a TFNC membrane with the three-tier structure: hydrophilic thin coating top layer, electrospun nanofiber scaffold mid-layer, and nonwoven microfibrous substrate bottom layer. Source: Wang et al. 2005 [93]. Reproduced with permission of American Chemical Society.

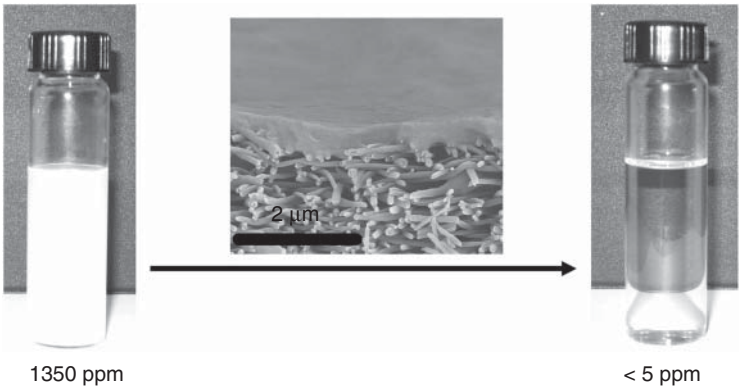


Figure 28.13 Purification of emulsified oil/water mixture with PVA-CN (1.25 wt%)-TFNC ultrafiltration membrane. Source: Yoon et al. 2009 [48]. Reproduced with permission of Elsevier.

[50, 131], PVA, or PVDF [132, 133]. The electrospun mid-layer can support a thin barrier layer (thickness of typically from 50 to 1000 nm). To reduce the fouling tendency, hydrophilic but water-resistant materials are usually considered, such as cross-linked PVA [48, 132], cross-linked PVA/cellulose nanofibers [134], cross-linked PEG/cellulose nanofibers [135], cross-linked polyamide [136], chitosan [50, 133], regenerated cellulose/chitin [137, 138], polysaccharide nanofibers [96, 131, 139], and even CNTs [93].

The performance of the three-layered TFNC membrane was found to be significantly better than conventional UF membranes. For example, in the system containing cross-linked PVA as the barrier layer supported by an electrospun PAN nanofiber scaffold, the permeation flux in separating emulsified oil droplets with diameter of 70–1000 nm and water (Figure 28.13) was 2–10 times higher than those of commercial membranes while being able to maintain a 99.0% rejection ratio [48, 124]. The system of emulsified oil droplets and water was used to simulate bilge water from ships or oily wastewater from oil fields.

Further improvement of the permeation flux could be achieved by incorporating nanofillers (e.g. cellulose nanofibers or CNTs) into the barrier layer of cross-linked PVA. This is because the naturally occurring interfacial gaps between the nanofibers and the polymer matrix in the barrier layer can serve as "water channels" to guide the water transport through the interconnected nanofiber scaffold, thus increasing the permeation flux [93, 134, 135]. Unfortunately, with GA cross-linked PVA as the membrane barrier layer, the coating process was ill-controlled due to the high viscosity, and the gel-like barrier has to be kept in the wet state before use. Alternately, bi-vinyl groups can be introduced into the PVA or PEG-based barrier layer, and the cross-linking reaction can be carried out by photoinitiation or heat initiation [135, 140]. In one study, chitosan without cross-linking was used as the barrier layer of a TFNC membrane [50]. The resulting membranes exhibited a good rejection ratio but relatively low permeation flux for the separation of oil emulsion and water, probably due to a relatively large barrier layer thickness. Cellulose and chitin regenerated from ionic liquids have also been used as the barrier layer

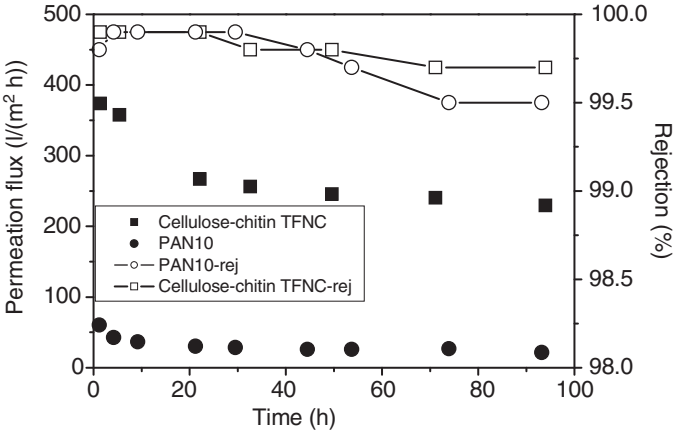


Figure 28.14 Cross-flow ultrafiltration of oil/water emulsion using TFNC membrane containing cellulose–chitin blend barrier layer and PAN10 membrane up to 100 hours. The applied pressure was 30 psi and temperature was 35 ± 2 °C. Source: Ma et al. 2010 [137]. Reproduced with permission of Elsevier.

to fabricate TFNC membranes. In this system, as the barrier thickness was optimized, 2–10 times higher flux was obtained in the TFNC membrane than the commercial counterparts while the membrane also maintained a good rejection ratio (>99.5%, seen in Figure 28.14) [137, 138].

The performance of the TFNC membranes has been reviewed recently [2]. For ultrafiltration applications, polysaccharide nanofibers were found to be very good candidates to fabricate the barrier layer, which led to good balance of filtration efficiency, i.e. high permeation flux, high rejection, and good antifouling tendency (due to the hydrophilicity) [131]. Furthermore, it is worthwhile to note that cellulose nanofiber-based TFNC membranes exhibited excellent chemical resistance, bacteria resistance, hypochlorite resistance, and applicability in a broad pH range [96]. The hierarchical structure of the cellulose nanofiber (CN) based TFNC membrane is illustrated in Figure 28.15, where a nonwoven microfibrous substrate (with fiber diameters in tens of microns) is used as the bottom support,

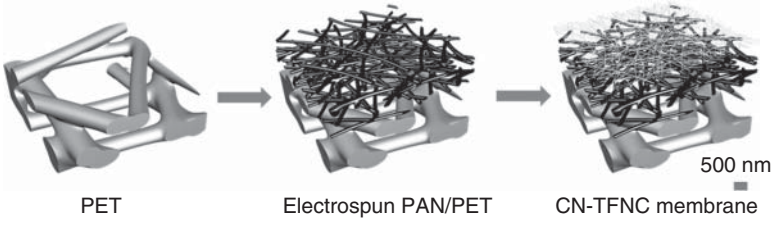


Figure 28.15 Schematic representation of the formation of a cellulose nanofiber (CN)-based TFNC membrane: nonwoven microfibrous substrate (with fiber diameters in the tens of micron size range) as the bottom support, electrospun nanofiber scaffold (with fiber diameters in the 100 nm to micron size range) as the mid-layer support, and cross-linked ultrafine cellulose nanofibers (with nominal fiber diameters in the five to tens of nanometer size range) as the top barrier layer.

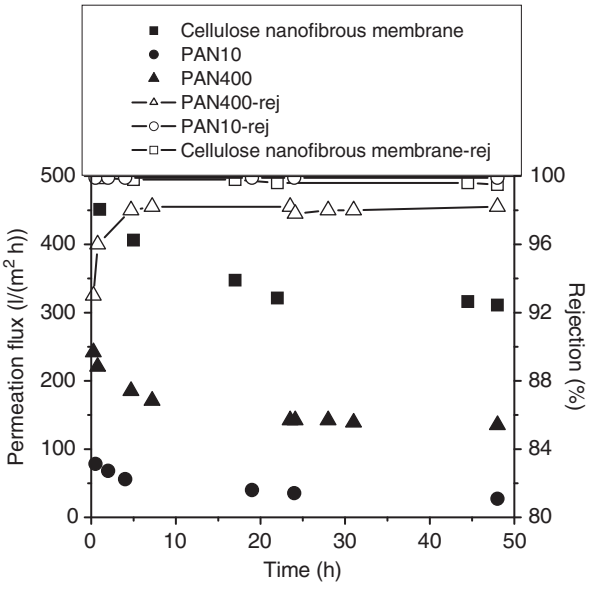


Figure 28.16 Permeation flux and rejection ratio of TFNC membrane containing cellulose nanofiber barrier layer as a function of time; measurement was carried out at a constant pressure of 30 psi and temperature of 37 °C in ultrafiltration of oil/water emulsions. The ultrafiltration performance of commercial PAN10 and PAN400 membranes was also included for comparison. Source: Ma et al. 2011 [131]. Reproduced with permission of American Chemical Society.

an electrospun nanofiber scaffold (with fiber diameters between 100 nm and few microns) as the mid-layer, and cross-linked ultrafine cellulose nanofibers (with fiber diameters between five and tens of nanometers) as the barrier layer.

The CN-TFNC membranes showed 3–11 times higher permeation flux compared with commercial ultrafiltration membranes, such as PAN10 and PAN400 (Sepro), and a rejection ratio higher than 99.5% (Figure 28.16), where the oil concentration in the permeate could exceed the environmental standard for wastewater disposal (i.e. less than 10 ppm) [131]. The high permeation flux could be attributed to the thinness and hydrophilicity of the CN barrier layer, leading to the reduction of hydraulic resistance and oil fouling tendency, but it was also due to the high porosity and interconnected pores in the electrospun nanofiber support.

In TFNC membranes, there is some integration between the barrier layer and the electrospun nanofibrous support, that is, the top part of the electrospun scaffold is partially impregnated in the nanofiber barrier layer [131, 137]. As evidence, the contour of electrospun nanofibers could be seen from the top view of the TFNC membrane (Figure 28.17). Such integration could increase the mechanical stability of the barrier layer and decrease the thickness of the barrier layer. The last effect would further increase the permeation flux [38]. In addition, the nanofiber scaffold embedded in the barrier layer can also serve as a way to introduce "water channels" to guide water transportation in the barrier layer, which is

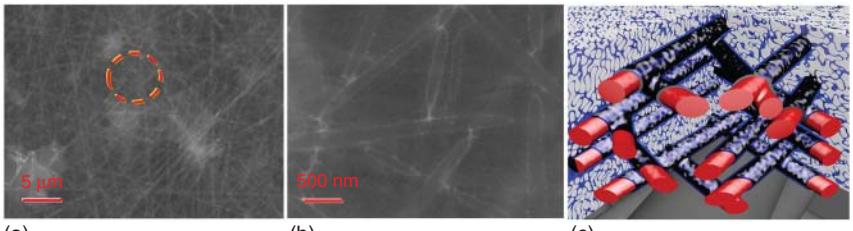


Figure 28.17 (a) SEM image of electrospun nanofibers embedded in the polymer matrix barrier layer of a TFNC membrane. (b) SEM image of magnification of the circle area in (a). (c) Representative of a fibrous network formed by electrospun nanofibers distributed in polymer matrix. Source: Ma et al. 2011 [131], 2010 [137]. Reproduced with permission of American Chemical Society.

also beneficial to increase the permeation flux and will be further discussed later [141].

As discussed earlier, in a pressure-driving filtration process, porosity of the porous membrane usually changes as a result of compaction, especially after a long-term and high-pressure operation. Thus, the permeation flux of the membrane often decreases significantly over time (e.g. 10–65% of the initial value) [97]. In general, a membrane with a very high porosity can be significantly compacted during the filtration process, independent of whether its porous structure is from the phase inversion process or from the electrospinning process. As a result, membranes with high porosity, such as electrospun nanofiber scaffolds (>80 vol%), are often more suitable to be used in low-pressure applications.

In TFNC membranes, electrospun PAN nanofiber scaffolds have been used as a mid-layer to support the cellulose nanofiber barrier layer. In this membrane system, the permeation flux was found to reduce to 42% after 21 hours of compaction using pure water at 30 psi. This was similar to the commercial membrane (PAN10), which was reduced to 48% under the same operating conditions. The compacted TFNC membrane, however, showed five times higher permeation flux than the compacted PAN10 membrane for removal of microparticle (diameter 100 nm) and a similar rejection ratio [96]. The electrospun PVDF membrane was also used as a mid-layer to support the barrier layer made of cross-linked chitosan. This TFNC membrane system also exhibited a significantly higher permeation flux and a lower fouling tendency than the commercial UF membranes for filtration of a BSA solution [133]. The low fouling tendency could be attributed to the hydrophilicity of the barrier layer. Finally, electrospun post-cross-linked PVA nanofiber scaffolds with GA were used as a support layer to support a relatively thick cross-linked PVA barrier layer, where the permeation flux of the resulting TFNC membrane, was quite stable and was over two times higher than that of the corresponding commercial membrane [93]. These studies clearly demonstrated that the high porosity and interconnected pore structure of the nanofiber scaffold played an essential role in improving the permeation flux of the membrane, even under the intense compaction conditions. The filtration performance of a variety of TFNC membranes is summarized in Table 28.1.

Table 28.1 Filtration performance of TFNC UF membranes.

Membranes	Top layer (thickness: nm)	Middle layer	Bottom layer	MWCO (kDa)	Permeability (l/(m^2 h)/psi)	Rejection ratio (%)	Applied pressure (psi)	References
PVA-TFNC	PVA (1800)	PVA e-spun	PET	—	1.30	>99.5	100	[132]
PVA-TFNC	PVA (500)	PAN e-spun	PET	40	2.56	99.0	90	[48]
PVA-TFNC	PVA (600)	PAN e-spun	PET	10	6.85	99.7	30	[134]
PVA-TFNC	PVA-MWCNT (1800)	PAN e-spun	PET	—	3.30	99.8	100	[93]
PVA-TFNC	PVA-UFCN (850)	PAN e-spun	PET	17.5	11.67	99.5	30	[134]
PVA-TFNC	PVA-UV (ND)	PVA e-spun	PET	—	1.83	99.5	30	[140]
PVA-TFNC	PVA (400)	PAN e-spun	N/A	—	4.67	99.5	45	[142]
Cellulose-TFNC	Cellulose (300)	PAN e-spun	PET	2000	9.30	99.8	30	[137]
Cellulose-TFNC	Microcrystal cellulose (600)	PAN e-spun	PET	5000	5.50	99.8	30	[138]
Chitin-TFNC	Chitin (600)	PAN e-spun	PET	5000	8.00	99.6	30	[138]
Cellulose/chitin-TFNC	Cellulose/chitin (600)	PAN e-spun	PET	5000	7.70	99.7	30	[138]
Chitosan-TFNC	Chitosan (1000)	PAN e-spun	PET	—	1.00	99.9	130	[50]
UFCN-TFNC	Cellulose nanofiber (100)	PAN e-spun	PET	2000	10.40	99.6	30	[131]
UFCN-TFNC	Cellulose nanowhisker (200)	PAN e-spun	PET	2000	9.10	99.7	30	[131]
UFCN-TFNC	Chitin nanofiber (450)	PAN e-spun	PET	2000	7.20	99.9	30	[131]
PEBAX-TFNC	PEBAX (800)	PVA e-spun	PET	—	0.57	>99.5	100	[132]
PEBAX-TFNC	PEBAX-MWCNT (800)	PVA e-spun	PET	—	1.61	99.8	100	[93]
PAN10	PAN (N/A)	N/A	PET	70	0.87	99.9	30	[137]
PAN400	PAN (N/A)	N/A	PET	2000	4.50	98.2	30	[137]

MWCNT, multiwalled carbon nanotube.

28.3.2.2 Nanofiltration and Reverse Osmosis

The pore sizes of nanofiltration membranes are usually less than 5 nm. When the pore size is less than 2 nm, the membrane can be used to remove divalent ionic compounds, such as $MgSO_4$, $MgCl_2$, Na_2SO_4, and dye molecules [128, 143]. The mechanism that normally describes the nanofiltration process is based on the combined effect of size exclusion and ionic repulsion interactions, or the so-called Gibbs–Donnan effect [144]. Typical commercially available nanofiltration membranes are fabricated with cellulose acetate using the phase inversion method [145] or with cross-linked polyamide by interfacial polymerization [146] on an ultrafiltration support.

The format of TFNC membranes based on electrospun nanofiber scaffolds has offered a new pathway to improve the filtration efficiency of nanofiltration [141]. In this format, electrospun nanofiber scaffolds (e.g. PAN and PES) could be used directly as the layer, instead of a UF support by the phase inversion method, to support the top barrier layer made by interfacial polymerization. For example, interfacial polymerization between trimesoyl chloride (TMC) in hexane and piperazine (PIP)/bipiperazine (BP) mixtures in water was carried out directly on the electrospun scaffold, where ionic liquids were also used as the inert additives in the water phase [141, 147]. The best performing TFNC nanofiltration membrane of this system exhibited 36% higher permeation flux than NF270, which was a top performing commercial membrane, for the removal of 2000 ppm of $MgSO_4$ (both membranes showed a similar rejection ratio of 97%). The higher permeation flux of the TFNC membrane was attributed to the combined effect of "water channels" due to the formation of nanocomposite structure and the high porosity of the electrospun nanofiber scaffold as the support layer. To reduce the compaction effect, a hot-pressed electrospun PAN nanofiber scaffold has been used as a support layer for fabrication of TFNC membranes, which exhibited a stable permeation flux even after a long operation [100]. In this system, high permeation flux (102 l/(m^2 h)) has been achieved for nanofiltration of $MgSO_4$ with 2000 ppm, which is about two times higher than for NF270. However, this system also exhibited a relatively low rejection ratio (86%). In another study, electrospun PVDF nanofiber scaffold was used as a support to carry an interfacially polymerized TMC and *p*-phenylenediamine (PPD) barrier layer, which also showed a relatively low rejection of 80.7% against to 2000 ppm of $MgSO_4$ [148].

In our opinion, the diameter of electrospun nanofibers (>100 nm) is relatively too large to support a thin barrier with thickness less than 100 nm and form a uniform nanocomposite structure. To overcome this problem, a three-layered TFNC membrane, containing a top layer of ultrafine cellulose nanofibers (fiber diameter ~ 5 nm), was used to host the interfacial polymerization process. There are several benefits to fabricating TFNC nanofiltration membranes with this approach [149]. The first benefit is that the cellulose nanofiber scaffold can retain the advantage of high porosity as in electrospun nanofiber scaffolds. Second, the effective pore size of the cellulose nanofiber scaffold is in the range of 20 nm, which is 1–2 orders of magnitude smaller than that of electrospun nanofiber scaffolds [150]. Third, as the average diameter of cellulose nanofibers is quite small (~5 nm), they can form an interconnected network in the barrier layer. The

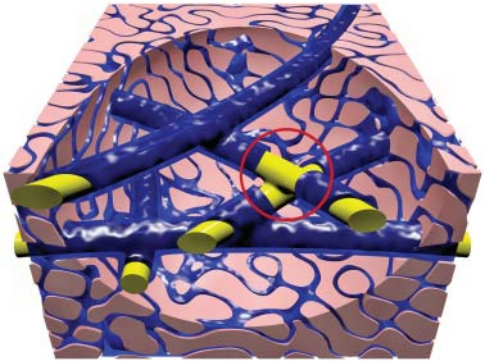


Figure 28.18 Schematic representation of the nature of water channels in the nanocomposite barrier layer. A skeleton of overlapped cellulose nanofibers (yellow) guides a continuously connected system of directed water channels (blue) formed by the connected hollow cylindrical gaps between the nanofibers and the polymer matrix (pink). The cutout in the red circle sketches the cross-linked nature of the nanofiber interconnects. The nanofiber skeleton is anchored at occasional direct contacts with the polymer matrix (not shown). Non-directed molecular cavities in the polymer matrix also contribute to the overall water flow through the barrier layer. Source: Ma et al. 2012 [151]. Reproduced with permission of American Chemical Society.

nanocomposite structure in the barrier layer thus would lead to interconnected water channels, created by the naturally occurring gap between the cellulose nanofiber and the matrix polyamide (Figure 28.18) [151]. The presence of these narrow water channels can greatly enhance the transportation of water molecules without sacrificing the selectivity.

The difference between using the regular interfacial polymerization pathway (i.e. the aqueous phase resides in the nanofiber scaffold) and the reversed interfacial polymerization pathway (i.e. the organic phase resides in the nanofiber scaffold) was investigated in the fabrication of TFNC membranes for NF and RO applications [149]. In this study, the initial scaffold possessed a three-layered structure, containing a top cellulose nanofiber layer and electrospun PAN nanofiber mid-layer. With the regular interfacial polymerization pathway (using TMC and PIP monomers), the loose part of the barrier layer was formed on top of the cellulose nanofiber scaffold, while the dense part was generated below the loose layer (Figure 28.19). The resulting TFNC membrane, exhibiting a high flux of about 40 l/(m^2 h) and 98% rejection ratio against 2000 ppm of $MgSO_4$, was better than that of the NF270 commercial nanofiltration membrane (having 72% rejection ratio under the same conditions). However, with the reversed interfacial polymerization pathway, smaller pore sizes in the barrier layer were obtained because the dense part of the barrier layer was left alone on top of the cellulose nanofiber scaffold. To transition from NF membranes to RO membranes, the barrier layer produced by the reversed interfacial polymerization pathway was further reacted with an excess amount of secondary amino groups (i.e. 1% TMC in hexane), which notably increased the NaCl rejection ratio from 74% to 91% (using 500 ppm NaCl feed solution under 100 psi applied pressure).

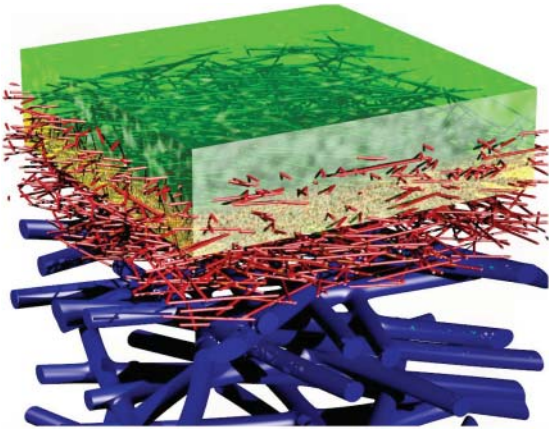


Figure 28.19 Schematic representative of TFNC-based nanofiltration membrane with nanocomposite barrier layer, made by typical interfacial polymerization process with the aqueous phase in the scaffold (the green region represents the barrier layer with loose structure, the yellow region represents the barrier layer with dense structure, the red fibers represent cellulose nanofibers, and the blue fibers represent electrospun nanofibers). Source: Wang et al. 2014 [149]. Reproduced with permission of Royal Society of Chemistry.

Recently, another method was demonstrated to fabricate TFNC RO membranes. In this approach, an electrospun cellulose acetate nanofiber scaffold was used to support multilayered polyelectrolytes of opposite charges in a layer-by-layer (LBL) manner [152]. Unfortunately the performance of this membrane system was not sufficient for practical considerations. For example, the rejection ratio of this composite membrane system for the removal of 2000 ppm NaCl was only in the range of 6–15%, while the corresponding water permeability of these membranes was about 40 l/(m^2 h).

28.3.2.3 Other Applications

TFNC membranes appear to be very suitable for forward osmosis (FO) applications due to the high permeability. However, the subject of this research is rarely reported in the literature [2, 153] and will surely be a subject of growing interest. Recently, two studies on the use of TFNC membranes for forward osmosis have been demonstrated [90, 154]. In these studies, PSU and PAN/cellulose acetate electrospun nanofiber scaffolds were used to support interfacially polymerized TMC-MPD polyamide barrier layers. The resulting TFNC membranes offered permeation fluxes two to five times higher than the commercial HTI osmotic membranes and high salt rejection for forward osmosis applications.

Electrospun PAN nanofiber scaffolds have also been used as the support layer for the fabrication of TFNC pervaporation membranes, where the barrier layer was either cross-linked PVA or graphene oxide (Figure 28.20) [155, 156]. These TFNC membranes were used to dehydrate an ethanol–water mixture, where higher flux and higher separation factors were obtained for both systems when compared with commercially available pervaporation membranes. The superior property of the TFNC format is due to the synergy of a highly porous substrate



Figure 28.20 The schematic diagram indicating the morphological arrangement of GO sheets (not shown in the correct scale, the red circle area represents a packing of GO sheets) and the supporting TFNC membrane scaffold. Source: Yeh et al. 2013 [156]. Reproduced with permission of Royal Society of Chemistry.

and a dense but thin barrier layer. It can be expected that a TFNC pervaporation membrane designed for the purification of volatile organics-contaminated water would also exhibit high flux and high separation factors.

Electrospun PAN nanofiber scaffolds also can play an important role for the membrane bioreactor (MBR) application. MBR is a facial water purification process, having a suspended growth bioreactor, typically used in municipal and industrial wastewater treatments. In this operation, the membrane is the most essential component in the system, where the issue of membrane fouling has been noted as the most pressing technology challenge. Typically, the MBR process can purify wastewater with sufficient quality to be discharged in the coastal areas or be used for urban irrigation [157, 158]. The membrane for MBR application, regarding nominal pore size, should be in the range of 0.05–0.20 μm, which falls into the categories between microfiltration and ultrafiltration. Therefore, a TFNC membrane with high porous structure, high pore interconnectivity, and appropriately designed pore size can be expected to be very useful in MBR, which would lead to high filtration efficiency. The use of suitable hydrophilic materials for electrospinning will be a critical component to produce membranes with good antifouling capability. Unfortunately, not much research has been carried out for this application.

Finally, electrospun nanofiber scaffolds have been proven very useful for MD applications. MD is a thermally driven approach for water purification, especially useful when there are substantial impurities with different nonvolatile contaminants (e.g. inorganics, organics, biological and polymeric materials) and different amount of contaminants in water [52, 159, 160] (e.g. the fracturing water from shale gas exploitation [161–163]) and when the pressure driven system is undesirable. The MD process is driven by a temperature gradient involving two phase transitions, i.e. liquid/vapor and vapor/liquid, subsequently taking place on the membrane surface. In this process, water in the feed solution passes through the

membrane in the vapor state, while the impurities are left behind. Compared with conventional distillation and pressure-driving membrane processes, MD shows the advantages in contaminant rejection (i.e. near 100% rejection for nonvolatile components) and lower operating pressures. However, the disadvantages of this operation also include low permeation flux and high scaling or fouling problems (as the operation is taken place at higher temperatures, it promotes the mineralization growth). For MD operations, the ideal electrospun nanofibrous membranes must have a superhydrophobic surface and an average pore size around 200 nm as conventional MD membranes. This was confirmed by several recent studies, indicating that hydrophobic electrospun scaffolds are very suitable for desalination of seawater by using the MD approach [164, 165], where high flux, high rejection, and low energy consumption have been achieved.

28.4 Conclusions

TFNC membranes, using electrospun nanofibers as a critical component, are a new generation of membranes with merits of high flux, high rejection, low fouling, and low energy consumption for water filtration. Electrospun nanofibers, either as a barrier component or as a supporting component, play a key role in improving the membrane performance. In specific, electrospun nanofiber scaffolds offer high porosity, high interconnectivity, adjustable pore size and distribution, high surface-to-volume ratio, and good mechanical properties. With the rapid development of scalable electrospinning processes and the ease to modify the surface property, electrospun nanofiber scaffolds can be expected to be implemented in new membrane systems for many different types of water purification.

28.5 Future Prospects

In spite of having many unique advantages over other filtration materials for water purification, electrospun nanofibrous membranes still face some challenges for implementation: (i) the quality and characteristics of the electrospun membranes need to be precisely controlled in large-scale production, (ii) the solvent (especially volatile organic solvent) used in industrial electrospinning process can be recycled and reused, and (iii) the surface modification of the nanofibrous membranes can be implemented in a green and economic manner. We believe all these challenges will be overcome in the near future where electrospun nanofibrous membranes will truly be implemented in many different types of water applications.

Acknowledgments

This work was supported by a SusChEM award from the National Science Foundation in the United States (DMR-1409507), the National Natural Science

Foundation of China (51673011), the State Key Laboratory of Organic-Inorganic Composites at Beijing University of Chemical Technology (oic-201503004), and the Fundamental Research Funds for the Central Universities (buctrc201501).

References

1 Shannon, M.A., Bohn, P.W., Elimelech, M. et al. (2008). *Nature* 452: 301–310.
2 Ma, H.Y., Hsiao, B.S., and Chu, B. (2012). *Functional Nanofibers and Applications*, Chapter 15 (ed. Q. Wei), 331–370. Cambridge, UK: Wood Publishing Limited.
3 Ramakrishna, S., Ma, Z., and Matsuura, T. (2011). *Polymer Membranes in Biotechnology: Preparation, Functionalization and Application*, 1–254. London: Imperial College Press.
4 Burger, C., Hsiao, B.S., and Chu, B. (2006). *Annual Review of Materials Research* 36: 333–368.
5 Thavasi, V., Singh, G., and Ramakrishna, S. (2008). *Energy & Environmental Science* 1: 205–221.
6 Yoon, K., Hsiao, B.S., and Chu, B. (2008). *Journal of Materials Chemistry* 18: 5326–5334.
7 Ma, H.Y., Burger, C., Hsiao, B.S., and Chu, B. (2011). *Journal of Materials Chemistry* 21: 7507–7510.
8 Meyyappan, M. and Sunkara, M.K. (2009). *Inorganic Nanowires: Applications, Properties, and Characterization*, 1–453. Florida: CRC Press, Inc.
9 Chakarvarti, S.K. and Vetter, J. (1998). *Radiation Measurements* 29: 149–159.
10 Lee, C.C., Grenier, C., Meijer, E.W., and Schenning, A.P.H.J. (2009). *Chemical Society Reviews* 38: 671–683.
11 Teo, W.E. and Ramakrishna, S. (2006). *Nanotechnology* 17: R89–R106.
12 Isogai, A., Saito, T., and Fukuzumi, H. (2011). *Nanoscale* 3: 71–85.
13 Huang, Z.M., Zhang, Y.Z., Kotaki, M., and Ramakrishna, S. (2003). *Composites Science and Technology* 63: 2223–2253.
14 Zong, X., Kim, K., Fang, D. et al. (2002). *Polymer* 43: 4403–4412.
15 Greiner, A. and Wendorff, J.H. (2008). *Advances in Polymer Science* 219: 107–171.
16 Reneker, D.H. and Chun, I. (1996). *Nanotechnology* 7: 216–223.
17 Greiner, A. and Wendorff, J.H. (2007). *Angewandte Chemie International Edition* 46: 5670–5703.
18 Reneker, D.H., Yarin, A.L., Fong, H., and Koombhongse, S. (2000). *Journal of Applied Physics* 87: 4531–4547.
19 Li, D. and Xia, Y. (2004). *Advanced Materials* 16: 1151–1170.
20 Shin, Y.M., Hohman, M.M., Brenner, M.P., and Rutledge, G.C. (2001). *Applied Physics Letters* 78: 1149–1151.
21 Ma, H.Y., Hsiao, B.S., and Chu, B. (2013). *Current Organic Chemistry* 17: 1361–1370.

22 There are numerous companies to produce electrospinning apparatus and products, e.g. http://www.elmarco.com/; http://www.donaldson.com/index.html; http://www.nabond.com/; http://holmarc.com/nano_fiber_electrospinning_station.html, etc.
23 Pham, Q.P., Sharma, U., and Mikos, A.G. (2006). *Tissue Engineering* 12: 1197–1211.
24 Sill, T.J. and von Recum, H.A. (2008). *Biomaterials* 29: 1989–2006.
25 Zeng, J., Xu, X., Chen, X. et al. (2003). *Journal of Controlled Release* 92: 227–231.
26 Liang, D., Hsiao, B.S., and Chu, B. (2007). *Advanced Drug Delivery Reviews* 59: 1392–1412.
27 Chase, G.G., Varabhas, J.S., and Reneker, D.H. (2011). *Journal of Engineered Fibers and Fabrics* 6: 32–38.
28 Park, H.S. and Park, Y.O. (2005). *Korean Journal of Chemical Engineering* 22: 165–172.
29 Qin, X. and Wang, S. (2006). *Journal of Applied Polymer Science* 102: 1285–1290.
30 Jo, S.M. (2012). *Hydrogen Storage*, Chapter 8 (ed. J. Liu), 181–210. Shanghai: InTech.
31 Miao, J., Miyauchi, M., Simmons, T.J. et al. (2010). *Journal of Nanoscience and Nanotechnology* 10: 5507–5519.
32 Ding, B., Wang, M., Wang, X. et al. (2010). *Materials Today* 13: 16–27.
33 Ding, B., Wang, M., Yu, J., and Sun, G. (2009). *Sensors* 9: 1609–1624.
34 Liu, Y., Ma, H.Y., Hsiao, B.S. et al. (2016). *Polymer* 107: 163–169.
35 Botes, M. and Cloete, T.E. (2010). *Critical Reviews in Microbiology* 36: 68–81.
36 Chu, B., Hsiao, B.S., and Yoon, K. (2008). *AATCC Review* 8: 31–33.
37 Graton, L.C. and Fraser, H.J. (1935). *Journal of Geology* 43: 785–909.
38 Chu, B. and Hsiao, B.S. (2009). *Journal of Polymer Science Part B: Polymer Physics* 47: 2431–2435.
39 Ulbricht, M. (2006). *Polymer* 47: 2217–2262.
40 Barhate, R.S., Loong, C.K., and Ramakrishna, S. (2006). *Journal of Membrane Science* 283: 209–218.
41 Zong, X., Ran, S., Kim, K. et al. (2003). *Biomacromolecules* 4: 416–423.
42 Wang, R., Shi, L., Tang, C.Y. et al. (2010). *Journal of Membrane Science* 355: 158–167.
43 Broens, L., Altena, F.W., Smolders, C.A., and Koenhen, D.M. (1980). *Desalination* 32: 33–45.
44 Cheryan, M. (1998). *Ultrafiltration and Microfiltration Handbook*, Chapter 3, 71–95. Pennsylvania, PA: Technomic Publishing Company, Inc.
45 Fane, A.G., Fell, C.J.D., and Waters, A.G. (1981). *Journal of Membrane Science* 9: 245–262.
46 Deniz, S. (2006). *Desalination* 200: 42–43.
47 Ho, C.C. and Zydney, A.L. (1999). *Journal of Membrane Science* 155: 261–275.
48 Yoon, K., Hsiao, B.S., and Chu, B. (2009). *Journal of Membrane Science* 338: 145–152.

49 Barhate, R.S., Loong, C.K., and Ramakrishna, S. (2007). *Journal of Membrane Science* 296: 1–8.

50 Yoon, K., Kim, K., Wang, X. et al. (2006). *Polymer* 47: 2434–2441.

51 Andrade, J.S. Jr., Costa, U.M.S., Almeida, M.P. et al. (1999). *Physical Review Letters* 82: 5249–5252.

52 Alkhudhiri, A., Darwish, N., and Hilal, N. (2012). *Desalination* 287: 2–18.

53 Fane, A.G., Fell, C.J.D., and Waters, A.G. (1983). *Journal of Membrane Science* 16: 211–224.

54 Genne, I., Kuypers, S., and Leysen, R. (1996). *Journal of Membrane Science* 113: 343–350.

55 Boure, T. and Vanholder, R. (2004). *Nephrology Dialysis Transplantation* 19: 293–296.

56 Fridrikh, S.V., Yu, J.H., Brenner, M.P., and Rutledge, G.C. (2003). *Physical Review Letters* 90: 144502.

57 Liu, Y., Wang, R., Ma, H.Y. et al. (2013). *Polymer* 54: 548–556.

58 Wang, R., Liu, Y., Li, B. et al. (2012). *Journal of Membrane Science* 392–393: 167–174.

59 Yang, S.Y., Ryu, I., Kim, H.Y. et al. (2006). *Advanced Materials* 18: 709–712.

60 Ma, H.Y., Burger, C., Hsiao, B.S., and Chu, B. (2012). *Biomacromolecules* 13: 180–186.

61 Zalusky, A.S., Olayo-Valles, R., Wolf, J.H., and Hillmyer, M.A. (2002). *Journal of the American Chemical Society* 124: 12761–12773.

62 Yan, F. and Goedel, W.A. (2004). *Advanced Materials* 16: 911–915.

63 Park, C., Yoon, J., and Thomas, E.L. (2003). *Polymer* 44: 6725–6760.

64 Apel, P. (2001). *Radiation Measurements* 34: 559–566.

65 Kuiper, S., van Rijn, C.J.M., Nijdam, W., and Elwenspoek, M.C. (1998). *Journal of Membrane Science* 150: 1–8.

66 Tracey, E.M. and Davis, R.H. (1994). *Journal of Colloid and Interface Science* 167: 104–116.

67 Saljoughi, E., Sadrzadeh, M., and Mohammadi, T. (2009). *Journal of Membrane Science* 326: 627–634.

68 Boland, E.D., Coleman, B.D., Barnes, C.P. et al. (2005). *Acta Biomaterialia* 1: 115–123.

69 Gibson, P., Schreuder-Gibson, H., and Rivin, D. (2001). *Colloids and Surfaces A: Physicochemical and Engineering Aspects* 187–188: 469–481.

70 Li, J., Sculley, J., and Zhou, H. (2012). *Chemical Reviews* 112: 869–932.

71 Yang, K. and Xing, B. (2010). *Chemical Reviews* 110: 5989–6008.

72 Yeh, E., Ostreicher, E., Sale, R. et al. (2002). Method for charge-modifying polyester. US Patent 2002/0155225; Pignot, C. and Artaud, L. Device for the diffusion of a volatile product and preparation process. US Patent 2002/0037385; Hou, K.C., Bretl, D.S., and Hembree, R.D. (2003). Microorganism filter and method for removing microorganism from water. US Patent 6, 565, 749; Ostreicher, E. (1992). Use of cationic charge modified filter media. US Patent 5, 085, 780.

73 Chu, B., Hsiao, B.S., and Ma, H.Y. (2011). High flux high efficiency nanofiber membranes and methods of production thereof. US Patent 2011/0198282;

Chu, B., Hsiao, B.S., Ma, H.Y., et al. (2012). High flux microfiltration membranes with virus and metal ion adsorption capability for liquid purification. WO Patent 2012/027242.
74 Ma, H.Y., Chu, B., and Hsiao, B.S. (2012). Functionalization of nanofibrous microfiltration membranes for water purification. WO Patent 2012/094407.
75 Barthlott, W. and Neinhuis, C. (1997). *Planta* 202: 1–8.
76 Sun, T., Feng, L., Gao, X., and Jiang, L. (2005). *Accounts of Chemical Research* 38: 644–652.
77 Feng, L., Li, S., Li, Y. et al. (2002). *Advanced Materials* 14: 1857–1860.
78 Tuteja, A., Choi, W., Ma, M. et al. (2007). *Science* 318: 1618–1622.
79 Wang, Z., Ma, H.Y., Chu, B., and Hsiao, B.S. (2017). *Separation Science and Technology* 52: 221–227.
80 Zhang, Y.Z., Su, B., Venugopal, J. et al. (2007). *International Journal of Nanomedicine* 2: 623–638.
81 Lin, J., Ding, B., Yu, J., and Hsien, Y. (2010). *ACS Applied Materials & Interfaces* 2: 521–528.
82 Ding, B., Kim, J., Kimura, E., and Shiratori, S. (2004). *Nanotechnology* 15: 913–917.
83 Min, M., Wang, X., Yang, Y. et al. (2011). *Journal of Nanoscience and Nanotechnology* 11: 6919–6925.
84 Martin, C.R. (1994). *Science* 266: 1961–1966.
85 Cheremisinoff, P.N. (1995). *Handbook of Water and Wastewater Treatment Technology*, Chapter 13, 506–510. New York: Marcel Dekker, Inc.
86 Witte, D., Dijkstra, P.J., Berg, J.W.A., and Feijen, J. (1996). *Journal of Membrane Science* 117: 1–31.
87 Golden, A.P. and Tien, J. (2007). *Lab on a Chip* 7: 720–725.
88 Ho, C.C. and Zydney, A.L. (2001). *Industrial and Engineering Chemistry Research* 40: 1412–1421.
89 Gao, K., Hu, X., Dai, C., and Yi, T. (2006). *Materials Science and Engineering B* 131: 100–105.
90 Bui, N.N., Lind, M.L., Hoek, E.M.V., and McCutcheon, J.R. (2011). *Journal of Membrane Science* 385–386: 10–19.
91 Gopal, R., Kaur, S., Ma, Z. et al. (2006). *Journal of Membrane Science* 281: 581–586.
92 Ma, H.Y., Hsiao, B.S., and Chu, B. (2014). *Journal of Membrane Science* 452: 446–452.
93 Wang, X., Chen, X., Yoon, K. et al. (2005). *Environmental Science and Technology* 39: 7684–7691.
94 Bohonak, D.M. and Zydney, A.L. (2005). *Journal of Membrane Science* 254: 71–79.
95 Park, N., Kwon, B., Kim, I.S., and Cho, J. (2005). *Journal of Membrane Science* 258: 43–54.
96 Ma, H.Y., Hsiao, B.S., and Chu, B. (2014). *Journal of Membrane Science* 454: 272–282.
97 Kallioinen, M., Pekkarinen, M., Manttari, M. et al. (2007). *Journal of Membrane Science* 294: 93–102.

98 Gopal, R., Kaur, S., Feng, C.Y. et al. (2007). *Journal of Membrane Science* 289: 210–219.
99 Yoon, K., Hsiao, B.S., and Chu, B. (2009). *Polymer* 50: 2893–2899.
100 Kaur, S., Barhate, R., Sundarrajan, S. et al. (2011). *Desalination* 279: 201–209.
101 Tang, Z., Qiu, C., McCutcheon, J.R. et al. (2009). *Journal of Polymer Science Part B: Polymer Physics* 47: 2288–2300.
102 Crittenden, J.C., Trussell, R.R., Hand, D.W. et al. (2005). *Water Treatment Principles and Design*, 2e, 1–1901. New Jersey: Wiley.
103 Yang, R., Aubrecht, K.B., Ma, H.Y. et al. (2014). *Polymer* 55: 1167–1176.
104 Yang, R., Su, Y., Burger, C. et al. (2015). *Polymer* 60: 9–17.
105 Liu, Y., Ma, H.Y., Liu, B. et al. (2015). *Film Sheeting* 31: 379–400.
106 facts about E. coli: dimensions, as discussed in "bacteria: diversity of structure of bacteria" in Britannica Online Encyclopedia. http://www.britannica.com/facts/5/463522/E-coli-as-discussed-in-bacteria (acceptable 22 September 2013).
107 Tolliver, D.L. and Schroeder, H.G. (1983). *Microcontamination* 1: 34–43.
108 Su, Y., Burger, C., Ma, H.Y. et al. (2015). *Biomacromolecules* 16: 1201–1209.
109 Su, Y., Burger, C., Ma, H.Y. et al. (2015). *Cellulose* 33: 3127–3135.
110 Sato, A., Wang, R., Ma, H.Y. et al. (2011). *Journal of Electron Microscopy* 60: 201–209.
111 Crini, G. (2006). *Bioresource Technology* 97: 1061–1085.
112 Mohan, D. and Pittman, C.U. (2007). *Journal of Hazardous Materials* 142: 1–53.
113 Busca, G., Berardinelli, S., Resini, C., and Arrighi, L. (2008). *Journal of Hazardous Materials* 160: 265–288.
114 Chanrai, N.G. and Burde, S.G. (2004). Recovery of oil from spent bleached earth. US Patent 6, 780, 321.
115 Ma, Z., Kotaki, M., and Ramakrishna, S. (2005). *Journal of Membrane Science* 265: 115–123.
116 Ma, Z. and Ramakrishna, S. (2008). *Journal of Membrane Science* 319: 23–28.
117 Ma, Z., Masaya, K., and Ramakrishna, S. (2006). *Journal of Membrane Science* 282: 237–244.
118 Ryu, Y.J., Kim, H.Y., Lee, K.H. et al. (2003). *European Polymer Journal* 39: 1883–1889.
119 Ding, B., Li, C., Miyauchi, Y. et al. (2006). *Nanotechnology* 17: 3685–3691.
120 Merck (2013). Microfiltration membranes for filtration and venting applications. http://www.millipore.com/publications.nsf/a73664f9f981af8c852569b9005b4eee/af9dca91de8ae07e852574fd004cf186/$FILE/PF1176EN00_EM.pdf (accessible 22 September 2013).
121 Wang, X., Ding, B., Yu, J. et al. (2010). *Nanotechnology* 21: 055502.
122 Schiffman, J.D. and Schauer, C.L. (2007). *Biomacromolecules* 8: 594–601.
123 Horzum, N., Boyaci, E., Eroglu, A.E. et al. (2010). *Biomacromolecules* 11: 3301–3308.
124 Fang, X., Xiao, S., Shen, M. et al. (2011). *New Journal of Chemistry* 35: 360–368.
125 Brady-Estevez, A.S., Kang, S., and Elimelech, M. (2008). *Small* 4: 481–484.

126 Brady-Estevez, A.S., Schnoor, M.H., Vecitis, C.D. et al. (2010). *Langmuir* 26: 14975–14982.
127 Koros, W.J., Ma, Y.H., and Shimidzu, T. (1996). *Journal of Membrane Science* 120: 149–159.
128 Fane, A.G. and Fell, C.J.D. (1987). *Desalination* 62: 117–136.
129 Rahimpour, A. and Madaeni, S.S. (2007). *Journal of Membrane Science* 305: 299–312.
130 Koops, G.H. (2013). *Encyclopedia of Desalination and Water Resources, Membrane Processes*, vol. II. Isle of Man: Eolss Publishers Co. Ltd. http://www.desware.net/Membrane-Processes.aspx.
131 Ma, H.Y., Burger, C., Hsiao, B.S., and Chu, B. (2011). *Biomacromolecules* 12: 970–976.
132 Wang, X., Fang, D., Yoon, K. et al. (2006). *Journal of Membrane Science* 278: 261–268.
133 Zhao, Z., Zheng, J., Wang, M. et al. (2012). *Journal of Membrane Science* 394–395: 209–217.
134 Ma, H.Y., Yoon, K., Rong, L. et al. (2010). *Industrial and Engineering Chemistry Research* 49: 11978–11984.
135 Wang, Z., Ma, H.Y., Hsiao, B.S., and Chu, B. (2014). *Polymer* 55: 366–372.
136 Zhang, H., Zheng, J., Zhao, Z., and Han, C.C. (2013). *Journal of Membrane Science* 442: 124–130.
137 Ma, H.Y., Yoon, K., Rong, L. et al. (2010). *Journal of Materials Chemistry* 20: 4692–4704.
138 Ma, H.Y., Hsiao, B.S., and Chu, B. (2011). *Polymer* 52: 2594–2599.
139 Wang, Z., Ma, H.Y., Chu, B., and Hsiao, B.S. (2017). *Journal of Applied Polymer Science* 134: 44583.
140 Tang, Z., Wei, J., Yung, L. et al. (2009). *Journal of Membrane Science* 328: 1–5.
141 Yoon, K., Hsiao, B.S., and Chu, B. (2009). *Journal of Membrane Science* 326: 484–492.
142 Wang, X., Zhang, K., Yang, Y. et al. (2010). *Journal of Membrane Science* 356: 110–116.
143 Hilal, N., Al-Zoubi, H., Darwish, N.A. et al. (2004). *Desalination* 170: 281–308.
144 Krasemann, L. and Tieke, B. (2000). *Langmuir* 16: 287–290.
145 Strathmann, H., Scheible, P., and Baker, R.W. (1971). *Journal of Applied Polymer Science* 15: 811–828.
146 Petersen, R.J. (1993). *Journal of Membrane Science* 83: 81–150.
147 Yung, L., Ma, H.Y., Wang, X. et al. (2010). *Journal of Membrane Science* 365: 52–58.
148 Kaur, S., Sundarrajan, S., Gopal, R., and Ramakrishna, S. (2012). *Journal of Applied Polymer Science* 124: E205–E215.
149 Wang, X., Yeh, T.M., Wang, Z. et al. (2014). *Polymer* 55: 1358–1366.
150 Ghosh, A.K. and Hoek, E.M.V. (2009). *Journal of Membrane Science* 336: 140–148.
151 Ma, H.Y., Burger, C., Hsiao, B.S., and Chu, B. (2012). *ACS Macro Letters* 1: 723–726.

152 Ritcharoen, W., Supaphol, P., and Pavasant, P. (2008). P. *European Polymer Journal* 44: 3963–3968.

153 Song, X., Liu, Z., and Sun, D.D. (2011). *Advanced Materials* 23: 3256–3260.

154 Bui, N.N. and McCutcheon, J.R. (2013). *Environmental Science and Technology* 47: 1761–1769.

155 Yeh, T.M., Yang, L., Wang, X. et al. (2010). *Journal of Renewable and Sustainable Energy* 4: 041406.

156 Yeh, T.M., Wang, Z., Mahajan, D. et al. (2013). *Journal of Materials Chemistry A* 1: 12998–13003.

157 Yang, W.B., Cicek, N., and Ilg, J. (2006). *Journal of Membrane Science* 270: 201–211.

158 Meng, F.G., Chae, S.R., Drews, A. et al. (2009). *Water Research* 43: 1489–1512.

159 Souhaimi, M.K. and Matsuura, T. (2011). *Membrane Distillation: Principles and Applications*, 1–460. London, UK: Elsevier.

160 Gryta, M. (2008). *Journal of Membrane Science* 325: 383–394.

161 Kerr, R.A. (2010). *Science* 328: 1624–1626.

162 McGlade, C., Speirs, J., and Sorrell, S. (2013). *Energy* 55: 571–584.

163 Vengosh, A., Warner, N., Jackson, R., and Darrah, T. (2013). *Procedia Earth and Planetary Science* 7: 863–866.

164 Feng, C., Khulbe, K.C., Matsuura, T. et al. (2013). *Separation and Purification Technology* 102: 118–135.

165 Maab, H., Francis, L., Al-saadi, A. et al. (2012). *Journal of Membrane Science* 423–424: 11–19.

29

Fibers for Filtration

Govindharajan Thilagavathi and Siddhan Periyasamy

PSG College of Technology, Department of Textile Technology, Coimbatore, 641004, India

29.1 Introduction

Textiles have been used as one of the important filter media from time as much as textiles were known for clothing. The use of textiles for filtration could be remembered from simple ancient people practices like separation of sand particles and other dirt while taking drinking water from river, ponds, etc. Textile like woven fabrics, by virtue, has the required structure for filtration, having structures with the openness on the orders of as close as to microns. The fabrics have good mechanical properties such as tensile, tear, and impact resistance good enough to withstand the normal course of forces. Hence textile fabrics could be used as an efficient filter media. Further, based on filtration requirements, the openness of the fabrics, gram per square meter (GSM), mechanical properties, etc. can be altered through the control of various governing parameters like type of fiber, yarn count, interlacement patterns, ends per inch (EPI) and picks per inch (PPI), number of layers of fabrics, etc. With the developments in high-performance and functional fibers and their use in technical textiles, filtration with specific requirements like high temperature, chemical, hot chemical, and micro- and nano-filtrations has become possible [1, 2].

The topic of textile filtration is extensive wherein numbers of variables can play its vital role based on the type of filtrations for which they are intended [3]. For example, textile filter media could be used in the form of fibers, rovings, yarns, and fabrics, which are made from yarns like interlaced (woven) fabrics and interloped (warp and weft knitted) fabrics and from fibers like the nonwoven fabrics. Nonwovens in particular can be constructed with varying degrees of porosity, thickness, and density coupled with structural isotropicity as it is made from random alignment of fibers [4]. Hence the nonwovens are promising textile structures to function as effective filter media. Apart from the structural diversity of textiles, considerations of filtration mechanisms too map well with the textile filter media for their effective performance in filtration applications.

Though the performance of the filter media would depend on various structural attributes, material-specific intensive properties are to be considered based on

Handbook of Fibrous Materials, First Edition. Edited by Jinlian Hu, Bipin Kumar, and Jing Lu.
© 2020 Wiley-VCH Verlag GmbH & Co. KGaA. Published 2020 by Wiley-VCH Verlag GmbH & Co. KGaA.

the types of filtration in question. In textiles, these intensive properties emanate from the fibers as they are the foundational building blocks of the textiles [5].

Filtration is one type of technical applications of the fibers. Most of the fibers could be a suitable candidate for developing filter media for any one type of filtration; however, the choice has to be obviously made based on the techno-economical requirements/considerations. Therefore, in this chapter, it is attempted to provide a comprehensive understanding of textile fibers for their suitability in filtration applications.

29.2 Filtration and Filter Media

The term filtration could be perceived as a classification under a broad term separation. Separation, hence, is a process of taking something apart from the mixture of either homogeneous or nonhomogeneous type belonging to solid–solid, solid–liquid, liquid–liquid, solid–gas, liquid–gas, and gas–gas. Based on the type of mixture, various principles could be employed for the separation. In such mixtures, high proportionate compound could be regarded as bulk phase, while the compound(s) in low proportion(s) could be regarded as mixed phase(s). Based on the kind of mixing, the mixtures could be classified as intimate and non-intimate mixing depending on the degree of chemical and physical interactions. If the mixture has spontaneous chemical interaction, such mixing could be classified as intimate and is classified as non-intimate if the chemical interaction between the mixed and bulk phase is nonspontaneous. In nonspontaneous mixtures interactions would be enacted mainly by physical forces coupled with some weak chemical forces. Among these kinds of separations, the term filtration is generally assigned to the separation of solid from liquid in the solid–liquid mixture. Such solid–liquid mixture could be a dispersion (non-intimate but made so by surface active agents) or a solution (intimate mixing) based on which the principle employed to remove the solid would differ. For example, if the solid–liquid mixture is a solution, the principle of separation of the dissolved solid could be by precipitation followed by straining while it could be simple straining or particle agglomeration followed by straining for dispersion type of solid–liquid mixture. Such similar separation principles could be used for other mixtures like liquid–liquid (solution or dispersion), liquid–gas, and solid–gas.

In the Handbook of Filter Media by Elsevier, the definition of filter medium is given as following [6]: *A filter medium is any material that, under the operating conditions of the filter, is permeable to one or more components of a mixture, solution or suspension, and is impermeable to the remaining components*. Hence, the filter media could be broadly regarded as the substrate/object through which the actual separation of the compound in question in the mixture is taking place. In most cases the mixed compound is having a distinct phase from the bulk phases. However, if both the mixed and bulk phases have a single phase like in the case of solutions, as stated above, it could be precipitated and then filtered through the filter media. Such separation of the particles through the filter media could be by simple straining (sieving) mechanism or by other mechanisms such as interception, Brownian diffusion, inertial separation, and electrostatic attraction that are

briefly described in Section 29.2.2. Based on the characteristics of the particles, any one of the mechanisms would dominate over the other in the filtration process. Accordingly, the filter media should be designed and selected. Additionally, there are other points such as cake formation aspects and its effect in particular type of filtration, its removal, temperature at which the filtration is carried out, reuse of the filter media, pressure considerations such as flow pressure and pressure drop, etc. based on which the design and selection of filter media would depend.

29.2.1 Types of Filtration

As briefed in Section 29.2, filtration types could be understood based on number of criteria such as based on the type of bulk and mixed phase. If the bulk phase is liquid, it is regarded as liquid filtration, and if it is gas, it is regarded as gas filtration. These two types are encountered in most cases under filtration while the other type of solid to solid comes more appropriately under separation than filtration. Further, based on the temperature of the mixture, the filtration could be regarded as hot/cold filtrations [7]; based on the type of filter media and the mixed phase, it could be regarded as surface or depth filtration [8, 9]. Based on the pressure difference/pressure drop due to filtration, it could be regarded as ambient pressure filtrations and vacuum/pressure filters [10]. Almost all the filtration applications could be brought under these categories [11].

29.2.2 Filtration Theories

Generally, a theory of filtration, by common perception, is considered due to the physical blocking effect based on the particle and filter media pore's average size and distribution that is generally referred to as straining theory/mechanism. However, there are situations wherein the filtration does happen outside the purview of this general theory of filtration. Hence, when the cause for such filtration effects is scientifically studied, distinct mechanisms such as interception, Brownian diffusion, inertial separation, and electrostatic attraction have been discovered in addition to the general straining theory. The schematic of the various mechanisms of particle filtration is shown in Figure 29.1. Interception mechanism is application to large particles that follows the streamline of the fluid carrying the particles, while the inertial mechanism is for the large particles, which travel off the streamline of the fluid.

In both cases the particle is arrested by the filter media when the particle strikes the media grain; however, such striking of particles takes place differently in these two mechanisms, i.e. in the interception mechanism, it happens when the particles flow very close to the media grain, while with the inertial it happens due to the random movement of the large particles due to the inertial force itself, leading to such particle striking and particle capturing. Brownian diffusion is applicable to the particles with diameter having less than 1 μm. Such small particles moving along with the flow of the fluid would exactly not have the straight line path as in the case of a large particle, which is due to the very small size and mass. Hence such particles like micro dusts and viruses would have a random

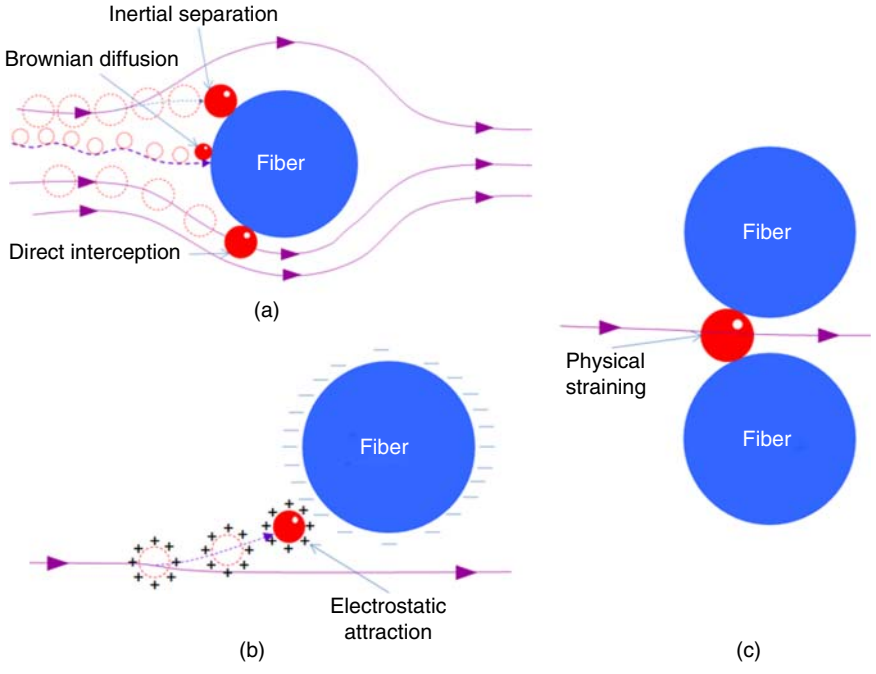


Figure 29.1 Schematic representation of various mechanisms of filtrations: (a) inertial separation, Brownian diffusion, and direct interception, (b) electrostatic attraction, and (c) physical straining.

motion within the flowing liquid that would be governed by the temperature of the fluid. Such randomly moving small particles are captured by the media grain through adherence, agglomeration, and consolidation by the subsequent particle capturing effects. In the case of electrostatic attraction, the particle capturing takes place due to the attractive forces between the filter media and the particles that are oppositely charged. Interception, inertial separation, Brownian diffusion, and straining types of mechanisms depend on the physical aspects of the particles and the filter media, and hence such effects could be the cause in various filtration applications. However, the electrostatic mechanism is possible through introduction of ionizing chemical elements in the filter media for specific filtration applications for which the chemistry of the particle to be filtered of is also known. Similar mechanisms have been reported in the literatures [12, 13].

29.2.3 Requirements of Filter Media

The specific requirements of the filter media for general kinds of fluid filtration could be listed as follows: high filtration efficiency; low pressure drop; no clogging; easy cleaning; easy maintenance; good dimensional stability under the filtration conditions; no change in filtration properties through change in pore size and distribution; versatility; durability; good cake formation; easy removal of cake; high performance to weight ratio; high performance to volume ratio;

good temperature and chemical stability; having good mechanical properties (strength, elastic recovery); good surface properties leading to good adsorption of the particles; good abrasion properties; no or required surface charges as per the filtration requirements; low resistance to fluid flow; no microbial growth or resistance to microbial attack; resistance to environmental factors like redox reactions, hydrolytic degradations, and any other corrosive reactions; resistance to reaction with the particles being filtered, which may be of polycompound belonging to organic and inorganic in nature or in certain cases in which the particles are known to be reactive; and automatic withering off of the filtered particles due to gravitation in appropriate applications [3].

29.3 Fibrous Materials as Filter Media

Textile fiber is unit of matter characterized by fineness, flexibility, and a high ratio of length to width. The fiber must also have sufficiently high temperature stability and a certain minimum strength, extensibility, and elasticity. The uniqueness of the fibrous substance is that it provides large surface area and interstices to the products made of it, due to the fact that the fibers are very small in its cross section, leading to large number of overlaps [14]. Such inherent porosity present in the fibrous substrates can be effectively used as a filter media.

29.3.1 Classification of Fibers

Understanding on classification of fibers would facilitate the fiber selection for developing textile filter media. Meeting the standard definition of a textile fiber, many fibers are naturally available, and man-made fibers using natural and synthetic polymer have been made imitating the natural fibers. Hence, fibers are broadly classified as natural fibers and man-made fibers. Under the man-made fiber categories, there are two major subdivisions, one being the regenerated fibers produced using natural polymers and the other being synthetic/artificial fibers produced using polymers synthesized by man. Cellulosics and polyamides are the two major categories of natural fibers. Examples of the fibers under cellulosic category are cotton, jute, flax, ramie, and hemp, while silk and wool are the major natural fibers under natural category. Regenerated polymer fibers are made first by dissolving the natural fibers in a suitable solvents and then extruding them in a spinneret to form fibers. Examples of the fibers belonging to this category are rayons (viscose, acetate, triacetate, polynosic, cuprammonium), lyocell, Tencel, and casein. Synthetic polymer fibers are produced first by synthesizing the polymer from organic and inorganic monomers and then converting them as fibers. Examples of the fibers belonging to this category are nylons (nylon 66, nylon 6, nylon 610, etc.), polyethylene terephthalate (PET), acrylic, polyethylene, polypropylene, glass, carbon, etc. [15, 16].

29.3.2 Fine and Morphological Structures of Fibers

In order to understand the effective role of the fiber as the building block material of the filter media, it is essential to understand the general structure of fibers.

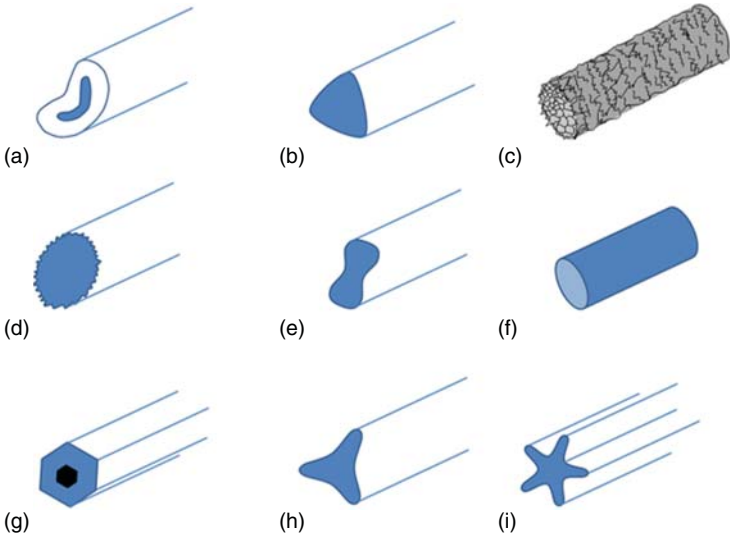


Figure 29.2 Schematic of surface macromorphology of various textile fibers: (a) kidney-shaped (cotton), (b) triangular (silk), (c) oval to round – scales overlapping (wool), (d) circular striated (rayon), (e) dog bone-shaped (acrylic), (f) circular (PET, nylon), (g) polygonal (flax), (h) trilobal (nylon), and (i) multilobular (acetate).

The structure of the fibers, like any materials, could be regarded as the macro surface morphological structure and the fine structure. The macro surface morphological structure is important in number of aspects as it decides the specific surface area of contact for a given mass/volume of materials. Such surface contacts would contribute for any one of the four filtration mechanisms, resulting in the filtration. Surface macromorphological structures of textile fibers are schematically presented in Figure 29.2. Generally, the natural and regenerated fibers have non-round cross section, while the synthetic fibers produced through melt spinning can have round cross section or any other shapes like triangular, trilobal, etc. based on the type of spinneret [17, 18]. Similarly the longitudinal shape of the natural fibers also has generally some irregular rough surface like in the case of wool; it has scaly surface, and with cotton it has twisted convolutions. However, in the case of man-made fibers, the longitudinal surface has generally smooth surface with some striations for noncircular cross-sectional fibers.

One of the important parameters apart from the cross-sectional and longitudinal forms of the fibers is the size of the fiber itself, which normally range about 10–70 μm. In the lower end range, cotton fiber varieties could be located, while on the higher end range, wool fiber varieties could be located. As far as the synthetic fibers are concerned, their diameter could be altered easily; however, producing finer fibers below 1 μm would be challenging in terms of stable structure development [17]. It is a known fact that for a given mass/volume, if the fiber size decreases, the total surface area would increase. Based on this fact, the size of the fibers would greatly influence the performance of the filtration. With the developments in synthetic fiber, the microdenier fibers (<1 denier) have high surface proportionately compared with that of the regular fiber fineness of about

1.5 denier [19]. The filter media developed with microdenier fiber could be made with the average pore size as low as 12–25 μm compared with the pore size of about 35–66 μm for those structures made with regular fibers. Such filter media made with microdenier fibers would yield high filtration efficiency as a result of high specific surface area [20].

In addition to the size/diameter of the fiber, its surface roughness would also have an effect, i.e. the rougher the surface, the more chances for the physical interactions of the particles through the various mechanisms of filtrations. For the purpose, the fibers could be given surface treatments through chemical or physical methods, which are other emerging areas of research [21, 22].

Besides the surface structures, the fine structure of the fibers could also play a significant role in the performance of the filter media. The fine structure of any material and also the fiber refers to the study of molecular arrangements. As it has been discussed in Section 29.3.1, fibers are made of polymers, which are regarded as the macromolecules. Like any other material, for being solids, it has to have crystalline regions (with few exceptions like glass); however, due to the macromolecular nature, it would not have 100% crystallinity but less than anything below, generally ranging about 30–60% for apparel and technical grade fibers and about 60% to <100% for high-performance grade fibers. Though the high degree of crystallinity would be preferred for a good mechanical performance, but it may not be preferred to have very high degree, leading to 100% as it would seriously affect the other unique properties of textile fibers such as the flexibility, extensibility along with elasticity, etc. [5]. Therefore, the semicrystalline nature of the fiber is the inherent advantages of the fibers meeting the functional requirements of a filter media and also for other textile-related applications. So, the partly crystalline and partly amorphous arrangements of the fibers form the fine structural aspects of the fibers.

Based on various parameters, polymer molecular arrangements in the fibers are depicted by two distinct models, namely, fibrillar model and micellar model as shown in Figure 29.3. The major difference in these two types of arrangements of polymer molecules inside the fiber is based on the length of the polymer chain. If the polymer chain is long like in the case of natural fibers and in high-performance fibers, they would run over relatively to a long distance inside the fiber, and hence, they would not form a definite short-range ordered structures but long-range orders in the fiber structures. In contrast, the micellar type of arrangement is for the short polymer chain. As the short chains cannot run over a long length, many chain ends could be seen in the amorphous regions. Moreover,

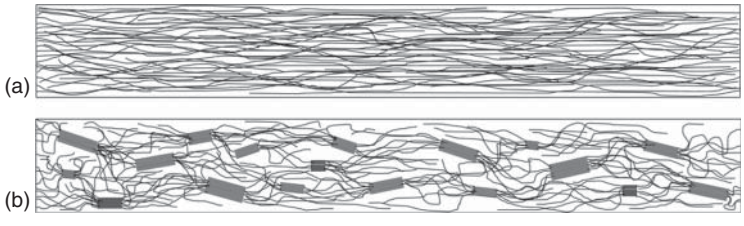


Figure 29.3 Fine structure models of fibers: (a) fibrillar model and (b) micellar model.

due to the relative high degree of freedom and movements, the short chains can adjust themselves to associate with the nearby polymer molecules, leading to a definite short-range order that is perceived as the clear crystalline regions [5].

Fibers belonging to these two models differ distinctly in their properties. Those belonging to fibrillar models exhibit good strength, modulus, and less extension with elasticity. In the case of natural fibers belonging to cellulosics, such arrangement is also one of the causes for increasing wet strength. The fibrillar model could be perceived as amorphous region dispersed in the ordered region, while the micellar model could be perceived as the crystalline regions dispersed in the amorphous regions. This implies that fiber belonging to micellar models would have high amorphous contents, while the fibers belonging to fibrillar model would have high crystalline/ordered regions. Hence the micellar model fibers would have generally low mechanical properties but would have good extensibility, flexibility, and good absorption. In filtration applications, the fine structure of the fiber would influence in terms of various property requirements. For example, if the filtration requires molecular absorption for the removal of the intimately mixed substance, then the choice of fiber would be from those belonging to the micellar model as it would have good absorption. However, if the filtration requirement emphasis is much on the mechanical properties, then the choice would be from those fibers belonging to fibrillar models.

It is evident that fibers remain as the only preferred material choice for various applications because of the aforementioned number of unique properties such as the fineness and flexibility along with the mechanical, thermal, chemical, and environmental properties. Particularly, the various possible fine and ultra/nano-fine sizes and the surface and fine structural aspects of fibers make them as good raw materials in the development of filter media. In Section 29.4, applications of fibers in various filtration applications would be discussed.

29.4 Forms of Fibrous Substrates for Filtration

Various forms of fibrous have been developed over a period of time for technical applications. Some of them are fiber assembly itself stuffed within a perforated cage, roving (it is a bulky strand of fiber twisted together with few twists/inch, an intermediate product prior to yarn formation), yarn, and fabrics. Of these, filter media made of fabrics find more applications as they can be used directly without special preparation as it would be required with rovings and yarns. There are different types of fabrics such as interlaced (woven), interloped (knitted), and entangled (nonwoven) with distinct properties based on the methods of manufacturing. They are briefly discussed below for a comprehensive understanding.

29.4.1 Roving and Yarns

The process of conversion of fiber into yarn is called as spinning process, which involves various stages. The yarn is produced in the final machine called ring

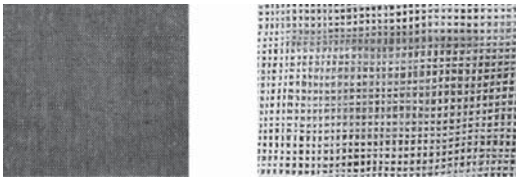


Figure 29.4 Cartridge filter media made of roving. (a) Roving package and (b) cartridge filter made of roving.

frame, which is the most popular way of manufacturing yarn. The feed material to this machine is the roving and is a bulky strand of fiber twisted together with few twists/inch, an intermediate product just prior to yarn formation. Such rovings could be wound in a particular pattern for obtaining the filter media for filtration applications (Figure 29.4). These kinds of filters are used in cartridge filters with the micron range of 0.5–100 μm. The filtration solution could be passed across the either inward to outward or outward to inward so that the mixed phase could be removed during the flow of the fluid through the media. These kinds of structures have its own advantage and disadvantages because of which the other types of fibrous filter media based on fabrics have become the choice. The main advantage of these kinds of filter would be that it would be suitable where the cylindrical type of filter media is preferred, and also on economical view point, these kinds of filter media are produced at a much earlier stages of fabric conversion (except the entanglement type of fabric), and so it may be cheaper. The possible disadvantages of these kinds of filters would be poor filtration performance due to preferential orientation of the fiber in the rove and yarn, and also there are chances for distorted shortcut flow of the fluid through the least resistant path as a result of structural distortion, which is more susceptible in these kinds of filter media.

29.4.2 Interlaced Fabrics

The fabrics made by interlacement of yarn through weaving machine are called woven/interlaced fabrics. Interlacement of yarns involves set of threads, one running along the length of the fabric, called as warp yarns, and the other one running across the fabric, called as weft yarns. Such threads interlace one over the other, and based on the type of interlacement, the fabric basic structures are classified as plain and twill, for which there are further derivatives such as matt, basket weaves as plan derivatives and satin, and sateen as twill derivatives. Apart from the weave structure aspects, the thread spacing that is expressed as EPI for warp yarns and PPI for weft yarns greatly governs the openness. Another important parameter of fabrics is called cover factor, derived from yarn size and thread spacing, also a measure of the openness of the fabric. Simple plain weave union fabrics with same yarn characteristics and thread spacing have the highest thread interaction for a given cover factor of the fabric. Schematics of fabrics are shown in Figure 29.5. Based on requirements of filter media fabric the types of openness required, various fabric parameters such as thread spacings, yarn count, and interlacement



(a) (b)

Figure 29.5 Interlaced fabric structures: (a) high cover factor and (b) low cover factor.

pattern could be altered. This type of filter media would have good mechanical properties and would be more appropriate for surface filtration.

29.4.3 Nonwovens

Nonwovens are a kind of fabrics made directly from fibers without undergoing the various intermediate processes of yarn and fabric manufacture. The process involves preparation of fibrous web through various techniques and then bonding the fibers by any one of the methods like mechanical, chemical, and thermal means based on the type of fiber and possibilities. Various methods of nonwoven preparation machines are available like needle punching machine for mechanical interlocking of fibers, wet laid nonwoven machine for chemical bonding, and spun bonding nonwoven machine for thermal bonding for thermoplastic polymer fibers. Essentially the fabrics of this type greatly differ from the fabrics made from interlacement in terms of mechanical properties, bulkiness, and porosity. For a given GSM of the fabrics, the mechanical strength of the interlaced fabrics would be the strongest as the fibers are well aligned in these structures compared with the nonwovens where the fibers are weakly bound comparatively. Due to the same factor of poor compact binding of fibers in the nonwoven, the nonwoven fabrics are bulkier and thicker for a given GSM, and hence, they would have more free space in its structure that makes it suitable for depth filtration. The mean flow pore ratings (MFPs) of typical nonwoven fabric for filtration media range from 1 to 500 μm. For the MFP of 15 μm and below, the fabric needs calendaring. Typical forms of the bulky nonwovens are shown in Figure 29.6. Because of the large porosity and the thick structures, the nonwoven fabrics could be used as effective filter media for depth filtration involving various types of filtration mechanisms.

29.4.4 Interloped Fabrics

Typical interloping patterns are shown in Figure 29.7. Figure 29.7a shows the interloping by weft knitting machine, and Figure 29.7b shows the microscopic view of the surface of the weft knitted fabrics, which indicate the presence of the



Figure 29.6 Needle-punched nonwoven.

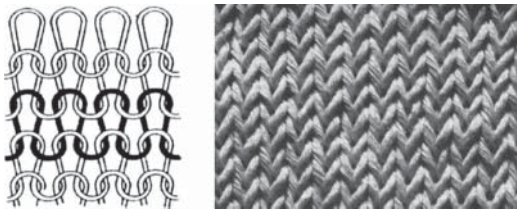


Figure 29.7 Interloped structures: (a) weft knitted structure and (b) microscopic view of weft knitted fabric surface.

looping pattern. As far as filtration is concerned, knitted structures find limited applications where there would be a need to undergo structure expansion of the media in order to take up the pressure fluctuations and protect the media failure and to regulate the pressure drop. However, such expansions could alter the physical dimensions of the interstices, affecting the filtration. Hence, this might be taken care if sufficient cake has formed to an extent that the filtration is actually effectuated by the cake rather than the fabrics. At this stage, the fabric mainly takes up the role of providing the support for the cake and undergoes extension as stated above. These structures are mainly used in air/dust filtrations.

29.4.5 Fibrous Membranes

Membrane is a substance characterized by very fine in thickness of the order of micron, and nanodimensions, flexible, have required mechanical, chemical, and temperature resistance. With the recent advent of technology developments in nanofiber spinning, one of the successful outcomes is the nanofibrous webs, which could be considered as the fibrous membranes with very fine pores for filtration purposes. Many research works have been initiated and reported in these areas that are discussed and presented in Section 29.5. Elsewhere the effect of nanoparticle-assisted nanomembrane filtration has been reported as an effective means of treating textile effluent water [23].

29.5 Fibers in Filtration Applications

Selection of the right fiber considering their material properties is the prime importance in filter fabric designing. As shown in the textile fiber classifications, many of the fibers belonging to the classifications like the natural fibers such as cotton and wool, man-made regenerated fibers like viscose rayon, and synthetic fibers like polyamides (nylons), polyesters (PET) (aromatic high-performance polyesters), polyolefins (polypropylene, polyethylene), glass (fiberglass), aramids (Nomex, Kevlar), and fluoropolymers (polytetrafluoroethylene [PTFE]) are used for filtration applications. Such textile filters are used in various areas such as metallurgical industries, foundries, cement industries, chalk and lime plants, brick works, ceramic industries, flour mills, medical, pharmaceutical, acoustics and screen printing, workshops, manufacturing halls, control stands to offices, schools, aerospace, automotives, bioclean, disk drives, flat panels, food, hospitals, medical devices, pharmaceuticals, and other electronics. In all these

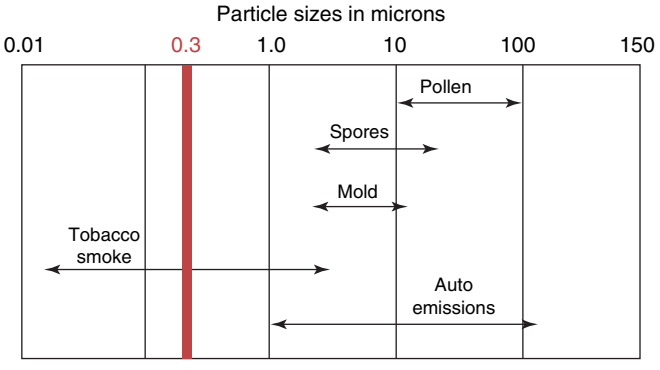


Figure 29.8 Typical class of particles and their physical size.

applications, the contaminants remain mostly in the form of particles whose typical size values are presented in Figure 29.8. It is claimed that the Bosch HEPA Premium Cabin Air Filters provide filtration efficiency of 99.97% at 0.3 μm [24].

Because of the typical nature of textile fibers being fine and flexible along with the other basic thermomechanical and chemical resistance, almost all the textile fibers are suitable candidates for all kinds of filtration in general. However from the historical perspective, before the advent of man-made/synthetic fibers, the natural fibers such as cotton and wool have been used for the development of filter media. Apart from the basic fineness and flexibilities, these two fibers are known for its inherent natural surface roughness and pores due to the polymeric fibril arrangement inside the fiber structures as shown in Figures 29.9 and 29.10 [25, 26].

In addition to the structural nonuniformity, these two fibers are known as the strong hydrophilic fibers, i.e. cotton has moisture regain of 8%, while the wool has 17% moisture regain. Such difference in moisture regain is because of the difference in the polymer molecules in cotton and wool, which are cellulose and protein, respectively. The cellulose molecules contain 6 –OH groups per repeat unit, and the wool protein has about 18 different amino acids in –R as side groups corresponding any one of the groups belonging to acidic, basic, hydroxyl, and hydrophobic type. Of the 18 amino acids, the major amino acids present in

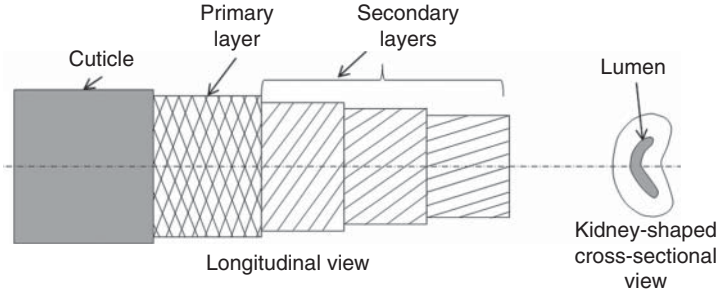


Figure 29.9 Structure of cotton fiber.

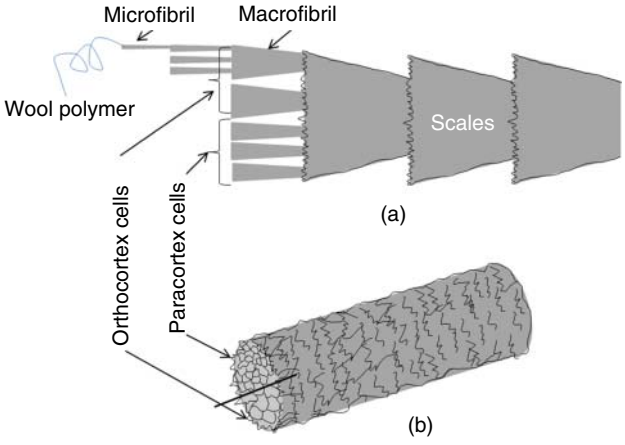


Figure 29.10 Schematic of wool fiber. (a) Scale and fibrils and (b) macroscopic rough surface.

wool fiber are glutamic acid (12%), cystine (11%), serine (10%), glycine (8%), and leucine (7.7%).

The difference is also due to the difference in the degree of crystallinity as in cotton it is 65% while in wool it is only 35%. Because of the structural complexity, wool has low crystallinity and high amorphous region, and hence, wool has high moisture regain. The moisture regain has a practical importance in terms of the diffusion of the water in the structures developed of these fibers. Generally the hydrophilic fibers would have a molecular absorption and transmission, while the hydrophobic fibers would have only surface-level adsorption and transmission as it is regarded as wicking. Additionally, such moisture properties also in general would facilitate biodegradation through the microorganisms. Hence such considerations while selecting the filter media fiber are important based on the kind of substance in the mixture to be separated and the disposal of the filter media.

However, some of the limitations of these fibers in filtration applications were the operating temperature and abrasion resistance. These fibers could be used only up to a temperature of 100 °C and had only average abrasion resistance. Of these two fibers, wool could withstand moisture very well and could be made into a thick felt due to the directional frictional effect.

After the advent of man-made and synthetic fibers, they were preferred the most as a result of improved properties with reference to temperature resistance and chemical and microbial stability. One of the most widely used synthetic fibers is the fiberglass or glass fiber. Some of the main properties that make them to be used in the filtration applications are the high temperature stability >1000 °C and chemical resistance along with the required mechanical properties. Additionally, fiberglass is comparatively cheap due to its raw material, the sand. The major chemical composition of the glass fiber is silica, generally above 50% with other inorganic oxides for the rest. The polymeric form of the silicon dioxide gives a random fine structural arrangement imparting the isotropic characteristics to the glass fiber unlike the other textile fibers that are anisotropic. Such inorganic polymeric fine structure form is responsible for the unique properties of the glass

fiber to be used in all the applications and particularly for high temperature (up to 255 °C for continuous operation) and chemical-resistant filtration applications. The glass fibers are lubricated with graphite so that it would not break as a result of rubbing action during handling and cleaning cycle. Graphite is used as lubricant because it can withstand the high operating temperature.

Further invention of the other synthetic fibers in the early twentieth century gave wide options of fibrous materials for developing filter media with techno-economical considerations. Nylon, the first synthetic fiber, has good abrasion resistance and so is more effective in filtering abrasive dusts than the other synthetic fibers invented later. However, nylon is considered to perform poorly under the acidic conditions and also with exposure to light and environment. Polyethylene terephthalate (PET) polyester fiber has superior acid and light resistance in addition to a comparable abrasion resistance. Hence the PET fiber is also used widely in many industrial filtration applications such as foundries, smelters, etc. However, PET is sensitive to alkali and so its use in alkaline environment should be avoided. Polypropylene being chemically more resistant than the other synthetic fibers is also an inexpensive fiber and hence is used in many industrial filtration applications. However, it is limited in its use only to low temperature conditions as its melting point is only 130 °C. The use of polypropylene fiber, in nonwoven form as against the existing roving form as cross-wound package form for textile industrial effluent treatment, has been studied. The study revealed that the nonwoven form resulted in similar particle filtration with lower pressure drop [27].

The synthetic fibers can also be physicochemically modified compared with glass fibers, which makes them more suitable for filtration applications [28]. Because of these multifunctional feasibilities in synthetic fibers, they are mostly preferred. Only on the ground of ecofriendly and sustainable products, natural fibers gain some importance [28]. Moreover, for healthcare applications natural fibers are preferred. For example, Texus Fibre, New Zealand, has created a range of filtration products for personal protective respirators such as face masks and home air purifiers using wool fiber [29]. The regenerated cellulosic fiber, viscose rayon, finds notable applications in filtration for filter paper applications where controlled porosity is required. This fiber has an irregular cross section, by virtue of the fiber formation, and hence it can provide high specific surface area. It is used in food filtration as the fiber is physiologically as well as hygienically safe and is having neutral taste [30]. Similarly, for milk filtration also, the natural fibers are preferred along with the combination of synthetics as a blend, which better meet the requirement of milk filtration than the individuals. The fiber combinations used for the purpose are cotton, viscose, and polyester [31]. As far as the bast fibers like jute and flax are concerned, they are being explored for potential applications. They are already in use for the purpose in geotextiles; however, their main stream use in filtration applications is yet to emerge on the ground of sustainable solutions [27].

Development of high-performance grade textile fibers that exhibit high degree of thermal, mechanical, and chemical properties has also led the way for their use in filtration applications that demand high continuous operating temperatures, which cannot be just met by the aliphatic organic polymer-based fibers, i.e. nylon, polypropylene, PET, etc. Nomex is one such aromatic polyamide fiber

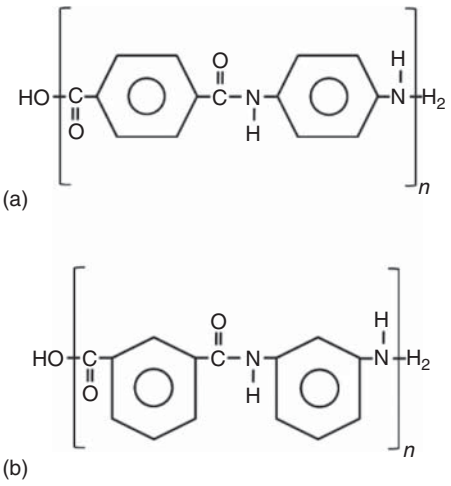


Figure 29.11 Chemical repeat unit structure of (a) Kevlar (poly-paraphenylene terephthalamide) and (b) Nomex (poly-metaphenylene isophthalamide).

whose chemical name is poly(*m*-phenylene isophthalamide), which is regarded as *meta*-aramid fibers. The Nomex, by trade name, fiber has high temperature stability having limiting oxygen index of 30, T_g of 275 °C, and T_m of 430 °C. Because of these thermal parameters, the Nomex fiber is used for continuous high temperature filtration applications like for filtering dusts from cement coolers, asphalt batch plants, ferroalloy furnaces, and coal dryers. The other well-known aramid is para-aramid fiber, which is known as Kevlar that has high mechanical properties, because of the para links, along with the thermal properties even higher than Nomex. Hence Kevlar can also be used for high temperature filtrations particularly even under certain mechanical strength requirements. The chemical structures of Nomex and Kevlar are shown in Figure 29.11, which are responsible for their superior properties.

Teflon, Ryton, P84, and carbon fibers are some of the other high-performance fibers, which are used for very high temperature filtrations. In addition to temperature stability, Teflon exhibits a very high resistance to acids (except fluorine) and can perform continuously up to 230 °C. Ryton is made from polyphenylene sulfide polymer fiber attached to a polyfluorocarbon scrim. It has good resistance to both acids and alkali and performs continuously at 177 °C. Teflon, Nomex, and Ryton have been used in coal-fired boilers to remove particulate emissions [32].

The use of membrane as a laminate over the fibrous structures has proved to be effective in filtrations. One such effective membrane is the expanded PTFE developed by the Gore-Tex. It has been stated that such structured filtrations used in metal industries, chemical industries, food industries, and coal-fired boilers result in very good emission reduction (99.9%), low pressure drops, increased bag life, and higher air to cloth ratio. Ceramic fibers are also very much found in filtration applications particularly for continuous very high temperature applications of >500 °C like in filters ahead of boiler superheater tube sections in order to remove particles and improve heat transfer in the boiler tubes [33].

Various fibers used in filtration applications and their properties are listed in Table 29.1. Based on these properties, one or more than one materials in combinations could be used for designing the filter bags based on the thermomechanical and chemical requirements. In one of the 1992 reports, the cost

Table 29.1 Fibers used in filtration applications and their properties [32–34].

Generic name	Fiber	Density (g/cc)	Maximum temperature		Resistance to					Tensile strength	Relative cost
			Cont.	Surge	Acid	Alkali	Flex abrasion resistance	Oxidizing agent	Hydrolysis		
Natural fiber	Cotton	1.54	82	107	Poor	Excellent	Average	—	—	Good	0.4
Polyolefin	Polypropylene	0.91	95	93	Excellent	Excellent	Good	Poor	Good	Excellent	0.5
	Polyethylene	0.95	85	—	Excellent	Excellent		Poor	Good	Excellent	—
Natural protein	Wool	1.36	93	121	Good	Poor	Average	—	—	Poor	0.8
Polyamide	Nylon	1.14	93	121	Poor to fair	Excellent	Excellent	Poor	Fair	Excellent	0.6
Acrylic	Orlon	1.20	116	127	Very good	Fair	Average	—	—	Excellent	0.7
Polyester	Dacron	1.38	135	163	Good	Fair	Excellent	Fair	Poor	Excellent	0.5
Aromatic polyamide	Nomex	1.14	204	218	Fair	Very good	Very good			Very good	2.0
Fluorocarbon	Teflon	—	232	260	Excellent[a)]	Excellent[a)]	Fair	—	—	Average	6.7
Glass	Fiberglass	2.58	260	260	Good	Poor	Poor to Fair	—	—	Excellent	1.0
Polymer	P84	—	232	260	Good	Fair	Fair	—	—	—	2.5
Polymer	Ryton	—	191	232	Excellent	Excellent	Good	—	—	—	2.5–4.0
Polymer	PBI	1.43	300	—	Very good	Very good	—	—	—	Average	—
Polymer	PBO	1.56	250	—	Excellent	Excellent	—	Good	Good	Excellent	—
Vinyl polymer	PVDC	1.70	85	—	Excellent	Good	—	Excellent	Good	—	—
	PVDF	1.78	100	—	Excellent	Excellent	—	Good	Excellent	—	—
	PTFE	2.10	150+	—	Excellent	Excellent	—	Excellent	Excellent	—	—
	PPS	1.37	150+	—	Excellent	Excellent	—	Fair	Excellent	—	—
	PVC	1.37	80	—	Excellent	Excellent	—	Fair	Excellent	—	—
	PEEK	1.30	150+	—	Good	Good	—	Fair	Excellent	—	—

PBI, polybenzimidazole; PBO, polybenzoxazole; PVDF, polyvinylidene fluoride; PTFE, polytetrafluoroethylene; PPS, poly(phenylene sulfide); PVC, polyvinylchloride.
a) Teflon acid resistance, excellent except poor for fluorine; Teflon alkaline resistance, excellent except poor for trifluoride, chlorine, and molten alkaline metals.

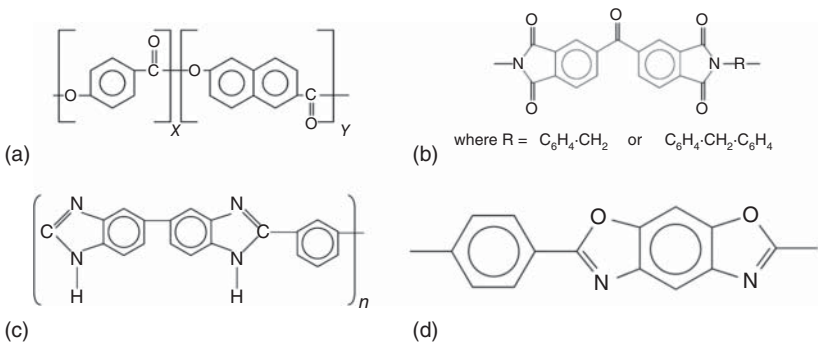


Figure 29.12 Chemical structure of some of the high-performance fibers for filtration applications. (a) Aromatic polyester (Vectron), (b) polyarimids (P84), (c) polybenzimidazole (PBI), and (d) polybenzoxazoles (PBOs, Zylon).

difference between fiberglass and Teflon filter bags could be noticed as much difference as about 220% [34]. The cost of a fiberglass bag 14 ft long and 6 in. in diameter is approximately $35–40, while the same size Teflon bag costs about $115–135. Hence, that the same size filter bag made of Teflon is about 220% higher than the one made of fiberglass. Chemical structure of some of the high-performance fibers is shown in Figure 29.12.

29.6 Factors Governing the Performance of Fibrous Filter Media

29.6.1 Role of Cross Section of the Fiber

Filtration application requires high surface area for a given volume so that the filter media could have large contact with the incoming fluid and have maximum particle contact. This would improve the particle filtration efficiency based on the principles of filtration. In general, natural fibers are having some irregularities over the surface except silk. However, synthetic fibers produced through melt spinning, in general, have round cross section because of the spinneret orifice. Of various mathematic geometries, round/sphere has the least circumference/surface area for a given diameter/volume. When the round and spherical shape is modified immediately, the circumference/surface area would increase according to the degree of cross-sectional deviation from round. These fibers are generally regarded as multilobed structures such as trilobal, octolobal, tape, diabolo (different solid shapes), channeled surface (Coolmax, Gcool), hollow, and bicomponent cross sections. Different types of noncircular cross sections of fibers along with their respective spinneret shapes are shown in Figure 29.13. Figure 29.14 shows the various types of bicomponent fibers produced for especially built-in properties.

Man-made fibers with irregular cross sections are used in filtration applications with some value-added functions [35]. It is reported that the multilobed cross-sectional fiber assists the particle and molecular filtration probably due to

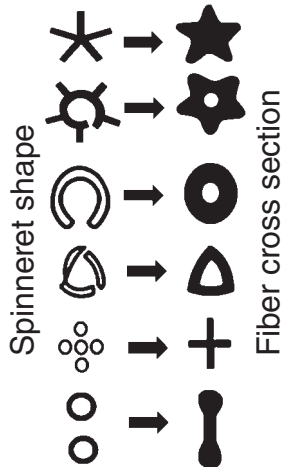


Figure 29.13 Various types of fiber cross sections along with the respective spinneret shapes.

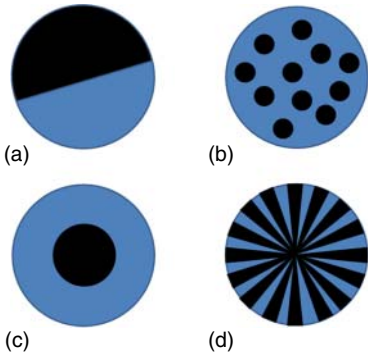


Figure 29.14 Types of bicomponent fiber: (a) side by side, (b) sea island, (c) core–sheath, and (d) splittable.

the increased surface area [36]. Active agents like acid or alkaline components are placed on the longitudinal slots of the multilobed fibers. These reactants react with the molecular and particle contaminants and fix them with the substrate. Such reagents could also be incorporated through some adsorptive particles in the slots of the fibers. In Cornell University, researchers have tried to study the Y fiber combinations on the packing density and found low packing density with relatively large area to volume ratio for triple Y fiber combinations. Such fiber combinations help particle trapping by Brownian motion [37].

Special channeled polyester fibers named as 4DG™, as one of the members of the Capillary Channel Polymer™ (CCP™), have many unique fiber geometries and have 2.3–2.8 times higher surface area compared with same denier round fibers because of the deep groove fibers with eight surface channels as shown in Figure 29.15 [38].

The CCP fibers have been used in tobacco smoke filters as its large surface channels could hold high content of tobacco smoke-modifying agents, such as flavorants [39]. Hence the channeled geometry could be an efficient way of capturing particles, and these kinds of structures are promising in filtration research [38].

Figure 29.15 Cross-sectional image of CCP™ fiber.



29.6.2 Role of Pore Size

The bulk properties of the filter media would depend on the type of material, the fibers used for its development, and hence the factors/properties of fibers are of importance in this context. Such properties of fibers mainly influence the kind of filtration applications, efficiency, and the durability of the filter media. For example, if the filtration requirement is to remove particles from hot chemicals, the choice of the fiber should be such that it has both chemical resistance and temperature resistance along with the high degree of chemical inertness even under hot conditions. This is an extreme example for which the fiber choice could be a fiberglass; however, for only chemical filtrations, the inert olefin fibers could be considered but not under hot conditions as they are sensitive to heat. Similarly fibers with high degree of mechanical performance such as strength, elongation, creep, and modulus might be required for pressure filtrations under ambient and elevated temperature conditions. Accordingly, the properties of fibers could be grouped and could be regarded as factors governing the choice and the performance of the fibrous filter media. The relevant properties of fibers can be classified as morphological properties, mechanical properties, thermal properties, chemical properties, and resistant properties to various environmental factors such as sunlight, microbes, and reactive particles in the atmosphere. There are other properties of textile fibers that might have an indirect influence on the filter media such as the moisture properties and electrical conductive properties [5, 26].

The morphological properties can be further subdivided into macromorphological properties and fine morphological properties and have notable influence on the filtration performance. Particularly, the macromorphological properties would decide the kind of pore surface profiles that has direct influence on the particle interaction. The other properties such as the mechanical properties could cover range of properties such as the strength, specific strength, modulus, elongation, elasticity, dimensional stability, abrasion resistance, creep, and stress relaxation. The mechanical properties are considered the most as it governs many of the filtration requirements. Thermal properties are mainly important to maintain the structural dimension under the intended working temperature.

Similarly, the other properties like chemical resistance are important, which again depend on the inherent nature of the polymer molecule. In this case the chemical groups involved in the polymer chains are expected not to respond in any one of the possible chemical reaction mechanisms such as the electrophilic–nucleophilic reactions and redox and free radical reactions. Polymer chains without any polar functional groups but with only the alkyl chains like polyethylene and polypropylenes are considered to have good resistance

to these kinds of chemical reaction mechanisms, and so they are considered good for chemical filtrations. Apart from this the polymers with cyclic structure, cross-linked structures, and high activation energy are also considered to have good chemical resistance along with the thermal resistance.

Generally, the microbial resistance of fibers made of artificial polymers like polyester (PET), nylon, acrylic, and other high-performance fibers is considered good and better than the natural fibers like cotton, silk, wool, etc. The possible reason could be not as simple as those given for thermal and chemical resistance but could be regarded as complex by virtue of the inherent growing and multiplying tendency of the microbes over the natural substances than those on the man-made substances. The other properties such as the resistance to sunlight and reactive particles in the atmosphere are also indirectly related with the chemical and thermal resistance. The properties like moisture and electrical properties do have a notable influence based on the type of filtration applications. In general, moisture properties impart the filter media to work with the principle of interaction with moisture in the incoming fluid at a molecular level and ensure moisture separation, for example, the removal of moisture from diesel in using cellulosic diesel filters. The electrical properties in turn influenced by moisture govern the kind and the quantity of surface charges, which might affect the particle through similar and opposite charge interaction effect, resulting in enhanced and/or selective particle separation.

29.7 Characterization of Filter Media

Characterization of filter media is a vast topic and could vary based on the particular applications. However, broadly, it can be listed as the dimensions, stiffness, mechanical properties such as tensile, tear strength, burst strength, elongation, and elasticity; density, porosity, pore size and structure – bubble point, mean flow pore size, image analysis, microscopy, X-ray microtomography, liquid extrusion porosimetry, liquid intrusion porosimetry, gas vapor adsorption; pressure drop, filtration efficiency – single pass, multi-pass efficiency, cumulative and fractional efficiency, dust loading capacity, cake release properties, etc. Some of the other properties are the moisture properties, formaldehyde contents, air permeability, fold endurance, water repellency, flammability and resistance to chemicals, redox reactions, and bacterial attack [13, 40, 41].

Standard test methods for these parameters have been established by many global organizations, some of which are the American Association of Textile Chemists and Colorists (AATCC); American National Standards Institute (ANSI); American Society of Heating, Refrigerating and Air-Conditioning Engineers (ASHRAE); ASTM International (ASTM); BSI British Standards (BSI); German Institute for Standardization (DIN); European Disposables and Nonwovens Association (EDANA); US Environmental Protection Agency (EPA); US Food and Drug Administration (FDA); Association of the Nonwoven Fabrics Industry (INDA); International Organization for Standardization (ISO); Japanese Standards Association (JSA); etc. Based on the country and the seller–buyer

interest, any one of the methods could be followed. The standard numbers under each of the organizations could be found in the respective web pages and are also summarized by Irwin M. Hutten [3].

29.8 Future Prospects

With the increasing thrust on technical textiles and technology developments, the need for filter media is increasing. With the matching material properties, textile fibers are found to be suitable candidates to prepare the filter media through any one form. Most suitable form in many cases is the nonwoven form as it turns out to be techno-economically viable. Among the varieties of fibers and the choices available, certainly the end-use application requirements have to be considered, and a suitable fiber has to be chosen accordingly. For general applications polypropylene, polyester (PET), and nylon are used; however, when the filters are expected to perform at high temperatures, the high-performance grade fibers may be preferred. Nowadays with the global emphasis on ecofriendly and sustainable products, natural fibers are also being revived for filtration applications. As of now, the global market potential for filtration nonwoven textiles is estimated to be $5.4 B with the market share as shown in Table 29.2 for each category of applications.

Among various filtration applications, automotive industry, water purification systems, and indoor air conditioning systems (heating, ventilation, and air conditioning [HVAC]) are the three major areas of applications. Healthcare industry and manufacturing industry requirements also go beyond 10% each. The other minor areas are the advanced technological sectors, hydrocarbon processing, and food and beverages.

With increasing use of commodity products, the need for filtration media is going to increase with higher rate ever year. Textile fibers along with the existing suitable properties, further feasibilities for modifications and functionalization based on the ever-increasing requirements makes them suitable ideal material for the filtration media, and hence their consumption would also be high.

Table 29.2 Market potential for filtration textiles.

Market application	Market share (%)
Transportation	22
Water filtration	20
HVAC	14
Food and beverage	2
Healthcare	11
Manufacturing	10
Advanced technology	6
Hydrocarbon processing	5

References

1 Hearle, J.W.S. (2001). *High-Performance Fibres*. New York: Woodhead Publishing Ltd.
2 Sundarrajan, S., Tan, K.L., Lim, S.H., and Ramakrishna, S. (2014). Electrospun nanofibers for air filtration applications. *Procedia Engineering* 75: 159–163.
3 Sutherland, K. (2008). *Filters and Filtration Handbook*, 5e. New York: Butterworth-Heinemann, Elsevier.
4 Tanchis, G. (2008). *The Nonwovens – Reference Books of Textile Technologies*. Italian Trade Commission.
5 Morton, W.E. and Hearle, J.W.S. (2008). *Physical Properties of Textile Fibres*. England: The Textile Institute, Woodhead Publishing Limited.
6 Purchas, D. and Sutherland, K. (2002). An introduction to filter media. In: *Handbook of Filter Media* (eds. Derek B Purchas and Ken Sutherland), Chapter 1, 2e, 1. Elsevier Advanced Technology. ISBN: 1856173755.
7 Chen, T., Wu, C., Liu, R. et al. (2011). Effect of hot vapor filtration on the characterization of bio-oil from rice husks with fast pyrolysis in a fluidized-bed reactor. *Bioresource Technology* 102 (10): 6178–6185.
8 Darby, J.L. and Lawler, D.F. (1990). Ripening in depth filtration textiles: effect of particle size on removal and head loss. *Environmental Science and Technology* 24 (7): 1069–1079.
9 Holdich, R.G., Cumming, I.W., and Smith, I.D. (1998). Crossflow microfiltration of oil in water dispersions using surface filtration with imposed fluid rotation. *Journal of Membrane Science* 143 (1–2): 263–274.
10 Sioutopoulos, D.C. and Karabelas, A.J. (2012). Correlation of organic fouling resistances in RO and UF membrane filtration under constant flux and constant pressure. *Journal of Membrane Science* 407–408 (15): 34–46.
11 Raoul, B. (1957). Pressure filters. US Patent 2, 799, 397 A.
12 Matteson, M.J. (1986). *Filtration Textiles: Principles and Practices*, 2e. CRC Press.
13 Hutten, I.M. (2007). Testing of nonwoven filter meida. In: *Handbook of Nonwoven Filter Media* (ed. Irwin M. Hutten), Chapter 6, 245–290. Elsevier Science and Technology.
14 Eichhorn, S., Hearle, J.W.S., Jaffe, M., and Kikutani, T. (2009). *Handbook of Textile Fibre Structure: Fundamentals and Manufactured Polymer Fibres*, vol. 1. Elsevier.
15 UNITEX (1971). Textile Fibres: Classification by Type – Terms and Definitions. Constitution.
16 Eichhorn, S., Hearle, J.W.S., Jaffe, M., and Kikutani, T. (2009). *Natural, Regenerated, Inorganic and Specialist Fibres*, vol. 2. Elsevier.
17 Gupta, V.B. and Kothari, V.K. (2012). *Manufactured Fibre Technology*. Springer Science & Business Media.
18 Wisniowski, M.-T. (2017). General properties of fiber polymers and fibers macro properties – Part V. http://artquill.blogspot.in/2013/08/general-properties-of-fiber-polymers.html (viewed 17 April 2017).

19 Yasuda, T. and Fujiwara, Y. (1970). Method of forming microfibers. US Patent 3, 549, 734 A.

20 Mukhopadhyay, A. and Choudhary, A.K. (2013). Performance of filter media as function of fibre fineness in pulse jet filtration system. *Textiles and Light Industrial Science and Technology (TLIST)* 2 (1): 13–26.

21 Periyasamy, S., Gupta, D., and Gulrajani, M.L. (2007). Nanoscale surface roughening of mulberry silk by monochromatic VUV excimer lamp. 103 (6): 4102–4106.

22 Periyasamy, S., Krishna Prasad, G., Chattopadhyay, S.K. et al. (2017). Micro-roughening of polyamide fabric using protease enzyme for improving adhesion strength of rubber-polyamide composite. 37 (3): 297–306.

23 Naidu, L.D., Saravanan, S., Goel, M. et al. (2016). A novel technique for detoxification of phenol from wastewater: nanoparticle assisted nano filtration (NANF). *Journal of Environmental Health Science and Engineering* 14 (9): 1–12.

24 BOSCH Invented for Life. HEPA premium cabin filter, USA. www .boschautoparts.com. (Accessed 18 April 2017)

25 Koushik, C.V. (1979). *The Helical Structure in the Secondary Wall of the Cotton Fibre*. University of Strathclyde. Department of Fibre Science.

26 Hearle, J.W.S. and Peters, R.H. (2013). *Fibre Structure*. Elsevier.

27 Harshavardhan, G., Kavin, P., and Krishnan, A. (2015). Development of non-woven filter for textile effluent filtration. B.Tech Project Work Thesis. Guided by Dr. G. Thilagavathi, Department of Textile Technology, PSG College of Technology.

28 Skomra, E. (2010). Production and characterization of novel air filtration media. All Dissertations. Paper 683. Clemson University, TigerPrints.

29 Texus Wool Fibre (2017). Natural Fibres That Improve Human Health, 111a Kerwyn Ave, East Tamaki, Auckland, New Zealand. http://lanaco.co.nz/texusfibre/assets/File/Texus_Brochure_August2015.pdf (viewed 18 April 2017).

30 Wimmer, P. and Zacharias, J. (2015). Viscose speciality fibres – bio-based fibres for filtration. *Filtration & Separation* 52 (3): 36–39.

31 Delaval. Efficient milk filtration. DeLaval International AB, 2008, Borosilicate Glass Fiber Filters Applications by Grade, Sterlitech Corporation, USA. www .sterlitech.com. (Accessed 18 April 2017)

32 Belba, V.H., Grubb, W.T., and Chang, R.L. (1992). The potential of pulse-jet baghouse for utility boilers. Part 1: A world-wide survey of users. *Journal of the Air and Waste Management Association* 42 (2): 209–218.

33 McKenna, J.D. and Turner, J.H. (1989). *Fabric Filter-Baghouses I, Theory, Design, and Selection*. Roanoke, VA: ETS.

34 Mohurle, N. and Thakare, N.R. (2013). Analysis on fabric filtration material for pulse jet fabric filter. *International Journal of Emerging Technology and Advanced Engineering* 3 (6): 603–609.

35 Zhang, W. and Yao, L. (2016). Review of the patented electrostatic air filter-materials and designs controlling technology. *BAOJ Nanotech* 2 (1): 9.

36 Rohrbach, R., Bause, D., Unger, P. et al. (2008). Complex shaped fiber for particle and molecular filtration. US Patent 7, 442, 223, B2.

37 Zhu, H. and Hinestroza, J.P. (2009). Collection efficiency for filters with staggered parallel Y and triple Y fibers: a numerical study. *Journal of Engineered Fibers and Fabrics* 4 (1): 16–25.
38 Vaughn, E. and Ramachandran, G. (2002). Fiberglass vs. synthetic air filtration media. *Journal of Engineered Fibers and Fabrics*: 41–53.
39 Phillips, B.M., Wilson, S.A., and Pollock, M.A. (1994). Tobacco smoke filter. US Patent 5, 356, 704.
40 Jena, A. and Gupta, K. *Characterization of Pore Structure of Filtration Media*. New York: Porous Materials, Inc.
41 Pike, R.D., Lassig, J.J., Shipp, P.W. Jr., and Williams, B.J. (2001). Nonwoven filter media. US Patent 6, 169, 045 B1.

30

Fibrous Materials for Thermal Protection

Gouwen Song[1] *and Yun Su*[2,3]

[1] *Department of Apparel, Events and Hospitality Management (AESHM), Iowa State University, Ames, IA 50011, USA*
[2] *College of Fashion and Design, Donghua University, Shanghai 200051, China*
[3] *Key Laboratory of Clothing Design and Technology, Donghua University, Ministry of Education, Shanghai 200051, China*

30.1 Introduction

Thermal hazardous environments are manifold and depend on the type of fire ground, for example, residential, manufacturing, wild land, storage, or mercantile fire [1]. Firefighters while exposed to fires and thermal environments encounter not only with the fatal injuries but also with nonfatal injuries, such as skin burn injuries, strain, bruise, and smoke or gas inhalation [2]. It is estimated that every year over 30 000 firefighters suffer injuries on the job in United States and many of them lose their lives while fighting fires, rescuing people, or responding to hazardous material incidents [2, 3]. Although extensive efforts have been dedicated to improve the health and safety of firefighters, this profession continues to be one of the world's most dangerous industries [4].

According to some reports [5, 6], thermal environmental conditions were usually identified as routine, hazardous, and emergency. An emergency thermal environment generally appears in a flashover condition that the temperature can rise above 600 °C with a heat flux range of 20–209.34 kW/m^2. Firefighter in this thermal environment has several seconds to react [7]. The routine and hazardous thermal environments can be defined as low-level radiative heat exposure, and the corresponding heat flux ranges from 5 to 20 kW/m^2 [5]. Even though the intensity of heat exposure does not cause the thermal degradation of protective material for longtime exposure, the majority of burn accidents occur in these thermal exposure situations [8, 9]. Therefore, in order to minimize or prevent fatal and nonfatal injuries from possible accidents, firefighters are required to wear protective clothing that is characterized by flame retardance and thermal insulation [10]. However, it is reported that thermal protection provided from thermal protective clothing is determined by various factors, such as fabric properties, air gap size, moisture content, and garment design. Additionally, the development of the proper type of fibrous materials is absolutely vital for the improvement of thermal protective performance of clothing against various heat exposures.

Handbook of Fibrous Materials, First Edition. Edited by Jinlian Hu, Bipin Kumar, and Jing Lu.
© 2020 Wiley-VCH Verlag GmbH & Co. KGaA. Published 2020 by Wiley-VCH Verlag GmbH & Co. KGaA.

In this chapter, an overview of the literature on performance requirements of thermal protective clothing is presented. Also, fibrous materials suitable for thermal protection are summarized in detail, including structure, properties, and theories. Assessment methods of thermal protective performance and applications of fibrous materials are discussed. The effect of various factors on thermal protective and comfort performance of clothing is reviewed. Finally, the future trends for thermal protection are given in order to develop advanced thermal protective clothing that can provide better occupational health and safety for firefighters.

30.2 Performance Requirements of Thermal Protective Clothing

According to standard NFPA 1971-97 and EN 469-05, a typical firefighting ensemble is usually composed of three different fabric layers, i.e. an outer shell, a moisture barrier, and a thermal liner (including a layer of apertured, closed cell foam and a layer of facecloth fabric). In order to minimize the flame burn, contact burn, and steam burn or scald, protective clothing should provide effective thermal and moisture protection from flash fires, high-intensity thermal radiation, and hot liquid and steam. The development in firefighting protective clothing changes the protective requirements from the single thermal hazard to multiple thermal hazards, attaching importance on human ergonomics and comfort. Thus, performance requirements of each layer fabric are presented in Figure 30.1.

The outer shell is designed to provide flame resistance, protection against heat radiation, and resistance to water and certain levels of abrasion, since the outer shell is directly exposed to flame, radiation, hot liquid, and hot steam. Thus, blended fabrics are generally selected as the outer shell in order to meet these performance requirements and reduce cost of production. The preferred fiber is constructed of a flame- and heat-resistant material, such as woven aramid and polybenzimidazole ("PBI," a trademark of Celanese Corp.) fibers. Commercially

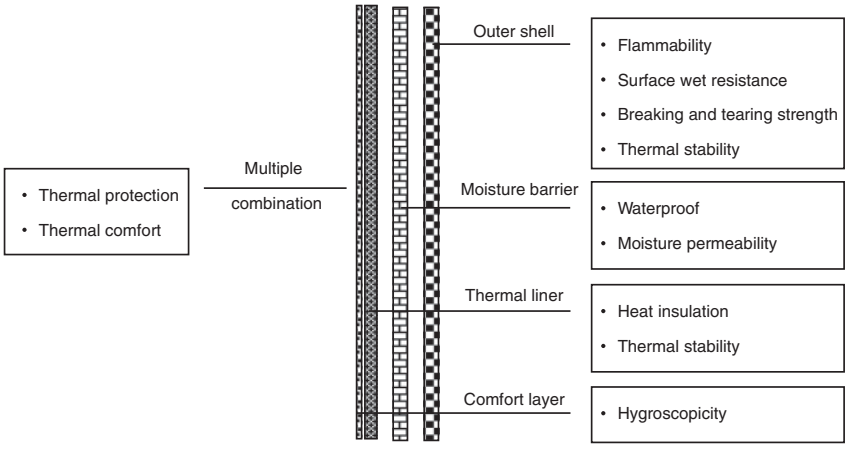


Figure 30.1 Performance requirements of thermal protective clothing.

available aramid materials mainly include Nomex and Kevlar (both are trademarks of E.I. DuPont, Inc.).

The vapor barrier is intended to protect the firefighter from steam and harmful chemicals. It was reported from the etiology of injuries to firefighters that flame burns just caused injury to 20% firefighters, while 65% patients received steam burns or scalds, especially for the poor sealing regions of clothing (such as the neck and hand) [11]. In addition, thermal protective clothing while providing thermal protection for wearer also brings about thermal stress due to the collection of moisture in the thermal liner and friction between the outer shell and the thermal liner layers. The design of moisture barrier also promotes water vapor transport outwardly from the wearer, which reduces wet weight gain from sources of moisture [12]. A moisture barrier commonly consists of a semipermeable membrane bonded or laminated to a fabric substrate, e.g. GORE-TEX (a trademark of W. L. Gore & Associates, Inc.). It was reported that GORE-TEX is a microporous polymeric film of polytetrafluoroethylene (PTFE), with pore volumes reaching 82% and maximum pore sizes of 0.2 μm [13]. Even though PTFE is hydrophobic, the extremely large number of pores and the thinness of the film allow the diffusion of gases [14]. Such moisture barriers are impermeable to liquid moisture but allow water vapor to pass through.

The thermal liner acts as an insulating medium against heat conduction, as well as providing thermal comfort for wearer. In order to reduce conduction heat transfer from thermal environment to human body, a thermal liner is typically made of a batting of aramid fiber quilted to a woven facecloth of spun yarn fiber. This is because the fabric structure can increase the amount of embedding air within thermal liner and reduce clothing weight to weaken the wearer's stress. The aramid fiber preferably is made of a flame- and heat-resistant material, such as Nomex and Kevlar. The preferred yarn fiber is fire-resistant cotton or viscose in order to provide better thermal comfort.

30.3 Fibrous Materials Suitable for Thermal Protection

Fire-retardant fibers can be classified into two types: chemically modified flame-resistant fiber and inherently flame-resistant fiber. The chemically modified flame-resistant fibers, including natural and synthetic fibers, are produced by a textile finishing process depending on the properties of flame retardant. The inherently flame-resistant fiber has special molecular structure to get high decomposition temperature, such as *meta*-aramid and *para*-aramid. The burning behavior of fibers is often determined by thermal transition temperatures and thermodynamic parameters, such as softening and melting temperature, and rate of heat release. The rate of heat release determines burning hazard, indicating the rate of fire spread and severity of burns. Table 30.1 shows the transition temperatures and thermodynamic parameters of the commonly fibrous materials. It can be found that the inherently flame-resistant fibers have higher thermal transition temperature compared with most fibers chemically modified flame retardant, since they have different mechanisms of flame resistance. The limiting oxygen index (LOI) of inherently flame-resistant fibers is more than 29%, meaning that they possess better flammability.

Table 30.1 Thermal transition of the commonly fibrous materials.

Category	Fiber type	Softening temperature (°C)	Melting temperature (°C)	Pyrolysis temperature (°C)	Igniting temperature (°C)	LOI (%)	Heat release rate (kg/J)	Flame-resistant mode
Chemically modified flame-resistant fiber	Cotton	—	—	350	350	18.4	19	Chemical finish
	Wool	—	—	245	600	25	27	
	Viscose	—	—	350	420	18.9	19	Additive introduced
	Polyester	80–90	255	420–447	480	20–21	24	Copolymeric modifications
	Nylon	50	215	431	450	20–21.5	39	
	Acrylic	100	>220	290	>250	18.2	32	
	Modacrylic	<80	>240	273	690	29–30	—	
Inherently flame-resistant fiber	*meta*-Aramid	275	375	410	>500	29–30	30	Acromatic homo- or copolymer
	para-Aramid	340	560	>590	>550	29	—	
	PBI	435	—	580	>600	>41	—	
	Kermel	285	—	411	—	30–32	—	

Source: Horrocks et al. 1988 [15]. Reproduced with permission of Taylor & Francis.

30.3.1 Chemically Modified Flame Retardant Fibers

Chemically modified fire-retardant fibers include natural (e.g. cotton, wool, and viscose) and synthetic fiber (e.g. polyester, acrylic, and nylon). There are various kinds of methods to improve the flame resistance of fibrous materials. Some flame retardant additives, such as halogen, nitrogen, silicon, and phosphorous, are usually incorporated into the spinning dopes during the manufacture of fire-resistant fibers [16]. Also, flame-retardant finishes can be applied on the surface of natural or synthetic substrate fibers. Generally speaking, these fire-resistant mechanisms involve in three aspects of burning behavior: fuel (from thermally degraded or pyrolyzed fibers), heat (from ignition and combustion), and oxygen (from the air), as described in Figure 30.2 [17].

The principles to improve flame resistance of fiber can be recognized as solid/condensed and gas/vapor phase (see Figure 30.3) [18, 19]. These flame-retardant strategies are related to combustion mechanism of fibrous materials, as can be seen from Figure 30.2. The solid/condensed phase strategies are to reduce the absorbed thermal energy from degradation reaction (a) or increase decomposition temperature by inserting inherently flame-resistant fibers (b). However, the most effective flame-retardant methods are to promote char

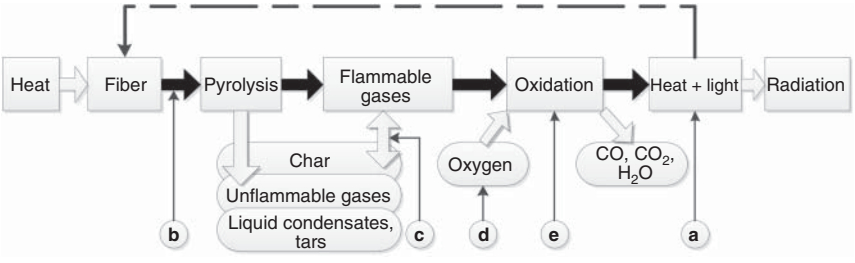


Figure 30.2 Combustion mechanism of fibrous materials.

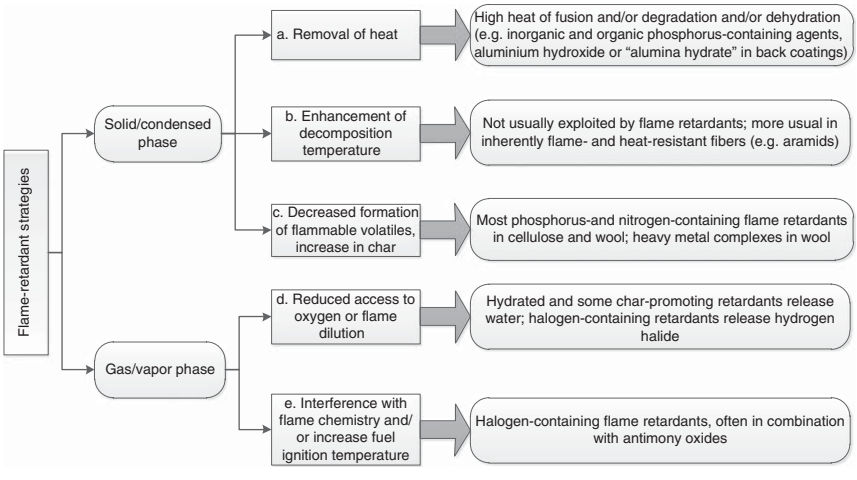


Figure 30.3 Flame-retardant strategies of fibrous materials.

formation by converting the organic fiber structure to a carbonaceous residue or char and hence reduce volatile formation (Figure 30.2c). Therefore, char-forming flame retardants offer both flame and heat resistance to a textile fiber. For example, most phosphorus- and nitrogen-containing retardants, when present in cellulose and wool, promote char formation and reduce volatile formation during heat exposure. In addition, the existence of elements like nitrogen and sulfur is known to enhance synergistically the performance of phosphorus-containing retardants by further increasing char-forming tendencies [19]. With regard to the gas/vapor-phase strategies, the flame-resistant principle is to affect the oxidation reaction of fibrous materials (see Figure 30.2). For one thing, hydrated and some char-promoting retardants can release water, while halogen-containing retardants produce hydrogen halide. These compounds can reduce the access to oxygen or flame dilution by forming protective barrier on the fiber surface (d) [20]. For another, the flammable gases generated from decomposition reaction can react with oxidation, which contributes to decrease the amount of oxygen used in combustion reaction (Figure 30.2e). The LOI of fibrous materials has an increase due to the reduced access to oxygen and increase of the igniting temperature.

All flame-retardant cottons are usually produced by after-treating fabrics chemically, depending on chemical character and cost of flame retardant. A textile finishing process also yields flame-retardant properties having varying degrees of durability to various laundering processes. The most effective flame retardants contain either phosphorus or antimony–bromine-based systems [19], such as Flacavon WP and Flacavon F12/97 (Schill & Seilacher), which can be applied to cotton fibers for improving the flammability. But this generates a perception of unacceptable environmental hazard and may cause wear casualties due to the inhalation of the toxic gases produced when the fibers catch fire.

Among the area of flammability of all the natural fibers, wool fiber has the highest inherent non-flammability and the pyrolyzing temperature. It has a relatively high LOI value of about 25% and a low flame temperature of about 600 °C. But wool fiber is not suitable for thermal protective clothing, since the pyrolyzing temperature is relatively low of around 245 °C. In order to meet performance requirement for thermal protection, zirconium hexafluoride complexes can be used to chemically finish wool fiber, such as Zirpro (IWS), Pyrovatex CP (Ciba) and Aflammit ZR (Thor).

The conventional synthetic fibers may be provided flame resistance during production by either incorporation of a flame retardant additive in the polymer melt or solution prior to extrusion. Also, the method of copolymeric modification can be used to improve fire retardance of synthetic fibers. Synthetic fibers produced in these ways are often said to be inherently flame retardant. However, the absence of polyamides reflects their high softening and melting reactivities and hence poor flame-retardant compatibilities. No char-promoting flame retardants exist for any of the conventional synthetic fibers so that it is not easy to offer high-performance flame and heat resistance.

30.3.2 Inherently Flame Retardant Fibers

The flame-retardant effect in chemically modified flame-retardant fibers can be reduced after several washing. However, the inherently flame-retardant fibers

have fundamentally combustion-resistant structures (i.e. all-aromatic polymer) that can better resist heat and flame for long-term usage. According to Table 30.1, most of inherently flame-retardant fibers decompose above 375 °C or so. Their all-aromatic structures are responsible for their low or non-thermoplasticity and high pyrolysis temperatures. In addition, their low flammabilities are dependent on their high char-forming potentials and LOI values.

Since high-performance *meta*-aramid was successfully developed by DuPont in the early 1960, Nomex fiber has been widely used for military, aerospace, and fire-fighting industry [21]. *meta*-Aramid possesses good tensile and other mechanical properties. The presence of aromatic groups can provide high thermal stability and flame resistance (see Figure 30.4). There has no aging under heat exposure of 220 °C for long time. The thermal transition temperatures of fiber are greatly more than that of the commonly natural and synthetic fibers (see Table 30.1). The char begins to form up to 400 °C, while the fabric can char quickly for high temperature of 900–1500 °C and thus lead to the increase of thickness to provide better thermal protection for wearer.

However, Nomex fiber easily shrinks when exposed to high-intensity heat flux, which can reduce thermal protective performance of protective materials. In order to avoid the drawback, Nomex fiber is usually blended with Kevlar fiber that has better strength and abrasion resistance, such as a blend of 95% Nomex and 5% Kevlar fibers [22]. Kevlar fiber developed by DuPont (Kevlar) and AKZO (Twaron) in the 1970s is one of *para*-aramid. The structure of *para*-aramid is given in Figure 30.5. The main difference between *meta*- and *para*-aramid is the positions of the aromatic groups along the backbone chain. Thus, *para*-aramid fibers comprise extreme symmetry within its polymer chains and have greater interchain links and crystallinity to provide higher tensile strength, rigidity, and moduli. Also, *para*-aramid fibers are high heat- and flame-resistant material. According to Table 30.1, its transition temperatures are larger than that of *meta*-aramid fibers. There exist no flame spread, shrinking, and melting phenomena when exposed to flash fire, which is appropriate for thermal protection.

Development work on aromatic PBI was conducted in 1960s. Later, PBI was used by NASA and the Air Force Materials Lab to make the astronaut's clothing. In 1983, the PBI fibers were manufactured commercially by Celanese Corporation [23, 24]. Figure 30.6 presents the molecular structure of PBI polymer. Table 30.1 shows that the decomposition of PBI in air occurs at

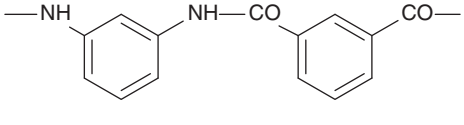


Figure 30.4 Structure of *meta*-aramid.

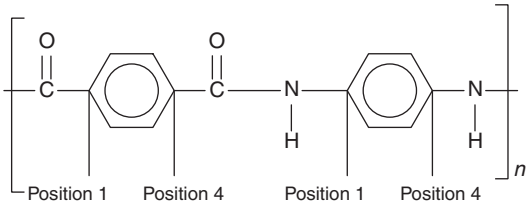


Figure 30.5 Structure of *para*-aramid.

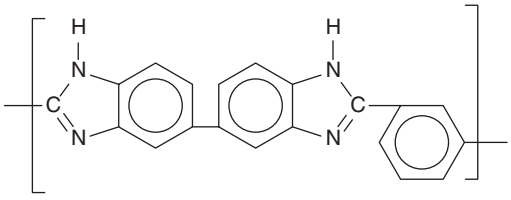


Figure 30.6 Structure of PBI polymer.

approximately 580 °C and the fiber can withstand high temperatures without severe loss of mechanical properties. In an inertial atmosphere, the temperature of weight loss occurs at 600 °C [25]. Long-term temperature aging can lead to rapid loss of mechanical properties owing to oxidative degradation, while PBI can durably maintain its properties in temperatures as low as −196 °C. The LOI value of PBI fiber is more than 41%. In addition, PBI is typically resistant to organic acids, chlorinated solvents, and strong acids. Due to the several attractive properties, such as high glass transition temperature, chemical resistance, and retention of good mechanical properties, PBI has been popularly used in high-performance polymer blends. PBI was generally introduced as an outer shell protective fabric that is typically composed of 40% PBI and 60% *para*-aramid.

Other popular type of *meta*-aramid fiber is poly(aramid-imide) fiber, like Kermel fiber. The molecular structure of poly(aramid-imide) consists of a high proportion of aromatic groups and combined double bonds (see Figure 30.7) that is similar with Nomex. Kermel fiber was developed by Rhone-Poulenc of France in 1971. The thermal properties of Kermel is also approximate to Nomex fiber, providing durable flame resistance even if for washing of 200 times. Meantime, Kermel fiber possesses excellent heat insulation and presents no melt and afterflame for long-time exposure of 250 °C. The Kermel fiber is developed through polycondensation of toluene diisocyanate and trimellitic anhydride [26]. A distinction of Kermel fiber is the circular transverse section that makes fabric soft for providing good comfort. The combustion of Kermel fiber just generates a small amount of smoke and toxic products, which is far less than most natural and synthetic fibers. But the Kermel fiber is commonly combined with cotton or viscose due to the expensive production costs. The most typical blended fabric is 50% Kermel and 50% flame-resistant viscose (Lenzing from Austria), which has excellent flame retardance and comfort.

Also worth mentioning is polybenzoxazole (PBO) from Dow Company in United States and Zylon (Toyobo), which comprises poly(*p*-phenylene-2 and 6-benzobisoxazole), as shown in Figure 30.8. The PBO fiber is a high modulus and high tenacity fiber that are about twice as high as respective values for

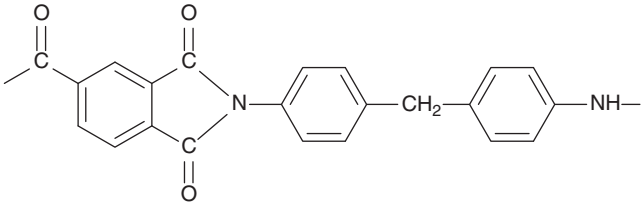


Figure 30.7 Structure of polyamide-imide.

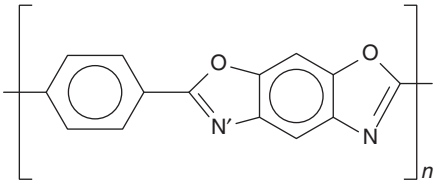


Figure 30.8 Structure of polybenzoxazole fiber.

meta-aramids and *para*-aramids [27]. Its LOI value is around 68%, which is far superior to other flame-retardant fibers. Liu et al. [26] compared the thermal property of three kinds of high-performance Kermel, Kevlar, and PBO. The results demonstrated that PBO fiber has the highest thermal degradation temperature. The initial temperatures of decomposition are, respectively, 556.5 °C (PBO), 464.2 °C (Kevlar), and 411.2 °C (Kermel). The mechanical property retention of PBO when heated is higher for providing a very high thermal stability compared with Kevlar and Kermel.

30.4 Performance Standards and Evaluation Method Development

The protective performance of fabric or clothing can be evaluated based on the laboratory simulation methods. Many related assessment standards and methods have been developed in recent decades. The evaluation of fibrous materials for potential use in thermal protective clothing generally involves two steps. First, the fibrous materials are tested to ensure their ability of flame resistance and thermal stability. Flammability test is carried out to evaluate this performance of protective materials that directly determine if the protective materials are suitable for thermal protection. Second, thermal protective performance of protective clothing should be evaluated for confirming the ability of resisting heat transfer, including conduction, convection, and radiation.

30.4.1 Flammability Test

Flammability is defined as the relative ease of ignition and relative ability to sustain combustion. The burning behavior of fabrics is influenced by a number of factors, such as the nature of the igniting source and time of its impingement, the fabric orientation and point of ignition (e.g. at the edge or face of the fabric or top or bottom), the ambient temperature and relative humidity, and the velocity of the air and fabric structural variables [19]. For flammability evaluation, various standardized test methods have been developed. The commonly evaluation methods include LOI, forty-five degree flammability test, vertical flammability test, and smoke concentration test.

The LOI is widely used to characterize the flammability of fibrous materials. The LOI represents the minimum volume percent of oxygen in a mixture of oxygen and nitrogen that can support flaming combustion of a material at 23 ± 2 °C. LOI is usually measured based on benchtop tester, as shown in Figure 30.9. A small test specimen is supported vertically by specimen holder. A mixture

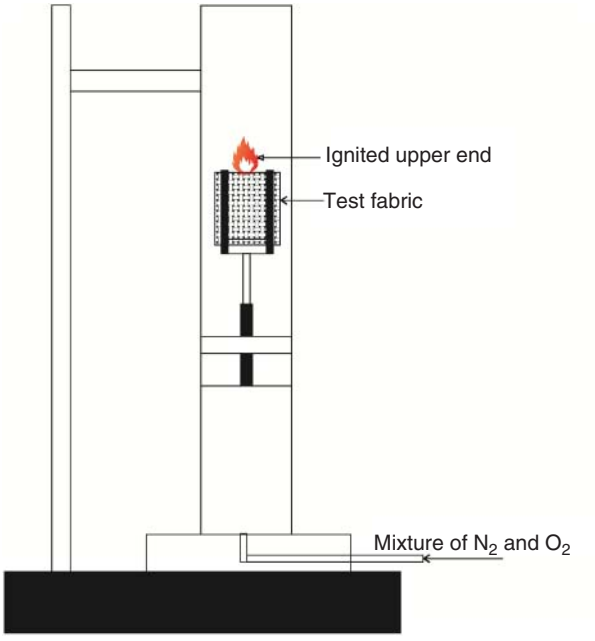


Figure 30.9 Frame design of LOI test apparatus from ASTM D2863.

of oxygen and nitrogen with 23 ± 2 °C is flowed upward through a transparent chimney at a rate 40 ± 2 mm/s. A flame igniter that consists of a tube with an inside diameter of 2 mm is inserted into the chimney to ignite the test specimen. The period for which burning continues and the length of specimen burnt is observed during each burning. By testing a series of specimens in different oxygen concentrations, the LOI is determined by gas measurement and control system. The larger LOI value means that the test specimen is characterized by better flammability and thermal stability. According to the LOI value of fibrous materials, the burning behavior can be divided into two types: fire-retardant fiber (LOI $\geqq$ 26%) and inflammable fiber (LOI $<$ 26%). The LOI value of the commonly fire-resistant fibers is given in Table 30.1.

LOI, while it proves to be a very effective indicator of ease of ignition, has not achieved the status of an official test within the textile field. This is because the sample ignition occurs at the top to give a vertically downward burning geometry, which is considered to be unrepresentative of the ignition geometry in the real situation. Furthermore, the exact LOI value is influenced by fabric structural variables for the same fiber type and is not single-valued for a given fiber type or blend [28]. However, it finds significant use in developing new flame retardants and optimizing levels of application to fibers and textiles.

The flammability of textile fabrics can be evaluated according forty-five degree and vertical flammability test as well (Figure 30.10), specified, respectively, by standard ASTM D1230 and ASTM D3659. According to standard ASTM D1230, a test specimen with 50 by 150 mm is held in the flammability tester at an angle of 45°. A standardized flame is applied to the surface near the lower end for

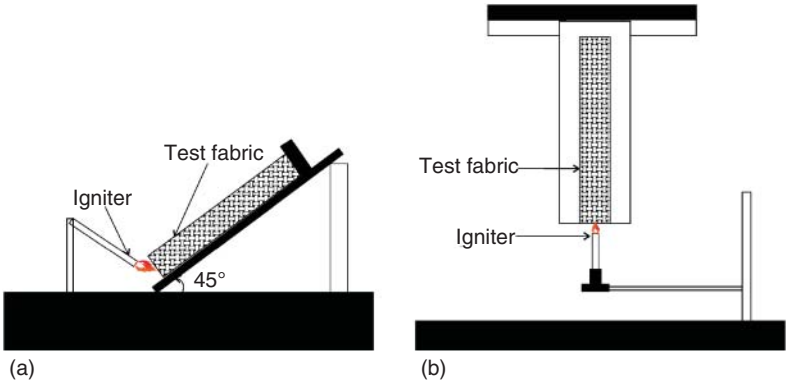


Figure 30.10 (a) Forty-five degree and (b) vertical flammability test apparatuses.

1 ± 0.1 seconds. An automatic electric timer is used to record the required time for the flame to spread up the fabric for a distance of 127 ± 0.2 mm, as an index of assessing the flaming degree of fibrous materials. The subsequent burning behavior of the specimen, such as ignites, chars, melts, or fuses, is observed to judge the ease of ignition and flammability.

Compared with forty-five degree flammability test, vertical flammability test is carried out for assessing the flammability properties of fabrics in a vertical configuration. The bottom edge of test specimen is ignited for three seconds using a small, open flame that can simulate the flaming process of an A-line-type garment on a manikin [20]. The afterflame and afterglow times are measured during the exposure. After the exposure, mass loss and char length of test specimen is calculated and used as an indicator of the material's ability to support combustion. In actual fire scenario, firefighter can be in a flame to perform emergency rescue so that protective clothing can be ignited at any angle. Therefore, the flammability properties of fabrics are extremely important for protecting them from flame exposure. In addition, protective clothing can be used to resist the spread of fire, or firefighter keeps a certain distance with an open fire. In view of the situation, the thermal insulation of protective materials that is the ability to resist convective, conductive, and radiative heat transfer is particularly important. Therefore, thermal protective performance of flame-retardant materials should be further evaluated.

30.4.2 Thermal Protective Performance Evaluation

Thermal protective clothing can resist heat transfer from thermal environment to human body. Thermal protective performance provided by clothing is directly related to worker's safety. Thus, assessment of thermal protective performance has a significant impact on the selection of protective materials. The laboratory simulation methods can be used to evaluate thermal protective performance of fabric or clothing, such as the benchtop tests [29–39] and the full-scaled manikin tests [40, 41], as shown in Table 30.2. The tested specimen is usually exposed to the simulated thermal environmental conditions, such as flame, thermal

Table 30.2 Standards for evaluating thermal protective performance (TPP) of clothing.

Standard	Test apparatus	Heat source	Evaluation index
NFPA 1971-2007 [33]	TPP test device	50/50 radiant/convective heat flux of 84 kW/m^2	TPP
ASTM F2700-2008 [36]	TPP test device	50/50 radiant/convective heat flux of 84 kW/m^2	HTP
ASTM F2703-2008 [38]	TPP test device	50/50 radiant/convective heat flux of 84 kW/m^2	TPE
NFPA 1977 [32]	RPP test device	100% radiant heat flux of 84 kW/m^2	RPP
ASTM F1939-2008 [35]	RPP test device	100% radiant heat flux of 21 and 84 kW/m^2	RHR
ASTM F2702-2008 [37]	RPP test device	100% radiant heat flux of 21 and 84 kW/m^2	RHP
ASTM F2731-2011 [39]	SET test device	100% radiant heat flux of 8.5 ± 0.5 kW/m^2	MET
ASTM F1060-2008 [34]	Hot contact tester	Hot surface with a temperature up to 360 and a pressure of 3 kPa	Skin burn time
ISO 6942-2002 [30]	RPP test device	100% radiant heat flux ranging from 20 to 80 kW/m^2	TF and RHTI
ISO 17492-2003 [31]	TPP test device	50/50 radiant/convective heat flux of 80 kW/m^2	TPI and HTI
ISO 9151-1995 [29]	Flame exposure apparatus	Flash fire of 80 kW/m^2	TF and HTI
ISO 13506-2008 [40]	Instrumented manikin	Flash fire of 84 ± 2.5 kW/m^2	Skin burn degree and burn area
ASTM F1930-2011 [41]	Instrumented manikin	Flash fire of 84 ± 2.5 kW/m^2	Skin burn degree and burn area

radiation, and hot surface. The thermal sensor at the rear of specimen records thermal histories in the process of heat exposure, which can be used to calculate the heat transfer rate through fabric (ISO 6942-2002 and ISO 17492-2003) or the required time to cause skin burn (NFPA 1971, ASTM F1939-2008, and ASTM F1060-2008).

30.4.2.1 Benchtop Testing

In the past decades, most researchers used TPP test device and RPP device to assess thermal protective performance of protective materials that are, respectively, confirmed with standards NFPA 1971 [33] and NFPA 1977 [32] (see Figure 30.11). The Stoll criterion developed by Stoll and Chianta [42] is employed in these test methods that are suitable to characterize performance of materials used in protective clothing in 50/50 radiant/convective heat flux of 84 kW/m^2 and 100% radiant heat flux of 21, 42, and 84 kW/m^2. The TPP and RPP

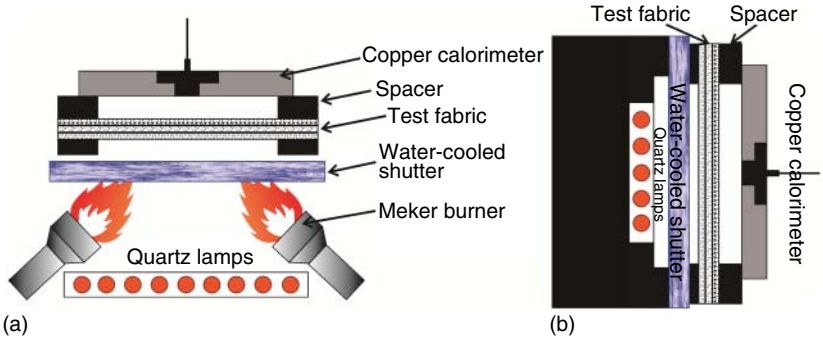


Figure 30.11 Thermal protective performance test apparatus. (a) TPP tester and (b) RPP tester.

values are employed to evaluate thermal and radiant protective performance, which can be obtained in Eq. (30.1):

$$\text{TPP/RPP} = \text{burn time} \times \text{calibrated burner or radiant heat flux value (cal/(cm}^2\text{ s))} \tag{30.1}$$

For meeting the performance requirement of standard NFPA 1971, a TPP rating of at least 35 is required for a fabric assembly used in firefighting protective clothing. It means that firefighter wearing this protective clothing can withstand a flash fire exposure (84 kW/m^2) for 17.5 seconds without causing second-degree burns. The RPP rating of fabric for thermal protection specified by NFPA 1977 is more than 20, which can provide 20 seconds protection time for firefighters under an approximately 42 kW/m^2 radiant exposure.

Although TPP and RPP tests have been widely used for characterize performance of materials, there are still many drawbacks. For instance, they are only suitable to copper disk calorimeter, constant heat flux intensity, and short-time thermal exposure as the measurement accuracy of metal sensors has a decrease tendency with prolonging duration time [10, 43, 44]. Furthermore, the discharge of the stored thermal energy in the fabric system after the exposure is not considered in the conventional TPP and RPP tests. Therefore, some new evaluation indexes have been put forward in order to effectively assess thermal protective performance of the clothing system.

As is described in Table 30.2, TPP, heat transfer performance (HTP), and thermal performance estimate (TPE) are used to evaluate thermal protection for the same heat exposure condition. The differences among the above three indexes lie in calculative methods of the second-degree burn time (see Figure 30.12). These calculative methods are based on Stoll criteria that speculate the relationship between thermal energy and tolerance time to second-degree burns under constant heat exposure level. Regarding to the TPP, it is defined as the relationship between the temperature rising worked out by a conversion equation according to ASTM E457 and second-degree burn time that is given by

$$T = 8.871t^{0.2905} + T_0 \tag{30.2}$$

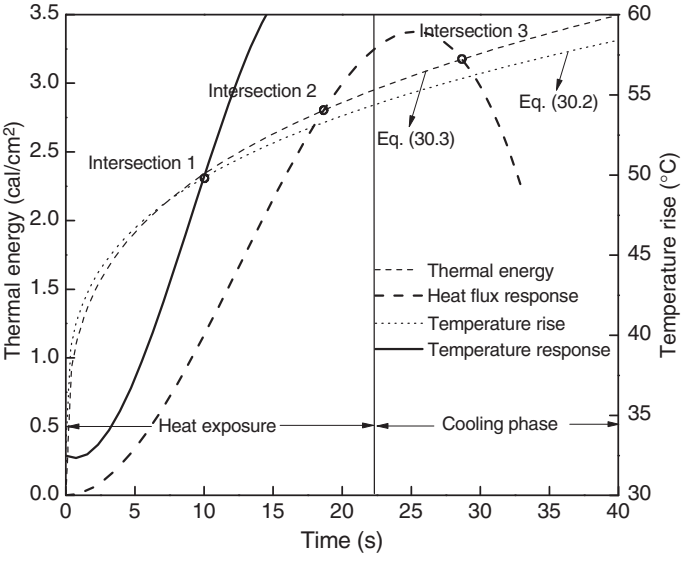


Figure 30.12 Comparison of different evaluation methods based on Stoll criteria.

where T_0 is the initial temperature of sensor. Its purpose is simpler to acquire second-degree burn injuries, but it is merely confined to the TPP sensors because different type sensors have different calculative formulas between the heat flux and the temperature. While the HTP is on the basis of the relationship between thermal energy transferred to human tissue and second-degree burn time, written as

$$q = 1.1991t^{0.2901} \tag{30.3}$$

therefore, the HTP has a larger range of application, which is not only for copper disk calorimeter but also for other sensors, e.g. skin-simulant sensor. But both the above two evaluation indexes are not used to investigate stored energy burns of skin tissues as the exposure duration does not include the cooling process. The TPE can be employed to account for skin burn resulting from the release of stored energy in clothing system during the cooling phase. That is to say, when there is merely an intersection between Eq. (30.2) and heat flux response curve in Figure 30.12, the obtained time is the burn time considering stored thermal energy. Compared with the TPP and the HTP, the TPE can provide the comprehensive skin burn data, including the heat transfer during heat exposure and stored heat transfer during cool down. In addition, a stored thermal energy test apparatus was employed to evaluate the transmitted and stored heat within fabrics under low heat flux conditions [39]. A new index called minimum exposure time (MET) was introduced to evaluate skin burn due to transferred and stored heat.

Other simple methods to assess thermal protection were developed without involving skin burn injuries, such as ISO 6942-2002, ISO 17492-2003, and ISO 9151-1995 (see Table 30.2). Among these standards, heat transmission factor (TF)

is the fraction of heat flux transmitted through a specimen exposed to a source of radiant heat, which is numerically equal to the ratio of the transmitted energy to the incident heat flux. In addition, heat transfer index (HTI) is the mean time in seconds to achieve a temperature rise of 12 ± 0.2 °C (or 24 ± 0.2 °C) when testing by this method with a specified incident heat flux density. Their principles are quite straightforward and suitable for all heat exposures owing to not involving skin heat transfer, but they are only used to rate the performance of different flame-retardant fabrics, not for assessing skin burns.

30.4.2.2 Full-Scaled Manikin Testing

Although these benchtop tests can effectively evaluate the heat transfer behavior of fabrics in various environmental conditions, it is extremely difficult to replace full-scaled manikin tests for evaluating thermal protection of the clothing. This is because manikin test can observe ignition and burning of the garment and heraldry, shrinkage or sagging in all directions after flaming, hole generation, smoke generation, and structural failure of seams. It can also be used to estimate the extent and nature of skin burn that a person would suffer if wearing the test garment under flash fire or radiant heat exposure. Thus, manikin experiments are great important tools to simulate the actual wearing state of clothing and present the heat and moisture transfer behavior in fire environment, protective clothing, and human body.

Over the years, full-scaled manikin test systems have been rapidly established for evaluating thermal protective performance of clothing. Most manikin test systems are employed to simulate a flash fire of 84 kW/m^2 using 8 or 12 propane gas torches, such as PyroMan of North Carolina State University [45], flame manikin Harry Burns of University of Alberta [46], and Thermo-Man of DuPont [47]. These manikins are tested in a standing position in initially quiescent air. Controlled air motion for simulating wind effects or body movement is not currently considered, but it is possible to move the manikin through a stationary flame. These manikins that represent an adult human using a flame-resistant, thermally stable, glass fiber-reinforced vinyl ester resin are equipped with more than 100 thermal energy sensors distributed uniformly within each area on the manikin surface. These sensor types mainly include copper, guarded copper slug, skin-simulant sensor, and embedded sensor, which can record the variation in skin temperature or heat flux over a preset time interval during and after heat exposure. These measurement data can be used to further calculate the time to cause second- or third-degree skin burn in different parts of human body and the overall percentage of burn area based on Henriques burn integral [48], as shown in Figure 30.13.

According to ASTM F1930-2011 and ISO 13506-2008, the test apparatus before dressing the manikin is essential to be calibrated. When the nude manikin is exposed to flames, the average exposure heat flux level is typically equal to 84 kW/m^2 with a standard deviation of 5%. A exposure duration with a range of 3–5 seconds is selected for the exposure of the dressed manikin, while the thermal sensors shall collect data for at least 60 seconds for ensuring the discharge of thermal energy stored in protective clothing.

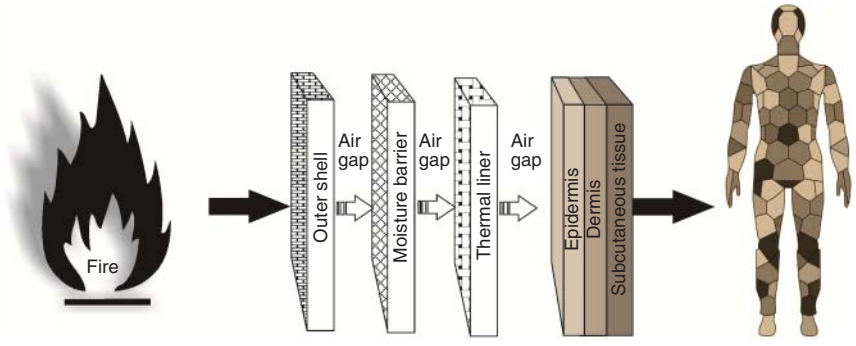


Figure 30.13 Thermal protective performance evaluation based on full-scaled manikin.

Even though the flash fire exposure is intense situation and extremely dangerous, most firefighters characteristically perform their duties at a relatively safe distance from the flame front and only require protection from low to moderate levels of radiant heat. Similar to flame manikin, RadMan test system was developed by North Carolina State University in order to evaluate radiant protective performance in a realistic radiant heat exposure that might be seen in the field for wildland firefighters [49]. As described in Figure 30.14, a radiant heat panel employed in RadMan system can produce a heat flux of 5–21 kW/m^2. The manikin is constructed of a metallic and fiber-layered structure for mimicking human skin. For further considering the effect of human physiology, a water-cooled system is introduced into RadMan skin surface to simulate the heat saturation and blood flow effects. Other than PyroMan, 70 RdF foil sensors are employed in RadMan system. This type of sensor can reduce the measurement errors for long duration exposure. By combining the skin heat transfer model and Henriques burn injury model, second- and third-degree burn times are obtained for evaluating the performance of clothing under a preset radiant heat exposure.

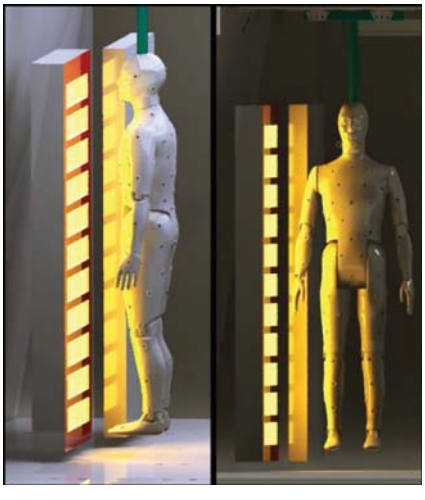


Figure 30.14 Thermal protective performance evaluation based on RadMan. Source: Watson 2014 [49]. Reproduced with permission of NC state university.

30.5 Influencing Factors of Thermal Protective Performance

Thermal protective performance of clothing is affected by fabric basic properties, such as physical properties and thermophysical properties [45]. Due to the specific geometry of human body shape and unique fabric properties, the air gap between the garment and human body is unevenly distributed over the body when the thermal protective clothing is worn on the human body [50]. Previous studies, including experimental investigation and numerical simulation, showed that the thermal performance of protective clothing also greatly depends on the air gap size [51, 52], the air volume [50], and the air gap position entrapped within the multilayer [53]. In addition, some studies indicated that moisture from high-humidity environment and body perspiration has a great influence on thermal protection as well [54]. The main reasons are that moisture can change thermophysical properties, such as thermal conductivity and specific heat capacity, and optical properties [55]. Moreover, moisture absorption/desorption and phase change can absorb or release a large amount of energy to affect heat transfer process in firefighter's clothing system, even resulting in skin steam burn or scald [10].

30.5.1 Effect of Fabric Basic Properties

Fabric physical properties play an important role in thermal protection of clothing, such as fabric structure, weight, thickness, porosity, and density. Many of these parameters are interrelated, and the dependence of protective performance of fabrics on these parameters is complex. These parameters can affect heat transfer rate in protective clothing, including conduction, radiation, and convection [56]. The convective heat transfer is generally ignored, since the porosity of fabric is enough small [57]. Conductive heat transfer in protective clothing mainly depends on thermal conductivity of fabric. Since thermal conductivity of air is so small (0.023 W/(m K) at 300 K) compared with most common insulating materials, the heat transfer rate can reduce if the air content embedded in clothing increases [58]. The radiative heat transfer is mostly determined by fabric's extinction coefficient that depends on fabric thickness and transmissivity [59]. Thus, thickness is the primary factor to determine thermal protective performance in radiant heat exposure and flash fire [60, 61]. A fabric with lower density and high weight can store more steady air to decrease conductive heat transfer [62, 63].

In addition, fabric's heat capacity affects thermal protection of clothing, as it can determine the capacity of storing thermal energy. During the firefighting operation, the thermal energy from the fire ground is transferred to the human skin through firefighting protective clothing, but a large amount of energy is stored in the clothing system [8]. The stored energy can be discharged to the ambient and the human skin in natural or forced ways due to body movement or external pressure after the exposure [64, 65]. It was reported that about 50% of the total energy to cause second-degree skin burn comes from the discharge of the stored thermal energy in the multilayer fabric under flash fire [9]. The

stored thermal burn can be reduced by increasing heat capacity or decreasing the discharged thermal energy to skin surface. Also, the optical properties of the fabric have an important influence on the thermal protective performance of firefighters' protective clothing, especially in intense thermal environments where radiation is the key mode of heat transfer in a fabric system with air gaps. Radiative heat transfer in a protective clothing is quite complex, involving absorbing, emitting, scattering, and transmitting [56]. The larger transmissivity and less reflectivity can increase the radiative heat transfer from the fabric system to the ambience and exacerbate skin burn.

30.5.2 Effect of Air Gap Size

The air gap size and volume between the clothing and human body can be obtained by using a portable three-dimensional (3D) body scanner [66]. The 3D images of the nude and clothed manikin can be captured and compared based on post-processing techniques. The results revealed that the air gap below the clothing is unevenly distributed, while the average air gap size in a protect clothing is approximate to 25 mm in real wearing situation [50]. The air gap size is dependent not only on the body shape but also on fabric properties and garment size [67].

Some researchers predicted that there exists an optimum air gap between the clothing and the body, which can provide the best thermal protection. Thus, different air gap sizes were employed to evaluate the thermal protective performance based on benchtop testers, such as TPP tester, RPP tester, and SET tester. It was found that the effect of the air gap size on thermal protection provided by the fabric system changed over the type of the heat source. For the flash fire of an 80 kW/m^2 heat flux, the rising of the air gap size could increase the thermal protective performance of flame-resistant fabrics [51, 52]. When the fabric system was exposed to an 84 kW/m^2 radiant heat flux, the thermal protective performance increased first and then reduced with the air gap size [68]. Furthermore, the effect of the air gap size in low-level thermal radiation (2, 5, 10 kW/m^2) was investigated using a self-designed bench-scale apparatus, showing that the thermal protective performance was greatly influenced by the size of the air gap and the location entrapped in multilayer fabric [53]. It was reported that the optimum air gap size was when the natural convection occurs [69]. Therefore, flow visualization experiments was conducted by Torvi and Dale [69] to investigate the occurrence of natural convection, predicting that the optimum air gap size was about 6–7 mm. The fabric system with air gaps of 9–12 mm in different moisture content seemed to provide maximum thermal protection from flash fire [70]. When the air gap presented different relative humidities, around 12–15 mm was the critical air gap size [71]. Therefore, it is found that the optimum air gap size has no certain value or does not exist, depending on the type of heat source, moisture content within fabric, and relative humidity in air gap. Additionally, most air gaps between the fabric sample and the test sensor were horizontally created in benchtop tests [33, 38]. But the air gap enclosure should be vertical in actual wearing state. There is a significant difference for the occurrence of natural convection under air gap enclosures

of different directions due to the location of hot surface and the buoyant force [58]. For example, the natural convection heat transfer in the vertical air gap enclosure should begin when the Rayleigh number is more than 1000, while the convective heat transfer within the air gap occurs when the Ra is more than 1708 [58]. Therefore, the effect of the vertical air gap should be further discussed.

30.5.3 Effect of Moisture Content

It is inevitable to sweat a lot for firefighters in fire ground while they suppress unwanted fires and rescue victims. Also, the firefighting lance is popularly used by firefighters to suppress fire. The presence of moisture from skin sweat or ambience can wet thermal protective clothing. Some studies reported that moisture content and distribution within the fabric system obviously affected thermal protection of fabric under various fire environments. Barker et al. [72] studied the impact of moisture content on the thermal protective performance under radiant heat flux of 6.3 kW/m^2 and found that multilayer fabrics with 15% moisture had the worst thermal protective performance. The study of Mäkinen et al. [73] showed that there was a decrease in thermal protective capacity with the increment of moisture content in radiant heat exposure of 20 kW/m^2. Furthermore, the thermal protective performance of single-layer fabrics that contains 70–80% moisture decreased to 35% under radiant heat exposure of 84 kW/m^2, while moisture had a positive effect on thermal properties in 50/50 radiant/convective heat flux of 84 kW/m^2 [74]. The main reason was that convective heat transfer between environment and clothing could speed up moisture evaporation and took away a section of heat. In contrast, radiant heat transfer had a complicated effect on moisture heat transfer with the variation of radiative intensity [55, 75].

Also, the moisture with different layer fabrics presented different influence tendencies on heat protection [76]. The moisture stored in the outer shell increased the thermal protective performance in low- and high-intensity thermal radiation [77]. But the moisture within the thermal liner, while providing the higher thermal protection in low-level radiation, increased the rate of heat transfer in protective clothing under high-level thermal radiation [76]. It can be attributed to the fact that moisture evaporation rate of outer shell is far larger than that of thermal liner and moisture barrier [77, 78]. Therefore, moisture applied in multilayer fabric system had an complex effect on thermal protection of the clothing, depending on the moisture content and distribution, the type of heat source, and the essential properties of flame-resistant fabric.

30.6 Future Trends

Significant research has been done in the field of thermal protective clothing to provide higher thermal protective, but the development in some smart materials and new technology creates new possible for further improvement of thermal protective clothing. These materials readily interact with human/environmental conditions to produce change in material properties. For example, shape memory materials can change their shapes with an increase of temperature, since the

shape memory effect results in an object reverting to a previously held shape when heated [79]. The selection of shape memory materials and its actuation temperature is key problem. Due to the importance of air gap size between different clothing layers, and clothing backside and body for thermal protection, the shape memory materials can be inserted in fabric layers to regulate the air gap size. But the rising of air gap size uncertainly increases thermal protective performance of clothing, as the occurrence of convective heat transfer for larger air gaps can speed up heat transfer from protective clothing to body [59]. Thus, the optimum air gap size should be further studied for different heat exposure conditions, especially for vertical air gap.

The development in intelligent thermal protective clothing has been introduced in past decades. The weaving of wires and sensors into protective clothing can monitor some fire environmental and physiological parameters, such as ambient temperature, skin temperature, heart rate, and heat stress. However, the time to cause skin burn or minimum heat exposure time was not predicted as an alert information for guiding the firefighting operations of firefighter. The monitoring data should be further analyzed for indicating the safety staying time and zone in fire ground conditions based on skin heat transfer model and Henriques burn model. Moreover, some active cooling methods (e.g. evaporative cooling, water-retaining fiber, ice pack, phase change materials, and ventilation cooling vest) should be combined with the intelligent monitoring system. These materials can be embedded in fabric layers to interact with a human body and produce thermoregulated effect by absorbing surplus body heat. But the cooling effect and duration of these methods is the urgent problem to be solved at present.

In addition, the relatively new technology of flame retardant is intumescent treatments. Most flame retardant are normally in the form of thin and low insulation coatings on a lining fabric, but these coatings will instantly form an inert insulative char to protect the wearer when activated by excessive heat or flame [27]. The flame retardant, its application technology, and the product must be environmentally acceptable for reducing inhalation of toxic fumes and gases. Furthermore, thermal hazards that firefighters are usually exposed not only include flash fire and high-intensity thermal radiation but also contact with hot objects, hot liquid splashes, and hot steam [80, 81]. The distinction of heat sources can result in the change of protective highlight. Protection from hot objects is to increase heat insulation of protective materials, while the reduction of hot liquid and steam penetration is a key method for protecting scalds or steam burns. Therefore, further study should develop multifunctional thermal protective clothing to meet multiple functional requirements.

References

1 Ali, A.H. and Mohmmed, R. (2015). A review of the firefighting fabrics for flashover temperature. *International Journal of Engineering Sciences and Research Technology* 4 (3): 247–257.

2 Karter, M.J. and NFP Association (2009). *Patterns of Firefighter Fireground Injuries*. National Fire Protection Association Quincy.

3 Fahy, R.F., LeBlanc, P.R., and Molis, J.L. (2006). *Firefighter Fatalities in the United States-2005*. National Fire Protection Association. Fire Analysis and Research Division.

4 Walton, S.M., Conrad, K.M., Furner, S.E., and Samo, D.G. (2003). Cause, type, and workers' compensation costs of injury to fire fighters. *American Journal of Industrial Medicine* 43 (4): 454–458.

5 Abbott, N.J. and Schulman, S. (1976). Protection from fire: nonflammable clothing — A review. *Fire Technology* 12 (3): 204–218.

6 Foster, J. and Roberts, G. (1995). Measurements of the firefighting environment – summary report. *Fire Engineers Journal* 55: 30–34.

7 Barker, R. (2005). A review of gaps and limitations in test methods for first responder protective clothing and equipment. *Report Presented to National Personal Protection Technology Laboratory*.

8 Guowen, S., Paskaluk, S., Sati, R. et al. (2010). Thermal protective performance of protective clothing used for low radiant heat protection. *Textile Research Journal* 81 (3): 311–323.

9 Song, G., Gholamreza, F., and Cao, W. (2011). Analyzing thermal stored energy and effect on protective performance. *Textile Research Journal* 81 (11): 1124–1138.

10 Barker, R.L. (2005). *A Review of Gaps and Limitations in Test Methods for First Responder Protective Clothing and Equipment*, 1–98. National Institute for Occupational Safety and Health.

11 Kahn, S.A., Patel, J.H., Lentz, C.W., and Bell, D.E. (2012). Firefighter burn injuries: predictable patterns influenced by turnout gear. *Journal of Burn Care and Research* 33 (1): 152–156.

12 Aldridge, D. (1997). Firefighter garment with combination facecloth and moisture barrier. Google Patents.

13 Gohlke, D.J. and Tanner, J.C. (1976). Gore-Tex® waterproof breathable laminates. *Journal of Industrial Textiles* 6 (1): 28–38.

14 Reischl, U. and Stransky, A. (1980). Comparative assessment of Goretex™ and Neoprene™ vapor barriers in a firefighter turn-out coat. *Textile Research Journal* 50 (11): 643–647.

15 Horrocks, A., Tune, M., and Cegielka, L. (1988). The burning behaviour of textiles and its assessment by oxygen-index methods. *Textile Progress* 18 (1–3): 1–186.

16 Tsukada, M., Khan, M.M.R., Tanaka, T., and Morikawa, H. (2011). Thermal characteristics and physical properties of silk fabrics grafted with phosphorous flame retardant agents. *Textile Research Journal* 81 (15): 1541–1548.

17 Horrocks, A. (1983). An introduction to the burning behaviour of cellulosic fibres. *Journal of the Society of Dyers and Colourists* 99 (7–8): 191–197.

18 Banks, M., Ebdon, J.R., and Johnson, M. (1993). Influence of covalently bound phosphorus-containing groups on the flammability of poly(vinyl alcohol), poly(ethylene-*co*-vinyl alcohol) and low-density polyethylene. *Polymer* 34 (21): 4547–4556.

19 Horrocks, A.R. and Price, D. (2001). *Fire Retardant Materials*. Woodhead Publishing.

20 Song, G. (2016). *Thermal Protective Clothing for Firefighters*. Woodhead Publishing.

21 Behnke, W.P., Chapin, R.S., and Fierro, J.F. (1978). Poly(*m*-phenylene isophthalamide) and poly(*p*-phenylene terephthalamide) fibers. Google Patents.

22 Wang, C.C. and Chen, C.C. (2005). Some physical properties of various amine-pretreated Nomex Aramid yarns. *Journal of Applied Polymer Science* 96 (1): 70–76.

23 Jackson, R.H. (1978). PBI fiber and fabric—properties and performance. *Textile Research Journal* 48 (6): 314–319.

24 Coffin, D.R., Serad, G.A., Hicks, H.L., and Montgomery, R.T. (1982). Properties and applications of celanese PBI—polybenzimidazole fiber. *Textile Research Journal* 52 (7): 466–472.

25 Chung, T.S., Glick, M., and Powers, E.J. (1993). Polybenzimidazole and polysulfone blends. *Polymer Engineering and Science* 33 (16): 1042–1048.

26 Liu, X.-Y., Tao, Y.-K., Wang, X.-L., and Yu, W.-D. (2009). The thermal property of high performance fiber. *Journal of Xi'an Polytechnic University* 23 (2): 267–271.

27 Shishoo, R. (2002). Recent developments in materials for use in protective clothing. *International Journal of Clothing Science and Technology* 14 (3/4): 201–215.

28 Hendrix, J., Drake, G., and Reeves, W. (1972). Effects of fabric weight and construction on OI values for cotton cellulose. *Journal of Fire and Flammability*: 338–345.

29 ISO/TC 94 ISO 9151 (1995). *I. Protective Clothing Against Heat and Flame Determination of Heat Transmission on Exposure to Flame*. Geneva, Switzerland: ISO, 2004.

30 ISO/TC 94 ISO 6942 (2002). *I. Protective Clothing-Protection Against Heat and Fire Method of Test: Evaluation of Materials and Material Assemblies When Exposed to a Source of Radiant Heat*. Geneva, Switzerland: ISO, 2004.

31 ISO/TC 94/SC13 ISO 17492 (2003). *I. Clothing for Protection Against Heat and Flame Determination of Heat Transmission on Exposure to Both Flame and Radiant Heat*. Geneva, Switzerland: ISO, 2004.

32 NFP Association (1998). *Standard on Protective Clothing and Equipment for Wildland Fire Fighting*. National Fire Protection Association.

33 NFP Association (2006). *Standard on Protective Ensembles for Structural Fire Fighting and Proximity Fire Fighting*. National Fire Protection Association.

34 ASTM F1060-08 A (2008). *Standard Test Method for Thermal Protective Performance of Materials for Protective Clothing for Hot Surface Contact*. West Conshohocken, PA: ASTM International.

35 ASTM F1939-15 A (2015). *Standard Test Method for Radiant Heat Resistance of Flame Resistant Clothing Materials with Continuous Heating*. West Conshohocken, PA: ASTM International.

36 ASTM F2700-13 A (2013). *Standard Test Method for Unsteady-State Heat Transfer Evaluation of Flame Resistant Materials for Clothing with Continuous Heating*. West Conshohocken, PA: ASTM International.

37 ASTM F2702-15 A (2013). *Standard Test Method for Radiant Heat Performance of Flame Resistant Clothing Materials with Burn Injury Prediction*. West Conshohocken, PA: ASTM International.

38 ASTM F2703-13 A (2013). *Standard Test Method for Unsteady-State Heat Transfer Evaluation of Flame Resistant Materials for Clothing with Burn Injury Prediction*. West Conshohocken, PA: ASTM International.

39 ASTM F2731-11 A (2011). *Standard Test Method for Measuring the Transmitted and Stored Energy of Firefighter Protective Clothing Systems*. West Conshohocken, PA: ASTM International.

40 ISO/TC 94 ISO/DIS 13506 (2004). *I. Protective Clothing Against Heat and Flame Test Method for Complete Garments Prediction of Burn Injury Using an Instrumented Manikin*. Geneva, Switzerland: ISO.

41 ASTM F1930-15 A (2015). *Standard Test Method for Evaluation of Flame Resistant Clothing for Protection Against Fire Simulations Using an Instrumented Manikin*. West Conshohocken, PA: ASTM International.

42 Stoll, A.M. and Chianta, M.A. (1968). A method and rating system for evaluation of thermal protection. DTIC Document.

43 DeMars, K., Henleson, W., and Lies, M. (2000). Thermal measurements for fire fighters' protective clothing. In: *Thermal Measurements: The Foundation of Fire Standards*, ASTM STP1427. West Conshohocken, PA: American Society for Testing and Materials.

44 Grimes, R., Mulligan, J., Hamouda, H. et al. (1996). The design of a surface heat flux transducer for use in fabric thermal protection testing. *ASTM Special Technical Publication* (1237): 607–624.

45 Song, G. (2003). Modeling thermal protection outfits for fire exposures. Doctoral Thesis. North Carolina State University.

46 Sipe, J.E. (2004). *Development of An Instrumented Dynamic Mannequin Test to Rate the Thermal Protection Provided by Protective Clothing*. Worcester Polytechnic Institute.

47 Behnke, W.P., Geshury, A.J., and Barker, R.L. Thermo-Man® and thermo-leg: large scale test methods for evaluating thermal protective performance. In: *Performance of Protective Clothing*, vol. 4, 1992. ASTM International.

48 Henriques, F. Jr. (1947). Studies of thermal injury; the predictability and the significance of thermally induced rate processes leading to irreversible epidermal injury. *Archives of Pathology* 43 (5): 489–502.

49 Watson, K.L. (2014). From radiant protective performance to RadManTM: the role of clothing materials in protecting against radiant heat exposures in wildland forest fires. Master Thesis. North Carolina State University.

50 Song, G. (2007). Clothing air gap layers and thermal protective performance in single layer garment. *Journal of Industrial Textiles* 36 (3): 193–205.

51 Torvi, D.A., Dale, J.D., and Faulkner, B. (1999). Influence of air gaps on bench-top test results of flame resistant fabrics. *Journal of Fire Protection Engineering* 10 (1): 1–12.

52 Sawcyn, C.M.J. (2003). Heat transfer model of horizontal air gaps in bench top testing of thermal protective fabrics. Master Thesis. University of Saskatchewan Saskatoon.

53 Fu, M., Weng, W., and Yuan, H. (2014). Effects of multiple air gaps on the thermal performance of firefighter protective clothing under low-level heat exposure. *Textile Research Journal* 84 (9): 968–978.

54 Su, Y. and Li, J. (2016). Analyzing steam transfer though various flame-retardant fabric assemblies in radiant heat exposure. *Journal of Industrial Textiles* https://doi.org/10.1177/1528083716674907.

55 Fu, M., Yuan, M.Q., and Weng, W.G. (2015). Modeling of heat and moisture transfer within firefighter protective clothing with the moisture absorption of thermal radiation. *International Journal of Thermal Sciences*: 96201–96210.

56 Su, Y., He, J., and Li, J. (2016). An improved model to analyze radiative heat transfer in flame-resistant fabrics exposed to low-level radiation. *Textile Research Journal* https://doi.org/10.1177/0040517516660892.

57 Fan, J.T., Luo, Z.X., and Li, Y. (2001). Heat and moisture transfer with sorption and condensation in porous clothing assemblies and numerical simulation (vol 43, pg 2989, 2000). *International Journal of Heat and Mass Transfer* 44 (5): 1079–1079.

58 Cengel, Y.A. (2003). *Heat Transfer: A Practical Approach*. McGraw-Hill.

59 Torvi, D.A. (1997). Heat transfer in thin fibrous materials under high heat flux conditions. Doctoral Thesis. University of Alberta.

60 Sun, G., Yoo, H., Zhang, X., and Pan, N. (2000). Radiant protective and transport properties of fabrics used by wildland firefighters. *Textile Research Journal* 70 (7): 567–573.

61 Day, M. and Sturgeon, P. (1987). Thermal radiative protection of fire fighters' protective clothing. *Fire Technology* 23 (1): 49–59.

62 Shalev, I. and Barker, R.L. (1984). Protective fabrics: a comparison of laboratory methods for evaluating thermal protective performance in convective/radiant exposures. *Textile Research Journal* 54 (10): 648–654.

63 Song, G., Paskaluk, S., Sati, R., and Crown, E.M. (2010). Thermal protective performance of protective clothing used for low radiant heat protection. *Textile Research Journal* https://doi.org/10.1177/0040517510380108.

64 Su, Y., He, J., and Li, J. (2016). Modeling the transmitted and stored energy in multilayer protective clothing under low-level radiant exposure. *Applied Thermal Engineering*: 931295–931303.

65 Su, Y., He, J., and Li, J. (2016). A model of heat transfer in firefighting protective clothing during compression after radiant heat exposure. *Journal of Industrial Textiles* https://doi.org/10.1177/1528083716644289.

66 Wang, M., Li, X., and Li, J. (2015). A new approach to quantify the thermal shrinkage of fire protective clothing after flash fire exposure. *Textile Research Journal* 86 (6): 580–592.

67 Lu, Y., Song, G., and Li, J. (2014). A novel approach for fit analysis of thermal protective clothing using three-dimensional body scanning. *Applied Ergonomics* 45 (6): 1439–1446.

68 Zhu, F.L. and Zhang, W.Y. (2006). Evaluation of thermal performance of flame-resistant fabrics considering thermal wave influence in human skin model. *Journal of Fire Sciences* 24 (6): 465–485.

69 Torvi, D.A. and Dale, J.D. (1999). Heat transfer in thin fibrous materials under high heat flux. *Fire Technology* 35 (3): 210–231.

70 Lu, Y., Li, J., Li, X., and Song, G. (2013). The effect of air gaps in moist protective clothing on protection from heat and flame. *Journal of Fire Sciences* 31 (2): 99–111.

71 Li, J., Lu, Y., and Li, X. (2012). Effect of relative humidity coupled with air gap on heat transfer of flame-resistant fabrics exposed to flash fires. *Textile Research Journal* 82 (12): 1235–1243.

72 Barker, R.L., Guerth-Schacher, C., Grimes, R.V., and Hamouda, H. (2006). Effects of moisture on the thermal protective performance of firefighter protective clothing in low-level radiant heat exposures. *Textile Research Journal* 76 (1): 27–31.

73 Mäkinen, H., Smolander, J., and Vuorinen, H. (1988). Simulation of the effect of moisture content in underwear and on the skin surface on steam burns of fire fighters. In: *Performance of Protective Clothing: Second Symposium, ASTM STP*, 415–421.

74 Lee, Y.M. and Barker, R.L. (1986). Effect of moisture on the thermal protective performance of heat-resistant fabrics. *Journal of Fire Sciences* 4 (5): 315–331.

75 Nazaré, S. and Madrzykowski, D. (2014). A Review of Test Methods for Determining Protective Capabilities of Fire Fighter Protective Clothing from Steam. NIST TN–1861, Gaithersburg, MD.

76 Keiser, C. and Rossi, R.M. (2008). Temperature analysis for the prediction of steam formation and transfer in multilayer thermal protective clothing at low level thermal radiation. *Textile Research Journal* 78 (11): 1025–1035.

77 Lawson, L.K., Crown, E.M., Ackerman, M.Y., and Dale, J.D. (2004). Moisture effects in heat transfer through clothing systems for wildland firefighters. *International Journal of Occupational Safety and Ergonomics* 10 (3): 227–238.

78 Rossi, R.M. and Zimmerli, T. (1996). *Influence of Humidity on the Radiant, Convective and Contact Heat Transmission Through Protective Clothing Materials*, ASTM Special Technical Publication 1237, 269–280. ASTM International.

79 Otsuka, K. and Wayman, C.M. (1999). *Shape Memory Materials*. Cambridge University Press.

80 Lu, Y., Song, G., Zeng, H., and Zhang, L. (2013). Characterizing factors affecting the hot liquid penetration performance of fabrics for protective clothing. *Textile Research Journal* 84 (2): 174–186.

81 Su, Y. and Li, J. (2016). Development of a test device to characterize thermal protective performance of fabrics against hot steam and thermal radiation. *Measurement Science and Technology* 27 (12): 1–9.

31

Comfort Management of Fibrous Materials

Chengjiao Zhang[1] *and Faming Wang*[2]

[1] *Soochow University, Department of Fashion Design and Engineering, Laboratory for Clothing Physiology and Ergonomics, Suzhou, China*
[2] *Department of Architecture, School of Architecture and Art, Central South University, Changsha, Hunan, China*

31.1 Introduction

Human beings are unique animals, and one of the most distinct differences between human beings and other species is the ability to bioengineer his thermal environment correspondingly to changes in the surrounding environment via adjusting clothing. The clothing, air temperature, radiant temperature, humidity, air movement, and metabolic heat have been regarded as the six fundamental factors that determine human thermal balance [1, 2].

This chapter focuses on human thermoregulation and shows the importance of clothing materials in maintaining the body thermal comfort. The interactions between the human body and the clothing will be discussed with a special emphasis on the materials and factors that could affect the comfort properties of the garment. Besides, the chapter also discusses the assessment techniques for comfort evaluation and the trends of clothing and materials for comfort management.

31.2 Human Thermal Regulation and Heat Transfer Mechanisms

Human beings are homoeothermic and needed to maintain body temperature by thermoregulatory and/or behavioral adjustments to adapt to changing environments. For a person at thermoneutral state, the internal temperature maintains at around 37.0 °C and indicates that a dynamic heat balance is built up between the body and its thermal environment. That is, numerically, the heat produced inside the body must be balanced by heat losses to the environments. The heat input source varies depending on the ambient temperature; the heat source within the body is generally the heat generated by metabolism in normal climatic conditions (see Figure 31.1). However, under extreme conditions, when the ambient temperature is higher than skin temperature, the heat input is combined by heat transfer

Handbook of Fibrous Materials, First Edition. Edited by Jinlian Hu, Bipin Kumar, and Jing Lu.
© 2020 Wiley-VCH Verlag GmbH & Co. KGaA. Published 2020 by Wiley-VCH Verlag GmbH & Co. KGaA.

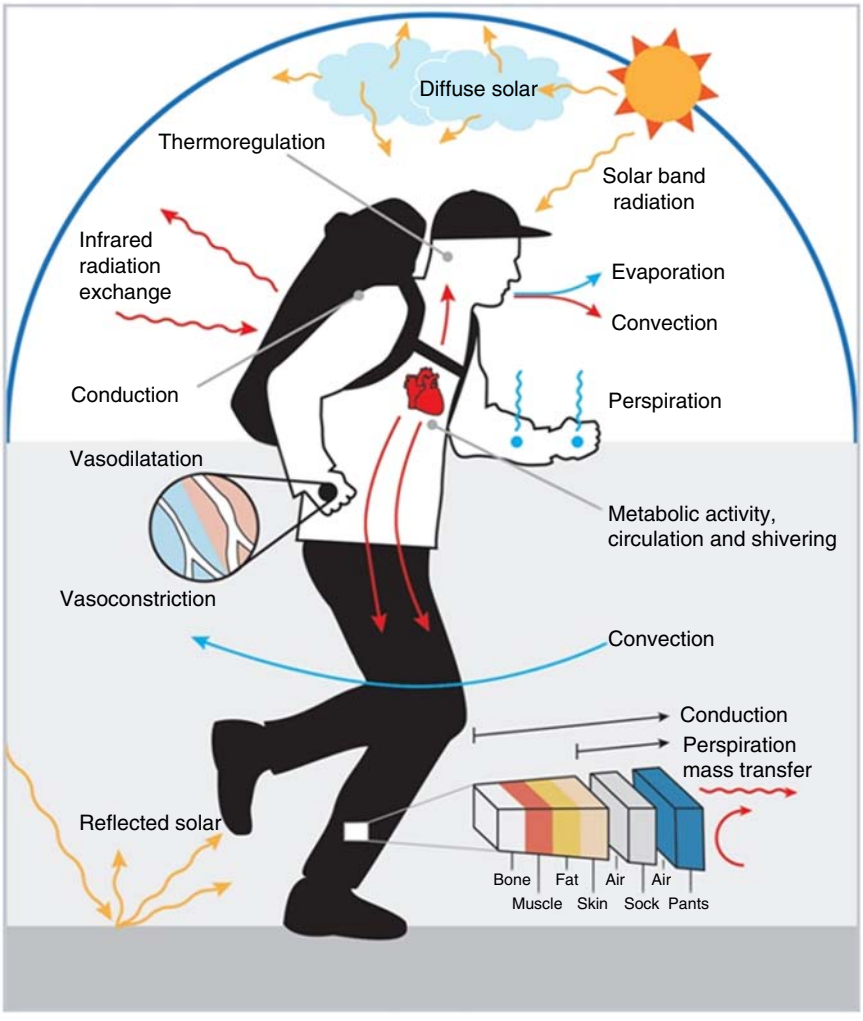


Figure 31.1 Human thermoregulation and heat transfer mechanisms.

from the surrounding environment and heat generated by metabolism within the body [2].

Heat transfers away from the body to the surrounding environment via several ways [3]:

- Dry heat transfer via conduction, convection, and radiation. Conductive heat transfer occurs between solid surfaces contacting with each other; convective heat transfer occurs between a solid surface and its surrounding fluid, e.g. air or water; radiation indicates heat transfer via emission or absorption of electromagnetic waves.
- Sweat evaporation.
- Heat transfer via respiration.

The body temperature would increase if the heat input sources were numerically greater than heat outputs, and it would decrease correspondingly if there was more heat drawn away from the body than the heat input. Ideally, the heat generation and heat loss should be equal. Thus a heat balance equation (in W or W/m^2) for the human body can be expressed based on this principle:

$$M \pm W = S \pm R \pm C \pm K - E \tag{31.1}$$

where M is the metabolic heat production, W is the energy consumed/absorbed by mechanical work, E is the heat transfer via evaporation, R is heat transfer by radiation, C is heat transfer via convection, K is heat transfer via conduction, and S is heat storage.

The heat balance equation for the human body can be expressed in many forms. However, all equations have the same underlying concept and involve three key elements; those for heat generation in the body, heat transfer, and heat storage (see Figure 31.2). The metabolic rate produces energy that enables a human to do mechanical work, and the resting energy is transferred into heat and mainly released into the environment via dry heat loss (i.e. conduction, convection, and radiation), sweat evaporation, and respiration. The heat storage S reflects the thermal debt situation of the body. When the body is in a thermally neutral state, S is zero. S becomes positive when the heat loss is less than the heat production, which causes rise in body temperature. On the other hand, the S will be negative when the heat loss is greater than the heat production, which leads to fall in body temperature.

Goldman [4] described that the heat production is about 1 met (defined as $58.15\ W/m^2$) for an average adult man (who has a body surface area of $1.8\ m^2$) at rest. Usually, about 12% of the resting heat production is drawn away by respiration; another 12% is taken away via evaporation on the skin surface. The remainder (about 76%) of the resting metabolic heat production is transferred from the body by convection and radiation in a comfortable environment; the relative proportion of convective to radiation losses is affected by the ambient air movement. With minimal clothing in still air, about 60% of the resting heat production is lost by radiation, and air movement can facilitate extra convective heat loss.

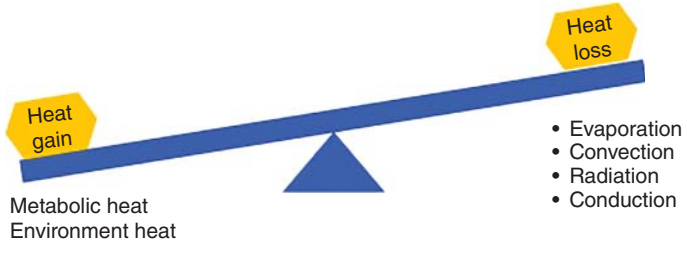


Figure 31.2 A schematic chart on human thermal balance.

31.3 Clothing Comfort

Clothing acts as both a barrier and a transporter between the human body and its surrounding environment. On one hand the clothing can protect the wearer from environmental hazards such as cold and heat. Besides, the clothing could also manage the heat and moisture balance the body needs. The interaction between the human body and clothing system involves four basic elements: physical processes between the clothing and surrounding environment, physiological processes within the body, and neurophysiological and psychological processes [5]. The physical process between the body, clothing, and environment involves heat and moisture transfer, which affects the level of thermal comfort for the human body [6].

Comfort indicates a complex state of mind that is affected by many physical, physiological, and psychological factors. Four different types of comfort may be classified from documented papers: thermal comfort, sensorial comfort, garment fit, and psychological comfort (e.g. esthetics [3]). As defined in ASHRAE 55 [7] and ISO 7730 [8], thermal comfort is indicated as the condition of mind that expresses satisfaction with the thermal environment. Comfort feeling is a psychological status, not directly related to physical environment or physiological state. Thermal comfort is affected by the six basic factors, among the six basic factors. Among the six basic factors, the air temperature, mean radiant temperature, air movement, and humidity represent the four key environmental factors that affect thermal comfort. These four parameters could directly affect the heat transfer between the body and its surrounding environment. The rate of convective heat transfer is a linear function of the temperature gradient between skin temperature and the ambient air temperature. The metabolic heat production is another major parameter defining thermal comfort because the individual metabolic heat production is the essential element of heat balance. The sixth parameter affecting thermal exchange between the human body and its environment is clothing, which acts as a thermal and moisture barrier between the body and the surrounding environment [4].

Many efforts have been made to develop thermal indexes to assess thermal comfort of environments. In the 1920s, researchers on the behalf of the American Society of Heating and Ventilating Engineers (ASHVE) proposed the effective temperature (ET) index based on a comprehensive series of studies [9, 10]. The ET index proposed the concept of standard environment as the comfort index value. ET is still used nowadays but is not generally recommended to use, although it has been found useful for assessing hot environments. Afterward, the resultant temperature [11] and the equivalent temperature [12, 13] were proposed to determine human thermal index.

In 1970, Fanger published the book "Thermal Comfort," and it was regarded as the most significant landmark in thermal comfort research and practice. The book outlines the conditions essential for thermal comfort and also describes methods and principles for thermal environment evaluation and

analysis with respect to thermal comfort. The methods that he proposed in the book are now the most influential and widely used throughout the world. In his book, he recognized that it is the combined thermal effect of all (six basic parameters) physical factors that determines human thermal comfort and three criteria should be fulfilled for human to reach the thermal comfort status: (i) the body is in heat balance; (ii) the sweat rate is within comfort limits; (iii) the mean skin temperature is within comfort limits [1].

31.4 Heat and Moisture Transfer Through Textiles

31.4.1 Heat Transfer Through Textiles

Heat transfer indicates that the energy transfers between two mediums because of the temperature gradient, e.g. the heat transfers from the medium with high-temperature to medium with lower temperature. Heat transfer will continue until the two media reach the same temperature, i.e. dynamic heat exchange equilibrium is reached. The amount of the transferred heat depends on temperature gradient and the thermal resistance between the two media. Heat can be transferred in fabrics by conduction through air and fibers, convection of the air within the fabric structure, and radiation from fiber to fiber.

Conductive heat transfer occurs at the interface between two physical contacting objects. The heat flow is depended by the temperature gradient, the larger the temperature gradient, the faster the heat flow between the two surfaces. In clothing system, conductive heat transfers between two contact fabrics or between fabrics and the human skin.

Convective heat transfer is caused by the molecular motion of a fluid or the air. The air density decreases after the heat absorption when it contacts to a high-temperature surface. The difference in air density induced by the temperature gradient forces warmed air to rise, and thus natural convective heat transfer occurs. Moreover, air movement could significantly impact convection and accelerate heat exchange and forced convective heat transfer. In clothing, convective heat flow mainly depends on the openness of the fabric and is not affected by the fabric thickness.

Radiative heat exchange indicates heat transferred by electromagnetic waves between objects with temperature gradient through space. The radiative heat transfer in textile materials could be significantly affected by the material density, construe, and finishing process of the fabrics [6].

The heat transfer in fabrics becomes much more complicated and is normally considered as coupled heat and moisture transfer when the presence of moisture or sweating [14]. Generally, the total heat transfer consists of a dry heat transfer component, moisture, and a liquid transfer component: dry heat loss includes conduction, radiation, and convection; the second form indicates insensible moisture diffusion; and the last form involves the diffusion of liquid water (e.g. sweat).

31.4.2 Moisture Transfer Through Textiles

Moisture exists in both liquid and vapor forms. The transfer of moisture through textiles is a complicated process, which could largely affect thermal comfort property of the fibrous materials. Textile products should exhibit an enough good moisture transfer ability to provide wearers thermal comfort. Water vapor transfer takes place by diffusion and forced convection. Vapor diffusion indicates the process that the water molecules migrate through the textile substance, driven by either the concentration gradient or by forced convection. Water vapor always moves from high vapor concentration regions to low vapor concentration areas. Forced convection also enhances water vapor transmission.

Moisture vapor diffusion is depended by the structure of the yarn and the fabric, as well as the interstices that are formed between fibers within yarns. Generally, fabrics with larger interstices normally allow rapid diffusion of water. In addition, vapor transfer is also affected by moisture adsorption, desorption between fibers and the surrounding air (see Figure 31.3). Adsorption indicates water molecules that are attracted to fabric surface, and it has a linear relationship with the fiber surface area within a fabric, e.g. a larger surface area promises larger amount of water adsorbed. Desorption is the process of molecular diffuses through the material through moisture adsorption and absorption. The heat absorption and release through moisture absorption or desorption further complicates the moisture transfer process within textile materials.

To characterize the vapor diffusion property, numerous methods have been proposed, and several international standards have been developed. The method proposed in the standards could be divided into two categories according to their principles, namely, the gravimetric method [15–17] and the hot plate method [18, 19]. For gravimetric methods, the water vapor transmission ability are obtained by measuring the mass transferred within in a certain time (usually 24 hours) and thus are usually time-consuming. For the hot plate method, the water vapor transmission ability is evaluated by measuring the water vapor resistance of a fabric.

Liquid water transfers through textiles via wetting and wicking. Wetting process indicates the displacement of the fiber–air interface with a fiber–liquid interface. Wicking is the process that liquid transfers into fiber assemblies via capillary effect. During wetting process, the liquid wets the fiber surface before transferring in and through the pores at the amorphous regions of fibers. The spreading of the liquid on the fiber surface depends on the surface energy

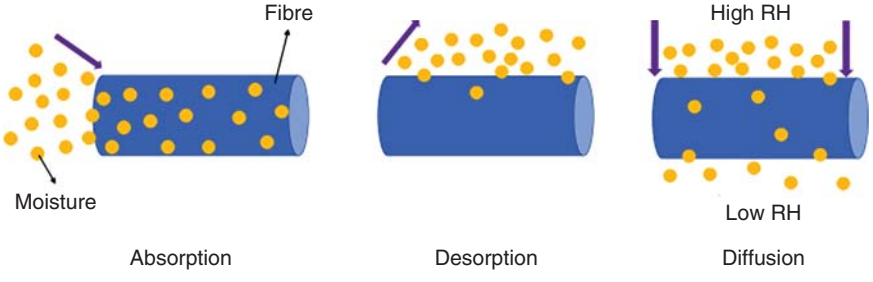


Figure 31.3 Absorption, diffusion, and desorption.

of the material and the liquid. The fabric will have a higher wettability if the surface energy of the fabric could overcome the free surface energy of the liquid. Otherwise, the fabric will have a lower wettability [20–22].

Wicking only occurs under the criteria that the fibers are wetted and there are capillary spaces between them, and it is drawn by capillary forces, and the wicking ability indicates the ability to maintain liquid flow in the capillaries. Depending on the direction of water flow, water flows in the plane of a fabric is always called "transverse wicking," "in-plane wicking," or "horizontal wicking." On the other hand, liquid flow perpendicular to the plane of the fabric is usually referred to as "vertical wicking" [23]. Both wetting and wicking behaviors are mainly determined by the surface tension of the fabric and the liquid. In addition, the wettability and wicking effect are also affected by the hydrophobicity of the fiber material [24]. Fabrics made of fibers with different hydrophobicity allow water molecules to penetrate into different fiber regions and thus affects the moisture regain. Fiber moisture regain affects wicking performance. Fibers with lower moisture regain tend to increase the wicking performance. Polyester fabric with a very low moisture regain can be developed to create a high wicking fabric. Besides, the capillary effect is also significantly affected by cross-sectional shapes of the fiber. Zhang et al. [25] compared the capillary effect of six types of fibers with different cross-sectional shapes and found that the best wicking effect was obtained from the concave cross-sectional shape. Currently, numerous methods have been proposed to characterize the wettability and wicking property of fabrics, and a number of standards are also available. For instance, the AATCC TM 197 [26] standard for testing fabric vertical wicking and AATCC TM 198 [27] for horizontal wicking, DIN 53924 [28] for the wicking height, the AATCC TM 39 [29], and ISO 4920 [30] standards are used to evaluate the fabric wettability.

31.5 Assessment of Materials and Clothing

With the advancement of textile technology, a shift of attention from using natural materials (cotton, fur) to man-made fiber or combinations of both has taken place. In clothing development, it is impossible to test all possible combinations because of the wide spectrum of material combinations at present. It requires a systematic approach in clothing development, and a five-stage evaluation system advocated by Goldman [31] and Umbach [32] provides a solution to the problem and has been widely used in the clothing research community. It is schematically presented in Figure 31.4. Prior to the evaluation process, a detailed analysis is necessary to be conducted on the requirements of the task of the intended clothing user. Then, a selection of fabrics and materials should be carried out, which are tested for a number of physical properties (Stage 1). During Stage 2, a prediction for the overall clothing characteristics can be made using the fabric characteristics, which can be put into the now-readily available thermal models that could analyze the heat exchange for a hypothetical user (e.g. such as the Required Insulation Index IREQ [33]), or actually combine this heat exchange approach with a physiological human thermoregulatory model, which allows a

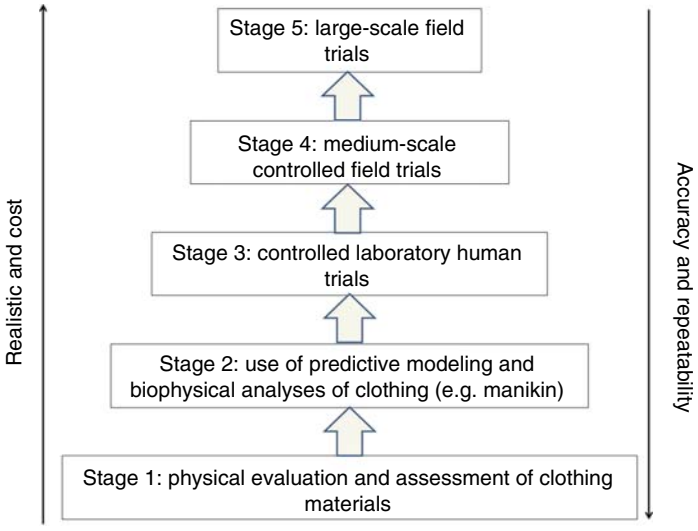


Figure 31.4 Five stages in the development and assessment of clothing systems proposed by Goldman [31] and Umbach [32].

prediction of the body's thermophysiological responses and the associated risks to the wearers' health or comfort (Stage 2) [34, 35].

In Stage 3, clothing wearing test will be conducted under defined conditions in a climatic chamber, and detailed data of the wearer will be collected. The outcome of this testing may help narrow down the material or fabric choices, which can then be evaluated in small- or large-scale field trials. Time and cost required in these two stages will increase over previous stages. Nevertheless, crucial information will be obtained in these two stages.

31.5.1 Material and Fabric Testing

For comparison of different fabrics, several tests on heat and vapor resistance are available, and many are now defined in international standards. A guarded hot plate is extensively used for heat resistance measurement of fabrics, which measures the amount of heat lost through a sample at a certain temperature gradient between the plate and the environment. From this, thermal resistance of the fabric can be calculated as

$$R_{\mathrm{ct}} = \frac{T_{\mathrm{plate}} - T_a}{H_{\mathrm{dry}}} - R_0 \tag{31.2}$$

where R_{ct} is the heat resistance of the fabric sample ($(\mathrm{m}^2\,\mathrm{K})/\mathrm{W}$), T_{plate} is the mean hot plate surface temperature (°C), T_a is the ambient temperature (°C), H_{dry} is the dry heat loss per square meter of plate area (W/m^2), and R_0·is the heat resistance measured without a sample present ($(\mathrm{m}^2\,\mathrm{K})/\mathrm{W}$).

Different equipment forms are in use for the fabric thermal insulation test and are presented in ISO 11092 [19], CAN/CGSB 4.2 No. 78.1-2001 [36], ASTM



Figure 31.5 The sweating guarded hotplate housed in a climate chamber.

D1518-85 [37], and BS 4745 [38]. However, the equipment styles are underlying the same principle, though the design differs a lot. Some clamp the fabric between a hot and a cold plate, others add an air layer between the sample and the cold plate, or use only a hot plate, while the other side of the sample is exposed to ambient air.

For the guarded hot plate (see Figure 31.5), the fabric's vapor resistance is calculated as

$$R_{\text{et}} = \frac{P_{\text{plate}} - P_a}{H - H_{\text{dry}}} - R_{\text{et0}} \tag{31.3}$$

where R_{et} is the heat resistance of fabric sample ($(\text{m}^2\ \text{Pa})/\text{W}$), P_{plate} is the mean hot plate surface vapor pressure (Pa), P_a is the ambient vapor pressure (Pa), H is the total heat loss per square meter of plate area (W/m^2), H_{dry} is the dry heat loss per square meter of plate area (W/m^2), and R_{et0} is the vapor resistance measured without a sample present ($(\text{m}^2\ \text{K})/\text{W}$).

A number of methods for determination of fabric vapor resistance are presented in BS 7209 [39], CAN/CGSB-4.2 No. 49-99 [40], ASTM F1868 [18], ASTM E96 [15], and ISO 11092 [19]. Test methods can vary dramatically in complexity and cost.

Besides the heat and vapor resistances, Woodcock [41] proposed the permeability index (i_m). The moisture permeability index of a material is defined as the ratio of the actual evaporative heat flow capability between the skin and the environment to the sensible heat flow capability as compared with the Lewis Ratio. The permeability index (i_m) is computed as

$$i_m = S \times \frac{R_{\text{ct}}}{R_{\text{et}}} \tag{31.4}$$

where S is the Lewis constant (60.6 Pa/K).

This permeability index varies between zero (totally impermeable) to the unity (air) (though the typical upper limit is due to its definition around 0.5). As mentioned before, in order to avoid moisture accumulation, the highest number is the best here. In addition to parameters aforementioned, the air permeability, waterproofness, and wicking property of the fabric are the characteristics that are usually evaluated.

31.5.2 Full-Scale Clothing Testing

As the step from fabric testing to laboratory human wear trials is quite big, it is necessary to have an intermediate step to evaluate the complete prototype of garments and ensembles on a physical apparatus. The thermal manikins developed during the last decades provide a practical solution to this problem. Thermal manikins are now available in a variety of sizes (baby or adult), shapes (male or female), and technologies (metal, resin shells, water filled fabric shells, etc.), and many of which now can "sweat" by applying uniformly wetted fabric "skin" or sweating output unit.

Moreover, with the technology development, thermal manikins (see Figure 31.6) available nowadays could be regulated regimentally; thus the local insulation can be studied and the whole body insulation. This allows a better analysis of "cold spots" in the clothing design. Most current manikins have 16–34 body segments, and each segment can be individually evaluated. Measurements are typically performed with the manikin standing static and with the manikin performing walking movements. Also measurements without wind (static) and with wind can be performed. In this way, effects of pumping, forced ventilation, and forced convection can be investigated, which is crucial for clothing evaluation [42, 43].

31.5.3 Clothing Thermal Insulation

Clothing thermal insulation is one of the most important parameters to characterize clothing thermal comfort. Thermal insulation of full-scale clothing is normally determined by a thermal manikin. Thermal manikins are manufactured in the human shape (see Figure 31.2), and the testing principle is the same as that of a guarded hot plate. Generally, three calculation methods might be used to



Figure 31.6 The Newton-type sweating thermal manikin (Thermetrics LLC, Seattle).

calculate clothing thermal insulation: the parallel method, the serial method, and the global method [44–46].

In the parallel method, thermal insulation is obtained by utilizing its reciprocal relation relationship with heat transfer coefficient. The heat transfer coefficient is calculated by averaging local heat transfer of each manikin segments. Thus the thermal insulation could be calculated as

$$I_t = \frac{1}{0.155} \sum_{i=1}^{i=n} \frac{a_i}{A} \frac{(T_{\mathrm{si}} - T_a)}{H_{\mathrm{ci}}} \tag{31.5}$$

where I_t is the total thermal insulation of the clothing (clo), n is the manikin's segment number, a_i is the surface area of the segment i (m^2), A is the total surface area of the manikin, T_{si} is the surface temperature of the segment i (°C), T_a is the air temperature (°C), and H_{ci} is the heat flux of the segment i (W/m^2).

Varies from the parallel method, the thermal insulation in the serial method is calculated by the averaged local insulation of each manikin segment, and the calculation is presented:

$$I_t = \frac{\sum a_i \cdot (t_i - t_a)}{\sum (a_i \cdot H_i)} \tag{31.6}$$

where a_i is ratio of the surface area of segment i to the total surface area of the manikin, t_a is the air temperature (°C), t_i is the segmental temperature (°C), and H_i is the heat flux of the segment i (W/m^2).

In addition to the parallel and the serial methods, the global method may also be used to calculate clothing thermal insulation [46]. It is calculated basing on the segmental heat loss, area-weighted surface temperature, and body segmental surface area, and the calculation is given as

$$I_g = \frac{\sum a_i \cdot t_i - t_a}{\sum (a_i \cdot H_i)} \tag{31.7}$$

where I_g is the global thermal insulation of the clothing, a_i is ratio of the surface area of segment i to the total surface area of the manikin, t_a is the air temperature (°C); t_i is the segmental temperature (°C), and H_i is the heat flux of the segment i (W/m^2).

Clothing insulation values calculated by different method may differ from each other depending on the clothing properties [47–49]. Generally speaking, thermal insulation values calculated by these three methods will be the same if clothing insulation distributes uniformly over the manikin body (i.e. homogeneous clothing insulation). However, if the clothing insulation is not evenly distributed over the manikin segments (i.e. inhomogeneous clothing insulation), the global and the serial methods will yield the same insulation value if the segmental heat flux is uniform over the manikin. In addition, the insulation calculated by the serial method is always higher than that calculated by the parallel method. Moreover, the global and parallel methods will result in the same thermal insulation value if the surface temperature is distributed uniformly over the manikin body; thus the insulation value obtained by the serial method will always be higher than that obtained by the global method [48–51].

31.5.4 Clothing Vapor Resistance

Evaporative resistance (or water vapor resistance) is the widely used physical parameter to quantify the moisture transfer property of full-scale clothing. The clothing evaporative resistance of a full-scale clothing ensemble can be calculated by either the heat loss option or the mass loss option [52]:

$$R_{\text{et}} = \frac{(p_s - p_a)A}{H_e - \frac{(T_s - T_a)A}{R_t}} \tag{31.8}$$

$$R_{\text{et}} = \frac{(p_s - p_a)A}{\lambda\left(\frac{dm}{dt}\right)} \tag{31.9}$$

where R_{et} is the total evaporative resistance of clothing ensemble and surface air layer ((kPa m^2)/W), p_s is water vapor pressure at the manikin's sweating surface (kPa), p_a is water vapor pressure in the air flowing over the clothing (kPa), A is area of the manikin's surface that is sweating (m^2), H_e is power required for sweating areas (W), T_s and T_a are fabric "skin" surface temperature and the ambient temperature, respectively (°C), and R_t is the total thermal resistance of the clothing ensemble and surface air layer ((°C m^2)/W). λ is the heat vaporization of water at the measured surface temperature (W); dm/dt is the evaporation rate of moisture leaving the manikin's sweating surface (g/min).

To determine clothing evaporative resistance, the simulation of human profuse sweating on the manikin is required (i.e. simulating a person with a fully wetted skin surface) [119]. In summary, three methods might be applied to achieve the simulation of human sweating [53–55]: pre-wet fabric "skin," manikins equipped with pumps and pipes to regulate water supply through sweat nozzles to the whole manikin body surface (a piece of highly stretchable fabric "skin" is also required for the purpose of distribution of sweat throughout the entire manikin body [see Figure 31.7]) and sweating fabric manikins featured with a water filled body covered by a waterproof but permeable fabric "skin." The pre-wetted fabric "skin" method is effective, but the "skin" tends to be dried out after a certain testing period, which is dependent upon the type of clothing tested, the test condition, and how much moisture the "skin" could hold with no dripping.

The second method (i.e. active sweating method) is the most often used, and this method solved the drying-out issue observed on the pre-wetted "skin" method. Cautions should be made on the adjustment of appropriate sweating rate for testing [56]. The sweating rate must be set to ensure the whole "skin" could maintain fully saturated throughout the entire testing period. Otherwise, partially dried out "skin" will significantly impact the determined clothing evaporative resistance, which tends to be significantly higher because the evaporative heat loss is much smaller [57–59]. Another issue with this method is that the surface temperature of the fabric "skin" is uncontrolled. Due to the sweat evaporation, the fabric "skin" surface temperature is found to be much lower than the controlled manikin surface [58, 59]. This will also largely impact the precision and accuracy of clothing evaporative resistance. Hence, it is highly recommended to future sweating manikins to control the fabric "skin" temperature rather than the manikin surface temperature during the wet tests.



Figure 31.7 A sweating manikin is wearing the saturated knitted fabric "skin."

The third typical type of commercialized sweating manikin is the "Walter" manikin [60]. From a technical viewpoint, the only merit of the "Walter" manikin is that, unlike many other sweating manikins that regulate the manikin surface temperature, "Walter" controls its fabric "skin" surface temperature. This design contributes to enhancing the measurement accuracy on clothing evaporative resistance. Nevertheless, the "Walter" sweating manikin has many limitations. First, this manikin has only one segment, and thus it is unable to measure clothing localized evaporative resistance. Second, the "Walter" manikin can only mimic human vaporous sweating. Hence, it fails to detect the effect of absorption of liquid sweat on clothing heat and mass transfer properties (unless intentionally wetting the tested clothing using additional water). Besides, the maximum perspiration rate of the waterproof and permeable Gore-Tex "skin" is a constant, and it is found that the perspiration rate is rather too low. It is found that the use of Gore-Tex "skin" changes the driving force for water evaporation. Normally, the main driving force for water evaporation is the water vapor pressure gradient between the skin surface and the environment [61]. However, in such test conditions where the environment permits much more sweat/water evaporation than the "skin," clothing evaporative resistance determined by the "Walter" manikin seems incorrect (i.e. the value tends to be much higher than those determined on other types of sweating manikin). Therefore, all these drawbacks greatly limit the application of the "Walter" manikin to determine clothing moisture transfer property of full-scale clothing.

It should be noted that the selection of two calculation options should be made with caution [57]. Otherwise, the reported clothing evaporative resistance data might be incorrect. For those manikins with a function of manikin surface temperature controlling (e.g. the "Newton" sweating manikin) and tests performed in isothermal conditions (i.e. $T_{\text{manikin}} = T_{\text{air}} = T_r$), the mass loss option is suggested.

The heat loss method significantly overestimates the real clothing evaporative resistance. If the manikin cannot record mass loss during the test period, the heat loss option should be corrected before use [62]. This correction model is found to be reliable and easy to use. Also, the fabric "skin" surface temperature should be used when computing the water vapor pressure at the saturated fabric "skin" surface. Wang et al. [63] established a universal equation to calculate the fabric "skin" temperature based on the heat loss observed from the test and the manikin surface temperature. This equation has been widely used by scientists to estimate the fabric "skin" temperature.

Though it is highly recommended to carry out clothing evaporative resistance in an isothermal condition, many published studies reported data from the tests performed in non-isothermal conditions. For tests performed in non-isothermal conditions, how to choose the options to calculate clothing apparent evaporative resistance (i.e. the evaporative resistance determined in non-isothermal conditions) becomes more complicated; further investigations are still required to explore this. It has been found that the condensation could significantly affect the heat exchange between the manikin and the test condition, especially for garments with limited vapor permeability [64, 65]. Thus, the mass loss method might be incorrect when being used to calculate clothing vapor resistance. Lastly, it should be emphasized that the clothing apparent evaporative resistance is only comparable with that determined at exactly the same test environmental condition.

31.5.5 Human Trials

Human wearing trials can provide valuable information that cannot be obtained from laboratory tests with test equipment (see Figure 31.8). The human wearing trials are mainly conducted in and out climatic chambers in laboratory. In climatic chambers, outdoor conditions could be mimicked with high accuracy, as well as if not more important reproducibly. In the controlled climatic chamber, it is possible to compare the performance of a number of garments on the same test subjects and thus get a good comparison of their properties in practical



Figure 31.8 Skin temperature measurements on human subjects.

applications. However, the human wearing trials are usually very time-consuming and therefore costly. Also the repeatability is lower compared with measurements carried out by thermal manikins. Besides, the measurement performed by human trials needs to be repeated by several participants in order to make the results and conclusions reliable and statistically comparable.

31.5.6 Fiber and Thermal Comfort

Fiber is the fundamental component of yarns, and usually it is the yarns that made into porous fabrics via weaving or knitting techniques. In addition, nonwoven fabrics can be constructed directly from fibers or filaments without the process of yarns. One key factor for fabrics is thermal resistance, and the trapped still air in the fabric structure contributes a lot to the heat barrier because the thermal resistance of air is eight times higher than that of fibers. According to Farnworth [66], the effective thermal conductivity of the fabric system is partly due to the air volume and partly due to the fiber fractions of the system. Thus using the effective thermal conductivity can be calculated with Eq. (31.10):

$$K_{\text{sys}} = (1 - P_{\varphi})K_a + P_{\varphi}K_f \tag{31.10}$$

where P_{φ} is the packing factor, K_a is the thermal conductivity of the air volume fraction, and K_f is the thermal conductivity of the fibrous component (Table 31.1 shows the typical thermal conductivity of various fibers).

From Eq. (31.10) it could be concluded that the more amount of still air trapped in the fabric structure, the higher the thermal insulation. Fibers affect the fabric thermal insulation via two approaches, namely, preventing air movement and providing a shield to radiative heat transfer. The thermal insulation of a fabric is determined by fiber physical properties, the structure of the fabric, and the

Table 31.1 Thermal conductivity of various fibers.

Textile fibers	Thermal conductivity (W/(m K))
Cotton	0.243
Nylon	0.171
Polyester staple	0.127
Polyester filament	0.157
Flax	0.344
Polypropylene	0.111
Rayon staple fiber	0.237
Wool	0.165
Silk	0.118
Aramid	0.192

Source: Hearle and Morton 2008 [67]. Reproduced with permission of Elsevier.

boundary air layer existing on the fabric surface. When air moves toward the fiber or fabric, its velocity of air adjacent to the fiber or fabric surface area keeps relative still to the fiber or fabric, which forms boundary air layer. Therefore, the existing boundary air layer, along with the existing still air, increases thermal insulation and provides considerable resistance to heat transfer through the fabric [6].

As mentioned above, the thermal insulation of the fabric depends on the physical structure of fiber, including its fineness, crimp, and length. Generally, the fineness of the fiber has a linear relationship with the thermal insulation because of the high surface-to-volume ratio of fine fibers. As a result of the high surface-to-volume ratio of fine fibers, many small spaces for still air between fibers can be formed, which limits the heat transfer through conduction and convection, resulting into a higher thermal insulation.

Microfiber has gained exclusive attention recently and has been used in clothing to improve clothing function because of its larger surface area. Fiber crimp can trap more still air by creating interstices in the yarn structure and thus increases the fabric thermal insulation. For example, the high thermal insulation of wool fibers can be explained by the natural crimp, which maintains a high volume of still air, explaining its traditional applications in cold weather clothing.

Additionally, Bogaty et al. [68] observed that fabric thermal insulation has close relation with the fiber arrangement. Fiber with parallel and perpendicular arrangements to the fabric surface showed improved thermal insulation. Besides, Kong et al. [69] described that fiber configuration, and its porosity can significantly impact the heat and moisture transfer. It was found that fabrics or garments made from hollow fibers could provide higher thermal insulation values because of the large still air volume trapped within the fabric. Because of its unique characteristics, hollow fibers can be used in applications like swimming suits. Hollow fibers can provide buoyancy for the body in the water and prevent human body from being cooled.

Besides the hollow fiber, with the developing of fiber technologies, functional fibers that are found growing importance may include the following:

- *Bicomponent or multicomponent fibers*: which are mainly obtained either via polymer blending or graft polymerization. For example, bicomponent synthetic fibers with low melting temperature sheath.
- Fibers manufactured by materials with inherent coloration and with a high degree of color fastness.
- Hollow fibers with a filled core or a core fiber spun with a sheath for protection or enhancement of the core properties. For example, glycol-based fillings that buffer heat changes [70].
- *Modified fibers*: fibers whose basic properties have been modified after certain physical or chemical process. For example, to increase the melting point of polyester fibers [71].

31.6 Fabric and Thermal Comfort

The heat and moisture transfer in a fabric depends on the yarn structure, the fiber geometry, and fabric construction. Compared with a flat filament, a spun yarn

or textured filament yarn can trap more still air and therefore can obtain better moisture and heat barrier, i.e. higher thermal insulation. The heat and moisture transport is also affected by the degree of yarn twist, the higher twist yarns, the more compact, resulting in lower thermal insulation because of less trapped air volume. On the other hand, the compact yarns may facilitate the capillary effect, resulting in improvement in moisture transfer.

It is proven by previous studies that the fabric thickness is the most important parameter in determining thermal insulation [72]. Generally, the thicker the fabric, the more amount of still air trapped in the fabric, providing higher thermal insulation. It is observed in some cases that there is a linear relation between the fabric thermal insulation and the fabric thickness. Compared with a single layer thick fabric, fabrics with multilayer present even higher insulation. For multilayer fabrics, however, the thermal resistance and thickness are not a linear relation [73].

The heat and moisture transfer capability is also affected by the fabric structures because different fabric structures have different levels of porosity, resulting in different volumes of still air entrapped in the fabric [118]. On average, knitted fabrics entrap more still air compared with woven fabrics, although the yarn density of weaving and knitting is a factor as well. Additionally, pile or napped constructions in fabrics can improve fabric thermal insulation, which is because the yarns or fibers perpendicular to the surface provide numerous spaces for entrapped air. These fabric insulation can be optimized when they are used as an inner layer next to the skin.

Furthermore, the fabric thermal insulation performance is also affected by its weight. However, clothing weight may deteriorate the comfort property, so it is important to balance high thermal insulation with low weight to improve comfort, and it is especially true for cold weather clothing. Lightweight fabrics can be obtained by bonding knitted fabric with woven fabric using polyurethane foam. The low density of polyurethane foam provides the sandwiched fabric-foam-fabric structure with high insulation and light weight.

In a study by Frydrych et al. [74], they compared fabrics made from regular cotton and man-made cellulose fibers. It was found that thermal insulation differed noticeably both with different types of fiber and different weaving patterns using same fiber. They also described a difference in the thermal absorption of the fabrics when different finishing processes were applied. A similar study was also performed on different clothing materials using a sweating cylinder [75]. In their study, the effectiveness of different material combinations on the thermal insulation was investigated, and significant different in thermal insulation was determined between different material combinations.

Multilayer fabrics increase the overall thickness of the garment, which contributes to increase in the total insulation of the clothing system. The multilayer clothing system normally comprises three layers: the outer layer, the middle layer, and the inner layer. The inner layer, together with the skin, forms the microclimate. Heat and moisture transport starts directly from this inner layer. The middle layer, usually made from fabrics that could entrap a large amount of air, normally contributes most to the thermal insulation. The main function of the outer layer is to provide sufficient protection to prevent the garment from being

injured. The outer layer is normally made of materials with excellent mechanical performance. In addition, functional or chemical finishing can be introduced to the outer layer in order to obtain some desirable properties such as self-cleaning. In addition to the physical properties of fiber, yarn and fabric, the thermal properties can be changed through functional coating and finishing applied to the surface of yarn or fabric.

31.7 Personal Conditioning Clothing for Improving Wear Comfort

31.7.1 Personal Cooling Clothing System

Heat strain has been regarded as one of the underlying causes for heat-related injuries and work accident, and even heat-associated high morbidity and mortality are attributed to the elicited body in extreme environments. When the ambient temperature is higher than that of the body skin in summer, sweat evaporation is the only avenue for human body to dissipate heat to environments [76]. Besides, human body may even receive conductive, convective, and radiative heat from the ambient in such extreme environments [77]. Thus, the body thermal balance would be easily disrupted in such conditions with the elevated body thermophysiological (such as core temperature rise) [78]. When the core temperature reaching 40 °C, cellular damage occurs rapidly, initiating a cascade of events that may lead to organ failure and possible fatality [79].

Recently, there has been a shift in attention from a focus on cooling the entire macro-environment (mainly using air conditioner) to cooling the microenvironment around the human body (using personal cooling strategies [PCSs]) [80]. Generally speaking, PCSs are energy saving, more flexible and user-friendly. Air fan (a type of PCS) is a direct cooling strategy and proved to be effective below some temperature limits [81, 82]. Besides the environmental limits, the less portability of the air fans limiting its use to active people. Regarding this, portable personal cooling clothing (PCC) may serve as an alternative to mitigate body heat strain in hot conditions [83, 84].

External cooling source may be incorporated into clothing to create a cooler the microenvironment between the human body and clothing to promote body heat dissipation. Various types of PCC have been developed during last few decades, and they could generally be divided into five categories: phase change materials (PCMs) for cooling clothing, evaporative cooling clothing (ECC), liquid cooling clothing (LCC), air cooling clothing (ACC), and the hybrid cooling clothing combining two or more cooling techniques [85–87]. The PCMs (such as frozen gels and ice packs) are usually placed closely to the body to absorb body heat during phase change. The cooling effect of PCMs mainly relies on their melting temperature and heat fusion, as well as their mass and the body coverage area. ACC utilizes the circulated natural or cold air to enhance evaporative or/and convective heat loss. The current existing ACC are generally configured in two forms: incorporating arrayed fine hoses with air pores into clothing to direct air flow (natural or cold air) to the body skin, powered by an external air compressor, and



Figure 31.9 (a) Phase change material pack and (b) the air ventilation fan.

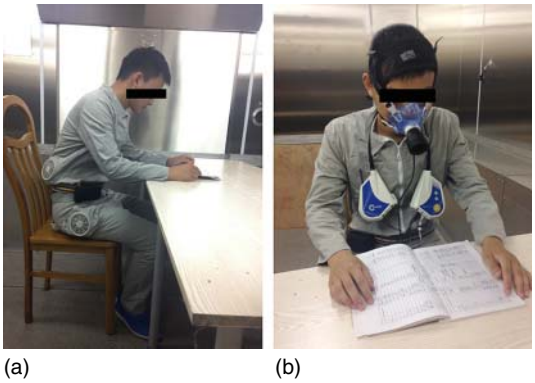


Figure 31.10 Hybrid personal cooling clothing incorporated with phase change materials and ventilation fans.

embedding air fans into clothing to make efficient air ventilation (natural air), powered by portable batteries (see Figure 31.9). ACC circulating natural air works on the same rational as air fans, both of which utilizes the increased air velocity around the body skin to enhance evaporative heat loss. LCC utilizes the positive temperature gradient between the human skin and the liquid to promote the conductive and convective heat dissipation. It was developed by incorporating a network of fine tubes into clothing in close contact with the body skin, and the circulating cold liquid (such as water) in tubes, pumps from a refrigerating system, removes excessive body heat. Hybrid cooling strategy (only one study was retrieved) combining liquid and air cooling sources has been shown to bring large cooling effects in reducing body physiological heat strain and improving human performance in hot and moderate humid environment [88–91] (see Figure 31.10). ECC utilizes water stored in the clothing to absorb heat from the human body to evaporate, and this type of PCC is normally light (lower than 1 kg), cheap, and convenient to use.

All the aforementioned studies focus on the cooling effects of PCC in specific fields such as firefighting, military, and biological and chemical protection fields where PCC is worn under protective clothing [92–94]. The cooling effect of the PCC worn as the outer layer might be different from that of PCC used as the interlayer, as the heat exchange between PCC and the ambient is more enhanced, and sweat evaporation is also less restricted compared with conditions where PCC is used as an outer layer [95].

31.7.2 Personal Heating Clothing System

Since there is no heating, ventilation, and air-conditioning (HVAC) system in some world spots such as Yangtze River urban areas in China, people there may experience cold discomfort at their ears, cheeks, hands, and feet while sitting in unheated cold environments in winter (below 10.0 °C). One possible way to minimize the body heat loss in cold environments is to wear high insulating traditional cold protective clothing or wear clothing in corporate with auxiliary heating [55]. Normally, traditional cold weather clothing has a multilayer structure and is usually thick and heavy. Besides, traditional cold weather clothing restricts the human body movement, reduces the manual dexterity, and thereby impairs the human work performance [96]. Moreover, the total thermal insulation of multilayer clothing has an upper limit, i.e. around 4.3 clo [97]. Hence, the usage of traditional clothing to improve body thermal comfort has been limited in extremely cold environments or long duration mild cold exposures [96]. Thereby, auxiliary heating sources implanted into clothing provide a promising solution to this problem. Properly designed heated clothing has been proven to be capable of providing the human body with sufficient protection in cold environments without sacrificing freedom of body movement.

The heating clothing currently available nowadays may be divided into four types: electrically heated clothing (EHC, see Figure 31.11); chemically heated clothing (CHC), harnessing heat generated via chemical reaction; phase change heating clothing incorporated with PCMs, and air/fluid flow heated clothing. Heated gloves and socks have been extensively examined, and they have evidently improved the thermal comfort in the hands/feet and manual dexterity in unconventional cryogenic environments [96]. Choi et al. [98] observed the clothing incorporated PCM exhibited higher microclimatic temperatures and improved thermal sensations compared with the non-heated clothing, but it had no effect on the rectal and mean skin temperatures. Coca et al. [99] described that a liquid heated garment (LHG), with 24 °C inletting water, could be useful in stabilizing the rectal temperature and maintaining comfort before and during exercise. Flouris et al. [100] also observed a higher mean body temperature during exercising in LHG compared with the non-heating and pre-heating (in LHG before exercise) scenarios, and the last two scenarios triggered higher frequency of cold-induced vasodilation (CIVD) in extremities. Chan and Burton [101] examined the performance of a CHC system (i.e. a jacket equipped with 30 heating pads and a pair of gloves incorporated with 4 chemical heating pads), and they observed that the CHC could maintain the torso skin temperature, but it

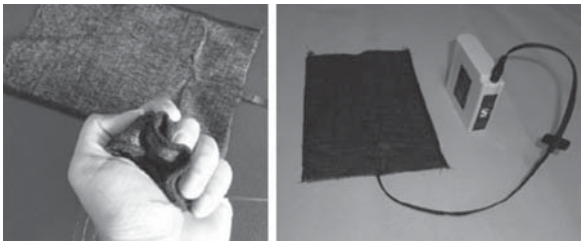


Figure 31.11 Heating fabric pads for engineering electrically heated clothing (EHC).

had no effect on other body parts that were not covered by the heating sachets in cold water. Kirsi et al. [102] investigated the performance of an electrically heated vest in a very cold environment (i.e. −15 °C) while having subjects standing or doing light work. The vest could significantly raise local skin temperatures and improve the thermal sensation of the torso but exhibited limited effect on both core and extremity temperatures. Furthermore, the effectiveness of the heated clothing mainly depends on the heating power and the exposing temperatures. For instance, Rantanen et al. [103] discovered that the electrically heated shirt provided sufficient protection to wearers in normal winter environment in Finland. However, decrease in the skin temperature was observed in wearers in extremely cold environments (i.e. from −14 to −20 °C). Heated clothing with a large heating power was also found to be able to improve both local and overall body thermal comfort (such as promoted finger blood flow and dexterity) when exposing to −25 °C for three hours [104].

31.7.3 Smart Heating Sleeping Bag

Sleeping bags have been regarded as essential protective products for sleeping outdoors, especially under cold environments. On applications, especially for expedition and mountaineering, the maximal thermal insulation with relatively lightweight is of the most important parameters for a sleeping bag [116]. Currently, sleeping bags have different shapes (e.g. mummy, rectangular, and quit shaped) and usually have a three-layer configuration, namely, the outer layer, an inner layer, and the filler [105]. The outer and inner layers are usually made of synthetic materials, and the filler material may be cotton, down, or synthetic fibers.

In order to characterize the performance of the sleeping bag, many models have been developed to estimate the minimal operating temperature of the sleeping bags, e.g. the Goldman's model, the KSU model, the Belding's model, the IREQ model, and the Havenith model [106]. In contrast to the minimal operating temperatures, the EN 13537 [107] standard proposed a model to predict the comfort operating temperature. The EN 13537 [107] listed out four label temperatures: maximum temperature, comfort temperature, limit temperature, and extreme temperature. Among the four above labeled temperatures, the comfort and limit temperatures are considered to be the most important temperatures. The comfort temperature is defined as the lower temperature threshold at which a standard woman could sleep for eight hours with a global thermal equilibrium state and just without feeling cold at a relaxed posture. The limit temperature is the lower temperature threshold at which a standard man could sleep for eight hours with a global thermal equilibrium state and just without feeling at a curved up posture [107]. Unfortunately, the EN 13537 [107] has not been widely adapted by sleeping bag manufacturers. Manufactures tend to label their products by different methods. For example, there are manufacturers labeling the temperatures based on customers' feedbacks, and others may label the temperatures based on the sleeping bag's physical properties such as the thickness, weight, and loftiness. Therefore, the thermal performance of sleeping bags labeled with same temperature ranges may vary greatly [108].

Even though there are quite a few models available for predicting minimal operating temperature, all those models have been questioned for mainly focusing on the global thermal comfort of the wearers. The models appear to have less consideration to the local thermal comfort, especially for the human feet. Compared with other body regions, such human extremities as the feet are more sensitive to cold environments, and their temperatures will decrease rapidly when being exposed to cold due to their larger specific surface area and relatively low local metabolic rate [109]. Compared with the other body parts, the specific surface area of human feet is around 2.5–3.0 times larger than that of the whole body, indicating it will lose heat more rapidly when exposing to cold. The decreased temperatures will lead to thermal discomfort, and further decrease may cause pain feeling in the toe and feet. Moreover, the accumulation of local thermal discomfort at the feet can significantly influence the whole body thermal comfort [110, 111].

Local thermal discomfort at the body extremities such as the feet has been widely reported, albeit that the mean skin temperature of the wearers is still within the thermoneutral range (i.e. 32–34 °C) when using sleeping bags at their predefined comfort temperatures [110, 112, 113, 119]. Huang [114] observed a similar tendency of decrease in toe temperatures on both male and female subjects when comparing the five models (i.e. the EN 13537 [107] model, the Goldman's model, the KSU model, the Belding's model, and the den Hartog's model). Lin et al. [112] reported that the foot temperature underwent a continuously and rapidly drop in sleeping bags under the EN 13537 [107] defined operating temperatures. Within the two hours exposure, the foot temperature dropped to almost 14 °C, at which strong cold sensations occurred even the mean skin temperature was well maintained within the thermal neutral range (i.e. 32–34 °C).

A series of studies have been conducted by the authors [110, 113, 115] to investigate the improvement in local and whole body thermal comfort using smart electrically heated sleeping bags. A smart heating sleeping bag that could response to the changes of the foot temperature was developed (see Figure 31.12). It was found that, compared with the traditional sleeping bag, the newly developed smart heating sleeping bag could maintain the foot temperature within the comfort range throughout the eight-hour trials under the EN 13537 [107] defined comfort temperatures, whereas linearly decreasing in foot



Figure 31.12 A smart electrical heating sleeping bag.

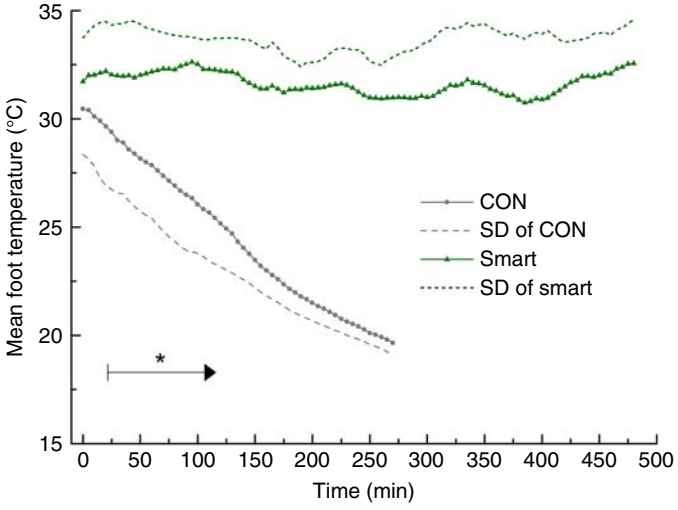


Figure 31.13 Time course changes in the mean foot temperature in CON (i.e. the traditional sleeping bag) and smart (i.e. the smart electrically heated sleeping bag). $^{*}p < 0.05$.

temperatures were observed in the traditional sleeping bags (see Figure 31.13). Additionally, it was noted that both local and overall thermal comfort were greatly improved in the smart heating sleeping bag.

31.8 Conclusions

Comfort management property plays an important role in fibrous materials, particularly for textiles and apparel. Comfort management includes regulation of body temperature and moisture transfer (including absorption, adsorption, desorption, wetting, wicking, drying, etc.). Due to advancing technology, more advanced intelligent and smart textiles will appear, which may greatly facilitate the improvement of the comfort property of textiles and clothing. In the future, flexible and small size sensors and actuators will be embedded into textiles, and this makes the textile even smarter. Personal cooling and heating clothing will be regulated based on the wearers' real-time physiological and psychological status. On the other hand, more advanced test equipment will be also developed. Measurements of heat and moisture transfer properties of textiles will become quicker, more precise, and more reproducible and thereby contribute to improving the precision of mathematical models.

References

1 Fanger, P.O. (1970). *Thermal Comfort*. Copenhagen: Danish Technical Press.
2 Parsons, K.C. (2002). *Human Thermal Environment*. London: Taylor & Francis.

3 Rossi, R. (2009). Comfort and thermoregulatory requirements in cold weather clothing. In: *Textiles for Cold Weather Apparel* (ed. J.T. Williams), 3–18. New York: CRC Press.

4 Goldman, R.F. (1988). *Biomedical Effects of Clothing on Thermal Control and Strain, Handbook on Clothing, Biomedical Effects of Military Clothing and Equipment Systems*, 1–18. Soesterberg: TNO Institute of Perception.

5 Li, Y. (2001). The science of clothing comfort. *Textile Progress* 31: 1–135.

6 Song, G. (2009). Thermal insulation properties of textiles and clothing. In: *Textiles for Cold Weather Apparel* (ed. J.T. Williams), 19–32. New York: CRC Press.

7 ASHRAE 55 (2013). Thermal Environmental Conditions for Human Occupancy. In: . Atlanta: American Society of Heating Refrigeration and Air Conditioning Engineers, American Society of Heating Refrigeration and Air Conditioning Engineers, Inc.

8 ISO 7730 (1984). *Moderate Thermal Environments-determination of the PMV and PPD Indices and Specification of the Conditions for Thermal Comfort*. Geneva: International Standards Organization.

9 Houghton, F.C. and Yagloglou, C.P. (1923). Determining equal comfort lines. *Transactions of American Society of Heating and Ventilation Engineers* 29: 165–176.

10 Houghton, F.C. and Yagloglou, C.P. (1924). Cooling effect on human beings produced by various air velocities. *Transactions of American Society of Heating and Ventilation Engineers* 30: 193–212.

11 Missenard, A. (1948). A thermique des ambiences: equivalences de passage, equivalences deséjours. *Chaleur et Industrie* 276: 159–172.

12 Dufton, A.F. (1929). The eupatheostat. *Journal of Scientific Instruments* 6: 249–251.

13 Dufton, A.F. (1936). The equivalent temperature of a warmed room. *Journal of the Institution of Heating & Ventilating Engineers* 4: 227–229.

14 Henry, P.S.H. (1939). Diffusion in absorbing media. *Proceedings of the Royal Society of London Series A* 171: 215–241.

15 ASTM E96 (2016). *Standard Test Methods for Water Vapor Transmission of Materials*. West Conshohocken, PA: American Society for Testing and Materials.

16 ISO 15496 (2004). *Textiles – Measurement of Water Vapor Permeability of Textiles for the Purpose of Quality Control*. Geneva: International Organisation for Standardisation.

17 ISO 2528 (1995). *Sheet Materials. Determination of Water Vapour Transmission Rate-Gravimetric (dish) Method*. Geneva: International Organisation for Standardisation.

18 ASTM F1868 (2014). *Standard Test Method for Thermal and Evaporative Resistance of Clothing Materials Using a Sweating Hot Plate*. West Conshohocken, PA: American Society for Testing and Materials.

19 ISO 11092 (2014). *Textiles-Physiological Effects-Determination of Physiological Properties-Measurement of Thermal and Water-vapour Resistance under Steady-state Conditions (Sweating Guarded-hotplate Test)*. Geneva: International Organisation for Standardisation.

20 Karppinen, T., Kassamakov, I., Haeggstrom, E., and Stor-Pellinen, J. (2004). Measuring paper wetting processes with laser transmission. *Measurement Science and Technology* 15: 1223–1229.

21 Rengasamy, R.S. (2006). Wetting phenomena in fibrous materials. In: *Thermal and Moisture Transport in Fibrous Materials* (eds. N. Pan and P. Gibson), 156–187. Cambridge: Woodhead Publishing.

22 Uddin, F. and Lomas, M. (2010). Wettability of easy-care finished cotton. *Fibres and Textiles in Eastern Europe* 18: 56–60.

23 Birrfelder, P., Dorrestijn, M., Roth, C., and Rossi, R.M. (2013). Effect of fiber count and knit structure on intra- and inter-yarn transport of liquid water. *Textile Research Journal* 83: 1477–1488.

24 Zhong, W. (2006). Surface tension, wetting and wicking. In: *Thermal and Moisture Transport in Fibrous Materials* (eds. N. Pan and P. Gibson), 136–155. Cambridge: Woodhead Publishing.

25 Zhang, Y., Wang, H., Zhang, C., and Chen, Y. (2007). Modeling of capillary flow in shaped polymer fiber bundles. *Journal of Materials Science* 42: 8035–8039.

26 AATCC TM 197 (2013). *Vertical Wicking of Textiles*. Research Triangle Park, NC: American Association of Textile Chemists and Colorists.

27 AATCC TM 198 (2013). *Horizontal Wicking of Textiles*. Research Triangle Park, NC: American Association of Textile Chemists and Colorists.

28 DIN 53924 (1997). *Testing of Textiles - Velocity of Soaking Water of Textile Fabrics (Method by Determining the Rising Height)*. Berlin: German Institute for Standardization.

29 AATCC TM 39 (1977). *Evaluation of Wettability*. Research Triangle Park, NC: American Association of Textile Chemists and Colorists.

30 ISO 4920 (2012). *Textile Fabrics -- Determination of Resistance to Surface Wetting (Spray Test)*. Geneva: International Standards Organization.

31 Goldman, R.F. (1974). Clothing design for comfort and work performance in extreme thermal environments. *Transactions of the New York Academy of Sciences* 36: 531–544.

32 Umbach, K.H. (1983). Evaluation of comfort characteristics of clothing by use of laboratory measurements and predictive calculations. *Proceedings of the 1981 International Conference on Protective Clothing Systems*, Stockholm, Sweden.

33 ISO 11079 (2007). *Ergonomics of the Thermal Environment-Determination and Interpretation of Cold Stress When Using Required Clothing Insulation (IREQ) and Local Cooling Effects*. Geneva: International Organisation for Standardisation.

34 Lotens, W.A. (1993). Heat transfer from humans wearing clothing. PhD destination. Netherland: Technische Universiteit Delft.

35 Wissler, E.H. and Havenith, G. (2009). A simple theoretical model of heat and moisture transport in multi-layer garments in cool ambient air. *European Journal of Applied Physiology* 105: 797–808.

36 CAN/CGSB 4.2 No. 78.1-2001 (2001). *Textile Test Methods-Thermal Protective Performance of Material for Clothing*. Quebec: Canadian General Standards Board.

37 ASTM D1518-85 (2003). *Standard Test Method for Thermal Transmittance of Textile*. West Conshohocken, PA: American Society for Testing and Materials.

38 BS 4745 (2005). *Determination of the Thermal Resistance of Textiles*. London: British Standards Institute.

39 BS 7209 (1990). *Specification for Water Vapour Permeable Apparel Fabrics*. London: British Standards Institute.

40 CAN/CGSB-4.2 No. 49-99 (1999). *Textile Test Methods Resistance of Materials to Water Vapour Diffusion*. Quebec: Canadian General Standards Board.

41 Woodcock, A.H. (1962). Moisture transfer in textile systems. *Textile Research Journal* 8: 628–633.

42 Lu, Y., Wang, F., Wan, X. et al. (2015). Clothing resultant thermal insulation determined on a moveable thermal manikin: Part I effects of wind and body movement on total insulation. *International Journal of Biometeorology* 59: 1475–1486.

43 Lu, Y., Wang, F., Wan, X. et al. (2015). Clothing resultant thermal insulation determined on a moveable thermal manikin: Part II effects of wind and body movement on localised insulation. *International Journal of Biometeorology* 59: 1487–1498.

44 ASTM F1291 (2015). *Standard Test Method for Measuring the Thermal Insulation of Clothing Using a Heated Manikin*. West Conshohocken, PA: American Society for Testing and Materials.

45 ISO 15831 (2004). *Clothing-Physiological Effects-Measurement of Thermal Insulation by Means of a Thermal Manikin*. Geneva: International Organisation for Standardisation.

46 ISO 9920 (2007). *Ergonomics of the Thermal Environment. Estimation of Thermal Insulation and Water Vapour Resistance of a Clothing Ensemble*. Geneva: International Organisation for Standardisation.

47 Huang, J. (2008). Calculation of thermal insulation of clothing from mannequin test. *Measurement Techniques* 51: 428–435.

48 Kuklane, K., Gao, C., Wang, F., and Holmér, I. (2012). Parallel and serial methods of calculating thermal insulation in European manikin standards. *International Journal of Occupational Safety and Ergonomics* 18: 171–179.

49 Xu, X., Endrusick, T., Gonzalez, J. et al. (2008). Comparison of parallel and serial methods for determining clothing insulation. *Journal of ASTM International* 5: 1–6.

50 Huang, J. (2012). Theoretical analysis of three methods for calculating thermal insulation of clothing from thermal manikin. *Annals of Occupational Hygiene* 56: 728–735.

51 Oliveira, A.V.M., Gaspar, A.R., and Quintela, D.A. (2008). Measurements of clothing insulation with a thermal manikin operating under the thermal comfort regulation mode: comparative analysis of the calculation methods. *European Journal of Applied Physiology* 104: 679–688.

52 ASTM F2370 (2015). *Standard Test Method for Measuring the Evaporative Resistance of Clothing Using a Sweating Manikin*. West Conshohocken, PA: American Society for Testing and Materials.

53 Wang, F. (2011). Clothing evaporative resistance: its measurements and application in prediction of heat strain. PhD dissertation. Lund, Sweden: Lund University.

54 Wang, F., Gao, C., Kuklane, K., and Holmér, I. (2009). A study on evaporative resistances of two skins designed for thermal manikin Tore under different environmental conditions. *Journal of Fiber Bioengineering and Informatics* 1: 301–305.

55 Wang, F., Gao, C., Kuklane, K., and Holmér, I. (2010). A review of technology of personal heating garments. *International Journal of Occupational Safety and Ergonomics* 16: 387–404.

56 Lu, Y., Wang, F., Peng, H. et al. (2016). Effect of sweating set rate on clothing real evaporative resistance determined on a sweating thermal manikin in a so-called isothermal condition ($T_{manikin}=T_a=T_r$). *International Journal of Biometeorology* 60: 481–488.

57 Wang, F., Gao, C., Kuklane, K., and Holmér, I. (2011). Determination of clothing evaporative resistance on a sweating thermal manikin in an isothermal condition: heat loss method or mass loss method? *Annals of Occupational Hygiene* 55: 775–783.

58 Wang, F., Gao, C., Kuklane, K., and Holmér, I. (2012). A comparison of three different calculation methods for clothing evaporative resistance. *Proceedings of The 5th European Conference on Protective Clothing and NOKOBETEF 10 (ECPC)*, Valencia, Spain.

59 Wang, F., Kuklane, K., Gao, C., and Holmér, I. (2012). Effect of temperature difference between manikin and wet fabric skin surfaces on clothing evaporative resistance: how much error is there? *International Journal of Biometeorology* 56: 177–182.

60 Fan, J., Chen, Y., and Zhang, W. (2001). A perspiring fabric thermal manikin: its development and use. In: *Proceedings of the Fourth International Meeting on Thermal Manikins*, September 2001, pp. 7–12.

61 Lu, Y., Wang, F., and Peng, H. (2016). Effect of two sweating simulation methods on clothing evaporative resistance in a so-called isothermal condition. *International Journal of Biometeorology* 60: 1041–1049.

62 Wang, F., Zhang, C., and Lu, Y. (2015). Correction of the heat loss method for calculating clothing real evaporative resistance. *Journal of Thermal Biology* 52: 45–51.

63 Wang, F., Kuklane, K., Gao, C., and Holmér, I. (2010). Development and validity of a universal empirical equation to predict skin surface temperature on thermal manikins. *Journal of Thermal Biology* 35: 197–203.

64 Havenith, G., Fogarty, A., Bartlett, R. et al. (2008). Male and female upper body sweat distribution during running measured with technical absorbents. *European Journal of Applied Physiology* 104: 245–255.

65 Havenith, G., Richards, M., Wang, X. et al. (2008). Apparent latent heat of evaporation from clothing: attenuation and 'heat pipe' effects. *Journal of Applied Physiology* 104: 142–149.

66 Farnworth, B. (1983). Mechanisms of heat flow through clothing insulation. *Textile Research Journal* 53: 717–725.

67 Hearle, J.W.S. and Morton, W.E. (2008). *Physical Properties of Textile Fibres*, 4e. Cambridge: Woodhead Publishing.

68 Bogaty, H., Hollies, N.R.S., and Harris, M. (1957). Some thermal properties of fabrics: Part I: The effect of fiber arrangement. *Textile Research Journal* 27: 445–449.

69 Kong, L.X., Li, Y., She, F.H. et al. (2001). Effect of fiber geometry and porosity on heat and moisture transfer in textiles. *Proceedings of the Textile Institute 81st World Conference - An Odyssey in Fibers and Spaces*, Melbourne, Australia.

70 Virgo, T.L. and Frost, C.M. (1985). Filled hollow fibres. *Textile Research Journal* 56: 737–743.

71 Zhu, S., Shi, M., Tian, M. et al. (2015). Burning behavior of irradiated PET flame-retardant fabrics impregnated with sensitizer. *Materials Letters* 160: 58–60.

72 Holcombe, B.V. and Hoschke, B.N. (1983). Dry heat transfer characteristics of underwear fabrics. *Textile Research Journal* 53: 368–374.

73 Wilson, C.A., Niven, B.E., and Laing, R.M. (1999). Estimating thermal resistance of the bedding assembly from thickness of materials. *International Journal of Clothing Science and Technology* 11: 262–267.

74 Frydrych, I., Dziworska, G., and Bilska, J. (2002). Comparative analysis of the thermal insulation properties of fabrics made of natural and man-made cellulose fibres. *Fibres & Textiles in Eastern Europe* 10 (4): 40–44.

75 Celcar, D., Meinander, H., and Gersak, J. (2008). A study of the influence of different clothing materials on heat and moisture transmission through clothing materials, evaluate using a sweating cylinder. *International Journal of Clothing Science and Technology* 20: 119–130.

76 Jay, O., Cramer, M.N., Ravanelli, N.M., and Hodder, S.G. (2015). Should electric fans be used during a heat wave? *Applied Ergonomics* 46: 137–143.

77 Cheung, S.S. and McLellan, T.M. (1998). Heat acclimation, aerobic fitness, and hydration effects on tolerance during uncompensable heat stress. *Journal of Applied Physiology* 84: 1731–1739.

78 Kenny, G.P. and Jay, O. (2013). Thermometry, calorimetry, and mean body temperature during heat stress. *Comprehensive Physiology* 3: 1689–1719.

79 Bowler, K. (1981). Heat death and cellular heat injury. *Journal of Thermal Biology* 6: 171–178.

80 Tham, K.W. and Pantelic, J. (2010). Performance evaluation of the coupling of a desktop personalized ventilation air terminal device and desk mounted fans. *Building and Environment* 45: 1941–1950.

81 Zhang, C., Song, W., and Wang, F. (2016). Evaporative cooling techniques to reduce body heat strain in heatwaves. *Proceedings of the 11th International Meeting on Thermal Manikin and Modelling (11i3m)*, Suzhou, China.

82 Ravanelli, N.M., Hodder, S.G., Havenith, G., and Jay, O. (2015). Heart rate and body temperature responses to extreme heat and humidity with and without electric fans. *JAMA* 313: 724–725.

83 Chan, A.P., Song, W., and Yang, Y. (2015). Meta-analysis of the effects of microclimate cooling systems on human performance under thermal stressful environments: potential applications to occupational workers. *Journal of Thermal Biology* 49–50: 16–32.

84 Gao, C., Kuklane, K., Wang, F., and Holmér, I. (2012). Personal cooling with phase change materials to improve thermal comfort from a heat wave perspective. *Indoor Air* 22: 523–530.

85 House, J.R., Lunt, H.C., Taylor, R. et al. (2013). The impact of a phase-change cooling vest on heat strain and the effect of different cooling pack melting temperatures. *European Journal of Applied Physiology* 113: 1223–1231.

86 Kenny, G.P., Schissler, A.R., Stapleton, J. et al. (2011). Ice cooling vest on tolerance for exercise under uncompensable heat stress. *Journal of Occupational and Environmental Hygiene* 8: 484–491.

87 Song, W. and Wang, F. (2016). The hybrid personal cooling system (PCS) could effectively reduce the heat strain while exercising in a hot and moderate humid environment. *Ergonomics* 59: 1009–1018.

88 Barhood, M.J., Davey, S., House, J.R., and Tipton, M.J. (2009). Post-exercise cooling techniques in hot, humid conditions. *European Journal of Applied Physiology* 107: 385–396.

89 Lai, D., Wei, F., Lu, Y., and Wang, F. (2017). Evaluation of a hybrid personal cooling system using a manikin operated in constant temperature mode and thermoregulatory model control mode in warm conditions. *Textile Research Journal* 87: 46–56.

90 Semeniuk, K.M., Dionne, J.P., Makris, A., and Medina, T. (2005). Evaluating the physiological performance of a liquid cooling garment used to control heat stress in hazmat protective ensembles. *Journal of ASTM International* 2: 1–9.

91 Song, W., Wang, F., and Wei, F. (2016). Hybrid cooling clothing to improve thermal comfort of office workers in a hot indoor environment. *Building and Environment* 100: 92–101.

92 Hadid, A., Yanovich, T., Erlich, T. et al. (2008). Effect of a personal ambient ventilation system on physiological strain during heat stress wearing a ballistic vest. *European Journal of Applied Physiology* 104: 311–319.

93 Reffeltrath, P.A. (2006). Heat stress reduction of helicopter crew wearing a ventilated vest. *Aviation Space and Environmental Medicine* 77: 545–550.

94 Vellerand, A.L., Michas, R.D., Frim, J., and Ackles, K.N. (1991). Heat balance of subjects wearing protective clothing with liquid or air-cooled vest. *Aviation Space and Environmental Medicine* 62: 383–391.

95 Teunissen, L.P.J., Wang, L., Chou, S.N. et al. (2014). Evaluation of two cooling systems under a firefighter coverall. *Applied Ergonomics* 45: 1433–1438.

96 Risikko, T. and Anttonen, H. (1997). Use of personal heaters in cold work. *Proceedings of the 1st International Symposium on Problems with Cold Work*, Stockholm, Sweden.

97 Hollies, N.R.S. and Goldman, R.F. (1977). *Clothing Comfort: Interaction of Thermal, Ventilation, Construction and Assessment Factors*. Ann Arbor, MI: Ann Arbor Science Publishers Inc.

98 Choi, K., Chung, H., Lee, B. et al. (2005). Clothing temperature changes of phase change material-treated warm-up in cold and warm environments. *Fibers and Polymers* 6: 343–347.

99 Coca, A., Koscheyev, V.S., Dancisak, M.J., and Leon, G.R. (2002). Optimization of thermal regimes within a liquid cooling/warming garment for body heat balance during exercise. *Medicine and Science in Sports and Exercise* 34: S220.

100 Flouris, A., Westwood, D., Mekjavic, I., and Cheung, S. (2008). Effect of body temperature on cold induced vasodilation. *European Journal of Applied Physiology* 104: 491–499.

101 Chan, C.Y.L. and Burton, D.R. (1982). A low level supplementary heating system for free dives. *Ocean Engineering* 9: 331–346.

102 Kirsi, H., Rissanen, S., Rintamaki, H., and Hzvarinen, V. (2013). Clothing and skin temperatures and heat flow while wearing far infrared heating vest in the cold-a thermal manikin and test subject study. *Proceedings of the 15th International Conference on Environmental Ergonomics (ICEE)*, Queenstown, New Zealand.

103 Rantanen, J., Vuorela, T., Kukkonen, K. et al. (2001). Improving human thermal comfort with smart clothing. *Proceedings of 2001 IEEE International Conference on System, Man and Cybernetics*, New York.

104 Brajkovic, D., Ducharme, M.B., and Frim, J. (1998). Influence of localized auxiliary heating on hand comfort during cold exposure. *Journal of Applied Physiology* 85: 2054–2065.

105 Zuo, J. (2004). Factors affecting the insulation value of sleeping bag systems. PhD dissertation. Manhattan, NY, USA: Kansas State University.

106 Huang, J. (2008). Prediction of air temperature for thermal comfort of people using sleeping bags: a review. *International Journal of Biometeorology* 52: 717–723.

107 EN 13537 (2012). *Requirements for Sleeping Bags*. Brussels: European Committee for Standardization.

108 McCullough, E.A., Huang, J., and Jones, B.W. (2005). Evaluation of EN 13537 and other models for predicting temperature ratings of sleeping bags. *The 11th International Conference on Environmental Ergonomics (ICEE)*, Ystad, Sweden.

109 Kuklane, K. (2009). Footwear for cold weather conditions. In: *Textiles for Cold Weather Apparel* (ed. J.T. Williams), 342–373. New York: CRC Press.

110 Zhang, C., Xu, P., Lai, D. et al. (2016). Electrically heated sleeping bags could improve the human feet thermal comfort in cold outdoor environments. *Industria Textila* 57: 164–173.

111 Song, W.F., Zhang, C.J., Lai, D.D., Wang, F.M., Kuklane, K. (2016). Use of a novel smart heating sleeping bag to improve wearers' local thermal comfort in the feet. *Scientific Report* 6: 19326.

112 Lin, L.Y., Wang, F., Kuklane, K. et al. (2013). A laboratory validation study of comfort and limit temperatures of four sleeping bags defined according to EN13537 (2002). *Applied Ergonomics* 44: 321–326.

113 Zhang, C., Ren, C., Li, Y. et al. (2016). Designing a smart electrical heating sleeping bag to improve wearers' feet thermal comfort while sleeping in a

cold ambient environment. *Textile Research Journal* https://doi.org/10.1177/0040517516651104.

114 Huang, J. (2003). Evaluation of heat loss models for predicting temperature ratings of sleeping bags. PhD dissertation. Manhattan, NY: Kansas State University.

115 Song, W., Zhang, C., Lai, D. et al. (2016). A novel smart heating sleeping bag to improve wearers' local thermal comfort in the feet. *Scientific Reports* 6: 19326.

116 Johnson, R. (2004). Pick the best sleeping bag. *Outdoor Life* 211: 132.

117 Ogulata, T. and Serin, M. (2010). Investigation of porosity and air permeability values of plain knitted fabrics. *Fibres & Textiles in Eastern Europe* 18: 7–10.

118 Taylor, N.A.S., Machado-Moreira, C.A., van den Heuvel, A.M.J. et al. (2009). The roles of hands and feet in temperature regulation in hot and cold environments. *Proceedings of the 13th International Conference on Environmental Ergonomics*, Boston, MA, USA.

119 Wang, F., Kuklane, K., Gao, C., and Holmér, I. (2010). Development and validity of a universal empirical equation to predict skin surface temperature on thermal manikins. *Journal of Thermal Biology* 35: 197–203.

32

Fibers for Radiation Protection

Boris Mahltig

Hochschule Niederrhein, University of Applied Sciences, Faculty of Textile and Clothing Technology, Webschulstraße 31, 41065 Mönchengladbach, Germany

32.1 Introduction

This chapter will present and discuss fibrous materials for radiation protection. For this, fibers for radiation protection are the aim of further discussion. However, at first, some important questions have to be checked before taking a view on different fibers and their properties. These questions are: what is the meaning of the term "radiation protection" and why a radiation protection is important?

Radiation protection can be easily described as protection of human, animals, or materials against destructive influences from electromagnetic radiation. This protection is gained by a decrease of the radiation intensity to lower values or in best case to zero intensity. This is also achieved by a protective material with low transmission properties for a specific type of radiation. The best way to describe is probably a material acting as a shield, and if you are behind this shield, radiation cannot reach you. Now, a second question comes into being: what may be the reason to avoid exposure to radiation? Simple and very general – it can be stated that by electromagnetic radiation a certain amount of energy is transmitted and the energy is transferred to the radiation-exposed material at a certain amount. Such an energy input can damage a living organism or a material to a certain degree. The kind of damage and its intensity are strongly determined by the type of radiation and its strength.

Different types of electromagnetic radiation are roughly summarized in Figure 32.1 and Table 32.1 [1, 2]. The types of radiation are distinguished by their wavelength λ (m), which is related to the frequency ν (s^{-1}) by the following equation: $\nu = c/\lambda$. In this equation, c is the speed of light with $c = 2.998 \times 10^8$ (m/s). The wavelength is also related to the quantum energy of light $E = h\nu$ with the Planck constant $h = 6.626 \times 10^{-34}$ J s [1].

In a simpler picture, the quantum energy can be understood as the energy that is carried by one single light particle called photon. For this, it is often mentioned that light with shorter wavelength contains higher energy. However, in a more exact description, it should be stated that this is the energy for one photon (photon energy) and not the energy of a radiation in total [2]. Of course, also the light

Handbook of Fibrous Materials, First Edition. Edited by Jinlian Hu, Bipin Kumar, and Jing Lu.
© 2020 Wiley-VCH Verlag GmbH & Co. KGaA. Published 2020 by Wiley-VCH Verlag GmbH & Co. KGaA.

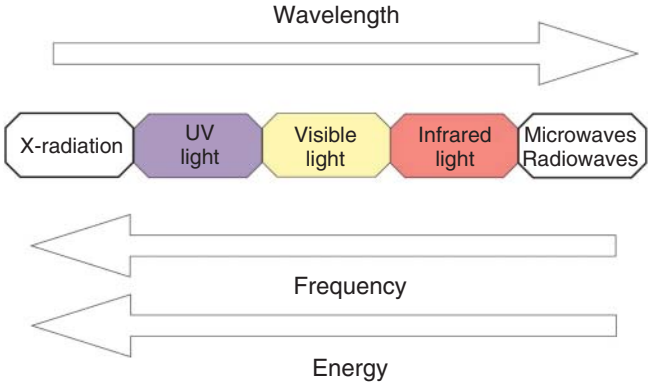


Figure 32.1 Schematic overview on different types of electromagnetic radiation, according to their wavelength, frequency, and energy.

Table 32.1 Overview on different types of radiation, their wavelength, and some potential reasons and applications for radiation protection.

Type of radiation	Range of wavelength (nm)	Reason for protection and potential applications	Protective functional component
Radiowaves, microwaves/ electrosmog	$>10^6$	EMI shielding, protection of electronic devices and identity	Electric conductive materials (e.g. elementary metals or carbon in conductive form as graphite, carbon black, or carbon nanotubes [CNTs])
Infrared radiation/IR light	$780–10^6$	Heat management, camouflage	IR reflective materials, e.g. metals or special metal oxides
Visible light/vis	400–780	Optical protection	Dyes or color pigments
Ultraviolet radiation/UV light	10–400	Prevention of sun burn, skin cancer/protection of UV sensitive materials	Organic UV absorbers (e.g. benzotriazoles as Tinuvin); inorganic UV absorbers (e.g. TiO_2, CeO_2, or ZnO)
X-radiation/X-rays	<10	Prevention of radiation damages and cancer	Components containing heavy chemical elements, as lead, $BaTiO_3$, $BaZrO_3$, $BaSO_4$, or Bi_2O_3

Also shown are principles and potential protective components.

intensity influences the energetic impact. This light intensity can be understood as the amplitude of the electromagnetic wave or as the number of photons transporting small units of energy. Many low-energy photons can have in sum the same energy as one high-energy photon.

In summary, electromagnetic radiation can be understood as a spreading wave or a photon containing beam [3]. Besides photons other particles can be part

of a beam and form radiation. The probably most prominent ones are α- and β-radiation. α-Radiation contains particles built up from two protons and two neutrons, while β-radiation is formed by electrons. α-, β-, and γ-Radiation are in common understanding often summarized to the general term radioactivity. γ-Radiation is electromagnetic radiation of low wavelength and extremely high photon energy [1].

Another particle radiation is a neutron beam containing neutron particles without any electrical charge. Neutrons have no electrostatic interaction potential to materials due to the absence of charge. For this, their transmission through materials is not hindered by Coulomb interactions to negatively charged electrons or positively charged atomic cores. Compared with other particle radiation, neutrons can transmit very well through most materials. Only if a neutron hits an atomic core its transmission is stopped [4]. Major neutron-absorbing chemical elements are boron and cadmium [5, 6].

An interesting overview on cosmic radiation and possible approaches for protection against them is given by Durante and Cucinotta [7]. In addition to α-, β-, and γ-radiation, cosmic radiation contains significant amounts of protons, muons, neutrons, and several types of heavy ions. It should be clear that this radiation is not just containing many different types of particles. Also these particles are of high energy impact, so a simple only textile based protection is obviously not suitable alone. Only in combination with other protective materials a fiber-based material could result in an suitable material.

After this broad summary according to different types of radiation, the question "why radiation protection is requested" should be picked up again. Now the focus of this question should be on content of these types of radiation, determined by their wavelength as shown in Table 32.1. In Table 32.1 it is clear that each type of radiation has few negative impacts, which makes a radiation protection necessary and in demand (Table 32.1). Roughly the damages caused by radiation can be sort into two categories - acting against human or materials and here especially electrical devices. Radiations with higher wavelength (lower photon energy) like radiowaves or infrared radiation are discussed along with protection and potential applications, e.g. for protection of electrical devices or for heat management systems. The modification of IR reflective properties of textiles is often used to realize a thermal IR camouflage, e.g. for uniforms and corporate wear. In this application a person carrying such a corporate wear is nearly invisible to IR cameras, which is an important issue for military clothes [8].

If this camouflage idea is formally transferred from infrared light to visible light, for visible light as one part of electromagnetic radiation, also the term optical protection can be introduced to the field of radiation protective textiles.

In comparison to these types of radiation, the reason for protection against UV light is much more serious. UV light can cause several serious effects on the skin such as sunburn or skin cancer. Further, the damaging of the eyes even until blindness is possible [9–11]. For this, the main purpose of UV protective fibers or fabrics is to prevent such health issues as skin cancer and sunburns [12].

Another important point is that UV radiation can damage also the fiber material. A UV protective functional fiber can improve the stability of the textile material under the influence of UV light. For example, a higher resistance polyester

fiber against UV-B light can be reached after spin doping with a UV protective agent [13].

For radiation with the highest photon energy listed in Table 32.1 (X-radiation), the reason for radiation protection is clear without any doubt. The exposure to X-radiation can cause radiation damages, cell mutation, and cancer and has to be avoided completely [14–16].

Following German law, if X-radiation is used, the operator and the X-radiation have to be in different rooms, separated by appropriate protective material. Only in exceptional cases, e.g. in medicine the in situ observation during an operation, this separation is not possible. However, in these cases personal protection like lead aprons has to be worn by the operator [17–20].

32.2 Structures and Properties of Fibers for Radiation Protection

Before describing and discussing the principles, it is better to discuss some principles of textiles in relation to interaction with radiation. Also, it is necessary to introduce some further fundamental terms to avoid possible misunderstanding in the following subchapters.

Generally, if a textile is exposed to radiation by an incoming beam, the incoming radiation can be roughly separated into three parts related to reflection, absorption, and transmission (Figure 32.2) [12, 21]. First, the transmission T (%) summarizes all radiation that is transmitted through the textile, and the aim of a radiation protective textile is of course to minimize the transmission, in best case to T zero.

Second, the reflection R (%) is related to radiation emitted back. For this, a high reflection will lead to low transmission, so the indication of reflection can be a method to realize radiation protective materials. However, if a dangerous radiation is reflected, it could hit other materials or living persons. Third, the absorption A (%) is the difference between incoming radiation and both reflection and transmission. If the incoming intensity is set to 100, the absorption A (%) can be calculated by $A\ (\%) = 100 - T\ (\%) - A\ (\%)$. The absorption can be understood as radiation uptake or energy uptake by the material, which is exposed to that radiation. For this reason, absorption is the best case to realize a radiation

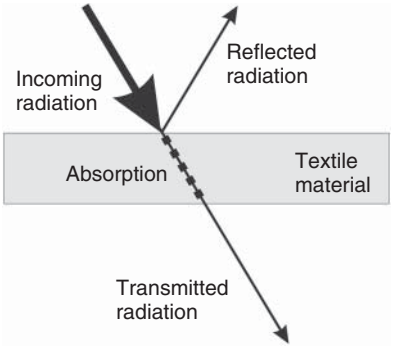


Figure 32.2 Schematic drawing of the radiation transfer through a textile material. The incoming radiation is divided by contact with the textile into reflected, absorbed, and transmitted radiation.

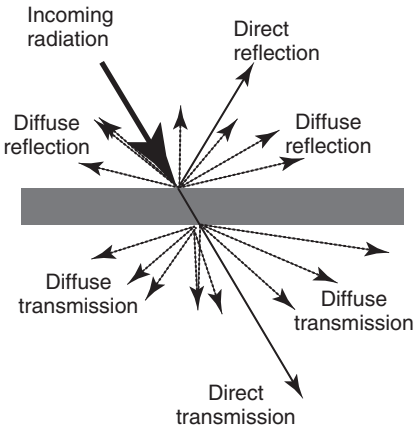


Figure 32.3 Schematic drawing and distinguishing of reflection and transmission (direct and diffuse) of radiation at a textile material.

protection. The absorbed radiation can be transferred to thermal energy, initiate photochemical reactions, or initiate again the emission of radiation in fluorescence or phosphorescence processes [22].

Because photochemical reactions can lead to destruction of materials, in most cases, the transfer of radiation energy to thermal energy is the most wished process for materials with radiation protective properties. This is necessary to gain a long-term stable and active protective material.

A further statement related to transmission and reflection has to be made, which is necessary for measurement arrangements determining the effectivity of a radiation protective material. Both transmission and reflection can be distinguished into a direct and a diffusive part (Figure 32.3) [23, 24].

Direct transmission goes through the textile without changing its direction. This can be described as a direct beam going through the textile material. Besides direct transmission diffuse transmission appears as a result of scattering process that happens during radiation transfer in contact with the textile. This is emitted in all directions, but of course it is similar to direct transmission, which is dangerous. To evaluate the radiation protection quality of a textile material, both direct and diffusive transmission have to be determined and summarized in one number. For this, a measurement arrangement has to be used, which enables the full capture and detection of all diffusive transmitted light. This arrangement can contain a so called integrated sphere, which is collecting the complete diffusive light to a detector [25, 26]. A schematic drawing of such a measurement arrangement is presented in Figure 32.4. Analogously to the transmission also the reflection can be distinguished into a direct reflection and diffusive one. The measurement of the diffuse reflection of visible light is also used to determine the color properties of textiles [27, 28].

The transmission of radiation through a textile is related to its protective function against this type of radiation. For measuring different types of radiation, different types of measurement setup should be used. A rough overview on some examples are given in Figure 32.4 with some schematic drawings in determining the transmission of textile samples for different types of radiation. The general principle for every type of radiation is the same, containing a source

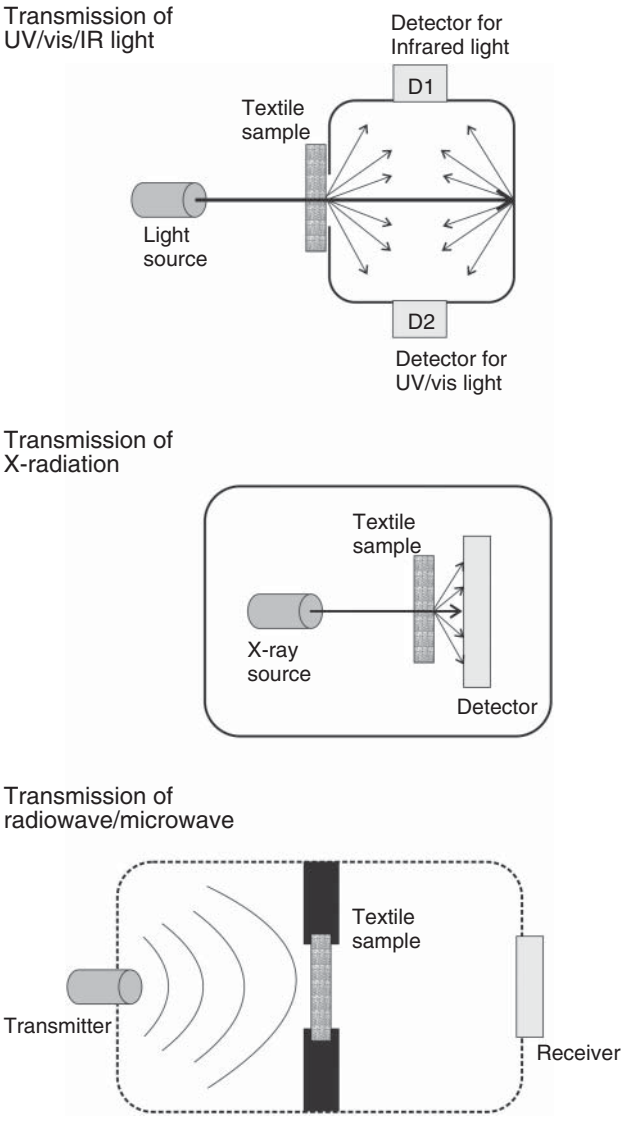


Figure 32.4 Schematic overview on different measurements to determine the transmission of a textile sample for different types of radiation.

for the radiation, a sample holder for the textile sample, and the detector for the radiation. Differences in the arrangements are realized to collect the optimum of transmitted light and for protective reasons.

The first setup is related to the measurement of UV light, visible light, and infrared light. The transmission of those three types of light with the range of wavelengths from 220 to 1400 nm can be determined in one single measurement. An important issue is that the whole transmission (direct and diffusive) is collected in an integrated sphere and recorded by the detectors. The interior of the

integrated sphere is equipped with the white pigment barium sulfate, which has also excellent reflective properties for UV and IR light. In the shown arrangement two detectors are used, one for UV and visible light and the other for IR light.

A possible setup for measuring the transmission against X-radiation is presented in Figure 32.4. In this setup the detector for the radiation is place in small distance behind the transmitted textile sample. This small distance is necessary to detect not only the direct but also the diffusive transmitted X-radiation. Another important point due to safety reasons is that the whole measurement setup is placed in a closed box. This protection is necessary to protect the operator from possibly scattered X-radiation.

In the case of measuring the transmission of radiowaves or microwaves, a full covering of the measurement setup is necessary. The reason for this is not only to protect the operator but also to prevent a distortion of the experiment by external radiation sources. Especially to the overall presence of mobile phones, disturbing radiation is nearly everywhere, so this experiment has to be shielded by a suitable coverage. Suitable materials for shielding are polymer materials with embedded carbon black particles as conductive component.

The most common fibers like cotton, polyester, polyamide, or acrylics do not contain any significant radiation protective property [29]. They have only low absorption capacity for any type of electromagnetic radiation. The reflection properties are low as well. Synthetic fibers as polyester or polyamide often contain titanium dioxide as white pigment. By this pigments, besides a high reflectivity for visible light, a certain absorption of UV light is introduced to the fiber. In this case, the fibers carry an additional component – the TiO_2 – containing the protective property [28]. In contrast wool fibers are reported to support UV protection by themselves. Wool is a protein fiber built up by 20 amino acids as natural monomers [30]. From these 20 amino acids, the amino acids tryptophan, tyrosine, and phenylalanine contain aromatic structures. These aromatic structures introduce UV absorption properties to the wool fiber. From those three mentioned amino acids, tryptophan exhibits the best UV absorption properties probable because it contains an aromatic ring system with nitrogen as heteroatom [31, 32]. The presence of aromatic amino acids is probably the reason why for wool high UV protection factor (UPF) values are reported [33]. It should be remarked here that silk mostly is of low UV protective potential, although it is a protein fiber [34, 35]. However, the silk protein is almost built up by the amino acid glycine. Depending on the origin of the silk, the glycine content is in the range of 20–66%. Other amino acids that are as well occurring in high amounts in different silk proteins are alanine, serine, glutamine, and lysine [34]. All those amino acids do not contain any aromatic structure leading to absorption of UV light with wavelength >250 nm. For this, no UV protection property is introduced to pure silk fibers.

Aramid fibers as technical fibers contain a chemical structure with conjugated aromatic systems as repeating unit, or this reason aramid absorbs strongly UV light and also significant amounts of visible light, clearly indicated by the yellow coloration of aramid fibers. However as UV protective fiber, aramid is not useful, due to its high decomposition rates under UV illumination. In contrast, different

methods are investigated to stabilize aramid fibers against the influence of UV light [36, 37].

A polymer from natural based resources reported for sun-blocking applications is lignin [38]. Lignin is a biopolymer occurring in higher plants and is present together with cellulose and hemicelluloses in wood [39]. Lignin is evaluated and reported for high-performance broad-spectrum sunscreens [38]. However, similar to aramid lignin exhibits a small stability under long-term exposition to UV light.

In general it should be concluded that if a radiation protection property is wished, a functional additive – carrying this protective property – has to be added, because most common fibers do not contain a radiation protection by themselves. An overview on different types of radiation protective components and additives is given in Table 32.1. In Table 32.1 it is distinguished into different types of radiation requiring different types of protective functional components.

Besides the chemical nature of the protective functional component, its placement in the fiber has a significant influence on its effectivity for radiation protection. A simple schematic overview on different possible arrangements is presented in Figure 32.5. Table 32.2 summarizes some production methods for each arrangement and gives some statements concerning fixation of the function and its durability.

The best radiation protection can be of course gained by a self-functional fiber containing a radiation protective material. In other words, the fiber material is the protective material itself. An example would be a fiber made from pure copper. Due to the high amount of active agent (the copper), the protection is excellent. In other cases, lower effectivity is reached by embedding the same radiation protective material, e.g. as copper pigments, into the fiber during the spinning process. Coating and traditional finishing processes yield to lower amounts of

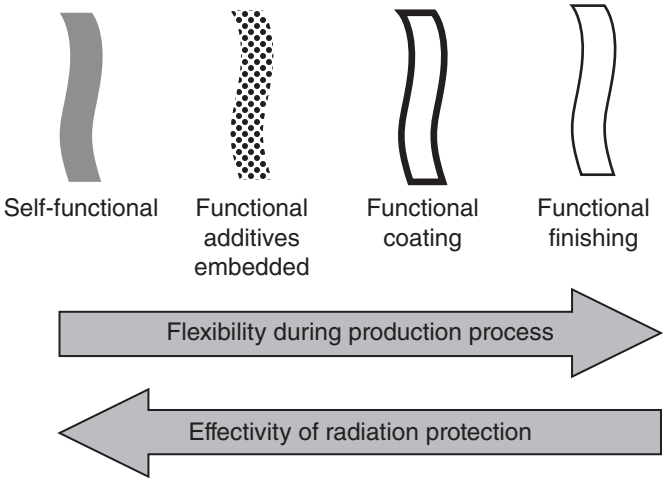


Figure 32.5 View on different positions of a functional component in a fiber. Shown is the relation to effectivity of functionalization – radiation protection – and the flexibility of the production process.

Table 32.2 Comparison of different positions of a functional component in a fiber according to possible production method and place in the textile production chain where the decision for the function is fixed.

Position of function in the fiber	Production method/realization of function	Fixation of function according to textile chain; limits
Self-functional	Selection of self-functional polymer or inorganic material for fiber production	Before fiber production; limited only to few materials
Embedded functional additives	Addition of functional pigments or particles during fiber production by melt spinning/dry or wet spinning	During fiber production; variations possible by combination of different pigments and fiber materials; limited to fiber production process
Functional coating	Coating deposition by different methods as wet chemical method, sol–gel coating, electrodeposition, deposition from gas phase	After fiber production; the mechanical properties of the fibers can be strongly influenced by the coating
Functional finishing	Finishing process analogously to yarn dyeing or fabric dyeing	After fiber or fabric production; the fiber/dye (additive) interaction has to be recognized to gain good fastness properties; compared with other methods smaller amounts of functional additive is applied

applied functional component. The amount of the active components applied is decreased in this order, and by this the effectivity of the protective functionalization is as well determined (Figure 32.5).

However, vice versa the flexibility of the application process is the highest for the finishing application and lowest for the self-functional fiber.

The term flexibility is related to the position in the textile production chain, where the functional additive is added. In other words, if the decision to apply a protective function has to be made in the beginning of the fiber production, the flexibility in the process is low. Vice versa, if the protective function is applied near the end of the textile chain by a dyeing or printing process, the flexibility of the whole application is quite high. An overview in relation to the textile chain is supported in Table 32.2.

The self-functional fiber is produced and dedicated mainly for only one or few types of application. The embedding of functional protective additives inside a synthetic or regenerated fiber enables the production of a fiber containing the advantageous properties of the functional additives and the organic fiber. These fibers contain higher flexibility, due to more possibilities in creation of new material combinations and properties. However, the decision for fiber properties has to be made in the beginning of the fiber production process. The properties are fixed for afterward performed production steps. The highest flexibility is gained

by functional finishing usually performed as treatment with an aqueous-based finishing agent at the already prepared yarn or fabric. In best case, a standard conventional polyester or cotton material is supplied and functionalized by a finishing agent, if a certain demand for a certain functional product is requested by the customer. The disadvantage here is that the amount of functional additives applied onto the fiber materials is lower compared with the cases "self-functional" or "embedded additives," so with finishing applications usually lower protection rates are realized. Also by finishing processes usually no inorganic pigments can be applied and fixed permanently onto the fiber surface.

The functional coating is in a certain way similar to the finishing process, because the coating is performed mostly onto already prepared fibers. However, the coating techniques, e.g. vapor deposition or electrochemical deposition, are more challenging and of higher technical effort compared with traditional textile finishing. For this, the coating is related to lower flexibility during production process. However, by coating usually higher amounts of functional additive can be applied to the fiber, so the finally gained effect is advantageous compared with the functional material prepared by finishing.

Radiowaves and microwaves require for effective shielding electric conductive materials [40, 41]. Appropriate materials are conductive metals and their alloys. Metallized fibers containing copper, nickel, silver, or different alloys are often mentioned and are used to produce knitted materials with conductive yarns. Alternatively to metals the coating with conductive polymers can be used [40, 42]. Also useful is carbon in its conductive forms as graphite, carbon black pigments, carbon nanotubes, or graphene and its modifications [43–46]. Carbon fibers with nickel coating are obtained by electroplating method and can be used for electromagnetic interference shielding [47].

Carbon nanotubes can be used as additive in fibers. However, yarns completely prepared from carbon nanotubes are realized [48] and combined in further modification with the carbon type of graphene [49]. Alternatively to carbon fibers, so-called carbonaceous fiber materials can be used to reach effective shielding against microwave radiation in the range of 30–1000 MHz [50]. The preparation starts here from PANOX fiber materials (supplier Carbon Fibers Inc.), which are partly pyrolyzed polyacrylonitrile fibers. On those fibers a further thermal treatment is done, probably to introduce graphite-like structure with electric conductive properties [50].

Protection mechanism against IR radiation is most commonly based on reflective materials [51]. High IR reflection is often gained with pure metals (especially aluminum pigments) [51, 52]. Alternatively special metal oxide pigments are used [53, 54].

Nevertheless, it should be mentioned that especially for near-IR light, organic IR absorbers are developed and described in patent literature [55, 56]. Prominent examples for such organic IR absorbers are metal complexes from dithiene type as depicted in Figure 32.6. The central metal in these complexes can be not only nickel but also other transition metals, e.g. palladium [55]. Other colorless organic IR absorbers are dithiolene metal complexes as presented in Figure 32.7 [56].

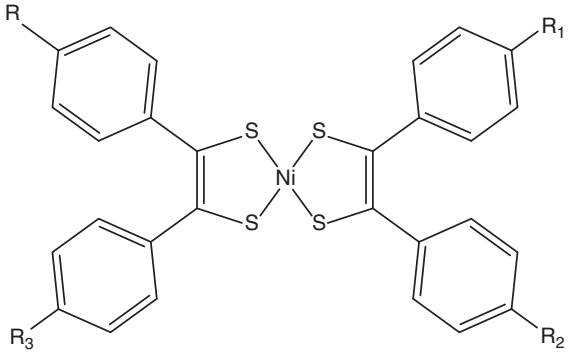


Figure 32.6 Chemical structure of an organic IR absorber – dithiene complex derivative. The central metal atom can be not only nickel but also palladium or platinum. The side groups R to R_3 are ether groups or amine groups [55].

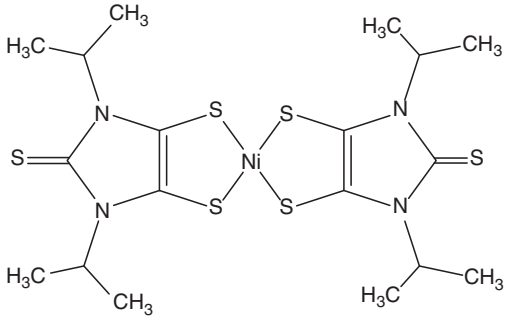


Figure 32.7 Chemical structure of an organic IR absorber – dithiolene metal complex derivative. The central metal atom can be not only nickel but also another metal [56].

Another interesting approach for IR protective materials based on absorption mechanisms are related to transparent conductive oxides (TCO). Such TCO materials are currently developed and modified for textile purposes by the DTNW (Krefeld, Germany) and the CHT (Tübingen, Germany). These institutions developed TCO nanoparticles prepared by a sol–gel process useful as textile finishing agents. By this, comparably high interactions with heat radiation and IR light is introduced to the treated fabric [57]. In further developments, these TCO nanoparticles could be also introduced into synthetic or regenerated fibers by spin doping.

While protection against IR light is realized in most applications by reflection, in most cases the absorption of UV light is used to introduce protection properties. One reason for this is probably that for UV light many excellent UV absorbers are available.

UV absorbers can be roughly distinguished into two groups – organic UV absorbers and inorganic UV absorbers [58]. Inorganic UV absorbers are usually white pigments of semiconductive nature. Prominent examples are titanium dioxide (TiO_2) and zinc oxide (ZnO) but also cerium(IV) oxide (CeO_2) [59]. These pigments can be added into synthetic or regenerated fibers by addition to the spinning mass. An alternative but not commercially used method is the application of TiO_2 or ZnO as sol–gel coating to apply UV protective function [60–63].

A sol–gel finishing agent based on TiO_2 was developed for UV protective purposes by the company CHT (Tübingen, Germany) under the name isys UVP. The

stability of this sol–gel system was excellent, so even hydrothermal processes were possible with it without starting gelation [64]. Recently developed TiO_2 materials for UV protective applications are prepared by hydrothermal methods. By this method, manifold different titania nanoparticles can be realized and applied in a sol–gel coating process [65, 66]. A further advantage is the possible combination with additional functional properties as self-cleaning or oil/water separation [66].

Most used UV absorber is the TiO_2, which is often used as white pigment in synthetic fibers (TiO_2; C.I. Pigment White 6) [67]. However, compared with UV protective applications for use as white pigment, only small amounts of titania are used; e.g. a white polyamide fiber is reported to contain only 0.012% titania. In contrast, different UV protective commercially available clothes for outdoor and sportswear contain titanium in the range of 0.22–0.85% [68]. These values are determined from the fibers by ICP-OES method. Further, it was stated that the TiO_2 in these investigated fibers is embedded inside the fibers as additive during the spinning production. For this, the washing stability of those products is almost excellent [68, 69].

Organic UV absorbers can occur in various chemical structures [58]. Some examples are given in Figures 32.8 and 32.9 [70–72]. These UV absorbers contain as basic functional component a chromophore for absorbing UV light as 2-hydroxybenzophenone or 2-(2-hydroxyphenyl)benzotriazole basic structures [70]. Another basic structure is from phenylacrylester derivatives (Figure 32.9) [71, 72].

Two main properties are the main requirements for an organic UV absorber. First, of course they have to absorb UV light over a broad range of wavelength and with high effectivity. Second, the UV absorber should not be decomposed under the exposure of UV light. The uptake of UV light by an organic molecule transfers this molecule to an excited electronic state [73].

Besides the return in the former ground state, this energy uptake can start a photochemical reaction leading to the decomposition of the organic molecule [73]. Organic components used as effective UV absorbers are containing a simple

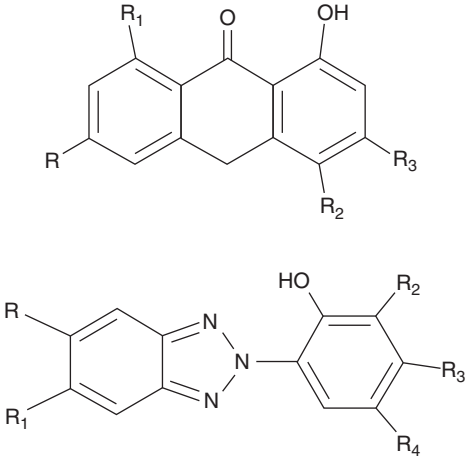


Figure 32.8 Chemical structures of organic UV absorbers with (a) 2-hydroxybenzophenone and (b) 2-(2-hydroxyphenyl)benzotriazole basic structures [70].

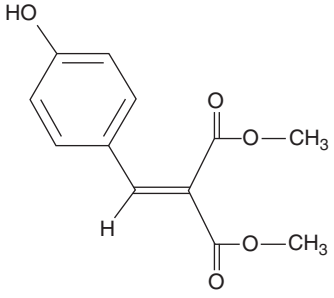


Figure 32.9 Chemical structure of an organic UV absorber – type phenylacrylester derivative. Source: Adapted from Rauch et al. 2004 [71] and Böttcher et al. 2006 [72].

mechanism that converts the uptaken UV light into heat energy; by this a destructive photochemical reaction is avoided [74].

Another important point related to the application of UV absorbers on textile materials is their fixation to the fiber material. This fixation is the main condition for washing stability. To reach an adequate fixation a strong interaction between fiber surface and the UV absorber has to be developed. For this, UV absorbers are developed containing not only the functional chromophore but also functional groups leading to interactions to different fiber surfaces.

Simply spoken, organic UV absorbers can be applied using finishing processes similarly used with traditional dyes. UV absorbers carrying a negative net charge in their molecular structure can be applied like an acid dye onto positively charged fibers as wool or polyamide [69]. The negative charge can be introduced to the UV absorber by a sulfonic group [70]. An example for such a dye is presented in Figure 32.10. This organic UV absorber has the basic structure of oxalic diarylamide. The sulfonic group $-SO_3Na$ is the negatively charged anchor group for application and fixation onto wool or polyamide fiber material. Also an application analogously to a direct dye onto cellulosic fibers is mentioned [70]. This UV absorber is useful not only for applications as clothes but also for other sun protective products as awnings or parasols.

UV absorbers with reactive anchor groups like chlorotriazine or vinylsulfone are dedicated for an application onto cotton or other cellulosic fibers, because of the formation of permanent covalent bonds between this reactive anchor group and the hydroxyl group onto the surface of the cellulosic fiber. An example for such a UV absorber containing both a chlorotriazine group and a vinylsulfone

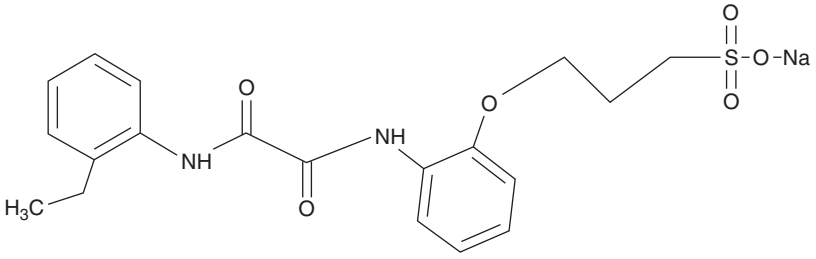


Figure 32.10 Chemical structure of an organic UV absorber with the basic structure of oxalic diacrylamide. The sulfonic group $-SO_3Na$ is the negatively charged anchor group for application and fixation onto wool or polyamide fiber material [70].

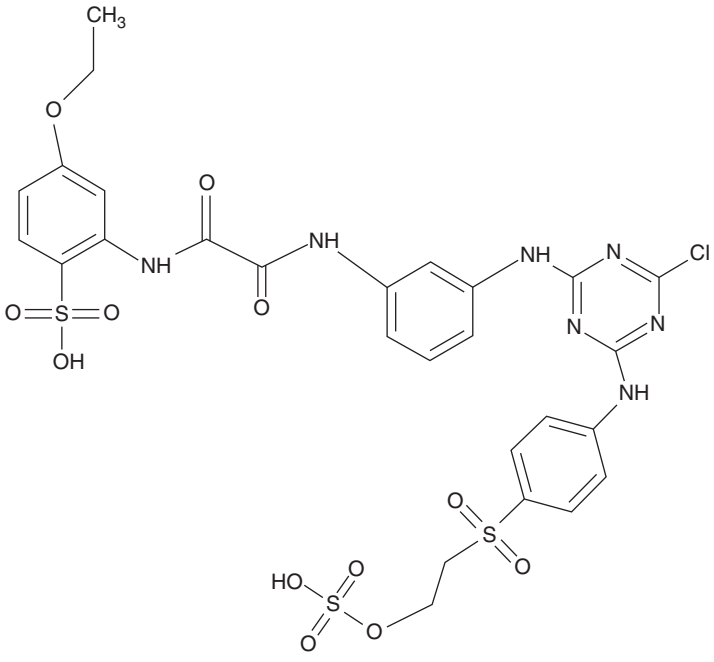


Figure 32.11 Chemical structure of an organic UV absorber with the basic structure of oxalic diacrylamide. This UV absorber contains chlorotriazine group and the vinylsulfone group, two reactive anchors useful especially for the application on cotton or other cellulosic fibers.

group is depicted in Figure 32.11. The basic structure of this UV absorber is of oxalic diacrylamide type [75]. The final vinylsulfone anchor group is formed under the alkaline conditions of the finishing bath, by splitting of a sulfate ion.

For application onto hydrophobic synthetic fibers as polyester, hydrophobic UV absorbers are applied as dispersion using conventional high-temperature (HT) processes.

This application process is similar to the application of conventional disperse dyes in an HT process. HT indicates a process temperature for the dyeing of $T > 100\,^{\circ}\mathrm{C}$, which should be significantly above the glass temperature of the synthetic polyester fiber. Usually process temperatures of 120–130 °C are used to promote the diffusion of the disperse dye into the polymer matrix of the polyester fiber [76]. For UV absorber application an aqueous dispersion based on 2-hydroxybenzophenone derivatives is reported, which is suitable for the application on polyester fabrics (Figure 32.12) [77].

A further mechanism is the transfer of UV light into visible light by fluorescence processes. In this case the energy of the UV light is not converted to heat, as it is the case for common UV absorbers. Instead fluorescence dyes transfer the UV light into visible light. Fluorescence dyes are most commonly used as optical brightener and are useful compounds for UV protective purposes. A prominent structure often found in fluorescence dyes and whitening agents is the stilbene structure. Especially triazinylaminostilbenes are mentioned to be excellent UV protective agents for textile treatment [29]. An example of such a stilbene

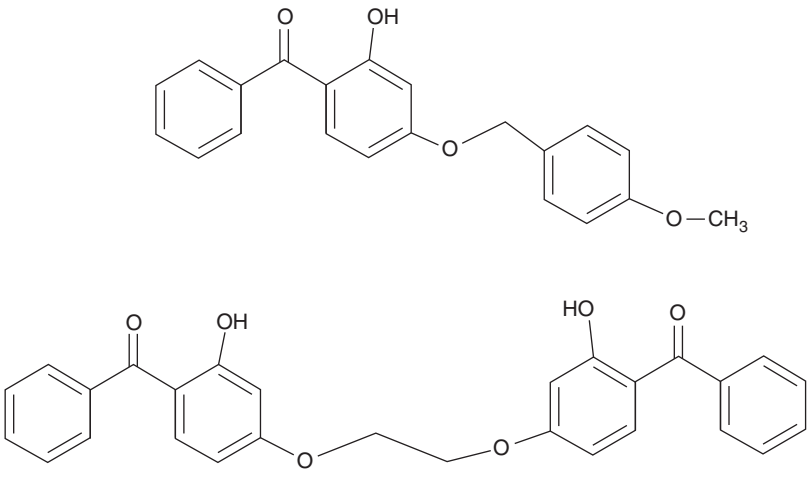
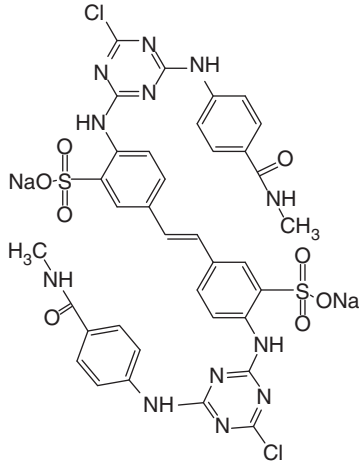


Figure 32.12 Chemical structures of organic UV absorbers. Different examples for UV absorbers of 2-hydroxybenzophenone derivatives for application in aqueous dispersions for the treatment of polyester fibers [77].

Figure 32.13 Chemical structure of a fluorescence whitening agent (optical brightener) with UV protective properties – stilbene type. Both monochlorotriazine rings are reactive anchors especially for fixation onto cellulosic fibers. The sulfonate groups $-SO_3Na$ support the solubility of this compound in water [78].



derivative is given in Figure 32.13 [78]. The depicted stilbene fluorescence dye contains two monochlorotriazine rings, which are acting as reactive anchor to fix the dye onto cellulosic fibers as cotton or viscose. The sulfonate groups $-SO_3Na$ support the solubility of this fluorescence dye in water [78].

A quite novel development in the field of UV protective materials is the application of graphene materials [79, 80]. Graphene nanoplates can be used as UV absorber onto cotton fibers. Even with amounts of 0.4 wt% applied graphene, significant UV protection can be realized [79]. Alternatively graphene oxide nanosheets can be used to realize UV protective materials based on cotton fibers. The combination with conductive synthetic polymers like polyaniline and this leads not only to the UV protection but also to conductive properties of the modified cotton materials [80].

The absorption capacity of a material for X-ray increases mostly as functions of the atomic weight of the chemical elements building up the material [81, 82]. Textile fibers are usually built up by lightweight atoms as hydrogen, carbon, oxygen, and nitrogen, so common textiles are almost completely transparent for X-ray. Effective X-ray absorbing components are containing heavy metals in elementary form, e.g. lead or in a component like HfO_2, $BaSO_4$, or Bi_2O_3 [83, 84]. For this, a functional component supporting X-ray protective properties to a fiber should contain chemical elements as lead, barium, or bismuth. However the decision which element or compound is the most appropriate has to be done under the aspects of toxicity and costs. Lead, which is traditionally used in lead aprons for X-ray protection purposes, is of high human toxicity and should be therefore not introduced in textile fibers [85]. Chemical element like gold or platinum are may be also effective X-ray absorbers, but their prize is far away from a possible textile application. In comparison, barium sulfate is a suitable compound. Soluble barium compounds like $BaCl_2$ or $Ba(NO_3)_2$ are toxic, because they release the toxic Ba^{2+} ion. However, the solubility of barium sulfate is extremely low, so it can be even used in medical applications [86]. Barium sulfate $BaSO_4$ is a white and nontoxic compound, which is used also as an X-ray contrast agent for medical applications. Its costs are in the range that is acceptable for textile applications. An analogous suitable material is bismuth oxide Bi_2O_3.

Because of the high photon energy of X-radiation and the high penetration depth of this radiation, usually a high amount of X-ray absorptive material is needed to gain a suitable protection against X-radiation. For this, in contrast to the UV protective application, for X-radiation an application of X-ray absorbers in a finishing process is not useful, because by finishing the amount of applied agents is too low. For suitable X-ray protection the functional additive has to be applied in high concentration inside the fiber or with a thick coating on the fabric material. The application of thick coatings with lead or other heavy metal compounds is the state of the art for actually commercialized products, as lead aprons [87–89]. The disadvantage of such thick coatings is that the textile properties are lost and the weight of the material is quite high. Besides the loss of the textile comfort, significant health problems can be the result from carrying high weight protective clothes [90]. Also cracks and defects can occur as results of long-term use and repeating of bending and folding [91–93].

As mentioned above, the durability of the textiles and its radiation protective properties is an important issue for usage. Beside the principal function, the durability is the most important parameter for successful commercialization of new materials. A schematic overview on the aspects of life cycle and durability of textiles for radiation protective purposes is given in Figure 32.14.

After preparation of the textile sample, the protective properties can be determined by transmission measurements with different setups as summarized in Figure 32.14. This measurement proves the principal function of the materials. The question for durability of this function is related to the point that the function be present in the future after a certain duration of usage. On this used sample the transmission measurement can be performed again, and the difference in transmission ΔT before and after usage is a parameter for the durability of the function. If ΔT is zero, best durability is realized.

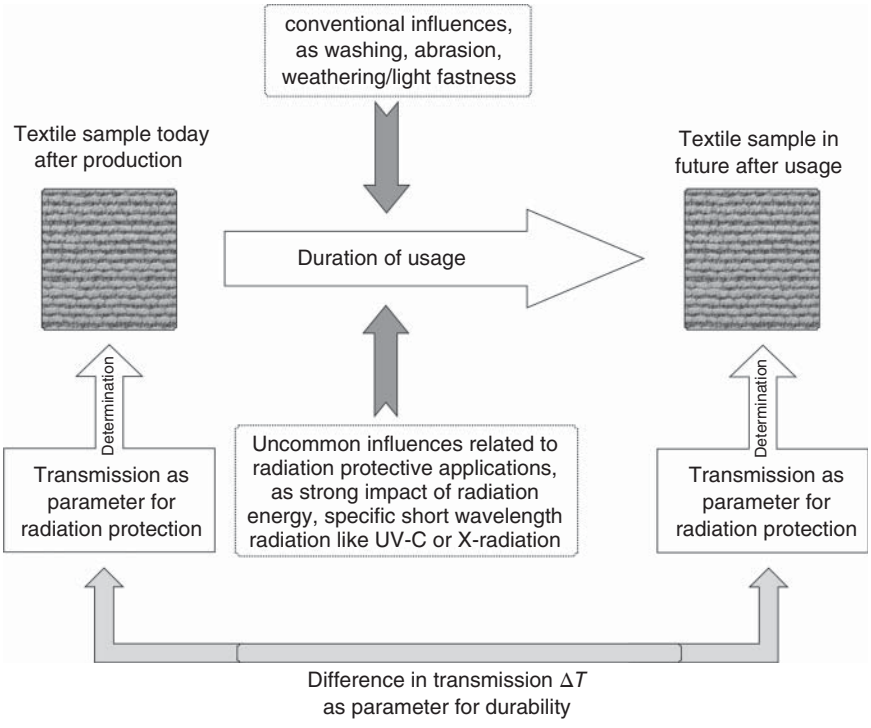


Figure 32.14 Schematic overview on aspects of life cycle and durability of textiles for radiation protective purposes.

For common textiles several conventional influences are taken into account for evaluation of the durability. Mainly these influences are the washing fastness, abrasion stability (crock fastness), and light fastness, which is also sometimes understood as weathering fastness. For durability investigations, usually the textile samples are intensively treated with one of those issues, and afterward the durability is graded with a number. An example could be the testing of the wash fastness of a UV absorber, which is applied in process related to a reactive dye. In this case, the transmission of UV light is tested before and after a repeating washing procedure, which is related to the conditions of usage, e.g. washing several times in a commercial washing machine at 40 °C with standard detergent.

One issue that is especially important for the durability of textile for radiation protective purposes are so-called uncommon influences, which are especially related to the situation of radiation exposition. Especially for applications related to protection against high-energy radiation of UV-C light or X-radiation, this is an important issue. This high-energy radiation with short wavelengths is absorbed by the textile material and can start photochemical reactions, which are able to destruct the textile sample. This important issue has to be tested and investigated especially for protective materials developed for long-term durations.

32.3 Functions, Performance, Evaluations, and Applications

In this section some typical examples for application of radiation protective fibers are summarized. These examples are related to different parts of the electromagnetic spectrum, and besides the principal action of the material also, hints on already successful commercialized materials are given.

32.3.1 Radiowave/Microwave Shielding

The shielding of radiowaves and microwaves is mostly done by electroconductive fibers or yarns [94–96]. Some important suppliers of metallized fibers, yarns, or fabrics are, e.g. Statex GmbH, Marktek Inc., Swicofil, and YSHIELD [97–101]. Often used are fibers from pure metals or synthetic fibers that are metallized – coated with a very thin metal layer [102]. Very prominently reported are silver-coated polyamide fibers, where the silver coating is deposited by electrochemical processes [103]. For electroplating of polyacrylonitrile fibers with silver, the application of primer compounds is useful to improve the durability of the silver coating. Advantageous primer compounds are aminosilanes or mercaptosilanes [104]. Even more exotic fiber materials are silver-coated polybenzoxazole (PBO) filament yarns [105].

The electrochemical deposition of copper or nickel is reported as well. For this, often at first, small amount of other noble is applied to the fiber, probably to promote an afterward copper deposition and especially the fixation of the copper on the fiber surface [106]. An overview on some metallized synthetic fibers and fabrics is given recently [107]. The electrochemical metal deposition is done from solution containing the required metal ions, so the solubility of an appropriate metal salt is a requirement for this deposition technique. Also more noble metals with higher redox potential are deposited by these electrochemical methods more easily. In contrast, metals like aluminum can be only deposited from solution, if strong reductive agents are present, e.g. $LiAlH_4$ [108].

In a US patent Okayasu et al. report on a method described as nonelectrolytically plating of a previously activated polyester textile [109]. The pretreatment is done with compounds of tin and palladium. Afterward metals like nickel, copper, cobalt, chromium, or their alloys are deposited. Twenty years later Onggar and Cherif try to repeat this wet chemical deposition of elementary silver onto polyester textile fabrics [110]. They used a combinatory deposition of silver ions with different amino compounds and a following reduction step with ascorbic acid. This type of deposition process leads normally to the formation of silver nanoparticles on the fiber surface [110]. However, to reach an appropriate conductivity for shielding purposes, the use of nanoparticles is usually not adequate, because of high specific surface area of the nanoparticles.

Another method to realize metallized fiber materials is the vacuum deposition [111–114]. This procedure is especially useful for metals with lower boiling point and less noble metals, which cannot be deposited easily by electrodeposition. Commercially available aluminum-coated fiber materials are usually prepared by

Table 32.3 Overview on products commercialized for EMI shielding by YSHIELD GmbH (Ruhstorf, Germany).

Product	Type	Color appearance	Shielding at 1 GHz (dB)	By EDS detected metals
Evolution	Woven fabric	White	30	Silver, copper
Steel twin	Woven fabric	Light gray	35	Iron, chromium, nickel
Steel gray	Woven fabric	Gray	35	Iron, chromium, nickel
Silver tricot	Knitted fabric	Gray	47	Silver
Silver tulle	Knitted fabric	Gray yellow	50	Silver
HEG03	Mesh	Metallic gray	55	Iron, chromium, nickel
Silver silk	Woven fabric	Metallic silver	60	Silver
HNG80	Woven fabric, netting	Metallic yellow silver	80	Copper, nickel
HNV80	Nonwoven, fleece	Metallic yellow silver	80	Copper, nickel

The shielding rate for radiation with frequency of 1 GHz is supported by the supplier.
Source: Data from YSHIELD GmbH 2016 [101].

this technique. One problem that can occur during vacuum deposition is related to the thermal energy of the evaporated metals. The impact of thermal energy can be transferred to the textile substrate, and by this a destruction of the textile material is possible.

Table 32.3 gives an overview on typical textiles currently offered for electromagnetic shielding [101]. The supplying company – YSHIELD, Germany – reports the shielding effectivity for radiation with 1 GHz frequency, which is in the range of microwave radiation. The shielding effectivity is in the range of 30–80 dB. The color of the fabrics differs from white and gray to a metallic appearance.

Different types of metals are detected on the fiber materials by using energy-dispersive spectroscopy (EDS). Mainly detected are silver, copper, and nickel. Also found are samples containing the metals iron, nickel, and chromium. These three metals are related to the occurrence of metal fibers from stainless steel. These materials are comparable with nonwoven fabrics made from stainless steel and polyester fibers reported by Ozen et al. [115]. From those products, mainly three categories should be distinguished, also shown as scanning electron microscopy (SEM) images in Figure 32.15.

First, there are standard fabrics containing only few metallic fibers. In the SEM images fibers containing chemical elements with higher atomic number are shown with stronger brightness, so the metal-containing fiber can be easily distinguished in these SEM images from standard textile fibers as polyester or cotton. This statement is proven by the EDS measurements supporting a lateral resolution of the element distribution onto the fiber surface (Figure 32.16).

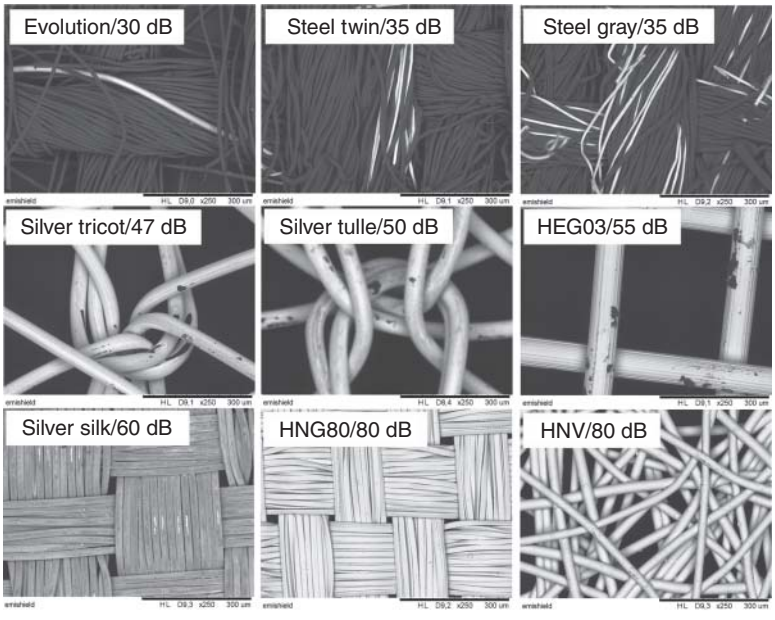


Figure 32.15 Overview on products commercialized for EMI shielding by YSHIELD GmbH (Ruhstorf, Germany); SEM images of different fabric samples recorded with a magnification of 250×. The type of fabric sample and the shielding effect against 1 GHz (supplier information) are directly indicated in each image.

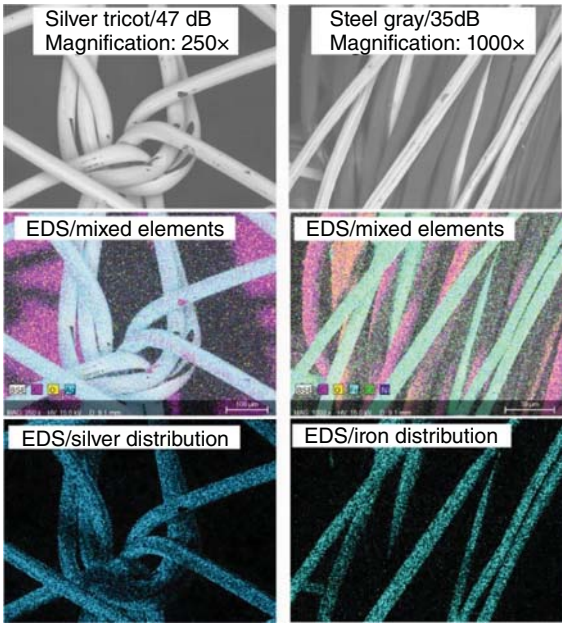


Figure 32.16 Overview on two products commercialized for EMI shielding by YSHIELD GmbH (Ruhstorf, Germany); SEM images and EDS images of different fabrics are shown. The type of fabric sample, the shielding effect against 1 GHz (supplier information), and the magnification for microscopic measurements are directly indicated in each image.

In the first category of shielding materials, shielding rates are in the range of 30–35 dB. These samples have a hand feeling and appearance comparable with common textiles. Their color is white or gray, and dyeability comparable with standard textiles can be expected. Altogether the application as a common textile for clothing and home textiles is possible.

The second category summarizes materials with a shielding rate around 50 dB. These fabrics are built up only from metallized fibers arranged in an open structure. These structures are knitted or an open mesh. Such metallized knitted net fabrics are known and developed in the early 1980s and dedicated especially for the protection against microwave radiation [116]. In an US patent from Ebneth et al., particularly nickel-coated knitted net fabrics are described, and the protective properties against microwave with frequencies from 1 GHz to 36 GHz are tested. A further important field of application is the eye protection [116]. These fabrics have a clearly metallic appearance and hand feeling. They have an open structure, so visible light can transmit in a certain amount. Altogether, these materials are certainly dedicated for application as curtains, window coverages, or technical applications.

The last third category is related to highest shielding rates from 60 to 80 dB. In this category, all fibers are metallized and form a dense structure as woven fabric or nonwoven felt. In summary for these three categories, the effectivity of EMI shielding increases by the number of metallized fibers on a certain area on the fabric, which could be also described as cover factor [117]. An example for a certain product is presented in Figure 32.17 with a bag containing EMI shielding properties commercialized for mobile phones. A mobile phone inside this bag is hidden and cannot reached by electromagnetic radiation. For this, the personal identity is covered. As shown the metal-plated fabric is placed inside the bag. This



Figure 32.17 Bag for mobile phones with EMI shielding properties with metal-plated fabric inside, product of company Electronic Wall (Kinding, Germany).

metal fabric seems to be similar to the silver silk fabric presented in Table 32.2 and Figure 32.17.

32.3.2 IR Shielding/Heat Management

The example of IR shielding is often related to the application in heat management. Those are textile materials like a metallized mesh proposed for the application of a heat protective curtain. If these fabrics are used as curtain for a window, their metallized surface reflects the IR radiation from sun back to outside of the building. By this, parts of the heat radiation are prevented from entering the building, and a heating indoors is avoided. Additionally the open structure of these materials supports still a certain transmittance for visible light, so an additional illumination indoors is not necessary. This fact is important, because illumination realized by artificial lamps is related to heat production and energy consumption. In winter time the situation is vice versa, the temperature inside the building is higher, and an aim would be to keep the heat indoors. Here a curtain with an infrared reflective side oriented to the room is useful.

An SEM images of a knitted fabric dedicated for heat management is presented in Figure 32.18. This fabric contains an open structure, to keep a certain transmittance for visible light. One side of the fabric is coated with aluminum and contains a metallic appearance. The other side is black. The reflection and transmission spectra of such knitted fabrics are presented in Figure 32.19.

Here two types of fabrics are compared. One is aluminum based, and the other one is steel based on the metal side. The transmission is over the investigated spectral range from 220 to 1400 nm wavelength nearly similar in the range of 35–45%. There is no significant difference if the aluminum- or steel-based fabric is measured and if the measurement is done from the metal or the black side of the fabric. A difference is observed by reflection measurement. The knitted fabric

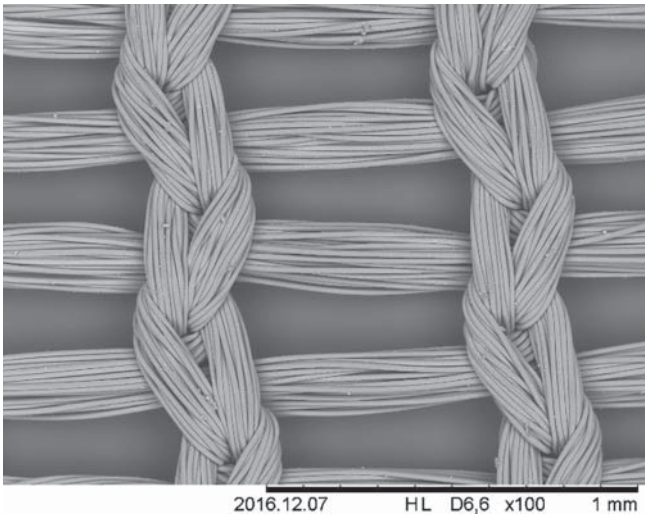
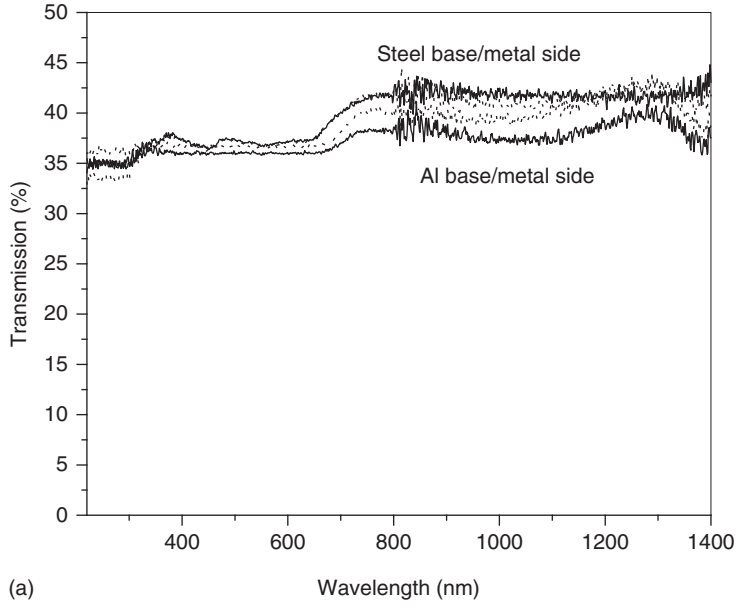


Figure 32.18 SEM image of knitted fabric dedicated for heat management, aluminum-based system.



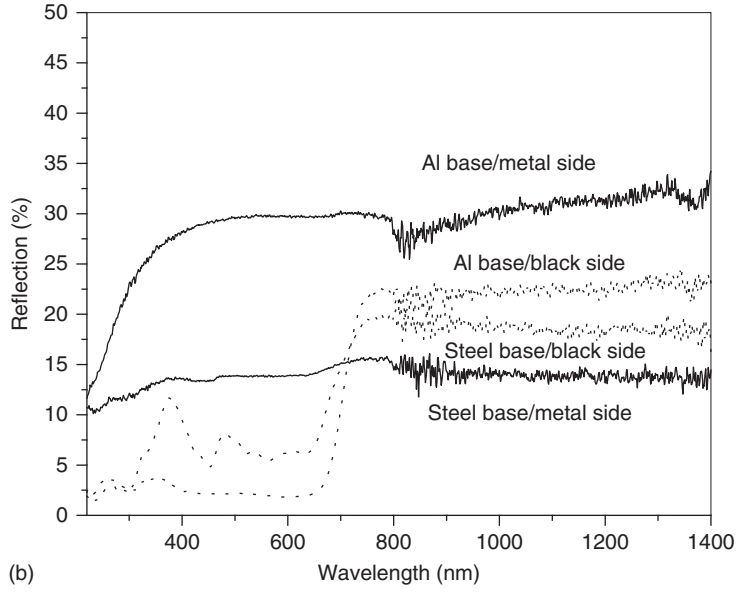


Figure 32.19 Spectra of diffuse transmission (a) and diffuse reflection (b) of fiber mesh from metallized fibers. The spectrum range summarizes UV, visible, and near-IR light. The metallized fiber meshes are measured from metal and from black side. The comparison is done with an aluminum-based mesh and a steel-based mesh.

with aluminum side exhibits the strongest reflection for visible and for infrared light (Figure 32.19). The steel-based system is of lower reflectance for IR light. Further, the reflection from the black side of both materials strongly depends on the type of light. For visible light only low reflection is observed, probably because of the absorption. However infrared light is still reflected in significant ration of around 20%.

32.3.3 UV and IR Protection

For an application supporting both UV and IR protection, a fiber containing a significant amount of TiO_2 can be mentioned. TiO_2 has excellent UV absorption and IR reflection properties, so a fiber with large amounts of this white pigment should be an effective material for this application.

In patent literature it is reported from ultraviolet protective fabrics based on regenerated cellulosic fibers [118]. These cellulosic fibers are prepared by modal or lyocell process and containing TiO_2 as UV absorber. The TiO_2 is applied in amount of 1 wt% and is originally supplied by the company Kronos [118]. Such UV protective cellulosic fibers with TiO_2 are commercialized under the name Tencel Sun by the company Lenzing. Appropriate products are on the market for outdoor apparel since the year 2009 [119].

Such a fiber could be a regenerated cellulosic fiber with incorporated TiO_2 as depicted in Figure 32.20. The SEM image of this fiber is recorded in a measurement mode giving not only the topography but also a material contrast. Areas containing the element titanium are shown brighter compared with the areas containing only cellulose. In fact, the embedded TiO_2 particles can be detected, and it can be also stated that the size of those particles is quite small compared with usually used pigment particles. The use of smaller inorganic particles improves the stability of the cellulosic fibers and enables further production

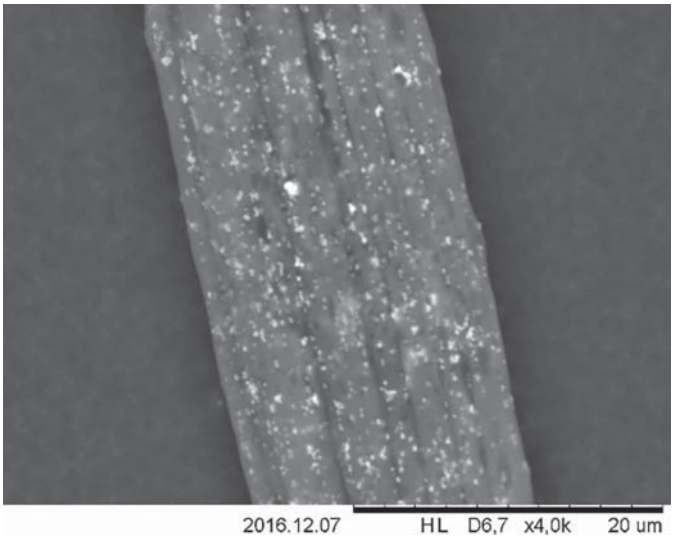


Figure 32.20 SEM image of a viscose fiber with embedded titania, useful for UV protective purposes.

processes as spinning, knitting, or weaving. The elementary content of titanium determined by EDS is around 5% on the fiber surface. This amount of titanium is roughly 10 times more as the amount of TiO_2 used in conventional synthetic fibers as polyester or polyamide. In conventional fiber TiO_2 is used to introduce a certain white color effect to the fiber.

A knitted structure produced form such TiO_2 containing cellulosic fibers contains transmission near to 0% for the complete UV range till 400 nm (Figure 32.21). This zero transmission is reached by the excellent absorption

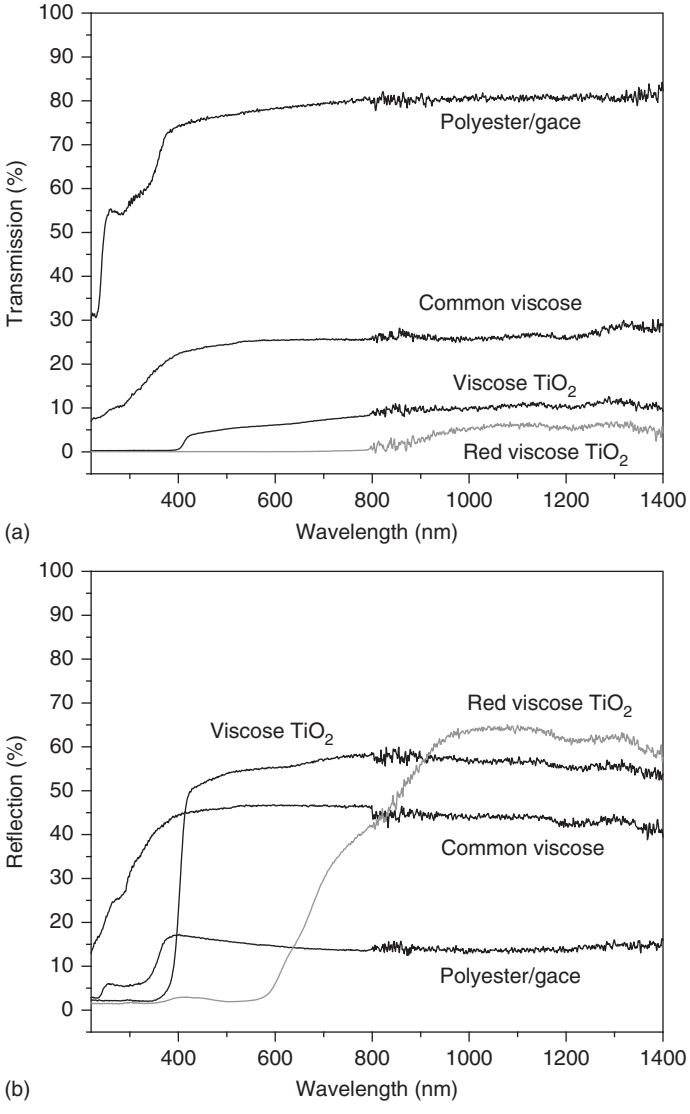


Figure 32.21 Spectra of diffuse transmission (a) and diffuse reflection (b) of different viscose fabrics and an open polyester gace. The spectra range summarizes UV, visible, and near-IR light. The titania containing viscose fibers are compared with a common viscose fabric and a common polyester.

behavior of TiO_2. The transmission of IR light (near-IR light 750–1400 nm is measured) is low with values of smaller 20%. However, the coloration of the textile substrate can have a certain influence. This is shown with spectra from that cellulosic fiber after dyeing with a red dye (Figure 32.21). The reflection of those colored samples depends strongly on the type of radiation. For UV light, the reflection is as well near zero, obviously because all UV light is absorbed by the TiO_2. For the IR light higher reflection of more than 50% are observed, probably because of the good reflectance properties of the embedded TiO_2 particles. For IR light mainly the reflective properties are responsible to gain the IR protective effect. An attractive development could be a combination with an organic absorber for near-IR light applied during a conventional dyeing process.

32.3.4 X-Ray Shielding

Figure 32.22 shows a SEM image of a cellulosic fiber containing $BaSO_4$ as X-ray absorber. The concentration of $BaSO_4$ is 40 wt%. This fiber is produced by the lyocell process at the TITK (Rudolstadt, Germany) [120, 121]. $BaSO_4$ is added to the spinning solution and embedded into the fiber during the wet spinning process. The SEM measurements are done in a measurement modus giving not only the topography information but also a certain material contrast. By this, chemical elements with higher atomic number are shown brighter, so $BaSO_4$ particles near

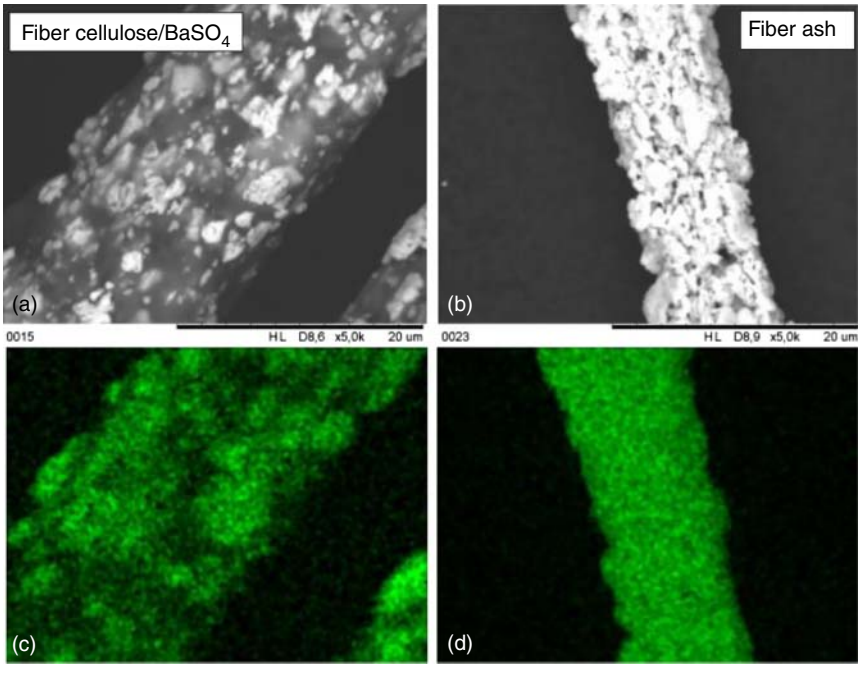


Figure 32.22 Comparison of cellulosic composite fiber with barium sulfate and the ash of this fiber. The images in panels (a, b) are recorded by SEM. The images in panels (c, d) present the distribution of the element barium mapped by EDS measurements.

the fiber surface can be clearly detected as white spots. The related EDS measurements show similar barium distribution on the fiber surface, so the estimation made from SEM investigations is proven.

After ignition of this cellulosic fiber by a flame, a fast burning follows, and a fibrous ash remained as residue. A SEM image of this fiber ash is shown in Figure 32.22. The linear structure of the fiber is still present, and the remaining structure could be well described as a kind of fiber skeleton built up by the non-burning inorganic compound $BaSO_4$. The structure of the ash seems to be denser, and the fiber diameter is slightly decreased. The denser structure is shown in the analogous EDS image presenting the barium distribution in the ash (Figure 32.22).

Such barium sulfate-containing cellulosic fibers are also described as composite fiber containing an organic component, cellulose, and an inorganic component, the barium sulfate as X-ray absorber [121, 122]. Not only barium sulfate but also other inorganic compounds can be embedded inside a cellulosic fiber to realize fiber materials for X-ray protection [84, 121]. An overview on SEM images of different fibers is shown in Figure 32.23. The idea of using barium titanate or barium zirconate instead of the barium sulfate is to replace the sulfur by a heavier element to improve the X-ray absorption properties.

It should be stated here that it is of course quite simple to produce a composite material built up from cellulose and barium sulfate. However, for X-ray

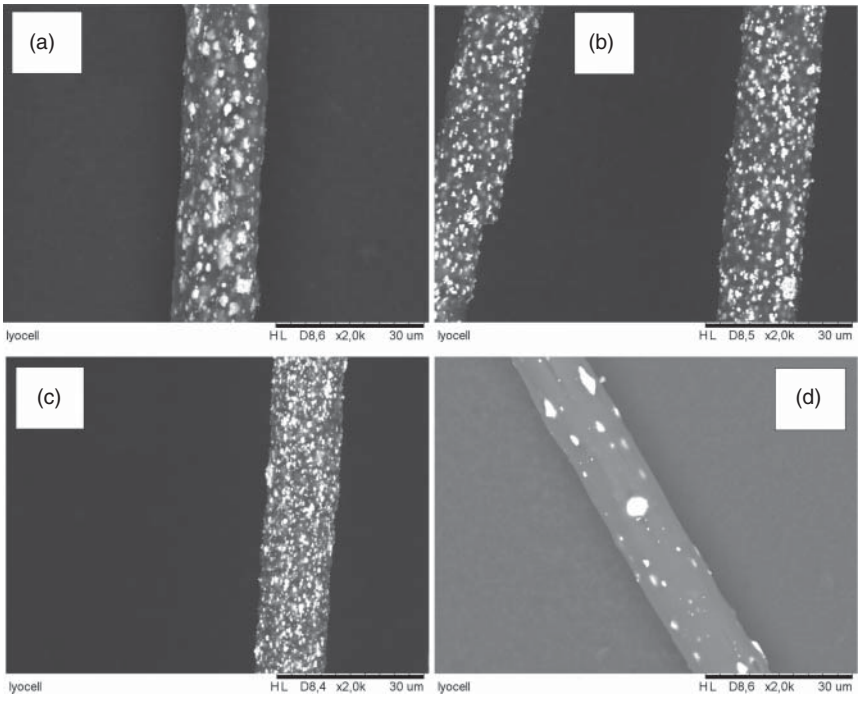


Figure 32.23 SEM images of cellulosic fibers with different embedded inorganic compounds as X-ray absorbers. (a) $BaSO_4$, (b) $BaTiO_2$, (c) $BaZrO_3$, and (d) Bi_2O_3.

protective purposes, fibers with high amounts of inorganic additive are needed, and for those fibers, disadvantageous changes in mechanical stability should be expected. For this, often after the fiber production, the preparation of a nonwoven material is described and investigated for X-ray protective properties [122]. In contrast the preparation of a yarn and later a fabric from those composite fibers is more challenging [84, 121, 123]. During spinning, knitting, or weaving processes, strong mechanical forces are working onto the fiber, and only if the preparation of composite fiber is especially developed and dedicated for textile production that the textile processes can be performed. Also the spinning processes have to be modified to realize an X-ray protective composite yarn [84].

However, the fabric production from such composite yarns is successfully realized, and some product examples are presented in Figures 32.24 and 32.25. It was demonstrated that the production process along the complete textile chain works to realize in the end a clothing product made from X-ray protective fibers [123]. A special idea for application was here to realize a hand protective device as shown in Figure 32.24 or a completely knitted glove for use in mobile X-ray analysis. Mobile analysis of elemental composition is often done by use of X-radiation to determine, for example, the amount of different metals building up an alloy. The operator is usually not exposed to the direct X-ray beam, but backscattering effects and fluorescence can lead to a certain exposition to radiation. For this, a certain protection for the hand and arms is quite suitable.



Figure 32.24 Hand protecting device constructed from a cellulose/inorganic composite fiber.



Figure 32.25 Protective jacket constructed from a cellulose/inorganic composite fiber.

The transmission of such textile materials against X-rays is presented in Figure 32.26. The X-ray transmission is shown as function of the photon energy of the X-rays, and it is clearly seen that the transmission is significantly decreased by the developed textile materials. In comparison an ordinary textile has a transmittance for X-ray of near 100%. However it is also obviously that the developed composite textile is not able to support a transmission near to zero. Especially for higher photon energies the transmission is decreases. This absorption behavior is caused by the absorption properties of the used inorganic materials. Also related to this are the marked absorption edges in Figure 32.26,

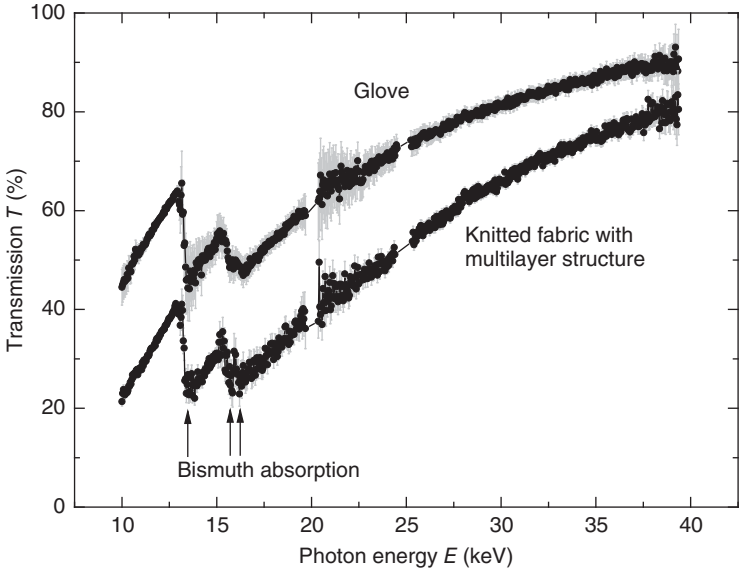


Figure 32.26 Transmission spectra for different knitted structures prepared from X-ray protective fibers.

which are typical for each chemical element. For this, the areas of applications have to be selected carefully, and not only the use as protective materials during material analytics but also the additional use together with traditional lead aprons could be a very perspective field for future applications.

32.4 Future Trends

Radiation protection is an important topic and a significant argument for technical applications and special clothes and of course in marketing. For each type of radiation, a certain reason and demand of radiation protection are raised and significant argument for usage. In general, it can be estimated that the demand for radiation protective fibers and textiles will be increased in the future, especially due to the increasing awareness of the customer to the fact of dangerous risks of radiation. Not only private customers but also the use in official facilities as hospitals, research institutes, police, or military organizations can benefit from radiation protective textile. Besides the protection itself, other applications are important as hiding the electronic identity or the heat camouflage.

A special prospective and attractive field of application will be probably the heat or light management, which is strongly related to radiation protection. The use of light management textile materials is a prospective method to lower the energy consumption for keeping buildings warm. Heating energy is cost saving, so this application is a very promising one.

To reach best protection properties, probable materials will be developed combining different types of functional additives in different arrangement and combinations. Special effective developments could be composite fibers combined with a coating and produced in knitted or woven materials.

Acknowledgments

For fruitful long-term cooperation, many helpful discussions, and experimental help, the presenter would like to thank many colleagues and students. Especially mentioned are Prof. Bendt, Prof. Breckenfelder, Prof. Kyosev, and Prof. Weide (all from Hochschule Niederrhein); Dr. Leisegang (from Saxray/Dresden); Dr. Krieg (from TITK/Rudolstadt); and Prof. Textor (Hochschule Reutlingen). Many thanks are also owed to K. Günther and A. Askani (yarn production); C. Giebing (fabric production); K. Bredlich, F. Bohnert, and N. Brinkert (knitting experiments); and M. Cont (help with the photographs). This work is partly financially supported by IGF project 17783BG/1 of the research association Forschungskuratorium Textil e.V. Reinhardtstraße 12-14, 10117 Berlin, and is supported by the AiF within the scope of the support program of the Industrielle Gemeinschaftsforschung und -entwicklung (IGF) of the Ministry of Economics and Technology due to a decision of the German Bundestag. For the funding of the electron microscope equipment, the author acknowledges very gratefully the program FH Basis of the German federal country North Rhine-Westphalia

NRW. All product and company names mentioned in this chapter may be trademarks of their respective owners, also without labeling.

References

1 Gerthsen, C. and Vogel, H. (1993). *Physik*, 17e. Berlin: Springer-Verlag.
2 Göpel, W. and Ziegler, C. (1994). *Struktur der Materie*. Stuttgart: B.G. Teubner Verlagsgesellschaft.
3 Atkins, P.W. (1993). *Quanten*. Weinheim: VCH-Verlagsgesellschaft.
4 Skoog, D.A. and Leary, J.J. (1996). *Instrumentelle Analytik*. Berlin: Springer-Verlag.
5 Carter, R.S., Palevsky, H., Myers, V.W., and Hughes, D.J. (1953). Thermal neutron absorption cross sections of boron and gold. *Physical Review* 92: 716.
6 Rainwater, J. and Havens, W.W. (1946). Neutron beam spectrometer studies of boron, cadmium, and the energy distribution from paraffin. *Physical Review* 70: 136.
7 Durante, M. and Cucinotta, F.A. (2011). Physical basis of radiation protection in space travel. *Reviews of Modern Physics* 83: 1245–1281.
8 Lottenbach, R. (2016). Innovative fabrics for uniforms, corporate wear and personal protection equipment. *Aachen-Dresden-Denkendorf International Textile Conference*, November 2016.
9 Horneck, G. (1995). Quantification of the biological effectiveness of environmental UV radiation. *Journal of Photochemistry and Photobiology B: Biology* 31: 43–49.
10 Brasch, D.E., Rudolph, J.A., Simon, J.A. et al. (1991). A role for sunlight in skin cancer. *Proceedings of the National Academy of Sciences of the United States of America* 88: 10124–10128.
11 Cerkova, J., Stipek, S., Crkovska, J. et al. (2004). UV rays, the prooxidant/antioxidant imbalance in the cornea and oxidative eye damage. *Physiological Reviews* 53: 1–10.
12 Saravanan, D. (2007). UV protection textile materials. *AUTEX Research Journal* 7: 53–62.
13 Teng, C. and Yu, M. (2003). Preparation and property of poly(ethylene terephthalate) fibers providing ultraviolet radiation protection. *Journal of Applied Polymer Science* 88: 1180–1185.
14 Albertini, R.J. and DeMars, R. (1973). Somatic cell mutation detection and quantification of X-ray induced mutation in cultured, diploid human fibroblasts. *Mutation Research* 18: 199–224.
15 Chambers, C.E., Fetterly, K.A., Holzer, R. et al. (2011). Radiation safety program for the cardiac catheterization laboratory. *Catheterization and Cardiovascular Interventions* 77: 546–556.
16 Chida, K., Kato, M., Kagaya, Y. et al. (2010). Radiation dose and radiation protection for patients and physicians during interventional procedure. *Journal of Radiation Research* 51: 97–105.

17 Fischer, F.M. (2009). Klinischer Vergleich computer-assistierter und konventioneller Implantationsverfahren. PhD thesis. Humboldt-Universität, Berlin.

18 Bohnsack, O. (2005). Reduktion der Strahlenexposition bei CT-Fluoroskopie-gesteuerten Interventionen: Möglichkeiten und Grenzen einer segmentalen Röhrenabschaltung. PhD thesis. Ludwig Maximilians Universität, München.

19 Dresing, K. (2011). Röntgen in Unfallchirurgie und Orthopädie. *Operative Orthopädie und Traumatologie* 1: 70–78.

20 Wucherer, M. and Loose, R. (2005). Berufliche Strahlenexposition. *Radiologie* 45: 291–303.

21 Mahltig, B., Zhang, J., Wu, L. et al. (2017). Effect pigments for textile coating – a review on the broad range of advantageous functionalization. *Journal of Coatings Technology and Research* 14: 35–55.

22 Hesse, M., Meier, H., and Zeeh, B. (2008). *Spectroscopic Methods in Organic Chemistry*. Stuttgart: Georg ThiemeVerlag.

23 Reinert, G., Fuso, F., Hilfiker, R., and Schmidt, E. (1997). UV-protecting properties of textile fabrics and their improvement. *Textile Chemist and Colorist* 29: 36–43.

24 Yu, Y., Hurren, C., Millington, K.R. et al. (2017). Research on the influence of yarn parameters on the ultraviolet protection of yarns. *The Journal of the Textile Institute* 108: 178–188.

25 Gambichler, T., Hatch, K.L., Avermaete, A. et al. (2002). Influence of wetness on the ultraviolet protection factor (UPF) of textiles: in vitro and in vivo measurements. *Photodermatology, Photoimmunology and Photomedicine* 18: 29–35.

26 Neumann, B. (2017). Von UV bis IR. *GIT-Labor-fachzeitschrift* 61: 12–17.

27 Alvarez, J. and Lipp-Symonowicz, B. (2003). Examination of the absorption properties of various fibres in relation to UV radiation. *AUTEX Research Journal* 3: 72–77.

28 Hoffmann, K., Laperre, J., Avermaete, A. et al. (2001). Defined UV protection by apparel textiles. *Archives of Dermatology* 137: 1089–1094.

29 Bajaj, P., Kothari, V.K., and Ghosh, S.B. (2000). Review article – some innovations in UV protective clothing. *Indian Journal of Fibre and Textile Research* 25: 315–329.

30 Asquith, R.S. and Garcia-Dominguez, J.J. (1968). New amino acids in alkali-treated wool. *Coloration Technology* 84: 155–158.

31 Lehninger, A.L., Nelson, D.L., and Cox, M.M. (1994). *Prinzipien der Biochemie*. Heidelberg: Spektrum Akademischer Verlag.

32 Jastorff, B., Störmann, R., and Wölcke, U. (2003). *Struktur-Wirkungs-Denken in der Chemie*. Bremen – Oldenburg: Universitätsverlag Aschenbeck & Isensee.

33 Algaba, I., Riva, A., and Crews, P.C. (2004). Influence of fiber type and fabric porosity on the UPF of summer fabrics. *AATCC Review* 4: 26–31.

34 Mongkholrattanasit, R., Krystufek, J., Wiener, J., and Vikova, M. (2011). Dyeing, fastness, and UV protection properties of silk and wool fabrics dyed

with eucalyptus leaf extract by the exhaustion process. *Fibres & Textiles in Eastern Europe* 19: 94–99.

35 Ebert, G. (1993). *Biopolymere*. Stuttgart: B.G. Teubner Verlagsgesellschaft.

36 Liu, X., Yu, W., and Xu, P. (2008). Improving the photo-stability of high performance aramid fibers by sol–gel treatment. *Fibers and Polymers* 9: 455–460.

37 Milford, J.G.N. (1972). Aromatic polyamide fibers containing ultraviolet light screeners. US Patent 3888821A, filed 2 November 1972 and issued 10 June 1975.

38 Qian, Y., Qiu, X., and Zhu, S. (2015). Lignin: a nature-inspired sun blocker for broad-spectrum sunscreens. *Green Chemistry* 17: 320–324.

39 Jakubke, H.-D. and Jeschkeit, H. (1993). *Concise Encyclopedia Chemistry*. Berlin: Walter de Gruyter.

40 Maity, S., Singha, K., Debnath, P., and Singha, M. (2013). Textiles in electromagnetic radiation protection. *Journal of Safety Engineering* 2: 11–19.

41 Wang, X., Liu, Z., and Zhou, Z. (2014). Virtual metal model for fast computation of shielding effectiveness of blended electromagnetic interference shielding fabric. *International Journal of Applied Electromagnetics and Mechanics* 44: 87–97.

42 Saini, P. and Choudhary, V. (2013). Electrostatic charge dissipation and electromagnetic interference shielding response of polyaniline based conducting fabrics. *Indian Journal of Pure and Applied Physics* 51: 112–117.

43 Azim, S.S., Satheesh, A., Ramu, K.K. et al. (2006). Studies on graphite based conductive paint coatings. *Progress in Organic Coatings* 55: 1–4.

44 Johnson, J.A., Barbato, M.J., Hopkins, S.R., and OMalley, M.J. (2003). Dispersion and film properties of carbon nanofiber pigmented conductive coatings. *Progress in Organic Coatings* 47: 198–206.

45 Singh, B.P., Bharadwaj, P., Choudhary, V., and Mathur, R.B. (2014). Enhanced microwave shielding and mechanical properties of multiwall carbon nanotubes anchored carbon fiber felt reinforced epoxy multiscale composites. *Applied Nanoscience* 4: 421–428.

46 Umrao, S., Gupta, T.K., Kumar, S. et al. (2015). Microwave-assisted synthesis of boron and nitrogen co-doped reduced graphene oxide for the protection of electromagnetic radiation in Ku-band. *ACS Applied Materials & Interfaces* 7: 19831–19842.

47 Wang, R., Yang, H., Wang, J., and Li, F. (2014). The electromagnetic interference shielding of silicone rubber filled with nickel coated carbon fiber. *Polymer Testing* 38: 53–56.

48 Jiang, K., Li, Q., and Fan, S. (2002). Spinning continuous carbon nanotube yarns. *Nature* 419: 801.

49 Foroughi, J., Spinks, G.M., Antiohos, D. et al. (2014). Highly conductive carbon nanotube-graphene hybrid yarn. *Advanced Functional Materials* 24: 5859–5865.

50 McCullough, F.P., Novak, L.R., and Hall, D.M. (1989). Camouflage material. US Patent 5, 312, 678, filed 6 October 1989 and issued 17 May 1994.

51 Gunde, M.K. and Kunaver, M. (2003). Infrared reflection-absorption spectra of metal-effect coatings. *Applied Spectroscopy* 57: 1266–1272.

52 Sutter, C.R., Petelinkar, R.A., and Reeves, R.E. (1998). Infrared reflective visually colored metallic compositions. US Patent 6468647B1, filed 17 February 1998 and issued 22 October 2002.

53 Bendiganavale, A.K. and Malshe, V.C. (2008). Infrared reflective inorganic pigments. *Recent Patents on Chemical Engineering* 1: 67–79.

54 George, G., Vishnu, V.S., and Reddy, M.I.P. (2011). The synthesis characterization and optical properties of silicon praseodymium Y_6MoO_{12} compounds: environmentally benign inorganic pigments with high NIR reflectance. *Dyes and Pigments* 88: 109–115.

55 Kauffman, M.H. (1985). Synthesis of transition metal dithiene complexes. US Patent 4, 593, 113, filed 14 January 1985 and issued 3 June 1986.

56 Lehmann, U. and Heizler, D. (2007). Dithiolene metal complex colorless IR absorbers. US Patent 2010/0021833A1, filed 18 December 2007 and issued 28 January 2010.

57 Straube, T., Mayer-Gall, T., Textor, T., and Gutmann, J.S. (2016). TCO-based nanoparticle coatings for heat-shielding applications in textile architecture. *Aachen-Dresden-Denkendorf International Textile Conference*, November 2016.

58 Hilfiker, R., Kaufmann, W., Reinert, G., and Schmidt, E. (1996). Improving sun protection factors by applying UV-absorbers. *Textile Research Journal* 66: 61–70.

59 Han, Y., Zhao, Y., Xie, C., and Powers, J.M. (2010). Color stability of pigmented maxillofacial silicone elastomer: effects of nano-oxides as opacifiers. *Journal of Color and Appearance in Dentistry* 38: 100–105.

60 Abidi, N., Hequet, E., Tarimala, S., and Dai, L.L. (2007). Cotton fabric surface modification for improved UV radiation protection using sol–gel process. *Journal of Applied Polymer Science* 104: 111–117.

61 Mahltig, B., Böttcher, H., Rauch, K. et al. (2005). Optimized UV protecting coatings by combination of organic and inorganic UV absorbers. *Thin Solid Films* 485: 108–114.

62 Mahltig, B. and Textor, T. (2008). *Nanosols and Textiles*. Singapore: World Scientific.

63 Ghamsari, M.S., Alamdari, S., Han, W., and Park, H.-H. (2017). Impact of nanostructured thin ZnO film in ultraviolet protection. *International Journal of Nanomedicine* 12: 2017–2216.

64 Mahltig, B. and Haufe, H. (2010). Biozidhaltige Nanosole zur Veredlung von weichen und temperaturempfindlichen Materialien. *Farbe & Lack* 116 (3): 27–30.

65 Alebeid, O.K. and Zhao, T. (2014). Anti-ultraviolet treatment by functionalizing cationized cotton with TiO_2 nano-sol and reactive dye. *Textile Research Journal* 85: 449–457.

66 Huang, J.Y., Li, S.H., Ge, M.Z. et al. (2015). Robust superhydrophobic TiO_2 fabrics for UV shielding, self-cleaning and oil–water separation. *Journal of Materials Chemistry A* 3: 2825–2832.

67 Christie, R.M. (2001). *Colour Chemistry*. Cambridge: The Royal Society of Chemistry.

68 Windler, L., Lorenz, C., von Goetz, N. et al. (2012). Release of titanium dioxide from textiles during washing. *Environmental Science and Technology* 46: 8181–8188.

69 Choudhury, A.K.R. (2006). *Textile Preparation and Dyeing*. Enfield: Science Publishers.

70 Reinert, G., Fuso, F., and Hilfiker, R. (1996). Process for increasing the sun protection factor of cellulosic fiber materials. US Patent 5, 914, 444, filed 4 March 1996 and issued 22 June 1999.

71 Rauch, K., Dieckmann, U., Böttcher, H., and Mahltig, B. (2004). UV-schützende transparente Beschichtungen für technische Anwendungen. German Patent DE102004027075A1, filed 2 June 2004 and issued 29 December 2005.

72 Böttcher, H., Mahltig, B., Haufe, H., and Henker, P. (2006). UV-licht absorbierendes material. German Patent DE102006002231A1, filed 17 January 2006 and issued 19 September 2007.

73 Schrader, B. and Rademacher, P. (2009). *Kurzes Lehrbuch der Organischen Chemie*. Berlin: Walter de Gruyter.

74 Küster, B. (1975). UV-Stabilisatoren für aromatische Polyamide. *Lenzinger Berichte* 38: 12–13.

75 Reinert, G., Fuso, F., and Hilfiker, R. (1996). Process for increasing the sun protection factor of cellulosic fibre materials. US Patent 5, 938, 793, filed 31 January 1996 and issued 17 August 1999.

76 Grethe, T., Haase, H., Natarajan, H.S. et al. (2015). Coating process for antimicrobial textile surfaces derived from a polyester dyeing process. *Journal of Coatings Technology and Research* 12: 1133–1141.

77 Heller, J. and Mura, J.-L. (1997). Aqueous dispersions and their use for treating textiles. US Patent 5, 955, 005, filed 23 July 1997 and issued 21 September 1999.

78 Eckhardt, C., Reinehr, D., Metzger, G., and Sauter, H. (1997). Triazine derivatives and their use. US Patent 5, 939, 379, filed 2 June 1997 and issued 17 August 1999.

79 Qu, L., Tian, M., Hu, X. et al. (2014). Functionalization of cotton fabric at low graphene nanoplate content for ultrastrong ultraviolet blocking. *Carbon* 80: 565–574.

80 Tang, X., Tian, M., Qu, L. et al. (2015). Functionalization of cotton fabric with graphene oxide nanosheet and polyaniline for conductive and UV blocking properties. *Synthetic Metals* 202: 82–88.

81 Prince, E., Fuess, H., Hahn, T. et al. (2006). *International Tables of Crystallography*, vol. C. International Union of Crystallography.

82 Hubbell, S.M. and Seltzer, J.H. (1996). *Tables of X-Ray Mass Attenuation Coefficients and Mass Energy-absorption Coefficients from 1 KeV to 20 MeV for Elements Z = 1 to 92 and 48 Additional Substances of Dosimetric Interest*. National Institute of Standards and Technology.

83 Mahltig, B., Haufe, H., Leisegang, T. et al. (2011). Verminderte Röntgentransmission durch beschichtete Textilien. *Melliand Textilberichte* 92: 36–39.

84 Günther, K., Giebing, C., Askani, A. et al. (2015). Cellulose/inorganic-composite fibers for producing textile fabrics of high X-ray absorption properties. *Materials Chemistry and Physics* 167: 125–135.
85 Martinez, T.P. and Cournoyer, M.E. (2001). Lead substitution and elimination study. *Journal of Radioanalytical and Nuclear Chemistry* 249: 397–402.
86 Willmes, A. (1993). *TaschenbuchChemischeSubstanzen*. Thun und Frankfurt am Main: Verlag Harri Deutsch.
87 Azman, N.Z.N., Siddiqui, S.A., and Low, I.M. (2013). Synthesis and characterization of epoxy composites filled with Pb, Bi or W compound for shielding of diagnostic X-rays. *Applied Physics A* 110: 137–144.
88 Lyra, M., Charalambatou, P., Sotiropoulos, M., and Diamantopoulos, S. (2011). Radiation protection of staff in radionuclide therapy. *Radiation Protection Dosimetry* 147: 272–276.
89 Schueler, B.A. (2010). Operator shielding. *Techniques in Vascular and Interventional Radiology* 13: 167–171.
90 Ross, A.M., Segal, J., Borenstein, D. et al. (1997). Prevalence of spinal disc disease among interventional cardiologists. *American Journal of Cardiology* 79: 68–70.
91 Finnerty, M. and Brennan, P.C. (2005). Protective aprons in imaging departments: manufacturer stated lead equivalence values require validation. *European Radiology* 15: 1477–1484.
92 Oyar, O. and Kislalioglu, A. (2012). How protective are the lead aprons we use against ionizing radiation? *Diagnostic and Interventional Radiology* 18: 147–152.
93 Nkubli, B.F., Nzotti, C.C., Nwobi, I.C. et al. (2013). Quality control in radiology units of tertiary healthcare centers in north eastern Nigeria. *Nigerian Journal of Medical Imaging and Radiation Therapy* 2: 26–31.
94 Han, E.G., Kim, E.A., and Oh, K.W. (2001). Electromagnetic interference shielding effectiveness of electroless Cu-plated PET fabrics. *Synthetic Metals* 123: 469–476.
95 Lai, K., Sun, R.J., Chen, M.Y. et al. (2007). Electromagnetic shielding effectiveness of fabrics with metallized polyester filaments. *Textile Research Journal* 77: 242–246.
96 Ziaja, J., Koprowska, J., and Janukiewicz, J. (2008). Using plasma metallisation for manufacture of textile screens against electromagnetic fields. *Fibres & Textiles in Eastern Europe* 16: 64–66.
97 Statex GmbH, Bremen, Germany. www.statex.de. (Accessed 14/01/2020).
98 Marktek Inc. Chesterfield, US. www.marktek-inc.com. (Accessed 14/01/2020).
99 Swicofil AG, Emmenbrücke, Switzerland. www.swicofil.com. (Accessed 14/01/2020).
100 YSHIELD GmbH, Ruhstorf, Germany. www.yshield.com. (Accessed 14/01/2020).
101 YSHIELD GmbH (2016). *Product Catalogue*. Ruhstorf, Germany: YSHIELD GmbH.

102 Marchini, F. (1991). Advanced applications of metallized fibres for electrostatic discharge and radiation shielding. *Journal of Coated Fabrics* 20: 153–166.

103 Bertuleit, K. (1991). Silver coated polyamide: a conductive fabric. *Journal of Coated Fabrics* 20: 211–215.

104 Wang, W., Li, W., Gao, C. et al. (2015). A novel preparation of silver-plated polyacrylonitrile fibers functionalized with antibacterial and electromagnetic shielding properties. *Applied Surface Science* 342: 120–126.

105 Odhiambo, S.A., de Mey, G., Hertleer, C. et al. (2014). Discharge characteristics of poly(3,4-ethylene dioxythiophene):poly(styrenesulfonate) (PEDOT:PSS) textile batteries, comparison of silver coated yarn electrode devices and pure stainless steel filament yarn electrode devices. *Textile Research Journal* 84: 347–354.

106 Orban, R.F. (1985). Continuous process for the sequential coating of polyamide filaments with copper and silver. US Patent 4645574A, filed 2 May 1985 and issued 24 February 1987.

107 Mahltig, B., Darko, D., Günther, K., and Haase, H. (2015). Copper containing coatings for metallized textile fabrics. *Journal of Fashion Technology & Textile Engineering* 3 (1): 1–10.

108 Lee, H.M., Choi, S.-Y., Jung, A., and Ko, S.H. (2013). Highly conductive aluminum textile and paper for flexible and wearable electronics. *Angewandte Chemie International Edition* 52: 7718–7723.

109 Okayasu, S., Shinichi, I., Kaga, U., and Nobatake, A. (1986). Process for producing an electromagnetic radiation-shielding, metallized polyester fiber textile material. US Patent 4, 681, 591, filed 22 May 1986 and issued 21 July 1987.

110 Onggar, T., Hund, H., Hund, R.-D., and Cherif, C. (2014). Silvering of inert PET-textile materials by means of one-bath and two-bath methods and their characteristics. *Fibres & Textiles in Eastern Europe* 22: 108–114.

111 Godley, P. (1948). Deposition of metal on a nonmetallic support. US Patent 2622041A, filed 3 August 1948 and issued 16 December 1952.

112 Manabe, K., Tsutsui, M. Suzuki, T. et al. (1983) Metal-coated fibrous objects. US Patent 4816124A, filed 19 December 1983 and issued 28 March 1989.

113 Yuranova, T., Rincon, A.G., Bozzi, A. et al. (2003). Antibacterial textiles prepared by RF-plasma and vacuum-UV meditated deposition of silver. *Journal of Photochemistry and Photobiology A: Chemistry* 161: 27–34.

114 Amberg, M., Kasdallah, C., Ritter, A., and Hegemann, D. (2012). Influence of residual oils on the adhesion of metal coatings to textiles. *Journal of Adhesion Science and Technology* 24: 123–134.

115 Ozen, M.S., Sancak, E., Beyit, A. et al. (2013). Investigation of electromagnetic shielding properties of needle-punched nonwoven fabrics with stainless steel and polyester fiber. *Textile Research Journal* 83: 849–858.

116 Ebneth, H., Fitzky, H.G., Wolf, G.D., and Giesecke, H. (1982). Use of metallized knitted net fabrics for protection against microwave radiation. US Patent 4, 572, 960, filed 1 November 1982 and issued 25 February 1986.

117 Dubrovski, P.D. and Golob, D. (2009). Effects of woven fabric construction and color on ultraviolet protection. *Textile Research Journal* 79: 351–359.

118 Bisjak, C., Gürtler, A., Dobson, P. et al. (2010). Ultraviolet protective fabrics based on man-made cellulosic fibers. US Patent 0156462A1, filed 3 May 2010 and issued 12 March 2012.

119 Ozgen, B. (2012). New biodegradable fibres, yarn properties and their applications in textiles: a review. *IndustriaTextila* 63: 3–7.

120 Wendler, F., Kosan, B., Krieg, M., and Meister, F. (2009). Possibilities for the physical modification of cellulose shapes using ionic liquids. *Macromolecular Symposia* 280: 112–122.

121 Mahltig, B., Günther, K., Giebing, C. et al. (2014). Inorganic/organic composite fibers for fabrics with X-ray protective properties. *Technical Textiles* 57: 56–58.

122 Qu, L., Tian, M., Zhang, X. et al. (2015). Barium sulfate/regenerated cellulose composite fiber with X-ray radiation resistance. *Journal of Industrial Textiles* 45: 352–367.

123 Mahltig, B., Günther, K., Askani, A. et al. (2016). Clothing form organic/inorganic composite fibers for reduction of X-ray exposition. *Technical Textiles* 59: 20–22.

33

Fibrous Materials for Antimicrobial Applications

Yue Deng, Yang Si, and Gang Sun

University of California Davis, Fiber and Polymer Science, Agricultural & Environmental Chemistry, 251 Everson Hall, Davis, CA 95616, USA

33.1 Introduction

33.1.1 Basic Principles

There are trillions of microorganisms that live in and on a human body [1]. Although some of them help to keep the body healthy, some of them can harm the body. Such kinds of microorganisms include pathogenic virus, gems, bacteria, and fungi. Textiles, which most of them are made of organic materials and have porous structures that hold moisture, provide the essential nutrients for microbes to live and create potentials for infections that can threat the health of human beings. Since textiles are so widely used in daily life, developing antimicrobial fibers becomes an important and valuable direction of research.

An "antimicrobial" is defined to be an agent that can either kill certain types of microbes or slow down their growth [2]. Antimicrobial agents work under different mechanisms and principles. When it comes to textiles, the more conventional way to make fibers antimicrobial is to treat them with some antimicrobial agents, such as *N*-halamines [3, 4], quaternary ammonium compounds (QACs) [5, 6], and photoactive chemicals [7–9]. In some cases, the natural materials themselves, which the fibers are made of, can inhibit the growth of microorganisms. Chitosans are an example of such natural polymers [10, 11]. This is another way to produce antimicrobial fibers. Antimicrobial fibers and their products, as mentioned before, have a variety of applications. For example, socks that claim to be antimicrobial can reduce the reproduction of fungi fed by human sweat and solve the unpleasing feet odor problem. Mildew-resistant shower curtains are another example of antimicrobial textiles as they have resistance against the growth of a type of fungus. Besides antifungals, textiles can also be combined with antibacterial agents and have a wide market in clinics, such as sterilized bandages.

33.1.2 Brief History

The earliest publication that can be found in the Web of Science Core Collection is published in 1972 by N. S. Plotkina, N. V. Vitulska, and V. A. Khokhl, while the

Handbook of Fibrous Materials, First Edition. Edited by Jinlian Hu, Bipin Kumar, and Jing Lu.
© 2020 Wiley-VCH Verlag GmbH & Co. KGaA. Published 2020 by Wiley-VCH Verlag GmbH & Co. KGaA.

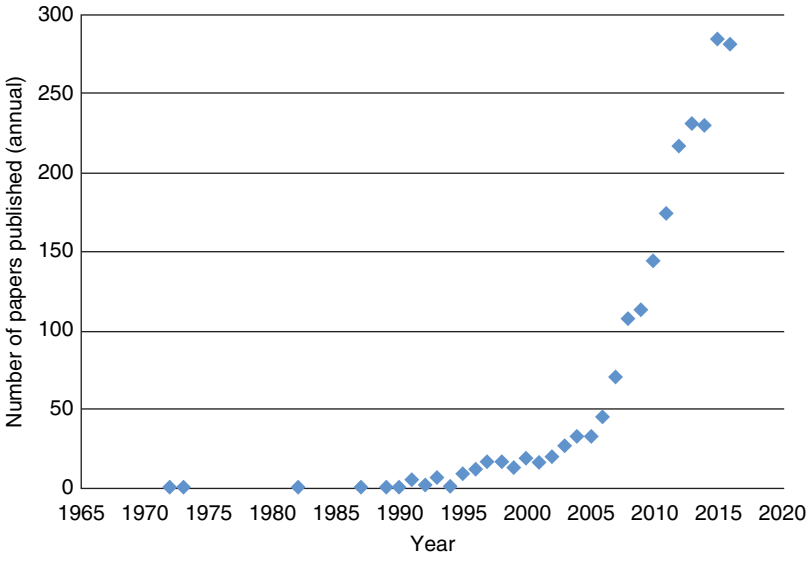


Figure 33.1 Number of publications each year that cover the topic of antimicrobial fibers.

application of antimicrobial textiles began years earlier. Military needs seem to be the main driving force for development of technology back in nineteen and first half of twenty centuries. Demand on microbial fibers was raised in World War II due to the surprisingly short duration of the military tents [2]. It was discovered that the reason that caused those tents to rot so fast is the rapid growth of a filamentous fungus (*Trichoderma reesei*) with the aid of the warm and wet weather in South Pacific.

However, antimicrobial fiber is not a very popular research topic compared with other topics in the biochemical related field. In 2015, one of its peak years, 285 journal papers were published. On the other hand, compared with only a handful publications in the 1980s, this application area is growing rapidly. Researches that were published around 2004 largely stimulated researchers to enter and devote into this field (Figure 33.1). Some of the inspiring studies including the rechargeable *N*-halamine textile [3, 4], applications of silver and other metal oxide nanoparticles on textiles [12–14], textile modification with quaternary ammonium salts [5, 6], and natural microbial agents [15–17]. This chapter will summarize some important discoveries and achievements in fiber modifications with antimicrobial agents. This chapter will also give a brief review on the process of incorporation of these major antimicrobial agents into fabrics and the advantages and disadvantages of each type of modified fibers.

33.2 Quaternary Ammonium Compound Modified Fabrics

QACs are one of the conventional agents that were applied on textiles as a surface treatment to grant the textiles antimicrobial property. Study on QACs started

about a hundred years ago, in the early twentieth century [18]. Its antimicrobial property began to draw scientists' attention in the 1960s [19, 20]. QACs were once widely used in communities for disinfections for its low toxicity and good bacteria-eliminating ability. However, later on, people discovered that overuse of QACs seemed to promote severe drug resistance among bacteria [21, 22]. This section will cover the bacterial killing mechanism of QACs to discover the reason why QACs would promote drug resistance based on the mechanism. This section will also discuss the environmental impacts of overusing QACs in late twentieth century.

33.2.1 Antimicrobial Mechanism of QACs

The ammonium group in a QAC brings a positive charge. It reacts with the negatively charged cell membranes and damaged their structures. This leads to a change in permeability of the membranes, causing the cells to lose vital liquids. In the end, the metabolism of the cells is severely disrupted, and the microbes get killed [6, 23].

QACs were once believed to be one of the best antimicrobial agents, because it is effective (at the right concentration), colorless, odorless, and aerobically biodegradable [24]. However, its biodegradability was challenged later on for there were evidences showing high concentration of QACs in natural water bodies [25, 26]. Besides the enrichment problem of QACs in lakes and rivers via sewage water, its bacteria-killing spectrum is also relatively narrow. QACs work better on Gram-positive bacteria than Gram-negative bacteria [27, 28]. It can barely deactivate *Pseudomonas* and cannot kill *Mycobacterium* [29].

In addition, its effectiveness is largely affected by the environment. QAC is a good surfactant and is easily absorbed onto all kinds of surfaces. In hospital practices, QACs can be absorbed onto surfaces of needles, gazes, cotton balls, and glass vessels [30, 31]. Those kinds of equipment can all reduce QAC solution's effective concentration. For example, while using QAC solution to sterilize cotton balls, 1 g of cotton ball can absorb approximately 1.58 g of QAC solution. The QAC solution would work great for sterilizing the cotton fibers. However, the concentration of QAC in the solution stored in the cotton ball would significantly drop to a level much lower than the effective concentration because large amount of QAC is absorbed onto the cotton fibers. Therefore, the cotton ball cannot be used to sterilize wound. The effectiveness of QACs can also be reduced by organic substances like proteins and serums. Since its antimicrobial mechanism is based on the positive charge on ammonium group, any compounds that bring negative charge will antagonize the disinfection ability of QACs. Such negatively charged substances include soap, milk, and washing powder. Any metal ions that can cause ammonium group to participate out will also decrease the activity of QACs [24].

33.2.2 Environmental Impact

The presence of QACs in natural water bodies is mainly influenced by its biodegradability and absorption of QACs onto variety of surfaces to pass through [22, 26].

As mentioned in Section 33.2.1, QACs are considered to be aerobically biodegradable. However, their half-lives are largely affected by factors such as their chemical structure, the oxygen abundance in the environment, and acclimatization of the microorganism that can degrade QACs [32, 33]. Generally, as the length of the alkyl chain increases, so does the time required for the QACs to degrade. On the other hand, longer alkyl chain is one of the popular modifications of QACs to increase its biocidal effectiveness. Therefore, many QACs found in natural water body are QACs with long alkyl chain, which require a considerably long time to be removed.

In addition to the accumulation of QACs in the nature, exposure of high concentration QACs also promote drug resistance in some bacteria. To survive in high concentration of QACs, some bacteria gain resistance to QACs. Main QAC resistance mechanisms include reducing expression of porins [34–36], mobilizing genetic units [37, 38], and elevating expression of efflux pumps [39–41]. These mechanisms could also help such bacteria to survive under some antibiotics. Therefore, the presence of QACs in the environment not only does generate the problem of high-level QAC intakes but also promote drug resistance.

33.2.3 Conclusions

QACs, which are once the most commonly used antimicrobial agents, are now facing many challenges. Its biocidal performance is largely influenced by the environment, which limits its applications. Efforts have been put on this topic to increase the stability of QACs in complex environment and to increase its effectiveness toward more bacteria species. Many new compounds have been synthesized, which have functional groups that can improve either the biocidal effect of QACs or the safety of QACs. For example, the United States Food and Drug Administration has approved that organosilicon quaternary ammonium salt is safe to be used on products that will get contact with the human body directly.

In general, QACs still have some advantages that make them still an important area to study in the field of antimicrobial textiles. They are effective to Gram-positive bacteria and can be strongly bounded onto surface of fabrics. As more novel researches on QACs get published and applied, QACs will be a kind of truly safe and broad-spectrum antimicrobial agent.

33.3 *N*-Halamine Modified Fabrics

The study of the antibacterial nature of *N*-halamine started in the 1980s [42–45]. This organic compound shows high efficiency in water disinfection and was soon applied to produce biocidal polymers in the late 1990s [4, 46–48]. It is still considered as one of the conventional antimicrobial agents for fiber modification, because nanotechnology entered the stage even later. Among all those conventional antimicrobial agents, such as QACs, chitosan, and polyhexamethylene biguanide, the rechargeable characteristic of *N*-halamine makes it stand out and still have many studies going on till today. *N*-Halamine can be bound onto polymers, thin films, and nanofibers and has applications in water disinfection, food packaging, and another antibacterial practices [49–51].

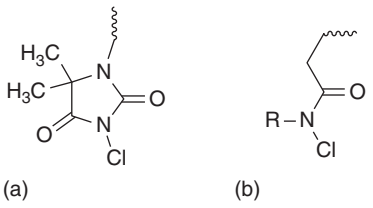


Figure 33.2 Some examples of possible structures of *N*-halamine compounds. (a) Example of a cyclic *N*-halamine and (b) example of an acyclic *N*-halamine.

33.3.1 Basic Principles

N-Halamine compounds have at least one nitrogen–halogen bond (shown in Figure 33.2). In most applications, this halogen is chloride. *N*-Halamine compounds kill microbes based on its oxidizing power provided by this N—X covalent bond. When it gets contact with the microbe, the N—X bond will be reduced to N–H and will release a free halogen ion (usually a Cl^+ ion as N–Cl is the mostly commonly used functional group in *N*-halamines). *N*-Halamine compounds also react with water to release halogen ions and show powerful water disinfection ability. This mechanism is shown in Figures 33.3 and 33.4. As illustrated, this oxidization reaction is also reversible. While putting the reduced functional groups in an environment with halogenating agent in abundance, they can regain the halogen atoms, and the antimicrobial ability can be restored. Dilute chlorine bleach is one of the widely used agents to help *N*-halamine compounds to be recharged with free Cl anions [4, 49, 52]. Since its bacterial killing mechanism is oxidizing, *N*-halamine will not promote microbial resistance.

33.3.2 Modification Method

The methods used for textile modification with *N*-halamine can be categorized into the following ones: cross-linking, grafting, coating, and reactive *N*-halamine treating.

33.3.2.1 Cross-linking

To add *N*-halamine onto surface of a textile via cross-linking, the reaction needs to start with a precursor of *N*-halamine. 1,3-Dimethylol-5,5-dimethylhydantoin (DMDMH) is a precursor of *N*-halamine that itself can also act as a cross-linker in basic environment. It was first successfully applied onto cotton cellulose by Y. Sun and G. Sun [47]. Y.Y. Sun and G. Sun then applied it onto other fabrics and the characteristics of the modified fabrics [3]. It was discovered that DMDMH

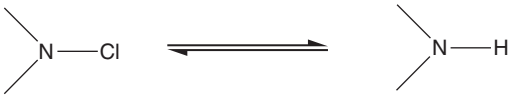


Figure 33.3 Reduce reaction of *N*-halamine (halogenated with chlorine), which is reversible.



Figure 33.4 Reaction of *N*-halamine (halogenated with chlorine) in water. This reaction is reversible.

modified fabrics gain a better durability [52]. However, it was also discovered that DMDMH-treated textiles would slowly release free formaldehyde, which raises safety concerns [51]. Therefore, researchers went on for more safety and reliable *N*-halamine precursors and found out several alternatives.

m-Aminophenylhydantoin (*m*-APH), a synthesized reagent, is one of the solutions to the safety problem of DMDMH. Unlike DMDMH, *m*-APH requires a polycarboxylic acid as a cross-linker to be bound onto the surface of a fabric. 1,2,3,4-Butanetetracarboxylic acid (BTCA) is a most commonly used polycarboxylic acid that gives the best wrinkle recovery with *m*-APH modified cotton in comparison with citric acid, tricarballylic acid, and other popular organic acids in industrial practice [53, 54]. BTCA can also act as the cross-linker for other *N*-halamine precursors to be added onto cellulose, such as 3-(2,3-dihydroxypropyl)-5,5-dimethylimidazolidine-2,4-dione [51], 3-(2,3-dihydroxypropyl)-7,7,9,9-tetramethyl-1,3,8-triazaspiro[4.5]decane-2,4-dione [55], 2-amino-2-methyl-1-propanol [14, 56], 2,2,6,6-tetramethyl piperidinol [56], 1-glycidyl-*s*-triazine-2,4,6-trione, and 1-(2,3-dihydroxypropyl)-*s*-triazine-2,4,6-trione [57].

33.3.2.2 Grafting

For *N*-halamines with vinyl groups, they can be grated onto fabrics through free radical polymerization reaction. For this reaction to happen, strong oxidative initiators, such as potassium persulfate, azobisisobutyronitrile, and ammonium cerium (IV) nitrate, are required.

N-Halamines containing vinyl groups can be further categorized into cyclic *N*-halamines and acyclic *N*-halamine. A typical cyclic *N*-halamine is 3-allyl-5,5-dimethylhydantoin, which has been successfully grafted onto many manmade and natural fabrics, including cotton, nylon, and polyester [4]. Acyclic *N*-halamines can be graded onto cellulose under similar mechanism [58–60]. However, due to its acyclic structure, its wash resistance and storage of chlorine are inferior to cyclic *N*-halamines.

33.3.2.3 Coating

Polymeric *N*-halamines can be applied onto many surfaces including textile via coating [61]. Chemical bonds form between the substrate and the coated polymeric layers, granting the composite reasonable durability. With the help of surfactants, water dispersible *N*-halamine polymers can be formed and be applied onto surfaces via emulsion polymerization. For a particular *N*-halamine monomer, 3-(4′-vinylbenzyl)-5,5-dimethylhydantoin, it can even be applied without using any organic solvent through admicellar polymerization [52, 62].

33.3.2.4 Reactive Reagent Treating

Reactive *N*-halamines refer to those *N*-halamine precursors that can chemically react with fibers to form covalent bonds. Therefore, textiles treated with reactive *N*-halamine have the best durability among all the modification methods. Cyclic *N*-halamines usually have good reactivities. Cyclic *N*-halamines such as 3-glycidyl-5,5-dialkylhydantoin and 1-glycidyl-*s*-triazine-2,4,6-trione are frequently used in reactive *N*-halamine treatments [63–65].

33.3.2.5 Electrospinning

All these processing methods listed in Sections 33.3.2.1 to 33.3.2.4 are embedding a layer or multiple layers of *N*-halamine onto the surface of textiles. However, there is another way to directly incorporate *N*-halamine into fabrics, which is via electrospinning. Electrospinning uses electric force to drive charged polymer solutions to form threads and spins threads to form fabrics. It produces fabrics with high specific surface area and high porosity and is a good method to generate nano- to microfibrous membranes [66–68]. Using water-soluble polymeric *N*-halamines (which were briefly introduced in Section 33.3.2.3), the obtained copolymer solution can be spun into fabrics that have direct incorporation of *N*-halamines. The large surface area makes this kind of fabrics has excellent bacterial killing effect right upon contacting. However, there is also a downside associates with the fast disinfection. *N*-Halamine nanofibrous membranes release chlorine too fast that they cannot stay effective for a long period of time and require frequently recharges.

33.3.3 Conclusions and Future Trend

N-Halamine is a powerful and special antimicrobial agent for fiber modification for the pathogen-killing functional group and can be recharged. Once the attached halogen is consumed, *N*-halamine compound can regain it by putting in an environment with sufficient amount of free halogen. Its bacterial killing mechanism is based on oxidation of the cell structure. Therefore, *N*-halamine works effectively for both Gram-positive and Gram-negative bacteria. It is a truly broad-spectrum antimicrobial agent that merely promotes microbial resistance. Furthermore, it has been discovered and confirmed that *N*-halamine compounds can also store the bacterial killing power until the substances they are in touch with oxidize the *N*-halamine compounds.

However, some conditions can cause *N*-halamine modified textiles to release the stored halogen in a fairly short period of time. Recent research focuses on increased stability of *N*-halamine, especially its durability after washing and under ultraviolet (UV) light. In addition to the effort put on researching its durability and stability, nanotechnology [68] is another direction that provides further space for the development of *N*-halamine. Nanostructures have greater specific area. Therefore, it can enhance the performance and efficiency of *N*-halamine in antimicrobial practices.

33.4 Metals and Metal Oxide Modified Fabrics

The applications of metals and metal oxides in antimicrobial textiles largely relied on the development of nanotechnology. Nanotechnology grants people ways to produce extremely small particles (to 10^{-7}~10^{-9} m), which creates large specific surface areas and largely increases the reactivity of those materials [69, 70]. More importantly, some materials would behave differently in nanoscale [71]. For example, some metal oxides, such as copper oxide [72, 73] and zinc

oxide [72–75], show antimicrobial property when they are in the forms of nanoparticles.

Most nanoparticles gain effective biocidal ability by the increased reactivity and contacting area. Their mechanisms of killing microorganisms are based on their own characteristics and are different from each other. This section will briefly talk about several commonly used metals and metal oxides for antimicrobial textile modification.

33.4.1 Silver

Silver has a long history of being used to sterilize water and food. Phoenicians used silver to keep their water clean and milk fresh. Chinese used silver to make food containers that can be used to test the toxicity of food. Today, silver is even applied in more products that people get contact with every day: toilet seats, refrigerator doors, drinking vessels, respirators, and water filters [76–78]. Production of some of those applications requires fibers treated with nanosized silver particles. Silver nanoparticles that can be used in fiber modification need to be inert and charge neutral [76].

There are several ways to produce nanosized silver particles. This section will introduce one of the most common methods. To make silver atoms, a silver salt is reduced in aqueous form with reducing agents. This method involves two agents: the silver salt is treated with a strong reducing agent and then a weak reducing agent. These two reducing agent controls the size of the silver nanoparticles and their dispersity [76, 79, 80].

33.4.2 Oligodynamic Effects of Metals

The antimicrobial nature of silver is called oligodynamic effect, which was discovered and named by Karl Wilhelm von Nägeli in 1893 [81]. Oligodynamic is a biocidal effect that is observed on many heavy metals. This means, not only silver but also other metals such as copper, zinc, gold, tin, and mercury have this biocidal effect [77, 82, 83]. Due to their toxicity toward human beings, besides silver, copper (II) oxide and zinc oxide are the two other metal oxides that are commonly used.

The mechanism of oligodynamic remains unknown. There are two major theories that try to explain this phenomenon. One theory suggests that silver nanoparticles release silver ions in a rate sufficient enough that can disrupt the DNA republication of microbes and so inhibit their growth. Another proposed mechanism believes that silver nanoparticles and ion can react with the cell walls and destroy microbes this way [71, 84–86].

33.4.3 Titanium Dioxide

Unlike copper (II) oxide, titanium dioxide kills bacteria through its photoactive power [72, 73], which will be discussed in Section 33.5. In general, metal oxides like titanium dioxide that has photocatalytic behavior can be made into nanoparticles and used in fiber modification [87–89]. Nanosizing helps them to achieve a

much faster reaction rate and a much greater contacting area. Therefore, titanium dioxide and similar metal oxides can kill bacteria effectively.

33.4.4 Conclusions and Future Trend

Nowadays, metals (particularly heavy metals) and metal oxides are a kind of important antimicrobial agent that is widely applied in textile modification. In order to make them work more effectively, in most cases, metals and metal oxides are made into nanoparticles while being used in fiber treatment. Metal oxides like titanium dioxide kill bacteria through photocatalysis, and heavy metals achieve similar result through oligodynamic effect. Since the mechanism of oligodynamic effect is yet not fully understood, a theoretical conclusion stating that metals will not promote resistance cannot be drawn. In general, through the observations in practice, silver nanoparticles are still the most effective and safe broad-spectrum antibacterial agent. However, just as other nanoparticles, nanoparticles of metals and metal oxides such as silver can penetrate human body and might cause damages inside [89–92]. Debate still goes on whether it is truly safe to use silver nanoparticles so widely in commercial products, yet silver nanoparticles are one of the most popular agents for industrial production.

33.5 Photoactive Chemical Modified Fabrics

As it was continuously brought up during this section, microbe infections have caused millions of death. Modified textiles and their products are a good way to control diseases caused by infections and are widely used in environments that require straight hygiene. Antimicrobial fibers usually gain their disinfection power through treatments with antimicrobial agents. A quick review: so far, three kinds of antimicrobial agents have been discussed in Sections 33.2, 33.3 and 33.4, which are QACs, *N*-halamine compounds, and metal (or metal oxide) nanoparticles. This section will cover one more category of agents that have biocidal effect: photoactive chemicals.

33.5.1 LAAAs and Photoinduced Biocidal Effect

LAAA refers to light-activated antimicrobial agent. LAAAs gain their antimicrobial power with the energy of light, so they are all photoactive. Photoactive chemicals can be organic or inorganic. Inorganic compounds, such as titanium dioxide (TiO_2, which was briefly mentioned in Section 33.4.3), and tin dioxide (SnO_2), are photocatalysts [93, 94]. Photocatalysts can speed up photoreaction under presence of light (both visible and invisible). For example, TiO_2 shows extraordinary photochemical activity under UV light.

In general, scientists believe that LAAAs kill cells of pathogenic microorganisms by the reactive oxygen species (ROS) they generate under illumination of light [95]. The mechanism of photoinduced disinfection of inorganic photoactive chemicals is still not yet fully understood. However, it is commonly believed

that the ROS generated will react with the cell membranes and break them apart. The deconstruction of cell membranes will lead to loss of vital substances from the inside of the cells and also allow more ROS to get into the cells and attack on more important functional structures. The damages on vital cell structures cause important cell functions and activities to stop and eventually kill the bacteria [96, 97]. Organic LAAAs are mostly strong oxidizing agents. Just like inorganic LAAAs, they produce huge amount of ROS upon shining on light. These ROS then oxidize microbes' cells and inactivate them.

33.5.2 Textile Modification with TiO_2

The photocatalytic nature of TiO_2 was first discovered and published by Prof. Fujishima in 1972 [98]. Many researches have been done on studying and applying its photochemical activity. When it comes to textile modification, TiO_2 has been successfully bound to several kinds of fibers [99–103]. Just like other metal oxides, in order to achieve a better performance, TiO_2 is turned into nanoparticles while being added onto the fibers.

The conventional method was pad-dry-cure [104]. However, since TiO_2 is inorganic yet fiber polymers are organic, the bonds formed between the inorganic and organic are quite weak. This leads to poor durability after washing. To improve the washing resistance of modified textile with TiO_2, lots of studies have been done on inventing a better modification process.

One of the newly discovered methods to immobilize TiO_2 nanoparticles onto textile surfaces is through sol–gel process [103]. Starting with a TiO_2 precursor, at the end of the sol–gel process, a gel, which is a three-dimensional porous structure, will form on the surface of the textile. Drying the gel to eliminate the liquid stored in the pores will leave nanosized TiO_2 particles on the surface that are more strongly bound compared with the conventional pad-dry-cure method.

Pretreating the fabrics with a cross-linker is another way to largely increase the durability of fabrics treated with TiO_2 nanoparticles. Among all possible cross-linkers, the ones with carboxylic acid groups are tested to be the best, because of the covalent bonds and hydrogen bonds that can be formed between TiO_2 nanoparticles and carboxylic acid groups [104–107].

Due to its relatively large bandgap, TiO_2 can only work under UV light. However, UV light does not always present in a sufficient amount. For example, glass can absorbed considerable amount of UV light, so the level of UV radiation is relatively low indoor. Therefore, efforts have also been put in to make TiO_2 nanoparticles work under visible light. Doping is a solution to this problem as the impurity prevents the light-generated active electrons and positive holes from joining together to form stable TiO_2 nanoparticles again [88].

33.5.3 Organic Photoactive Reagents

Most oxidative organic chemicals are more or less having biocidal effect. This section will introduce two major kinds: chemicals that generate ROS through type I photochemical reaction and chemicals that generate oxygen and ROS though type II photochemical reaction.

Anthraquinone and benzophenone derivatives are two representative species that gain biocidal ability through type I photochemical reaction under UV light [108–113]. The ROS production rate of a derivative depends on the structure of the anthraquinone or benzophenone derivative and the available functional groups on the substrate. In general, derivatives with electron-withdrawing groups produce ROS at a higher efficiency. Substrates with good hydrogen-donating ability also help the derivatives to have a better ROS yield. Some benzophenone derivatives are also precursors of perfumes and dyes [112, 113]. Therefore, in addition to produce antimicrobial textiles, they can be used to add color to the processed textiles to make the finished products even more marketable.

Porphyrins and phthalocyanines, on the other hand, generate oxygen and ROS under visible light (with wavelength in the range of 400–800 nm depending on the structure of the particular derivate) via type II photochemical reaction [114–118]. The porphyrin and phthalocyanine derivatives can be excited by visible light at the desired wavelength and then react with oxygen present in the surroundings to generate ground state oxygen and ROS.

ROS has relatively short half-lives. Therefore, even though they are effective in terms of killing Gram-positive bacteria, they show very weak power in inactivating Gram-negative bacteria [115, 116]. The thicker outer cell membrane structure of Gram bacteria prevents ROS from getting into the cell and destroying the vital cell organelles.

33.5.4 Conclusions and Future Trend

This section discussed both inorganic and organic photoactive chemicals that can be used in antimicrobial fiber modification. Since the modified fibers gain their biocidal ability through illumination of light, in general, most photoactive antimicrobial textiles are recyclable and rechargeable. This characteristic of photoactive antimicrobial textiles also raises concerns on their durability.

Semiconductor agents such as TiO_2 have shown poor results after washing, because of the weak bonds formed between the inorganic doping materials and the organic substrates. However, stability is also a problem to organic agents, even though they can form stronger covalent bonds with the textile surface. As photosensitive species, illumination of light will alter the structure of the critical functional groups and eventually cause these agents to lose their bacterial-inactivating ability [115, 119].

Besides stability toward wearing, washing, and light, safety is another issue that is driving scientists and researchers to invest more time and effort on photoactive antimicrobial agents. For inorganic chemicals, nanotechnology is widely applied to increase the efficiency of biocidal performance. However, there is an ongoing debate if nanoparticles are safe to be in contact with the human body directly [120, 121]. There are similar concerns on ROS, which are the major bacterial killing species in LAAA mechanism. It is worried that the bacterial inactivation mechanism is not selective in that those nanoparticles or ROS would not only destroy pathogens but also may attack human cells when they get contact with the cells. There should be more researches studying the actual effects of using photoactive chemical modified textiles on human bodies.

In conclusion, photoactive sensitizers are effective broad-spectrum antimicrobials. Depending on the particular chemical, it can get excited and gain the biocidal effect at a wavelength in the range from visible to UV. Since the bacteria are inactivated by oxidization, photoactive chemicals that can be used in textile modification generally do not promote resistance.

33.6 Natural Antimicrobial Polymers

Sections 33.2, 33.3 and 33.4 cover major antimicrobial agents that can be used to treat fibers to give them disinfection abilities. However, not only synthesized chemicals can inhibit the growth of microorganisms, but also nature-generated chemicals have excellent biocidal effect for animals to use as well. Ancient Egyptians, Ancient Indians, and Chinese started to use herbs to treat diseases and prevent infections thousands of years ago [122–124].

Nature materials tend to have good biocompatibility and low toxicity. Because of these unique properties compared with other synthesized polymers, nature textiles have big advantages in medical practice. They are frequently made into hygiene products and implantable products. This section will focus on natural antimicrobial polymers and discuss their structures, applications, and drawbacks.

33.6.1 Hyaluronic Acid

Hyaluronic acid (HA), which is also known as hyaluronan, is a conjugate base of hyaluronate. HA is a unique glycosaminoglycan for its nonsulfated structure [125, 126]. Figure 33.5 is an illustration of the skeletal formula for HA. Unlike many other glycosaminoglycans, HA is produced in the plasma membrane rather than in the Golgi apparatus. HA is a naturally produced large molecule in which its molecular weight can reach millions. HA is one of the crucial components of the extracellular matrix and can be found in many parts of a body, such as neural and epithelial tissues. In fact, HA was first discovered and isolated from cows' eyes [127].

Due to its excellent biocompatibility, HA is widely used to aid wound healing and repairing. Since HA is vital for cell immigration, it is also seen as an important indicator of tumor development. HA fabrics would be an ideal material for tissue engineering since it is very common in living organs and tissues [128, 129]. However, the fast turnover speed of HA makes it harder to use HA fabrics as a stable constructive material. This situation can be improved by cross-linking

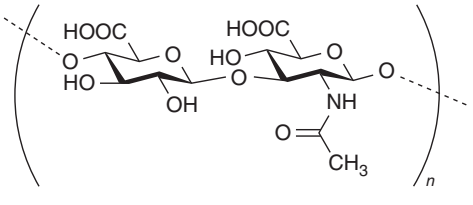


Figure 33.5 Skeletal formula of hyaluronic acid. In each monomer unit, on the left structure is D-glucuronic acid, and on the right is *N*-acetyl glucosamine. They are linked together by alternating β-(1→4) and β-(1→3) glycosidic bonds.

HA fibers and modified HA fibers with other polymers or hydrogels [127–129]. Some successfully commercial examples include Perlane (R), Hylaform (R), and Restylane (R).

33.6.2 Gelatin

Gelatin is a derivative of collagen, which is an abundant protein in mammals that can be found in the extracellular space in many connective tissues [130]. Gelatin can be derived under both acidic and alkaline conditions. Acidic hydrolysis gives gelatin type A, which is positively charged. Basic hydrolysis gives gelatin type B, which is negatively charged [131]. Under specific conditions, the final gelatin product can be transparent. Due to its abundance, gelatin is also very cost-efficient. It also has good biocompatibility and solubility in water. Research shows gelatin can promote cell growth as well [131, 132]. Therefore, gelatin is widely used in medical and cosmetic products. It is also commonly used as gelling agent in food production since gelatin is nontoxic and safe for human intake. Just as HA, gelatin and modified gelatin are one of the most popular materials for tissue engineering and drug delivery research [131, 133].

33.6.3 Alginate

Alginate, which is also called alginic acid or algain, is a natural polysaccharide. (1→4)-Linked β-D-mannuronate and (1→4)-linked α-L-guluronate linked together covalently to form Alginate [134]. Figure 33.6 shows the structure of (1→4)-linked β-D-mannuronate, and Figure 33.7 shows the structure of (1→4)-linked α-L-guluronate. Figure 33.8 is a diagram showing the alginate polymer. Alginates are mostly extracted from brown seaweeds. Alginate refined from different species of brown seaweeds would have small derivatives in their structures [135]. However, those minor differences between alginates do not alter the properties of alginate in general.

Alginate has extraordinary ability of absorbing water [134]. Therefore, it is commonly used in dehydrating process. Alginate is also a gelling agent and is applied in medication for wound healing [134, 136–138]. It can form a gel covering the wound to prevent further infection and keep moisture at a level that is perfect for the damaged tissue to regenerate itself.

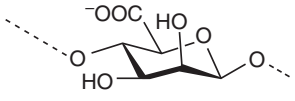


Figure 33.6 Chemical structure of (1→4)-linked β-D-mannuronate.

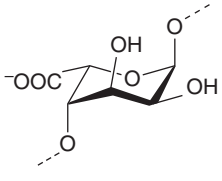


Figure 33.7 Chemical structure of (1→4)-linked α-L-guluronate.

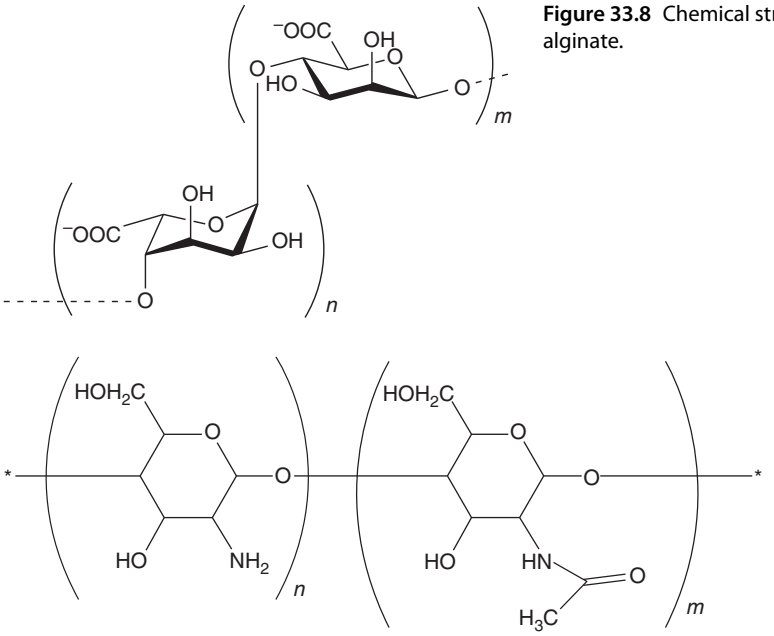


Figure 33.8 Chemical structure of alginate.

Figure 33.9 Chemical structure of chitosan, which is a copolymer consisting of β-(1→4)-linked 2-acetamido-2-deoxy-D-glucopyranose (shown on the left) and 2-amino-2-deoxy-D-glucopyranose (shown on the right).

33.6.4 Chitosan

Chitosan is a linear nature copolymer that is composed of β-(1→4)-linked 2-acetamido-2-deoxy-D-glucopyranose and 2-amino-2-deoxy-D-glucopyranose, as shown in Figure 33.9 [139]. Chitosan is a derivative of chitin, which is an abundant component in exoskeletons of crustaceans and insects [140]. In industry, chitin is produced from the seafood waste, where the shells of shrimps, crabs, and other marine exoskeletons are processed to get refined chitin. Deacetylation of chitin gives chitosan. This change in the structure of this natural copolymer also makes it more soluble in water, which makes the further processing and modification easier [139].

Similar to other natural polymers, chitosan has good biocompatibility and bioadhesivity. It is also believed to be nontoxic and biodegradable. Combined with its biocidal ability, chitosan has applications in variety of fields, such as medication, food additives, cosmetics, and bioengineering. In addition, due to its structure and available functional groups, chitosan can be processed to take different forms, including hydrogels, fibers, aerogels, thin films, powders, micro- or nanoparticles, and composite [141–144].

The antimicrobial effect of chitosan is highly related to its primary amine groups, which is formed during the deacetylation. Therefore, the acetylation process can affect the antimicrobial ability of chitosan. Its bacterial killing mechanism is based on electrostatic. The primary amine group is electron donating and easily picks up a positive charge [140]. Positively charged amines

interact with cell membranes of microbes, which have negative charges, and damage the structures of cells, which can eventually disrupt the DNA replication and other vital functions of the microbe cells and deactivate them.

33.6.5 Conclusions and Future Trend

Natural antimicrobial polymers, just like many other inorganic or organic synthesized antimicrobial agents, show effective biocidal power. Many natural antimicrobials are broad-spectrum bacterial killing agents that work for both Gram-positive and Gram-negative bacteria and fungi. Moreover, until now, it has not yet been reported that any natural microbial has promoted microbial resistance.

Compared with other synthesized antimicrobial agents, the natural agents have a huge advantage that they are biodegradable and have good biocompatibility. This unique characteristic of natural antimicrobial polymers grants them applications in biomaterial and tissue engineering field. Materials like alginate and HA have been proved that they help wounds to heal. Polymers such as chitosan and gelatin have wide usage in drug delivery.

As natural polymers, they present in abundance in living creatures. Therefore, many researchers are studying the method to effectively extract and purify them from plant or animal tissues. Since they can be made into fibers themselves, modifying those natural antimicrobial textiles with other antimicrobial agents is another direction that has great potential and has drawn many attentions.

33.7 Conclusions

Pathogens, a treat to public health and the safety of many other human activities, need to be properly controlled especially in an era when the global population is greater than ever before. Antimicrobial textiles are a good way to deactivate pathogenic bacteria and fungi, because they can be easily made into applications, such as clothes, filters, covering materials, and gaze, which protect people from infections in daily lives.

There are many kinds of antimicrobial agents that can be used in fiber modification to grant fibers biocidal effects. This chapter mainly discussed five kinds of them: quaternary ammonium salts (QACs), *N*-halamine compounds, metals, photoactive chemicals, and natural polymers. Table 33.1 is a summary comparing the biocidal performances of some agents.

Each of these antimicrobial agents has their own advantages. QACs can also soften the fabrics to make them more comfortable to wear. *N*-Halamine compounds can be recharged. Silver nanoparticles have the best bacterial killing effectiveness of all kinds. Photoactive chemicals gain energy from sunlight (300–700 nm), which make the products greener. Natural antimicrobials have applications in tissue engineering and wound healing for their good biocompatibility.

In general, there is not a single antimicrobial agent that is better than everything else in all the aspects. Therefore, an important trend of this industry is

Table 33.1 Comparison among some common antimicrobial agents.

Agents	Effectiveness[a] against			Microbial resistance	Toxicity[b]
	Gram-positive bacteria	Gram-negative bacteria	Fungi		
Quaternary ammonium compounds	+	−	−	Yes	3
N-Halamine	+	+	+	Not reported	1
Silver	+++	+++	+++	Not reported	1
Copper	+	+	+	Yes	2
Chitosan	+	+	+	Not reported	1, b

a) For the biocidal effectiveness evaluation: + means the chemical shows the ability to deactivate the particular kind of microorganisms; − means the chemical does not show the ability to deactivate the particular kind of microorganisms; +++ means the chemical shows outstanding microbial effect at extremely low concentration.

b) For toxicity ranking: 1 means the chemical is lightly toxic or nontoxic, safe for human during regular uses; 2 means the chemical could be toxic if it is used in large amount; 3 means the chemical is toxic and can cause damage to human body and the environment; b means the chemical is biodegradable and biocompatible.

to combine those agents together, along with other novel technology, such as nanotechnology, to further develop antimicrobial fibers with better performance. In the meanwhile, innovation of safer materials that cause less damage to both the environment and the users is another hot direction that much work has been done.

References

1 Sender, R., Fuchs, S., and Milo, R. (2016). Revised estimates for the number of human and bacteria cells in the body. *PLoS Biology* 14 (8): 1–14.

2 Hardin, I.R. and Kim, Y. (2016). Nanotechnology for antimicrobial textiles. In: *Antimicrobial Textiles* (ed. G. Sun), pp. 87–97. Wiley.

3 Sun, Y.Y. and Sun, G. (2001). Novel regenerable N-halamine polymeric biocides. III. Grafting hydantoin-containing monomers onto synthetic fabrics. *Journal of Applied Polymer Science* 81 (6): 1517–1525.

4 Sun, Y. and Sun, G. (2002). Durable and regenerable antimicrobial textile materials prepared by a continuous grafting process. *Journal of Applied Polymer Science* 84 (8): 1592–1599.

5 Son, Y.A. and Sun, G. (2003). Durable antimicrobial nylon 66 fabrics: ionic interactions with quaternary ammonium salts. *Journal of Applied Polymer Science* 90 (8): 2194–2199.

6 Yao, C., Li, X., Neoh, K.G. et al. (2008). Surface modification and antibacterial activity of electrospun polyurethane fibrous membranes with quaternary ammonium moieties. *Journal of Membrane Science* 320 (1–2): 259–267.

7 Mercs, L. and Albrecht, M. (2010). Beyond catalysis: N-heterocyclic carbene complexes as components for medicinal, luminescent, and functional materials applications. *Chemical Society Reviews* 39 (6): 1903–1912.

8 Evans, P. and Sheel, D.W. (2007). Photoactive and antibacterial TiO_2 thin films on stainless steel. *Surface and Coatings Technology* 201 (22–23): 9319–9324.

9 Pant, H.R., Pandeya, D.R., Nam, K.T. et al. (2011). Photocatalytic and antibacterial properties of a TiO_2/nylon-6 electrospun nanocomposite mat containing silver nanoparticles. *Journal of Hazardous Materials* 189 (1–2): 465–471.

10 Rabea, E.I., Badawy, M.E.T., Stevens, C.V. et al. (2003). Chitosan as antimicrobial agent: applications and mode of action. *Biomacromolecules* 4 (6): 1457–1465.

11 Pillai, C.K.S., Paul, W., and Sharma, C.P. (2009). Chitin and chitosan polymers: chemistry, solubility and fiber formation. *Progress in Polymer Science* 34 (7): 641–678.

12 Sharma, V.K., Yngard, R.A., and Lin, Y. (2009). Silver nanoparticles: green synthesis and their antimicrobial activities. *Advances in Colloid and Interface Science* 145 (1–2): 83–96.

13 Melaiye, A., Sun, Z.H., Hindi, K. et al. (2005). Silver(I)-imidazole cyclophane gem-diol complexes encapsulated by electrospun tecophilic nanofibers: formation of nanosilver particles and antimicrobial activity. *Journal of the American Chemical Society* 127 (7): 2285–2291.

14 Duran, N., Marcato, P.D., De Souza, G.I.H. et al. (2007). Antibacterial effect of silver nanoparticles produced by fungal process on textile fabrics and their effluent treatment. *Journal of Biomedical Nanotechnology* 3 (2): 203–208.

15 Cleveland, J., Montville, T.J., Nes, I.F., and Chikindas, M.L. (2001). Bacteriocins: safe, natural antimicrobials for food preservation. *International Journal of Food Microbiology* 71 (1): 1–20.

16 Saleem, M., Nazir, M., Ali, M.S. et al. (2010). Antimicrobial natural products: an update on future antibiotic drug candidates. *Natural Product Reports* 27 (2): 238–254.

17 Singh, R., Jain, A., Panwar, S. et al. (2005). Antimicrobial activity of some natural dyes. *Dyes and Pigments* 66 (2): 99–102.

18 Sisson, W.A. and Saner, W.R. (1939). An X-ray diffraction study of the swelling action of several quaternary ammonium hydroxides on cellulose fibers. *Journal of Physical Chemistry* 43 (6): 687–699.

19 Reck, R.A. and Harwood, H.J. (1953). Antimicrobial activity of quaternary ammonium chlorides – derived from commercial fatty acids. *Industrial and Engineering Chemistry* 45 (5): 1022–1026.

20 Weiner, N.D. and Zografi, G. (1965). Interfacial properties of antimicrobial long-chain quaternary ammonium salts. I. Soluble films at air-water interface. *Journal of Pharmaceutical Sciences* 54 (3): 436–442.

21 Hegstad, K., Langsrud, S., Lunestad, B.T. et al. (2010). Does the wide use of quaternary ammonium compounds enhance the selection and spread

of antimicrobial resistance and thus threaten our health? *Microbial Drug Resistance* 16 (2): 91–104.

22 Buffet-Bataillon, S., Tattevin, P., Bonnaure-Mallet, M., and Jolivet-Gougeon, A. (2012). Emergence of resistance to antibacterial agents: the role of quaternary ammonium compounds–a critical review. *International Journal of Antimicrobial Agents* 39 (5): 381–389.

23 Lu, G., Wu, D., and Fu, R. (2007). Studies on the synthesis and antibacterial activities of polymeric quaternary ammonium salts from dimethylaminoethyl methacrylate. *Reactive and Functional Polymers* 67 (4): 355–366.

24 Chen, C.Z.S., Beck-Tan, N.C., Dhurjati, P. et al. (2000). Quaternary ammonium functionalized poly(propylene imine) dendrimers as effective antimicrobials: structure-activity studies. *Biomacrobolecules* 1 (3): 473–480.

25 Tezel, U. and Pavlostathis, S.G. (2015). Quaternary ammonium disinfectants: microbial adaptation, degradation and ecology. *Current Opinion in Biotechnology* 33: 296–304.

26 Zhang, C., Cui, F., Zeng, G.-M. et al. (2015). Quaternary ammonium compounds (QACs): a review on occurrence, fate and toxicity in the environment. *Science of the Total Environment* 518–519: 352–362.

27 Heir, E., Sundheim, G., and Holck, A.L. (1999). Identification and characterization of quaternary ammonium compound resistant staphylococci from the food industry. *International Journal of Food Microbiology* 48 (3): 211–219.

28 Ioannou, C.J., Hanlon, G.W., and Denyer, S.P. (2007). Action of disinfectant quaternary ammonium compounds against *Staphylococcus aureus*. *Antimicrobial Agents and Chemotherapy* 51 (1): 296–306.

29 Harrison, J.J., Turner, R.J., Joo, D.A. et al. (2008). Copper and quaternary ammonium cations exert synergistic bactericidal and antibiofilm activity against *Pseudomonas aeruginosa*. *Antimicrobial Agents and Chemotherapy* 52 (8): 2870–2881.

30 Antonucci, J.M., Zeiger, D.N., Tang, K. et al. (2011). Synthesis and characterization of dimethacrylates containing quaternary ammonium functionalities for dental applications. *Dental Materials* 28 (2): 219–228.

31 Tseng, C.-C., Pan, Z.-M., and Chang, C.-H. (2016). Application of a quaternary ammonium agent on surgical face masks before use for predecontamination of nosocomial infection-related bioaerosols. *Aerosol Science and Technology* 50 (3): 199–210.

32 Games, L.M., King, J.E., and Larson, R.J. (1982). Fate and distribution of a quaternary ammonium surfactant, octadecyltrimethyammonium chloride (OTAC) in wasterwater-treatment. *Environmental Science and Technology* 16 (8): 483–488.

33 Tezel, U., Tandukar, M., Martinez, R.J. et al. (2012). Aerobic biotransformation of *n*-tetradecylbenzyldimethylammonium chloride by an enriched *Pseudomonas* spp. Community. *Environmental Science and Technology* 46 (16): 8714–8722.

34 Tabata, A., Nagamune, H., Maeda, T. et al. (2003). Correlation between resistance of *Pseudomonas aeruginosa* to quaternary ammonium compounds and expression of outer membrane protein OprR. *Antimicrobial Agents and Chemotherapy* 47 (7): 2093–2099.

35 Bore, E., Hebraud, M., Chafsey, I. et al. (2007). Adapted tolerance to benzalkonium chloride in *Escherichia coli* K-12 studied by transcriptome and proteome analyses. *Microbiology-SGM* 153: 935–946.

36 Karatzas, K.A.G., Randall, L.P., Webber, M. et al. (2008). Phenotypic and proteomic characterization of multiply antibiotic-resistant variants of *Salmonella entetica* serovar typhimurium selected following exposure to disinfectants. *Applied and Environmental Microbiology* 74 (5): 1508–1516.

37 Bjorland, J., Steinum, T., Sunde, M. et al. (2003). Novel plasmid-borne gene qacJ mediates resistance to quaternary ammonium compounds in equine *Staphylococcus aureus*, *Staphylococcus simulans*, and *Staphylococcus intermedius*. *Antimicrobial Agents and Chemotherapy* 47 (10): 3036–3052.

38 Gillings, M.R., Duan, X.J., Hardwick, S.A. et al. (2008). Gene cassettes encoding resistance to quaternary ammonium compounds: a role in the origin of clinical class 1 integrons? *ISME Journal* 3 (2): 209–215.

39 Littlejohn, T.G., Paulsen, I.T., Gillespie, M.T. et al. (1992). Substrate-specificity and energetics of antiseptic and disinfectant resistance in *Staphylococus aureus*. *FEMS Microbiology Letters* 95 (2–3): 259–266.

40 McMurry, L.M., Oethinger, M., and Levy, S.B. (1998). Overexpression of marA, soxS, or acrAB produces resistance to triclosan in laboratory and clinical strains of *Escherichia coli*. *FEMS Microbiology Letters* 166 (2): 305–309.

41 Pages, J.-M., Amaral, L., and Fanning, S. (2011). An original deal for new molecule: reversal of efflux pump activity, a rational strategy to combat gram-negative resistant bacteria. *Current Medicinal Chemistry* 18 (19): 2969–2980.

42 Worley, S.D., Williams, D.E., and Barnela, S.B. (1987). The stabilities of new N-halamine water disinfectants. *Water Research* 21 (8): 983–988.

43 Barnela, S.B., Worley, S.D., and Williams, D.E. (1987). Syntheses and antibacterial activity of new N-halamine compounds. *Journal of Pharmaceutical Sciences* 76 (3): 245–247.

44 Worley, S.D. and Williams, D.E. (1988). Disinfecting water with a mixture of free chlorine and an organic N-halamine. *Journal American Water Works Association* 80 (1): 69–71.

45 Tsao, T., Worley, S.D., and Williams, D.E. (1990). New N-halamine water disinfectants. *Abstracts of Papers of the American Chemical Society 199, 28-BIOT*.

46 Eknoian, M.W., Worley, S.D., Bickert, J., and Williams, J.F. (1999). Novel antimicrobial N-halamine polymer coatings generated by emulsion polymerization. *Polymer* 40: 1367–1371.

47 Sun, Y. and Sun, G. (2001). Novel regenerable N-halamine polymeric biocides. II. Grafting hydantoin-containing monomers onto cotton cellulose. *Journal of Applied Polymer Science* 81: 617–624.

48 Lin, J., Winkelmann, C., Worley, S.D. et al. (2002). Biocidal polyester. *Journal of Applied Polymer Science* 85: 177–182.

49 Si, Y., Cossu, A., Nitin, N. et al. (2017). Mechanically robust and transparent N-halamine grafted PVA-co-PE films with renewable antimicrobial activity. *Macromolecular Bioscience* 17: 1600304.

50 Kenawy, E.-R., Worley, S.D., and Broughton, R. (2007). The chemistry and applications of antimicrobial polymers: a state-of-the-art review. *Biomacromolecules* 8 (5): 1359–1384.

51 Ren, X.H., Kocer, H.B., Worley, S.D. et al. (2009). Rechargeable biocidal cellulose: synthesis and application of 3-(2,3-dihydroxypropyl)-5,5-dimethylimidazolidine-2,4-dione. *Carbohydrate Polymers* 75 (4): 683–687.

52 Sun, Y. and Sun, G. (2001). Durable and refreshable polymeric N-halamine biocides containing 3-(4′-vinylbenzyl)-5,5-dimethylhydantoin. *Journal of Polymer Science Part A: Polymer Chemistry* 39: 3348–3355.

53 Liang, J., Wu, R., Wang, J.W. et al. (2007). N-halamine biocidal coatings. *Journal of Industrial Microbiology and Biotechnology* 34 (2): 157–163.

54 Lee, J., Broughton, R.M., Akdag, A. et al. (2007). Antimicrobial fibers created via polycarboxylic acid durable press finishing. *Textile Research Journal* 77 (8): 604–611.

55 Ren, X.H., Akdag, A., Zhu, C. et al. (2009). Electrospun polyacrylonitrile nanofibrous biomaterials. *Journal of Biomedical Materials Research Part A* 91A: 385–390.

56 Cerkez, I., Kocer, H.B., Worley, S. et al. (2012). Multifunctional cotton fabric: antimicrobial and durable press. *Journal of Applied Polymer Science* 124: 4230–4238.

57 Li, R., Dou, J., Jiang, Q. et al. (2014). Preparation and antimicrobial activity of beta-cyclodextrin derivative copolymers/cellulose acetate nanofibers. *Chemical Engineering Journal* 248: 264–272.

58 Li, R., Sun, M., Jiang, Z. et al. (2014). N-Halamine-bonded cotton fabric with antimicrobial and easy-care properties. *Fibers and Polymers* 15: 234–240.

59 Liu, S. and Sun, G. (2006). Durable and regenerable biocidal polymers: acyclic N-halamine cotton cellulose. *Industrial and Engineering Chemistry Research* 45: 6477–6482.

60 Liu, S. and Sun, G. (2008). New refreshable N-halamine polymeric biocides: N-chlorination of acyclic amide grafted cellulose. *Industrial and Engineering Chemistry Research* 48: 613–618.

61 Luo, J. and Sun, Y. (2008). Acyclic N-halamine coated Kevlar fabric materials: preparation and biocidal functions. *Industrial and Engineering Chemistry Research* 47: 5291–5297.

62 Ren, X., Kou, L., Kocer, H.B. et al. (2008). Antimicrobial coating of an N-halamine biocidal monomer on cotton fibers via admicellar polymerization. *Colloids and Surfaces A: Physicochemical and Engineering Aspects* 317: 711–716.

63 Jiang, J., Chen, Y., Ren, X. et al. (2007). Fabric treated with antimicrobial N-halamine epoxides. *Industrial and Engineering Chemistry Research* 46: 6425–6429.

64 Ma, K., Liu, Y., Xie, Z. et al. (2013). Synthesis of novel N-halamine epoxide based on cyanuric acid and its application for antimicrobial finishing. *Industrial and Engineering Chemistry Research* 52 (22): 7413–7418.

65 Ma, K., Jiang, Z., Li, L. et al. (2014). N-halamine modified polyester fabrics: preparation and biocidal functions. *Fibers and Polymers* 15: 2340–2344.

66 Fong, H., Chun, L., and Reneker, D. (1999). Beaded nanofibers formed during electrospinning. *Polymer* 40: 4585–4592.

67 Greiner, A. and Wendorff, J.H. (2007). Electrospinning: a fascinating method for the preparation of ultrathin fibers. *Angewandte Chemie International Edition* 46: 5670–5703.

68 Si, Y., Li, J., Zhao, C. et al. (2017). Biocidal and rechargeable N-halamine nanofibrous membranes for highly efficient water disinfection. *ACS Biomaterials Science & Engineering* 3 (5): 854–862.

69 MacNaught, A.D. and Wilkinson, A.R. (eds.) (1997). *Compendium of Chemical Terminology: IUPAC Recommendations*, 2e. Blackwell Science.

70 Alemán, J., Chadwick, A.V., He, J. et al. (2007). Definitions of terms relating to the structure and processing of sols, gels, networks, and inorganic-organic hybrid materials (IUPAC Recommendations 2007). *Pure and Applied Chemistry* 79 (10): 1801.

71 Kim, J.S., Kuk, E., Yu, K.N. et al. (2007). Antimicrobial effects of silver nanoparticles. *Nanomedicine: Nanotechnology, Biology and Medicine* 3: 95–101.

72 Heinlaan, M., Ivask, A., Blinova, I. et al. (2008). Toxicity of nanosized and bulk ZnO, CuO and TiO_2 to bacteria *Vibrio fischeri* and crustaceans *Daphnia magna* and *Thamnocephalusplatyurus*. *Chemosphere* 71: 1308–1316.

73 Aruoja, V., Dubourguier, H.-C., Kasemets, K., and Kahru, A. (2009). Toxicity of nanoparticles of CuO, ZnO and TiO_2 to microalgae *Pseudokirchneriella subcapitata*. *Science of the Total Environment* 407: 1461–1468.

74 Wang, R., Xin, J.H., Tao, X.M., and Daoud, W.A. (2004). ZnO nanorods grown on cotton fabrics at low temperature. *Chemical Physics Letters* 398: 250–255.

75 Yadav, A., Prasad, V., Kathe, A.A. et al. (2006). Functional finishing in cotton fabrics using zinc oxide nanoparticles. *Bulletin of Materials Science* 29: 641–645.

76 Marambio-Jones, C. and Hoek, E.M.V. (2010). A review of the antibacterial action of silver nanoparticles. *Journal of Proteome Research* 5: 916–924.

77 Tortora, G.J., Funke, B.R., and Case, C.L. (2004). *Microbiology An Introduction*, 10e. San Francisco, CA: Pearson Benjamin Cummings.

78 Cowan, M.M., Abshire, K.Z., Houk, S.L., and Evans, S.M. (2003). Antimicrobial efficacy of a silver-zeolite matrix coating on stainless steel. *Journal of Industrial Microbiology and Biotechnology* 30: 102–106.

79 Pillai, Z.S. and Kamat, P.V. (2004). What factors control the size and shape of silver nanoparticles in the citrate ion reduction method? *The Journal of Physical Chemistry B* 110: 16248–16253.

80 Gulrajani, M.L., Gupta, D., Periyasamy, S., and Muthu, S.G. (2008). Preparation and application of silver nanoparticles on silk for imparting antimicrobial properties. *Journal of Applied Polymer Science* 108: 614–623.

81 Nägeli, K.W. (1893). Übero ligodynamische Erscheinungen in lebenden Zellen. *Neue Denkschriften der allgemeinen Schweizerischen Gesellschaft für die gesamte Naturwissenschaft*, XXXIII (1).

82 Bauman, R.W. (2012). *Microbiology with Diseases by Body System*, 3e. Benjamin Cummings.

83 Cowan, M.K. (2012). *Microbiology: A Systems Approach*, 3e. Pearson Education, Inc.

84 Choi, O., Deng, K.K., Kim, N.-J. et al. (2008). The inhibitory effects of silver nanoparticles, silver ions, and silver chloride colloids on microbial growth. *Water Research* 42: 3066–3074.

85 Smetana, A.B., Klabunde, K.J., Marchin, G.R., and Sorensen, C.M. (2008). Biocidal activity of nanocrystalline silver powders and partcles. *Langmuir* 24: 7457–7464.

86 Hwang, E.T., Lee, J.H., Chae, Y.J. et al. (2008). Analysis of the toxic mode of action of silver nanoparticles using stress-specific bioluminescent bacteria. *Small* 4: 746–750.

87 Armelao, L., Barreca, D., Bottaro, G. et al. (2007). Photocatalytic and antibacterial activity of TiO_2 and Au/TiO_2 nanosystems. *Nanotechnology* 18 (37): 1–7.

88 Li, Q., Xie, R.C., Ll, Y.W. et al. (2007). Enhanced visible-light-induced photocatalytic disinfection of *E-coli* by carbon-sensitized nitrogen-doped titanium oxide. *Environmental Science and Technology* 41 (14): 5050–5056.

89 Nowack, B. and Bucheli, T.D. (2007). Occurrence, behavior and effects of nanoparticles in the environment. *Environmental Science and Technology* 45: 1177–1183.

90 Wijnhoven, S.W.P., Peijnenburg, W.J.G.M., Herberts, C.A. et al. (2009). Decreasing uncertainties in assessing environmental exposure, risk, and ecological implications of nanomaterials. *Environmental Science and Technology* 43: 6458–6462.

91 Nowack, B. (2010). Nanosilver revisited downstream. *Science* 330: 1054–1055.

92 Nowack, B., Krug, H.F., and Height, M. (2011). 120 years of nanosilver history: implications for policy makers. *Environmental Pollution* 150: 5–22.

93 Foster, H.A., Ditta, I.B., Varghese, S., and Steele, A. (2011). Photocatalytic disinfection using titanium dioxide: spectrum and mechanism of antimicrobial activity. *Applied Microbiology and Biotechnology* 90 (6): 1847–1868.

94 Gil-Tomas, J., Dekker, L., Narband, N. et al. (2011). Lethal photosensitisation of bacteria using a tin chlorin e6-glutathione-gold nanoparticle conjugate. *Journal of Materials Chemistry* 21 (12): 4189–4196.

95 Omar, G.S., Wilson, M., and Nair, S.P. (2008). Lethal photosensitization of wound-associated microbes using indocyanine green and near-infrared light. *BMC Microbiology* 8: Article Number 111.

96 Tung, W.S. and Daoud, W.A. (2011). Self-cleaning fibers via nanotechnology: a virtual reality. *Journal of Materials Chemistry* 21 (22): 7858–7869.

97 Lu, Z.X., Zhou, L., Zhang, Z.L. et al. (2003). Cell damage induced by photocatalysis of TiO_2 thin films. *Langmuir* 19 (21): 8765–8768.

98 Fujishima, A. and Honda, K. (1972). Electrochemical photolysis of water at a semiconductor electrode. *Nature* 238 (5358): 37–38.

99 Daoud, W.A., Xin, J.H., and Zhang, Y.H. (2005). Surface functionalization of cellulose fibers with titanium dioxide nanoparticles and their combined bactericidal activities. *Surface Science* 559 (1–3): 69–75.

100 Qi, K.H., Xin, J.H., Daoud, W.A., and Mak, C.L. (2007). Functionalizing polyester fiber with a self-cleaning property using anatase TiO_2 and low-temperature plasma treatment. *International Journal of Applied Ceramic Technology* 4 (6): 554–563.

101 Tung, W.S. and Daoud, W.A. (2008). Photocatalytic formulations for protein fibers: experimental analysis of the effect of preparation on compatibility and photocatalytic activities. *Journal of Colloid and Interface Science* 326 (1): 283–288.

102 Pakdel, E., Daoud, W.A., and Wang, X.G. (2013). Self-cleaning and superhydrophilic wool by TiO_2/SiO_2 nanocomposite. *Applied Surface Science* 275: 397–402.

103 Mahltig, B., Haufe, H., and Bottcher, H. (2005). Functionalisation of textiles by inorganic sol–gel coatings. *Journal of Materials Chemistry* 15 (41): 4385–4398.

104 Qi, K.H., Daoud, W.A., Xin, J.H. et al. (2006). Self-cleaning cotton. *Journal of Materials Chemistry* 16 (47): 4567–4574.

105 Bozzi, A., Yuranova, T., and Kiwi, J. (2005). Self-cleaning of wool-polyamide and polyester textiles by TiO_2-rutile modification under daylight irradiation at ambient temperature. *Journal of Photochemistry and Photobiology A: Chemistry* 172 (1): 27–34.

106 Kiwi, J. and Pulgarin, C. (2010). Innovative self-cleaning and bactericide textiles. *Catalysis Today* 151 (1–2): 2–7.

107 Yuranova, T., Mosteo, R., Bandara, J. et al. (2006). Self-cleaning cotton textiles surfaces modified by photoactive SiO_2/TiO_2 coating. *Journal of Molecular Catalysis A: Chemistry* 244 (1–2): 160–167.

108 Hong, K.H., Liu, N., and Sun, G. (2009). UV-induced graft polymerization of acrylamide on cellulose by using immobilized benzophenone as a photo-initiator. *European Polymer Journal* 45 (8): 2443–2449.

109 Hong, K.H. and Sun, G. (2007). Photocatalytic functional cotton fabrics containing benzophenone chromophoric groups. *Journal of Applied Polymer Science* 106 (4): 2661–2667.

110 Hong, K.H. and Sun, G. (2007). Preparation and properties of benzophenone chromophoric group branched polymer for self-decontamination. *Polymer Engineering and Science* 47 (11): 1750–1755.

111 Hong, K.H. and Sun, G. (2008). Poly(styrene-*co*-vinylbenzophenone) as photoactive antimicrobial and selfdecontaminating materials. *Journal of Applied Polymer Science* 109 (5): 3173–3179.

112 Zhuo, J. and Sun, G. (2013). Antimicrobial functions on cellulose materials introduced by anthraquinone vat dyes. *ACS Applied Materials & Interfaces* 5 (21): 10830–10835.

113 Zhuo, J. and Sun, G. (2014). Light-induced surface graft polymerizations initiated by an anthraquinone dye on cotton fibers. *Carbohydrate Polymers* 112: 158–164.

114 Malik, Z., Hanania, J., and Nitzan, Y. (1990). Bactericidal effects of photoactivated porphyrins – an alternative approach to antimicrobial drugs. *Journal of Photochemistry and Photobiology B: Biology* 5 (3–4): 281–293.

115 Banfi, S., Caruso, E., Buccafurni, L. et al. (2006). Antibacterial activity of tetraaryl-porphyrin photosensitizers: an in vitro study on Gram negative and Gram positive bacteria. *Journal of Photochemistry and Photobiology B: Biology* 85 (1): 28–38.

116 Lambrechts, S.A.G., Aalders, M.C.G., and Van, M.J. (2005). Mechanistic study of the photodynamic inactivation of candida albicans by a cationic porphyrin. *Antimicrobial Agents and Chemotherapy* 49 (5): 2026–2034.

117 Mantareva, V., Kussovski, V., Angelov, I. et al. (2011). Non-aggregated Ga(III)-phthalocyanines in the photodynamic inactivation of planktonic and biofilm cultures of pathogenic microorganisms. *Photochemical & Photobiological Sciences* 10 (1): 91–102.

118 Griffiths, M.A., Wren, B.W., and Wilson, M. (1997). Killing of methicillin-resistant *Staphylococcus aureus* in vitro using aluminium disulphonated phthalocyanine, a light-activated antimicrobial agent. *Journal of Antimicrobial Chemotherapy* 40 (6): 873–876.

119 Segalla, A., Borsarelli, C.D., Braslavsky, S.E. et al. (2002). Photophysical, photochemical and antibacterial photosensitizing properties of a novel octacationic Zn(II)-phthalocyanine. *Photochemistry & Photobiological Sciences* 1 (9): 641–648.

120 Geppert, M., Hohnholt, M., Gaetjen, L. et al. (2009). Accumulation of iron oxide nanoparticles by cultured brain astrocytes. *Jounral of Biomedical Nanotechnology* 5 (3): 285–293.

121 Murr, L.E. (2009). Nanoparticulate materials in antiquity: the good, the bad and the ugly. *Materials Characterization* 60 (4): 261–270.

122 Colegate, S.M. and Molyneux, R.J. (2007). *Bioactive Natural Products: Detection, Isolation, and Structural Determination*. CRC Press.

123 Aboelsoud, N.H. (2010). Herbal medicine in ancient Egypt. *Journal of Medicinal Plant Research* 4 (2): 82–96.

124 Sun, H., Zhang, A., and Wang, X. (2012). Potential role of metabolomic approaches for Chinese medicine syndromes and herbal medicine. *Phytotherapy Research* 26 (10): 1466–1471.

125 Tan, H.P., Ramirez, C.M., Miljkovic, N. et al. (2009). Thermosensitive injectable hyaluronic acid hydrogel for adipose tissue engineering. *Biomaterials* 30 (36): 6844–6853.

126 Schante, C.E., Zuber, G., Herlin, C., and Vandamme, T.F. (2011). Chemical modifications of hyaluronic acid for the synthesis of derivatives for a broad range of biomedical applications. *Carbohydrate Polymers* 85 (3): 469–489.

127 Fakhari, A. and Berkland, C. (2013). Applications and emerging trends of hyaluronic acid in tissue engineering, as a dermal filler and in osteoarthritis treatment. *Acta Biomaterialia* 9 (7): 7081–7092.

128 Burdick, J.A. and Prestwich, G.D. (2011). Hyaluronic acid hydrogels for biomedical applications. *Advanced Materials* 23 (12): H41–H56.

129 Leach, J.B., Bivens, K.A., Patrick, C.W., and Schmidt, C.E. (2003). Photocrosslinked hyaluronic acid hydrogels: natural, biodegradable tissue engineering scaffolds. *Biotechnology and Bioengineering* 82 (5): 578–589.

130 Djagny, K.B., Wang, Z., and Xu, S.Y. (2001). Gelatin: a valuable protein for food and pharmaceutical industries: review. *Critical Reviews in Food Science and Nutrition* 41 (6): 481–492.

131 Siqueira, N.M., Paiva, B., Camassola, M. et al. (2015). Gelatin and galactomannan-based scaffolds: characterization and potential for tissue engineering applications. *Carbohydrate Polymers* 133: 8–18.

132 Li, M.Y., Guo, Y., Wei, Y. et al. (2006). Electrospinning polyaniline-contained gelatin nanofibers for tissue engineering applications. *Biomaterials* 27 (13): 2705–2715.

133 Young, S., Wong, M., Tabata, Y., and Mikos, A.G. (2005). Gelatin as a delivery vehicle for the controlled release of bioactive molecules. *Journal of Controlled Release* 109 (1–3): 256–274.

134 Lee, K.Y. and Mooney, D.J. (2012). Alginate: properties and biomedical applications. *Progress in Polymer Science* 37 (1): 106–126.

135 Wong, T.Y., Preston, L.A., and Schiller, N.L. (2000). Alginate lyase: review of major sources and enzyme characteristics, structure-function analysis, biological roles, and applications. *Annual Review of Microbiology* 54: 289–340.

136 Sun, J. and Tan, H. (2013). Alginate-based biomaterials for regenerative medicine applications. *Materials* 6 (4): 1285–1309.

137 Balakrishnan, B., Mohanty, M., Umashankar, P.R., and Jayakrishnan, A. (2005). Evaluation of an in situ forming hydrogel wound dressing based on oxidized alginate and gelatin. *Biomaterials* 26 (32): 6335–6342.

138 Choi, Y.S., Hong, S.R., Lee, Y.M. et al. (1999). Study on gelatin-containing artificial skin: I. Preparation and characteristics of novel gelatin-alginate sponge. *Biomaterials* 20 (5): 409–417.

139 Dash, M., Chiellini, F., Ottenbrite, R.M., and Chiellini, E. (2011). Chitosan-A versatile semi-synthetic polymer in biomedical applications. *Progress in Polymer Science* 36 (8): 981–1014.

140 Berger, J., Reist, M., Mayer, J.M. et al. (2004). Structure and interactions in covalently and ionically crosslinked chitosan hydrogels for biomedical applications. *European Journal of Pharmaceutics and Biopharmaceutics* 57 (1): 19–34.

141 Agnihotri, S.A., Mallikarjuna, N.N., and Aminabhavi, T.M. (2004). Recent advances on chitosan-based micro- and nanoparticles in drug delivery. *Journal of Controlled Release* 100 (1): 5–28.

142 Suh, J.K.F. and Matthew, H.W.T. (2000). Application of chitosan-based polysaccharide biomaterials in cartilage tissue engineering: a review. *Biomaterials* 21 (24): 2589–2598.

143 Renault, F., Sancey, B., Badot, P.M., and Crini, G. (2009). Chitosan for coagulation/flocculation processes - an eco-friendly approach. *European Polymer Journal* 45 (5): 1337–1348.

144 Lim, S.H. and Hudson, S.M. (2003). Review of chitosan and its derivatives as antimicrobial agents and their uses as textile chemicals. *Journal of Macromolecular Science Polymer Reviews* C43 (2): 223–269.

34

Fibers for Auxetic Applications

Hong Hu and Adeel Zulifqar

The Hong Kong Polytechnic University, Institute of Textiles and Clothing, Hung Hom, Kowloon, Hong Kong, China

34.1 Introduction

Poisson's ratio (PR) is a measure of the Poisson effect, the phenomenon in which a material tends to expand in directions perpendicular to the direction of compression. Conversely, if the material is stretched rather than compressed, it usually tends to contract in the directions transverse to the direction of stretching. It is a common observation when a rubber band is stretched, it becomes noticeably thinner. The PR is denoted by ν and named after Siméon Poisson. It is the signed ratio of transverse strain to axial strain or transversal expansion to axial compression and calculated by using Eq. (34.1):

$$\nu = -\frac{\varepsilon_y}{\varepsilon_x} \tag{34.1}$$

where ε_x is the axial strain and ε_y is the transverse strain.

The PR is one of the fundamental properties of any engineering materials and represents important mechanical characteristics for many applications including in engineering systems, which incorporate textile fibers as structural elements. Mostly the traditional engineering materials (TEMs) have positive PR. In certain rare cases, a material will actually shrink in the transverse direction when compressed (or expand when stretched), which yields a negative value of the PR as shown in Figure 34.1. This occurs due to their specific core structure and the mode of their deformation when the sample is uniaxially loaded. This behavior is termed as auxeticity, and such materials are known as auxetic materials.

The term auxetic was derived from the Greek word auxetikos, which means "that which tends to increase" by K. Evans of the University of Exeter [1]. The known naturally and manmade auxetic materials include metals, silicates, zeolites, laminates, gels, composites foams, fibers, polymers, etc. These materials are incorporated as core materials to produce sandwich panels, drug release systems, and energy absorbance textiles. These materials can also be used for vibration damping and to reduce creep buckling failure. It is claimed that auxetic materials have enhanced mechanical properties like shear modulus, energy

Handbook of Fibrous Materials, First Edition. Edited by Jinlian Hu, Bipin Kumar, and Jing Lu.
© 2020 Wiley-VCH Verlag GmbH & Co. KGaA. Published 2020 by Wiley-VCH Verlag GmbH & Co. KGaA.

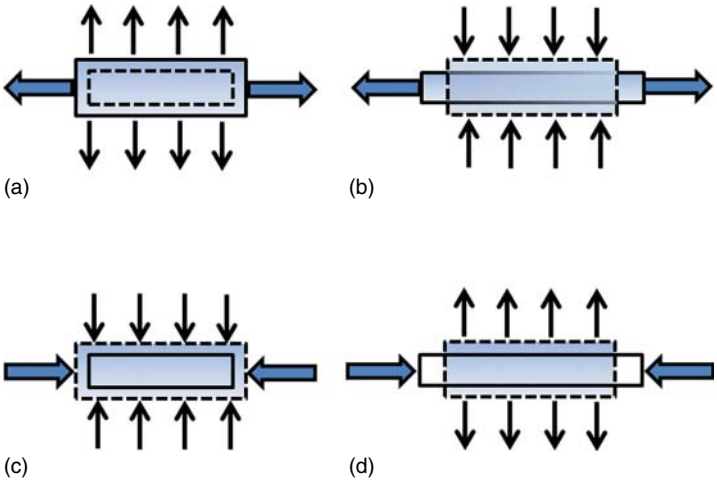


Figure 34.1 Deformation behavior of materials when stretched: (a) auxetic and (b) conventional; deformation behavior of materials when compressed: (c) auxetic and (d) conventional.

absorbance, vibration damping [1–4], sound absorption [5], indentation resistance [6], sync-elastic behavior, and better formability [7]. In recent past years the auxetic fibers have been developed and investigated by many researchers including, polymeric auxetic fibers, auxetic filaments, and moisture-sensitive auxetic fibers.

34.2 Auxetic Structures and Geometries

Auxetic materials have been known for over a hundred years but have only gained attention in recent decades. The PR is an elastic constant and is independent of the material scale. Thus auxetic materials can be single molecules or a particular structure of macroscopic to microscopic level [8–13]. Auxetic materials can be produced by modifying the macrostructure of the material. These materials possess hinge-like features, which can change shape when a force is applied. For example, when a tensile force is applied, the hinge-like structures extends, causing the material to expand in lateral direction. While on application of a compressive force, the hinge-like structure folds even further, and the material contracts in lateral direction. At the macroscale, the auxetic behavior can be exemplified with an elastic cord having an inelastic string wound around it. When a pulling force is applied, the inelastic string gets straight, while the elastic cord stretches and winds helically around it, and the volume of the structure is increased. Auxetic materials usually have open cell structure and have a relatively low density. It is the open cell structure that can be modified to give the desired properties.

Auxetic materials can be made based on two different approaches: firstly, the top-down approach, which involves the manipulation of everyday polymers to give the desired structure and properties, and secondly, the bottom-up approach,

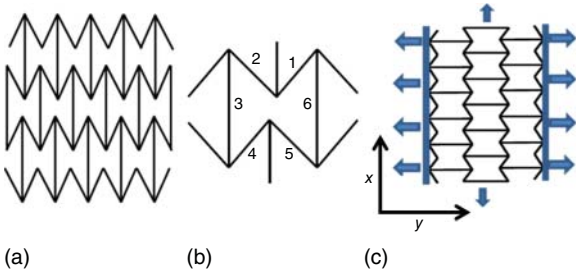


Figure 34.2 Re-entrant hexagon auxetic geometry (a) re-entrant hexagon structure, (b) unit cell, and (c) the structure under stretch.

in which the material is built molecule by molecule on a very small scale. In both techniques the main objective is to create a repeating pattern of unit cells, which possess the hinge-like features. Rod Lakes created the first ever polymer-based auxetic material in 1987 by employing the top-down approach. He applied heat and pressure to ordinary polyurethane foam, which consisted of a honeycomb of hexagonal cells, which resulted in auxetic hexagon [14].

34.2.1 Auxetic Geometries

In past few years, various geometrical structures capable of inducing auxetic behavior into the material have been developed and tested to realize their mechanical properties. These structures include re-entrant model, rotating model, nodule and fibril model, and chiral model. These auxetic structures can be used to develop various fibrous-based auxetic materials. These geometrical structures are explained briefly below.

34.2.1.1 Re-entrant Geometries

Auxetic structures based on re-entrant geometries achieve their auxetic behavior due to the deformation of diagonals along with the rotation around the hinge joints when stretched. Figure 34.2 illustrates one such example of an existing auxetic geometry named as re-entrant hexagonal geometry. The minimal repeating unit or unit cell is shown in Figure 34.2b. When the fabric is subjected to extension as shown in a direction, the fabric also expands in a direction that is perpendicular to the extension direction as shown in Figure 34.2c resulting in the negative PR effect.

34.2.1.2 Rotating Rigid Geometry

Auxetic materials based on rotational rigid geometry are based on deformation theory of geometrical configurations linked at some point of the unit. When such materials are axially stretched in a certain direction, the angles between the edges of adjacent triangles or squares or rectangles may change, and units rotate expanding in both directions. One such geometry is illustrated in Figure 34.3a; the architecture is a rotating rectangles.

The four rigid rectangles are connected at their vertices by hinges, in such a way that the empty spaces between the rectangles form rhombi. The minimal repeating unit or unit cell is highlighted in black color. It is assumed that the rectangle units are rigid and do not change their shape under loading and can

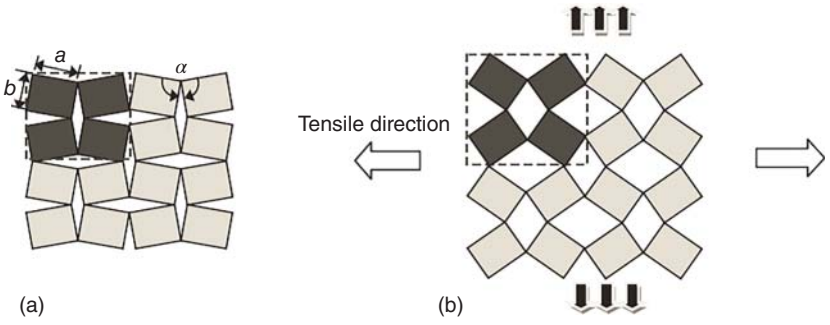


Figure 34.3 Rotating rectangles geometry (a) free state and (b) stretched state. Source: Hu et al. 2011 [15]. Reproduced with permission of SAGE.

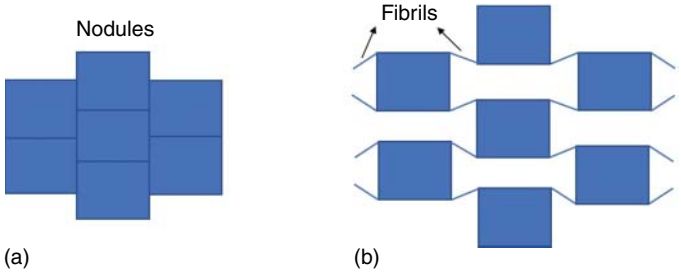


Figure 34.4 Schematic of nodule–fibril model representing microstructure of typical auxetic microporous polymer. (a) The polymer at rest and (b) the polymer at the tensile load. Source: Adapted from Liu and Hu 2010 [17].

rotate freely under loading. When the structure is subjected to an extension in a direction, the structure also expands in a direction that is perpendicular to the extension direction due to the free rotation of the rectangle units as shown in Figure 34.3b resulting in the negative PR effect. The auxetic effect depends on the strain and dimensions of the rectangles [16].

34.2.1.3 Nodule and Fibril-Based Structure

Auxetic materials based on nodule and fibrils achieve auxetic behavior due to the transition of nodes connected by fibrils under tension. One such example is illustrated in Figure 34.4.

In the stress-free state, the nodules overlap with the fibrils wound around them as shown in Figure 34.4a. When the material is stretched in the direction of the fibrils, they get straight, and the nodules rotate and snap into a rigid grid-like arrangement as shown in Figure 34.4b [17].

34.2.1.4 Chiral-Based Auxetic Geometries

Chiral structures are another kind of structures that have been developed for auxetic honeycombs. As shown in Figure 34.5, in this kind of structures, basic chiral units (highlighted in bold) are firstly formed by connecting straight ligaments (ribs) to central nodes, which may be circles or rectangles or other geometrical

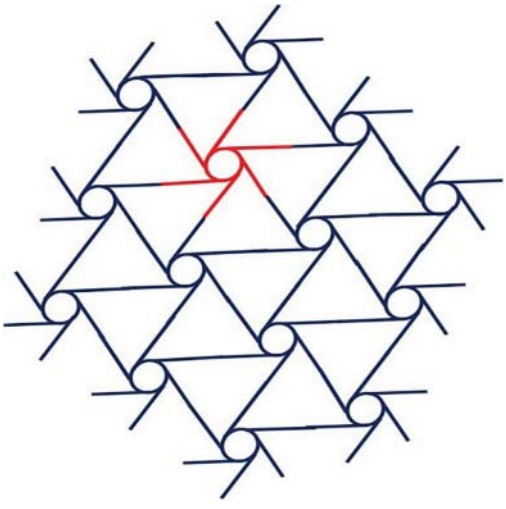


Figure 34.5 Chiral honeycombs formed with the same chiral units. Source: Adapted from Liu and Hu 2010 [17].

forms. The whole chiral structures are then formed by joining the chiral units. The auxetic effects are achieved through wrapping or unwrapping of the ligaments around the nodes in response to an applied force [17].

34.2.1.5 Foldable Geometries

The principle of using foldable structures to create an auxetic effect is that a folded structure can be unfolded when stretched in one direction, increasing the dimensions in lateral direction, thus yielding auxetic effect. One such geometry is illustrated in Figure 34.6. As shown in Figure 34.6a, the geometrical structure used to generate the auxetic effect is a three-dimensional structure formed with parallelogram planes of the same shape and size. These parallelogram planes are connected side to side in a zigzag form.

When stretched in the horizontal or vertical direction, each parallelogram can change its inclined position related to the surface plane of the structure, which

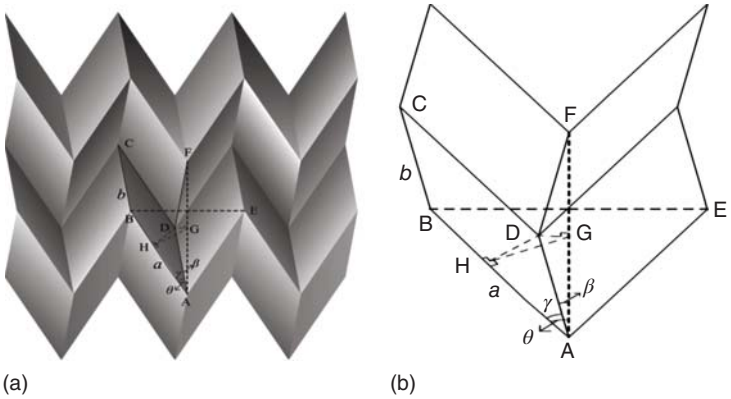


Figure 34.6 Geometrical structure: (a) three-dimensional structure and (b) unit cell. Source: Liu et al. 2009 [18]. Reproduced with permission of SAGE.

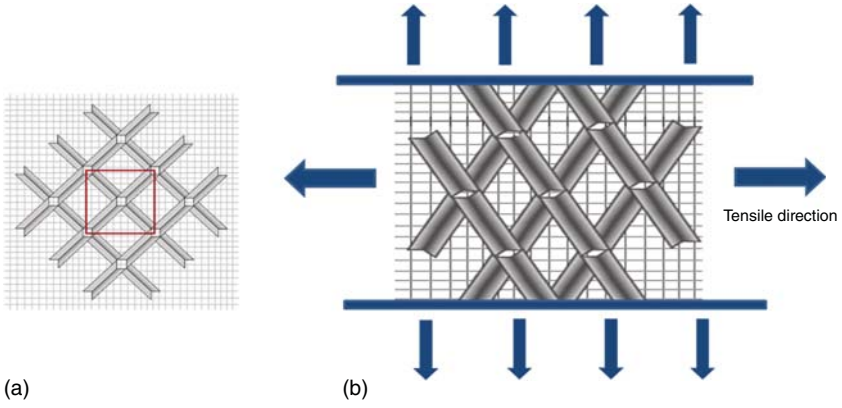


Figure 34.7 Foldable geometries: folded stripes in the oblique fashion in the free state (a) and stretched state (b). Source: Zulifqar et al. 2017 [19]. Reproduced with permission of SAGE.

results in an opening of the whole structure by increasing its dimensions in both the horizontal and vertical directions. Consequently, the auxetic effect can be achieved without changing the shape and size of the parallelogram planes. As the auxetic effect mainly comes from the position change of the parallelogram planes, it is assumed that their shape and size remain unchanged during extension. This means that a, b, and γ are kept constant.

Figures 34.7 and 34.8 illustrate two more foldable geometries that can be used to create the auxetic effect. The architecture of the geometry in Figure 34.7 is formed by placing re-entrant folded stripes in oblique fashion, which means that the stripes intersect each other in diagonal fashion as shown in Figure 34.7a. The empty spaces formed between these stripes are flat and may form a parallelogram shape. The architecture of the geometry in Figure 34.8 is re-entrant in-phase parallel folded stripes in zigzag fashion. This geometry consists of folded stripes placed in zigzag manner running along warp direction or weft direction as shown in Figure 34.8a. The minimal repeating unit or unit cell for both geometries is highlighted by red color box. When the structure is subjected to an extension in a direction, the structure also expands in a direction that is perpendicular to the extension direction due to the flattening of the re-entrant folded oblique stripes, and the transverse dimensions of the structure may remain unchanged or increase resulting in the zero or negative PR effect as shown in Figures 34.7b and 34.8b [19].

34.3 Auxetic Polymeric Fibers and Materials

34.3.1 Liquid Crystalline Polymers and Auxetic Monofilaments

Liquid crystalline polymer (LCP) exhibiting auxetic behavior was also developed. The arrangement of laterally attached rods in a main chain of LCP is shown in

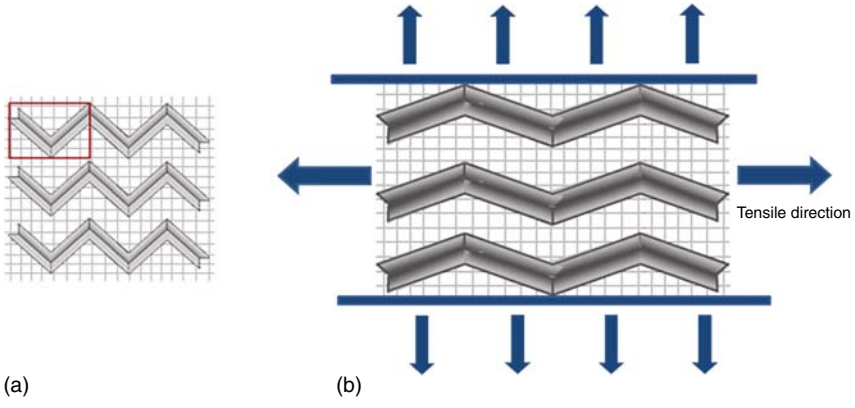


Figure 34.8 Foldable geometries: folded stripes in parallel in-phase zigzag fashion along the weft in the free state (a) and stretched state (b). Source: Zulifqar et al. 2017 [19]. Reproduced with permission of SAGE.

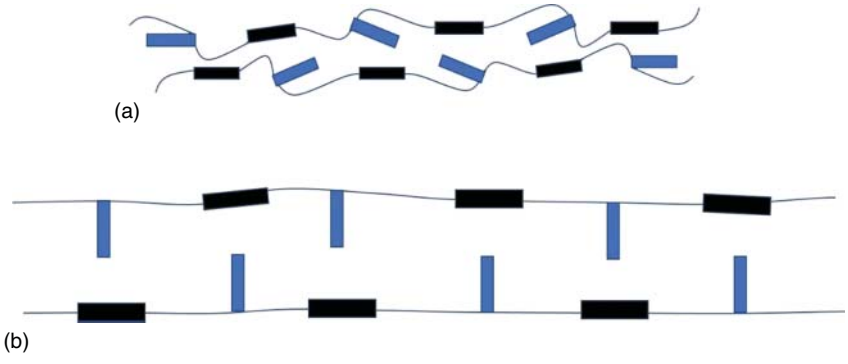


Figure 34.9 Liquid Crystalline Polymer (LCP), arrangement of main chain (a) without deformation; (b) due to stretch along horizontal direction. Source: Adapted from Liu et al. 1998 [20].

Figure 34.9. The nematic field leads to orientation of the laterally attached rods parallel to the polymer chain axis. Under tensile stress as shown in Figure 34.9, full extension of the polymer main chain forces the laterally attached rods normal to the chain axis leading to an expansion in the direction normal to the chain axis and hence to auxetic behavior. It is important to consider that the laterally attached rods should be sufficiently long, in order to increase the interchain distance and ultimately induce the auxetic behavior [20]. Polymeric monofilaments displaying auxetic behavior were also produced. The produced filaments had a microstructure of interconnected surface-melted powder particles. The structure and deformation mechanisms at the microscale, rather than at the molecular level (as compared with conventional filaments extruded from a fully molten polymer), are responsible for enhanced mechanical properties, including the auxetic effect [21].

34.3.2 Auxetic Polymeric Fibers

The auxetic polymeric fibrous material is an area that has a great potential for development. Up until today, auxetic fibers developed include ultra-high molecular weight polyethylene (UHMWPE), polyethylene (PE), polyester, nylon, and polypropylene (PP) fibers. Among these fibers only PP fibers are produced on large scale, and all others were produced on laboratory scale. Auxetic fibers have a wide range of potential applications including fiber-reinforced composites, drug delivery systems, and systems for personal protection. In this section, the auxetic fibers produced and characterized to date are discussed briefly in terms of processing conditions and manufacturing methods.

34.3.3 Auxetic Polypropylene Fibers

Alderson et al. were the first to successfully produce auxetic fibers. They developed a kind of auxetic PP fiber by employing a novel thermal processing technique, based on modified conventional melt spinning technique. This enabled a continuous fabrication process of auxetic PP fibers with diameters of less than 1 mm, and a large value of PR ($\nu = -0.6$) was obtained when measured by using video extensometer. The conventional melt spinning method with some novel modifications is adopted to produce auxetic PP fibers. The set of processing conditions are described including temperature, screw speed, and takeoff speed. It was observed that at a temperature of 159 °C with a screw speed of 1.05 rad/s and takeoff speed of 0.03 m/s, the produced fibers exhibited auxetic behavior. It is important to note that the temperature should be constant throughout the length of the extruder and there should be no drawing. Figure 34.10 shows that the fibers obtained via this processing route have in-phase length and width data, which confirms the auxetic behavior of produced fibers [22].

34.3.3.1 Large-Scale Production of Auxetic PP Fibers

Previously, the auxetic fibers were produced only on laboratory scale. Recently, Kim Alderson et al. produced auxetic PP fibers on large scale, by using a big scale extruder machine as shown in Figure 34.11. The extruder used for this process

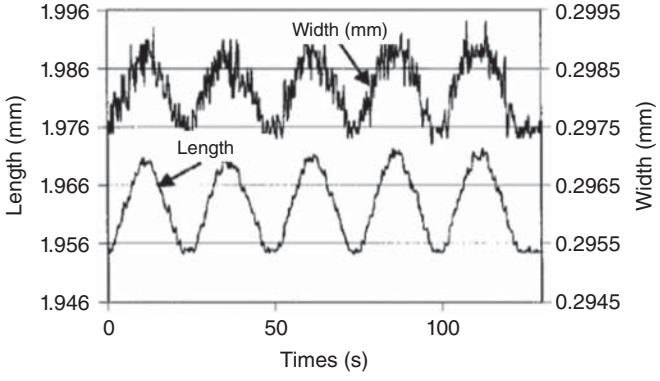


Figure 34.10 Width–length data for polypropylene fibers. Source: Alderson et al. 2002 [22]. Reproduced with permission of Taylor & Francis.

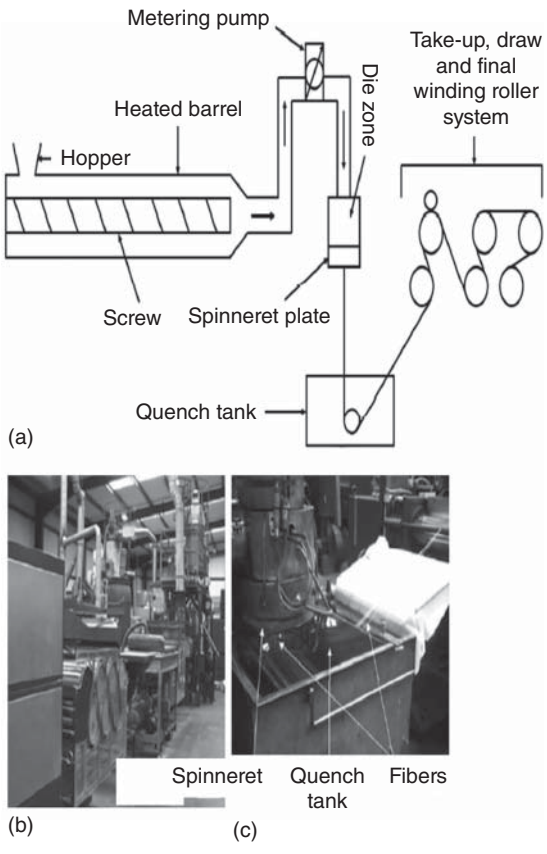


Figure 34.11 (a) Schematic of a general melt extruder, (b) the Davis-Standard thermatic extruder used in the large-scale extrusion, and (c) spinneret and quench tank of the Davis-Standard thermatic extruder. Source: Alderson et al. 2016 [23]. Reproduced with permission of John Wiley & Sons.

was Davis-Standard thermatic extruder by Shakespeare Monofilament UK Ltd., as shown in Figure 34.11b. The auxetic PP fibers produced in this process had good reproducibility, and it was reported that fibers exhibited auxetic behavior over large strain range as compared with the fibers produced in laboratory. The processing conditions to produce auxetic fibers were barrel temperature 200 °C, a screw speed of 12.5 rpm, and a take-up speed of either 1.5 or 3.5 rpm. It is important to mention that the extruded fibers also require ambient air quenching. It is important to consider that unlike laboratory scale production, the barrel temperature of 200 °C was identified in this work to produce auxetic fibers on large scale by using industrial-size extruders. The authors aimed to focus on the thermal characteristics of the polymer in the large-scale extruder and the resulting fiber microstructure, as future work. It is reported that the physical state of the polymer in the larger barrel during extrusion at 200 °C will be determined and will be related to the corresponding state in the smaller barrel laboratory extruder at the 159 °C conditions established for auxetic fibers and also the additional 180–190 °C conditions established for auxetic PP films. It will be necessary to establish the effects of dwell time and thermal equilibration on the nature of the polymer in situ (e.g. homogeneous melt or a partially melted, heterogeneous state). A postproduction assessment of fiber morphology and

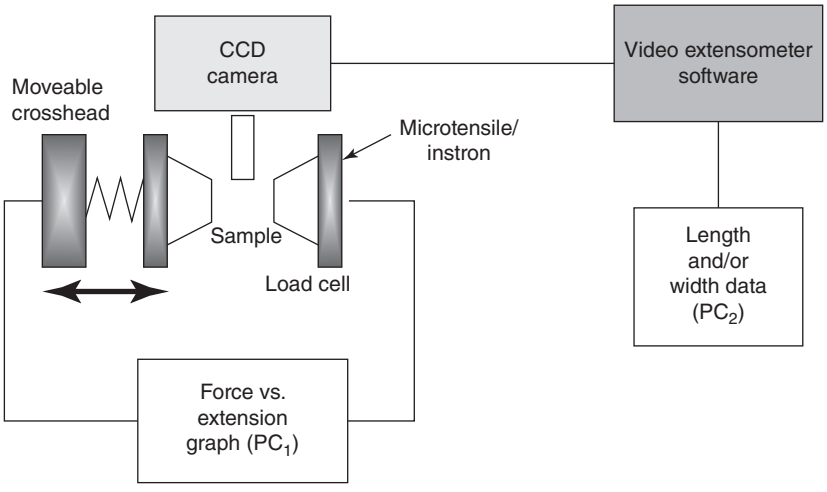


Figure 34.12 Schematic of the video extensometer setup. Source: Alderson et al. 2016 [23]. Reproduced with permission of John Wiley & Sons.

crystallinity will also be undertaken to determine the microstructural features and size scale responsible for the auxetic effect [23].

34.3.3.2 Testing of Auxetic Behavior of PP Fibers

Instron 4300 mechanical testing machine with a 100 N load cell, at a crosshead speed of 2 mm/min, was used to test the auxetic behavior of fibers. The PR was measured using a Messphysik ME46 video extensometer. This consists of a computer software package, which simultaneously measures length and width data from changes in the contrast between markers attached to the fibers along their lengths and the edges of the fibers, which gave the width measurement. The schematic setup of the equipment is shown in Figure 34.12. The software splits the length defined by the fiducial markers into 10 segments, the widths of which are then tracked throughout the test. Occasionally, individual segments can be tracked incorrectly due to features on the fiber surface, lighting issues, and such like. This is evident through the recorded segment width being significantly different to the actual fiber diameter (i.e. adjacent segment widths) or displaying markedly different trends to other segments. In such cases, the identified segment data were removed from the subsequent analysis [23].

Figure 34.13a shows the raw data for conventional PP fiber. This clearly shows as the length increases (bold line), the width decreases. This is conventional behavior and is found in all sections of the fiber. To get the PR from these data, an average true transverse strain vs. true axial strain plot is constructed, and the slope of this gives PR as shown in Figure 34.13b. Figure 34.14a shows the same analysis for auxetic fiber. It can be seen clearly that as the fiber is pulled, it increases in diameter, giving the negative PR by analysis as above as −0.82 as shown in Figure 34.14b. The auxetic effect is then shown for the first time in a fiber produced on a large-scale extruder and persists over the full 5% axial strain range covered in the test. This is an increase in the strain range for auxetic behavior

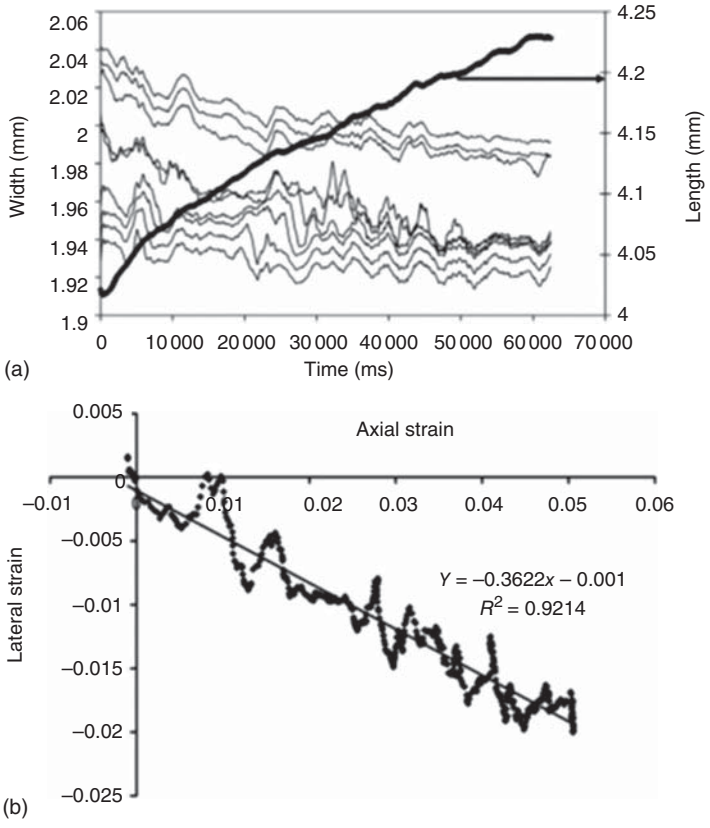


Figure 34.13 (a) Raw width and length data, showing conventional behavior; (b) plot of lateral strain against axial strain, showing Poisson's ratio, +0.36. Source: Alderson et al. 2016 [23]. Reproduced with permission of John Wiley & Sons.

found in melt extruded auxetic fibers, which persists typically up to 1–2% strain in fibers produced previously on a lab-scale extruder [23].

34.3.4 Auxetic Polyethylene

Alderson and Evans produced a microporous form of UHMWPE, capable of exhibiting large negative PR as low as −1.2 depending on the degree of anisotropy in the material. The manufacturing process consisted of three stages including compaction, sintering, and extrusion of UHMWPE fine powder. The function of the compaction is to induce structural integrity to the polymer. The set of compaction conditions including compaction pressure and temperature were described in order to produce auxetic polymer. The investigation revealed that the compaction pressure and temperature must be kept at 0.04 GPa and 110–125 °C, respectively, while holding at these conditions for 10–20 minutes. It was observed that the modulus of the resulting exudate is reduced if the temperature and compaction pressure are lower than the mentioned limits and if higher than the mentioned limits, the polymer particle are deformed. The

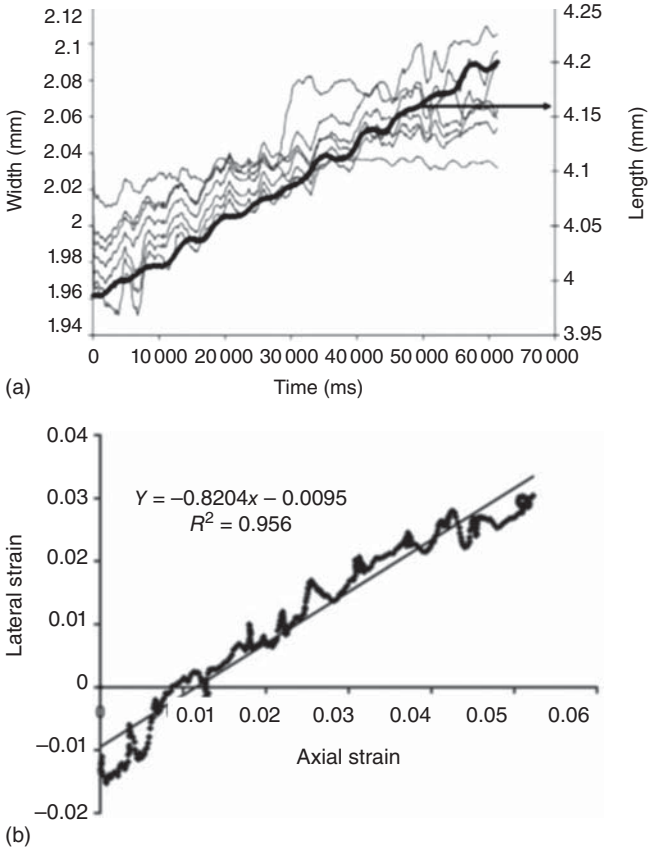


Figure 34.14 (a) Raw width and length data, showing auxetic behavior; (b) plot of lateral strain against axial strain showing Poisson's ratio, −0.82. Source: Alderson et al. 2016 [23]. Reproduced with permission of John Wiley & Sons.

compacted polymer is then reheated up to 160 °C and held at this temperature for 20 minutes. The polymer is then extruded with a speed of 500 mm/min. The geometry of die must be a cone die with a cone semi angle of 30° and a small die capillary length. The die entry diameter of 15 mm and exit diameter of 7–7.5 mm must also be used in order to achieve auxetic extrudate with high structural integrity. The output of these processing conditions is found to be an extrudate as shown in Figure 34.15, with strain-dependent negative PR [24–27].

34.3.5 Auxetic Polyester Fibers

A novel method to produce auxetic polyester fibers has been described. The polyester granules were grinded by using an in-house cryogenic grinding, and particles of less than 150 μm were collected to carry out the extrusion. The extrusion was carried out at higher temperature (230 °C) profile and gradually decreased the temperature to 210 °C until the viscosity of the powder bulk was too high to allow free flow through the die zone. An important consideration for the production of auxetic fibers is maintaining the minimum draw ratio and

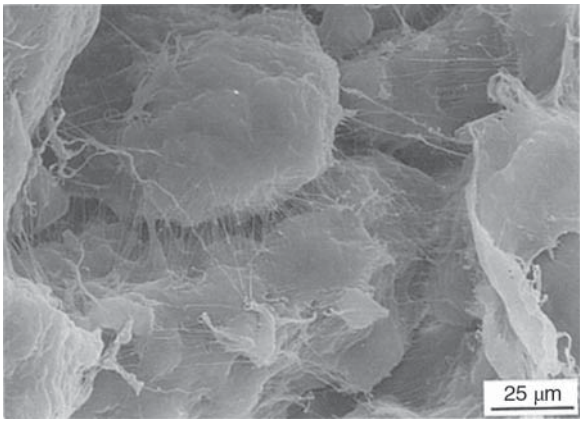


Figure 34.15 Scanning electron microscopy (SEM) images of auxetic microporous UHMWPE. Source: Alderson and Evans 1992 [24]. Reproduced with permission of Elsevier.

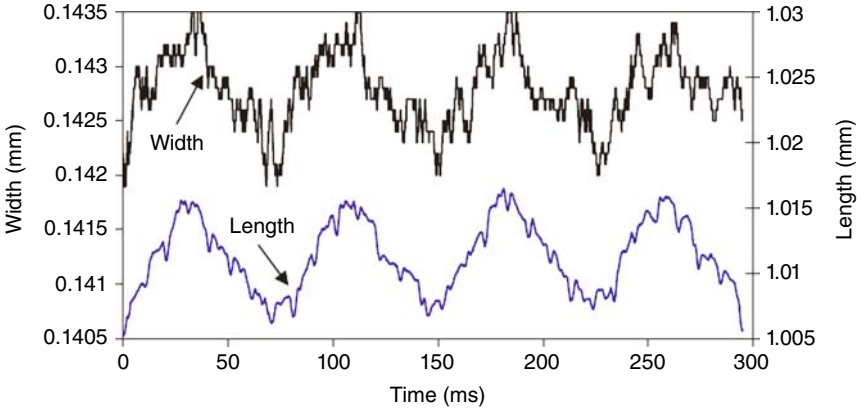


Figure 34.16 Width–length data for polyester fibers processed at temperature of 225 °C. Source: Ravirala et al. 2005 [28]. Reproduced with permission of John Wiley & Sons.

viscosity of the powder bulk. Therefore, the viscosity, take-up speed, and screw speed are critical factors, which influence the production of auxetic fibers. The take-up speed during extrusion has direct impact on screw speed, and optimum processing conditions for extrusion could only be achieved only at a screw speed of 0.525 rad/s with minimum take-up speed of 0.075 m/s. The fibers produced at 225 °C with screw speed 0.525 rad/s and take-up speed 0.075 m/s were found to exhibit auxetic behavior. They have an in-phase length–width data as shown in Figure 34.16. It can be observed that the width increased as the length increases in response to the applied force along the length of the fiber. Similarly, the width decreased as the length decreased on removal of the tensile load. Thus the fiber was confirmed to be auxetic [28, 29].

34.3.6 Auxetic Polyamide Fibers

The nylon powder was successfully used to produce auxetic polyamide fiber. One such development used the nylon powder supplied by nylon colors with 43 µm as average size of powdered particles. First of all, the nylon powder was oven

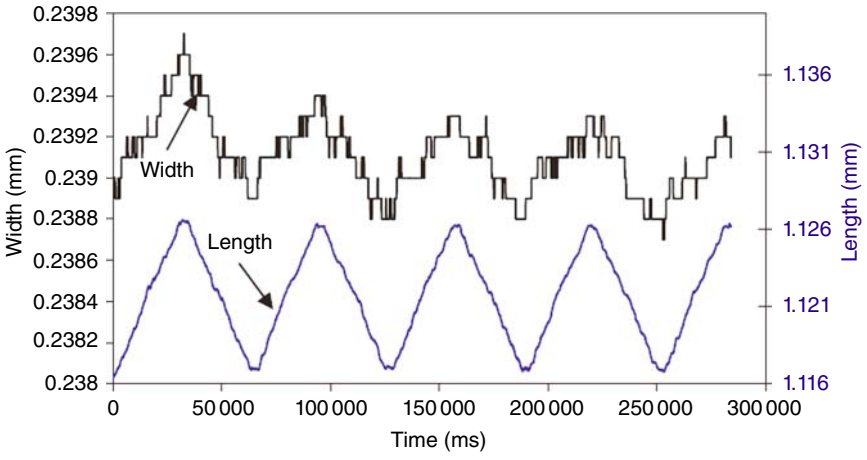


Figure 34.17 Width–length data for polyamide fibers. Source: Ravirala et al. 2005 [28]. Reproduced with permission of John Wiley & Sons.

dried for two days in low vacuum at 80 °C to avoid hydrolysis during extrusion. The powder was then extruded through the melt extruder maintaining constant temperature at 195 °C with screw speed 10 rpm (1.05 rad/s) and take-up speed 2 m/min (0.03 m/s). Figure 34.17 shows the length and width data of the obtained fibers at these processing conditions. It was reported that the length of the fiber increased when the load is applied with increase in width also. When the load was removed, the fiber length decrease combined with the decrease in the width as well. Since the fiber has shown these features in all the continuous cycles of load application and removal, this particular fiber was found to be auxetic [28].

34.3.7 Moisture-Sensitive Auxetic Fibers

The moisture-sensitive auxetic fiber has been invented, which responds not only to external force but also to moisture by using moisture-activated shrinking filament. The invented fiber is a combination of two components, one component is a moisture-sensitive shrinking filament with relatively high modulus of elasticity such as modified cellulosic fibers, e.g. cotton or rayon. The other component is an elastic material of lower modulus of elasticity, for example, siloxane. The fiber is straight in its dry state with no tensile load. When the fiber is in wet state, the moisture-sensitive shrinking component shrinks, and a pulling force is applied along to the elastic component causing it to deform and form helices, and pores are created. When the load (tensile or due to shrinking in wet state) is applied along the length of the auxetic fiber, the wrapped component gets straight, and the diameter of helices formed by the elastic components is increased especially in areas where pores are created. The elastic component of auxetic fibers undergoes opposite displacement in y-direction as compared with the displacement of the elastic component of the adjacent auxetic fiber. These opposite displacements cause the thickness of material to be increased leading to auxetic behavior. The important consideration in development of such yarn is that there must be

enough difference between the modulus of elasticity of the materials for two components. Further, the auxetic moisture sensitive yarn can only be produced by arranging two components at different handedness. Helical auxetic yarns made of moisture-sensitive auxetic materials were suggested for functional garment [30]. More advanced work is required in order to increase the range of the materials that can be finished in auxetic fiber form together with the development of predictive models to understand the deformation mechanisms leading to auxetic behavior in fibers.

34.4 Properties and Applications of Auxetic Fibers

The unusual property of auxetic materials is that they are relatively resistant to denting. When an auxetic material is impacted, the compression caused by the impact results in the material compressing toward the point of the impact, thus becoming much denser and resisting the force. When a composite material fractures, the fibers are pulled out of the matrix. This results in the reinforcing effect being lost as the bond between the fiber and the matrix fails. It has been suggested that an auxetic fiber within a composite would resist fiber pullout. When the fiber is pulled, it will expand and effectively lock into the matrix rather than contracting and pulling out easily as a conventional fiber would do as shown in Figure 34.18 [31]. Therefore, the fracture toughness of a composite can be enhanced by using auxetic fiber reinforcements. Auxetic materials are also more resistant to fracture; they expand laterally as a force is applied, and this restricts the growth of any potential cracks in the material.

With the invention of auxetic PP fibers [22], the concept of using embedded auxetic fibers in a softened epoxy resin was employed to produce a single fiber composite [32]. The fiber pullout resistance and energy absorption were tested. In comparative tests with specimens containing positive PR fibers, the auxetic

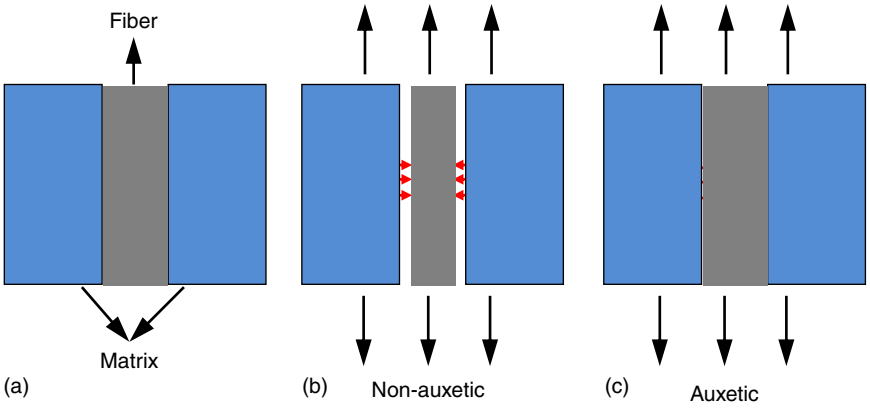


Figure 34.18 Fiber reinforced composites. (a) Fiber Matrix interface; (b) contraction in conventional fibers during stretching; (c) expansion in auxetic fibers during stretching. Source: Wang et al. 2016 [1]. Reproduced with permission of Elsevier.

fiber-locking mechanism is shown to enable the specimen to carry more than twice the maximum load; and in terms of energy absorption, the auxetic fiber is up to three times more difficult to extract than the equivalent positive PR fiber. It has been reported that with auxetic fibers, pullout is resisted because the fibers expand perpendicular to the pullout force. This could help to resist potential failure mechanisms in the composite, such as crack growth. In another study it was reported that in the case of auxetic fiber, the negative PR will induce radial expansion and the tip of the de-bonded fiber during pulling out, to close up, and the stress concentration at that region will be reduced. The radial expansion of the de-bonded fiber increases the contact between the unbonded fiber and matrix leading to an enhanced frictional contact, and more force is required to pull the fiber out [33, 34].

Another potential application for auxetic fibers is in drug delivery systems. The microporous auxetic fibers can be employed to fabricate a wound healing bandage. The drug agent can be entrapped into the microspores of the fiber, and during wound swelling the bandage will receive a stress, and the microspores of auxetic fibers will be opened and release the drug to the infected region. After wound healing the stress on the bandage will be reduced, and drug release will be stopped [35]. The auxetic composites may also find application in the aircraft.

The aircrafts undertake very high shear force when flying. The materials with higher shear strength can optimize the performance of the aircraft. The auxetic composites can have higher shear modulus, and another property worthy to mention, among others, is they have better formability, enabling them easier to make the shape needed. Therefore, the auxetic composites can be good candidate instead of the conventional composites to be used on the aircraft in the future [1]. Nevertheless, other mechanical properties like strength and very high modulus are essential in order to replace conventional fibers with auxetic fibers in these and other applications.

34.5 Conclusions

This chapter mainly discussed the fibers for auxetic applications. The auxetic fibers are very good materials to be used in fiber-reinforced composites; the advantages they possess make them very useful in designing of smart composites. For example, enhanced vibration damping, higher shear modulus, higher energy absorbance, and fracture toughness make them an ideal candidate to be used to fabricate composites for high-profile application areas including aerospace. Although this new breed of composites is not yet mature enough, it is believed that they will be developed and good enough to be used in aerospace engineering instead of conventional composites. However, the disadvantage just like with the auxetic materials is that they are too porous and are not stiff enough to bear the load. Therefore, the auxetic materials are suitable for certain specific applications. Moreover, there are only a few auxetic fibers developed including UHMWPE, PE, polyester, nylon, and PP fibers. Among these fibers only PP fibers are produced on large scale, and all others were produced on laboratory scale.

Therefore, continuous processes to produce auxetic fibers on large scale must be developed. Another important feature that auxetic fibers must have is that they should have the possibility of blending with other materials and spinning them into yarns. In this way the spectrum of fibers for auxetic applications could be broadened. More advanced work is required in order to increase the range of the materials that can be finished in auxetic fiber form together with the development of predictive models to understand the deformation mechanisms leading to auxetic behavior in fibers.

References

1 Wang, Z., Zulifqar, A., and Hu, H. (2016). Auxetic composites in aerospace engineering. In: *Advanced Composite Materials for Aerospace Engineering: Processing, Properties and Applications* (eds, S. Rana and R. Fangueiro), p. 213. Woodhead Publishing.

2 Steffens, F., Rana, S., and Fangueiro, R. (2016). Development of novel auxetic textile structures using high performance fibres. *Materials and Design* 106: 81–89.

3 Jiang, L., Gu, B., and Hu, H. (2016). Auxetic composite made with multilayer orthogonal structural reinforcement. *Composite Structures* 135: 23–29.

4 Bezazi, A. and Scarpa, F. (2007). Mechanical behaviour of conventional and negative Poisson's ratio thermoplastic polyurethane foams under compressive cyclic loading. *International Journal of Fatigue* 29: 922–930.

5 Scarpa, F. and Smith, F. (2004). Passive and MR fluid-coated auxetic PU foam–mechanical, acoustic, and electromagnetic properties. *Journal of Intelligent Material Systems and Structures* 15: 973–979.

6 Chan, N. and Evans, K. (1998). Indentation resilience of conventional and auxetic foams. *Journal of Cellular Plastics* 34: 231–260.

7 Wang, Z. and Hu, H. (2016). Tensile and forming properties of auxetic warp-knitted spacer fabrics. *Textile Research Journal* https://doi.org/10.1177/0040517516660889.

8 Alderson, K., Pickles, A., Neale, P., and Evans, K. (1994). Auxetic polyethylene: the effect of a negative Poisson's ratio on hardness. *Acta Metallurgica et Materialia* 42: 2261–2266.

9 Baughman, R.H., Shacklette, J.M., Zakhidov, A.A., and Stafström, S. (1998). Negative Poisson's ratios as a common feature of cubic metals. *Nature* 392: 362–365.

10 Caddock, B. and Evans, K. (1989). Microporous materials with negative Poisson's ratios. I. Microstructure and mechanical properties. *Journal of Physics D: Applied Physics* 22: 1877.

11 Evans, K., Nkansah, M., and Hutchinson, I. (1994). Auxetic foams: modelling negative Poisson's ratios. *Acta Metallurgica et Materialia* 42: 1289–1294.

12 Lim, T.-C. (2009). Out-of-plane modulus of semi-auxetic laminates. *European Journal of Mechanics - A/Solids* 28: 752–756.

13 Yeganeh-Haeri, A., Weidner, D.J., and Parise, J.B. (1992). Elasticity of a-cristobalite: a silicon dioxide with a negative Poisson's ratio. *Science* 257: 650–652.
14 Lakes, R. (1987). Foam structures with a negative Poisson's ratio. *Science* 235: 1038–1040.
15 Hu, H., Wang, Z., and Liu, S. (2011). Development of auxetic fabrics using flat knitting technology. *Textile Research Journal* 81: 1493–1502.
16 Grima, J.N. and Evans, K.E. (2006). Auxetic behavior from rotating triangles. *Journal of Materials Science* 41: 3193–3196.
17 Liu, Y. and Hu, H. (2010). A review on auxetic structures and polymeric materials. *Scientific Research and Essays* 5: 1052–1063.
18 Liu, Y., Hu, H., Lam, J.K., and Liu, S. (2010). Negative Poisson's ratio weft-knitted fabrics. *Textile Research Journal* 80 (9): 856–863.
19 Zulifqar, A., Hua, T., and Hu, H. (2017). Development of uni-stretch woven fabrics with zero and negative Poisson's ratio. *Textile Research Journal* https://doi.org/10.1177/0040517517715095.
20 Liu, P., He, C., and Griffin, A. (1998). Liquid crystalline polymers as potential auxetic materials: Influence of transverse rods on the polymer mesophase. In: *Abstracts of Papers of the American Chemical Society*, U108.
21 Alderson, A. and Alderson, K. (2005). Expanding materials and applications: exploiting auxetic textiles. *Technical Textiles International* 777: 29–34.
22 Alderson, K., Alderson, A., Smart, G. et al. (2002). Auxetic polypropylene fibres: Part 1-Manufacture and characterisation. *Plastics, Rubber and Composites* 31: 344–349.
23 Alderson, K., Nazaré, S., and Alderson, A. (2016). Large-scale extrusion of auxetic polypropylene fibre. *Physica Status Solidi B* 253: 1279–1287.
24 Alderson, K. and Evans, K. (1992). The fabrication of microporous polyethylene having a negative Poisson's ratio. *Polymer* 33: 4435–4438.
25 Pickles, A., Webber, R., Alderson, K. et al. (1995). The effect of the processing parameters on the fabrication of auxetic polyethylene. *Journal of Materials Science* 30: 4059–4068.
26 Alderson, K., Kettle, A., Neale, P. et al. (1995). The effect of the processing parameters on the fabrication of auxetic polyethylene. *Journal of Materials Science* 30: 4069–4075.
27 Neale, P., Pickles, A., Alderson, K., and Evans, K. (1995). The effect of the processing parameters on the fabrication of auxetic polyethylene. *Journal of Materials Science* 30: 4087–4094.
28 Ravirala, N., Alderson, A., Alderson, K., and Davies, P. (2005). Expanding the range of auxetic polymeric products using a novel melt-spinning route. *Physica Status Solidi B* 242: 653–664.
29 Ravirala, N., Alderson, K.L., Davies, P.J. et al. (2006). Negative Poisson's ratio polyester fibers. *Textile Research Journal* 76: 540–546.
30 Lee, W., Lee, S., Koh, C., and Heo, J. (2010). Moisture sensitive auxetic material. Google Patents.
31 Evans, K.E. and Alderson, A. (2000). Auxetic materials: functional materials and structures from lateral thinking! *Advanced Materials* 12: 617–628.

32 Alderson, K., Simkins, V., Coenen, V. et al. (2005). How to make auxetic fibre reinforced composites. *Physica Status Solidi B* 242: 509–518.
33 Donoghue, J., Alderson, K., and Evans, K. (2009). The fracture toughness of composite laminates with a negative Poisson's ratio. *Physica Status Solidi B* 246: 2011–2017.
34 Simkins, V., Alderson, A., Davies, P., and Alderson, K. (2005). Single fibre pullout tests on auxetic polymeric fibres. *Journal of Materials Science* 40: 4355–4364.
35 Alderson, A., Rasburn, J., Ameer-Beg, S. et al. (2000). An auxetic filter: a tuneable filter displaying enhanced size selectivity or defouling properties. *Industrial and Engineering Chemistry Research* 39: 654–665.

Index

a

accordion 487
acetal copolymer 342
acetate fibers 10
Acetobacter xylinum 106
acid extraction 160, 161
acrylic based superabsorbent fiber 324, 326
activated UHMWPE yarn 304
active sweating method 868
acyclic *N*-halamine 931, 932
Adaptive Network Based Fuzzy Inference System (ANFIS)
  architecture 541, 542
  back-propagation learning 541
  hybrid learning 541, 544
  parameters 543
adherent polydopamine film 349
advanced applications of textile materials 22–23
advanced composites 207, 224
aerogels 27, 119, 372, 373, 940
aggregation 56, 159, 538
ahimsa silk 81
air cooling clothing (AFC) 874
air filtration technology 175
air-jet looms 480
air-jet weaving machines 480
airlaid nonwoven fabrics 328
airlaying 490
air pollution 118, 175
air vortex spun yarn
  prominent features 447–448
  structure 446–447
Alcantara® 297
alginate 29, 324, 503, 939–940
alginate fibers 5, 29, 324
aligned MWCNT/Si fiber synthesis 661
alkali extraction 160, 161
α-amino acids in naturalproteins 48
α-keratin 8, 48–50, 59, 69
American Society of Heating and Ventilating Engineers (ASHVE) 860
amino acid composition
  of fibroin 77
  of sericin 77
  of silk fibers 86
amplified spontaneous emission (ASE) 399
Anaphe silk 82
ANF modified polysulphone membranes 224
animal fibers 2, 37, 78
anionic polymer brushes 732–733
Antheraea assamensis 82
Antheraea pernyi 82
Antheraea proylei J 81
anti-bacterial fibers 28, 362
antimicrobial agent 348–349, 503, 505, 518, 927–930, 933, 935, 937, 938, 941, 942
antimicrobial fibers
  chitosans 927
  definition 927
  history of 927–928
  metals and metal oxides modified fabrics
    oligodynamic effect 934

Handbook of Fibrous Materials, First Edition. Edited by Jinlian Hu, Bipin Kumar, and Jing Lu.
© 2020 Wiley-VCH Verlag GmbH & Co. KGaA. Published 2020 by Wiley-VCH Verlag GmbH & Co. KGaA.

antimicrobial fibers (*contd.*)
silver 934
titanium dioxide 934–935
natural polymers
alginate 939–940
chitosan 940–941
gelatin 939
hyaluronic acid (HA) 938
N-halamine
coating 932
cross-linking 931–932
electrospinning 933
grafting 932
principles of 931
reactive reagent treating 932
photoactive chemicals
LAAA 935–936
organic photoactive reagents 936–937
photo-induced biocidal effect 935–936
textile modification with TiO_2 936
QACs
environmental impact 929–930
mechanism of 929
aperture angle, of glass and optical fibers 601
apparel manufacturing industries 21
Aquaform 329
Aquasorb 329
aqueous counter collision (ACC) 102–103, 112
aramid-boehmite 224
aramid fibers 5, 10, 895
advanced composites 224
aramid solutions 211
ballistics 225
chemical properties 219–220
communication 226–227
composites with soft materials 222–223
copolyaramids 211
direct polycondensation 210
dry-jet-wet spinning 215–216
dry spinning 214
electrical application 226
future trends 227
haemodialysis 224
heat treatment 216–217
historical developments of 207
industrial protective apparel 225
low temperature polycondensation 208
mechanical/tensile properties 220–221
nanofibers 216
permselective use 225–226
ropes and cables 224–225
structure 217–219
thermal properties 221–222
ultrafiltration 224
wet spinning 214
aramid nanofibers (ANFs) 216, 224
aromatic bi-carboxylic acid 340
aromatic polyamides 25, 28, 207–211
artificial neural network (ANN) 530
back-propagation algorithm 532–533
characteristics 530
functioning 531
learning rate and momentum 534–535
Levenberg–Marquardt algorithm 533–534
multilayered structure 530–531
number of hidden layers 534
number of nodes 534
prediction accuracy 532
yarn engineering 544
artificial turf 298–299
asbestos 225, 227, 437
atomic force microscopy (AFM) 101, 515
attenuation profiles 611, 620–627, 638
defined 609
of PPMA optical fiber 602, 603
of silica optical fiber 602
Australia wool, inspection and evaluation 61
Australian Wool Testing authority (AWTA) 61
autumn wool 45
auxetic effect 25, 956–959, 962

auxetic geometries
chiral structures 956–957
foldable geometry 957–958
nodule and fibril-based structure 956
re-entrant hexagonal geometry 955
rotational rigid geometry 955–956
auxetic moisture sensitive yarn 967
auxetic monofilaments 959
auxetic polyamide fiber 965–966
auxetic polyester fibers 964–965
auxetic polyethylene 963–964
auxetic polymeric fibers and materials
auxetic monofilaments 959
auxetic polyamide fiber 965–966
auxetic polyester fibers 964–965
auxetic polyethylene 963–964
auxetic polypropylene (PP) fiber 960–963
liquid crystalline polymer 958–959
moisture sensitive auxetic fiber 966–967
properties and applications 967–968
auxetic polypropylene (PP) fiber 960–963

b

backing yarn 249
back-propagation algorithm 532–533, 535
bacterial cellulose 107
fibril dimensions 105
hierarchical structure 107
mechanical property 101
synthesis 106
TEMPO oxidation 106
Young's modulus 107
ball wool 44
bandgap fibers 6
basic warp knitted structures 487
bast fibers 437, 820
bave/filament 78
bayberry tannin immobilized collagen fiber (BTICF) membrane 168
bayberry tannins 168
Bekinox BK50 235
bendable conductive yarn structure 246
β-(1-4)-D-glucosamine units 503
bi-component cross-sections 823–824
bi-component elastic fiber 338, 350–351
bicomponent electrospun fibers 136
bicomponent fibers 5
bicomponent melt-spinning 282
biocomponent spinning 288–295
biodegradable fibers 300–301
as bonding elements 296
cross-section geometry 284–285
electrically conducting fibers 301–302
with functional surface 299–300
high-performance core 298–299
liquid-core fibers 302–303
melt-spinning equipment 285–286
microfibers 297
PA66-random copolymer side-by-side hosiery yarn 282
polymer optical fibers 301
post-treatment of 295–296
shape-memory fibers 304
with special cross-sections 297–298
special spin pack design 286–288
spin pack design 282–284
thermoplastic fiber-reinforced composites 303
bicomponent melt-spinning 282, 286, 288–290, 293
bicomponent (conjugated) spinning 281
bicomponent thermoplastic core-sheath fibers 287
bio-absorbable materials 503
bio-based polyamide-56 nanofiber/nets (PA-56 NF/N) membranes 191
biocomponent spinning
coextrusion instabilities 291–292
encapsulation 292–293
interfacial adhesion 290–291
orientation and crystallization 288–290
simulation and modeling 293–295

biocomponent spinning (*contd.*)
structure formation 288
volatiles 293
biodegradable fibers 300–301
bio-medical measurement 392, 397
biomimetic scaffolds 150
Biopol™ 71
biopolymers 71, 72, 127, 151, 169
1,1′-bis(4-vinylbenzyl)-4,4′-bipyridinium dinitrate (VBVN) 731, 732
bivoltines 80
bleaching 20
blended polyester staple fiber (PES) 320
blow room section 16
Bombyx mori 75, 78, 86
botany wool 41
Bragg reflector 616
braiding
applications 495–496
processes and machines 493–494
structures and properties 494–495
braiding machines 493–496
Brillouin optical time domain reflectometry (B-OTDR) 395–397
brin 76, 78
Brownian diffusion 116, 808–810
brush-protruding' configuration 726, 728
bulk polymerization technique 608
bulk resistivity 234
1,4-butanediol 425, 767
1,2,3,4-butanetetracarboxylic acid (BTCA) 932

C

calfskin 163, 167, 168
capacitance 381, 564, 572–575, 650, 666, 667, 699, 700, 739, 740
capacitive fiber-based sensors 700
capacitive humidity sensors 705
capacitive sensors 699, 700
Capillary Channel Polymer™ (CCP™) 824
carbonaceous fiber materials 898
carbon black 30, 148, 242–243, 302, 347, 895, 898
carbon fibers 5, 10, 821
containing nanoparticles 654
continuous fiber network of 653–654
carbonization 46, 654, 655, 659, 660, 663
carbon nanotubes (CNTs) 135, 242–243, 347, 422, 564, 689–693, 723, 788, 790, 898
carboxymethylated chitosans 129, 130
carboxymethylation 105, 129, 130, 141
carded yarn 443, 444
carding 16, 490
catalytic moiety ink patterning 736–737
cationic polymer brushes 731–732
cellulose 95
degree of polymerization 96
Iα and Iβ, unit cells for 98
molecular formula 95
molecular structure 96
cellulose acetate butyrate (CAB) 346, 366
cellulose acetate nanofibers 110, 797
cellulose acetate propionate (CAP) 346
cellulose biosynthesis 96, 99
cellulose ester (CE) 346, 788
cellulose fibers 95, 119
applications of 118
in energy storage devices 118
macro-scaled continuous 114–117
nanocellulose fibers in biomedical applications 118
nano-scaled 100–107
sub-micron-scaled 107–114
wood, hierarchical structure of 101
cellulose microfibrils 96, 97, 100–102, 106, 113
cellulose nanofibrils 105, 106
cellulose synthase enzyme (CeSA) 96
cellulosic fibers 3, 7, 10, 319, 437, 901–903, 912, 913, 915, 966
cellulosics 245, 811, 814
centrifugal electrospinning system 148
centrifugal spinning 657, 658, 662–667

centriod method 538
ceramic fibers 5, 10, 821
ceramics 182, 411, 682
channeled surface 823
chemically bonded nonwovens 493
chemically heated clothing (CHC) 876
chemically modified flame resistant fiber 833, 835–836
chemically stable chitosan membranes 148
chemical sensors 26, 705–709
China's wool 38
  average diameter of 54
  quality 39–40
  types 38
chiral-based auxetic geometries 956–957
chitin 29, 125, 127–129, 135, 150, 182, 503, 790, 940
chitin nanocrystals 135
chitosan 29, 127, 165, 182, 503, 504, 940, 941
  apparent viscosities 128
  centrifugal electrospinning system 148
  characteristics of 127
  chemically stable membranes 148
  composite fibrous scaffold 136
  deacetylation of 128
  enzymatic method 129
  extracted *vs.* commercial, characteristics of 128–131
  extraction/modification of 127
  forms and applications 127
  FTIR spectra of 127
  market value 127
  moisture sorption changes 141
  N-carboxymetylation 144
  primary applications of 127
  production,sources used for 127
  structure 127
  three-dimensional electrospun mats 150
chitosan based heart valve scaffold 142
chitosan fibers
  antioxidant activity 146
  application of 140–145
  blend fibers 135–139
  carboxymethylation 141
  cellulose/O-hydroxyethyl fibers *vs.* viscose rayon 136
  chitosan based heart valve scaffold 142
  Cu(II) removal efficiency 142
  dissolved in acetic acid-methanol mixture 132
  electrospun 145–151
  electro-wet-spinning 134
  glyoxal crosslinking agent 133
  hollow chitosan fiber preparation 139–140
  hydroxyapatite/tricalcium phosphate effect on 138
  mechanical properties and fineness 131
  microfluidic approach for 140
  moisture absorption capacity changes 143
  morphological analysis 144
  osteoblast cell proliferation on 145
  pH response 135
  production 131–135
  properties 132
  regenerated 151
  scaffolds 141, 144
  wet spinning 134
  wound dressings 141
chitosan/nylon 6 hybrid fibers 137
chitosan-poly (vinyl alcohol) blend fibers 139
chitosan-poly(lactide-co-glycolide) (PLGA) composite fibers 138
chitosan/PVA/PEDOT blend fibers 150, 151
chitosans 129, 131, 141, 927
chitosan solvent/solvent mixtures 127
chlorotriazine 901–903
Chord modulus 758
chromatographic analysis 512
chronic venous diseases 751
closed fleece hair 44
clothing comfort 860–861
clothing development
  five-stage evaluation system 863

clothing development (*contd.*)
full-scale clothing testing 866
human trials 870–871
material and fabric testing 864–865
thermal insulation 866–867
water vapour resistance 868–870
clothing system 844, 847, 860, 861, 864, 873–877
CNT/graphene based fiber actuators 691–693
CNT/PANI composite fiber-based textiles 669
CNT/PANI composite textiles 667
CNT-PDDA artificial muscles 368
CNT/polydiacetylene fibres 578
coan silk 83
coarse wool 41, 43, 45, 51, 58
coated textile electrode 243
coextrusion instabilities 291–292
collagen 29, 503
collagen composite fiber 165
collagen fiber
bioapplication 167
fiber as enhancer 167
isolation of 160
metal adsorption application 167–168
metal nanoparticle support 169
perspectives 171
source and structure of 157–160
spinning 160–165
template for synthetic metal fiber 168
collagen fibril 29, 157–160, 162, 165
collagen triple helix 158
color-changed fibers 362, 376
color-changed textiles 372
colored poly(trimethylene terephthalate) fibers 353
combed yarn 443–444
combined weaves 481–482
combing process 45, 47, 443
commercial cross-linked polyacrylic acid based SAP 316
commercially available poly-*p*-subsituted phenylene terephthalamide based aramid films 226
compact spinning 444
compact yarn 444, 873
composite electrospun fibers 149
compound weaves 482–483
compression bandages 753, 757–760, 765
compression molded thermoset polymers 24
compression stockings 428–430, 753, 759
compression therapy
chronic venous disorders 750–752
external pressure 752–753
fibrous material and construction 758–762
innovations 762–765
pressure prediction 756–758
role of fibers
fibrous based compression products 753–754
practical challenges 755–756
requirements 754–759
shape memory fibers for 765–768
conducting nanofibers 150
conducting polymers 239, 499, 565, 572, 686–688
conductive fibers 500
carbon based fibres 242–243
combined different concepts 243–244
conductivity 233–234
embroidery/sewing 248–249
fabric production 248
fibre material selection/yarn production 245–248
flexible devices 253
future trends 253–254
as industrial materials 30
intrinsically conducting polymer and coating 239–241
metal fibres, coating and deposition 234–239
printing techniques 249–250
textile electrodes 252–253

washable sensors 251–252
wearable electronics 253
conductive inks 253, 500–501
conductive polymer based fiber actuators 689, 690
conductive polymeric fibers 26
conductive textiles 233, 242, 722–723
conductive yarn 27, 235, 243, 246–248, 253, 500, 898
continuous fiber network, of carbon fiber 653
continuous filament yarn 441, 442, 450, 486
convective heat transfer 847, 849, 850, 861
conventional ELD 724
conventional fiber structure 368
conventional spinning 271–272, 365, 437
copolyaramids 210–211
co-polymer ink patterning 738–739
copper-doped $Li_4Ti_5O_{12}$/CNF composite 654
core diameter, of glass and optical fibers 601
core-sheath yarn 759
core-shell polylactic acid/chitosan fibers 150
core-shell structured nano fibers 422
core-shell yarns 247, 248
cortical layer 51–52, 56
cotton 437
cotton fibers 7, 512, 739, 903, 929
coulombic efficiency 650
count wool 41, 60
crimp 53–55, 350, 438, 455, 458, 463–466, 473, 484, 613, 872
crimped fibers 350, 438
crimpness, of wool 55–56
crisp set 536
cross-linked acrylic copolymers 319, 331
cross linked polyethylene elastic fibers 352
crystal-coil-crosslink model 424
crystalline aliphatic polyester 340
crystalline silicon (c-Si) 364
crystal transformation mechanism 377
cultivated silk 78
cuticle layer 51
cyclic *N*-halamines 932
cyclic-olefin polymer (COP) 301
cyclic transparent optical polymer (CYTOP) 606
Cyphrex™ 297

d

decorative textile motifs 248
defuzzification 538
depth filtration 785, 786, 809, 816
desizing 20
deuterated polymer 607
deuterinated polymers 607
diacids 210
dielectric elastomer based fiber actuators 691
dielectric electroactive polymers (D-EAPs) 688–689
1,3-Dimethylol-5,5-dimethylhydantoin (DMDMH) textiles 932
4,4′-diphenylmethane diisocyanate 425
directional frictional effect 56, 819
direct polycondensation 208, 210
direct/polymer laying 490
direct yarn count systems 17
disperse dyed PTT 343
disposable nonwovens 493
dithiolene metal complexes 898
domestic silkworm 75, 85
double-layer capacitor 651, 652
down wool hair 41
drawing machines 16
draw resonance 292
dry-jet-wet spinning of aramid fibers 215
dry SAP particles 329
dry spinning 117, 151, 214, 322, 335–337, 412, 415, 430
dry spinning of aramid fibers 214
dry spun cellulose nanofibrils 117
dry superabsorbent polymer 317
dual nozzle coaxial electrospinning setup 655

dyeing 20, 21, 52, 59, 62, 250, 346, 352, 353, 357, 734, 745, 902, 914
dyes 20
dye-sensitized solar cells (DSCs) 568, 667

e

EastOne 297
eccentric core-sheath bicomponent fibers 284
effective temperature (ET) index 860
EGCG-CF nanocatalyst 169
elastane fibers 343
elastic core yarn 235
elastic fibers
  bi-component 350–351
  classification 335–338
  definition 335
  future trends 356–357
  hard 353
  polyester 353
  polyether-ester 352–353
  polyolefin 351–352
  polyurethane 344–350
  structure & principle in elasticity 338–343
  structure & principle in other performances 343–344
elastic stress 355, 424
elastomeric fibers 6
elastomeric yarns 759, 761
electreted PVDF/ PTFE nanofibrous membranes 188
electrical conductive polymer based fiber actuators 690
electrically conducting fibers 301, 515, 518
electrically conducting polymers 686–688
electrically heated clothing (EHC) 876
electroactive materials 560, 562, 568, 581
electrochemical properties of cable battery 576
electrochromic fibres 577–580
electrode materials, for fibrous electronic devices 562
  carbon-based materials 564
  conducting polymers 565
  metals and metal oxides 562–564
electrohydrodynamic processing 145
electroless deposition technique 246
electroless metal deposition (ELD)
  aqueous-and air-compatible process 724
  catalytic moiety ink patterning 736
  conventional 724
  metal-deposited polymeric surface 724
  non-conductive textile materials 724
  polymer brushes
    advantages of 733–734
    anionic 732–733
    cationic 731–732
    fabricated metallic textiles 734–736
    nonionic 733
electroluminescence 370, 371, 375, 376, 378
electroluminescent device, fibre-shaped 581
electromagnetic radiation 597, 599, 889–891, 909
electro-netting process 176–178, 180–181
electronic textiles 499
  conductive fibres 500
  conductive inks 500–501
  fashion statements 515
  medical 518–519
  military 515
  pragmatic applications 518
  safety 518
electron spectroscopy for chemical analysis (ESCA) 511
electro responsive MPU fibers 421
electro-spinning 108, 162, 176, 177, 272, 366, 657, 773
  core-shell polylactic acid/chitosan fibers 150
  fundamental theory of 179
electro-spinning/netting (ESN) process 177

electrospinning set-up 657
electrospun cellulosic acetate (CA) fibers 273
electrospun chitosan fibers 145–151
electro spun composite phase change polyethylene terephthalate (PET) fibers 274
electro-spun fibers 422
electrospun fibers for filtration
  electro-netting 177–178
  electro-spinning 176–177
  future trends 199
  medium-high temperature filter 196–198
  normal temperature filter 185
  principles and theories 178–181
  structures and properties 182
electrospun nanofiber scaffolds
  mechanical properties 781–782
  polymer materials 782
  pore size 777–778
  porosity 775–777
  surface area 778–779
electrospun nanofibers/nets (NF/N) membranes 178
electrospun nanofibrous composite membranes
  barrier layer
    adsorption 785–788
    size exclusion 783–785
  challenges 799
  support layer
    nanofiltration and reverse Osmosis 795–797
    ultrafiltration (UF) membranes 789–794
electrospun nanofibrous membranes 176, 784, 799
electrospun PAN nanofiber scaffold 784, 790, 793, 795, 797, 798
electrospun substituted Kevlar nanofibers 216
electrospun trilayer non-woven mats 656
electrostatic attraction 63, 808–810
electrostatic spinning 176
elementary fibrils 100–102, 104–107
embroidered carbon fibers 244
embroidered textile current collector 252
embroidery/sewing 248–249
encapsulated PCM 270, 271
encapsulation 238, 292–293, 641, 745
end emitting optical fiber 595, 597, 612, 613, 623, 643
energy density 576, 650
energy dispersive X-ray analysis (EDX) 500, 513–514
energy harvesters
  mechanical 570–572
  thermal 566–568
energy harvesting devices 667–671, 700, 745
energy storage systems (ESS) 263, 653, 657, 665, 672
environmental pollution 175
enzyme 161
epigallocatechin-3-gallate (EGCG) 169
ericulture 81
eri silk 81, 84, 87
ethylene glycol diacrylate 319
ethylene maleic anhydride copolymer 319
1-ethyl-3-methylimidazolium acetate 108, 109
eutectic PCMs 267
evaporative cooling clothing (ECC) 874
external quantum efficiency (EQE) spectra 745
extrinsic sources of attenuation 603, 604

f

fabricated metallic textiles, PAMD 734
fabric making technologies
  braiding 493–496
  future trends 496
  knitting 485–490
  nonwovens 490–493
  weaving 479–481
fabrics 872
  apparent faults 61
  definition 477

fabrics (*contd.*)
embroidery techniques 248
and fiber based membranes 372–373
production 248
structures 477
thermal insulation performance 873
wettability 863
Fagara silk 83
far infrared bi-component elastic fiber 350
fashion statements 515
fiber based actuators 374, 683
carbon nanotubes 689–693
dielectric electroactive polymers 688–689
electrically conducting polymers 686–688
piezoelectric materials 684–686
shape memory materials 683
twisted/coiled fibers 694
types 694
fiber-based energy generators 557
fiber based functional fabrics 372
fiber-based piezoelectric materials 381
fiber-based sensors 694
scaling up of 710
strain and pressure sensors 696–705
working principle 695
fiber Bragg grating (FBG) 704
human vital signs 398
multi-vital sign measurement 404
sensing method 391, 395
smart textiles 405
fiber electrode wrapped fibre devices (FEWFDs) 560–561
fiber material selection 245–248, 250–251
fiber-mat thermoplastics 24
fiber-optic biosensors (FOBS) 26
fiber-optic chemical sensors (FOCS) 26
fiber optic gyroscope 391, 683
fiber-optic sensors
advantages 394
bio-medical measurement 397
human vital signs 398
multi-vital sign measurement 404
oxygen concentration measurement 395
partial least squares regression calibration for blood pressure measurement 402
pulse rate measurement 400
pulse wave measurement 399
respiratory rate measurement 400
smart textiles 405
strain measurement 395
temperature measurement 395
fiber optics principle 595
fibers 435
consumption 436–438
defined 2
effects of time, temperature, and moisture 440
elastic recovery 440
as electronic devices 26–27
for flame and thermal protection 28
health/stress/comfort management 27–28
historical evolution 2
for medical compression garments 27
parameters 438
for radiation protection 28–29
requirements 2
resilience 440
stiffer 436
stress–strain curve 438–440
for tissue engineering 29–30
in water treatment process 25–26
work of rupture 440
fiber sensors 682
fiber shaped actuators 362, 688
fiber shaped electronic devices 557–561
fibre electrode wrapped fibre devices 560–561
mechanical energy harvesters 570–572
parallel coil fibre devices 561–562
sheath-core single fibre devices 561
solar cells 568–570

thermal energy harvesters 566–568
twisted fibre devices 559–560
fiber-shaped electronic devices
characterization techniques and key parameters 583
electroluminescent device 581
lithium ion batteries 575–577
sensors 581–583
structures of 559
supercapacitors 572–575
transistors 580–581
fiber shaped OLED 371
fibrillar model 813, 814
fibrillogenesis of collagen 158
fibroin 78, 84
amino acid composition 78
amino acid residues 78
in *Bombyx mori* 78
molecular weight 78
molecule 8
fibrous based compression products 753
fibrous energy materials
centrifugal spinning 657, 658
characterization techniques 653–656
electrodes, fibrous structure of 653
electrospinning 657
fabrication approach 657–659
porous fiber structure 654
separators 656–657
tubular fiber structure 654
fibrous filter media 176
cross-section, role of 823–825
pore-size, role of 825–826
fibrous materials
advantages 30–31
antimicrobial 927
atomic force microscopy 515
biological properties 14
categories 2
characteristics 6–7
chemical properties 14–15
chromatographic analysis 512–513
classification of 2
desirable properties 15
electronic textiles 499, 500
energy dispersive X-ray analysis 513–514
fashion statements 515
Fourier transform infrared (FTIR) spectroscopy 507–509
medical textiles 501–506, 518–519
military 515
morphological and structural properties 7–10
performance tests 521
photocatalytic self-cleaning 499
physical properties 10–11
polymeric chains, phases of 5
pragmatic applications 518
safety 518
scanning electron microscope 515
self-cleaning textiles 506–507, 519
superhydrophobicity 499
thermal properties 14
X-ray diffraction 509–511
X-ray fluorescence 512
X-ray photoelectron spectroscopy 511–512
fibrous materials, origin of 2
filter media
characterization of f 826–827
clothing 807
definition of 808
fibrous 823
fibrous materials
classification of 811
fine and morphological structures of 811–814
interception mechanism 809
mixed and bulk phase 808
nonwovens 807
requirements 810–811
filtration textiles
bulk and mixed phase 809
fibers in 817
forms of fibrous substrates
interloped fabrics 816–817
membrane 817
nonwovens 816
roving 815
woven/interlaced fabrics 815
yarn 814

filtration textiles (*contd.*)
hot/cold 809
intimate and non-intimate mixing 808
market potential 827
non-spontaneous mixtures 808
pressure difference/pressure drop 809
solid-liquid mixture 808
theory of 809
fineness of wool 52, 53, 58
fine wool 52
from domestic and modified sheep breeds 60
domestic fine wool tops 60
finishing process 21
fire-retardant fibers
chemically modified flame resistant fiber 833, 835, 836
inherently flame resistant fiber 833, 836–839
first-generation Li-ion cell 650
fish wool 83
flame-resistant viscose fibers 28
flammability 836, 839–841
flax 1–3, 7, 25, 245, 811, 820
fleece wool 44, 58
flexible devices 253, 557
flexible double rapier looms 479
flexible electronics 681, 682, 709, 736
fluorescent silk thread 91
fluoroolefins 608
fluoropolymers 606, 608, 817
foldable geometry 957–959
forward osmosis (FO) 780, 789, 797
Fourier transform infrared (FTIR) spectroscopy 500, 507–509
four-layer bandaging systems 757
free radical polymerization (FRP) 319, 728, 932
freeze-drying assisted self-assembly 114
freshly spun GO fiber hydrogel 362
frictional spun yarns 448
friction spinning 15, 17, 247, 448
fringed micelle model 7
full-scale clothing testing 866
functional textiles 22
properties 22
water repellent 22–23
water vapor permeability 23–24
fuzzification 537
fuzzy inference system (FIS) 538–539
fuzzy linguistic rules 551
fuzzy logic 535
fuzzy sets 536
membership function 536–538
fuzzy modeling 538, 539
fuzzy sets 536–538, 541–543, 548

g

gas sensors 518, 705
Gaussian membership function 537, 548
gelatin 160, 939
genetic algorithm (GA) 529, 539–541
genetically engineered silks 91
genetic inheritance operators 540
Georgia Tech Wearable Motherboard (GTWM) 722
glass fibres 26, 222, 437, 478, 594, 601, 622, 820
glass optical fibers (GOFs) 392, 394, 406, 594, 704
glutaraldehyde vapors 147, 150
glycine 76, 85, 132, 158, 895
gold nanoparticles (AuNPs) 169, 241
GORE-TEX 821, 833, 869
Grace-flexi fibers 610
graded-index (GI) POFs 301
graded index profile optical fiber 598, 599
grade wool 60
grafting-to' strategy 726, 727
GranuGel 329
graphene 242, 564
fibers 365
nanoplates 903
woven fabrics 242
graphite nanoplatelets (GNP) 242
gravimetric specific capacity/capacitance 650
grease of wool 59

"green" fiber 167
guard hairs 39

h

Hagen–Poiseuille equation 776
hair fibers 3, 5, 7, 8, 37, 44, 45
hand protecting device 916
hard computing 529
hard elastic fibers 338, 341, 342, 356
Havenith model 877
heating textiles 248
Heating Ventilation and Air-Conditioning system (HVAC) 194, 827, 876
heat management 891, 910–912
heat transfer performance (HTP) 843, 844
heat transfers 858
heat transfer through textiles 861
helical auxetic yarns 967
helical (non-α spiral) polypeptide chains 157
heterogeneous hair 44
heterotypical wool fiber 43
hierarchically arranged helical fibrous actuators 362
highly absorbing polyelectrolyte polymer-based materials 315
highly designed ZnO nanowire arrays 364
highly sensitive textile-based pressure sensor 238
high performance fibers 1, 5, 7, 221, 821, 823, 826
high performance fibrous materials 24
  for automobile composite 24
  auxetic applications 25
  as building materials 25
  environmental protection 25–26
  optical applications 26
high purity medical grade chitosan 125, 127
high temperature ceramic fibers 5
hollow core Bragg fiber 616
Hollow cross sections 823
hollow fibers 5, 27, 139, 226, 285, 421, 872
homogeneous wool 44, 60
horizontal wicking 863
Huggies® 329
human civilization, evolution of 2–3
human thermal balance 859
human thermoregulation 857–858
humidity and temperature sensing fibers 705, 707
hyaluronic acid (HA) 938–939
hybrid cooling clothing 874
hybrid cooling strategy 875
hybridization 26, 39, 541
hybrid PVDF/ZnO dual components device 572
hybrid soft computing systems 541
hydrogen-bond networks in cellulose Iα 99, 100
hydrogen bonds 50, 67, 99, 104, 105, 159, 217, 218, 224, 338, 340
hydrolyzed starch-graft-polyacrylonitrile product 316
hydrophilic fibers 25, 818, 819
hydrophilic sodium polyacrylate powder 317
hydrophobic bonds 159
hydrostatic pressure 752
hydroxyalkyl methacrylate based hydrogels 316
hydroxyapatite (HAP) 137–138, 149, 150, 165
hydroxylysine 158
hydroxyproline 158, 159
hygroscopic fibers 25

i

immobilized avidin 241
immobilized bayberry tannins 168
impurities of wool 59
incident photon-to-current conversion efficiency (IPCE) 670
indirect yarn counting system 18
individual microfibrils 101, 158
individual TC monomers 158
industrial grade chitosan 125, 127
industrial protective apparel 225

inherently flame resistant fiber 833, 836–839
ink-jet printing 238, 243, 249, 250, 736–739
inorganic fibres 1, 6, 207, 437
inorganic nonmetallic materials 364
inorganic PCMs 266–267
in-plane wicking 863
intelligentization method 356
interface modification layer (IML) 744
interface pressure 749, 756–763, 765
interfacial adhesion 167, 290–291
interlaced fabrics 815–816
intermittent pneumatic compression (IPC) 754, 756
intertwining among branching jets 180
inter-yarn friction 455
intrasite 329
intrinsically conducting polymers (ICPs) 239, 500, 723
intrinsic sources of attenuation 603
ionic bonds 159
IREQ model 877
irregular woven structure 457
IR shielding 910–912
islands-in-the-sea fibers 285, 297
islands-in-the-sea filaments 283, 284, 297

j

jet looms 479, 480

k

Kemp's racetrack model 465
keratin 8
  extraction, from wool 70–71
  protein 70
Kevlar 208, 821
Kevlar 29 217, 220, 225
Kevlar 49 217–219
Kevlar 117 217
Kevlar 147 217, 220
Kevlar aramid yarn 220
Kevlar reinforced 80/20 PBA/PU composite panel 225
Knee Sleeve 518, 519
knitted construction 759
knitted fabric structures 428, 486–488, 546
knitting
  applications 489–490
  knitted fabric structures 486–488
  knitting machines 485–486
  properties 488–489
knitting machines 19, 485–489, 546, 816
knitting process 19, 248, 435, 477, 759

l

lanolin 46, 53, 57, 58
Laplace's Law 756, 757
latent heat storage (LHS) 263, 264
LED lifetime 639, 640
left-handed helical (non-α spiral) polypeptide chains 159
"leveling effect," 778
Levenberg–Marquardt algorithm 533–534, 548
Lewis Ratio 865
$LiFePO_4$/CNF freestanding cathodes 663
LiF/Fe/CNF cathodes 663
Li-ion batteries
  carbon coated Si/CNF composite nanofibers 660
  carbonized $SnCl_2$/PAN nanofibers 662
  electrodeposited SnO_2 662
  electrospun PAN-based CNFs 659
  graphite 659
  hematite iron oxide 662
  Li_2MnSiO_4 cathode 663
  Si/CNF composites 660
  Sn/Cu/CNF core-shell structures 662
  twisted aligned MWCNT fiber 661
  twisted aligned MWCNT/Si composite fiber 661
limiting oxygen index (LOI) 221, 821, 833, 839, 840
linear density of fiber 438
linearity (LT) 464, 465, 634
linear programming problem, for yarn 544, 545

line illumination hybrid system (LIHS) 595, 637
active illumination 638
advantages 642
for clothing and accessories 642
for fashion 642
portable powering structure 640
structure 637
lipid content, of wool fiber 59–60
liquid cooling clothing (LCC) 874
liquid-core fibers (LCF) 302–303
liquid crystalline polymer (LCP) 293, 958–959
liquid sorption mechanism 318
liquid water transfers 862
Li-S batteries 663, 665
lithium chloride/dimethylacetamide (LiCl/DMAc) solvent system 108
lithium-ion battery (LIB) 640
fibre-shaped 575–577
principles of 650–651
silica/PAN membrane separator 656
lithium phosphorus oxynitride electrolyte (LiPON) 642
long wool 41, 54
loose wool 44
low density cross-linked SAP 316
low self-discharge nickel–metal hydride (NiMH) rechargeable batteries 641
low temperature polycondensation 208–210
lumen fluid 285
luminescence fibers 375–376
lyotropic solution 212, 213, 215, 217

m

Mach–Zehnder interferometry 398
macrobend sensors 704
macro-scaled continuous cellulose fibers 114
maleic anhydride polypropylene (MAPP) 321
Mamdani FIS 538, 539
m-aminophenylhydantoin (m-APH) 932
man-made fibers 2, 4, 6, 163, 245, 293, 328, 415–416, 811–812, 823
manufactured fibers 4, 15, 207, 438
m-aramid fibers 207, 227
m-aramid nanofibers 216
m-aramid nanofibrous membrane 225
materials-based actuation technologies 682
matrix-assisted catalytic printing (MACP) 736
Maxwell stress 688
Maypole braiding machines 493, 494
mechanical energy harvesters 570–572
mechanical humidity sensors 705
mechanically derived microfibrillated cellulose 104
medical compression 773
fibers for 27
stockings 753
medical textiles 492, 499, 501–506, 518–522
medium wool 41
medullary layer 52
medullated wool 44
meltblowing process 491
meltblown fabrics 492
melted/semi-melted PCM 268
melt-spinning 281
melt-spinning equipment 285–286
melt spinning method 343, 365, 425, 960
melt-spun bicomponent fiber 293
membrane bioreactor (MBR) application 798
membrane distillation (MD) 789, 798, 799
memory fibrous materials 30
memory polymers (MPs) 765, 766
characterization of 428
components 424–425
electro-spun fibers 422
evaluation of shape-memory properties 413–414
future trends 430
mechanism of stress memory 423–424

memory polymers (MPs) (*contd.*)
morphology and molecular mechanism 412–413
post spinning operations 417
potential application of 428–429
recent advances 430
smart hollow fibers 421
stress-memory 422–423
stress-memory behaviour 425–427
wer or melt spun fibers 415–417
memory polyurethanes 28, 412, 422, 423
memory stress 422–429, 765
meso-tetra(4-carboxyphenyl) porphyrin (TCPP) 507
Messphysik ME46 video extensometer 962
meta-aramid 28, 821, 833, 837–839
metabolic heat production 859, 860
metal-deposited textile 724
metal fibers 168, 234–239, 246, 247, 437, 907
metallic fiber sensors 705
metal related smart fibers 363
metals and metal oxides modified fabrics
oligodynamic effect 934
titanium dioxide 934–935
metal staple fibres 437
meta-oriented phenylene rings 219
micellar model 813, 814
microbend sensors 704
Microdictyon tenuous cellulose 98
microfibers 165, 285, 297, 658, 662, 789
microfibrillated cellulose (MFC) 102, 104
microfibrils 7, 96, 97, 100–103, 106–108, 113, 158–160, 219, 338
microfiltration 783, 784, 786, 788, 789, 798
microfluidic approach for chitosan fiber preparation 140
microfluidic spinning 164–165
microfluidizer 103, 104
micronaire 544
microporous auxetic fibers 968
microstructured optical fibers 604
microwave irradiation 129, 216
microwave shielding 906–910
Mildew resistant 927
milk filtration 820
mineral fibers 1, 4, 437
miniaturized sensors 233
moisture bed sensor 251–252
moisture sensitive auxetic fiber 966–967
moisture transfer through textiles 861–863
moisture vapour diffusion 862
monochlorotriazine 903
montmorillonite (MMT) clay 324
Morphotex® 298, 299
molting 80
MPU filaments (MPFs) 415
MPU–MWNT fiber 422
muga silk 76, 82, 87
mulberry silks 85
defined 78
non-mulberry 80–81
types of 79–80
worms and cocoons 78
multifilament yarn 441
multilayer compression bandaging system 759, 764
multi-layer multicomponent bandaging system 758
multimode optical fibers 593, 599, 600
multivoltines 79, 80
mussel silk 83

n

nanocellulose assembly 110, 111, 119
nanocellulose fibers
biomedical applications 118
freze drying 112
nanocellulose self-assembly 110
nanofiber filters
functional properties 189–191
with high-efficiency and low pressure drop 185–189

nanofiber membranes
  structure and species of 183–185
  types and structure of 181–183
nanofibers 285
  aramid 216
  systems 773
nanofiltration 788, 795–797
Nanofront™ 297
nanogenerators 667, 671
nanoscale aramid fibers 216
nano-scaled cellulose fibers 100, 118
nano-scaled silk fibroin 347
nanosized sensors 233
NaOH/urea solvent systems 109, 114
native cellulose I crystalline structure 97, 114, 115, 119
natural collagen fiber 157, 160, 167, 171
natural fibers 2, 7
  advantages 30–31
  as building materials 25
  drawbacks 2
  feature 7
  historical evolution 2
natural fibrous materials 3
natural length 53, 54
natural materials 92, 167, 863
natural microfibrils 7
natural polymers
  alginate 939–940
  chitosan 940–941
  gelatin 939
  hyaluronic acid (HA) 938–939
natural protein fibers 37, 38, 50
natural silk fibroin 347
NatureWorks™ 71
near field electrospinning (NFES) 686
needled nonwoven materials 329
needlepunched nonwoven fabrics 552
needle punching technique 491
net raw wool rate 59
Newton-type sweating thermal manikin 866
N-halamine
  coating 932
  cross-linking 931–634
  electrospinning 933
  grafting 932
  principles of 931
N-halamine textile 928
nickel-titanium (NiTi) alloy 683
Ni core-shell NPs 169, 170
Nitinol 683
nitrogen-doped carbon nanofibers (N-CNFs) 653
N,N'-methylene bisacrylamide 319
nodule and fibril-based structure 956
Nomex 5, 207, 208, 214, 219, 226, 821
non-circular cross-sections of fibres 823
non conductive standard textile fibres 248
non-covalent crosslinkers 150
nonionic polymer brushes 733
non-miscible polymers 291
non-mulberry silks 80
  Anaphe silk 82
  coan silk 83
  eri silk 81–82
  Fagara silk 83
  muga silk 82
  mussel silk 83
  oak tasar 81
  spider silk 83
  tasar silk 80–81
non-mulberry silks 80, 83–88
non mulberry silkworms 75, 78
non-polar solvent 323
non-structural composites 24
non-textile fibers 2, 3, 10
nonwoven fabrics 19, 25, 437, 551
nonwoven fabric technology 478
nonwoven fibrous membranes 175, 785
non-woven meta aramids 28
non-woven nanofiber scaffolds
  electrospinning 778
  morphology of 776
  polyester 779
  pore size 777–778
  porosity 775–777, 781
nonwovens 759, 816
  applications 493
  manufacture of 490–492
  properties 492

normal temperature filtration media 185
N6–PAN NNB composite membranes 193
N-substituted Kevlar 216
Nu-Gel 329
numerical aperture 598, 605, 606, 614, 619
nylon-6 182
nylon fibres 25, 759
nylon 6–polyacrylonitrile nanofiber-nets binary (N6–PAN NNB) structured membrane 192

o

oak tasar 81
Oasis 100 329
OASIS Super Absorbent Fibre (SAF) 316, 328
Oasis superabsorbent yarn 319
oil super-absorbent polymer (oil-SAP) 318
olefin-based stretch fiber 337, 338
oncotic pressure 752
open fleece hair 44
optical fibers 6, 26, 593
  advantages 593
  cladding, refractive index 596
  classification 392
  fiber-optic sensors 394
  future trends 406
  general characteristics 394
  inorganic 593
  internal reflection 597
  manufacturing process 392
  multimode 599, 600
  properties and functionality 596
  single-mode 599
optical fiber sensors 394–404, 406, 704–706, 709
optical material 391
optical total internal reflection 704
organic electrochemical transistors (OECTs) 241, 580–581
organic field effect transistors (OFETs) 241, 580–581
organic PCMs 265–267
oriented carbon nanotube fibers 365
oxidation method 57
4,4′-oxydianiline 210
oxygen concentration measurement 395

p

P84 28, 821, 823
PA-6/boehmite nanofibrous membranes 187–188
PA-6 electrospun nanofibers 185
palladium (Pd) nanoparticle catalyst 169
Pampers® 329
PA-66 nanofibrous membranes 185
PA-6 NF/N membranes 193–195
PANI/CNT fibre supercapacitor 572
PAN micro/nano fiber 658
PA-6/oligomer system 180
para-aramid 28, 821, 833, 837–839
paraboloid reflector system 619
parallel coil fibre devices (PCFDs) 558–559, 561–562
PA66-random copolymer side-by-side hosiery yarn 282
p-aramid 207–209, 212, 214, 219, 221, 222, 226, 227
partial least squares regression (PLSR) 402–404
particle filtration 190, 199, 809, 820, 823
particle radiation 891
particulate matter (PM) 175
patterned hybrid nanofiber membrane 372
PBI polymer 837, 838
PBT/PBAT core-sheath fibers 289
PBT/PET three-dimensional crimped fibers 350
PCM/polymer hollow fibres 271
PEDOT-based dual functional fibre 579
Peirce geometrical model of cloth 613
Peirce's geometrical model 458–459
pentamolters 80
perovskite solar cells 568, 570

personal cooling clothing (PCC) system 874–875
personal cooling strategies (PCSs) 874
personal heating clothing system 876–877
PET embedded PA-6 NF/N filter 195
PET/PE bicomponent fibers 289
PET/poly(butylene succinate/L-lactate) (PBSL) 290
PET/poly(L-lactic acid) (PLLA) 290
PET/polyamide 6 (PA6) bicomponent fibers 290
PET/poly(phenylene sulfide) (PPS) bicomponent fibers 290
phase change cooling clothing (PCMs) 874
phase change fibers 6, 263–276
phase change materials (PCMs)
  automotive industries 275
  beddings and accessories 275
  coating process 270
  conventional spinning 271, 272
  electrical applications 275–276
  electrospinning 272–274
  eutectic 267
  in fibrous structure 267–268
  gloves 275
  hospital applications 274–275
  inorganic 266–267
  microencapsulation 268–270
  organic 266
  principle of 264–265
  shoes and accessories 276
  space suits 275
  sports wear 274
phase separation of charged droplets 180, 788
photoactive chemicals modified fabrics
  LAAA 935–936
  organic photoactive reagents 936–937
  photo-induced biocidal effect 935–936
  textile modification with TiO_2 936
photoluminescence 370, 375
photonic band gap (PBG) fibers 616
Pierce geometric model, of cloth 613
Pierce's geometrical model 465
piezoelectric devices 570–571
piezoelectric effect 251, 671, 684
piezoelectric fiber-based actuators 686, 687
piezoelectric fibers 362, 365, 686
piezoelectric fiber sensors 700
piezoelectric material based fiber actuators 687, 688
piezoelectric nanogenerator 27, 671
piezoelectric sensors 700, 703
piezoresistive fiber based sensors 696, 697, 699
Pinna squamosa 83
plain, twill and satin/sateen weaves 481
plain weave 456, 460, 463, 473, 481, 484, 567, 815
plain woven fabric 464
  anisotropy 464–465
  crimp in warp and weft yarns 463–464
  extended in a bias direction 463
  extended in principal direction 462–463
plain woven fibrous assembly 13
plastic optical fiber (POF) 301, 391, 395, 593, 601, 704
ploy ether sulfone (PES) 196, 781
PMETAC 731–733, 735
PMETAC brushes 730–732, 734, 737
Poisson, Siméon 953
Poisson's ratio (PR) 463, 629, 953, 963, 964
poly(1,6-hexanediol adipate) 425, 767
poly(3,4-ethylenedioxithiophene) (PEDOT) 26, 30, 150–151, 241, 243, 501, 518, 565, 572, 578–579, 710
poly(3-hexylthiophene) (P3HT) 241, 581
poly(4-vinylpyridine) (P4VP) 733
poly(acrylic acid) (PAA) 29, 180, 189, 316–317, 324, 374, 659, 666, 705, 731, 732
poly(benzophenone isophthalamide) (DBF/ISO) 226

poly(ethylene oxide) (PEO) 29, 185, 189–190, 340, 504
poly (fluoroalkyl acrylates) (PFA) 608
poly(lactic acid) (PLA) 29, 90, 136–137, 139, 144, 150, 165, 241, 300, 686, 687
poly(*m*-phenylene isophthalamide) (*m*-DPI) 194, 208, 212, 219, 821
poly(methacryloyl ethyl phosphate) (PMEP) 730, 732–733
poly(*N* isopropyl acrylamide) 165
poly(*N*-isopropylacrylamide) (PNIPAm) 165, 369, 374–375, 380
poly(*N*-vinyl pyrrolidone) (PVP) 29, 198, 504, 654, 659
poly (*p*-benzamide) (PBA) 212, 225
poly(*p*-phenylene) (PPP) 239, 240
poly(*p*-phenylene benzobisthiazole) 221
poly(*p*-phenylene terephthalamide) (PPTA) 10, 209–210, 212–214, 217–219, 221–222
poly(*p*-phenylene vinylene) (PPV) 239
poly (propylene) (PP) 175, 191–192, 241, 243, 285, 289–290, 292, 296, 318, 321, 329, 338, 342, 344, 786, 960–962, 967–968
poly(trimethylene terephthalate) (PTT) 291, 337, 341–343, 350, 353, 401–402
poly(vinyl alcohol) (PVA) 29, 109, 136, 139, 144, 150–151, 184–185, 224, 242, 249, 297, 319, 324, 381, 504, 572, 659, 705, 740, 782, 784, 788, 790, 793, 797
poly (fluoroalkyl methacrylates) 608
polyacetylene (PA) 180, 184–188, 191–196, 239–240, 291–292, 298–299, 302, 351
polyacrylamide copolymer 319
polyacrylic acid 316–317, 374, 705
polyacrylonitrile (PAN) 182, 271, 316, 653, 733, 782, 898
polyacrylonitrile/poly(acrylic acid) (PAN/PAA) nanofibrous membranes 189
polyalkylene terephthalate 352
polyamide (Nylon) fibre 437
polyamide-imide 838
Polyamide/Lycra 235
polyamide-66 (PA-66) NF/N membrane 191
polyamide 6 nonwoven 235
polyamide-6/poly(m-phenylene isophthalamide) nanofiber/net (PA-6/PMIA NF/N) membranes 194
polyamides 1, 10, 25, 27–28, 207–211, 226, 243, 245, 291, 299, 302, 343, 491, 759, 790, 795–797, 811, 817, 820, 836, 895, 900–901, 906, 913, 965–966
polyaniline (PAn or PANi) 239–241, 518, 572, 574, 580, 667–669, 686, 689, 705, 709, 903
polybenzimidazole (PBI) 182, 659, 823, 832, 837–838
polybenzoxazine (PBA)/urethane prepolymer (PU) alloys 225
poly[1,1′-bis(4-vinylbenzyl)-4,4′-bipyridinium dinitrate] (PVBVN) 731–732
polybutene-1 342
polybutylene terephthalate (PBT) 289, 337, 340–343, 350–353
polycaprolactone (PCL) 29, 165
polycaprolactone (PCL) composites 167
polycaprolactone(PCL) loaded nattokinase (NK) 369
poly (hexane-1 6-carbonate) diol, 348
poly (pentane-1 5-carbonate) diol, 348
polydioxanone (PDO) 165
polyester elastic fibers 335, 337, 341, 343, 353, 356
polyester fabrics 241–242, 246, 735, 863, 902, 903
polyesters polylactide (PLA) 29, 136–137, 139, 144, 150, 165, 240–241, 300, 686–687
polyether-ester (PEE) elastic fiber 337–338, 340–341, 344, 352–353, 357
polyetherimide 196

polyetherimide-silica (PEI-SiO_2) nanofibrous membrane 196
polyethersulfone (PES) electrospun nanofiber scaffolds 781
polyethylene (PE) 5, 109, 175, 194, 243, 271, 285, 304, 341–344, 352, 430, 496, 607, 694, 817, 826, 960, 963–964
polyethylene (POE) jacket 351, 609
poly-(3,4-ethylenedioxythiophene) (PEDOT) 26, 30, 150–151, 241, 243, 501, 518, 565, 572, 578–579, 710
polyethylene terephthalate (PET) filaments 194, 243, 273, 343, 518, 783, 811, 820, 826–827
poly(trimethylene terephthalate) (PTT) fiber 291, 337, 341–343, 350–351, 353, 401–402
polyfluorene (PF) 239–240
poly(vinylidene fluoride) (PVDF) hard elastic fiber 344
polyhexamethylene biguanide (PHMB) 504, 930
poly(benzophenone-5-tert-butylisophthalamide) (DBF/TERT) homopolymers 226
polyhydroxyalkanoate (PHA) 300, 767
polyimide 196, 371, 659, 732
polyimide fibers 28
polylactic acid (PLA) fiber actuators 686
polymer-assisted metal deposition (PAMD)
  ELD
    advantages of 733–734
    anionic polymer brushes 732–733
    catalytic moieties 736–737
    cationic polymer brushes 731–732
    fabricated metallic textiles 734–736
    nonionic polymer brushes 733
  mechanism of 728–731
  metallic trace in
    catalytic moiety ink patterning 736–737
    co-polymer ink patterning 738–739
    R2R printing technology 736
  polymer brushes 725, 726
polymer based fibers 365, 684, 689–690, 820
polymer-based sensors 709
polymer brush
  cationic 731–732
  nonionic 733
polymer brushes 725
  advantages of 728, 733
  anionic 732–733
  grafting 730
  macromolecular chains 726
  organosilane initiators 730
  PAMD 725, 726
  surface modification of materials 725
polymeric micro/nanofibers
  electrospinning 108
polymeric N-halamines 932, 933
polymeric/plastic optical fiber (POF) 593, 704, 706
  characteristics 594
  cladding material requirements 608
  core attenuation 607
  CYTOP 606
  fabrication materials 604
  illumination systems 636–642
  jacket selection requirements 608–609
  light transfer rate 607
  local side emission 620–622
  maximum operating temperature 607
  mechanical properties 627–635
  optical attenuation 623–627
  PMMA core 604–608
  polycarbonate core 605, 606
  with polymethylmethacrylate 593
  polystyrene core 606
  thermal properties 635–636

polymerization 4, 96, 163, 208, 238, 268, 316, 340, 367, 412, 415, 500, 603, 667, 726, 784, 872, 932
polymer materials 319, 603–604, 782, 895
polymer optical fibers (POFs) 301, 391–392, 601, 618
polymer solar cells (PSCs) 560, 564, 568, 742, 744–745
polymeta-phenylene isophthalamide 196, 821
poly-4-methyl pentene 342
poly-(4-methyl-1-pentene) (PMP) (TPX) 344
polynanocrystalline yttria-stabilized zirconia (YSZ) nanofibrous membranes 198
poly (vinyl alcohol) nanofiber 109, 139, 242, 273, 297, 319, 504, 659, 705, 782
polyolefin based bicomponent fibers 298
polyolefin elastic fibers 341, 351–352
polyolefin elastomer 351–352, 607
polyolefin-fibres 341, 351, 357, 437
polyolefin plastomer (POP) matrix 304
polyoxyethylene 338, 352
polyoxymethylene (POM) 344
poly(4-methacryloyl benzophenone-*co*-2-methacryloyloxy ethyltrimethylammonium chloride) [P(MBP-*co*-METAC)] 739
polypivalotactone 342
poly(3,4-ethylenedioxythiophene) poly(styrene sulfonate) (PEDOT + PSS) 243
poly(butylene terephthalate) (PBT)/poly(butylene adipate-co-terephthalate) (PBAT) 289
poly (3-methylthiophene) (P3MT) polyester fabric 241
poly(ethylene terephthalate) (PET)/polystyrene (PS) bicomponent spinning 289
polypropylene (PP) 2, 25, 175, 191–192, 241–243, 271, 285, 289–290, 292, 296, 318, 321, 329, 338, 342, 344, 437, 491, 694, 786, 811, 817, 820, 826–827, 960–963, 967–968
polypropylene monofilament fibers 271
polypropylene oxide 338
poly(3,4-ethylene dioxythiophene) p-toluenesulfonic acid (PEDOT + PTSA) 241
polypyrrole (PPy) 26, 239–241, 243–244, 363, 501, 509–511, 518, 565, 686
polysaccharide pullulan (PULL) 324
polystyrene 182, 241, 268–269, 289, 297, 394, 565, 593, 606, 704, 782
poly[styrene-*block*-(ethylene-*co*-butylene)-*block*-styrene] 304
polysulfone/polyacrylonitrile/polyamide-6 (PSU/PAN/PA-6) filtration medium 194
polytetrafluoroethylene (PTFE) 188, 225, 607, 618, 733, 817, 821, 833
polytetrafluoroethylene nanoparticles (PTFE NPs) 188
polytetrahydrofuran 338
polytetramethylene oxide (PTMO) 340
polythiophene (PT or PTh) 239–240
polytrimethylene terephthalate (PTT) fiber 291, 337, 341–343, 350–351, 353, 401–402
polydimethylsiloxane (PDMS) 164, 242, 340, 351, 514, 518, 577, 671, 702
polyurethane (PU) 6, 67, 165, 184, 225, 238, 326, 335, 370, , 582, 683, 873, 955
polyurethane elastic fibers 344, 346–350
polyurethane raw materials 336

polyvinyl alcohol (PVA) 29, 109, 136, 139, 144, 150–151, 184–185, 224, 242, 249, 297, 319, 324, 381, 504, 572, 659, 705, 740, 782, 784, 788, 790, 793, 797
polyvinyl alcohol copolymers 319
polyvinylidene fluoride (PVDF) 148, 184, 188, 302, 344, 514, 572, 665, 685–687, 694, 700, 733, 782, 784, 789–790, 793, 795
porosity ratio 11
porous carbon nanofiber 655, 656, 670
porous CNFs production 667
porous 1D α-Fe_2O_3/CNF nanofiber production 662
post spinning operations 412, 417–421
power density 572, 576, 640, 650–651, 653, 665
pressure-driving filtration process 781, 793
pressure drop 176, 185–192, 194–199, 293, 547, 750, 760–762, 768, 779, 785, 809–810, 817, 820–821, 826
pressure relaxation 761
pressure sensing 381, 696, 699–700, 704, 765
primary fiber structure 367–369
printing techniques 238, 249–250, 736–737
pristine *m*-aramid polymer 216
projectile weaving machines 480
protective jacket 917
protein fibers 3, 7–8, 14, 20, 37–38, 50, 163, 895
PRS® paraffin wax 269
pseudocapacitors 579, 651–652
Pt doped porous carbon nanofibers (Pt/N-PCNF) 670
Pt-supported N-doped porous CNF 671
PU56-118 415
PU66-118 415
pulse rate measurement 400
pulse transit time (PTT) 291, 337, 341–343, 350–351, 353, 401–402
pulse wave measurement 399
pulse wave velocity (PWV) 401
Purilon 329
PVA-co-PE nanofibers 381
PVA (polyvinyl alcohol)/PAA (poly acrylic acid)-AM (acrylamide) based superabsorbent fibers 324

q

quantum energy 889
quaternary ammonium compounds (QACs)
  environmental impact 929–930
  mechanism of 929

r

radiation protection, fibers
  absorption 892
  aramid fibers 895
  durability 905
  future aspects 918
  IR shielding/heat management 910–912
  organic IR-absorber
    dithiene complex derivative 898, 899
    dithiolene metal complex derivative 898, 899
  organic UV-absorbers 901
    2-hydroxybenzophenone 900
    2-hydroxybenzophenone derivatives 902, 903
    2-(2-hydroxyphenyl)benzotriazol 900
    oxalic diacrylamide 901, 902
    phenylacrylester derivative 900, 901
  radiowave/microwave shielding 906–910
  reflection 892, 898
  self-functional fiber 896, 897
  transmission 892, 894
  UV and IR-protection 912–914
  X-ray absorbers 904
  X-ray shielding 914–918
radiowaves shielding 906–910
RadMan system 846
rapier weaving machines 479, 615

raw wool, from sheep 60
reactive N-halamines 931–932
recycled poly (vinyl butyral) (PVB) 167
redox reaction mechanism 377
re-entrant hexagonal geometry 955
refractive index 26, 88, 301, 593–598, 604, 606, 608–612, 614, 616, 619, 704
regenerated chitosan fibers 126, 151–152
regenerated fibers 1, 4, 10, 811–812, 817, 897, 899
regenerated polymer fibres 811
regular weaves 456–457
renewable energy resources 649
resilience 19, 70, 83, 298–299, 350, 354, 357, 440, 464, 465, 488, 492, 704–705, 764
resin method 57
resistive humidity sensors 705
respiratory rate measurement 400–401
reverse osmosis 25, 225, 788, 795–797
rewet property 326
RGO-PPy coated samples 244
ring spinning process 16, 442
  blow room section 16
  carding 16
  combing 16
  cone winding 17
  drawing 16
  objectives 16
  roving 16
ring spun yarn
  prominent features 444–445
  structure 443–444
ripple-like PA-6 NF/N membrane 195
roll-to-roll (R2R) printing technology 736
rosette-shaped terminal complexes 96, 107
rotational rigid geometry 955
rotor spinning 15, 17, 445–446
rotor spun yarn
  prominent feature 446
  structure 446
Roulette wheel selection 540
roving 16–17, 47, 442, 447, 814–815, 820
Ryton 821

S

SAF™ 323
sandwich structured polyamide-6/polyacrylonitrile/polyamide-6 (PA-6/PAN/PA-6) composite membrane 193
sateen/satin weaves 482
scanning electron microscope (SEM) 43, 101, 110, 112, 115–117, 145, 164, 169, 178, 189, 192–193, 195, 239, 269–270, 368, 372, 375, 377, 382, 422, 515, 578, 619, 636, 653, 655, 661, 664, 667, 669–670, 685, 689, 702, 735, 741, 743, 775, 784, 787, 793, 907–908, 910, 912, 914–915, 965
scouring 20, 58
screen printing 21, 238, 249, 736–739, 817
"segmented arc" spinnerets 285
segmented pie fibers 291, 295, 297
segmented pie technique 285
segmented polyurethanes 6, 27, 414–415
selective laser melting (SLM) 288
self-assembled monolayer (SAM) 507, 726–727, 733–734
self-assembled sub-micron fibers 112
self-assembling 366–367, 369
self-cleaning textiles 499, 506–507, 519–522
self-crimping yarns 284
self-sensing actuators 682, 700
sensible heat storage (SHS) 263
sensors 380–381
  fiber-based 709
  fibre-shaped 582–583
sensory detection method 61
sericin 76, 84
  amino acid composition 77
  amino acids in 76
  molecular weight 76

shape memory alloys (SMAs) 364, 373–374, 411, 682–683, 685, 694
shape memory ceramics (SMCs) 24, 411
shape memory fibers 6, 27, 304, 335, 362, 364, 373–374, 765–768
shape memory hybrids (SMHs) 374
shape memory materials (SMMs) 25, 27, 30, 374, 411, 683–685, 849–850
shape memory polymers (SMPs) 6, 67–69, 374, 411, 422, 683–685
  fiber actuators 684
shape memory polyurethane (SMP–MWNT) composite 422
shape-memory properties 15, 63–70, 413–415, 425, 430
shearing and sorting process, of wool 44–45
sheath-core single fibre devices (SCSFDs) 558–559, 561–562, 568–570, 575
sheet molded compounds (SMC) 24, 411
shuttleless looms 479
shuttle looms 479, 480
Si/carbon nanofiber (Si/C) 654–655, 660–661
Si/C–C core–shell nanofiber structure 654–655
Si/C/CNF nanofiber production 660
Si/C composite nanofibers 655
side-by-side bicomponent fibers 284
side emitting plastic optical fibers (SEPOF) 594, 595, 609
  abrasion 620, 621
  active illumination 638
  Al_2O_3 particles in core 617
  attenuation profile 609
  based on difference between refractive indexes 610–612
  illumination intensity 611, 612
  micro-cuts/notches in cladding 618
  micro-mirrors formation 619
  multiple micro-bending 612–616
  structure modifications 616–620
  with TiO_2 particles 619
  ZnO particles in cladding 617
silica glass fiber optics 394
silica nanofibrous (SNF) membranes 197, 329
silica optical fiber, attenuation profile of 602
silica/PAN membranes 656
silicon based pastes 250
silicon-based p-i-n photodiode junction fibre 570
silicon oxide fibers 364
silk 78, 182
  amino acid composition 85–86
  applications 88
  biomedical applications 90
  characterization 78
  creep and stress relaxation behavior 88
  cross-sectional view, SEM 84
  fibre reinforced composites 90
  fine structure 83–85
  fluorescent silks 91
  genetically engineered 91
  inverse stress relaxation phenomenon 88
  longitudinal views, SEM 84
  mechanical properties of 88
  mulberry silk 78–80
  non-mulberry silk 80–83
  optical properties 87–88
  place of origin 79–80
  structure 78
  tensile properties 86–87
  textile and apparels 89–90
  types and importance 78
  viscoelastic behavior 88
silk fibres 2, 8, 37, 50, 76, 83–88, 90, 895
  amino acid composition of 86
silk filament 76, 78–79
silk worm races
  Chinese 79–80
  European 80
  Indian 79
  Japanese 79
  molting 80
  voltinism 80

single crystal silicon fibers 364
single fiber structure 182–183
single-mode optical fibers 599, 601
single plain jersey knitting 487
single point crossover and mutation operator 540
SiO_2/PAN membranes 665, 666
"skin-core" effect 215
skin-core fibers 369
sleeping bag 877–879
slip effect 176, 186–187
smart anti-bacterial fiber 362
smart antibacterial textiles 372
smart clothing 377
smart fibers 2, 6
  aerogels 373
  classification 362
  coating with no less than double layers 370
  coating with single layer 370
  color-changed fibers 376–377
  definition 361
  energy conversion 381
  fabrics and fiber based membranes 372
  fiber-based actuator 374–375
  future trends 381–383
  inorganic nonmetallic materials 364–365
  intelligentization method 366–367
  luminescence fibers 375–376
  medical supplies 378–380
  metal related 363–364
  other uses 381
  primary fiber structure 368–371
  research status 361–362
  sensors 380–381
  shape memory fibers 373–374
  smart clothing 377–378
  spinning methods 365–366
  thermo-regulated fiber 377
  wearable electronics 378
smart heating sleeping bag 877–879
smart hollow fibers 421
smart robots 372
smart textile 30, 251
smart textiles 21, 26, 30, 233, 244, 251, 253–254, 267, 274, 349, 361, 375, 377–378, 391, 404–407, 557, 570, 684, 750, 879
SnO_2-TiO^2-NF photoanode 669
sodium storage mechanism in N-CNFs 654
soft computing 529
  advantage 529
  artificial neural network 530–535
  fabric property prediction 545–551
  fuzzy logic 535–539
  genetic algorithm 539–540
  yarn manufacturing 544–545
solar cells, fibre-shaped 568
solid core Bragg photonic fiber 617
solution spinning 10, 151, 212, 215, 272, 323–324, 365–366
solution-spinning polyurethane elastomers 336
Soutache techniques 249
spacer fabrics 489–490, 759
special spin pack design 285–288
spider silk 31, 76, 83
spider *vs.* mulberry silkworm silks 76
spider-web-like NF/N structured membranes 183
spinning 6, 41, 75, 108, 132, 157, 176, 207, 235, 271, 281, 319, 335, 365, 412, 436, 478, 544, 608, 655, 683, 735, 759, 779, 812, 835, 896, 960
spinning consistency index (SCI) 544
spinning of collagen fiber
  acid extraction 161
  alkali extraction 161
  collagen composite fiber 165
  electrospinning 162
  enzyme 160–161
  microfluidic spinning 164–165
  wet spinning 162–164
spinning process 15–17, 46–47, 52, 54, 214–216, 219, 242, 245, 285, 288–291, 293, 302, 304, 336, 344, 347, 365, 419, 443, 478, 491, 780, 814, 896, 914
spinning, textile manufacturing 15–18
  friction spinning 17

ring spinning 16–17
rotor spinning 17
yarn numbering system (count) 17–18
spin pack design 282–284, 286–288
splittable fibers 295
spring wool 45
spunbonded and thermal bonded nonwovens 493
spunbond fabrics 327, 492
stainless steel yarns 235, 251
standardised textile processes 233
staple spun yarn structure 438, 441, 443
stearic acid (SA) fiber 266, 271
step index profile optical fiber 598, 599
Sterigel 329
stilbene derivative 902–903
Stoll criterion 842, 844
strain fabric sensing technology 27
strain gauge 518, 696
strain measurement 392, 395, 397, 696, 710
strain sensors 235, 350, 395–396, 518, 696, 700, 705
stress–strain curve 438–440
stress memory 422–423
behaviour 425–427
components 424–425
cycle 423
mechanism 423–424
programming 423
stress relaxation 88, 290, 419–420, 423, 425, 429, 440, 760–761, 825
stretched length 53–54
sub-bandage pressure 749
sub-micron fibers 110–113, 134
sub-micron-scaled cellulose fibers 107–114
Sugeno FIS 539
summer wool 45
super-absorbent fibers 5
application 327–329
future scope and challenges 329–330
history of 316
mixing with hydrophobic/hydrophilic material 320
polymer materials 319
principle of 316–319
test methods 325–327
using uperabsorbent polymer 322
super absorbent polymer (SAP) 315–322, 326–329
superabsorbent textiles 318, 325–329
superabsorbent yarn 319–320
supercapacitors 665–667, 739
fibre-shaped 572–575
principles of 651–652
superfine wool 52–53
surface-initiated atom transfer radical polymerization (SI-ATRP) 728, 730, 732–734
sweating manikin 868–869
Swellcoat™ 328
switch-spring-frame model 423–425
SWNTs coated cotton yarn 370–371
swollen superabsorbent yarn 320
synthetic fibers 2, 5, 7, 10, 25, 820
advantages 30–31
as building materials 25
synthetic filament yarn 247
synthetic polymer fibres 811

t

tasar silk 80–81, 88
Taylor Cone 109, 179–180, 657, 774
Technical Absorbents (TAL) 316, 320, 323, 327–328
technical fabrics 480, 530
technical textiles 6, 21–22, 37, 52, 227, 478, 484–485, 489, 496, 529, 750, 807, 827
Teflon 658, 821, 823
Teijinconex 207, 214
temperature measurement 392, 395, 870
TEMPO mediated oxidation of native cellulose 104–105
tensile elongation (EMT) 464–465
tensile resilience (RT) 464–465
tensile work (WT) 464–465
tert-butanol 113, 114

tetrafluoroethylene-hexafluoropropylene-vinylidene fluoride terpolymer (THV) 301
tetramoulters 80
textile-based CNT/PEDOT + PSS composite conductors 243
textile-based electronics
  applications in
    polymer solar cells (PSCs) 742, 744–745
    supercapacitor 739–741
    triboelectric nanogenerator 742, 743
  fabricated metallic textiles 723–724
  flexible and stretchable material 721
  high-performance conductive textiles 722–723
  metal/textile interfacial 724–726
  PAMD 725
  wearable electronics 721, 722
textile based superabsorbent products 318
textile electrodes 243, 252, 253
textile-embedded electronics 709
textile fibers 1–3, 6, 11–12, 14–15, 28, 38, 63, 235, 243, 247–249, 436, 438, 440, 630, 671, 683, 723–724, 745, 750, 760, 808, 811–813, 817–820, 825, 827, 836, 891, 904, 907, 953
  evolution of 3
textile fibrous assembly 11–14
  mechanical behaviour 11
textile filter media 807, 811
textile manufacturing/processing 15
  dyeing 20
  dyes used 20
  finishing 21
  knitting 19
  nonwoven fabrics 19
  pretreatment process 20
  printing 21
  spinning process 15–18
  weaving process 18–19
  wet processing technology 20
textile printing 21
Thai silk 80
thermal comfort 264, 275, 833, 857, 860–862, 866, 872–874, 876–879
  fibre 871–872
thermal energy harvesters 566–572
thermal energy storage (TES) 263, 265–266, 276
thermal insulation bi-component elastic fiber 350
thermal performance estimate (TPE) 843, 844
thermal protective performance clothing
  air gap size effect 848–849
  evaluation of
    bench top testing 842–845
    full-scaled manikin testing 845–846
    standards 842
  fabric physical properties 847–848
  fibrous materials
    chemically modified flame resistant fiber 833, 835–836
    inherently flame resistant fiber 833, 836–839
  flame retardant 850
  flammability 839–841
  moisture content 849
  requirements of 832
  shape memory materials 849
thermal-regulated fibers 362, 377–378
thermal sensitive memory polyurethane 422–423, 425
thermal stress 270, 274, 424–425, 833
thermo-bondable core-sheath bicomponent fibers 296
thermobonded nonwoven fabrics 282
thermo-chemical heat storage processes 263
thermoplastic elastomer (TPE) 304, 337, 843–844
thermoplastic fiber-reinforced composites 303–304
thermo-regulated fiber 362, 377–378
thermo-regulating textiles 264
thermotropic liquid crystalline polymer (TLCP)/PP 289

thin-film nanofibrous composite (TFNC) membrane 781, 782
barrier layer and the electrospun nanofibrous 792
cellulose and chitin 790
cellulose nanofiber 791, 792
filtration performance of 793, 794
forward osmosis (FO) applications 797
permeation flux 793
polymer matrix barrier layer 793
three-tier structure 789, 790
Thorp, John 442
three-dimensional electrospun chitosan mats 150
3D rotary braiding machines 494
TiO_2 nanofibers 668
tissue engineering, fibers for 29–30
TLCP/PP bicomponent fibers 289
total internal reflection 593, 596–597, 704
tournament selection 540
traditional engineering materials (TEM) 101, 104, 106, 422, 461, 653, 667, 953
transistors 26–27, 240–241, 557, 566, 580–581
transverse wicking 863
trapezoidal membership function 537
triazinylaminostilbenes 902
tri-block A-B-C copolymer 763
triboelectric nanogenerator 379, 742
triclosan 503
1,1,1-trimethylol-propane triacrylate 319
trimolters 80
tripolyphosphate (TPP) 150, 842–844, 848
tropocollagen (TC) 29, 96–97, 158–159
"tube in orifice" spinneret 285
Twaron 10, 207, 837
twill weaves 456, 482
twisted and/or coiled polymeric fibers 694
twisted CNT yarn actuator 690
twisted fibre devices (TFDs) 558–562, 568, 570
twist GO hydrogel fibers 381
type I collagen fiber 157
tyrosine 8, 85, 895

u

ultracapacitors 651
ultrafiltration (UF) membranes 789–793
ultra-fine nano fibers 137, 272, 422, 778
ultra-high molecular weight polyethylene (UHMWPE) fibers 304, 960, 963, 965, 968
ultrathin conductive layer wrapped polyurethane yarns 370
ultraviolet protective fabrics 912
univoltines 79–80
US 20070292684 A1 349
UV protection factor (UPF) of plain woven fabrics 547–551
ANFIS model 548–551
ANN model 548, 549
nonlinear regression model 547–549
trend analysis 549

v

valine 85
Valonia cellulose 97, 98
van der Waals forces 7, 110–111, 159, 216, 338, 436, 515
vapour diffusion 862
vegetabel tannins 167–168
Velcro patches 764
vinylsulfone 901–902
viscose rayon 4, 9, 10, 114–115, 136, 163, 817, 820
viscous stress 424, 425
volatiles 109, 293–294, 322, 363, 513, 518, 779, 798–799, 835–836
voltinism 79, 80

w

Walter' manikin 869
warp 455
and weft satins 457

warp (*contd.*)
knitting 19
yarn 248, 815
washable sensors 251
washable wetness sensor 252
washing and weeding process, of wool 46
water-jet looms 479, 480
water purification
electrospun nanofiber scaffolds
mechanical properties 781–782
polymer materials 782
pore geometry 779–780
pore size 777–778
porosity 775–777
surface area 778–779
electrospun nanofibrous composite membranes 783–799
water soluble chitosan 125, 127
water vapor permeability property 23
wearable electronic devices 557, 565, 681, 722
wearable electronics 26–27, 118, 250, 253, 349, 378, 558, 566, 568, 584, 640, 721, 740, 745
weave factor 455, 457–458
weaving
applications 484–485
properties 484
weaving machines 479–481
woven structures 481–484
weaving machines 479–481
weaving process 18
beating 19
picking 19
shedding 18
sizing/slashing 18
taking up and letting off 19
warping 18
weft 455
and warp knitting machines 485
yarns 248, 815
weft knitting 19
jacquard fabrics 487
machine 816, 817
wer or melt spun fibers 415
wet blue leather fiber PVB 167
wet-extrusion of aqueous cellulose nanofibrils suspensions 115
wetlaying 490–491
wet processing technology 20–21
wet spinning 6, 114, 116–117, 134, 136–137, 139, 161–165, 215–216, 242, 271, 322–324, 335–337, 366, 412, 415, 430, 683, 686, 705, 914
of aramid fibers 214
wet spun method 366
wet spun polyurethane (PU) fibres 242
wet-stretching induced cellulose nanofibrils orientation 116, 117
wicking 819, 862–863, 865, 879
wicking parameter 326
wild silks 75, 80
winding process 17
wood cellulose fibers, hierarchical structure of 101
wool
acid resistance 59
classification methods 41–45
composition 48
count tops 61
crimpness 55–56
fabric inspection and evaluation 61
fineness of 52–53
friction and felting property 56–57
grease 57–58
hygroscopicity 59
impurities of 59
keratin extraction 70
keratins, future advanced uses of 71
length of 53–55
macromolecular structure 49–50
morphology and hierarchical structure 50–52
physical properties 68
primary processing 45–46
properties 37, 52–60
quality count 53
received by Australian brokers and dealers 39
shape memory properties 63
shearing and sorting process 45
twin-net-switch structural model 69

type and property 42
uses 37
warmth retention 60
washing and weeding process 46
yarn spinning process 46–48
wool fibers 2, 37, 356, 812, 836, 872, 895
lipid content 59
wool quality count *vs.* China's wool average diameter 54
wool worsted fabric
color fatness requirements 64
physical requirements 63
wool worsted products 62, 70
appearance of defects, evaluation and grading 65
work of rupture 440
World raw silk production 79
worsted wool fabrics
dimensional stability to washing requirements 64
length of 62
quality grading 62
technical and safety requirements 62
woven aramid 832
woven construction 759
woven fabrics 815
compression deformation 465–468
constitutive laws 470–471
continuum models 471
crimp 458
discontinuum models 471
energy methods 472–473
geometric models 458
irrecoverable deformation 14
irregular woven structure 457
non-linear stress-strain trend 11
plain weave 456
regular weave structure 456–457
shearing deformation 468–469
stress-strain plots for 11, 13
tensile deformation 461–465
twill weaves 456–457
UV protection modeling 547
warp and weft satins 457
weave factor 457–458
woven structures 11, 182, 247, 440, 477, 481–484, 615, 618, 743

x

Xinjiang wool 39
X-ray diffraction (XRD) 67, 69, 105, 116, 218, 417, 500, 509–511, 653
X-ray fluorescence 500, 512
X-ray photoelectron spectroscopy (XPS) 500, 511–513, 653
X-ray protective fibers 915–917
Xtrasorb® 327

y

yarn 435, 759, 814
air vortex spun 446
classification 440–441
frictional spun 448
mechanical properties 448
ring spun 442–443
rotor spun 445
strength–comfort–twist relationship 451–453
structure 441–448
tensile strength 448–451
yarn-based thermoelectric generator 566
yarn crimp 463–464, 484
yarn manufacturing, soft computing applications in 544
yarn production 245–248, 250, 447
yarn spinning process, of wool 46–48
yarn tenacity 537–538
membership functions of 538
Young's modulus 107, 116–117, 119, 165, 194, 226, 244, 401, 439, 465
YSZ nanofibrous membranes 198

z

zirconate titanate (PZT) nanofiber 381, 671, 685
ZnO nanowires fibre-shaped piezoelectric device 571
ZnO paper-based piezoelectric device 571